FINAL REPORT

An Ecohydrological Approach to Managing Intermittent and Ephemeral Streams on Department of Defense Lands in the Southwestern United States

SERDP Project RC-1727

JANUARY 2015

Lainie Levick
Samantha Hammer
Russell Lyon
Phillip Guertin
University of Arizona

Joel Murray
Amy Birtwistle
Brian Bledsoe
Melinda Laituri
Colorado State University

David Goodrich
USDA-ARS

Distribution Statement A
This document has been cleared for public release

SERDP
DOD ▪ EPA ▪ DOE

This report was prepared under contract to the Department of Defense Strategic Environmental Research and Development Program (SERDP). The publication of this report does not indicate endorsement by the Department of Defense, nor should the contents be construed as reflecting the official policy or position of the Department of Defense. Reference herein to any specific commercial product, process, or service by trade name, trademark, manufacturer, or otherwise, does not necessarily constitute or imply its endorsement, recommendation, or favoring by the Department of Defense.

REPORT DOCUMENTATION PAGE

Form Approved
OMB No. 0704-0188

The public reporting burden for this collection of information is estimated to average 1 hour per response, including the time for reviewing instructions, searching existing data sources, gathering and maintaining the data needed, and completing and reviewing the collection of information. Send comments regarding this burden estimate or any other aspect of this collection of information, including suggestions for reducing the burden, to Department of Defense, Washington Headquarters Services, Directorate for Information Operations and Reports (0704-0188), 1215 Jefferson Davis Highway, Suite 1204, Arlington, VA 22202-4302. Respondents should be aware that notwithstanding any other provision of law, no person shall be subject to any penalty for failing to comply with a collection of information if it does not display a currently valid OMB control number.

PLEASE DO NOT RETURN YOUR FORM TO THE ABOVE ADDRESS.

1. REPORT DATE *(DD-MM-YYYY)*	2. REPORT TYPE	3. DATES COVERED *(From - To)*
01-30-2015	Final Report	Mar 2010 - Jan 2015

4. TITLE AND SUBTITLE

An Ecohydrological Approach to Managing Intermittent and Ephemeral Streams on Department of Defense Lands in the Southwestern United States

5a. CONTRACT NUMBER
W912HQ-10-C-0009

5b. GRANT NUMBER
NA

5c. PROGRAM ELEMENT NUMBER
NA

6. AUTHOR(S)

L. Levick, S. Hammer, R. Lyon, J. Murray, A. Birtwistle, D. Goodrich, B. Bledsoe, P. Guertin, M. Laituri

5d. PROJECT NUMBER
RC-1727

5e. TASK NUMBER
NA

5f. WORK UNIT NUMBER
NA

7. PERFORMING ORGANIZATION NAME(S) AND ADDRESS(ES)

University of Arizona, Tucson, AZ 85721
Colorado State University, Fort Collins, CO 80523
USDA ARS, 2000 E Allen Rd, Tucson, AZ 85719

8. PERFORMING ORGANIZATION REPORT NUMBER
NA

9. SPONSORING/MONITORING AGENCY NAME(S) AND ADDRESS(ES)

Strategic Environmental Research and Development Program
4800 Mark Center Drive, Suite 17D08
Alexandria, VA 22350

10. SPONSOR/MONITOR'S ACRONYM(S)
SERDP

11. SPONSOR/MONITOR'S REPORT NUMBER(S)
RC-1727

12. DISTRIBUTION/AVAILABILITY STATEMENT

Unlimited Distribution

13. SUPPLEMENTARY NOTES

NA

14. ABSTRACT

The objective of this project was to develop an ecohydrologically-based stream type classification and methodology for four military reservations in the southwestern United States representing the four Level III ecoregions that occur here: Fort Irwin (Mojave Basin and Range), Yuma Proving Ground (YPG; Sonoran Desert), Fort Huachuca (Madrean Archipelago), and Fort Bliss (Chihuahuan Desert). The goals of this project were to: (1) characterize ephemeral and intermittent streams using vegetation, hydrologic, and geomorphic attributes and develop a stream type classification based on those attributes, (2) associate wildlife habitat with the variables and stream type classification to improve management of TER-S and species of concern, and (3) provide a tool that allows Department of Defense (DoD) managers to evaluate the impacts of perturbations (e.g. climate change, military activities) on the hydrologic regimes of these systems and the species that depend on them.

15. SUBJECT TERMS

military, ephemeral, intermittent, arid, ecohydrology, classification, geomorphology, riparian vegetation, xeroriparian, hydrology, wildlife, cluster analysis, species richness, gray vireo, desert tortoise, owl

16. SECURITY CLASSIFICATION OF:			17. LIMITATION OF ABSTRACT	18. NUMBER OF PAGES	19a. NAME OF RESPONSIBLE PERSON
a. REPORT	b. ABSTRACT	c. THIS PAGE			Lainie Levick
U	U	U	U	577	19b. TELEPHONE NUMBER *(Include area code)* 520-647-9153 x176

Reset

Table of Contents

List of Figures ..... **iii**

List of Tables ..... **v**

List of Acronyms ..... **vii**

Keywords ..... **ix**

Acknowledgements ..... **ix**

Abstract **1**

1.0 Objective **3**

2.0 Background **4**

Ephemeral and Intermittent Stream Characteristics 6

Study Site Selection 12

General Descriptions by Installation 14

Classification Techniques 21

Hydrologic Rainfall-Runoff Models 23

3.0 Materials and Methods **25**

Task 1: Data Mining and Cataloging 25

Task 2: Characterization of the Study Watersheds and Stream Systems 26

Unit of Analysis and Riparian Zone 27

Variables for the Ecohydrologic Stream Type Classification 28

Hydrologic Modeling Using AGWA 31

Riparian Vegetation Characterization 39

Task 3: Field Data Acquisition 46

Geomorphic Data 47

Riparian and Upland Vegetation Data 47

Hydrologic Data 48

Wildlife and Wildlife Sign, Habitat Features 48

Longitudinal Channel Walks 48

Task 4: Classification of Ephemeral and Intermittent Stream Types 49

Analysis Methods 49

Task 4a: Wildlife Associations 51

Species Distribution Modeling Methods 51

Mesquite Bosque Species Richness Methods 57

Nesting Habitat Index Methods 62

Species Richness Analysis Methods 64

Task 5: Field Test and Verification 66

Hydrologic Modeling Verification 66
Riparian Vegetation Data Verification 70
Task 6: Assessment Methodology 72
Task 7: Technology Transfer Workshops with DoD Managers 73
4.0 Results and Discussion 76
Ecohydrological Stream Type Classification 77
Fort Irwin 80
Yuma Proving Ground 83
Fort Huachuca 87
Fort Bliss 90
Special Conditions 93
Wildlife Associations 94
Fort Irwin 95
YPG 112
Fort Huachuca 129
Fort Bliss 146
Discussion 164
4.1 Action Items 169
Classification Coordination with Projects RC-1725 and RC-1726 169
Valley Bottom Floodplain Complex, Growler Wash 174
Channel Incision 180
5.0 Conclusions and Implications for Future Research/Implementation 185
6.0 Literature Cited 191
7.0 Appendices 204
Appendix A: Scientific and Technical Publications, Theses, and Presentations 1
Appendix B: Stream Type Classification Results B-1
Fort Irwin 2
Yuma Proving Ground 5
Fort Huachuca 8
Fort Bliss 11
Appendix C: Wildlife Tables C-1
Appendix D: AGWA Hydrologic Modeling Results for Flow Permanence and Peak Flows D-1
Appendix E: Maps of Field Site Locations E-1
Appendix F: Samantha Hammer Master's Thesis F-1
Appendix G. Russell Lyon Master's Thesis G-1
Appendix H. AGWA Tool Guidance Document H-1

Appendix I: Stream Type Classification Guidance Document.....I-1
Appendix J: Vegetation Analysis and Methods Guidance Document..... J-1
Appendix K: Geomorphology Analysis Guidance Document..... K-1

List of Figures

Figure 1. Conceptual model. 5
Figure 2. Project tasks and schedule. 6
Figure 3. Map of the Department of Defense Southwest Region, ecoregions and study locations: Fort Irwin, Yuma Proving Ground, Fort Huachuca, and Fort Bliss. 13
Figure 4. Fort Irwin landcover, field sites, and springs. 14
Figure 5. Photos at Fort Irwin showing "floodout zones." 15
Figure 6. Photos at Fort Irwin showing No Name Spring (left), and Brinkman Wash where the channel bottom is vegetated and creosote indicates uplands (right). 15
Figure 7.Yuma Proving Ground vegetation communities and field sites. 16
Figure 8. Photos at YPG showing riparian vegetation located in swales between desert pavement covered hills (left) and in a large incised alluvial wash (right). 17
Figure 9. Photos at Fort Huachuca study sites showing bedrock dominated channel (left) and wide incised alluvial channel (right). 18
Figure 10. Photos at Fort Huachuca study sites showing riparian vegetation at an upland intermittent stream reach (left) and a mid-elevation ephemeral stream reach (right). 18
Figure 11. Fort Huachuca land cover and field sites. 19
Figure 12. Fort Bliss ecological management areas and field sites. 20
Figure 13. Photos at Fort Bliss in areas without defined channel formation: Otero Mesa swales (left), and coppice sand dunes (right). 21
Figure 14. Images showing the 1 km stream reach polygon representing water surface width at 3 m inundation depth, overlain on an orthophoto, at Fort Huachuca. 28
Figure 15. Automated Geospatial Watershed Assessment Tool (AGWA) work flow and model outputs. 32
Figure 16. Hydrograph comparing modeled (SWAT) and observed (USGS) discharge for Upper Garden Canyon, Fort Huachuca, using met station precipitation in the SWAT model. 35
Figure 17. Map of Upper Garden Canyon Watershed and USGS stream gauge location. 37
Figure 18. Plots of simulated vs. observed average monthly volume totals at Upper Garden Canyon using NEXRAD-MPE precipitation input for (a) calibration and (b) validation. . 38
Figure 19. Map showing flow permanence for all 1 km stream reaches at Fort Irwin. 39
Figure 20. Illustration of vegetation structure layers. 41
Figure 21. Map of vegetation structure group 1 - 4 m for Fort Irwin streams. 42
Figure 22. Map and table of vegetation structure classes for Fort Irwin stream reaches. 42
Figure 23. Map image at Bitter Springs, Fort Irwin, showing MSAVI2 values (left), and a photo of Bitter Springs (right). 44
Figure 24. Map image of Bitter Springs area, Fort Irwin, showing MSAVI2 mean values for the 1 km stream reach polygons (left), and MSAVI2 values classified for percent cover (right). 44
Figure 25. Dendrograms for YPG clustering, 4 clusters, with (left) and without (right) the SVRI index. 45

Figure 26. NMDS plots for YPG clustering with (left) and without (right) the SVRI index. . 46
Figure 27. YPG - Overview of 7 of the 12 modeled bosques. 59
Figure 28. Fort Irwin, field site *NLBL1*: Qp100 = 0.001 m^3/s, flow permanence = 4.1%. 67
Figure 29. Fort Huachuca, field site *BRHC1*: Qp100 = 124 m^3/s, flow permanence = 33.1%.68
Figure 30. Fort Bliss, field site *THGC1*: Qp100 = 728.2 m^3/s, flow permanence = 28.3%. ... 69
Figure 31. YPG, field site *MW002*: Qp100 = 1458.4 m^3/s, flow permanence = 0.10%. 70
Figure 32. Fort Huachuca's East Range riparian vegetation height categories, comparison of field data with LiDAR analysis results 71
Figure 33. Map of Fort Huachuca's East Range, with study sites and the LiDAR-derived vegetation height categories clipped to a 75 m wide stream buffer (total 150 m wide). 72
Figure 34. Mean and maximum flow permanence (%) for each installation. 78
Figure 35. Fort Irwin dendrogram and map for 8 stream types. 81
Figure 36. Fort Irwin stream types, percent of total stream reaches and total stream lengths. 81
Figure 37. YPG dendrogram and map for 10 stream types. 84
Figure 38. YPG stream types, percent of total stream reaches and total stream lengths. 84
Figure 39. Fort Huachuca dendrogram and map for 8 stream types. 87
Figure 40. Fort Huachuca stream types, percent of total stream reaches and total stream lengths. 88
Figure 41. Fort Bliss dendrogram and map for 8 stream types. 90
Figure 42. Fort Bliss stream types, percent of total stream reaches and total stream lengths.. 91
Figure 43. Probability of tortoise presence as a function of each individual variable. 96
Figure 44. Correlation of desert tortoise probability of presence from our unbiased prior model (SEDRP model) and the USGS model. 97
Figure 45. MaxEnt modeling results for the desert tortoise with an unbiased prior (top) and a biased prior (bottom). 98
Figure 46. Probability of presence for burrowing owl as a function of each individual variable. 99
Figure 47. MaxEnt modeling results for the burrowing owl with an unbiased prior (top) and a biased prior (bottom). 101
Figure 48. Correlation of desert tortoise and burrowing owl probability of presence for the unbiased prior model. 102
Figure 49. Fort Irwin - Richness of riparian-associated species. 103
Figure 50. Fort Irwin - Richness of riparian-associated TER-S species. 104
Figure 51. Fort Irwin - Richness of riparian-associated species in the eight stream types. ... 105
Figure 52. Fort Irwin - Richness of riparian-associated TER-S in the eight stream types. ... 107
Figure 53. YPG - Richness of riparian-associated species. 118
Figure 54. YPG - Richness of riparian-associated TER-S species. 119
Figure 55. YPG - Richness of riparian-associated species in the ten stream types. 121
Figure 56. YPG - Richness of riparian-associated TER-S in the ten stream types. 123
Figure 57. Fort Huachuca – Mexican Spotted Owl probability of presence as a function of four variables. 129
Figure 58. Fort Huachuca - MaxEnt modeling results for Mexican spotted owl. 130
Figure 59. Fort Huachuca - Probability of presence for Mexican spotted owls in stream types within the modeling area. 131
Figure 60. Fort Huachuca – Owl probability of presence as a function of two variables. 132
Figure 61. Fort Huachuca - MaxEnt modeling results for screech owls. 133

Figure 62. Fort Huachuca - Probability of presence for screech owls in stream types within the modeling area. 134
Figure 63. Fort Huachuca richness of riparian-associated species. 135
Figure 64. Fort Huachuca richness of riparian-associated TER-S species. 136
Figure 65. Fort Huachuca richness of riparian-associated species in the eight stream types. 138
Figure 66. Fort Huachuca - richness of riparian-associated TER-S in the eight stream types. 140
Figure 67. Logistic modeling results for gray vireo. 148
Figure 68. Probability of presence for gray vireos in stream types within the modeling area. 149
Figure 69. Values across stream reaches on Fort Bliss, NM/TX of the overall nesting habitat value metric, NH_a (top) and the width-adjusted nesting habitat value metric, NH_w (bottom). 151
Figure 70. Total stream lengths at Fort Bliss, NM/TX of values of the overall nesting habitat metric, NH_a and width-adjusted metric, NH_w. 152
Figure 71. Fort Bliss - Richness of riparian-associated species. 154
Figure 72. Fort Bliss - Richness of riparian-associated TER-S. 156
Figure 73. Fort Bliss - Richness of riparian-associated species in the eight stream types. 158
Figure 74. Fort Bliss - Richness of riparian-associated TER-S in the eight stream types. 160
Figure 75. Map showing the difference in water surface extent derived from the 10 m DEM and 1 m LiDAR for the 3 m inundated depth at Fort Huachuca. 167
Figure 76. Preliminary coordinated classification for flow permanence at Fort Huachuca... 170
Figure 77. Comparison of flow permanence (%) at all four installations. 170
Figure 78. Comparison of average annual precipitation (mm and inches) at all four installations. 170
Figure 79. Comparison of 25-yr 1-hr peak flow (m^3/s) at all four installations. 171
Figure 80. Map of Mohave Wash, Yuma Proving Ground, showing variability based on SWReGAP land cover and Arizona Geology. 172
Figure 81. Map of Cabeza Prieta Growler and San Cristobal Washes, with data points. 176
Figure 82. Photos from Growler Wash area, Valley Bottom Floodplain Complex (top), and YPG mesquite bosque (bottom). 178
Figure 83. Location of the majority of mesquite bosques at YPG. 179
Figure 84. Illustrations of bank slope, with the outline of the 0.5 m and 2 m water surface width polygons. 182
Figure 85. Map of stream reaches displayed with “Mean Bank Slope” (blue = lowest to red = highest) and photos of selected field sites. 184

List of Tables

Table 1. Statistical results for Upper Garden Canyon SWAT-NEXRAD, rain gauge and met tower simulations with coefficient of determination (R^2) and Nash-Sutcliffe Efficiency (NSE) values for calibration and validation time periods. 37
Table 2. Ecohydrological variables using in modeling individual species occurrence at each installation. Codes used here were also used for species richness modeling. 53
Table 3. YPG - Species or groups of species included in species richness, relative abundance index (RAI) and bird relative abundance index. 60
Table 4. YPG - Predictor variables for bosque species richness estimators. 61

Table 5. Variable importance, CART analysis, Fort Irwin. 82
Table 6. Fort Irwin stream type classification analysis, prediction success, 8 stream types. .. 82
Table 7. Fort Irwin thresholds for input variables, percent of each stream type for 8 stream types. 83
Table 8. Variable importance, CART analysis, YPG. 85
Table 9. YPG stream type classification analysis, prediction success, 10 stream types. 85
Table 10. YPG thresholds for input variables, percent of each stream type for 10 stream types. 86
Table 11. Variable importance, CART analysis, Fort Huachuca. 88
Table 12. Fort Huachuca stream type classification analysis, prediction success, 8 stream types. 89
Table 13. Fort Huachuca thresholds for input variables, percent of each stream type for 8 stream types. 89
Table 14. Variable importance, CART analysis, Fort Bliss. 91
Table 15. Fort Bliss stream type classification analysis, prediction success, 8 stream types. . 91
Table 16. Fort Bliss thresholds for input variables, percent of each stream type for 8 stream types. 93
Table 17. Fort Irwin - Effect of ecohydrological variables on all pooled TER-S riparian-associated species richness. 108
Table 18. Fort Irwin - Effect of ecohydrological variables on reptile TER-S riparian-associated species richness. 109
Table 19. Fort Irwin - Effect of ecohydrological variables on bird TER-S riparian-associated species richness. 110
Table 20. Fort Irwin - Effect of ecohydrological variables on mammal TER-S riparian-associated species richness. 111
Table 21. YPG – Mesquite bosques P-values <0.3 from poisson GLM for predictor variables as a function of species richness estimators. Values 0.2-0.3 are in gray 112
Table 22. Effect of each parameter on the species richness estimator, JK1. 113
Table 23. Effect of each parameter on the species richness estimator, JK2. 113
Table 24. Effect of each parameter on the species richness estimator, Chao1. 113
Table 25. Effect of each parameter on the overall RAI. 114
Table 26. Effect of each parameter on the bird RAI. 114
Table 27. Effect of each parameter on the mule deer RAI. 115
Table 28. Effect of each parameter on the kit fox RAI. 115
Table 29. YPG - Effect of ecohydrological variables on All TER-S riparian-associated species richness. 124
Table 30. YPG - Effect of ecohydrological variables on Amphibian TER-S riparian-associated species richness. 125
Table 31. YPG - Effect of ecohydrological variables on Reptile TER-S riparian-associated species richness. 126
Table 32. YPG - Effect of ecohydrological variables on Bird TER-S riparian-associated species richness. 127
Table 33. YPG - Effect of ecohydrological variables on Mammal TER-S riparian-associated species richness. 128
Table 34. Fort Huachuca - Results of Mann-Whitney U Tests for each ecohydrological variable in Critical Habitat for spotted owls. 131

Table 35. Fort Huachuca - Effect of ecohydrological variables on all TER-S riparian-associated species richness. 141
Table 36. Fort Huachuca - Effect of ecohydrological variables on amphibian TER-S riparian-associated species richness. 142
Table 37. Fort Huachuca - Effect of ecohydrological variables on reptile TER-S riparian-associated species richness. 143
Table 38. Fort Huachuca - Effect of ecohydrological variables on bird TER-S riparian-associated species richness. 144
Table 39. Fort Huachuca - Effect of ecohydrological variables on mammal TER-S riparian-associated species richness. 145
Table 40. Fort Bliss - Effect of ecohydrological variables used in the averaged top set of gray vireo models. 146
Table 41. Confusion matrix and accuracy rates for overall gray vireo modeling (training and test sets combined). 147
Table 42. Number of species nesting in each vegetation layer at Fort Bliss (left) and percent of species nesting in each vegetation layer (right) 150
Table 43. Results of GLM regression of estimated breeding bird richness derived from stacked GAP models against breeding bird richness measures derived from Kozma and Mathews (1995) and Myers et al. (1998) for 13 stream reaches on Fort Bliss, NM. 152
Table 44. Fort Bliss - Effect of ecohydrological variables on all riparian-associated TER-S richness. 161
Table 45. Fort Bliss - Effect of ecohydrological variables on riparian-associated reptile TER-S richness. 162
Table 46. Fort Bliss - Effect of ecohydrological variables on riparian-associated mammal TER-S richness. 162
Table 47. Fort Bliss - Effect of ecohydrological variables on riparian-associated bird TER-S richness. 163
Table 48. Statistical comparison of derived water surface widths from a 10 m DEM vs. 1 m LiDAR at different inundation depths. 167
Table 49. Watershed, valley and reach scale attributes. 173
Table 50. Use of USGS DEM and LiDAR-derived DEM data in the analyses 188

List of Acronyms

AGWA: Automated Geospatial Watershed Assessment Tool, http://www.tucson.ars.ag.gov/agwa/
AICc: Akaike's Information Criterion adjusted for small sample size
ArcGIS: Geographic Information System software product from ESRI, http://www.esri.com
ARS: Agricultural Research Service, http://www.ars.usda.gov
AUC: area under the curve of the receiver operating plot
AZGFD: Arizona Game and Fish Department
BNA: Birds of North America Online
CART: Classification and Regression Tree
CN: Curve Number
CSU: Colorado State University
DEM: Digital Elevation Model

DISDI: Defense Installation Spatial Data Infrastructure
DoD: Department of Defense, http://www.defenselink.mil/
ER: Entrenchment Ratio
ERDAS Imagine: image analysis software from ERDAS, http://www.erdas.com/products/ERDASIMAGINE/ERDASIMAGINE/Details.aspx
FUSION: U.S. Forest Service software for analysis and processing of LiDAR data, http://forsys.cfr.washington.edu/fusion/fusionlatest.html
GIS: Geographic Information Systems
GLM: Generalized linear model
HGVC: Hydro-Geomorphic Valley Classification tool
HRU: Hydrologic response unit
HSD: Honestly significant difference test, Tukey's
KINEROS2: Kinematic Runoff and Erosion Model, http://www.tucson.ars.ag.gov/kineros/
LiDAR: Light Detection and Ranging
MSAVI2: Modified Soil Adjusted Vegetation Index (Qi et al., 1994)
NCDC: National Climatic Data Center
NDVI: Normalized Difference Vegetation Index
NEXRAD-MPE: Next-Generation Radar-Multisensor Precipitation Estimation, high-resolution Doppler weather radars operated by the National Weather Service
NLCD: National Land Cover Dataset
NHD: National Hydrography Dataset
NMDS: Nonmetric Multidimensional Scaling
NRCS: Natural Resources Conservation Service
OHWM: Ordinary High Water Mark
OR: Omission rate
PAC: Protected Activity Centers
QuickBird: satellite imagery, http://www.digitalglobe.com/
R-G-B-NIR: Red, Green, Blue and Near Infra-red bands in satellite imagery
RAI: Relative abundance index
RapidEye: satellite imagery, http://www.rapideye.net/
RENDVI: Red Edge Normalized Difference Vegetation Index
RS: Remote sensing
RSI: Rainfall Seasonality Index
SAVI: Soil Adjusted Vegetation Index
SPM: Salford Predictive Modeler Suite, http://www.salford-systems.com/spminfo.html
SSURGO: Soil Survey Geographic Database
SVRI: Seasonal Vegetation Response Index
SWAT: Soil and Water Assessment Tool, http://swat.tamu.edu/
SWReGAP: Southwest Regional Gap Analysis Program
T&E: Threatened and Endangered Species
TER-S: Threatened, Endangered and At-Risk Species
TSP: Total Stream Power
UA: University of Arizona
U.S.: United States
USDA: United States Department of Agriculture, http://www.usda.gov
USLE: Universal Soil Loss Equation, http://topsoil.nserl.purdue.edu/usle/

USGS: United States Geological Survey
YPG: Yuma Proving Ground

Keywords
military, ephemeral, intermittent, arid, ecohydrology, classification, geomorphology, riparian vegetation, xeroriparian, hydrology, wildlife, cluster analysis, species richness, gray vireo, desert tortoise, owl

Acknowledgements
The funding for this research was provided by the Department of Defense, Strategic Environmental Research and Development program (SERDP), under the Resource Conservation and Climate Change program area. We greatly appreciate the opportunity to conduct this research, and thank the Program Manager, John Hall, his staff, and the staff at HydroGeoLogic for their support and guidance. We also acknowledge and thank the USDA-ARS Southwest Watershed Research Center, Tucson, AZ, for providing extensive in-kind support, including field vehicles for our many exciting excursions onto the installations. We would like to thank the Environmental/Natural Resources and Range Operations personnel at Fort Bliss, Fort Huachuca, Fort Irwin and Yuma Proving Ground for their logistical and technical support, and for granting us access to their installations. We especially appreciate the support and feedback from Dallas Bash, Brian Locke and David Black at Fort Bliss; Liana Aker and Dave Housman at Fort Irwin; Sheridan Stone, Tom Runyon, and Justin Nixon at Fort Huachuca; and Laura Merrill and John Glover at YPG. We thank Patty Guertin for her excellent help in plant identification and field data collection on our early field trips. We thank Chandra Collins-Holifield at the Southwest Watershed Research Center for her very valuable help with the remote sensing analyses. We acknowledge Steve Amesbury for his help in field data collection on the early field trips. We also thank Susan Howe for her efforts in getting this project started.

Abstract

Objectives.
Ephemeral and intermittent streams are the predominant fluvial forms in arid and semi-arid environments, yet knowledge of how these streams function is limited; specifically the linkages between wildlife and ecosystem characteristics in these environments are not well documented. Various studies have shown biological and habitat diversity in arid and semi-arid lands to be considerably higher along ephemeral and intermittent stream corridors in comparison to adjacent uplands. The central premise of this research is that the ecological integrity of these streams and the species that depend on them (including threatened, endangered, and at-risk species; TER-S) is inextricably linked to their hydrologic regime and that managing these systems is best addressed within an ecohydrological framework. The objective of this project was to develop an ecohydrologically-based stream type classification and methodology for four military reservations in the southwestern United States representing the four Level III ecoregions that occur here: Fort Irwin (Mojave Basin and Range), Yuma Proving Ground (YPG; Sonoran Desert), Fort Huachuca (Madrean Archipelago), and Fort Bliss (Chihuahuan Desert). The goals of this project were to: (1) characterize ephemeral and intermittent streams using vegetation, hydrologic, and geomorphic attributes and develop a stream type classification based on those attributes, (2) associate wildlife habitat with the variables and stream type classification to improve management of TER-S and species of concern, and (3) provide a tool that allows Department of Defense (DoD) managers to evaluate the impacts of perturbations (e.g. climate change, military activities) on the hydrologic regimes of these systems and the species that depend on them.

Technical Approach.
Existing climatic, physical, and biological data from GIS and ground-based methods were acquired for each military installation to characterize the stream channels across that installation. Digital elevation models and imagery (including multi-return LIDAR and high resolution multispectral imagery) were used to quantify riparian vegetation cover, density, and structure. The Automated Geospatial Watershed Assessment Tool (AGWA) and its two embedded hydrologic models (Soil and Water Assessment Tool, SWAT; and the Kinematic Runoff and Erosion Model, KINEROS2) were used to develop hydrologic gradients of peak flow and flow permanence. The USGS National Hydrography Plus Version 2 Dataset was used as the basis for the stream network and to derive the variables. Agglomerative hierarchical cluster analysis was used to classify ephemeral and intermittent streams by the ecohydrologic properties, and CART was used to determine thresholds for each variable for the predictive model. Various types of wildlife data, including species richness and occurrence of particular species, were analyzed in relation to the classified stream types and the ecohydrologic properties to provide information for managing species of concern. The AGWA tool was used to evaluate the impacts of climate change, training activities, and land management actions on flow permanence and peak flows.

Results.
Ephemeral and intermittent stream reaches at Fort Irwin, YPG, Fort Huachuca and Fort Bliss were classified based on their hydrologic, geomorphic and vegetation characteristics. Because these four installations have different hydrologic regimes and physical characteristics, each stream type classification is unique and represents the variability of stream reaches within that

installation. The classification procedure was developed and applied using data specific to each installation and the data and methodologies are appropriate for use in extending the classification to streams not on the NHD stream network within each installation. The final ecohydrologic stream types were determined for each installation from statistical analyses, cluster validity tests, examination of the mapped clusters, and site knowledge. Fort Irwin, Fort Huachuca and Fort Bliss had 8 final stream types, and YPG had 10 stream types. A CART classification tree was used to evaluate the clustering results for each installation to identify the thresholds for the input variables for each stream type. Results generally were explained in terms of the climate regime and geomorphology for YPG and Fort Irwin where annual rainfall amounts are relatively low or are largely confined to one season per year. Fort Bliss and Fort Huachuca experience higher annual rainfall amounts with a bimodal pattern, and vegetation variables were more important in those classifications. Vegetation density and cover were strongly related to elevation at all installations. The AGWA tool can be used immediately to evaluate management actions or climate change scenarios that modify the input variables, to determine if and how the stream type and wildlife associations might be affected. All variables and results are spatially referenced using a "Unique ID" and can be used immediately to evaluate individual stream reaches for management needs.

The stream type classifications and input variables were associated with wildlife in two ways. Species richness models were developed using habitat models for each installation. Species distribution models that evaluated the use of streams by single species of concern were developed that may guide management of and future surveys for those species. At Fort Bliss, a model was created for the New Mexico state threatened Gray Vireo (*Vireo vicinor*). At Fort Huachuca, models were created for the federally threatened Mexican Spotted Owl (*Strix occidentalis lucida*) and Screech Owls (Western, *Megascops kennicottii*; and Whiskered, *Megascops trichopsis*). At Fort Irwin, models were created for the federally threatened Desert Tortoise (*Gopherus agassizi*) and the Western Burrowing Owl (*Athene cunicularis*).

To assist management decision-making, datasets and tutorials were developed for evaluation of various land cover, land use, and climate change scenarios in AGWA. Technology transfer workshops were conducted at the installations to train personnel in the use of AGWA and to present project datasets and results. Feedback from the workshops was positive, indicating participants' interest in using the tools generated by the project.

Benefits.
The classifications and wildlife associations will assist natural resource managers by providing a method of identifying similar stream types, as well as stream reaches with similar characteristics, and for use in developing sampling schemes or surveys for wildlife and land use management. This research provides benefits to the DoD that include: (1) advancement in scientific understanding of how ephemeral and intermittent streams function, (2) a procedure for producing an ecohydrologic classification of ephemeral and intermittent streams to guide management activities and decision making and that can be applied over large areas using remotely sensed data and watershed modeling tools, (3) associations of the classification and variables with wildlife habitat for improved understanding of habitat requirements and management of species of concern and TER-S, and (4) a tool for assessing impacts of perturbations (e.g. climate change, military activities) on the hydrologic regimes and species that depend upon these streams on DoD installations in the southwestern United States.

1.0 Objective

This project is in response to the SERDP FY2010 Statement of Need (SON), Sustainable Infrastructure (SI) Focus Area entitled "Managing and Restoring Southwest Intermittent and Ephemeral Stream Systems on Department of Defense Lands". The SON outlined several issues that were of interest in improving management of DoD's southwestern installations including characterizing the variation of intermittent and ephemeral stream systems, potential altered hydrology and projected climate change, and the impacts on these systems and the threatened, endangered, and at-risk species (TER-S) that depend on them. The Southwest desert region is currently experiencing the effects of climate change and prolonged drought, and the impacts to wildlife and vegetation communities are already evident.

The main objective of this research was to develop an ecohydrologically-based stream type classification for Southwest desert military installations that distinguishes ephemeral and intermittent stream types by a set of ecohydrologic attributes (vegetation, hydrology and geomorphology). This objective addresses the need to characterize the variation of these stream systems, and creates the foundation for addressing the need to determine impacts from projected climate change on these systems and their management.

A second objective was to link the stream type classification with wildlife habitat characteristics, species habitat models, and wildlife species observation data to improve their management. The results address this objective, and create the foundation for understanding how variations in these stream systems may impact TER-S, for improved management of those species.

The final objective was to provide a tool that allows DoD managers to evaluate the impacts of natural and anthropogenic perturbations (e.g. climate change, military activities) on the hydrologic regimes of these systems and the species that depend on them. The Automated Geospatial Watershed Assessment (AGWA; http://www.tucson.ars.ag.gov/agwa) tool was applied to address this need, and includes tools to perform climate or land use change analyses.

Conventional stream classifications based on flow attributes and/or channel morphology have primarily been focused on perennial stream networks common to mesic environments (Rosgen, 1994; Montgomery and Buffington, 1997; Puckridge et al., 1998). In arid to semi-arid systems where ephemeral and intermittent streams are the dominant fluvial features, scarce observational data has hindered most attempts to perform similar stream classifications. While ephemeral and intermittent streams perform similar hydrologic and ecologic functions as their perennial counterparts (Levick et al., 2008) they generally are not incorporated in most watershed-based assessments. Few studies have addressed a comprehensive set of vertebrate species across a range of ephemeral and intermittent streams, or the effects of hydrology on wildlife and their use of xeroriparian systems. Doing so could elucidate which characteristics of these systems are important to particular species or groups of species of wildlife and would allow for better management and more effective conservation efforts. This research addresses these issues by producing a stream type classification for ephemeral and intermittent streams that can be related to wildlife habitat and used in defining ecohydrological relationships.

With these tools, DoD managers will be able to identify stream reaches with specific properties that are of interest for management actions, and will be able to predict changes in the hydrologic regime due to land cover or climate change to guide management decision-making, for sustained land use in the context of military training and testing.

2.0 Background

The Department of Defense (DoD) manages over 35,600 km^2 (3.56 million ha) of arid and semi-arid land in their Southwest Region, to meet its mission of providing national defense, and to maintain its commitment to stewardship of its lands. This includes compliance with the Endangered Species Act to conserve the federally listed threatened and endangered species that occur on those lands (Rubinoff et al., 2006), and conservation of biological diversity through various programs such as the Sustainment of Ranges and Operating Areas (DoD Directive 3200.15; Benton et al., 2008). The DoD Southwest Region is comprised of four distinct desert ecoregions, each with unique characteristics and climate regimes: the Mojave Desert, Sonoran Desert, Madrean Archipelago, and Chihuahuan Desert. Nineteen military installations are operational in this landscape, and as of October 2006, twenty-six federally listed threatened or endangered species were documented as occurring on or contiguous to these installations. In 2006, the United States Army alone spent over $40 million on the management of threatened and endangered (T&E) species and their habitat (Rubinoff et al., 2006).

Ephemeral and intermittent streams are the predominant fluvial forms in these deserts, but their ecological function is not well understood; most riparian studies are conducted on perennial systems, and in wetter, more humid locations. Knowledge of how these dryland streams function has improved in recent years (see Graf, 1988b; Bull and Kirkby, 2002; and D'Odorico and Porporato, 2006); however, linkages between wildlife and ecosystem characteristics are not well documented. Various studies have shown that biological and habitat diversity in arid and semi-arid lands are considerably higher along ephemeral and intermittent stream corridors in comparison to adjacent uplands (Warren and Anderson, 1985; DeBano et al., 2003). Riparian areas are clearly important for wildlife, but most conservation efforts and ecohydrological research (Stromberg et al., 2009, Steward et al., 2012) have focused on the riparian areas of perennial streams rather than ephemeral or intermittent streams. These streams are critical in maintaining overall watershed health, and their proper management will aid in sustaining long-term military testing and training in the DoD's Southwest Region. A better understanding of these ecosystems is needed for management of the streams, natural resources, TER-S, other species of concern, and for sustaining military training and testing.

Natural resource managers at military installations face a number of challenges related to their need to balance natural resource protection with the military mission. They must manage and protect TER-S and their habitat, while at the same time providing for military use and access to training areas. This includes identifying stream reaches that might be important to wildlife, or roads that might become impassable during high runoff events. Managers are knowledgeable about their installation but the large land areas and diversity of terrain, flora, and fauna can make it difficult to know where specific landscape or habitat features might occur. They need to be able to identify locations with specific characteristics required for TER-S (e.g. riparian areas with dense vegetation 1 m to 4 m tall) and for other management priorities (e.g. areas that might

flood frequently). To achieve their management goals, certain areas might be recommended for closure to military use. Managers require defensible science-based information to present to commanders to support their recommendations, and methods to rank the relative importance of landscape characteristics. This research provides that information in the form of a set of ecohydrological variables for describing stream reaches, a stream type classification and methodology that identifies groups of similar stream reaches, and associations with wildlife groups to identify important stream reaches.

The central premise of this research is that the ecological integrity of dryland streams and the species that depend on them (including threatened, endangered, at-risk species, and species of concern) are best addressed within an ecohydrological framework that includes vegetation, geomorphologic and hydrologic characteristics (Figure 1). In other words, wildlife habitat and stream types are a function of the hydrologic, geomorphic, and vegetation characteristics present there. Along riparian corridors, the timing, frequency, and duration of flow greatly influence the relative amount of water, sediment, nutrient load, and organic matter that is available to establish and maintain fluvial forms and their associated biological communities. Vegetation is typically denser and more diverse along streams in comparison to uplands, especially in arid and semi-arid regions. As a result, riparian areas have more habitat diversity for wildlife because they provide food, cover, nesting, and movement corridors that may not be available in the uplands.

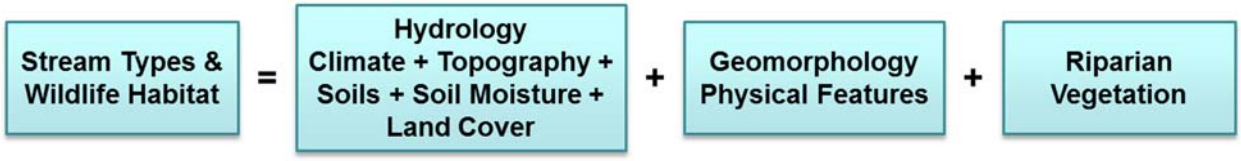


Figure 1. Conceptual model.

To address DoD's need for better understanding and management of Southwestern ephemeral and intermittent streams, and how they might be impacted by military training and testing activities, we developed a methodology that 1) classifies ephemeral and intermittent stream types by a set of biotic and abiotic attributes: hydrologic, geomorphic and vegetation; 2) associates the stream types and variables to wildlife habitat, and 3) provides a tool that allows DoD managers to evaluate the impacts of perturbations (e.g. climate change, military activities) on the hydrologic regimes of these systems that can be used to evaluate impacts to the species (TER-S; threatened, endangered, and at-risk) that depend on them. These objectives were organized into 7 main tasks (Figure 2), described in Methods and Materials Section 3. The final task, Task 8, is this report.

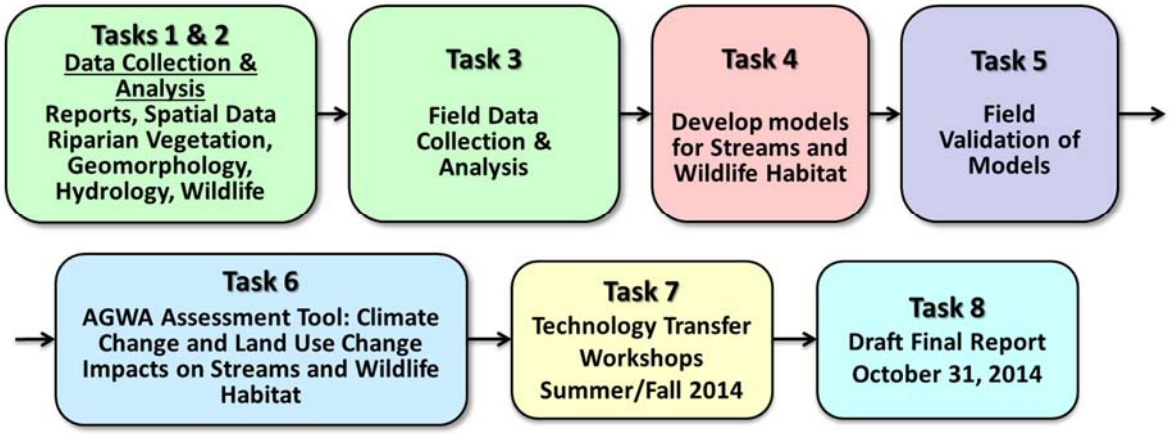


Figure 2. Project tasks and schedule.

Ephemeral and Intermittent Stream Characteristics

Ephemeral and intermittent streams are found across the Earth's land surface and are prevalent in watersheds in arid and semi-arid regions, also known as drylands. In the Southwestern U.S., the ephemeral nature of most streams often obscures the importance of the underlying ecohydrological processes that occur within them. These streams perform essential functions in the maintenance and protection of the biological resources of drylands even though they do not have permanent flow. Dry riverbeds tightly retain organic matter and nutrients (Wagener et al., 1998) and can harbor water underground that is not available elsewhere (Levick et al., 2008). Consequently, dry riverbeds and their floodplains often contain the most dense and diverse vegetation in arid landscapes, contrasting strongly with the sparse vegetation of their adjacent uplands (Steward et al., 2012; Levick et al., 2008). Ephemeral and intermittent streams have hydrologic regimes that are distinct from perennial streams primarily in the episodic nature of their flows, and are distinct from each other in the localized sources from which they derive their flows, which in part determines their resulting channel forms and vegetative characteristics.

The terms ephemeral and intermittent are hydrological classifications that were originally developed by the US Geological Society in the 1920's (Gebhardt et al., 2005). Ephemeral streams are defined as dry channels which flow for only brief periods in direct response to localized precipitation, and are at all times above the groundwater reservoir (i.e. no baseflow component), whereas intermittent streams are characterized as having continuous flow for some portion of a seasonal year, usually in response to changes in surface and subsurface hydrology (e.g. snowmelt, spring flow, or contact with the water table), or due to geologic controls that force groundwater to the surface. Particularly in arid and semi-arid environments, channel systems are highly dynamic, and often out of equilibrium with moderate to low flows (Soar and Thorne, 2001) which occur on annual or interannual cycles. Historically, large-scale geomorphic changes to arid channel networks have occurred during runoff events with recurrence intervals over decadal time scales, and incremental adjustments are made in response to smaller scale flows that bracket these larger, channel forming events.

Scientists have recently begun to embrace a more interdisciplinary approach to improve our understanding of the links between hydrological, biogeochemical, and ecological processes (Rodriguez-Iturbe, 2000; Newman et al., 2006). As a result, ecohydrology has emerged as a branch of science that explores the interactions between hydrological and ecological processes and their associated feedbacks across both spatial and temporal scales. The study of ecohydrology in arid and semi-arid ecosystems is of particular importance because the lack of water and the tight coupling of hydrological partitioning and ecological dynamics is more evident yet not as clearly understood (Jackson et al., 2009). Ecohydrological research offers a more holistic approach to ecosystem studies, but a solid understanding of each underlying process must be in place prior to making any attempts to establish relationships between the processes.

Riparian areas are a unique part of the landscape where hydrologic connectivity is maintained throughout the watershed to supply the water and nutrients needed to fuel downstream biogeochemical reactions, and to provide nutrients, critical habitat, and migration routes for many species of wildlife. Riparian ecology is controlled largely by local and regional flow patterns determined by the variability in the intensity, timing, and duration of precipitation interacting with terrain, soil texture, and evapotranspiration (Poff et al., 1997). The interaction between a stream's flow regime and riparian communities are largely determined by how precipitation translates into moisture stored in the soil and other components of the water budget expressed in the equation:

$$P = R + ET + S + D$$

where P = precipitation, R = runoff, ET = evapotranspiration, S = storage in soil, and D = deep aquifer recharge. The following section summarizes how each component of the water budget is tied to a stream's flow regime and how they influence riparian vegetation communities.

Arid and semi-arid systems are characterized by mean annual precipitation that is less than potential evapotranspiration rates (Allison and Hughes, 1983). These conditions limit how much water is present at the surface resulting in ephemeral streams being the dominant fluvial features of the landscape. An ephemeral stream's flow regime is not influenced by groundwater inflow but is solely tied to the timing and magnitude of precipitation pulses that are in turn driven by seasonal to decadal climatic patterns (Loik et al., 2004). In semi-arid regions of the United States the majority of precipitation events are small (<5 mm) events with most of the rainfall returning to the atmosphere via evaporation, resulting in less water available for plant uptake (Lauenroth and Bradford, 2009). More important are the less frequent, higher intensity precipitation events that are responsible for initiating overland flow that determines the flow regime and have the greatest influence on riparian vegetation.

Riparian vegetation is influenced by flow regime characteristics such as presence of surface or groundwater flows and high and low flow conditions (Stromberg et al., 2005). Distinct vegetation patterns have been observed along ephemeral and intermittent streams where greater soil moisture concentrations allow for increased plant biomass or the establishment of more mesic species, and tend to follow soil moisture across a horizontal gradient away from the stream channel. A decline in species cover, richness and diversity can be observed as well as a transition

from mesic to more xeric species, travelling outward, perpendicular to the stream channel. The degree to which these transitions take place is primarily regulated by the flow regime, which determines how much subsurface moisture travels from the hyporheic and parafluvial zones beneath the active channel to the riparian zone. It's in these areas where the majority of ecohydrological processes occur and where the other components of the water budget determine riparian characteristics.

Runoff is typically the smallest component of the water budget in arid and semi-arid rangelands, often accounting for less than 5% of the total annual budget (Wilcox et al., 2006). In regions of the southwestern United States subject to the North American Monsoon, runoff is most often associated with high intensity, summer thunderstorms (Stone et al., 2008). Runoff can also be generated from late summer and fall tropical depressions. In higher elevations where shallow soils and bedrock are common, runoff also occurs with rapid snowmelt and low intensity, longer duration winter rainfall enhanced by El Niño conditions (Woolhiser et al., 1993). While topography and soil texture can influence runoff behavior, how runoff responds once it encounters vegetation is an important determinant of ecohydrological processes. Upland vegetation patches help slow runoff, leading to sediment deposition and infiltration, facilitating their own growth and promoting greater biological activity (Ludwig et al., 2005). Riparian areas perform in a manner similar to upland vegetation patches, but are tied directly to the stream channel where the additional soil moisture supports more vegetation growth and/or can influence the flow regime.

Determining the frequency and magnitude of streamflow events is an essential component of any assessment of riparian vegetation productivity and characteristics (Poff and Ward, 1989; Hupp and Osterkamp, 1996; Snelder et al., 2005). Flow permanence and peak flow are two key metrics that have been used to describe the flow regime in dryland environments; however, the lack of observational data collected from ephemeral or intermittent streams due to infrequent flow events makes characterization difficult. Characterizing the hydrology of ephemeral and intermittent stream channels can allow land managers to better assess riparian conditions and may be used to predict response to changes in the hydrologic regime associated with human disturbances. It can also be used to direct land use activities away from ecologically sensitive areas to help preserve ecosystem health and take into consideration some of the environmental concerns associated with future land use and climate change.

Quantifying the relationship between flow regime and stream ecology in dryland ecosystems requires a measurement that captures the stochastic nature of flow pulses and accurately describes hydrologic connectivity throughout the stream. Flow permanence offers this by determining the degree of stream intermittency by quantifying the amount of time in a given period that flow is present in the channel (Leenhouts et al., 2006). Aside from providing soil moisture for transpiration, flow pulses are responsible for initiating biogeochemical processes by stimulating microbial activity, cycling nutrients and organic matter, and transporting these resources to downstream areas where they are available to the adjacent riparian zone (Larned et al., 2010). Riparian areas exposed to longer periods of flow duration (higher values of flow permanence), should display predictable patterns, such as increased vegetation biomass and height. A stream classification that includes flow permanence can be used as an indicator of soil

moisture available for riparian vegetation uptake and used to assign different levels of ecological importance among various stream reaches.

Several studies have looked at the importance of the relationship between flow permanence and vegetation or aquatic species ecology. Hupp (2000) showed that for low-gradient coastal rivers a similar metric known as the hydroperiod, or the annual period of inundation, controls riparian vegetation distribution and was useful for assessing plant ecological patterns. Stromberg et al. (2005) showed that in a semi-arid environment stream flow and soil moisture are positively associated with plant species richness and that flow permanence might be used in ephemeral and intermittent streams as an indicator of riparian species composition. Arscott et al. (2010) found a direct relationship between variations in flow permanence and benthic invertebrate species' richness and density along temporary rivers of New Zealand.

Large flood events that are common to ephemeral and intermittent streams are responsible for much of the sediment transport and channel formation and can have considerable influence on riparian species. Peak flow represents the maximum discharge of a stream after a precipitation event and is a useful metric for describing the magnitude of a flow. It is also often used to assess the hydrologic response of a watershed to a particular storm event and can be used as a measurement of watershed condition. Estimates of peak flows can also be made using a rainfall-runoff model and design storms generated from precipitation frequency maps. These estimates can point to areas within a watershed that may experience large alterations in channel morphology and/or high loads of sediment transport. These areas can then be considered in directing site or road development to more stable locations or used to justify culvert construction for existing roadways, for example.

Three storm types characterize the seasonal precipitation patterns in the Southwest, which give rise to differences in flow regime: winter-early spring North Pacific frontals (November-March), summer convective precipitation enhanced by the North American Monsoon (July-August), and occasional late summer/early fall (September-October) North Pacific tropical rains. Interannual variability in fall, winter and spring precipitation is modulated by the El Niño Southern Oscillation (ENSO), but variability in monsoonal precipitation is less clearly tied to these large-scale climatic indices, and the importance of monsoonal rainfall decreases westward (Betancourt, 2007; Ely, 1997). Fall tropical systems can produce extreme floods (Webb and Betancourt, 1992), and in some years, they contribute most of the annual rainfall in southwestern Arizona. In addition to these three seasonal precipitation patterns, decadal-to-multidecadal variability, characterized by alternating and widespread droughts and pluvials is evident in both the instrumental and tree-ring climatic records for the western US. Notable examples include the megadrought in the late 1500s followed by the megapluvial in the early 1600s, and the bracketing of epic droughts in the 1930s and 1950s by two of the wettest episodes (1905-1920 and 1965-1995) in the last millennium (Betancourt, 2007).

Channels adjust to changing climatic conditions and other perturbations (e.g. changes in land use) in generally predictable ways, with a tendency toward equilibrium through minimization of energy expenditure along their course. The large variability in frequency and magnitude of flow gives rise to ephemeral and intermittent channel and network properties in arid and semi-arid lands that are distinct from properties of perennial streams in more humid regions. Dryland

stream properties include: 1) high drainage densities due to a combination of intense precipitation and low vegetation cover, 2) a proportionately large number of disaggregated and compound channels resulting from highly variable, localized runoff and sediment that is transported in pulses, 3) convex or straight slopes due to decreasing downstream discharge, 4) large width to depth ratios due to non-cohesive soils and sparse vegetation on channel banks, and 5) high sediment transport capacities (Knighton, 1998). Numerous authors have cited these properties and others when discussing the difficulty in determining the channel-forming flow or bankfull discharge in dryland rivers, suggesting a range from the <1- to 32-yr flood event as the channel forming flow depending on these properties (see Graf, 1988a; Bull and Kirkby, 2002; Lopez-Bermudez et al., 2002; Curtis et al., 2011). Dust and Wohl (2010) suggested that "flow events with return periods of approximately 25 years and greater are the flow events primarily responsible for forming and maintaining the geometry of a floodplain in the semi-arid environment."

Various studies have shown that as watershed area and stream length increase in dryland streams, drainage density, slope, and discharge tend to decrease (Leopold and Miller, 1956; Schumm, 1977; Graf, 1988a; and others). Graf (1983; 1988b) illustrated the coexistence of different channel patterns in active flood zones as interactions between channel slope and stream power at different flow magnitudes by documenting shifts in channel form from braided (during high flows) to meandering (at low flows) along the Gila and Salt Rivers in Arizona. Compound channel forms are among the most common in arid and semi-arid lands where there is a high ratio of record peak discharge to average annual discharge (Graf, 1988b). While anastomosing channels might appear similar to braided channels in planform, there are distinct differences. Braided channels tend to develop in basins where high variability, low frequency runoff events move large amounts of sediment as bedload; geologic weathering results in a large percentage of non-cohesive, sandy soils as the primary bed and bank material; and low nutrient availability combined with infrequent precipitation preclude vegetation from establishing in densities great enough to stabilize channel banks. Lateral channel migration is thus common in braided systems. Anastomosing channels tend to form in regions where geologic weathering results in a higher percentage of fine grained bed and bank material that is transported primarily as suspended or mixed load during runoff events. Relative to braided channels, width to depth ratios tend to be lower in anastomosing networks, sinuosities higher, and vegetation, once established, tends to stabilize channels and thus preclude continuous lateral migration (Field and Lichvar, 2007). The combined requirements of dense vegetation and more cohesive soils tend to lessen the prevalence of anastomosing channel types in the Southwest.

Ephemeral streams are quite commonly discontinuous in the Southwest, forming a distinct planform of alternating erosional and depositional zones, where the erosional reaches are sometimes referred to as arroyos and depositional reaches as sheetflood zones (Field and Lichvar, 2007). Discontinuous ephemeral streams occur most commonly in semi-arid regions where non-cohesive sediment transport is high, but sufficient vegetation is present to trap sediment in sheetflood zones, and transmission loss to channel beds results in episodic pulses of sediment transported discontinuously throughout the channel network (Bull, 1997; Tooth, 2000). Sheetflood zones may correspond to the NatureServe or Southwest GAP Land cover class of Chihuahuan-Sonoran Desert Bottomland and Swale Grassland (Lowry et al., 2005).

Numerous studies have found ephemeral and intermittent streams to be important to specific wildlife species or groups of species. It has been estimated that in the Southwest U.S., 80% of all animals use riparian resources and habitats at some life stage, and more than 50% of breeding bird species nest chiefly in riparian habitats (Krueper, 1993). The patterns of xeroriparian vegetation and the associated faunal communities that establish within and along ephemeral and intermittent stream systems, and the biological responses that occur as channels adjust to natural and human-induced perturbation, are not fully understood. Riparian vegetation plays a pivotal role in determining the timing and magnitude of runoff in fluvial systems, which modifies the hydro-geomorphic processes and resulting forms associated with dryland streams (Graf, 1988a). Vegetation provides the functional services of moderating soil and air temperatures, stabilizing channel banks and interfluves, seed banking and trapping of silt and fine sediment favorable to the establishment of diverse floral and faunal species, and dissipating stream energy which aids in flood control (Howe et al., 2008). Development of the xeroriparian corridor is a response to these inputs, and provides features for wildlife that are not as available in the adjacent uplands such as food, cover, nesting and breeding habitat, and movement/migration corridors.

Vegetation structure and diversity play crucial roles in wildlife use of any specific location. Habitat complexity can be divided into vertical structure and horizontal structure. In general, there is a positive relationship between high horizontal habitat structure (habitat heterogeneity) and biodiversity (Tews et al., 2004). In the Western U.S., Vale et al. (1989) used principal component analysis (PCA) on presence/absence information of mammal, reptile, and amphibian species by vegetation association and by physiographic region to explore factors influencing species richness. They found that species richness for five of the nine guilds they examined - ground carnivores of vertebrates, ground carnivores of invertebrates, ground seed-eaters, ground omnivores, and aerial carnivores of invertebrates (bats) - increased as vegetation structure became more complex (increasing height and volume) and environmental conditions became more varied. In southern Africa, an area with a significant amount of drylands, plant species richness, particularly woody plant species richness, is a very strong predictor of mammal species richness (Andrews and O'Brien, 2000; Qian et al., 2009).

In Warren and Anderson's (1985) study of xeroriparian vegetation in a Sonoran Desert wash, they described four floristic classes associated with increases in watershed area and controlled by frequency and amount of flow, shading, and channel scouring. As watershed area increased, riparian facultative and obligate species appeared and increased, larger shrubs and trees became common, and structural complexity increased. Similarly, Zimmerman et al. (1999) found that vegetation distribution and composition in an ephemeral canyon system in central Arizona were best explained by a complex temperature/moisture - substrate gradient. Strongly echoing Warren and Anderson (1985), Shaw and Cooper (2008) found that in northeastern Arizona, decreased disturbance potential and increased moisture availability in the downstream direction were related to greater abundance of obligate riparian vegetation and increasing structural importance of shrubs and trees.

Multi-return LiDAR data has become an important tool in wildlife habitat analyses, especially with respect to vegetation structure. On the Consumes River in central California, Seavy et al. (2009) created logistic regression occupancy models for sixteen riparian bird species using only LiDAR-derived canopy height and canopy heterogeneity (standard deviation of height). Using

only these vegetation structure variables, the authors were able to achieve fair to good models (Area Under the Curve, AUC >0.75) for ten, or nearly two-thirds of these species. In an area of sand-dunes, heathlands, and dry forests in the Netherlands, Ficetola et al. (2014) tested whether land cover or LiDAR-derived vegetation structure measures were better at predicting the distribution of nine bird species. For seven of the nine species, the best model included LiDAR-derived vegetation structure, and for five of these species, the best model included only these variables. Both vertical structure diversity and horizontal environmental heterogeneity determine what areas are suitable habitat for particular species, and in turn influence species richness.

The importance of vegetation structure to avian richness and diversity in particular, stems from the importance of structure for individual bird species. Vertical structure determines the distribution and availability of perching, foraging, and nesting sites (Brokaw and Lent, 1999), so areas with greater vertical structure provide more niches for more species. MacArthur and MacArthur (1961) discovered that breeding bird species richness in the eastern U.S. increased as foliage height diversity of the 0-2' (0-0.6 m), 2-25' (0.6-7.6 m), and >25' (7.6m) vegetation layers increased. Parker (1986) found that thorn trees, along with stem succulents, enhanced avian diversity in desert shrublands by providing a structural framework that facilitated subdivision of foraging space. Thorn trees were much more abundant in the wash than in the uplands. At 21 sites scattered across the drylands of Arizona and New Mexico, total vegetation volume is strongly and positively correlated with breeding bird density (Mills et al., 1991).

Since vegetation structure and diversity are important determinants of wildlife diversity and abundance (Anderson and Ohmart, 1977), ephemeral and intermittent streams could be expected to be crucial habitat for wildlife species. Riparian zones are traditionally valued for wildlife for their ability to provide water and their increased vegetation diversity and structure, which provide food, cover, nesting habitat, and breeding habitat. Their unique vegetation and geomorphology provide shade and a moister and cooler microclimate. The linear nature of streams, as well as the open center created by the stream itself, provide abundant edge environments, as well as ideal migration routes and travel corridors (Thomas et al., 1979). While xeroriparian areas in drylands only rarely provide water, they retain other values, especially the vegetation and microclimate components. Hammer (2014) and Levick et al. (2008) noted numerous studies that document the significance of xeroriparian areas to wildlife.

This project addresses DoD's need for improved understanding and management of ephemeral and intermittent stream systems by 1) characterizing them in terms of their hydrologic, vegetation, and geomorphic properties, 2) creating a stream type classification system using those properties, 3) linking wildlife habitat to both the classification and ecohydrologic properties, and 4) providing a tool that can be used to evaluate the impacts of climate change and land use change on these systems.

Study Site Selection

The DoD has adopted an ecoregional approach for evaluating military lands in terms of their ability to sustain military training and testing (Bailey, 2002; Doe et al., 1999, 2006). We used this ecoregion approach to select our study sites to best represent the diversity of species and

communities that exists (Olson et al., 2001) in DoD's Southwest Region (Figure 3). Ecoregions represent areas with similar biological communities that can be related to climate, elevation, vegetation, and geology (Bailey and Hogg, 1986; Omernik, 1995; Omernik and Bailey, 1997; and others). Furthermore, it has been noted that wildlife assemblages can be associated with vegetation structure and other ecosystem features (Vestal, 1914; Dasmann, 1972; Udvardy, 1975; Bailey and Hogg, 1986; Olson et al., 2001; Kreft and Jetz, 2010).

Our study sites, which represent the four major ecoregions (Omernik, 1995) across the Southwest U.S., are Fort Irwin (Mojave Desert), Yuma Proving Ground (Sonoran Desert), Fort Huachuca (Madrean Archipelago), and Fort Bliss (Chihuahuan Desert) (Figure 3). These ecoregions correspond to Bailey's Ecoregion Sections: the Mojave Desert, the Sonoran Mojave Desert Sections of the American Semi-Desert Province, and the Basin and Range section of the Chihuahuan Semi-Desert Province (includes Madrean Archipelago and Chihuahuan Desert) (Bailey, 1976). The four sites have unique physical and biological characteristics, resulting in unique datasets, stream type classifications, and wildlife analyses.

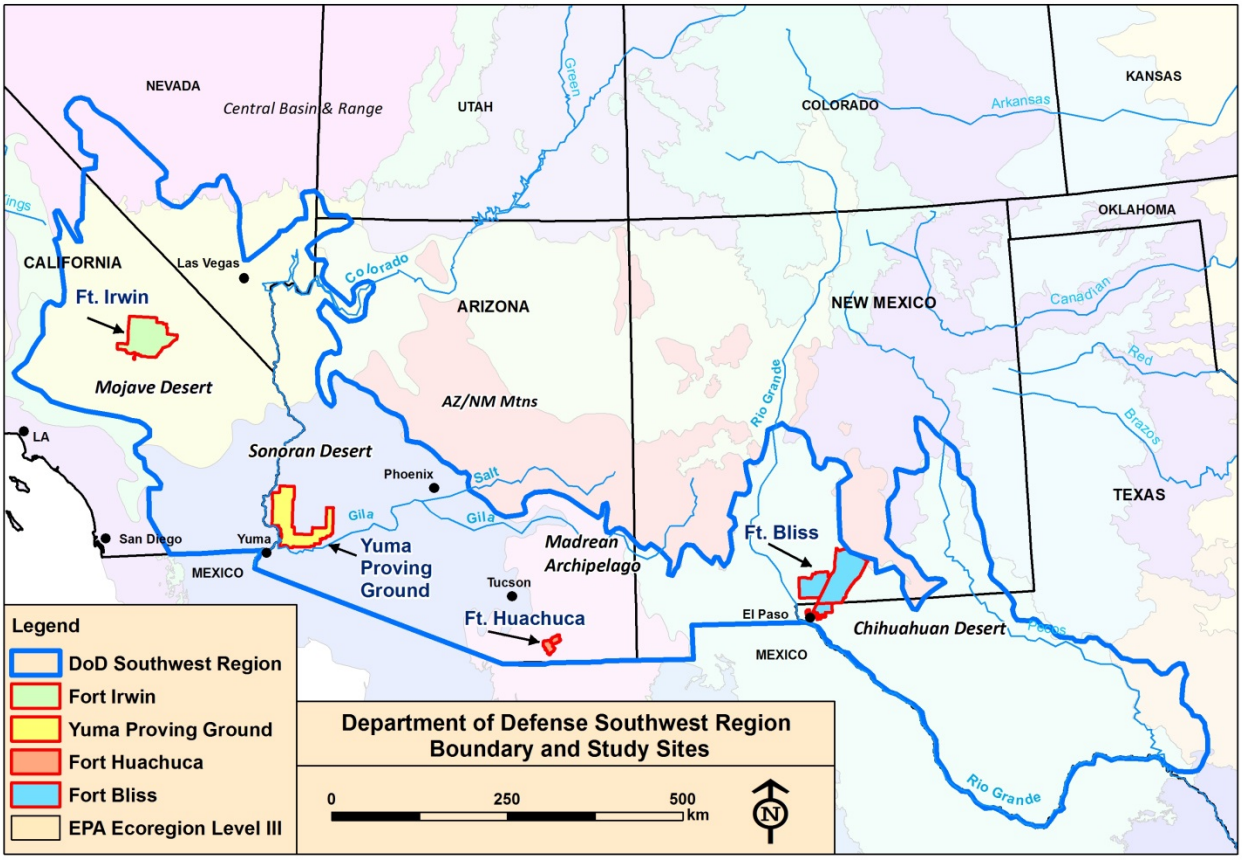


Figure 3. Map of the Department of Defense Southwest Region, ecoregions and study locations: Fort Irwin, Yuma Proving Ground, Fort Huachuca, and Fort Bliss.

General Descriptions by Installation

Fort Irwin, California (2,590 km^2)

Fort Irwin is located in the Mojave Desert ecoregion, just south of Death Valley National Park, and north of Barstow. Elevations range from 240 to 1,860 m. Terrain is varied, and includes steep, rugged mountains, broad alluvial fans and bajadas, sandy plains, rolling hills, and playas. Fort Irwin receives approximately 110 mm (4.13 in) of annual precipitation, mainly from October through April. Hereford et al. (2006) in their analysis of Mojave Desert precipitation estimated that 66% of total annual precipitation occurs during these months, and noted that this cool-season precipitation is widespread, of relatively long duration, and the most important and dependable for most of the vascular plants, directly affecting resource availability for small herbivores, small mammals and certain reptiles.

Fort Irwin does not contain any perennial surface flows; however, there are 14 (fourteen) springs that are monitored regularly by Fort Irwin staff (Figure 4). Large areas of creosote-dominated alluvial fans and sandy, gently sloping surfaces, identified as Sonoran-Mojave Creosotebush-White Bursage Desert Scrub occur here (Figure 4). Distinct riparian vegetation zones are not easily visible on these surfaces, where overland flow spreads out over a wide area, forming a network of small ephemeral flow paths that change with subsequent flows. Several of our field sites are located in these areas, and although they are not included in the stream type classification, they are included in our field data and noted as "Floodout" zones (Figure 5).

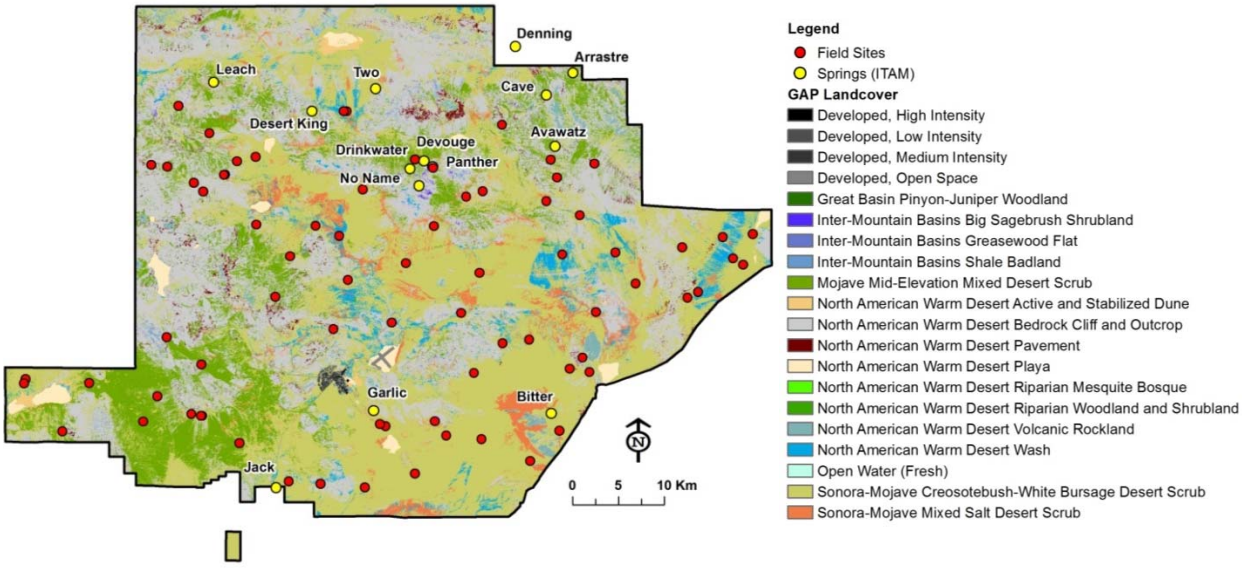


Figure 4. Fort Irwin landcover, field sites, and springs.



Figure 5. Photos at Fort Irwin showing "floodout zones."

Vegetation at Fort Irwin is shrub-dominated. Common plants found at our field sites include creosote bush (*Larrea tridentata*), white bursage (*Ambrosia dumosa*), brittlebush (*Encelia farinosa*), four-wing and shadscale saltbush (*Atriplex canescens* and *Atriplex confertifolia*), ephedra (*Ephedra nevadensis*), crucifixion thorn (*Castela emoryi*), catclaw acacia (*Acacia greggii*), desert willow (*Chilopsis linearis*), blackbush (*Coleogyne ramosissima*), buckwheat (*Erigonum inflatum*), cholla cactus (*Opuntia sp.*), beavertail prickly pear (*Opuntia basilaris*), cottontop cactus (*Echinocactus polycephalus*) and Joshua tree (*Yucca brevifolia*).

Riparian vegetation may be restricted to the channel banks, located only within the stream channel, or may not be present at all. Creosote frequently marks the division between the upland and channel, and is sometimes the upland vegetation identifier (Figure 6). Vegetation along the channel is frequently taller and denser than the same vegetation on the uplands, and is another method of defining the riparian zone.


Figure 6. Photos at Fort Irwin showing No Name Spring (left), and Brinkman Wash where the channel bottom is vegetated and creosote indicates uplands (right).

Yuma Proving Ground, Arizona (3,367 km^2)

Yuma Proving Ground (YPG) is located in the Lower Colorado River Valley Subdivision of the Sonoran Desert ecoregion, with elevations ranging from 54 to 868 m. Most of YPG is classified as Sonoran-Mojave Creosotebush-White Bursage Desert Scrub, and Sonoran Paloverde-Mixed Cacti Desert Scrub (Figure 7). Mesquite bosques are found in some areas, and are discussed in the wildlife analysis section. Riparian vegetation may be restricted to the channel banks, located only within the stream channel, or may not be present at all. Plants normally restricted to the uplands in wetter areas may only be found along the channels at YPG (Figure 8). Landforms include steep rugged mountains, alluvial fans, bajadas, sandy plains, sand dunes, and desert pavement covered piedmonts (fan terraces).

YPG receives only about 92.7 mm (3.65") of rainfall per year, and is our driest location. There is no perennial surface flow at YPG; however, we located a tinaja (natural water tank in bedrock) along one of our transects in the Trigo Mountains along the far western arm of YPG, and smaller pools of water in some of the upper reaches in Mojave Wash. Tinajas may be found in the mountains in various locations at YPG.

Common plants found at our field sites include ironwood (*Olneya tesota*), creosote (*Larrea tridentata*), blue paloverde (*Parkinsonia florida*), littleleaf paloverde (*Parkinsonia microphylla*), white bursage (*Ambrosia dumosa*), desert lavender (*Hyptis emoryi*), wolfberry (*Lycium sp.*), smoke tree (*Psorothamnus spinosus*), catclaw acacia (*Acacia greggii*), velvet mesquite (*Prosopis velutina*), four-wing saltbush (*Atriplex canescens*), brittlebush (*Encelia farinosa*), ephedra (*Ephedra nevadensis*), jojoba (*Simmondsia chinensis*), saguaro (*Carnegia gigantea*), ocotillo (*Fouquieria splendens*), cholla (*Opuntia sp.*), and prickly pear (*Opuntia sp.*).

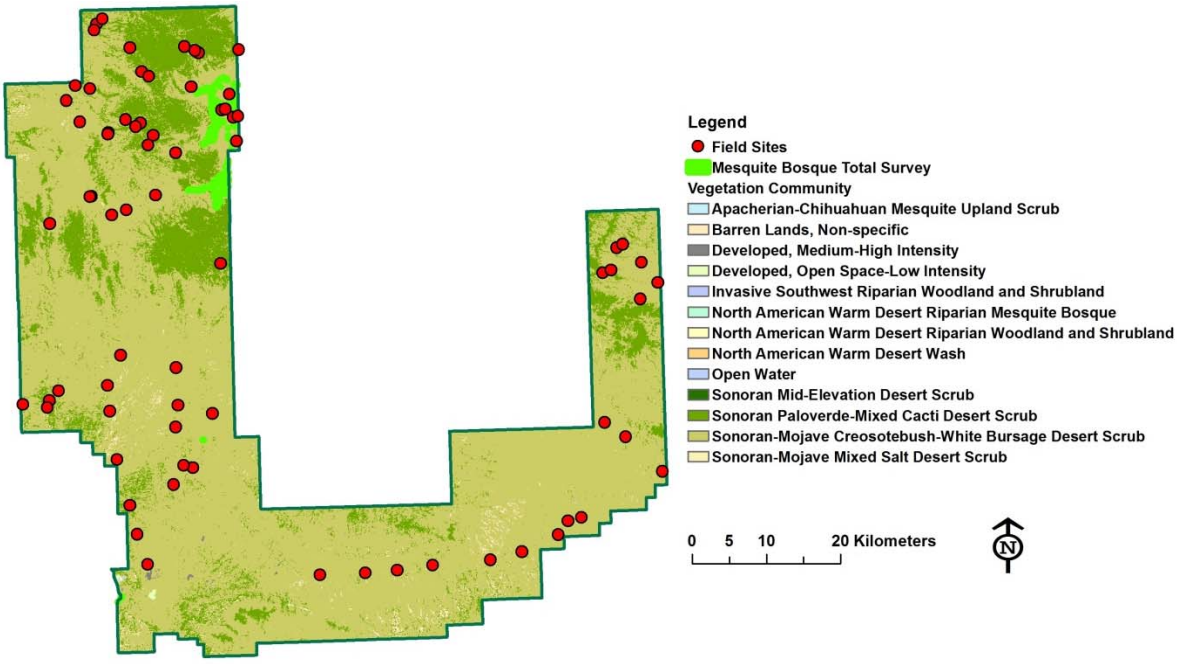


Figure 7.Yuma Proving Ground vegetation communities and field sites.



Figure 8. Photos at YPG showing riparian vegetation located in swales between desert pavement covered hills (left) and in a large incised alluvial wash (right).

Fort Huachuca, Arizona (291 km^2)

Fort Huachuca is situated on the eastern flanks of the Huachuca Mountains in southeastern Arizona, and ranges in elevation from about 1,220 to over 2,560 m. It is located in the transition zone between the Sonoran Desert and Chihuahuan Desert, known as the Madrean Archipelago ecoregion. Fort Huachuca receives approximately 381 mm (15.6") of annual precipitation and is our only installation with permanent surface flow. Garden Canyon and Huachuca Canyon Creeks flow out of the Huachuca Mountains, and contain intermittent reaches in the upper portions fed from springs and snowmelt. Stream channels in the upper reaches tend to be bedrock dominated or bedrock with alluvium. The middle and lower stream reaches are generally incised alluvium and become wider and shallower with distance from the mountain front (Figure 9). Streams on Fort Huachuca flow into the San Pedro River to the east, or the Babocomari River to the north, a tributary to the San Pedro. Both the San Pedro and Babocomari contain perennial reaches, and host numerous threatened, endangered, and sensitive species of flora and fauna, some of which use the channels on Fort Huachuca for foraging or movement corridors.

Vegetation consists of semi-desert mixed grasslands with mesquite, yucca and agave in the lower elevations, through Encinal pinyon-oak scrub and mixed deciduous in the middle elevations, to ponderosa pine forests in the higher elevations of the mountains. Riparian vegetation is present as sycamore, maple and various shrubs in and along the upper stream channels, mixed in with conifers, oaks and juniper. The canopy in the upper channels is closed, with a well-defined structure of upper canopy, mid canopy, shrub, and ground cover layers. Riparian vegetation in the middle to lower elevations is generally denser and taller than the adjacent uplands, and includes willow, mesquite and grasses along the channel banks, and a generally higher diversity of shrubs and grasses than the uplands (Figure 10). There is a distinct change in slope and land cover at the base of the Huachuca Mountains (Figure 11). We sampled 61 locations across Fort Huachuca to capture the variability of channel types, vegetation, land cover and geomorphology (Figure 11).



Figure 9. Photos at Fort Huachuca study sites showing bedrock dominated channel (left) and wide incised alluvial channel (right).

Common plants found at our field sites include (from upper elevations to lower) pinyon pine (*Pinus discolor*), alligator juniper (*Juniperus deppeana*), various oaks (*Quercus spp.*), agave (*Agave palmeri*), Arizona sycamore (*Platanus wrightii*), bigtooth maple (*Acer grandidentatum*), madrone (*Arbutus arizonica*), velvet ash (*Fraxinus velutina*), Arizona walnut (*Juglans major*), velvet mesquite (*Prosopis velutina*), littleleaf sumac (*Rhus microphylla*), desert willow (*Chilopsis linearis*), four-wing saltbush (*Atriplex canescens*), yucca sp., and various grasses, cacti and forbs.



Figure 10. Photos at Fort Huachuca study sites showing riparian vegetation at an upland intermittent stream reach (left) and a mid-elevation ephemeral stream reach (right).

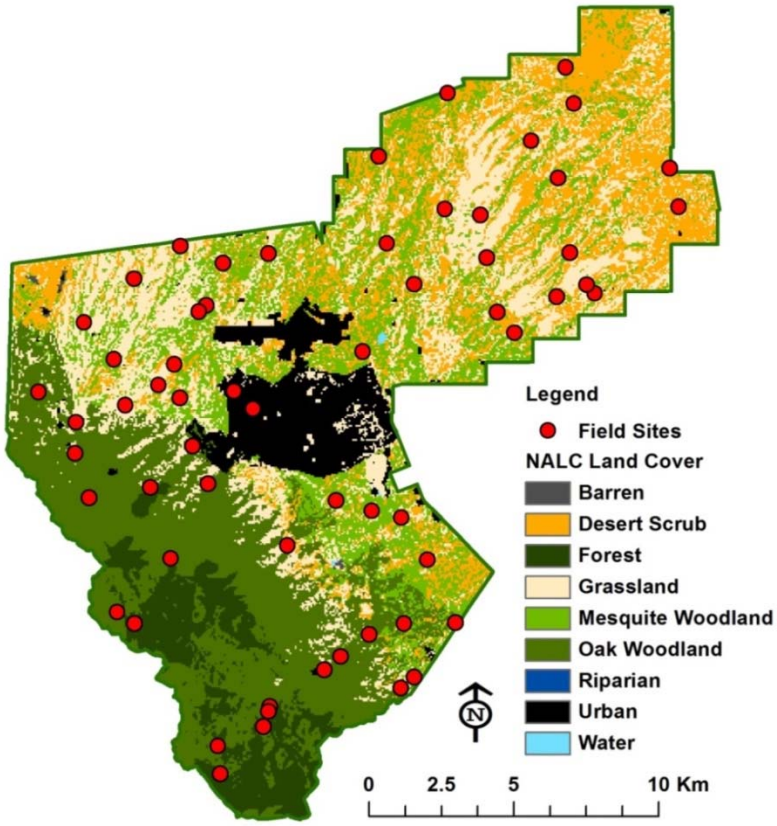


Figure 11. Fort Huachuca land cover and field sites.

Fort Bliss, Texas/New Mexico (4,530 km^2)

Fort Bliss is the largest of our study locations and the most challenging for stream type classification because of its large size and diversity of landforms. It is located in the Chihuahuan Desert ecoregion, with elevations ranging from approximately 1,170 to 2,700 m. Fort Bliss receives approximately 220 mm (8.66") of annual precipitation. Vegetation is dominated by semi-desert grassland and steppe community, followed by stabilized coppice dune and sand flat scrub, creosote mixed desert scrub, and small areas of pinyon-juniper woodland in the mountains. The ecological management areas defined by the installation are (in order of largest area): Basin Aeolian, Basin Alluvial, Sacramento Mountains, Organ Mountains, Hueco Mountains, Otero Mesa, Franklin Mountains and Foothill-Bajada Complex (Figure 12).

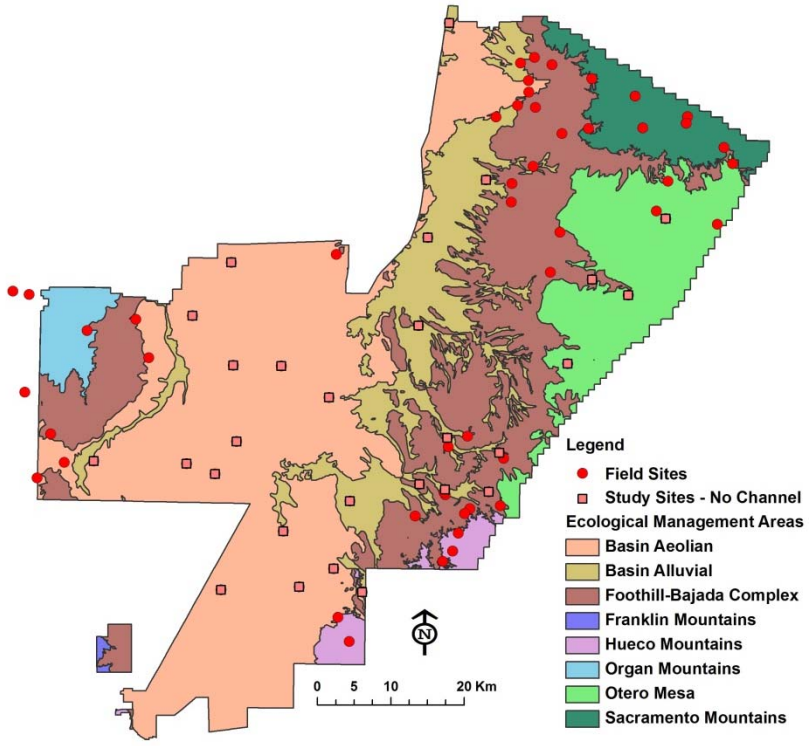


Figure 12. Fort Bliss ecological management areas and field sites.

Over half of Fort Bliss falls under the Basin Aeolian management area which is mostly composed of stabilized coppice dunes that have no stream channel formation (Figure 12). The dunes are stabilized primarily with honey mesquite (*Prosopis glandulosa*) and four-wing saltbush (*Atriplex canescens*), but have little to no vegetation between dunes. Although no distinct riparian vegetation zones exist, these dune areas support a wide variety of wildlife. Some parts of the Basin Aeolian management area have more active dunes, where small channels form but disappear quickly into the sands. This is evident in areas close to other land cover or management types.

Otero Mesa is a large area of grasslands where the flow paths are visible as wide swales containing vegetation assemblages distinct from the adjacent uplands, generally graminoids with scattered shrubs (Figure 13). These areas are defined as sheetflood zones of discontinuous streams or from NatureServe (http://www.natureserve.org), *Chihuahuan – Sonoran Desert Bottomland and Swale Grassland (Tobosa Swales)*. The remainder of Fort Bliss stream channels range from small incised channels to large arroyos and wide braided systems.

Common plants found at our study sites include: creosote (*Larrea tridentata*), yucca (*Yucca elata*, *Yucca torreyi*, and *Yucca baccata*), honey mesquite (*Prosopis glandulosa*), four-wing saltbush (*Atriplex canescens*), ephedra (*Ephedra sp.*), desert willow (*Chilopsis linearis*), cholla (*Opuntia imbricata*), purple prickly pear (*Opuntia macrocentra*), broom snakeweed (*Gutierrezia sarothrae*), tarbush (*Flourensia cernua*), ocotillo (*Fouquieria splendens*), agave (*Agave lechugilla*), pinyon pine (*Pinus edulis*), acacia (*Acacia neovernicosa*), mountain mahogany (*Cercocarpus montanus*), desert ceanothus (*Ceanothus greggii*), oaks (*Quercus spp.*), and various grasses.



Figure 13. Photos at Fort Bliss in areas without defined channel formation: Otero Mesa swales (left), and coppice sand dunes (right).

Classification Techniques

Several classification techniques were used in this project to analyze individual variables, and to create the stream type classifications for each installation. Classification schemes provide a mechanism for identifying features with similar characteristics. Referred to as "machine learning," these techniques are applied to categorical, binary or continuous data, and include supervised (discriminant analysis) and unsupervised (clustering) classification techniques. Supervised classification employs a training set of data where the class or label is known, to classify or label an additional set of data, while unsupervised classification groups unlabeled data into similar clusters using pattern recognition (Jain, 1999; Kotsiantis, 2007). We used a cluster analysis, a decision tree (CART) analysis, an unsupervised classification, and a RandomForests analysis in this project, described below.

Cluster analysis, a type of unsupervised classification, is a term applied to a variety of statistical techniques and algorithms used to explore a set of variables or multivariate data for the purpose of identifying groups or clusters of variables that are most similar and meaningful (Everitt and Hothorn, 2010; Rai, 2011: Jain, 1999; and others). Clustering is used in exploratory data mining in a variety of fields, including medical research, natural resources, image analysis, and psychology, to identify patterns in a dataset. There are numerous clustering techniques and models that can be applied depending on the type of data to be analyzed and the desired final outcome. A common clustering procedure that was used in this research is agglomerative hierarchical clustering. This method was used to develop the ecohydrologic stream type classification for this project, and is described in more detail below.

Agglomerative hierarchical clustering creates groups from the data based on similarity starting with each data point as its own cluster, and merges them, building a dendrogram or tree that can include nested clusters. Clusters in the data are determined using the relative distance between the points to create homogeneous groups that minimize the distance between points within a

cluster and maximizes the distance between clusters. Distance measures include Euclidean, Manhattan, kernelize, and others. Clustering methods include Ward's, complete linkage, median, centroid and others. The data may be split into any number of clusters. The resulting clusters are visualized in a dendrogram that includes all data points and consists of a hierarchy of clusters. This technique was used to determine the ecohydrological stream types in this project using the vegetation, hydrologic, physical and geomorphic variables for each stream reach. The analysis was performed in the R statistical package version 3.1.1 (R Core Team, 2014), using the *hclust* function for agglomerative hierarchical clustering, with the Euclidean distance function (ordinary distance), and Ward's method (minimizing total within-cluster variance, centroid based, producing compact, spherical clusters). These methods were chosen as most appropriate based on the complex nature and diversity of the input variables.

Hierarchical clustering is useful for determining patterns and natural groupings in data; however, one of its limitations is the lack of a mechanism for determining the "optimum" number of final clusters (Heller and Ghahramani, 2005). For example, if the number of clusters is too small the result is too general to be useful; however, if it is too large then the model may be too difficult to interpret and be overfitted, reducing its usefulness. To determine the optimum number of groups, another algorithm, *k*-means clustering, can be used. It is based on obtaining the lowest within-group sum of squares when partitioning the data into a specified number of clusters, using a centroid model. It produces a plot of the within-group sum of squares where a bend or elbow in the resulting curve indicates an optimum number of clusters (Everitt and Hothorn, 2010). *K*-means clustering is not as effective on very complex datasets (Jain, 1999) as the resulting curve can be difficult to interpret (i.e. lacking obvious bends or elbows); however, it can provide useful information regarding potential clustering. *K*-means clustering was applied in R using various numbers of clusters; however, the results were unclear, indicating that there were multiple acceptable cluster arrangements. The final number of clusters (stream types) for each installation was selected by cluster validity indices (described in the next section), examination of the mapped clusters, inspection of the resulting dendrograms from the agglomerative hierarchical clustering, and site knowledge.

Classification and regression trees (CART) (Breiman et al., 1984; Clark and Pregibon, 1992) are modern statistical techniques ideally suited for both exploring and modeling complex multivariate interactions (Baker, 1993; Rejwan et al., 1999). CART models produce decision trees through binary recursive partitioning that can be used for interactive exploration and description or prediction of non-linear patterns and processes (De'ath and Fabricius, 2000). CART models have been applied in remote sensing studies to extract land cover information (Borak and Strahler, 1999) and have been used along with object-oriented methods in urban mapping (Thomas et al., 2003), and rangeland mapping (Laliberte et al., 2007). CART is a type of supervised classification that requires a target variable and explanatory or predictive variables, and does not require spatial information. CART repeatedly splits the predictor variables into more homogeneous groups, aiming to predict or explain the target variable, creating a tree that is categorical (classification trees) or numeric (regression trees). Trees complement or represent an alternative to many traditional statistical techniques, including multiple regression, analysis of variance, logistic regression, log-linear models, and linear discriminate analysis (Mallinis et al., 2008). A CART classification analysis was used in this project to determine the thresholds or breaks for each variable for each stream type identified from the cluster analysis, using the

Salford Predictive Modeler software suite. The classification or decision tree can be used to predict stream types in unclassified reaches.

Combining cluster analysis with decision trees has been described by various researchers as a hybrid data mining technique that improves accuracy and results (Aviad and Roy, 2011; Gothai and Balasubramanie, 2012; Sharma and Kaler, 2013). The cluster analysis provides a means of examining the structure of the data and combines it into meaningful groupings; however, cluster analysis does not provide thresholds for the input variables used to form the clusters. CART analysis fills in this gap by identifying the threshold for each variable that places a data point into one cluster or another.

RandomForests (RF) is a type of unsupervised learning that selects the training set by *sampling with replacement*. This method generally excludes a third of the data that is subsequently used to evaluate each model. RF creates hundreds of classification trees and predicts class membership for the remaining data. It is based on CART concepts, but is different in that it combines data and grows each tree using a random variable to split the data during tree construction. The resulting final classes are derived from the mode of each class from all trees. RF requires a target and predictor variables, and will automatically identify the best predictors. Additional advantages of RF are that the input data do not require preprocessing (i.e. scaling), it includes self-testing (out-of-bag error estimation), and can be used to generate tree-based clusters (Salford Systems, 2004). The RF model in Salford Systems Predictive Modeler Suite (SPM; Salford Systems, 2004) was used to produce a geomorphic reach type classification using a suite of hydrologic, geomorphic, and physical variables. This approach was used to enable coordination with SERDP project RC-1726 (D. Cooper, PI), and for possible use in the stream type classification. The reach classes were not used in the final stream type classification; additional information on this analysis is included in Section 4.1 Action Items, Classification Coordination with Projects RC-1725 and RC-1726.

The Iterative Self-Organizing Data Analysis Technique (ISODATA) unsupervised classification is a clustering algorithm commonly used in remote sensing applications. This technique evaluates multispectral data for natural groupings to create clusters or classes (Jensen, 1996). The maximum number of desired classes is specified, but the algorithm may return fewer classes. This technique was used in this project in ERDAS Imagine (ERDAS, 2013) to create vegetation structure classes derived from multi-return LiDAR data (Light Detection and Ranging). The vegetation structure classes were ultimately not used in the stream type classification, but are included to provide additional vegetation-based information for each stream reach for use by the installations managers.

Hydrologic Rainfall-Runoff Models

Hydrologic rainfall-runoff models are often utilized to simulate streamflow characteristics where observations are unavailable. Rainfall-runoff models calculate stream discharge and other metrics by employing mathematical equations that partition rainfall into each of the hydrologic components based on the interactions with various watershed characteristics including topography, soil type, and vegetation cover. The output from these models can be used to create runoff hydrographs that are useful for measuring and evaluating streamflow patterns.

Rainfall-runoff models are also useful for determining flow permanence because they report discharge values at a daily time-step; the smallest practical unit of time that can be used to determine the percent of time when flow is present in a stream channel. One major challenge in determining flow permanence in ephemeral and intermittent channels is the lack of observed data; however, new methods that use hydrologic models to simulate flow regimes have recently emerged. Kirkby et al. (2011) used a hydrological model to create flow duration curves from which ecologically sensitive, low-flow frequencies were derived for semi-arid rivers across Europe. Gallart et al. (2012) used rainfall-runoff simulations to develop flow-permanence and seasonal predictability of zero flow period metrics that were used to classify ephemeral streams into distinct aquatic regimes.

Hydrologic models have also been useful in determining additional streamflow metrics such as runoff depth and peak discharge. Hernandez et al. (2000) used two rainfall-runoff models to assess watershed condition by measuring runoff response to land cover change. Wollmuth and Eheart (2000) used a rainfall-runoff model to calculate discharge volumes so they could distribute water allocations to meet both irrigation demand and environmental flows necessary to sustain riparian vegetation. Both of these studies indicate that with the absence of measured data, model simulated results can be used as a substitute, though some discretion must be used in the quantitative results of such efforts depending on whether model calibration and validation are possible.

3.0 Materials and Methods

We developed a methodology to create an ecohydrological stream type classification for Fort Irwin, YPG, Fort Huachuca, and Fort Bliss, that includes three distinct types of data: geomorphic, hydrologic, and vegetation. Each data type was analyzed separately for all stream reaches at each installation. The unit of analysis was the 1 km stream reach, and the USGS National Hydrography Dataset (NHD; U.S. Geological Survey, 2006; McKay et al., 2012) Plus Version 2 dataset was used as the stream network. The most explanatory metrics from each dataset were used in the final classification of ephemeral and intermittent stream types. Subsequently, the classified stream types were linked to wildlife habitat, and species observation data were linked to the variables. AGWA was used for the hydrologic modeling and to evaluate the effect of climate and land cover changes on stream types.

The project included 8 major tasks: 1) data collection, 2) data analysis, 3) field data collection, 4) model development, 5) model validation, 6) AGWA tool application, 7) technology transfer workshops, and 8) final report. The methods and materials for each task are described in order.

Task 1: Data Mining and Cataloging

This task involved collecting data necessary for the analyses, and creating a data catalog (or database) for those data. Initial data collection included reconnaissance visits to each installation, meetings with their natural resource managers (to introduce the project and identify their management and TER-S issues and concerns), and collection of geographic information systems (GIS) data, remotely sensed data, and reports (wildlife studies, management plans, etc.). Publicly available data were also collected via the internet for the region. Satellite imagery was purchased when it was not available from the installations. Using these data, characterization of the general variability of stream channel features at each installation was performed to guide the selection of initial sites for field data collection, to develop a general approach for the types of data to collect, and to produce the stream type classifications.

GIS and remotely sensed data collected for each installation include:

- National Hydrography Dataset (NHD) Plus Version 2 Dataset (http://www.horizon-systems.com/nhdplus/NHDPlusV2_home.php)
- Land cover: National Land Cover (NLCD) database (http://www.mrlc.gov/nlcd2006.php); Southwest Regional GAP Analysis Project (SWReGAP; http://fws-nmcfwru.nmsu.edu/swregap/), and National Gap Analysis Program http://www.gapanalysis.usgs.gov)
- NRCS major land resource areas (www.nrcs.usda.gov)
- Soils: SSURGO and STATSGO soils databases (www.nrcs.usda.gov)
- GAP animal habitat models (http://swregap.nmsu.edu/HabitatModels and http://gapanalysis.usgs.gov/species/)
- Wildlife species observational data
- USGS Seamless Digital Elevation Model (DEM) data
- Ecoregion data (Omernik,1995; Bailey, 1976)
- Multi-return LiDAR
- Remotely sensed multispectral imagery (QuickBird and RapidEye)

- Site-specific datasets from the individual installations (training areas, roads, springs, wildlife data, etc.)

Climate data obtained for the hydrologic modeling include:

- USGS precipitation and streamflow data, where available
- Local meteorological station data from the installations, where available
- National Climatic Data Center (NCDC) rain gage data (http://www.ncdc.noaa.gov/data-access/land-based-station-data)
- Next-generation Radar-Multisensor Precipitation Estimation (NEXRAD-MPE) precipitation data (http://water.weather.gov/precip/p_download_new/)

Data catalogues of all relevant spatial and tabular information for each installation have been created as ArcGIS 10.1 (ESRI, http://www.esri.com/software/arcgis) geodatabases and folders. All data will be delivered to each installation on a stand-alone laptop.

Task 2: Characterization of the Study Watersheds and Stream Systems

Characterization of the stream systems and watersheds at each installation was performed using vegetation, hydrologic, geomorphic and physical data. All data were derived for the 1 km stream reaches, and were georeferenced to the stream reaches using a "Unique ID" based on the NHD flowline reach codes. Selected data were used for the stream type classification, hydrologic modeling, vegetation analysis, and geomorphic reach type analysis. The methods used to derive the data are described here briefly, and in more detail below.

Hydrologic modeling was performed using the AGWA tool (Miller et al., 2007; Goodrich et al., 2012; http://www.tucson.ars.ag.gov/agwa), which parameterizes and runs two rainfall-runoff models within a GIS interface: the Soil Water Assessment Tool (SWAT; Arnold et al., 1994), and the KINEmatic Runoff and EROSion (KINEROS2; Smith et al., 1995).

SWAT was used to obtain stream flow permanence (from water yield, mm), and KINEROS2 was used to obtain peak flows (m^3/s) from design storms. Contributing watershed area above each stream reach was obtained from the KINEROS2 output data, and is included as an input variable georeferenced to each stream reach using the Unique ID. The models require land cover, soils, topographic and climate data. The vegetation characteristics were derived from satellite imagery and multi-return LiDAR (when available), to characterize vegetation structure, cover and density (from vegetation indices). The geomorphic data were derived from the GIS and LiDAR data at the reach, valley and watershed scale. All data types were evaluated for use in the Stream Type Classification.

Although antecedent soil moisture is recognized as a key variable in surface hydrologic processes, the hydrologic models as used in this project, SWAT and KINEROS2, do not produce soil moisture as a model output, although it is accounted for in the models. SWAT, a continuous simulation model, simulates antecedent soil moisture on a daily basis, based on soil and land cover properties, assuming average basin wetness and using the SCS runoff curve number (CN) for antecedent moisture group II (average condition). The initial soil water content used to compute CN can be retrieved from a model output file (output.hru file, the SW_INIT variable),

but is not included in the output tables in the version used with AGWA, nor is it available as a daily value (although antecedent soil moisture is calculated by the model on a daily basis).

KINEROS2, an event-based model, does not calculate antecedent soil moisture. This value defaults to 0.2 or is set by the user (0 – 1.0) as an input variable, as the saturation index (SI). Setting SI = 0.2 represents an approximate median initial pre-storm soil moisture condition based on CREAMS (Knisel et al., 1980) daily water balance simulations at 11 rain gages within the USDA-ARS Walnut Gulch Experimental Watershed over approximately 50 rainfall events.

Unit of Analysis and Riparian Zone

To produce the variables for the stream type classification, a unit of analysis was required, in addition to delineation of a riparian zone for the vegetation analyses. One (1) kilometer (km) was selected as the unit of analysis based on our field experience as the average stream length that captures the overall variability along a stream, and all data were derived at that scale. Stream reaches are based on the NHDPlus V2 flowline for all natural water courses; flowlines were split into +/- 1 km reaches using the ET GeoWizards tool (ET SpatialTechniques, http://www.ian-ko.com/). This tool splits a line into equal segments as close to the specified length as possible, adjusting the length to eliminate any remainders. Therefore, the stream reaches are not all exactly 1 km in length.

Delineation of the riparian zone was accomplished using the streamline and a DEM in the Hydro-Geomorphic Valley Classification Tool (HGVC; Carlson, 2009). This tool runs in ArcMap, and creates a polygon by inundating the DEM to a specified depth above the thalweg, delineating the water surface extent at that depth. Because the NHD flowline was used to inundate the DEM, it was first compared to the actual stream course visible in the hillshades and orthophotos, and manually edited to improve the location accuracy and the water surface extent polygons derived from them. The riparian vegetation variables and the riparian widths were derived from the inundated polygons.

The split and edited streamline was inundated using a LiDAR bare earth DEM or 10 m USGS DEM depending on the installation to various depths (0.25 m, 0.5 m, 1 m, 2 m, and 3 m) to create the polygons representing water surface extent at those depths. The vegetation variables were derived using the water surface extent for the 3 m inundation depth. This depth was selected using aerial imagery and field photographs as the depth that resulted in the most accurate water surface extent to delineate the extent of vegetation most likely influenced by stream flow when it occurs. The resulting polygon map delineates the areas around the channels that might be influenced during streamflow (i.e. indicating a riparian zone). When viewed using a base map or aerial photos, it generally includes the denser vegetation associated with the channel. We did not attempt to include forbs and grasses resulting from seasonal rainfall or episodic stream flow since we were aiming to identify the more permanent vegetation structure and abundance for use in wildlife habitat analyses.

Using this water surface extent for the analyses assumes that vegetation located more than 3 m above the thalweg would not be able to readily access soil water associated with stream flow. Although various authors (see for example Cable, 1969; Canadell et al., 1996; Gibbens and Lenz,

2001) have noted that root systems of many plants can extend much deeper than 3 m, many plant roots are within the 2-3 m depth range. This inundation depth captured the extent of riparian-associated vegetation most consistently across all four study locations, and was selected to represent the riparian zone (Figure 14). The resulting polygons for each installation provided a suitable zone within which to calculate relative vegetation metrics.

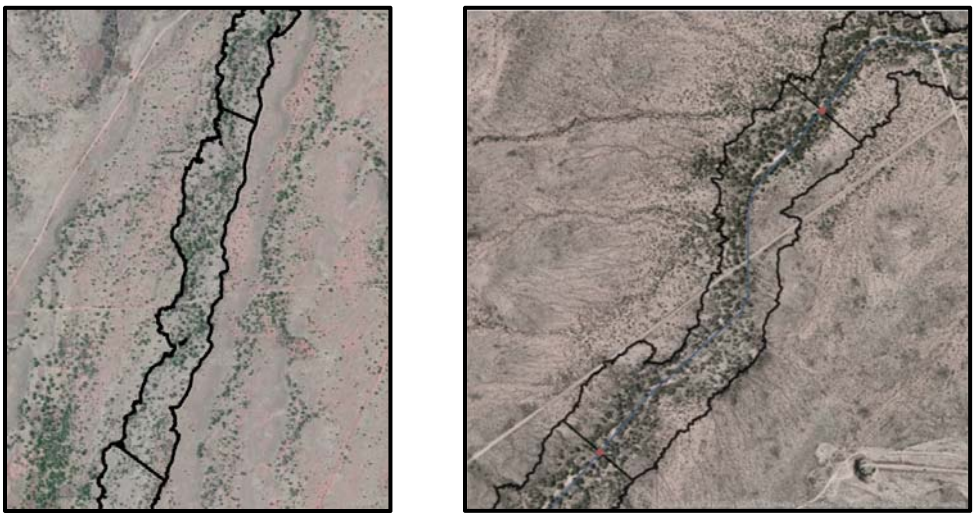


Figure 14. Images showing the 1 km stream reach polygon representing water surface width at 3 m inundation depth, overlain on an orthophoto, at Fort Huachuca.

Variables for the Ecohydrologic Stream Type Classification

A suite of variables were derived to develop the stream type classifications at each installation. The majority of the work done for this project was focused on identifying and developing these variables. To represent the ecohydrology of the four installations, we chose variables that would characterize the hydrologic flow regime, vegetation, physical features, and geomorphology of the stream reaches. The input variables derived for each 1 km stream reach are listed below with a description of the significance of the variable and how it was derived. More details are included in the Guidance Documents for each variable type. All variables are geo-referenced to an individual stream reach using a "Unique ID".

1. Hydrologic variables (see Lyon (2013) and the AGWA Tool Guidance Document for more detail on the hydrologic modeling). The values obtained from the AGWA/KINEROS2 and SWAT simulations were transferred from the AGWA-generated streamlines to the NHD Plus Version 2 flowlines used for the stream network in this research.
    a. Flow Permanence (%): Percent of the year there is flow in the channel, derived from the AGWA/SWAT model output for water yield (mm), using the Next-Generation Radar Multi-Sensor Precipitation Estimates (NEXRAD-MPE) from 2005-2012, obtained as a 4x4 km grid (one precipitation value per 4 km^2 per day) from the NOAA Advanced Hydrologic Prediction Service as a series of daily shapefiles for the conterminous United States. Flow permanence is calculated as the number of days with flow above a certain cutoff value divided by the total number of days. Three watershed size classes were assigned different cutoffs based on their contributing watershed area. Watersheds with an area <10 km^2 were assigned a cutoff of 0.0001 m^3/sec; between 10-34.9 km^2 a cutoff of

0.001 m^3/sec; and >35 km^2 a cutoff of 0.35 m^3/sec. SWAT is a curve-number-based model that uses hydrologic group, hydrologic condition, cover type, and antecedent moisture condition to calculated CN; therefore, these variables are implicit in the model simulations for flow permanence.

b. Peak flow or discharge (Qp, m^3/s): Obtained from the AGWA/KINEROS2 model outputs for the 5-, 10-, 25-, and 100-yr 1-hr design storms. Design storms were derived from the precipitation depths obtained from the pre-defined table of precipitation frequency estimates based on a specific return interval and duration from NOAA's Precipitation Frequency Data Server (NOAA, 2012). The 25-yr 1-hr peak flow was used in the classification as the representative value for the wide range of conditions at our study sites, and relates to the range of channel-forming flows in this region (1-32 yr return period), and is the minimum flow likely to inundate the overbank areas (Dust and Wohl, 2010).

2. Vegetation variables

a. Vegetation cover (%): Derived from the QuickBird or RapidEye satellite imagery, using a vegetation index to classify the 1 km stream reaches into vegetation vs. bare ground or ground cover, with aerial photography and field photos as guides to verify vegetation pattern, density and cover. Calculated as total area of vegetation pixels divided by total area of the 1 km stream reach polygon.
   i. QuickBird satellite imagery, 2.4 m multispectral resolution and 0.6 m panchromatic resolution, R-G-B-NIR bands (provided by Fort Huachuca and purchased for Fort Irwin), used to derive the Modified Soil Adjusted Vegetation Index (MSAVI2; Qi et al., 1994).
   ii. RapidEye satellite imagery, 5 m resolution, R-G-B-NIR and Red Edge bands (purchased for Fort Bliss and YPG), used to derive the Red Edge-NDVI vegetation index. RapidEye imagery was considerably less expensive than QuickBird imagery, and also included an additional band, the Red Edge band, that has been shown to improve vegetation analysis (Weichelt, 2012). We were interested in determining if this type of data could enhance this analysis.

b. Mean Vegetation Index: Describes the relative vegetation density for each 1 km stream reach, calculated using only the pixels classified as vegetation cover from the satellite imagery (i.e. the pixels classified as bare ground or ground cover were not used to derive this variable). In areas of sparse vegetation, both vegetation and soil properties are represented by the vegetation index, and can indicate the overall sparseness or density of vegetation.

c. Vegetation structure: Describes the vertical vegetation features, derived from the multi-return LiDAR vegetation height layer (calculated by differencing the canopy or first return layer and the ground or last return layer) and classified into vegetation height categories based on typical vegetation structure (i.e. <1 m, 1-4 m, 4-12 m, >12 m; Stromberg – personal communication). Vegetation Structure represents the various areas of vegetation that are typically used by wildlife, and the total amount of vegetation that is within that height layer. Note that these values do not account for vegetation that is beneath that height category (i.e. the 1-4 m high vegetation underneath the 4-12 m high vegetation), but represent only the vegetation within that height range.
   i. Fort Huachuca provided 1 m, bare earth and first return LiDAR data.

ii. Fort Irwin provided 1 m, bare earth and first return LiDAR data (note that their LiDAR does not cover the northern portion of the installation, the Leach Lake Impact Area, therefore this analysis is restricted to that extent).
iii. Fort Bliss provided 1.5 m, canopy and ground LiDAR data.
iv. YPG and DISDI provided limited LiDAR data at various resolutions for a few small areas. LiDAR was flown for all of YPG in 2013 but was not available to us in time for this analysis; therefore we do not have vegetation structure data for YPG. To add another vegetation variable in place of vegetation structure, we calculated a variable to represent vegetation response to seasonal monsoonal storms using Landsat 5 TM data, described next.

d. Seasonal Vegetation Response Index (SVRI): YPG Landsat 5 TM analysis for vegetation seasonal response to monsoonal storms, used to enhance the classification in the absence of LiDAR vegetation structure data. Calculated from the mean vegetation index MSAVI2 value for each 1 km stream reach, for a wet monsoon season (2008), as a percent change index from June 11 to Oct. 1.

3. Geomorphic and physical variables
   a. Elevation (m): Derived from LiDAR bare earth DEM and from the 10 m USGS DEM for YPG at the midpoint of each 1 km stream reach.
   b. Slope (%): Derived from the LiDAR bare earth DEM, or the 10 m USGS DEM for YPG, as the percent slope for each 1 km stream reach.
   c. Total stream power (kW/m): The rate of energy dissipation against the bed and banks of a channel; estimates the ability of the stream to transport sediment or cause erosion. Calculated using peak flow from the AGWA/KINEROS2 hydrologic modeling results, and LiDAR or 10 m DEM derived slope, using the same return periods as those used for peak flow (the 25-yr return period was used as the representative value for the range of conditions at our study sites), with the following equation:

      Stream Power□□ = □gQS

      where□□ is the density of water (1000 kg/m^3), g is acceleration due to gravity (9.8 m/s^2), Q is discharge (m^3/s), and S is channel slope (percent)
   d. Cumulative area above the reach (m^2): Represents the watershed area above the reach that contributes to stream flow at that reach, and is related to channel geometry and vegetation community differences; obtained from the AGWA model outputs.
   e. Mean Riparian Width (m): Water surface width at inundation depths of 0.25 m, 0.5 m, 1 m, 2 m, and 3 m, represents the distance from edge to edge of the riparian vegetation including the channel, or the channel bottom; derived using the HGVC tool in ArcMap, to create a polygon delineating the water surface extent at the specified depth; requires a filled DEM and a stream network (the edited NHD stream line), calculated as the area of each 1 km stream reach polygon divided by the actual length of the stream reach. The polygons inundated to 3 m depth were used to derive the vegetation variables; the widths from the 2 m inundated polygons were used for the stream type classification; the 3 m and 0.5 m widths were used to calculate the entrenchment ratio (see section g. below).
   f. Rainfall seasonality index: Describes precipitation characteristics and indicates the intensity of erosion potential due to precipitation characteristics, derived from PRISM

30 year normals (PRISM Climate Group, 2010), for the 30 year period 1980-2010, calculated as the mean precipitation of the wettest month divided by the mean annual precipitation, for the mid-point of each stream reach.

g. Entrenchment Ratio: A ratio indicating the degree of channel entrenchment or the vertical containment of the river; usually calculated as Flood Prone Width divided by Bankfull Width from field data (Rosgen, 1994), calculated here using mean riparian widths: 3 m / 0.5 m. Lower values (closer to 1) for the entrenchment ratio indicate higher entrenchment. This calculation assumes Water Surface Width at 3 m inundation depth approximates Flood Prone Width, and Water Surface Width at 0.5 m inundation depth approximates Bankfull Width. For the wildlife analysis at Fort Bliss only, a different entrenchment ratio was used because this analysis was part of Hammer's thesis (2014). The entrenchment ratio at Fort Bliss was derived by dividing the 0.5 m width by the 2 m width; therefore, the ratio is inverted and higher values of this variable indicate higher entrenchment.

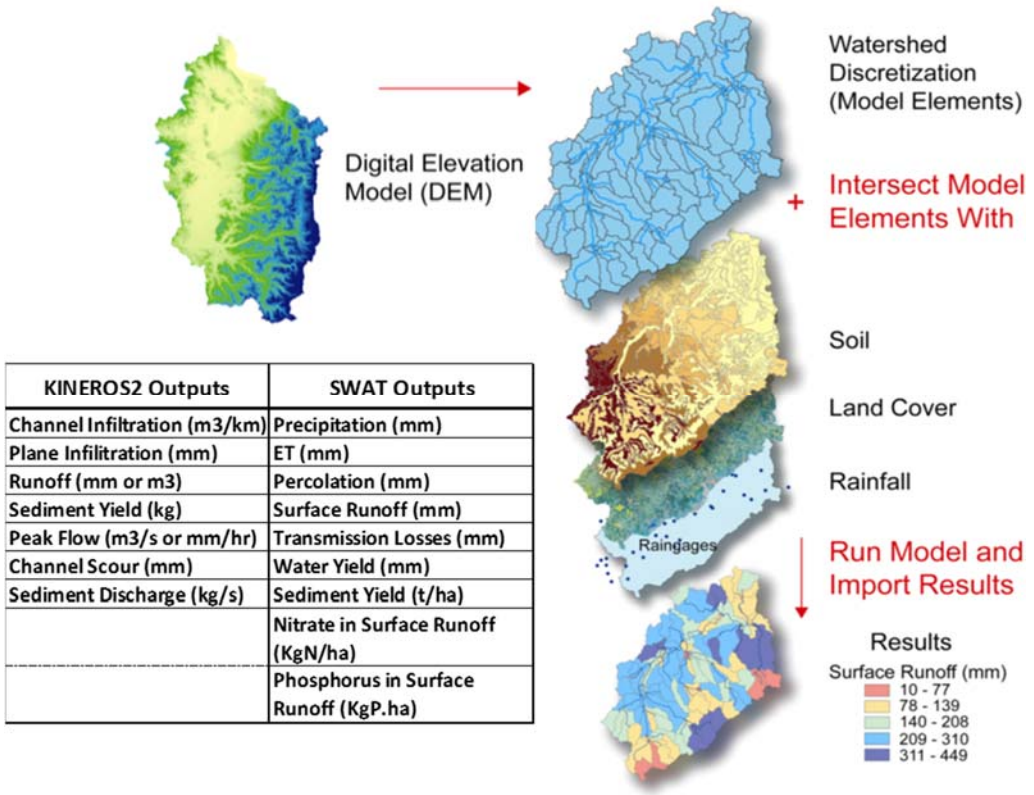
Hydrologic Modeling Using AGWA

The Automated Geospatial Watershed Assessment (AGWA) tool was used to perform the hydrologic analyses to obtain the peak flow and flow permanence variables. It was also used to model climate and land cover change impacts. We have obtained a Certificate of Networthiness for the AGWA tool, Cert#201418208.

AGWA is a GIS-based hydrologic analysis system for use by watershed, natural resource, and land use managers and scientists in performing watershed- and basin-scale studies (Miller et al., 2007; Goodrich et al., 2012; http://www.tucson.ars.ag.gov/agwa). AGWA was jointly developed by the USDA Agricultural Research Service, the Environmental Sciences Division of the U.S. Environmental Protection Agency Office of Research and Development, the University of Arizona, and the University of Wyoming to automate the parameterization and execution of two runoff and erosion models: the SWAT and KINEROS2 hydrologic models. SWAT is a continuous simulation model for use in large (~1,000 km^2) watersheds. KINEROS2 is an event-driven model designed for intermediate sized watersheds (<100 km^2) characterized by predominantly overland flow. These two models provide the capability for hydrologic modeling and watershed assessments at multiple temporal and spatial scales. AGWA uses nationally available GIS data layers to fully parameterize, execute, and visualize results from both SWAT and KINEROS2. It runs as an add-in to ESRI's ArcGIS desktop 9.x, 10.x and ArcView 3.x software platforms (http://www.esri.com/products/index.html).

The AGWA tool was developed for use on arid and semi-arid rangelands, and has been applied world-wide and intensively in the San Pedro watershed, Arizona. In 2006, AGWA/KINEROS was used to predict connectivity of ephemeral stream channels to the perennial reaches of the San Pedro River (Levick et al., 2006). In 2004, AGWA/KINEROS was used to estimate infiltration from detention basins in the Sierra Vista subwatershed (GeoSystems Analysis, Inc., 2004). In 2003, a customized version of AGWA was developed by members of the study team to support land management activities at Fort Huachuca such as closure and revegetation of existing roads, and expansion of the cantonment area into undeveloped land (Levick et al., 2003).

AGWA is mainly designed to provide qualitative estimates of runoff and erosion for use as a relative change tool for scenario analysis; however, with careful model calibration using high quality observations of precipitation and streamflow data, it can provide quantitative estimates as well. To run either model the user employs the AGWA interface to delineate the watershed boundary from a chosen outlet based on a digital elevation dataset. The watershed is then discretized into smaller hydrologic response units for SWAT (HRUs) or overland and channel model elements for KINEROS2 that are parameterized by intersecting soil, landcover and precipitation data. AGWA creates the required input files for the selected model, and displays the results in tabular, hydrograph and map form. Figure 15 is a schematic of the AGWA workflow. All results were applied to the 1 km stream reaches for each installation.



KINEROS2 Outputs	SWAT Outputs
Channel Infiltration (m3/km)	Precipitation (mm)
Plane Infilitration (mm)	ET (mm)
Runoff (mm or m3)	Percolation (mm)
Sediment Yield (kg)	Surface Runoff (mm)
Peak Flow (m3/s or mm/hr)	Transmission Losses (mm)
Channel Scour (mm)	Water Yield (mm)
Sediment Discharge (kg/s)	Sediment Yield (t/ha)
	Nitrate in Surface Runoff (KgN/ha)
	Phosphorus in Surface Runoff (KgP.ha)

Figure 15. Automated Geospatial Watershed Assessment Tool (AGWA) work flow and model outputs.

All data required to run AGWA is freely available from a variety of federal and state websites. For this analysis, we used 10 m DEMs for the delineation and discretization of the watersheds, acquired for all four installations from the USGS Seamless Data Warehouse (http://seamless.usgs.gov/index.php). Fine scale Soil Survey Geographic (SSURGO) soil datasets were obtained where available and coarser State Soil Geographic Database (STATSGO) data layers were acquired for the remaining areas, both available from the National Resource Conservation Service's Soil Data Mart (http://soildatamart.nrcs.usda.gov/Default.aspx). A landcover classification dataset based on Landsat ETM+ imagery was acquired for Arizona and New Mexico from the Southwest Regional Gap website (SWREGAP; http://fws-nmcfwru.nmsu.edu/swregap/default.htm). The Northwest Gap Analysis data for California was

obtained from the website http://gap.uidaho.edu/index.php/gap-home/Northwest-GAP/california-land-cover.

In this research, AGWA was used with the KINEROS2 model to develop values for peak flow, and with the SWAT model for flow permanence. Flow permanence refers to the percent of time per year where surface flow is present within each individual reach. It is determined by averaging the daily water yield (mm) values for each year over the period of record, and dividing by the total number of days to get the average percent of time per year there is flow present in the channel. Peak flow is the maximum discharge value for a stream reach following a precipitation event. A summary of the hydrologic modeling and calibration will be presented here; for a more thorough description see the M.S. Thesis by Lyon (2013), and Appendix D for maps showing the values for flow permanence and the 25-yr 1-hr peak flows for each installation.

It is widely known that soil moisture has a key role in surface hydrology; however, because of the extremely large and diverse study area for this project (approx. 10,770 km2; 2,661,000 acres) field measurements of soil moisture were not feasible. Various methods for predicting or estimating soil moisture exist, including the recently deployed Soil Moisture and Ocean Salinity (SMOS) satellite. These products are not necessarily appropriate at the scale of our project (e.g. SMOS resolution is approx. 35 – 50 km, while our stream reaches can be as small as 1 m wide), and generally require post-processing and analyses not within the scope of this project. In addition, AGWA is not currently configured to incorporate these types of data.

AGWA estimates or predicts soil moisture using known data sets, and these predictions are unique to each of the embedded models, KINEROS2 and SWAT. Miller et al. (2002) describe how AGWA addresses antecedent soil moisture in the two models as follows. KINEROS2 is an event-based model and does not compute inter-storm soil moisture conditions. This information is provided as an initial condition, and defaults to 0.2 initial soil water content or saturation index, SI (Goodrich, 1990). This value can be modified by the user, but was left at the default value for this project because the model uses design storms instead of observed data. Holding soil moisture constant in this way allowed us to compare relative differences across stream reaches, and produce this stream type classification and methodology. In these water-limited environments soil moisture tends to be very low except immediately following a precipitation event. The saturation index, SI = 0.20 is an approximate median initial pre-storm soil moisture condition based on CREAMS (Knisel et al., 1980) daily water balance simulations at 11 rain gages within the USDA-ARS Walnut Gulch Experimental Watershed in southeastern Arizona over approximately 50 rainfall events. An option would have been to bracket the KINEROS2 simulations using an SI of ~ 0.1 for dry conditions, and SI of ~ 0.5 for wet conditions. No sensitivity analyses were conducted for the KINEROS2 model for this project; however, Goodrich et al. (1991; 1994; Yatheendradas et al., 2008) investigated the effect of initial soil water content on runoff simulations at the Walnut Gulch Experimental Watershed, and suggested that the spatial variation of rainfall in small watersheds (i.e. approximately 0.04 km2) has a larger effect on runoff characteristics than initial soil moisture. For medium sized watersheds (i.e. approximately 6.3 km2) results indicated that a single basin average for SI did not seriously limit runoff simulations. Simulated watersheds for this project varied in size from 0.28 km2 to 1368 km2. Walnut Gulch has an average annual precipitation of approximately 312 mm

(Goodrich et al., 2008), and all streams are ephemeral. The default values were used for all variables in the KINEROS2 simulations.

For the SWAT model, soil moisture is addressed as part of the Curve Number (CN) which is a function of the hydrologic group, hydrologic condition, cover type and antecedent soil moisture for average basin wetness; CN is adjusted on a daily time step (Miller et al., 2002). Soil hydrologic group is obtained from soils data, and cover type is from classified land cover data. This is a conservative estimate for our study sites given their arid to semi-arid climate regimes. Lyon (2013) calibrated SWAT for peak flow at Fort Huachuca using USGS stream flow gage data. Fort Huachuca is the only one of our study sites with gage data that could be used to calibrate the model. Lyon found that to match observed peak flow amounts, the Curve Number must be decreased by 15%, in addition to other adjustments to input values. This indicated that the default assumptions in AGWA over-estimated the amount of moisture in the soil, which resulted in an over-estimation of the amount of runoff. The sensitivity analysis conducted for the SWAT simulations showed that the Curve Number (CN) was one of the most important input variables in the model. SWAT assumes antecedent moisture condition II (average basin wetness) for calculation of the Curve Number, and adjusts CN on a daily time step based on modeled soil moisture.

However, it should be stressed that in arid and semiarid environments, the additional water gathered by drainage systems is critical for supporting riparian systems. Numerous studies (Lite et al. 2005, Levick et al. 2008, Stromberg et al. 2007, Stromberg et al. 1991) have shown that riparian type and condition are correlated to streamflow amount and magnitude. In turn, streamflow characteristics can be significantly influenced by disturbance and climate.

Precipitation is one of the more important inputs to these models. SWAT requires average daily precipitation values for several years as input, and KINEROS2 requires design storm data. Because of the high degree of spatiotemporal variability in rainfall and runoff in the southwest, and the lack of actual measurement data in these regions (only a thinly scattered network of rain gages and very few stream gages exist), various data sources were evaluated to identify the most appropriate rainfall data. Fort Huachuca had the best network of rain gages, and USGS stream flow gages at Upper Garden (USGS 09470800), and Huachuca (USGS 09471310) Canyons that allowed for model calibration to improve accuracy. Thus, Fort Huachuca was used as the test case to determine if nationally available climate datasets were suitable for use in the models for all installations included in this study.

At Fort Huachuca, daily precipitation data from 1998 to 2010 were obtained from seven meteorological stations (met stations) located within the installation boundary. Daily precipitation data were also obtained from the National Climatic Data Center's (NCDC) TD3200 U.S. Cooperative Summary of Day dataset for all gages located in or near Fort Huachuca from the date the gage became operable through 2011. The models were run with both precipitation datasets, and simulations in Garden Canyon showed an average difference in surface flow of less than 4%, suggesting that precipitation data from the NCDC datasets could be used for model inputs at the other installations (Fort Irwin, YPG, and Fort Bliss) where local raingage data are unavailable or sparse.

Results from Garden Canyon were also compared to tidbit sensor data acquired by SERDP project RC-1725 (J. Stromberg, PI), which recorded presence of flow during 2011 in both Upper and Lower Garden Canyon. This comparison confirmed that simulated flow permanence in Upper Garden Canyon was comparable but overestimated in Lower Garden Canyon, suggesting that calibration and validation were necessary. To calibrate SWAT, actual streamflow measurements were needed; Garden Canyon was chosen due to the presence of a stream gage in its upper section. Calibration involved comparing average annual surface flow, baseflow and total water yield between observed and estimated flows. The model calibration determined that a 15% reduction in Curve Number (CN) values, originally calculated during parameterization, and a decrease in the groundwater "revap" coefficient (GW_REVAP) from the default of 0.2 to 0.02, were necessary to get equivalent results. The next step in calibration was to compare individual storm hydrographs for observed and estimated flows. For a more detailed description of the calibration methods, see Lyon (2013). The adjusted values were used for all SWAT simulations at all four installations.

The hydrograph plots showed that the model failed to pick up some storms using both the NCDC and met station precipitation data (Figure 16), suggesting that the low resolution of rain gauges was not capturing the spatial variability typical of convective summer storms in the area. This led to the use of the finer resolution (4 km^2) NEXRAD-MPE radar data to better account for these storm characteristics by providing improved representation of the spatial variability of summer convective storms, than the NCDC rain gage network which has sparse coverage around our project locations.

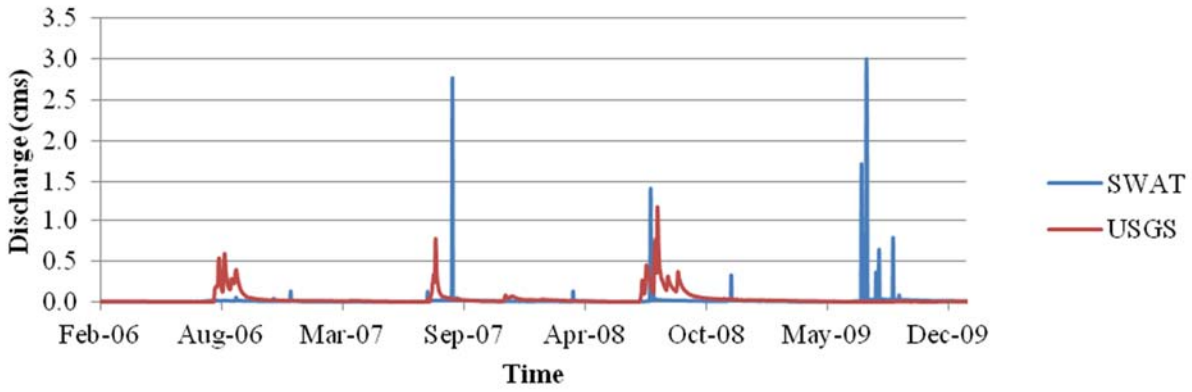


Figure 16. Hydrograph comparing modeled (SWAT) and observed (USGS) discharge for Upper Garden Canyon, Fort Huachuca, using met station precipitation in the SWAT model.

NEXRAD data is collected through a network of 159 high-resolution Weather Surveillance Radar-1988 Doppler (WSR-88D) radars that constantly scan the near surface detecting precipitation and atmospheric movement using a Precipitation Processing System (PPS) algorithm described in detail in Fulton et al. (1998). The data is organized to provide spatially continuous precipitation estimates over a 4x4 km^2 grid projected in the Hydrologic Rainfall Analysis Project (HRAP) coordinate system. The quality of NEXRAD data has evolved through various stages (I-IV), as new algorithms have been developed to remove bias and enhance accuracy (Young et al., 2000). NEXRAD Stage IV observed precipitation data, also known as Multi-sensor Precipitation Estimation (NEXRAD-MPE) data, were downloaded from the NOAA

Advanced Hydrologic Prediction Service as a series of daily shapefiles from 2005-2012 for the conterminous United States. An open source Python script designed by Mehmat Ercan at the University of South Carolina was used to create a table of daily precipitation values for the central point of each HRAP grid cell that intersected any part of the study area watersheds. Center points were then used as virtual rain gauge locations and used to drive SWAT.

To confirm that the NEXRAD data were acceptable for input to SWAT, a statistical comparison was performed on the model outputs at Fort Huachuca using the NCDC rain gage data, the met tower data, and the NEXRAD-MPE data. The model was calibrated at both the Upper Garden Canyon (Figure 17) and Huachuca Canyon stream flow gages, using each precipitation input for a subset of years and validated using the remaining data. Results for Upper Garden Canyon are shown below.

Both SWAT-NEXRAD and SWAT-rain gauge simulations obtained acceptable levels of accuracy based on R^2 and NSE values for average monthly totals during both calibration and validation time periods (

Table 1 and Figure 18). The similarity between rain gauge and radar results observed at Upper Garden and Huachuca Canyons suggested that the NEXRAD-MPE data can serve as an accurate substitute for field observations where rain gauges are absent or possibly achieve better results where they are scarce (for more details, see Lyon, 2013, included as an attachment). The higher resolution of NEXRAD-MPE data (4 km^2) provides improved representation of the spatial variability of summer convective storms, than the NCDC rain gauge network which has sparse coverage around our project locations.

NEXRAD-MPE data were used for the precipitation inputs for the final simulations for SWAT for all installations. An example map showing flow permanence values for the 1 km stream reaches at Fort Irwin are presented in Figure 19. Maps for flow permanence for all installations showing the AGWA streamlines and the NHDPlus Version 2 streamlines are in Appendix D.

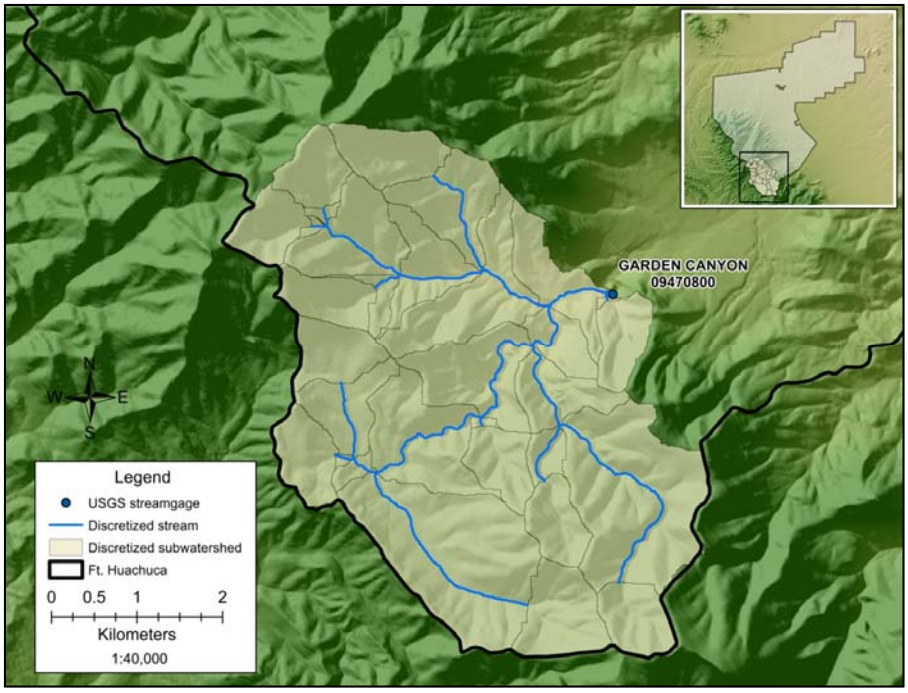
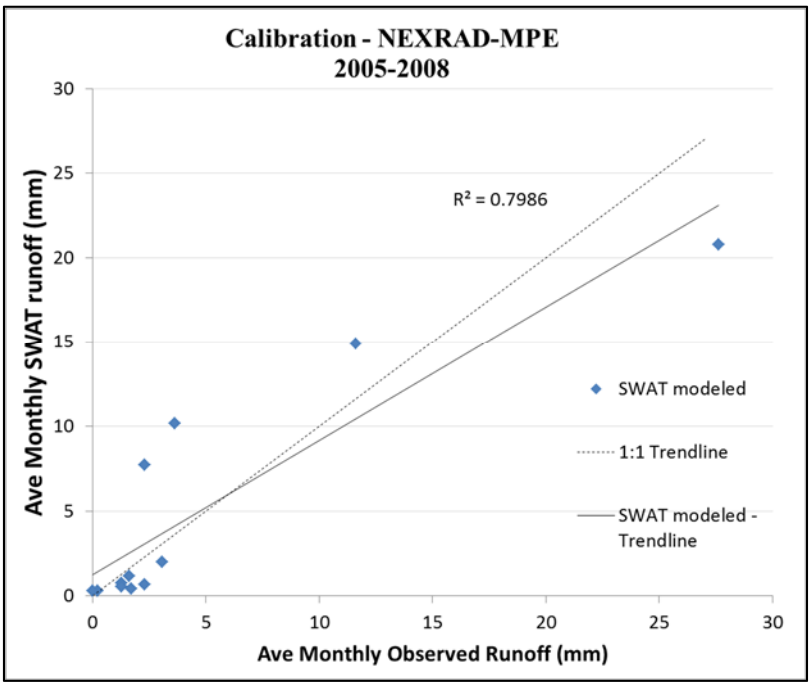


Figure 17. Map of Upper Garden Canyon Watershed and USGS stream gauge location.

Table 1. Statistical results for Upper Garden Canyon SWAT-NEXRAD, rain gauge and met tower simulations with coefficient of determination (R^2) and Nash-Sutcliffe Efficiency (NSE) values for calibration and validation time periods.

Precipitation Data	Calibration					Validation				
	Years	Daily		Monthly		Years	Daily		Monthly	
		R^2	NSE	R^2	NSE		R^2	NSE	R^2	NSE
Nexrad-MPE	2005-2008	0.50	-0.01	0.80	0.80	2009-2012	0.57	-0.38	0.90	0.86
Rain gage	2000-2005	0.46	0.44	0.95	0.92	2006-2011	0.34	-0.24	0.97	0.73
Met Tower	2000-2004	0.02	-6.9	0.06	-0.3	2005-2008	0.37	-0.21	0.99	0.78

a)



b)

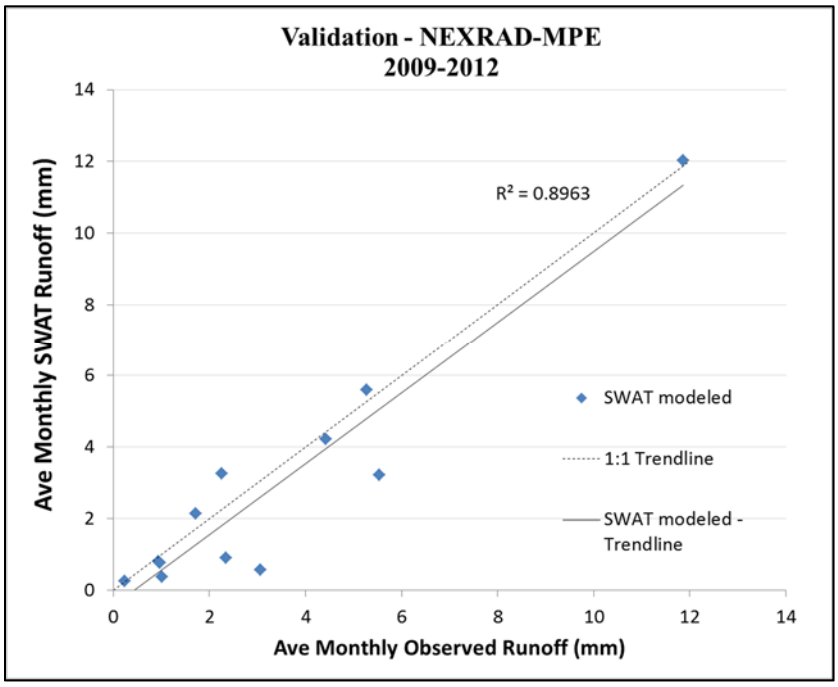


Figure 18. Plots of simulated vs. observed average monthly volume totals at Upper Garden Canyon using NEXRAD-MPE precipitation input for (a) calibration and (b) validation.

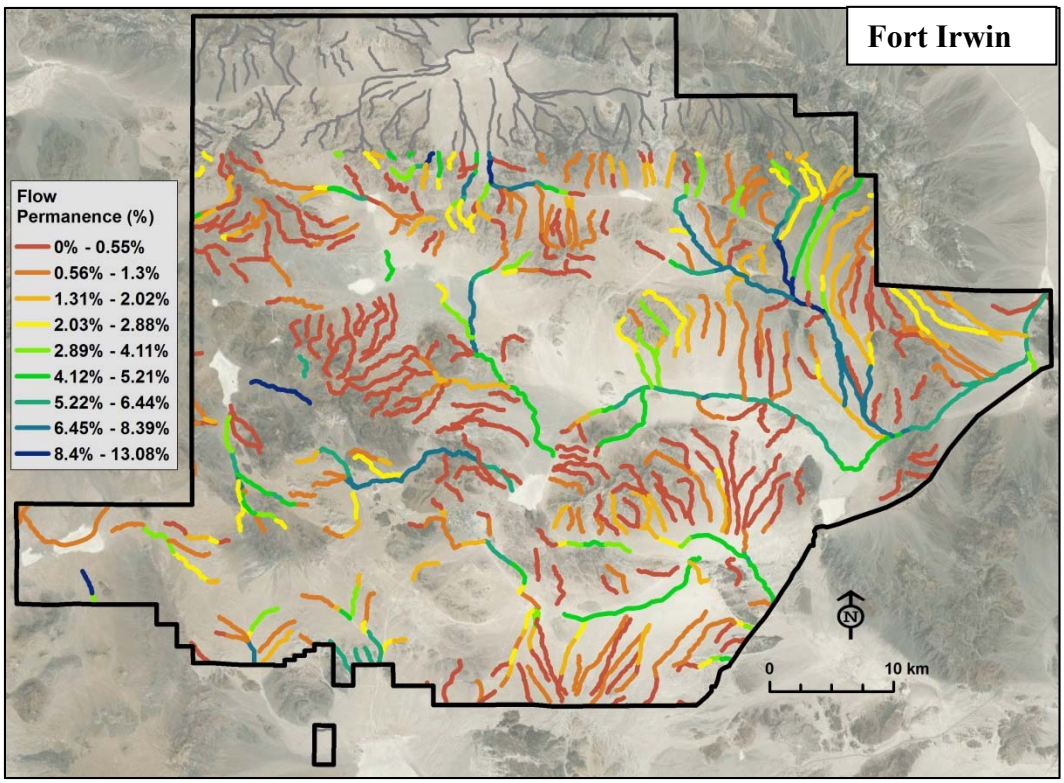


Figure 19. Map showing flow permanence for all 1 km stream reaches at Fort Irwin.

KINEROS2 was used to obtain peak flow for a variety of storm durations and return intervals for each HRU in the study areas. KINEROS2 requires precipitation frequency estimates for specific return intervals and durations. Estimates of these values were acquired for each watershed center from NOAA's National Weather Service Hydrometeorological Design Studies Center Precipitation Frequency Data Server (NOAA PFDS, 2012; http://hdsc.nws.noaa.gov/hdsc/pfds/index.html).

The PFDS allows for the input of geographical coordinates of each watershed center to determine precipitation depths based on a frequency analysis of partial duration series. Design storms based on several storms were created from the PFDS data using the centroid coordinate for each watershed in the study areas. Applying a design storm created from a single point estimate across an entire watershed tends to result in an overestimation of runoff due to the failure to account for spatial heterogeneity of the input data (Miller et al., 2002). To account for discrepancies an aerial reduction factor was applied to the depth values based on Osborn et al. (1980) and expanded in NOAA's Technical Memorandum NWS HYDRO-40 (Zehr and Myers, 1984) to average the depths over the entire watershed. Peak flows for the 5-, 10-, 25- and 100-yr 1-hr storms were modeled for all watersheds at all four installations.

Riparian Vegetation Characterization

The purpose of the vegetation analysis was to characterize the vegetation along the stream channels for analysis of wildlife habitat use and value, and for use in the stream type

classification. Riparian vegetation is important in determining the value of the stream reach to wildlife. The criteria used to select the appropriate characteristics for analysis were based on features that wildlife require for nesting, breeding, foraging, and movement. Vegetation height (structure), cover, abundance, biomass, and connectivity (patchiness) are some of the more important features for wildlife habitat. Different species of wildlife use different types of vegetation and prefer different structural elements. Ground dwelling birds, small mammals and reptiles depend on ground cover, while some birds have a preference for foraging or nesting in shrubs, mid-canopy or upper canopy. Larger mammals (i.e. deer) depend on the taller vegetation to provide cover and protection from predators.

Our analysis used vegetation structure (height), cover and density to characterize the riparian vegetation. Vegetation structure represents the vertical bands in vegetation that are typically used by wildlife. Vegetation cover represents the horizontal extent of the vegetation, and vegetation density is an indication of vegetation abundance or lushness. These characteristics were chosen because they are important to wildlife, and were obtainable from our data. All vegetation data were derived for the 1 km stream reach polygons created by inundating the DEM to 3 m depth.

Riparian vegetation cover and density were obtained from satellite imagery (QuickBird or RapidEye) in ERDAS Imagine. Multi-return LiDAR (canopy or first return, and bare earth or ground; where available) data in ArcGIS were used to derive vegetation structure for use in the stream type classification, and also to create a separate structure-based classification. FUSION (LiDAR analysis and processing software; http://www.fs.fed.us/eng/rsac/fusion/launch/fusionbkg.htm) was used to process some of the LiDAR datasets. LiDAR data were not available for most of YPG at the start of the project; however, small tiles were available that were used to analyze vegetation structure at mesquite bosques for analysis of wildlife camera data. Field data and photos were used to check riparian vegetation width, height, and cover.

We did not attempt to identify plant species from the LiDAR or satellite imagery since this information can be obtained from existing vegetation mapping and reports at each military installation, and vegetation species cannot be determined using our methods and data.

Vegetation Structure (height)

Vegetation height was obtained from multi-return LiDAR data by differencing the first return and bare earth layers, and extracting individual structure groups (Farid et al., 2006; Bork and Su, 2007). Structure categories were based on the general types of vegetation found in these deserts, and relate to the general height bands of vegetation used by wildlife: <1 m, 1-4 m, 4-12 m, and >12 m (Figure 20).

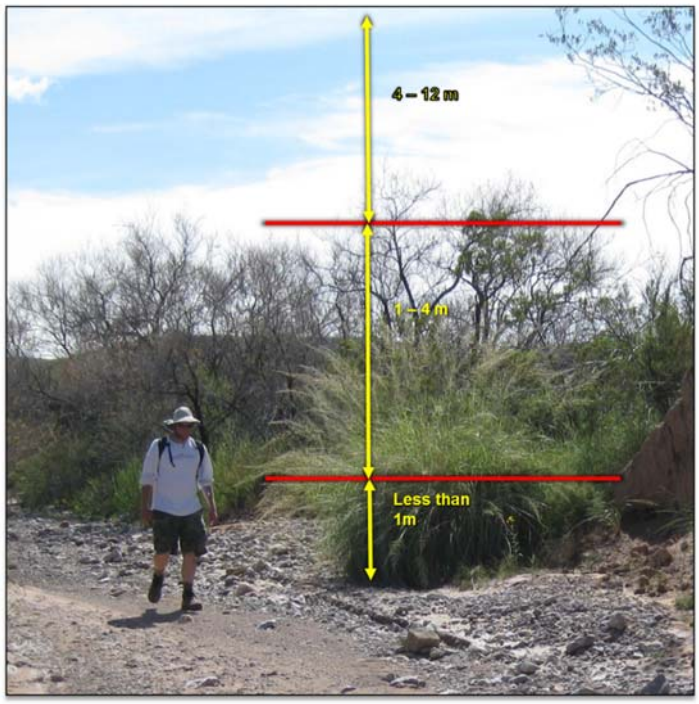


Figure 20. Illustration of vegetation structure layers.

The lowest structure category was determined by selecting the vegetation height that best distinguished bare earth or ground cover from more permanent woody vegetation. This varied by installation as follows and was confirmed from field data and photos:

Fort Huachuca: 1 m (extensive grass cover)
Fort Bliss: 0.25 m (very small shrubs, ground cover and forbs)
Fort Irwin: 0.5 m (small shrubs, ground cover, small creosote, rocks)
YPG: 0.2 m (ground cover, available for only a small area, used for wildlife analysis)

The percent of each structure category within each 1 km reach was calculated, and these values were used in the stream type classification. An example map of the "vegetation 1-4 m" structure category is shown in Figure 21 for Fort Irwin.

In addition, a vegetation structure-based classification was performed using the Isodata Unsupervised Classification function in ERDAS Imagine. This classification can provide additional information to managers for use in creating sampling schemes and wildlife surveys. An example map of this result for Fort Irwin is shown in Figure 22.

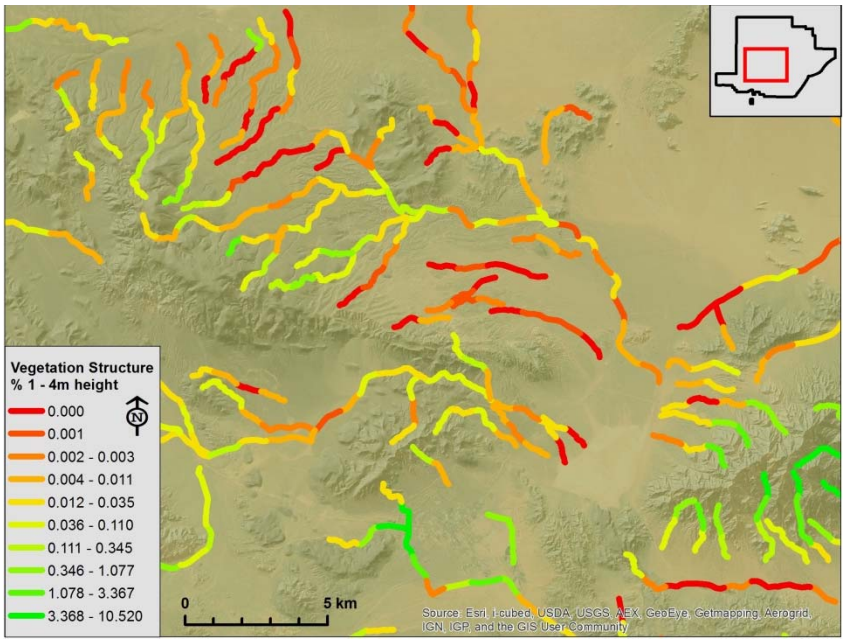
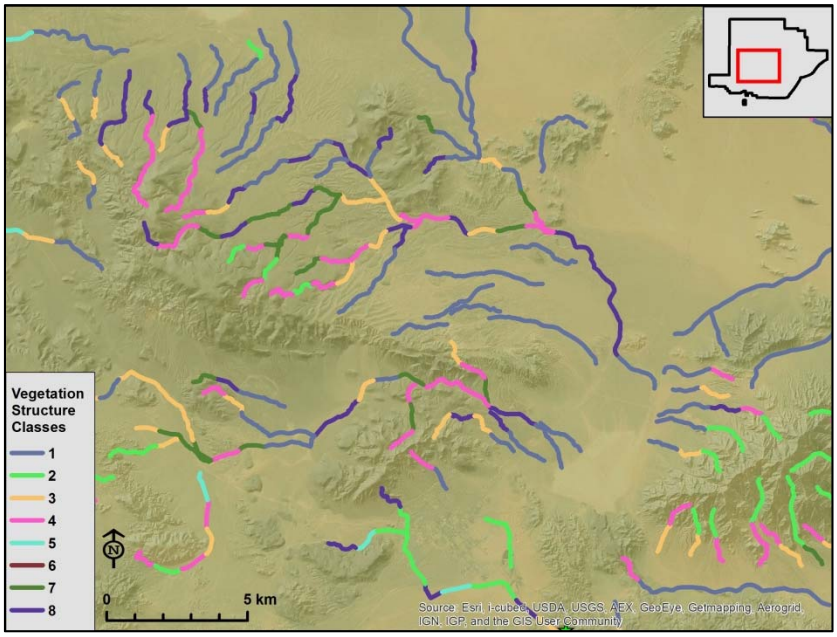


Figure 21. Map of vegetation structure group 1 - 4 m for Fort Irwin streams.



Fort Irwin Vegetation Structure Classes and Percent of each structure category				
Class	>0.25m	>1m	>4m	>12m
1	0.25	0.01	0.00	0.00
2	9.91	2.43	0.27	0.00
3	1.09	0.08	0.00	0.00
4	3.16	0.26	0.00	0.00
5	1.25	0.28	0.04	0.00
6	0.34	0.02	0.00	0.00
7	1.32	0.01	0.00	0.00
8	0.73	0.01	0.00	0.00

Figure 22. Map and table of vegetation structure classes for Fort Irwin stream reaches.

In the above figures, the locations with higher percentages of vegetation cover between 1 - 4 m (Figure 21, brightest green) are the same locations of structure classes with high percentages of vegetation taller than 1 m (Figure 22, Class 2, bright green).

Vegetation Cover and Density

Vegetation cover and density were obtained from vegetation indices derived from the QuickBird and RapidEye satellite imagery, using ERDAS Imagine image processing software. Vegetation

indices are ratios of the reflectance properties of vegetation, and were used to classify the images into vegetation vs. bare ground or ground cover. Several commonly used indices were tested to determine which yielded the best results across the varied terrain of our study locations for each type of imagery.

QuickBird imagery contains Red, Green, Blue and Near-Infrared bands. Vegetation indices that were tested include Normalized Difference Vegetation Index (NDVI), Simple Ratio Index (SI), Enhanced Vegetation Index (EVI), Greenness Index (GI), Soil Adjusted Vegetation Index (SAVI), and Modified Soil Adjusted Vegetation Index (MSAVI2). See Appendix F for more information and the equations for these indices.

The MSAVI2 vegetation index produced the best results for both Fort Irwin and Fort Huachuca. Soil reflectance is one of the main independent variables influencing a vegetation index, in addition to the amount of vegetation (leaf area index, LAI), and the canopy architecture (mean leaf inclination angle) (Rondeaux et al., 1996). Various studies have shown that MSAVI2 has the best result in areas with sparse vegetation and bare soil, found in arid and semi-arid regions (Qi et al., 1994; Rondeaux et al., 1996; Purevdorj et al., 1998; Jiang et al., 2007). It was derived from the Soil Adjusted Vegetation Index (SAVI) but does not require prior knowledge of the soil brightness value that is required for SAVI. This index is calculated using the Red and Near-Infrared (NIR) bands:

$$MSAVI2 = \frac{\left(2*NIR+1-\sqrt{(2*NIR+1)^2-8*(NIR-RED)}\right)}{2}$$

RapidEye imagery includes an additional spectral band, the Red Edge band, which is located between the Red and Near Infra-red (NIR) bands. It provides additional information on plant chlorophyll content and leaf structure reflection, improving the ability to distinguish plant types, cover and abundance (Weichelt, et al., 2012). Schuster et al. (2012) tested the use of the red edge band for land use classification and found that this band improved accuracy in areas of open landscapes such as bush vegetation. The Red Edge band is used in narrowband greenness indices and several of these were tested at Fort Bliss and YPG by converting narrowband greenness indices to broad-band (The ENVI User Guide, http://geol.hu/data/online_help/Vegetation_Indices.html , accessed Nov. 27, 2012). The indices tested include Red Edge Normalized Difference Vegetation Index (RENDVI), Modified Red Edge Simple Ratio Index (Re-Mod-SRI), Modified Red Edge Normalized Difference Vegetation Index, Modified Chlorophyll Absorption in Reflectance Index (MCARI; Daughtry et al., 2000), and Transformed Chlorophyll Absorption in Reflectance Index (TCARI; Haboudane et al., 2002). See Appendix F for more information and the equations for these indices. The Red Edge NDVI produced the best results across all terrain types at Fort Bliss and YPG, and is calculated using the standard NDVI equation with the Red Edge band replacing the red band:

RE-NDVI = (NIR - RE) / (NIR + RE)

The vegetation indices were calculated for each installation (MSAVI2 at Fort Huachuca and Fort Irwin, and RENDVI at Fort Bliss and YPG), and then classified into vegetation vs. bare ground or ground cover (Figure 23). The vegetation index values were extracted for each 1 km stream reach polygon to obtain vegetation density as the mean value of the vegetation pixels for each 1

km polygon. Vegetation cover was derived as the total area of pixels in each polygon classified as vegetation, divided by the area of the 1 km stream reach polygon (Figure 24).

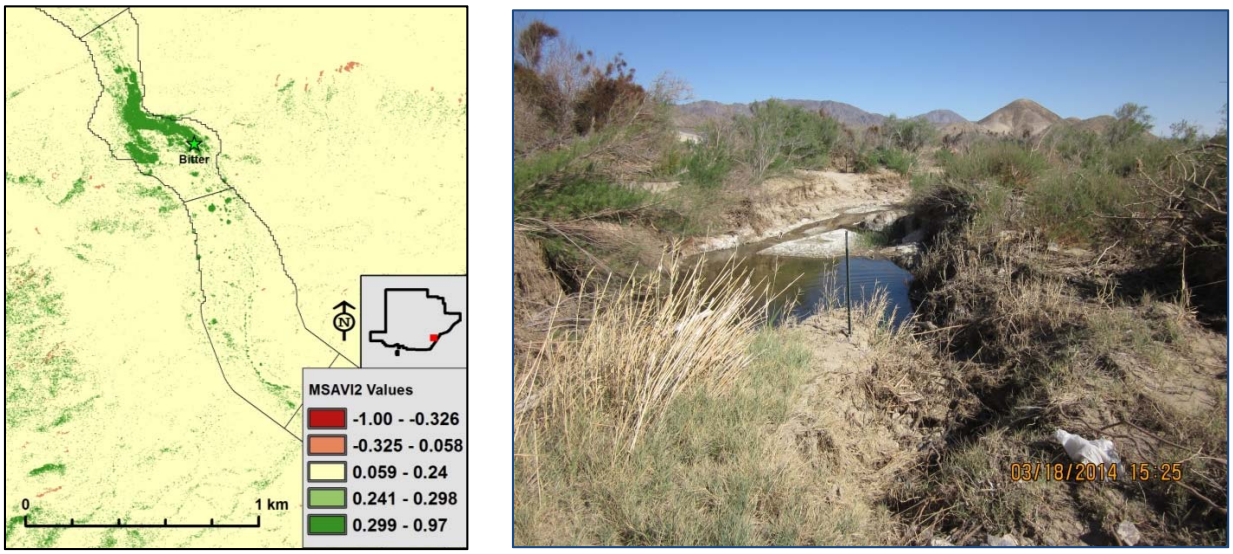


Figure 23. Map image at Bitter Springs, Fort Irwin, showing MSAVI2 values (left), and a photo of Bitter Springs (right).

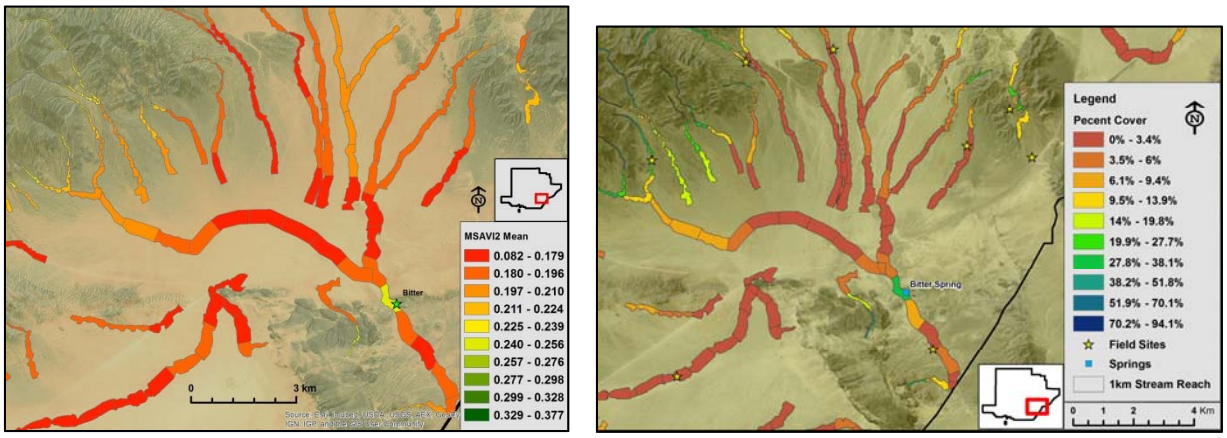


Figure 24. Map image of Bitter Springs area, Fort Irwin, showing MSAVI2 mean values for the 1 km stream reach polygons (left), and MSAVI2 values classified for percent cover (right).

Seasonal Vegetation Response to Monsoonal Precipitation

Because we were unable to perform the LiDAR vegetation structure analysis at YPG due to lack of LiDAR data, we investigated the use of Landsat 5 Thematic Mapper (TM) data to enhance the vegetation characterization. Landsat data are freely available with a temporal resolution of 16 day intervals. We obtained Landsat 5 TM data for several dates bracketing the summer months from 2006 through 2010. Based on the National Weather Service monsoon statistics (http://www.wrh.noaa.gov/twc/monsoon/monsoon.php), 2008 was a wet monsoon for Yuma, Phoenix and Tucson (37.8, 144.8, and 140.2 mm respectively). Using all three locations to select the year was important to ensure that most if not all of YPG received precipitation during the

months of July, August and September. The goal was to select a year that would experience the greatest change in vegetation response by the end of the summer months throughout YPG. While 2008 was not the highest total monsoonal precipitation, all three locations experienced relatively high amounts of rainfall during the summer, and rainfall was the most likely evenly distributed for those months for Yuma.

Using scenes from a pre-monsoon and post-monsoon date (June 11, 2008 and Oct. 1, 2008) we calculated the MSAVI2 vegetation index for YPG, to represent vegetation condition before and after the monsoon season. The percent difference of the mean MSAVI2 values for each 1 km stream reach polygon was used to indicate the vegetation response to the monsoonal precipitation and was used as input to the classification, as a seasonal vegetation response index (SVRI).

Various statistical analyses were performed to evaluate whether this index, SVRI, improved the stream type classification. Correlation analysis indicated that the index was not correlated to any of the other variables. Principal components analysis (PCA) indicated that SVRI was significant in the second and third principal components. Cluster analysis in R was performed using both datasets, for 3 to 12 clusters. Dendrograms and nonmetric multidimensional scaling (NMDS) in R were used to view the structure of the datasets with and without the index for each cluster result (Figure 25 and Figure 26), and indicated that the addition of the index resulted in more distinct clusters. A one-way analysis of variance (ANOVA) indicated that the clusters were statistically significantly different for most of the other input variables with and without the SVRI.

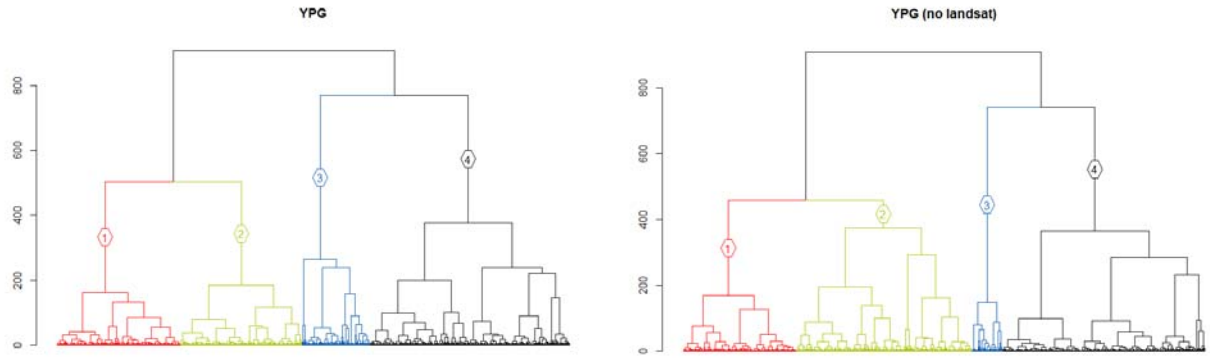


Figure 25. Dendrograms for YPG clustering, 4 clusters, with (left) and without (right) the SVRI index.

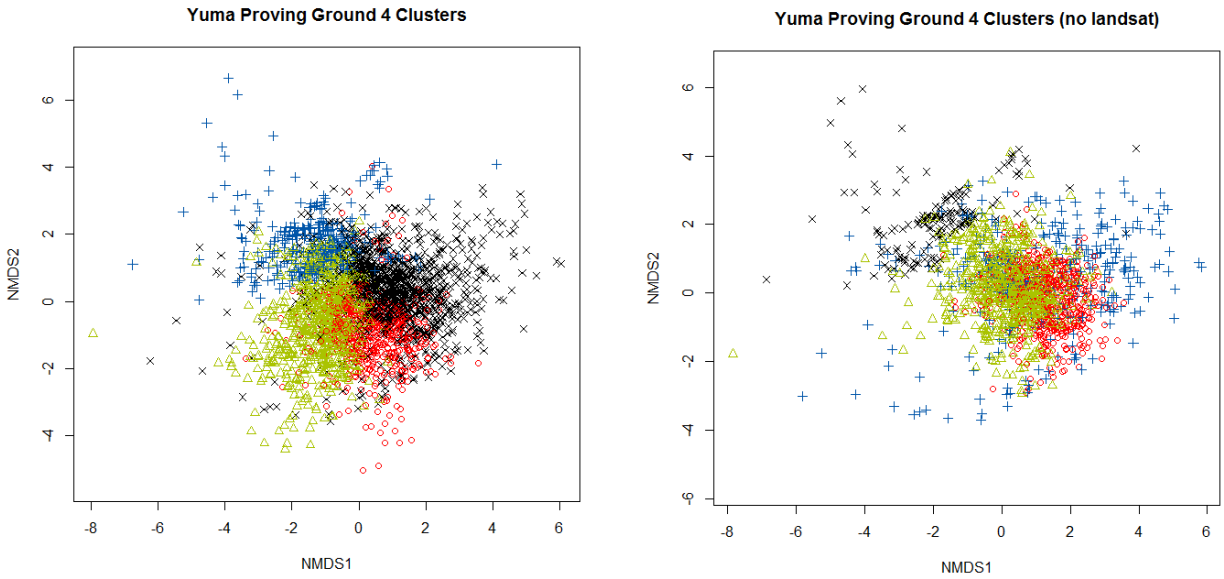


Figure 26. NMDS plots for YPG clustering with (left) and without (right) the SVRI index.

This approach is appropriate for arid locations where vegetation response to rainfall is noticeable. The best results will be obtained if the images used are from before and after a growing season, unless temperature also defines the growing season. This method assumes that a significant increase in vegetation greenness occurs following a growing (rainy) season; therefore it will not be as effective in locations where rainfall is evenly distributed throughout the year. The type of vegetation (i.e. woody vs. herbaceous) should also be taken into consideration as the change in the vegetation index from herbaceous plants may be stronger than woody plant species, especially for bare areas.

Although this analysis used a single year, optimal analyses should incorporate average changes in MSAVI2 values by using multiple years of remote sensing imagery. In this analysis, the Landsat derived MSAVI2 index was used as it reduces the effects of bare ground common in arid settings; however, other indices such as the normalize difference vegetation index (NDVI) or the enhanced vegetation index (EVI) may be used in a similar manner.

Task 3: Field Data Acquisition

The main goal of the field data collection was to obtain geomorphic and vegetation characteristics from a variety of stream types for use in field checking the GIS and other derived data. Our field data collection methods evolved as we obtained more data and understood more about the variability of stream reaches across our study locations. Following review of the field data from the initial field trips, we revised our data collection methodologies to target the most relevant types of field data that were an appropriate scale for this analysis and that could be used to confirm the GIS and remotely sensed data. The original field data collection methodologies are described below, along with the revised methodology for each type of data. Copies of all data collection forms are included as attachments. Maps of the field data locations are included as Appendix E.

To sample the variability of stream types across each installation, we used two different methods. During the initial site visits we selected field sites based on observed visual differences in the field, such as channel width, depth, substrate, vegetation density and species, etc. These sites represented the general variability we observed. Subsequent field sites were selected using the ArcMap random point generator to create a set of 100 sample points to capture the overall variability of stream types. Each point was constrained to a minimum allowable distance of 1 km between points and within 100 m of a streamline.

Geomorphic Data

Geomorphic data were taken along a 100 m transect using a tape placed down the center of the channel. The original data collection protocol included channel characterization, sketches, and descriptions of pattern, planform, bedform, banks, terraces, cross section, particle size distribution estimate (Wolman Pebble Count), GPS channel cross sections, GPS longitudinal profile, and photographs. After analyzing these data, we determined that we did not require that level of detail for the classification. The revised field data collection protocol eliminated planform and cross-sectional sketches and intensive GPS surveys, but included channel planform and bedform, bank attributes, a modified particle size distribution estimate, and an estimate of the channel bottom width and bank depth. By eliminating the most time-intensive activities that were also not an appropriate scale for this analysis, more focused field data were collected, thus increasing the overall sample size. In almost all cases, a larger sample size increases accuracy.

Riparian and Upland Vegetation Data

Vegetation data were taken along the same 100 m transect as the geomorphic data. The original data collection included the riparian vegetation outline (using a GPS), canopy density (using a densiometer), vegetation structure (using a modified stadia rod), detailed lists of the common plant species present, and photographs. The canopy density and structure data were taken at every 5 m, on the uplands and in the riparian zone on both right and left sides of the channel, and along the center of the channel. We also used an Abney Level to obtain the height of various trees and shrubs for ground truthing the LiDAR.

After reviewing the field data for riparian vegetation we determined that we did not need that level of detail, and so revised our methodology accordingly. Subsequent data were collected only along the 100 m transect at the same location as the geomorphic data. Visual estimates of riparian vegetation structure (height classes) for the entire transect were recorded as percent of woody vegetation cover less than 1 m, 1 – 4 m, 4 – 12 m, and greater than 12 m. These height classes represent the general vegetation structure required by wildlife and correspond with the vegetation height classes obtained from the multi-return LiDAR. Along with percent cover for each height class, we recorded patch density based on a scale of 1-5 (no patches to almost continuous dense cover) that we attempted to convert to percentages based on analysis of the imagery; however, we did not have enough field data to complete this analysis. For the overall transect, we recorded the dominant vegetation form (tree, shrub, grass or cactus), the dominant tree and shrub species, the most common plant species, maximum vegetation height, and average riparian vegetation width. We took a series of photographs at the 0 m, 50 m and 100 m points on the transect. The fourth and final field data protocol collected only the data required to ground

truth the vegetation analysis from the LiDAR and satellite imagery: percent cover for each structure class, overall percent cover, average riparian zone width, maximum vegetation height, photos, and general notes on species composition.

Hydrologic Data

Hydrologic data were taken as visual observation during the last round of trips to validate the AGWA model results for flow permanence. This was performed by evaluating evidence of recent flows, flood debris, channel features (harrow marks), channel geometry, and vegetation characteristics, in relation to the estimates of flow permanence from the AGWA/SWAT model. No other hydrological data were taken in the field.

Wildlife and Wildlife Sign, Habitat Features

Wildlife data were taken along the same 100 m transect as the geomorphic and vegetation data, and included the uplands. Data collection originally included information on wildlife observations (visual and audio), presence and abundance of scat, tracks, trails, ground disturbance, nests, burrows, perches, plants fruiting or flowering, amount of debris/litter, dead trees, horizontal cover, and the difference between the upland and riparian canopy cover. The revised field data included, for both the riparian zone and the adjacent upland, qualitative estimates on the abundance of wildlife trails and other wildlife evidence and a qualitative estimate of how amenable conditions at the transect are to observing evidence of wildlife (e.g. a gravel bed that would show the tracks of very few wildlife species would be rated 'low,' compared to a 'high' rating for a fine sandy bed that would show many species' tracks). Other notes, such as dominant plant species and details on wildlife evidence were also recorded. These data were used to inform us of the general amount and diversity of wildlife that use these riparian areas.

Longitudinal Channel Walks

During the earlier field trips we included "longitudinal channel walks" which involved walking along the channel and recording observations at every 100 m (200 m for longer walks). The purpose was to observe changes in geomorphology, vegetation and wildlife habitat features over a longer distance than the typical 100 m transect to aid us in determining an appropriate stream length for our unit of analysis, and to inform us of the variability of stream reaches. These walks varied in length from 1 km to 4 km, depending on the location. The features of very large braided channels that did not change noticeably over several kilometers were captured with a 1 km walk, while steep mountain channels or alluvial fan channels that had noticeable changes in several hundred meters required a longer distance to understand their overall variability. The data collected from these channel walks increased the total number of sites, and also improved our understanding of the variability of stream types at each installation.

Data collected included the following visual observations and photographs:

1. Geomorphology: channel planform, channel bedform, left and right bank characteristics, presence or absence of flow, particle size distribution estimate, and woody debris.

2. Riparian Vegetation: upland vegetation type, tallest and most abundant riparian tree and shrub species, other tree and shrub species, grass and forb abundance, and dominant vegetation form (tree, shrub, forb, grass).
3. Wildlife habitat features: species visibly present, species audibly present, presence of scat, tracks, trails, burrows, ground disturbance, nests, perches, flowering/fruiting plants, debris, horizontal cover percent, and difference in upland vs. riparian zone canopy.

Task 4: Classification of Ephemeral and Intermittent Stream Types

A unique stream type classification was created for each installation based on the hydrologic, vegetation, physical and geomorphic variables, using an agglomerative hierarchical clustering technique. The resulting stream type classes and input variables were associated with wildlife habitat for each installation.

Analysis Methods

In preparation for the classification, we developed a large dataset of variables during Task 2 at each installation for each 1 km stream reach. The majority of the analyses were related to identifying and deriving the variables that would best distinguish stream types. The variables developed for the stream type classifications were derived from readily available GIS data, satellite imagery, and LiDAR data (when available). A combination of statistical techniques were utilized to select the final input variables and to create the stream type classifications for each installation.

Analyses were performed in EXCEL, the R statistical software (www.r-project.org) within the R-Studio interface (www.rstudio.com), and SPM. Correlation analysis (Pearson correlation analysis in EXCEL) was used to reduce the number of input variables. Principal components analysis (PCA) was used to determine which variables were most significant, and which were related (varied together). PCA is a form of multidimensional scaling, and is a linear transformation of the variables into a lower dimensional space that retains the greatest amount of information about the variables.

We used an agglomerative hierarchical clustering technique in R, *hclust*, with the Euclidean distance function and Ward's method, to create the stream type classifications. Euclidean distance is the ordinary distance between two points. Ward's method is a minimum variance method that finds compact, spherical clusters (http://stat.ethz.ch/R-manual/R-patched/library/stats/html/hclust.html). Nonmetric multidimensional scaling (NMDS) in R was used to view the structure of the datasets for each cluster result. Cluster validity tests were performed in R to aid in the identification of the optimal number of clusters for each installation. Over 30 tests were performed, including silhouette widths, generalized minimum distance of distributions, dissimilarity measure, Dindex index, and Hubert index. These analyses produced either a plot or index that identifies the optimum number of clusters as an abrupt change, bend or elbow in the data. We selected the strongest tests from Milligan and Cooper's (1985) review of procedures for determining the number of clusters in a data set.

The validity tests indicated that while there was usually one optimal cluster arrangement, there were several acceptable cluster configurations. Therefore, the results from the validity tests were used to guide the selection of the optimal number of clusters, but site knowledge, field data, photos, and examination of the mapped data were used to select the final arrangement that best described the variability across each installation. A one-way analysis of variance (ANOVA) and Tukey's Honestly Significant Difference (HSD) tests were used to determine if the variables within each cluster (stream type) were statistically significantly different for each level of clustering. The tests compared the means and assigned a letter to each cluster that indicated its similarity to or difference from the other clusters. Clusters that do not share a letter have significantly different means. Boxplots were used to visualize the cluster statistics and also identify the variables most important in defining each cluster. This information was also used in selecting the final number of clusters.

The thresholds or breaks for each variable for each stream type were determined using a CART classification decision tree, using the Salford Predictive Modeler software suite. The final stream types were used as the target variables, and all defaults were kept for the initial tree (Gini method, 10-fold cross validation, no limits on tree size or minimum cases per terminal node, no weighting, and equal priors). The stream type classifications are unique for each installation, with no overlap across installations; however, the classification procedure may be applied within the same ecoregion. Thresholds can be used by management as a predictive tool to place streams not on the NHD stream network (new data) into one of the stream types. Combining cluster analysis with decision trees has been described by various researchers as a data mining technique that improves accuracy and results (Aviad and Roy, 2011; Gothai and Balasubramanie, 2012; Sharma and Kaler, 2013).

Summary documents with mapped clusters, dendrograms, NMDS plots and boxplots for each installation are included as Appendix B. A GIS data layer with the classified stream types was produced for each installation that includes all variables (geomorphology, riparian vegetation and hydrology) for each stream reach.

The input variables (described in more detail previously) used in the cluster analysis for the stream type classifications were:

1. Elevation (m)
2. Slope (%)
3. Flow Permanence (%)
4. Peak flow for the 25-yr 1-hr storm (Qp, m^3/s)
5. Vegetation structure (heights) groups (% cover of each layer), from the LiDAR vegetation height layer, varies by installation (not available for YPG)
6. Vegetation cover (%), derived using the vegetation index
7. Vegetation density, derived from the mean vegetation index
8. Total stream power for the 25-yr 1-hr storm (kW/m)
9. Cumulative area above the reach (m^2)
10. Water surface width at inundation depth of 2 m
11. Rainfall seasonality index (RSI)

12. Entrenchment Ratio, calculated from the water surface widths at 3 m and 0.5 m inundation depths (ER_3m_05m)
13. Seasonal Vegetation Response Index (SVRI), Landsat 5 TM MSAVI2, percent difference from June, 11, 2008 to Oct. 1, 2008, for YPG only

Task 4a: Wildlife Associations

This part of the research explored wildlife use patterns of ephemeral and intermittent streams using the geomorphic, hydrologic, and vegetation variables and the stream type classes. The research was conducted in detail at Fort Bliss, and the methods were applied at the other three installations. Additional analyses were conducted if other types of wildlife data were available. Wildlife use patterns were examined at three levels: single species, an entire group of species (e.g. mammals), and all species. For more detail, see the Master's Thesis by Hammer (2014).

To address whether habitat for particular vertebrate wildlife species of concern is associated with particular stream reaches, species distribution models were created using the ecohydrological input variables that evaluated the use of streams by single species of concern. At Yuma Proving Ground, there were not enough data on any one species in the stream reaches to model, so species richness in the bosques was modeled. Wildlife camera data, available for the mesquite bosques at YPG from the Arizona Game & Fish Department (AZGFD), were used with multi-return LiDAR to examine wildlife use of those areas.

At an intermediate level, multi-return LiDAR data were used at Fort Bliss to assign a nesting habitat index for all breeding birds and for just TER-S breeding birds to each stream reach in the study area. This index was tested using field data provided by the installation. The field data also allowed us to conduct a small test of estimated species richness derived from stacked animal habitat distribution models (described next).

To gain the broadest perspective, stacked Gap Analysis Program (USGS, 2014; USGS, 2007) animal habitat distribution models were created to explore patterns of terrestrial vertebrate species richness in the stream types at each installation. Richness of all species, birds, mammals, reptiles, and amphibians were examined. In addition, the richness of the TER-S species in each of these groups was examined. We created models to understand what particular ecohydrological characteristics were associated with TER-S richness.

Species Distribution Modeling Methods

An objective of the project was to link the stream classification to TER-S species. All installations except for YPG were able to provide enough point data for modeling the occurrence of at least one species in stream reaches on their installation.

Fort Bliss was able to provide an excellent data set to model one species. Gray vireos (*Vireo vicinor*) have a regional NatureServe rank in New Mexico of Apparently Secure (S4) for their breeding range and Vulnerable (S3) in their non-breeding range. They are listed by New Mexico as Threatened.

Fort Irwin was able to provide enough point data to model two species. Mohave desert tortoises (*Gopherus agassizi*) have a global NatureServe rank of G3, Vulnerable, and a regional rank in California of S2, Imperiled. They are also listed as Threatened under the Endangered Species Act. Burrowing owls (*Athene cunicularis*) have a regional NatureServe rank of S3, Vulnerable, in California. They are also listed as a Species of Special Concern by the California Department of Fish and Wildlife. Though not exclusive to streams, these species use the banks of washes for burrows. Wildlife managers at Fort Irwin have found them to be somewhat associated with washes and expressed interest in understanding better which washes are important for these species.

Fort Huachuca was also able to provide enough point data to model two to three species. Mexican spotted owls (*Strix occidentalis lucida*) have a global NatureServe rank of G3, Vulnerable, and a regional rank in Arizona of S3S4, Imperiled to Apparently Secure. They are also listed as Threatened under the Endangered Species Act. Whiskered screech owls (*Megascops trichopsis*) have a regional NatureServe rank of S3, Vulnerable, in Arizona. They are also listed as a Species of Greatest Conservation Need by the Arizona Department of Game and Fish. Western screech owls (*Megascops kennicotti*) do not have any special designations in Arizona, but at times have been considered conspecific with whiskered screech owls. Wildlife managers at Fort Huachuca expressed interest in understanding better which canyons are important for these species.

Environmental data

Seventeen of our ecohydrological variables were used for species distribution modeling: 7 vegetation, 3 hydrologic, and 7 geomorphic/physical variables (Table 2). We used one additional geomorphic variable from our data catalog and derived 5 additional variables that could be important for species occurrence. The additional variable from our data catalog used in species distribution modeling was rock type at Fort Huachuca, from the Arizona Geology dataset. For Fort Huachuca and Fort Bliss, we derived two measures of vegetation structure complexity using the LiDAR data: the Shannon diversity index (Shannon and Weaver, 1949) and the Simpson (1-D) diversity index (Burnham and Overton, 1979; Magurran and McGill, 2011). For both measures, higher values correspond to increasing structural diversity. For Fort Bliss, we used the land cover variety variable derived for the species richness analysis at that installation (see Species Richness Analysis Methods section below for more detail). This variable indicates the number of different ecological systems occurring in a stream reach. Because both desert tortoises and burrowing owls use wash banks for burrows, we derived a measure of bank slope at Fort Irwin by calculating the average slope of the area between the 0.25 m inundated depth polygon and the 2 m inundated polygon. Surface roughness has been shown to be a good predictor of desert tortoise presence (Nussear et al., 2009), so we derived an average surface roughness variable following the method used by Wallace and Gass (2008). We used DEM Surface Tools for ArcGIS (Jenness, 2013) to calculate the Surface Ratio of the LiDAR DEM . We then derived the average surface roughness by calculating the mean Surface Ratio within the 2 m inundated depth stream reaches using the ZonesWOverlap tool (Clark, 2012) in ArcGIS 10.

Table 2. Ecohydrological variables using in modeling individual species occurrence at each installation. Codes used here were also used for species richness modeling.

Variable	Code	Huachuca	Irwin	Bliss
Cumulative area above reach	Cum_area	•	•	•
Elevation	LidElevMidPts	•	•	•
Entrenchment ratio	ER_3m_05m	•	•	•
Slope	PCTslope	•	•	•
Rainfall Seasonality Index	RSI	•	•	•
Mean riparian width (2m deep)	Width2m	•	•	•
Mean riparian width (3m deep)	Width3m	•		•
Rock type	Rocktype	•		
Flow permanence	FlowPerm	•	•	•
Total stream power (25-yr)	Q25TSP	•	•	•
Peak flow (25-yr)	Qp25	•	•	•
LiDAR % cover, ground cover	veg0_025m		•	
LiDAR % cover, low veg	veg0_1m/veg025_1/veg05_1	•	•	•
LiDAR % cover, veg 1-4m	veg1_4m	•	•	•
LiDAR % cover, veg 4-12m	veg4_12m	•	•	•
LiDAR % cover, veg >12m	veg12m/veg12mPA	•		•
Mean vegetation index	msavi2/rendvi_mean	•	•	•
Percent cover	msavi2/rendvi_pct	•	•	•
Average surface roughness	AvSurfRough		•	
Bank slope	Slope2_025_m		•	
Number of land cover types	Landcover_variety			•
Shannon structural diversity	Shannon	•		•
Simpson structural diversity	Simpson1_D	•		•

Each variable was linked to the appropriate stream polygons (3 m inundated depth at Fort Huachuca and Fort Bliss, 2 m inundated depth at Fort Irwin). At Fort Huachuca and Fort Irwin, each variable linked to the polygons was then converted into a raster with a cell size of 5 square meters for use in MaxEnt. Only the area within the 2 or 3 m flooded zone of the stream reaches was modeled for each species.

For all species, locations were spatially filtered to no more than one per stream reach and usually at least 1 km apart by selecting all stream reaches within either 50 m, 100 m, or 200 m of a species location. Stream reaches were represented by the 3 m inundated depth riparian polygons. Spatial filtering helps reduce the effect of spatial autocorrelation, reduce overfitting, and prevent overly complex models (Radosavljevic and Anderson, 2013; Shcheglovitova and Anderson, 2013). The presence input used for MaxEnt was the center point of each of the selected streams.

Fort Bliss – Logistic Regression

From 2007-2012, most stream reaches in the gray vireo's range on Fort Bliss were surveyed for the species (White Sands, 2007; Zia, 2010, 2012a, 2012b, 2013). Observations, nests, and male territories were documented. Survey locations were recorded and whether or not vireos were

observed, yielding a dataset of both presence and absence, assuming lack of detection was true absence.

At Fort Bliss, the gray vireo was found in streams in the Organ and Sacramento Mountains, so the modeled region included the 3 m flooded depth stream reaches in these areas. Because the dataset had both presence and absence, the modeled area only included surveyed streams in these mountains. The modeled area included 199 stream reaches, representing 10% of the reaches on the installation.

For gray vireos, stream reaches within 50 m of a species location were selected. Out of 2844 total survey points, 1094 were within this distance of one of our stream reaches. We used both the point locations and male territory polygons to assign each stream reach a presence or absence value. These steps resulted in 62 stream reaches used by vireos, 3.1% of the total number of reaches on the installation and 31.2% of the stream reaches in the modeling area.

For model validation, we split the data into a training set and a testing set. We used a random number generator to reserve 23.6% (n=47) (Huberty, 1994) of the stream reaches in the modeling area for testing.

We used the training set to create a binomial generalized linear model (GLM) with a log link, also known as logistic regression. Occurrence (presence or absence) was modeled as a function of the ecohydrological variables. The top models for gray vireo occurrence were generated through a process modified from Grueber et al. (2011). Akaike's Information Criterion adjusted for small sample size (AICc) was used to evaluate model performance. Because the Shannon index of vegetation structural diversity had a lower AICc value than the Simpson (1-D) index when each variable was used independently to predict gray vireo presence (ΔAICc = 2.7), only the Shannon index was used in modeling.

An initial global model that included all possible predictor variables was built and then standardized by centering on the mean and dividing by 2 standard deviations (Gelman, 2008) using the *arm* package in R (Gelman et al., 2009). The package MUMIN (Bartoń, 2009) was used to generate all model subsets of the global model. All models within 2 ΔAICc of the top model were examined for uninformative parameters. Models that simply added one or two variables to another model in the top set were only retained if they had a lower AICc than simpler model. A second global model was created that contained only those variables found in the reduced top model set. MUMIN was used to generate all model subsets of the second global model. Parameter estimates of all models in the top 2 ΔAICc were model averaged using the natural averages method to generate estimates of effect size. Standardized parameter estimates are reported as effect sizes with unconditional standard errors. Estimates were transformed to an odds ratio and adjusted using the standard deviation of each variable from the training set to correspond with a meaningful change in each predictor variable. All models subsets of the second global model were used to generate measures of relative variable importance to ensure that it was calculated from a balanced set (Burnham and Anderson2002: 167–169).

We calculated predicted values for both the training and testing sets using the model-averaged estimates. Predicted values from a logistic regression range from 0 – 1. We determined what

value was the most appropriate threshold to consider presence when converting predicted values to presence/absence by calculating overall accuracy of the training and testing sets for different threshold values. For the most appropriate threshold value, we built confusion matrices for the training and testing sets, and calculated overall accuracy, omission and commission rates for both presence and absence, and the Kappa coefficients (Cohen, 1960) for both sets, which measures how much better than random a model is. An early guideline for interpretation of Kappa by Landis and Koch (1977) suggested that values < 0.4 indicated poor agreement that the model was better than random, 0.41–0.80 as moderate agreement that the model was better than random, and >0.80 as strong agreement that the model was better than random. Using the package ROCR (Sing et al., 2005) in R, we also obtained AUC values for both sets. AUC (area under the curve of the receiver operating plot) reveals the models discriminatory ability. When both presence and absence are known, it measures the probability that the model correctly ranks a random presence locality higher than a random absence locality.

To assess whether gray vireos were associated with a particular stream type, we performed a Kruskal-Wallis test for differences in probability of presence among the 8 stream types at Fort Bliss. Tukey HSD tests were used to examine pairs of stream types to determine which were significantly different from each other.

Fort Huachuca and Fort Irwin – MaxEnt

Data provided by Fort Huachuca and Fort Irwin were in the form of presence-only data. We used MaxEnt (version 3.1; http://www.cs.princeton.edu/~schapire/maxent/; Phillips et al., 2004, 2006) to model species at this installation because it has been widely used for this application.

At Fort Irwin, both species modeled were found across the installation, so the modeled region included the 3 m inundated depth stream reaches on the entire installation with the exception of the Leach Lake Impact Area. The modeled area included 1427 stream reaches, 82.1% of the reaches on the installation.

At Fort Huachuca, both species were confined to the mountains. The lowest elevation GAP land cover (Lowry et al., 2005) that either species occurred in was Madrean Encinal. The lower elevation limit of this land cover was approximately 1600 m. The modeling area included all stream reaches which reached an elevation of 1600 m anywhere along their length. Any stream reaches that did not meet this criteria but were at least partially within the USFWS designated critical habitat for Mexican spotted owls were also added to the modeling area. The modeled area included 69 stream reaches, 27.0% of the reaches on the installation.

Study species and occurrence records

Fort Huachuca provided us with 94 Mexican spotted owl locations collected from 1991-2010 from a number of yearly inventories. For spotted owls, stream reaches within 200 m of a species location were selected. This step resulted in 11 stream reaches used by spotted owls, 4.3% of the total number of reaches on the installation and 15.9% of the stream reaches in the modeling area.

Fort Huachuca provided us with 94 whiskered, 8 screech owl and western, and 9 screech owl locations observed during the 2009 and 2010 Mexican spotted owl surveys. For screech owls,

stream reaches within 200 m of a species location were selected. This step resulted in 8 stream reaches used by whiskered screech owls and 7 stream reaches used by western screech owls. Modeling for the two species was combined because both species were observed in only 9 stream reaches total, 3.5% of the total number of reaches on the installation and 13.0% of the stream reaches in the modeling area.

The Natural Resources section of the Department of Public Works at Fort Irwin provided us with 201 burrowing owl observation locations collected in 2005 and 2010-2013. These locations were mostly from surveys, with some incidental observations. For burrowing owls, stream reaches within 200 m of a species location were selected. This step resulted in 34 stream reaches used by burrowing owls, 1.9% of the total number of reaches on the installation and 2.4% of the stream reaches in the modeling area.

The Natural Resources section of the Department of Public Works at Fort Irwin provided us with 1086 tortoise observation locations collected from 1994-2013. These locations were mostly incidental observations of live and dead animals. For desert tortoises, stream reaches within 100 m of a species location were selected. This step resulted in 165 stream reaches used by desert tortoises, 9.4% of the total number of reaches on the installation and 11.6% of the stream reaches in the modeling area.

Model parameters

The models for each species were tuned by testing multiple settings for a number of MaxEnt parameters. We evaluated model performance using four criteria. The average evaluation/test AUC reveals the models discriminatory ability. It "quantifies the probability that the model correctly ranks a random presence locality higher than a random background pixel" (Phillips et al., 2006). Models with a higher AUC were preferred; the maximum AUC value is 1. The average difference between the calibration/training and evaluation/test AUCs (ΔAUC) "quantifies the degree of over-fitting to noise" (Radosavljevic and Anderson, 2013) and should be minimized. As in Radosavljevic and Anderson (2013), we used the minimum training presence threshold test omission rate (Zero OR) and the 10^{th} percentile training presence threshold test omission rate (Ten OR) to quantify over-fitting. Zero OR should be as close to zero as possible, while Ten OR should be as close to 0.1 as possible. When results were similar at different regularization levels, we chose the lower regularization to reduce under-fitting.

For Fort Irwin modeling, we used k-fold cross validation (k=4). Each model was tested with regularization multipliers of 0.5, 1, 1.5, 2, 2.5, 3, 3.5, and 4. Feature classes were restricted to H (hinge), L (linear), LQ (linear and quadratic), LQH (linear, quadratic, and hinge), and no restriction (LQPTH; linear, quadratic, product, threshold, and hinge). For desert tortoises, the optimal model parameters were a regularization value of 2.0 and feature class H. For burrowing owl, the optimal model parameters were a regularization value of 1.0 (the default) and feature classes LQ.

Since a visual inspection of tortoise and burrowing owl localities revealed that many fell along roads, we created a biased prior by calculating the distance of each 5 square meter pixel in the modeled region from a road and rescaling the result from 1-5 where cells with a value of 5 were closest to the road and cells with a value of 1 were farthest from the road, implying that

probability of having visited a cell adjacent to a road is 5 times as high as it would be far from any road.

For Fort Huachuca, we used a delete-one jackknife approach for validation (Pearson et al, 2007, Peterson et al., 2011). This approach has shown to produce good models using <10 occurrence records (Anderson and Gonzalez, 2011, Shcheglovitova and Anderson, 2013). Each model was tested with regularization multipliers of 1, 2, 3, and 4. Feature classes were restricted to H, LQ, and LQH. For both species, the optimal model parameters were a regularization value of 3.0 and feature class H.

Modeling was initially performed with the full set of variables for that installation (Table 2). To arrive at the optimal model, we examined the result of jackknife tests performed in MaxEnt. When removing a variable would increase training gain, test gain, or AUC, especially if its percent contribution and permutation importance were low, this was done. Results are presented using the default logistic output from MaxEnt.

To assess whether each species was associated with a particular stream type, we performed Kruskal-Wallis tests for differences in probability of presence among groups. Tukey HSD tests were used to examine pairs of stream types to determine which were significantly different from each other. In addition, Fort Huachuca uses Protected Activity Centers (PACs) to manage Mexican spotted owl habitat. For the subset of streams within the USFWS Designated Critical Habitat for spotted owls, we used a Mann-Whitney U Test to determine if streams within PACs had significantly different values of each ecohydrological variable than streams outside of PACs. Since rock type was a categorical variable, we used a Pearson's chi-squared test to determine if streams in PACS were found in different rock types.

Mesquite Bosque Species Richness Methods

At Yuma Proving Ground, LiDAR data were available for only a portion of the installation, so it was not possible to investigate the connection between GAP riparian species richness (described in a later section) and vegetation structure along streams. However, LiDAR data were available for an area in which many of YPG's mesquite bosques are found. The bosques on YPG are made up of honey mesquite, creosote, range ratany, white bursage, galleta grass, bush muhly, and a variety of forbs (Jason Associated Corp., 2008). The composition of these bosques is very similar to the xeroriparian areas along streams at YPG and, like the xeroriparian areas, they are highly productive and species rich relative to the surrounding uplands, providing important cover and habitat for a variety of animals.

Arizona Game and Fish conducted a camera-trapping study on bosques from April 2009 to May 2011 to identify which wildlife species use bosques, seasonal patterns of use, how use is influenced by bosque size, shape, and proximity to permanent water (<http://www.azgfd.gov/w_c/WildlifeUseMesquiteBosque.shtml>). There are 182 mapped bosques in the northeast corner of the Cibola Range of YPG. AZGFD placed 50 cameras in 16 of these bosques; 12 are ones for which LiDAR data were available. An additional 69 bosques are covered by the LiDAR data. Through an Interagency Service Agreement (ISA), AZGF provided the number of each species recorded in each of these 12 bosques. We analyzed how vegetation

structure, proximity to other bosques, and hydrologic variables of the closest streams influenced species richness, overall wildlife abundance, and abundance of birds, mule deer, and kit fox in these 12 bosques.

Ecohydrological variables

We used ArcGIS 10.1 to process the LiDAR tiles provided by DISDI (Defense Installation Spatial Data Infrastructure). We subtracted the bare-earth raster layer from the first-return raster layer to get vegetation height for eleven of the bosques for which there were camera data. There was no bare-earth file for Bosque 108, so we clipped the appropriate tile to just the extent of the bosque polygon, and examined it visually for the average ground-level elevation. The value 352.4 meters produced reasonable values for the vegetation structure. We subtracted this value from the first-return values to get vegetation height for Bosque 108. We classified the vegetation height raster into -500-0.2 m, 0.2-1 m, 1-2 m, 2-3 m, 3-4 m, 4-5 m, >5 m and calculated the percent of each height class in the bosques in two ways. Percent of each class present in each bosque was calculated by dividing the number of pixels in a class by the total number of pixels in the bosque. Cumulative percent of each class was calculated by summing the number of pixels in a class and all those physically above it, and dividing by the total number of pixels in a bosque. Cumulative percent cover can be interpreted in two ways. It can be thought of as an estimate of the total amount of vegetation cover in that class in the bosque, because most pixels with taller vegetation also contain vegetation in each height class below the tallest vegetation. It can also be interpreted as the percent cover in the bosque of vegetation above a certain height.

Because the surrounding area could have an effect on wildlife use of a bosque, we used ArcMap to find the number of other bosques within 250, 500, and 1000 m of the edge of each bosque. We also calculated the percent of the area within those same distance bands that was classified as bosque. This was done by converting the bosque polygon layer into a raster where cells in polygons had a value of one, running the tool ZonesWOverlap (Clark, 2012) to get the sum of the bosque raster layer in each buffer zone, and dividing the sum of the bosque raster layer by the area of the buffer zone.

Most bosques were found along streamlines (Figure 27) for which peak flows and flow permanence were modeled with the AGWA tool for ArcGIS (Lyon, 2013). We included the flow permanence from NEXRAD data and peak flows for the 10 year, 1-hour storm that were closest to each bosque in the analysis. We also included the area in square meters of each bosque.

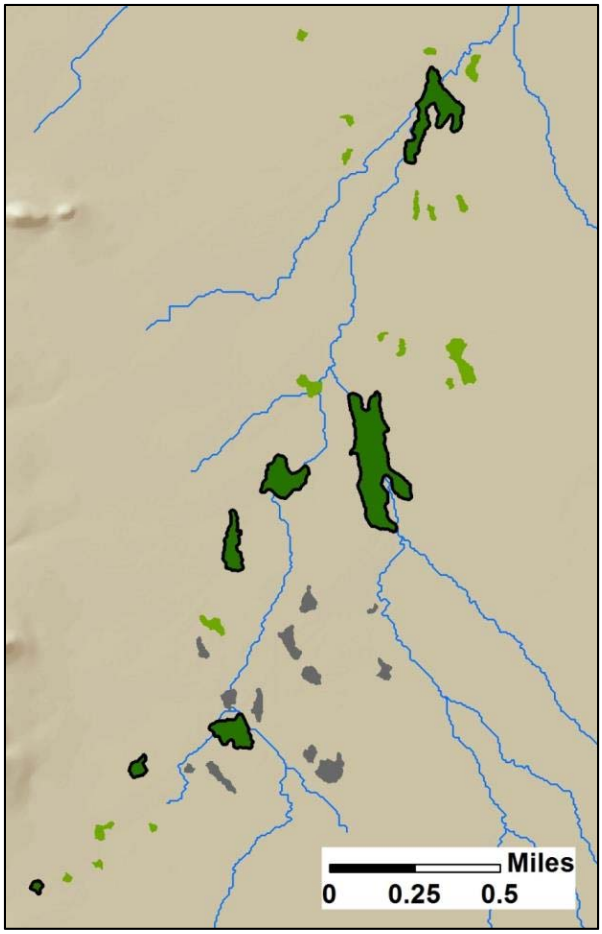


Figure 27. YPG - Overview of 7 of the 12 modeled bosques.
Blue lines are stream lines generated by Lyon (2013). Dark green polygons with black outlines are bosques with wildlife camera data used to generate models. Bright green polygons are bosques for which LiDAR were available, but no camera data, and gray polygons are bosques for which neither type of data were available.

Species Richness

Since detection of all species present in an area is rarely possible, we used several estimators to approximate total species richness of each bosque.

Table 3 provides a list of species included in the analysis.

Accipiter, Lizard, Unknown Raptor, Unknown Rodent, Snake, and Unknown Bird were provided by AZGFD, but excluded from species richness estimation. Dove, Ground Squirrel, and Small Owl may have included multiple species but were each treated as a species. These three also are not common targets for camera-trapping because they can be difficult to detect reliably, but were included because they had substantial numbers in multiple bosques, indicating the cameras at YPG did an adequate job capturing their presence. We calculated the first- and second-order jackknife richness estimators $S_{jackknife1}$ (JK1) and $S_{jackknife2}$ (JK2) (Burnham and Overton, 1979; Magurran and McGill, 2011). We used EstimateS (Colwell, 2013) to calculate the Chao 1

species richness estimator, S_{Chao1}. Values of the Chao 1 species richness estimator were rounded to be used as counts in modeling.

Table 3. YPG - Species or groups of species included in species richness, relative abundance index (RAI) and bird relative abundance index.

Species	Richness	RAI	Bird RAI
Accipiter		•	•
Badger	•	•	
Black-tailed Jackrabbit	•	•	
Bobcat	•	•	
Coyote	•	•	
Desert Cottontail	•	•	
Dove	•	•	•
Grey Fox	•	•	
Ground squirrel	•	•	
Kit Fox	•	•	
Lizard		•	
Mule deer	•	•	
Poorwill	•	•	•
Quail	•	•	•
Red-tailed Hawk	•	•	•
Road Runner	•	•	•
Small Owl	•	•	•
Snake		•	
Turkey Vulture	•	•	•
Unknown Bird		•	•
Unknown Raptor		•	•
Unknown Rodent		•	

We used R (R Core Team, 2014) to model each predictor variable (Table 4) as a function of each species richness estimator using a poisson GLM with a log link.

Next, we generated the top models for each species richness estimator through the following process, modified from Grueber et al. (2011). We used Akaike's Information Criterion adjusted for small sample size (AICc) to evaluate model performance. We built an initial global model that included all possible predictor variables, and used the package *MUMIN* to generate all model subsets that had a maximum of three predictor variables. We allowed models to have only one measure of number of bosques and one measure of percent cover of bosques within a certain distance. We also excluded combinations of the LiDAR-derived variables that did not make biological sense, e.g., layers that were nested closely within each other, highly correlated adjacent layers, and layers that were mutually exclusive. We examined the models within 4 AICc units of the top model generated by this process, and chose one measure of number of bosques and one measure of percent cover of bosques within a certain distance to retain based on the number of times the predictor occurred in the top models and where those models ranked. Variables occurring in models of higher rank and more frequently were preferred. We also chose

a set of LiDAR-derived variables to retain based on the same criteria, and avoiding any combination precluded in the subset-generation.

Table 4. YPG - Predictor variables for bosque species richness estimators.

Variable	Code
Area (m2)	Area
Cumulative % >0.2 m / Vegetation >0.2 m % cover in bosque	Cm % >0.2m
Cumulative % >1 m / Vegetation >1 m % cover in bosque	Cm % >1m
Cumulative % >2 m / Vegetation >2 m % cover in bosque	Cm % >2m
Cumulative % >3 m / Vegetation >3 m % cover in bosque	Cm % >3m
Cumulative % >4 m / Vegetation >4 m % cover in bosque	Cm % >4m
Cumulative % >5 m / Vegetation >5 m % cover in bosque	Cm % >5m
Percent of the bosque with vegetation reaching 0.2-1 m	% 0.2-1 m
Percent of the bosque with vegetation reaching 1-2 m	% 1-2 m
Percent of the bosque with vegetation reaching 2-3 m	% 2-3 m
Percent of the bosque with vegetation reaching 3-4 m	% 3-4 m
Percent of the bosque with vegetation reaching 4-5 m	% 4-5 m
Peak Flow 10 year, 1 hour storm	10-yr Peak Flow
Flow Permanence, from NEXRAD	NexradFP
Percent of area w/i 250 m that is bosque	% Cover Bosques
Percent of area w/i 500 m that is bosque	% Cover Bosques
Percent of area w/i 1000 m that is bosque	% Cover Bosques
Number of bosques w/i 250 m	# Bosques w/i
Number of bosques w/i 500 m	# Bosques w/i
Number of bosques w/i 1000 m	# Bosques w/i

We created a second global model with just the retained variables, generated all model subsets that had a maximum of three predictor variables, and examined the models within 4 AICc units of the top model. We checked for uninformative parameters to drop by determining if any nested models did not have a marked decrease in maximized log likelihood over the next simplest model. We created a third and final global model with all the retained parameters, and standardized the global model by centering on the mean and dividing by 2 standard deviations (Gelman, 2008) using the *arm* package in R (Gelman et al., 2009). We generated all subsets of the standardized model with a maximum of three predictor variables. We model averaged all models in this subset to generate measures of relative variable importance (Burnham and Anderson, 2002: 167–169). When the number of models within 2 ΔAICc of the top model was greater than one, we model averaged parameter estimates of all models in the top 2 ΔAICc using the natural averages method to generate estimates of effect size. Unconditional standard errors are reported when parameters were model-averaged.

Wildlife Abundance

We estimated overall abundance of wildlife in each bosque using a relative abundance index (RAI). We summed the counts in each species category, divided by the number of cameras in the bosque, and divided by 7.9, our best estimate of hundreds of camera days based on cameras operating from April 2009 – May 2011. The results were rounded to use as a count in modeling. We also estimated total bird abundance (Bird RAI) in each bosque using an RAI. We summed the counts in each species category and divided by the number of cameras in the bosque. We did

not divide these values by 7.9 because they were much smaller numbers. We rounded the result to use as a count in modeling. We estimated abundance for two individual species. Mule Deer RAI was calculated in the same manner as overall RAI with only mule deer counts. We initially attempted to model kit fox presence/absence with a binomial GLM, but the sample size was too small for this to work. We estimated Kit Fox RAI as the counts of kit foxes divided by the number of cameras in each bosque. We multiplied this value by 4 so that rounding caused minimal changes to the very low initial values. We used the process described for species richness to generate a set of best models, relative variable importance, and effect size for each RAI.

Nesting Habitat Index Methods

The availability of multi-return LiDAR data for the structure of vegetation in ephemeral streams across the installations gave us detailed information about vegetation that would normally require extensive field work to collect. Vegetation structure is arguably the most important, factor in defining nesting habitat for birds. Each species has a preference for where it nests within the vegetation structure layers. We have attempted to create a metric for each stream reach at Fort Bliss only that indicates how "valuable" it is as bird nesting habitat. We performed this analysis at Fort Bliss because Kozma and Matthews (1995) and Myers et al. (1998) collected data on bird use of "arroyo-riparian" areas in a focused area of Fort Bliss from 1993-1997. They used mist-netting and point-counts to survey birds within the riparian zone and in the adjacent uplands. Observational data on bird occurrence was collected from 1 May – 9 June, 1993; 3 May – 15 June, 1994; 6 May – 16 June, 1995; 29 April – 16 June 1996; and 2 May – 6 June 1997. Searches for nests were performed in 1996 and 1997. This data set allowed us to ground-truth the nesting-habitat metric.

We narrowed the riparian-associated bird list (see Species Richness Analysis Methods section below) to species that had distribution models with summer or year-round habitat on or very near Fort Bliss (Appendix C, Table 1). We eliminated four species from this list that had a small amount of their GAP distribution models present near or on the installation, but had never been observed on the installation based on the INRMP (U.S. Army, 2001) and the online eBird database (ebird.org). We also added eight species to the list that we had not categorized as riparian-associated, but which Kozma et al. (1995) and Myers et al. (1998) had listed.

Based on the description of their nest site requirements from Birds of North America Online (BNA; http://bna.birds.cornell.edu/bna/), each species received a score for each vegetation structure layer: a two (2) indicated the species preferred to nest in that layer, a one (1) indicated that they sometimes used that layer but it was just outside their strongest preference, and zero (0) indicated that the species did not use that layer. For a few species with little information on nesting habitat, we also consulted the Biota Information System of New Mexico online database (BISON-M; http://www.bison-m.org/). We calculated the number of species using each layer as the sum of all species scores for the layer, divided by two (Appendix C, Table 1). Since not all species are found everywhere, we also used the habitat descriptions from BNA to note whether the species would be found in the lowlands, foothills, or mountains of Fort Bliss; we calculated subscores for the number of species using each layer in each of these three broad categories. We also calculated subscores for the subset of birds that were TER-S species.

Because tall vegetation at Fort Bliss usually has shorter vegetation beneath it and it was important not to miss the availability of the lower layers for nesting, we calculated the percent cover of vegetation in each structure layer (C_i) as the percent cover of that layer in each stream reach plus the percent cover of all higher layers (this is equivalent to the cumulative percent cover measures calculated at YPG for the bosque analysis, described previously):

$C_{0.5\text{-}1}$ = veg05_1m + veg 1_4m + veg4_12m + veg12m
$C_{1\text{-}4}$ = veg 1_4m + veg4_12m + veg12m
$C_{4\text{-}12}$ = veg4_12m + veg12m
$C_{>12}$ = veg12m

Fort Bliss provided shapefiles of all observations made during both Kozma and Mathews' (1995) and Myers et al.'s (1998) arroyo-riparian studies and all nests found during the 1996-1997 study. Their transects overlapped substantially with 13 of our stream reaches. We shortened the stream reach polygons when necessary to match the length surveyed by Kozma and Mathews and Myers et al., and recalculated the area of the modified polygons and lengths of the streams within them. For the observational data, we extracted the subset of observations made at survey points within the 13 stream reaches. For the nest data, we counted the number of nests within 5 m of the stream reach polygons, to account for small differences in vegetation in the time since the study was done and prevent eliminating nests due to small location recording errors. This increased the total number of nests by 13 (from 137), but only two nests were from species not classified as riparian-associated, indicating this buffer did not include inappropriate areas.

From both datasets, we recorded the number of riparian-associated species that were observed (S_o) and nesting (S_n) in each stream reach. To account for imperfect detection, we used the first-order jackknife species richness estimator $S_{jackknife1}$ (JK1; Burnham and Overton, 1979; Magurran and McGill, 2011) to derive the estimated number of species observed ($JK1_o$) and nesting ($JK1_n$) in each stream reach. To adjust for stream reaches being different lengths, we divided each species richness metric by the surveyed stream length (km).

As part of the assessment of the nesting habitat value metric, NH_a, we created Gaussian general linear models (GLM) with an identity link in R. Regressing the ecohydrological variables against the species/km metrics revealed that the 3-m flooded depth riparian width was a significant or marginally significant predictor for all metrics (S_o/km, p=0.025; S_n/km, p=0.12; $JK1_o$/km, p=0.02; $JK1_n$/km, p=0.028). Greater width was associated with increased values of all species richness measures. Based on these results, we created a width-adjusted nesting habitat metric. We rescaled riparian width from 0-100 to match the range of the percent cover variables. The width adjusted metric (nh_w) was calculated as:

$$nh_w = 4*(N_{0.5\text{-}1}*C_{0.5\text{-}1} + N_{1\text{-}4}*C_{1\text{-}4} + N_{4\text{-}12}*C_{4\text{-}12} + N_{>12}*C_{>12}) + Width_{scaled}$$

The multiplication of the original score by four ensured that width had a contribution equal to that of one structure layer. We rescaled nh_w from 0-10 (NH_w) to improve interpretability.

We also used the Kozma and Mathews and Myers et al. datasets to ground-truth the species richness that we calculated from the GAP animal habitat models (see Species Richness Analysis section).

Species Richness Analysis Methods

To gain the broadest understanding of the importance of different ephemeral and intermittent streams to wildlife, we created xeroriparian-associated species lists for each installation, used GAP models to derive species richness in stream reaches for various taxa groups and TER-S, compared species richness of these groups between stream types, and examined which ecohydrological variables influence TER-S richness in stream reaches.

Riparian-associated species

Using documents provided by the four installations, as well as other sources, an initial list of all vertebrate species occurring on the four installations was generated (Appendix C, Table 2). Shorebirds and waterfowl were not included, since these species are mostly vagrants or use urbanized areas on the installations. Non-native species were also not included. Each species was categorized as riparian-associated or not riparian-associated using the Ecology and Life History descriptions in NatureServe Explorer (NatureServe, 2014), supplemented when necessary with information from other sources. Species were classified as riparian-associated if the description explicitly mentioned riparian areas, water, canyons, streams or a similar term, or if the species' habitat was described with words such as brush, forest, shrub, thicket, dense undergrowth, and similar descriptors that typically are only found in the xeroriparian areas of the installations. When a species had a description that matched upland areas, such as species that primarily use open grasslands or desert, it was categorized as not riparian-associated.

Species Distribution Models

The National Gap Analysis Program (USGS-GAP, 2014) and the Southwest Regional Gap Analysis Program (SWReGAP; Boykin et al., 2007) have created distribution models for numerous species found in the United States. Based on literature-cited information about habitat associations, GAP distribution models are deductive models that predict areas suitable for occupation within a species' range (Boykin et al., 2007). Information used to define habitat associations includes GAP National Land Cover data of ecological systems, elevation, hydrology, human avoidance, forest edge, and ecotone widths. The resulting models are rasters with a 30x30 meter pixel size. All available species distribution models for riparian-associated species from USGS-GAP (2014) were obtained. Many species were not available from this program. Some were not modeled, while others species' models were still being developed. For these species, distribution models from the older Southwest Regional GAP (USGS-GAP, 2007) were obtained. A number of species were excluded from the analysis at this point because no model was available for them, or none of their modeled habitat occurred on a particular installation.

All models were reclassified so that a value of one (1) indicated presence of habitat for the species and a value of zero (0), absence. Models were stacked using the Raster Calculator tool in

ArcGIS 10 to create rasters with species richness values for specific groups. Known and potential occurrence, breeding and non-breeding habitat, and seasonal habitat were pooled. For each installation richness rasters were created for all riparian-associated species pooled, all birds that are resident for at least part of the year, all passage migrant birds, all amphibians, all reptiles, and all mammals. Only USGS-GAP models were available for Fort Irwin. Many of the reptile models for this installation were not yet available, so only Bird and Mammal rasters were created for Fort Irwin. Richness rasters for species of concern (TER-S) were created by stacking models of species that met one of these criteria: federally listed, state listed, or ranked by NatureServe as 3 (Vulnerable) at a global, national, or regional scale in the state in which the installation being analyzed was located. TER-S richness rasters included all species, just amphibians, just reptiles, just mammals, and just birds.

The ZonesWOverlap tool (Clark, 2012) in ArcGIS 10 was used to calculate the mean species richness values for each group in the 3 m inundated depth stream reach polygons at Fort Bliss, Fort Huachuca, and Yuma Proving Ground. At Fort Irwin, the 2 m inundated depth polygons were used. At Fort Bliss, species richness was not calculated for reaches in Texas, because SWReGAP models did not extend into that state.

Richness Analysis

To determine whether stream types had different potential species richness for each of the riparian-associated species groups and riparian-associated TER-S groups, Kruskal-Wallis tests for differences among groups were performed. Tukey HSD tests were used to examine pairs of stream types to determine which were significantly different from each other. Correlation analysis was done on the average species richness values of each stream reach to determine which species groups had similar patterns of richness. Correlation analysis was also done on the species richness values of each stream type to determine which species groups had similar patterns of richness in regard to the stream types. The average richness of each species group in each stream type was ranked; the ranks were tested for correlation between groups.

To further understand what ecohydrological characteristics of stream reaches were associated with the species richness of TER-S, generalized linear models (GLM) were created in R (R Core Team, 2014). Because the Fort Bliss analysis was part of Hammer's thesis, several other variables were also included. An additional entrenchment ratio was tested (0.5m/2m) using a gaussian GLM with an identity link to model species richness. The percent cover of each vegetation structure layer was used to calculate a structural diversity measure using the Shannon Index (Magurran and McGill, 2011). Landcover Variety was calculated to describe the horizontal habitat heterogeneity of a stream reach, another important feature for wildlife. It was calculated by using the ZonesWOverlap tool (Clark, 2012) in ArcGIS 10 to determine the number of different ecological systems in the GAP National Land Cover dataset (Lowry et al., 2005) present in each stream reach. For the other installations, only the ecohydrological variables used to create the stream types were used to model species richness.

A Gaussian GLM with an identity link was used for all modeling. The top models for each species richness estimator (e.g. birds, reptiles) were generated through a process modified from Grueber et al. (2011). Akaike's Information Criterion adjusted for small sample size (AICc) was

used to evaluate model performance. An initial global model that included all possible predictor variables was built and then standardized by centering on the mean and dividing by 2 standard deviations (Gelman, 2008) using the *arm* package in R (Gelman et al., 2009). The package *MUMIN* (Bartoń, 2009) was used to generate all model subsets that had a maximum of ten predictor variables. All models that had a maximum of ten predictor variables were used to generate measures of relative variable importance (Burnham and Anderson, 2002: 167–169). When the number of models within 2 ΔAICc of the top model was greater than one, parameter estimates of all models in the top 2 ΔAICc were model averaged using the natural averages method to generate estimates of effect size. Standardized parameter estimates are reported as effect sizes. Unconditional standard errors are reported when parameters were model-averaged.

Task 5: Field Test and Verification

During the fall and winter of 2013/2014 we visited each installation to present our results to installation managers for their feedback, and to check our data in the field. Vegetation and geomorphic field data were taken to validate geomorphic planform, vegetation structure, vegetation cover, and reach width (based on the 3 m inundated water surface width). Hydrologic modeling results were checked by visual observation for peak flow and flow permanence, by evaluating evidence of recent flows, channel features and geometry, and vegetation characteristics, in relation to the results from the AGWA simulations.

Hydrologic Modeling Verification

Various observations were used to verify the AGWA hydrologic model results, including evidence of flood debris, characteristics of channel banks, identification of the Ordinary High Water Mark (OHWM:, Lichvar and McColley, 2008), including the most common OHWM indicators: change in bank slope, sediment size and color, vegetation type and cover, and the presence of flood debris (Lefebvre et al., 2013). No attempt was made to estimate the actual peak flows or flow permanence in the field; the purpose was to determine if features corresponding to the relative model results (i.e. high flow permanence, low peak flows) were visible.

Many of the larger channels at YPG, Fort Irwin and Fort Bliss are used as roads because of the infrequent flows. Dry streambeds provide obvious routes through the desert, and in many cases it is difficult to determine which came first: the road or the channel. Nevertheless, we used OHWM indicators to evaluate our modeling results at each installation during the Fall 2012/Spring 2013 field trips, and found generally good correlation with model results. An example at each installation is included below.

The KINEROS2 model was used to simulate peak flow, using a default value of 0.2 for initial soil moisture, an important variable in surface hydrologic processes. Holding soil moisture constant in this way allowed us to compare relative differences across stream reaches, and produce this stream type classification and methodology. In these water-limited environments soil moisture tends to be very low except immediately following a precipitation event. Therefore, a stream reach might experience large peak flows but still have low flow permanence (and low soil moisture) due to the low frequency of the large flows as seen at YPG (Figure 31).

An exception to this concept would be if a stream reach were consistently wet (i.e. at a spring), this modeling approach would not reflect that. However, in a water- limited environment the long term presence of increased soil moisture from a spring would be reflected by a more robust vegetative growth detectable by the multi-return LiDAR vegetation height analysis, and by the vegetation indices. Our experience is that all springs and other permanent waters are well known to base managers.

Figure 28 is a photo taken at Fort Irwin at field site *NLBL1*. Simulated flow permanence at Fort Irwin ranges from 0% to 13.1%, and the simulated 100yr-1hr peak discharge ranges from 0 - 163 m^3/s. This channel is often used as a road, has very low peak flows (Qp100 = 0.001 m^3/s), and relatively moderate (for Fort Irwin) flow permanence (4.1%). Minor changes in vegetation along the channel are visible, as well as a small change in bank slope and substrate color and texture. Flood debris is visible along the channel banks indicating recent flow.

Figure 29 is a photo of field site *BRHC1* at Fort Huachuca. Simulated flow permanence at Fort Huachuca ranges from 0% - 92.5%, and the simulated 100-yr 1-hr peak discharge ranges from 0 – 1,702 m^3/s. This channel reach has fairly high peak flows (Qp100 = 577 m^3/s) and high flow permanence (33.1%), evidenced by the large trees along the channel, large cobbles in the channel bottom, and well defined banks.



Figure 28. Fort Irwin, field site *NLBL1*: Qp100 = 0.001 m^3/s, flow permanence = 4.1%.



Figure 29. Fort Huachuca, field site *BRHC1*: Qp100 = 124 m^3/s, flow permanence = 33.1%.

Figure 30 is a photo of field site *THGC1* at Fort Bliss. Simulated flow permanence at Fort Bliss ranges from 0% - 33.5%, and the simulated 100yr-1hr peak discharge ranges from 0 – 2,898 m^3/s. This channel reach has a high peak flow (Qp100 = 1,912 m^3/s) and high flow permanence (28.3%), as shown by the well-defined channel banks and dense shrub cover along the channel.



Figure 30. Fort Bliss, field site *THGC1*: Qp100 = 728.2 m^3/s, flow permanence = 28.3%.

Figure 31 is a photo of field site *MW002* at YPG. Simulated flow permanence at YPG ranges from 0% - 14.8%, and the simulated 100yr-1hr peak discharge ranges from 0 – 3,233 m^3/s. This channel reach has a high peak flow (Qp100 = 1,458 m^3/s) and very low flow permanence (0.10%).



Figure 31. YPG, field site *MW002*: Qp100 = 1458.4 m^3/s, flow permanence = 0.10%.

Riparian Vegetation Data Verification

The vegetation cover, vegetation structure and riparian width variables were verified with field data from each installation to the extent practicable. The vegetation structure from LiDAR was compared with field data and is described in more detail below. Vegetation cover derived from the classified satellite imagery was checked using visual estimates of the overall vegetation cover for the 100 m transect. Riparian widths from the 3 m inundated polygons at 3 m depth were checked using the GPS and shapefiles of the inundated polygons, by walking the outline of the polygon to confirm that it adequately represented the extent of riparian-associated vegetation.

LiDAR-derived Vegetation Height Validation

Field data were used to verify the LiDAR-derived vegetation heights. Figure 32 shows a comparison of this analysis at Fort Huachuca's East Range for the percentage of riparian vegetation types by height category (<1 m, 1-4 m, 4-12 m and >12 m). The green bars represent the average of the riparian vegetation field survey results from 11 field sites in the East Range (Figure 33). The blue bars show the percent of each height category within a 150 m wide stream buffer for the entire East Range based on LiDAR-derived vegetation heights. The 150 m wide

buffer (75 m on each side of the channel) was chosen so the transition from stream influenced vegetation could be distinguished from upland vegetation, and most closely represented the extent of the field surveys in this location. The LiDAR was classified into the four vegetation height categories previously noted. This comparison plot shows that the LiDAR results under-estimated percent cover when compared to field data. This may be because field data collection enables a more detailed estimate of tree height, canopy extent and understory that may not show up in the LiDAR due to resolution of the LIDAR data acquisition, sparseness of desert foliage or irregular shapes of the trees and shrubs.

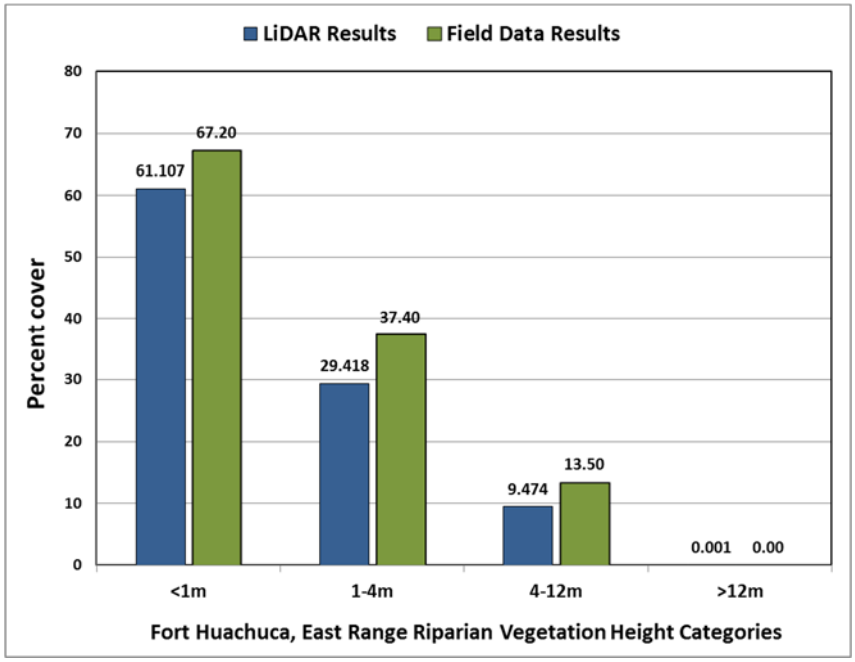


Figure 32. Fort Huachuca's East Range riparian vegetation height categories, comparison of field data with LiDAR analysis results

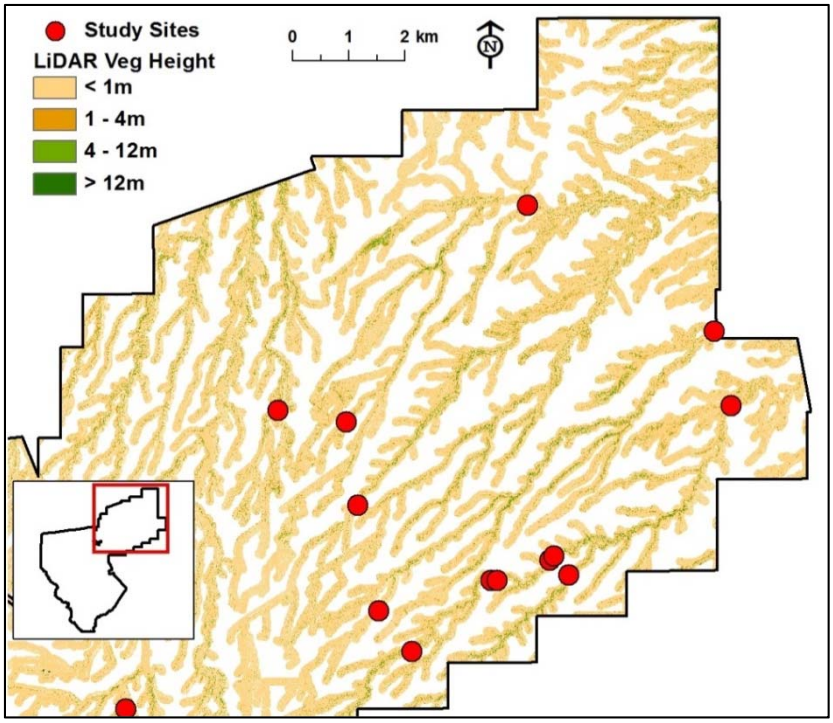


Figure 33. Map of Fort Huachuca's East Range, with study sites and the LiDAR-derived vegetation height categories clipped to a 75 m wide stream buffer (total 150 m wide).

Task 6: Assessment Methodology

The AGWA tool provides the ability to evaluate impacts from land cover, land use and climate change scenarios (see Task 2, Hydrologic Modeling for more information on the AGWA tool). AGWA was used to produce peak flows (m^3/s) and water yield (mm; used to calculate flow permanence) from the KINEROS2 and SWAT models, respectively (see Section 3, Task 2, Hydrologic Modeling, for more information on AGWA). Both variables were used in this project in the cluster analysis to obtain stream types. Thresholds for both values related to the stream types were obtained from the CART analysis.

AGWA may be used as an assessment tool either by running SWAT or KINEROS2 with revised climate or land cover data to obtain new values for peak flow or water yield, or by modifying those outputs directly. The new values may be applied to the classification decision tree to determine if the revised land cover or climate causes the stream type to change, which could potentially change the wildlife associations or habitat values. AGWA is best used as a relative change tool unless the models are carefully calibrated using observed data. Comparing model results from current and future scenarios provides an assessment methodology to improve management decision making.

Changes in land cover or land use can be simulated in AGWA using the land cover modification tool. New training areas can be changed from a vegetated land cover to barren, or disturbed. An expansion of a cantonment area can be changed from vegetated to urban or built-up land cover. Alternatively, simulating the rehabilitation of a training area might be modeled by changing that area from disturbed to grasslands. Resulting impacts to runoff, peak flow, or water yield, are then

simulated using AGWA, and used directly in management, or used in the decision tree and tables to determine changes to stream types and wildlife habitat. For example, the relative change to peak flows at roads downstream from a new training area that would remove vegetation and compact soil could be simulated to determine if modifications to a road crossing are necessary.

Evaluating impacts from climate change can be performed with AGWA by modifying the precipitation inputs (e.g. increase or decrease intensity, volume, or timing) or temperature inputs. We evaluated a climate change scenario using NOAA's Geophysical Fluid Dynamics Laboratory Global Circulation Model 2.1 (GFDL CM2.1) for daily precipitation and temperature forecast values, which are based on the Intergovernmental Panel on Climate Change (IPCC) Emission Scenario A2 that predicts a global temp increase of 3.4^{o} C by 2100. We compared the absolute change in historic flow permanence from 1981-2000 to projected flow permanence for 2081-2100 for each installation. The results of the comparison show a wide variance in absolute and percent changes of flow permanence values. One pattern that emerged was a noticeable decrease in flow permanence in the higher elevation mountainous areas. These patterns indicate that these areas might be more sensitive to climate change and could be used to justify the directing of adaptation strategies to focus on species located in these areas first. Overall, flow permanence is very low at these locations resulting in only a small change that was not enough to impact our models. The precipitation and temperature input files will be provided to each installation, as well as the flow permanence values, for their use and analysis.

A step-by-step tutorial and dataset were developed for each installation that illustrates a land use change scenario and a climate change scenario. The tutorials were used in the Technology Transfer Workshops and AGWA trainings, and will be included in the final data delivery to each installation. An example tutorial is included as an attachment to this report.

Other management tools included in AGWA are the ability to simulate buffer strips, detention/retention ponds or reservoirs, and post-fire effects using a burn severity map. AGWA is routinely being updated with new management tools based on feedback from users. While our Tucson ARS office is not set up to provide full time support for AGWA, we are available to assist with questions, time permitting.

Task 7: Technology Transfer Workshops with DoD Managers

Throughout the project we met with DoD managers to keep them involved in this research and to receive their feedback and comments. This proved to be very valuable in guiding our research.

Annual meetings and presentations

During each site visit to each installation we scheduled a meeting and presentation with the staff. Attendees included natural resource managers, GIS staff, and consultants. We provided an update on our research, and an opportunity for discussion regarding our progress to date, and on our future directions. Participation and feedback at these presentations were especially useful. For example, the wildlife biologist at Fort Bliss indicated that he would be able to use the results of the stream type classification and also the riparian vegetation structure classification in developing surveys and sampling schemes.

Interim workshop

A manager's workshop was held on May 16, 2012, in Tucson, to bring together all SERDP funded teams working on Southwest Region installations with the managers at each installation to facilitate information exchange. The workshop included presentations by each team, discussion sessions and workshops on the technologies being applied, and a discussion of the method of delivery for the final data products. Attendance included representatives from Fort Huachuca, Fort Irwin, White Sands Missile Range, YPG, Barry M. Goldwater/Luke Air Force Range, and Yuma Marine Corps Air Station (MCAS). In addition, SERDP staff, several SERDP Technical Advisory Committee members, and other SERDP funded researchers were in attendance. The emphasis was on two thematic areas: climate change and ephemeral streams, and fire and invasive species. A few conclusions from this workshop are as follows:

1) Internet access is a major challenge. Thus, the managers prefer to receive data and tools that do not require internet access. They prefer the data to be in SDSFIE format, in geodatabases, using the NHD identifiers to reference stream reaches. They requested that the word "military" be included as a keyword in scientific papers.

2) Fire and Invasive species: There is a general need for better regional fire models that are based on thresholds for change and ability to translate fuel load into risk. The models also should be informed by information such as post-fire recovery time of vegetation, locations of fire-sensitive taxa, and better understanding of the environmental costs of fighting fires vs. allowing them to burn. Given that fuel loads and temperature change seasonally, an ideal tool would be threshold-based "risk" maps based on recent (prior 2 weeks) remote sensing information such as NDVI. This would be coupled with decision support systems that allow mangers to determine when to take action (such as fire fighting or fuel thinning).

3) Climate change. The general consensus is that the Southwest region will become hotter and more arid, although changes in precipitation have higher uncertainty than do changes in temperature. Overarching questions revolved around ecosystem resiliency, identifying and monitoring indicators of climate change, and preparing for future management of new/novel ecosystems that may result as climates in the region shift.

4) Roads. Another issue that arose was the need for greater understanding of road effects on natural resources. On some bases, roads are cutting across ephemeral washes, resulting in development of mesquite bosques on the upstream side of the road. Questions regarding the environmental consequences, and roads management (e.g., via culverts) were raised.

Final Technology Transfer Workshops

Technology transfer workshops and AGWA trainings were conducted at each installation. Attendees included natural resource managers (ecologists, wildlife biologists, archeologists, hydrologists, botanists, etc.), GIS staff, and consultants. The format was casual, encouraged discussion, and lasted 1 or 1.5 days. The schedule for the first morning included presentations on the overall project goals and objectives, the stream type classification results, the vegetation,

geomorphic, and hydrologic analyses, and the wildlife linkages results. The AGWA training encompassed the first afternoon, and next morning for the 1.5 day workshop. It utilized a tutorial representing a land cover change scenario that the installation suggested or one that we developed based on our knowledge of the site. The AGWA training included the use of both the KINEROS2 and SWAT models, use of the land cover modification tool, and a climate change scenario using projected climate data. The workshop continued to the second morning if necessary.

Workshop participants were asked to fill out a short questionnaire about the presentations and AGWA trainings. Questions were regarding the level of detail presented, the difficulty of the AGWA training, and their intention to use our tools (AGWA, the stream type and vegetation structure classifications, wildlife analysis, etc.) in their work. Responses were favorable overall, although some participants with little GIS experience had some difficulty using the AGWA tool. Most participants were enthusiastic about using the tools, datasets, and methods developed during this project.

4.0 Results and Discussion

Natural resource managers at military installations face a number of challenges related to their need to balance natural resource protection with the military mission. They must manage and protect TER-S and their habitat, while at the same time providing for military use and access to training areas. This includes identifying stream reaches that might be important to wildlife, or roads that might become impassable during high runoff events. Managers are knowledgeable about their installation but the large land areas and diversity of terrain, flora, and fauna can make it difficult to know where specific landscape or habitat features might occur. They need to be able to identify locations with specific characteristics required for TER-S (i.e. riparian areas with dense vegetation 1 m to 4 m tall) and for other management priorities (i.e. areas that might flood frequently). To achieve their management goals, certain areas might be recommended for closure to military use. Managers require defensible science-based information to present to commanders to support their recommendations, and methods to rank the relative importance of landscape characteristics. This research provides that information in the form of a set of ecohydrologic variables for describing stream reaches, a stream type classification and methodology that identifies groups of similar stream reaches, and associations with wildlife groups to identify important stream reaches.

The stream type classification and methodology will be useful for managers because it will improve their understanding of the spatial variability of ecohydrological characteristics of stream reaches on their installation, and their understanding of how these features relate to wildlife habitat. The individual vegetation, hydrologic, and geomorphic variables are georeferenced to each stream reach, allowing managers to identify specific features of concern and locations for management actions. All of the data are delivered in a GIS and in tabular form. In addition, the data layers derived from the satellite imagery and multi-return LiDAR for the vegetation variables are provided to the managers for additional analyses, including extending these results to specific areas of interest not on the NHD stream network (i.e. small tributaries).

The classification results and variables are spatially linked to specific stream reaches using a Unique ID, allowing managers to use the data to identify locations with specific attributes to guide surveys for wildlife management, to develop sampling schemes or protocols, to locate reaches with high peak flows or flow permanence for transportation management, and to support other management activities. While we cannot anticipate the needs of managers with regard to wildlife or other management actions, we have provided a suite of information from which they can select the data they need in the form of the variables attributed to each stream reach. The analyses we have done for the wildlife can be used as is for management, but it may hold addition value as an example of how managers can use this dataset. For example, creating distribution models for other species of concern or richness maps for a particular group of species we did not include, or methods of analyzing species observation data with respect to stream types or ecohydrological variables. Stream reaches containing a higher proportion of vegetation in the 1 to 4 m height range can be identified as potential habitat for a specific species, such as the Gray Vireo that prefers that structure layer for nesting. Stream reaches with high peak flows at road crossings can be located and appropriate culverts or modifications can be applied. An invasive species such as buffelgrass could be mapped in relation to our dataset to analyze patterns or identify potential new locations that species might spread to or be found. A

particular stream type might be characterized as having very high flow permanence, indicating both valuable wildlife habitat and potential problems for training activities. By re-classifying flow permanence to high-medium-low, roads could be prioritized for management and training uses. Each stream type is characterized in terms of its most important variables, enabling managers to use the stream type classifications for similar management actions or decision making.

This information provides managers with science-based support for their recommendations to military commanders for management of the resource. During our numerous meetings with resource managers they have identified the above examples of specific needs and potential uses for our data and methodologies. The classifications are specific to the installation and ecoregion in which they were developed. Successful application of the classification methodology to other installations is dependent on the availability of the data required to derive the variables, and the ability to perform the required analyses. However, if the variables can be derived, and the area being extrapolated to is located near one of the project installations and has similar environmental characteristics, the predictive CART models can be used to identify the stream types and ecohydrological variables, which can then be used with the species richness models.

Ecohydrological Stream Type Classification

Ephemeral and intermittent streams at Fort Irwin, YPG, Fort Huachuca and Fort Bliss were classified based on their hydrologic, geomorphic and vegetation characteristics described earlier in this report. Because these four installations have very different hydrologic regimes and physical characteristics, each classification is unique and represents the variability of stream reaches within that installation; however, the classifications may be applicable within the same ecoregion using the variables and thresholds. Fort Irwin, Fort Huachuca and Fort Bliss have 8 final stream types, and YPG has 10 stream types. The final stream types and input variables were associated with wildlife habitat and species observation data, where available. The classifications will assist natural resource managers by providing a method of identifying similar stream types, and stream reaches with similar characteristics, for use in developing sampling schemes or surveys for wildlife and land use management.

The final stream types were determined for each installation from statistical and cluster analyses, cluster validity tests, examination of the mapped clusters, and site knowledge. A CART classification tree was used to evaluate the clustering results for each installation to determine the thresholds for the input variables for each stream type. The final stream types from the cluster analysis were used as the target variables, and all defaults were kept (Gini method, 10-fold cross validation, no limits on tree size or minimum cases per terminal node, no weighting, and equal priors). Fort Irwin, YPG, and Fort Bliss, have large land areas with very diverse terrain, and multiple distinct mountain ranges, their associated foothills, sand dunes, grasslands, creosote flats, playas and alluvial fans. As a result, those classification trees were more complex. Fort Huachuca is a small installation by comparison, with only one mountain range, its associated foothills, and lower elevation grasslands, and is the only installation with permanent flow and extensive forested areas. This classification tree was simpler than the others.

The optimal tree, identified as the tree with the least cost, was selected for determining thresholds for the input variables. For all installations except Fort Huachuca, the optimal tree was limited to a depth of 7 nodes to avoid terminal nodes with very few cases and create a more usable model for management; however, the complete tree will also be provided to each installation. The optimal tree for Fort Huachuca was simple enough that it did not need to be limited in depth.

Flow permanence is very low at Fort Irwin, YPG and Fort Bliss, with very subtle differences between stream reaches. Maximum flow permanence is 92.5% at Fort Huachuca, but only 13.1% at Fort Irwin, 14.8% at YPG, and 33.5% at Fort Bliss (Figure 34). Thus, the hydrologic variables were more significant in determining the stream types at Fort Huachuca, while the geomorphic variables (elevation, slope, reach width, and watershed area) were more significant at the other installations. Elevation and slope (or total stream power) were important variables for all installations because of the varied terrain and the strong influence of these geomorphic factors on hydrologic and vegetative characteristics.

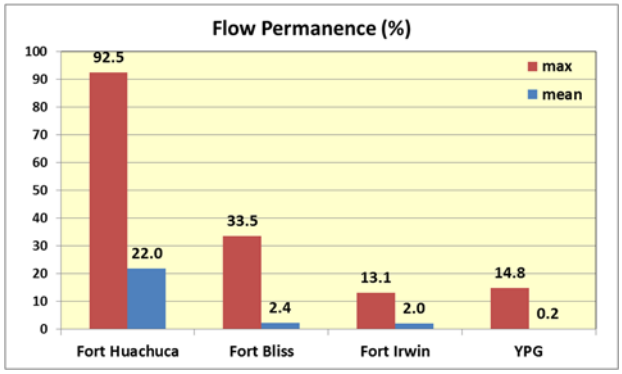


Figure 34. Mean and maximum flow permanence (%) for each installation.

Appendix B shows the final mapped stream types, dendrogram, NMDS plot, and box plots of the variables for each installation. A GIS feature class will be provided to each installation that includes all stream reaches, their stream type, and values for each of the variables. A discussion of the results for the stream types for each installation is included below. Misclassification errors (prediction success) are reported below for each installation, and generally occur where one stream type transitions to another or in stream types on the same branch of the dendrogram, indicating that those stream types are similar in many respects. Errors are likely due to heterogeneity of the input variables within the 1km stream reaches, which were determined graphically and not based on vegetation, geomorphic or hydrologic characteristics.

One of the basic premises for this research was that hydrology and geomorphology influence the vegetation characteristics. For example, it was presumed that higher flow permanence would result in increased vegetation cover or density in these water limited regions. Although our dataset is limited to the NHD Plus V2 stream reaches, which excludes many kilometers of lower-order stream channels, we were able to see some minor trends in the data. Fort Huachuca had a positive but weak relationship between flow permanence and vegetation cover ($R^2 = 0.28$). As noted previously, Fort Huachuca is our only location with any permanent stream flow. At Fort Bliss and YPG there was a very weak positive relationship between flow permanence and vegetation cover ($R^2 = 0.02$ and 0.006 respectively). Fort Irwin had a slight negative relationship.

The strongest relationships, although generally weak, between hydrology/geomorphology and vegetation were as follows:

Fort Irwin:

Percent slope and vegetation structure 0.25 m – 1 m, $R^2 = 0.41$
Elevation and vegetation cover, $R^2 = 0.41$
Elevation and mean vegetation index/vegetation density, $R^2 = 0.36$

YPG:

Elevation and vegetation cover, $R^2 = 0.11$
Elevation and SVRI, $R^2 = 0.11$

Fort Huachuca:

Flow Permanence and
veg 0 - 1 m, $R^2 = 0.25$
veg 4 - 12 m, $R^2 = 0.24$
vegetation cover, $R^2 = 0.28$
mean vegetation index/vegetation density, $R^2 = 0.26$

Elevation and
veg 0 – 1 m, $R^2 = 0.57$ (negative)
veg 1 – 4 m, $R^2 = 0.40$
veg 4 – 12 m, $R^2 = 0.62$
vegetation cover, $R^2 = 0.48$
mean vegetation index/vegetation density, $R^2 = 0.57$

Slope and
veg 0 – 1 m, $R^2 = 0.41$ (negative)
veg 1 - 4 m, $R^2 = 0.47$
veg 4 – 12 m, $R^2 = 0.39$
vegetation cover, $R^2 = 0.24$
mean vegetation index/vegetation density, $R^2 = 0.32$

Width 2m and
veg 0 – 1 m, $R^2 = 0.34$
veg 1 – 4 m, $R^2 = 0.34$
vegetation cover, $R^2 = 0.25$
mean vegetation index/vegetation density, $R^2 = 0.24$

RSI and
veg 0 – 1 m, $R^2 = 0.42$
veg 1 - 4 m, $R^2 = 0.37$ (negative)
veg 4 – 12 m, $R^2 = 0.33$ (negative)
vegetation cover, $R^2 = 0.46$ (negative)
mean vegetation index/vegetation density, $R^2 = 0.50$ (negative)

Fort Bliss:

Slope and veg 0.5 – 1 m, $R^2 = 0.33$
Slope and veg 1 – 4 m, $R^2 = 0.29$

Elevation and
- veg 1 – 4 m, $R^2 = 0.35$
- veg 4 – 12 m, $R^2 = 0.25$
- vegetation cover, R^2 0.32
- mean vegetation index/vegetation density, $R^2 = 0.25$

Attempts to correlate the biotic and abiotic variables did not produce satisfactory results. We performed a CART analysis to predict the vegetation structure (biotic) variables from the geomorphology and hydrology (abiotic), but except at Fort Huachuca, the predictive capability was weak. Although flow permanence, one of the hydrologic variables, can be considered as a surrogate for soil moisture, the hydrologic properties likely influence vegetation composition more than vegetation structure.

Lyon (2013) included a detailed discussion of the interactions of hydrologic and biotic processes in his master's thesis. He noted that the increased biodiversity and ecological function of riparian areas are attributed in part to the dynamic nature of the flow regime's regulation of soil moisture. Species richness in riparian zones varies greatly both spatially and temporally along the stream channel and the degree to which these vegetation changes occur is primarily regulated by the flow regime (Naiman et al., 1993), which determines how much subsurface moisture travels from the hyporheic and parafluvial zones beneath the active channel to the riparian zone. It is within these areas where the majority of ecohydrological processes occur and where the other components of the water budget determine riparian characteristics (Naiman & Decamps, 1997). Riparian vegetation is influenced by flow regime characteristics such as presence of surface or groundwater flows and high and low flow conditions (Stromberg et al., 2005).

Fort Irwin

The cluster validity tests for Fort Irwin suggested five or twelve stream types as optimal. However, five stream types did not adequately describe the range of conditions we found across the installation, and twelve clusters created several groups with very small differences based mainly on elevation. Eight stream types were selected using site knowledge in addition to the statistical tests to capture the variability that was not well discerned using only the statistical methods.

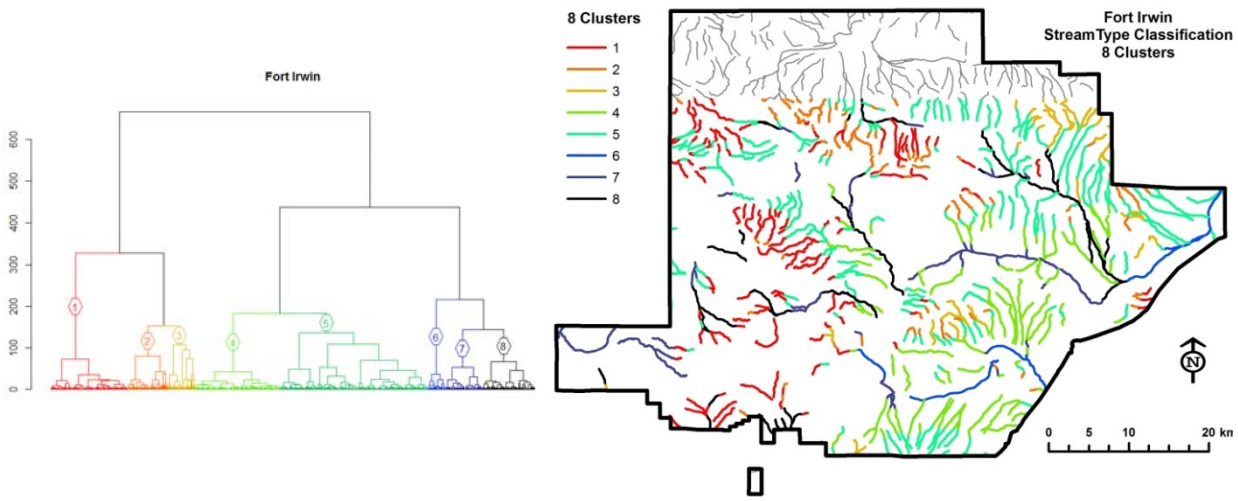


Figure 35. Fort Irwin dendrogram and map for 8 stream types.

The stream types fell into 3 main groups that were further split into 8 stream types (Figure 35). Stream types 1, 2 and 3 form one of the main groups, and represent 29.9% of stream reaches. Stream types 4 and 5 form the second group, representing nearly half of all stream reaches (17.7% and 30.4% respectively). Stream types 6, 7 and 8, the third group, are the remaining 22% of reaches. Figure 36 includes graphs showing the percentage of total stream reaches and total stream lengths for each stream type.

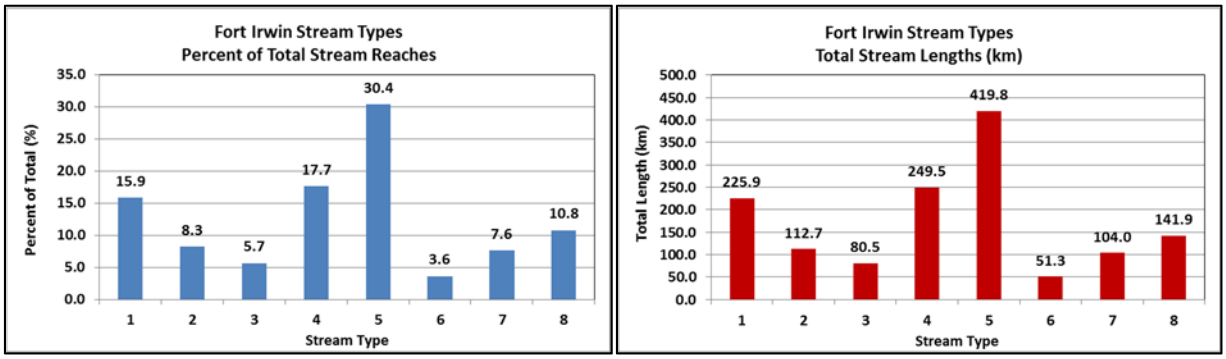


Figure 36. Fort Irwin stream types, percent of total stream reaches and total stream lengths.

Slope, vegetation cover, smaller vegetation (<1 m), reach width and elevation were significant variables in the PCA first principal component, and these variables varied the most among the 8 stream types (see Appendix B). Vegetation structure (0.25 m – 4 m), entrenchment ratio (3 m / 0.5 m), cumulative area and elevation were significant in the second principal component. Variable importance was similar in the CART analysis, although the vegetation structure was not as important (Table 5). The classification tree is included as an attachment to this report.

Table 5. Variable importance, CART analysis, Fort Irwin.

Variable	Score		Variable	Score
Watershed Area (m^2)	100.0		Total Stream Power 25-yr 1-hr (kW/m)	47.5
Elevation (m)	95.9		Flow Permanence (%)	47.1
Width 2m (m)	92.8		Veg 0 - 0.25m (%)	44.1
Vegetation Cover (%)	82.9		Entrenchment Ratio 3m/0.5m	43.0
Percent Slope (%)	72.7		Veg 1 - 4 m (%)	42.2
Veg 0.25 - 1m (%)	55.6		Peak Flow 25-yr 1-hr (m^3/s)	42.0
MSAVI2 Mean	55.0		Veg 4 - 12 m (%)	1.1
RSI	49.0			

The optimal classification tree for Fort Irwin included 67 terminal nodes, a relative cost of 0.142, and a prediction success of 84.72%. This tree was limited to a depth of 7 nodes to represent most of the variability, resulting in 21 terminal nodes, a relative cost of 0.196, and a prediction success of 76.73%. Accuracy for each stream type obtained from the limited tree is reported in Table 6.

Table 6. Fort Irwin stream type classification analysis, prediction success, 8 stream types.

Actual Class	Total Class	Percent Correct	1 N = 300	2 N = 125	3 N = 89	4 N = 255	5 N = 331	6 N = 52	7 N = 130	8 N = 145
1	227.00	89.43%	203.00	10.00	0.00	0.00	13.00	0.00	0.00	1.00
2	118.00	78.81%	14.00	93.00	4.00	0.00	5.00	0.00	2.00	0.00
3	81.00	83.95%	6.00	4.00	68.00	0.00	2.00	0.00	1.00	0.00
4	252.00	76.98%	1.00	0.00	0.00	194.00	48.00	0.00	7.00	2.00
5	434.00	59.45%	68.00	17.00	16.00	60.00	258.00	0.00	7.00	8.00
6	52.00	100.00%	0.00	0.00	0.00	0.00	0.00	52.00	0.00	0.00
7	109.00	90.83%	2.00	0.00	0.00	0.00	2.00	0.00	99.00	6.00
8	154.00	83.12%	6.00	1.00	1.00	1.00	3.00	0.00	14.00	128.00
Total:	1,427.00									
Average:		82.82%								
Overall % Correct:		76.73%								

Table 7 lists the thresholds and percentages for each variable for each stream type from that tree, in general order of importance. Values in the table indicate the percent of stream reaches in each stream type for each variable range. The largest percentages are shown in a bold font, indicating the majority of stream reaches. From this table, the general characteristics of each stream type can be determined. For example, stream reaches classified as Stream Type 1 are characterized by average reach widths <=228.02 m, TSP <=1.28 kW/m, RSI >0.20, with 95.2% of those reaches having <=3.89% of vegetation from 0.25 and 1 m in height, and 98.7% with flow permanence <=3.94%.

Most stream reaches at Fort Irwin are characterized by low flow permanence (less than 3.94% of the year), and low total stream power (TSP <=1.28 kW/m). Stream type 3 has the highest total stream power, with 81.5% of reaches having TSP >1.28 kW/m. Stream type 6 is characterized by having the largest watershed area and relatively high flow permanence, but low elevation. Stream type 7 has the widest reaches.

Table 7. Fort Irwin thresholds for input variables, percent of each stream type for 8 stream types.

Stream Type	Watershed Area (m^2)				Width 2m (m)		TSP 25-yr 1-hr (kW/m)		ER 3m/0.5m	
	<=1,589,301	<=327,136,256	<=517,404,360	>517,404,360	<=228.02	>228.02	<=1.28	>1.28	<=4.78	>4.78
1	17.2	**82.8**	0.0	0.0	**100.0**	0.0	**100.0**	0.0	44.1	**55.9**
2	28.0	**72.0**	0.0	0.0	**98.3**	1.7	**91.5**	8.5	**96.6**	3.4
3	4.9	**95.1**	0.0	0.0	**98.8**	1.2	18.5	**81.5**	**70.4**	29.6
4	10.3	**89.7**	0.0	0.0	**93.3**	6.7	**100.0**	0.0	20.2	**79.8**
5	13.6	**86.4**	0.0	0.0	**95.9**	4.1	**96.3**	3.7	28.6	**71.4**
6	0.0	0.0	0.0	**100.0**	48.1	**51.9**	**92.3**	7.7	**69.2**	30.8
7	2.8	**97.2**	0.0	0.0	5.5	**94.5**	**100.0**	0.0	**97.2**	2.8
8	0.0	**94.8**	5.2	0.0	**77.3**	22.7	**96.8**	3.2	41.6	**58.4**

Stream Type	Veg 0.25 - 1m (%)		Flow Permanence (%)					RSI	
	<=3.89	>3.89	<=3.94	<=4.74	<=6.95	<=7.00	>7.00	<=0.20	>0.20
1	**95.2**	4.8	**98.7**	1.3	0.0	0.0	0.0	0.0	**100.0**
2	16.1	**83.9**	**92.4**	0.8	3.4	0.0	3.4	0.0	**100.0**
3	**66.7**	33.3	**91.4**	0.0	8.6	0.0	0.0	48.1	**51.9**
4	**100.0**	0.0	**96.8**	2.8	0.4	0.0	0.0	0.0	**100.0**
5	**96.3**	3.7	**96.1**	3.2	0.7	0.0	0.0	5.3	**94.7**
6	**98.1**	1.9	0.0	23.1	**76.9**	0.0	0.0	0.0	**100.0**
7	**100.0**	0.0	**58.7**	5.5	31.2	1.8	2.8	0.0	**100.0**
8	**99.4**	0.6	2.6	13.0	37.7	3.9	**42.9**	0.0	**100.0**

Stream Type	Elevation (m)			MSAVI2 Mean			Vegetation Cover (%)		Veg 1 - 4m (%)	
	<=838.69	<=897.65	>897.65	<=0.24	<=0.29	>0.29	<=3.58	>3.58	<=0.05	>0.05
1	5.7	4.4	**89.9**	1.3	**51.5**	47.1	0.0	**100.0**	**62.1**	37.9
2	20.3	5.9	**73.7**	28.0	**51.7**	20.3	0.8	**99.2**	0.8	**99.2**
3	35.8	6.2	**58.0**	43.2	**44.4**	12.3	0.0	**100.0**	14.8	**85.2**
4	**92.9**	4.4	2.8	**99.6**	0.4	0.0	25.0	**75.0**	**92.5**	7.5
5	32.9	10.6	**56.5**	**71.7**	24.2	4.1	0.9	**99.1**	**74.2**	25.8
6	**100.0**	0.0	0.0	**98.1**	1.9	0.0	44.2	**55.8**	**80.8**	19.2
7	44.0	6.4	**49.5**	**80.7**	19.3	0.0	36.7	**63.3**	**81.7**	18.3
8	39.0	13.0	**48.1**	**64.3**	23.4	12.3	2.6	**97.4**	**66.2**	33.8

Yuma Proving Ground

The cluster validity tests indicated that ten stream types were optimal at YPG, and this agreed with our knowledge of the installation and examination of the data and clustering results. YPG is our driest location, but experiences monsoon season storms which decrease towards the west. YPG wraps around the Kofa and Castle Dome Mountains, resulting in a complex climate and geography with numerous areas with distinct features. The western arm of YPG is dominated by rugged, igneous mountains and foothills, draining west towards the Colorado River. The southwestern and southern areas are alluvial, draining south and southwest towards the Gila River (Figure 3).

The cluster analysis grouped the data at YPG into five main groups that were further split into 10 stream types (see the dendrogram Figure 37). Nearly half of all stream reaches (47.9%) are classified as stream types 1 or 2, representing nearly half the total stream length. Stream type 6 is the next largest group, representing 13.5% of stream reaches. Figure 38 includes graphs showing the percentage of total stream reaches and total stream length for each stream type.

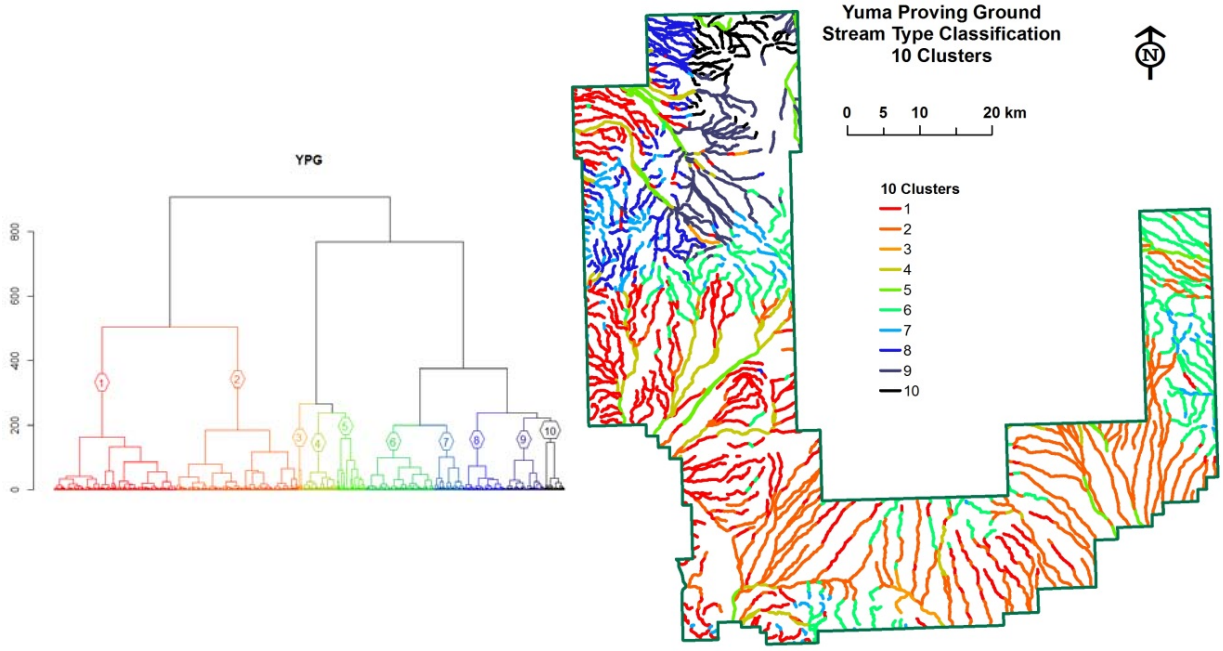


Figure 37. YPG dendrogram and map for 10 stream types.

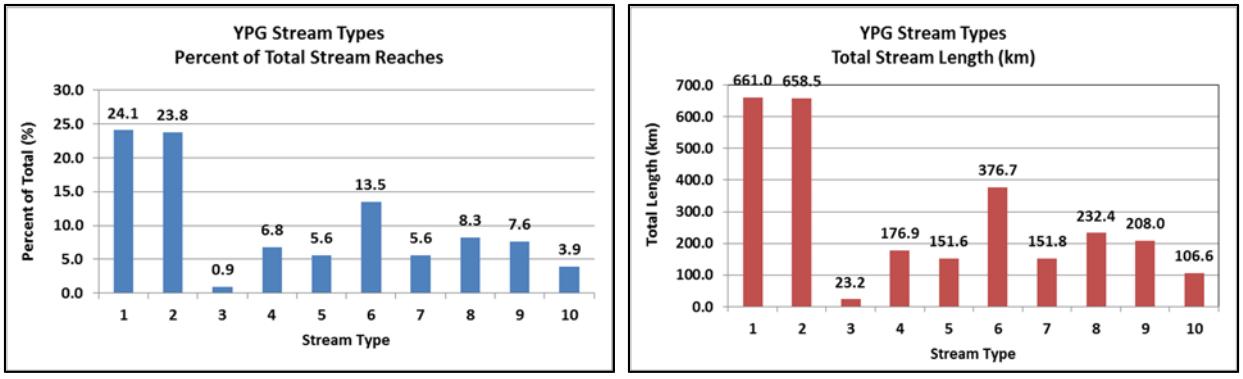


Figure 38. YPG stream types, percent of total stream reaches and total stream lengths.

Peak flow, watershed area, reach width, and slope were the most significant variables in the first principal component in the PCA. Total stream power, elevation and seasonal vegetation response to monsoon precipitation index (SVRI) were significant in the second principal component. The vegetation variables, percent cover and mean RENDVI, became significant in the third principal component. Peak flow and the geomorphic variables had a stronger influence on stream types than vegetation or flow permanence. Variable importance from the CART classification analysis was slightly different, with RSI being most important, followed by reach width and percent slope (Table 8).

Table 8. Variable importance, CART analysis, YPG.

Variable	Score		Variable	Score
RSI	100.0		Peak Flow 25-yr 1-hr (m^3/s)	72.1
Width 2m (m)	90.1		Elevation (m)	53.6
Percent Slope (%)	89.4		Flow Perm (%)	53.5
Watershed Area (m^2)	78.9		RENDVI Mean	53.0
TSP 25yr 1hr (kW/m)	78.2		Seasonal Vegetation Response Index (SVRI)	47.5
Vegetation Cover (%)	75.7		Entrenchment Ratio 3m/0.5m	21.2

The optimal classification tree for YPG had 86 terminal nodes, a relative cost of 0.140, and 84.83% prediction success. To produce a usable predictive model, the tree was limited to a depth of 7 nodes, resulting in 35 terminal nodes, a relative cost of 0.167, and 80.75% prediction success (Table 9). This tree was selected as representative of most of the variability, and will be more useful to managers applying this classification system as a predictive tool as opposed to the 86 terminal nodes in the complete tree. Most of the misclassification errors occur at transitions from one stream type to another, most likely due to data representation. The classification tree is included as an attachment to this report.

Table 9. YPG stream type classification analysis, prediction success, 10 stream types.

Actual Class	Total Class	Percent Correct	1 N = 617	2 N = 619	3 N = 25	4 N = 211	5 N = 158	6 N = 435	7 N = 189	8 N = 245	9 N = 220	10 N = 123
1	684.00	72.81%	498.00	39.00	0.00	11.00	2.00	92.00	7.00	26.00	7.00	2.00
2	675.00	82.52%	75.00	557.00	0.00	13.00	4.00	25.00	1.00	0.00	0.00	0.00
3	25.00	100.00%	0.00	0.00	25.00	0.00	0.00	0.00	0.00	0.00	0.00	0.00
4	192.00	85.42%	4.00	3.00	0.00	164.00	3.00	6.00	8.00	1.00	2.00	1.00
5	159.00	93.71%	0.00	1.00	0.00	6.00	149.00	0.00	1.00	0.00	1.00	1.00
6	384.00	75.26%	34.00	19.00	0.00	1.00	0.00	289.00	33.00	0.00	7.00	1.00
7	160.00	76.88%	3.00	0.00	0.00	9.00	0.00	9.00	123.00	7.00	5.00	4.00
8	235.00	85.96%	3.00	0.00	0.00	2.00	0.00	10.00	9.00	202.00	3.00	6.00
9	217.00	86.64%	0.00	0.00	0.00	5.00	0.00	4.00	4.00	8.00	188.00	8.00
10	111.00	90.09%	0.00	0.00	0.00	0.00	0.00	0.00	3.00	1.00	7.00	100.00
Total:	2,842.00											
Average:		84.93%										
Overall % Correct:		80.75%										

This tree was used to determine the thresholds for each input variable, and the percentages for each stream type, which are shown in Table 10. Values in the table indicate the percent of stream reaches in each stream type for each variable range. Because YPG has a great diversity of landforms many of the variables have numerous thresholds, and frequently there is no single value representing the majority of stream reaches; however, the value representing the largest percentage of reaches is shown in a bold font.

Table 10. YPG thresholds for input variables, percent of each stream type for 10 stream types.

Stream	Flow Perm (%)		Qp25 (m^3/s)			RSI				Width 2m (m)			
Type	<= 3.32	> 3.32	<=208.10	<=354.06	>354.06	<=0.16	<=0.17	<=0.18	>0.18	<=226.10	<=230.04	<=266.46	>266.46
1	**100.0**	0.0	**99.4**	0.3	0.3	47.7	**48.0**	3.7	0.7	**70.9**	1.9	7.7	18.9
2	**100.0**	0.0	**97.2**	2.4	0.4	**83.3**	16.6	0.1	0.0	5.5	0.3	5.6	**87.9**
3	0.0	**100.0**	**80.0**	20.0	0.0	**68.0**	0.0	32.0	0.0	44.0	4.0	8.0	44.0
4	**100.0**	0.0	16.1	**75.0**	8.9	40.1	**46.9**	13.0	0.0	31.8	2.6	16.7	**49.0**
5	**100.0**	0.0	1.9	10.7	**87.4**	27.7	27.7	29.6	15.1	13.8	0.0	9.4	**76.1**
6	**100.0**	0.0	**99.7**	0.3	0.0	**77.1**	20.8	1.8	0.3	**88.5**	0.8	3.1	7.0
7	**100.0**	0.0	**94.4**	5.0	0.6	38.8	24.4	14.4	22.5	**99.4**	0.0	0.0	0.0
8	**100.0**	0.0	**100.0**	0.0	0.0	0.0	9.4	**51.9**	38.7	**96.6**	0.4	1.7	1.3
9	**100.0**	0.0	**94.5**	5.5	0.0	0.0	7.4	**73.3**	19.4	46.5	0.9	7.4	43.3
10	**100.0**	0.0	**100.0**	0.0	0.0	0.0	0.0	4.5	**95.5**	**100.0**	0.0	0.0	0.0

Stream	RENDVI Mean					Vegetation Cover (%)				
Type	<=0.11	<=0.12	<=0.13	<=0.15	>0.15	<=0.23	<=0.23	<=0.46	<=0.51	>0.51
1	**50.0**	33.0	12.0	4.8	0.1	**85.8**	1.0	13.0	0.1	0.0
2	5.3	20.3	36.1	34.2	4.0	**86.7**	1.3	11.4	0.3	0.3
3	0.0	20.0	16.0	**56.0**	8.0	24.0	4.0	**64.0**	8.0	0.0
4	26.0	30.7	21.9	19.8	1.6	**63.5**	2.6	28.1	1.6	4.2
5	17.6	14.5	22.0	39.0	6.9	**64.2**	1.9	28.3	1.3	4.4
6	3.1	19.0	29.2	40.9	7.8	22.7	7.3	**65.1**	3.1	1.8
7	35.0	27.5	13.1	16.9	7.5	5.6	0.6	43.8	14.4	35.6
8	**80.4**	17.9	1.7	0.0	0.0	**64.3**	1.3	30.6	1.7	2.1
9	0.0	9.2	16.6	**51.6**	22.6	**59.4**	1.8	35.5	2.8	0.5
10	3.6	2.7	18.0	**70.3**	5.4	**92.8**	1.8	5.4	0.0	0.0

Stream	Elevation (m)						Slope (%)			
Type	<=207.65	<=236.65	<=237.23	<=349.33	<=400.63	>400.63	<= 3.25	<=4.82	<=17.88	>17.88
1	**51.8**	14.0	0.6	32.0	1.3	0.3	**93.0**	4.7	2.3	0.0
2	**66.5**	11.1	0.4	16.6	2.2	3.1	**100.0**	0.0	0.0	0.0
3	**56.0**	8.0	0.0	4.0	20.0	12.0	**96.0**	4.0	0.0	0.0
4	**46.9**	14.6	0.5	36.5	1.6	0.0	**99.5**	0.5	0.0	0.0
5	40.3	10.1	0.0	35.2	7.5	6.9	**96.9**	1.3	1.9	0.0
6	4.2	7.6	0.3	**41.9**	16.7	29.4	**96.9**	3.1	0.0	0.0
7	5.0	6.9	0.0	**41.3**	15.6	31.3	**83.1**	16.9	40.0	0.0
8	12.3	12.8	0.0	**44.7**	21.7	8.5	**86.8**	12.3	0.9	0.0
9	0.0	0.0	0.0	**51.2**	36.9	12.0	**97.7**	1.8	0.5	0.0
10	0.0	0.0	0.0	39.6	30.6	29.7	**78.4**	21.6	27.0	7.2

Stream	ER 3m/05m		Watershed Area (m^2)				SVRI				
Type	<= 3.55	> 3.55	<=31429012	<=103478288	<=358500096	>358500096	<= -0.83	<=0.28	<=0.42	<=0.83	>0.83
1	26.0	**74.0**	**97.5**	2.0	0.4	0.0	**72.2**	27.5	0.0	0.3	0.0
2	**62.5**	37.5	**81.5**	16.4	1.9	0.1	38.5	**54.5**	1.2	2.7	3.1
3	44.0	**56.0**	**60.0**	24.0	12.0	4.0	8.0	**68.0**	0.0	16.0	8.0
4	38.5	**61.5**	15.1	**60.4**	24.5	0.0	46.4	45.8	3.6	3.1	1.0
5	**67.3**	32.7	1.3	18.9	**58.5**	21.4	38.4	**57.2**	0.6	2.5	1.3
6	16.1	**83.9**	**98.7**	1.3	0.0	0.0	15.9	**66.4**	5.5	10.4	1.8
7	**63.8**	36.3	**98.8**	1.3	0.0	0.0	20.6	**46.9**	13.8	11.9	6.9
8	23.0	**77.0**	**100.0**	0.0	0.0	0.0	31.1	**68.1**	0.9	0.0	0.0
9	47.5	**52.5**	**84.8**	15.2	0.0	0.0	38.2	**60.8**	0.0	0.5	0.5
10	48.6	**51.4**	**100.0**	0.0	0.0	0.0	0.9	**58.6**	8.1	19.8	12.6

Most stream types are generally characterized by low slope, low peak flow and low flow permanence, except for stream type 3 which has the highest mean flow permanence, and stream type 5 which has the highest mean peak flow and total stream power. Intermediate peak flows are found in Stream Type 4, where 75% of the stream reaches have a 25-yr 1-hr Peak Flow (Qp25) of between 208.1 and 354.05 m^3/s. All stream reaches classified as Stream Type 3 have greater than 3.32% flow permanence. Stream types 1 and 2 are characterized by low elevation, low slope, low vegetation cover and low SVRI. Both have a wide range of widths, although stream type 2 has the highest mean width, and stream type 1 has the lowest SVRI. Stream type 3 has moderately high vegetation cover. Stream types 4 and 5 have the highest peak flows and total stream power of all stream types. Stream types 6 through 10 are the highest elevation reaches, with stream types 7 and 10 having the greatest slopes of all stream types.

Fort Huachuca

The cluster validity tests indicated that five stream types exist at Fort Huachuca. Based on our site knowledge and the other statistical analyses we identified eight stream types. Although Fort Huachuca is a small installation, it has a wide range of elevation, slopes, vegetation communities, and a much wider range of flow permanence; eight clusters adequately characterize that variability here.

The stream types fell into 4 main groups that were further split into 8 stream types, representing the high elevation mountains, mid elevation foothills, lower elevation grasslands, and the main-stem channel reaches (Figure 39). Stream types 1 and 2 constitute 18.3% of stream reaches, all located in the upper elevation mountains. Stream types 3 and 4 represent 12.5% of stream reaches and are the main stem channels of the larger watersheds, Garden Canyon, Huachuca Canyon, Slaughterhouse Wash, and Rock Spring/Soldier Canyon. Lower Garden Canyon is separated to form stream type 3 due to its higher flow permanence, peak flows, entrenchment ratio, and vegetation cover and heights. It drains to a different outlet from the other main stem channels, to the east to the San Pedro River, instead of to the north to the Babocomari River.

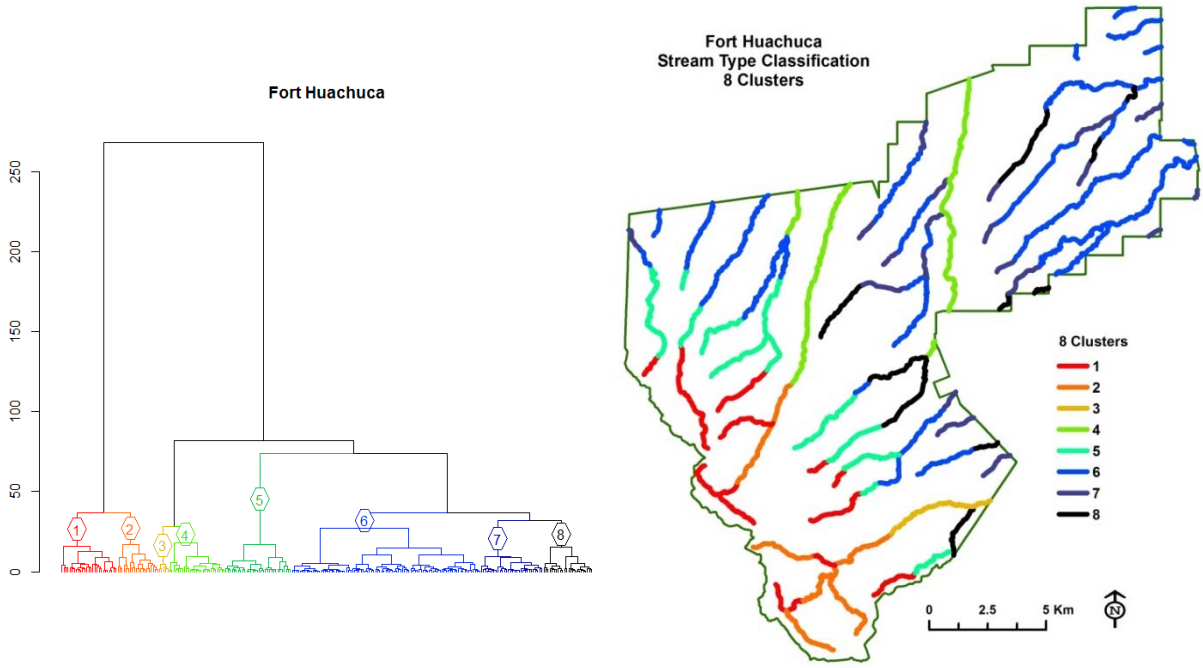


Figure 39. Fort Huachuca dendrogram and map for 8 stream types.

Stream type 5 represents the middle elevation foothill channels that transition from the mountains to the grasslands, and comprises 12.5% of stream reaches. Stream types 6, 7 and 8 are located in the grasslands and East Range, and comprise the remaining stream reaches. Stream type 6 is the largest group with 35.5% of all stream reaches. Figure 40 includes graphs showing the percentage of total stream reaches and total stream lengths for each stream type.

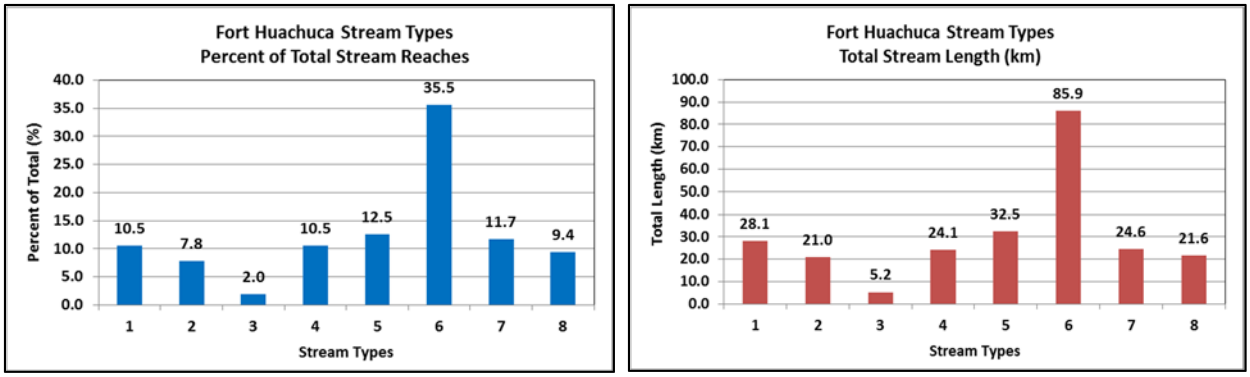


Figure 40. Fort Huachuca stream types, percent of total stream reaches and total stream lengths.

PCA analysis indicated that the first principal component is strongly correlated with vegetation structure (vegetation <1 m, and 4 - 12 m), elevation, vegetation density, RSI, slope and vegetation cover. Stream types at Fort Huachuca are clearly delineated on these variables, especially elevation and slope (Figure 39). The second principal component is strongly correlated with peak flow, TSP, cumulative area, entrenchment ratio, flow permanence and width, indicating the importance of these variables in further defining the stream types.

Variable importance from the CART classification analysis indicated that peak flow, vegetation between 4 – 12 m, RSI, and elevation were the most important variables (Table 11). The optimal classification tree for Fort Huachuca had 11 terminal nodes, a relative cost of 0.188, and 81.25% prediction success (Table 12). This tree was used to determine the thresholds for each input variable, and the percentages for each stream type, shown in Table 13. Values in this table indicate the percent of stream reaches in each stream type for each variable range. Values shown with a bold font indicate the majority of stream reaches for each variable. For example, 100% of the stream reaches classified as Stream Type 1 have more than 2.54% of all vegetation between 4 – 12 m in height, and are over 1423.65 m in elevation. The classification tree is included as an attachment to this report.

Table 11. Variable importance, CART analysis, Fort Huachuca.

Variable	Score		Variable	Score
Peak Flow 25-yr 1-hr (m^3/s)	100.0		MSAVI2 Mean	39.4
Veg 4-12m (%)	64.4		Veg 1-4m (%)	38.9
RSI	55.4		Flow Perm (%)	35.2
Elevation (m)	51.2		Percent Slope (%)	26.8
Total Stream Power 25-yr 1-hr (kW/m)	48.9		Width 2m (m)	21.0
Watershed Area (m^2)	48.1		Veg >12m (%)	17.6
Veg 0-1m (%)	45.9		Vegetation Cover (%)	11.9
Entrenchment Ratio 3m/0.5m	39.4			

Table 12. Fort Huachuca stream type classification analysis, prediction success, 8 stream types.

Actual Class	Total Class	Percent Correct	1 N = 25	2 N = 24	3 N = 5	4 N = 26	5 N = 31	6 N = 89	7 N = 31	8 N = 25
1	27.00	81.48%	22.00	4.00	0.00	0.00	1.00	0.00	0.00	0.00
2	20.00	95.00%	1.00	19.00	0.00	0.00	0.00	0.00	0.00	0.00
3	5.00	100.00%	0.00	0.00	5.00	0.00	0.00	0.00	0.00	0.00
4	27.00	96.30%	0.00	1.00	0.00	26.00	0.00	0.00	0.00	0.00
5	32.00	71.88%	2.00	0.00	0.00	0.00	23.00	5.00	0.00	2.00
6	91.00	81.32%	0.00	0.00	0.00	0.00	5.00	74.00	6.00	6.00
7	30.00	80.00%	0.00	0.00	0.00	0.00	0.00	4.00	24.00	2.00
8	24.00	62.50%	0.00	0.00	0.00	0.00	2.00	6.00	1.00	15.00
Total:	256.00									
Average:		83.56%								
Overall % Correct:		81.25%								

Table 13. Fort Huachuca thresholds for input variables, percent of each stream type for 8 stream types.

Stream Type	Peak Flow 25-yr 1-hr (m^3/s)				Vegetation 0 - 1 m (%)			Vegetation 4 - 12 m (%)	
	<=112.07	<=262.24	<=350.71	<=785.56	>785.56	<=66.98	>66.98	<=2.54	>2.54
1	12.5	**45.8**	20.8	20.8	0.0	**100.0**	0.0	0.0	**100.0**
2	**93.1**	6.9	0.0	0.0	0.0	**75.9**	24.1	6.9	**93.1**
3	0.0	0.0	0.0	16.7	**83.3**	16.7	**83.3**	33.3	**66.7**
4	0.0	6.5	6.5	**87.1**	0.0	3.2	**96.8**	**83.9**	16.1
5	**75.0**	25.0	0.0	0.0	0.0	4.2	**95.8**	8.3	91.7
6	**81.4**	18.6	0.0	0.0	0.0	0.0	**100.0**	**95.3**	4.7
7	**97.3**	2.7	0.0	0.0	0.0	0.0	**100.0**	**81.1**	18.9
8	**88.7**	11.3	0.0	0.0	0.0	0.0	**100.0**	**98.4**	1.6

Stream Type	Elevation (m)		ER 3m / 0.5m		Width 2m (m)		Flow Permanence (%)	
	<=1423.65	>1423.65	<=9.15	>9.15	<=90.8	>90.8	<=26.32	>26.32
1	0.0	**100.0**	**100.0**	0.0	**100.0**	0.0	8.3	**91.7**
2	0.0	**100.0**	**100.0**	0.0	**100.0**	0.0	44.8	**55.2**
3	0.0	**100.0**	0.0	**100.0**	**83.3**	16.7	16.7	**83.3**
4	**74.2**	25.8	**83.9**	16.1	**51.6**	48.4	48.4	**51.6**
5	4.2	**95.8**	**95.8**	4.2	**100.0**	0.0	16.7	**83.3**
6	44.2	**55.8**	48.8	**51.2**	44.2	**55.8**	**74.4**	25.6
7	**100.0**	0.0	**100.0**	0.0	**67.6**	32.4	**100.0**	0.0
8	**75.8**	24.2	**95.2**	4.8	**79.0**	21.0	**93.5**	6.5

Stream types 1 and 2 are characterized by high percentages of vegetation taller than 4 m, and high flow permanence, although stream type 2 has higher flow permanence than stream type 1. Reaches in stream type 3 have high peak flow, the highest flow permanence, and a high entrenchment ratio. Stream type 5 represents the middle elevation foothill channels that transition from the mountains to the grasslands. Stream types 6, 7 and 8 have high amounts of vegetation below 1 m, and very little above 4 m high. They have low peak flow, flow permanence and stream power.

Fort Bliss

The cluster validity tests indicated that seven clusters were the optimum number for Fort Bliss. This cluster arrangement did not separate streams above and below Otero Mesa which, based on our field experience have different characteristics. The next cluster level split those stream reaches, so we selected eight stream types for Fort Bliss.

The stream types fell into three main groups: high elevation - high slope mountain reaches, mid-elevation reaches, and lower elevation - low slope reaches (Figure 41). Stream types 1, 2 and 3 are higher elevation - high slope reaches, and represent 16.2% of all stream reaches. Stream types 4, 5 and 6 are the second group of stream reaches, are mid-elevation with moderate slopes and comprise 57.3% of reaches. Stream types 7 and 8, the lower elevation - low slope reaches, make up the remaining 26.4% of stream reaches. Figure 42 is a graph showing the percentage of total stream reaches and total stream lengths for each stream type.

Fort Bliss has numerous discontinuous sheetflood reaches identified as Chihuahuan-Sonoran Desert Bottomland and Swale Grassland (Tobosa Swales) by NatureServe (http://www.natureserve.org), characterized by wide, shallow flow paths with vegetation distinct from the adjacent uplands (see Figure 13). These reaches were not identified as a separate stream type using our methods; however, most of these reaches are classified as stream type 7 (widest and lowest slopes) or stream type 5 (lowest peak flow, low vegetation cover, and least amount of vegetation taller than 0.5 m in height). In addition, many of these reaches may not have been included on the NHD stream network, due to the way that network was created (note the large areas of Otero Mesa in the northeast area of the installation with no stream lines). This reach type is discussed in the next section.

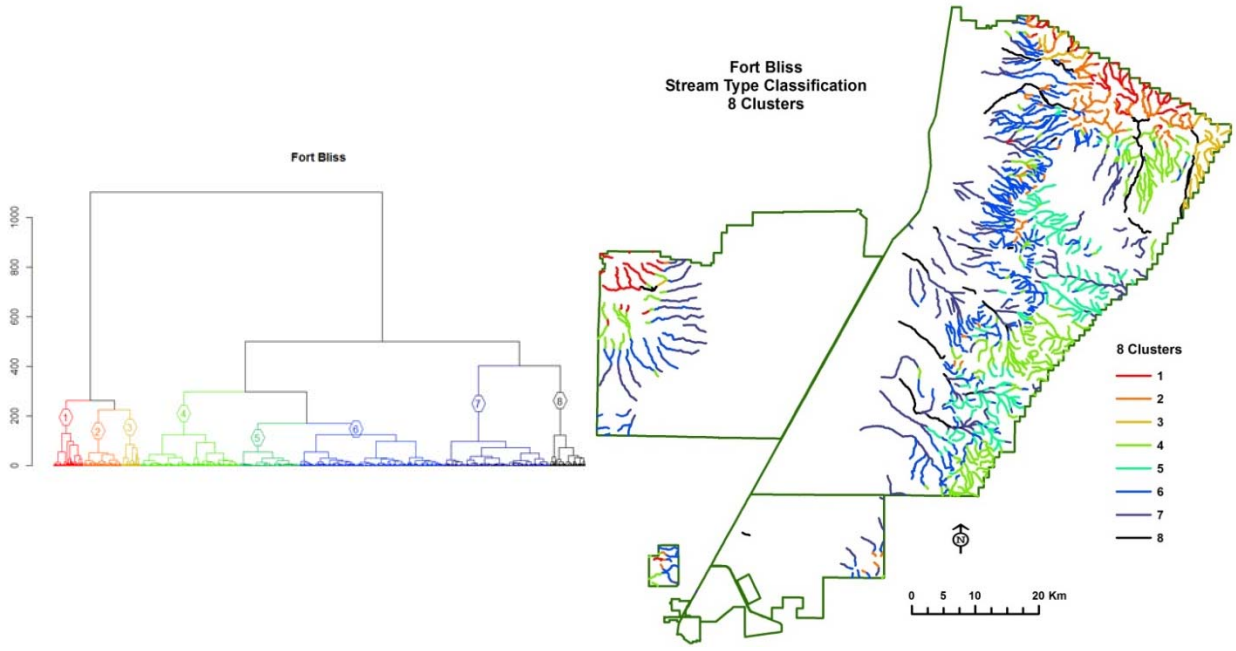


Figure 41. Fort Bliss dendrogram and map for 8 stream types.

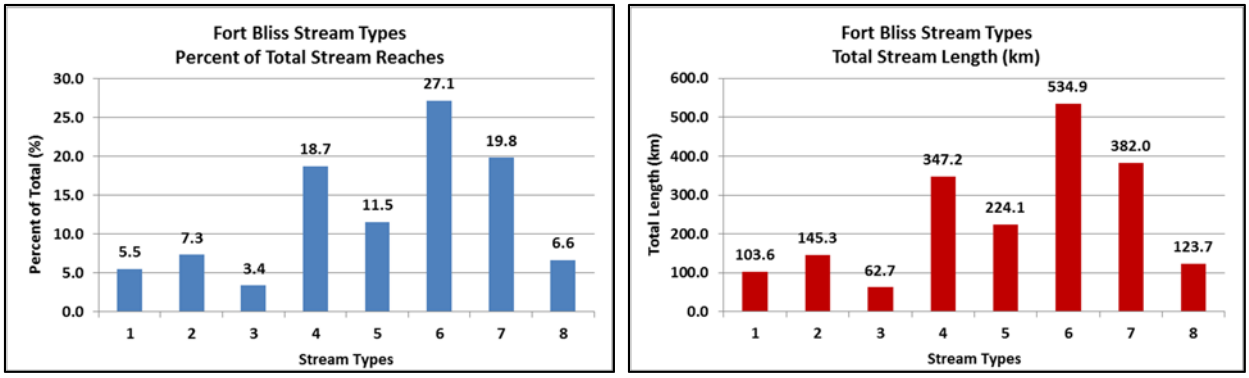


Figure 42. Fort Bliss stream types, percent of total stream reaches and total stream lengths.

PCA analysis confirmed that the vegetation variables were most significant in the first principal component, followed by slope and elevation. The hydrologic and physical variables were significant in the second principal component.

The optimal classification tree for Fort Bliss included 63 terminal nodes, a relative cost of 0.136, and a prediction success of 85.41%. Variable importance in CART was similar to the PCA results, indicating that vegetation structure and elevation were the most important (Table 14). This tree was limited to a depth of 7 nodes to represent most of the variability and create a more useful prediction model. This resulted in a tree with 29 terminal nodes, a relative cost of 0.176, and prediction success of 80.59% (Table 15). The classification tree is included as an attachment to this report.

Table 14. Variable importance, CART analysis, Fort Bliss.

Variable	Score		Variable	Score
Veg <0.5m (%)	100.0		Peak Flow 25-yr 1-hr (m^3/s)	56.1
Elevation (m)	90.4		RENDVI Mean	52.4
Veg 1-4m (%)	90.0		Watershed Area (m^2)	47.8
Width 2m (m)	72.9		Percent Slope (%)	31.8
Veg 4 - 12m (%)	69.9		TSP 25-yr 1-hr (kW/m)	28.7
Vegetation Cover (%)	60.4		RSI	11.6
Veg 0.5 - 1m (%)	59.1		ER 3m / 0.5m	7.2
Flow Perm (%)	56.1			

Table 15. Fort Bliss stream type classification analysis, prediction success, 8 stream types.

Actual Class	Total Class	Percent Correct	1 N = 112	2 N = 162	3 N = 69	4 N = 354	5 N = 290	6 N = 493	7 N = 380	8 N = 134
1	110.00	90.00%	99.00	4.00	3.00	2.00	0.00	1.00	0.00	1.00
2	146.00	83.56%	10.00	122.00	0.00	7.00	0.00	6.00	0.00	1.00
3	67.00	98.51%	0.00	1.00	66.00	0.00	0.00	0.00	0.00	0.00
4	373.00	80.16%	3.00	8.00	0.00	299.00	29.00	22.00	9.00	3.00
5	230.00	82.17%	0.00	0.00	0.00	3.00	189.00	20.00	18.00	0.00
6	541.00	74.31%	0.00	25.00	0.00	39.00	40.00	402.00	34.00	1.00
7	395.00	79.24%	0.00	0.00	0.00	4.00	31.00	36.00	313.00	11.00
8	132.00	88.64%	0.00	2.00	0.00	0.00	1.00	6.00	6.00	117.00
Total:	1,994.00									
Average:		84.57%								
Overall % Correct:		80.59%								

Table 16 lists the thresholds and percentages for each variable for each stream type from that tree, in general order of importance. Values in the table indicate the percent of stream reaches in each stream type for each variable range. The largest percentages are shown in a bold font, indicating the majority of stream reaches. From this table, the general characteristics of each stream type can be determined. For example, 98.5% of all stream reaches in stream type 3 have a flow permanence of greater than 14.16%, and this stream type has the highest flow permanence for Fort Bliss. Stream type 8 has the highest peak flows of all stream reaches, with 82.6% estimated to have peak flows greater than 544.3 m^3/s.

In general, stream types 1, 2 and 3 have the greatest amount of vegetation cover, most of which is between 0.5 - 1 m in height. These three stream types also have the greatest amount of vegetation between 1 – 4 m, and relatively higher slopes than the other stream types. Stream type 1 has 90.9% of reaches with more than 20.11% of vegetation between 1 – 4 m in height. Stream reaches in types 7 and 8 are the widest reaches, with the majority wider than 188.99 m. Most of the vegetation in stream types 4 through 8 is less than 4 m in height, and these stream reaches are less entrenched than reaches in stream types 1 to 3. Stream types 6, 7, and 8 are low elevation reaches.

Table 16. Fort Bliss thresholds for input variables, percent of each stream type for 8 stream types.

Stream Types	Flow Perm (%)		Peak Flow Qp25 (m3/s)				Veg <0.5 m (%)		Veg 1-4m (%)		
	<=14.16	>14.16	<=317.35	<=438.91	<=544.30	>544.30	<=82.93	>82.93	<=12.75	<=20.11	>20.11
1	**99.1**	0.9	**97.3**	1.8	0.9	0.0	**99.1**	0.9	3.6	5.5	**90.9**
2	**100.0**	0.0	**96.6**	2.7	0.7	0.0	**99.3**	0.7	**60.3**	30.8	8.9
3	1.5	**98.5**	**74.6**	0.0	3.0	22.4	**50.7**	49.3	**67.2**	9.0	23.9
4	**100.0**	0.0	**98.7**	1.3	0.0	0.0	4.8	**95.2**	**100.0**	0.0	0.0
5	**100.0**	0.0	**100.0**	0.0	0.0	0.0	0.0	**100.0**	**100.0**	0.0	0.0
6	**100.0**	0.0	**98.0**	1.7	0.4	0.0	10.2	**89.8**	**99.8**	0.2	0.0
7	**100.0**	0.0	**87.1**	7.3	3.8	1.8	2.8	**97.2**	**100.0**	0.0	0.0
8	**100.0**	0.0	5.3	3.0	9.1	**82.6**	13.6	**86.4**	**97.7**	2.3	0.0

Stream Types	RENDVI Mean (vegetation density)				RSI			Width 2m (m)		
	<=0.15	<=0.16	<=0.19	>0.19	<=0.19	<=0.22	>0.22	<=162.42	<=188.99	>188.99
1	0.9	2.7	26.4	**70.0**	**41.8**	30.0	28.2	**99.1**	0.0	0.9
2	12.3	14.4	**37.0**	36.3	**56.8**	43.2	0.0	**100.0**	0.0	0.0
3	4.5	7.5	35.8	**52.2**	32.8	**67.2**	0.0	**77.6**	3.0	19.4
4	3.8	7.2	**54.4**	34.6	6.4	**85.0**	8.6	**76.4**	7.2	16.4
5	**90.0**	6.5	3.5	0.0	30.0	**70.0**	0.0	**88.3**	8.3	3.5
6	**56.4**	20.0	22.7	0.9	42.5	**57.1**	0.4	**87.6**	5.9	6.5
7	**89.1**	9.1	1.8	0.0	15.7	**84.3**	0.0	9.4	8.9	**81.8**
8	**37.1**	11.4	34.1	17.4	28.8	**69.7**	1.5	34.8	7.6	**57.6**

Stream Types	ER 3m/05m		Percent Slope (%)						Veg 4-12m (%)		
	<=6.43	>6.43	<=2.85	<=3.07	<=8.56	<=11.07	<=23.72	>23.72	<=1.11	<=4.52	>4.52
1	**100.0**	0.0	1.8	0.0	**51.8**	7.3	25.5	13.6	8.2	13.6	**78.2**
2	**99.3**	0.7	1.4	7.5	**71.2**	10.3	9.6	0.0	**66.4**	30.1	3.4
3	**95.5**	4.5	34.3	3.0	**46.3**	4.5	9.0	3.0	**68.7**	11.9	19.4
4	**95.4**	4.6	**47.7**	6.7	37.3	5.1	3.2	0.0	**99.7**	0.3	0.0
5	**100.0**	0.0	**62.6**	6.5	30.9	0.0	0.0	0.0	**100.0**	0.0	0.0
6	**90.9**	9.1	34.8	4.4	**53.6**	3.1	4.1	0.0	**99.8**	0.2	0.0
7	**96.2**	3.8	**94.9**	2.0	3.0	0.0	0.0	0.0	**100.0**	0.0	0.0
8	**85.6**	14.4	**68.9**	5.3	23.5	0.0	2.3	0.0	**97.7**	1.5	0.8

Stream Types	Veg 0.5-1m (%)		Watershed Area (m2)		Elevation (m)			Veg. Cover (%)	
	<=3.23	>3.23	<=164494480	>164494480	<=1404.74	<=1466.43	>1466.43	<=51.65	>51.65
1	2.7	**97.3**	**100.0**	0.0	0.9	1.8	**97.3**	2.7	**97.3**
2	0.7	**99.3**	**100.0**	0.0	11.0	10.3	**78.8**	42.5	**57.5**
3	25.4	**74.6**	**91.0**	9.0	3.0	3.0	**94.0**	44.8	**55.2**
4	**62.5**	37.5	**100.0**	0.0	8.3	6.4	**85.3**	**50.7**	49.3
5	**95.7**	4.3	**100.0**	0.0	0.9	10.0	**89.1**	**100.0**	0.0
6	17.4	**82.6**	**100.0**	0.0	43.8	26.6	29.6	**97.0**	3.0
7	**75.2**	24.8	**100.0**	0.0	**65.6**	9.6	24.8	**100.0**	0.0
8	47.0	**53.0**	**77.3**	22.7	**40.9**	20.5	38.6	**81.1**	18.9

Special Conditions

Two conditions that we were not able to adequately describe with our methods are described here: discontinuous sheetflood zones, and springs.

Discontinuous Sheetflood Zones

Stream segments that terminate in playas or sand dunes, or are discontinuous sheetflood zones (vegetated swales), like those found at Fort Bliss or Fort Irwin, were difficult to delineate as a separate reach type using our methods. We are using the NHD Plus V2 flowline for our stream

network that delineates only those stream segments that could be defined in terms of flow direction, and this method generally did not include those terminal stream reaches in playas or dunes. However, in our analysis we restricted maximum stream width to 400 m (200 m on either side of the flowline) to confine the width of streams ending in those areas. Using ratios of our variables for water surface widths these terminal stream reaches may be identified, i.e. for the 3 m and 2 m inundations, the ratio will be 1 or close to 1. The best results would be achieved using a combination of ratios to avoid errors resulting from entrenched reaches that would also have a ratio of close to 1.

This method may also be used to identify discontinuous or vegetated swale stream reaches, which were often included in the NHD stream network. A concern with this method is that the NHD flowlines do not follow the drainages very well, and we used a relatively coarse 10 m DEM for the inundation depths at Forts Irwin and Bliss. Even with the stream line editing done for this project, it is still not adequate for creating highly accurate water surface widths. This issue needs further study, to include more careful streamline editing with LiDAR data, and using the LiDAR bare earth DEM in the inundation step. Experimenting with various depths and ratios could possibly identify the discontinuous sheetflood reaches or vegetated swales more accurately.

Springs

Fort Irwin contains numerous springs that are monitored regularly. While we were not able to delineate them as a separate stream type using our methods, we are able to identify them using the vegetation structure variables, 1-4 m and 4-12 m. When the springs fall on our stream network (the NHD Flowline), those stream reaches exhibit a higher percentage of vegetation in the taller height classes, and can be identified in this manner. The vegetation structure classification can also be used in general to identify stream reaches that contain a higher percentage of taller vegetation, indicating higher moisture content.

Wildlife Associations

The DoD manages a vast amount of arid and semi-arid land in their Southwest Region that contains mainly ephemeral or intermittent stream reaches. Although knowledge and understanding of how these systems function is slowly increasing, there is a general lack of knowledge regarding the interaction between arid and semi-arid ecosystem features and wildlife needs. Most research on stream systems focus on perennial streams, and most stream type classifications focus on a particular type of data such as hydrologic or vegetation. This project addresses these knowledge gaps by combining vegetation, geomorphic and hydrologic data to classify and describe ephemeral and intermittent stream reaches, and associates the results to wildlife habitat, resulting in a broader overview and understanding of these interactions.

These results address whether habitat for particular vertebrate wildlife species of concern is associated with particular stream reaches, using species distribution models that evaluated the use of streams by single species of concern. We also evaluated which ecohydrological variables

were associated with TER-S richness and whether stream types were good indicators of species richness.

Fort Irwin

At Fort Irwin, we modeled desert tortoise and burrowing owl occurrence in ephemeral and intermittent streams and tested their probability of occurrence in relation to stream type. We mapped species richness of riparian associated birds and mammals, and tested whether stream type was related to richness of these two groups. We mapped species richness of all riparian-associated TER-S, bird TER-S, mammal TER-S, and reptile TER-S, and tested whether stream type was related to richness of these groups. We modeled species richness of the TER-S groups as a function of ecohydrological variables to better understand why richness varied in stream reaches.

Desert Tortoise

This species was modeled with MaxEnt. Probability of presence predicted for desert tortoise with an unbiased prior was highly correlated with presence predicted by the biased prior incorporating distance from roads ($r = 0.996$, $p<0.001$). We report the modeling results for the unbiased prior.

When desert tortoise presence was modeled without a biased prior, seven variables were retained for the final model: riparian width (27.4% contribution, 15.4% permutation importance), elevation (24.1% contribution, 29.1% permutation importance), bank slope (24% contribution, 22.6% permutation importance), total stream power (15.7% contribution, 15.1% permutation importance), percent cover (3.6% contribution, 7.6% permutation importance), peak flow (3.2% contribution, 7.6% permutation importance),and RSI (2.1% contribution, 8.2% permutation importance). Higher probability of presence was generally related to elevations between 600 - 900m, RSI values near 0.225, and narrower riparian widths. Three variables showed a more threshold-like response: probability of presence dropped substantially once total stream power and peak flow exceeded zero, and probability of presence increased substantially once percent slopes exceeded about 5%. Generally, lower percent covers increased probability of presence, but percent cover below 5% was associated with low probability of presence (Figure 43).

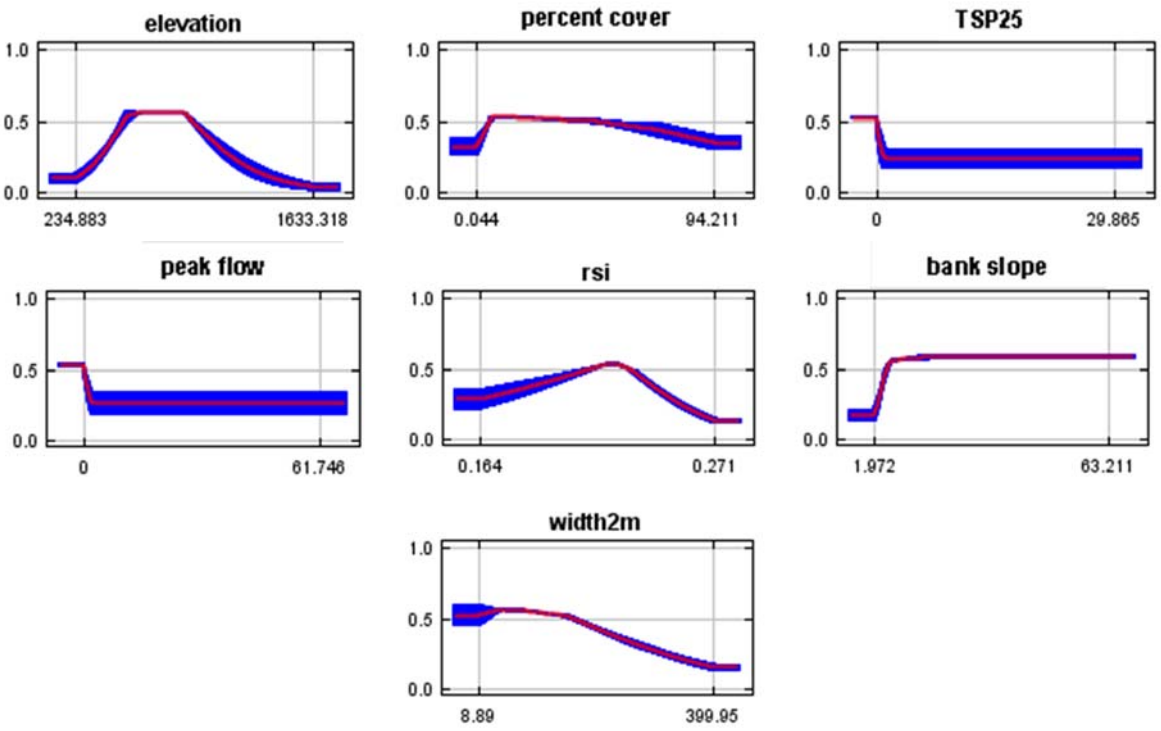


Figure 43. Probability of tortoise presence as a function of each individual variable. The x-axis shows the range of values of the variable, while the y-axis shows the resulting probability of presence when just that variable was used to predict presence.

The AUC value of the model was acceptable for the testing sets ($\mu = 0.728$, $s = 0.028$). Zero OR for the testing set was 0.03 ($s = 0.04$, expected mean of 0) and Ten OR for the testing set was 0.18 ($s = 0.10$, expected mean of 0.10).

Desert tortoise probability of presence was significantly correlated with average values in each stream reach for probability of presence predicted by the 1-km resolution USGS desert tortoise model (Nussear et al., 2009) (Figure 44). Correlation was slightly higher for the unbiased prior ($r = 0.42$, $p<0.001$) than the biased prior ($r = 0.38$, $p<0.001$). This is not surprising since the USGS model was not created with a biased prior. While Nussear et al. (2009) did not include how the variables in their final model affected probability of presence, three of the seven variables in their final model are similar to the ecohydrological variables in our final model. They included elevation, as did we. They included a measure of average surface roughness, which may relate to our bank slope measure. Lastly, they included a measure of perennial plant cover, which is likely very similar to our measure of percent cover derived from MSAVI2 values.

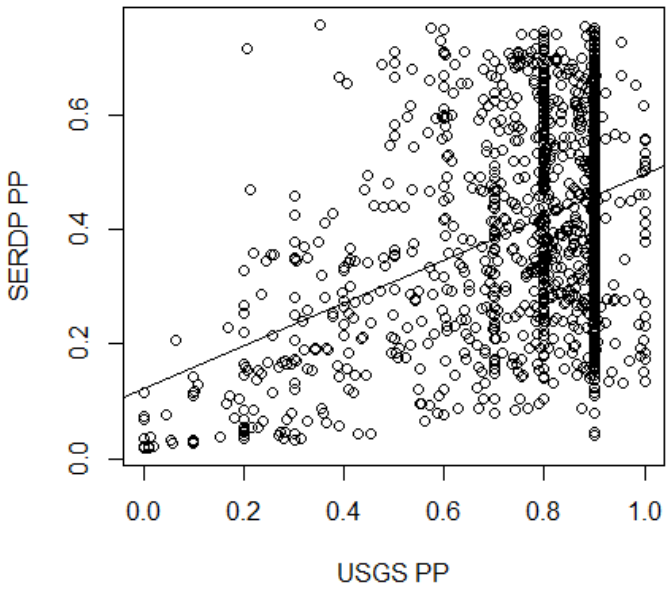


Figure 44. Correlation of desert tortoise probability of presence from our unbiased prior model (SEDRP model) and the USGS model.

A visual inspection of the results (Figure 45) shows that tortoise richness tends to be highest in mid-elevation streams. Probability of presence changes slightly in some streams when a biased prior is used, but is overall very similar across the installation. This model may help detect areas that are especially valuable for desert tortoise.

Desert tortoise probability of presence was not significantly different between stream types for either an unbiased prior or a biased prior. Stream types had about equal probability of tortoise presence; they were not a good predictor of where desert tortoises may occur.

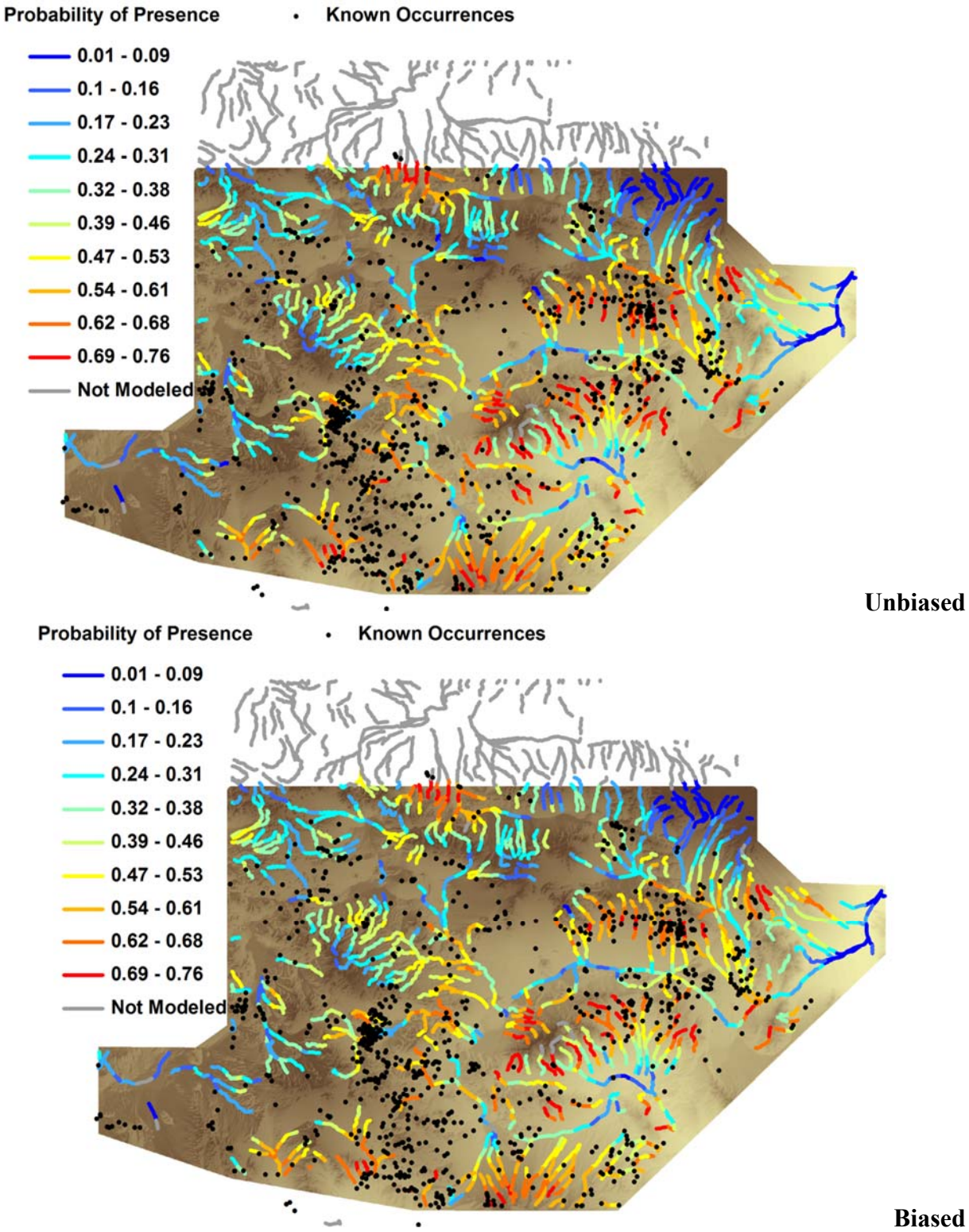


Figure 45. MaxEnt modeling results for the desert tortoise with an unbiased prior (top) and a biased prior (bottom).

Western Burrowing Owl

This species was modeled with MaxEnt. Probability of presence predicted for burrowing owl with an unbiased prior was highly correlated with presence predicted by the biased prior incorporating distance from roads (r = 0.995, p<0.001). We report the modeling results for the unbiased prior.

When burrowing owl presence was modeled without a biased prior, seven variables were retained for the final model: veg 1-4 m (21.4% contribution, 14.3% permutation importance), veg 4-12 m (19.8% contribution, 0.2% permutation importance), percent cover (14.6% contribution, 8.9% permutation importance), bank slope (14.1% contribution, 18.4% permutation importance), flow permanence (11.1% contribution, 26.1% permutation importance), percent slope (9.6% contribution, 19.6% permutation importance), and peak flow (9.3% contribution, 12.5% permutation importance). Higher probability of presence was associated with increasing percent cover of veg 1 - 4 m, veg 4 – 12 m, percent cover, and flow permanence (Figure 46). Probability of presence peaked sharply when bank slope was about 15% and more broadly when percent slope of the streamline was about 12%. Probability of presence was highest at the very lowest peak flow values and dropped rapidly once peak flow increased.

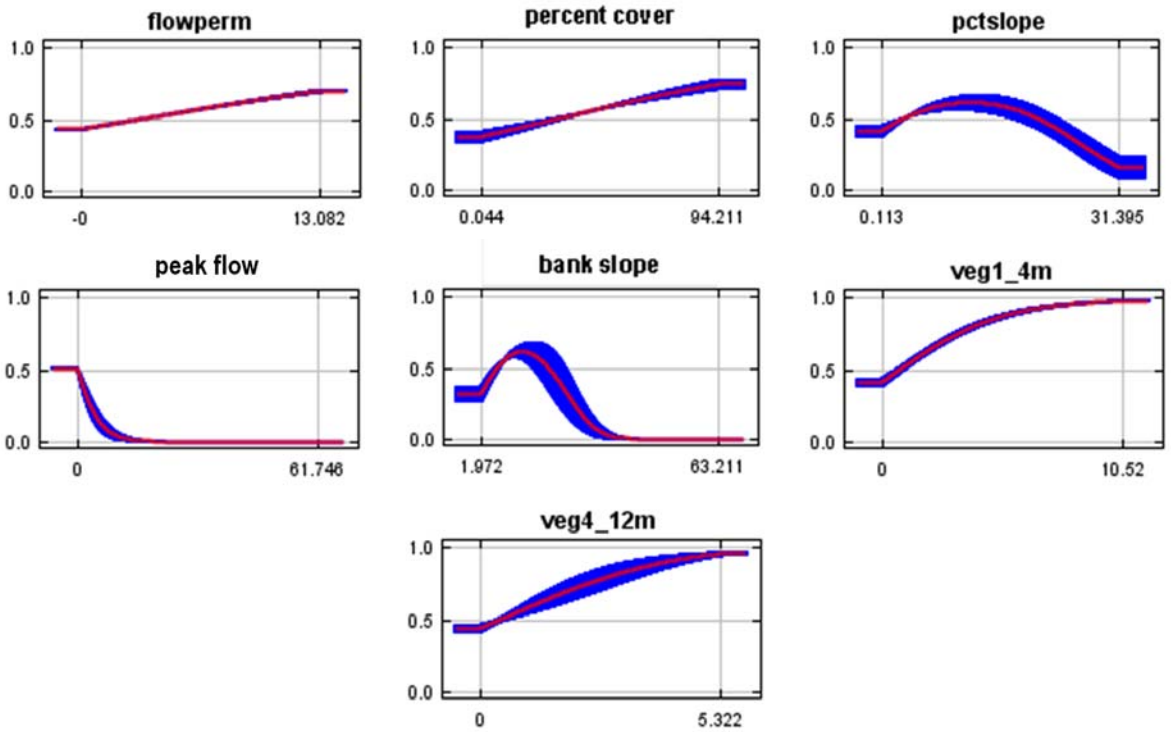


Figure 46. Probability of presence for burrowing owl as a function of each individual variable. The x-axis shows the range of values of the variable, while the y-axis shows the resulting probability of presence when just that variable was used to predict presence.

The AUC value of the model was acceptable for the testing sets (μ = 0.751, s = 0.069). Zero OR for the testing set was 0.06 (s = 0.07, expected mean of 0) and Ten OR for the testing set was 0.26 (s = 0.19, expected mean of 0.10).

A visual inspection of the results (Figure 47) shows that the best habitat for burrowing owls may cluster in several areas of the installation. Values for the biased prior are nearly identical with those for the unbiased prior.

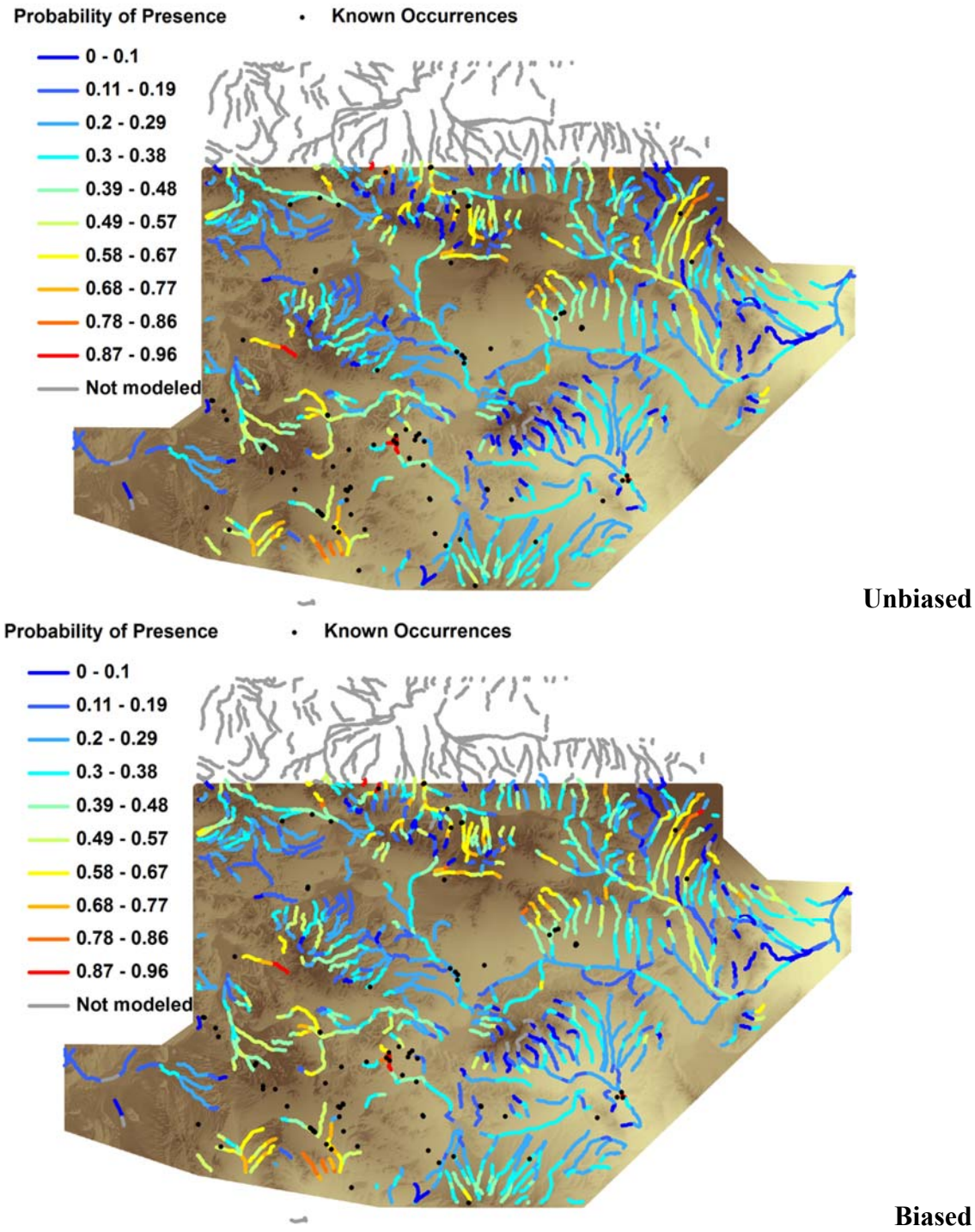


Figure 47. MaxEnt modeling results for the burrowing owl with an unbiased prior (top) and a biased prior (bottom).

Burrowing owl probability of presence was not significantly different between stream types for either an unbiased prior or a biased prior. Stream types had about equal probability of owl presence; they were not a good predictor of where burrowing owls may occur.

Desert tortoise and burrowing owl probability of presence were slightly, but significantly correlated with each for both the unbiased prior ($r = 0.22$, $p<0.001$, Figure 48) and the biased prior ($r = 0.21$, $p<0.001$).

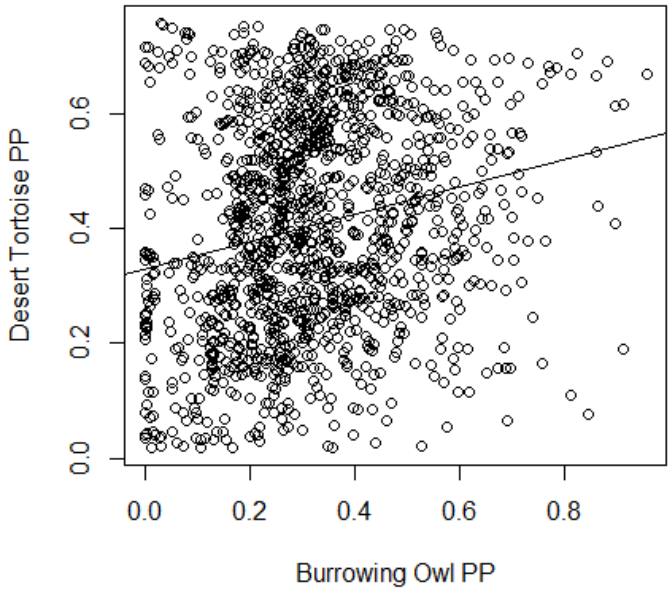


Figure 48. Correlation of desert tortoise and burrowing owl probability of presence for the unbiased prior model.

Geographic distribution of species richness

Fort Irwin was the least species rich installation, with a total of 242 possible species, 142 of which (59%) were riparian-associated (Appendix C, Table 2). For the riparian-associated species, models were available for 19 reptiles, 20 mammals, 72 birds, and no amphibians (there are three species of amphibians that could potentially occur on the installation, but none have ever been observed there).

For riparian-associated species, only bird and mammal richness were calculated. Bird and mammal richness were not correlated ($r = -0.22$). Richness of birds was often highest in mid-elevation reaches between the higher mountain reaches and the main valley drainages (Figure 49). Richness of mammals was often high in the higher mountain stream reaches, but did not follow a clear pattern geographically.

Fort Irwin had 32 potential TER-S: 21 birds, 7 mammals, and 4 reptiles (Appendix C, Table 3) for which models were available. For riparian-associated TER-S, bird, mammal, reptile, and pooled richness of the three groups were calculated. Pooled richness of all TER-S was correlated with reptile richness ($r = 0.73$). Richness of all TER-S species and TER-S reptiles was generally highest in stream reaches in the southeastern area of the installation (Figure 50). Bird richness for

TER-S followed a similar geographic pattern as all riparian-associated bird richness. TER-S mammal richness was generally highest in the highest elevation stream reaches, particularly in a mountainous area in the far eastern area of the installation.

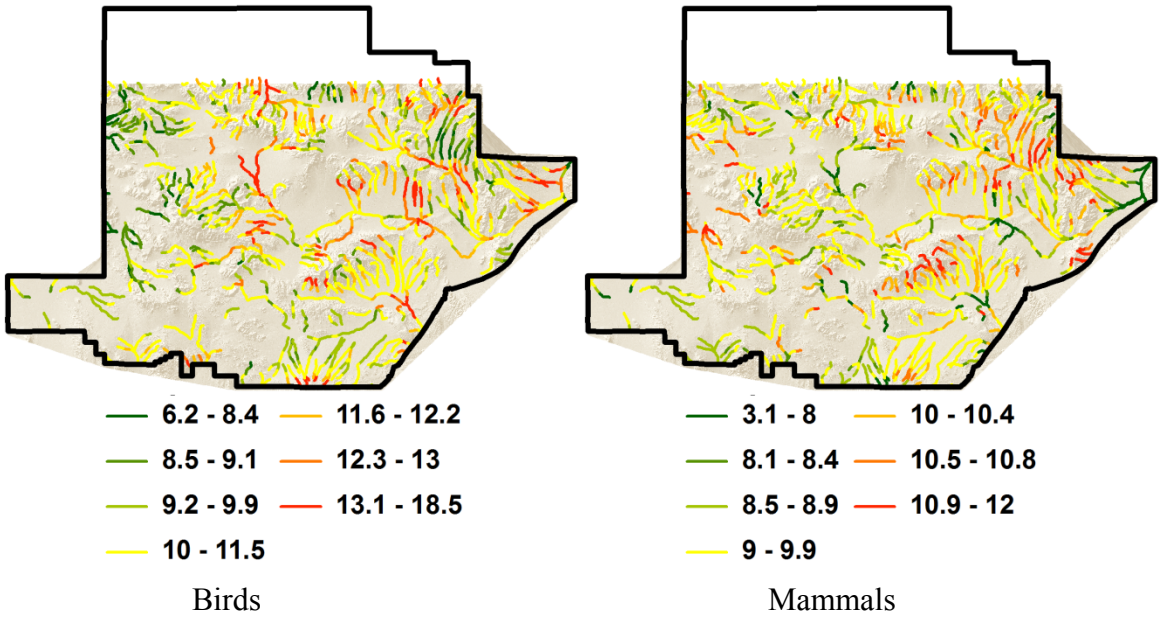


Figure 49. Fort Irwin - Richness of riparian-associated species.
Dark green reaches have a value less than 1.5 standard deviations (SD) below the mean value for the group, medium green reaches are 1-1.5 SD below the mean, light green are 0.5-1 SD below the mean, yellow are within 0.5 SD of the mean, light red are between 0.5-1 SD above the mean, medium red are 1-1.5 SD above the mean, and bright red are >1.5 SD above the mean.

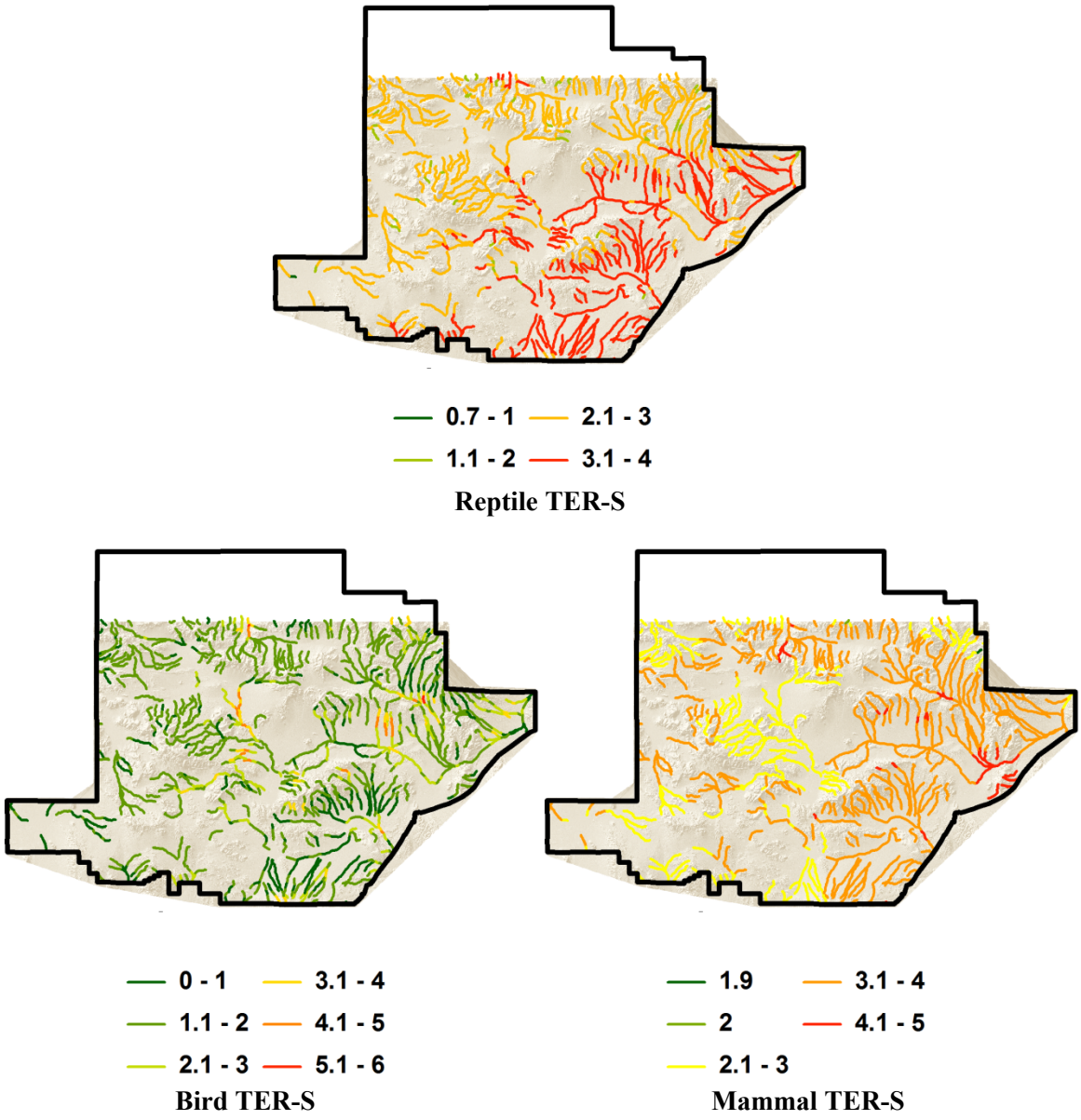


Figure 50. Fort Irwin - Richness of riparian-associated TER-S species.
Darker green reaches have lower richness, yellow have intermediate richness, and dark red have the highest richness.

Species richness and stream types

When the average riparian-associated species richness in each stream type was ranked, the distribution of bird richness into the stream types at Fort Irwin was not correlated with the distribution of mammal (r = -0.17) richness in stream types (Figure 51).

Stream type 1 – Moderately low bird richness and moderate mammal richness.

Stream type 2 – Moderate bird richness and moderately high mammal richness, significantly higher than in stream type 1.

Stream types 3, 4 & 5 – Moderately high bird richness, significantly higher than in stream type 1, moderately high mammal richness, significantly higher in stream types 3 and 5 than in stream type 1.

Stream types 6, 7 & 8 – Moderate to moderately high bird richness, significantly higher in stream type 8 than in stream type 1, and low to moderate mammal richness. Mammal richness is significantly lower in stream type 7 than in type 2 – 5.

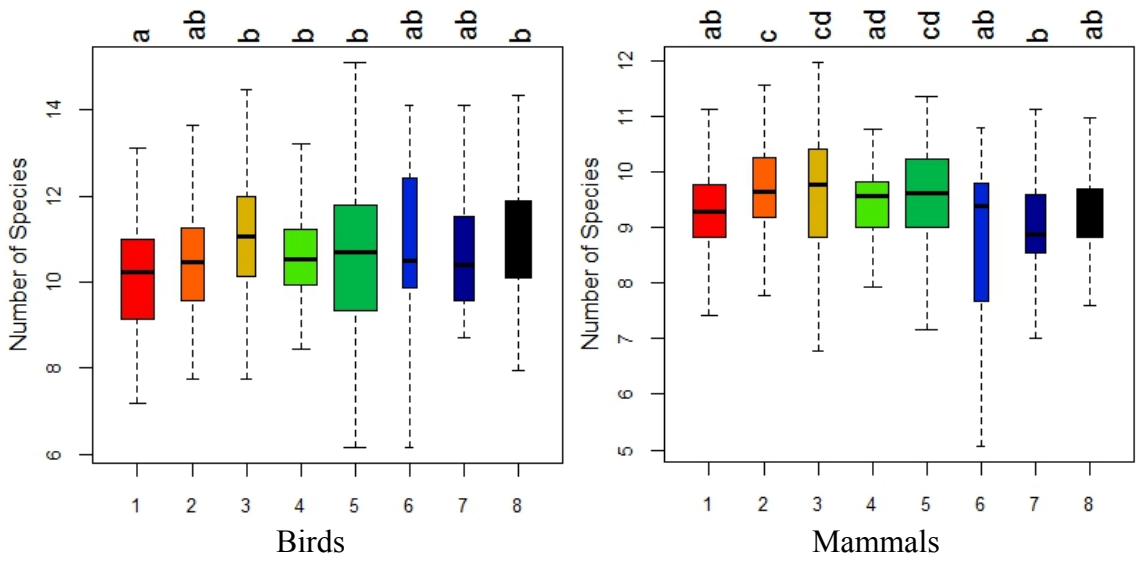


Figure 51. Fort Irwin - Richness of riparian-associated species in the eight stream types. Colors match those shown on stream type maps. Width is proportional to number of streams in each type.

When the average riparian-associated species richness of TER-S in each stream type was ranked, the distribution of pooled richness into the stream types at Fort Irwin was correlated with reptile ($r = 0.93$) and mammal ($r = 0.81$) richness. Mammal and reptile TER-S richness were somewhat correlated ($r = 0.62$). Richness of all TER-S, reptiles, and mammals shows very similar patterns within the stream types, with the highest richness in stream types 4 and 6, intermediate richness in stream types 5, 7, and 8, and the lowest richness in stream type 1. Bird richness for TER-S shows few differences between the stream types, with higher average richness in types 3 and 8 than in type 4 (Figure 52).

Stream type 1 – Low overall and reptile TER-S richness, low bird richness, and low mammal richness.

Stream types 2 & 3 – Low overall and reptile TER-S richness in stream type 2 to moderate richness in stream type 3, low bird richness in stream type 2, moderate bird richness in stream type 3 that is significantly higher than in type 4, and moderate mammal richness, significantly higher in stream type 2 and in type 1.

Stream types 4 & 6– Significantly higher overall and reptile TER-S richness than any other stream types, low to moderate bird richness, and high mammal richness, along with stream type 5, significantly higher than in any other stream type but 8.

Stream types 5, 7 & 8 – Moderate to high overall and reptile TER-S richness, with a few stream reaches having the highest values for overall richness on the installation, moderate bird richness in stream types 5 and 7, moderately high bird richness in stream type 8, significantly greater than in stream type 4, and moderately high mammal richness, significantly higher than in stream type 1 but significantly lower than in stream type 4.

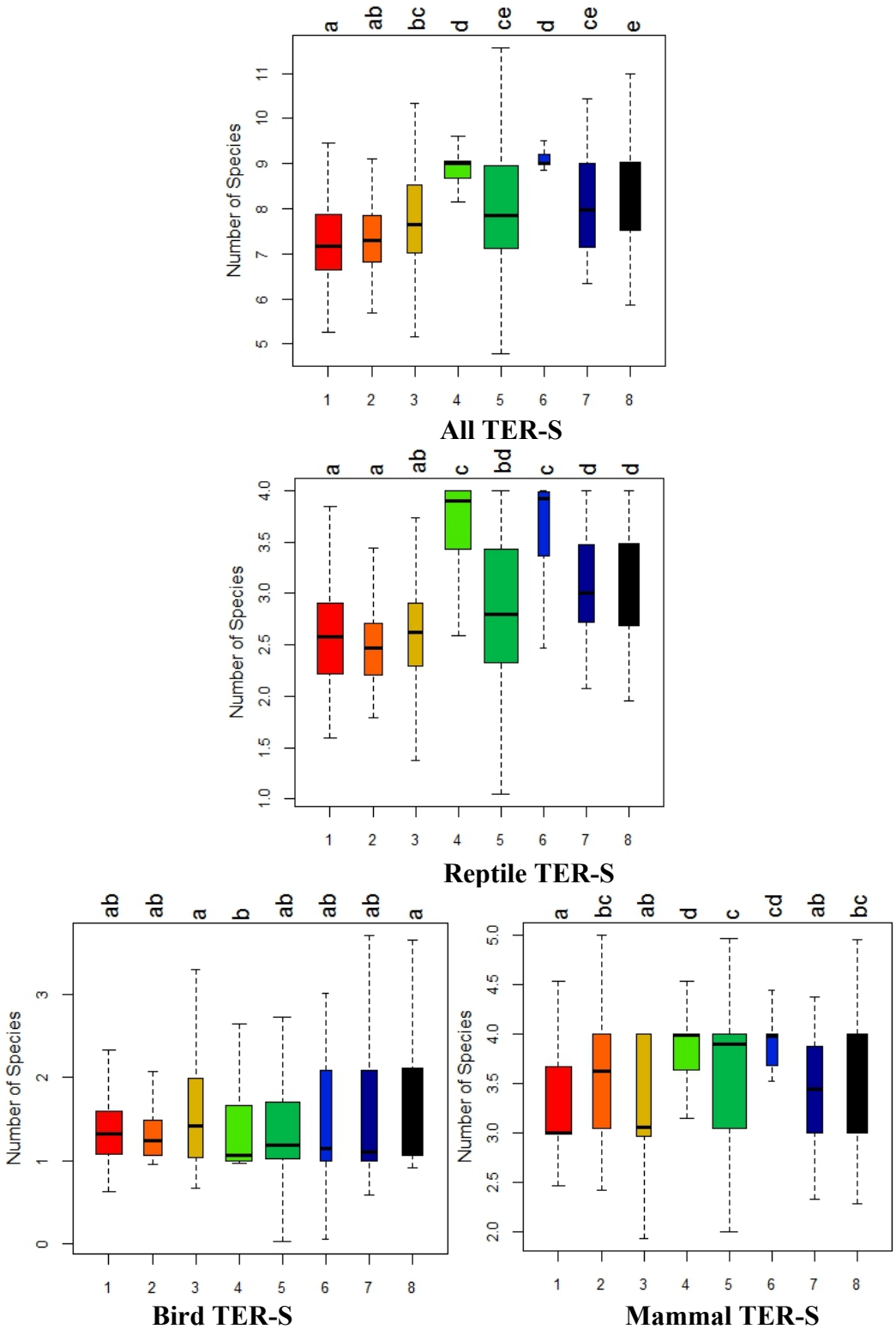


Figure 52. Fort Irwin - Richness of riparian-associated TER-S in the eight stream types. Colors match those shown on stream type maps. Width is proportional to number of streams in each type.

In individual stream reaches, richness of general riparian-associated species was correlated with richness of TER-S for birds ($r = 0.79$), but less strongly for mammals ($r = 0.56$) At Fort Irwin, planning management for the general riparian-associated bird group should benefit TER-S bird richness also, and vice versa. It is less clear whether this would be true for mammals. The correlation held for birds when the average species richness in each stream type was examined, but not for mammals.

TER-S response to ecohydrological variables

When pooled TER-S richness was modeled as a function of the ecohydrological variables, the largest effect was that of elevation (Table 17). Higher elevations caused species richness to decrease. The mean vegetation index value had the second largest effect; higher values of it also tended to decrease species richness, indicating the TER-S richness at Irwin is higher in less dense vegetation. Percent cover also had a large effect, but increased richness, indicating TER-S richness may be higher in reaches with more, but low density, vegetation.

Table 17. Fort Irwin - Effect of ecohydrological variables on all pooled TER-S riparian-associated species richness.

Parameter	*Effect Size*	*Relative Effect Size*	*SE*	95% Confidence Interval		*Relative Importance*
				Lower	*Upper*	
LidElevMidPts	-1.55	35.9	0.09	-1.57	-1.54	1.00
msavi2_mean	-0.64	14.7	0.10	-0.65	-0.63	1.00
msavi2_pct	0.45	10.3	0.10	0.43	0.46	1.00
FlowPerm	0.34	7.8	0.06	0.33	0.34	1.00
Width2m	-0.32	7.5	0.06	-0.33	-0.31	1.00
veg0_025m	-0.29	6.7	0.06	-0.30	-0.28	1.00
RSI	-0.29	6.6	0.08	-0.30	-0.28	0.99
CumArea	-0.16	3.6	0.06	-0.16	-0.15	0.87
ER3m_05m	0.14	3.3	0.05	0.14	0.15	0.86
veg4_12m	-0.08	1.9	0.05	-0.09	-0.08	0.35
Qp25	-0.07	1.6	0.05	-0.08	-0.06	0.24

When reptile TER-S richness was modeled as a function of the ecohydrological variables, the largest effect was again that of elevation (Table 18). Higher elevations caused species richness to decrease. The RSI value had the second largest effect; higher values of it also tended to decrease species richness, indicating the TER-S richness at Irwin is higher where rainfall is more evenly spread throughout the year. Percent of the stream reach with vegetation 0-0.25 m also had a substantial effect, decreasing richness, indicating TER-S richness may be higher in reaches with a higher percent cover of vegetation >0.25 m.

Table 18. Fort Irwin - Effect of ecohydrological variables on reptile TER-S riparian-associated species richness.

Parameter	*Effect Size*	*Relative Effect Size*	*SE*	95% Confidence Interval		*Relative Importance*
				Lower	*Upper*	
LidElevMidPts	-1.15	48.5	0.04	-1.16	-1.14	1.00
RSI	-0.27	11.4	0.04	-0.28	-0.27	1.00
veg0_025m	-0.22	9.2	0.03	-0.22	-0.21	1.00
veg4_12m	-0.13	5.6	0.03	-0.14	-0.13	1.00
CumArea	-0.12	5.0	0.03	-0.12	-0.12	1.00
msavi2_pct	0.10	4.2	0.04	0.09	0.10	0.74
msavi2_mean	0.07	2.8	0.05	0.06	0.07	0.37
Qp25	-0.06	2.7	0.03	-0.07	-0.06	0.76
Width2m	-0.06	2.5	0.03	-0.06	-0.06	0.64
ER3m_05m	0.04	1.6	0.03	0.03	0.04	0.37
Q25TSP	-0.04	1.6	0.04	-0.04	-0.03	0.31
PCTSlope	-0.03	1.4	0.04	-0.04	-0.03	0.22
FlowPerm	0.03	1.4	0.03	0.03	0.04	0.26
veg1_4m	-0.03	1.1	0.03	-0.03	-0.02	0.23
veg025_1m	-0.02	0.9	0.03	-0.03	-0.02	0.21

When bird TER-S richness was modeled as a function of the ecohydrological variables, the largest effect was that of the mean MSAVI2 value (Table 19). Higher values caused species richness to decrease, indicating the bird TER-S richness at Irwin is higher in less dense vegetation. Flow permanence had the second largest effect; higher values of it tended to increase species richness. RSI and elevation also had substantial effect sizes. Higher values of both variables were associated with increased bird richness.

Table 19. Fort Irwin - Effect of ecohydrological variables on bird TER-S riparian-associated species richness.

Parameter	*Effect Size*	*Relative Effect Size*	*SE*	95% Confidence Interval		*Relative Importance*
				Lower	*Upper*	
msavi2_mean	-0.26	16.6	0.06	-0.27	-0.25	0.99
FlowPerm	0.24	15.5	0.04	0.24	0.25	1.00
RSI	0.17	10.7	0.06	0.16	0.18	0.73
LidElevMidPts	0.16	10.4	0.07	0.15	0.17	0.62
Width2m	-0.15	9.8	0.05	-0.16	-0.15	0.94
veg025_1m	-0.11	7.3	0.05	-0.12	-0.11	0.67
veg4_12m	0.11	7.3	0.04	0.11	0.12	0.87
Q25TSP	0.09	6.0	0.05	0.09	0.10	0.65
msavi2_pct	0.06	3.9	0.08	0.05	0.07	0.28
CumArea	0.06	3.7	0.05	0.05	0.06	0.36
veg1_4m	0.05	3.3	0.09	0.04	0.06	0.36
Qp25	-0.05	3.0	0.05	-0.05	-0.04	0.29
veg0_025m	0.02	1.5	0.05	0.02	0.03	0.25
ER3m_05m	0.02	1.0	0.04	0.01	0.02	0.27

When mammal TER-S richness was modeled as a function of the ecohydrological variables, the largest effect was that of elevation (Table 20). Higher elevations caused species richness to decrease. The mean vegetation index value had the second largest effect; higher values of it also tended to decrease species richness, indicating that mammal TER-S richness at Irwin is higher in less dense vegetation. Percent cover also had a large effect, but increased richness, indicating TER-S richness may be higher in reaches with more, but low density, vegetation. The ecohydrological variables with the largest effect on TER-S mammal richness were essentially the same as for all TER-S richness.

Table 20. Fort Irwin - Effect of ecohydrological variables on mammal TER-S riparian-associated species richness.

Parameter	*Effect Size*	*Relative Effect Size*	*SE*	95% Confidence Interval		*Relative Importance*
				Lower	*Upper*	
LidElevMidPts	-0.57	25.4	0.04	-0.57	-0.56	1.00
msavi2_mean	-0.36	16.0	0.05	-0.36	-0.35	1.00
msavi2_pct	0.31	13.8	0.05	0.30	0.31	1.00
RSI	-0.17	7.4	0.04	-0.17	-0.16	1.00
veg1_4m	0.12	5.3	0.04	0.11	0.12	0.96
veg4_12m	-0.11	4.9	0.03	-0.11	-0.11	1.00
CumArea	-0.10	4.3	0.03	-0.10	-0.09	0.99
Width2m	-0.10	4.3	0.04	-0.10	-0.09	0.93
ER3m_05m	0.09	4.1	0.03	0.09	0.10	0.99
FlowPerm	0.09	3.9	0.03	0.08	0.09	0.98
veg0_025m	-0.08	3.7	0.03	-0.09	-0.08	0.85
PCTSlope	0.06	2.8	0.04	0.06	0.07	0.61
veg025_1m	-0.04	1.7	0.06	-0.05	-0.03	0.35
Qp25	-0.03	1.2	0.02	-0.03	-0.02	0.40
Q25TSP	-0.02	1.1	0.03	-0.03	-0.02	0.32

There are several variables that had a large effect on the species richness of multiple TER-S taxa groups. Elevation was one of the largest effects for mammals and reptiles and the fourth largest effect for birds, with a relative variable importance of 10 – 49%. Higher elevations were associated with decreased richness of mammals and reptiles, but increased richness of birds. Mean vegetation index value was one of the top two largest effects for mammals and birds, with a relative variable importance of 16 – 17%. Higher values were associated with decreased richness for both groups. RSI was one of the four largest effects for all groups, with a relative variable importance of 7 – 11%. Higher values were associated with decreased richness of mammals and reptiles, but increased richness of birds.

YPG

At Yuma Proving Ground, we modeled species richness of bosques and overall relative abundance of vertebrates, birds, mule deer, and kit fox in bosques with camera-trapping data provided by the Arizona Game and Fish Department. We mapped species richness of all riparian-associated species, riparian associated birds, passage migrant birds, mammals, reptiles, and amphibians, and tested whether stream type was related to richness of these groups. We mapped species richness of all riparian-associated TER-S, TER-S birds, TER-S mammals, TER-S reptiles, and TER-S amphibians, and tested whether stream type was related to richness of these groups. We modeled species richness of the TER-S groups as a function of ecohydrological variables to better understand why richness varied in stream reaches.

Mesquite Bosques

For each species richness predictor tested separately, p-values < 0.3 are reported in Table 21. No variables were found to be significant on their own for Chao1 or JK1, though the percent of area within 500 m classified as bosque was marginally significant at p = 0.10. Nexrad flow permanence (NexradFP) was marginally significant at p = 0.10 for JK1. The percent of area within 500 m classified as bosque and the number of bosques within 500 m were significant (p <0.05) predictors of JK2. The percent of area within 250 m classified as bosque, the number of bosques within 250 m, and the Nexrad flow permanence were marginally significant (0.05<p<0.1) for JK2. The peak flow of the 10-yr storm was also marginally significant (p=0.2).

Table 21. YPG – Mesquite bosques P-values <0.3 from poisson GLM for predictor variables as a function of species richness estimators. Values 0.2-0.3 are in gray.

Predictor	Chao1	JK1	JK2
Area			0.19
Cm % >0.2m	0.24	0.25	
Cm % >1m			
Cm % >2m			
Cm % >3m			
Cm % >4m			
Cm % >5m		0.22	0.22
% 0.2-1 m			
% 1-2 m	0.25	0.28	
% 2-3 m			
% 3-4 m			
% 4-5 m			
10-yr Peak Flow			0.20
NexradFP	0.25	0.18	0.07
% Cover Bosques w/i 250m	0.20	0.23	0.07
% Cover Bosques w/i 500m	0.10	0.10	0.05
% Cover Bosques w/i 1000m			
# Bosques w/i 250m		0.20	0.06
# Bosques w/i 5000m			0.05
# Bosques w/i 1000m			

The top models (Table 22, Table 23, Table 24) for all three species richness estimators all included the percent of vegetation reaching 2-3 m and the percent cover in the bosque of vegetation above 5 m (Cm % >5m). The effect of Cm % >5m on species richness was negative and the largest effect for all three response variables (-0.83 to -0.95). The effect of % 2-3 m on species richness was positive and nearly equal to that of Cm % >5 m for all three response variables (0.72 - 0.85). Percent cover of bosques within 500 m (% Cover Bosques w/i 500m) was an important predictor for Chao1 and JK2, with a relative importance comparable to Cm % >5 m and % 2-3 m, but a smaller effect size of about 0.28. The number of bosques within 500 m (# Bosques w/i 500m) and flow permanence (NexradFP) were also important predictors for JK2, with positive effects on species richness. Chao1 was positively affected by the total amount of vegetation (Cm % >0.2m), but this variable was less important than others in the top set of models.

Table 22. Effect of each parameter on the species richness estimator, JK1.

			95% Confidence Interval		
Parameter	*Estimate*	*SE*	*Lower*	*Upper*	*Relative Importance*
(Intercept)	2.49	0.08	2.44	3.90	
Cm % >5 m	-0.95	0.34	-1.15	-0.75	0.74
% 2-3 m	0.85	0.33	0.66	1.04	0.69

Table 23. Effect of each parameter on the species richness estimator, JK2.

			95% Confidence Interval		
Parameter	*Estimate*	*SE*	*Lower*	*Upper*	*Relative Importance*
(Intercept)	2.57	0.09	2.52	2.62	
% Cover Bosques w/i 500m	0.29	0.18	0.19	0.40	0.31
# Bosques w/i 500m	0.29	0.19	0.18	0.40	0.32
Cm % >5 m	-0.83	0.38	-1.04	-0.61	0.28
% 2-3 m	0.72	0.36	0.51	0.93	0.23
NexradFP	0.27	0.19	0.16	0.38	0.24

Table 24. Effect of each parameter on the species richness estimator, Chao1.

			95% Confidence Interval		
Parameter	*Estimate*	*SE*	*Lower*	*Upper*	*Relative Importance*
(Intercept)	2.45	0.10	2.40	2.51	
Cm % >5 m	-0.85	0.40	-1.08	-0.62	0.31
% 2-3 m	0.80	0.39	0.58	1.02	0.27
% Cover Bosques w/i 500m	0.27	0.19	0.16	0.38	0.24
Cm % >0.2 m	0.22	0.21	0.10	0.34	0.16

The top models for overall wildlife abundance showed that area of the bosque and percent of the bosque with vegetation reaching 3-4 m (% 3-4 m) had a positive effect, while the amount of vegetation over 5 m had a negative effect (Table 25). All three variables were equally important. Cm % >5m had the greatest effect (-1.48), followed by % 3-4m (1.24) and Area (0.96).

Table 25. Effect of each parameter on the overall RAI.

			95% Confidence Interval		
Parameter	*Estimate*	*SE*	*Lower*	*Upper*	*Relative Importance*
(Intercept)	3.70	0.05	3.67	3.73	
Area	0.96	0.07	0.92	1.00	1
Cm % >5 m	-1.48	0.21	-1.60	-1.36	1
% 3-4 m	1.24	0.20	1.13	1.36	1

The top models for overall bird abundance showed that flow permanence of the nearest stream (NexradFP) and the percent of the bosque with vegetation reaching 1-2 m (% 1-2m) had a positive effect, while 10-yr peak flow of the nearest stream (10-yr Peak Flow), the number of bosques within 1000 m, and the amount of vegetation over 5 m had a negative effect (Table 26). Percent 1-2m, NexradFP, and 10-yr Peak Flow were the three most important variables with the largest effect sizes.

Table 26. Effect of each parameter on the bird RAI.

			95% Confidence Interval		
Parameter	*Estimate*	*SE*	*Lower*	*Upper*	*Relative Importance*
(Intercept)	2.79	0.09	2.74	2.85	
NexradFP	2.19	0.37	1.98	2.40	0.69
10-yr Peak Flow	-1.71	0.34	-1.91	-1.51	0.69
% 1-2 m	1.61	0.20	1.49	1.72	1.00
Cm % >5 m	-1.20	0.24	-1.34	-1.07	0.31
# Bosques w/i 1000m	-0.53	0.13	-0.61	-0.46	0.31

For mule deer (Table 27), the top models showed that the peak flow of the 10 year storm in the nearest stream and the number of bosques within 1000 m had a positive effect on relative abundance. These two variables had equal importance, with number of bosques within 1000 m having a slightly larger effect size (1.06 versus 0.85). The percent cover of bosques within 1000 m was nearly equal in importance to the other two predictors, but it had a smaller and negative effect (-0.71) on mule deer relative abundance.

Table 27. Effect of each parameter on the mule deer RAI.

Parameter	Estimate	SE	95% Confidence Interval		Relative Importance
			Lower	Upper	
(Intercept)	2.69	0.08	2.64	2.73	
10-yr Peak Flow	0.85	0.14	0.77	0.93	1.00
# Bosques w/i 1000m	1.06	0.21	0.94	1.18	1.00
% Cover Bosques w/i 1000m	-0.71	0.20	-0.82	-0.59	0.97

Kit fox relative abundance (Table 28) was positively associated with the percent cover of bosques within 250 m and negatively associated with the amount of vegetation over 2 m. The two predictor variables were equal in importance, but the effect of Cm % >2m (-4.43) was nearly twice that of % Cover Bosques w/i 250m (2.35).

Table 28. Effect of each parameter on the kit fox RAI.

Parameter	Estimate	SE	95% Confidence Interval		Relative Importance
			Lower	Upper	
(Intercept)	0.15	0.50	-0.13	0.44	
Cm % > 2 m	-4.43	1.23	-5.14	-3.73	1.00
% Cover Bosques w/i 250m	2.35	0.45	2.09	2.61	1.00

The top models for all three species richness estimators all included the percent of vegetation reaching 2 - 3 m and the percent cover in the bosque of vegetation above 5 m. Both Chao1 and JK2 were also predicted by the percent cover of bosques within 500 m. The similarity in the results from the three estimators is strong evidence that these three characteristics of bosques are quite important to wildlife. It is not surprising that the percent of the bosque with vegetation reaching 2 - 3 m is important to species richness.

A number of studies have found that vertebrate species richness increases with increasing structural diversity (e.g. Vale et al. 1989, Goetz et al. 2014). The 2 - 3% layer represents where the vegetation becomes taller than is typically found in the surrounding desert scrub, and higher layers > 3 m have decreasing amounts of cover, so this layer probably does a good job of representing the increased structural diversity of the bosques. The presence of more bosques within 0.5 km is reasonable, too, because it should support the presence of species that are more reliant on the unique environments bosques provide, increasing species richness. The upper vegetation layer (5-7 m) had a negative relationship to species richness, which is less easily explainable. This vegetation layer does not occur in over half of the bosques modeled and is very rare in the ones in which it occurs. The tallest trees may serve as hunting perches for raptors, who in turn deter other species, or it could be a proxy for a variable I did not consider.

It seems reasonable that overall wildlife abundance is higher in larger bosques. Larger bosques provide more area for more individual home ranges. Bosques with a higher percent of their area with vegetation reaching 3-4 m was another important variable, most likely for similar reasons that the percent cover of vegetation reaching 2-3 m had a positive effect on species richness. As

with species richness, the percent cover in the bosque of vegetation above 5 m had a negative effect on relative abundance of wildlife.

Bird abundance appears to be higher in bosques with more vegetation reaching 1-2 m, which suggests this vegetation layer is heavily used by the species at YPG for roosting or nesting. This also fits with the finding that breeding bird density is positively associated with vegetation volume (Mills et al. 1991). The fact that higher flow permanence is associated with greater abundance could be caused by these bosques remaining a bit moister and cooler, making them an important refuge in this hot, dry climate. Areas with higher flow permanence might also have more fruit on their shrubs and more forage in general, providing food for more individuals. Ten-year peak flows of the nearest stream had a negative effect on bird relative abundance. Areas that experience higher peak flows may have less mature vegetation to provide food and shelter. Once again, the percent cover in the bosque of vegetation above 5 m had a negative effect on relative abundance of birds. The number of bosques within 1 km having a negative effect on bird abundance is unexpected. This is one of the less important variables, and has only a quarter to one half of the effect of the other variables. One possible explanation is that in areas with few bosques, many birds that have their home ranges in the surrounding desert scrub congregate in isolated bosques for specific habitat values it provides, while in areas with more bosques, birds have more places spread out into to seek these values, resulting in a lower numbers of birds per bosque. Alternatively, its smaller effect and importance could indicate it is a spurious variable that would not be supported if the sample size was larger.

Mule deer in the King Valley in the adjacent Kofa National Wildlife Refuge use xeroriparian habitat in washes almost exclusively because they provide more food, cover, and travel corridors than adjacent uplands (Krausman et al., 1985). The bosques in this study have a very similar composition, and while they lack obvious stream channels, many are in fact along drainage routes. Bosques are essentially xeroriparian habitat. This information about mule deer habitat corresponds well to the finding that mule deer abundance is positively affected by the number of bosques within 1 km. More patches within the area should also increase their utility as travel corridors. The 1 km distance band seems appropriate for a larger animal with bigger home range size. Unlike birds, mule deer abundance is positively associated with 10-yr peak flows. Bosques with larger peak flows may have more clearings in underbrush that increase ease of movement for these larger animals. The negative effect of percent cover of bosques within 1 km on mule deer abundance is puzzling, but in conjunction with their greater abundance where more bosques are found, could mean areas with higher numbers of small bosques are ideal for supporting mule deer populations. These areas would have shorter average distances between bosques, decreasing travel distances and making it easier for deer to stay in their preferred habitat.

The percent cover of vegetation >2 m had a very strong negative effect on relative abundance of kit fox. While kit foxes use bosques, they avoid those with much tall vegetation cover. This result is supported by the fact that kit foxes are primarily animals of open desert, shrub, or shrub-grass environments (NatureServe, 2014). Since kit foxes spend much of their time in burrows, which are usually well hidden by thick brush (Meaney et al., 2006), denning may be one way in which they use bosques. It is interesting that they preferred bosques with a higher percent cover of other bosques within 250 m. Higher percent cover of bosques most likely corresponds to higher prey availability for kit foxes, since their rodent prey reaches its highest density in mixed

riparian scrub (Kepner, 1978). However, the 250 m distance is surprising. A 250 m radius circle has an area of only ~0.2 km^2, while typical home range size for kit fox ranges from >2 km^2 (O'Neal et al., 1987) in Utah to > 12 km^2 in habitat in western Arizona similar to YPG (Zoellick and Smith, 1992). The smaller number here could just mean kit foxes prefer to hunt where travel distances are short, or the bosques could be core-use areas for them.

While species richness estimators are a sound approach to analyzing this camera data, relative abundance indices (RAIs) are not generally recommended for analysis of camera data because there is no way to separate detection probability from the actual probability of an animal being present. We have presented our interpretations of the model results, but the results for overall, bird, mule deer, and kit fox RAI should be viewed with caution. We are optimistic about the results because many of them fit with what is known about the ecology of the groups or species, but some of these could just be a due to detection probability differences, rather than real differences in abundance.

Geographic distribution of species richness

Yuma Proving Ground had with a total of 315 possible species, 195 of which (62%) were riparian-associated (Appendix C, Table 2). For the riparian-associated species, models were available for 34 reptiles, 34 mammals, 94 birds, and 6 amphibians. Pooled richness of all riparian-associated species was correlated with richness of birds (r = 0.75), mammals (r = 0.65), and reptiles (r = 0.65), but not amphibians or passage migrant birds. Pooled richness, mammal richness, and bird richness was greatest in many of the higher elevation areas on the Cibola Range and the East Arm (Figure 53), though bird richness was not high in all mountainous areas or most of the East Arm. None of the richness values for the taxa-specific groups were correlated with each other. Richness of passage migrant birds was highest in stream reaches of the East Arm and scattered reaches elsewhere, particularly in some stream reaches close to the Gila River, just south of the installation. Most of the streams on the installation might provide habitat for 3-5 amphibian species, but richness was typically lower in the highest elevations.

Yuma Proving Ground had 57 potential TER-S: 1 amphibian (Colorado River toad, *Incilius alvarius*), 29 birds, 17 mammals, and 10 reptiles (Appendix C, Table 3). For TER-S richness, pooled richness of all species was not correlated with richness of any taxa-specific group. Pooled richness of all TER-S species was not distributed across the installation with any clear pattern (Figure 54), but values tended to be somewhat higher in lower elevation stream reaches. Reptile richness was highest in the East Arm and streams draining south into the Gila River. Mammal richness tended to be grouped by watershed. Bird TER-S richness was relatively uniform across the installation. Because there was only one amphibian TER-S, the values for mean TER-S richness for that group actually represent the percent of each stream reach that had habitat modeled for that species.

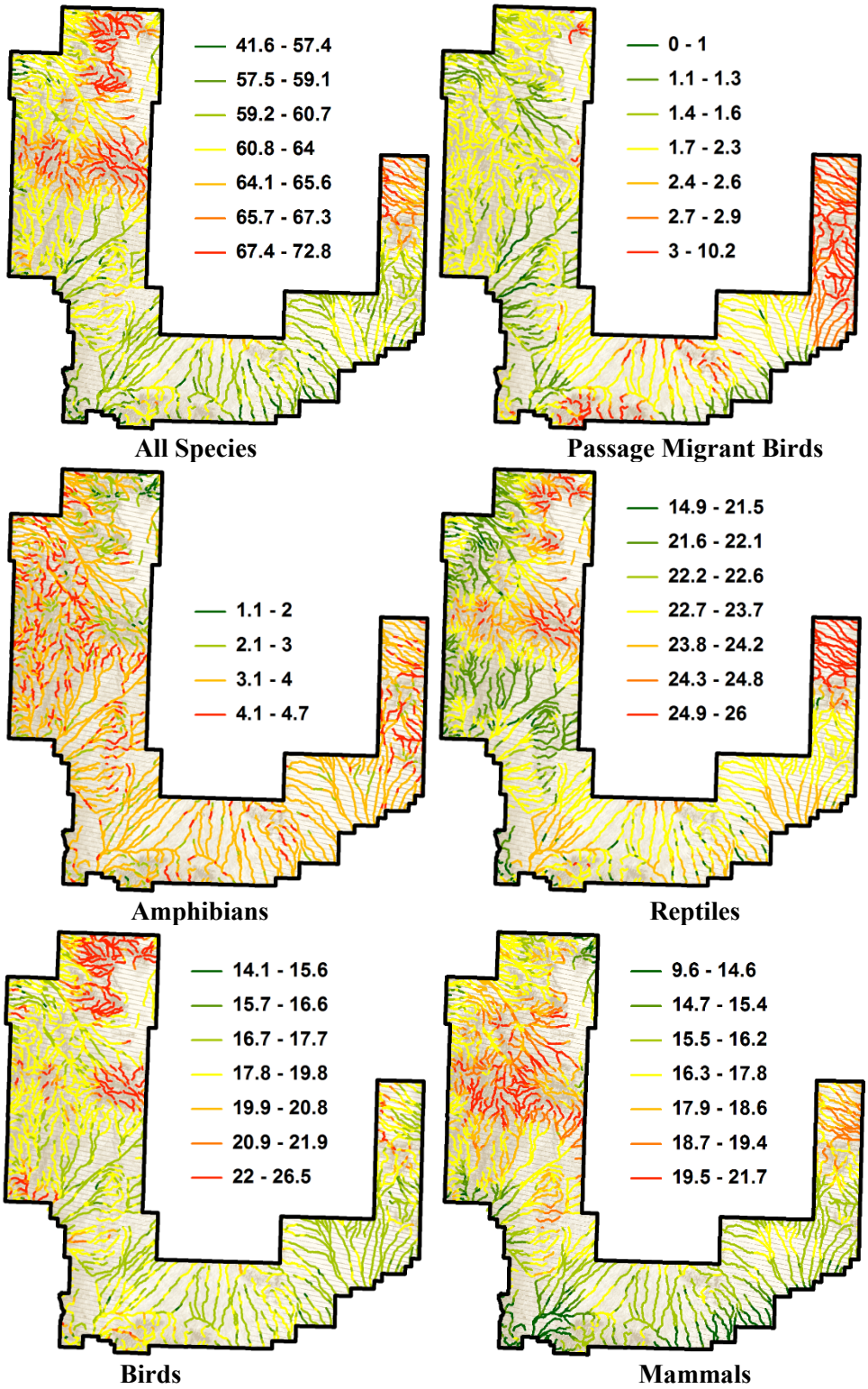


Figure 53. YPG - Richness of riparian-associated species.
Dark green reaches have a value less than 1.5 standard deviations (SD) below the mean value for the group, medium green reaches are 1-1.5 SD below the mean, light green are 0.5-1 SD below the mean, yellow are within 0.5 SD of the mean, light red are between 0.5-1 SD above the mean, medium red are 1-1.5 SD above the mean, and bright red are >1.5 SD above the mean.

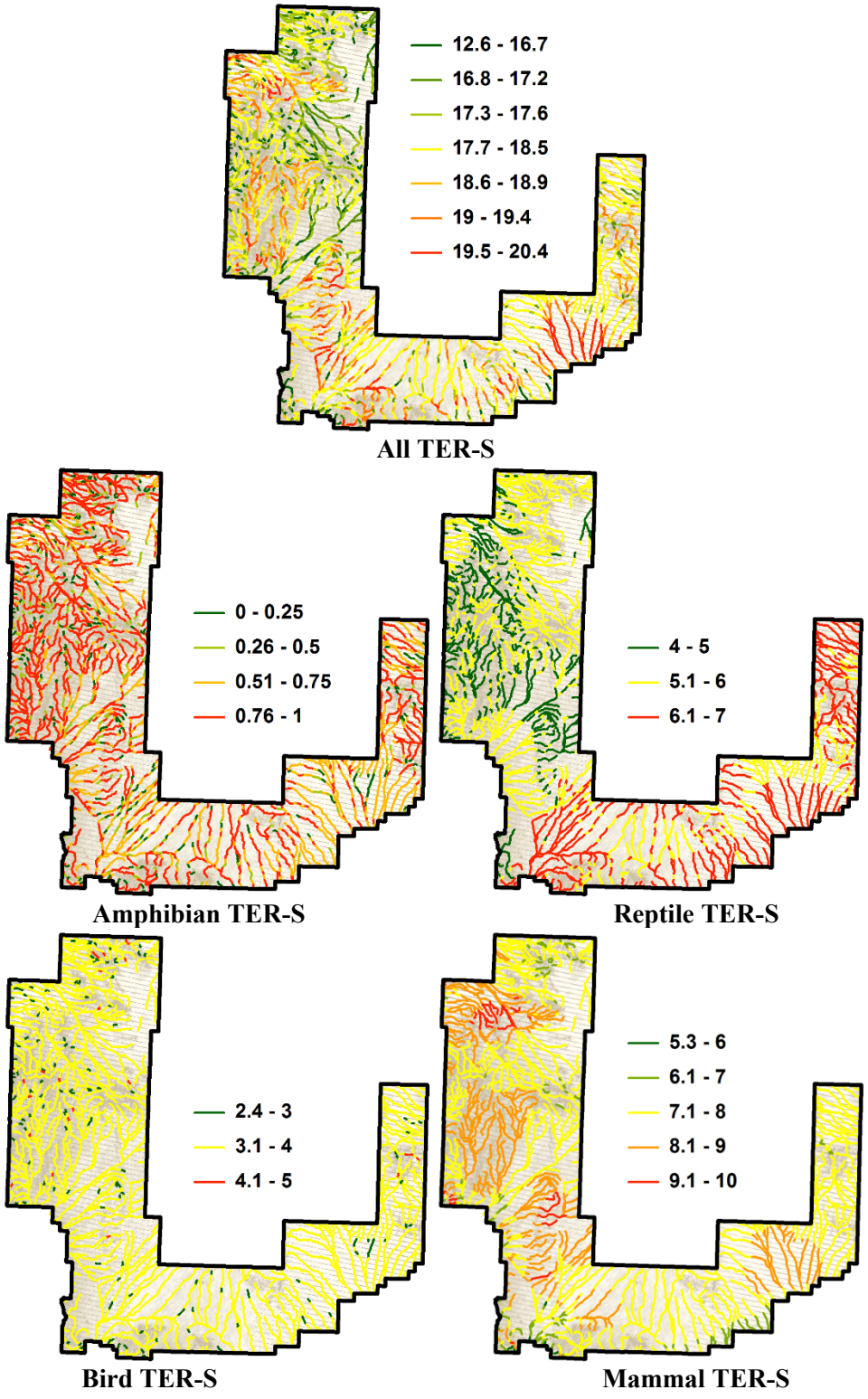


Figure 54. YPG - Richness of riparian-associated TER-S species.
Darker green reaches have lower richness, yellow have intermediate richness, and dark red have the highest richness.

Species richness and stream types

When the average riparian-associated species richness in each stream type was ranked, the distribution of pooled richness into the stream types at Yuma Proving Ground was correlated positively with the distribution of bird (r = 0.90), mammal (r = 0.79), and reptile (r = 0.79) richness in stream types (Figure 55). Average bird and mammal richness in each stream type were correlated (r = 0.76). Richness of reptile and passage migrant bird species in the ten stream types were also correlated (r = 0.64).

Stream types 1, 4, & 5 – Low overall species richness, though significantly higher than that in stream type 2, low passage migrant bird richness, particularly in stream type 4, high amphibian richness, the lowest reptile richness, low bird richness, moderate mammal richness.

Stream types 2 & 3 – Lowest overall species richness, though some reaches in type 3 have moderate overall richness, low passage migrant bird richness, high amphibian richness, moderately high reptile richness, low bird richness, moderately low mammal richness.

Stream type 6 – Moderate overall species richness, though some reaches have high overall richness, the highest passage migrant bird richness, along with stream type 7, the highest amphibian richness, high reptile richness, low bird richness, moderately high mammal richness.

Stream types 7 & 9 – Moderate overall species richness, though some reaches have high overall richness, the highest passage migrant bird richness in stream type 7, along with type 6, low passage migrant bird richness in stream type 9, moderate amphibian richness, moderate reptile richness, moderate bird richness, higher mammal richness.

Stream type 8 – Moderate overall species richness, moderate passage migrant bird richness, moderate reptile richness, moderate bird richness, higher mammal richness.

Stream type 10 – Significantly higher overall species richness than any other stream types, potential habitat for 2 migrant bird species, significantly lower amphibian richness than any other stream type, high reptile richness, significantly higher bird richness than any other stream type, moderate mammal richness.

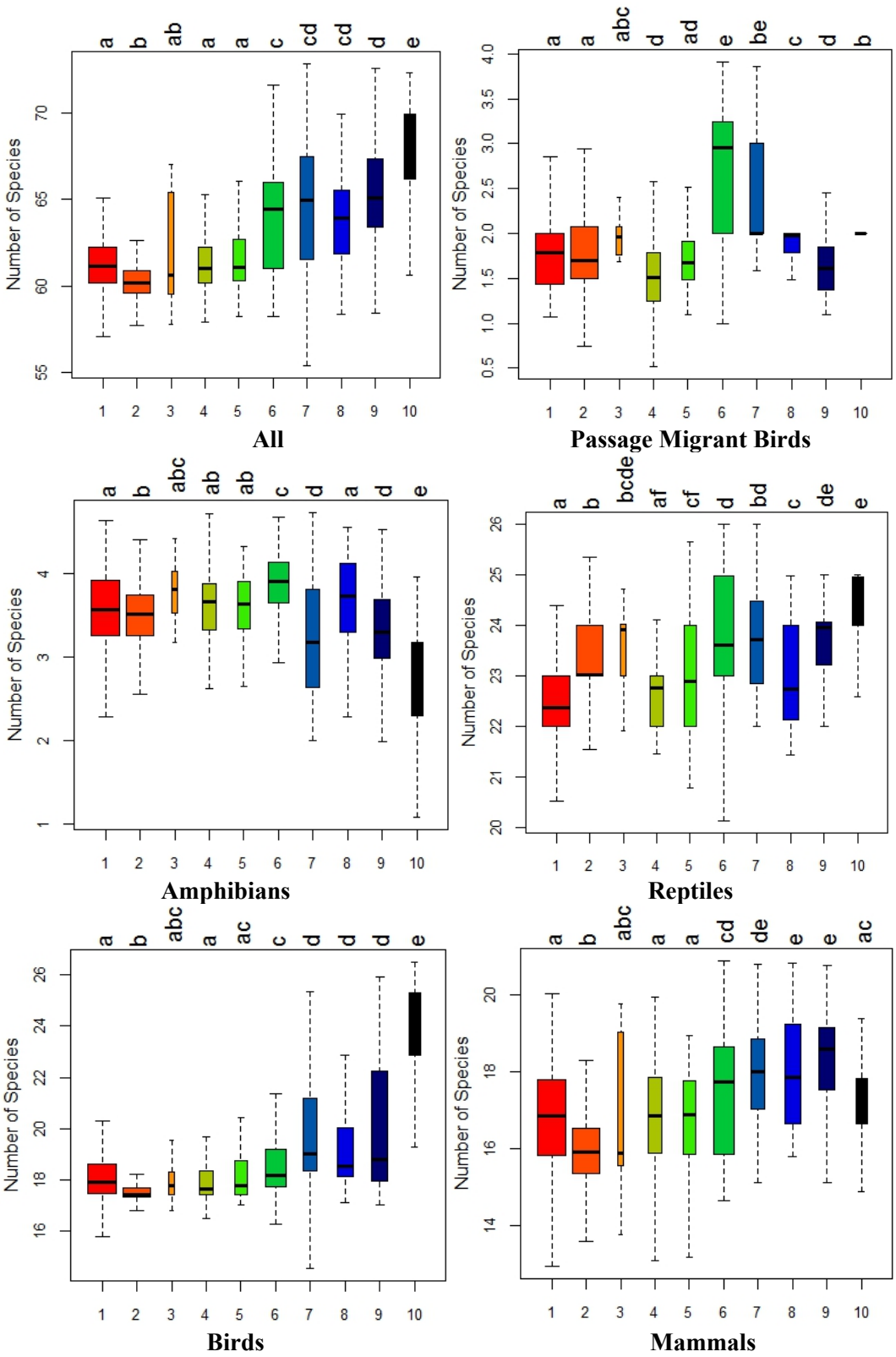


Figure 55. YPG - Richness of riparian-associated species in the ten stream types. Colors match those shown on stream type maps. Width is proportional to number of streams in each type.

When the average riparian-associated species richness of TER-S in each stream type was ranked, richness of any of the groups was not correlated with richness of any other group. There were significant differences between some stream types in TER-S richness, but many were quite similar and had broad ranges of richness for the different groups (Figure 56). Overall, stream type at Yuma Proving Ground did not seem to predict TER-S richness very well.

Stream type 1 – Moderate overall TER-S richness, a broad range of reptile richness, but low on average, moderate bird richness, higher mammal richness.

Stream types 2 & 3 – Moderate overall TER-S richness in stream type 3 to moderately high overall richness in stream type 2, high reptile richness, particularly in stream type 2, low to moderate bird richness, moderate mammal richness.

Stream type 4– Moderate overall TER-S richness, lower reptile richness, moderate bird richness, moderate mammal richness.

Stream type 5 – Moderate overall TER-S richness, lower reptile richness, moderate bird richness, moderate mammal richness.

Stream type 6 – Moderately high overall TER-S richness, moderate reptile richness, high bird richness, moderate mammal richness.

Stream type 7 – Moderate overall TER-S richness, lower reptile richness, high bird richness, moderate mammal richness.

Stream type 8 – Moderately low overall TER-S richness, very low reptile richness, high bird richness, moderate mammal richness.

Stream type 9 – Lower overall TER-S richness, very low reptile richness, moderate bird richness, moderate mammal richness.

Stream type 10 – Lower overall TER-S richness, moderate reptile richness, high bird richness, low mammal richness.

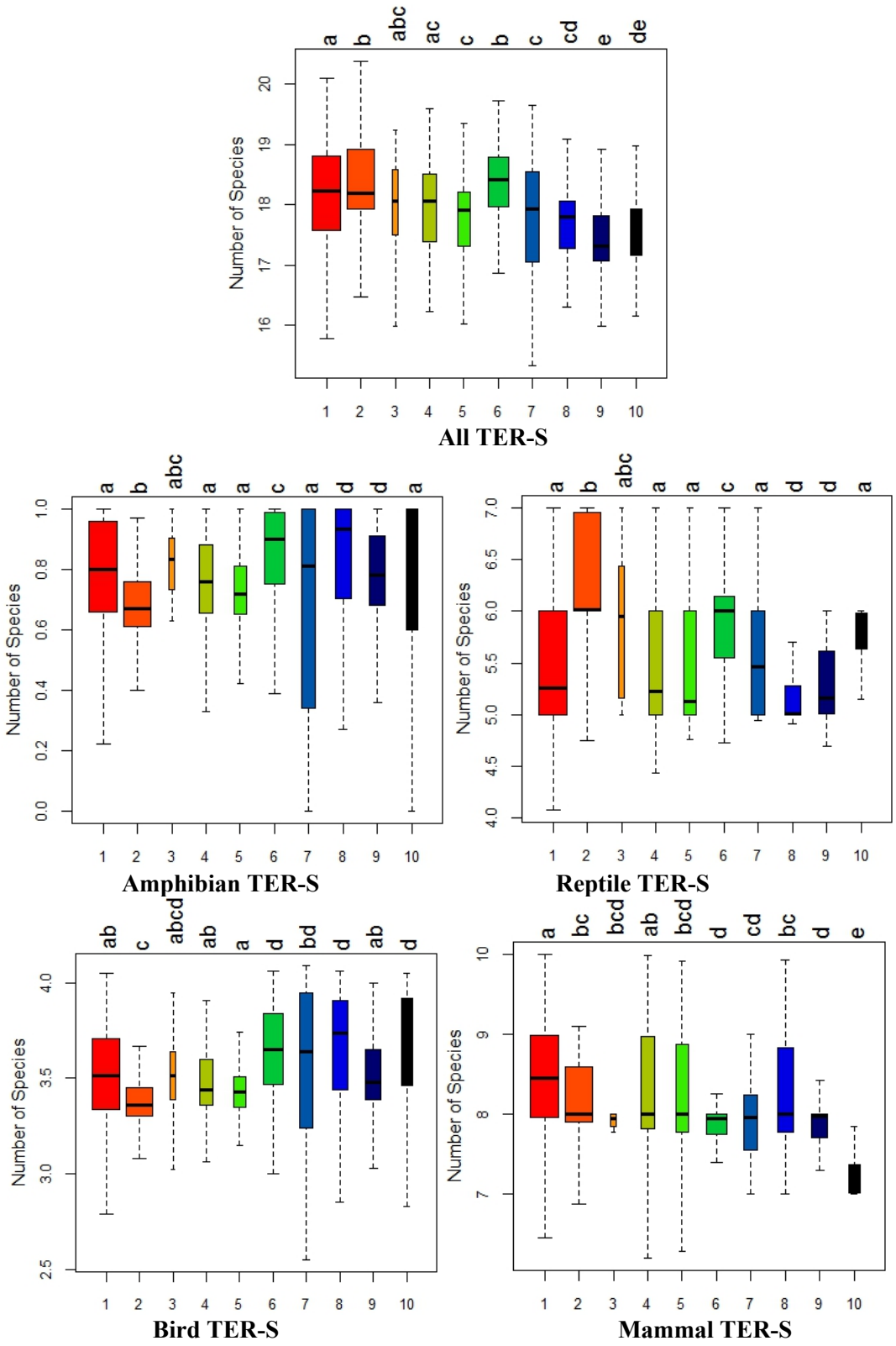


Figure 56. YPG - Richness of riparian-associated TER-S in the ten stream types. Colors match those shown on stream type maps. Width is proportional to number of streams in each type.

In individual stream reaches, richness of general riparian-associated species was correlated with richness of TER-S for two groups. All riparian-associated species richness and all TER-S richness were negatively correlated (r = -0.76). Riparian-associated bird species richness and bird TER-S richness were positively correlated (r = 0.65). For birds, planning management for riparian-associated species should benefit TER-S also, and vice versa. However, for mammals and reptiles, it is important to plan for TER-S specifically. This pattern did not hold when the average species richness in each stream type was examined. For stream types average richness was only correlated between the richness of riparian-associated amphibians and the amount of habitat for the one amphibian TER-S (r = 0.64).

TER-S response to ecohydrological variables

When pooled TER-S richness was modeled as a function of the ecohydrological variables, the largest effect was that of elevation (Table 29). Higher elevations caused species richness to decrease. Percent slope of the stream reach, peak flow, RSI, and riparian width all had about equal effect sizes, with higher values of all four variables tending to decrease species richness.

Table 29. YPG - Effect of ecohydrological variables on All TER-S riparian-associated species richness.

Parameter	*Effect Size*	*Relative Effect Size*	*SE*	95% Confidence Interval		*Relative Importance*
				Lower	*Upper*	
CumArea	0.26	8.7	0.05	0.26	0.27	1.00
SVRI	0.22	7.2	0.03	0.21	0.22	1.00
rendvi_mean	0.21	6.9	0.03	0.20	0.21	1.00
rendvi_pct	0.12	4.1	0.04	0.12	0.13	0.99
Q25TSP	0.05	1.8	0.06	0.05	0.06	0.36
FlowPerm	-0.06	2.1	0.03	-0.07	-0.06	0.78
ER_3m_05m	-0.17	5.5	0.03	-0.17	-0.16	1.00
Width2m	-0.34	11.2	0.04	-0.34	-0.33	1.00
RSI	-0.34	11.4	0.03	-0.35	-0.34	1.00
Qp25	-0.36	12.1	0.06	-0.37	-0.36	1.00
PCTSlope	-0.37	12.3	0.04	-0.38	-0.37	1.00
ypg_elev	-0.50	16.6	0.04	-0.51	-0.50	1.00

When percent of the stream reaches with habitat for the single amphibian TER-S was modeled as a function of the ecohydrological variables, the largest effects were that of riparian width and slope (Table 30). Greater widths and higher slopes caused species richness to decrease.

Table 30. YPG - Effect of ecohydrological variables on Amphibian TER-S riparian-associated species richness.

Parameter	*Effect Size*	*Relative Effect Size*	*SE*	95% Confidence Interval		*Relative Importance*
				Lower	*Upper*	
Width2m	-0.23	28.1	0.01	-0.24	-0.23	1.00
PCTSlope	-0.21	25.6	0.01	-0.21	-0.21	1.00
ypg_elev	-0.08	9.7	0.01	-0.08	-0.08	1.00
rendvi_mean	0.07	9.0	0.01	0.07	0.08	1.00
rendvi_pct	0.06	7.6	0.01	0.06	0.06	1.00
RSI	0.06	6.6	0.01	0.05	0.06	1.00
SVRI	0.04	5.1	0.01	0.04	0.04	1.00
Qp25	0.03	4.2	0.02	0.03	0.04	0.87
CumArea	-0.02	2.3	0.01	-0.02	-0.02	0.47
FlowPerm	-0.01	1.2	0.01	-0.01	-0.01	0.41
ER_3m_05m	0.00	0.4	0.01	0.00	0.00	0.28
Q25TSP	0.00	0.3	0.02	0.00	0.00	0.36

When reptile TER-S richness was modeled as a function of the ecohydrological variables, the largest effect was that of peak flow (Table 31); higher peak flows caused species richness to decrease. The second largest effect was that of mean RE-NDVI, with higher values increasing species richness. This indicates that, once peak flow is adjusted for, reptile TER-S richness at YPG may be greatest in stream with dense vegetation. RSI was also an important variable, with higher values decreasing reptile richness.

Table 31. YPG - Effect of ecohydrological variables on Reptile TER-S riparian-associated species richness.

Parameter	*Effect Size*	*Relative Effect Size*	*SE*	95% Confidence Interval		*Relative Importance*
				Lower	*Upper*	
Qp25	-0.65	20.1	0.05	-0.66	-0.64	1.00
rendvi_mean	0.49	15.2	0.02	0.49	0.49	1.00
RSI	-0.44	13.5	0.02	-0.44	-0.43	1.00
ypg_elev	-0.30	9.4	0.02	-0.31	-0.30	1.00
CumArea	0.30	9.2	0.03	0.29	0.30	1.00
Q25TSP	0.26	8.2	0.04	0.26	0.27	1.00
Width2m	0.21	6.7	0.03	0.21	0.22	1.00
rendvi_pct	-0.20	6.3	0.02	-0.21	-0.20	1.00
SVRI	0.19	6.0	0.02	0.19	0.20	1.00
PCTSlope	0.12	3.6	0.03	0.11	0.12	1.00
ER_3m_05m	-0.04	1.3	0.02	-0.05	-0.04	0.75
FlowPerm	0.02	0.5	0.02	0.01	0.02	0.33

When bird TER-S richness was modeled as a function of the ecohydrological variables, the largest effects were that of riparian width and slope (Table 32). These two variables combined accounted for 56% of the total effect. Greater widths and higher slopes caused species richness to decrease.

Table 32. YPG - Effect of ecohydrological variables on Bird TER-S riparian-associated species richness.

Parameter	*Effect Size*	*Relative Effect Size*	*SE*	95% Confidence Interval		*Relative Importance*
				Lower	*Upper*	
Width2m	-0.37	37.0	0.01	-0.37	-0.37	1.00
PCTSlope	-0.21	21.0	0.01	-0.21	-0.21	1.00
rendvi_pct	0.07	7.3	0.01	0.07	0.07	1.00
RSI	0.07	6.5	0.01	0.06	0.07	1.00
rendvi_mean	0.06	6.2	0.01	0.06	0.06	1.00
ypg_elev	-0.06	5.6	0.01	-0.06	-0.05	1.00
ER_3m_05m	-0.06	5.5	0.01	-0.06	-0.05	1.00
SVRI	0.05	4.9	0.01	0.05	0.05	1.00
Qp25	0.02	2.3	0.01	0.02	0.02	0.65
Q25TSP	0.02	1.8	0.01	0.02	0.02	0.47
FlowPerm	-0.01	1.3	0.01	-0.01	-0.01	0.55
CumArea	-0.01	0.6	0.01	-0.01	0.00	0.31

When mammal TER-S richness was modeled as a function of the ecohydrological variables, the largest effect was that of mean RE-NDVI (Table 33); higher values caused species richness to decrease. This indicates that mammal TER-S richness at YPG may be greatest in streams with a low density of vegetation. Peak flow was the second largest effect size, with higher values associated with decreased mammal richness. Percent cover and peak flow also had substantial effects. Higher values of both tended to increase mammal richness. Mammal richness appears to be highest in streams with greater percent cover of vegetation, but where that vegetation is more sparse, rather than dense.

Table 33. YPG - Effect of ecohydrological variables on Mammal TER-S riparian-associated species richness.

Parameter	*Effect Size*	*Relative Effect Size*	*SE*	95% Confidence Interval		*Relative Importance*
				Lower	*Upper*	
rendvi_mean	-0.42	28.7	0.03	-0.42	-0.41	1.00
Q25TSP	-0.21	14.3	0.05	-0.21	-0.20	1.00
rendvi_pct	0.19	13.1	0.03	0.19	0.20	1.00
Qp25	0.18	12.5	0.05	0.18	0.19	0.98
PCTSlope	-0.10	6.8	0.04	-0.10	-0.09	0.91
SVRI	-0.07	4.9	0.03	-0.08	-0.07	0.92
ER_3m_05m	-0.07	4.9	0.03	-0.07	-0.07	0.92
Width2m	0.07	4.6	0.04	0.06	0.07	0.72
FlowPerm	-0.06	3.8	0.02	-0.06	-0.05	0.83
ypg_elev	-0.06	3.8	0.03	-0.06	-0.05	0.70
RSI	-0.03	2.1	0.03	-0.03	-0.03	0.42
CumArea	0.01	0.5	0.04	0.00	0.01	0.29

There are several variables that had large effects on the species richness of multiple TER-S taxa groups. Riparian width was the largest effect for both birds and the amphibian species, with a relative variable importance of 28 - 37%. Greater reach widths were associated with decreased richness for both groups. The second largest effect for both of these groups was also the same – percent slope - with a relative variable importance of 21 – 26%. Higher slopes were associated with decreased richness. Mammal and reptile TER-S richness shared two of their most important variables. Mean RE-NDVI had the largest effect size for mammals (29%) and the second largest effect size for reptiles (15%). While higher values of this variable increased reptile richness, they decreased mammal richness. Peak flow was also important for both mammals and reptiles (13 – 20%), but again with an opposite effect on the two groups; higher peak flows decreased reptile richness and increased mammal richness.

Fort Huachuca

At Fort Huachuca, we modeled Mexican spotted owl and screech owl occurrence in ephemeral and intermittent streams and related their probability of occurrence to stream types. We mapped species richness of all riparian-associated species, riparian associated birds, passage migrant birds, mammals, reptiles, and amphibians, and tested whether stream type was related to richness of these groups. We mapped species richness of all riparian-associated TER-S, bird TER-S, mammal TER-S, reptile TER-S, and amphibian TER-S, and tested whether stream type was related to richness of these groups. We modeled species richness of the TER-S groups as a function of ecohydrological variables to better understand why richness varied in stream reaches.

Mexican Spotted Owl

This species was modeled with MaxEnt. For Mexican spotted owls, only four variables were retained for the final model: percent slope (43% contribution, 45.1% permutation importance), veg 0-1 m (31.5% contribution, 9.2% permutation importance), veg 4-12 m (0% contribution, 0.2% permutation importance), and veg >12 m (25.5% contribution, 45.4% permutation importance). Higher probability of presence was generally related to steeper slopes, lower percent cover of veg 0-1 m, and higher percent cover of veg 4-12 m and veg >12 m (Figure 57).

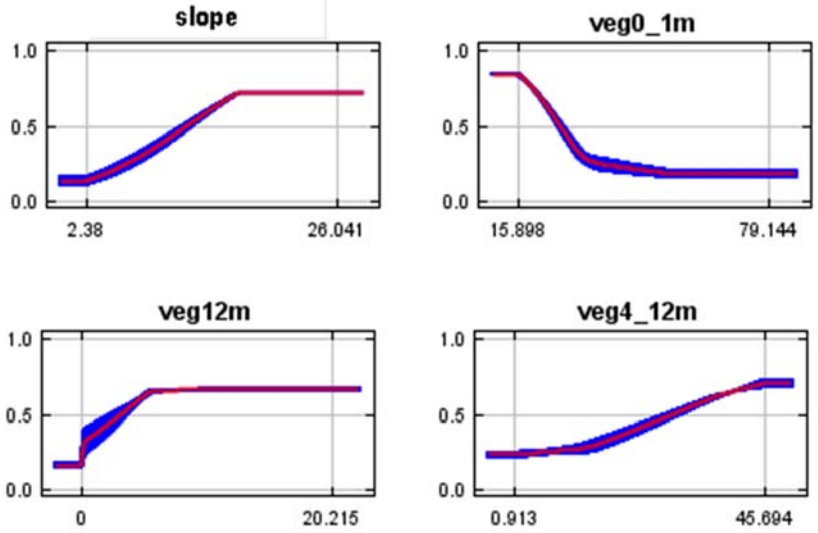


Figure 57. Fort Huachuca – Mexican Spotted Owl probability of presence as a function of four variables.
The x-axis shows the range of values of the variable, while the y-axis shows the resulting probability of presence when just that variable was used to predict presence.

The AUC value of the model was quite high for the testing sets ($\mu = 0.908$, $s = 0.075$). Zero OR for the testing set was 0.18 ($s = 0.40$, expected mean of 0) and Ten OR for the testing set was 0.36 ($s = 0.50$, expected mean of 0.10). A visual inspection of the results (Figure 58) shows that the Protected Activity Centers (PACs) used by Huachuca for management correspond very closely to higher probability of presence predicted by MaxEnt. This model may help detect areas that are especially valuable for spotted owls.

Mexican spotted owl probability of presence was significantly different between stream types (Kruskal Wallis $\chi^2 = 24.8$, $p = <0.001$) (Figure 59). Only stream type 5 was significantly different from stream types 1 and 2. However, stream type 7 did not occur within the modeling area, and stream types 3,4, 6, and 8 have only 1-2 reaches each in the modeling area. As a result, statistical tests could not detect a difference between any types but stream types 1, 2, and 5. This suggests that stream type is actually a good predictor of spotted owl presence, with these owls only likely to occur in stream types 1 or 2.

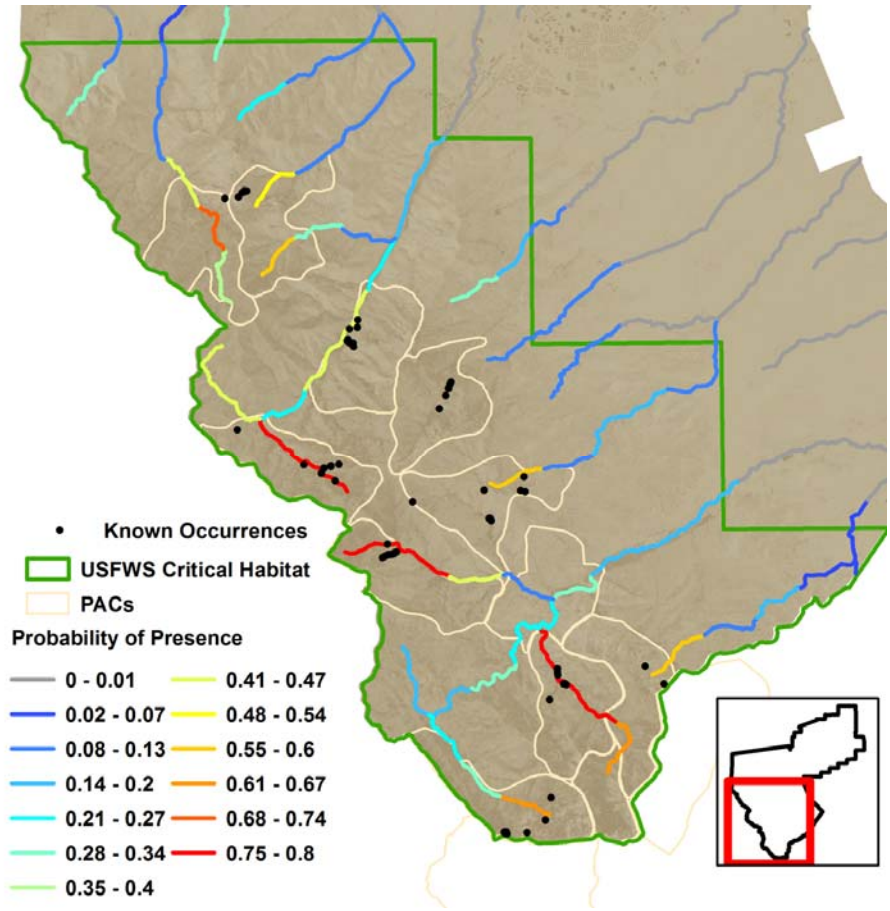


Figure 58. Fort Huachuca - MaxEnt modeling results for Mexican spotted owl. PACs are Protected Activity Centers used by the installation for management.

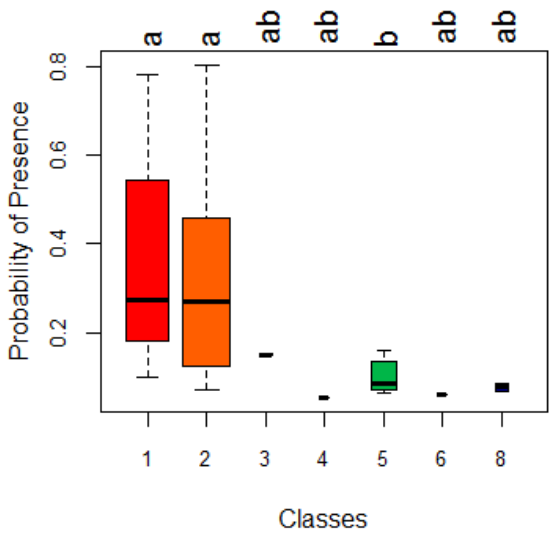


Figure 59. Fort Huachuca - Probability of presence for Mexican spotted owls in stream types within the modeling area.
Pairs of streams not sharing a letter indicates a significant difference between the pair.

For the subset of streams within the USFWS Designated Critical Habitat for spotted owls, streams within PACs had significantly different values for many of the ecohydrological variables than streams outside of PACs (Table 34). Only peak flow, flow permanence, Shannon structural diversity, and cumulative area were not significantly different. PACs were preferentially located in areas of sandstone and limestone, but occurred much less frequently than expected in areas of granite ($\chi^2 = 96.4$, $p<0.001$).

Table 34. Fort Huachuca - Results of Mann-Whitney U Tests for each ecohydrological variable in Critical Habitat for spotted owls.

Variable	In PACs	W	p
Slope	greater	315	0.003
Q25TSP	greater	288	0.001
LidElevMidPts	greater	160	<0.001
msavi2_mean	greater	175	<0.001
msavi2_pct	greater	262	<0.001
veg1_4m	greater	319	0.004
veg4_12m	greater	85	<0.001
Simpson1_D	greater	84	<0.001
veg0_1m	less	998	<0.001
Width3m	less	752	0.007
RSI	less	716	0.015
ER3m_05m	less	751	0.007
Qp25	same		
FlowPerm	same		
Shannon	same		
CumArea	same		

Western and Whiskered Screech Owls

This species was modeled with MaxEnt. For screech owls, only two variables were retained for the final model: rocktype (92% contribution, 68.9% permutation importance) and RSI (8% contribution, 31.1% permutation importance). Higher probability of presence was generally related to lower RSI values (Figure 60). Probability of presence was lower in stream reaches located in granite.

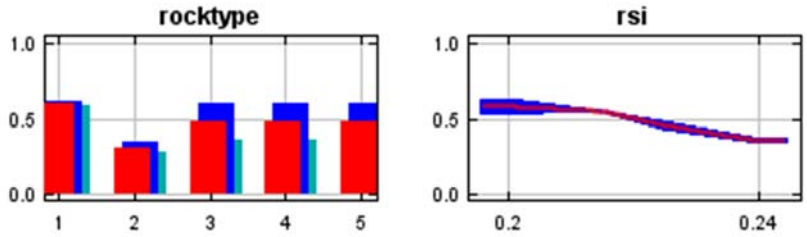


Figure 60. Fort Huachuca – Owl probability of presence as a function of two variables. The x-axis shows the range of values of the variable, while the y-axis shows the resulting probability of presence when just that variable was used to predict presence. Rock type 1 = sandstone, 2 = granite, 3 = sand, 4 = conglomerate, and 5 = limestone.

The AUC value of the model was high for the testing sets ($\mu = 0.831$, $s = 0.183$). Zero OR for the testing set was 0.11 ($s = 0.33$, expected mean of 0) and Ten OR for the testing set was 0.11 ($s = 0.33$, expected mean of 0.10). A visual inspection of the results (Figure 61) shows most of the high elevation areas on the installation have relatively high probability of presence for screech owls. Screech owl and Mexican spotted owl probability of presence were correlated with each other (0.82).

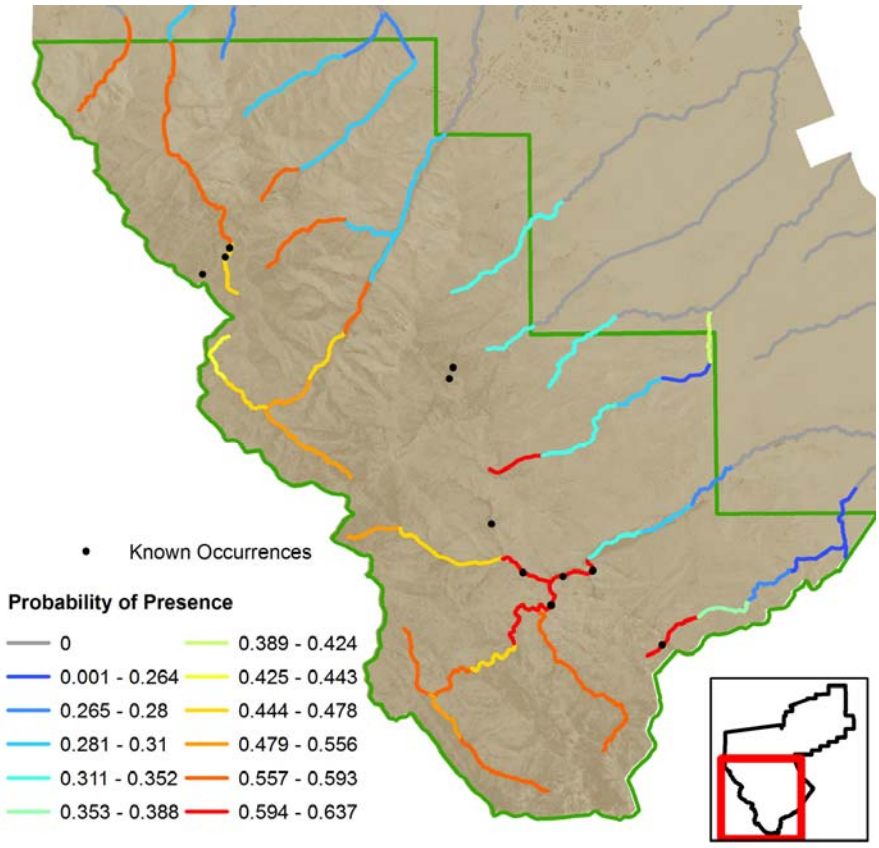


Figure 61. Fort Huachuca - MaxEnt modeling results for screech owls.

Screech owl probability of presence was significantly different between stream types (Kruskal Wallis $\chi^2 = 23.7$, $p = <0.001$). Only stream type 5 was significantly different from stream type 1. As for Mexican spotted owls, stream type 7 did not occur within the modeling area, and stream types 3, 4, 6, and 8 have only 1-2 reaches each in the modeling area. This suggests that stream type is actually a good predictor of spotted owl presence, with these owls only likely to occur in stream types 1 or 2. Visualizing the probability of presence in the boxplot (Figure 62) suggests that screech owls may be slightly more likely to occur in stream type 1 than 2.

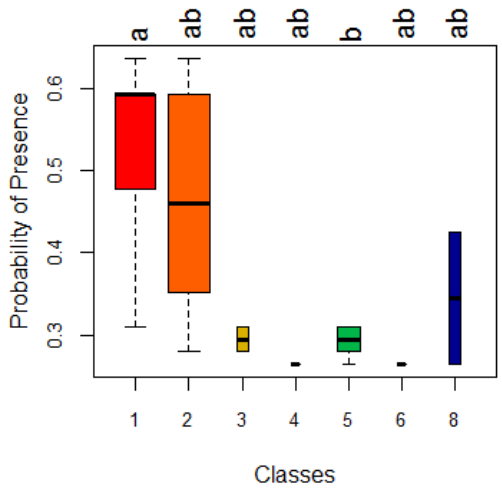


Figure 62. Fort Huachuca - Probability of presence for screech owls in stream types within the modeling area.
Pairs of streams not sharing a letter indicates a significant difference between the pair.

Geographic distribution of species richness

Fort Huachuca was the most species rich installation, with a total of 438 possible species, 258 (59%) of which were riparian-associated (Appendix C, Table 2). For the riparian-associated species, models were available for 45 reptiles, 47 mammals, 116 birds, and 14 amphibians. Pooled richness of all riparian-associated species was highly correlated with richness of birds (r = 0.83), and also correlated with richness of mammals (r = 0.78) and reptiles (r = 0.70), but not amphibians or passage migrant birds. Pooled richness was highest in the mid-elevation mountain canyons, but also high in other streams across the Fort (Figure 63). Reptile and amphibian richness were correlated (r = 0.77) with each other; both had lower values in the mountains and higher values in the lower elevation streams. Bird and mammal richness were somewhat correlated (r = 0.63), with a pattern opposite from the herpetofauna. Richness of birds and mammals was highest in the mountains and average to below-average in the low-elevation streams. Richness of passage migrant birds was usually highest in certain mountain stream reaches. For all groups, Garden Canyon had average to above-average richness and often stood out compared to other reaches.

Fort Huachuca had 98 potential TER-S: 7 amphibians, 47 birds, 23 mammals, and 21 reptiles (Appendix C, Table 3). For TER-S richness, pooled richness of all species was correlated with bird (r = 0.80), mammal (r = 0.63), and reptile (r = 0.81) richness. For all three groups, richness was generally highest in mid-elevation mountain streams (Figure 64). Bird TER-S richness was also high in higher elevation streams, mammal TER-S richness values were more variable across the installation, and reptile TER-S richness was high in just one mountain canyon. The highest values for both reptile and amphibian TER-S groups were found in Garden Canyon. Amphibian TER-S richness was generally high in all other non-mountain streams. Reptile TER-S richness was average across much of the installation, with high richness in specific lowland streams.

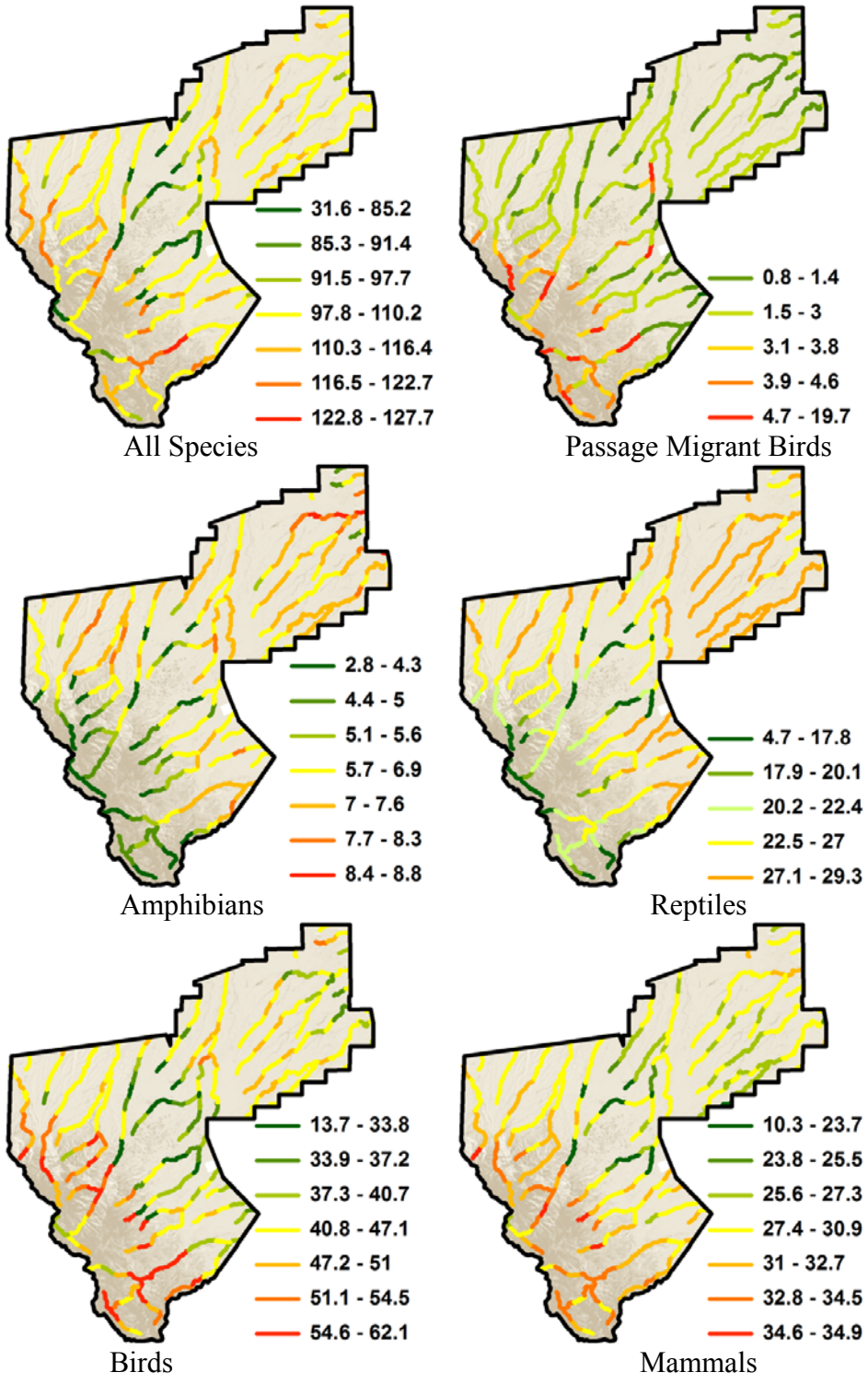


Figure 63. Fort Huachuca richness of riparian-associated species.
Dark green reaches have a value less than 1.5 standard deviations (SD) below the mean value for the group, medium green reaches are 1-1.5 SD below the mean, light green are 0.5-1 SD below the mean, yellow are within 0.5 SD of the mean, light red are between 0.5-1 SD above the mean, medium red are 1-1.5 SD above the mean, and bright red are >1.5 SD above the mean.

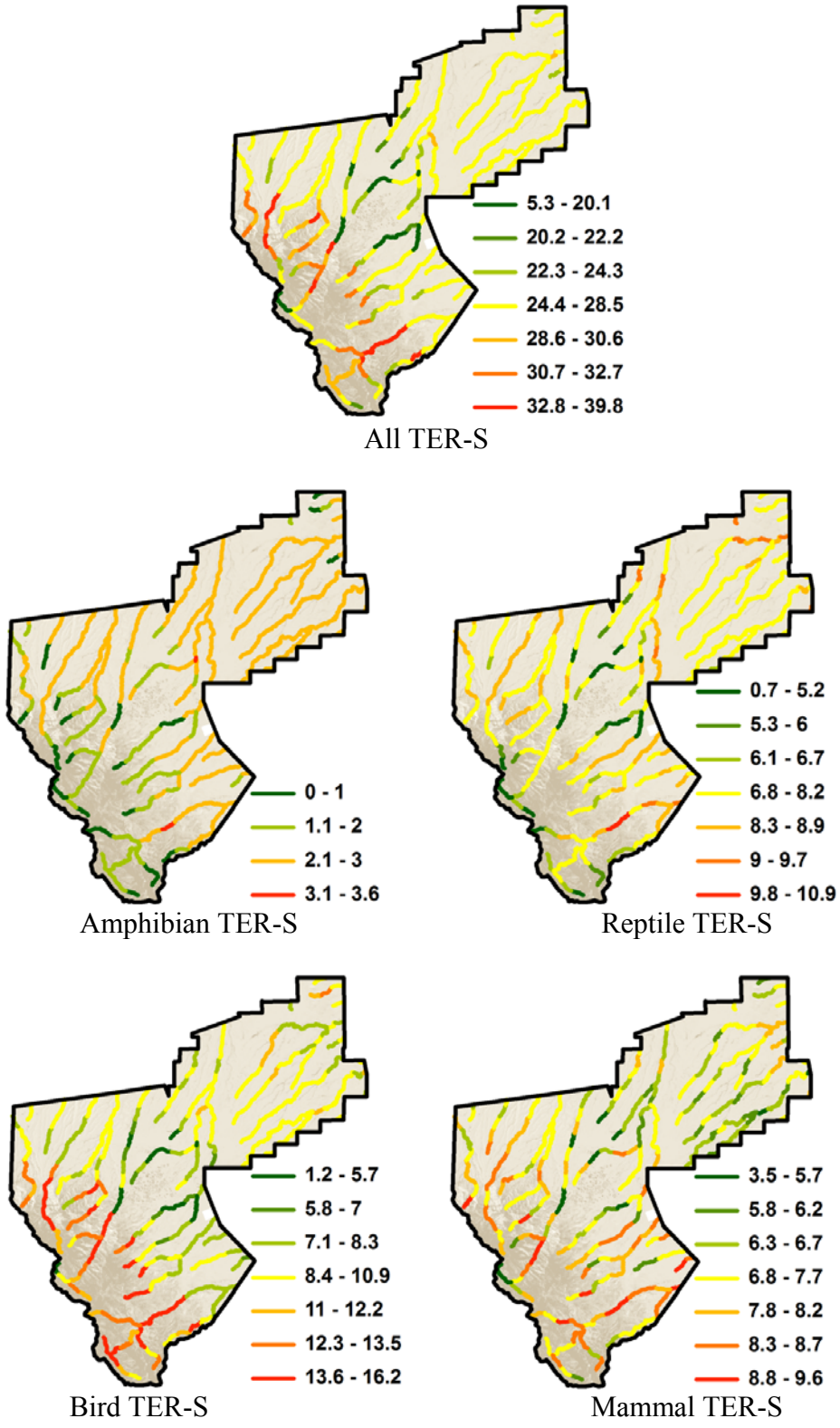


Figure 64. Fort Huachuca richness of riparian-associated TER-S species.
Darker green reaches have lower richness, yellow have intermediate richness, and dark red have the highest richness.

Species richness and stream types

When the average riparian-associated species richness in each stream type was ranked, the distribution of pooled richness in the stream types at Fort Huachuca was correlated positively with the distribution of bird (r = 0.71) and passage migrant bird (r = 0.67) richness in stream types (Figure 65). For all three groups, richness of stream type 1 is significantly greater than that of stream type 6. Richness of amphibian and reptile species in the eight stream types was highly correlated (r = 1.00). For both groups, richness is significantly lower in stream types 1 and 2 than in all other stream types. The distribution of bird, passage migrant bird, and mammal richness in stream types were all highly correlated with each other (bird-mammal, r = 0.81, bird-passage migrant, r = 0.93, mammal-passage migrant, r = 0.93). For these groups, richness was highest in stream types 1 and 2. Though not highly correlated, amphibian and reptile richness were generally opposite that of bird and mammal richness in the stream types.

Stream types 1 & 2 – Moderately high overall richness, very high passage migrant bird richness highest bird richness on average, highest mammal richness, lowest reptile and amphibian richness.

Stream type 3 – Moderately high overall richness, with some reaches having the highest values on the installation, a broad range of bird and passage migrant bird richness, high amphibian richness, quite high reptile richness, and moderately high mammal richness.

Stream type 4, 6, and 8 – Generally low overall richness, lowest passage migrant bird richness, moderately high amphibian richness, with some type 8 reaches having the highest values on the installation, high reptile richness, the lowest bird richness, and low mammal richness, though type 8 has significantly higher richness than type 7.

Stream type 5 – Along with type 1, the highest overall species richness, moderately low passage migrant bird richness (between types 1/2 and type 8), moderately high amphibian richness, moderate reptile richness, though significantly lower than type 7, moderately high bird richness that is significantly greater than types 6 and 8, and high mammal richness.

Stream type 7 – Moderate overall species richness, low passage migrant bird richness, moderately high amphibian richness, high reptile richness, moderate bird richness that is significantly greater than type 6, and low mammal richness.

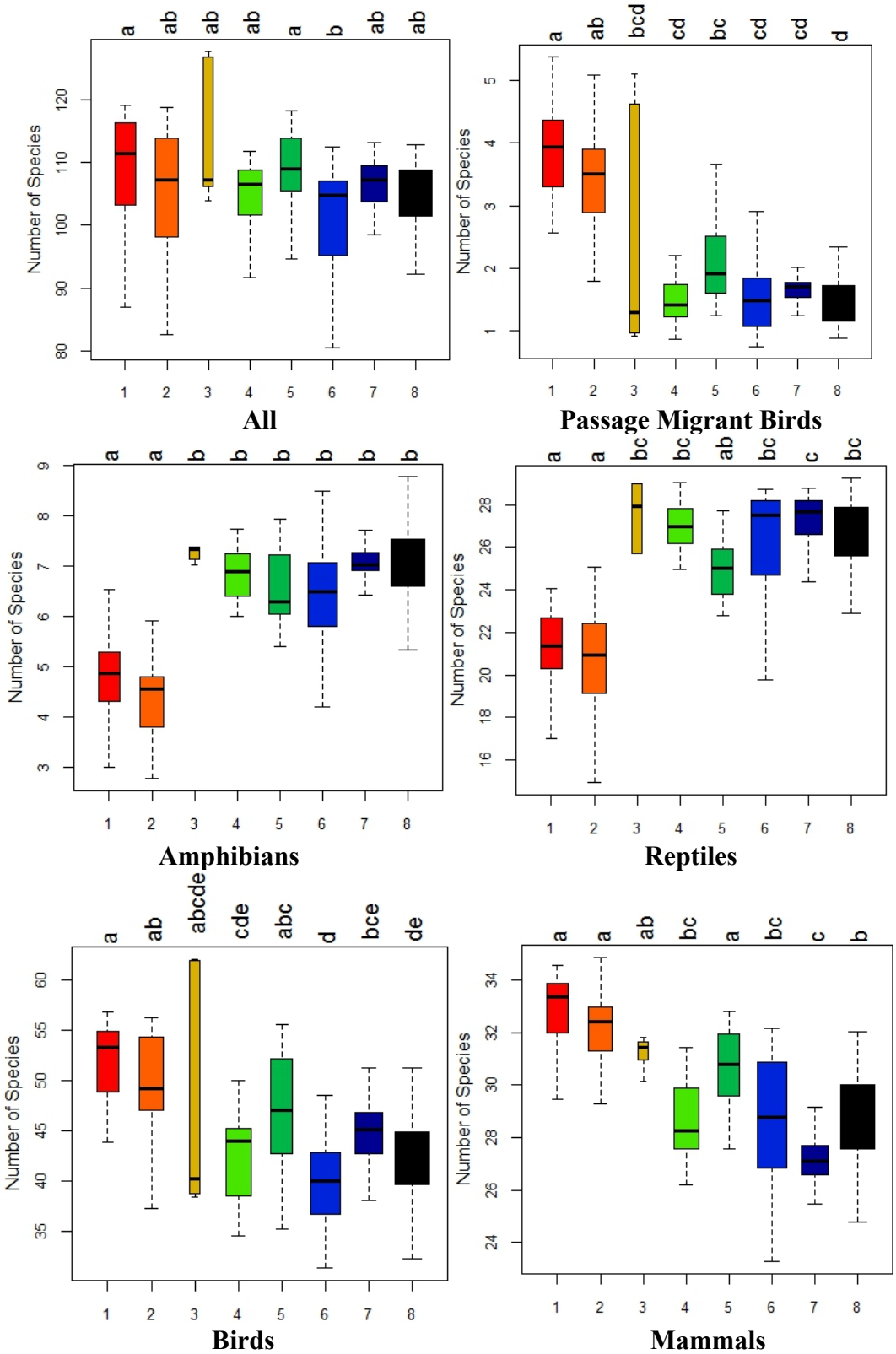


Figure 65. Fort Huachuca richness of riparian-associated species in the eight stream types. Colors match those shown on stream type maps. Width is proportional to number of streams in each type.

When the average riparian-associated species richness of TER-S in each stream type was ranked, the distribution of pooled richness into the stream types at Fort Huachuca was correlated with only bird (r = 0.83) and mammal (r = 0.76) richness. For all species pooled and birds, type 1 stream reaches had significantly higher richness than types 4, 6, and 8. Mammals followed this pattern, but only the difference between stream types 1 and 8 was significant. Unlike the riparian-associated groups including non TER-S, reptile and amphibian TER-S richness were somewhat negatively correlated (r = -0.64). These groups had somewhat similar distribution of richness values into the stream types, with types 1 and 2 having the lowest richness, and type 3 having the highest richness. However, though not significant, richness of amphibians tended to be higher in type 7 than type 5, while reptile richness tended to be higher in type 5 than type 7 (Figure 66).

Stream types 1 & 2 – Moderately high overall richness, though some type 2 reaches have the lowest values on the installation, moderate mammal richness, high bird richness, particularly in type 1, lowest reptile and amphibian richness.

Stream type 3 – High overall and mammal richness, with some reaches having the highest values for those groups on the installation, a broad range of bird richness, high amphibian richness, and the highest reptile richness.

Stream type 4, 6, and 8 – Moderately low overall richness, moderately high amphibian richness, with some type 8 reaches having the highest values on the installation, moderate reptile richness, the lowest bird richness, and low mammal richness.

Stream type 5 – Moderately high overall species richness, moderately high amphibian and reptile richness, moderately high bird richness that is significantly greater than types 4 and 6, and moderate mammal richness.

Stream type 7 – Moderate overall species richness, moderately high amphibian richness, moderate reptile richness, moderate bird richness that is significantly greater than types 4 and 6, and low mammal richness, significantly less than in types 1, 2, 3, 5, and 6.

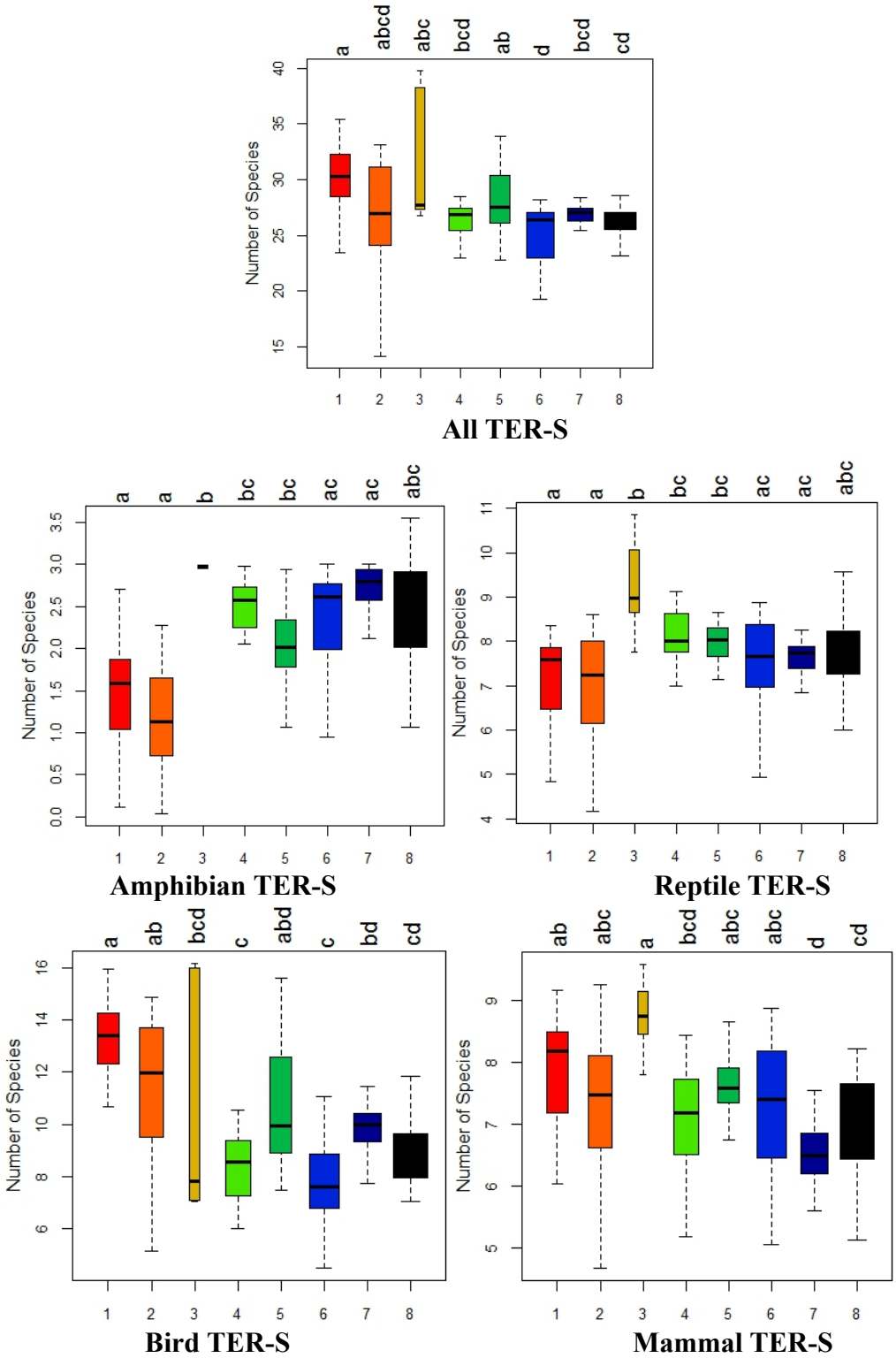


Figure 66. Fort Huachuca - richness of riparian-associated TER-S in the eight stream types. Colors match those shown on stream type maps. Width is proportional to number of streams in each type.

In individual stream reaches, richness of general riparian-associated species was highly correlated with richness of TER-S for all groups (all species, 0.92; amphibians, 0.87; birds, 0.90; mammals, 0.77; and reptiles, 0.88). At Fort Huachuca, planning management for each riparian-associated general group should benefit TER-S also, and vice versa. The same patterns held when the average species richness in each stream type was examined.

TER-S response to ecohydrological variables

When pooled TER-S richness was modeled as a function of the ecohydrological variables, the largest effect was that of elevation (Table 35). Higher elevations caused species richness to decrease. Examination of the distribution of pooled richness on the installation (Figure 64) shows that there is actually a mid-elevation peak in overall species richness. The mean vegetation index value had nearly as large an effect as elevation, but higher values of the index tended to increase species richness, indicating the TER-S at Huachuca may prefer more dense vegetation. RSI also had a large effect, but decreased richness, indicating TER-S may prefer stream reaches where rainfall is more evenly distributed throughout the year. Interestingly, the effect of the percent cover of 4-12 m vegetation was negative, while the effect of the percent cover of 1-4 m vegetation was positive.

Table 35. Fort Huachuca - Effect of ecohydrological variables on all TER-S riparian-associated species richness.

Parameter	*Effect Size*	*Relative Effect Size*	*SE*	95% Confidence Interval		*Relative Importance*
				Lower	*Upper*	
LidelevMidPts	-4.94	20.5	1.05	-5.07	-4.81	1.00
msavi2_mean	4.07	16.9	1.15	3.93	4.22	0.99
RSI	-3.54	14.7	0.93	-3.66	-3.42	0.99
veg4_12m	-1.86	7.7	1.37	-2.04	-1.69	0.42
veg1_4m	1.55	6.4	0.88	1.44	1.66	0.60
PercentSlope	-1.28	5.3	1.04	-1.41	-1.15	0.38
CumArea	1.24	5.1	0.55	1.17	1.31	0.67
Q25TSP	1.17	4.9	0.92	1.06	1.29	0.35
Width2m	-1.05	4.3	0.67	-1.13	-0.96	0.48
Qp25	1.02	4.2	0.67	0.94	1.11	0.40
veg12m	-0.84	3.5	0.64	-0.92	-0.76	0.40
msavi2_pct	0.70	2.9	0.83	0.60	0.81	0.29
ER3m_05m	-0.43	1.8	0.52	-0.50	-0.37	0.33
FlowPerm	0.43	1.8	0.63	0.35	0.51	0.26

When amphibian TER-S richness was modeled as a function of the ecohydrological variables, the largest effects were that of elevation and slope (Table 36). Higher elevations and slopes caused species richness to decrease. Three vegetation structure layer variables were also important; higher percent covers of the 0 - 1 m, 1 - 4 m, and 4 - 12 m layers increased amphibian richness, with the largest influence from the 1 - 4 m layer. High peak flows tended to decrease amphibian richness, though high total stream power tended to increase it. Increased cumulative area and mean vegetation index also tended to increase species richness for amphibians.

Table 36. Fort Huachuca - Effect of ecohydrological variables on amphibian TER-S riparian-associated species richness.

Parameter	*Effect Size*	*Relative Effect Size*	*SE*	95% Confidence Interval		*Relative Importance*
				Lower	*Upper*	
LidelevMidPts	-0.62	15.6	0.18	-0.64	-0.60	0.98
PercentSlope	-0.62	15.5	0.17	-0.64	-0.59	0.99
veg1_4m	0.46	11.5	0.15	0.44	0.48	0.92
veg0_1m	0.32	8.1	0.17	0.30	0.34	0.69
Qp25	-0.31	7.9	0.21	-0.34	-0.29	0.35
Q25TSP	0.25	6.4	0.20	0.23	0.28	0.45
veg4_12m	0.23	5.8	0.17	0.21	0.25	0.29
CumArea	0.23	5.7	0.09	0.21	0.24	0.83
msavi2_mean	0.23	5.7	0.16	0.21	0.25	0.38
RSI	0.18	4.4	0.15	0.16	0.20	0.39
ER3m_05m	0.15	3.8	0.08	0.14	0.16	0.60
Width2m	-0.13	3.4	0.11	-0.15	-0.12	0.34
msavi2_pct	0.12	3.1	0.12	0.11	0.14	0.32
FlowPerm	-0.12	3.1	0.12	-0.14	-0.11	0.36

When reptile TER-S richness was modeled as a function of the ecohydrological variables, the largest effect was again that of elevation (Table 37); higher elevations caused species richness to decrease. The effect of the 4-12m vegetation structure layer was quite strong, but unlike for amphibians, higher percent covers of this layer decreased reptile richness. The mean vegetation index had a strong effect on reptile richness, with higher values increasing richness, indicating that more reptile TER-S occur in dense vegetation at Huachuca. RSI also had a significant effect, but decreased richness, indicating TER-S reptiles may prefer stream reaches where rainfall is more evenly distributed throughout the year. Greater cumulative area and total stream power also tended to increase species richness for reptiles.

Table 37. Fort Huachuca - Effect of ecohydrological variables on reptile TER-S riparian-associated species richness.

Parameter	*Effect Size*	*Relative Effect Size*	*SE*	95% Confidence Interval		*Relative Importance*
				Lower	*Upper*	
LidelevMidPts	-1.79	20.2	0.35	-1.83	-1.74	1.00
veg4_12m	-1.39	15.7	0.55	-1.46	-1.32	0.70
msavi2_mean	1.24	14.0	0.46	1.18	1.29	0.73
RSI	-1.07	12.1	0.34	-1.12	-1.03	0.96
Q25TSP	0.54	6.2	0.31	0.51	0.58	0.42
CumArea	0.54	6.1	0.22	0.51	0.57	0.80
Qp25	0.46	5.2	0.31	0.42	0.50	0.39
Width2m	-0.42	4.7	0.23	-0.44	-0.39	0.59
veg12m	-0.31	3.5	0.26	-0.34	-0.28	0.47
veg0_1m	0.31	3.5	0.41	0.26	0.36	0.27
msavi2_pct	0.30	3.4	0.33	0.26	0.34	0.41
ER3m_05m	-0.29	3.3	0.19	-0.32	-0.27	0.52
FlowPerm	0.18	2.0	0.25	0.15	0.21	0.29

When bird TER-S richness was modeled as a function of the ecohydrological variables, the largest effect was that of the mean vegetation index (Table 38); higher vegetation index values caused species richness to increase. More bird TER-S may occur in dense vegetation at Huachuca. As with the other TER-S groups, elevation also had a strong and negative effect on bird richness. As with reptile TER-S, RSI had a large effect, with higher values decreasing bird richness. The most important vegetation structure layer for TER-S birds was the 1-4 m layer. Higher percent cover of this layer increased bird richness. Higher percent cover of the 0-1 m layer tended to decrease bird richness. Because of the way these layers were derived, higher values of the 0-1 m layer indicate lower values of the any vegetation >1 m, so bird richness at Huachuca seems to be associated with higher percent cover of tall vegetation.

Table 38. Fort Huachuca - Effect of ecohydrological variables on bird TER-S riparian-associated species richness.

Parameter	*Effect Size*	*Relative Effect Size*	*SE*	95% Confidence Interval		*Relative Importance*
				Lower	*Upper*	
msavi2_mean	2.11	18.2	0.49	2.04	2.17	1.00
LidelevMidPts	-2.07	17.9	0.53	-2.14	-2.00	0.99
RSI	-1.83	15.8	0.42	-1.88	-1.77	1.00
veg1_4m	1.68	14.5	0.43	1.63	1.74	1.00
veg0_1m	-0.70	6.0	0.50	-0.76	-0.64	0.42
PercentSlope	-0.59	5.1	0.49	-0.65	-0.53	0.41
veg4_12m	-0.50	4.3	0.67	-0.59	-0.42	0.28
ER3m_05m	-0.48	4.1	0.26	-0.51	-0.44	0.64
Width2m	-0.34	2.9	0.33	-0.38	-0.30	0.36
msavi2_pct	-0.31	2.7	0.43	-0.37	-0.26	0.31
Qp25	0.27	2.3	0.25	0.23	0.30	0.28
Q25TSP	0.25	2.1	0.33	0.21	0.29	0.27
CumArea	0.20	1.7	0.25	0.17	0.23	0.26
FlowPerm	0.15	1.3	0.31	0.11	0.19	0.25
veg12m	0.12	1.1	0.32	0.08	0.16	0.25

When mammal TER-S richness was modeled as a function of the ecohydrological variables, the largest effect was that of RSI (Table 39); higher values caused species richness to decrease. More predictable rainfall spread throughout the year is associated with higher mammal richness. Unexpectedly, the next strongest effect is that of the 1-4 m vegetation structure layer, though higher percent cover of this layer is actually associated with decreased mammal TER-S richness. Both the mean vegetation index and percent cover derived from it have a substantial and positive effect on mammal richness. This would indicate that richness for this group is higher where there is more and denser vegetation. This seems to be at odds with the vegetation structure results, where higher percent cover of the 4-12 m layer also decreases richness. Higher values of total stream power, peak flow, and percent slope are all associated with increased mammal richness.

Table 39. Fort Huachuca - Effect of ecohydrological variables on mammal TER-S riparian-associated species richness.

Parameter	*Effect Size*	*Relative Effect Size*	*SE*	95% Confidence Interval		*Relative Importance*
				Lower	*Upper*	
RSI	-0.73	15.0	0.19	-0.75	-0.70	1.00
veg1_4m	-0.51	10.4	0.19	-0.53	-0.48	0.74
msavi2_mean	0.47	9.7	0.28	0.44	0.51	0.55
msavi2_pct	0.43	8.9	0.20	0.41	0.46	0.67
Q25TSP	0.35	7.3	0.21	0.33	0.38	0.45
veg4_12m	-0.33	6.7	0.38	-0.37	-0.28	0.35
Qp25	0.30	6.2	0.13	0.28	0.32	0.47
PercentSlope	-0.29	6.1	0.21	-0.32	-0.27	0.51
veg12m	-0.28	5.8	0.15	-0.30	-0.26	0.55
CumArea	0.26	5.4	0.14	0.24	0.28	0.48
veg0_1m	0.22	4.6	0.25	0.19	0.26	0.34
LidelevMidPts	-0.17	3.6	0.23	-0.20	-0.15	0.29
ER3m_05m	0.17	3.6	0.13	0.16	0.19	0.48
FlowPerm	0.16	3.3	0.15	0.14	0.18	0.28
Width2m	0.16	3.3	0.16	0.14	0.18	0.37

There are several variables that had large effect on the species richness of multiple TER-S taxa groups. Elevation was one of the two largest effects for all groups except mammals, with a relative variable importance of 16 – 20%. Higher elevations were associated with decreased richness for all these groups. Mean vegetation index value was one of the three largest effects for all groups except amphibians, with a relative variable importance of 8 – 18%. Higher values were associated with increased richness for all these groups. RSI was one of the four largest effects for all groups except amphibians, with a relative variable importance of 12 – 16%. Higher values were associated with decreased richness for all these groups. Percent cover of the 1-4 m vegetation layer was one of the four largest effects for all groups except reptiles, with a relative variable importance of 10 – 15%. Higher values were associated with increased richness of amphibians and birds, but decreased richness of mammals. Total stream power had a substantial effect on all groups except birds, with a relative variable importance of 6-16%. Higher values were associated with increased richness of all of these groups.

Fort Bliss

At Fort Bliss, we modeled gray vireo occurrence in ephemeral and intermittent streams and related their probability of occurrence to stream types. We created a nesting habitat metric and tested it against previously-collected field data. We used this same field data to conduct a test of breeding bird species richness derived from stacked GAP models. We mapped species richness of all riparian-associated species, riparian associated birds, passage migrant birds, mammals, reptiles, and amphibians, and tested whether stream type was related to richness of these groups. We mapped species richness of all riparian-associated TER-S, bird TER-S, mammal TER-S, and reptile TER-S, and tested whether stream type was related to richness of these groups. We modeled species richness of the TER-S groups as a function of ecohydrological variables to better understand why richness varied in stream reaches.

Gray Vireo Model

For gray vireos, twelve variables were retained for the final model (Table 40). Higher probability of presence was generally related to smaller cumulative watershed area, lower 10-yr peak flows, higher percent cover of veg 0.5 - 1 m, and lower mean RE-NDVI. Other interesting effects include the avoidance of streams with vegetation >12 m, higher probability of presence in streams with higher flow permanence, and a negative effect of percent cover.

Table 40. Fort Bliss - Effect of ecohydrological variables used in the averaged top set of gray vireo models.
Odds can be interpreted as the increase or decrease in probability of presence for a change in units as indicated in the unit change column (e.g., increasing RSI by 0.01 units increases the probability of presence by 202%, while increasing the cumulative area by 10 km^2 decreases the probability of presence by 31%).

Parameter	*Effect Size*	*Relative Effect Size*	95% CI Effect		*Relative Importance*	*Unit Change for Odds*	*Odds*	95% CI Odds	
			Lower	*Upper*				*Lower*	*Upper*
(Intercept)	-2.06		-2.12	-2.01					
Cum_Area	-4.41	13.4	-4.79	-4.02	0.39	10 (km2)	0.69	0.67	0.72
Qp10	-3.72	11.3	-3.87	-3.57	0.99	10	0.91	0.91	0.92
veg05_1m	3.70	11.2	3.58	3.81	1.00	1	1.35	1.34	1.37
rendvi_mean	-3.36	10.2	-3.52	-3.19	0.89	0.01	0.70	0.68	0.72
LidElevMidPts	-2.97	9.0	-3.08	-2.85	0.98	100	0.21	0.19	0.22
RSI	2.96	9.0	2.83	3.09	0.94	0.01	2.02	1.94	2.11
veg12m_PA	-2.87	8.7	-3.09	-2.65	0.50	N to Y	0.06	0.04	0.08
FlowPerm	2.46	7.5	2.36	2.56	0.98	1	1.17	1.16	1.18
rendvi_pct	-2.16	6.5	-2.28	-2.03	0.81	0.1	0.63	0.61	0.65
Landcvr_variety	1.93	5.8	1.83	2.02	0.92	1	2.28	2.16	2.40
PCTSlope	-1.29	3.9	-1.37	-1.20	0.61	1	0.84	0.83	0.85
Q25TSP	-1.15	3.5	-1.24	-1.06	0.43	10	0.95	0.94	0.95

The AUC value of the model was quite high for both the training (0.905) and the testing set (0.822). Overall accuracy was highest with a threshold value of 0.207. This threshold resulted in

an overall accuracy of 74.5% for the test set and 76.3% for the training set, for a weighted accuracy for both sets combined of 75.9%. Kappa coefficients were 0.447 for the test set and 0.519 for the training set, indicating the model was at least moderately better than a random model. Confusion matrices and omission and commission rates are reported in Table 41. Of the 62 stream reaches in which gray vireos were found, the model predicted they would be present in 52 of these, as well as 38 additional stream reaches in which they were not observed.

Table 41. Confusion matrix and accuracy rates for overall gray vireo modeling (training and test sets combined).

		Observed		
		Presence	Absence	Sum
Predicted	Presence	52	38	90
	Absence	10	99	109
	Sum	62	137	199

Accuracy	Omission	Comission
Presence	83.9%	57.8%
Absence	72.3%	90.8%

A visual inspection of the results (Figure 67) shows that the model had trouble predicting gray vireo occurrence in the Organ Mountains. Different factors may affect vireo occurrence in different mountain ranges. This model may be best suited for managing gray vireos in the Sacramento Mountains.

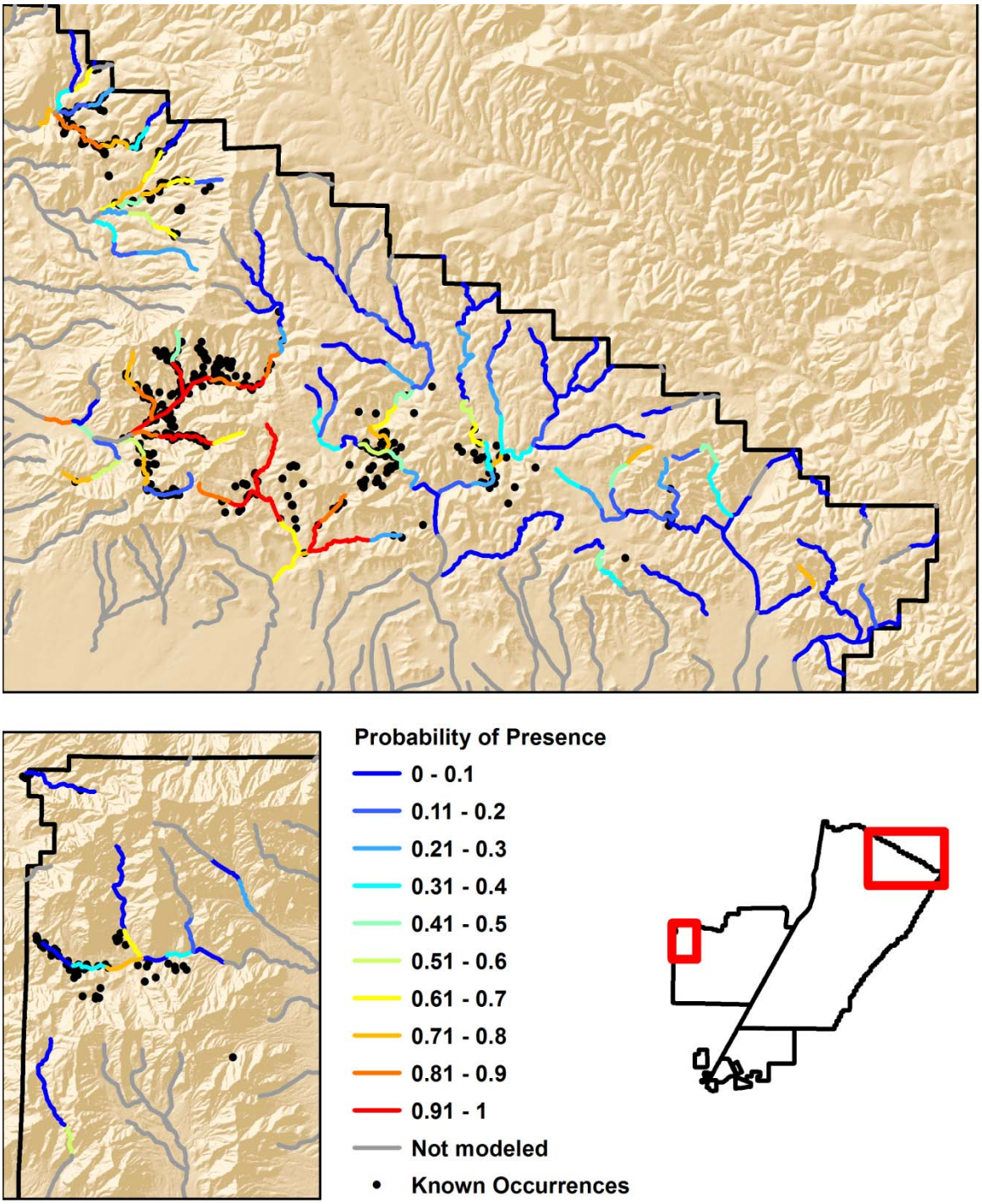


Figure 67. Logistic modeling results for gray vireo.
The Sacramento Mountains modeling area is shown above, and the Organ Mountains modeling area is shown below to the left. Using the 0.207 threshold as indicating presence, streams that are at symbolized with light blue to red could be habitat for vireos.

Figure 68 shows that gray vireo probability of presence was significantly different between stream types (Kruskal-Wallis $\chi^2 = 73.2$, $p < 0.001$). Stream type 2 had a significantly higher

probability of presence than stream types 1, 3, and 4. However, stream types 5 and 7 did not occur within the modeling area, and stream type 6 had only 3 reaches each in the modeling area. This suggests that stream type is actually a good predictor of gray vireo presence, with these birds only likely to occur in stream type 2, and possibly in stream type 6.

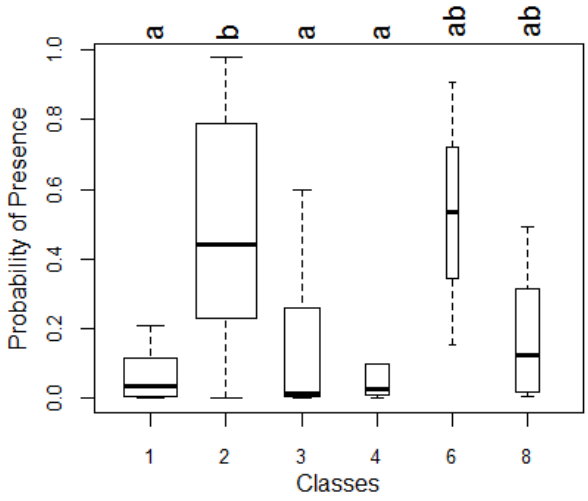


Figure 68. Probability of presence for gray vireos in stream types within the modeling area. Pairs of stream not sharing a letter indicates a significant differences between the pair.

Nesting Habitat

Including the species Kozma and Mathews and Myers et al. found to be riparian-associated, Fort Bliss had 84 birds which are likely to nest in xeroriparian areas, 41 (49%) of which are summer-only residents (Appendix C, Table 1). Nine of the 84 species were not included in the nesting habitat metric because their nest site requirements were not primarily vegetation associated; some species used burrows or cliffs, or nested on the ground. Cowbirds were excluded because they are nest parasites. Twenty-two of the 75 birds included in the metric were TER-S species. Fifty-six of the 75 species occur in the lowlands, 68 in the foothills, and 50 in the mountains. Overall, the 1 - 4 m and 4 - 12 m vegetation structure layers were the most heavily used by birds nesting at the installation, with about 40% and 30% of species using each layer, respectively (Table 42). The lowest and highest layers see use by only about 15 - 20% of birds each. Creating sub-lists for lowlands, foothills, and mountains had only very small effects on the distribution of use. Mountains showed the greatest change in use of the vegetation layers from the overall metric; use of the two lower layers decreased while use of the upper layers increased. TER-S use of the vegetation layers was also very similar to overall use. Because values for the subsets and overall were so close, overall calculations were used for all subsequent analyses.

Table 42. Number of species nesting in each vegetation layer at Fort Bliss (left) and percent of species nesting in each vegetation layer (right).

	Vegetation Layer					Vegetation Layer			
Subset	0.5-1m	1-4m	4-12m	>12m	Subset	0.5-1m	1-4m	4-12m	>12m
Overall	27	54.5	39	19	*Overall*	19.4%	39.1%	28.0%	13.6%
Overall Lowlands	21	41	27	12	Overall Lowlands	20.8%	40.6%	26.7%	11.9%
Overall Foothills	22	49.5	36.5	18	Overall Foothills	17.5%	39.3%	29.0%	14.3%
Overall Mountains	16	34	29	16.5	Overall Mountains	16.8%	35.6%	30.4%	17.3%
TERS	8	13.5	9.5	6	TERS	21.6%	36.5%	25.7%	16.2%
TERS Lowlands	7	11	8.5	5.5	TERS Lowlands	21.9%	34.4%	26.6%	17.2%
TERS Foothills	6	11.5	9	5.5	TERS Foothills	18.8%	35.9%	28.1%	17.2%
TERS Mountains	3.5	5.5	4	3.5	TERS Mountains	21.2%	33.3%	24.2%	21.2%

From 1993-1997, Kozma and Mathews and Myers et al. made 8341 observations of 51 riparian-associated species in the 13 reaches that corresponded to those in our study. Reaches were observed to have 20 – 34 species each.

From 1996-1997, Myers et al. found 150 nests belonging to 22 species of birds in 13 reaches that corresponded to those in the SERDP study. Five species, accounting for 11% of all nests (17) were not on the riparian-associated species list. Stream reaches contained nests belonging to 4-10 different species.

The original overall metric, NH_a, was not a significant predictor of S_o/km ($p=0.221$), S_n/km ($p=0.503$), $JK1_o$/km ($p=0.309$), or $JK1_n$/km ($p=0.247$), but the estimates for its effect on these measures was positive (S_o/km, 7.96; S_n/km, 1.67; $JK1_o$/km, 8.67; $JK1_n$/km, 4.94). However, once width was included in the metric, NH_w, it was a significant predictor of S_o/km (estimate = 11.08, $p=0.014$), $JK1_o$/km (estimate = 13.67, $p=0.021$), and $JK1_n$/km (estimate = 7.04, $p=0.018$) and a marginally significant predictor of S_n/km (estimate = 2.75, $p=0.132$). NH_w was a slightly better predictor of breeding bird richness than width alone for S_o/km ($\Delta AIC = 1.34$) and $JK1_n$/km ($\Delta AIC = 0.97$), while width alone was a slightly better predictor of S_n/km ($\Delta AIC = 0.20$) and $JK1_o$/km ($\Delta AIC = 0.11$).

The original metric, NH_a, and the width-adjusted metric, NH_w, are distributed differently across the installation (Figure 69). For the original overall metric, NH_a, nearly all values above 2.5 are in the mountainous areas of Fort Bliss, values between 1 and 2.5 are found in the foothills and some of the lowlands, and values below 1 account for the rest of the area, primarily lowlands. Over half of the stream-km on the installation (56.6%, 1089 km) are between 0 – 0.249, while values 2 or greater account for only 7.2% (138 km) of all stream-km (Figure 70).

The distribution of the nesting height metric changes for the width-adjusted metric, NH_w. The highest values, those over 5, are still primarily in the mountains, but some downstream reaches draining into the Tularosa Basin and on Otero Mesa also have higher values of 2.5 or more (the *widest* streams). Values from 0.5-2.5 are scattered throughout the area, while values below 0.5 make up the rest of the streams, mostly in the lowlands and foothills. The distribution of stream length values is more "normal," but still skewed to the left (Figure 70). Streams with a value of 1-1.49 are the most common (27.1%, 521 km), and values 2 or greater have increased to 30.6% of stream-km (589 km).

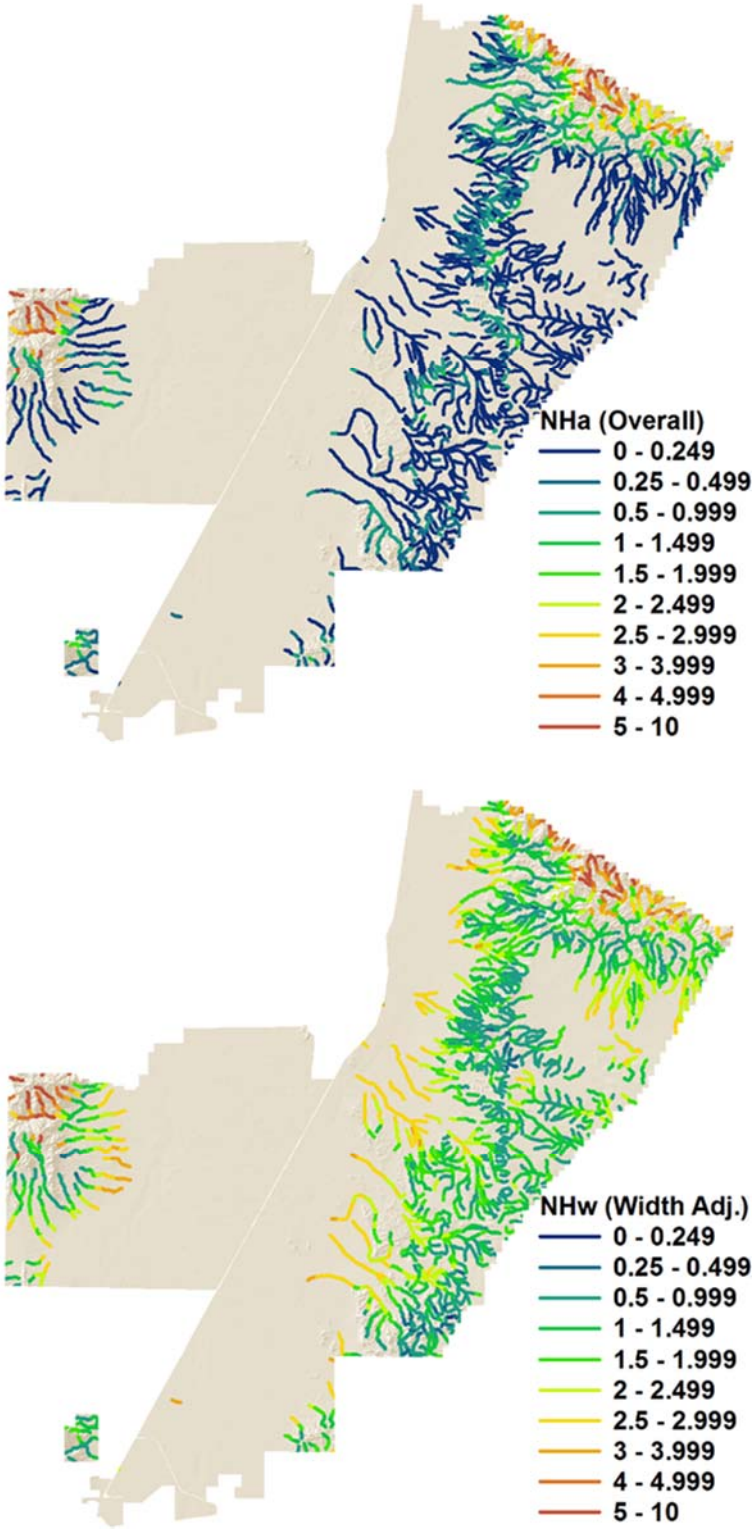


Figure 69. Values across stream reaches on Fort Bliss, NM/TX of the overall nesting habitat value metric, NH_a (top) and the width-adjusted nesting habitat value metric, NH_w (bottom).

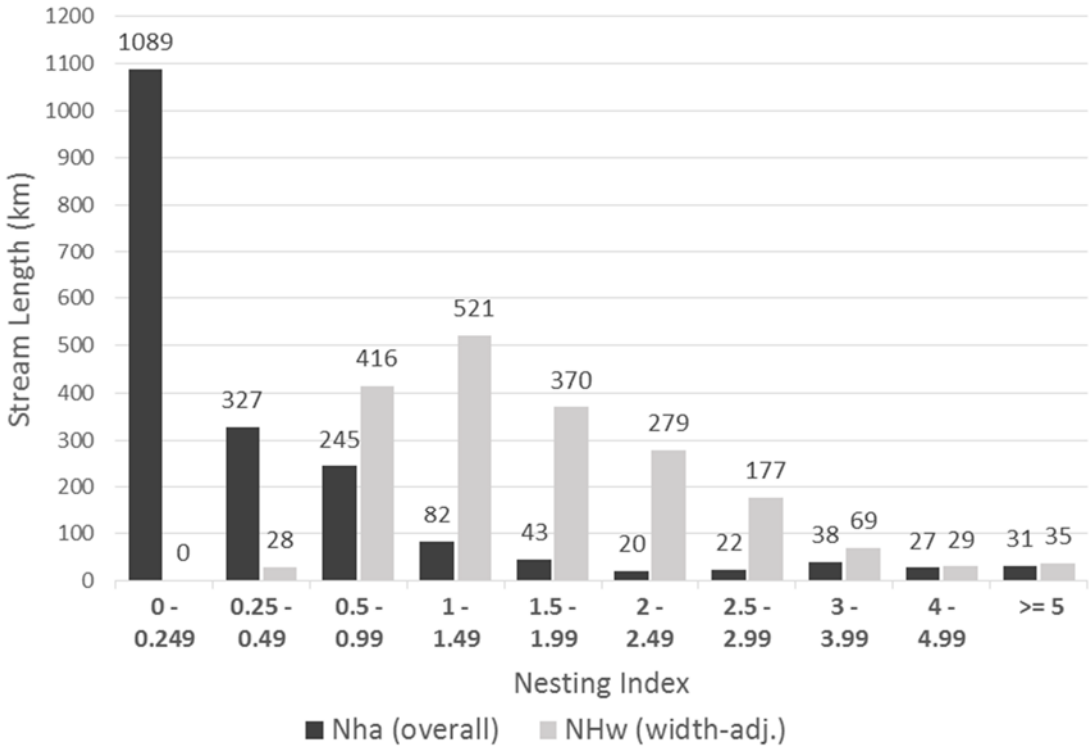


Figure 70. Total stream lengths at Fort Bliss, NM/TX of values of the overall nesting habitat metric, NH_a and width-adjusted metric, NH_w.
Number above column indicates distance in stream-km for that range of metric values.

Species richness of breeding birds (birds with only summer or year-round habitat) derived from the stacked GAP models was not a significant predictor of any measure of breeding bird richness derived from the Kozma and Mathews and Myers et al. data (Table 43). Since only 13 stream reaches in one small area of the installation were used to ground-truth, it is difficult to determine whether this actually indicates a problem with the stacked GAP model richness.

Table 43. Results of GLM regression of estimated breeding bird richness derived from stacked GAP models against breeding bird richness measures derived from Kozma and Mathews (1995) and Myers et al. (1998) for 13 stream reaches on Fort Bliss, NM.

Richness Measure	Estimate	p-value
S_o/km	-0.10	0.16
$JK1_o$/km	-0.06	0.32
S_n/km	-0.19	0.34
$JK1_n$/km	-0.14	0.19

Geographic distribution of species richness

Fort Bliss had a total of 378 possible species, 218 of which (58%) were riparian-associated (Appendix C, Table 2). For the riparian-associated species, models were available for 42 reptiles, 37 mammals, 100 birds, and 9 amphibians. Pooled richness of all riparian-associated species was correlated with richness of birds ($r = 0.77$), mammals ($r = 0.78$), and reptiles ($r = 0.71$), but not amphibians or passage migrant birds. Pooled richness was highest in the Organ Mountains, Hueco Mountains, the Castner Draw/School Tank area, and the Grapevine and Culp Canyons area (Figure 71). The escarpment of Otero Mesa was also relatively rich, while Otero Mesa itself was of average richness. The Sacramento Mountains had average to below average richness. Bird and mammal richness were correlated ($r = 0.78$). Bird richness values were distributed similarly to pooled richness, but with higher values in the Sacramento and Organ Mountains, and particularly low richness values in the Tularosa Basin and parts of Otero Mesa. Mammal richness was close to average in many of the stream reaches across the installation, but was much higher in the Organ and Sacramento Mountains.

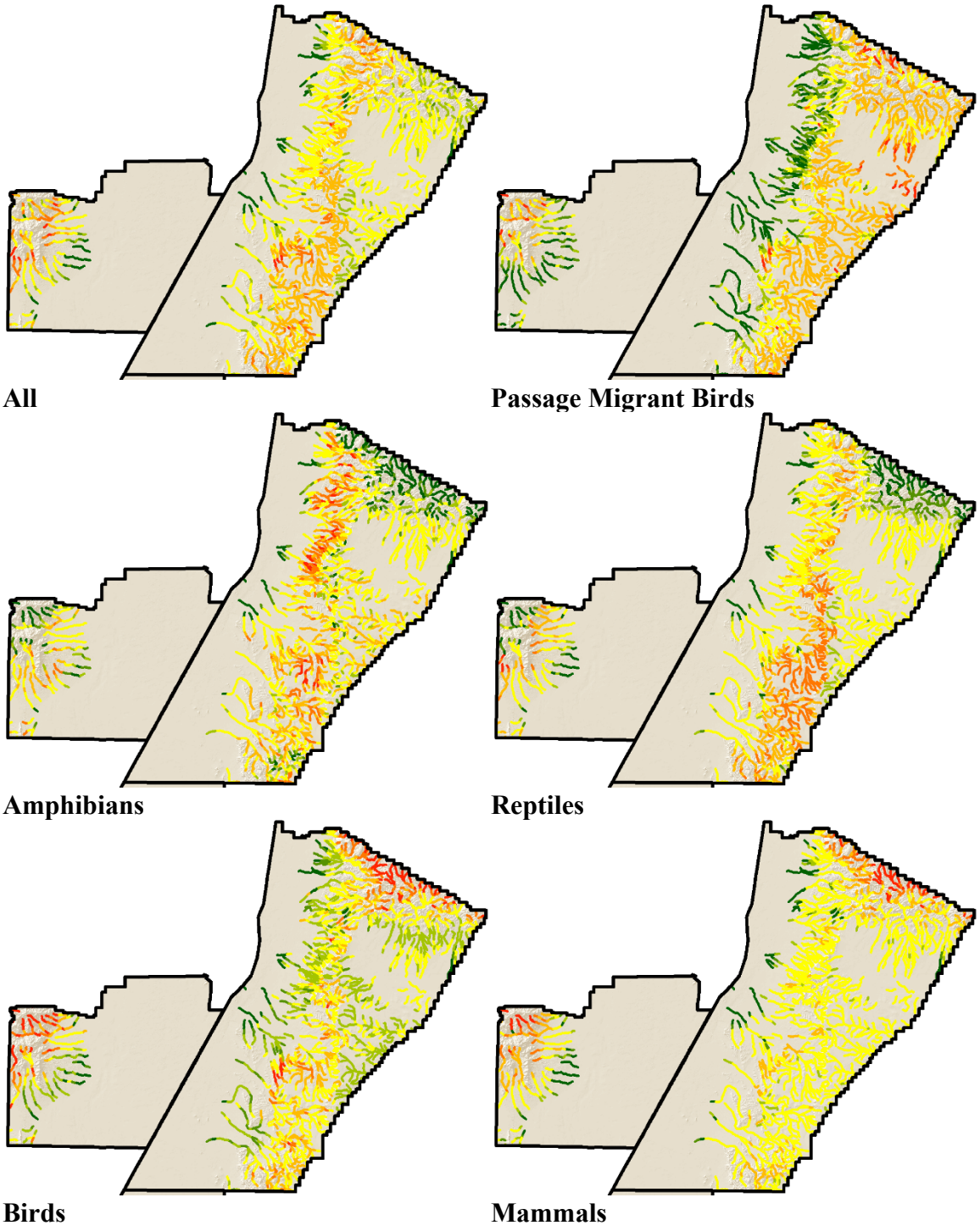


Figure 71. Fort Bliss - Richness of riparian-associated species.
Dark green reaches have a value less than 1.5 standard deviations (SD) below the mean value for the group, medium green reaches are 1-1.5 SD below the mean, light green are 0.5-1 SD below the mean, yellow are within 0.5 SD of the mean, light red are between 0.5-1 SD above the mean, medium red are 1-1.5 SD above the mean, and bright red are >1.5 SD above the mean.

Reptile and amphibian richness were correlated ($r = 0.66$) with each other – both had lower values in the Organ and Sacramento Mountains and higher values in the Hueco Mountains, escarpment of Otero Mesa, and the Castner Draw/School Tank area. Herpetofauna richness followed an opposite pattern from birds and mammals in the higher Organ and Sacramento Mountains, but was similar to these groups in the Hueco Mountains and Castner Draw/School Tank area.

Richness of passage migrant birds was highest in the mountains and east of the Otero Mesa escarpment, with particularly high richness in small areas of the Organ and Sacramento Mountains, as well as the El Paso Draw area of Otero Mesa. Streams draining off of the escarpment to the west and into Tularosa Basin had well-below-average richness.

Fort Bliss had 43 potential TER-S: 27 birds, 9 mammals, and 7 reptiles (Appendix C, Table 3). None of the amphibian species that might occur on the base fit any of the TER-S criteria. For TER-S richness, pooled richness of all species was highly correlated with bird ($r = 0.92$) richness and also correlated with mammal ($r = 0.78$) richness.

Pooled TER-S richness was highest in the Grapevine and Culp Canyons area, the Organ Mountains, parts of the Hueco Mountains, and the escarpment of Otero Mesa (Figure 72). Parts of the Sacramento Mountains and the Castner Draw/School Tank area were also high in habitat for TER-S, while Otero Mesa and the Tularosa Basin had habitat for the fewest species.

Bird TER-S richness was correlated with mammal ($r = 0.66$) TER-S richness. Bird TER-S richness was highest in the Organ Mountains, Grapevine Canyon area, and short stretches of streams on the Otero Mesa escarpment. The rest of the Sacramento Mountains, the Hueco Mountains, the Castner Draw/School Tank area, and the northern part of Otero Mesa also had above average richness. For mammals, the most species rich areas were the middle- to lower-elevation areas of the Sacramento Mountains, the escarpment of Otero Mesa, the Hueco and Organ Mountains, and a few reaches in the Castner Draw/School Tank area.

Reptile TER-S richness was distributed quite differently than and somewhat opposite from the bird and mammal groups. Streams draining the Otero Mesa escarpment, in the Tularosa Basin, and the lowest streams of the Doña Ana range had much higher-than-average richness. A few slightly higher elevation streams and scattered streams in other areas had average richness, while the rest of the installation had below average richness.

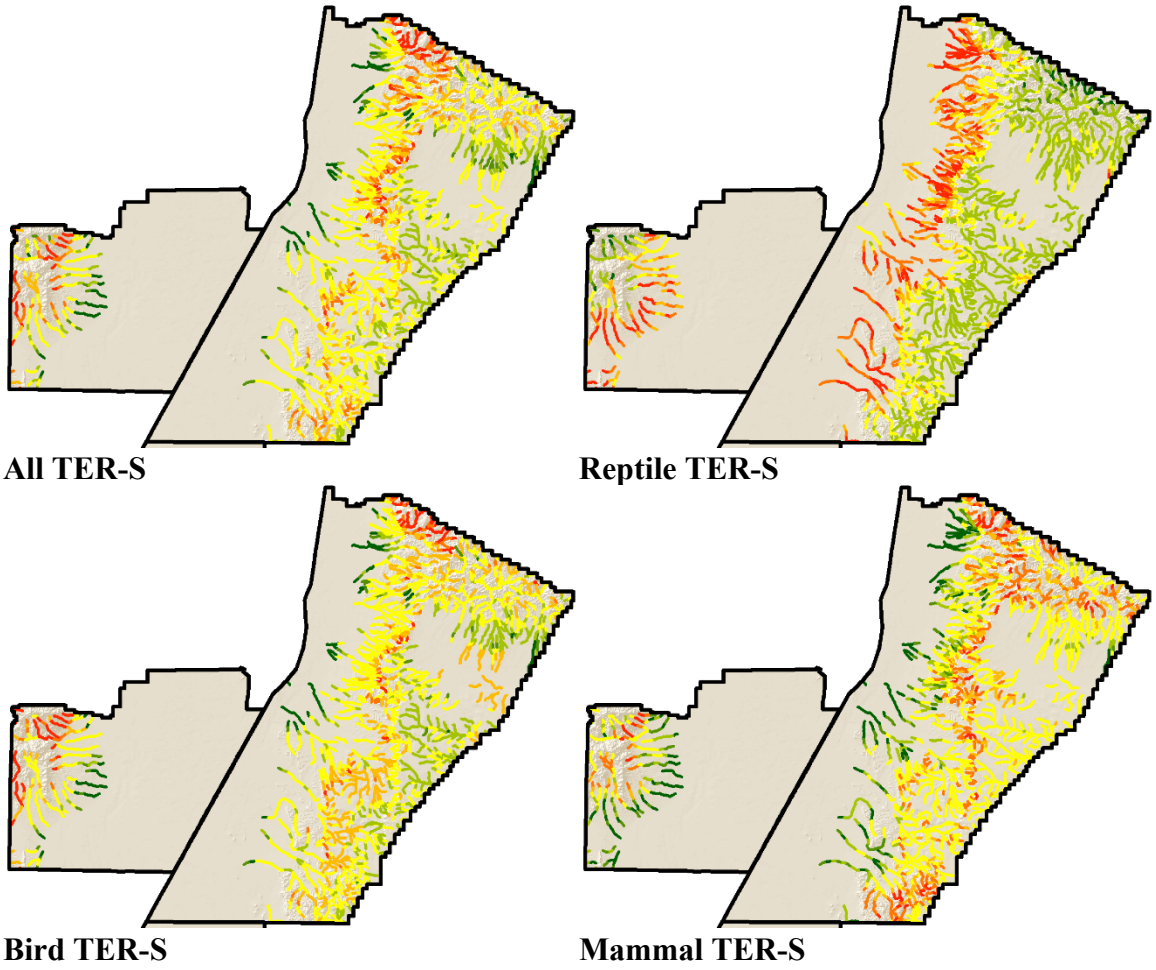


Figure 72. Fort Bliss - Richness of riparian-associated TER-S.
Dark green reaches have a value less than 1.5 standard deviations (SD) below the mean value for the group, medium green reaches are 1-1.5 SD below the mean, light green are 0.5-1 SD below the mean, yellow are within 0.5 SD of the mean, light red are between 0.5-1 SD above the mean, medium red are 1-1.5 SD above the mean, and bright red are >1.5 SD above the mean.

Species richness and stream types

When the average riparian-associated species richness in each stream type was ranked, the distribution of pooled richness into the stream types at Fort Bliss was correlated positively with the distribution of bird ($r = 0.64$) and mammal ($r = 0.71$) richness in stream types (Figure 73). For all three groups, stream types 1 and 2 have high richness and 7 and 8 have the lowest richness. Richness of amphibian and reptile species in eight stream types was highly correlated ($r = 1.00$). For both groups, stream type 1 has significantly lower richness than almost every other stream type. Both also have significantly higher richness in stream types 5 and 6 than all types but type 4, while types 2 and 3 have intermediate richness. The distribution of bird, passage migrant bird, and mammal richness in stream types were all correlated with each other (bird-mammal, $r = 0.98$, bird-passage migrant, $r = 0.81$, mammal-passage migrant, $r = 0.74$). For these groups, richness was highest in stream types 1,2, and 3, and lowest in 6, 7, and 8. Both

amphibian and reptile richness were negatively correlated with bird richness ($r = 0.60$ for both pairs), and also generally opposite that of mammal richness and passage migrant bird richness in the stream types.

Stream type 1 – Moderately high overall richness, high passage migrant bird richness, lowest reptile and amphibian richness, highest bird and mammal richness.

Stream types 2 & 3 – Moderately high overall richness in type 2, significantly lower overall richness in type 3 (moderately low), high passage migrant bird richness, moderate reptile and amphibian richness, moderate mammal richness, moderate bird richness, though significantly higher in stream type 1 than type 2.

Stream types 4 & 5 – Moderate to moderately low overall richness, high passage migrant bird richness, high amphibian and reptile richness, moderately low bird richness, low mammal richness.

Stream type 6 – High overall richness, significantly greater than all types than 1 and 2, a broad range of passage migrant bird richness, but significantly lower than types 1-5, the highest reptile and amphibian richness, significantly greater than all but stream type 5, moderately low bird richness, moderately low mammal richness, but significantly higher than stream types 4/5 and 7/8.

Stream types 7 & 8 – Significantly lower overall richness than any other stream types, a broad range of passage migrant bird richness, but generally the lowest of the stream types, moderately high amphibian and reptile richness, between that of stream types 2/3 and 6, very low bird and mammal richness, significantly lower than almost all other stream types.

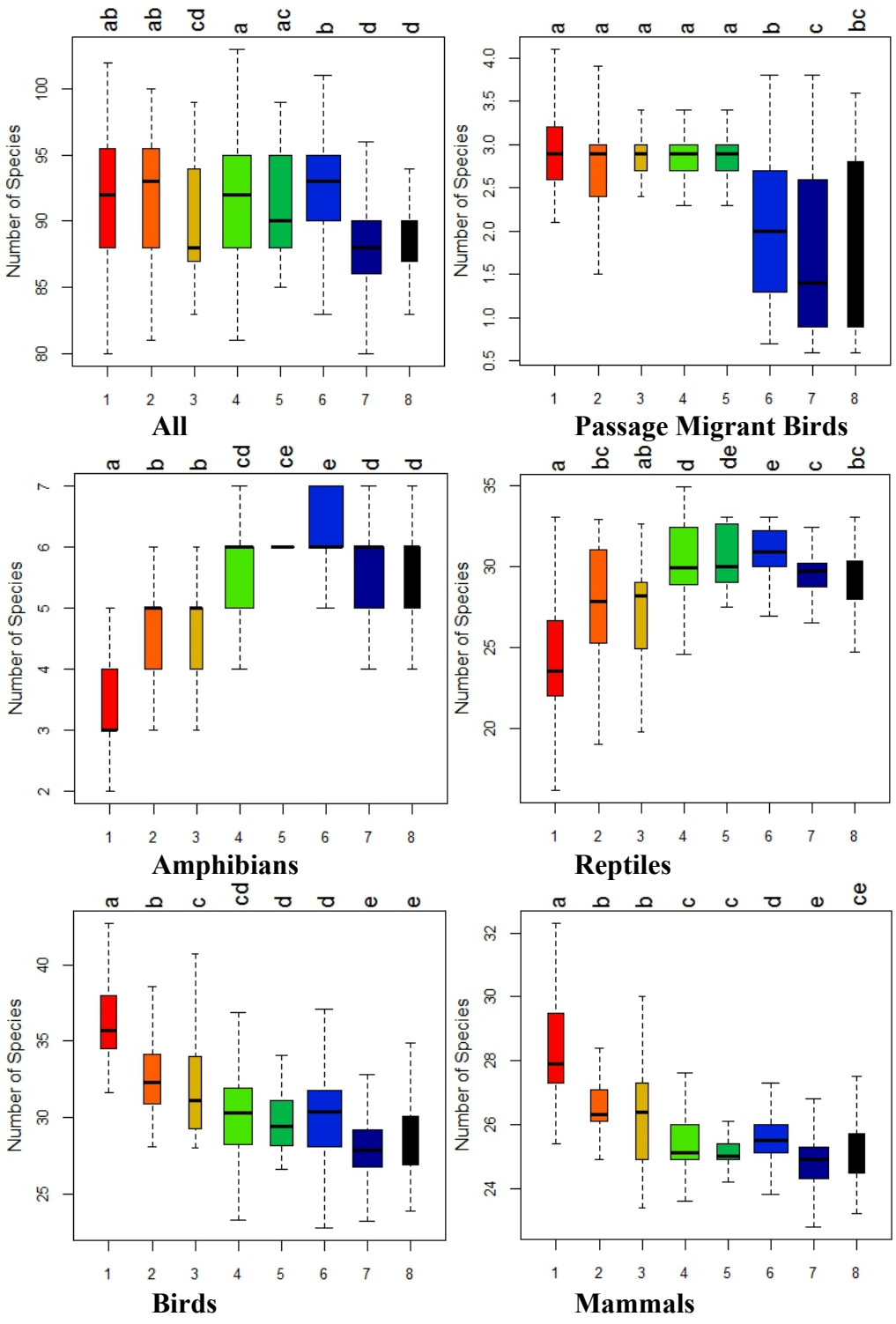


Figure 73. Fort Bliss - Richness of riparian-associated species in the eight stream types. Colors match those shown on stream type maps. Width is proportional to number of streams in each type.

When the average riparian-associated species richness of TER-S in each stream type was ranked, the distribution of pooled richness in the stream types at Fort Bliss was correlated with only bird (r = 0.88) and mammal (r = 0.74) richness (Figure 74). Bird and mammal TER-S richness were also highly correlated with each other (r = 0.86). For these three groups, type 1 and 2 stream reaches typically have the highest richness, while types 7 and 8 have the lowest richness. Reptile TER-S richness was negatively correlated with both mammal TER-S (r = -0.71) and bird TER-S (r = -0.67) richness, typically having richness low richness in stream types where mammal and bird richness were high.

Stream type 1 – Moderate overall TER-S richness, significantly higher than types 4, 5, 7, and 8, though with some streams having the highest richness on the installation, lowest reptile richness, highest bird richness, high mammal richness.

Stream type 2 – Highest overall TER-S richness on average, significantly greater than all other stream types, moderate reptile richness, highest bird richness, highest mammal richness, significantly higher than in nearly all stream types.

Stream type 3 – Broad range of overall TER-S richness, on average moderate values, moderate reptile richness, moderately high bird richness intermediate between stream types 1/2 and all other types but 6, which it is similar to, very high mammal richness.

Stream type 4 – Moderate overall TER-S richness, significantly lower than stream types 1, 2, and 6 but higher than stream types 5, 7, and 8, moderate reptile richness, low bird richness but higher than in types 5 and 7, high mammal richness.

Stream type 5 – Low overall TER-S richness, along with types 7 and 8, moderate reptile richness, lowest bird richness, high mammal richness.

Stream type 6 – Moderate overall TER-S richness, significantly higher than types 4, 5, 7, and 8, high reptile richness, moderately high bird richness intermediate between stream types 1/2 and all other types but 3, which it is similar to, high mammal richness.

Stream type 7 – Low overall TER-S richness, along with types 5 and 8, high reptile richness, lowest bird richness, lowest mammal richness.

Stream type 8 – Low overall TER-S richness, along with types 5 and 7, high reptile richness, low bird richness, very low mammal richness, but significantly higher than in stream type 7.

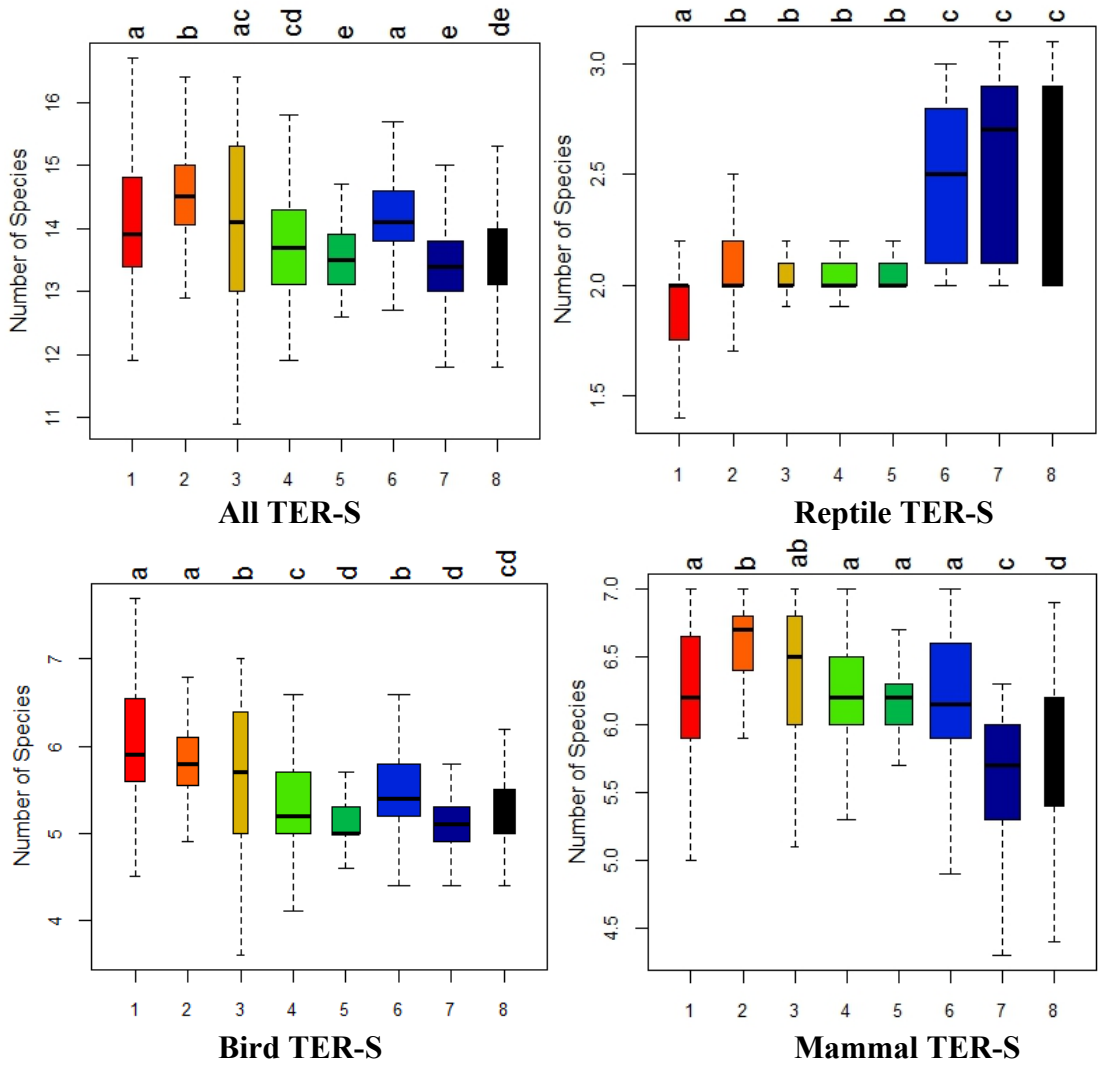


Figure 74. Fort Bliss - Richness of riparian-associated TER-S in the eight stream types. Colors match those shown on stream type maps. Width is proportional to number of streams in each type.

In individual stream reaches, richness of all riparian-associated species was highly correlated with richness of all TER-S (0.81). This was also true for the riparian-associated and TER-S mammals (0.67) and riparian-associated and TER-S birds (0.76). However, reptile TER-S richness was not correlated with general riparian-associated reptile richness (0.12). For birds and mammals, planning management for each riparian-associated general groups should benefit TER-S also, and vice versa. However, for reptiles, it is important to plan for TER-S specifically. The same patterns held when the average species richness in each stream type was examined.

TER-S response to ecohydrological variables

As a reminder, the entrenchment ratio for the wildlife analysis at Fort Bliss only was calculated by dividing the 0.5 m width by the 2 m width, resulting in higher values corresponding to greater entrenchment, the inverse of the ratio used in the rest of the study.

When pooled TER-S richness was modeled as a function of the ecohydrological variables, the largest effect was that of riparian width (Table 44). Greater riparian widths caused species richness to decrease. Elevation had the second largest effect, with higher values associated with decreased species richness. Percent cover had a substantial effect size; streams with higher percent cover had higher overall TER-S richness. The variety of landcover types had a substantial negative effect on richness.

Table 44. Fort Bliss - Effect of ecohydrological variables on all riparian-associated TER-S richness.

Parameter	*Effect Size*	*Relative Effect Size*	*SE*	95% Confidence Interval		*Relative Importance*
				Lower	*Upper*	
Width3m	-1.12	26.1	0.06	-1.12	-1.11	1.00
LidElevMidPts	-0.63	14.7	0.07	-0.63	-0.63	1.00
rendvi_pct	0.41	9.7	0.12	0.41	0.42	1.00
Landcvr_var	-0.38	8.9	0.04	-0.38	-0.38	1.00
veg05_1m	0.28	6.7	0.09	0.28	0.29	0.94
rendvi_mean	-0.27	6.3	0.08	-0.27	-0.27	0.64
CumArea	-0.26	6.1	0.05	-0.26	-0.26	1.00
Q25TSP	0.26	6.0	0.05	0.26	0.26	1.00
RSI	0.20	4.7	0.04	0.20	0.20	1.00
veg1_4m	-0.20	4.7	0.07	-0.21	-0.20	0.38
PCTSlope	0.14	3.4	0.05	0.14	0.15	0.32
FlowPerm	0.11	2.6	0.04	0.11	0.11	0.52

When reptile TER-S richness was modeled as a function of the ecohydrological variables, the largest effect by a substantial margin was that of elevation (Table 45). Higher elevations caused species richness to decrease. Two vegetation structure layer variables were also important. Higher percent covers of the 0.5-1 m and 4-12 m layers increased reptile richness, with the largest influence from the 0.5-1 m layer.

Table 45. Fort Bliss - Effect of ecohydrological variables on riparian-associated reptile TER-S richness.

Parameter	Effect Size	Relative Effect Size	SE	95% Confidence Interval		Relative Importance
				Lower	Upper	
LidElevMidPts	-0.67	44.7	0.02	-0.67	-0.67	1.00
veg05_1m	0.20	13.1	0.02	0.19	0.20	1.00
veg4_12m	0.14	9.1	0.02	0.14	0.14	1.00
rendvi_mean	-0.10	7.0	0.02	-0.10	-0.10	1.00
ER05m_2m	-0.10	6.5	0.02	-0.10	-0.10	1.00
Width3m	-0.06	4.3	0.02	-0.07	-0.06	0.99
veg1_4m	0.04	3.0	0.03	0.04	0.05	0.27
rendvi_pct	0.04	2.7	0.02	0.04	0.04	0.21
Shannon	0.03	2.1	0.01	0.03	0.03	0.55
Landcvr_var	0.03	2.1	0.01	0.03	0.03	0.69
PCTSlope	-0.03	1.9	0.02	-0.03	-0.03	0.37
Qp25	0.03	1.8	0.01	0.03	0.03	0.63
FlowPerm	0.03	1.8	0.01	0.03	0.03	0.64

When mammal TER-S richness was modeled as a function of the ecohydrological variables, the largest effect was that of riparian width (Table 46). Greater riparian widths were associated with decreased mammal richness. The 1-4 m vegetation structure layer had the second-strongest effect size. Higher percent cover of this layer decreased mammal richness. As with the TER-S reptile group, elevation was also an important variable. However, the effect of elevation was opposite that for reptiles; higher elevations were associated with increased mammalian TER-S richness.

Table 46. Fort Bliss - Effect of ecohydrological variables on riparian-associated mammal TER-S richness.

Parameter	Effect Size	Relative Effect Size	SE	95% Confidence Interval		Relative Importance
				Lower	Upper	
Width3m	-0.60	32.7	0.02	-0.60	-0.60	1.00
veg1_4m	-0.34	18.4	0.03	-0.34	-0.33	1.00
LidElevMidPts	0.28	15.1	0.02	0.28	0.28	1.00
Landcvr_var	-0.14	7.6	0.02	-0.14	-0.14	1.00
rendvi_pct	0.10	5.7	0.02	0.10	0.10	1.00
Q25TSP	0.09	5.0	0.02	0.09	0.09	1.00
PCTSlope	0.08	4.5	0.02	0.08	0.08	0.97
veg4_12m	-0.08	4.3	0.02	-0.08	-0.08	0.91
ER05m_2m	0.07	3.6	0.02	0.06	0.07	0.84
CumArea	-0.06	3.1	0.02	-0.06	-0.06	0.78

When bird TER-S richness was modeled as a function of the ecohydrological variables, the largest effect was that of elevation (Table 47). As was found for mammals, higher elevations were associated with decreased bird richness. Landcover variety had the second strongest effect, with a negative relationship with bird richness. Percent cover also had a strong effect – higher values were associated with higher species richness, indicating that stream reaches with more vegetation may support more bird TER-S at Bliss. About equal in effect was cumulative area, with higher values associated with lower bird richness. RSI also had a substantial positive effect, suggesting areas that receive more concentrated periods of precipitation host more bird TER-S at this installation.

There are several variables that had large effects on the species richness of multiple TER-S taxa groups at Fort Bliss. Bird and mammal richness in particular responded to the same ecohydrological variables. For these two groups, riparian width had the strongest effect, with a relative variable importance of 20 – 33%; greater widths were associated with decreased richness for both groups. Landcover variety was one of the four largest effects for both groups, with a relative variable importance of 8 – 13%; higher values were associated with decreased richness for both groups. Percent cover was one of the five largest effects for both groups, with a relative variable importance of 6 – 12%; higher values were associated with increased richness for both groups. Mammal and reptile richness were both strongly affected by elevation, with a relative variable importance of 15 – 45%. However, higher elevations were associated with increased richness of mammals, but decreased richness of reptiles. The 0.5-1 m vegetation structure layer had a substantial effect on birds and reptiles, with a relative variable importance of 9-13%; higher values were associated with increased richness of both groups.

Table 47. Fort Bliss - Effect of ecohydrological variables on riparian-associated bird TER-S richness.

Parameter	*Effect Size*	*Relative Effect Size*	*SE*	95% Confidence Interval		*Relative Importance*
				Lower	*Upper*	
Width3m	-0.37	19.5	0.04	-0.38	-0.37	1.00
Landcvr_var	-0.24	12.6	0.03	-0.24	-0.24	1.00
rendvi_pct	0.22	11.5	0.04	0.22	0.22	1.00
CumArea	-0.21	11.0	0.03	-0.21	-0.21	1.00
RSI	0.20	10.5	0.03	0.20	0.20	1.00
veg05_1m	0.17	8.9	0.04	0.17	0.17	0.98
LidElevMidPts	-0.15	8.0	0.04	-0.15	-0.15	0.99
PCTSlope	0.13	7.0	0.04	0.13	0.14	0.95
Q25TSP	0.12	6.3	0.03	0.12	0.12	0.95
FlowPerm	0.09	4.7	0.03	0.09	0.09	0.86

Discussion

Analysis of the stream type classification results and input variables provides an improved understanding of the ecohydrology of the ephemeral and intermittent streams and the relationships between variables at each installation. Results were unique for each installation, as expected, and could generally be explained in terms of the climate regime and geomorphology for YPG and Fort Irwin where annual rainfall amounts are very small or are largely confined to one season per year. Fort Bliss and Fort Huachuca experience higher annual rainfall amounts with a bimodal pattern, and vegetation variables are more important in those classifications. Vegetation density and cover are strongly related to elevation at all installations. Some observations for each installation are discussed below.

Fort Irwin receives approximately 110 mm (4.13 in) of annual precipitation, mainly from October through April, as widespread, long duration events, enhanced by El Niño conditions. Flow permanence at Fort Irwin is estimated at a maximum 13.1%, and a mean of approximately 2%. Peak flows are also low, with a maximum of 61.8 m^3/s, and a mean of 0.7 m^3/s for the 25-yr 1-hr event. Due to the low annual cool-season rainfall, low flow permanence and peak flows, vegetation tends to be sparse and small, and geomorphic factors become more important in distinguishing stream types. Watershed area, elevation, and reach width were the three most important variables in the CART analysis, and slope was the fifth most important (Table 5). Vegetation cover was the fourth most important. In the PCA analysis, slope, vegetation cover, vegetation less than 1 m in height, reach width and elevation were the most significant variables for the first principal component.

YPG receives approximately 92.7 mm (3.65”) of rainfall per year, with nearly half occurring during the summer monsoon season as high-intensity, short-duration thunderstorms. Although flow permanence is low (14.8% maximum, 0.2% mean), peak flows can be high with a maximum 25-yr 1-hr peak flow of 1145.2 m^3/s and a mean of 98.2 m^3/s. Geomorphic and climatic factors were the most important in determining stream types, with RSI, channel width, slope, watershed area and total stream power being the most important.

Fort Huachuca receives approximately 381 mm (15.6 in) of annual precipitation, with about 58% occurring during July – September. Peak flows are high, at 1146.9 m^3/s for the maximum 25-yr 1-hr event, and an average of 137.2 m^3/s. Flow permanence is also high at 92.5% maximum and 22.0% mean. As expected, vegetation cover is also high, and these variables were very significant in the classification. In the PCA, vegetation taller than 1m, RSI , slope and TSP were the most significant variables in the first component. Peak flow, vegetation from 4-12 m, RSI, elevation, and TSP were the most important in the CART analysis.

Fort Bliss receives approximately 220 mm (8.66 in) of annual rainfall, with about half falling during July – September. Peak flows can be very high with a maximum of 1481.2 m^3/s and a mean of 145.1 m^3/s for the 25-yr 1-hr event. Flow permanence reaches a maximum of 33.5% in the upper reaches of the Organ Mountains, with an overall mean of 2.4%. Vegetation ground cover, elevation, vegetation from 1 – 4 m height, channel width, and vegetation from 4 – 12 m height were the most important variables in this classification. The PCA results showed all

vegetation variables as being the most significant in the first principal component, followed by slope and elevation.

Overall, we found a number of the ecohydrological variables we derived to be significant predictors of wildlife richness in ephemeral and intermittent streams across the study areas. We were able to create adequate to very good models of stream use for all five species with primarily the original ecohydrological variables. Even when supplemental variables were important, they were still related to the ecohydrological characteristics of the stream. Similarly, we were able to create models of species richness for all groups we considered from our ecohydrological variables. Richness of every group was significantly related to several of these variables.

The stream types created through clustering were also useful in understanding wildlife linkages with ephemeral and intermittent streams. Stream type was a significant predictor of occurrence of gray vireos, screech owls, and Mexican spotted owls. However, desert tortoise and burrowing owl occurrences were not linked to stream type. This may have been because of the ecohydrological variables we chose to use in clustering the reaches into types, or because of where we chose to split the tree to determine the number of types. Stream type was also a significant predictor of species richness for all the species groups we examined. These results indicate classifying ephemeral and intermittent streams could potentially be a powerful tool for understanding their importance to wildlife.

Our supplemental analyses of the bosque data at YPG and breeding bird data at Fort Bliss emphasized the importance of vegetation structure to wildlife, a key ecohydrological variable influenced by climate, hydrology, and geomorphology. Both analyses also found that hydrological variables added information not provided by the vegetation variables; riparian width improved the prediction of breeding bird richness and flow permanence was important for species richness in bosques. The prevalence of the measures of the number and amount of bosques used in modeling species richness and relative abundance in the bosques also demonstrated that connectivity is critical for wildlife. Ephemeral and intermittent streams connect wildlife habitats across these larger, arid landscapes.

As noted earlier, the majority of the time spent on this project was spent in determining the most informative variables, the best methods of creating those variables, and the most appropriate methods for relating the variables and stream types to the wildlife data. As we progressed through the project we altered and improved our methods, resulting in some of the earlier methods being discarded. Some of the lessons learned and take away messages are described below.

1. Using the NHD Plus V2 flowline as the stream network limited the analysis. This dataset was originally chosen because of the rich underlying data that we planned to utilize in the geomorphic analysis. By the time we determined that the original geomorphic analysis would not produce useful results, we were too far into the project to select another stream network. Some of the issues with the NHDPlus flowline are: 1) it does not accurately reflect the total extent of ephemeral and intermittent streams, 2) it does not include stream segments less than 1 mile in length, 3) it is based on the 1:100,000 scale topographic maps which leaves out many stream reaches, especially headwater stream channels and other small streams, 4) dry streambeds that

contain water only during or after a rain event are not consistently demarcated, and 5) streams in which the flow direction could not be definitively determined were left out (stream reaches with very low slope). The resulting stream network limited the number of stream segments included in this analysis. Using the AGWA generated stream network or streams derived from the LiDAR bare earth DEMs would have greatly improved this analysis.

2. Resolution of the RapidEye imagery and QuickBird imagery for vegetation analysis may have been inadequate to capture desert vegetation. Both types of imagery provided good results for vegetation cover and density; however, the lower resolution of the RapidEye (5 m vs. 2.4 m for QuickBird) meant that smaller plants were possibly not adequately represented. In arid locations this could include a large amount of vegetation on the landscape, and might result in under-estimating the vegetation cover or density. The 2.4 m resolution of the QuickBird data was also likely too large to capture most of the smaller plants, especially at Fort Irwin where small shrubs dominate most of the landscape. Future analyses should pan-sharpen the QuickBird data to the 0.6 m resolution of the panchromatic band to improve the analysis. We tested this by pan-sharpening one tile at Fort Irwin, and comparing the difference in total amount of classified vegetation cover per stream reach. Although we speculate that this might have improved the results in some respects or in some locations, the difference in cover was not significant for this tile.

3. The method used to create the inundated polygons used for the vegetation analysis and stream reach widths could be improved. The method used was the HGVC Inundation Depth tool using a filled DEM (LiDAR bare earth or USGS 10 m DEM), a streamline, and a specified depth. To improve the results, the flowlines from the NHD Plus V2 dataset were manually edited to more closely follow the channels based on aerial imagery and the DEM or LiDAR hillshade before being used in the HGVC. We used the LiDAR bare earth DEM at Fort Huachuca, and a 10 m DEM at the other 3 installations. Possible improvements include using only LiDAR for all installations, and creating the streamline from the LiDAR data. For example, the analysis performed for the Spring 2014 IPR comparing the resulting 3 m inundated polygons generated using LiDAR vs. a 10 m DEM showed that the LiDAR gave a superior result (Figure 75, Table 48). Vertical accuracy of the USGS-NED 10 m DEM is approximately 1.55 m, while the approximate vertical accuracy of LiDAR varies depending on land cover type from 36 – 72.5 cm (from the documentation for the LiDAR acquisition for Fort Huachuca, 2009). Additionally, resolution of the LiDAR DEM is up to ten times better than the 10 m DEMs, providing a more accurate depiction of the shape of the channel and its valley. Using LiDAR for all analyses would greatly improve the resulting polygons and vegetation analyses. While we found significant differences in LiDAR vs. 10 m DEM for all widths, the 3 m inundation depth used in our vegetation analyses had the smallest percent difference and highest correlation. This minimized the possible discrepancies we might have created by using the 10 m DEM instead of LiDAR.

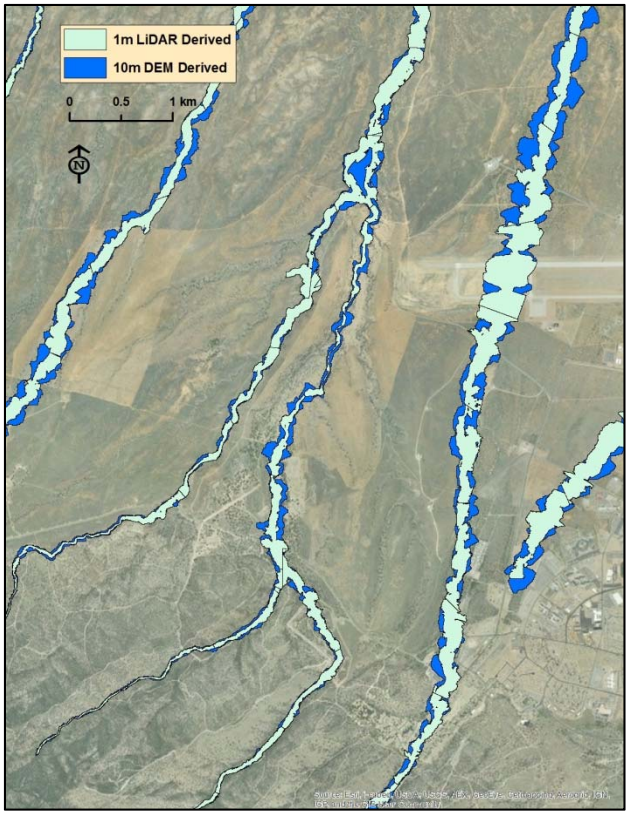


Figure 75. Map showing the difference in water surface extent derived from the 10 m DEM and 1 m LiDAR for the 3 m inundated depth at Fort Huachuca.

Table 48. Statistical comparison of derived water surface widths from a 10 m DEM vs. 1 m LiDAR at different inundation depths.

Inundation Depth (m)	Width Mean Difference (m)	Percent Difference (%)	Wilcoxon Signed Rank Test	Spearman Correlation	
			P-Value	Coefficient	P-Value
3	45.17	32.19	<0.001	0.83	<0.001
2	46.1	45.88	<0.001	0.79	<0.001
1	31.42	59.84	<0.001	0.74	<0.001
0.5	21.56	76.06	<0.001	0.72	<0.001
0.25	15.63	94.25	<0.001	0.7	<0.001

4. GAP animal habitat distribution models are intended to be used on a broad scale and are based primarily on habitat associations reported in the literature. As such, the species richness values we report should be regarded with some caution and thought of as the number of species a stream reach could potentially provide habitat for. The accuracy of our potential species richness values depends on how well species were categorized as riparian or non-riparian and the accuracy of the GAP models used to calculate richness. By using the GAP models to focus just on which stream reaches may be habitat for a species and agglomerating many species models,

we hope to have minimized the effect of any inaccuracies in the models. The GAP data provided a way to examine a broad suite of species across a large landscape. As better models at finer scale are produced in the future, our methods may yield even better results.

4.1 Action Items

Classification Coordination with Projects RC-1725 and RC-1726

The Program Office has requested that we coordinate with projects RC-1725 (D. Cooper, PI) and RC-1726 (J. Stromberg, PI) to "reconcile your various approaches to stream classification so that final proposed classification schemes are consistent and complementary, as appropriate." We have been in contact with the teams from both projects throughout this research; however, the three classifications are at different spatial scales with different methods and objectives, making it difficult to truly combine our classifications. Two efforts at classification coordination are described below.

Coordination with project RC-1726 (J. Stromberg, PI)

We coordinated with Dr. Julie Stromberg and her colleagues on project RC-1726 to examine how our AGWA flow permanence results compared to their tidbit results for flow permanence, to create a flow permanence classification at Fort Huachuca. Five of her sites corresponded with our stream network, and we used the data from those sites. Using our modeled flow permanence values where NEXRAD 2005-2012 precipitation data were used in the model inputs, and in-stream sensor results from the Stromberg team we were able to extrapolate their classification to all of Fort Huachuca. Stromberg's preliminary class names were Hyper-ephemeral (non-phreatic), Ephemeral (deep to non-phreatic), Dry Intermittent (deep to shallow phreatic), Wet Intermittent (shallow phreatic), and Quasi-Perennial (shallow phreatic). These names were ultimately not used; only the range of values was used for each class (Figure 76). However, the names provide an indication of the potential range of values for "ephemeral" vs. "intermittent" reaches.

However, extending this classification breakdown to our other sites (Fort Irwin, YPG and Fort Bliss), was not appropriate because the climate regimes are too different from Fort Huachuca (Figure 77, Figure 78, Figure 79) to be usable as defined here. Fort Huachuca has much higher precipitation and flow permanence than our other locations. Fort Irwin and YPG have similar precipitation and flow permanence, but not peak flows. Fort Irwin does not have a summer monsoon, and is dominated by frontal systems from the Pacific that typically have lower rainfall intensities. Fort Bliss has the highest peak flows of the four installations and intermediate flow permanence. Using Stromberg's preliminary classes would result in YPG and Fort Irwin having only two flow permanence classes, and Fort Bliss having three. Our goal for a classification is to be able to distinguish ephemeral and intermittent stream types beyond just two or three classes. We have not done anything further on this, but may pursue it in the future.

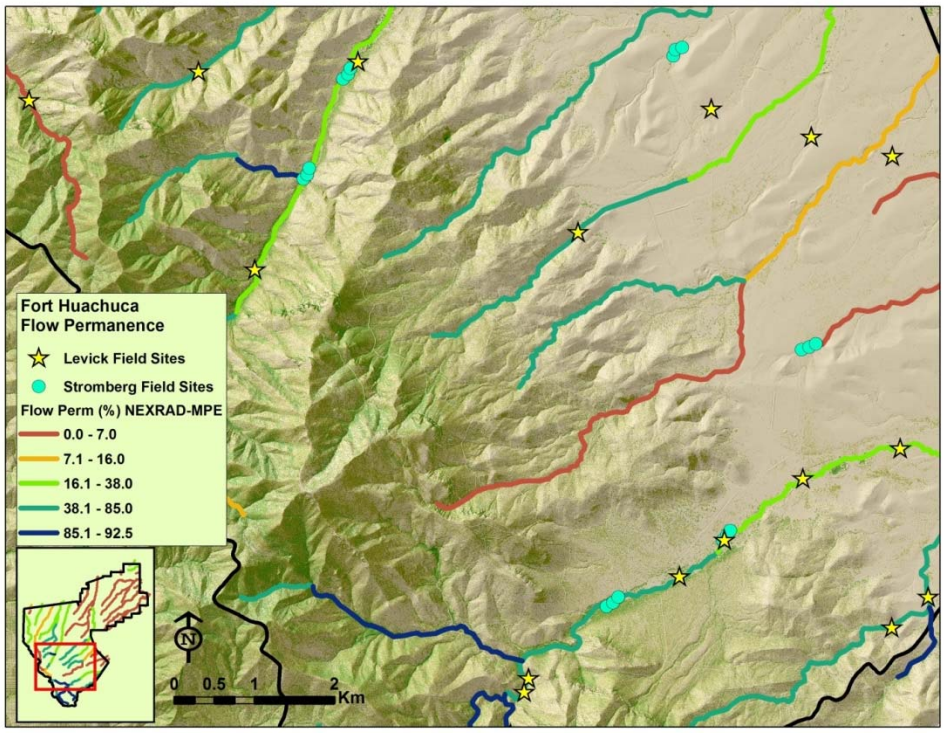


Figure 76. Preliminary coordinated classification for flow permanence at Fort Huachuca.

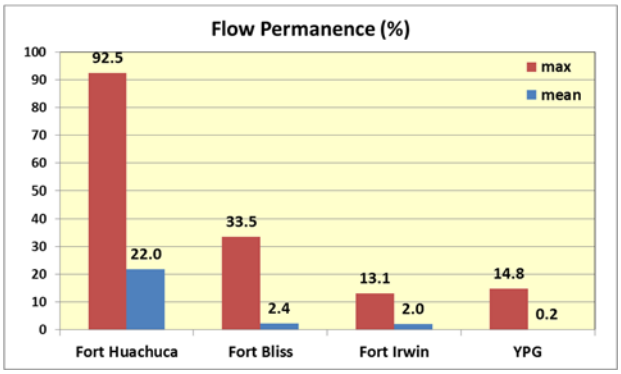


Figure 77. Comparison of flow permanence (%) at all four installations.

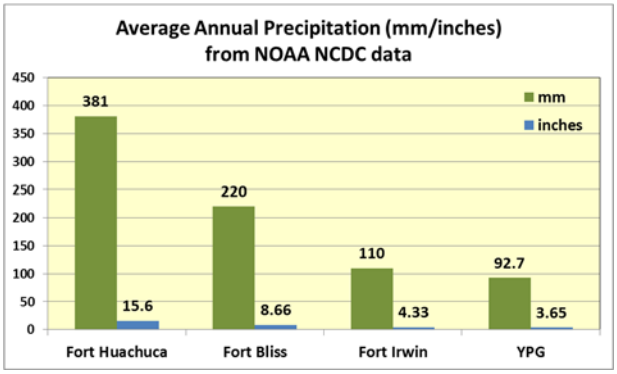


Figure 78. Comparison of average annual precipitation (mm and inches) at all four installations.

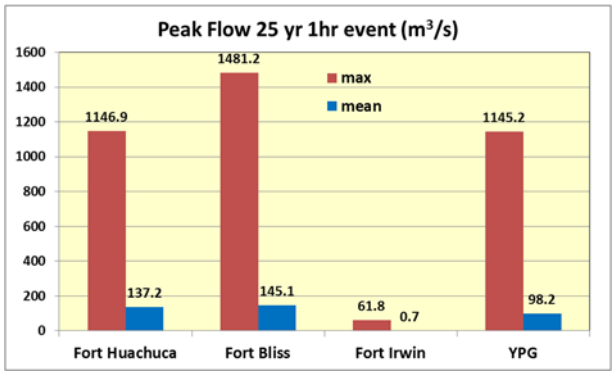


Figure 79. Comparison of 25-yr 1-hr peak flow (m^3/s) at all four installations.

Coordination with project RC-1725 (D. Cooper, PI)

Early in the project we coordinated with Dr. Cooper's team (Project RC-1725) and met out in the field at YPG to review their geomorphic data collection methods and possibly coordinate field sites. At that time, neither of us had finalized our geomorphic reach type classifications or the variables used to define the classes, and therefore we were unable to combine our classifications. However, in preparation for that field trip a preliminary analysis was conducted to characterize our stream network in terms of geology and land cover. The characterization consisted of a GIS analysis of the unique combinations of geology or rock type and land cover (SWReGAP) on a buffered stream map. Figure 80 shows an example at Mohave Wash, YPG. The unique GAP-Rock Type combinations are shown as colored lines, the yellow dots represent the Cooper Team's study locations, and the magenta dots represent the Levick Team's study sites as of January 2011. This analysis assisted us in understanding their classification goals, enabled us to assess the overall variability of stream types, and guided our selection of initial field sites to represent unique combinations of geology and land cover. This information was used to select field sites for all spring 2011 field trips, with the goal of capturing the variability in land cover and geology.

While in the field, we quickly realized that the level of detail of their data collection was much more intense than ours, and they were sampling at a much finer scale than we were and over a much smaller area. For example, their goal, as described to us, was to sample 100 sites representing the five pre-defined geomorphic stream types (braided, bedrock, bedrock with alluvium, single-thread, and piedmont headwaters) in the Mohave and Yuma Wash watersheds. Their data collection methods were aimed at geomorphic properties (cross sections, pebble counts, width/depth ratios, etc.). Our field data collection methods were geared towards understanding the variability of stream characteristics across all of YPG, Fort Irwin, Fort Huachuca and Fort Bliss, and were necessarily less detailed.

Upon finalizing our classifications, we compared our reach type classification with Project RC-1725. They produced a geomorphic classification of ephemeral channels in mountainous regions of southwestern Arizona, and developed their dataset in the Yuma and Mojave Washes of YPG. From Sutfin et al. (2014) they surveyed 86 stream reaches at YPG and took detailed geomorphic data for the purpose of characterizing five geomorphic reach classes: piedmont headwater, bedrock, bedrock with alluvium, incised alluvium, and braided channels. Their study sites were

selected to represent these five geomorphic types. They tested their results at Barry M. Goldwater Air Force Range, but did not extend their classification at YPG beyond their study sites. In contrast, our project produced an ecohydrological stream type classification that included geomorphic, hydrologic, and vegetation variables, and also attempted a geomorphic reach classification (see next section). We surveyed 74 stream reaches distributed across all of YPG, selected randomly to capture the variability in stream types, and assigned a geomorphic reach class in the field based on visual inspection. We had only 7 common sites with Project RC-1725, making a statistical comparison of results not feasible.

The two projects had different approaches, methods, goals, and spatial extents. Project RC-1725 reach characteristics were obtained mainly from field data, while our variables were obtained via GIS analyses. Our field data were used to determine the best methodology for selecting and developing the vegetation and other ecohydrological variable analyses, for assigning geomorphic reach class, and for developing a database of photographs, geomorphic and vegetation data to support our GIS analyses. The most important difference between our two projects is Project RC-1726's classification is a geomorphic classification limited to ephemeral mountainous regions in the Sonoran Desert, while our classification is ecohydrological and includes all terrain types. Our methods were developed for and applied to the four desert ecoregions across the southwest U.S., and is therefore more applicable to wildlife and natural resources management on a broader scale.

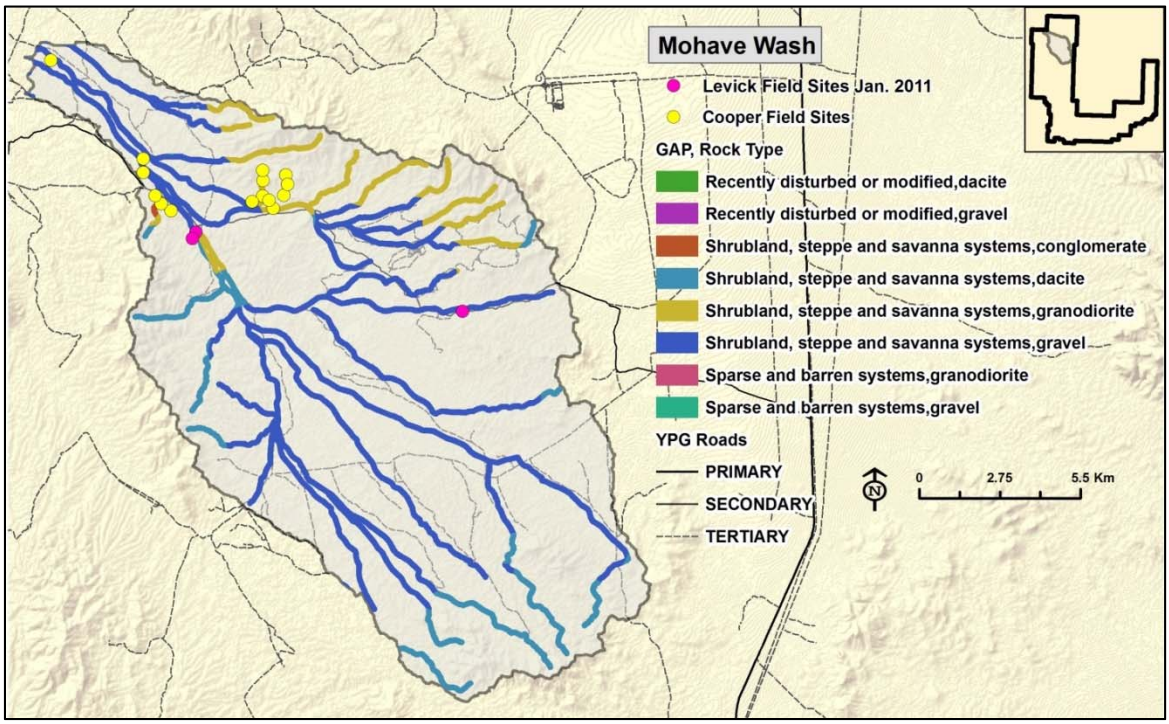


Figure 80. Map of Mohave Wash, Yuma Proving Ground, showing variability based on SWReGAP land cover and Arizona Geology.

Geomorphic Reach Type Classification

We performed a geomorphic reach type classification based on a suite of variables derived from the NHD Plus V2 dataset and other data (see Section 1, Data Mining). The geomorphic data were used to create a geomorphic-based reach type classification for each installation, for potential use in the stream type classification, and for possible coordination with David Cooper's SERDP Project (RC-1725). Our initial reach classes were based on their reach classes (Sutfin et al., 2014; Ellen Wohl, personal communication, 2011): bedrock, bedrock with alluvium, braided, incised alluvium, and piedmont headwater. These classes were developed for ephemeral mountainous regions in southwestern Arizona (i.e. the western arm of YPG; Sutfin et al., 2014).

For our analysis, we used the RandomForests (RF) model in the SPM software package, to classify all 1 km stream reaches in our stream network, using the stream reaches classified from field work to train the model. All of our field sites were identified as one of the 5 Sutfin et al. (2014) reach types based on field data and visual observation. The NHDPlus V2 and other datasets were used to derive the predictor variables, and the reach type was used as the target variable. RandomForests was used to predict reach class for all remaining reaches besides the reaches with our field sites. Depending on the installation, we used 46-50 geomorphic variables in the model, derived from various sources (Table 49) at three scales based on the NHD Plus V2 dataset: watershed (HUC12), valley (catchment) and reach.

Table 49. Watershed, valley and reach scale attributes.

Watershed Scale Attributes	Valley Scale Attributes	Reach Scale Attributes
1) Area, Width, Length	1) Area, Width, Length	1) Slope
2) Drainage Density	2) Slope	2) Mean Stream Widths
3) Slope	3) GAP Land Cover (Majority)	3) Rock Types and Lithology
4) GAP Land Cover (Majority)	4) Flooding Frequency	4) Rainfall Seasonality Index
5) Weathered Products Texture	5) Hydrological Group	5) Modified Fournier Index
6) NOAA Flood-Frequency-Duration	6) Soil Drainage Class	6) Contributing Area
7) Rainfall Seasonality Index	7) USLE - K Factor	7) Flood-Peak Discharge
8) Modified Fournier Index		8) Total Stream Power
		9) Unit Stream Power

After visiting each of the installations several times we identified stream types that were not adequately described using the five Sutfin et al. (2014) classes. This is particularly true at Fort Irwin, where large alluvial fans and broad flow-production zones dominate the landscape, and at Fort Bliss where discontinuous streams with vegetated swales or sheetflood zones are widespread. To include these unique reach types and improve prediction accuracy, we revised the classes to better represent the variability we observed at our study locations: bedrock, single-thread, braided, discontinuous, and floodout (where channelized flow stops; Tooth, 1999). We also added additional training sites using GoogleEarth (www.earth.google.com) to identify reach type. Since Fort Bliss had the greatest number of discontinuous and floodout type reaches, we tested these reach classes on that dataset.

Original prediction accuracy from the RF model was generally low (20-35% for all installations). Overall prediction accuracy for Fort Bliss improved to 50% from 32% after the modifications to

reach type and input variables. Most of the misclassification in this analysis was between bedrock and single-thread, and between discontinuous and floodout. Our dataset was not adequate to distinguish these reach types, so we combined them into single-thread and discontinuous/sheetflood, resulting in three geomorphic reach types: single-thread, discontinuous/sheetflood, and braided. In addition, we revised the predictor variables to improve predictive accuracy by adding mean riparian widths at different depths, and removing highly correlated variables and those with low predictive capability based on model output. This improved the model accuracy to approximately 80%; however we determined that our dataset was still not adequate for the model to distinguish these stream types, and that more intensive and detailed field data collection would be required to more accurately assign reach types. In addition, the model was not able to correctly classify transition zones or mixed stream reaches, indicating that our stream reaches need to be shorter in some areas. Stream reaches based on changes in vegetation, hydrology, or geomorphology might be especially useful in improving geomorphic reach classification. Our final geomorphic reach classes for each 1 km stream reach are based on field data, the RF model, and aerial imagery. Although the stream reaches at Fort Bliss were assigned a reach class, this information was not used in the stream type classification because: (1) it was only 80% accurate, and (2) it was categorical data and not compatible with the rest of our variables. Other studies have experienced similar issues with attempts to classify southwestern stream reaches based on geomorphic features (see, for example, Lichvar and McColley, 2008, and Lefebvre et al., 2013), suggesting that these streams are too variable with respect to flow regime and watershed characteristics, including location on the landscape to classify at the reach scale (Lefebvre et al., 2013).

Valley Bottom Floodplain Complex, Growler Wash

The Valley Bottom Floodplain Complex is a natural community conservation element identified in the Nature Conservancy document “Conservation Elements of and a Biodiversity Management Framework for the Barry M. Goldwater Range, Arizona” (Hall et al., 2001). From that report, Table 6.1, “Natural Community Elements of the Barry M. Goldwater Range”, this community type exhibits a spatial pattern described as a “linear/large patch system, with linear xeroriparian areas embedded within the complex, and is characterized by a shifting mosaic of vegetation patches spread across a floodplain, which may also be considered a large patch system.”

In response to a request from the Program Office to address this type occurrence, on Nov. 21, 2013, L. Levick, S. Hammer and R. Lyon visited the Growler Valley and San Cristobal Wash in Organ Pipe Cactus National Monument and Cabeza Prieta National Wildlife Refuge to sample this natural community type. The purpose of this site visit was to determine if and how this community compared to others we have seen at our other study locations.

Access was via Bates Well Road and El Camino del Diablo. Growler Wash in this area is a well-defined channel, and not representative of the Valley Bottom Floodplain Complex, so this channel was not surveyed. Instead, the valley between Growler and San Cristobal Washes was surveyed at three patch locations: two about 2.6 km north of El Camino, and one about 150 m south of El Camino. A vegetation strand/patch in San Cristobal Wash was surveyed at one

location about 2.5 km north of El Camino, and at one upland area between vegetation strands about 700 m north of El Camino (Figure 81).

Detailed vegetation and geomorphic characteristics were recorded and photographs taken for a total of five (5) locations that included patches, linear strands, and uplands. General notes and photos were taken at two (2) additional locations.

Each site is summarized below. A summary of field data from one of our study sites at a mesquite bosque at YPG are included, along with photos for comparison (Figure 82).

CP01

Located in the Growler Valley, approximately 2.6 km north of El Camino del Diablo, west of the Organ Pipe Cactus National Monument boundary road in an area of patchy bosque-like features. Two data points were taken at this location, with additional photos and notes at two other locations.
Geomorphic description: sheetflood with some discontinuous channeling, less than 1 m deep, soil 90% silt/clay, 10% sand.

CP01.1: UTM Zone 12 WGS 84 3559568.6 303048.0, elev. 332.5 m
Vegetation description: linear riparian feature with dense vegetation and standing dead trees, located in a swale, no defined channel, dominated by mesquite and creosote, with wolfberry, bursage and grasses (galleta).
Vegetation structure: 7% bare ground, 30% < 1 m, 25% 1-4 m, 2% 4-12 m, 0% >12 m
Average width 71 m, Maximum vegetation height 4.5 m

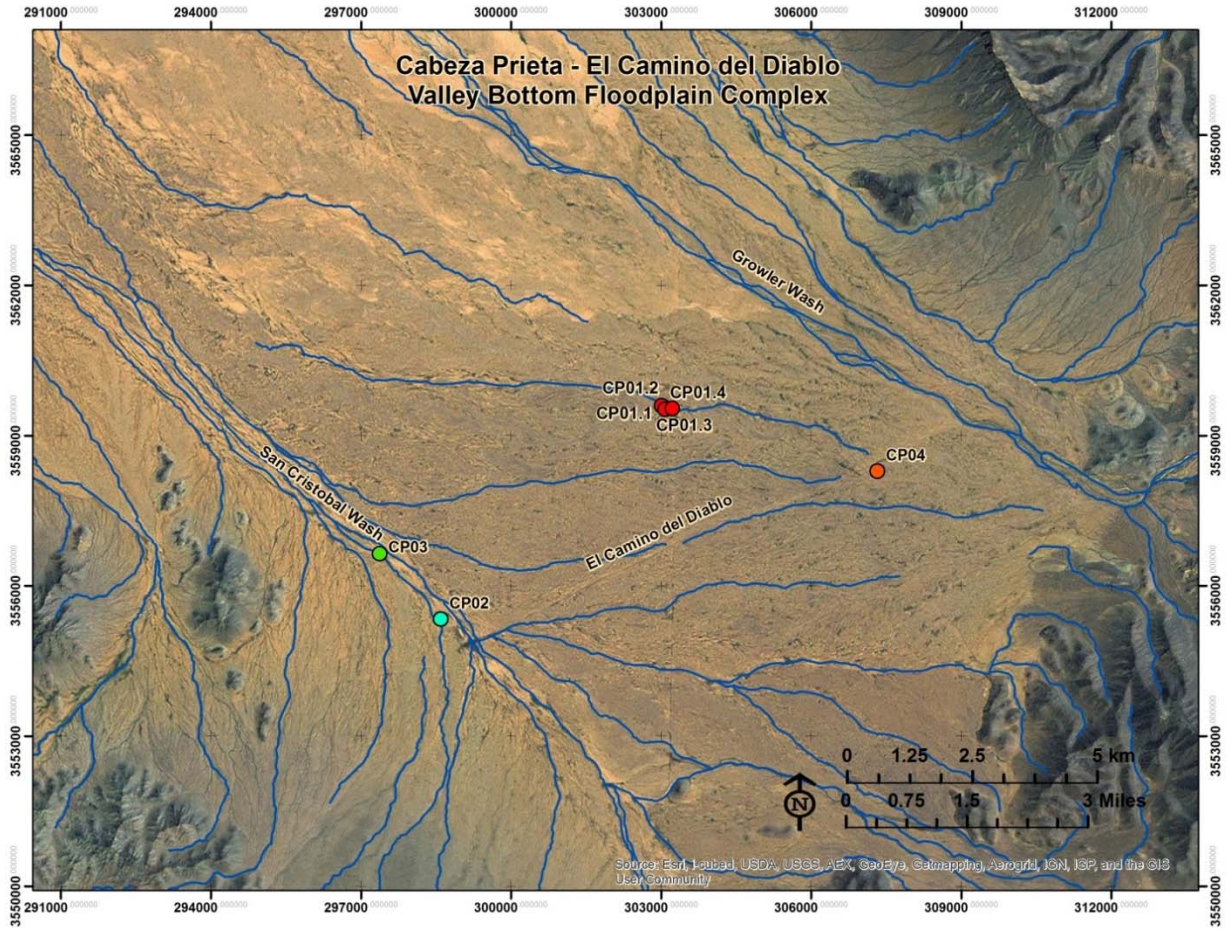


Figure 81. Map of Cabeza Prieta Growler and San Cristobal Washes, with data points. Colored dots refer to individual site locations.

CP01.2: UTM Zone 12 WGS 84 3559600.4 303011.7
Vegetation description: channel feature downstream from CP01.1, with smaller vegetation patches
Bursage, grasses (galleta), creosote, dead mesquite
Uplands: sparse creosote

CP01.3: UTM Zone 12 WGS 84 3559528.6 303077.6, Uplands adjacent to vegetation strand, start point walking back to truck, photos are for the entire walk back
Vegetation description: sparse creosote, bursage and grasses, isolated mesquite, dead mesquite and creosote

CP01.4: UTM Zone 12 WGS 84 3559542.6 303220.4
Vegetation description: Swale/patch, denser and taller vegetation than CP01.1, more defined channel, mesquite, wolfberry, grass (galleta), creosote, bursage
Vegetation structure: 10% bare ground, 25% <1 m, 30% 1-4 m, 5% 4-12 m, 0% >12 m
Average width 70 m, Maximum vegetation height 5 m

CP02: UTM Zone 12 WGS 84 3555331.0 298587.2, elev. 311.8 m
San Cristobal Wash Uplands area between vegetation strands, about 700 m north of El Camino del Diablo.
Geomorphic description: sheetflood, no defined channel, mostly silt, mudcracks, soil 90% silt/clay, 10% sand.
Vegetation description: creosote with sparse forbs and grasses, abundant dead vegetation
Vegetation structure: 80% bare ground, 10% < 1 m, 3% 1-4 m, 0% 4-12 m, 0% >12 m
Maximum vegetation height 2 m

CP03: UTM Zone 12 WGS 84 3556640.5 297365.9, elev. 304.7 m
San Cristobal Wash, vegetation strand/patch about 2.5 km north of El Camino del Diablo in an area of linear vegetation features. This was one of the more dense areas within one of the longer vegetation strands.
Geomorphic description: sheetflood with some discontinuous channeling, less than 1 m deep, mudcracks, sand bed (60% silt/clay, 39% sand, 1% gravel).
Vegetation description: dense vegetation strand, defined flow path <1 m wide/deep, mesquite, creosote, bursage, shrubs, grasses (galleta)
Vegetation structure: 5% bare ground, 5% <1 m, 50% 1-4 m, 10% 4-12 m, 0% >12 m
Average width 35 m, Maximum vegetation height 6 m
Uplands/walk back to truck: sparse creosote, barrel cactus, dead creosote and small mesquite, pencil cholla, saguaro, ground cover

CP04: UTM Zone 12 WGS 84 3558289.3 307321.9, elev. 348.0 m
Bosque, isolated patch 150 m south of El Camino, possibly associated with a longer flow path.
Geomorphic description: sheetflood, no defined channel, 100% silt/clay at GPS point.
Vegetation description: mesquite, bursage, grasses (galleta), creosote
Vegetation structure: 20% bare ground, 35% <1 m, 20% 1-4 m, 5% 4-12 m, 0% >12 m
Average width 40 m, Maximum vegetation height 7 m
Uplands: small creosote, desert pavement, dead mesquite and creosote

Data from YPG Mesquite Bosque:
Bosque1, YPG, located in the northeast portion of the Western Arm of YPG, near Tyson Wash.
No defined channel, within a creosote flat, approx. 40 m wide.
Dominant vegetation: mesquite, creosote, shrubs, grasses.
Vegetation structure: 30% <1 m, 5% 1-4 m, 30% 4-12 m, 0% >12 m



CP01.1



CP01.4





YPG Bosque1

Figure 82. Photos from Growler Wash area, Valley Bottom Floodplain Complex (top), and YPG mesquite bosque (bottom).

Summary

In general these areas within the Valley Bottom Floodplain Complex are very similar to the mesquite bosques at YPG, and to a lesser extent the discontinuous streams at Fort Bliss, in that they are patches of dense vegetation that differ from the surrounding areas in species composition, height and density, and are topographic low areas usually related to flow paths.

YPG has numerous mesquite bosques which are similar in density and vegetation diversity, but are restricted to relatively small areas, mainly in the northeast portion of the western arm of YPG (Figure 83). They follow the stream network, but do not have defined channels and are probably located in topographic low areas. The vegetation species are very similar to the community in the Growler/San Cristobal area.


Figure 83. Location of the majority of mesquite bosques at YPG.

Fort Bliss has many discontinuous stream systems, with sheetflood zones interspersed with channelized segments where the vegetation is different in composition, height and density from the uplands; however, the vegetation there is sparser, not as tall or as diverse. These features at Fort Bliss can be described as linear only because they generally follow flow paths; the patches themselves are not necessarily linear.

We do not have LiDAR or satellite imagery for the Growler Wash/San Cristobal Wash area so are unable to analyze these sites to fit them into a vegetation structure or stream type class.

Channel Incision

This section addresses an Action Item from the Spring 2014 IPR and the follow-up comments. Our response submitted with the July 15, 2014 Quarterly Progress Report is copied here, followed by our response to the follow-up comments regarding a pilot test of our proposed alternative, and an additional method of determining channel incision, which may be more feasible to apply.

QPR July 15, 2014, Suggested Method of Determining Channel Incision

Channel entrenchment or incision is a common adjustment pattern for ephemeral and intermittent streams in the Southwest. The method to create channel widths combined with the GIS slope methodology can be used to evaluate channel incision. Channel incision is useful for identifying gulleys that might impede training activities, determining steep banks that may provide habitat for wildlife, or identifying down-cutting which may indicate a watershed issue upstream (i.e. anthropogenic impacts such as urban development, cattle grazing, etc.). The degree of channel incision was not included as a variable in this classification because we did not develop it until after the classification was performed. Degree of channel incision could be a useful addition to the set of variables for the reasons mentioned above, or as an analysis variable on its own. Having more direct measures of incision in our variable set (as opposed to surrogates) could have potentially enhanced the ability to link hydro-geomorphic and biological characteristics. However, a simplistic one-size-fits all threshold of incision depth is not recommended given the wide range of channel sizes considered in this study. Instead, methods that account for the degree of incision relative to the scale and watershed position of channels are more likely to provide useful information related to ecological characteristics.

Investigations of the causal mechanisms of entrenchment (Schumm and Hadley, 1957; Mosley, 1972; Patton and Schumm, 1975; Cooke and Reeves, 1976; Bull, 1997; Pelletier and DeLong, 2004; and others) have revealed three broad classes of perturbations that can initiate the process of downcutting: land management, climate change, and internal adjustments (Graf, 1988b; Cooke and Reeves, 1976; Graf, 1983). Long term decreases in sediment to water ratio, loss of flow resistance associated with climate change, and artificial flow concentrations have all been cited as conditions favorable to erosion over aggradation (Field and Lichvar, 2007). Eventually, the increasing vertical extent of incised channels creates instability, causing the bank soils and vegetation to collapse, resulting in increased bed roughness, reducing stream power, and initiating a cyclic phase of aggradation. The alluvial water table generally drops as a result of channel incision, causing die back or death of woody vegetation along the high banks (Webb and Leake, 2006). While the process of erosion can occur quite rapidly (years to decades), phases of infilling can take much longer (decades to centuries).

Channel incision is typically determined via field methods and can be described using various ratios such as flood-prone width/bankfull width, or lowest bank height/maximum bankfull depth. These ratios describe the degree of channel incision as opposed to defining an incised channel vs. one that is not. However, since we are unable to determine bankfull depth from our dataset, we suggested the following alternative method to determine degree of channel incision (although performing this analysis at all installations is beyond the scope and timeframe of this project).

As part of the analysis for this project we have developed mean channel widths for each 1 km stream reach based on a series of inundation depths: 0.25 m, 0.5 m, 1 m, 2 m, and 3 m using the HGVC tool in ArcMap. The HGVC floods a digital elevation model given an input inundation depth or discharge / Manning *n* value. Outputs include a polygon delineating water surface extent from which we calculated the mean width for each 1 km stream reach. These widths may be used in various combinations and ratios to determine the degree of channel incision, which can also be described as valley entrenchment. We attempted to perform this analysis using a discharge value without success, due to the very complex nature of the HGVC model and inputs (i.e., we could not get it to complete the analysis without crashing). More time would be required to trouble-shoot this problem. However, we describe the general multi-stepped methodology below.

1. Stratify all stream reaches by geomorphic setting across an installation. For example, bedrock dominated areas could be separated from alluvial channels using geologic, geomorphic and soils data. Field data, slope and elevation could be used to stratify the channels further.

2. Use the HGVC tool to create inundated polygons using a reference peak discharge value obtained from USGS flood frequency regression equations for each stream reach, and calculate the mean water surface width of each 1 km stream reach at the reference discharge.

3. Test various ratios of inundation width by creating a ratio of the water surface width at the reference peak discharge (e.g., the 10-yr. USGS peak discharge, Qp10) to the water surface width at some multiple of the reference peak discharge. Different return intervals could be tested with field or LiDAR topographic data to identify the ratio that best describes the degree of incision relevant to the management question of interest. For the desert southwest, the dominant discharge based on field indicators often corresponds to a peak flow with a 10 to 20 year return period. Thus, an example ratio might be:

$$\text{Entrenchment ratio} = \frac{\text{Inundated width using LiDAR with the } 10-\text{yr peak discharge (Qp10)}}{\text{Inundated width using LIDAR with (Qp10 x 3)}}$$

Given that depth often scales with approximately $Q^{0.4}$ in at-a-station hydraulic geometry relationships (Knighton, 1998); a discharge multiplier of approximately three in the denominator would be a reasonable starting point for creating a ratio of water surface widths. Alternatively, depths corresponding to the reference discharge could be used to construct the ratio. For example, Dodov and Foufoula-Georgiou (2006) used a depth multiplier of 1.6 to construct an entrenchment ratio based on water surface width.

This approach would account for both geomorphic context through an initial stratification of channel types and the scale-dependency of incision depth across a broad range of drainage areas and dominant discharges.

<u>Alternative method of determining channel incision using GIS slope analysis</u>

This method is based on the concept that changes in slope or percent slope at channel banks can be used as a measure of incision. This method was tested in ArcGIS using the “slope” function

on a LiDAR bare earth 1 m DEM to get the slope of channel banks. We tested this method for a subset of streams in the East Range at Fort Huachuca, and the approach is described below. The accuracy of this method is largely dependent on the accuracy of the stream line used to create the inundated polygons. The best result would be obtained if the streamlines were generated using the LiDAR DEM, and the inundated polygon generated from the LiDAR DEM and that streamline. The difference in slope or height from top of bank to channel bottom can also be used to determine degree of incision. This example illustrates using the mean bank slope.

1. Using the 0.5 m and 2 m inundated polygons created with the HGVC Inundation tool, erase the 0.5 m water surface width polygon from inside of the 2 m (or other) polygon to isolate the channel banks from the bottom and floodplain.

2. Run the Slope tool using the LiDAR bare earth DEM to get a layer of the bank slopes.

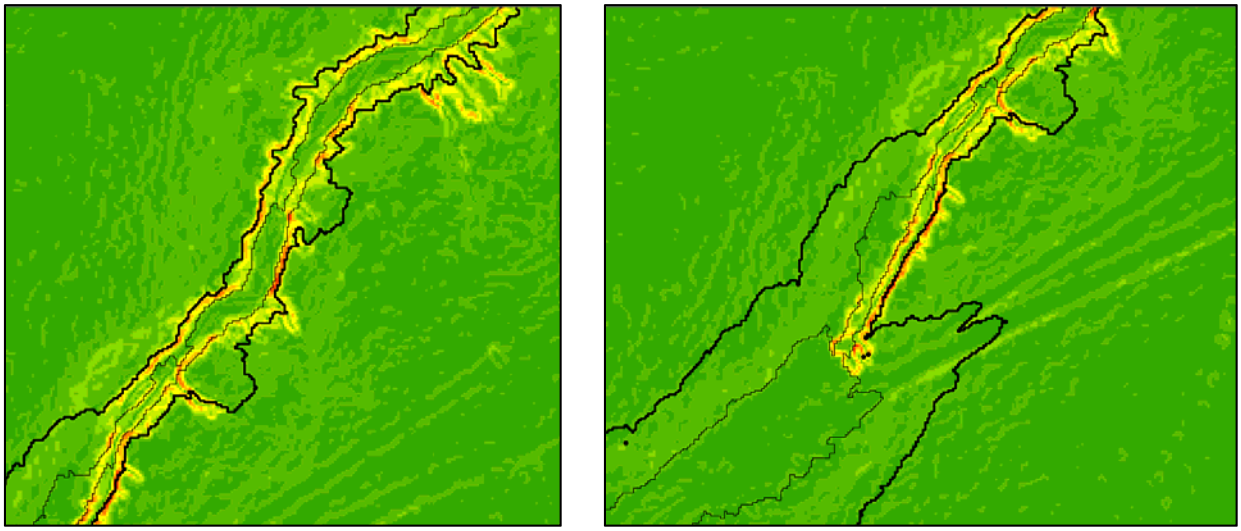


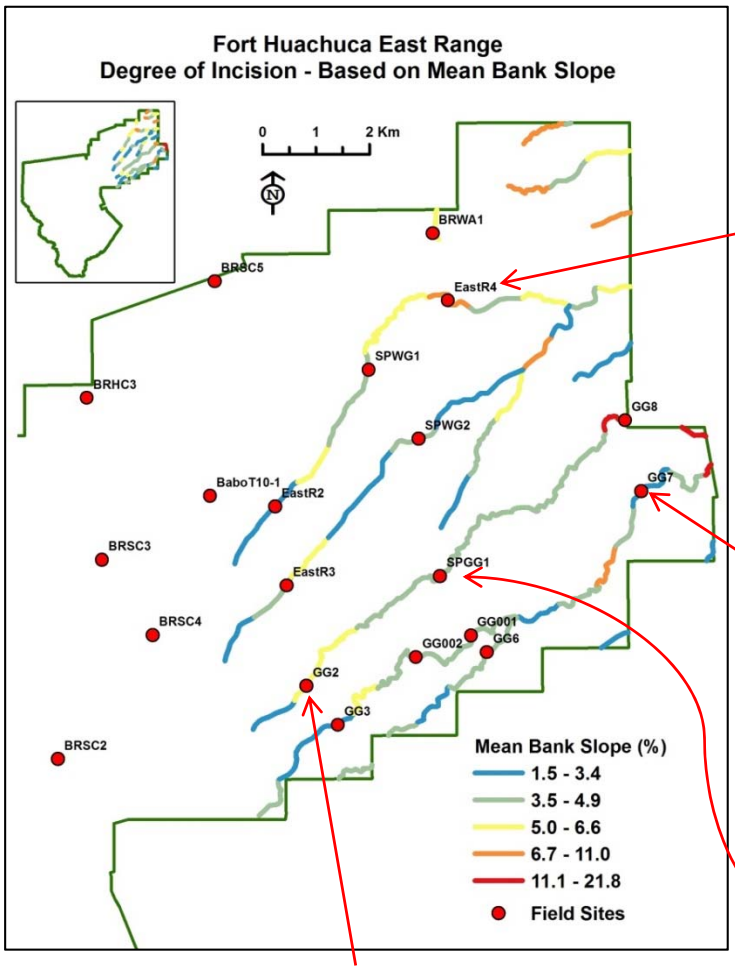
Figure 84. Illustrations of bank slope, with the outline of the 0.5 m and 2 m water surface width polygons.

Figure 84 illustrates the bank slope where slope increases from dark green (lowest slope) through yellow to red (highest slope). The difference in the polygons captures the channel banks fairly well. Notice the headcut in the stream section in the image on the right.

3. Run "ZonesWOverlap" tool (Clark, 2012) in ArcMap using the erased polygon layer as the zonal feature class, and the slope layer as the value raster. This will output a table of the summary statistics for slope for each 1 km polygon, including mean and maximum values. Note that these values reflect both sides of the channel for the entire 1 km stream reach.

4. Map the "mean bank slope" results on the stream network for each 1 km stream reach (Figure 85). Lower values for slope indicate less incised (blue lines); higher values indicate more incised (red lines). Green lines represents stream reaches with a slope of at least 3.5, which is where we estimate streams begin to be incised. Photos of field sites illustrate the range of values from "un-incised" to "highly incised." For stream reaches that have a head-cut and transition from un-

incised to incised, the degree to which the mean bank slope is affected depends on how far up the stream reach the nick-point is found.





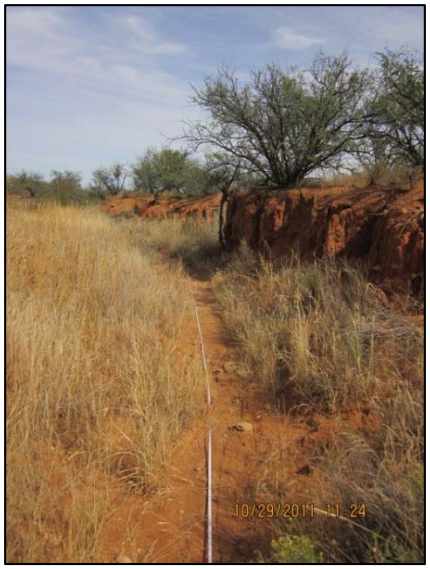
EastR4: Mean Bank Slope 8.9%



GG7: Mean Bank Slope 2.8%



SPGG1: Mean Bank Slope 4.0%



GG2: Mean Bank Slope 5.2%

Figure 85. Map of stream reaches displayed with "Mean Bank Slope" (blue = lowest to red = highest) and photos of selected field sites.

5.0 Conclusions and Implications for Future Research/Implementation

A stream type classification procedure was developed and applied at four military installations located in four southwestern ecoregions, using a cluster analysis of a set of variables specific to each installation. A CART analysis of the classification results defined the range of the most important variables for each class, providing a method of placing a new stream reach at each installation into the classification. This predictive model is summarized in tables for each installation, where the percentage of stream reaches that fall within the thresholds (range of values) for each variable is shown for each stream type. The threshold that represents the largest percentage of reaches is highlighted using a bold font and is a good predictor for that stream type; when the percentages for all ranges are similar that variable is not a good predictor for that stream type (see Section 4). The Guidance Documents included as appendices explain how to obtain each variable, which are necessary to obtain to be able to use the tables. Many variables can be derived from commonly available GIS data or LiDAR (elevation, slope, and watershed area), or from USGS gage data (rainfall). Once the stream type is identified, the wildlife analyses can be used to determine the relative richness of the different wildlife groups (mammals, birds, amphibians, reptiles, TER-S, etc.). The methodologies used to analyze wildlife observation data can be applied to other species of concern to evaluate their habitat requirements or potential habitat locations with respect to our variables.

The data layers derived for each installation that are required to develop the input variables are included in the data catalogue, and can be used to perform this analysis on stream reaches not on the NHD stream network used in this project. A limitation of applying the classification to other installations is the availability of the data required to derive the variables, and the ability to perform the required analyses. For example, a LiDAR DEM may be available to derive reach elevation and slope, but multi-return LiDAR data are required for the vegetation structure variables. Satellite imagery and the ability to process and analyze it are required for the vegetation cover and mean vegetation index variables. Ability to run the AGWA hydrologic model and compute flow permanence is also required. In addition, the predictive models and classifications are specific to the ecoregion in which they were developed, and should only be applied within the installation for which they were developed, or in the areas immediately surrounding that installation and within the same ecoregion. The Guidance Documents included as appendices to this report include the methodologies to perform these analyses. The installations were provided with all data derived for this project.

The field procedures, modeling methods, and classification system will be useful for determining ephemeral and intermittent stream features and wildlife habitat for base resource management needs. Resource managers at each installation will receive a broad range of physical and biological attributes that are spatially referenced to stream reaches in a GIS database. These attributes can be used to assess relative susceptibility to disturbance using the database and multi-criteria decision analysis. The ecohydrological classification, GIS database, and mapping tools provide for flexibility and adaptive management as information availability and objectives evolve over time.

We have provided several sets of information about wildlife for managers. We developed distribution models for how five species of management concern use stream reaches. These

provide better maps of which areas species use than were previously available and elucidate which ecohydrological characteristics are associated with their occurrence. Managers can use the maps to adjust high-impact training away from streams important for these species and better plan future surveys for the species. They could potentially use the information on which ecohydrological characteristics are important for the species to plan habitat improvements to marginal areas and prevent activities that might lower the habitat value of currently good habitat. Occurrence of the three species at Forts Huachuca and Bliss was associated with stream type; this could be used to simplify implementation of the previous suggested uses.

We also developed maps of species richness in stream types, associated species richness with stream types, and examined the correlation of species richness between the species groups, and created models to show which ecohydrological characteristics were associated with TER-S richness. As with the data on individual species, managers can use the maps to adjust high-impact training away from streams high in overall species richness or species richness of a particular group of species, including TER-S. The richness maps may also identify valuable areas that have been overlooked. Managers could potentially use the information on which ecohydrological characteristics are important for TER-S richness to plan habitat improvements to marginal areas and prevent activities that might decrease potential richness of valuable stream reaches. Additionally, the correlations of species richness between groups should help managers better understand how a planned action will influence other groups.

The analysis of the bosque camera data also provided some potentially useful insights. Vegetation structure above 2m and measures of bosque connectivity (number of bosques and amount of bosque environments) consistently were important variables that positively influenced species richness and abundance. This information can be used to help direct training and development of new training areas to locations that minimize loss of connectivity and bosques with the most valuable vegetation characteristics.

The nest height metric developed for Fort Bliss provides an estimate of the value to breeding birds of stream reaches across the installation. It requires further verification, but should serve as a useful tool for planning surveys and other studies. Even in its current form, it could be used to avoid high-impact activities in areas very likely to be breeding habitat for many bird species.

In addition to these suggested uses, we have developed methods of understanding the link between ephemeral and intermittent streams and wildlife that can be applied by managers seeking to do more detailed analyses. For example, managers could develop richness maps for a select group of species in which they are interested, create distribution models for other species of concern with the ecohydrological variables we have provided, or predict which stream reaches provide habitat for a select group of breeding birds.

A new method of using LiDAR to explore vegetation structure was developed that increases knowledge about riparian vegetation by adding a vertical component for describing vegetation features. It also provides a new tool to define potential wildlife value based on their use of vegetation structure. Classification schemes are becoming widely used as a tool to improve understanding and prediction of complex ecological data and patterns; however, these tools are best used as supplements to local ecological knowledge (Olden, et al., 2008).

The tools and products from this research meet specific needs for improved management of military lands in support of sustained land use for testing and training. Specifically, the AGWA tool provides the ability to evaluate the effects of land cover and climate change scenarios on the hydrologic flow regime, identifying areas of increased or decreased flows or sediment yield that could interfere with the use of some roads or training areas. This information can aid in planning new training areas, or in designing road modifications. Complete datasets with tutorials for performing these analyses are provided to each installation. The wildlife species richness models and specific species distribution models provide information on locations that are important to wildlife, and that could be included in future wildlife surveys, or protected from training activities. The input variables and stream type classifications are delivered in tabular and spatial formats with a Unique ID for each stream reach, allowing managers to evaluate individual variables. As examples, they will be able to select all stream reaches with vegetation cover greater than 50%, or slopes less than 1%, or peak flow greater than 100 m3/s, and so on. The stream type classification can be used in a similar manner. Having this type of information readily available will be a benefit to natural resource managers by supporting their management activities for protection of the resources needed for both wildlife management and for sustaining land use in the context of military training and testing. We have provided tools and datasets that are ready to use as is, and also training workshops, tutorials and guidance documents that will support continued and expanded use of these tools

Remaining Research Questions/Future Research

While collecting and analyzing the data for this project, and developing the methods to produce the stream type classification and wildlife associations, numerous issue arose that point to the need for additional research. Some of those issues are listed here.

a. A better method is needed to delineate homogeneous stream reaches for use in ecological studies. The streams for this project were split into 1 km segments by dividing the stream reach into equal segments as close to 1 km as possible. As a result the stream reach breaks did not correspond with on-the-ground changes in geomorphology, vegetation or hydrology. Additional research is needed to determine an improved method to split stream reaches based on those features. For example, in mountainous areas reaches might be split based on change in slope, or sinuosity. This would improve the input variables and resulting classifications developed for this project.

b. Additional research is needed as a follow-up to this project to field test the species richness estimates, and determine if they are useful. This project did not include time or funding for these tasks.

c. This research used a method to estimate mean channel width that encompasses the riparian vegetation zones; however, other methods of defining channel or riparian zone widths exist (various equations, Soar and Thorne, 2001) that could be investigated using channel forming flows and TSP values, for example. Related to that, a method to define the width/extent of just the riparian vegetation either on the banks of the channel or within it would be useful for relating vegetation to wildlife use. Since these streams provide

movement corridors for wildlife, measures of patchiness or connectivity would also be helpful in future studies. Degree of channel incision, combined with channel width could potentially enhance the ability to link hydro-geomorphic and biological characteristics (see Section 4.1, Action Items, Channel Incision for more information on deriving channel incision).

d. This project used USGS 10 m DEM data and LiDAR-derived DEM data for the analyses (see Table 50 below). Future research could determine the impact on the vegetation variables and resulting stream type classifications when using only LiDAR-derived DEM data to delineate the riparian zone (via the HGVC inundation tool) rather than the lower-resolution DEMs. We speculate that using LiDAR data for all analyses might produce different results. The HGVC tool produces a polygon layer that was used to calculate reach widths (water surface extent for a given depth above the thalweg), and also to derive the vegetation variables (vegetation height from multi-return LiDAR, and vegetation indices and cover from satellite imagery). We used the LiDAR-derived DEM to delineate the riparian zone at Fort Huachuca only; a USGS DEM was used at the other installations. Additionally, multi-return LiDAR data were used to develop the vegetation structure variables, but were not available for YPG in time for use in these analyses. We evaluated the difference in producing inundated polygon areas with LiDAR vs. USGS data for a small area and found a small but noticeable difference (for the 3 m inundation depth); however, we did not compute and compare the vegetation variables. The resolution of the LiDAR data is much finer than the USGS data (1 m vs. 10 m), and its use in the HGVC tool would create riparian polygons that more closely approximated the topography on the ground, resulting in a better approximation of the riparian vegetation extent and resulting calculations.

Table 50. Use of USGS DEM and LiDAR-derived DEM data in the analyses

	Type of Data	
	Riparian Zone Polygons*	Vegetation Structure variables
Fort Irwin	10 m USGS DEM	1 m Multi-return LiDAR
YPG	10 m USGS DEM	n/a
Fort Huachuca	1 m LiDAR-derived DEM	1 m Multi-return LiDAR
Fort Bliss	10 m USGS DEM	1.5 m Multi-return LiDAR

*Riparian Zone Polygons were used to derive input variables: reach widths, vegetation cover, mean vegetation indices, entrenchment ratios from the reach widths, and SVRI from the mean vegetation index at YPG.

e. Further research could be conducted that combines all data developed for this project to determine if a combined classification is possible for the entire southwest as opposed to the ecoregion – specific classifications that were developed here. A preliminary analysis indicated that this could be accomplished; however, additional data and processing time would be required so that all datasets were uniform. Currently we do not have LiDAR-derived vegetation structure data for YPG, and the data derived from the different types of satellite imagery would need to be standardized.

f. Further research might determine if the LiDAR vegetation structure data and the vegetation indices can be combined to improve the extraction of the riparian vegetation zone for ephemeral and intermittent streams.

   Both vegetation structure and vegetation greenness can indicate more dense or lush vegetation suggestive of riparian areas, and by combining these two data types, a better delineation of riparian zones might be accomplished. While both on their own can be used to do this, combining them should be more effective. The MSAVI2 vegetation index and the Red Edge NDVI both use spectral data to identify areas of higher greenness, usually found along riparian zones. The LiDAR structure data can also indicate riparian areas by identifying taller vegetation than in the adjacent upland areas. Vegetation is generally taller and denser along stream channels in arid regions than in the uplands due to increased moisture. Both of these data types were used in the project; however, they weren't combined in such a way that would improve identification of riparian zones. By thresholding or classifying both types of data, the location where vegetation transitions from riparian to uplands might be distinguished. The difference in greenness and structure in combination should be able to delineate riparian vegetation as distinct from the uplands or channel bed. Our efforts to perform this type of analysis were not successful, and we found the HGVC tool to be more efficient for our large study area. However, further investigation might produce a more efficient methodology.

Potential for direct implementation for DoD and others

The stream type classifications, wildlife analyses, and input variables can be used as presented here for supporting and informing management actions. The AGWA tool can be used immediately to evaluate management actions or climate change scenarios that modify the input variables, to determine if and how the stream type and wildlife associations might be affected. All data and results were delivered to each installation with guidance documents to facilitate their use. All variables and results are spatially referenced to each stream reach using a "Unique ID" and can be used immediately to evaluate individual stream reaches for management needs.

Although the AGWA results for flow permanence and peak flows were not tested or validated at each installation, the AGWA tool and its embedded models have been tested and validated at numerous locations around the world. See Goodrich et al. (2012) regarding KINEROS2 and AGWA, model use, calibration and validation. For the SWAT model, see Arnold et al. (2012) regarding SWAT, model use, calibration and validation, and Baker and Miller (2013). For this project, AGWA/SWAT was calibrated at Fort Huachuca (Lyon, 2013) where 2 USGS streamflow gages were available. No gages were available at the other 3 installations; therefore Fort Huachuca was used to perform the calibration.

The stream type classification was not tested or validated in the field primarily due to lack of time; however, field data, photos, and site knowledge were used extensively in selecting the methodology to create the stream type classification and verifying the number of final classes to represent the variability of stream reaches across each installation. The CART predictive models

(regression analysis) included cross-validation which withholds portions of the dataset for validation.

The wildlife species richness models were not tested or validated except for the small test case at Fort Bliss using the 13 stream reaches for which breeding bird data were available. The mesquite bosque data were not tested with an independent set due to the very small sample size. The breeding bird nest height data at Fort Bliss were verified with the field data. The species distribution models for specific species of concern at Forts Bliss, Huachuca, and Irwin all were tested or built with a test set or cross-validation.

The classification procedure was developed and applied using data specific to each installation and the data and methodologies are appropriate for use in extending the classification to streams not on the NHD stream network within each installation. The threshold values related to the classifications may be used to apply the classifications in areas with similar hydrologic regime and geomorphology (i.e. the same ecoregion) surrounding each installation. The methodology and procedures are broadly applicable; however, a limitation of applying the classification procedure to other locations is the availability of the data required to derive the input variables, and the ability to perform the required analyses. This classification methodology should be reviewed and tested if applied beyond the ecoregion for which it was developed.

6.0 Literature Cited

Allison, G., and Hughes, M. 1983. Journal of Hydrology, 60(1-4), 157-173.

Anderson, R.P., Gonzalez Jr., I., 2011. Species-specific tuning increases robustness to sampling bias in models of species distributions: an implementation with MaxEnt. Ecological Modelling 222: 2796–2811.

Anderson, B.W., and Ohmart, R.D. 1977. Vegetation Structure and Bird Use in the Lower Colorado River Valley. In: Importance, Preservation and Management of Riparian Habitat: A Symposium, July 9, 1977. U.S. Forest Service General Technical Report RM-43, p. 23-34.

Andrews, P. and O'Brien, E.M. 2000. Climate, vegetation, and predictable gradients in mammal species richness in southern Africa. Journal of Zoology, London, 251:205-231.

Arnold, J.G., Williams, J. R., Srinivasan, R., King, K.W. and Griggs, R. H. 1994. SWAT-Soil Water Assessment Tool. USDA, Agricultural Research Service, Grassland, Soil and Water Research Laboratory, Temple, Texas.

Arnold, J.G., Moriasi, D.N., Gassman, P.W., Abbaspour, K.C., White, M.J., Srinivasan, R., Santhi, C., Harmel, R.D., van Griensven, A., Van Liew, M.W., Kannan, N., Jha, M.K. 2012. SWAT: Model use, calibration, and validation. Transactions of the ASABE, 55(4): 1491-1508. See also http://swat.tamu.edu/ for SWAT documentation and publications.

Arscott, D.B., Larned, S., Scarsbrook, M.R., Lambert, P. 2010. Aquatic invertebrate community structure along an intermittence gradient: Selwyn River, New Zealand. Journal of the North American Benthological Society, 29(2):530-545.

Aviad, B., and Roy, G. 2011. Classification by clustering decision tree-like classifier based on adjusted clusters. Expert Systems with Applications, 38:8220-8228.

Bailey, R.G. 1976. "Ecoregions of the United States" map, Aug. 17, 2001, unnumbered publication. Intermountain Region, USDA Forest Service, Ogden, Utah. http://www.fs.fed.us/land/ecosysmgmt/ecoreg1_home.html

Bailey, R.G. 2002. Ecoregion-Based Design for Sustainability. Springer-Verlag, New York, NY.

Bailey, R.G. and Hogg, H.C. 1986. A world ecoregions map for resource partitioning. Environmental Conservation, 13: 195–202.

Baker, F. A. 1993. Classification and regression tree analysis for assessing hazard of pine mortality caused by Heterobasidion annosum. Plant Disease, 77 (2):136–139.

Baker, T.J. and Miller, S.N. 2013. Using the Soil and Water Assessment Tool (SWAT) to assess land use impact on water resources in an East African watershed. Journal of Hydrology, 486: 100-111.

Bartoń, K. 2009. MuMIn: multi-model inference. R package, version 0.12.2. Available at: <http://r-forge.r-project.org/projects/mumin/>.

Benton, J., Ripley, J.D., and Powledge, F., eds. 2008. Conserving Biodiversity on Military Lands: A Guide for Natural Resources Managers. 2008 edition. Available at http://www.dodbiodiversity.org. Arlington, Virginia: NatureServe.

Betancourt, J. 2007. Climate Variability and change in the Southwest. In: Proceedings from the Southwest Region Threatened, Endangered, and At-Risk Species Workshop, 22-25 October 2007, Tucson, Arizona. Prepared for the Legacy Resource Management Program, Strategic Environmental Research and Development Program, and Environmental Security Technology Certification Program by HydroGeoLogic, Inc., Reston, Virginia.

Borak, J.S. and Strahler, A.H. 1999. Feature selection and land cover classification of a MODIS-like data set for a semi-arid environment. International Journal of Remote Sensing 20 (5): 919–938.

Bork, E.W. and Su, J.G. 2007. Integrating LIDAR data and multispectral imagery for enhanced classification of rangeland vegetation: A meta analysis. Remote Sensing of Environment 111:11–24.

Boykin, K. G., B. C. Thompson, R. A. Deitner, D. Schrupp, D. Bradford, L. O'Brien, C. Drost, S. Propeck-Gray, W. Rieth, K. A. Thomas, W. Kepner, J. Lowry, C. Cross, B. Jones, T. Hamer, C. Mettenbrink, K.J. Oakes, J. Prior-Magee, K. Schulz, J. J.Wynne, C. King, J. Puttere, S. Schrader, and Z. Schwenke. 2007. Predicted animal habitat distributions and species richness. Chapter 3 in J.S. Prior-Magee, et al., eds. Southwest Regional Gap Analysis Final Report. U.S. Geological Survey, Gap Analysis Program, Moscow, ID.

Breiman, L., Friedman, J.H., Olshen, R.A. and Stone, C.J. 1984. Classification and Regression Trees. Wadsworth and Brooks Publishing, Monterey, California.

Brokaw, N.V.L. and Lent, R.A. 1999. Vertical structure. In: Hunter M.L. (Ed), Maintaining biodiversity in forest ecosystems. Cambridge, UK: Cambridge University Press. pp. 373-399.

Bull, W.B. 1997. Discontinuous ephemeral streams. Geomorphology 19: 227–276.

Bull, L.J. and Kirkby, M.J. 2002. Dryland river characteristics and concepts. In: Dryland Rivers: Hydrology and Geomorphology of Semi-Arid Channels. L.J. Bull and M.J. Kirkby (eds.), John Wiley & Sons Ltd., Chichester, England. p. 3-15.

Burnham, K.P. and Anderson, D.R. 2002. Model Selection and Multimodel Inference: A Practical Information-Theoretic Approach, 2nd edn. Springer, Berlin.

Burnham, K.P. and Overton, W.S. 1979. Robust estimation of population size when capture probabilities vary among animals. Ecology 60:927–936.

Cable, D.R. 1969. Competition in the Semidesert Grass-shrub Type as Influenced by Root Systems, Growth Habits, and Soil Moisture Extraction. Ecology, 50(1); 27-38.

Canadell, J., Jackson, R.B., Ehleringer, J.R., Mooney, H.A., Sala, O.E., Schulze, E.D. 1996. Oecologia, 108(4); 583-595.

Carlson, E.A. 2009. Fluvial Riparian Classifications for National Forests in the Western United States. M.S. Thesis. Colorado State University, Fort Collins, CO; 194 pp.

Clark, L. A. and D. Pregibon. 1992. Tree-based models. In: J. M. Chambers and T. J. Hastie, (eds). Statistical models in S. Wadsworth and Brooks, Pacific Grove, California, USA, pp. 377–420.

Clark, S. 2012. ZonalStatsOverlappingPolys, Tool to Calculate Zonal Stats using Zonal Statistics as Table with an overlapping polygon feature class. Available from ESRI http://www.arcgis.com/home/item.html?id=b859b33c616a47d2b99b5e133942db02. Accessed August 30, 2013.

Cohen, J. 1960. A coefficient of agreement for nominal scales. Educational and Psychological Measurement 20(1):37–46.

Colwell, R.K. 2013. EstimateS: Statistical estimation of species richness and shared species from samples. Version 9. User's Guide and application published at: <http://purl.oclc.org/estimates>.

Cooke, R.U. and Reeves, R.W. 1976. Arroyos and Environmental Change in the American Southwest. Clarendon Press, Oxford.

Curtis, K.E., Lichvar, R.W., Dixon, L.E. 2011. Ordinary High Flows and the Stage-Discharge Relationship in the Arid West Region. ERCD/CRREL TR-11-12. Hanover, NH, US Army Engineer Research and Development Center, Cold Regions Research and Engineering Laboratory.

D'Odorico, P. and Porporato, A. (eds.). 2006. Dryland Ecohydrology. Springer: Dordrecht, The Netherlands.

Dasmann, R.F. 1972. Towards a system for classifying natural regions of the world and their representation by national parks and reserves. Biological Conservation, 4, 247–255.

Daughtry, C.S.T., Walthall, C.L., Kim, M.S., Brown de Colstoun, E., McMurtrey, J.E. III. 2000. Estimating Corn Leaf Chlorophyll Concentration from Leaf and Canopy Reflectance. Remote Sensing of Environment, 74: 229-239.

De'ath, G. and Fabricius, K.E. 2000. Classification and regression trees: A powerful yet simple technique for the analysis of complex ecological data. Ecology 81:3178-3192.

DeBano, L.F., Rinne, J.N., Baker, M.B. Jr. 2003. Management of Natural Resources in Riparian Corridors. Journal of the Arizona-Nevada Academy of Science, Watershed Management in Arizona, vol. 35 (1): 58-70.

Dodov, B.A. and Foufoula-Georgiou, E. 2006. Floodplain Morphometry Extraction from a High Resolution Digital Elevation Model: a Simple Algorithm for Regional Analysis Studies. http://static.msi.umn.edu/rreports/2005/1.pdf

Doe, W.W. III, Shaw, R.B., Bailey, R.G., Jones, D.S. and T. E. Macia. 1999. Locations and Environments of U.S. Army Training and Testing Lands: An Ecoregional Framework for Assessment. Federal Facilities Environmental Journal, Autumn 1999: 9-26.

Doe, W.W. III, Bailey, R.G., Harmon, R., King, BG W.C., Palka, COL E.J. 2006. Natural Environments for Testing and Training: Developing Geographic Analogs for an Expeditionary Army. SERDP paper ADA481238.

Dust, D.W. and Wohl, E.E. 2010. Quantitative technique for assessing the geomorphic thresholds for floodplain instability and braiding in the semi-arid environment. Natural Hazards, 55:145-160.

Ely, L.L. 1997. Response of extreme floods in the southwestern United States to climatic variations in the late Holocene. Geomorphology, 19:175-201.

ERDAS. 2013. ERDAS Imagine. Intergraph Corporation, Huntsville, AL.

Everitt, B.S. and Hothorn, T. 2010. A Handbook of Statistical Analyses Using R. Second Edition. Chapman & Hall/CRC Press, Taylor & Francis Group, Boca Raton, FL.

Farid, A., Rautenkranz, D., Goodrich, D.C., Marsh, S.E. and Sorooshian, S. 2006. Riparian vegetation classification from airborne laser scanning data with an emphasis on cottonwood trees. Canadian J. of Remote Sensing. 32(1): 15-19.

Ficetola, G.F., Bonardi, A., Mücher, C.A., Gilissen, N.L.M., Padoa-Schioppa, E. 2014. How many predictors in species distribution models at the landscape scale? Land use versus LiDAR-derived canopy height. International Journal of Geographical Information Science, 28(8):1723-1739.

Field, J.J. and Lichvar, R.W. 2007. Review and Synopsis of Natural and Human Controls on Fluvial Channel Processes in the Arid West. U.S. Army Corps of Engineers, Engineer Research and Development Center, Cold Regions Research and Engineering Laboratory, internal report #ERDC/CRREL TR-07-16.

Fulton, R.A., Breidenbach, J.P., Seo, D.J., Miller, D.A., O'Bannon, T. 1998. The WSR-88D rainfall algorithm. Weather and Forecasting, 13(2), 377-395.

Gallart, F., Prat, N., Garcia-Roger, E.M., Latron, J., Rieradevall, M., Llorens, P., . . . Froebrich, J. 2012. A novel approach to analyzing the regimes of temporary streams in relation to their controls on the composition and structure of aquatic biota. Hydrology and Earth System Sciences, 16(9): 3165-3182.

Gebhardt, K., Prichard, D., Cowley, E. and Stevenson, M. 2005. Riparian area management: Riparian and wetland classification review and application. Technical reference 1737-21. U.S. Dept. of the Interior, Bureau of Land Management, Denver, CO. BLM/ST/ST-05/002+1737.

Gelman, A. 2008. Scaling regression inputs by dividing by two standard deviations. Statistics in Medicine. 27: 2865–2873.

Gelman, A., Su, Y.S., Yajima, M., Hill, J., Pittau, M.G., Kerman, J. et al. 2009. arm: data analysis using regression and multilevel/hierarchical models. R package, version 9.01.

Gibbens, R.P. and Lenz, J.M. 2001. Root systems of some Chihuahuan Desert Plants. Journal of Arid Environments, 49: 221-263.

Goetz, S.J., Sun, M., Zolkos, S., Hansen, A., and Duayah. R. 2014. The relative importance of climate and vegetation properties on patterns of North American breeding bird species richness. Environmental Research Letters 9: 1:18.

Goodrich, D.C. 1990. Geometric simplification of a distributed rainfall-runoff model over a range of basin scales. PhD Dissertation, Univ. of Arizona, Tucson.

Goodrich, D.C., Bach, L.B., Weltz, M.A., Jackson, T.J., Schmugge, T.J., Keefer, T.O., Amer, S.A., Unkrich, C.L. 1991. Preliminary runoff simulation sensitivity to various measures of soil water content. Tenth Conference on Biometeorology and Aerobiology and the Special Sessions on Hydrometeorology, Sept. 10-13, 1991, Salt Lake City, Utah.

Goodrich, D.C., Burns, I.S., Unkrich, C.L., Semmens, D., Guertin, D.P., Hernandez, M., Yatheendradas, S., Kennedy, J.R., Levick, L. 2012. KINEROS2/AGWA: Model Use, Calibration, and Validation. Transactions of the ASABE. 55(4): 1561-1574.

Goodrich, D.C., Keefer, T.O., Unkrich, C.L., Nichols, M.H., Osborn, H.B., Stone, J.J., Smith, J.R. 2008. Long-term precipitation database, Walnut Gulch Experimental Watershed, Arizona, United States. Water Resources Research, 44.

Goodrich, D.C., Schmugge, T.J., Jackson, T.J., Unkrich, C.L, Keefer, T.O., Parry, R., Bach, L.B, Amer, S.A. 1994. Runoff simulation sensitivity to remotely sensed initial soil water content. Water Resources Research, 30(5): 1393-1405.

Gothai, E. and Balasubramanie, P. 2012. An Efficient Way for Clustering Using Alternative Decision Tree. American Journal of Applied Sciences, 9(4):531-534.

Graf, W.L. 1983. Flood-related channel change in an arid region river. Earth Surface Processes and Landforms 8: 125-39.

Graf, W.L. 1988a. Fluvial Processes in Dryland Rivers. Springer-Verlag, New York. p. 346

Graf, W.L. 1988b. Definitions of flood plains along arid region rivers. In: Flood Geomorphology, V.R. Baker, R.C. Kochel, P.C. Patton (eds), 231-42. John Wiley & Sons Ltd, Chichester, England.

Grueber, C.E., Nakagawa, S., Laws, R.J., and Jamieso, I.G. 2011. Multimodel inference in ecology and evolution: challenges and solutions. Journal of Evolutionary Biology 24: 699-711.

Haboudane, D., Miller, J.R., Tremblay, N., Zarco-Tejada, P.J., Dextraze, L. 2002. Integrated narrow-band vegetation indices for prediction of crop chlorophyll content for application to precision agriculture. Remote Sensing of Environment, 81: 416-426.

Hall, J.A., Comer, P., Gondor, A., Marshall, R., and Weinstein, S. 2001. Conservation Elements of and a Biodiversity Management Framework for the Barry M. Goldwater Range, Arizona. The Nature Conservancy of Arizona, Tucson. 199 pp.

Hammer, S. 2014. Ephemeral and intermittent streams as wildlife habitat at Fort Bliss, New Mexico/Texas. M.S. Thesis. University of Arizona, Tucson, AZ.

Heller, K.A. and Ghahramani, Z. 2005. Bayesian Hierarchical Clustering. In: Proceedings of the 22nd International Conference on Machine Learning, University of Bonn, Germany, Aug. 7-11, 2005. Downloaded Oct. 9, 2013 from http://www.machinelearning.org.

Hereford, R., Webb, R.H., Longpre, C.I. 2006. Precipitation history and ecosystem response to multidecadal precipitation variability in the Mojave Desert region, 1893-2001. Journal of Arid Environments, 67:13-34.

Hernandez, M., Miller, S.N., Goodrich, D.C., Goff, B.F., Kepner, W.G., Edmonds, C.M., Jones, K.B. 2000. Modeling runoff response to land cover and rainfall spatial variability in semi-arid watersheds. Environmental Monitoring and Assessment, 64(1): 285-298.

Howe, S., Levick, L.R. and Hautzinger, A. 2008. Hydrology and Ecology of Southwestern Intermittent Streams, Dry Washes, and Adjacent Riparian Zones. In: Proceedings from the Southwest Region Threatened, Endangered, and At-Risk Species Workshop, 22-25 October 2007, Tucson, Arizona. Prepared for the Legacy Resource Management Program, Strategic Environmental Research and Development Program, and Environmental Security Technology Certification Program by HydroGeoLogic, Inc., Reston, Virginia.

Huberty, C. J. (1994c). Applied Discriminant Analysis. New York, Wiley. (282,306,337)

Hupp, C. 2000. Hydrology, geomorphology and vegetation of Coastal Plain rivers in the south-eastern USA. Hydrological Processes, 14(16-17): 2991-3010.

Hupp, C.R. and Osterkamp, W.R. 1996. Riparian vegetation and fluvial geomorphic processes. Geomorphology 14:277-295.

Jackson, R.B., Jobbagy, E.G., Nosetto, M.D. 2009. Ecohydrology in a human-dominated landscape. Ecohydrology, 2(3), 383-389.

Jain, A.K., Murty, M.N., Flynn, P.J. 1999. Data Clustering; A Review. ACM Computing Surveys, 31(3): 264-323.

Jason Associated Corporation. 2008. Mesquite bosque survey of the Cibola and Laguna regions. Prepared for: U.S. Army Garrison Yuma Proving Ground, Environmental Sciences, IMWE-YMA-PWE. Yuma, Arizona.

Jenness, J. 2013. DEM Surface Tools for ArcGIS (surface_area.exe). Jenness Enterprises. Available at: http://www.jennessent.com/arcgis/surface_area.htm.

Jensen, J.R. 1996. Introductory Digital Image Processing: A Remote Sensing Perspective. 2nd edition. Prentice Hall, N.J.

Jiang, Z., Huete, A.R., Li, Jing, Qi, J. 2007. Interpretation of the modified soil-adjusted vegetation index isolines in red-NIR reflectance space. Journal of Applied Remote Sensing, v.1.

Kepner, W.G. 1978. Small mammals of the Black Canyon and Skull Valley planning units, Maricopa and Yavapai Counties, Arizona. U.S. Dept. of Interior, Bureau of Land Management. Technical Note 350.

Kirkby, M.J., Gallart, F., Kjeldsen, T.R., Irvine, B.J., Froebrich, J., Lo Porto, A., De Girolamo, A., and the MIRAGE Team. 2011. Classifying low flow hydrological regimes at a regional scale. Hydrology and Earth System Sciences, 15(12), 3741-3750.

Knighton, A.D. 1998. Fluvial Forms and Processes: A New Perspective. John Wiley and Sons, Inc., New York. p. 165.
Knisel, W. G. (Editor), 1980. CREAMS: A Field Scale Model for Chemicals, Runoff, and Erosion from Agricultural Management Systems, U.S. Department of Agriculture, Science and Education Administration, Conservation Research Report, 26, 643 p.
Kotsiantis, S.B. 2007. Supervised Machine Learning: A Review of Classification Techniques. Informatica, 31(3): 249-268.
Kozma, J.M. and Mathews, N.E. 1995. Long-term monitoring of Neotropical migrants in Chihuahuan Desert arroyo-riparian habitat and adjacent upland.
Krausman, P.R, Rautenstrauch, K.R., and Leoplold. B.D. 1985. Xeroriparian systems used by desert mule deer in Texas and Arizona. Pages 144-148 in R. R. Johnson, C. D. Ziebell, D. R. Patton, P. F. Ffolliott, and R. H. Hamre, eds. Riparian ecosystems and their management: Reconciling conflicting uses. U.S. Forest Serv. Gen. Tech. Rept., RM-120:1-523.
Kreft, H. and Jetz, W. 2010. A framework for delineating biogeographical regions based on species distributions. Journal of Biogeography, 37(11): 2029-2053.
Krueper, D.J. 1993. Conservation priorities in naturally fragmented and human-altered riparian habitats of the arid West. USDA Forest Service. General Technical Report RM-43. Available online: www.birds.cornell.edu/pifcapemay/krueper.htm.
Laliberte, A.S., Fredrickson, E.L. and Rango, A. 2007. Combining decision trees with hierarchical object-oriented image analysis for mapping arid rangelands. Photogrammetric Engineering and Remote Sensing, 73(2): 197–207.
Landis, J.R. and G.G. Koch. 1977. The measurement of observer agreement for categorical data. Biometrics 33(1):159–174.
Larned, S.T., Datry, T., Arscott, D.B., Tockner, K. 2010. Emerging concepts in temporary-river ecology. Freshwater Biology, 55(4).
Lauenroth, W.K., and Bradford, J.B. 2009. Ecohydrology of dry regions of the United States: precipitation pulses and intraseasonal drought. Ecohydrology, 2(2).
Leenhouts, J.M., Stromberg, J.C., Scott, R.L. 2006. United States. Bureau of Land Management and Geological Survey (U.S.). Hydrologic requirements of and consumptive ground-water use by riparian vegetation along the San Pedro River, Arizona. Reston, Va.: U.S. Geological Survey, Scientific Investigations Report 2005-5163.
Leopold, L.B. and Miller, J.P. 1956. Ephemeral streams - hydraulic factors and their relation to the drainage net. US Geological Survey Professional Paper 282-A.
Lefebvre, L., Lichvar, R., Curtis, K., Gillrich, J. 2013. Channel Classification across Arid West Landscapes in Support of OHW Delineation. ERDC/CRREL TR-13-3. Hanover, NH: US Army Engineer Research and Development Center, Cold Regions Research and Engineering Laboratory.
Levick, L.R., Scott, S.N., Semmens, D.J., Miller, S.N., Guertin, D.P., Goodrich D.C. 2003. Application of a Land Cover Modification Tool and the Automated Geospatial Watershed Assessment Tool (AGWA) at Fort Huachuca, AZ. 6th Annual SCGIS (Society for Conservation GIS) Conference, Asilomar Conference Center, Monterey, California, July 4-6, 2003.
Levick, L., Semmens, D., Goodrich, D., Kepner, W., Brush, J., Leidy, R.A., Goldmann, E. 2006. Simulated Changes in Runoff and Sediment in Developing Areas near Benson, Arizona. U.S. Environmental Protection Agency, Office of Research and Development, Las

Vegas, NV, and USDA/ARS Southwest Watershed Research Center, Tucson, AZ. EPA/600/R-06/158; ARS/1873.
Levick, L., Fonseca, J., Goodrich, D., Hernandez, M., Semmens, D., Stromberg, J., Leidy, R., Scianni, M., Guertin, D.P., Tluczek, M., and Kepner, W. 2008. The Ecological and Hydrological Significance of Ephemeral and Intermittent Streams in the Arid and Semi-arid American Southwest. U.S. Environmental Protection Agency and USDA/ARS Southwest Watershed Research Center. EPA/600/R-08/134, ARS/233046, 116 pp.
Lichvar, R.W., and McColley, S.M. 2008. A field guide to the identification of the Ordinary High Water Mark (OHWM) in the Arid West region of the western United States. ERDC/CRREL TR-08-12. Hanover, NH: US Army Engineer Research and Development Center, Cold Regions Research and Engineering Laboratory.
Lite, S.J., K.J. Bagstan, and J.C. Stromberg. 2005. Riparian plant species richness along lateral and longitudinal gradients of water stress and flood disturbance, San Pedro River, Arizona, USA. Journal of Arid Environments 63(4): 785-813.
Loik, M.E., Breshears, D.D., Lauenroth, W.K., Belnap, J. 2004. A multi-scale perspective of water pulses in dryland ecosystems: climatology and ecohydrology of the western USA. Oecologia, 141(2).
Lopez-Bermudez, F., Conesa-Garcia, C, Alonso-Sarria, A. 2002. Floods: Magnitude and Frequency in Ephemeral Stream of the Spanish Mediterranean Region. In: Dryland Rivers: Hydrology and Geomorphology of Semi-Arid Channels. L.J. Bull and M.J. Kirkby (eds.), John Wiley & Sons Ltd., Chichester, England. P. 329-350.
Lowry, J.H, Jr., Ramsey, R.D., Boykin, K., Bradford, D., Comer, P., Falzarano, S., Kepner, W., Kirby, J., Langs, L., Prior-Magee, J., Manis, G., O'Brien, L., Sajwaj, T., Thomas, K.A., Rieth, W., Schrader, S., Schrupp, D., Schulz, K., Thompson, B., Velasquez, C., Wallace, C., Waller E. and Wolk, B. 2005. Southwest Regional Gap Analysis Project: Final Report on Land Cover Mapping Methods, RS/GIS Laboratory, Utah State University, Logan, Utah.
Ludwig, J.A., Wilcox, B.P., Breshears, D.D., Tongway, D.J., and Imeson, A.C. 2005. Vegetation patches and runoff-erosion as interacting ecohydrological processes in semi-arid landscapes. Ecology, 86(2).
Lyon, R. 2013. Using rainfall-runoff models to characterize the flow regime of desert streams in the U.S. southwest. M.S. Thesis, University of Arizona, Tucson.
MacArthur, R.H., and MacArthur. J.W. 1961. On bird species diversity. Ecology 42:594–598
Magurran, A.E. and McGill. B.J. 2011. Biological diversity: frontiers in measurement and assessment. Oxford University Press, New York.
Mallinis, G., Koutsias, N., Tsakiri-Strati, M. and Karteris, M. 2008. Object-based classification using QuickBird imagery for delineation of forest vegetation polygons in a Mediterranean test site. ISPRS J. Photogrammetry & Remote Sensing, 63: 237-250.
McKay, L., Bondelid, T., Dewald, T., Rea, A., Johnston, C., Moore, R. 2012. NHDPlus Version 2.1. Horizon Systems Corporation, Herndon, VA.
Meaney, C.A., M. Reed-Eckert, and Beauvais. G.P. 2006. Kit Fox (Vulpes macrotis): a technical conservation assessment. [Online]. USDA Forest Service, Rocky Mountain Region. Available: http://www.fs.fed.us/r2/projects/scp/assessments/kitfox.pdf
Miller, S.N., Semmens, D.J., Hernandez, M., Goodrich, D.C., Miller, W.P., Kepner, W.G., Ebert, D. 2002. GIS-based hydrologic modeling: the Automated Geospatial Watershed

Assessment tool. In: Proceeding of the Second Federal Interagency Hydrologic Modeling Conference, July 28 - August 1, 2002, Las Vegas NV, CD-ROM, 12 p.
Miller, S.N., Semmens, D.J., Goodrich, D.C., Hernandez, M., Miller, R.C., Kepner, W.G. and Guertin, D.P. 2007. The Automated Geospatial Watershed Assessment Tool. J. Environmental Modeling and Software, 22:365.377
Milligan, G.W. and Cooper, M.C. 1985. An Examination of Procedures for Determining the Number of Clusters in a Data Set. Psychometrika. 50(2):159.179.
Mills, G.S., Dunning, J.B. and Bated, J.M. 1991. The relationship between breeding bird density and vegetation volume. Wilson Bulletin. 103(3):468-479.
Montgomery, D., and Buffington, J. 1997. Channel-reach morphology in mountain drainage basins. Geological Society of America Bulletin, 109(5): 596-611.
Mosley, M.P. 1972. Evolution of a discontinuous gully system. Annuals of the Association of American Geographers 62:655-663.
Myers, L.M., Mathews, N.E., and Kozma, J.M. Final report: long term monitoring of Neotropical migrant and breeding bird populations in arroyos and uplands on Fort Bliss Military Reservation.
NatureServe. 2014. NatureServe Explorer: An online encyclopedia of life [web application]. Version 7.1. NatureServe, Arlington, Virginia. Available http://explorer.natureserve.org.
Nussear, K.E., Esque, T.C., Inman, R.D., Gass, L., Thomas, K.A., Wallace, C.S.A., Blainey, J.B., Miller, D.M., Webb R.H. 2009. Modeling habitat of the desert tortoise (Gopherus agassizii) in the Mojave and parts of the Sonoran Deserts of California, Nevada, Utah, and Arizona. U.S. Geological Survey Open-File Report 2009-1102, 18 p.
Newman, B.D., Wilcox, B.P., Archer, S.R., Breshears, D.D., Dahm, C.N., Duffy, C.J., McDowell, N.G., Phillips, F.M., Scanlon, B.R., Vivoni, E.R. 2006. Ecohydrology of water-limited environments: A scientific vision. Water Resources Research, 42(6), W06302.
NOAA. 2012. National Oceanic and Atmospheric Administration's Precipitation Frequency Data Server. Precipitation dataset. Retrieved 04/25/2012, from http://dipper.nws.noaa.gov/hdsc/pfds/
O'Neal, G.T., Flinders, J.T., and Clary, R.P. 1987. Behavioral ecology of the Nevada kit fox (Vulpes macrotis nevadensis) on a managed desert rangeland. Pp. 443-481in Current mammalogy (H.H. Genoways, ed.). Plenum Press, New York, 1:1-519.
Olden, J.D., Lawler, J.J., Poff, N.L. 2008. Machine Learning Methods Without Tears: A Primer for Ecologists. The Quarterly Review of Biology, 83(2):171-193.
Olson, D.M., Dinerstein, E., Wikramanayake, E.D., Burgess, N.D., Powell, G.V.N., Underwood, E.C., D'Amico, J.A., Itoua, I., Strand, H.E., Morrison, J.C., Loucks, C.J., Allnutt, T.F., Ricketts, T.H., Kura, Y., Lamoreux, J.F., Wettengel, W.W., Hedao, P., Kassem, K.R. 2001. Terrestrial ecoregions of the world: a new map of life on earth. BioScience, 51: 933–938.
Omernik, J.M. 1995. Ecoregions: A Spatial Framework for Environmental Management. In: Biological assessment and criteria: tools for water resource planning and decision making. W.S. Davis and T.P. Simon (eds.), CRC Press, Boca Raton, Florida, pp. 49-62.
Omernik, J.M. and Bailey, R.G. 1997. Distinguishing between watersheds and ecoregions. J. American Water Resources Association, 33 (5): 935-949.
Osborn, H. B., Lane, L. J., Myers, V. A. 1980. Rainfall-Watershed Relationships for Southwestern Thunderstorms. Transactions of the ASAE, 23(1):82.

Parker, K.C. 1986. Partitioning of foraging space and nest sites in a desert shrubland bird community. American Midland Naturalist, 115:255-267.
Patton, P.C. and Schumm, S.A. 1975. Gully erosion, northwestern Colorado: A threshold phenomenon. Geology, 3:88–90.
Pearson, R.G., Raxworthy, C.J., Nakamura, M., Peterson, A.T. 2007. Predicting species distributions from small numbers of occurrence records: a test case using cryptic geckos in Madagascar. Journal of Biogeography, 34(1):102-117.
Pelletier, J.D. and DeLong, S. 2004. Oscillations in arid alluvial-channel geometry. Geology 32:8, p. 713-716.
Peterson, A.T., Soberón, J., Pearson, R.G., Anderson, R.P., Martínez-Meyer, E., Nakamura, M., Araújo, M.B., 2011. Ecological niches and geographic distributions. Monographs in Population Biology, Princeton University Press, Princeton, NJ.
Phillips, S.J., Dudik, M., Schapire, R.E. 2004. A maximum entropy approach to species distribution modeling. In: Proceedings of the Twenty-First International Conference on Machine Learning. ACM Press, New York, pp. 472-486.
Phillips, S.J., Anderson, R.P., Schapire, R.E. 2006. Maximum entropy modeling of species geographic distributions. Ecological Modelling 190:231-259.
Poff, N.L, and Ward, J.V. 1989. Implications of streamflow variability and predictability for lotic community structure: a regional analysis of streamflow patterns. Canadian Journal of Fisheries and Aquatic Sciences, 46:1805-1818.
Poff, N.L., Allan, J.D., Bain, M.B., Karr, J.R., Prestegaard, K.L., Richter, B.D., Sparks, R.E., Stromberg, J.C. 1997. The Natural Flow Regime. Bioscience, 47(11).
Polaka, I., and Borisov, A. 2010. Clustering-Based Decision Tree Classifier Construction. Technological and Economic Development of Economy, 16(4):765-781.
PRISM Climate Group. 2010. Oregon State University, http://prism.oregonstate.edu
Puckridge, J., Sheldon, F., Walker, K., Boulton, A. 1998. Flow variability and the ecology of large rivers. Marine and Freshwater Research, 49(1): 55-72.
Purevdorj, T.S., Tateishi, R., Ishiyama, T., Honda, Y. 1998. Relationships between percent vegetation cover and vegetation indices. International Journal of Remote Sensing, 19:3519-3535.
Qi, J., Chehbouni, A., Huete, A.R., Kerr, Y.H., Sorooshian, S. 1994. A Modified Soil Adjusted Vegetation Index. Remote Sensing of Environment, 48:119-126
Qian, H., Kissling, W.D., Wang, X., and Andrews. P. 2009. Effects of woody plant species richness on mammal species richness in southern Africa. Journal of Biogeography 36:1685–1697
R Core Team (2014). R: A language and environment for statistical computing. R Foundation for Statistical Computing, Vienna, Austria <http://www.R-project.org >
Radosavljevic, A., and Anderson, R.P. 2013. Making better MAXENT models of species distributions: complexity, overfitting and evaluation. Journal of Biogeography, 41(4):629-643.
Rai, P. 2011. Data Clustering: K-means and Hierarchical Clustering. Downloaded May 17, 2014 from http://www.cs.utah.edu/~piyush/teaching/4-10-print.pdf
Rejwan, C., Collins, N.C., Brunner, L.J., Shuter, B.J. and Ridgway, M.S. 1999. Tree regression analysis on the nesting habitat of smallmouth bass. Ecology 80:341–348.
Rodriguez-Iturbe, I. 2000. Ecohydrology: A hydrologic perspective of climate-soil-vegetation dynamics. Water Resources Research, 36(1), 3-9.

Rondeaux, G., Steven, M., Baret, F. 1996. Optimization of Soil-Adjusted Vegetation Indices. Remote Sensing of Environment, 55:95-107.
Rosgen, D. 1994. A Classification of Natural Rivers. Catena, 22(3): 169-199.
Rubinoff, J., Wills, T., Sekscienski, S. and Belfit, S. 2006. Installation Summaries from the FY2006 Survey of Threatened and Endangered Species on Army Lands. U.S. Army Environmental Command Aberdeen Proving Ground, Maryland.
Salford Systems, SPM. 2004. RandomForests; An Implementation of Leo Breiman's RF, by Salford Systems. http://salford-systems.com
Schumm, S.A. 1977. The Fluvial System. John Wiley and Sons, New York. p. 338.
Schumm, S.A. and Hadley, R.F. 1957. Arroyos and the Semi-arid Cycle of Erosion. American Journal of Science, 255:161-174.
Schuster, C., Forster, M., Kleinschmit, B. 2012. Testing the red edge channel for improving land-use classifications based on high-resolution multi-spectral satellite data. International Journal of Remote Sensing, 33(17): 5583-5599. http://dx.doi.org/10.1080/01431161.2012.666812
Seavy, N.E., Viers, J.H., Wood, J.K. 2009. Riparian bird response to vegetation structure: a multiscale analysis using LiDAR measurements of canopy height. Ecological Applications, 19(7):1848-1857.
Shannon, C.E. and W. Weaver. 1949. The mathematical theory of communication. The University of Illinois Press, Urbana, 117pp.
Sharma, H. and Kaler N.K. 2013. Data Mining with Improved and Efficient Mechanism in Clustering Analysis and Decision Tree as a Hybrid Approach. International Journal of Innovative Technology and Exploring Engineering (IJITEE), 2(5):58-60.
Shaw, J.R. and D.J. Cooper. 2008. Linkages among watersheds, stream reaches, and riparian vegetation in dryland ephemeral stream networks. Journal of Hydrology 350: 68-82.
Shcheglovitova, M. and Anderson, R. P. 2013. Estimating optimal complexity for ecological niche models: a jackknife approach for species with small sample sizes. Ecological Modelling, 269:9-17
Sing, T., Sander, O., Beerenwinkel, N., Lengauer, T. 2005. ROCR: visualizing classifier performance in R. Bioinformatics 21(20):3940-3941.
Snelder, T.H., Biggs, G.J.F., Woods, R.A. 2005. Improved Eco-hydrological Classification of Rivers. River Res. Applic. 21:609-628.
Soar, P.J. and Thorne, C.R. 2001. Channel Restoration Design for Meandering Rivers. ERDC/CHL CR-01-1. U.S. Army Engineer Research and Development Center, Flood Damage Reduction Research Program, Vicksburg, MS.
Steward, A.L., von Schiller, D., Tockner, K., Marshall, J.C., Bunn, S.E. 2012. When the river runs dry: human and ecological values of dry riverbeds. Front. Ecol. Environ, 10(4):202-209.
Stromberg, J.C., Bagstad, K.J., Leenhouts, J.M., Lite, S.J., Makings, E. 2005. Effects of stream flow intermittency on riparian vegetation of a semi-arid region river (San Pedro River, Arizona). River Research and Applications, 21(8).
Stromberg, J.C., Beauchamp, V.B., Dixon, M.D., Lite, S.J. and Paradzick, C. 2007. Importance of low-flow and high-flow characteristics to restoration of riparian vegetation along rivers in arid south-western United States. Freshwater Biology 52(4): 651-679.
Stromberg, J.C., Pattern, D.T. and Richter, B.D. 1991. Flood flows and dynamics of Sonoran riparian forests. Rivers 2(3): 221-235.

Stromberg, J.C., Hazelton, A.F., White, M.S. 2009. Plant species richness in ephemeral and perennial reaches of a dryland river. Biodiversity Conservation, 18:663-677.
Stone, J.J., Nichols, M.H., Goodrich, D.C., and Buono, J. 2008. Long-term runoff database, Walnut Gulch Experimental Watershed, Arizona, United States. Water Resources Research, 44(5), W05S05.
Sutfin, N.A., Shaw, J., Wohl, E.E., Cooper, D. 2014. A geomorphic classification of ephemeral channels in a mountainous, arid region, southwestern Arizona, USA. Geomorphology, 221: 164-175.
Tews, J., Borse, U., Grimm, V., Tielborger, K., Wichmann, M.C., Schwager, M., Jeltsch, F. 2004. Animal species diversity driven by habitat heterogeneity/diversity; the importance of keystone structures. Journal of Biogeography, 31(1):79-92.
Thomas, J.W., Maser, C. and Rodiek, J.E. 1979. Edges. In: J.W. Thomas (Ed.), Wildlife Habitats in Managed Forest: the Blue Mountains of Oregon and Washington. USDA Forest Service Agricultural Handbook Number 553.
Thomas, N., Hendrix, C. and Congalton, R.G. 2003. A comparison of urban mapping methods using high-resolution digital imagery, Photogrammetric Engineering & Remote Sensing, 69(9):963–972.
Tooth, S. 1999. Floodouts in Central Australia. In: Varieties of Fluvial Form. Eds. A.J. Miller and A. Gupta. John Wiley & Sons Ltd.
Tooth, S. 2000. Process, form and change in dryland rivers: A review of recent research. Earth-Science Reviews, 51: 67–107.
Udvardy, M.D.F. 1975. A classification of the biogeographical provinces of the world. International Union for Conservation of Nature (IUCN), Morges, Switzerland.
U.S. Army, Fort Bliss Integrated Natural Resources Management Plan, 2001. Prepared by Fort Bliss Directorate of Environment Conservation Division; Science Applications International Corp.; Center for Ecological Management of Military Lands; U.S. Army Corps of Engineers; and Geo-Marine, Inc.
U.S. Army, Fort Bliss Mission and Master Plan Supplemental Programmatic Environmental Impact Statement, Final SEIS. 2007. Lead Agency: U.S. Army, Installation Management Agency.
U.S. Geological Survey (USGS). 2006. National Hydrography Dataset (NHD) website, http://nhd.usgs.gov/index.html.
U.S. Geological Survey (USGS) National Gap Analysis Program (USGS-GAP). 2007. Digital Animal-Habitat Models for the Southwestern United States. Version 1.0. Center for Applied Spatial Ecology, New Mexico Cooperative Fish and Wildlife Research Unit, New Mexico State University
U.S. Geological Survey Gap Analysis Program (USGS-GAP). 2014. National Species Distribution Models. Available: http://gapanalysis.usgs.gov. Accessed 2013, 2014, various dates.
Vale, T.R., Parker, K.C., and Parker, A.J. 1989. Terrestrial vertebrates and vegetation structure in the western United States. The Professional Geographer, 41:450-64.
Vestal, A.G. 1914. Internal relations of terrestrial associations. The American Naturalist, 48: 413–445.
Wagener, S.M., Oswood, M.W., and Schimel, J.P. 1998. Rivers and soils: parallels in carbon and nutrient processing. BioScience 48: 104–08.

Wallace, C.S.A., and Gass, L. 2008. Elevation derivatives for Mojave Desert Tortoise Habitat models: U.S. Geological Survey Open-File Report 2008-1283, 7 p. http://pubs.usgs.gov/of/2008/1283/.

Warren, P.L. and Anderson, L.S. 1985. Gradient analysis of a Sonoran Desert wash. In: Riparian Ecosystems and Their Management: Reconciling Conflicting Uses. First North American Riparian Conference, April 16-18, 1985. U.S.D.A. Forest Service General Technical Report RM-120, p. 150-155.

Webb, R.H. and Betancourt, J.L. 1992. Climatic variability and flood frequency of the Santa Cruz River, Pima County, Arizona. U.S. Geological Survey Water-Supply Paper, 2379, 40 p.

Webb, R. H., and Leake, S. A. 2006. Ground-water surface-water interactions and long-term change in riverine riparian vegetation in the southwestern United States. Journal of Hydrology, 320(3):302-323.

Weichelt, H., Rosso, P., Marx, A., Reigber, S., Douglass, K., Heynen, M. 2012. The RapidEye Red Edge Band White Paper. Accessed Nov. 26, 2012 http://blackbridge.com/rapideye/upload/Red_Edge_White_Paper.pdf

White Sands Technical Services. Britt, C. and Lundblad, C. 2007.Gray vireo status and distribution on Fort Bliss: 2007.

Wilcox, B.P., Dowhower, S.L., Teague, W.R., Thurow, T.L. 2006. Long-term water balance in a semi-arid shrubland. Rangeland Ecology and Management, 59:600-606

Wollmuth, J., and Eheart, J. 2000. Surface water withdrawal allocation and trading systems for traditionally riparian areas. Journal of the American Water Resources Association, 36(2): 293-303.

Woolhiser, D., Keefer, T., Redmond, K. 1993. Southern Oscillation Effects on Daily Precipitation in the Southwestern United-States. Water Resources Research, 29(4): 1287-1295.

Young, C. B., Bradley, A. A., Krajewski, W. F., Kruger, A., and Morrissey, M. L. 2000. Evaluating NEXRAD Multisensor Precipitation Estimates for Operational Hydrologic Forecasting. Journal of Hydrometeorology, 1(3), 241.

Zehr, R. M., Myers, V. A., and United States National Weather Service. 1984. Depth-area ratios in the semi-arid southwest United States. Vol. 40 of NOAA technical memorandum NWS HYDRO. U.S. Dept. of Commerce, National Oceanic and Atmospheric Administration, National Weather Service.

Zia Engineering and Environmental Consultants. Hobert, J., Hartsough, M., and Burkett, D. 2010. Gray Vireo Status and Distribution on Sacramento Mountains Portions of Fort Bliss – 2008.

Zia Engineering and Environmental Consultants. Griffin, D., Burkett, D., and Wu, R. 2012a. Surveys for Avian Species of Concern in the Organ Mountains on Fort Bliss.

Zia Engineering and Environmental Consultants. Hanks, T., Schielke, B., and Burkett, D. 2012b.Gray Vireo Surveys and Nest Monitoring on Ft. Bliss, Otero County New Mexico.

Zia Engineering and Environmental Consultants. Griffin, D. and Stabinsky, K. 2013. 2012 Gray Vireo Surveys & Nest Monitoring on Fort Bliss Military Reservation.

Zimmerman, J.A.C., DeWald, L.E., and P.G. Rowlands. 1999. Vegetation diversity in an interconnected ephemeral riparian system of north-central Arizona, USA. Biological Conservation. 90:217-228.

Zoellick, B.W. and Smith, N.S. 1992. Size and Spatial Organization of Home Ranges of Kit Foxes in Arizona. Journal of Mammalogy 73(1): 83-88.

7.0 Appendices

Appendix A: Scientific and Technical Publications, Theses, and Presentations

Hammer, S. 2014. Ephemeral and intermittent streams as wildlife habitat at Fort Bliss, New Mexico/Texas. M.S. Thesis, University of Arizona, Tucson, AZ

Lyon, R. 2013. Using rainfall-runoff models to characterize the flow regime of desert streams in the US Southwest. Russ Lyon, M.S. Thesis, University of Arizona, Tucson, AZ.

Lyon, R. 2013. Using rainfall-runoff models to characterize the flow regime of desert streams in the US Southwest (oral presentation). International Association of Landscape Ecology Annual Symposium, Landscape Dynamics along Climatic Gradients: Models for a Changing World, Austin, TX, April 14 -18, 2013.

Murray, J.G., L.R. Levick, B. Bledsoe, R. Lyon, S. Hammer, D.P. Guertin, D. Goodrich and M. Laituri. 2012. An Ecohydrological Assessment of Dryland Riparian Ecosystems in the Southwestern United States (poster). AWRA 2012 Summer Specialty Conference, Riparian Ecosystems IV: Advancing Science, Economics and Policy, June 27-29, 2012, Denver, Colorado.

Levick, L.R., D.P. Guertin, D. Goodrich, J.G. Murray, R.A. Lyon, S. Hammer, B. Bledsoe, and M. Laituri. A classification of intermittent and ephemeral streams on Department of Defense land (poster and abstract). Biodiversity and Management of the Madrean Archipelago III, May 1-5, 2012, Tucson, AZ.

Levick, L.R., J.G. Murray, R.A. Lyon, S. Hammer, D.P. Guertin, D. Goodrich, B. Bledsoe, and M. Laituri. 2012. An Ecohydrological Assessment of Dryland Riparian Ecosystems in the Southwestern United States (poster and abstract). AWRA Spring Specialty Conference, Geographic Information Systems (GIS) and Water Resources VII, March 26-28, 2012, New Orleans, LA.

Proposed Publications

Levick et al. 2015. Ecohydrologic classification of stream types on DoD lands in the southwest U.S.

Hammer et al. 2015. Ephemeral stream attributes as predictors of wildlife habitat.

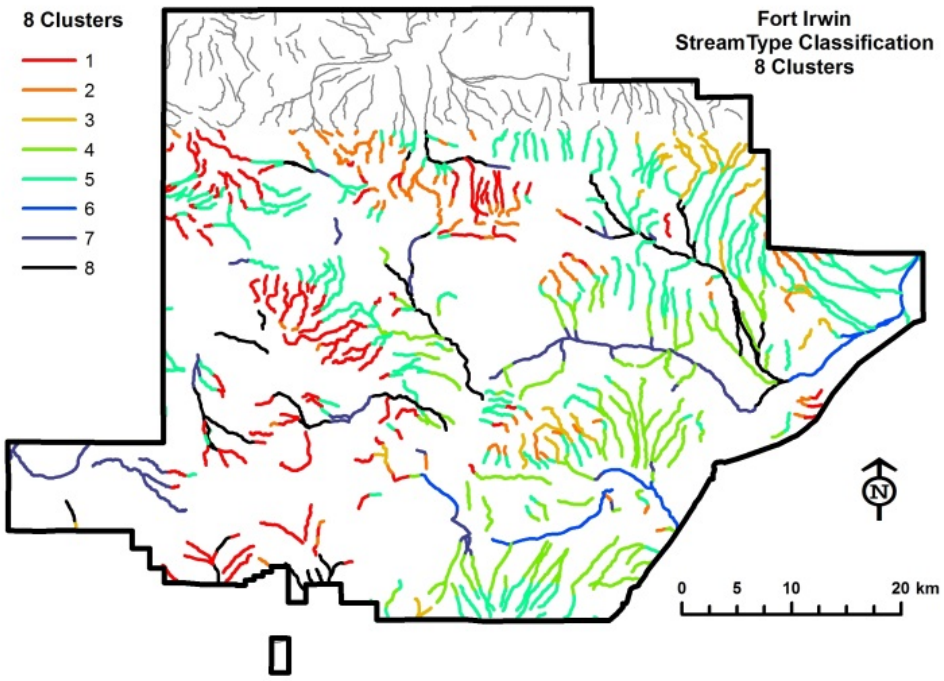
Levick and Hammer. 2015. Use of remotely sensed data to classify gradients of riparian vegetation for an ephemeral and intermittent stream type classification to improve wildlife management.

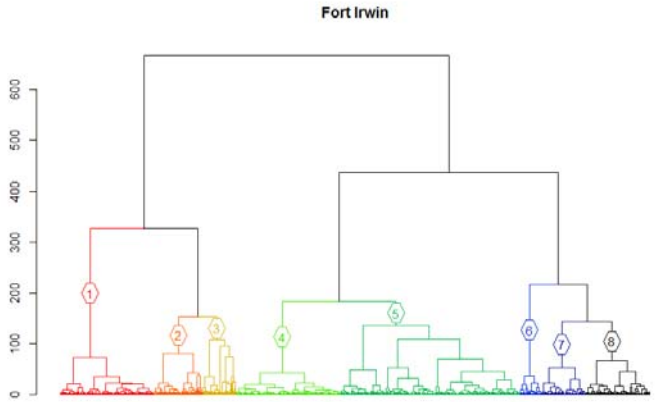
Levick et al. 2015. Potential effects of climate change and land use impacts on ephemeral and intermittent streams

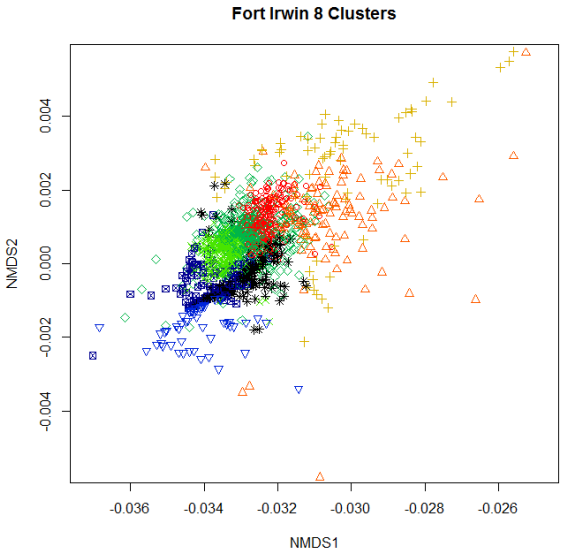
Appendix B: Stream Type Classification Results

Fort Irwin

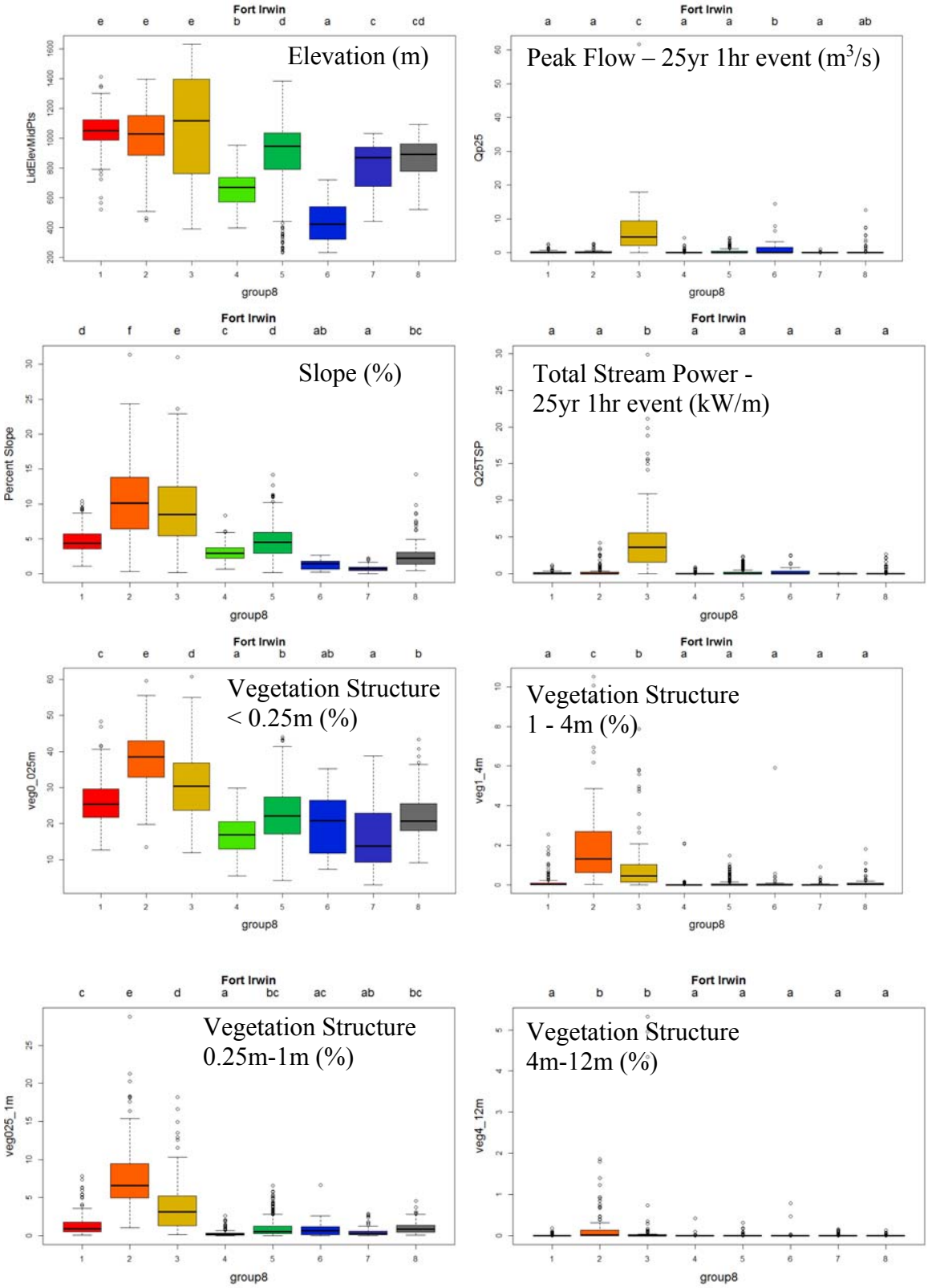
Stream Type Classification Results – 8 Classes
Mapped Clusters, Dendrogram, NMDS plot, Box Plots for Input Variables

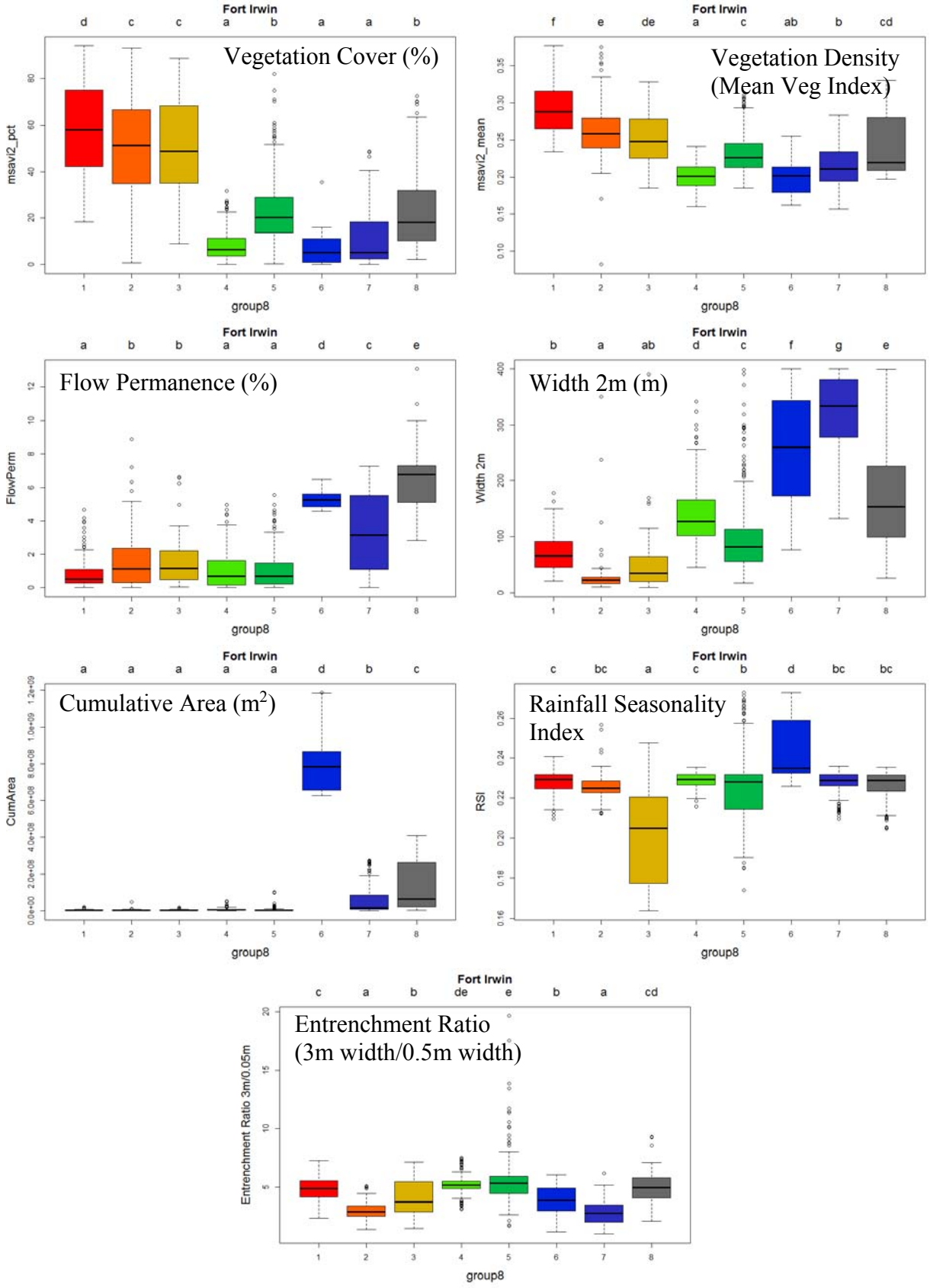






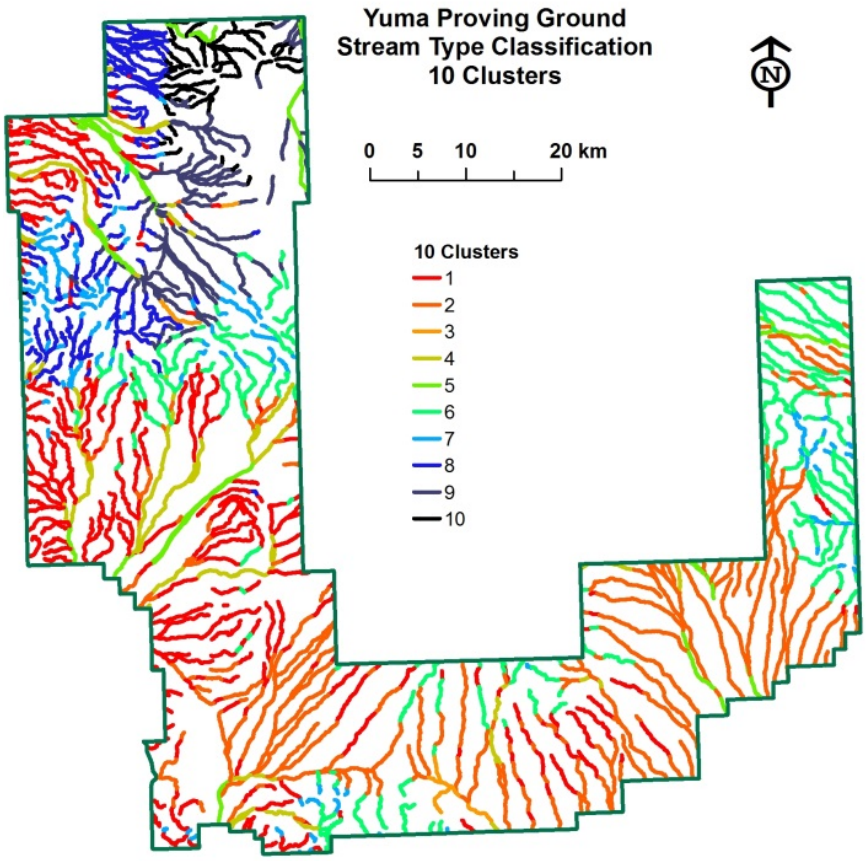
Boxplots, 8 Stream Types

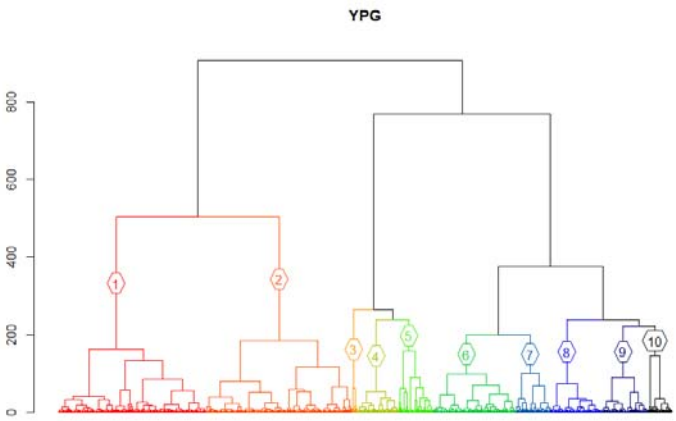


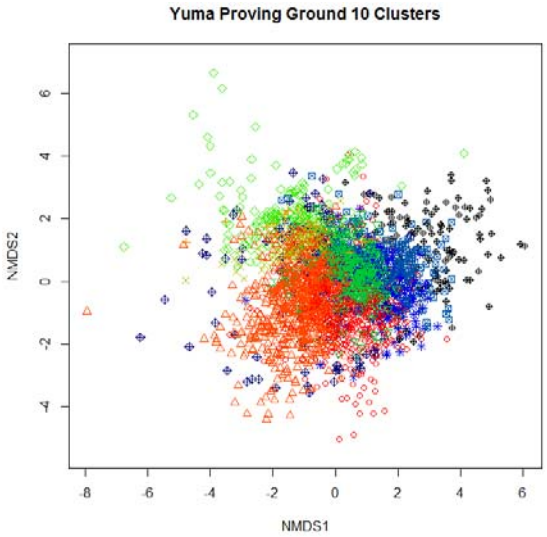

Fort Irwin
Vegetation Cover (%)
msavi2_pct
group8
Fort Irwin
Vegetation Density
(Mean Veg Index)
msavi2_mean
group8
Fort Irwin
Flow Permanence (%)
FlowPerm
group8
Fort Irwin
Width 2m (m)
Width 2m
group8
Fort Irwin
Cumulative Area (m2)
CumArea
group8
Fort Irwin
Rainfall Seasonality
Index
RSI
group8
Fort Irwin
Entrenchment Ratio
(3m width/0.5m width)
Entrenchment Ratio 3m/0.05m
group8

Yuma Proving Ground

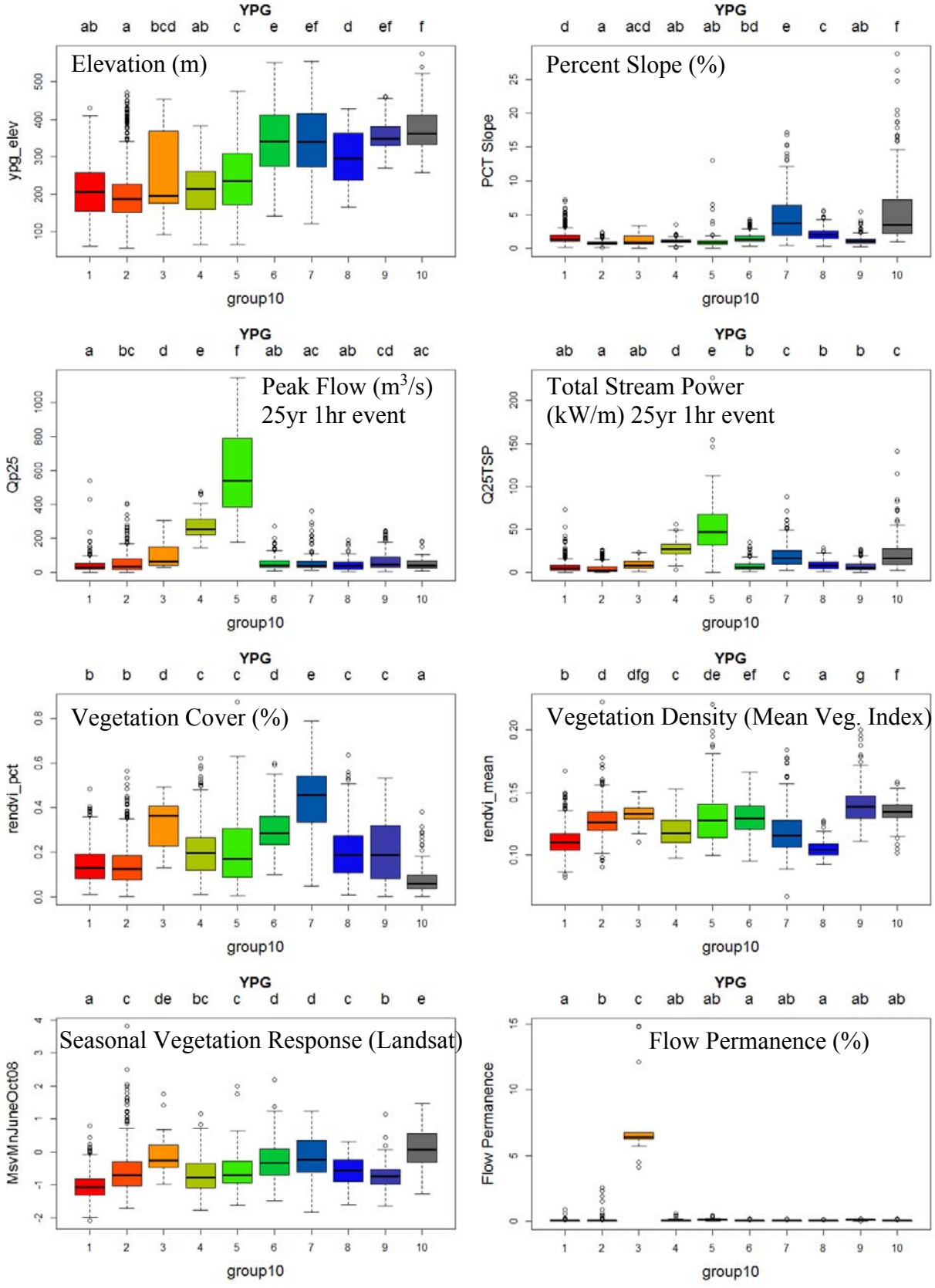
Stream Type Classification Results – 10 Classes
Mapped Cluster, Dendrogram, NMDS plot, Box Plots for Input Variables

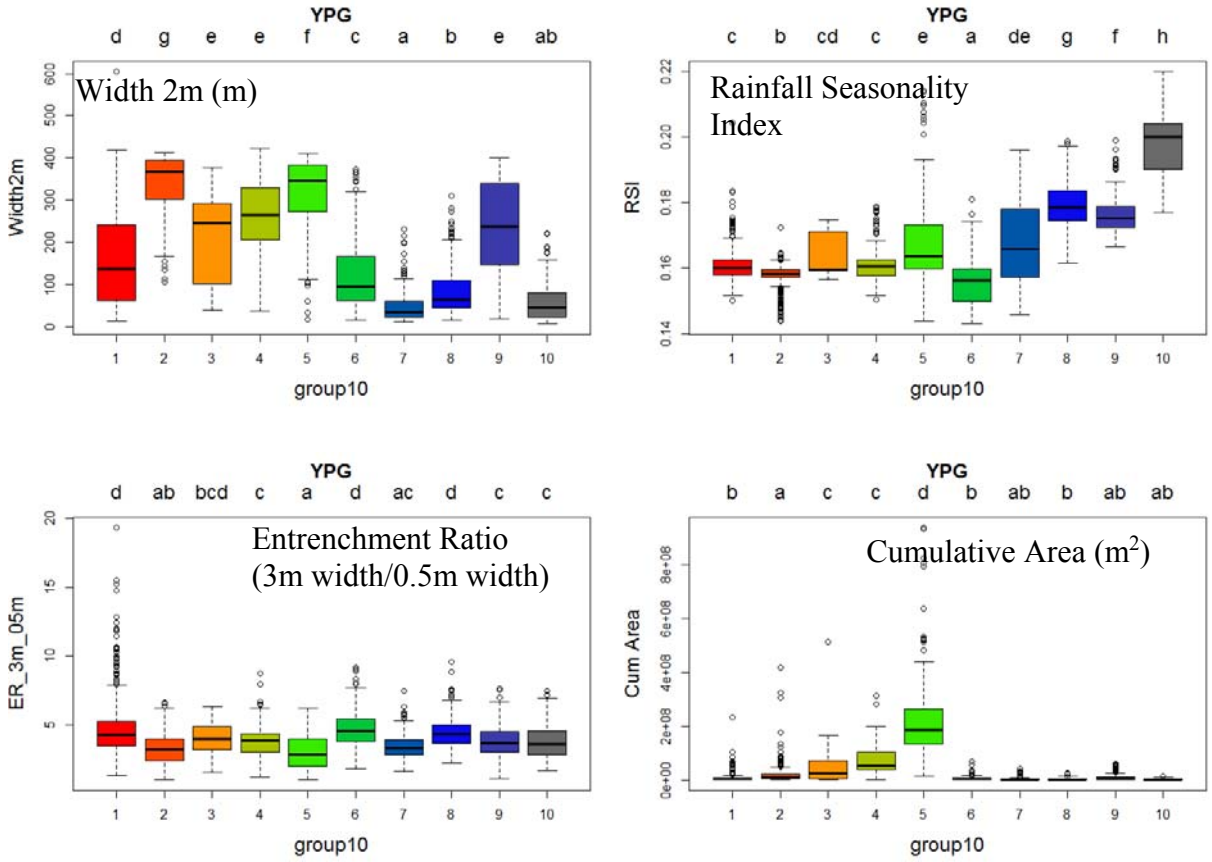






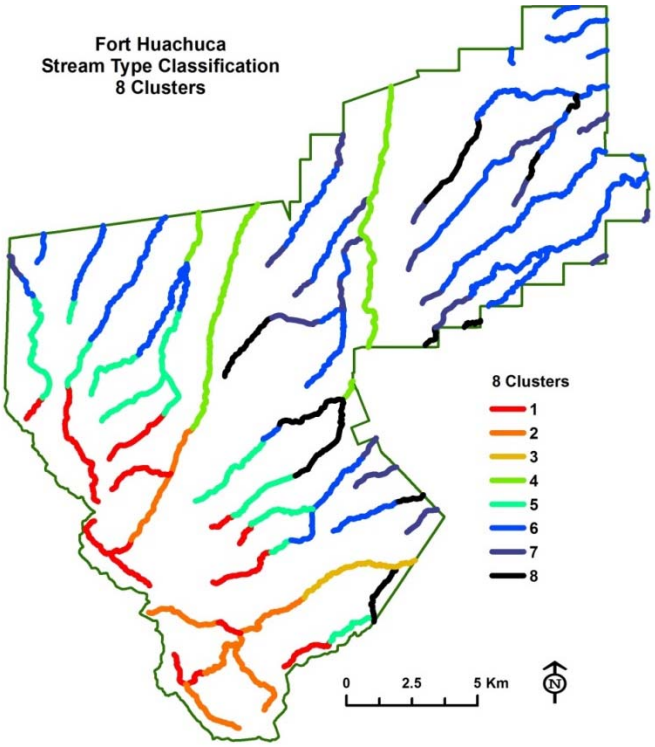
Boxplots, 10 Clusters

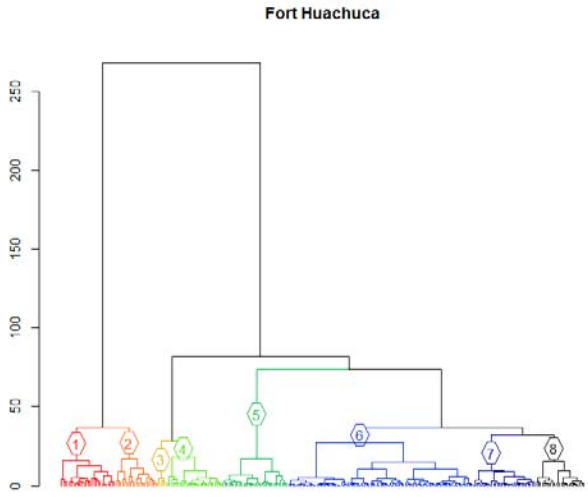


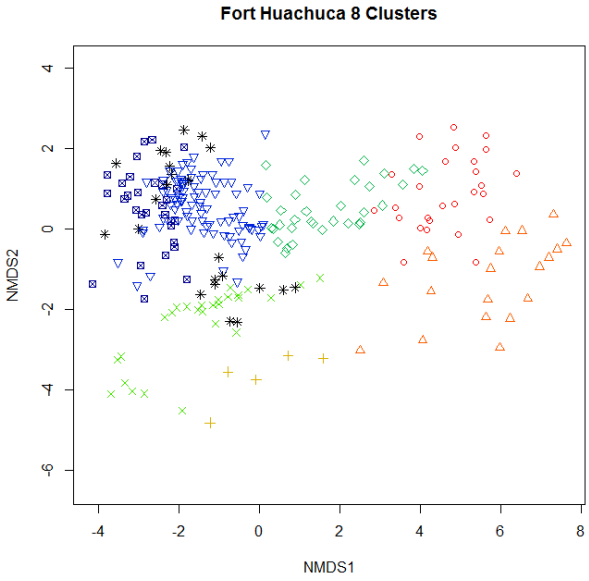

YPG
d g e e f c a b e ab
Width 2m (m)
Width2m
group10
YPG
c b cd c e a de g f h
Rainfall Seasonality Index
RSI
group10
YPG
d ab bcd c a d ac d c c
Entrenchment Ratio (3m width/0.5m width)
ER_3m_05m
group10
YPG
b a c c d b ab b ab ab
Cumulative Area (m2)
Cum Area
group10

Fort Huachuca

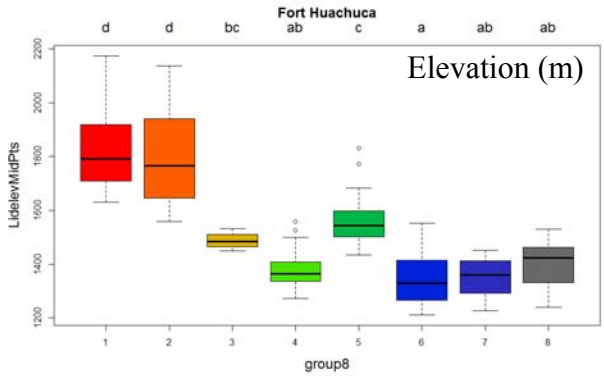
Stream Type Classification Results – 8 Clusters
Mapped Clusters, Dendrogram, NMDS plot, Box Plots for Input Variables



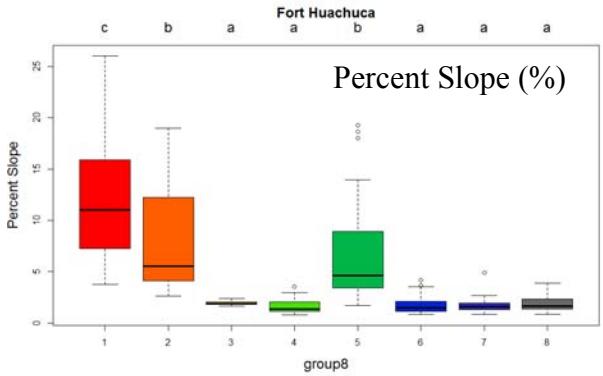




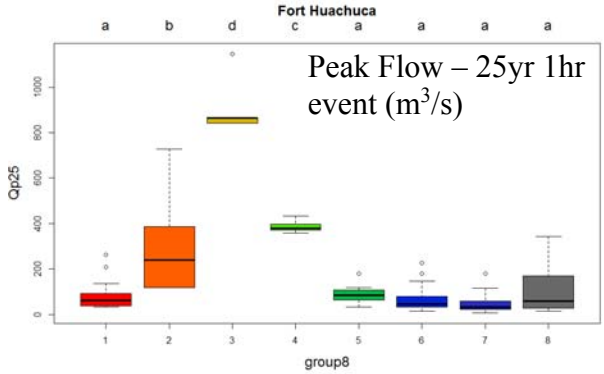
Boxplots, 8 Clusters



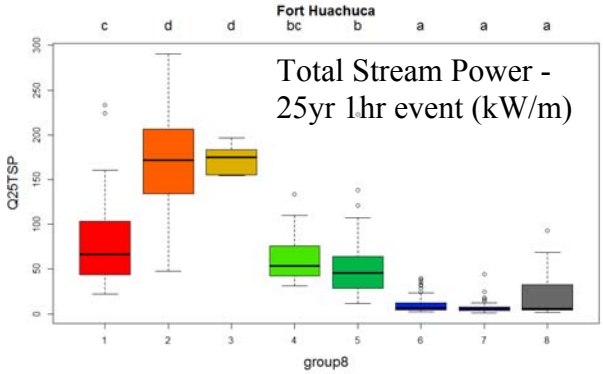
Elevation (m)



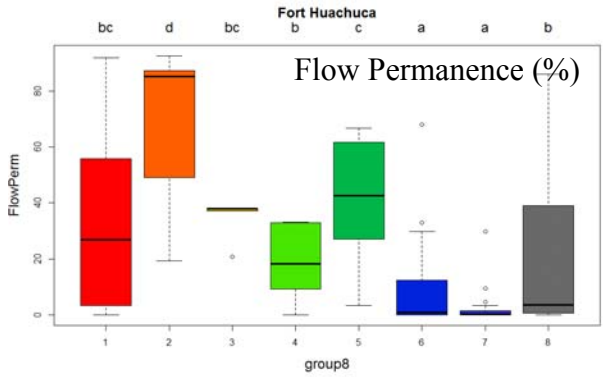
Percent Slope (%)



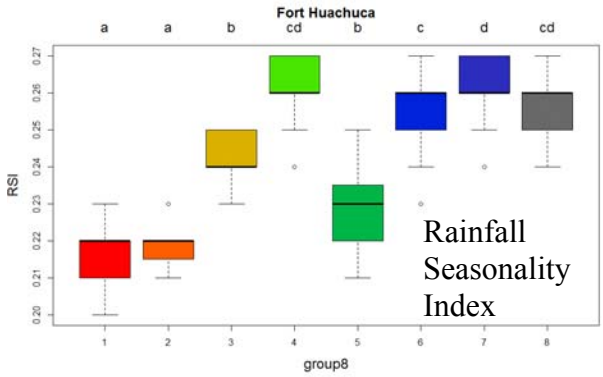
Peak Flow – 25yr 1hr event (m^3/s)



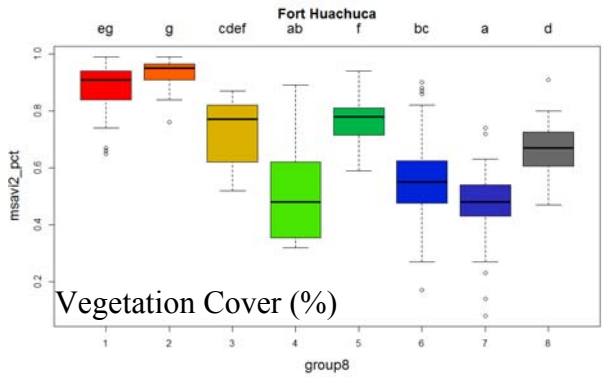
Total Stream Power - 25yr 1hr event (kW/m)



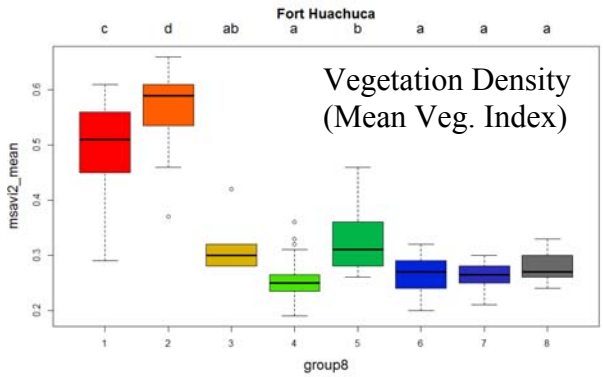
Flow Permanence (%)



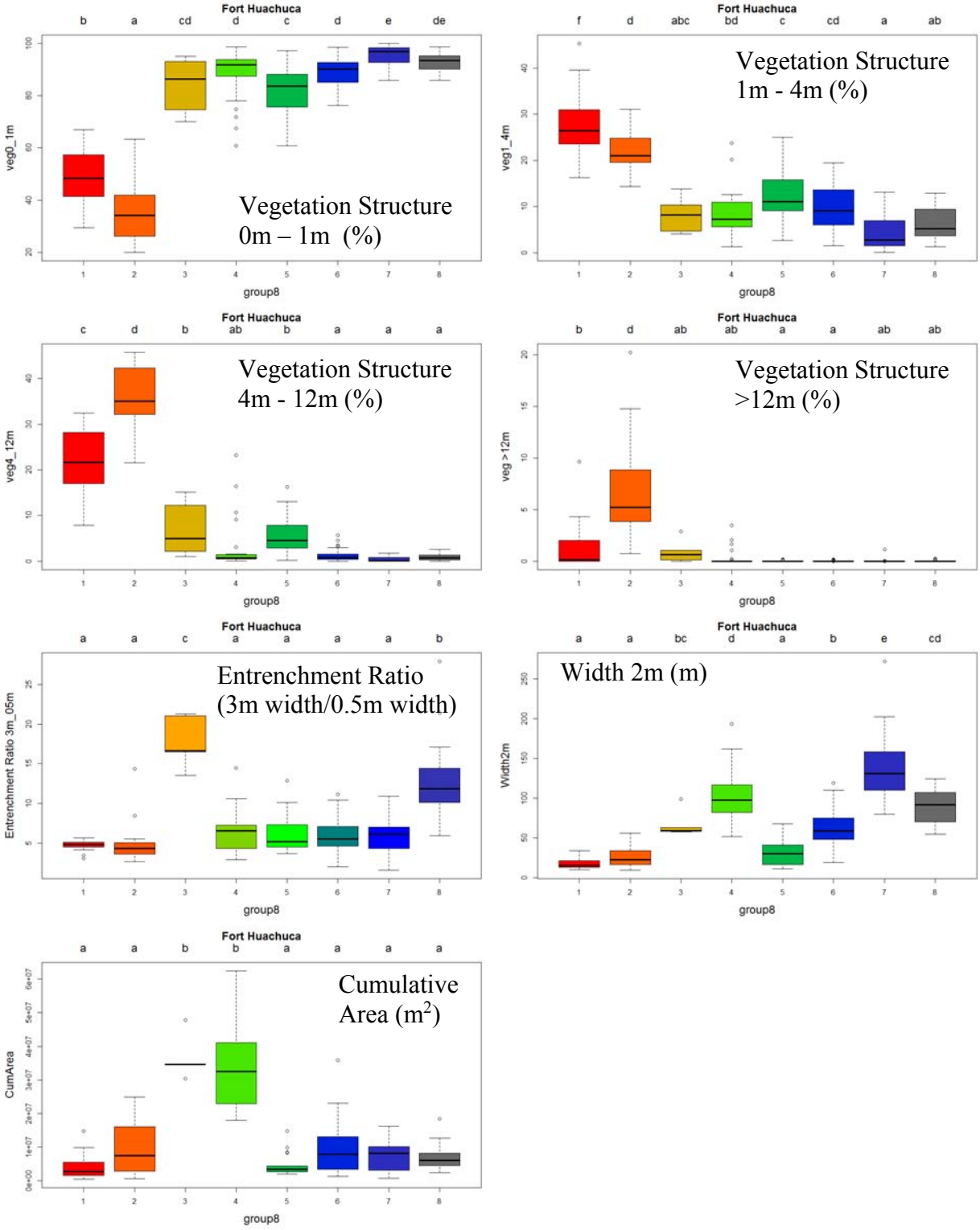
Rainfall Seasonality Index



Vegetation Cover (%)

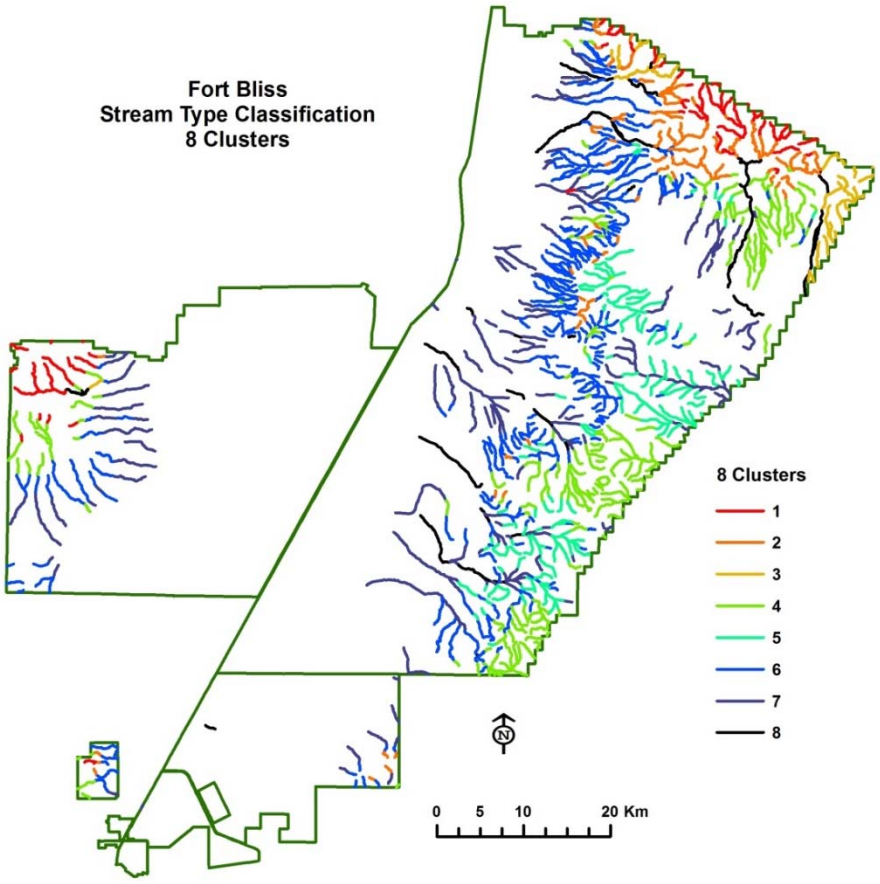


Vegetation Density (Mean Veg. Index)

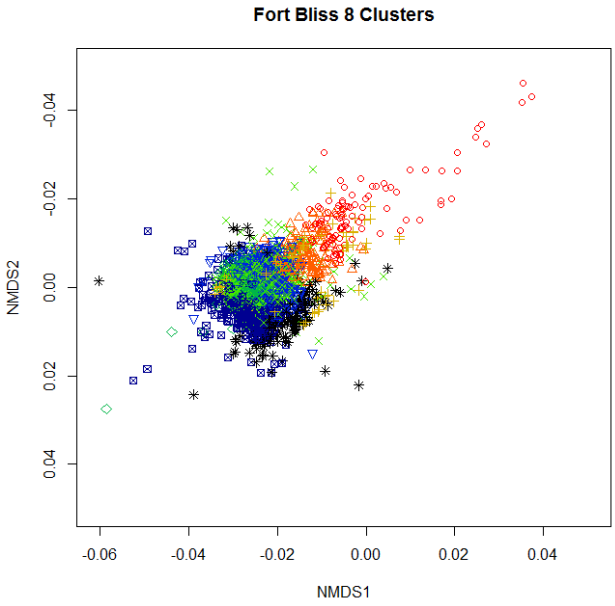

Fort Huachuca
b a cd d c d e de
veg0_1m
Vegetation Structure
0m – 1m (%)
group8
Fort Huachuca
f d abc bd c cd a ab
veg1_4m
Vegetation Structure
1m - 4m (%)
group8
Fort Huachuca
c d b ab b a a a
veg4_12m
Vegetation Structure
4m - 12m (%)
group8
Fort Huachuca
b d ab ab a a ab ab
veg > 12m
Vegetation Structure
>12m (%)
group8
Fort Huachuca
a a c a a a a b
Entrenchment Ratio 3m_05m
Entrenchment Ratio
(3m width/0.5m width)
group8
Fort Huachuca
a a bc d a b e cd
Width2m
Width 2m (m)
group8
Fort Huachuca
a a b b a a a a
CumArea
Cumulative
Area (m2)
group8

Fort Bliss

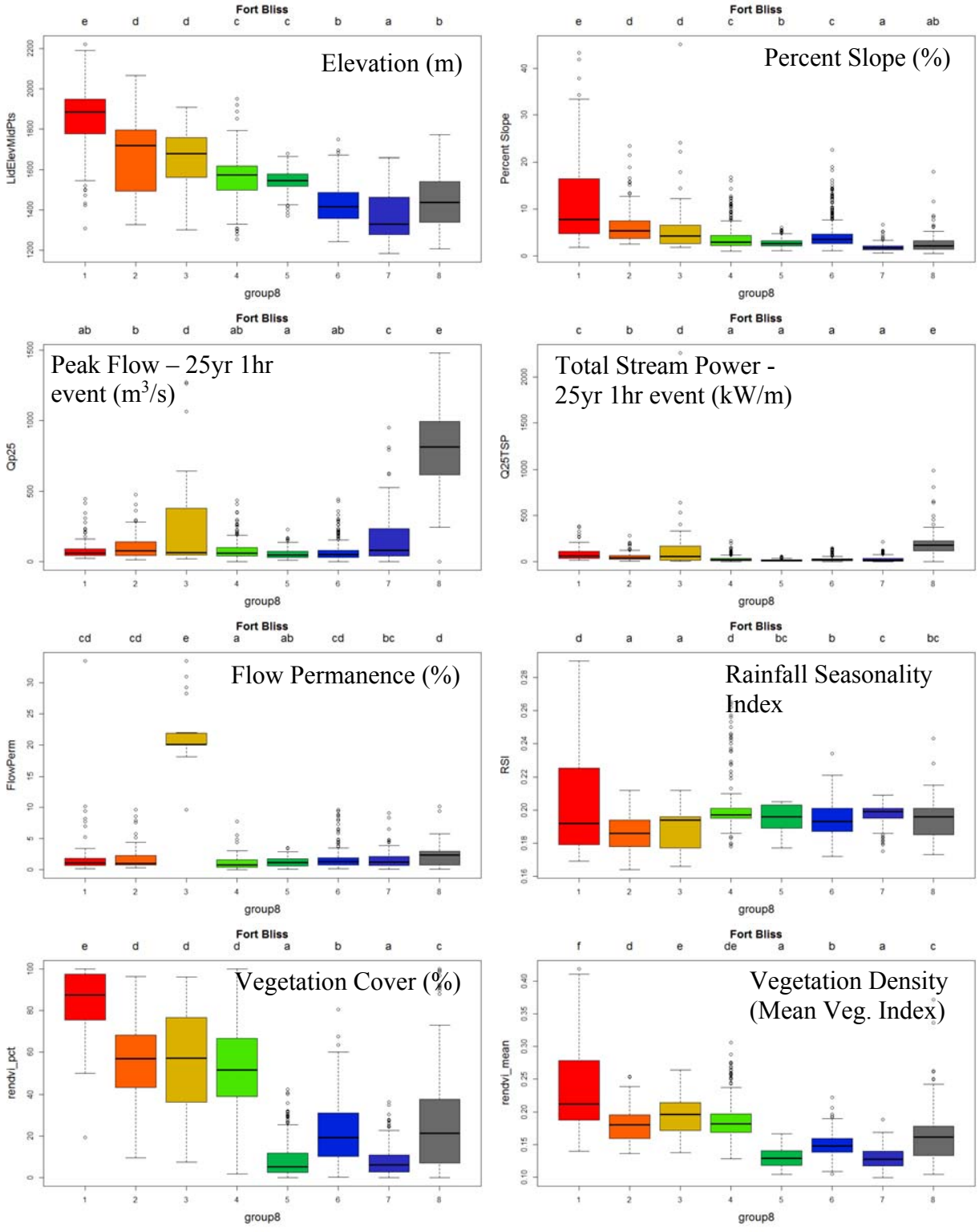
Stream Type Classification Results – 8 Classes
Mapped Clusters, Dendrogram, NMDS plot, Box Plots for Input Variables

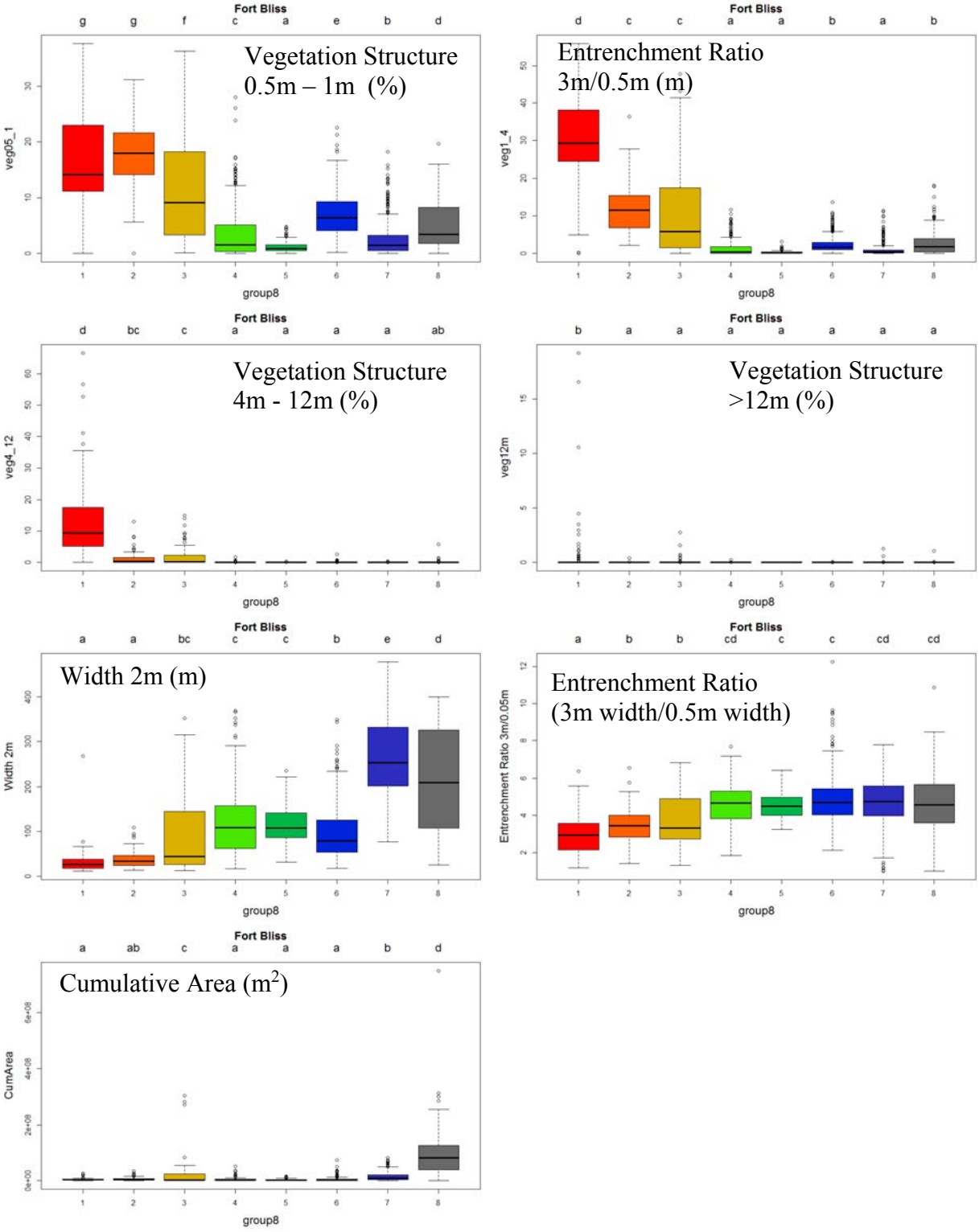






Boxplots, 8 Clusters




Fort Bliss
g g f c a e b d
Vegetation Structure
0.5m – 1m (%)
veg05_1
group8
Fort Bliss
d c c a a b a b
Entrenchment Ratio
3m/0.5m (m)
veg1_4
group8
Fort Bliss
d bc c a a a a ab
Vegetation Structure
4m - 12m (%)
veg4_12
group8
Fort Bliss
b a a a a a a a
Vegetation Structure
>12m (%)
veg12m
group8
Fort Bliss
a a bc c c b e d
Width 2m (m)
Width 2m
group8
Fort Bliss
a b b cd c c cd cd
Entrenchment Ratio
(3m width/0.5m width)
Entrenchment Ratio 3m/0.05m
group8
Fort Bliss
a ab c a a a b d
Cumulative Area (m2)
CumArea
group8

Appendix C: Wildlife Tables

Table 1. Riparian-associated breeding birds at Fort Bliss, NM. Nests were found for species highlighted in gray by Myers et al. (1998). Species marked with a * were added to the riparian associated list based on Myers' findings. Scores for use of each structure layer, season of presences, and occurrence in lowlands, foothills, or mountains are indicated. Season YR = year-round occurrence, S = summer occurrence. Riparian rank was used in Hammer's thesis.

		Vegetation Layer					Rip.				
Common Name	Scientific Name	0.5-1m	1-4m	4-12m	>12m	Season	Rank	TERS	Lowlands	Foothills	Mountains
Cooper's hawk	*Accipiter cooperii*			2	2	YR	F or I	N		●	●
Sharp-shinned hawk	*Accipiter striatus*		1	2	2	YR	F or I	N		●	●
Red-winged blackbird	*Agelaius phoeniceus*	2	2	1		YR	O	N	●	●	
*Rufous-crowned sparrow	*Aimophila ruficeps*	1				YR	KM RA	N	●	●	●
Black-throated sparrow	*Amphispiza bilineata*	2	1			YR	N	N	●	●	
Western scrub-jay	*Aphelocoma californica*		2	1		YR	F	N		●	●
Black-chinned hummingbird	*Archilochus alexandrinus*		2	2		S	I or O	N	●	●	●
Long-eared owl	*Asio otus*		2	1		YR	I	N	●	●	
Gray Hawk	*Asturina nitidus*			1	2	S	O	Y	●	●	
*Verdin	*Auriparus flaviceps*	1	2	1		YR	KM RA	N	●	●	
Great horned owl	*Bubo virginianus*	1	1	2	2	YR	F	N	●	●	●
Zone-tailed hawk	*Buteo albonotatus*			1	2	S	I	Y	●	●	●
Swainson's hawk	*Buteo swainsoni*		2	1		S	F	N	●	●	
Common black-hawk	*Buteogallus anthracinus*				2	S	O	Y	●	●	●
Gambel's quail	*Callipepla gambelii*	2	1			YR	I	N	●	●	
Scaled quail	*Callipepla squamata*	2	1			YR	F	Y	●	●	
Costa's Hummingbird	*Calypte costae*	2	2			S	F	Y	●	●	
Pyrrhuloxia	*Cardinalis sinuatus*		2			YR	F or I	N	●	●	
Lesser goldfinch	*Carduelis psaltria*		2	2	1	YR	O	N		●	●
*House finch	*Carpodacus mexicanus*		2	1		YR	KM RA	N	●	●	
Turkey vulture	*Cathartes aura*				1	S	F	N	●	●	●
Hermit thrush	*Catharus guttatus*	2	1			YR	KM RA	N		●	●
Canyon wren	*Catherpes mexicanus*					YR	I	Y			
Lesser nighthawk	*Chordeiles acutipennis*	1	1	1		S	F	N	●	●	
American dipper	*Cinclus mexicanus*					YR	O	Y			

Appendix C

Common Name	Scientific Name	Vegetation Layer				Season	Rip. Rank	TERS	Lowlands	Foothills	Mountains
		0.5-1m	1-4m	4-12m	>12m						
Western Yellow-billed cuckoo	*Coccyzus americanus*		2	1	1	S	O	Y	●	●	
Western wood-pewee	*Contopus sordidulus*	1	2	2	2	S	F	N		●	●
White-tailed kite	*Elanus leucurus*		1	2	2	YR	F	Y	●	●	
Cordilleran flycatcher	*Empidonax occidentalis*	1	2	1		S	O	N			●
Willow Flycatcher	*Empidonax traillii*	1	2	1		S	O	Y		●	●
Gray flycatcher	*Empidonax wrightii*	1	2	1		S	I	Y	●	●	●
Brewer's blackbird	*Euphagus cyanocephalus*	2	2	1		YR	I	N	●	●	●
Northern Aplomado Falcon	*Falco femoralis*			2		YR	N	Y	●	●	
American kestrel	*Falco sparverius*		1	2	1	YR	F	N	●	●	●
*Greater roadrunner	*Geococcyx californicus*		2			YR	KM RA	N	●	●	-
Common yellowthroat	*Geothlypis trichas*					S	O	N			
Blue grosbeak	*Guiraca/Passerina caerulea*	2	2	1		S	F	N	●	●	
Yellow-breasted chat	*Icteria virens*	2	1			S	I	Y	●	●	●
Bullock's oriole	*Icterus bullockii*		2	2	1	S	F	N	●	●	●
Hooded oriole	*Icterus cucullatus*		2	2		S	I	Y	●	●	●
Scott's oriole	*Icterus parisorum*		2	1		S	N	N	●	●	
Mississippi kite	*Ictinia mississippiensis*		1	2	2	S	I	Y	●	●	●
Northern mockingbird	*Mimus polyglottos*	1	2	1	1	YR	N	N	●	●	●
*Brown-headed cowbird	*Molothrus ater*					YR	KM RA	N	●	●	●
*Ash-throated flycatcher	*Myiarchus cinerascens*	1	2	1		S	KM RA	N	●	●	-
MacGillivray's warbler	*Oporornis tolmei*	2	1	1		S	I	N			●
Western screech-owl	*Otus kennicotti*		1	2		YR	I	N	●	●	●
Harris's hawk	*Parabuteo unicinctus*		2	2		YR	I	Y	●	●	
Painted bunting	*Passerina ciris*	2	2			S	F	N	●	●	●
Indigo bunting	*Passerina cyanea*	2				S	I	N	●	●	●
Varied bunting	*Passerina versicolor*	2	2			S	O	Y	●		
Cave swallow	*Petrochelidon fulva*					S	I	Y			
Cliff swallow	*Petrochelidon pyrrhonota*					S	I	N			
Phainopepla	*Phainopepla nitens*		2	1		S	I	N	●	●	●

Appendix C

Common Name	Scientific Name	Vegetation Layer				Season	Rip. Rank	TERS	Lowlands	Foothills	Mountains
		0.5-1m	1-4m	4-12m	>12m						
Black-headed grosbeak	*Pheucticus melanocephalus*		2	2		S	I	N	●	●	●
Downy woodpecker	*Picoides pubescens*		1	2	1	YR	F	N		●	●
Hairy woodpecker	*Picoides villosus*		2	2	2	YR	F	N		●	●
Canyon towhee	*Pipilo fuscus*	1	2			YR	I	N	●	●	●
Spotted towhee	*Pipilo maculatus*	2	2			YR	F or I	N	●	●	●
Summer tanager	*Piranga rubra*		2	2	1	S	O	N	●	●	●
Blue-gray gnatcatcher	*Polioptila caerulea*		1	2	1	S	F	N		●	●
Black-tailed gnatcatcher	*Polioptila melanura*	1	2	1		YR	I	Y	●	●	
Great-tailed grackle	*Quiscalus mexicanus*		1	2	2	YR	I	N	●	●	●
*Ruby-crowned kinglet	*Regulus calendula*	1	1	2	1	YR	KM RA	N			●
Bank Swallow	*Riparia riparia*					S	I	N	●		
Rock wren	*Salpinctes obsoletus*					YR	F	N			
Black phoebe	*Sayornis nigricans*		1			YR	O	N	●	●	●
Red-naped sapsucker	*Sphyrapicus nuchalis*		2	2	1	YR	F	N		●	●
Black-chinned sparrow	*Spizella atrogularis*	2				S	F	Y	●	●	●
Northern rough-winged swallow	*Stelgidopteryx serripennis*					S	I	N			
Mexican spotted owl	*Strix occidentalis*			1	1	YR	I	Y			●
Bewick's wren	*Thryomanes bewickii*	1	2	1		YR	F	N	●	●	●
Crissal thrasher	*Toxostoma dorsalis/crissale*	2	2			YR	O	N	●	●	
Brown thrasher	*Toxostoma rufum*	2	2			YR	I	N	●	●	●
House wren	*Troglodytes aedon*		2	2		YR	F	N	●	●	●
Cassin's kingbird	*Tyrannus vociferans*			2	2	S	I	N	●	●	●
Orange-crowned warbler	*Vermivora celata*	2	2			YR	F or I	N			●
Lucy's warbler	*Vermivora luciae*		2	2		S	O	Y	●	●	
Virginia's warbler	*Vermivora virginiae*	1	1			S	F	Y		●	●
Bell's vireo	*Vireo bellii*	2	2			S	I	Y	●		
Warbling vireo	*Vireo gilvus*		2	2	2	S	F or I	N	●	●	●
Plumbeous/Solitary vireo	*Vireo plumbeus*	1	2	1		S	F or I	N		●	●
Gray vireo	*Vireo vicinior*		2			S	N	Y		●	●
White-winged dove	*Zenaida asiatica*		2	2		YR	F	N	●	●	●

Table 2. Riparian-associated species occurring or possible in the study area. Source of model or lack of availability indicated by USGS (National GAP), SW (Southwest Regional GAP), or None. Species with an asterisk in the model column were subspecies represented by the full species model, or species represented by another GAP model because taxonomy changed. Riparian-association indicated in the RA? column. Inclusion in TER-S group indicated with a Y (yes) or N (no). B = Bliss, H = Huachuca, I = Irwin, Y = YPG.

Model			Occurs						TERS			
Source	Scientific Name	Common Name	B	H	I	Y	RA?	Taxon	B	H	Y	I
*	*Ambystoma tigrinum stebbinsi*	Sonoran tiger salamander		•			RA	A		Y		
USGS	*Ambystoma tigrinum/mavortium*	Tiger salamander	•	•			RA	A				
None	*Anaxyrus/Bufo boreas*	Western toad			•		RA	A				
SW	*Anaxyrus/Bufo cognatus*	Great Plains toad	•	•		•	RA	A				
SW	*Anaxyrus/Bufo debilis*	Green toad	•	•			RA	A		Y		
SW	*Anaxyrus/Bufo punctatus*	Red-spotted toad	•	•	•	•	RA	A				
SW	*Anaxyrus/Bufo woodhousii*	Woodhouse's toad	•	•		•	RA	A				
None	*Gastrophryne olivacea*	Great Plains narrow-mouthed toad		•			RA	A				
SW	*Hyla arenicolor*	Canyon tree frog	•	•			RA	A				
None	*Hyla regilla*	Northern pacific chorus frog			•		RA	A				
SW	*Hyla wrightorum*	Huachuca/Arizona tree frog		•			RA	A		Y		
USGS	*Incilius alvarius*	Colorado River toad		•		•	RA	A		Y	Y	
SW	*Lithobates blairi*	Plains leopard frog		•			RA	A		Y		
USGS	*Lithobates chiricahuensis*	Chiricahua leopard frog		•			RA	A		Y		
USGS	*Lithobates yavapaiensis*	Yavapai/Lowland leopard frog		•		•	RA	A		Y		
SW	*Scaphiopus couchii*	Couch's spadefoot	•	•		•	RA	A				
SW	*Spea bombifrons*	Plains spadefoot	•	•			RA	A				
SW	*Spea multiplicata*	New Mexico/Mexican spadefoot	•	•			RA	A				
USGS	*Accipiter cooperii*	Cooper's hawk	•	•	•	•	RA	B				Y
USGS	*Accipiter striatus*	Sharp-shinned hawk	•	•	•	•	RA	B				Y
USGS	*Aegolius acadicus*	Northern saw-whet owl		•		•	RA	B				
SW	*Agelaius phoeniceus*	Red-winged blackbird	•	•	•	•	RA	B				
None	*Amazilia beryllina*	Berylline Hummingbird		•			RA	B				
USGS	*Amazilia violiceps*	Violet-crowned Hummingbird		•			RA	B		Y		
USGS	*Amphispiza belli/Artemisiospiza nevadens*	Sage sparrow	•	•	•	•	RA	B	N			

Model Source	Scientific Name	Common Name	Occurs B	Occurs H	Occurs I	Occurs Y	RA?	Taxon	TERS B	TERS H	TERS Y	TERS I
USGS	*Amphispiza bilineata*	Black-throated sparrow	•	•	•	•	RA	B				
USGS	*Amphispiza quiquestriata*	Five-striped sparrow		•			RA	B		Y		
USGS	*Aphelocoma californica*	Western scrub-jay	•	•		•	RA	B				
USGS	*Archilochus alexandrinus*	Black-chinned hummingbird	•	•	•	•	RA	B				
USGS	*Asio otus*	Long-eared owl	•	•	•	•	RA	B		Y	Y	Y
USGS	*Asturina nitidus/Buteo plagiatus*	Gray hawk	•	•			RA	B	Y	Y		
USGS	*Baeolophus wollweberi*	Bridled titmouse		•			RA	B				
None	*Basileuterus rufifrons*	Rufous-capped warbler		•			RA	B				
USGS	*Bubo virginianus*	Great horned owl	•	•	•	•	RA	B				
USGS	*Buteo albonotatus*	Zone-tailed hawk	•	•		•	RA	B	Y			
None	*Buteo lineatus*	Red-shouldered hawk				•	RA	B				
None	*Buteo platypterus*	Broad-winged hawk		•			RA	B				
USGS	*Buteo regalis*	Ferruginous hawk	•	•	•	•	RA	B		Y	Y	Y
USGS	*Buteo swainsoni*	Swainson's hawk	•	•	•	•	RA	B		Y	Y	Y
USGS	*Buteogallus anthracinus*	Common black-hawk	•	•			RA	B	Y	Y		
USGS	*Callipepla californica*	California quail			•		RA	B				
USGS	*Callipepla gambelii*	Gambel's quail	•	•	•	•	RA	B				
USGS	*Callipepla squamata*	Scaled quail	•	•			RA	B	Y			
USGS	*Calothorax lucifer*	Lucifer hummingbird		•			RA	B		Y		
USGS	*Calypte costae*	Costa’s hummingbird	•	•	•	•	RA	B	Y			Y
None	*Camptostoma imberbe*	Northern beardless-tyrannulet		•			RA	B				
USGS	*Cardinalis cardinalis*	Northern cardinal		•		•	RA	B				
USGS	*Cardinalis sinuatus*	Pyrrhuloxia	•	•		•	RA	B				
USGS	*Carduelis lawrencei*	Lawrence’s goldfinch	•	•	•	•	RA	B	Y	Y	Y	Y
USGS	*Carduelis psaltria*	Lesser goldfinch	•	•	•	•	RA	B				
USGS	*Carduelis tristis*	American goldfinch	•	•	•	•	RA	B	N	N	N	
USGS	*Cathartes aura*	Turkey vulture	•	•	•	•	RA	B				
None	*Catharus ustulatus*	Swainson’s thrush	•	•	•	•	RA	B				
USGS	*Catherpes mexicanus*	Canyon wren	•	•	•	•	RA	B				
USGS	*Ceryle alcyon*	Belted kingfisher	•	•	•	•	RA	B		Y	Y	
USGS	*Chloroceryle americana*	Green kingfisher		•			RA	B		Y		
USGS	*Chordeiles acutipennis*	Lesser nighthawk	•	•	•	•	RA	B				

Model Source	Scientific Name	Common Name	Occurs B	Occurs H	Occurs I	Occurs Y	RA?	Taxon	TERS B	TERS H	TERS Y	TERS I
USGS	*Cinclus mexicanus*	American dipper	•	•			RA	B	Y	Y		
USGS	*Cistothorus palustris*	Marsh wren	•	•	•	•	RA	B	N	Y	Y	
USGS	*Coccyzus americanus*	Yellow-billed cuckoo	•	•	•	•	RA	B	Y	Y	Y	Y
USGS	*Colaptes chrysoides*	Gilded flicker				•	RA	B				
USGS	*Columbina passerina*	Common ground-dove		•		•	RA	B				
USGS	*Contopus sordidulus*	Western wood-pewee	•	•	•	•	RA	B				
USGS	*Corvus brachyrhynchos*	American crow	•				RA	B				
None	*Crotophaga sulcirostris*	Groove-billed ani	•				RA	B				
USGS	*Cyanthus latirostris*	Broad-billed hummingbird		•			RA	B		Y		
None	*Dendroica fusca*	Blackburnian warbler	•				RA	B				
None	*Dendroica occidentalis*	Hermit warbler	•	•	•	•	RA	B				
None	*Dendroica palmarum*	Palm warbler	•			•	RA	B				
None	*Dendroica pensylvanica*	Chestnut-sided warbler	•				RA	B				
None	*Dendroica striata*	Blackpoll warbler	•			•	RA	B				
None	*Dendroica virens*	Black-throated green warbler	•				RA	B				
None	*Dolichonyx oryzivorus*	Bobolink	•		•		RA	B				
None	*Dumetella carolinensis*	Gray catbird		•		•	RA	B				
USGS	*Elanus leucurus*	White-tailed kite	•	•		•	RA	B	Y	Y	Y	
None	*Empidonax difficilis*	Pacific-slope flycatcher		•	•	•	RA	B				
USGS	*Empidonax fulvifrons*	Buff-breasted flycatcher		•			RA	B		Y		
None	*Empidonax minimus*	Least flycatcher	•				RA	B				
USGS	*Empidonax oberholseri*	Dusky flycatcher	•	•	•	•	RA	B				
USGS	*Empidonax occidentalis*	Cordilleran flycatcher	•	•		•	RA	B		Y		
USGS	*Empidonax traillii extimus*	Southwestern Willow flycatcher	•	•	•	•	RA	B	Y	Y	Y	Y
USGS	*Empidonax wrightii*	Gray flycatcher	•	•	•	•	RA	B	Y			
USGS	*Eugenes fulgens*	Magnificent hummingbird		•			RA	B		Y		
None	*Euphagus carolinus*	Rusty blackbird	•		•	•	RA	B				
USGS	*Euphagus cyanocephalus*	Brewer's blackbird	•	•	•	•	RA	B				
USGS	*Falco femoralis*	Aplomado Falcon	•	•			RA	B	Y	Y		
USGS	*Falco sparverius*	American kestrel	•	•	•	•	RA	B				
USGS	*Geothlypis trichas*	Common yellowthroat	•	•	•	•	RA	B				
None	*Geothlypis/Oporornis formosa*	Kentucky warbler		•			RA	B				

Model Source	Scientific Name	Common Name	Occurs B	Occurs H	Occurs I	Occurs Y	RA?	Taxon	TERS B	TERS H	TERS Y	TERS I
USGS	*Haliaeetus leucocephalus*	Bald eagle	•	•		•	RA	B	Y	Y	Y	
USGS	*Icteria virens*	Yellow-breasted chat	•	•	•	•	RA	B	Y			Y
USGS	*Icterus bullockii*	Bullock's oriole	•	•	•		RA	B		Y		
USGS	*Icterus cucullatus*	Hooded oriole	•	•	•	•	RA	B	Y			
None	*Icterus galbula*	Baltimore oriole	•			•	RA	B				
USGS	*Icterus parisorum*	Scott's oriole	•	•	•	•	RA	B				
USGS	*Ictinia mississippiensis*	Mississippi kite	•	•			RA	B	Y	Y		
None	*Ixoreus naevius*	Varied thrush				•	RA	B				
USGS	*Junco hyemalis*	Dark-eyed junco	•	•	•	•	RA	B				
USGS	*Lampornis clemenciae*	Blue-throated Hummingbird		•			RA	B		Y		
USGS	*Lanius excubitor*	Northern shrike	•				RA	B				
USGS	*Melanerpes uropygialis*	Gila woodpecker		•	•	•	RA	B		Y	Y	Y
USGS	*Melospiza georgiana*	Swamp sparrow	•	•		•	RA	B		Y	Y	
USGS	*Melospiza lincolnii*	Lincoln's sparrow	•	•	•	•	RA	B	N	Y	Y	
USGS	*Melospiza melodia*	Song sparrow	•	•	•	•	RA	B				Y
USGS	*Melozone aberti*	Abert's towhee		•		•	RA	B		Y	Y	
USGS	*Micrathene whitneyi*	Elf owl		•		•	RA	B				
USGS	*Mimus polyglottos*	Northern mockingbird	•	•	•	•	RA	B				
USGS	*Myiarchus tuberculifer*	Dusky-capped flycatcher		•			RA	B		Y		
USGS	*Myiarchus tyrannulus*	Brown-crested flycatcher		•	•	•	RA	B				Y
USGS	*Myiodynastes luteiventris*	Sulphur-bellied flycatcher		•			RA	B		Y		
USGS	*Oporornis tolmei*	MacGillivray's warbler	•	•	•	•	RA	B		Y	Y	
USGS	*Oreoscoptes montanus*	Sage thrasher	•	•	•	•	RA	B	N			
USGS	*Otus/Megascops kennicotti*	Western screech-owl	•	•	•	•	RA	B				
USGS	*Pachyramphus aglaiae*	Rose-throated becard		•			RA	B		Y		
USGS	*Pandion haliaetus*	Osprey	•	•		•	RA	B	Y	Y	Y	
USGS	*Parabuteo unicinctus*	Harris's hawk	•	•		•	RA	B	Y			
None	*Parula americana*	Northern parula	•			•	RA	B				
USGS	*Passerella iliaca*	Fox sparrow	•	•	•	•	RA	B		Y	Y	
USGS	*Passerina amoena*	Lazuli bunting	•	•	•	•	RA	B				
USGS	*Passerina caerulea*	Blue grosbeak	•	•		•	RA	B				
USGS	*Passerina ciris*	Painted bunting	•				RA	B				

Model Source	Scientific Name	Common Name	Occurs B	Occurs H	Occurs I	Occurs Y	RA?	Taxon	TERS B	TERS H	TERS Y	TERS I
USGS	*Passerina cyanea*	Indigo bunting	•	•	•	•	RA	B		Y	Y	
USGS	*Passerina versicolor*	Varied bunting	•	•			RA	B	Y	Y	Y	
USGS	*Petrochelidon fulva*	Cave swallow	•				RA	B	Y			
USGS	*Petrochelidon pyrrhonota*	Cliff swallow	•	•	•	•	RA	B				
USGS	*Phainopepla nitens*	Phainopepla	•	•	•	•	RA	B				
None	*Pheucticus ludovicianus*	Rose-breasted grosbeak	•	•			RA	B				
USGS	*Pheucticus melanocephalus*	Black-headed grosbeak	•	•	•	•	RA	B				
USGS	*Picoides arizonae*	Arizona woodpecker		•			RA	B		**Y**		
USGS	*Picoides pubescens*	Downy woodpecker	•				RA	B				
USGS	*Picoides villosus*	Hairy woodpecker	•	•			RA	B				
USGS	*Pipilo chlorurus*	Green-tailed towhee	•	•	•	•	RA	B	N	N	N	
None	*Pipilo erythrophthalmus*	Eastern towhee	•				RA	B				
USGS	*Pipilo maculatus*	Spotted towhee	•	•	•	•	RA	B				
USGS	*Pipilo/Melozone fuscus*	Canyon towhee	•	•		•	RA	B				
USGS	*Piranga rubra*	Summer tanager	•	•		•	RA	B				
USGS	*Polioptila caerulea*	Blue-gray gnatcatcher	•	•	•	•	RA	B				
USGS	*Polioptila melanura*	Black-tailed gnatcatcher	•	•	•	•	RA	B	Y			
None	*Polioptila nigriceps*	Black-capped gnatcatcher		•			RA	B				
None	*Protonotaria citrea*	Prothonotary warbler	•			•	RA	B				
USGS	*Pyrocephalus rubinus*	Vermilion flycatcher		•	•	•	RA	B				Y
USGS	*Quiscalus mexicanus*	Great-tailed grackle	•	•	•	•	RA	B				
USGS	*Riparia riparia*	Bank swallow	•	•		•	RA	B				Y
USGS	*Salpinctes obsoletus*	Rock wren	•	•	•	•	RA	B				
USGS	*Sayornis nigricans*	Black phoebe	•	•	•	•	RA	B				
USGS	*Sayornis phoebe*	Eastern phoebe	•			•	RA	B				
None	*Selurus aurocapilla*	Ovenbird		•			RA	B				
None	*Seiurus noveboracensis*	Northern waterthrush	•	•		•	RA	B				
None	*Setophaga ruticilla*	American redstart	•	•		•	RA	B				
USGS	*Sphyrapicus nuchalis*	Red-naped sapsucker	•	•	•	•	RA	B	N			
None	*Spizella arborea*	American tree sparrow			•		RA	B				
USGS	*Spizella atrogularis*	Black-chinned sparrow	•	•		•	RA	B	Y			
USGS	*Spizella pallida*	Clay-colored sparrow	•	•			RA	B		Y		

Model Source	Scientific Name	Common Name	Occurs B	Occurs H	Occurs I	Occurs Y	RA?	Taxon	TERS B	TERS H	TERS Y	TERS I
USGS	*Stelgidopteryx serripennis*	Northern rough-winged swallow	•	•	•	•	RA	B				
None	*Stellula calliope*	Calliope hummingbird		•		•	RA	B				
USGS	*Strix occidentalis lucida*	Mexican spotted owl	•	•			RA	B	Y	Y		
USGS	*Tachycineta bicolor*	Tree swallow	•	•	•	•	RA	B	N	Y	Y	
USGS	*Thryomanes bewickii*	Bewick's wren	•	•	•	•	RA	B				
USGS	*Toxostoma dorsalis/crissale*	Crissal thrasher	•	•	•	•	RA	B				Y
USGS	*Toxostoma rufum*	Brown thrasher	•			•	RA	B				
USGS	*Troglodytes aedon*	House wren	•	•		•	RA	B				
USGS	*Trogon elegans*	Elegant trogon		•			RA	B		Y		
None	*Tyrannus tyrannus*	Eastern kingbird	•				RA	B				
USGS	*Tyrannus vociferans*	Cassin's kingbird	•	•	•	•	RA	B				
USGS	*Tyranus crassirostris*	Thick-billed kingbird		•			RA	B		Y		
USGS	*Tyranus melancholicus*	Tropical kingbird		•		•	RA	B		Y	Y	
None	*Vermivora chrysoptera*	Golden-winged warbler	•			•	RA	B				
USGS	*Vermivora/Oreothlypis celata*	Orange-crowned warbler	•	•	•	•	RA	B		Y		
USGS	*Vermivora/Oreothlypis luciae*	Lucy's warbler	•	•	•	•	RA	B	Y			Y
USGS	*Vermivora/Oreothlypis virginiae*	Virginia's warbler	•	•	•	•	RA	B	Y			Y
*	*Vireo bellii arizonae*	Arizona Bell's vireo		•	•	•	RA	B		Y	Y	Y
USGS	*Vireo bellii medius*	Bell's vireo	•				RA	B	Y			
*	*Vireo bellii pusillus*	Least Bell's vireo			•	•	RA	B			Y	Y
USGS	*Vireo gilvus*	Warbling vireo	•	•	•	•	RA	B				
USGS	*Vireo huttoni*	Hutton's vireo	•	•	•	•	RA	B				
USGS	*Vireo plumbeus*	Plumbeous vireo	•	•	•		RA	B				
USGS	*Vireo vicinior*	Gray vireo	•	•	•	•	RA	B	Y	Y	Y	Y
None	*Wilsonia citrina*	Hooded warbler	•	•			RA	B				
USGS	*Xanthocephalus xanthocephalus*	Yellow-headed blackbird	•	•	•	•	RA	B				Y
USGS	*Zenaida asiatica*	White-winged dove	•	•	•	•	RA	B				
USGS	*Zonotrichia atricapilla*	Golden-crowned sparrow			•	•	RA	B			Y	
None	*Zonotrichia querula*	Harris's sparrow	•				RA	B				
None	*(Xero)Spermophilus mohavensis*	Mohave ground squirrel			•		RA	M				
SW	*Ammospermophilus interpres*	Texas antelope squirrel	•				RA	M	Y			
None	*Ammospermophilus leucurus*	White-tailed antelope squirrel			•	•	RA	M				

Model Source	Scientific Name	Common Name	Occurs B	Occurs H	Occurs I	Occurs Y	RA?	Taxon	TERS B	TERS H	TERS Y	TERS I
USGS	*Antrozous pallidus*	Pallid bat	•	•	•	•	RA	M				Y
USGS	*Baiomys taylori*	Northern pygmy mouse		•			RA	M		Y		
USGS	*Bassariscus astutus*	Ringtail	•	•	•	•	RA	M				
None	*Chaetodipus eremicus*	Chihuahuan pocket mouse	•				RA	M				
None	*Chaetodipus formosus*	Long-tailed pocket mouse			•	•	RA	M				
SW	*Chaetodipus hispidus*	Hispid pocket mouse	•	•			RA	M	Y			
USGS	*Chaetodipus intermedius*	Rock pocket mouse	•	•		•	RA	M				
USGS	*Choeronyctis mexicana*	Mexican long-tongued bat		•			RA	M		Y		
USGS	*Corynorhinus townsendii*	Townsend's big-eared bat	•	•	•	•	RA	M	Y	Y	Y	Y
*	*Corynorhinus townsendii pallescens*	Pale lump-nosed bat	•	•	•	•	RA	M	Y	Y	Y	Y
SW	*Dicotyles/Pecari tajacu*	Javelina / Collared peccary	•	•		•	RA	M				
SW	*Didelphis virginiana*	Virginia opossum (includes mexican opossum)	•				RA	M		Y		
USGS	*Eptesicus fuscus*	Big brown bat	•	•	•	•	RA	M				
SW	*Erethizon dorsatum*	Porcupine	•	•		•	RA	M				
USGS	*Euderma maculatum*	Spotted bat		•	•	•	RA	M		Y	Y	Y
USGS	*Eumops perotis*	Greater bonneted/mastiff bat		•	•	•	RA	M		Y	Y	Y
None	*Felis pardalis*	Ocelot		•			RA	M				
None	*Felis yagouroundi*	Jaguarundi		•			RA	M				
USGS	*Idionycteris phyllotis*	Allen's big-eared/lappet-browed bat		•		•	RA	M		Y	Y	
USGS	*Lasionycteris noctivagans*	Silver-haired bat	•	•	•	•	RA	M		Y	Y	Y
USGS	*Lasiurus blossevillii*	Western red bat	•	•	•	•	RA	M	Y	Y	Y	Y
USGS	*Lasiurus cinereus*	Hoary bat	•	•	•	•	RA	M				
USGS	*Lasiurus xanthinus*	Western yellow bat		•		•	RA	M		Y	Y	
USGS	*Lynx rufus*	Bobcat	•	•	•	•	RA	M				
USGS	*Macrotus californicus*	Californian leaf-nosed bat		•	•	•	RA	M		Y	Y	Y
USGS	*Mephitis macroura*	Hooded skunk		•			RA	M				
SW	*Mephitis mephitis*	Striped skunk	•	•		•	RA	M				
SW	*Microtus mogollonensis*	Mogollon vole	•				RA	M				
None	*Mormoops megalophylla*	Peter's ghost-faced bat		•			RA	M				
USGS	*Mustela frenata*	Long-tailed weasel	•	•			RA	M				
USGS	*Myotis auriculus*	Southwestern myotis		•			RA	M		Y		
USGS	*Myotis evotis*	Long-eared myotis			•		RA	M				

Model Source	Scientific Name	Common Name	Occurs B	Occurs H	Occurs I	Occurs Y	RA?	Taxon	TERS B	TERS H	TERS Y	TERS I
USGS	*Myotis lucifugus*	Little brown myotis	•		•		RA	M	Y	Y		
USGS	*Myotis occultus*	Occult little brown bat / Arizona myotis	•	•		•	RA	M		Y	Y	
USGS	*Myotis velifer*	Cave myotis	•	•		•	RA	M	Y	Y	Y	
USGS	*Myotis volans*	Long-legged myotis	•	•	•	•	RA	M		Y	Y	
USGS	*Myotis yumanensis*	Yuma myotis	•	•	•	•	RA	M		Y	Y	
USGS	*Nasua narica*	White-nosed coati		•			RA	M				
None	*Neotoma lepida*	Desert woodrat			•	•	RA	M				
USGS	*Nyctinomops macrotis*	Big free-tailed bat	•	•		•	RA	M	Y	Y	Y	
SW	*Odocoileus hemionus*	Mule deer	•	•		•	RA	M				
SW	*Odocoileus virginanus*	White-tailed deer	•	•			RA	M		Y		
SW	*Ondatra zibethicus*	Muskrat				•	RA	M				
USGS	*Peromyscus boylii*	Brush mouse	•	•	•	•	RA	M				
SW	*Peromyscus leucopus*	White-footed mouse	•	•			RA	M				
USGS	*Peromyscus truei*	Pinyon mouse			•		RA	M				
SW	*Pipi/parastrellus hesperus*	Western pipistrelle / Canyon bat	•	•	•	•	RA	M				
SW	*Procyon lotor*	Raccoon	•	•		•	RA	M				
USGS	*Puma concolor*	Mountain lion	•	•	•	•	RA	M	Y			
*	*Puma concolor browni*	Yuma mountain lion				•	RA	M			Y	
SW	*Reithrodontomys megalotis*	Western harvest mouse	•	•			RA	M				
USGS	*Sciurus arizonensis*	Arizona gray squirrel		•			RA	M		Y		
USGS	*Sigmodon arizonae*	Arizona cotton rat		•		•	RA	M		Y	Y	
USGS	*Sigmodon fulviventer*	Tawny-bellied cotton rat		•			RA	M				
SW	*Sigmodon hispidus*	Hispid cotton rat	•			•	RA	M				
*	*Sigmodon hispidus eremicus*	Yuma hispid cotton rat				•	RA	M			Y	
USGS	*Sorex arizonae*	Arizona shrew		•			RA	M		Y		
USGS	*Sorex tenellus*	Inyo shrew			•		RA	M				
USGS	*Spilogale gracilis*	Western spotted skunk	•	•		•	RA	M				
SW	*Sylvilagus audubonii*	Desert cottontail	•	•	•	•	RA	M				
SW	*Sylvilagus floridanus*	Eastern cottontail	•	•			RA	M				
USGS	*Tadarida brasiliensis*	Brazilian/Mexican free-tailed bat	•	•	•	•	RA	M	Y	Y	Y	
SW	*Urocyon cinereoargenteus*	Gray fox	•	•	•	•	RA	M				
USGS	*Ursus americanus*	Black bear	•	•			RA	M				

Model Source	Scientific Name	Common Name	Occurs B	Occurs H	Occurs I	Occurs Y	RA?	Taxon	TERS B	TERS H	TERS Y	TERS I
USGS	*Arizona elegans*	Glossy snake	•	•	•	•	RA	R				
USGS	*Aspidoscelis burti*	Canyon spotted whiptail		•			RA	R		Y		
USGS	*Aspidoscelis exsanguis*	Chihuahuan spotted whiptail	•				RA	R				
USGS	*Aspidoscelis inornata*	Little striped whiptail	•				RA	R				
USGS	*Aspidoscelis neomexicana*	New Mexico whiptail	•				RA	R				
USGS	*Aspidoscelis sonorae*	Sonoran spotted whiptail		•			RA	R				
*	*Aspidoscelis stictogrammus*	Giant spotted whiptail		•			RA	R				
USGS	*Aspidoscelis tesselata*	Checkered whiptail	•				RA	R				
USGS	*Aspidoscelis tigris*	Western/Tiger whiptail	•		•	•	RA	R	Y			
USGS	*Aspidoscelis uniparens*	Desert grassland whiptail	•	•			RA	R				
USGS	*Callisaurus draconoides*	Zebra-tailed lizard		•	•	•	RA	R				
SW	*Chilomeniscus stramineus*	Variable sand snake				•	RA	R			Y	
None	*Chrysemys picta*	Painted turtle	•				RA	R				
None	*Coluber constrictor*	Racer	•		•		RA	R				
USGS	*Cophosaurus texanus*	Greater earless lizard	•	•			RA	R				
SW	*Crotalus atrox*	Western diamondback rattlesnake	•	•		•	RA	R				
USGS	*Crotalus cerastes*	Sidewinder			•	•	RA	R				
SW	*Crotalus lepidus*	Rock rattlesnake	•	•			RA	R				
*	*Crotalus lepidus klauberi*	Banded rock rattlesnake	•	•			RA	R	Y	Y		
*	*Crotalus lepidus lepidus*	Mottled rock rattlesnake	•				RA	R	Y			
USGS	*Crotalus mitchelli*	Speckled rattlesnake			•	•	RA	R				
USGS	*Crotalus molossus*	Black-tailed rattlesnake	•	•		•	RA	R				
USGS	*Crotalus willardi*	Ridge-nosed rattlesnake		•			RA	R		Y		
*	*Crotalus willardi obscurus*	New Mexico ridge-nosed rattlesnake		•			RA	R		Y		
*	*Crotalus willardi willardi*	Arizona ridge-nosed rattlesnake		•			RA	R		Y		
USGS	*Crotaphytus collaris*	Eastern collared lizard	•	•			RA	R				
None	*Crotaphytus nebrius*	Sonoran collared lizard				•	RA	R				
SW	*Diadophis punctatus*	Ringneck snake	•	•	•	•	RA	R				
USGS	*Dipsosaurus dorsalis*	Desert iguana			•	•	RA	R				
SW	*Elaphe gutatta/Pantherophis guttatus*	Red cornsnake / Great Plains ratsnake	•				RA	R				
USGS	*Elgaria kingi*	Sonoran/Madrean alligator lizard		•			RA	R				
None	*Elgaria panamintina*	Panamint alligator lizard			•		RA	R				

Model Source	Scientific Name	Common Name	Occurs B	Occurs H	Occurs I	Occurs Y	RA?	Taxon	TERS B	TERS H	TERS Y	TERS I
USGS	*Gopherus agassizii*	Mohave desert tortoise			•		RA	R			Y	
*	*Gopherus morafkai*	Sonoran desert tortoise		•		•	RA	R		Y		Y
None	*Gyalopion quadrangulare*	Thornscrub hook-nosed snake		•			RA	R				
USGS	*Heloderma suspectum*	Gila monster		•		•	RA	R		Y	Y	
USGS	*Holbrookia maculata*	Lesser earless lizard	•	•			RA	R				
SW	*Hypsiglena chlorophaea*	Night snake	•	•	•	•	RA	R				
*	*Hypsiglena chlorophaea sp. nov.*	Hooded night snake		•			RA	R		Y		
SW	*Kinosternon flavescens*	Yellow mud turtle	•	•			RA	R		Y		
USGS	*Kinosternon sonoriensi*	Sonoran mud turtle		•		•	RA	R		Y	Y	
USGS	*Lampropeltis alterna*	Gray-banded kingsnake	•				RA	R	Y			
USGS	*Lampropeltis getula*	Common kingsnake	•	•	•	•	RA	R				
*	*Lampropeltis californiae*	California kingsnake			•	•	RA	R			(Y)	
*	*Lampropeltis nigrita*	Western black kingsnake		•			RA	R		Y		
*	*Lampropeltis splendida*	Desert kingsnake	•	•			RA	R	(Y)			
USGS	*Lampropeltis pyromelana*	Sonoran mountain kingsnake		•			RA	R		Y		
SW	*Leptotyphlops/Rena dulcis*	Texas blind/thread snake	•			•	RA	R				
SW	*Leptotyphlops/Rena humilis*	Western blind/thread snake	•	•	•	•	RA	R	Y			
	Lichanura orcutti	Northern Three-lined boa (Rosy boa)			•	•	RA	R			Y	Y
USGS	*Masticophis/Coluber flagellum*	Western coachwhip	•	•	•	•	RA	R				
SW	*Masticophis/Coluber taeniatus*	Striped whipsnake	•		•	•	RA	R				
USGS	*Micruroides euryxanthus*	Sonoran coral snake		•		•	RA	R		Y	Y	
USGS	*Phrynosoma modestum*	Roundtail horned lizard	•	•			RA	R		Y		
USGS	*Phrynosoma platyrhinos*	Desert horned lizard			•	•	RA	R				
USGS	*Plestiodon callicephalus*	Mountain skink		•			RA	R		Y		
USGS	*Plestiodon gilberti*	Gilbert's skink			•		RA	R				
USGS	*Plestiodon obsoletus*	Great Plains skink	•	•			RA	R				
USGS	*Rhinocheilus lecontei*	Longnose snake	•	•	•	•	RA	R				
SW	*Salvadora grahamiae*	Mountain/Eastern patchnose snake	•	•			RA	R				
SW	*Salvadora hexalepis*	Western patchnose snake	•	•	•	•	RA	R				
*	*Salvadora hexalepis deserticola*	Big bend patchnose snake	•	•			RA	R		Y		
SW	*Sceloporus clarkii*	Clark's spiny lizard		•			RA	R				
USGS	*Sceloporus magister*	Desert spiny lizard	•	•	•	•	RA	R				

Model Source	Scientific Name	Common Name	Occurs B	Occurs H	Occurs I	Occurs Y	RA?	Taxon	TERS B	TERS H	TERS Y	TERS I
USGS	*Sceloporus poinsettii*	Crevice spiny lizard	•				RA	R				
SW	*Sceloporus undulatus(?)*	Prairie lizard	•	•			RA	R				
USGS	*Senticolis triaspis*	Green ratsnake		•			RA	R		Y		
USGS	*Sistrurus catenatus*	Massasauga	•	•			RA	R	Y	Y		
SW	*Sonora semiannulata*	Western Ground snake	•	•	•	•	RA	R				
SW	*Tantilla hobartsmithi*	Smith's/Southwestern black-headed snake	•	•	•	•	RA	R				
SW	*Tantilla nigriceps*	Plains black-headed snake	•	•			RA	R		Y		
None	*Tantilla planiceps*	Western black-headed snake			•		RA	R				
USGS	*Tantilla willcoxi*	Chihuahuan black-headed snake		•			RA	R		Y		
USGS	*Tantilla yaquia*	Yaqui black-headed snake		•			RA	R		Y		
SW	*Thamnophis cyrtopsis*	Blackneck garter snake	•	•			RA	R				
USGS	*Thamnophis eques*	Mexican garter snake		•			RA	R				
*	*Thamnophis eques megalops*	Brown garter snake		•			RA	R		Y		
SW	*Thamnophis marcianus*	Checkered garter snake	•	•		•	RA	R				
USGS	*Thamnophis sirtalis*	Common garter snake	•				RA	R				
USGS	*Trimorphodon biscutatus*	Western/Texas lyresnake	•	•	•	•	RA	R				
*	*Trimorphodon lambda*	Sonoran lyresnake	?	•	?	•	RA	R	Y	Y	Y	
*	*Trimorphodon lyrophanes*	California lyresnake			•		RA	R				
USGS	*Trimorphodon vilkinsonii*	Texas lyresnake	•				RA	R	Y			
USGS	*Uma notata*	Colorado Desert fringe-toed lizard				•	RA	R			Y	
USGS	*Uma scoparia*	Mojave fringe-toed lizard			•	•	RA	R			Y	Y
USGS	*Urosaurus graciosus*	Long-tailed brush lizard			•	•	RA	R				
USGS	*Urosaurus ornatus*	Ornate tree lizard	•	•		•	RA	R				
USGS	*Uta stansburiana*	Common side-blotched lizard	•	•	•	•	RA	R				
USGS	*Xantusia vigilis*	Common/Desert night lizard			•	•	RA	R				
na	*Craugastor augusti*	Western barking frog	•	•			N	A				
na	*Accipiter gentilis*	Northern (Apache) goshawk	•	•	•	•	N	B				
na	*Aeronautes saxatilis*	White-throated swift	•	•	•	•	N	B				
na	*Aimophila carpalis*	Rufous-winged Sparrow		•			N	B				
na	*Aimophila cassinii*	Cassin’s sparrow	•	•			N	B				
na	*Aimophila ruficeps*	Rufous-crowned sparrow	•	•	•		N	B				
na	*Aimophila/Peucaea botterii*	Botteri's sparrow		•			N	B				

Model Source	Scientific Name	Common Name	Occurs B	H	I	Y	RA?	Taxon	TERS B	H	Y	I
na	*Ammodramus bairdii*	Baird's sparrow	•	•			N	B				
na	*Ammodramus leconteii*	Le Conte's sparrow	•				N	B				
na	*Ammodramus savannarum*	(Arizona) Grasshopper sparrow	•	•		•	N	B				
na	*Anthus rubescens*	American pipit	•	•	•	•	N	B				
na	*Anthus spraguei*	Sprague's pipit	•	•		•	N	B				
na	*Aphelocoma ultramarina*	Mexican jay		•			N	B				
na	*Aquila chrysaetos*	Golden eagle	•	•	•	•	N	B				
na	*Asio flammeus*	Short-eared owl	•	•	•	•	N	B				
na	*Athene cunicularia*	Western burrowing owl	•	•	•	•	N	B				
na	*Auriparus flaviceps*	Verdin	•	•	•	•	N	B				
na	*Baeolophus ridgwayi*	Juniper titmouse	•	•	•		N	B				
na	*Bombycilla cedrorum*	Cedar waxwing	•	•	•	•	N	B				
na	*Buteo jamaicensis*	Red-tailed hawk	•	•	•	•	N	B				
na	*Buteo lagopus*	Rough-legged hawk	•	•	•	•	N	B				
na	*Calamospiza melanocorys*	Lark bunting	•	•		•	N	B				
na	*Calcarius lapponicus*	Lapland longspur	•		•	•	N	B				
na	*Calcarius mccownii*	McCown's longspur	•	•			N	B				
na	*Calcarius ornatus*	Chestnut-collared longspur	•	•		•	N	B				
na	*Calypte anna*	Anna's hummingbird		•	•	•	N	B				
na	*Campylorhynchus brunneicapillus*	Cactus wren	•	•	•	•	N	B				
na	*Caprimulgus ridgwayi*	Buff-collared Nightjar		•			N	B				
na	*Caprimulgus vociferus*	Whip-poor-will	•	•			N	B				
na	*Caracara cheriway*	Crested caracara		•			N	B				
na	*Cardellina rubrifrons*	Red-faced warbler	•	•			N	B				
na	*Carduelis pinus*	Pine siskin	•	•	•	•	N	B				
na	*Carpodacus cassini*	Cassin's finch	•	•		•	N	B				
na	*Carpodacus mexicanus*	House finch	•	•	•	•	N	B				
na	*Carpodacus purpureus*	Purple finch	•			•	N	B				
na	*Catharus guttatus*	Hermit thrush	•	•	•	•	N	B				
na	*Certhia americana*	Brown creeper	•	•	•	•	N	B				
na	*Chaetura vauxi*	Vaux's swift		•	•	•	N	B				
na	*Chondestes grammacus*	Lark sparrow	•	•	•	•	N	B				

Model Source	Scientific Name	Common Name	Occurs B	Occurs H	Occurs I	Occurs Y	RA?	Taxon	TERS B	TERS H	TERS Y	TERS I
na	*Chordeiles minor*	Common nighthawk	•	•			N	B				
na	*Circus cyaneus*	Northern harrier	•	•	•	•	N	B				
na	*Coccothraustes vespertinus*	Evening grosbeak	•	•	•		N	B				
na	*Colaptes auratus*	Northern flicker	•	•	•	•	N	B				
na	*Columba fasciata*	Band-tailed pigeon	•	•		•	N	B				
na	*Columbina inca*	Inca dove	•	•		•	N	B				
na	*Contopus cooperi*	Olive-sided flycatcher	•	•	•	•	N	B				
na	*Contopus pertinax*	Greater pewee		•			N	B				
na	*Coragyps atratus*	Black vulture		•			N	B				
na	*Corvus corax*	Common raven	•	•	•	•	N	B				
na	*Corvus cryptoleucus*	Chihuahuan raven	•	•			N	B				
na	*Cyanocitta stelleri*	Steller's jay	•	•		•	N	B				
na	*Cypseloides niger*	Black swift	•				N	B				
na	*Cyrtonyx montezumae*	Montezuma quail	•	•			N	B				
na	*Dendroica coronata*	Yellow-rumped warbler	•	•	•	•	N	B				
na	*Dendroica graciae*	Grace's warbler	•	•			N	B				
na	*Dendroica nigrescens*	Black-throated gray warbler	•	•	•	•	N	B				
na	*Dendroica petechia*	Yellow warbler	•	•	•	•	N	B				
na	*Dendroica townsendi*	Townsend's warbler	•	•	•	•	N	B				
na	*Empidonax hammondii*	Hammond's flycatcher	•	•		•	N	B				
na	*Eremophila alpestris*	Horned lark	•	•	•	•	N	B				
na	*Euptilotis neoxenus*	Eared quetzal		•			N	B				
na	*Falco columbarius*	Merlin	•	•	•	•	N	B				
na	*Falco mexicanus*	Prairie falcon	•	•	•	•	N	B				
na	*Falco peregrinus*	Peregrine falcon	•	•	•	•	N	B				
na	*Geococcyx californicus*	Greater roadrunner	•	•	•	•	N	B				
na	*Glaucidium gnoma*	Northern pygmy-owl	•	•			N	B				
na	*Gymnorhinus cyanocephalus*	Pinyon jay	•		•	•	N	B				
na	*Hirundo rustica*	Barn swallow	•	•	•	•	N	B				
na	*Hylosharis leucotis*	White-eared hummingbird		•			N	B				
na	*Icterus pustulatus*	Streak-backed oriole		•			N	B				
na	*Junco phaeonotus*	Yellow-eyed junco		•			N	B				

Model Source	Scientific Name	Common Name	Occurs B	H	I	Y	RA?	Taxon	TERS B	H	Y	I
na	*Lanius ludovicianus*	Loggerhead shrike	•	•	•	•	N	B				
na	*Loxia curvirostra*	Red crossbill	•	•	•		N	B				
na	*Melanerpes formicivorus*	Acorn woodpecker	•	•			N	B				
na	*Melanerpes lewis*	Lewis woodpecker	•	•		•	N	B				
na	*Meleagris gallopavo*	Gould's wild turkey	•	•			N	B				
na	*Mniotilta varia*	Black-and-white warbler	•	•			N	B				
na	*Molothrus ater*	Brown-headed cowbird	•	•	•	•	N	B				
na	*Molothus aeneus*	Bronzed cowbird	•	•			N	B				
na	*Myadestes townsendi*	Townsend's solitaire	•	•	•	•	N	B				
na	*Myiarchus cinerascens*	Ash-throated flycatcher	•	•	•	•	N	B				
na	*Myioborus pictus*	Painted redstart	•	•		•	N	B				
na	*Nucifraga columbiana*	Clark's nutcracker		•		•	N	B				
na	*Otus flammeolus*	Flammulated owl		•		•	N	B				
na	*Otus/Megascops trichopsis*	Whiskered screech-owl		•			N	B				
na	*Passerculus sandwichensis*	Savannah sparrow	•	•	•	•	N	B				
na	*Peucedramus taeniatus*	Olive warbler		•			N	B				
na	*Phalaenoptila nuttallii*	Common poorwill	•	•	•	•	N	B				
na	*Picoides scalaris*	Ladder-backed woodpecker	•	•	•	•	N	B				
na	*Piranga bidentata*	Flame-colored tanager		•			N	B				
na	*Piranga flava*	Hepatic tanager	•	•		•	N	B				
na	*Piranga ludoviciana*	Western tanager	•	•	•	•	N	B				
na	*Poecile gambeli*	Mountain chickadee	•				N	B				
na	*Pooecetes gramineus*	Vesper sparrow	•	•		•	N	B				
na	*Progne subis*	Purple martin	•			•	N	B				
na	*Psaltriparus minimus*	Bushtit	•	•	•		N	B				
na	*Regulus calendula*	Ruby-crowned kinglet	•	•	•	•	N	B				
na	*Regulus satrapa*	Golden-crowned kinglet	•	•		•	N	B				
na	*Ridgwayia pinicola*	Aztec thrush		•			N	B				
na	*Sayornis saya*	Say's phoebe	•	•	•	•	N	B				
na	*Selasphorus platycercus*	Broad-tailed hummingbird	•	•			N	B				
na	*Selasphorus rufus*	Rufous hummingbird	•	•	•	•	N	B				
na	*Selasphorus sasin*	Allen's hummingbird		•			N	B				

Model Source	Scientific Name	Common Name	Occurs B	Occurs H	Occurs I	Occurs Y	RA?	Taxon	TERS B	TERS H	TERS Y	TERS I
na	*Sialia currucoides*	Mountain bluebird	•	•	•	•	N	B				
na	*Sialia mexicana*	Western bluebird	•	•		•	N	B				
na	*Sialia sialis*	Eastern bluebird	•	•			N	B				
na	*Sitta canadensis*	Red-breasted nuthatch	•	•	•	•	N	B				
na	*Sitta carolinensis*	White-breasted nuthatch	•	•		•	N	B				
na	*Sitta pygmaea*	Pygmy nuthatch	•	•	•		N	B				
na	*Sphyrapicus thyroideus*	Williamson's sapsucker	•	•			N	B				
na	*Sphyrapicus varius*	Yellow-bellied sapsucker	•				N	B				
na	*Spiza americana*	Dickcissel	•				N	B				
na	*Spizella breweri*	Brewer's sparrow	•	•	•	•	N	B				
na	*Spizella passerina*	Chipping sparrow	•	•	•	•	N	B				
na	*Sturnella magna*	Eastern meadowlark	•	•			N	B				
na	*Sturnella neglecta*	Western meadowlark	•	•	•	•	N	B				
na	*Tachycineta thalassina*	Violet-green swallow	•	•	•	•	N	B				
na	*Toxostoma bendirei*	Bendire's Thrasher		•	•	•	N	B				
na	*Toxostoma curvirostre*	Curve-billed thrasher	•	•		•	N	B				
na	*Toxostoma lecontei*	LeConte's thrasher			•	•	N	B				
na	*Troglodytes hiemalis*	Winter wren		•			N	B				
na	*Turdus migratorius*	American robin	•	•	•	•	N	B				
na	*Tyrannus verticalis*	Western kingbird	•	•	•	•	N	B				
na	*Tyto alba*	Barn owl	•	•	•	•	N	B				
na	*Vermivora peregrina*	Tennessee warbler	•				N	B				
na	*Vermivora ruficapilla*	Nashville warbler	•	•	•	•	N	B				
na	*Vireo cassinii*	Cassin's vireo	•	•		•	N	B				
na	*Vireo olivaceus*	Red-eyed vireo	•	•		•	N	B				
na	*Vireo philadelphicus*	Philadelphia vireo	•				N	B				
na	*Wilsonia pusilla*	Wilson's warbler	•	•	•	•	N	B				
na	*Zenaida macroura*	Mourning dove	•	•	•	•	N	B				
na	*Zonotrichia albicollis*	White-throated sparrow	•	•		•	N	B				
na	*Zonotrichia leucophrys*	White-crowned sparrow	•	•	•	•	N	B				
na	*(Neo)Tamias minimus*	Least chipmunk	•				N	M				
na	*(Xero)spermophilus tereticaudus*	Round-tailed ground squirrel		•	•	•	N	M				

Model Source	Scientific Name	Common Name	Occurs B	Occurs H	Occurs I	Occurs Y	RA?	Taxon	TERS B	TERS H	TERS Y	TERS I
na	*Ammospermophilus harrisii*	Harris's antelope squirrel		•		•	N	M				
na	*Antilocapra americana*	Pronghorn	•	•		•	N	M				
na	*Canis latrans*	Coyote	•	•	•	•	N	M				
na	*Canis lupus*	Mexican gray wolf		•			N	M				
na	*Chaetodipus baileyi*	Bailey's pocket mouse		•		•	N	M				
na	*Chaetodipus penicillatus*	Desert pocket mouse	•	•	•	•	N	M				
na	*Conepatus mesoleucus*	Hog-nosed skunk		•			N	M				
na	*Cratogeomys castanops*	Yellow-faced pocket gopher	•				N	M				
na	*Cynomys ludovicianus*	Black-tailed prairie dog	•	•			N	M				
na	*Dipodomys deserti*	Desert kangaroo rat			•	•	N	M				
na	*Dipodomys merriami*	Merriam’s kangaroo rat	•	•	•	•	N	M				
na	*Dipodomys microps*	Great Basin/Chisel-toothed kangaroo rat			•		N	M				
na	*Dipodomys ordii*	Ord’s kangaroo rat	•	•			N	M				
na	*Dipodomys panamintinus*	Panamint kangaroo rat			•		N	M				
na	*Dipodomys spectabilis*	Banner-tailed kangaroo rat	•	•			N	M				
na	*Geomys bursarius*	Plains pocket gopher	•				N	M				
na	*Leptonycteris curasoae*	Lesser/Curasoan long-nosed bat		•		•	N	M				
na	*Lepus alleni*	Antelope jackrabbit		•			N	M				
na	*Lepus californicus*	Black-tailed jackrabbit	•	•	•	•	N	M				
na	*Myotis californicus*	California myotis	•	•	•	•	N	M				
na	*Myotis leibii/ciliolabrum*	(western) Small-footed myotis	•	•	•	•	N	M				
na	*Myotis thysanodes*	Fringed myotis	•	•	•		N	M				
na	*Neotoma albigula*	White-throated wood rat	•	•		•	N	M				
na	*Neotoma mexicana*	Mexican woodrat		•			N	M				
na	*Neotoma micropus*	Gray (southern plains) wood rat	•				N	M				
na	*Notiosorex cockrumi*	Cockrum's gray shrew		•			N	M				
na	*Notiosorex crawfordi*	Desert/Crawford's Gray shrew	•	•	•	•	N	M				
na	*Onychomys arenicola*	Mearn’s/CHIHUAHUAN grasshopper mouse	•				N	M				
na	*Onychomys leucogaster*	Northern (short-tailed) grasshopper mouse	•	•			N	M				
na	*Onychomys torridus*	Southern grasshopper mouse		•	•	•	N	M				
na	*Ovis canadensis*	Desert bighorn sheep	•		•	•	N	M				
na	*Panthera onca*	Jaguar		•			N	M				

Model Source	Scientific Name	Common Name	Occurs B	H	I	Y	RA?	Taxon	TERS B	H	Y	I
na	*Perognathus amplus*	Arizona pocket mouse				•	N	M				
na	*Perognathus flavescens*	Plains/Apache pocket mouse	•				N	M				
na	*Perognathus flavus*	Silky pocket mouse	•	•			N	M				
na	*Perognathus longimembris*	Little pocket mouse			•	•	N	M				
na	*Perognathus parvus*	Great Basin pocket mouse			•		N	M				
na	*Peromyscus crinitus*	Canyon mouse			•	•	N	M				
na	*Peromyscus eremicus*	Cactus mouse	•	•	•	•	N	M				
na	*Peromyscus maniculatus*	Deer mouse	•	•	•	•	N	M				
na	*Peromyscus nasutus*	Northern rock mouse	•				N	M				
na	*Reithrodontomys fulvescens*	Fulvous harvest mouse		•			N	M				
na	*Reithrodontomys montanus*	Plains harvest mouse	•	•			N	M				
na	*Sciurus nayaritensis chiricahuae*	Chiricahua/Mexican fox squirrel		•			N	M				
na	*Sigmodon ochrognathus*	Yellow-nosed cotton rat		•			N	M				
na	*Sorex merriami*	Merriam's shrew			•		N	M				
na	*Sorex monticolus*	Dusky shrew		•			N	M				
na	*Spermophilus mexicanus/ Ictidomys parvi*	Mexican ground squirrel	•				N	M				
na	*Spermophilus spilosoma*	Spotted ground squirrel	•	•			N	M				
na	*Spermophilus variegatus*	Rock squirrel	•	•		•	N	M				
na	*Spermophilus/Ictidomys tridecimlineatus*	Thirteen-lined ground squirrel	•				N	M				
na	*Tadarida/Nyctinomops femorosacca/us*	Pocketed free-tailed bat	•	•		•	N	M				
na	*Tamias canipes*	Gray-footed chipmunk	•				N	M				
na	*Tamias cinereicollis*	Gray-collared chipmunk	•				N	M				
na	*Tamias quadrivittatusaustralis*	Organ Mountain Colorado chipmunk	•				N	M				
na	*Taxidea taxus*	Badger	•	•	•	•	N	M				
na	*Thomomys bottae*	Botta's/Mearns' pocket gopher		•	•	•	N	M				
na	*Thomomys umbrinus*	Southern pocket gopher		•			N	M				
na	*Vulpes macrotis*	Kit fox	•	•	•	•	N	M				
na	*Vulpes vulpes*	Red fox	•				N	M				
na	*Bogertophis subocularis*	Trans-pecos (rat) snake	•				N	R				
na	*Chionactis occipitalis*	Western shovel-nosed snake			•	•	N	R				
na	*Cnemidophous/Aspidoscelis arizonae*	Arizona striped whiptail		•			N	R				
na	*Coleonyx brevis(variegatus)*	western banded gecko	•	•	•		N	R				

Model Source	Scientific Name	Common Name	Occurs B	H	I	Y	RA?	Taxon	TERS B	H	Y	I
na	*Crotalus pricei*	Twin-spotted rattlesnake		•			N	R				
na	*Crotalus scutulatus*	Mojave rattlesnake	•	•	•	•	N	R				
na	*Crotalus viridis viridis*	Prairie rattlesnake	•				N	R				
na	*Crotaphytus bicinctores*	Great Basin collared lizard			•	•	N	R				
na	*Gambelia wislizenii*	leopard lizard	•	•	•	•	N	R				
na	*Gyalopion canum*	(Chihuahuan) western hooknose snake	•	•			N	R				
na	*Heterdon nasicus*	(Mexican) Western hognose snake	•	•			N	R				
na	*Holbrookia elegans*	elegant earless lizard		•			N	R				
na	*Lampropeltis triangulum*	(New Mexico) Milk snake	•	•			N	R				
na	*Leptotyphlops dissectus*	New Mexico threadsnake		•			N	R				
na	*Masticophus bilineatus*	Sonoran whipsnake		•			N	R				
na	*Phrynosoma cornutum*	Texas horned lizard	•	•			N	R				
na	*Phrynosoma douglasii(hernandesi)*	(Greater) short-horned lizard	•	•			N	R				
na	*Phrynosoma mcallii*	Flat-tailed horned lizard				•	N	R				
na	*Phrynosoma solare*	Regal horned lizard		•		•	N	R				
na	*Phyllorhynchus decurtatus*	Western/Spotted leaf-nosed snake			•	•	N	R				
na	*Pituophis catenifer*	Bullsnake/Gophersnake	•	•	•	•	N	R				
na	*Sauromalus obesus/ater*	Chuckwalla			•	•	N	R				
na	*Sceloporous occidentalis*	Western fence lizard			•		N	R				
na	*Sceloporus jarrovi*	Yarrow's/mountain spiny lizard		•			N	R				
na	*Sceloprous graciosus*	Common sagebrush lizard			•		N	R				
na	*Scelporous slevini*	Slevin's bunchgrass lizard		•			N	R				
na	*Terrapene ornata*	(Desert/)ornate box turtle	•	•			N	R				
na	*Uma rufopunctata*	Yuman desert fringe-toed lizard				•	N	R				

Table 3. Conservation status of riparian-associated species occurring or possible in the study area. Source of model or lack of availability indicated by USGS (National GAP), SW (Southwest Regional GAP), or None. Inclusion in TER-S group indicated with a Y (yes) or N (no); species marked with an N fit the TER-S criteria, but not in their range on that installation. Natureserve conservation ranks are G5, N5, and S5, unless otherwise noted. Details on ranking can be found at http://explorer.natureserve.org/granks.htm; ranks are 5 (Secure), 4 (Apparently Secure), 3 (Vulnerable), 2 (Imperiled), 1 (Critically Imperiled), or H (Possibly Extinct or Presumed Eliminated), and are sometimes split by breeding (B) and non-breeding (N) range. Federal and State listing status is indicated by T (threatened), E (endangered), or P (proposed). Arizona uses SGCN (Species of Greatest Conservation Need). California uses WSC (Wildlife Species of Concern) and SSC (Species of Special Concern). B = Bliss, H = Huachuca, I = Irwin, Y = YPG.

Scientific Name	Common Name	Occur				Tax.	Species of Concern Status								TERS			
							NatureServe				Listing							
		B	H	I	Y		G/N	NM	AZ	CA	Fed	NM	AZ	CA	B	H	I	Y
Ambystoma tigrinum/mavortium	Tiger salamander	•	•			A										Y		
Anaxyrus/Bufo debilis	Green toad	•	•			A	N4	S4	S3							Y		
Hyla wrightorum	Huachuca/Arizona tree frog		•			A	G4		T2, S1S2		P		SGCN			Y		
Incilius alvarius	Colorado River toad		•		•	A			S3S4				SGCN			Y		Y
Lithobates blairi	Plains leopard frog		•			A			S1				SGCN			Y		
Lithobates chiricahuensis	Chiricahua leopard frog		•			A	G2G3		S2		T		SGCN			Y		
Lithobates yavapaiensis	Yavapai/Lowland leopard frog		•		•	A	G4		S3				SGCN			Y		
Accipiter cooperii	Cooper's hawk	•	•	•	•	B		S4	S4	S3				WL			Y	
Accipiter striatus	Sharp-shinned hawk	•	•	•	•	B		S4	S4	S3				WL			Y	
Amazilia violiceps	Violet-crowned Hummingbird		•			B			S3				SGCN			Y		
Amphispiza quiquestriata	Five-striped sparrow		•			B	G4		S1S2				SGCN			Y		

Scientific Name	Common Name	Occur				Tax.	Species of Concern Status								TERS			
							NatureServe				Listing							
		B	H	I	Y		G/N	NM	AZ	CA	Fed	NM	AZ	CA	B	H	I	Y
Asio otus	Long-eared owl	•	•	•	•	B		S4	S2B, S3S4N	S3?				SSC		Y	Y	Y
Asturina nitidus/Buteo plagiatus	Gray hawk	•	•			B	N1N,N3B		S3				WSC		Y	Y		
Buteo albonotatus	Zone-tailed hawk	•	•		•	B	G4	S3	S4						Y			
Buteo regalis	Ferruginous hawk	•	•	•	•	B	G4	S2B, S4N	S2B, S4N	S3S4			SGCN	WL		Y	Y	Y
Buteo swainsoni	Swainson's hawk	•	•	•	•	B		S4	S3	S2				T		Y	Y	Y
Buteogallus anthracinus	Common black-hawk	•	•			B	G4G5/ N3B	S2B, S3N	S3			T	SGCN		Y	Y		
Callipepla squamata	Scaled quail	•	•			B		S3B, S4N							Y			
Calothorax lucifer	Lucifer hummingbird		•			B	G4G5		S2							Y		
Calypte costae	Costa's hummingbird	•	•	•	•	B	N4N	S1		S3?		T			Y		Y	
Carduelis lawrencei	Lawrence's goldfinch	•	•	•	•	B	G3G4		S1S3N	S3					Y	Y	Y	Y
Ceryle alcyon	Belted kingfisher	•	•	•	•	B		S4	S2B, S5N				WSC			Y		Y
Chloroceryle americana	Green kingfisher		•			B	N4		S2							Y		
Cinclus mexicanus	American dipper	•	•			B		S3B, S4N	S3				SGCN		Y	Y		
Cistothorus palustris	Marsh wren	•	•	•	•	B		S1B, S5N	S2B, S3S4N						N	Y		Y
Coccyzus americanus	Yellow-billed cuckoo	•	•	•	•	B		S3	S3	S1	PT		SGCN	E	Y	Y	Y	Y

Scientific Name	Common Name	Occur				Tax.	Species of Concern Status								TERS			
							NatureServe				Listing							
		B	H	I	Y		G/N	NM	AZ	CA	Fed	NM	AZ	CA	B	H	I	Y
Cyanthus latirostris	Broad-billed hummingbird		•			B			S3				SGCN			Y		
Elanus leucurus	White-tailed kite	•	•		•	B	N4	S2N	S2B, S2S3N						Y	Y		Y
Empidonax fulvifrons	Buff-breasted flycatcher		•			B	N1B		S1				SGCN			Y		
Empidonax occidentalis	Cordilleran flycatcher	•	•		•	B		S5B, S4N	S2S3B							Y		
Empidonax traillii extimus	Southwestern Willow flycatcher	•	•	•	•	B	G5T2	S1	S1	S1	E	E	SGCN	E	Y	Y	Y	Y
Empidonax wrightii	Gray flycatcher	•	•	•	•	B		S3B, S5N							Y			
Eugenes fulgens	Magnificent hummingbird		•			B	N4B		S4				SGCN			Y		
Falco femoralis	Aplomado Falcon	•	•			B	G4T2/N1	SHB, S1N	SH		E	E	SGCN		Y	Y		
Haliaeetus leucocephalus	Bald eagle	•	•		•	B		S1B, S4N	S2S3B, S4N			T	SGCN		Y	Y		Y
Icteria virens	Yellow-breasted chat	•	•	•	•	B		S3B, S4N	S4	S3				SSC	Y		Y	
Icterus bullockii	Bullock's oriole	•	•	•		B		S4B, S5N	S4B, S1N							Y		
Icterus cucullatus	Hooded oriole	•	•	•	•	B		S3B, S4N							Y			
Ictinia mississippiensis	Mississippi kite	•	•			B		S2B, S3N	S3				SGCN		Y	Y		
Lampornis clemenciae	Blue-throated Hummingbird		•			B			S4				SGCN			Y		
Melanerpes uropygialis	Gila woodpecker		•	•	•	B				S1S2			SGCN	E		Y	Y	Y

Scientific Name	Common Name	Occur				Tax.	Species of Concern Status								TERS			
							NatureServe				Listing							
		B	H	I	Y		G/N	NM	AZ	CA	Fed	NM	AZ	CA	B	H	I	Y
Melospiza georgiana	Swamp sparrow	•	•		•	B		S4N	S2S3N							Y		Y
Melospiza lincolnii	Lincoln's sparrow	•	•	•	•	B		S2B, S5N	S3B, S5N				SGCN		N	Y		Y
Melospiza melodia	Song sparrow	•	•	•	•	B		S4B, S5N		S3?							Y	
Melozone aberti	Abert's towhee		•		•	B	G3G4		S3				SGCN			Y		Y
Myiarchus tuberculifer	Dusky-capped flycatcher		•			B	N4B		S4				SGCN			Y		
Myiarchus tyrannulus	Brown-crested flycatcher		•	•	•	B	N4B		S4	S2S3				WL			Y	
Myiodynastes luteiventris	Sulphur-bellied flycatcher		•			B	N3B		S3				SGCN			Y		
Oporornis tolmei	MacGillivray's warbler	•	•	•	•	B			S4				SGCN			Y		Y
Pachyramphus aglaiae	Rose-throated becard		•			B	G4G5		S1				SGCN			Y		
Pandion haliaetus	Osprey	•	•		•	B	N4N	S2B, S4N	S2B, S4N				WSC		Y	Y		Y
Parabuteo unicinctus	Harris's hawk	•	•		•	B		S2B, S3N							Y			
Passerella iliaca	Fox sparrow	•	•	•	•	B		S4N	S2N							Y		Y
Passerina cyanea	Indigo bunting	•	•	•	•	B			S3							Y		Y
Passerina versicolor	Varied bunting	•	•			B	N4B	S1	S3			T	SGCN		Y	Y		Y
Petrochelidon fulva	Cave swallow	•				B	N4B	S3							Y			

Scientific Name	Common Name	Occur				Tax.	Species of Concern Status								TERS			
							NatureServe				Listing							
		B	H	I	Y		G/N	NM	AZ	CA	Fed	NM	AZ	CA	B	H	I	Y
Picoides arizonae	Arizona woodpecker		•			B			S3				SGCN			**Y**		
Polioptila melanura	Black-tailed gnatcatcher	•	•	•	•	B		S3		S4					Y			
Pyrocephalus rubinus	Vermilion flycatcher		•	•	•	B				S2S3				SSC			Y	
Riparia riparia	Bank swallow	•	•		•	B			S4M	S2S3							Y	
Spizella atrogularis	Black-chinned sparrow	•	•		•	B		S3							Y			
Spizella pallida	Clay-colored sparrow	•	•			B	N4N5B, N4N	S4N	S1N							Y		
Strix occidentalis lucida	Mexican spotted owl	•	•			B	G3T3	S2	S3S4		T		SGCN		Y	Y		
Tachycineta bicolor	Tree swallow	•	•	•	•	B		S3B, S4N	S3						N	Y		Y
Toxostoma dorsalis/crissale	Crissal thrasher	•	•	•	•	B		S4B, S5N		S3				SSC			Y	
Trogon elegans	Elegant trogon		•			B	N1N2N, N3B		S3				SGCN			Y		
Tyranus crassirostris	Thick-billed kingbird		•			B	N2B		S2				SGCN			Y		
Tyranus melancholicus	Tropical kingbird		•		•	B	N3B		S3				WSC			Y		Y
Vermivora/Oreothlypis celata	Orange-crowned warbler	•	•	•	•	B		S4B, S5N	S3B, S5N							Y		
Vermivora/Oreothlypis luciae	Lucy's warbler	•	•	•	•	B		S3B, S4N		S2S3				SSC	Y		Y	
Vermivora/Oreothlypis virginiae	Virginia's warbler	•	•	•	•	B		S3B, S4N		S2S3				WL	Y		Y	

Scientific Name	Common Name	Occur				Tax.	Species of Concern Status								TERS			
							NatureServe				Listing							
		B	H	I	Y		G/N	NM	AZ	CA	Fed	NM	AZ	CA	B	H	I	Y
Vireo bellii medius	Bell's vireo	•				B	N4B	S2B, S3N	S4		PS	T			Y	Y	Y	Y
Vireo vicinior	Gray vireo	•	•	•	•	B	G4/ N4B	S4B, S3N	S4	S2		T	SGCN	SSC	Y	Y	Y	Y
Xanthocephalus xanthocephalus	Yellow-headed blackbird	•	•	•	•	B		S4B, S5N		S3				SSC			Y	
Zonotrichia atricapilla	Golden-crowned sparrow			•	•	B			S1S2N									Y
Ammospermophilus interpres	Texas antelope squirrel	•				M	G4G5/ N4N5	S3							Y			
Antrozous pallidus	Pallid bat	•	•	•	•	M		S4S5	S4	S3				SSC			Y	
Baiomys taylori	Northern pygmy mouse		•			M	G4G5/ N4		S3							Y		
Chaetodipus hispidus	Hispid pocket mouse	•	•			M		S3							Y			
Choeronyctis mexicana	Mexican long-tongued bat		•			M	G4		S3				SGCN			Y		
Corynorhinus townsendii	Townsend's big-eared bat	•	•	•	•	M	G3G4/ N3N4	S3	S3S4	S2S3				PT/ SSC	Y	Y	Y	Y
Didelphis virginiana	Virginia/Mexican opossum		•			M			S3							Y		
Euderma maculatum	Spotted bat		•	•	•	M	G4/ N3N4		S2S3	S2S3			SGCN	SSC		Y	Y	Y
Eumops perotis	Greater bonneted/mastiff bat		•	•	•	M	G5T4/N 3		S3	S3?			SGCN	SSC		Y	Y	Y
Idionycteris phyllotis	Allen's big-eared/lappet-browed bat		•		•	M	G4/ N3N4		S2S3				SGCN			Y		Y
Lasionycteris noctivagans	Silver-haired bat	•	•	•	•	M		S4	S3S4	S3S4						Y	Y	Y

Scientific Name	Common Name	Occur				Tax.	Species of Concern Status								TERS			
							NatureServe				Listing							
		B	H	I	Y		G/N	NM	AZ	CA	Fed	NM	AZ	CA	B	H	I	Y
Lasiurus blossevillii	Western red bat	•	•	•	•	M	N3	S3	S3	S3?			SGCN	SSC	Y	Y	Y	Y
Lasiurus xanthinus	Western yellow bat		•		•	M	N2		S2S3				SGCN			Y		Y
Macrotus californicus	Californian leaf-nosed bat		•	•	•	M	G4		S3	S2S3			SGCN	SSC		Y	Y	Y
Myotis auriculus	Southwestern myotis		•			M	N4		S3							Y		
Myotis lucifugus	Little brown myotis	•		•		M	G3/N3			S2S3					Y	Y		
Myotis occultus	Occult little brown bat/ Arizona myot	•	•		•	M	G4/N4	S4	S3				SGCN			Y		Y
Myotis velifer	Cave myotis	•	•		•	M	N4	S3S4	S3S4				SGCN		Y	Y		Y
Myotis volans	Long-legged myotis	•	•	•	•	M		S4S5	S3S4	S4?						Y		Y
Myotis yumanensis	Yuma myotis	•	•	•	•	M		S4	S3S4	S4?			SGCN			Y		Y
Nyctinomops macrotis	Big free-tailed bat	•	•		•	M	N3N4	S3	S3						Y	Y		Y
Odocoileus virginanus	White-tailed deer	•	•			M							SGCN			Y		
Puma concolor	Mountain lion	•	•	•	•	M		S3?	S4						Y			Y
Sciurus arizonensis	Arizona gray squirrel		•			M	G4/N4		S4				SGCN			Y		
Sigmodon arizonae	Arizona cotton rat		•		•	M	N4		S4				SGCN			Y		Y
Sigmodon hispidus	Hispid cotton rat	•			•	M												Y

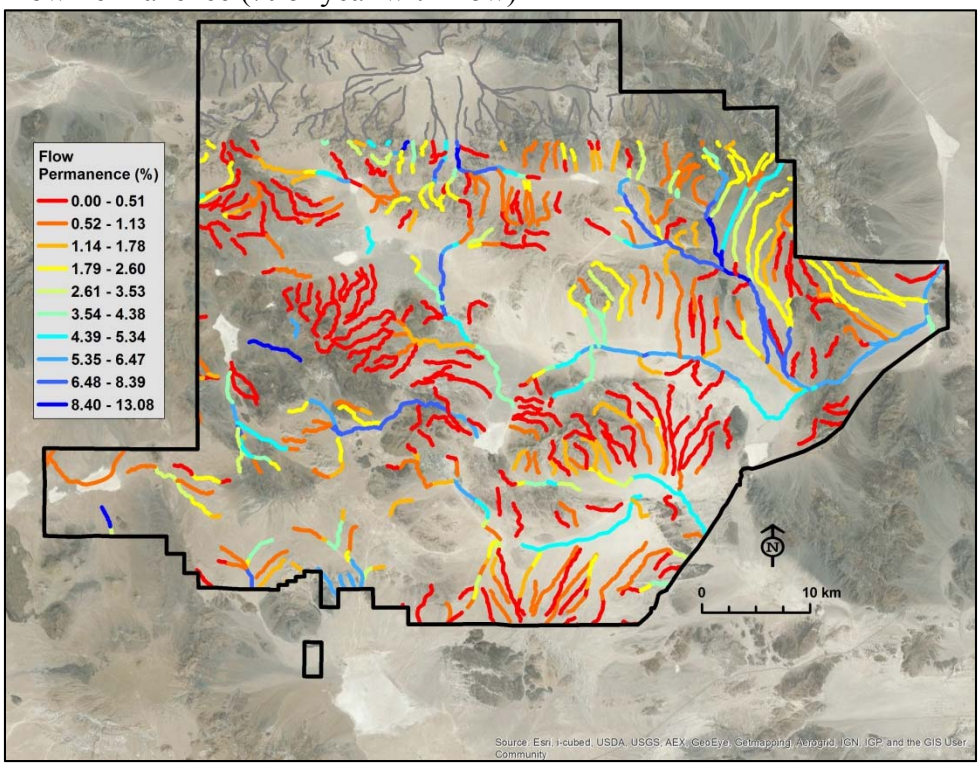
Scientific Name	Common Name	Occur				Tax.	Species of Concern Status								TERS			
							NatureServe				Listing							
		B	H	I	Y		G/N	NM	AZ	CA	Fed	NM	AZ	CA	B	H	I	Y
Sorex arizonae	Arizona shrew		•			M	G3/ N2N3		S2				SGCN			Y		
Tadarida brasiliensis	Brazilian/Mexican free-tailed bat	•	•	•	•	M		S3S4	S3S4				SGCN		Y	Y		Y
Aspidoscelis burti	Canyon spotted whiptail		•			R										Y		
Aspidoscelis tigris	Western/Tiger whiptail	•		•	•	R		S3							Y			
Chilomeniscus stramineus	Variable sand snake				•	R			S4				SGCN					Y
Crotalus lepidus	Rock rattlesnake	•	•			R		S4	S3						Y	Y		
Crotalus willardi	Ridge-nosed rattlesnake		•			R	N2N3		S2				SGCN			Y		
Gopherus agassizii	Mohave desert tortoise			•		R	G3		S2	S2	T		SGCN	T		Y	Y	Y
Heloderma suspectum	Gila monster		•		•	R	G4T4		S4				SGCN			Y		Y
Hypsiglena chlorophaea	Night snake	•	•	•	•	R										Y		
Kinosternon flavescens	Yellow mud turtle	•	•			R		S4	S1				SGCN			Y		
Kinosternon sonoriensi	Sonoran mud turtle		•		•	R	G4/N4		S4				SGCN			Y		Y
Lampropeltis alterna	Gray-banded kingsnake	•				R	N4	S1				E			Y			
Lampropeltis getula	Common kingsnake	•	•	•	•	R									Y	Y		Y
Lampropeltis pyromelana	Sonoran mountain kingsnake		•			R	G4/N4		S3							Y		

Scientific Name	Common Name	Occur				Tax.	Species of Concern Status								TERS			
							NatureServe				Listing							
		B	H	I	Y		G/N	NM	AZ	CA	Fed	NM	AZ	CA	B	H	I	Y
Leptotyphlops/Rena humilis	Western blind/thread snake	•	•	•	•	R		S3?							Y			
Lichanura orcutti	Northern Three-lined/Rosy boa			•	•		G4/N4		S3S4	S3S4							Y	Y
Micruroides euryxanthus	Sonoran coral snake		•		•	R							SGCN			Y		Y
Phrynosoma modestum	Roundtail horned lizard	•	•			R			S3							Y		
Plestiodon callicephalus	Mountain skink		•			R	G4G5/ N2N3		S2							Y		
Salvadora hexalepis	Western patchnose snake	•	•	•	•	R										Y		
Senticolis triaspis	Green ratsnake		•			R	G5		S3				SGCN			Y		
Sistrurus catenatus	Massasauga	•	•			R	G3G4	S3S4	S1				SGCN		Y	Y		
Tantilla nigriceps	Plains black-headed snake	•	•			R			S2							Y		
Tantilla willcoxi	Chihuahuan black-headed snake		•			R	G4/ N1N2		S1				SGCN			Y		
Tantilla yaquia	Yaqui black-headed snake		•			R	G4/N2		S2				SGCN			Y		
Thamnophis eques	Mexican garter snake		•			R	G4		S1							Y		
Trimorphodon biscutatus	Western/Texas lyresnake	•	•	•	•	R									Y	Y	Y	Y
Uma notata	Colorado Desert fringe-toed lizard				•	R	G3/ N2N3			S2?								Y
Uma scoparia	Mojave fringe-toed lizard			•	•	R	G3G4		S1	S3S4			SGCN	SSC			Y	Y

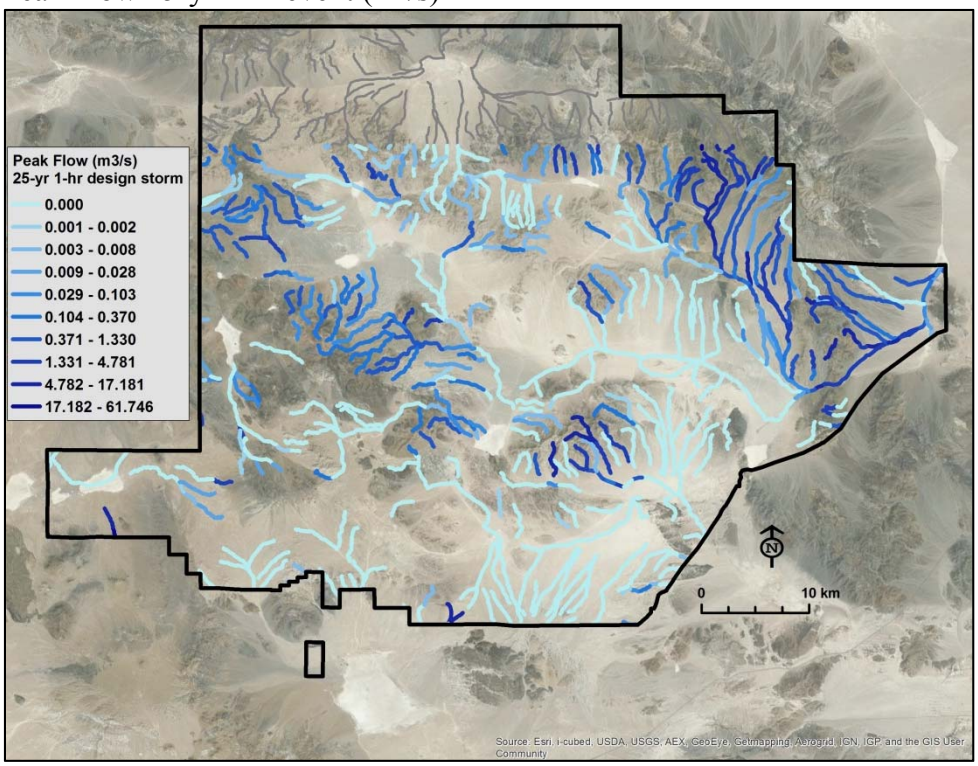
Appendix D: AGWA Hydrologic Modeling Results for Flow Permanence and Peak Flows

Fort Irwin

Flow Permanence (% of year with flow)

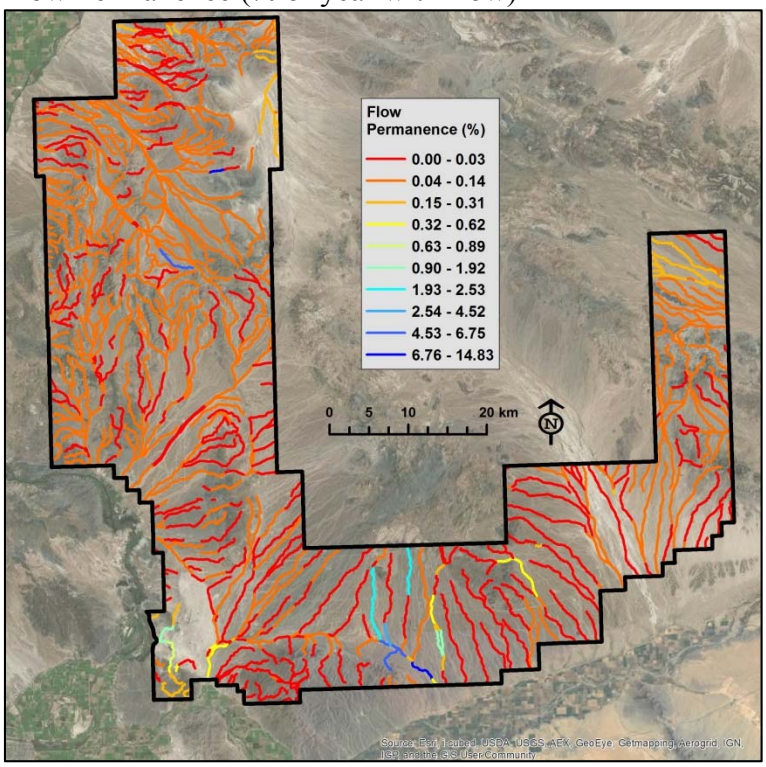


Peak Flow 25-yr 1-hr event (m^3/s)

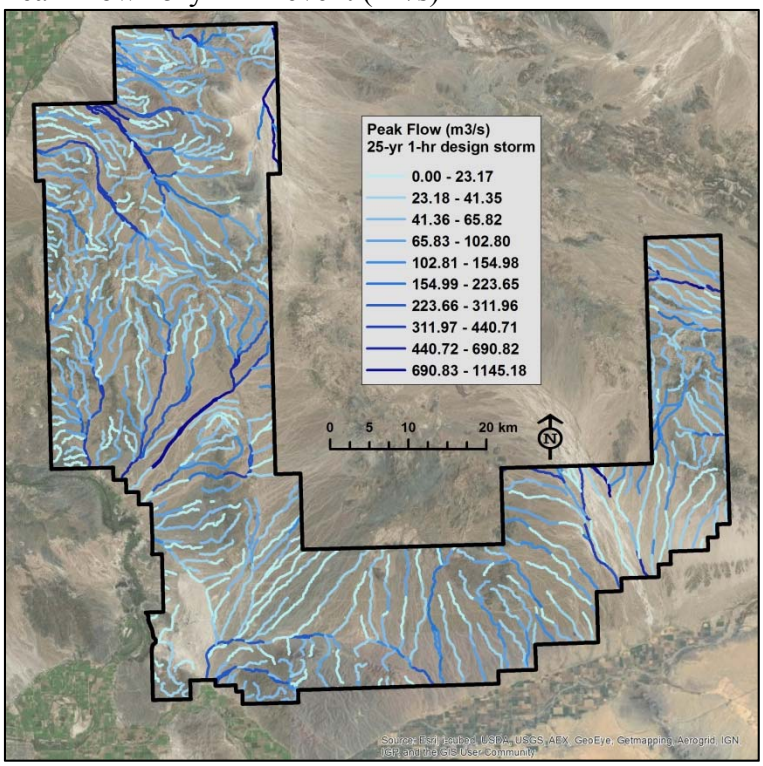


YPG

Flow Permanence (% of year with flow)

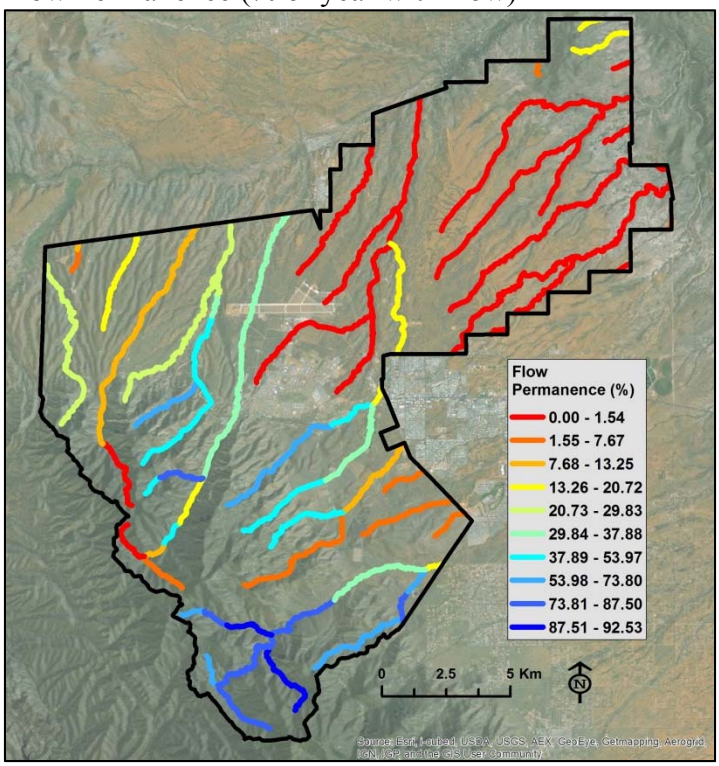


Peak Flow 25-yr 1-hr event (m^3/s)

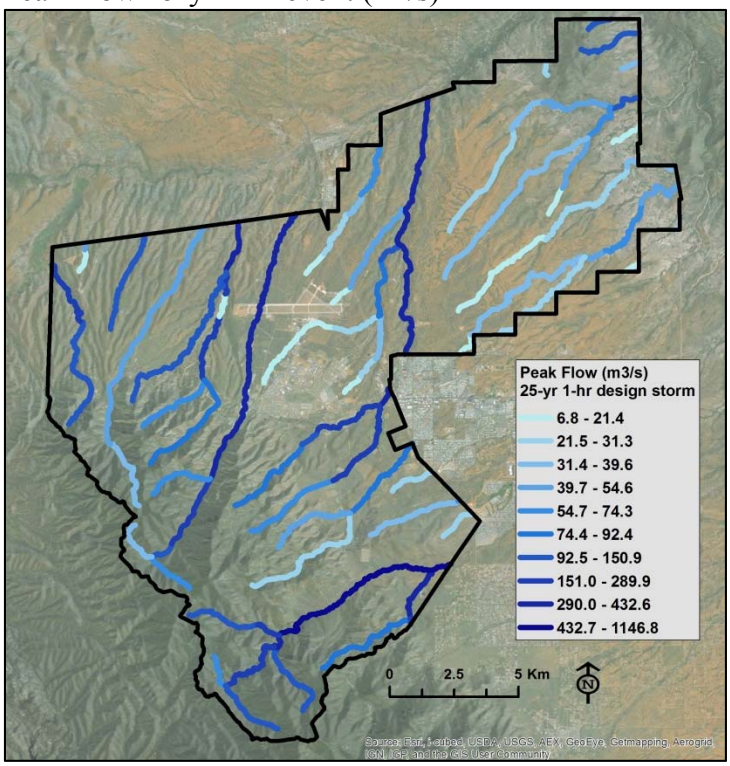


Fort Huachuca

Flow Permanence (% of year with flow)

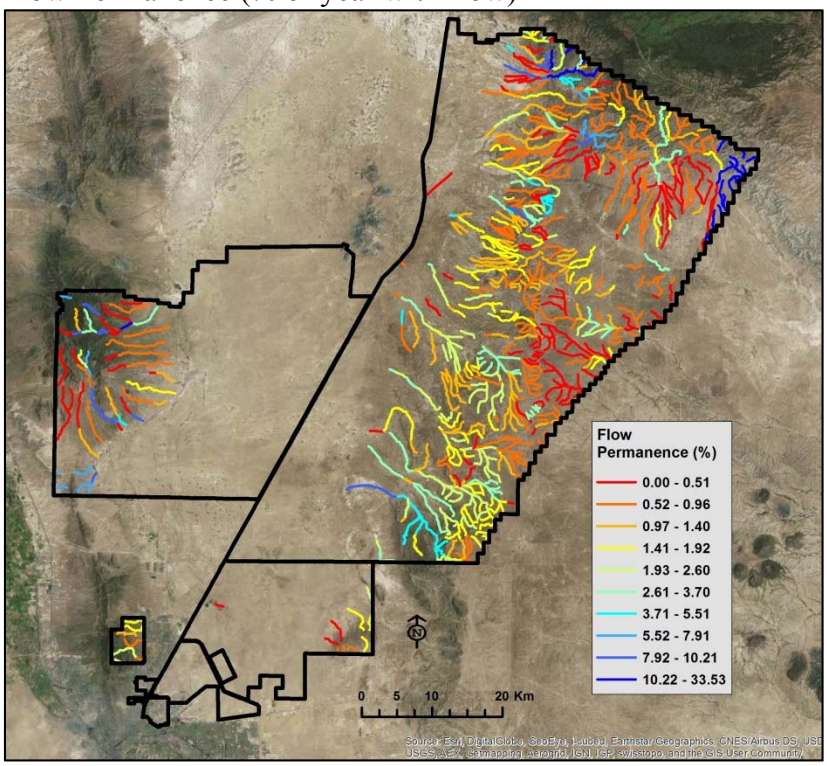


Peak Flow 25-yr 1-hr event (m^3/s)

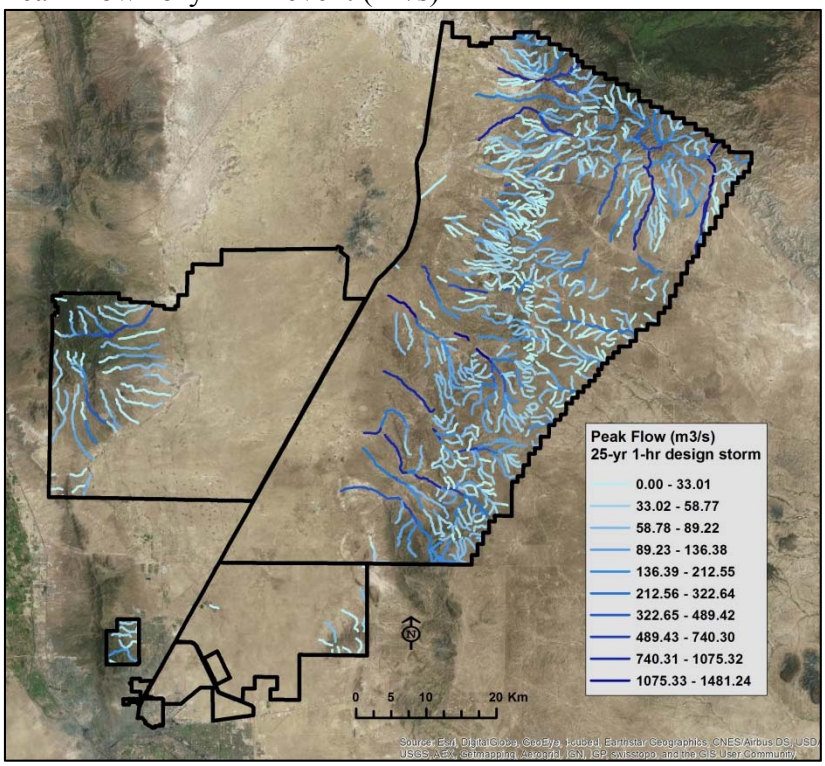


Fort Bliss

Flow Permanence (% of year with flow)

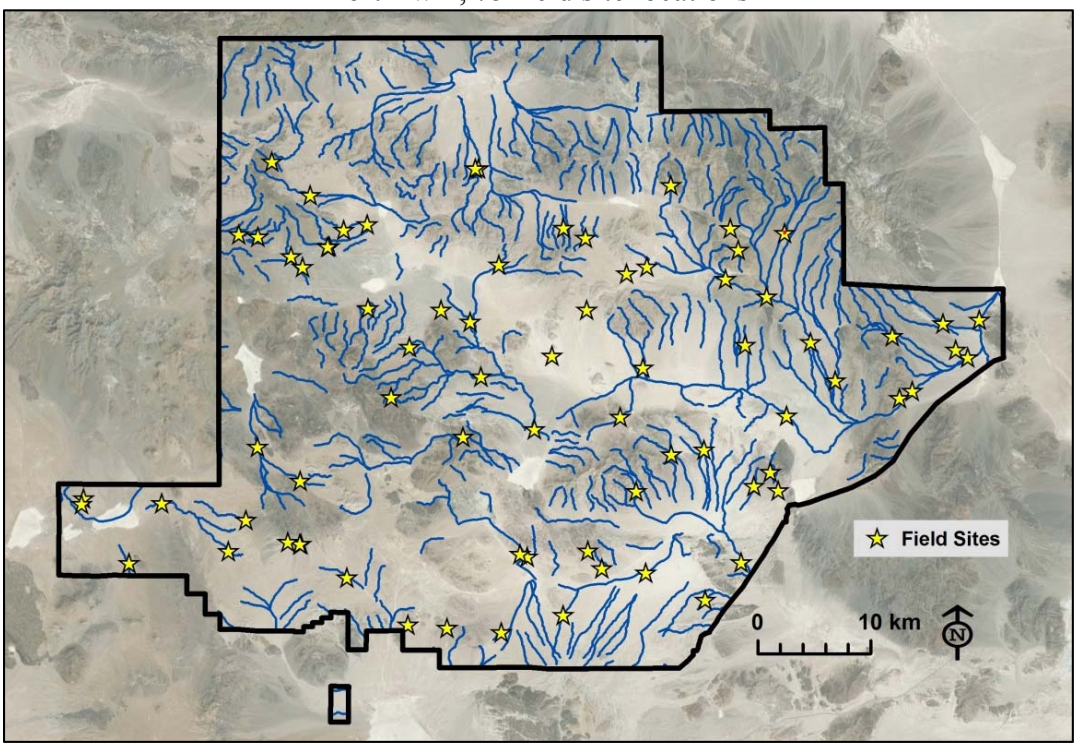


Peak Flow 25-yr 1-hr event (m^3/s)

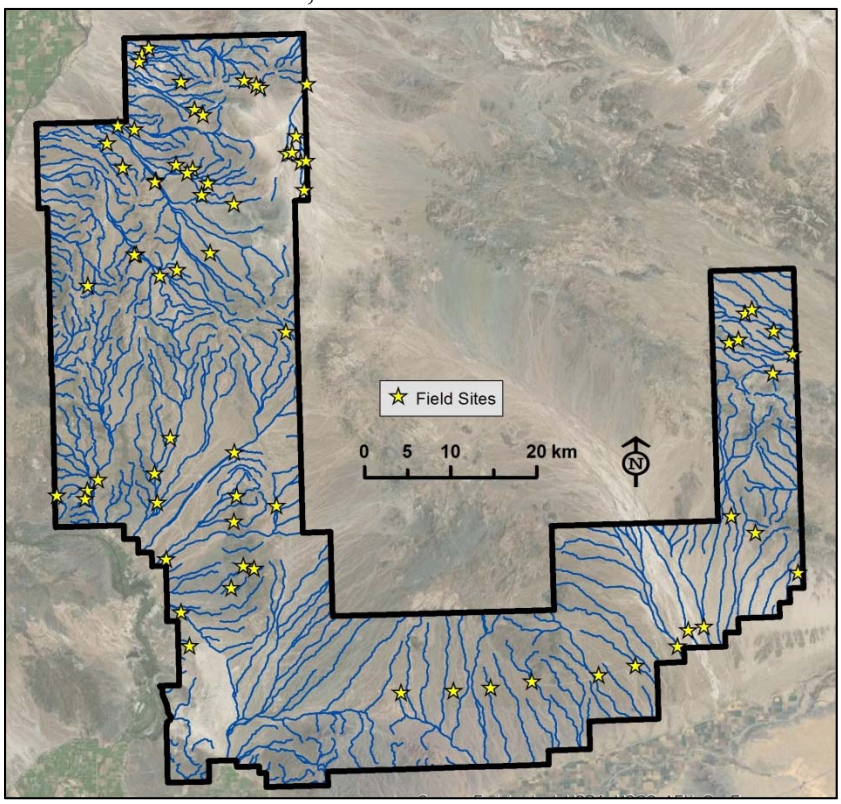


Appendix E: Maps of Field Site Locations

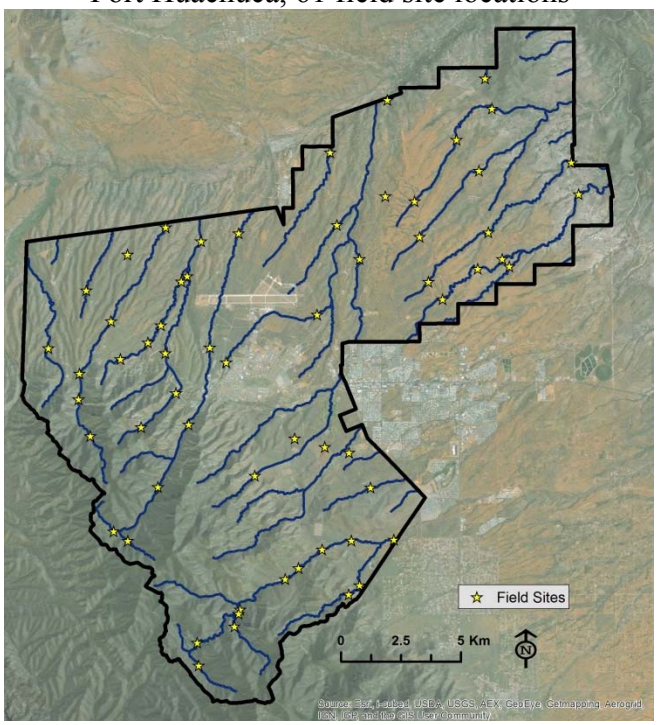
Fort Irwin, 75 field site locations



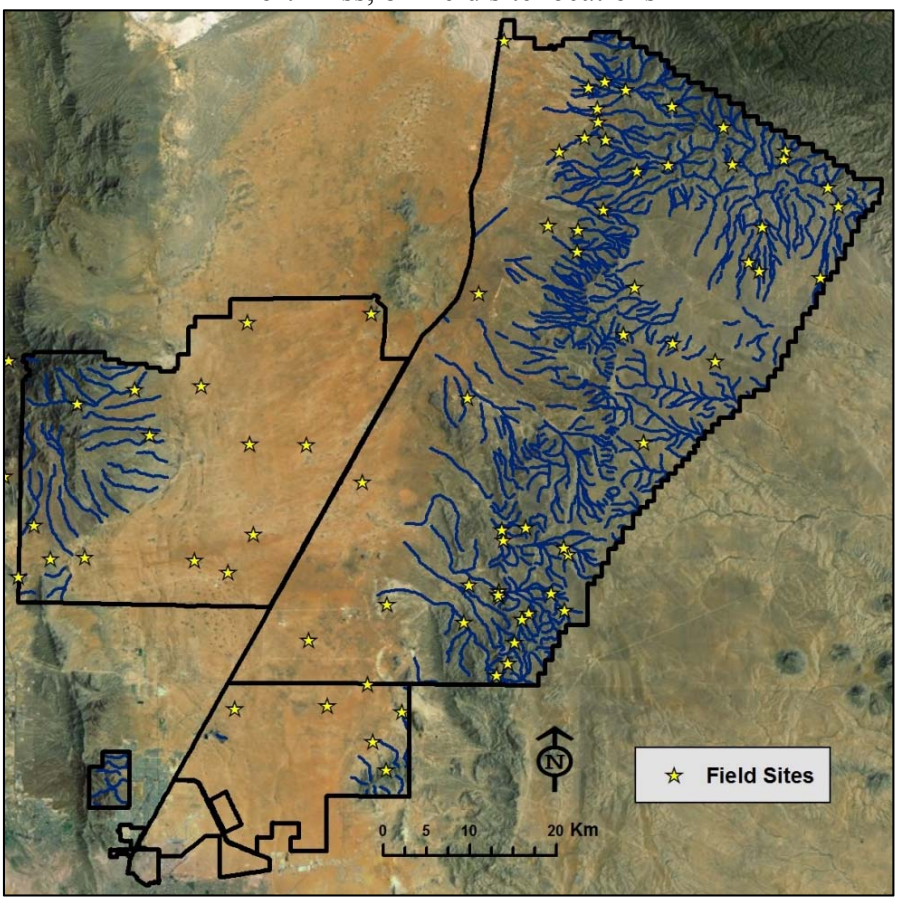
YPG, 71 field site locations



Fort Huachuca, 61 field site locations



Fort Bliss, 82 field site locations



Appendix F: Samantha Hammer Master's Thesis

CHARACTERISTICS OF EPHEMERAL AND INTERMITTENT STREAMS IMPORTANT FOR USE BY WILDLIFE AT FORT BLISS, NEW MEXICO/TEXAS

by

Samantha J. Hammer

A Thesis Submitted to the Faculty of the

SCHOOL OF NATURAL RESOURCES AND THE ENVIRONMENT

In Partial Fulfillment of the Requirements

For the Degree of

MASTER OF SCIENCE

In the Graduate College

THE UNIVERSITY OF ARIZONA

2014

STATEMENT BY AUTHOR

This thesis has been submitted in partial fulfillment of requirements for an advanced degree at the University of Arizona and is deposited in the University Library to be made available to borrowers under rules of the Library.

Brief quotations from this thesis are allowable without special permission, provided that an accurate acknowledgement of the source is made. Requests for permission for extended quotation from or reproduction of this manuscript in whole or in part may be granted by the head of the major department or the Dean of the Graduate College when in his or her judgment the proposed use of the material is in the interests of scholarship. In all other instances, however, permission must be obtained from the author.

SIGNED: Samantha J. Hammer

APPROVAL BY THESIS DIRECTOR

This thesis has been approved on the date shown below:

16 December 2014
Date

D. Phillip Guertin
Professor of Watershed Management

Acknowledgements

I would like to acknowledge the Strategic Environmental Research and Development Program (SERDP) for providing funding for the project that my thesis was a part of, as well as feedback on my research. The Tucson ARS/SWRC provided vehicles for field work and an office in which to work. My co-workers on the project all provided great support, advice, and camaraderie: Russ Lyon, Joel Murray, Amy Birtwistle, Brian Bledsoe, Dave Goodrich, and especially Lainie Levick. Lainie was also on my committee and coordinated the SERDP study. She was always available as a sounding board for ideas and to help guide my research. My advisor, Phil Guertin, helped guide me through the process and gave me valuable feedback on my thesis drafts. Bill Mannan, my other committee member, was especially helpful in making sure my approach to understanding the wildlife use of streams was appropriate. Fort Bliss personnel, especially Brian Locke, as well as personnel at the other SERDP project installations (Fort Huachuca, Fort Irwin, and Yuma Proving Ground) provided me with excellent field data sets that were vital to my thesis and constructive criticism while I developed my thesis.

I particularly want to thank my good friends, Diane Faircloth and Jeff Van Maren, who were extremely supportive and invaluable over the last four years. Leila Gass and Brigette Beasley were also great. All my other friends all provided a great support network and kept me happy during a stressful time. I also thank my family, especially my mom.

TABLE OF CONTENTS

List of Figures 5
List of Tables 6
Abstract 11
Introduction 12
Literature Review 14
Species Richness
    Methods 29
    Results 32
    Discussion 59
Bird Nest Height
    Methods 66
    Results 67
    Discussion 71
Gray Vireo Habitat Model
    Methods 73
    Results 76
    Discussion 82
Conclusion 85
Literature Cited 86
Appendix A – Wildlife tables 98
Appendix B – Distribution of potential species richness 122

LIST OF FIGURES

Figure 1. World distribution of warm drylands (from Tooth 2000). 14
Figure 2. Ecological Management Areas at Fort Bliss, Texas/New Mexico, from Levick et al. (*in progress*). 25
Figure 3. Comparison of relative effect size of ecohydrological variables in Gaussian GLM regression models of potential species richness of several TER-S groups in stream reaches at Fort Bliss, NM. Ecohydrological variables were derived from data collected during or previous to 2012. Potential species richness was derived by stacking GAP animal habitat distribution models downloaded on or before October 2014. Input variables were standardized so estimates are one the same scale; relative effect size was calculated by converting the estimates to a percentage. 53
Figure 4. Plot of the average of the relative effect sizes of ecohydrological variables used to model potential species richness of 21 species groups in stream reaches at Fort Bliss, NM versus the number of groups in which the variable was used for modeling. 56
Figure 5. Map of the areas of the Fort Bliss, NM used in describing the distribution of potential species richness in stream reaches. Richness was derived by stacking GAP animal habitat distribution models downloaded on or before October 2014. 57
Figure 6. Map of the location of data collected by Kozma and Mathews (1995) and Myers et al. (1998) on breeding birds in arroyo-riparian areas of Fort Bliss, NM from 1993-1997. Riparian zone indicates the extent of the 3-m flooded depth polygons used in the SERDP project to derive ecohydrological variables. 65
Figure 7. Values across stream reaches on Fort Bliss, NM/TX of the overall nesting habitat value metric, NH_a (top) and the width-adjusted nesting habitat value metric, NH_w (bottom). Metrics were created by combining information on preferred nest height of bird species occurring on the installation and information on the vegetation structure of each stream reach collected by Levick et al. (*in progress*). 69
Figure 8. Total stream lengths at Fort Bliss, NM/TX of values of the overall nesting habitat metric, NH_a and width-adjusted metric, NH_w. Number above column indicates distance in stream-km for that range of metric values. 70
Figure 9. Maps showing the literature-based model for Gray Vireo habitat in streams at Fort Bliss, NM. Colored streams identify streams with >28.8% cover in the 1-4 meter vegetation layer from LiDAR that contain some Gray Vireo land cover types. Gray streams represent all other streams (no identified habitat). 77
Figure 10. Receiver-operating curves (ROC) for the survey-based model test set (a) and training set (b). ROC curves were the result of modeling gray vireo presence in streams at Fort Bliss, NM based on field data collected from 2007-2012. 79
Figure 11. Maps of logistic modeling results for gray vireo in stream reaches at Fort Bliss, NM based on field data collected from 2007-2012. The Sacramento Mountains modeling area is shown above, and the Organ Mountains modeling area is shown below to the left. The 0.207 threshold for presence resulted in the greatest model accuracy. By this threshold, streams that are symbolized with light blue (0.21 – 0.3) or greater, toward the red end of the spectrum, could be habitat for vireos. 81

LIST OF TABLES

Table 1. Effect of ecohydrological variables on potential richness of all riparian-associated species in stream reaches at Fort Bliss, NM. Results are from using a Gaussian GLM regression to model species richness as a function of the ecohydrological variables. Ecohydrological variables were derived from data collected during or previous to 2012. Potential species richness was derived by stacking GAP animal habitat distribution models downloaded on or before October 2014. Input variables were standardized so estimates are one the same scale; relative effect size was calculated by converting the estimates to a percentage. 32
Table 2. Effect of ecohydrological variables on potential richness of all obligate riparian-associated species in stream reaches at Fort Bliss, NM. Results are from using a Gaussian GLM regression to model species richness as a function of the ecohydrological variables. Ecohydrological variables were derived from data collected during or previous to 2012. Potential species richness was derived by stacking GAP animal habitat distribution models downloaded on or before October 2014. Input variables were standardized so estimates are one the same scale; relative effect size was calculated by converting the estimates to a percentage. 33
Table 3. Effect of ecohydrological variables on potential richness of all TER-S riparian-associated species in stream reaches at Fort Bliss, NM. Results are from using a Gaussian GLM regression to model species richness as a function of the ecohydrological variables. Ecohydrological variables were derived from data collected during or previous to 2012. Potential species richness was derived by stacking GAP animal habitat distribution models downloaded on or before October 2014. Input variables were standardized so estimates are one the same scale; relative effect size was calculated by converting the estimates to a percentage. 34
Table 4. Effect of ecohydrological variables on potential richness of riparian-associated amphibians in stream reaches at Fort Bliss, NM. Results are from using a Gaussian GLM regression to model species richness as a function of the ecohydrological variables. Ecohydrological variables were derived from data collected during or previous to 2012. Potential species richness was derived by stacking GAP animal habitat distribution models downloaded on or before October 2014. Input variables were standardized so estimates are one the same scale; relative effect size was calculated by converting the estimates to a percentage. 35
Table 5. Effect of ecohydrological variables on potential richness of obligate riparian-associated amphibians in stream reaches at Fort Bliss, NM. Results are from using a Gaussian GLM regression to model species richness as a function of the ecohydrological variables. Ecohydrological variables were derived from data collected during or previous to 2012. Potential species richness was derived by stacking GAP animal habitat distribution models downloaded on or before October 2014. Input variables were standardized so estimates are one the same scale; relative effect size was calculated by converting the estimates to a percentage. 36
Table 6. Effect of ecohydrological variables on potential richness of riparian-associated reptiles in stream reaches at Fort Bliss, NM. Results are from using a Gaussian GLM regression to model species richness as a function of the ecohydrological variables. Ecohydrological variables were derived from data collected during or previous to 2012. Potential species

richness was derived by stacking GAP animal habitat distribution models downloaded on or before October 2014. Input variables were standardized so estimates are one the same scale; relative effect size was calculated by converting the estimates to a percentage. 37
Table 7. Effect of ecohydrological variables on potential richness of obligate riparian-associated reptiles in stream reaches at Fort Bliss, NM. Results are from using a Gaussian GLM regression to model species richness as a function of the ecohydrological variables. Ecohydrological variables were derived from data collected during or previous to 2012. Potential species richness was derived by stacking GAP animal habitat distribution models downloaded on or before October 2014. Input variables were standardized so estimates are one the same scale; relative effect size was calculated by converting the estimates to a percentage. 38
Table 8. Effect of ecohydrological variables on potential richness of TER-S riparian-associated reptiles in stream reaches at Fort Bliss, NM. Results are from using a Gaussian GLM regression to model species richness as a function of the ecohydrological variables. Ecohydrological variables were derived from data collected during or previous to 2012. Potential species richness was derived by stacking GAP animal habitat distribution models downloaded on or before October 2014. Input variables were standardized so estimates are one the same scale; relative effect size was calculated by converting the estimates to a percentage. 39
Table 9. Effect of ecohydrological variables on potential richness of riparian-associated mammals in stream reaches at Fort Bliss, NM. Results are from using a Gaussian GLM regression to model species richness as a function of the ecohydrological variables. Ecohydrological variables were derived from data collected during or previous to 2012. Potential species richness was derived by stacking GAP animal habitat distribution models downloaded on or before October 2014. Input variables were standardized so estimates are one the same scale; relative effect size was calculated by converting the estimates to a percentage. 40
Table 10. Effect of ecohydrological variables on potential richness of obligate riparian-associated mammals in stream reaches at Fort Bliss, NM. Results are from using a Gaussian GLM regression to model species richness as a function of the ecohydrological variables. Ecohydrological variables were derived from data collected during or previous to 2012. Potential species richness was derived by stacking GAP animal habitat distribution models downloaded on or before October 2014. Input variables were standardized so estimates are one the same scale; relative effect size was calculated by converting the estimates to a percentage. 41
Table 11. Effect of ecohydrological variables on potential richness of riparian-associated TER-S mammals in stream reaches at Fort Bliss, NM. Results are from using a Gaussian GLM regression to model species richness as a function of the ecohydrological variables. Ecohydrological variables were derived from data collected during or previous to 2012. Potential species richness was derived by stacking GAP animal habitat distribution models downloaded on or before October 2014. Input variables were standardized so estimates are one the same scale; relative effect size was calculated by converting the estimates to a percentage. 42
Table 12. Effect of ecohydrological variables on potential richness of riparian-associated birds in stream reaches at Fort Bliss, NM. Results are from using a Gaussian GLM regression to model species richness as a function of the ecohydrological variables. Ecohydrological

variables were derived from data collected during or previous to 2012. Potential species richness was derived by stacking GAP animal habitat distribution models downloaded on or before October 2014. Input variables were standardized so estimates are one the same scale; relative effect size was calculated by converting the estimates to a percentage. 43
Table 13. Effect of ecohydrological variables on potential richness of obligate riparian-associated birds in stream reaches at Fort Bliss, NM. Results are from using a Gaussian GLM regression to model species richness as a function of the ecohydrological variables. Ecohydrological variables were derived from data collected during or previous to 2012. Potential species richness was derived by stacking GAP animal habitat distribution models downloaded on or before October 2014. Input variables were standardized so estimates are one the same scale; relative effect size was calculated by converting the estimates to a percentage. 44
Table 14. Effect of ecohydrological variables on potential richness of riparian-associated TER-S birds in stream reaches at Fort Bliss, NM. Results are from using a Gaussian GLM regression to model species richness as a function of the ecohydrological variables. Ecohydrological variables were derived from data collected during or previous to 2012. Potential species richness was derived by stacking GAP animal habitat distribution models downloaded on or before October 2014. Input variables were standardized so estimates are one the same scale; relative effect size was calculated by converting the estimates to a percentage. 45
Table 15. Effect of ecohydrological variables on potential richness of riparian-associated birds summering in stream reaches at Fort Bliss, NM. Results are from using a Gaussian GLM regression to model species richness as a function of the ecohydrological variables. Ecohydrological variables were derived from data collected during or previous to 2012. Potential species richness was derived by stacking GAP animal habitat distribution models downloaded on or before October 2014. Input variables were standardized so estimates are one the same scale; relative effect size was calculated by converting the estimates to a percentage. 46
Table 16. Effect of ecohydrological variables on potential richness of obligate riparian-associated birds summering in stream reaches at Fort Bliss, NM. Results are from using a Gaussian GLM regression to model species richness as a function of the ecohydrological variables. Ecohydrological variables were derived from data collected during or previous to 2012. Potential species richness was derived by stacking GAP animal habitat distribution models downloaded on or before October 2014. Input variables were standardized so estimates are one the same scale; relative effect size was calculated by converting the estimates to a percentage. 47
Table 17. Effect of ecohydrological variables on potential richness of riparian-associated birds wintering in stream reaches at Fort Bliss, NM. Results are from using a Gaussian GLM regression to model species richness as a function of the ecohydrological variables. Ecohydrological variables were derived from data collected during or previous to 2012. Potential species richness was derived by stacking GAP animal habitat distribution models downloaded on or before October 2014. Input variables were standardized so estimates are one the same scale; relative effect size was calculated by converting the estimates to a percentage. 48
Table 18. Effect of ecohydrological variables on potential richness of obligate riparian-associated birds wintering in stream reaches at Fort Bliss, NM. Results are from using a

Gaussian GLM regression to model species richness as a function of the ecohydrological variables. Ecohydrological variables were derived from data collected during or previous to 2012. Potential species richness was derived by stacking GAP animal habitat distribution models downloaded on or before October 2014. Input variables were standardized so estimates are one the same scale; relative effect size was calculated by converting the estimates to a percentage. 49
Table 19. Effect of ecohydrological variables on potential richness of riparian-associated birds found year-round in stream reaches at Fort Bliss, NM. Results are from using a Gaussian GLM regression to model species richness as a function of the ecohydrological variables. Ecohydrological variables were derived from data collected during or previous to 2012. Potential species richness was derived by stacking GAP animal habitat distribution models downloaded on or before October 2014. Input variables were standardized so estimates are one the same scale; relative effect size was calculated by converting the estimates to a percentage. 50
Table 20. Effect of ecohydrological variables on potential richness of obligate riparian-associated birds found year-round in stream reaches at Fort Bliss, NM. Results are from using a Gaussian GLM regression to model species richness as a function of the ecohydrological variables. Ecohydrological variables were derived from data collected during or previous to 2012. Potential species richness was derived by stacking GAP animal habitat distribution models downloaded on or before October 2014. Input variables were standardized so estimates are one the same scale; relative effect size was calculated by converting the estimates to a percentage. 51
Table 21. Effect of ecohydrological variables on potential richness of riparian-associated passage migrant birds in stream reaches at Fort Bliss, NM. Results are from using a Gaussian GLM regression to model species richness as a function of the ecohydrological variables. Ecohydrological variables were derived from data collected during or previous to 2012. Potential species richness was derived by stacking GAP animal habitat distribution models downloaded on or before October 2014. Input variables were standardized so estimates are one the same scale; relative effect size was calculated by converting the estimates to a percentage. 52
Table 22. Number of bird species potentially nesting in each vegetation layer at Fort Bliss, NM/TX (left) and percent of bird species potentially nesting in each vegetation layer (right). Derived from data on bird nest height available from Birds of North America Online obtained by October 2014. 68
Table 23. Results of GLM regression of estimated breeding bird richness derived from stacked GAP models against breeding bird richness measures derived from Kozma and Mathews (1995) and Myers et al. (1998) for 13 stream reaches on Fort Bliss, NM. 70
Table 24. Ecological systems identified by the gray vireo GAP model as habitat for that species on Fort Bliss, NM/TX. Model downloaded on October 2014..... 74
Table 25. Confusion matrix and accuracy rates for literature-based model of gray vireo distribution in streams at Fort Bliss, NM. 76
Table 26 . Effect of ecohydrological variables on gray vireo probability of presence in streams on Fort Bliss, NM. Gray vireo presence was determined based on field data collected from 2007-2012 and modeled with a logistic regression. Parameter estimates are the average of all models within 2 AICc units of the top model. Input variables were standardized so estimates are one the same scale; relative effect size was calculated by converting the

estimates to a percentage. Odds can be interpreted as the increase or decrease in probability of presence for a change in units as indicated in the unit change column (e.g., increasing RSI by 0.01 units increases the probability of presence by 202%, while increasing the cumulative area by 10 km^2 decreases the probability of presence by 31%). 78
Table 27. Accuracy measures for three tested presence thresholds of output from the model of gray vireo stream use at Fort Bliss, NM. 80
Table 28 . Confusion matrix and accuracy rates for gray vireo modeling (training and test sets combined). The presence/absence of gray vireos in streams at Fort Bliss, NM was modelled as a function of ecohydrological characteristics of the stream with logistic regression. 80

ABSTRACT

The importance of riparian areas for wildlife is well known, but even in drylands most research has focused on perennial systems. Most of the streams in drylands are intermittent or ephemeral. The xeroriparian areas of these streams have been shown to be important to wildlife, but wildlife use of these systems has rarely been linked to their ecohydrological characteristics. In addition, most studies are limited to a small area and a limited set of species. As part of a Strategic Environmental Research and Development Program (SERDP) project to classify intermittent and ephemeral streams by their ecohydrological characteristics, I investigated which characteristics were related to wildlife use of streams at Fort Bliss, New Mexico and Texas. I found that use of streams by a single species, the Gray Vireo (*Vireo vicinor*), could be modeled with good accuracy using watershed area, peak flow, flow permanence, elevation, rainfall seasonality, and several vegetation variables. At a broader scale, I used vegetation structure data to assign a nesting habitat index to each stream reach and found that vegetation structure and riparian width could be combined to predict the number of breeding bird species using the 13 stream reaches for which field data were available. At the broadest scale, I used stacked GAP animal habitat distribution models to measure potential species richness. Potential richness of various vertebrate groups and TER-S species was related to a number of ecohydrological variables, particularly riparian width, land cover variety, elevation, and percent cover. Mammals and birds often had the opposite response from reptiles and amphibians. Understanding differences between xeroriparian areas, where those different values are, and what ecohydrological characteristics are associated with those differences is an important step in understanding and managing these resources.

INTRODUCTION

The importance of riparian areas for wildlife is well known, but even in drylands most research has focused on perennial systems. Most of the streams in drylands of the world are temporary, and since drylands comprise nearly 50% of total land area (UNEP 1992), temporary streams make up a substantial proportion of the total number, length, and discharge of the world's rivers (Larned et al. 2010, Tooth 2000). In the Southwest, an estimated 81% of streams are intermittent or ephemeral (Levick et al. 2008).

While numerous researchers have documented the importance of the xeroriparian areas of these temporary streams to wildlife, there is still a need to understand how the biological diversity of intermittent and ephemeral streams may be linked to hydro-ecological conditions (Howe et al. 2008). Most studies only examine the differences between riparian areas and uplands, focus on particular species or a narrow group of species (e.g. breeding birds), or have a small spatial extent. Research is needed on the differences in wildlife use between different xeroriparian areas. By examining a comprehensive set of vertebrate species across a range of ephemeral and intermittent streams, the important characteristics of these systems to particular species or groups of species may be revealed. Understanding important characteristics of these systems would allow for better management and more effective conservation efforts. The recent availability of widespread and finer-scale remote sensing data makes a comprehensive study feasible.

An ephemeral and intermittent stream classification based on geomorphic, hydrologic, and vegetation characteristics has recently been developed for the Southwest by a group based in Tucson, Arizona, at the University of Arizona and the USDA-ARS Southwest Watershed Research Center, in collaboration with Colorado State University in Ft. Collins, Colorado (Levick et al., *in progress*). This research was funded by the Strategic Environmental Research and Development Program (SERDP) of the U.S. Department of Defense. Study areas included Fort Bliss, in the Chihuahuan Desert of Texas and New Mexico, Fort Huachuca, AZ, in the transition zone from the Chihuahuan to the Sonoran Desert, Yuma Proving Ground, AZ, in the Lower Sonoran Desert, and Fort Irwin, CA, in the Mojave Desert. Geomorphic characteristics of the streams on the study areas are from the National Hydrography Dataset (USGS 2006). Lyon (2013) used the Automated Geospatial Watershed Assessment tool (AGWA, Miller et al. 2007; Goodrich et al. 2012; http://www.tucson.ars.ag.gov/agwa) to model flow permanence and peak flows for the streams in the study areas. LiDAR data and satellite images collected for the study provided detailed information on vertical vegetation structure and vegetation cover.

My objective was to use the ecohydrological (geomorphic, hydrologic, and vegetation) variables to explore wildlife use patterns of the ephemeral and intermittent streams at Fort Bliss in the Chihuahuan Desert of New Mexico. I examined wildlife use patterns at three levels. As a test case to understand whether habitat for one wildlife species of concern is associated with particular stream reaches, I created a distribution model of a single species of concern in stream reaches at Fort Bliss. At an intermediate scale, I used vegetation structure data to assign a nesting habitat index to each stream reach in the study area. To gain the broadest perspective, I used stacked Gap Analysis Program (USGS 2007, USGS 2014) animal habitat distribution models to explore what ecohydrological characteristics were associated with terrestrial vertebrate species richness of the ephemeral and intermittent streams at Fort Bliss.

This thesis begins with a literature review of ephemeral and intermittent streams, focusing on the prevalence this stream type, the contrast between the vegetation of these streams

and their adjacent uplands, the importance of vegetation to wildlife, and the existing knowledge of the importance of the xeroriparian areas of these streams to wildlife. I discuss how my research contributes to understanding the importance of ephemeral and intermittent streams to wildlife. A description of the study area and data sources of the ecohydrological variables follows.

The body of the thesis is divided into three sections. In the first I detail the methods and results for an analysis of species richness of stream reaches at Fort Bliss and discuss the results. The second section contains the methods, results, and discussion of creating a breeding bird nesting habitat index for stream reaches from LiDAR-derived vegetation structure. In the final section, I explain the methods for the creation of a distribution model for the New Mexico-threatened Gray Vireo in the stream reaches of Fort Bliss, and discuss the results. In the conclusion, I integrate the results of the three main sections and discuss my findings.

LITERATURE REVIEW

Importance of xeroriparian areas

While riparian areas comprise 5% or less of total land area (NRC 2002), conservation efforts often focus on riparian areas because they harbor a disproportionate number of species relative to their spatial extent. The species richness or diversity of riparian areas can be thought of as having three components – α-, β-, and γ-diversity (Whittaker 1960, Magurran and McGill 2011). Alpha (α-) diversity is the diversity of a site, β-diversity is the difference in composition between two sites, and γ-diversity is the diversity of a landscape produced by the combination of α- and β-diversity. Riparian areas are frequently cited as providing habitat for a greater number of species (α-diversity) than their adjacent uplands (Naiman et al. 1993 in Hylander 2006). However, a meta-analysis by Sabo et al. (2005) found that riparian areas do not provide habitat for more species than adjacent uplands. Instead, they provide habitat for different species, resulting in higher turnover of species pools (β-diversity). As a result, riparian zones increase regional richness (γ) by an average of 50% globally. In an analysis in response to Hylander (2006), Sabo and Soykan (2006) revised that figure down to 38%, but found that it could be as high as 150% in some regions. Furthermore, riparian zones and uplands share about half of the regional species pool, with the percentage of unique riparian species averaging 24%, but reaching as high as 60%.

Riparian areas are clearly important for wildlife, but most conservation efforts and ecohydrological research (Stromberg et al. 2009, Steward et al. 2012) have focused on the riparian areas of perennial streams rather than ephemeral or intermittent streams (temporary streams). Temporary streams are known by over forty names – washes, creeks, arroyos, gulches, gullies, wadis, among others (Steward et al. 2012). Most of the streams in drylands of the world are temporary, and since drylands comprise nearly 50% of total land area (UNEP 1992, Figure 1), temporary streams make up a substantial proportion of the total number, length, and discharge of the world's rivers (Larned et al. 2010, Tooth 2000).

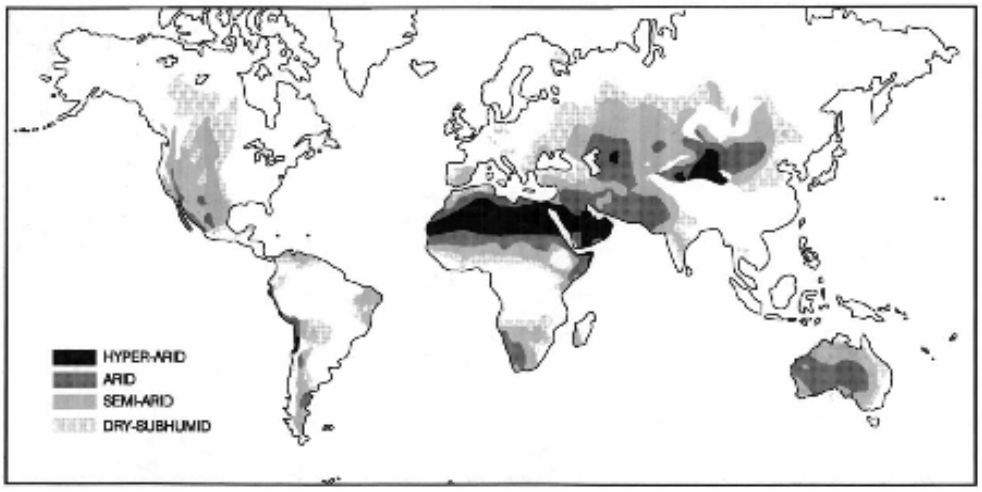


Figure 1. World distribution of warm drylands (from Tooth 2000).

In the contiguous United States, at least 59% of streams are estimated to be ephemeral or intermittent (US EPA 2005, in Levick et al. 2008). In the Southwest, these estimates range from

66% in California to 88% in New Mexico, reaching a maximum of 94% in Arizona and averaging 81% (Levick et al. 2008). The spatial and temporal extent of these temporary streams is likely to increase in the future due to climate change, altered land-use patterns, and increased water extraction for human use (Larned et al. 2010, Steward et al. 2012). Given their broad extent and likelihood of expanding, understanding how these systems function is an important task. These systems are threatened because of how little we know of their societal and ecological value (Steward et al. 2012). Research on temporary rivers has greatly increased in the past eight years (Datry et al. 2011), yet most of it has focused on topics such as nutrient cycling, stream chemistry, sediment movement, and aquatic organisms (Larned et al. 2010), rather than their importance for vegetation and wildlife.

Xeroriparian areas and vegetation

Dry riverbeds tightly retain organic matter and nutrients (Wagener et al. 1998) and can harbor water underground that is not available elsewhere (Levick et al. 2008). Consequently, dry riverbeds and their floodplains often contain the most dense and diverse vegetation in arid landscapes, contrasting strongly with the sparse vegetation of their adjacent uplands (Steward et al. 2012, Levick et al. 2008). The vegetation along these temporary streams is often referred to as xeroriparian for ephemeral streams and mesoriparian for intermittent streams – terms first defined by Johnson et al. (1984). One of the earliest descriptions in the literature of xeroriparian areas was presented by Kassas and Imam (1954) on the vegetation of wadi beds in the Egyptian desert. They reported that the bed of the wadi was usually bare and vegetation was restricted to long, narrow strips along the sides. Wadi xeroriparian areas contained richer vegetation than any other desert vegetation type and were classified into five types based on plant species and soil characteristics: barren rock surfaces dominated by the woody shrub *Stachys aegyptiaca* with plant cover <30%, shallow soils dominated by the succulents *Zygophyllum coccineum* or *Anabasis setifera* with plant cover <30%, soils deeper than 0.5m dominated by the thorny shrub *Zilla spinosa* with plant cover <30%, bunch grasslands where the plant cover may exceed 80% and soils are > 1m deep, and wadi terraces with climax vegetation dominated by four different woody shrubs with plant cover from <50% to >90%. The *Tamarix*-dominated wadi terrace type showed the most complex structure, with trees reaching 10m high, a bushy layer of *Atriplex*, a lower layer of associated plants, and a ground cover of ephemeral plant species.

Most research during the first three-quarters of the 20th century in the Southwestern U.S. focused on riparian zones of perennial streams (Warren and Anderson 1985). In one of the earliest studies of a temporary stream riparian zone in the U.S., Warren and Anderson (1985) studied the xeroriparian vegetation along ~30 miles (48 km) of a Sonoran Desert wash in southwestern Arizona. They found that β-diversity was higher along the upstream to downstream riparian gradient than the adjacent upland gradient. In southeastern Arizona, plant species richness was higher throughout the year along the floodplain of an intermittent/perennial stream than in the adjacent uplands (Stromberg 2007). In the Mojave Desert, shrub cover and density was higher than average adjacent to washes (Schwinning et al. 2011).

In addition to the strong contrast between xeroriparian areas and their adjacent uplands, dryland streams exhibit a vegetation gradient along the stream. A number of studies have also focused on this longitudinal gradient. In Warren and Anderson's (1985) study of xeroriparian vegetation in a Sonoran Desert wash, they described four floristic classes associated with increases in watershed area and controlled by frequency and amount of flow, shading, and

channel scouring. As watershed area increased, riparian facultative and obligate species appeared and increased, larger shrubs and trees became common, and structural complexity increased. Similarly, Zimmerman et al. (1999) found that vegetation distribution and composition in an ephemeral canyon system in central Arizona were best explained by a complex temperature/moisture - substrate gradient. Strongly echoing Warren and Anderson (1985), Shaw and Cooper (2008) found that in northeastern Arizona, decreased disturbance potential and increased moisture availability in the downstream direction were related to greater abundance of obligate riparian vegetation and increasing structural importance of shrubs and trees. In southeastern Arizona, richness at ephemeral sites along Cienega Creek was equal to or greater than that at perennial sites during seasons with greater precipitation (Stromberg et al. 2009). Katz et al. (2012) studied three rivers in Arizona, and found that the riparian zones of intermittent-flow sites had higher long-term plant species richness than either ephemeral or perennial sites. Xeroriparian zones have important variation in their vegetation structure and plant species richness across a range of scales.

Vegetation and wildlife

Vegetation structure and diversity play crucial roles in wildlife use of any specific location. Vegetation complexity can be divided into vertical structure and horizontal structure. Vertical structure is the distribution of the vegetation from ground-level to canopy-level, while horizontal structure is the distribution of vegetation, plant types, and plant species across the landscape. In general, there is a positive relationship between high horizontal structure, often referred to as habitat heterogeneity, and biodiversity (Tews et al. 2004). In the Western U.S., Vale et al. (1989) used principal component analysis (PCA) on presence/absence information of mammal, reptile, and amphibian species by vegetation association and by physiographic region to explore factors influencing species richness. They found that species richness of five of the nine guilds they examined - ground carnivores of vertebrates, ground carnivores of invertebrates, ground seed-eaters, ground omnivores, and aerial carnivores of invertebrates (bats) - increased as vegetation structure became more complex (increasing height and volume) and environmental conditions became more varied. In southern Africa, another region with a significant area of drylands, plant species richness, particularly woody plant species richness, is a very strong predictor of mammal species richness (Andrews and O'Brien 2000, Qian et al. 2009). Boone and Krohn (2000) examined the relative importance of geomorphology, climate, and woody plant species richness for amphibians, reptiles, mammals, and birds in Maine. They used range maps gridded into 324 km^2 blocks. They found that woody plants were the most important variable for reptiles, moderately important for amphibians and birds, and least important for mammals. Climate was the most important variable for mammals and birds.

The importance of vegetation structure to avian species richness in particular has been established since MacArthur and MacArthur (1961) discovered that breeding bird species richness in the eastern U.S. increased as foliage height diversity, a measure of vertical structure, of the 0-2' (0-0.6 m), 2-25' (0.6-7.6 m), and >25' (7.6m) vegetation layers increased. Parker (1986) found that thorn trees, along with stem succulents, enhanced avian diversity in desert shrublands by providing a structural framework that facilitated subdivision of foraging space. Thorn trees were much more abundant in the wash located on the site than in the uplands. At 21 sites scattered across the drylands of Arizona and New Mexico, total vegetation volume is strongly and positively correlated with breeding bird density (Mills et al. 1991).

More recently, the availability of large national datasets, such as the North American Breeding Bird Survey (BBS, Pardieck et al. 2014) and remotely-sensed datasets, has shown that the response of bird diversity to vegetation structure is ubiquitous. Culbert et al. (2013) used species richness information from BBS routes, vertical vegetation structure information from the National Biomass and Carbon Dataset (Kellendorfer et al. 2012), and horizontal structure information from the 2001 National Land Cover Database (Homer et al. 2007). They found that the best models of species richness included measures of both horizontal and vertical structure. In another study using BBS data in the contiguous U.S. and southern Canada, Goetz et al. (2014) found that vegetation properties were usually the strongest determinants of breeding bird species richness, while more detailed vertical structure metrics were of importance to only some guilds, though this may have been influenced by sparse sampling by the LiDAR (Light Detection and Ranging; Dubayah and Drake 2000) data used to measure vertical structure.

The importance of vegetation structure to avian richness and diversity stems from the importance of structure for individual bird species. Vertical structure determines the distribution and availability of perching, foraging, and nesting sites (Brokaw and Lent 1999 in Culbert et al. 2013), so areas with greater vertical structure provide more niches for more species. On the Consumes River in central California, Seavy et al. (2009) created logistic regression occupancy models for sixteen riparian bird species using only LiDAR-derived canopy height and canopy heterogeneity (standard deviation of height). Using only these vegetation structure variables, the authors were able to achieve fair to good models (AUC >0.75) for ten, or nearly two-thirds, of these species. In an area of sand-dunes, heathlands, and dry forests in the Netherlands, Ficetola et al. (2014) tested whether land cover or LiDAR-derived vegetation structure measures were better at predicting the distribution of nine bird species. For seven of the species, the best model included LiDAR-derived vegetation structure, and for five of these species, the best model included only these variables. Both vertical structure diversity and horizontal environmental heterogeneity determine what areas are habitat for particular species, and in turn influence species richness.

Xeroriparian areas and wildlife

Levick et al. (2008) discussed the value of ephemeral and intermittent streams as wildlife support and habitat, and the following material draws heavily from that report. In their report, they noted that Anderson and Ohmart (1977) found that vegetation structure and diversity are important determinants of wildlife diversity and abundance. Therefore, ephemeral and intermittent streams could be expected to be habitat for many wildlife species. Riparian zones are traditionally valued for wildlife for their ability to provide water and their increased vegetation diversity and structure, which provide food, cover, nesting habitat, and breeding habitat. Their unique vegetation and geomorphology provide shade and a moister and cooler microclimate. The linear nature of streams, as well as the open center created by the stream itself, provide abundant edge environments, as well as ideal migration routes and travel corridors (Thomas et al. 1979). While xeroriparian areas in drylands only rarely provide water, they retain all these other values, especially the vegetation and microclimate components. There has been some research on the value to wildlife of ephemeral and intermittent streams. Numerous studies have found ephemeral and intermittent streams to be important to specific wildlife species or groups of species. It has been estimated that in the Southwest, 80% of all animals use riparian zones at some life stage, and more than 50% of breeding bird species nest chiefly in riparian areas (Krueper 1993).

Herpetofauna

Herpetofauna in xeroriparian systems tend to be the least well studied. Along a reach of the Gila River in south-central Arizona, reptile and amphibian species diversity and richness were highest in the desert wash portion of the study area, and of seven species trapped in only one type of vegetation, five were trapped only in the desert wash (Jakle and Gatz 1985). The desert wash also had equal abundance to the desert upland area. Additionally, the mesquite bosque area had higher richness and diversity than the riparian salt cedar area, which was likely due to the well-developed herbaceous and shrub layer that the salt cedar area lacked.

Levick et al. (2008) noted a much more comprehensive report by Jones (1988) that detailed the results of a BLM survey from 1977-1981 of herpetofauna in Arizona. The study covered sixteen vegetation types in 27,885 array-nights on 8.5 million acres (3.4 million ha). The xeroriparian zones, called Mixed Riparian Scrub, had the third highest species richness (41 species) and diversity of all vegetation types, exceeded only by Sonoran Desert (49 species), closed chaparral and cottonwood-willow riparian (44 species). Mesquite bosques, a type of temporary stream riparian zone, and desert grasslands had the richest amphibian fauna. Mesquite Bosque also had the highest diversity of snakes, the highest richness of turtles, the greatest abundance of amphibians, and the second highest diversity of amphibians. Mesquite Bosque and Mixed Riparian Scrub had the highest abundance of snakes. These two vegetation types were consistently among the most rich and diverse vegetation types in several of the analyses.

In an exhaustive survey of the 340,000 acre (138,000 ha) Organ Pipe Cactus National Monument, Rosen and Lowe (1996) found that lizards and some snake species preferred xeroriparian areas over valley-floor floodplains and the surrounding desertscrub, hypothesizing that it was due to higher prey abundance and relative humidity, and the cover afforded by the dense vegetation. Lizard abundance was highest in mesquite woodland or bosque along ephemeral streams and in xeroriparian areas, and almost all non-riparian snake species used xeroriparian areas as refugia during droughts.

There is also some information about the importance of xeroriparian zones to specific species. On 66 transects in the Mojave Desert, Heaton et al. (2006) found that zebra-tailed lizard, *Callisaurus draconoides,* abundance was greater in sandy and rocky washes than on alluvial plains or deposits. Though they had similar or less total vegetation cover, washes had significantly greater percent cover of shrubs and lower cover of ground vegetation than the alluvial environments. Desert tortoises use washes in the Mojave Desert for foraging (Baxter 1988, in Levick et al. 2008). Particular reaches of washes with more shrubs and rougher topography were preferred for desert tortoise den sites and sources of succulent forage in Utah (McArthur and Sanderson 1992, in Levick et al. 2008), and in Arizona Upland Sonoran desertscrub, tortoises occur only along major middle and upper bajada washes and not in valleys (Van Devender 2002, in Levick et al. 2008). Of all known occurrences, of the California red-legged frog, 64% were found in intermittent, rather than perennial, streams (Hayes and Jennings 1988, in Levick et al. 2008).

Mammals

While a few studies have been done on groups of species, even less information seems to be available about overall mammalian species richness of xeroriparian zones. Most information

about mammalian use of ephemeral and intermittent streams comes from studies of individual species. Some work has been done on small mammal groups. In the desert northwest of Phoenix, AZ, Kepner (1978) conducted a large study of 64 sites with 18,000 trap nights on 338,000 acres (137,000 ha) of BLM land. Sites were classified as chaparral, desert grassland, Sonoran desertscrub, riparian deciduous woodland, mesquite/acacia bosque, mixed broadleaf, cottonwood-willow, or mixed riparian scrub. Mixed-riparian scrub is limited to desert washes and arroyos, while riparian deciduous woodland is found in perennial and intermittent watercourses and bosques are found on alluvium of old floodplains. Of these eight vegetation communities, the mixed riparian scrub of temporary streams had the highest rodent species richness and density of individuals, and was also important to two lagomorph species. Other types of riparian vegetation actually had the lowest richness and density values, perhaps because most desert rodents do not require free water. However, desert shrews were only trapped in mixed riparian scrub, mesquite/acacia bosques, cottonwood-willow, and mixed broadleaf communities, all riparian zones. In incidental observations made during the study, all types of vegetation along perennial and intermittent drainages were important to pocket gophers, bats, mustelids, procyonids, deer, and javelina.

Jorgensen et al. (1996) sampled vegetation types in and out of arroyos of the Sacramento Mountain foothills in the Chihuahuan Desert of New Mexico. Rodent diversity was highest in arroyos, which may have been related to lower temporal variation of seed abundance in arroyos relative to out of arroyos. Mist-netting for bats at three dry wash sites across the 345,000 ha Yuma Proving Ground in southwestern Arizona resulted in captures of three of the seven bat species caught at water sources on the installation (Castner et al. 1995). In a study of just one rodent species, Cudworth and Koprowski (2011) examined nest site selection of Arizona gray squirrels, a species endemic to the mountains of the southwestern U.S. and northwestern Mexico. They found that nest densities were 2.6 times higher in riparian woodlands than in pine-oak woodlands. Nest sites had more large trees, snags, logs, and canopy cover and lower slope.

Numerous studies of desert mule deer have elucidated the importance of xeroriparian areas for this species. Krausman et al. (1985) studied desert mule deer use of xeroriparian systems in west Texas and Arizona. They collected 750 visual observations in west Texas, 1180 locations from 12 radio-collared deer in central Arizona, and 870 locations of 15 radio-collared deer in southwest Arizona. They found that while deer actually avoided washes in Texas, in central Arizona they used washes an average of 71.4% of the time year-round and 83.3% of the time in the summer. In southwestern Arizona, over 99% of locations were in washes, all but six of 870. Plant species diversity at Arizona study areas was twice as high in xeroriparian washes as it was in the uplands, and food and cover were less abundant or scarce outside of the washes. In the mesquite-grass shrublands and dry washes of southeastern Arizona, Ragoztkie and Bailey (1991) again found that 19 desert mule deer preferred dry washes over all other environments, especially in summer, and noting that the pattern was much stronger in females than males.

Birds

In contrast to mammals, reptiles, and amphibians, numerous studies have examined bird use of xeroriparian areas, many of which examined bird richness, diversity, or abundance. Two studies have looked at birds during multiple seasons – summer breeding birds, wintering birds, and passage migrants in the spring and fall. An early study by Johnson and Haight (1985) covered a wide area of the U.S. Southwest and Mexico, including the Mohave, Chihuahuan, and

several subdivisions of the Sonoran Desert. The authors surveys revealed that bird species diversity and/or population density was five to ten times greater in xeroriparian plots than in adjacent upland plots during summer, winter, and migration, except for at one site. Levick et al. (2008) noted a number of breeding bird surveys that examined data from 66 study plots on desert BLM lands in California. Species richness of breeding birds in dry washes was about 1.5 times that of the surrounding desertscrub, while wintering bird richness was about 2 times as high. Strong and Bock (1990) studied differences in use of 132 small riparian plots by summer and winter birds in the Huachuca Mountains of southeastern Arizona. The streams in this study were either perennial or intermittent, with reliable seasonal flow. For summer birds, they found that the dominant riparian tree species influenced bird species richness and total density, with cottonwood plots having the greatest richness and both cottonwood and sycamore plots having the greatest density of birds. High elevation areas had different communities than low-elevation and foothill vegetation types. For winter birds, upland vegetation influenced species richness and abundance, with riparian plots in open grasslands having higher values than riparian plots in wooded areas.

More commonly, studies focus on just the breeding bird community. Kirkpatrick et al. (2007) surveyed seventeen higher-order stream reaches in southeastern Arizona that covered a continuum from perennial to ephemeral flow. Relative abundance of birds was 75-136% greater along the riparian areas than in the uplands. Species richness was 68-120% greater (44-82% for breeding species and 205-371% for non-breeding species). Even for ephemeral sites, avian richness and abundance was significantly higher than in the surrounding uplands. At a species level, 31 of 97 species showed significantly different abundance in riparian versus upland areas, 97% of which were more abundant in the riparian areas. While the presence of surface water did not influence richness or abundance, the volume of velvet mesquite did have a positive association with these metrics. Velvet mesquite supports high densities of arthropods, a primary food resource for birds. In a study in Tucson, AZ, distance from undisturbed washes best explained native breeding bird species richness (Germaine et al. 1998). Richness decreased as distance from washes increased. Shanahan et al. (2011) found that richness of forbs and grass-like plants, invertebrate mass, and percent shade were important in explaining breeding bird community composition along Las Vegas Wash in Nevada. At an individual species level, Powell and Steidl (2002) quantified patterns of nest-site selection of seven riparian songbirds. Most species strongly selected Arizona sycamore and netleaf hackberry at the nest-patch scale. At the canyon scale, most species nested in areas with higher vegetation density and volume, a finding that underlines how the vegetation structure of temporary streams' is key to their importance to wildlife.

In southwestern Arizona, the importance of xeroriparian zones to migratory bird species is well documented. In the Lower Colorado River Valley, Rosenberg et al. (1991) found that in upland areas, migrating birds concentrated in xeroriparian vegetation along the extensive network of ephemeral streams. Hardy et al. (2004) surveyed neotropical migrants from February to June in three large washes on the Barry M. Goldwater Air Force Range, along which the vegetation types could be characterized as xeroriparian scrub, creosote-bursage, mixed-cacti, or rocks/cliffs. Ninety-seven percent of all detections of passage migrant birds were from xeroriparian scrub, which covered less than 55% of the area surveyed; 87% of passage migrant birds were classified as xeroriparian specialists. Passage migrant species richness was strongly associated with the presence of mesquite and palo verde >2.5 m. Higher species richness of non-passage breeding neotropical migrants was associated with wider xeroriparian corridors, along

with the presence of mature (>2.5m) palo verde, mesquite, desert willow, and catclaw acacia. Several other studies have documented the use of xeroriparian areas by passage migrants (Lynn et al. 2006; Skagen et al. 2005 and Ohmart and Zisner 1993 in Levick et al. 2008).

Study Objectives

A recent review of temporary river ecology highlighted the need for research on what ecosystem components of ephemeral and intermittent streams support the diversity of terrestrial taxa (Datry et al. 2011). At a U.S. Department of Defense workshop on threatened, endangered, and at-risk species in the Southwest Region (http://www.serdp-estcp.org/News-and-Events/Conferences-Workshops/Past-RC-and-CC-Workshops), participants noted that there was particular need to understand how the biological diversity of intermittent and ephemeral streams may be linked to hydro-ecological conditions (Howe et al. 2008). While the studies I have reviewed have clearly shown that xeroriparian areas are important to wildlife, most only examined the differences between riparian areas and uplands. There are a few exceptions. For example, Strong and Bock (1990) examined differences between riparian plots, but studied only streams in a single small mountain range, most of which had more frequent and reliable flow then the majority of streams in the Southwest. Kepner's (1978) study of small mammals and Jones' (1988) study of herpetofauna looked at differences between riparian deciduous woodland, mesquite/acacia bosque, mixed broadleaf, cottonwood-willow, and mixed riparian scrub. However, the mixed-riparian scrub type comprises the vast majority of ephemeral streams. Research is needed on wildlife use differences within this type. Hardy et al.'s (2004) study did this to some extent by separating vegetation types of the washes into xeroriparian scrub, creosote-bursage, mixed-cacti, or rocks/cliffs, but still only examined three washes.

None of these studies have looked at a comprehensive set of vertebrate species across a range of ephemeral and intermittent streams. Doing so could elucidate what characteristics of these systems are important to particular species or groups of species. Research is also lacking on the effects of hydrology on wildlife and their use of xeroriparian systems. Understanding important characteristics of these systems would allow for better management and more effective conservation efforts. The recent availability of widespread and finer-scale remote sensing data makes a comprehensive study feasible.

To better understand the ephemeral and intermittent streams of the Southwest and their importance for wildlife, the Strategic Environmental Research and Development Program (SERDP) funded a study whose objectives were to characterize the ecohydrological variation of intermittent and ephemeral stream systems based on their vegetation, hydrology, and geomorphology, to produce a stream type classification, to develop associations of stream types to wildlife habitat characteristics, and to provide a tool to simulate climate change and land use change (Levick et al., *in progress*). The project was conducted at four military installations across the Southwest: Fort Irwin in the Mojave Desert of California, Yuma Proving Ground in the Lower Sonoran Desert of western Arizona, Fort Huachuca in the transition zone between the Sonoran and Chihuahuan Deserts of southeastern Arizona, and Fort Bliss in the Chihuahuan Desert of New Mexico and west Texas. The study encompassed over 8000 km of streams distributed across 1.1 million ha. Because of this broad scope and limited funding, research focused on remote sensing data and using previously collected field data. My thesis was produced as part of this project, and so was built around existing data sets, including GIS data and field data.

My objective was to use the geomorphic, hydrologic, and vegetation information developed by Levick et al. (*in progress*) to explore wildlife use patterns of the ephemeral and intermittent streams at one of these installations, Fort Bliss. I examined wildlife use patterns at three levels. To gain the broadest perspective, I used stacked Gap Analysis Program (USGS

2007, USGS 2014) animal habitat distribution models to explore what ecohydrological characteristics were associated with terrestrial vertebrate species richness of the ephemeral and intermittent streams at Fort Bliss. At an intermediate scale, I used LiDAR data to assign a nesting habitat index for all breeding birds and just TER-S breeding birds to each stream reach in the study area. As a test case to understand whether habitat for one wildlife species of concern is associated with particular stream reaches, I created a distribution model for the use of streams by a single species of concern, the Gray Vireo, which is a New Mexico Threatened species. I chose the Gray Vireo because the installation had collected a substantial dataset on where it occurred on post, its Threatened Status makes it of particular conservation interest, and personnel at the Fort had found it to be somewhat riparian-associated at their installation.

These methodologies – GAP distribution models, AGWA hydrological modeling, LiDAR vegetation information, and geomorphology data – have not been combined to study differences in xeroriparian systems. I found only one study that used two of these to some extent - GAP animal data and, instead of LiDAR, land use data - to examine species richness patterns between riparian areas. In that study, Ekness and Randhir (2007) examined potential species richness in the Westfield River watershed in Massachusetts. They found that different order subwatersheds had different potentials for overall richness, with the highest richness occurring in headwaters and lower order subwatersheds. Furthermore, patterns varied for reptiles, amphibians, mammals, and birds. However, this study was not conducted on the intermittent and ephemeral streams of drylands, and did not incorporate hydrology, geomorphology, or the more detailed information about vegetation structure that LiDAR provides.

I will use geomorphic, hydrologic, and vegetation information to explore wildlife use patterns of the ephemeral and intermittent streams at Fort Bliss at three scales. This comprehensive approach will add to our understanding of the importance of dryland xeroriparian areas for wildlife by highlighting differences in wildlife use between xeroriparian areas and the characteristics of these systems that may be related to those differences. This in-depth understanding of the important characteristics of these systems will allow for better management and more effective conservation efforts.

General methods

Site Description

Parts of this description are drawn from Levick et al. (*in progress*). Fort Bliss covers 453,000 ha of the semi-arid Chihuahuan Desert in south-central New Mexico and far western Texas. Elevations range from approximately 1,170 to 2,700 meters. Prominent physiographic features include the higher elevation Sacramento and Organ Mountains, the mid-elevation Franklin and Hueco Mountains, the low-elevation Tularosa Basin, and the gently rolling grasslands of Otero Mesa (U.S. Army 2001). Summers are hot and dry and winters are moderate. Temperatures range from -22.2 to 45.6° C with a daily average of 17.8° C. Fort Bliss receives an annual average of 20.3 cm of precipitation in the valley to 50.8 cm in the mountains. Most rainfall occurs from July to September during intense thunderstorms.

The installation is comprised of a diversity of landforms. Vegetation is dominated by semi-desert grassland and steppe community, followed by stabilized coppice dune and sand flat scrub, creosote mixed desert scrub, and small areas of pinyon-juniper woodland in the mountains. Common plants found in the study area include: creosote (*Larrea tridentata*), yucca (*Yucca elata*, *Yucca torreyi*, and *Yucca baccata*), honey mesquite (*Prosopis glandulosa*), four-wing saltbush (*Atriplex canescens*), ephedra spp. (*Ephedra spp.*), desert willow (*Chilopsis linearis*), cholla (*Opuntia imbricata*), purple prickly pear (*Opuntia macrocentra*), broom snakeweed (*Gutierrezia sarothrae*), tarbush (*Flourensia cernua*), ocotillo (*Fouquieria splendens*), agave (*Agave lechugilla*), pinyon pine (*Pinus edulis*), acacia (*Acacia neovernicosa*), mountain mahogany (*Cercocarpus montanus*), desert ceanothus (*Ceanothus greggii*), oaks (*Quercus spp.*), and various grasses.

The ecological management areas defined by the installation are (in order of largest area): Basin Aeolian, Basin Alluvial, Sacramento Mountains, Organ Mountains, Hueco Mountains, Otero Mesa, Franklin Mountains and Foothill-Bajada Complex (Figure 2).

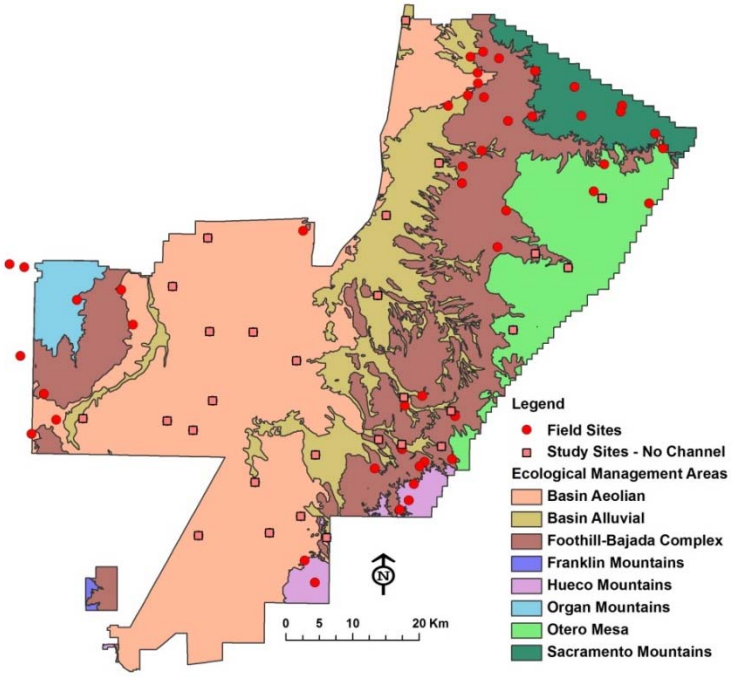


Figure 2. Ecological Management Areas at Fort Bliss, Texas/New Mexico, from Levick et al. (*in progress*).

Over half of Fort Bliss falls under the Basin Aeolian management area which is mostly composed of stabilized coppice dunes that have no stream channel formation. The dunes are stabilized primarily with honey mesquite (*Prosopis glandulosa*) and four-wing saltbush (*Atriplex canescens*), but have little to no vegetation between dunes. Although no distinct riparian vegetation zones exist, these dune areas support a wide variety of wildlife. Some parts of the Basin Aeolian management area have more active dunes, where small channels form but disappear quickly into the sands. This is evident in areas close to other land cover or management types.

Otero Mesa is a large area of grasslands where the flow paths are visible as wide swales containing vegetation assemblages distinct from the adjacent uplands. These areas are defined as sheetflood zones of discontinuous streams. In the remainder of Fort Bliss stream channels range from small incised channels to large arroyos and wide braided systems.

Ecohydrological Data

Most variables used in this thesis were derived as part of the SERDP classification of ephemeral and intermittent streams in the Southwest (Project RC-1727, Levick et al., *in progress*). More detailed descriptions of these variables can be found in the documentation for that project but are included briefly here.

I derived two additional variables that could be important for species occurrence. One was a measure of vegetation structure complexity derived from the LiDAR data, the Shannon diversity index (Shannon and Weaver 1949). For this measure, higher values correspond to increasing structural diversity. I also derived a variable that measures land cover variety. This variable indicates the number of different ecological systems occurring in a stream reach.

Unit of Analysis

One kilometer stream reaches were selected as the unit of analysis based on field surveys as the average stream length that captures the overall variability along a stream, and all data were derived at that scale. Stream reaches are based on the NHDPlus V2 streamline that was split into +/- 1km reaches with the ET GeoWizards tool (ET Spatial Techniques, http://www.ian-ko.com/).

The streamline and a DEM were used to delineate the riparian zone in the Hydro-Geomorphic Valley Classification Tool (HGVC; Carlson 2009). This tool runs in ArcMap, and creates a polygon by inundating the DEM to a specified depth, delineating the water surface extent at that depth. The polygons representing the water surface extent of the polygons for the 3m inundation depth were used to derive the riparian vegetation variables and riparian widths. This depth was selected through the examination of aerial imagery and field photographs as the most accurate water surface extent to delineate the extent of vegetation most likely influenced by stream flow when it occurs (i.e. indicating a riparian zone). When viewed on a base map or aerial photos, it generally includes the obvious denser vegetation associated with the channel. These polygons are the 1 km stream reaches, which are the unit of analysis.

Hydrology

The two hydrologic variables I used were derived by Lyon (2013) via hydrologic modeling with the Automated Geospatial Watershed Assessment tool (AGWA; Miller et al. 2007, Goodrich et al. 2012). AGWA parameterizes and runs two rainfall-runoff models, Soil and Water Assessment Tool (SWAT) and Kinematic Runoff and Erosion Model (KINEROS2), within a GIS interface. The models require land cover, soils, topographic and climate data. The values obtained from the AGWA/KINEROS2 and AGWA/SWAT simulations were transferred from the AGWA-generated streamlines to the NHD Plus Version 2 (USGS 2006) streamlines used for the stream network in this research.

Flow Permanence (%) is defined as the percent of the year there is flow in the channel. It was derived from the AGWA/SWAT model output for water yield (mm). The Next-Generation Radar Multi-Sensor Precipitation Estimates (NEXRAD-MPE) from 2005-2012 were obtained as a 4x4 km grid (one precipitation value per 4 km^2 per day) from the NOAA Advanced Hydrologic Prediction Service as a series of daily shapefiles for the conterminous United States. These estimates were used to model water yield in AGWA/SWAT.

Peak flow or discharge (Qp, m^3/s) was obtained from the AGWA/KINEROS2 model outputs for the 25-year 1-hour design storm. Design storms were derived from the precipitation depths obtained from the pre-defined table of precipitation frequency estimates based on a specific return interval and duration from NOAA's Precipitation Frequency Data Server (NOAA 2012). I used the 10 and 25-year peak flow values (Qp10 and Qp25) and corresponding total stream power of the 10 and 25-year storms (Tsp 10 and Tsp25) because recurrence intervals for channel-forming flows of streams in arid lands a are typically 10-32 years (Graf 1988, Bull and Kirkby 2002), rather than the 1.5 year recurrence interval common in temperate climates. This is also the minimum flow likely to inundate the overbank areas (Dust and Wohl 2010).

GEOMORPHOLOGY AND PHYSICAL VARIABLES

Elevation (m) was derived from a LiDAR bare earth DEM, at the midpoint of each 1km stream reach. Slope along the length of the stream reach was derived from the LiDAR bare earth DEM for each 1km stream reach.

Total Stream Power (kW/m) is defined as the rate of energy dissipation against the bed and banks of a channel; it estimates the ability of the stream to transport sediment or cause erosion. It was derived from the 25-year peak flow output by the AGWA/KINEROS2 hydrologic modeling, and LiDAR-derived slope with the following equation:

$$\text{Stream Power } \Omega = \rho g Q S$$

where ρ is the density of water (1000 kg/m^3), g is acceleration due to gravity (9.8 m/s^2), Q is discharge (m^3/s), and S is channel slope

Watershed Area above the reach (m^2) represents the area above the reach that contributes to stream flow at that reach, and is related to channel geometry and vegetation community differences. It was obtained from the AGWA model outputs.

Riparian Width (m) is defined as the water surface widths at inundation depths of 1m, 2m, and 3m. The 1m flooded depth often represents the extent of the channel bottom. The 2m and 3m flooded depths represent the extent of riparian vegetation from edge to edge, including the channel bottom. As such, it does not directly measure the width of the vegetation bands that are found along each edge of many temporary streams. Additionally, vegetation in these streams is sometimes found directly in the channel. Riparian width was derived with the HGVC tool as described earlier. To calculate riparian width from these polygons, the area of each 1km stream reach polygon was divided by the actual length of the stream reach.

The Rainfall Seasonality Index describes the precipitation characteristics of the stream reach and indicates the intensity of erosion potential due to precipitation characteristics. It was derived from PRISM 30 year normals (PRISM Climate Group 2010), for the 30-year period 1980-2010, calculated as the mean precipitation of the wettest month divided by the mean annual precipitation.

The Entrenchment Ratio indicates the degree of channel entrenchment or the vertical containment of the river; usually calculated as Flood Prone Width divided by Bankfull Width from field data (Rosgen 1994), calculated here from mean riparian widths: 0.5m/2m, 0.5m/3m, 1m/2m, 1m/3m, and 2m/3m. Higher values (closer to 1) for the entrenchment ratio indicate more entrenched reaches.

Vegetation and Land Cover

Vegetation cover (%) was derived from satellite imagery. A vegetation index was used to classify the 1km stream reaches into vegetation vs. bare ground or ground cover. Aerial photography and field photos were used as guides to verify vegetation pattern, density and cover. It was calculated as total area of vegetation pixels divided by total area of the 1km stream reach polygon. Red Edge-NDVI values were derived from 5m-resolution RapidEye satellite imagery, with R-G-B-NIR and Red Edge bands (ENVI User Guide; http://geol.hu/data/online_help/Vegetation_Indices.html).

Mean Vegetation Index describes the relative vegetation density for each 1km stream reach, calculated only from the pixels classified as vegetation cover from the satellite imagery (i.e. the pixels classified as bare ground or ground cover were not used to derive this variable). In areas of sparse vegetation, both vegetation and soil properties are represented by the vegetation index. Therefore, the Mean Vegetation Index can indicate the overall sparseness or density of vegetation.

Vegetation structure variables that describe the vertical vegetation features were derived from a multi-return LiDAR vegetation height layer with 1.5m resolution. The height layer was calculated by differencing the canopy and ground layers. The height layer was classified into vegetation height categories of 0.5-1m, 1-4m, 4-12m, >12m.The classification was converted into four variables that represents the percent of each stream reach with vegetation within one height layer. Since few streams had vegetation >12m, I converted the >12m variable into a binary presence/absence measure. Vegetation structure represents the various zones or regions in vegetation that are typically used by wildlife. Note that these values do not account for vegetation that is beneath that height category (i.e. the 1-4m high vegetation underneath the 4-12m high vegetation), but represents the vegetation that reaches about its maximum height within that height range. I also used the percent cover of each structure layer to calculate a structural diversity measure with the Shannon Index (Shannon and Weaver 1949).

Landcover Variety describes the horizontal structure heterogeneity of a stream reach, another important feature for wildlife. The ZonesWOverlap (Clark 2012) tool in ESRI ArcGIS 10.1 was used to determine the number of different ecological systems in the GAP National Land Cover dataset (USGS 2011).

SPECIES RICHNESS

My objective for this section was to explore the differences in terrestrial vertebrate species richness of ephemeral and intermittent stream reaches across Fort Bliss, and to understand what ecohydrological characteristics were associated with species richness.

Methods

Riparian-associated species

I used the Integrated Natural Resources Management Plan provided by Fort Bliss to create an initial list of all vertebrate species occurring on the installation (U.S. Army 2001). I used the USGS GAP species viewer (http://gapanalysis.usgs.gov/species/viewer/species-viewer/) to add to this list by checking the ranges of all species distribution models with habitat in Otero and Doña Ana counties. I also checked whether species range maps provided by NatureServe indicated that other species might be found on the installation (NatureServe 2014, Patterson et al. 2003, Ridgely et al. 2003, IUCN et al. 2004). Once I created an exhaustive list of species in the study area (Appendix A, Table 1), I used the Ecology and Life History descriptions in NatureServe Explorer (NatureServe 2014) to classify each species as riparian-associated (RA) or not riparian-associated. When this description was not sufficient, I referred to other sources (BISON-M 2013, Brennan 2012, RHJV 2004). I did not include any of the shorebirds or waterfowl, since these species are mostly vagrants or use urbanized areas on the installations. I also excluded non-native species. I classified species as riparian-associated if the description explicitly mentioned riparian areas, water, canyons, streams or a similar term, and also if it described the species' habitat with words such as brush, forest, shrub, thicket, dense undergrowth, and similar descriptors that typically are only found in the riparian areas of Fort Bliss. I excluded species that had descriptions that matched upland areas, such as species that primarily use open grasslands or desert. For riparian-associated species, I identified their level of xeroriparian-dependence at Fort Bliss as "No", "Facultative," "Important, but not obligate," and "Obligate." For species classified as No, their habitat description had no mention of streams, canyons, water, or other terms indicative of riparian areas, but did mention something that suggested they would use the type of vegetation typical of xeroriparian areas. For species classified as Facultative, their habitat description explicitly mentioned one of the terms indicative of riparian areas, but did not indicate it was preferred over other habitat types listed. For species classified as Important, but not obligate, their habitat description indicated a moderate to somewhat strong preference for riparian areas, water, streams, canyons, or similar areas. For species classified as Obligate, their habitat description indicated that the species required riparian areas, water, streams, canyons, or similar areas. The resulting list can be found in Appendix A, Table 2.

Species distribution models

The National Gap Analysis Program (USGS 2014) and the Southwest Regional Gap Analysis Program (Boykin et al. 2007, USGS 2007) have created distribution models for numerous species found in the United States. Based on literature-cited information about habitat associations, GAP distribution models are deductive models that predict areas suitable for

occupation within a species' range. Information used to define habitat associations includes GAP National Land Cover data of ecological systems, elevation, hydrology, human avoidance, forest edge, and ecotone widths. The resulting models are rasters with a 30x30 meter pixel size. I obtained all available species distribution models for riparian-associated species from USGS (2014). Many species were not available from this program. Some were not modeled, while others species' models were still being developed. For these species, I obtained distribution models from the older Southwest Regional GAP (USGS 2007). A number of species were excluded from the analysis at this point because no model was available for them, or none of their modeled habitat occurred on the installation. I converted all Southwest GAP models to GRID format to manipulate them.

Distribution models from the National GAP include summer, winter, and year-round habitat, while models from the Southwest GAP include, summer, winter, year-round, and migratory habitat, sometimes subdivided by breeding and non-breeding or known and potential. I separated all models so that each included only one habitat type and reclassified them so that a value of one indicated presence and a value of zero, absence. I used the Raster Calculator tool in ESRI ArcGIS 10.1 to stack models to create rasters with species richness values for specific groups. Known and potential occurrences were pooled, as well as breeding and non-breeding habitat. Only birds and some bats had summer or winter habitat.

I created riparian-associated richness layers for all species pooled, all birds with summer, winter, or year-round habitat, all birds with summer habitat, all birds with winter habitat, all birds with year-round habitat, all birds with migratory habitat, all amphibians, all reptiles, and all mammals.

By including only species with Obligate or Important, but not obligate dependence on riparian areas, I created riparian-obligate species richness layers for all species pooled, all birds with summer, winter, or year-round habitat, all birds with summer habitat, all birds with winter habitat, all birds with year-round habitat, all amphibians, all reptiles, and all mammals.

I created richness layers for just species of concern (TER-S species) by stacking models of species that met one of these criteria: federally listed, state listed, or ranked by NatureServe as 3 (Vulnerable) at a global, national, or regional scale in New Mexico. TER-S richness layers included all species, just mammals, just reptiles, and just summer, winter, and year-round birds.

Calculating species richness at Bliss

I used the Project Raster tool in ESRI ArcGIS 10.1 to re-project the species richness rasters into WGS 1984, Zone 13N for analysis at Fort Bliss. From the SERDP project layer of all stream reach polygons at Fort Bliss, I eliminated all reaches in Texas, because the Southwest GAP models used for some species did not include that state. I also checked all reaches with a stream length less than one standard deviation below the mean (775.5 meters). I eliminated reaches that were small fragments and those that were mostly overlapped by other reaches. While doing this, I found four reaches >775.5 meters that had almost complete overlap with other reaches and eliminated them. I used the ZonesWOverlap (Clark 2012) in ESRI ArcGIS 10.1 to calculate the mean species richness values for each group in the remaining stream reaches at Fort Bliss.

Analysis

I used generalized linear models (GLM) in R (R Core Team 2014) to explore which vegetative, hydrologic, and geomorphic variables of the stream reaches (Appendix A, Table 4) were correlated with the species richness of the various groups. For modeling each measure of species richness, I included one measure of riparian vegetation width (width of stream when flooded to 1, 2, or 3 meters) and one measure of entrenchment ratio (2m/3m ER, 1m/3m ER, 0.5m/3m ER, 1m/2m ER, or 0.5m/2m ER). I chose which riparian width and entrenchment ratio to use by modeling the species richness as a function of each variable individually with a Gaussian GLM with an identity link. In each set, I retained the variable that resulted in the lowest Akaike's Information Criterion (AIC; Akaike 1973, Burnham and Anderson 2002), adjusted for small sample size (AICc). AIC estimates how much information is lost when a model is used to approximate the true data, so lower values are indicative of better performing models. In general, any model within 2 AIC units of the best-performing model is considered as competitive with that model.

Though a Poisson GLM is usually used for count data, I used a Gaussian GLM with an identity link for all modeling because all data were under-dispersed and a Gaussian GLM resulted in much lower AIC values of the global model for all measures of species richness.

I generated the top models for each species richness estimator through the following process, modified from Grueber et al. (2011). I used Akaike's Information Criterion adjusted for small sample size (AICc) to evaluate model performance. I built an initial global model that included all possible predictor variables, and used the *arm* package in R (Gelman et al. 2009) to standardize the global model by centering on the mean and dividing by 2 standard deviations (Gelman 2008). I used the package MUMIN (Bartoń 2009) to generate all model subsets that had a maximum of ten predictor variables. I checked the models within 2 ΔAICc of the top model for uninformative parameters by determining if any nested models did not have a marked decrease in maximized log likelihood over the next simplest model. I model-averaged all models that had a maximum of ten predictor variables to generate measures of relative variable importance (Burnham and Anderson 2002: 167–169). When the number of models within 2 ΔAICc of the top model was greater than one, I model-averaged parameter estimates of all models in the top 2 ΔAICc by the natural averages method to generate estimates of effect size. Unconditional standard errors are reported when parameters were model-averaged.

Results of the models included an estimate for each parameter; since the input variables were standardized, the estimates indicate the effect size of each variable on the same scale. The term parameter estimate and effect size are used interchangeably. I report relative effect size as percent of the sum of the parameter estimates to compare the change in contribution of each variable between models of different richness measures. When parameter estimates are positive, this indicates an increase in the value of that ecohydrological variable is associated with an increase in richness, and the reverse when the parameter estimate is negative. Effect direction is sometimes indicated by a (+) or (-). Standard errors and 95% confidence intervals calculated from them are given. Relative importance, calculated as the sum of the Akaike weights over all models in which the variable was included, are also reported for each variable. In tables of model results, variables are ranked from greatest relative effect size to least.

Results

Groups including all riparian-associated species

Fort Bliss had a total of 372 possible species, 218 of which (58%) were riparian-associated. Models were available for 187 of the riparian-associated species at Fort Bliss. Stream reaches could potentially provide habitat for a mean of 90.5 riparian associated species (s = 6.6, range = 37.2 - 102.9). Forty-five percent (n = 99) of the riparian-associated species were riparian-obligate. Stream reaches could potentially provide habitat for a mean of 33.0 riparian-obligate species (s = 2.6, range = 15.1 – 42.7). Twenty percent (n = 42) of the riparian-associated species were TER-S species. Stream reaches could potentially provide habitat for a mean of 13.8 TER-S species (s = 1.1, range = 7.1 – 17.0).

Species with any level of riparian-association

For the All RA species group, there was only one top model. The strongest effect (Table 1) was a negative response to increasing riparian width (1m flooded depth). Percent cover had a strong positive effect, followed by a strong negative effect of mean vegetation index. Watershed area, elevation, percent of the stream reach with vegetation 0.5-1 m tall, and landcover variety all had negative effects, while the rainfall seasonality index (RSI), 2m/3m entrenchment ratio, and total stream power of the 25-year storm had positive effects.

Table 1. Effect of ecohydrological variables on potential richness of all riparian-associated species in stream reaches at Fort Bliss, NM. Results are from using a Gaussian GLM regression to model species richness as a function of the ecohydrological variables. Ecohydrological variables were derived from data collected during or previous to 2012. Potential species richness was derived by stacking GAP animal habitat distribution models downloaded on or before October 2014. Input variables were standardized so estimates are one the same scale; relative effect size was calculated by converting the estimates to a percentage.

Parameter	*Estimate*	*Relative Effect Size*	*SE*	95% Confidence Interval		*Relative Importance*
				Lower	*Upper*	
1m Width	-7.65	29.9	0.47	-7.67	-7.63	1.00
Percent Cover	3.61	14.1	0.57	3.59	3.64	1.00
Veg_Ind Mean	-2.71	10.6	0.54	-2.73	-2.68	1.00
RSI	2.08	8.1	0.27	2.07	2.10	1.00
W_Area	-2.08	8.1	0.30	-2.09	-2.06	1.00
Elevation	-2.07	8.1	0.35	-2.08	-2.05	1.00
LiDAR 0.5-1m	-1.64	6.4	0.34	-1.66	-1.63	0.99
Landcover_var	-1.36	5.3	0.27	-1.38	-1.35	1.00
ER 2/3	1.22	4.7	0.36	1.20	1.23	0.90
TSP25	1.20	4.7	0.30	1.19	1.22	0.92

Obligate riparian-associated species

For the All Obligate RA species group, there were two competing models. Many of the same variables were important and relative effect sizes and directions were similar, but elevation was not important (Table 2). Instead, obligate species were influenced positively by the percent of the stream reach with vegetation 4-12 m tall and flow permanence. In addition land cover variety changed direction to become a positive predictor of species richness and increased in relative effect size from 5.3% to 9.2%.

Table 2. Effect of ecohydrological variables on potential richness of all obligate riparian-associated species in stream reaches at Fort Bliss, NM. Results are from using a Gaussian GLM regression to model species richness as a function of the ecohydrological variables. Ecohydrological variables were derived from data collected during or previous to 2012. Potential species richness was derived by stacking GAP animal habitat distribution models downloaded on or before October 2014. Input variables were standardized so estimates are one the same scale; relative effect size was calculated by converting the estimates to a percentage.

Parameter	*Estimate*	*Relative Effect Size*	*SE*	95% Confidence Interval		*Relative Importance*
				Lower	*Upper*	
1m Width	-1.42	16.8	0.14	-1.43	-1.42	1.00
Percent Cover	1.29	15.2	0.23	1.28	1.30	1.00
W_Area	-0.99	11.8	0.12	-1.00	-0.99	1.00
RSI	0.96	11.3	0.11	0.95	0.96	1.00
Veg_Ind Mean	-0.79	9.3	0.23	-0.80	-0.78	0.96
Landcover_var	0.78	9.2	0.11	0.77	0.78	1.00
LiDAR 4-12	0.77	9.1	0.12	0.76	0.77	0.98
Tsp25	0.52	6.2	0.13	0.52	0.53	1.00
LiDAR 0.5-1	-0.37	4.4	0.16	-0.38	-0.37	0.37
ER 0.5/2	0.33	3.9	0.16	0.32	0.34	0.52
FP	0.23	2.7	0.11	0.22	0.23	0.47

Riparian-associated TER-S species

For the All TER-S RA species group, there were four competing models. Effect sizes were generally smaller than those for the All RA group (Table 3). Most of the same variables were used in the models as for All RA, though the effect size of elevation and land cover variety increased relative to the other variables. Riparian width remained in the models, but changed from the 1-m flooded depth to the 3-m. Notably, the effect of LiDAR 0.5-1m changed from negative to positive. Entrenchment ratio was not important for TER-S species. Three variables with relative small effect sizes and importance that not used for All RA were added for TER-S species: LiDAR 1-4 (-), slope (+), and flow permanence (+).

Table 3. Effect of ecohydrological variables on potential richness of all TER-S riparian-associated species in stream reaches at Fort Bliss, NM. Results are from using a Gaussian GLM regression to model species richness as a function of the ecohydrological variables. Ecohydrological variables were derived from data collected during or previous to 2012. Potential species richness was derived by stacking GAP animal habitat distribution models downloaded on or before October 2014. Input variables were standardized so estimates are one the same scale; relative effect size was calculated by converting the estimates to a percentage.

Parameter	*Effect Size*	*Relative Effect Size*	*SE*	95% Confidence Interval		*Relative Importance*
				Lower	*Upper*	
3m Width	-1.12	26.1	0.06	-1.12	-1.11	1.00
Elevation	-0.63	14.7	0.07	-0.63	-0.63	1.00
Percent Cover	0.41	9.7	0.12	0.41	0.42	1.00
Landcover_var	-0.38	8.9	0.04	-0.38	-0.38	1.00
LiDAR 0.5-1	0.28	6.7	0.09	0.28	0.29	0.94
Veg_Ind Mean	-0.27	6.3	0.08	-0.27	-0.27	0.64
W_Area	-0.26	6.1	0.05	-0.26	-0.26	1.00
Tsp25	0.26	6.0	0.05	0.26	0.26	1.00
RSI	0.20	4.7	0.04	0.20	0.20	1.00
LiDAR 1-4	-0.20	4.7	0.07	-0.21	-0.20	0.38
Slope	0.14	3.4	0.05	0.14	0.15	0.32
FP	0.11	2.6	0.04	0.11	0.11	0.52

Groups including riparian-associated amphibian species

Models were available for 9 of the riparian-associated amphibians at Fort Bliss. Stream reaches could potentially provide habitat for a mean of 5.6 riparian associated amphibians (*s* = 1.0, range = 1.8 – 7.4). Sixty-seven percent (n = 6) of the riparian-associated amphibians were riparian-obligate. Stream reaches could potentially provide habitat for a mean of 3.7 riparian-obligate amphibians (*s* = 0.8, range = 1.2 – 5.0). None of the riparian-associated species were TER-S amphibians.

Species with any level of riparian-association

For the Amphibian RA species group, there were two competing models. The strongest effects (Table 4) were negative responses to increasing elevation, riparian width, entrenchment, slope, percent cover of vegetation from 0.5-4 meters, and land cover variety. Only rainfall seasonality, mean vegetation index, and total stream power for the 25-year storm had positive effects, but the effect of these three variables on richness was small compared to the variables with negative effects.

Table 4. Effect of ecohydrological variables on potential richness of riparian-associated amphibians in stream reaches at Fort Bliss, NM. Results are from using a Gaussian GLM regression to model species richness as a function of the ecohydrological variables. Ecohydrological variables were derived from data collected during or previous to 2012. Potential species richness was derived by stacking GAP animal habitat distribution models downloaded on or before October 2014. Input variables were standardized so estimates are one the same scale; relative effect size was calculated by converting the estimates to a percentage.

Parameter	*Estimate*	*Relative Effect Size*	*SE*	95% Confidence Interval		*Relative Importance*
				Lower	*Upper*	
Elevation	-1.00	24.4	0.05	-1.00	-1.00	1.00
3m Width	-0.85	20.8	0.05	-0.86	-0.85	1.00
ER 0.5/2	-0.41	10.1	0.05	-0.41	-0.41	1.00
Slope	-0.40	9.7	0.05	-0.40	-0.40	1.00
LiDAR 1-4	-0.36	8.7	0.06	-0.36	-0.35	0.98
LiDAR 0.5-1	-0.34	8.3	0.06	-0.34	-0.34	1.00
Landcover_var	-0.28	6.9	0.04	-0.28	-0.28	1.00
RSI	0.14	3.3	0.04	0.13	0.14	0.97
Veg_Ind Mean	0.11	2.7	0.04	0.11	0.11	0.48
Tsp25	0.11	2.6	0.04	0.10	0.11	0.33
W_Area	-0.10	2.5	0.04	-0.11	-0.10	0.61

Obligate riparian-associated species

For the Amphibian Obligate RA species group, there were two competing models. Many of the variables had the same effect on obligate species richness (Table 5) as they did on general species richness, but elevation decreased in greatly in relative effect size (24.4% to 8.1%). Elevation and riparian width changed from decreasing species richness to increasing it. The relative effect size of the 0.5-1m vegetation approximately doubled. The effect of watershed area and LiDAR 1-4m were not used in the model for obligate amphibians, while LiDAR 4-12m, 25-year peak flow, and the presence of vegetation >12m all had a negative effect on obligate amphibian richness that was not found for riparian-associated amphibian richness.

Table 5. Effect of ecohydrological variables on potential richness of obligate riparian-associated amphibians in stream reaches at Fort Bliss, NM. Results are from using a Gaussian GLM regression to model species richness as a function of the ecohydrological variables. Ecohydrological variables were derived from data collected during or previous to 2012. Potential species richness was derived by stacking GAP animal habitat distribution models downloaded on or before October 2014. Input variables were standardized so estimates are one the same scale; relative effect size was calculated by converting the estimates to a percentage.

Parameter	*Estimate*	*Relative Effect Size*	*SE*	95% Confidence Interval		*Relative Importance*
				Lower	*Upper*	
3m Width	0.61	18.0	0.04	0.61	0.61	1.00
LiDAR 0.5-1	-0.55	16.3	0.04	-0.56	-0.55	1.00
Slope	-0.38	11.2	0.07	-0.38	-0.38	1.00
LiDAR 4-12	-0.31	9.1	0.03	-0.31	-0.31	1.00
Elevation	0.28	8.1	0.03	0.27	0.28	1.00
LiDAR >12Y - N	0.24	6.9	0.06	0.23	0.24	0.47
Landcover_var	-0.21	6.3	0.03	-0.22	-0.21	1.00
Qp25	-0.21	6.2	0.04	-0.21	-0.21	0.51
Tsp25	0.19	5.7	0.04	0.19	0.20	0.49
ER 0.5/2	-0.16	4.8	0.03	-0.17	-0.16	0.59
Veg_Ind Mean	0.14	4.0	0.03	0.13	0.14	0.87
RSI	0.11	3.3	0.03	0.11	0.11	0.87

Groups including riparian-associated reptile species

Models were available for 42 of the riparian-associated reptiles at Fort Bliss. Stream reaches could potentially provide habitat for a mean of 29.5 riparian associated reptiles (s = 3.1, range = 14.4 - 34.9). Thirty-one percent (n = 13) of the riparian-associated reptiles were riparian-obligate. Stream reaches could potentially provide habitat for a mean of 7.1 riparian-obligate reptiles (s = 0.7, range = 3.8 – 8.0). Seventeen percent (n = 6) of the riparian-associated reptiles were TER-S species. Stream reaches could potentially provide habitat for a mean of 2.3 TER-S reptiles (s = 0.4, range = 0.3 – 3.1).

Species with any level of riparian-association

For the Reptile RA species group, there was only one top model. The strongest effects by far (Table 6) were the negative ones of riparian width and elevation. These effects were trailed by negative effects of the vegetation layers from 0.5-12 m and land cover variety. The strongest positive effect was that of slope, followed by the entrenchment ratio, rainfall seasonality, and percent cover.

Table 6. Effect of ecohydrological variables on potential richness of riparian-associated reptiles in stream reaches at Fort Bliss, NM. Results are from using a Gaussian GLM regression to model species richness as a function of the ecohydrological variables. Ecohydrological variables were derived from data collected during or previous to 2012. Potential species richness was derived by stacking GAP animal habitat distribution models downloaded on or before October 2014. Input variables were standardized so estimates are one the same scale; relative effect size was calculated by converting the estimates to a percentage.

Parameter	*Estimate*	*Relative Effect Size*	*SE*	95% Confidence Interval *Lower*	95% Confidence Interval *Upper*	*Relative Importance*
1m Width	-3.04	22.2	0.19	-3.05	-3.03	1.00
Elevation	-3.00	22.0	0.16	-3.00	-2.99	1.00
LiDAR 0.5-1	-1.46	10.7	0.20	-1.46	-1.45	1.00
Landcover_var	-1.39	10.2	0.11	-1.40	-1.39	1.00
LiDAR 4-12	-1.20	8.8	0.17	-1.21	-1.19	1.00
LiDAR 1-4	-1.14	8.3	0.25	-1.15	-1.13	1.00
Slope	0.95	6.9	0.14	0.94	0.95	1.00
ER 1/3	0.56	4.1	0.14	0.55	0.56	0.94
RSI	0.49	3.6	0.11	0.48	0.49	1.00
Percent Cover	0.44	3.2	0.14	0.44	0.45	0.72

Obligate riparian-associated species

For the Reptile Obligate RA species group, there were three competing models. Again, nearly all of the same variables were important for obligate species (Table 7) as were important for the general riparian-associated reptiles. All had the same direction and similar importance relative to the RA group, except for LiDAR 1-4m, which increased its influence relative to other variables for riparian-obligate reptiles, and LiDAR 4-12m, which decreased its influence. One new variable was added for the obligate group – Shannon diversity of LiDAR vegetation structure, which had a small but negative effect.

Table 7. Effect of ecohydrological variables on potential richness of obligate riparian-associated reptiles in stream reaches at Fort Bliss, NM. Results are from using a Gaussian GLM regression to model species richness as a function of the ecohydrological variables. Ecohydrological variables were derived from data collected during or previous to 2012. Potential species richness was derived by stacking GAP animal habitat distribution models downloaded on or before October 2014. Input variables were standardized so estimates are one the same scale; relative effect size was calculated by converting the estimates to a percentage.

		Relative		95% Confidence Interval		
Parameter	*Estimate*	*Effect Size*	*SE*	*Lower*	*Upper*	*Relative Importance*
1m Width	-0.65	21.4	0.04	-0.66	-0.65	1.00
Elevation	-0.56	18.2	0.04	-0.56	-0.56	1.00
LiDAR 1-4	-0.42	13.7	0.08	-0.42	-0.41	1.00
LiDAR 0.5-1	-0.27	8.8	0.07	-0.27	-0.27	1.00
Slope	0.26	8.5	0.04	0.26	0.26	1.00
Landcover_var	-0.25	8.1	0.03	-0.25	-0.25	1.00
Percent Cover	0.15	5.0	0.04	0.15	0.16	0.98
ER 1/3	0.15	4.9	0.03	0.15	0.15	0.97
LiDAR 4-12	-0.14	4.5	0.04	-0.14	-0.14	0.65
Shannon_LiDAR	-0.13	4.1	0.04	-0.13	-0.13	0.62
RSI	0.08	2.8	0.03	0.08	0.09	0.50

Riparian-associated TER-S

For the Reptile TER-S RA species group, there were five competing models. The variables associated with high species richness for TER-S reptiles (Table 8) were quite different from those associated with all riparian-associated reptiles. The influence of elevation, one of the strongest effects for riparian-associated reptile richness, dominated the TER-S reptile richness. Riparian width changed from 1m to 3m, but decreased tremendously in its effect size. RSI dropped from the models, while mean vegetation index (-), flow permanence (+), peak flow (+), and the Shannon index for vertical structure (+) were added. Many variables changed the direction of their effect. LiDAR 0.5-1m, LiDAR 1-4m, LiDAR 4-12m, and land cover variety all switched from a negative to a positive effect on richness; LiDAR 0.5-1m was still one of the most influential variables, while land cover variety moved from being one of the larger effect sizes to one of the smallest. Entrenchment ratio changed from the 1m/3m ratio to the 0.5m/2m ratio and from a positive to a negative effect. Slope also changed from a positive to a negative effect.

Table 8. Effect of ecohydrological variables on potential richness of TER-S riparian-associated reptiles in stream reaches at Fort Bliss, NM. Results are from using a Gaussian GLM regression to model species richness as a function of the ecohydrological variables. Ecohydrological variables were derived from data collected during or previous to 2012. Potential species richness was derived by stacking GAP animal habitat distribution models downloaded on or before October 2014. Input variables were standardized so estimates are one the same scale; relative effect size was calculated by converting the estimates to a percentage.

Parameter	*Effect Size*	*Relative Effect Size*	*SE*	95% Confidence Interval		*Relative Importance*
				Lower	*Upper*	
Elevation	-0.67	44.7	0.02	-0.67	-0.67	1.00
LiDAR 0.5-1	0.20	13.1	0.02	0.19	0.20	1.00
LiDAR 4-12	0.14	9.1	0.02	0.14	0.14	1.00
Veg_Ind Mean	-0.10	7.0	0.02	-0.10	-0.10	1.00
ER 0.5/2	-0.10	6.5	0.02	-0.10	-0.10	1.00
3m Width	-0.06	4.3	0.02	-0.07	-0.06	0.99
LiDAR 1-4	0.04	3.0	0.03	0.04	0.05	0.27
Percent Cover	0.04	2.7	0.02	0.04	0.04	0.21
Shannon_lidar	0.03	2.1	0.01	0.03	0.03	0.55
Landcover_var	0.03	2.1	0.01	0.03	0.03	0.69
Slope	-0.03	1.9	0.02	-0.03	-0.03	0.37
Qp25	0.03	1.8	0.01	0.03	0.03	0.63
FP	0.03	1.8	0.01	0.03	0.03	0.64

Groups including riparian-associated mammal species

Models were available for 37 of the riparian-associated mammals at Fort Bliss. Stream reaches could potentially provide habitat for a mean of 25.3 riparian associated mammals (*s* =

1.9, range = 10.4 – 32.3). Forty-nine percent (n = 18) of the riparian-associated mammals were riparian-obligate. Stream reaches could potentially provide habitat for a mean of 11.1 riparian-obligate mammals (*s* = 0.7, range = 6.1 – 14.7). Twenty-four percent (n = 9) of the riparian-associated mammals were TER-S species. Stream reaches could potentially provide habitat for a mean of 6.1 TER-S mammals (*s* = 0.5, range = 3.1 – 7.0).

Species with any level of riparian-association

For the Mammal RA species group, there were seven competing models. The strongest effects were a negative effect of riparian width (1m) and mean vegetation index, and positive effects of percent cover, elevation, and LiDAR 4-12 m (Table 9). Also included were watershed area (-) and RSI (+).

Table 9. Effect of ecohydrological variables on potential richness of riparian-associated mammals in stream reaches at Fort Bliss, NM. Results are from using a Gaussian GLM regression to model species richness as a function of the ecohydrological variables. Ecohydrological variables were derived from data collected during or previous to 2012. Potential species richness was derived by stacking GAP animal habitat distribution models downloaded on or before October 2014. Input variables were standardized so estimates are one the same scale; relative effect size was calculated by converting the estimates to a percentage.

Parameter	*Estimate*	*Relative Effect Size*	*SE*	95% Confidence Interval		*Relative Importance*
				Lower	*Upper*	
1m Width	-1.23	18.0	0.09	-1.23	-1.22	1.00
Veg_Ind Mean	-0.93	13.6	0.16	-0.94	-0.93	1.00
Percent Cover	0.92	13.4	0.15	0.91	0.92	1.00
Elevation	0.84	12.4	0.10	0.84	0.85	1.00
LiDAR 4-12	0.68	10.0	0.10	0.68	0.69	1.00
W_Area	-0.44	6.4	0.08	-0.44	-0.43	1.00
RSI	0.39	5.8	0.07	0.39	0.40	1.00
Tsp25	0.30	4.4	0.08	0.30	0.31	0.93
Landcover_var	-0.23	3.3	0.08	-0.23	-0.22	0.91
LiDAR >12Y - N	-0.19	2.8	0.17	-0.20	-0.19	0.09
LiDAR 1-4	0.18	2.6	0.12	0.17	0.19	0.13
Slope	0.15	2.2	0.09	0.15	0.16	0.25
FP	0.12	1.8	0.07	0.12	0.12	0.20
ER 0.5/2	0.12	1.7	0.08	0.11	0.12	0.13
Shannon_LiDAR	0.11	1.6	0.09	0.10	0.11	0.09

Obligate riparian-associated species

For the Obligate Mammal RA species group, there were six competing models. Most of the same variables were important for obligate species (Table 10) in a similar manner as they were for all riparian-associated species, but the importance of vegetation >12m disappeared, the relative effect size of the riparian width (1m) dropped dramatically from largest for riparian-

associated mammals to second-to-last for riparian-obligate mammals. The relative effect size of LiDAR 1-4 (+) increased from 2.6% for riparian-associated mammals to 12.4% for riparian-obligate mammals. Additionally, both entrenchment ratio and elevation became negative influences on richness rather than positive. Elevation also decreased greatly in importance.

Table 10. Effect of ecohydrological variables on potential richness of obligate riparian-associated mammals in stream reaches at Fort Bliss, NM. Results are from using a Gaussian GLM regression to model species richness as a function of the ecohydrological variables. Ecohydrological variables were derived from data collected during or previous to 2012. Potential species richness was derived by stacking GAP animal habitat distribution models downloaded on or before October 2014. Input variables were standardized so estimates are one the same scale; relative effect size was calculated by converting the estimates to a percentage.

Parameter	*Estimate*	*Relative Effect Size*	*SE*	95% Confidence Interval		*Relative Importance*
				Lower	*Upper*	
LiDAR 4-12	0.34	15.1	0.04	0.33	0.34	1.00
Percent Cover	0.30	13.6	0.06	0.30	0.31	1.00
Veg_Ind Mean	-0.30	13.4	0.06	-0.30	-0.29	1.00
LiDAR 1-4	0.28	12.4	0.05	0.27	0.28	1.00
W_Area	-0.22	9.9	0.03	-0.22	-0.22	1.00
Landcover_var	0.22	9.7	0.03	0.21	0.22	1.00
Slope	0.14	6.1	0.04	0.13	0.14	0.84
ER 0.5/2	-0.10	4.6	0.04	-0.11	-0.10	0.70
RSI	0.10	4.6	0.03	0.10	0.10	0.99
Elevation	-0.07	2.9	0.04	-0.07	-0.06	0.34
Shannon_LiDAR	0.05	2.4	0.04	0.05	0.05	0.15
Tsp25	0.05	2.0	0.03	0.04	0.05	0.22
1m Width	-0.04	1.8	0.03	-0.04	-0.04	0.27
FP	0.03	1.4	0.03	0.03	0.03	0.09

Riparian-associated TER-S

For the Mammal TER-S RA species group, there was only one top model. Several variables had the same effect as for the general riparian-associated group, including entrenchment ratio, slope, and watershed area, though the last decreased in effect size (Table 11). While percent cover decreased in effect size, it and elevation remained the two top positive influences on richness for mammalian TER-S species. No new variables were used, but five were dropped: mean vegetation index, LiDAR >12, the Shannon index, flow permanence, and RSI. As for the All and Reptile TERS RA groups, riparian width switched from the 1m to the 3m flooded depth. It also became a positive rather than a negative effect. LiDAR 1-4m and LiDAR 4-12m switched from positive to negative effects on richness, and the 1-4m variable substantially increased its effect size, going from being the twelfth largest to the second largest.

Table 11. Effect of ecohydrological variables on potential richness of riparian-associated TER-S mammals in stream reaches at Fort Bliss, NM. Results are from using a Gaussian GLM regression to model species richness as a function of the ecohydrological variables. Ecohydrological variables were derived from data collected during or previous to 2012. Potential species richness was derived by stacking GAP animal habitat distribution models downloaded on or before October 2014. Input variables were standardized so estimates are one the same scale; relative effect size was calculated by converting the estimates to a percentage.

Parameter	*Effect Size*	*Relative Effect Size*	*SE*	95% Confidence Interval		*Relative Importance*
				Lower	*Upper*	
3m Width	-0.60	32.7	0.02	-0.60	-0.60	1.00
LiDAR 1-4	-0.34	18.4	0.03	-0.34	-0.33	1.00
Elevation	0.28	15.1	0.02	0.28	0.28	1.00
Landcover_var	-0.14	7.6	0.02	-0.14	-0.14	1.00
Percent Cover	0.10	5.7	0.02	0.10	0.10	1.00
Tsp25	0.09	5.0	0.02	0.09	0.09	1.00
Slope	0.08	4.5	0.02	0.08	0.08	0.97
LiDAR 4-12	-0.08	4.3	0.02	-0.08	-0.08	0.91
ER 0.5/2	0.07	3.6	0.02	0.06	0.07	0.84
W_Area	-0.06	3.1	0.02	-0.06	-0.06	0.78

Groups including all riparian-associated bird species

Models were available for 100 of the riparian-associated birds at Fort Bliss. Stream reaches could potentially provide habitat for a mean of 30.1 riparian associated birds (*s* = 3.3, range = 10.4 – 42.7). Sixty-two percent (n = 62) of the riparian-associated birds were riparian-obligate. Stream reaches could potentially provide habitat for a mean of 11.1 riparian-obligate birds (*s* = 2.1, range = 3.2 – 21.2). Twenty-seven percent (n = 27) of the riparian-associated birds were TER-S species. Stream reaches could potentially provide habitat for a mean of 5.4 TER-S birds (*s* = 0.7, range = 1.1 – 8.6).

Species with any level of riparian-association

For the All Bird RA species group, there was only one top model. The strongest effects were percent cover (+), riparian width (3m, -), and elevation (+, Table 12). Also quite influential were mean vegetation index (-), watershed area (-), LiDAR 4-12 (+), and RSI (+). The smallest positive effects included LiDAR 0.5-1, land cover variety, and total stream power.

Table 12. Effect of ecohydrological variables on potential richness of riparian-associated birds in stream reaches at Fort Bliss, NM. Results are from using a Gaussian GLM regression to model species richness as a function of the ecohydrological variables. Ecohydrological variables were derived from data collected during or previous to 2012. Potential species richness was derived by stacking GAP animal habitat distribution models downloaded on or before October 2014. Input variables were standardized so estimates are one the same scale; relative effect size was calculated by converting the estimates to a percentage.

Parameter	*Estimate*	*Relative Effect Size*	*SE*	95% Confidence Interval		*Relative Importance*
				Lower	*Upper*	
Percent Cover	1.79	15.9	0.25	1.78	1.80	1.00
3m Width	-1.74	15.5	0.16	-1.75	-1.73	1.00
Elevation	1.64	14.6	0.16	1.63	1.64	1.00
Veg_Ind Mean	-1.20	10.7	0.24	-1.22	-1.19	1.00
W_Area	-1.18	10.5	0.13	-1.19	-1.18	1.00
LiDAR 4-12	1.03	9.2	0.14	1.03	1.04	1.00
RSI	0.98	8.7	0.11	0.97	0.98	1.00
LiDAR 0.5-1	0.61	5.4	0.15	0.60	0.62	0.65
Landcover_var	0.57	5.1	0.12	0.56	0.57	1.00
Tsp25	0.50	4.4	0.12	0.49	0.50	0.81

Obligate riparian-associated species

For the Obligate Bird RA species group, there were two competing models. Very similar ecohydrological characteristics seem to be associated with riparian-obligate bird richness (Table 13) as were associated with riparian-associated bird richness. All the variables used for the overall group were retained for the obligate subset, and one variable LiDAR 1-4 (+) with a moderate effect size was added. The effect of land cover variety did get quite a bit larger, while elevation became much smaller. The effect of watershed area, vegetation index, and percent cover also decreased, though percent cover remained the positive influence with the largest effect size.

Table 13. Effect of ecohydrological variables on potential richness of obligate riparian-associated birds in stream reaches at Fort Bliss, NM. Results are from using a Gaussian GLM regression to model species richness as a function of the ecohydrological variables. Ecohydrological variables were derived from data collected during or previous to 2012. Potential species richness was derived by stacking GAP animal habitat distribution models downloaded on or before October 2014. Input variables were standardized so estimates are one the same scale; relative effect size was calculated by converting the estimates to a percentage.

Parameter	*Estimate*	*Relative Effect Size*	*SE*	95% Confidence Interval		*Relative Importance*
				Lower	*Upper*	
3m Width	-1.31	16.7	0.12	-1.31	-1.30	1.00
Percent Cover	0.93	11.9	0.15	0.92	0.93	1.00
LiDAR 4-12	0.92	11.7	0.13	0.91	0.92	1.00
Landcover_var	0.91	11.6	0.08	0.90	0.91	1.00
LiDAR 0.5-1	0.66	8.5	0.19	0.65	0.67	0.98
RSI	0.64	8.1	0.07	0.63	0.64	1.00
W_Area	-0.61	7.8	0.08	-0.61	-0.61	1.00
Veg_Ind Mean	-0.57	7.3	0.14	-0.57	-0.56	0.95
LiDAR 1-4	0.56	7.1	0.14	0.55	0.56	0.46
Elevation	0.36	4.7	0.09	0.36	0.37	0.44
Tsp25	0.36	4.6	0.08	0.35	0.36	0.91

Riparian-associated TER-S

For the All Bird TER-S RA species group, there was only one top model. The effects of riparian width, percent cover, and watershed area on the TER-S subset (Table 14) were very similar to their effects on all riparian-associate birds. Two new variables with small but positive effects were added, flow permanence and slope, while mean vegetation index and LiDAR 4-12 were dropped. The effect of two variables flipped from positive to negative for TER-S; land cover variety, which increased in effect size from 5.1% to 12.6%, and elevation, which about halved in relative effect size.

Table 14. Effect of ecohydrological variables on potential richness of riparian-associated TER-S birds in stream reaches at Fort Bliss, NM. Results are from using a Gaussian GLM regression to model species richness as a function of the ecohydrological variables. Ecohydrological variables were derived from data collected during or previous to 2012. Potential species richness was derived by stacking GAP animal habitat distribution models downloaded on or before October 2014. Input variables were standardized so estimates are one the same scale; relative effect size was calculated by converting the estimates to a percentage.

Parameter	*Effect Size*	*Relative Effect Size*	*SE*	95% Confidence Interval		*Relative Importance*
				Lower	*Upper*	
3m Width	-0.37	19.5	0.04	-0.38	-0.37	1.00
Landcover_var	-0.24	12.6	0.03	-0.24	-0.24	1.00
Percent Cover	0.22	11.5	0.04	0.22	0.22	1.00
W_Area	-0.21	11.0	0.03	-0.21	-0.21	1.00
RSI	0.20	10.5	0.03	0.20	0.20	1.00
LiDAR 0.5-1	0.17	8.9	0.04	0.17	0.17	0.98
Elevation	-0.15	8.0	0.04	-0.15	-0.15	0.99
Slope	0.13	7.0	0.04	0.13	0.14	0.95
Tsp25	0.12	6.3	0.03	0.12	0.12	0.95
FP	0.09	4.7	0.03	0.09	0.09	0.86

Groups including riparian-associated summering bird species

Models were available for 42 of the riparian-associated summering birds at Fort Bliss. Stream reaches could potentially provide habitat for a mean of 9.5 riparian associated summering birds (s = 1.4, range = 3.1 – 17.1). Sixty-seven percent (n = 28) of the riparian-associated summering birds were riparian-obligate. Stream reaches could potentially provide habitat for a mean of 3.5 riparian-obligate summering birds (s = 1.0, range = 0.2 – 8.3).

Species with any level of riparian-association

For the Summering Bird RA species group, there were two competing models. The strongest effects were positive ones of elevation, LiDAR 4-12 m, and percent cover (Table 15). Mean vegetation index had a fairly large negative effect. Also important were riparian width (-), land cover variety (+), RSI (+), and watershed area (-). Other variables with a smaller effect size or variable importance that helped predict richness of this group were absence of vegetation >12m (-), entrenchment ratio, (+), and slope (+).

Table 15. Effect of ecohydrological variables on potential richness of riparian-associated birds summering in stream reaches at Fort Bliss, NM. Results are from using a Gaussian GLM regression to model species richness as a function of the ecohydrological variables. Ecohydrological variables were derived from data collected during or previous to 2012. Potential species richness was derived by stacking GAP animal habitat distribution models downloaded on or before October 2014. Input variables were standardized so estimates are one the same scale; relative effect size was calculated by converting the estimates to a percentage.

Parameter	*Estimate*	*Relative Effect Size*	*SE*	95% Confidence Interval		*Relative Importance*
				Lower	*Upper*	
Elevation	1.01	18.1	0.07	1.00	1.01	1.00
LiDAR 4-12	0.83	14.8	0.06	0.82	0.83	1.00
Percent Cover	0.78	14.0	0.11	0.78	0.79	1.00
Veg_Ind Mean	-0.64	11.6	0.11	-0.65	-0.64	1.00
1m Width	-0.47	8.4	0.07	-0.47	-0.47	1.00
Landcover_var	0.41	7.3	0.05	0.40	0.41	1.00
RSI	0.39	6.9	0.05	0.38	0.39	1.00
W_Area	-0.34	6.1	0.05	-0.34	-0.34	0.98
LiDAR >12Y - N	-0.30	5.4	0.12	-0.30	-0.29	0.57
Slope	0.21	3.7	0.06	0.20	0.21	0.29
ER 0.5/2	0.20	3.6	0.05	0.20	0.20	0.73

Obligate riparian-associated species

For the Obligate Summering Bird RA species group, there were seven competing models. Ten of the eleven variables that were important for all riparian-associated summering birds were also important for the subset of obligate species; the presence of >12m tall vegetation was dropped (Table 16). However, the riparian width changed from the narrower 1m flooded depth to the wider 3m flooded depth. The effect of percent cover and LiDAR 4-12m decreased moderately, and the effect of mean vegetation index decreased more. Three new variables were helpful in predicting riparian-obligate species richness, all with negative effects: Shannon diversity of vegetation structure, LiDAR 0.5-1m, and 25-year peak flow. The latter two variables, along with the vegetation index mean, had lower relative importance than most other variables, though.

Table 16. Effect of ecohydrological variables on potential richness of obligate riparian-associated birds summering in stream reaches at Fort Bliss, NM. Results are from using a Gaussian GLM regression to model species richness as a function of the ecohydrological variables. Ecohydrological variables were derived from data collected during or previous to 2012. Potential species richness was derived by stacking GAP animal habitat distribution models downloaded on or before October 2014. Input variables were standardized so estimates are one the same scale; relative effect size was calculated by converting the estimates to a percentage.

Parameter	*Estimate*	*Relative Effect Size*	*SE*	95% Confidence Interval		*Relative Importance*
				Lower	*Upper*	
Elevation	0.70	21.1	0.05	0.70	0.70	1.00
Landcover_var	0.43	13.0	0.04	0.43	0.44	1.00
3m Width	-0.36	10.7	0.05	-0.36	-0.35	1.00
Percent Cover	0.31	9.3	0.08	0.31	0.31	1.00
RSI	0.29	8.8	0.04	0.29	0.30	1.00
LiDAR 4-12	0.27	8.1	0.05	0.27	0.27	1.00
W_Area	-0.21	6.2	0.04	-0.21	-0.20	0.93
Shannon_LiDAR	-0.14	4.4	0.04	-0.15	-0.14	0.77
Veg_Ind Mean	-0.14	4.2	0.08	-0.14	-0.14	0.20
LiDAR 0.5-1	-0.14	4.1	0.07	-0.14	-0.13	0.29
ER 0.5/2	0.13	4.0	0.05	0.13	0.14	0.68
Slope	0.12	3.5	0.05	0.11	0.12	0.54
Qp25	-0.08	2.6	0.05	-0.09	-0.08	0.20

Groups including riparian-associated wintering bird species

Models were available for 31 of the riparian-associated wintering birds at Fort Bliss. Stream reaches could potentially provide habitat for a mean of 7.6 riparian associated wintering birds (s = 1.0, range = 2.1 – 13.3). Fifty-five percent (n = 17) of the riparian-associated wintering birds were riparian-obligate. Stream reaches could potentially provide habitat for a mean of 2.0 riparian-obligate wintering birds (s = 0.8, range = 0.9 – 6.2).

Species with any level of riparian-association

For the Wintering Bird RA species group, there was only one top model. The largest effects were RSI (+), riparian width (3m, -), and elevation (+, Table 17). Moderate effect sizes were found for watershed area (-), LiDAR 0.5-1 (+), LiDAR 1-4 (-), and total stream power (+). Percent cover, entrenchment ratio, and land cover variety had less strong, but positive, effects.

Table 17. Effect of ecohydrological variables on potential richness of riparian-associated birds wintering in stream reaches at Fort Bliss, NM. Results are from using a Gaussian GLM regression to model species richness as a function of the ecohydrological variables. Ecohydrological variables were derived from data collected during or previous to 2012. Potential species richness was derived by stacking GAP animal habitat distribution models downloaded on or before October 2014. Input variables were standardized so estimates are one the same scale; relative effect size was calculated by converting the estimates to a percentage.

Parameter	*Estimate*	*Relative Effect Size*	*SE*	95% Confidence Interval		*Relative Importance*
				Lower	*Upper*	
RSI	0.57	16.5	0.04	0.57	0.57	1.00
3m Width	-0.56	16.1	0.05	-0.56	-0.56	1.00
Elevation	0.50	14.5	0.05	0.50	0.50	1.00
W_Area	-0.39	11.1	0.04	-0.39	-0.38	1.00
LiDAR 0.5-1	0.36	10.2	0.06	0.35	0.36	1.00
LiDAR 1-4	-0.34	9.8	0.06	-0.34	-0.34	1.00
Tsp25	0.33	9.4	0.04	0.32	0.33	1.00
Percent Cover	0.18	5.3	0.05	0.18	0.19	0.85
ER 0.5/2	0.14	4.0	0.05	0.14	0.14	0.73
Landcover_var	0.10	3.0	0.04	0.10	0.11	0.74

Obligate riparian-associated species

For the Obligate Wintering Bird RA species group, there were two competing models. The predictors for the riparian-obligate subset of birds (Table 18) were very different than for riparian-associated wintering birds. Elevation switched from being positively associated with richness to being negatively associated and the second strongest effect overall. The effect of the entrenchment ratio also switched from positive to negative, but it had the smallest effect size of all the variables used to predict obligate richness. The five variables used for both riparian-associated wintering birds and the riparian-obligate subset all changed their effect sizes; riparian width, watershed area, and RSI all decreased, while LiDAR 0.5-1 and land cover variety increased substantially. Percent cover, total stream power, and the negative effect of LiDAR 1-4 all dropped from the models. Four new variables were important for riparian-obligate species – LiDAR 4-12m (+), with the third greatest effect size of all variables, peak flow (+), flow permanence (+), and Shannon diversity of vegetation structure (+).

Table 18. Effect of ecohydrological variables on potential richness of obligate riparian-associated birds wintering in stream reaches at Fort Bliss, NM. Results are from using a Gaussian GLM regression to model species richness as a function of the ecohydrological variables. Ecohydrological variables were derived from data collected during or previous to 2012. Potential species richness was derived by stacking GAP animal habitat distribution models downloaded on or before October 2014. Input variables were standardized so estimates are one the same scale; relative effect size was calculated by converting the estimates to a percentage.

Parameter	*Estimate*	*Relative Effect Size*	*SE*	95% Confidence Interval		*Relative Importance*
				Lower	*Upper*	
LiDAR 0.5-1	0.59	18.2	0.05	0.58	0.59	1.00
Elevation	-0.56	17.4	0.04	-0.56	-0.56	1.00
LiDAR 4-12	0.50	15.6	0.04	0.50	0.51	1.00
Landcover_var	0.38	11.8	0.03	0.38	0.38	1.00
RSI	0.29	9.1	0.03	0.29	0.30	1.00
3m Width	-0.26	8.0	0.04	-0.26	-0.26	1.00
W_Area	-0.17	5.4	0.04	-0.17	-0.17	0.95
Qp25	0.17	5.2	0.04	0.17	0.17	0.93
FP	0.12	3.8	0.03	0.12	0.12	1.00
Shannon_LiDAR	0.09	2.8	0.04	0.09	0.09	0.41
ER 0.5/2	-0.08	2.6	0.04	-0.09	-0.08	0.33

Groups including riparian-associated year-round bird species

Models were available for 27 of the riparian-associated year-round birds at Fort Bliss. Stream reaches could potentially provide habitat for a mean of 13.0 riparian associated year-round birds (s = 1.2, range = 5.1 – 17.0). Seventy-nine percent (n = 21) of the riparian-associated year-round birds were riparian-obligate. Stream reaches could potentially provide habitat for a mean of 5.7 riparian-obligate year-round birds (s = 0.9, range = 1.1 – 9.2).

Species with any level of riparian-association

For the Year-round Bird RA species group, there were two competing models. The strongest effects were percent cover (+), riparian width (3m, -), and mean vegetation index (-, Table 19). Moderate effects were found for LiDAR 1-4 (+), watershed area (-), the absence of vegetation >12m (-), and LiDAR 4-12 (+). Total stream power, Shannon structural diversity, land cover variety, and flow permanence had smaller positive effects on species richness.

Table 19. Effect of ecohydrological variables on potential richness of riparian-associated birds found year-round in stream reaches at Fort Bliss, NM. Results are from using a Gaussian GLM regression to model species richness as a function of the ecohydrological variables. Ecohydrological variables were derived from data collected during or previous to 2012. Potential species richness was derived by stacking GAP animal habitat distribution models downloaded on or before October 2014. Input variables were standardized so estimates are one the same scale; relative effect size was calculated by converting the estimates to a percentage.

Parameter	*Estimate*	*Relative Effect Size*	*SE*	95% Confidence Interval		*Relative Importance*
				Lower	*Upper*	
Percent Cover	0.93	20.5	0.10	0.93	0.94	1.00
3m Width	-0.77	16.8	0.06	-0.77	-0.76	1.00
Veg_Ind Mean	-0.69	15.2	0.10	-0.70	-0.69	1.00
LiDAR 1-4	0.49	10.7	0.09	0.48	0.49	0.99
W_Area	-0.46	10.1	0.05	-0.46	-0.46	1.00
LiDAR >12Y - N	-0.41	9.0	0.12	-0.41	-0.40	0.98
LiDAR 4-12	0.27	6.0	0.07	0.27	0.28	0.99
Tsp25	0.17	3.8	0.06	0.17	0.17	0.82
Shannon_LiDAR	0.13	2.8	0.07	0.12	0.13	0.38
Landcover_var	0.12	2.7	0.05	0.12	0.13	0.57
FP	0.11	2.4	0.05	0.11	0.11	0.49

Obligate riparian-associated species

For the Obligate Year-round Bird RA species group, there were two competing models. The effect of the ecohydrological variables was overall very similar to that for the general year-round bird group, but the effect of the Shannon index and LiDAR 4-12m disappeared (Table 20). Two new variables were added to the models, slope and elevation, with positive but relatively small effect sizes.

Table 20. Effect of ecohydrological variables on potential richness of obligate riparian-associated birds found year-round in stream reaches at Fort Bliss, NM. Results are from using a Gaussian GLM regression to model species richness as a function of the ecohydrological variables. Ecohydrological variables were derived from data collected during or previous to 2012. Potential species richness was derived by stacking GAP animal habitat distribution models downloaded on or before October 2014. Input variables were standardized so estimates are one the same scale; relative effect size was calculated by converting the estimates to a percentage.

Parameter	*Estimate*	*Relative Effect Size*	*SE*	95% Confidence Interval		*Relative Importance*
				Lower	*Upper*	
Percent Cover	0.64	19.4	0.07	0.64	0.65	1.00
3m Width	-0.60	18.0	0.04	-0.60	-0.59	1.00
Veg_Ind Mean	-0.56	16.9	0.07	-0.56	-0.56	1.00
LiDAR 1-4	0.42	12.6	0.05	0.42	0.42	1.00
W_Area	-0.27	8.2	0.04	-0.27	-0.27	1.00
LiDAR >12Y - N	-0.19	5.8	0.07	-0.20	-0.19	0.47
Elevation	0.16	4.8	0.04	0.16	0.16	0.89
Tsp25	0.14	4.1	0.04	0.13	0.14	0.91
Landcover_var	0.13	4.0	0.03	0.13	0.13	0.93
Slope	0.13	4.0	0.04	0.13	0.13	0.67
FP	0.08	2.3	0.03	0.07	0.08	0.33

Riparian-associated passage migrant bird species

Stream reaches could potentially provide habitat for a mean of 2.3 riparian associated passage migrant bird species (s = 0.8, range = 0.6 – 5.0).

For the Passage Migrant Bird RA species group, there were six competing models. The strongest effect by far was a positive influence of elevation (Table 21). Also with relatively large effects, LiDAR 0.5-1m (-), mean vegetation index (+), LiDAR 1-4m (-), and LiDAR 4-12m (-), were used in the models. Entrenchment ratio (+), peak flow (-), the Shannon index (-), and total stream power (+) had weak effects, but relative importance close to that of the stronger contributing variables. Absence of vegetation >12m (+), percent cover (-), land cover variety (-), riparian width (3m, -), and flow permanence (-) had the least effect and lowest relative importance of the variables in the top models of riparian-associated passage migrant species richness.

Table 21. Effect of ecohydrological variables on potential richness of riparian-associated passage migrant birds in stream reaches at Fort Bliss, NM. Results are from using a Gaussian GLM regression to model species richness as a function of the ecohydrological variables. Ecohydrological variables were derived from data collected during or previous to 2012. Potential species richness was derived by stacking GAP animal habitat distribution models downloaded on or before October 2014. Input variables were standardized so estimates are one the same scale; relative effect size was calculated by converting the estimates to a percentage.

Parameter	*Estimate*	*Relative Effect Size*	*SE*	95% Confidence Interval		*Relative Importance*
				Lower	*Upper*	
Elevation	1.38	39.4	0.04	1.38	1.39	1.00
LiDAR 0.5-1	-0.33	9.4	0.05	-0.33	-0.33	1.00
Veg_Ind Mean	0.33	9.3	0.04	0.33	0.33	1.00
LiDAR 1-4	-0.30	8.6	0.07	-0.30	-0.30	1.00
LiDAR 4-12	-0.27	7.6	0.05	-0.27	-0.26	1.00
ER 0.5/2	0.19	5.3	0.04	0.18	0.19	1.00
Qp25	-0.15	4.2	0.04	-0.15	-0.15	0.93
Shannon_LiDAR	-0.13	3.7	0.04	-0.13	-0.13	0.96
Tsp25	0.11	3.2	0.04	0.11	0.12	0.86
LiDAR >12Y - N	0.10	3.0	0.07	0.10	0.11	0.18
Percent Cover	-0.08	2.3	0.06	-0.08	-0.08	0.13
Landcover_var	-0.05	1.5	0.03	-0.05	-0.05	0.28
3m Width	-0.05	1.4	0.04	-0.05	-0.05	0.14
FP	-0.04	1.1	0.03	-0.04	-0.04	0.13

Comparison of variables for TER-S groups

The species richness of the three TER-S groups - birds, mammals, and reptiles – were all affected by riparian width (3m flooded depth), land cover variety, percent cover, elevation, and

slope. Riparian width had a negative effect on all TER-S groups. It was the most important variable for both mammals and birds, while it was not as important for reptiles (Figure 3). Land cover variety was the second-most important variable for bird TER-S richness, while it was less important for mammals, and had a negative effect on both groups. It had a positive but very small effect on reptile TER-S richness. Elevation was the strongest variable for reptiles, with a moderate effect on birds. It had a negative influence on both groups, while it had a positive effect on mammals, where it was also the third largest effect. Percent cover had a positive effect on richness of all three TER-S groups, with relatively large effects on mammals and birds, and a small effect on reptiles. Slope had a positive effect on mammal and bird richness, while for reptiles it was negative, but it was the variable with the smallest effect size. When a variable was in the models for all three groups, it generally had a similar effect on mammals and birds, and an opposite effect on reptiles.

Both mammal and bird TER-S richness responded to watershed area and total stream power negatively. Both mammal and reptile richness responded to LiDAR 1-4m, LiDAR 4-12m, and the entrenchment ratio, but with opposite effects for all three variables. Bird and reptile richness were both associated positively with LiDAR 0.5-1m and flow permanence. Only bird TER-S richness was associated with the rainfall seasonality index (RSI). Only reptile TER-S richness was associated with peak flow, the vegetation index mean, and the Shannon vegetation structural diversity index.

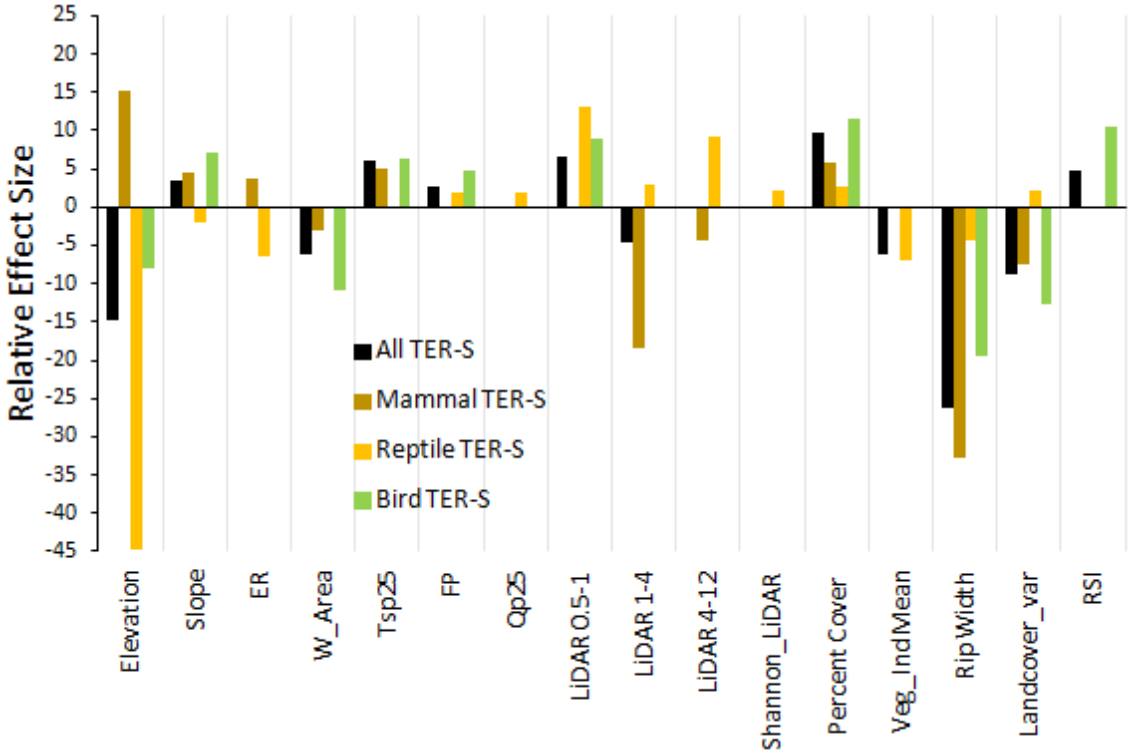


Figure 3. Comparison of relative effect size of ecohydrological variables in Gaussian GLM regression models of potential species richness of several TER-S groups in stream reaches at Fort Bliss, NM. Ecohydrological variables were derived from data collected during or previous to 2012. Potential species richness was derived by stacking GAP animal habitat distribution models

downloaded on or before October 2014. Input variables were standardized so estimates are one the same scale; relative effect size was calculated by converting the estimates to a percentage.

Summering birds versus WINTERING birds

Summering bird richness had some similarities and some differences from wintering bird species richness in its response to the input variables. The patterns across seasonality also changed some when considering species with any level of riparian-association ("all"), or just obligate riparian-associated species ("obligate"). The difference in response of summering versus wintering species richness of "all" birds and only "obligate" birds was similar for riparian width (all -), watershed area (all -), rainfall seasonality (all +), and land cover variety (all +). For both the "all" and "obligate" groups, only summering birds responded negatively to mean vegetation index and positively to slope. The presence of vegetation >12m (-), which was important for "all" summering birds, was not important for "obligate" summering birds. LiDAR 4-12m (+) had a strong effect for "all" summering birds, while for "obligate" birds, it had a very strong effect on wintering birds also. LiDAR 1-4m (-) and TSP25 (+) were used to model "all" wintering bird richness, but were not used for "obligate" wintering birds, which added an effect of flow permanence (+). For "all" birds, both summering and wintering species responded positively to percent cover, while for "obligate" birds, only summering birds responded to percent cover, still positively. Conversely, for "all" birds, only wintering species responded positively to LiDAR 0.5-1m, while for "obligate" birds summering birds also responded to low vegetation, but in the opposite direction (-). Two variables were used in models for both "all" and "obligate" groups in both summering and wintering subsets, but changed from having the same effect for both seasons to opposite effects. Elevation and the entrenchment ratio had a positive effect in both seasons for the "all" group, while for the "obligate" group, their effect remained the same for summering birds, but became negative for wintering birds. Two variables that were not important for either seasonality of "all" birds became important for both seasonalities of "obligate" species richness – peak flow and the Shannon structural diversity index, which both had a negative effect for summering birds and a positive effect for wintering birds.

General observations

I made several other interesting observations about the species richness results. Looking at all species, subsets of taxa, subsets of vulnerability, subsets of seasonality, and subsets of riparian-association level resulted in 21 sets of species whose richness was modeled as a function of the input variables. Three variables always had the same effect direction when they were included in models. Total stream power, included in 15 sets, and rainfall seasonality index, included in 16 sets, always had a positive effect on species richness. Watershed area, included in 16 sets, always had a negative effect on richness.

Several variables had the same effect direction for almost all 21 sets of species, but differed for one or a few sets. Riparian width, which was included for all 21 sets of species, had a positive effect only for riparian-obligate amphibian richness; for all others it was negative. Similarly, mean vegetation index was included for 15 sets of species, but had a positive effect only for 3 sets – passage migrant birds and both riparian-associated and riparian-obligate amphibians. Conversely, percent cover was included for 18 sets, but had a negative effect only on passage migrant birds. Slope was included for 13 sets, but had a negative effect only on

reptiles and both riparian-associated and riparian-obligate amphibians. Flow permanence was included for 10 sets, but was negative only for passage migrant birds, where it also had a very small effect size.

Three other variables had effect directions typically weighted in one direction, but with the opposite effect on the richness of a third of the sets in which they were included. Entrenchment ratio, which typically had a positive effect on the richness of the 15 sets it was included for, had a negative effect on TER-S reptiles, riparian-obligate mammals, riparian-obligate wintering birds, and both riparian-associated and riparian-obligate amphibians. LiDAR 4-12m, which typically had a positive effect on the richness of the 15 sets it was included for, had a negative effect on passage migrant birds, TER-S mammals, riparian-obligate amphibians, and both riparian-associated and riparian-obligate reptiles. The presence of vegetation >12m, which typically had a negative effect on the richness of the 6 sets it was included for, had a positive effect on passage migrant birds and riparian-obligate amphibians.

When I examined the average effect size of the input variables across all 21 sets of species, an interesting trend emerged. The variables that were most commonly included in modeling also tended to have the largest effect size (Figure 4). Land cover variety is an exception to this. It was included in all 21 sets, but had only a moderate average effect size. Riparian width, land cover variety, elevation, percent cover, and vegetation index mean were the five most frequently used variables.

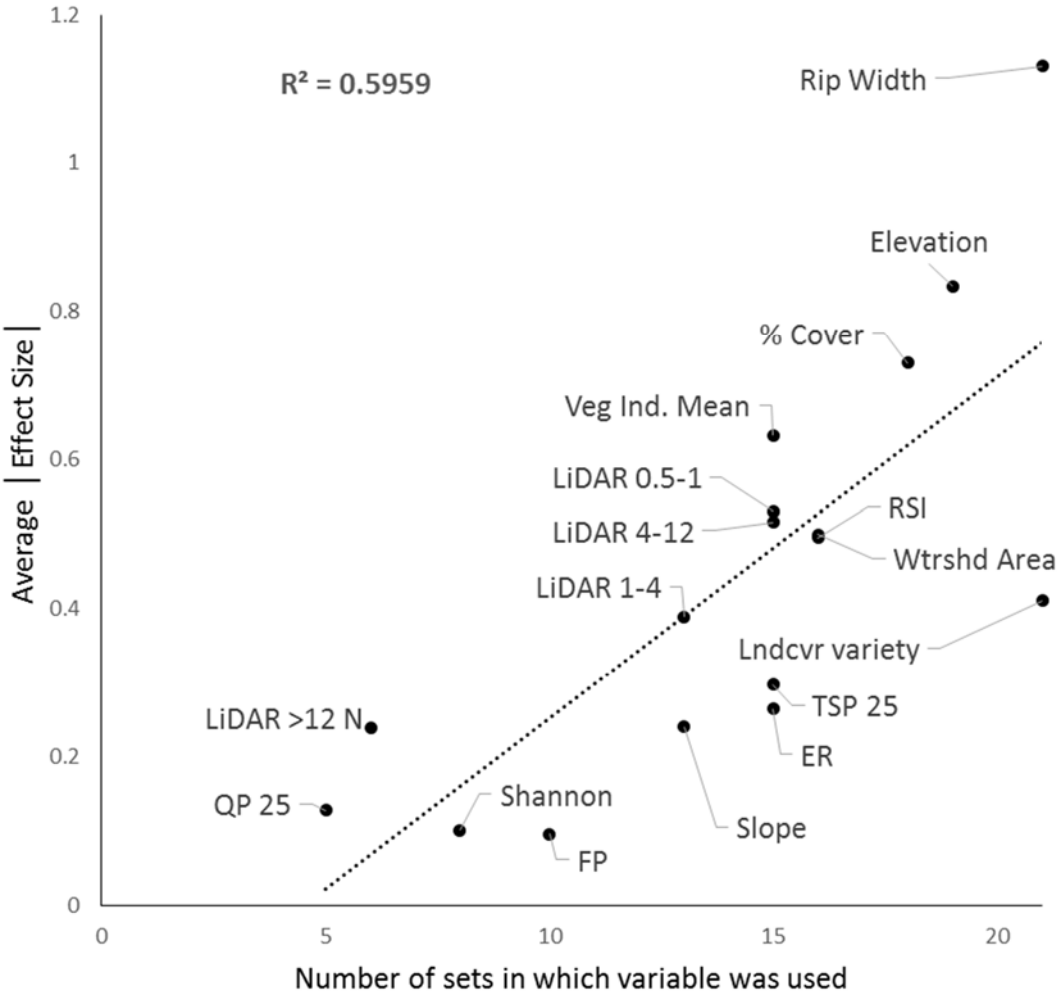


Figure 4. Plot of the average of the relative effect sizes of ecohydrological variables used to model potential species richness of 21 species groups in stream reaches at Fort Bliss, NM versus the number of groups in which the variable was used for modeling.

Spatial distribution of richness

I describe the distribution of species richness of the various groups below. Maps of species richness are provided in Appendix B. For all stream reaches, richness is indicated by color, with green reaches having the lowest richness and red the highest richness. Specifically, dark green reaches have a value less than 1.5 standard deviations (SD) below the mean value for the group, medium green reaches are 1-1.5 SD below the mean, yellow-green are 0.5-1 SD below the mean, yellow are within 0.5 SD of the mean, orange are between 0.5-1 SD above the mean, medium red are 1-1.5 SD above the mean, and dark red are >1.5 SD above the mean. Figure 5 provides a key to the areas described in the text.

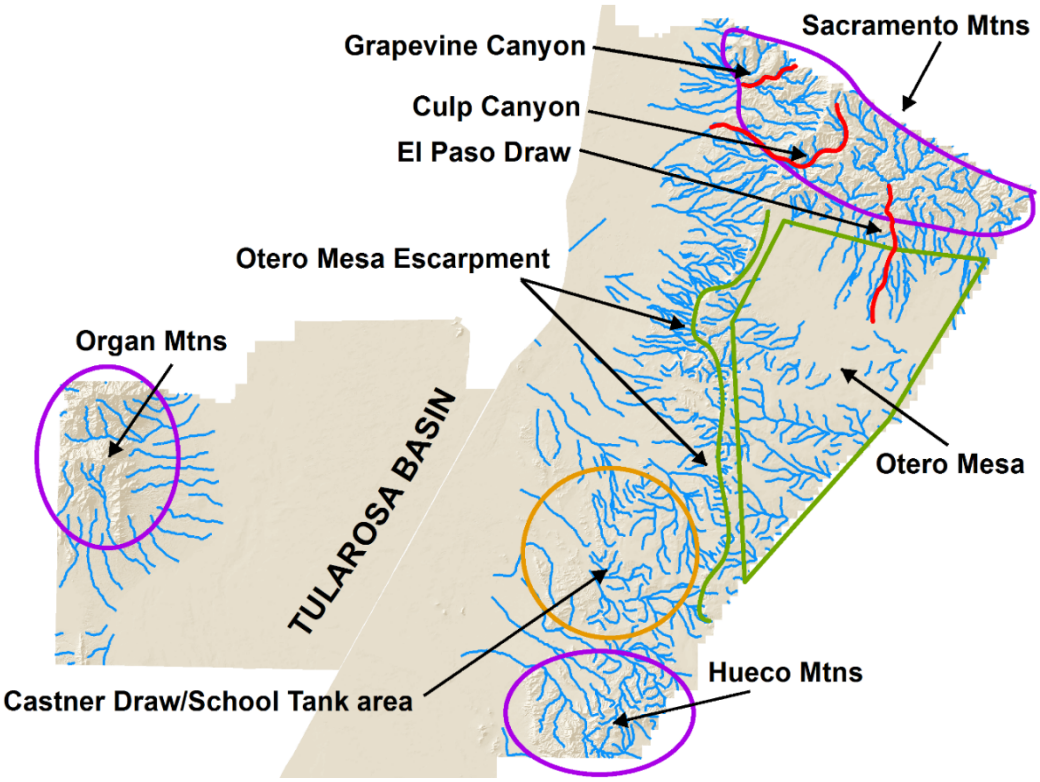


Figure 5. Map of the areas of the Fort Bliss, NM used in describing the distribution of potential species richness in stream reaches. Richness was derived by stacking GAP animal habitat distribution models downloaded on or before October 2014.

The distribution of species richness across stream reaches at Fort Bliss varies by group. When all taxa were grouped, the most species rich areas were in the Organ Mountains, Hueco Mountains, the Castner Draw/School Tank area, and the Grapevine and Culp Canyons area (Appendix B, Figure 1). The escarpment of Otero Mesa was also relatively rich, while Otero Mesa itself was of average richness. The Sacramento Mountains had average to below average richness, while the Tularosa Basin had the lowest richness. When just riparian-obligate species were considered, the Organ Mountains, western Sacramento Mountains (Culp Canyon area), and the Castner Draw/School Tank area became even more species rich relative to other areas (Appendix B, Figure 2). Most of the escarpment of the mesa became average to below average. For all taxa grouped, richness of TER-S species was highest in the Grapevine and Culp Canyons area, the Organ Mountains, parts of the Hueco Mountains, and the escarpment of Otero Mesa (Appendix B, Figure 3). Parts of the Sacramento Mountains and the Castner Draw/School Tank area were also high in habitat for TER-S species, while Otero Mesa and the Tularosa Basin had habitat for the fewest species.

For amphibians, the escarpment of Otero Mesa was a particularly species-rich area (Appendix B, Figure 4). The Hueco and southern Organ Mountains were also rich areas, while the northern Organ Mountains and the Sacramento Mountains had very low potential for amphibian richness. Otero Mesa was intermediate to a bit higher in richness. When just riparian-obligate amphibians were considered, the distribution of richness changed some (Appendix B,

Figure 5). Species richness concentrated in the Otero Mesa and Castner Draw/School tank area, while other areas had relatively lower potential for amphibian richness.

For summering birds, a relatively simple pattern emerged (Appendix B, Figure 6). The Organ Mountains, Sacramento Mountains, and a small area near Castner Draw/School Tank were very species rich. Otero Mesa, its escarpment, and the Hueco Mountains had average richness, while streams closest to the Tularosa Basin had below-average richness. When just riparian-obligate species were considered, the pattern remained about the same, except for increases in richness for the Hueco Mountains and the area just off the southwestern edge of Otero Mesa (Appendix B, Figure 7).

For wintering bird species potential richness was highest in the Organ Mountains, Hueco Mountains, Castner Draw/School Tank area, and parts of the Sacramento Mountains (Appendix B, Figure 8). Richness was lowest in the Tularosa Basin and on Otero Mesa. When just riparian-obligate wintering birds were considered, richness was still highest in the Organ Mountains, but it was also quite high on the escarpment and increased to average to above-average in the Tularosa Basin (Appendix B, Figure 9). Richness decreased relatively on Otero Mesa, much of the Hueco Mountains, and in parts of the Castner Draw/School Tank area.

For year-round resident bird species, richness was highest in all of the Sacramento Mountains, Grapevine Canyon, the northern Organ Mountains, and the Castner Draw/School Tank area (Appendix B, Figure 10). It was also higher than average in the Hueco Mountains. Otero Mesa and the Tularosa Basin were average to below-average. The pattern for just riparian-obligate resident birds remained very similar to that found for all riparian-associated resident birds (Appendix B, Figure 11).

When all seasonalities of birds were considered as a group, the distribution of richness was very similar to the distribution for just year-round resident birds (Appendix B, Figure 12). This pattern also held for just the riparian-obligate subset (Appendix B, Figure 13). When just TER-S species were considered, the pattern shifted somewhat (Appendix B, Figure 14). The Organ Mountains, Grapevine Canyon area, and short stretches of streams on the Otero Mesa escarpment became the most species-rich areas. The rest of the Sacramento Mountains, the Hueco Mountains, the Castner Draw/School Tank area, and the northern part of Otero Mesa also had above average richness. Some stream reaches near the Tularosa Basin increased to near-average richness.

For mammals, the streams with habitat for the most species were concentrated in the Sacramento and Organ mountains (Appendix B, Figure 15). Some hot spots were also scattered along the escarpment, in the Castner Draw/School Tank area, and in the Hueco Mountains. Most stream reaches on the installation had about average richness for mammals, with the exception of streams closest to Tularosa Basin, which had much lower richness. When just riparian-obligate mammals were considered, the distribution of richness became much more varied (Appendix B, Figure 16). When just TER-S species were considered, the most species rich areas were the middle- to lower-elevation areas of the Sacramento Mountains, the escarpment of Otero Mesa, the Hueco and Organ Mountains, and a few reaches in the Castner Draw/School Tank area (Appendix B, Figure 17).

Reptiles displayed a pattern very different from that of other taxa, with the most species rich streams located in the Castner Draw/School Tank area, the escarpment of Otero Mesa, the Hueco Mountains, and lower-order streams of the Organ Mountains (Appendix B, Figure 18). The Grapevine and Culp Canyons area also had above-average richness. Many streams had average richness, but the Sacramento Mountains and Tularosa Basin had the lowest richness.

When just riparian-obligate reptiles were considered, the pattern remained the same as for all riparian-associated reptiles, but differences became more pronounced (Appendix B, Figure 19). The pattern for the subset of TER-S reptiles was quite different than for other reptile groups. Streams draining the Otero Mesa escarpment, in the Tularosa Basin, and the lowest streams of the Dona Ana range had much higher-than-average richness (Appendix B, Figure 20). A few slightly higher elevation streams and scattered streams in other areas had average richness, while the rest of the installation had below average richness.

The distribution of richness for passage migrant birds was unique (Appendix B, Figure 21). Much of the installation had above-average richness, with particularly high richness in small areas of the Organ and Sacramento Mountains, as well as the El Paso Draw area of Otero Mesa. Streams draining off of the escarpment and into Tularosa Basin had well-below-average richness.

When only the richness of the TER-S species subsets were considered, mammals and birds, as well as all TER-S grouped, showed similar distributions of species richness, while reptiles followed a distinctly different pattern.

Discussion

Ecohydrological variables

In terms of frequency of use and average effect size, the most important variables related to species richness of stream reaches were riparian width, land cover variety, elevation, percent cover, and vegetation index mean.

Riparian width had a negative effect on richness of all groups except for riparian-obligate amphibians. This relationship seems counterintuitive; wider riparian zones might be expected to host more species because they have more area for a variety of niches. The only study I found on how this variable affects species richness was by Hardy et al. (2004), who found a positive effect of riparian width on summering birds. Shaw and Cooper (2008) found that increased channel width best explained saturation frequency of channel deposits. Because of the way riparian width was calculated in this study, streams with wider channels generally have greater riparian widths. Since saturation frequency could be expected to have a positive effect on richness, my result is still opposite from what would be expected. Because streams with greater riparian widths in this study generally have wider channels, riparian width is not a reliable indicator of the amount of riparian vegetation. In fact, correlation between percent cover or the LiDAR variables and the riparian widths ranges from -0.20 to -0.57. In particular, streams with very wide channels may have little vegetation. The lack of a direct relationship between riparian width and the amount of riparian vegetation is the most likely reason that I found the opposite relationship between riparian width and species richness that has been found previously and would be expected.

Riparian width may also have shown this relationship to richness because of its relationship with other factors. Narrower riparian zones tend to occur in smaller watersheds; in all the models watershed area was included in, richness was higher in smaller watersheds. Similarly, narrower riparian zones almost always occur at higher elevation, which has a positive effect on richness of some groups. My results also indicate that a 3m flooded width is generally a good choice for delineating the riparian zone.

In the literature, measures of horizontal vegetation structure, such as land cover variety, generally have a positive effect on species richness (Tews et al. 2004). I found this to be the case

for only about half of the groups of species I examined. This was true for most of the bird groups, except the TER-S subset. It was also true for the riparian-obligate mammals, the all riparian-obligate species subset, and the TER-S reptiles. My results are in line with those of Culbert et al. (2013), who found that land cover diversity measures had a positive relationship with forest and shrubland bird richness. Generally, amphibians and reptiles responded negatively to increased land cover variety. This could be due to the fact that, in this semi-arid setting, stream reaches with greater landcover variety include more non-riparian vegetation that hosts fewer species. This would be particularly true for amphibians, which require more moisture.

Elevation had the second greatest average effect size and was used for modeling richness of 19/21 subsets. Boone and Krohn (2000) used range-maps to evaluate species richness patterns in Maine and found that climate explained a substantial proportion of the variation in richness for all four taxa. Elevation is the primary determinant of climate on Fort Bliss, so my results mesh well with these previous findings. This variable generally had a positive effect on bird richness, except for riparian-obligate wintering birds, which supports previous findings in the Southwest that higher elevation is positively associated with bird richness (Mcfarland et al. 2012). Mammal richness tended to behave like bird richness, but switched to a negative response to elevation when just the riparian-obligate species were considered. Elevation had a negative effect on reptile and amphibian richness, except for the riparian-obligate amphibian subset. This is consistent with studies of riparian areas in the Southwest that found herpetofauna richness to be highest in environments common in lower elevations. Jones (1988) found that mesquite bosque environments, a type not found at higher elevations, were the vegetation type richest in amphibians, turtles, and snakes. In the Huachuca Mountains of southeastern Arizona, Morrison et al. (1995) found that herpetofauna richness was highest in pinyon-oak-juniper and oak-juniper environments, typically found in the mid- to lower-elevation reaches of the canyons they studied.

Percent cover was included in models for many groups, and had a positive relationship with species richness for all subsets but passage migrant birds. This generally positive relationship is as expected, because more area with vegetation should provide more niches for different species. Percent cover has been found to be important to breeding birds (Shanahan et al. 2011) in xeroriparian areas, but information for other groups is lacking.

The vegetation index used here was Red-Edge NDVI, which is more appropriate for drylands than the typical NDVI measure reported in most research because it was designed for use in locations with bright soil background and high percentages of bare ground. It can be interpreted to represent the density of vegetation. Unexpectedly, it had a negative relationship with richness for most groups; it was only positive for passage migrant birds and amphibians. Since Mean Vegetation Index was only calculated from pixels classified as vegetation, this result combined with the percent cover results would suggest that most species prefer stream reaches with higher percent cover of vegetation, but sparse vegetation where it occurs, a seemingly contradictory situation. Pixels containing only ground cover or grasses were not included in the mean vegetation index calculation, which may have contributed to this result. However, desert vegetation tends to have small leaves, which means there is ground visible through the plant to the satellite. It seems reasonable that mean vegetation index is an indirect measure of the plant community present in a stream reach. Certain plant species or communities with less dense canopies may provide habitat for more vertebrate species, while migrant birds key in on dense vegetation when selecting stopover sites. Dense vegetation might provide habitat for more amphibian species because it creates cooler and wetter microclimate for animals that lose water

more easily. Other studies of birds have not found NDVI measures to add much information to models (Goetz et al. 2007, Mcfarland et al. 2012).

Another variable included in modeling for most sets of species was Watershed Area, with a negative effect on richness for all groups. To my knowledge, only Ekness and Randhir's (2007) similar study looked at watershed area and species richness. In agreement with my findings, they found that headwaters and lower order subwatersheds had higher levels of species diversity compared to higher order subwatersheds. The relationship of watershed area to species richness may be driven by the effect watershed area has on vegetation properties. Ephemeral stream networks in Arizona show predictable changes in vegetation as watershed area increases (Warren and Anderson 1985, Shaw and Cooper 2008). Obligate riparian taxa increase in relative abundance, moisture availability increases, and shrub and tree species become more structurally important. However, in contrast with my findings and those of Ekness and Randhir (2007), these attributes would tend to increase vertebrate species richness. Perhaps there is a more complex pattern, such as a peak at mid-sized watersheds, that my modeling approach was not able to capture, or an interaction with another variable that caused this counter-intuitive result.

Rainfall seasonality and total stream power had positive effects on richness of many groups, which has not been reported for xeroriparian systems to my knowledge. These are interesting results that warrant further study.

The LiDAR structure variables were moderately important based on their frequency of use and effect size. The most consistent relationship of LiDAR structure with richness was for the 4-12m layer, which had a positive effect on most of the bird and mammal groups and a negative effect on reptile, amphibian, and passage migrant bird groups. The 0.5-1m and 1-4m layers had roughly the same effects. Most studies that used LiDAR or vertical structure measures to predict species richness have been confined to birds. One older study of other taxa by Vale et al. (1989) found that most feeding guilds of mammals, reptiles, and amphibians were positively associated with more complex vegetation structure. Their study did not separate by taxa and compared vegetation across the entire western U.S., not just streams in one region. Jakle and Gatz (1985) attributed the high herpetofauna richness of the mesquite bosque portion of their study area to its well-developed herbaceous and shrub layer. A multitude of studies have found that bird species richness increases as vegetation volume of measures of vertical structure increase (e.g. MacArthur and MacArthur 1961, Kirkpatrick et al. 2007, Culbert et al. 2013, Goetz et al. 2014). Overall, my results for birds are congruent with previous studies, with the exception of the negative response of passage migrants to all LiDAR variables. The results for other taxa are harder to verify.

The entrenchment ratio was a moderately important variable that was included in about three-quarters of the modeled groups. It had a variable effect, usually positive. No previous studies have examined this variable, but more entrenched streams may provide habitat for more species because of their cooler, shadier microclimate and banks that can be used for burrows. Of the six ratios tested, the 0.5m/2m ratio explained richness the best for most groups.

Flow permanence could be expected to be quite an important variable for species richness, but was only used for about half of the groups, usually with one of the smallest effect sizes. However, it was positive for almost all these groups. In general, flow permanence was very low ($\mu = 2.35\%$, $s = 4.34\%$), which may explain why it was not a very important variable. Two studies have used variables related to this one. The presence of surface water was not found to influence bird richness along higher-order streams in southeastern Arizona (Kirkpatrick et al. 2007), while dominant tree species did influence bird richness in lower-order streams in the same

region (Strong and Bock 1990). Dominant tree species is influenced by flow permanence; this study found richness to be highest in cottonwood plots, which require the greatest flow permanence, concurring with my findings.

The three least-used variables were peak flow, the presence of vegetation >12m, and the Shannon structural diversity measure. While it is rarely used, the LiDAR >12m binomial variable did have a moderate effect size for riparian-obligate amphibians (presence of vegetation >12m decreased richness) and riparian-associated year-round birds (presence of vegetation >12m increased richness). I expected the Shannon diversity index to be a more important variable and a positive influence for all groups, but for all the groups it was used for, it had the smallest or one of the smallest effect sizes. It was sometimes positive, but nearly as often negative. Interestingly, the models that included the Shannon index always had at least one LiDAR variable that was among the larger effect sizes of all variables in the model. This suggests that just as LiDAR data have been shown to be more effective than older, less detailed, vegetation metrics, LiDAR information from different vegetation layers is more effective than a summary structural diversity statistic. In fact, all 21 sets of species included at least one, and more often two to three, of the LIDAR structure layer variables.

In summary, species richness appears to be most correlated with physical and vegetation variables, but hydrologic variables, in particular total stream power, are also important. When including all riparian-associated species, all four taxa respond in the same way to several variables. Birds and mammals, endothermic species, tend to have similar patterns as each other and opposite from reptiles and amphibians, ectothermic species. When just riparian-obligate subsets of species are considered, the alliances are blurred somewhat.

Some of my results on the effect of ecohydrological variables on species richness agree with previous work. Others disagree or have little relevant previous work to be compared to. This disagreement could indicate some of my findings based on the GAP data are spurious, but could just as well mean that patterns are different for streams in this region. The areas of disagreement and the new findings I report can be used as a guide for management and future research, but should be corroborated with field work.

Riparian-obligate subsets

Creating models for just the subset of riparian-associated species that were more dependent on the riparian zone, the riparian-obligates, did not change the results substantially with the exception of the wintering birds group. Most of the same variables were included in both sets of models, typically with similar relative effect sizes and directions.

The variables whose effects changed the most were elevation and the LiDAR variables. Elevation was particularly unstable between the riparian-associated group and the riparian-obligate subset. For all taxa groups except reptiles, it changed the direction of its effect, disappeared for riparian-obligates, or decreased in importance. The 4-12m LiDAR layer was added to models of riparian-obligate richness for all groups that did not use it for their corresponding riparian-associated group, except for year-round birds. Half of the groups showed changes in the effect of the 1-4m layer, which was either dropped, added, or increased in importance for riparian-obligates. The Shannon structural diversity index derived from the LiDAR data was used more often for the riparian-obligate subsets. Curiously, the effect size of percent cover decreased or actually disappeared for the four bird groups, though it increased for reptiles.

The hydrological variables were more important for the riparian-obligate subset than the riparian-associated groups, as might be expected for species tied more closely to the stream zones. Flow permanence was added to models of all species richness and wintering bird richness. Peak flow, which was only used in the passage migrant bird models of riparian-associated species richness, was added for three taxa groups: amphibians, summering birds, and wintering birds.

Shifts in the effect of two variables caused their relationships with richness to behave more like I would have expected based on previous studies. Entrenchment ratio, which had a positive association with richness of all riparian-associated groups but amphibians, had a negative association with mammals and wintering birds also when just riparian-obligates were considered. Land cover variety, a factor generally expected to increase species richness, but which I found had a positive association with only the bird riparian-associated groups, also had a positive association with mammal richness when just riparian-obligates were considered.

Overall, since results are generally similar and more information about hydrological variables is added when just riparian-obligates are considered, it is probably more useful to restrict studies of riparian-zone species richness to this more limited group.

TER-S subsets

Since most management activities focus on TER-S species, it is important to know whether these species have the same relationship with the ecohydrological attributes of stream reaches. While taxa groups of TER-S species show some similarities to their corresponding riparian-associated and riparian-obligate groups, they are quite different overall. Reptile and mammal TER-S richness tend to react in opposing directions to the ecohydrological variables, while bird richness parallels mammal richness about half the time and reptile richness about half the time. Because of their different responses to the ecohydrological variables and their different spatial distribution of richness, examining TER-S species independently from larger species groups is important to understand their richness in xeroriparian zones.

Utility of GAP data for species richness in xeroriparian zones

Though they have been verified with existing data and expert opinions, GAP species distribution models are based on wildlife habitat relationships with land cover, not directly on field surveys. Land cover itself tends to have an accuracy >60% (Boykin et al. 2010). The habitat models are also at a relatively coarse scale of 30x30 meter pixels. As such, they are intended for use at the landscape scale (areas the size of square km). The average size of the stream reaches in this study was 0.17 km^2, with a total stream reach area of 332 km^2. This is probably near the limit of how small an area can be studied with these models. In general though, I found ecohydrological variables had relationships with species richness that often corresponded to what has been reported in the literature. I also was able to report some undescribed relationships for ecohydrological attributes of xeroriparian areas.

When GAP species distribution models were used to derive species lists for national parks in Utah, accuracy was lowest for amphibians (69%) and reptiles (78%) and highest for birds (91%) and mammals (84%; Edwards et al. 1996). Commission error rates were greater than omission error rates, which is probably desirable for planning conservation, as it would be better to plan for a species not present than to fail to consider a species that was actually there. Based

on these results, my findings for birds and mammals are more likely to be accurate than my findings for reptiles and amphibians. Despite the shortcomings of GAP distribution models, they are a tool that makes it possible to examine patterns of species richness across much broader areas and groups of taxa than would be possible with field surveys. This can be done with considerably less cost, time, and effort. GAP models also represent a significant improvement over the use of coarser range maps for these types of studies. These results should be used with some caution and ideally verified by field work, but they serve as a good starting point for management, planning of field surveys, and hypothesis generation.

BIRD NEST HEIGHT

The availability of LiDAR data about the structure of vegetation in ephemeral streams across Fort Bliss made available information about vegetation structure that would normally require extensive field work to collect. Vegetation structure is one of the most important factors in defining nesting habitat for birds. Each species has a preference for where it nests within the vegetation structure layers. I have attempted to create a metric for each stream reach that indicates how "valuable" it is as bird nesting habitat. Kozma and Mathews (1995) and Myers et al. (1998) collected data on bird use of "arroyo-riparian" areas in a focused area of Fort Bliss from 1993-1997 (Figure 6). They used mist-netting and point-counts to survey birds within the riparian zone and in the adjacent uplands. Observational data on bird occurrence was collected from 1 May – 9 June, 1993; 3 May – 15 June, 1994; 6 May – 16 June, 1995; 29 April – 16 June 1996; and 2 May – 6 June 1997. Searches for nests were performed in 1996 and 1997. This data set allowed me to ground-truth the nesting-habitat metric.

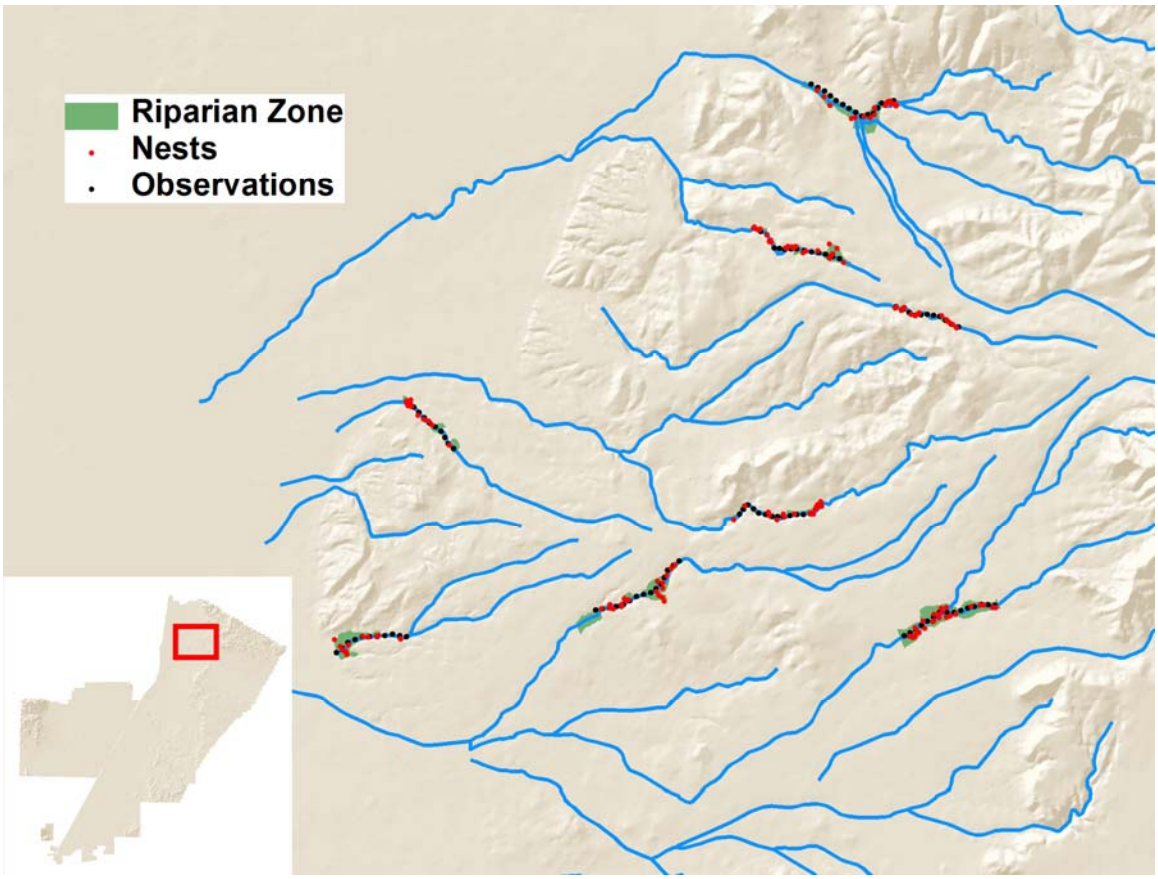


Figure 6. Map of the location of data collected by Kozma and Mathews (1995) and Myers et al. (1998) on breeding birds in arroyo-riparian areas of Fort Bliss, NM from 1993-1997. Riparian zone indicates the extent of the 3-m flooded depth polygons used in the SERDP project to derive ecohydrological variables.

Methods

I narrowed the riparian-associated bird list developed for the species richness analysis to species that had distribution models with summer or year-round habitat on or very near Fort Bliss (Appendix A, Table 1). I eliminated four species from this list that had a small amount of their GAP distribution models present on or near the installation, but had never been observed on the installation based on the INRMP (U.S. Army 2001) and the online eBird database (Sullivan et al. 2009, eBird 2014). I also added eight species to the list that I had not categorized as riparian-associated, but which Kozma and Mathews (1995) and Myers et al. (1998) found to be.

Based on the description of their nest site requirements from Birds of North America Online (Poole 2014), I gave each species a score for each vegetation structure layer: a two (2) indicated the species preferred to nest in that layer and a one (1) indicated that they sometimes used that layer but it was just outside their strongest preference. For a few species with little information on nesting habitat, I also consulted the Biota Information System of New Mexico (BISON-M 2013). I calculated the number of species using each layer as the sum of all species scores for the layer, divided by two (Appendix A, Table 3). Since not all species are found everywhere, I also used the habitat descriptions from BNA to note whether the species would be found in the lowlands, foothills, or mountains of Fort Bliss; I calculated subscores for the number of species using each layer in each of these three broad categories. I also calculated subscores for the subset of birds that were TER-S species.

Because tall vegetation at Fort Bliss usually has shorter vegetation beneath it and it was important not to miss the availability of the lower layers for nesting, I calculated the percent cover of vegetation in each structure layer (C_i) as the percent cover of that layer in each stream reach plus the percent cover of all higher layers:

$C_{0.5\text{-}1}$ = veg05_1m + veg 1_4m + veg4_12m + veg12m
$C_{1\text{-}4}$ = veg 1_4m + veg4_12m + veg12m
$C_{4\text{-}12}$ = veg4_12m + veg12m
$C_{>12}$ = veg12m

I combined the information on number of species (N_i) using each structure layer and the percent cover of each structure layer (C_i) in stream reaches to create a metric (nh_a) for each stream reach that indicates how "valuable" it is as bird nesting habitat:

$$nh_a = N_{0.5\text{-}1}*C_{0.5\text{-}1} + N_{1\text{-}4}*C_{1\text{-}4} + N_{4\text{-}12}*C_{4\text{-}12} + N_{>12}*C_{>12}$$

I rescaled nh_a from 0-10 (NH_a) to improve interpretability. I calculated metrics for the lowland (NH_l), foothill (NH_f), mountain (NH_m), and TER-S (NH_t) subsets from their respective subscores.

Fort Bliss provided shapefiles of all observations made during both Kozma and Mathews' (1995) and Myers et al.'s (1998) arroyo-riparian studies and all nests found during the 1996-1997 study. Their transects overlapped substantially with 13 of the SERDP project stream reaches (Levick et al., *in progress*). I shortened the stream reach polygons when necessary to match the length surveyed by Kozma and Mathews and Myers et al., and recalculated the area of the modified polygons and lengths of the streams within them. For the observational data, I extracted the subset of observations made at survey points within the 13 stream reaches. For the

nest data, I counted the number of nests within 5 m of the stream reach polygons, to account for small differences in vegetation in the time since the study was done and prevent eliminating nests due to small location recording errors. This increased the total number of nests by 13 (from 137), but only two nests were from species not classified as riparian-associated, indicating this buffer did not include inappropriate areas.

From both datasets, I recorded the number of riparian-associated species that were observed (S_o) and nesting (S_n) in each stream reach. To account for imperfect detection, I used the first-order jackknife species richness estimator $S_{jackknife1}$ (JK1; Burnham and Overton 1979, Magurran and McGill 2011) to derive the estimated number of species observed ($JK1_o$) and nesting ($JK1_n$) in each stream reach. To adjust for stream reaches being different lengths I divided each species richness metric by the surveyed stream length (km).

To analyze the utility of the nesting habitat value metric, NH_a, I created Gaussian general linear models (GLM) with an identity link in R. Regressing the ecohydrological variables against the species/km metrics revealed that the 3-m flooded depth riparian width was a significant or marginally significant predictor for all metrics (S_o/km, p=0.025; S_n/km, p=0.12; $JK1_o$/km, p=0.02; $JK1_n$/km, p=0.028). Greater width was associated with increased values of all species richness measures. Based on these results, I created a width-adjusted nesting habitat metric. I rescaled riparian width from 0-100 to match the range of the percent cover variables. The width adjusted metric (nh_w) was calculated as:

$$nh_w = 4*(N_{0.5\text{-}1}*C_{0.5\text{-}1} + N_{1\text{-}4}*C_{1\text{-}4} + N_{4\text{-}12}*C_{4\text{-}12} + N_{>12}*C_{>12}) + Width_{scaled}$$

The multiplication of the original score by four ensured that width had a contribution equal to that of one structure layer. I rescaled nh_w from 0-10 (NH_w) to improve interpretability.

I used the Kozma and Mathews and Myers et al. datasets to ground-truth the species richness that I calculated from the GAP animal habitat models (see Species Richness Analysis section).

Results

Including the species Kozma and Mathews and Myers et al. found to be riparian-associated, Fort Bliss had 84 birds which were likely to nest in xeroriparian areas, 41 (49%) of which are summer- only residents (Appendix A, Table 3). Nine of the 84 species were not included in the nesting habitat metric because their nest site requirements were not primarily vegetation associated; some species used burrows or cliffs, or nested on the ground. Cowbirds were excluded because they are nest parasites. Twenty-two of the 75 birds included in the metric were TER-S species. Fifty-six of the 75 species occur in the lowlands, 68 in the foothills, and 50 in the mountains. Overall, the 1-4 m and 4-12 m vegetation structure layers were the most heavily used by birds nesting at the installation, with about 40% and 30% of species using each layer, respectively (Table 22). The lowest and highest layers see use by only about 15-20% of birds each. Creating sub-lists for lowlands, foothills, and mountains had only very small effects on the distribution of use. Mountain locations showed the greatest change in use of the vegetation layers from the overall metric; use of the two lower layers decreased while use of the upper layers increased. TER-S use of the vegetation layers was also very similar to overall use. Because values for the subsets and overall were so close, overall calculations were used for all subsequent analyses.

Table 22. Number of bird species potentially nesting in each vegetation layer at Fort Bliss, NM/TX (left) and percent of bird species potentially nesting in each vegetation layer (right). Derived from data on bird nest height available from Birds of North America Online obtained by October 2014.

Subset	Vegetation Layer			
	0.5-1m	1-4m	4-12m	>12m
Overall	27	54.5	39	19
Overall Lowlands	21	41	27	12
Overall Foothills	22	49.5	36.5	18
Overall Mountains	16	34	29	16.5
TERS	8	13.5	9.5	6
TERS Lowlands	7	11	8.5	5.5
TERS Foothills	6	11.5	9	5.5
TERS Mountains	3.5	5.5	4	3.5

Subset	Vegetation Layer			
	0.5-1m	1-4m	4-12m	>12m
Overall	19.4%	39.1%	28.0%	13.6%
Overall Lowlands	20.8%	40.6%	26.7%	11.9%
Overall Foothills	17.5%	39.3%	29.0%	14.3%
Overall Mountains	16.8%	35.6%	30.4%	17.3%
TERS	21.6%	36.5%	25.7%	16.2%
TERS Lowlands	21.9%	34.4%	26.6%	17.2%
TERS Foothills	18.8%	35.9%	28.1%	17.2%
TERS Mountains	21.2%	33.3%	24.2%	21.2%

From 1993-1997, Kozma and Mathews and Myers et al. made 8341 observations of 51 riparian-associated species in the 13 reaches that corresponded to those in the SERDP study (Levick et al. *in progress*). Reaches were observed to have 20 – 34 species each.

From 1996-1997, Myers et al. found 150 nests belonging to 22 species of birds in 13 reaches that corresponded to those in the SERDP study. Five species, accounting for 11% of all nests (17) were not on the riparian-associated species list. Stream reaches contained nests belonging to 4-10 different species. The original overall metric, NH_a, was not a significant predictor of S_o/km (p=0.221), S_n/km (p=0.503), $JK1_o$/km (p=0.309), or $JK1_n$/km (p=0.247), but the estimates for its effect on these measures was positive (S_o/km, 7.96; S_n/km, 1.67; $JK1_o$/km, 8.67; $JK1_n$/km, 4.94). However, once width was included in the metric, NH_w, it was a significant predictor of S_o/km (estimate = 11.08, p=0.014), $JK1_o$/km (estimate = 13.67, p=0.021), and $JK1_n$/km (estimate = 7.04, p=0.018) and a marginally significant predictor of S_n/km (estimate = 2.75, p=0.132). NH_w was a slightly better predictor of breeding bird richness than width alone for S_o/km (ΔAIC = 1.34) and $JK1_n$/km (ΔAIC = 0.97), while width alone was a slightly better predictor of S_n/km (ΔAIC = 0.20) and $JK1_o$/km (ΔAIC =0.11).

The original metric, NH_a, and the width-adjusted metric, NH_w, are distributed differently across the installation (Figure 7). For the original overall metric, NH_a, nearly all values above 2.5 are in the mountainous areas of Fort Bliss, values between 1 and 2.5 are found in the foothills and some of the lowlands, and values below 1 account for the rest of the area, primarily lowlands. Over half of the stream-km on the installation (56.6%, 1089 km) are between 0 – 0.249, while values 2 or greater account for only 7.2% (138 km) of all stream-km (Figure 8).

The distribution of the nesting height metric changes for the width-adjusted metric, NH_w. The highest values, those over 5, are still primarily in the mountains, but some downstream reaches draining into the Tularosa Basin and on Otero Mesa also have higher values of 2.5 or more (the *widest* streams). Values from 0.5-2.5 are scattered throughout the area, while values below 0.5 make up the rest of the streams, mostly in the lowlands and foothills. The distribution of stream length b values is more "normal," but still skewed to the left (Figure 8). Streams with a value of 1-1.49 are the most common (27.1%, 521 km), and values 2 or greater have increased to 30.6% of stream-km (589 km).

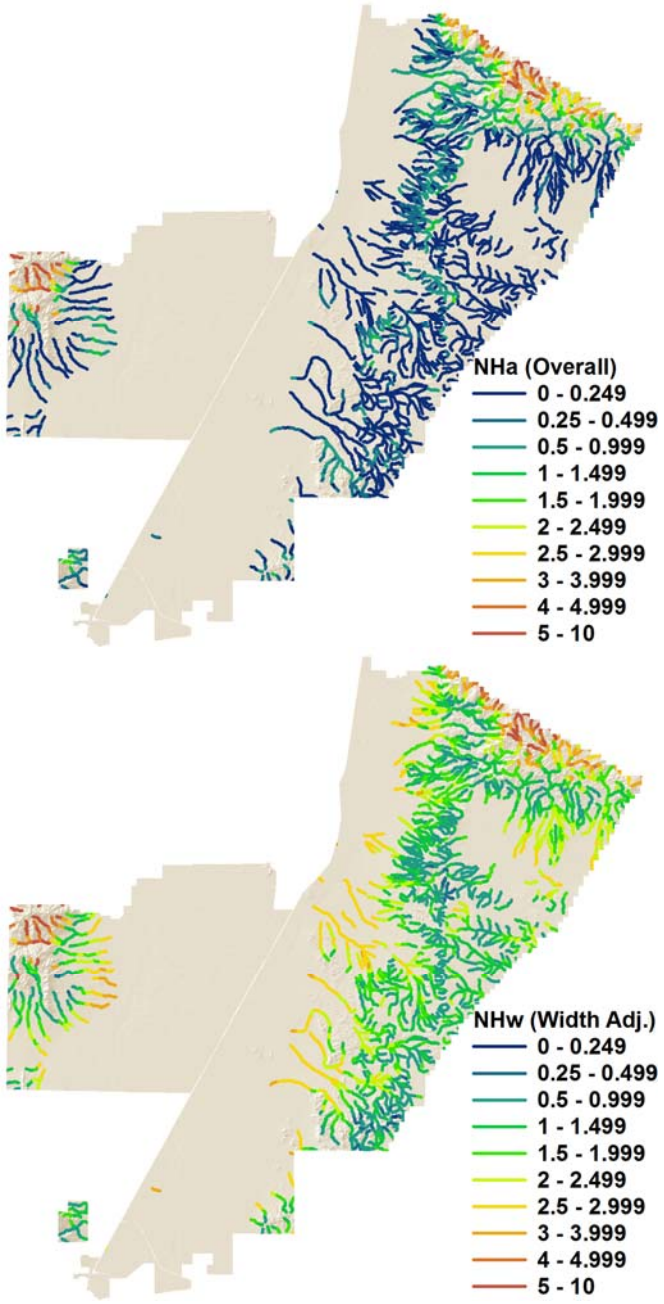


Figure 7. Values across stream reaches on Fort Bliss, NM/TX of the overall nesting habitat value metric, NH_a (top) and the width-adjusted nesting habitat value metric, NH_w (bottom). Metrics were created by combining information on preferred nest height of bird species occurring on the installation and information on the vegetation structure of each stream reach collected by Levick et al. (*in progress*).

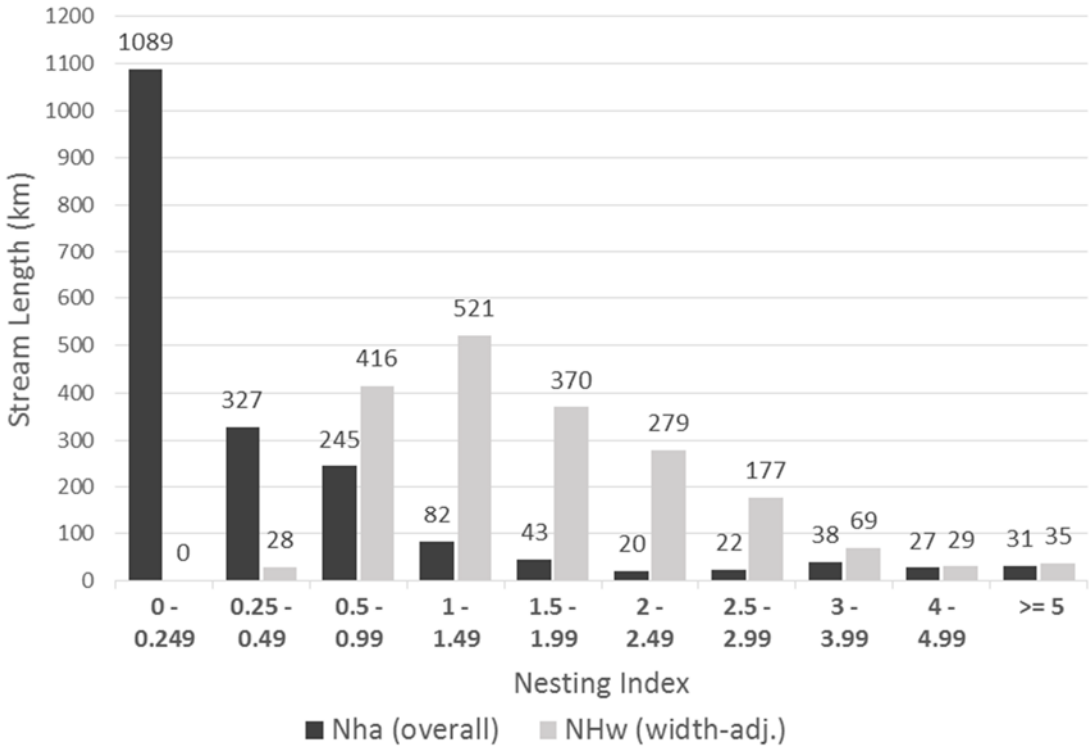


Figure 8. Total stream lengths at Fort Bliss, NM/TX of values of the overall nesting habitat metric, NH_a and width-adjusted metric, NH_w. Number above column indicates distance in stream-km for that range of metric values.

Species richness of breeding birds (birds with only summer or year-round habitat) derived from the stacked GAP models was not a significant predictor of any measure of breeding bird richness derived from the Kozma and Mathews and Myers et al. data (Table 23). Since only 13 stream reaches in one small area of the installation were used to ground-truth, it is difficult to determine whether this actually indicates a problem with the stacked GAP model richness.

Table 23. Results of GLM regression of estimated breeding bird richness derived from stacked GAP models against breeding bird richness measures derived from Kozma and Mathews (1995) and Myers et al. (1998) for 13 stream reaches on Fort Bliss, NM.

Richness Measure	Estimate	p-value
S_o/km	-0.10	0.16
$JK1_o$/km	-0.06	0.32
S_n/km	-0.19	0.34
$JK1_n$/km	-0.14	0.19

Discussion

The importance of vegetation structure to breeding bird richness has been well established. Because locations with greater vertical structure provide more niches for more species, greater vertical structural complexity increases richness (MacArthur and MacArthur 1961). Total vegetation volume is strongly and positively correlated with breeding bird density (Mills et al. 1991) and vertical vegetation structure is a one of the primary influences on occupancy of individual bird species (Seavy et al. 2009, Ficetola et al. 2014). Once the nesting height metric was adjusted for the width of the riparian-corridor, it was a significant predictor of three out of four measures of breeding bird richness, even with a small sample of only 13 stream reaches. While structure alone is very important, it is reasonable that adjusting for width improved the predictive power of the nesting height metric. Wider streams have more area for more breeding territories of different species. With larger areas, wider streams might also be expected to have greater vegetation volume, important for breeding bird richness (Mills et al. 1991) and higher horizontal structure complexity, another factor that has also been tied to increased breeding bird richness (Culbert et al. 2013).

It may seem to be a contradiction that riparian width had a positive influence on breeding bird richness from Kozma and Mathews and Myers et al.'s studies while it had a negative influence on all species richness measures derived from the GAP models. However, this is most likely an issue of scale. The field data were collected from a small set of only 13 of the 1908 stream reaches I analyzed with the GAP data. Across the broad scale of all stream reaches, riparian width is not well correlated with the amount of riparian vegetation. At the smaller extent of these field studies, the vegetation and streams are quite similar to each other and riparian width may serve as a better indicator of the amount of riparian vegetation. Correlations for the 3m riparian width and the vegetation variables in just these 13 reaches are closer to zero than they were for the entire set of streams, or even positive (-0.18 to +0.32), which lends some support to this interpretation. However, the opposite influence of riparian width for the nest height metric underscores the caution that should be shown with the application of the nest height metric to other areas of the Fort.

I used two types of measures of species richness to assess the nesting habitat metric: the actual number of species, S, and the estimated number of species, JK1. Assuming that the NH_w was a good predictor of the number of breeding birds in the stream reaches studied by Kozma and Mathews and Myers et al., I can make some observations about the use of S versus JK1. For species observed during the studies, S had a somewhat smaller p-value than JK1, while for species found nesting, JK1 had a much smaller p-value than S. For the observation data, pooling 5 years of thousands of observations may have resulted in very good detection of the actual number of species breeding in stream reaches. Since finding nests can be quite difficult and there were only two years of this type of data, it seems reasonable that detection of the true number of species nesting in stream reaches would be better measured by the JK1 species richness estimator.

The results of ground-truthing the nesting habitat metric with the data Kozma and Mathews and Myers et al. is promising, but is based on a very small sample from a small area of the installation. The stream reaches they sampled covered 10.8 km of stream, 0.56% of all the streams on the installation. Their study area covered 43.3 km^2 (minimum convex polygon) of the installation, approximately 1.6% of the installation in which stream are found. Other areas of the installation may be better understood by nesting habitat metrics calculated with the geographic

sub-scores or without the width adjustment. For example, the range of widths in the 13 stream reaches studied by Kozma and Mathews and Myers at al. was 55-197m, while the range of widths across the installation is 15-498m. Outside the range found in those 13 reaches, the relationship of breeding bird richness to width may be different – either nonexistent or opposite. Adjusting the metric for width only caused a change of 0.35 - 1.27 in the 13 reaches, but caused changes of 0-3.23 in all reaches. For management, it may be more appropriate to consider the unadjusted metric, NH_a, or a version of it calculated for the appropriate geographic setting, as a good indicator of where vegetation structure may favor high breeding bird richness, but to realize that other factors may influence or dominate breeding bird richness in specific locations.

Another important issue that I did not address in the nesting habitat metric was the rarity or commonness of the breeding bird species. This information is available in Fort Bliss' INMRP (U.S. Army 2001). Taking this into account could change the results. Managers might also want to create a metric for just the rare species, incorporating geographic location of streams.

A final issue is the time elapsed since the data Kozma and Mathews and Myers et al. were collected. The LiDAR data the nesting habitat metric is based on were collected in November 2006, a minimum of 9 years since the field data on breeding birds were collected. Vegetation structure may have changed in that time period, particularly because Fort Bliss has experienced a marked increase in use for military training since the 2005 Base Realignment and Closure, as well as drought in combination with warmer temperatures from 2000-2003. It is impossible to know if or how this may have affected my results.

The species richness data from Kozma and Mathews and Myers et al. did not support or undermine the estimated breeding bird species richness derived from the stacked GAP models. It is a concern that the estimates were negative, but the values of the estimate were very small (< 0.2). Values close to zero in regression have more uncertainty around their sign. It is not surprising that a small sample of only 13 reaches did not have a significant result. The range of GAP-derived breeding bird richness in the 13 reaches was only 16.5-23.7 species, while the range across the entire installation is 8.26-32.88 species ($\mu = 22.51$, $s = 2.51$). No conclusion can be drawn about the GAP richness estimates from this analysis.

On the whole, the nesting habitat metric would require further research to understand its accuracy and utility, but the results from this small test were promising.

GRAY VIREO HABITAT MODEL

In this section, I use field data to determine whether a single species is associated with particular streams, and what ecohydrological characteristics of those streams are important for its occurrence. Fort Bliss was able to provide an excellent data set to model one species. Gray vireos (*Vireo vicinor*) have a regional NatureServe rank in New Mexico of Apparently Secure (S4) for their breeding range and Vulnerable (S3) in their non-breeding range. The species is listed by New Mexico as Threatened.

From 2007-2012, most stream reaches in the gray vireo's range on Fort Bliss were surveyed for the species (White Sands, 2007; Zia, 2010, 2012a, 2012b, 2013). Observations, nests, and male territories were documented. Survey locations were recorded and whether or not vireos were observed, yielding a dataset of both presence and absence, assuming lack of detection was true absence.

Methods

Literature-based model

I used the data summarized in the Birds of North America Online (Poole 2014) entry for the Gray Vireo (Barlow et al. 1999) to create the literature-based model. Barlow et al. indicated that the most important factor for Gray Vireo occurrence was "continuous" shrub cover from 0.5-2 meters in height. Most foraging occurs in the 1-4 m vegetation layer, and the birds are found from 914-2380 meters in elevation in West Texas, the region closest to Fort Bliss. Because all the streams at Fort Bliss are in this elevation range, no streams were excluded due to elevation. The 1-4 meter LiDAR structure layer includes most of the 0.5-2 meter layer that Barlow et al. identified as important for vireos, as well as all of the layer in which they prefer to forage. The mean percent cover of this layer in riparian zones at Fort Bliss is only 5.2% (s = 11.8%). To approximate what gray vireos might perceive as continuous cover of this vegetation layer, I selected all streams with a cumulative 1-4 m percent cover equal to or greater than the mean value plus 2 standard deviations, or 28.8% cover. The cumulative 1-4m percent cover was derived by adding the percent covers of the >12m and 4-12m layers to the 1-4m layer because most stream reaches at Fort Bliss with the higher canopy layers also had vegetation in the vegetation layers below those. I eliminated stream reaches that did not have any of the National GAP (USGS 2014) land cover types listed in the National GAP Gray Vireo species distribution model (Table 24). The remaining stream reaches indicate where Gray Vireos may occur based on the literature.

Table 24. Ecological systems identified by the gray vireo GAP model as habitat for that species on Fort Bliss, NM/TX. Model downloaded on October 2014.

Code	Ecological System	Percent Cover	Area (ha)
5201	Chihuahuan Creosotebush, Mixed Desert and Thornscrub	18.2	81859.1
5309	Inter-Mountain Basins Semi-Desert Shrub Steppe	10.0	449.3
3201	North American Warm Desert Bedrock Cliff and Outcrop	8.4	380.8
4512	Colorado Plateau Pinyon-Juniper Woodland	8.0	0.4
5604	Madrean Juniper Savanna	7.5	337.5
9822	North American Warm Desert Wash	6.2	281.4
9833	North American Warm Desert Lower Montane Riparian Woodland and Shrubland	6.1	275.4
5809	Rocky Mountain Gambel Oak-Mixed Montane Shrubland	4.9	22.1
9835	North American Warm Desert Riparian Woodland and Shrubland	4.8	215.9
4143	Madrean Encinal	4.8	215.1
3202	Rocky Mountain Cliff, Canyon and Massive Bedrock	4.0	179.5
5211	Apacherian-Chihuahuan Mesquite Upland Scrub	3.0	13534.0
5308	Inter-Mountain Basins Montane Sagebrush Steppe	1.2	5.4
5603	Inter-Mountain Basins Juniper Savanna	1.2	0.5
4518	Madrean Pinyon-Juniper Woodland	1.1	5119.0
5407	Mogollon Chaparral	0.8	3435.9
4534	Southern Rocky Mountain Pinyon-Juniper Woodland	0.6	2581.9
5606	Southern Rocky Mountain Juniper Woodland and Savanna	0.2	915.9

I used survey data provided by Fort Bliss, described below, to evaluate the literature-based model. I evaluated accuracy with a confusion matrix, and calculated overall accuracy, omission and commission rates for both presence and absence, and the Kappa coefficient (Cohen 1960), which measures how better than random a model is. An early guideline for interpretation of Kappa by Landis and Koch (1977) suggested that values < 0.4 indicated poor agreement that the model was better than random, 0.41–0.80 as moderate agreement that the model was better than random, and >0.80 as strong agreement that the model was better than random.

Survey-based model

At Fort Bliss, White Sands (2007) and Zia (2010, 2012a, 2012b, 2013) found the gray vireo in streams in the Organ and Sacramento Mountains. Because the dataset had both presence and absence, the modeled region only included surveyed streams in these mountains. The modeled area included 199 stream reaches, 10% of the reaches on the installation.

I spatially filtered presence/absence locations to no more than one per stream reach and usually at least 1 km apart by selecting all stream reaches within 50m of a survey point. Stream reaches were represented by the 3m flooded-depth riparian polygons. Spatial filtering helps reduce the effect of spatial autocorrelation, reduce overfitting, and prevent overly complex models (Radosavljevic and Anderson 2013, Shcheglovitova and Anderson 2013). Out of 2844 total survey points, 1094 were within 50m of one of the stream reaches. I used both the point locations and male territory polygons to assign each stream reach a presence or absence value. These steps resulted in 62 stream reaches used by vireos, 3.1% of the total number of reaches on the installation and 31.2% of the stream reaches in the modeling area.

Twenty ecohydrological variables were considered for modeling – 9 vegetative, 5 hydrologic, and 6 geomorphic/physical variables (Levick et al., *in progress*). The variables used were watershed area, elevation, entrenchment ratio (2m/3m), slope, rainfall seasonality index, 3m riparian width, flow permanence, 10-year total stream power, 25-year total stream power, 10-year peak flow, 25-year peak flow, LiDAR 0.5-1m, LiDAR 1-4m, LiDAR 4-12m, LiDAR >12m (presence/absence), mean vegetation index, percent cover, landcover variety, Shannon vertical vegetation structural diversity, and Simpson vertical vegetation structural diversity.

For model validation, I split the data into a training set and a testing set. I used a random number generator to reserve 23.6% (n=47) of the stream reaches in the modeling area for testing (Huberty 1994).

I used the training set to create a binomial generalized linear model (GLM) with a log link, also known as logistic regression. Occurrence (presence or absence) was modeled as a function of the ecohydrological variables. The top models for gray vireo occurrence were generated through a process modified from Grueber et al. (2011). Akaike's Information Criterion adjusted for small sample size (AICc) was used to evaluate model performance. The Shannon index of vegetation structural diversity had a lower AICc value than the Simpson (1-D) index when each variable was used independently to predict gray vireo presence (ΔAICc = 2.7); only the Shannon index was used in modeling. The 10-year peak flow had a lower AICc value than the 25-year peak flow when each variable was used independently to predict gray vireo presence (ΔAICc = 1.1); only the 10-year peak flow was used in modeling. The 25-year total stream power had a lower AICc value than the 10-year total stream power when each variable was used independently to predict gray vireo presence (ΔAICc = 0.7); only the 25-year total stream power was used in modeling.

An initial global model that included all possible predictor variables was built and then the *arm* package in R (Gelman et al. 2009) was used to standardize by centering on the mean and dividing by 2 standard deviations (Gelman 2008). The package MUMIN (Bartoń 2009) was used to generate all model subsets of the global model. All models within 2 ΔAICc of the top model were examined for uninformative parameters. Models that simply added one or two variables to another model in the top set were only retained if they had a lower AICc than the simpler model. A second global model was created that contained only those variables found in the reduced top model set. MUMIN was used to generate all model subsets of the second global model. Parameter estimates of all models in the top 2 ΔAICc were model averaged by the natural averages method to generate estimates of effect size. Standardized parameter estimates are reported as effect sizes with unconditional standard errors. Estimates were transformed to an odds ratio and adjusted by the standard deviation of each variable from the training set to correspond with a meaningful change in each predictor variable. All models subsets of the second global model were used to generate measures of relative variable importance to ensure that it was calculated from a balanced set (Burnham and Anderson 2002: 167–169).

I calculated predicted values for both the training and testing sets from the model-averaged estimates. Predicted values from a logistic regression range from 0 to 1. I determined what value was the most appropriate threshold to consider as presence by calculating overall accuracy of the training and testing sets for different threshold values. A threshold value is the minimum value required to consider the gray vireo present in a stream reach. The value refers to the prediction made by the logistic regression equation. I tested threshold values of 0.118, 0.142, and 0.207. For the most appropriate threshold value, I built confusion matrices for the training and testing sets, and calculated overall accuracy, omission and commission rates for both

presence and absence, and the Kappa coefficients for both sets. Using the package ROCR (Sing et al. 2005) in R, I also obtained AUC values for both sets. AUC (area under the curve of the receiver operating plot) reveals the models discriminatory ability. When both presence and absence are known, it measures the probability that the model correctly ranks a random presence locality higher than a random absence locality.

Results

Literature-based model

Excluding all stream reaches with <28.8% cover left 109 streams reaches, nearly all of which were located in the Sacramento and Organ Mountains. Eliminating reaches without land cover suitable for Gray Vireos eliminated 7 of these reaches, resulting in 102 stream reaches that could provide habitat for Gray Vireos (Figure 9).

However, overall accuracy for this model was poor at 44.8% (Table 25). Presence omission rate was 20.4%, indicating that many streams where gray vireos were actually present were not included in the model. Many streams where vireos were predicted to be did not have any observed vireos, resulting in a presence commission rate of only 17.5%. Absence omission rate was 55.9% and the absence commission rate was 60.6%. The Kappa coefficient for this model was -0.227; the model was significantly worse than a random model.

Cumulative percent cover of the 1-4m vegetation layer in streams in which the gray vireo occurred, based on the survey data, was actually between 2.4% and 49.9% ($\mu = 18.2$, $s = 12.7$), while the range in the survey area was 1.4% to 97.1% ($\mu = 23.5$, $s = 19.5$). While not significantly different, gray vireos tended to occur in areas with lower percent cover of this vegetation layer.

Table 25. Confusion matrix and accuracy rates for literature-based model of gray vireo distribution in streams at Fort Bliss, NM.

		Observed		
		Presence	Absence	Sum
Predicted	Presence	11	52	63
	Absence	43	66	109
	Sum	54	118	172

Accuracy	Omission	Comission
Presence	20.4%	17.5%
Absence	55.9%	60.6%

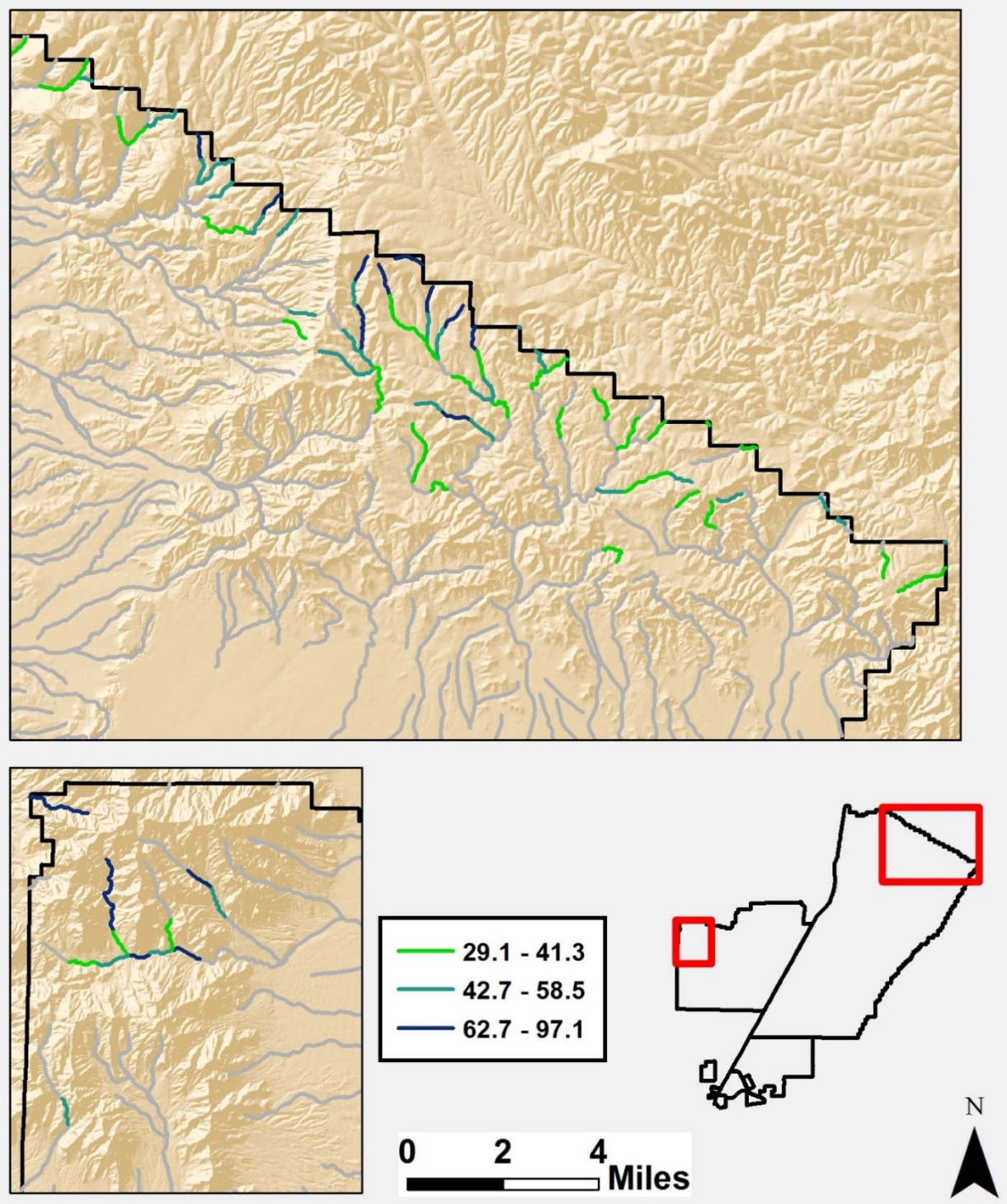


Figure 9. Maps showing the literature-based model for Gray Vireo habitat in streams at Fort Bliss, NM. Colored streams identify streams with >28.8% cover in the 1-4 meter vegetation layer from LiDAR that contain some Gray Vireo land cover types. Gray streams represent all other streams (no identified habitat).

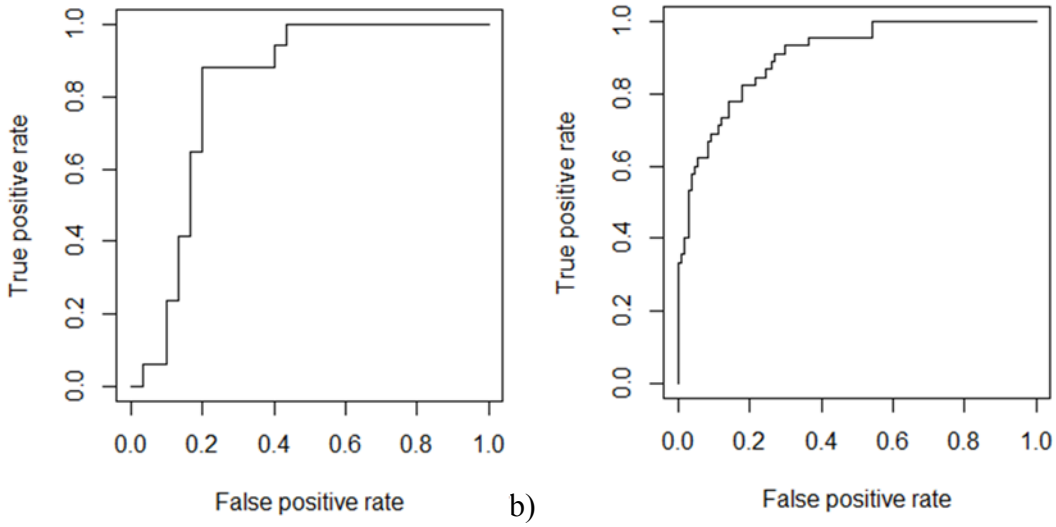
Survey-based model

Twelve variables were retained for the final model (Table 26). Higher probability of presence was generally related to smaller cumulative watershed area, lower 10-year peak flows, higher percent cover of veg 0.5-1m, and lower mean RENDVI. Other interesting effects include the avoidance of streams with vegetation >12m and streams at higher elevations, higher probability of presence in streams with higher flow permanence and higher RSI values, and a negative effect of percent cover.

Table 26 . Effect of ecohydrological variables on gray vireo probability of presence in streams on Fort Bliss, NM. Gray vireo presence was determined based on field data collected from 2007-2012 and modeled with a logistic regression. Parameter estimates are the average of all models within 2 AICc units of the top model. Input variables were standardized so estimates are one the same scale; relative effect size was calculated by converting the estimates to a percentage. Odds can be interpreted as the increase or decrease in probability of presence for a change in units as indicated in the unit change column (e.g., increasing RSI by 0.01 units increases the probability of presence by 202%, while increasing the cumulative area by 10 km^2 decreases the probability of presence by 31%).

Parameter	*Effect Size*	*Relative Effect Size*	95% CI Effect		*Relative Importance*	*Unit Change for Odds*	*Odds*	95% CI Odds	
			Lower	*Upper*				*Lower*	*Upper*
(Intercept)	-2.06		-2.12	-2.01					
W_Area	-4.41	13.4	-4.79	-4.02	0.39	10 (km2)	0.69	0.67	0.72
QP 10	-3.72	11.3	-3.87	-3.57	0.99	10	0.91	0.91	0.92
LiDAR 0.5-1 m	3.70	11.2	3.58	3.81	1.00	1	1.35	1.34	1.37
Veg_Ind Mean	-3.36	10.2	-3.52	-3.19	0.89	0.01	0.70	0.68	0.72
Elevation	-2.97	9.0	-3.08	-2.85	0.98	100	0.21	0.19	0.22
RSI	2.96	9.0	2.83	3.09	0.94	0.01	2.02	1.94	2.11
LiDAR >12m (P/A	-2.87	8.7	-3.09	-2.65	0.50	N to Y	0.06	0.04	0.08
Flow Perm	2.46	7.5	2.36	2.56	0.98	1	1.17	1.16	1.18
Percent Cover	-2.16	6.5	-2.28	-2.03	0.81	0.1	0.63	0.61	0.65
Landcover_var	1.93	5.8	1.83	2.02	0.92	1	2.28	2.16	2.40
Slope	-1.29	3.9	-1.37	-1.20	0.61	1	0.84	0.83	0.85
TSP 25	-1.15	3.5	-1.24	-1.06	0.43	10	0.95	0.94	0.95

The AUC value of the model was quite high for both the training (0.905) and the testing set (0.822; Figure 10). Overall accuracy was highest with a threshold value of 0.207 (Table 27).



a) b)

Figure 10. Receiver-operating curves (ROC) for the survey-based model test set (a) and training set (b). ROC curves were the result of modeling gray vireo presence in streams at Fort Bliss, NM based on field data collected from 2007-2012.

Table 27. Accuracy measures for three tested presence thresholds of output from the model of gray vireo stream use at Fort Bliss, NM.

		Threshold		
		0.118	0.142	0.207
Overall	*Test*	80.9	78.7	74.5
Accuracy	*Train*	72.4	73.0	76.3
Weighted Accuracy		74.4	74.3	75.9
Presence	*Test*	82.4	76.5	64.7
Omission	*Train*	95.6	93.3	91.1
Weighted P Omission		92.5	89.3	84.9
Presence	*Test*	70.0	68.4	64.7
Commission	*Train*	51.8	52.5	56.2
Weighted P Comission		56.1	56.3	58.2
Absence	*Test*	80.0	80.0	80.0
Omission	*Train*	62.6	64.5	70.1
Weighted A Omission		66.7	68.2	72.4
Absence	*Test*	88.9	85.7	80.0
Comission	*Train*	97.1	95.8	94.9
Weighted A Comission		95.2	93.4	91.4
Kappa	*Test*	0.601	0.551	0.447
Coefficient	*Train*	0.467	0.472	0.517
Weighted Kappa		0.499	0.491	0.500

This threshold resulted in an overall accuracy of 74.5% for the test set and 76.3% for the training set, for a weighted accuracy for both sets combined of 75.9% (Table 27). Kappa coefficients were 0.447 for the test set and 0.519 for the training set, indicating the model was at least moderately better than a random model. Confusion matrices and omission and commission rates are reported in Table 28. Of the 62 stream reaches in which gray vireos were found, the model predicted they would be present in 52 of these, as well as 38 additional stream reaches in which they were not observed.

Table 28. Confusion matrix and accuracy rates for gray vireo modeling (training and test sets combined). The presence/absence of gray vireos in streams at Fort Bliss, NM was modelled as a function of ecohydrological characteristics of the stream with logistic regression.

		Observed		
		Presence	Absence	Sum
Predicted	Presence	52	38	90
	Absence	10	99	109
	Sum	62	137	199

Accuracy	Omission	Comission
Presence	83.9%	57.8%
Absence	72.3%	90.8%

A visual inspection of the results (Figure 11) shows that the model had trouble predicting gray vireo occurrence in the Organ Mountains. Different factors may affect vireo occurrence in

different mountain ranges. This model may be best suited for managing gray vireos in the Sacramento Mountains.

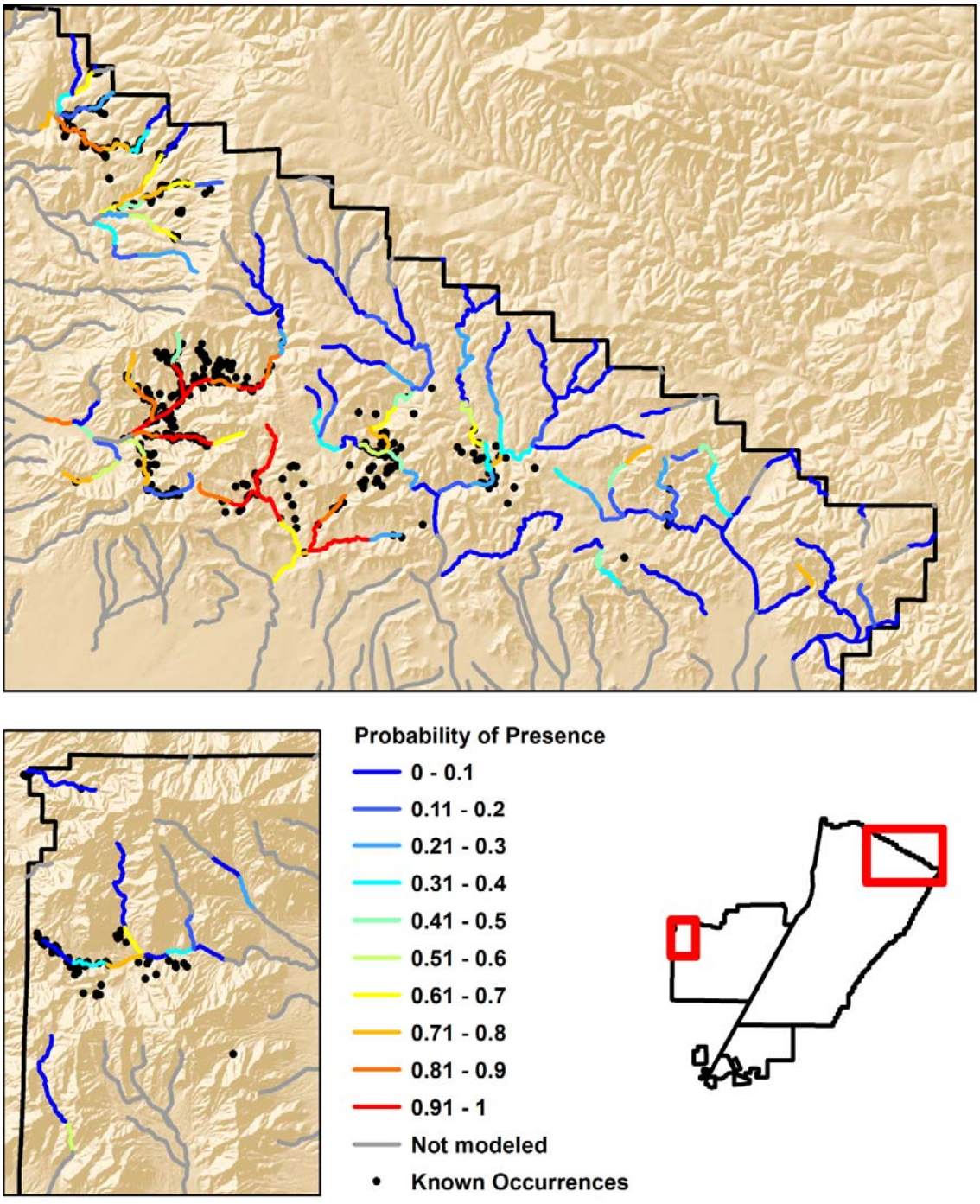


Figure 11. Maps of logistic modeling results for gray vireo in stream reaches at Fort Bliss, NM based on field data collected from 2007-2012. The Sacramento Mountains modeling area is shown above, and the Organ Mountains modeling area is shown below to the left. The 0.207 threshold for presence resulted in the greatest model accuracy. By this threshold, streams that are

symbolized with light blue (0.21 – 0.3) or greater, toward the red end of the spectrum, could be habitat for vireos.

Discussion

The poor results of the literature-based model highlight the shortcomings of models based only on habitat associations rather than directly on field data. The literature-based model was based on percent cover of the 1-4m vegetation layer and land cover categories. However, the survey data showed that gray vireos actually seemed to prefer slightly lower percent cover of this layer than was available in the environment. One of the shortcomings of species-habitat association models is their basis on short-term localized studies (Wolff 1995). The literature-based model may have failed partly because, while this structural layer is important in some areas of the vireo's range, it is not important for the vireo at Fort Bliss. Environmental associations with occurrence at the biogeographic scale do not always correspond to associations at the local scale.

Another component that may be responsible for the failure of the literature-based model may be the use of land cover associations from the GAP distribution model. Cablk et al. (2002) explain that linking species occurrence to environmental categories can mask the true relationships that exist between species and their environments. These relationships are with compositional landscape features or other characteristics of certain vegetation types, such as productivity, vertical vegetation complexity, or temperature and light gradients. Moreover, mapping species occurrence based on environmental categories will result in different outcomes when the number of environmental categories changes. When the actual survey data were considered, a majority of the gray vireo occurrences were actually in streams which were characterized as predominantly Apacherian-Chihuahuan Semi-Desert Grassland and Steppe. This ecological system was not included in the GAP model as potential habitat for the gray vireo. Two sources of error are possible: the GAP land cover may have been miscategorized in the areas where gray vireos were found in this ecological system, or this ecological system may have been inappropriately excluded from the gray vireo habitat associations. This problem with the gray vireo GAP model does cast some doubt on the species richness estimates derived from the stacked GAP models.

Regardless of the exact cause, the survey-based model based on actual locations and the environmental conditions at those locations far surpassed the performance of the literature-based model. I included several environmental variables that have not previously been included in habitat models for the gray vireo. Watershed area, with a relative effect size of 13.4%, was the most important variable. While this variable initially seems to be difficult to interpret, as discussed in the literature review, watershed area in drylands has a strong link to changes in the plant community composition (Warren and Anderson 1985, Shaw and Cooper 2008). It is likely that this variable is similar to land cover, but better approximates gradual changes in the plant community that is a key factor in determining what areas are habitat for the gray vireo. Peak flow of the 10-year storm and percent cover of the 0.5-1m layer were nearly tied as the second-largest effects (11% relative effect size). Peak flow had a negative effect, suggesting gray vireos avoid streams with higher peak flows. While flow permanence had a smaller influence on the model (relative effect size, 7.5%), increasing it by 1% increased probability of presence for gray vireos by 17%. These are interesting results that are likely related to the impact of these hydrological variables on vegetation, but would require further investigation to explain.

Four direct measures of vegetation were included in the model. Higher percent cover of the 0.5-1m vegetation layer increased the probability of presence for gray vireos. This result is in agreement with the BNA description of the importance of vegetation 0.5-2m high and the findings of Schlossberg (2006), discussed below. Two other vegetation variables included in the model are noteworthy. Higher values of mean RE-NDVI (relative effect size, 10.2%) and the presence of vegetation >12m (relative effect size, 8.7%) were both associated with decreased probability of vireo presence; vireos avoid streams with more dense and very tall vegetation within the modeling area at Fort Bliss. This is also supported by the inclusion of percent cover as a negative effect. As a bird of the open woodlands, this is a somewhat surprising result. As Guisan and Zimmerman (2000) point out, creating a distribution model from field data results in a model of a species realized niche rather than its fundamental niche (Hutchinson 1957). The presence of gray vireos in streams with less dense and shorter vegetation at Fort Bliss could be related to interactions with other species.

Two other physical variables had some effect on gray vireo occurrence. Elevation was the strongest of these (relative effect size, 9.0%); an increase of stream elevation by 100m caused gray vireo probability of presence to decrease by nearly 80%. This was also found to be a very important negative influence on gray vireos by Schlossberg (2006). Several studies have noted that the gray vireos and plumbeous vireos are segregated elevationally, with gray vireos restricted to the lower elevations in areas where both species occur (Johnson 1972, Oberholser 1974, and Sedgwick 1987, in Barlow et al. 1999). The rainfall seasonality index had the same relative effect size as elevation, but higher values increased the probability of vireo presence. Higher values of RSI indicate rainfall is more concentrated in one month within the year. As with peak flow, this probably impacts the vegetation community, but would require further investigation.

In the only study exclusively on the distribution of the gray vireo in the last 25 years, Schlossberg (2006) studied the species in pinyon-juniper woodlands on the Colorado Plateau of southern Utah and northern Arizona. He found that vireos preferred areas with a higher proportion of junipers relative to pinyon pine, and areas with some shrub cover, particularly sagebrush where it was present. While my model had no measure of junipers or pinyon pine, it is possible watershed area corresponds to a change in abundance of these trees. My finding of the positive influence of vegetation 0.5-1m does agree nicely with Schlossberg's finding that some shrub cover is important for vireos.

As in my model, Schlossberg also found vireos to be more common at the lower elevations in his studied range of 1370 - 2290m. His interpretation of this was that, because junipers are more drought tolerant, they are the dominant trees at lower elevations of the gray vireo range; gray vireos prefer junipers, and therefore lower elevations. However, he found much stronger support for a vegetation-elevation model (Akaike weight of 0.5) and an elevation-only model (Akaike weight of 0.35) than a vegetation-only model (Akaike weight of 0.13). He found that vireos were most abundant from 1500-1900m, and rare above 1900m. That elevation range is remarkable similar to were vireos were found in the surveys of Fort Bliss – vireos were present in streams with an elevation of 1626.8 – 1887.0 m ($\mu = 1762.4$, $s = 56.2$m), compared to the range of all surveyed streams of 1588.6 – 2084.7 ($\mu = 1796.9$, $s = 96.9$). Again, this could be due to competitive exclusion by plumbeous vireos, but eBird (eBird 2014) observation data indicate that this species has been found in some of the same stream reaches as gray vireos at Fort Bliss, making that unlikely. More likely is Schlossberg's suggestion based on Cooper and Gessaman (2004) that gray vireos are physiologically adapted to the warmer temperatures of lower

elevations. This hypothesis seems to be supported by the close correspondence of the upper elevation limit of 1900m found both by Schlossberg and the Fort Bliss surveys.

Overall, it is clear that the model based on survey data performed well. Measures of accuracy and error were acceptable to good, the effect of several variables agreed well with the findings of a recent study, and I reported effects of several other variables not yet reported to be associated with gray vireo occurrence.

CONCLUSION

By examining species richness, bird nesting patterns, and occurrence of the gray vireo, I was able to explore wildlife use patterns in ephemeral and intermittent streams at Fort Bliss. Ecohydrological components of these streams that appear to be most important to the diversity of terrestrial taxa are generally the vegetative and physical characteristics, such as riparian width, elevation, percent cover, and vegetation density as measured by RE-NDVI. However, I did find that some hydrological characteristics of the stream were associated with species richness and occurrence of the gray vireo. As Ekness and Randhir (2007) found, species richness was highest in smaller watersheds. Watershed area had at least a 10% relative effect size for five species richness measures, was included in eleven other measures, and had the largest effect size in the model of gray vireo occurrence. While they were rarely among the most important variables, total stream power and flow permanence were frequently included in models of species richness, and were both moderately important for gray vireos. It is clear that hydrological conditions are associated with species richness and occurrence, but my results can not reveal whether species are responding directly to hydrological conditions, or if these variables were good surrogates for some unmeasured characteristic of streams to which species were actually responding.

Using the survey data of Kozma and Mathews (1995) and Myers et al. (1998) and recently collected LiDAR data, I was able to confirm the importance of vegetation structure and riparian width on species richness of breeding birds. I used this relationship to extrapolate the potential nesting value of stream reaches across the installation. Vegetation structure and riparian width vary greatly between xeroriparian stream reaches, resulting in differences in their potential as habitat for breeding birds.

Creating the model of gray vireo occurrence showed that a single species of concern was indeed associated with particular stream reaches and ecohydrological conditions. In fact, hydrology had about equal influence on occurrence of this species as did vegetative and other abiotic characteristics of streams.

While most previous studies had focused on differences between riparian or xeroriparian zones and their adjacent uplands, I demonstrated that xeroriparian stream reaches are also different from each other in their potential species richness, their ability to provide nesting habitat for breeding birds, and their likelihood to host a particular species of concern. I linked these differences to the ecohydrological characteristics of individual stream reaches, and also mapped the differences in a GIS. Understanding differences between xeroriparian areas, where those different values are, and what ecohydrological characteristics are associated with those differences should give managers much greater ability to manage these important areas and to avoid high-impact activities in the areas most valuable to wildlife.

LITERATURE CITED

Akaike, H. 1973. Information theory and an extension of the maximum likelihood principle. International Symposium on Information Theory, 2:267-281.

Anderson, B.W., and R.D. Ohmart. 1977. Vegetation structure and bird use in the Lower Colorado River Valley. In: Importance, Preservation and Management of Riparian Habitat: A Symposium, July 9, 1977. U.S. Forest Service General Technical Report RM-43, p. 23-34.

Andrews, P. and E.M. O'Brien. 2000. Climate, vegetation, and predictable gradients in mammal species richness in southern Africa. Journal of Zoology, London, 251:205-231.

Barlow, Jon C., Leckie, S.N., and C.T. Baril. 1999. Gray Vireo (*Vireo vicinor*), The Birds of North America Online (A. Poole, Ed.). Ithaca: Cornell Lab of Ornithology; Retrieved from the Birds of North America Online: <http://bna.birds.cornell.edu/bna/species/447>

Bartoń, K. 2009. MuMIn: multi-model inference. R package, version 0.12.2. Available at: <http://r-forge.r-project.org/projects/mumin/>.

Baxter, R.J. 1988. Spatial distribution of desert tortoises (*Gopherus agassizii*) at Twentynine Palms, California: implications for relocations. In: Management of Amphibians, Reptiles, and Small Mammals in North America. Proceedings of the Symposium, July 19-21, 1988. U.S. Forest Service General Technical Report RM-166, p. 180-189.

[BISON-M] Biota Information System of New Mexico. 2013 version. BISON-M home page. http://www.bison-m.org. Accessed February 2013.

Boone, R.B. and W.B Krohn. 2000. Partitioning sources of variation in vertebrate species richness. Journal of Biogeography 27(2):457-470.

Boykin, K.G., B.C. Thompson, R.A. Deitner, D. Schrupp, D. Bradford, L. O'Brien, C. Drost, S. Propeck-Gray, W. Rieth, K. Thomas, W. Kepner, J. Lowry, C. Cross, B. Jones, T. Hamer, C. Mettenbrink, K.J. Oakes, J. Prior-Magee, K. Schulz, J. J. Wynne, C. King, J. Puttere, S. Schrader, and Z. Schwenke. 2007. Predicted animal habitat distributions and species richness. Chapter 3 in J.S. Prior-Magee, ed. Southwest Regional Gap Analysis Final Report. U.S. Geological Survey, Gap Analysis Program, Moscow, ID.

Boykin, K.G., Thompson, B.C., and S. Propeck-Gray. 2010. Accuracy of gap analysis habitat models in predicting physical features for wildlife-habitat associations in the southwest U.S. Ecological Modelling 221:2769-2775.

Brennan, T.C. 2012. Online field guide to the reptiles and amphibians of Arizona. <http://www.reptilesofaz.org/>

Brokaw, N.V.L. and R.A. Lent. 1999. Vertical structure. In: Hunter M.L. (Ed), Maintaining biodiversity in forest ecosystems. Cambridge, UK: Cambridge University Press. pp. 373-399.

Bull, L.J. and M.J. Kirkby. 2002. Dryland rivers: hydrology and geomorphology of semi-arid channels. John Wiley and Sons Ltd., Chichester.

Burnham, K.P. and D.R. Anderson. 2002. Model selection and multimodel inference: a practical information-theoretic approach, 2nd ed. Springer, Berlin.

K. P. Burnham and W. S. Overton. 1979. Robust estimation of population size when capture probabilities vary among animals. Ecology 60:927–936.

Cablk, M., White, D., and A.R. Kiester. 2002. Assessment of spatial autocorrelation in empirical models in ecology. In: Scott, J.M., Heglund, P.J., Morrison, M.L., Haufler, J.B., Raphael, M.G., Wall, W.A., Samson, F.B. (Eds.), Predicting Species Occurrences—Issues of Accuracy and Scale. Island Press, Washington, pp. 429–440.

Carlson, E.A. 2009. Fluvial riparian classifications for national forests in the western United States. M.S. Thesis. Colorado State University, Fort Collins, CO; 194 pp.

Castner, S. V., T. K. Snow, and D. C. Noel. 1995. Bat inventory of the U.S. Army Yuma Proving Ground, Arizona: 1995. Nongame and Endangered Wildlife Program Technical Report 90. Phoenix: Arizona Game and Fish Department.

Clark, S. 2012. ZonalStatsOverlappingPolys, Tool to calculate zonal stats using Zonal Statistics as Table with an overlapping polygon feature class. <http://www.arcgis.com/home/item.html?id=b859b33c616a47d2b99b5e133942db02>. Accessed August 30, 2013.

Cohen, Jacob. 1960. A coefficient of agreement for nominal scales. Educational and Psychological Measurement 20(1):37–46.

Cooper, S. J. and J. A. Gessaman. 2004. Thermoregulation and habitat preference in Mountain Chickadees and Juniper Titmice. Condor 106:852–861.

Cudworth, N.L. and J.L. Koprowski. 2011. Importance of scale in nest-site selection in Arizona gray squirrels. Journal of Wildlife Management 75:1668–1674.

Culbert, P. D., V. C. Radeloff, C. F. Flather, J. M. Kellndorfer, C. D. Rittenhouse, and A. M. Pidgeon. 2013. The influence of vertical and horizontal habitat structure on nationwide patterns of avian biodiversity. Auk 130(4):656-665.

Datry, T., Arscott, D.B., and S. Sabater. 2011. Recent perspectives on temporary river ecology FOREWORD. Aquatic Sciences 73:453-457.

Dubayah, R. O. and J. B. Drake. 2000. Lidar remote sensing for forestry. Journal of Forestry 98:44–46.

Dust, D.W. and E.E. Wohl. 2010. Quantitative technique for assessing the geomorphic thresholds for floodplain instability and braiding in the semi-arid environment. Natural Hazards 55:145-160.

eBird. 2014. eBird: An online database of bird distribution and abundance [web application]. eBird, Cornell Lab of Ornithology, Ithaca, New York. Available: <http://www.ebird.org>. (Accessed: October 2014)

Edwards, T. C., Jr., E. Deshler, D. Foster, and G. G. Moisen. 1996. Adequacy of wildlife habitat relation models for estimating spatial distributions of terrestrial vertebrates. Conservation Biology 10:263-270.

Ekness, P. and T. Randhir. 2007. Effects of riparian areas, stream order, and land use disturbance on watershed-scale habitat potential: an ecohydrologic approach to policy. Journal of the American Water Resources Association 43:1468–1482.

Ficetola, G.F., Bonardi, A., Mücher, C.A., Gilissen, N.L.M., and E. Padoa-Schioppa. 2014. How many predictors in species distribution models at the landscape scale? Land use versus LiDAR-derived canopy height. International Journal of Geographical Information Science 28(8):1723-1739.

Gelman, A. 2008. Scaling regression inputs by dividing by two standard deviations. Statistics in Medicine 27: 2865–2873.

Gelman, A., Su, Y.-S., Yajima, M., Hill, J., Pittau, M.G., and J. Kerman, et al. 2009. arm: data analysis using regression and multilevel/ hierarchical models. R package, version 9.01.

Germaine, S.S. Rosenstock, S.S., Schweinsburg, R.E., and W.S. Richardson. 1998. Relationships among breeding birds, habitat, and residential development in greater Tucson, Arizona. Ecological Applications 8:680–691.

Goetz, S., Steinberg, D., Dubayah, R., and B. Bryan. 2007. Laser remote sensing of canopy habitat heterogeneity as a predictor of bird species richness in an eastern temperate forest, USA. Remote Sensing of Environment 108: 254-263.

Goetz, S.J., Sun, M., Zolkos, S., Hansen, A., and R. Dubayah. 2014. The relative importance of climate and vegetation properties on patterns of North American breeding bird species richness. Environmental Research Letters 9:1-18.

Goodrich, D.C., Burns, I.S., Unkrich, C.L., Semmens, D., Guertin, D.P., Hernandez, M., Yatheendradas, S., Kennedy, J.R., and L. Levick. 2012. KINEROS2/AGWA: model use, calibration, and validation. Transactions of the ASABE. 55(4): 1561-1574.

Graf, W.L. 1988. Fluvial processes in dryland rivers. Springer-Verlag, Berlin.

Grueber, C.E., Nakagawa, S., Laws, R.J., and I.G. Jamieson. 2011. Multimodel inference in ecology and evolution: challenges and solutions. Journal of Evolutionary Biology 24:699-711.

Guisan, A. and N.E. Zimmerman. 2000. Predictive habitat distribution models in ecology. Ecological Modeling 135(2-3):147-186.

Hardy, P.C., D.J. Griffin, K.A. Juenzi, and M.L. Morrison. 2004. Occurrence and habitat use of passage neotropical migrants in the Sonoran Desert. Western North American Naturalist 64:59-71.

Hayes, M.P. and M.R. Jennings. 1988. Habitat correlates of distribution of the California red-legged frog (*Rana aurora draytonii*) and the foothill yellow-legged frog (*Rana boylii*): Implications for Management. In: Management of Amphibians, Reptiles, and Small Mammals in North America. Proceedings of the Symposium, July 19-21, 1988. U.S. Forest Service General Technical Report RM-166, p. 144-158.

Heaton, J.S., A.R. Kiester, and M. Meyers. 2006. The LizLand model: a geomorphic approach to lizard habitat modeling in the Mojave Desert. Journal of Arid Environments 67(Supplemental 1):202-225.

Homer, C., Dewitz, J., Fry, J., Coan, M., Hossain, N., Larson, C., Herold, N., McKerrow, A., VanDriel, J.N., and J. Wickham. 2007. Completion of the 2001 National Land Cover Database for the Conterminous United States. Photogrammetric Engineering and Remote Sensing, Vol. 73, No. 4, pp 337-341.

Howe, S., Levick, L.R., and A. Hautzinger. 2008. Hydrology and ecology of Southwestern intermittent streams, dry washes, and adjacent riparian zones. In: Proceedings from the Southwest Region Threatened, Endangered, and At-Risk Species Workshop, 22-25 October 2007, Tucson, Arizona. Prepared for the Legacy Resource Management Program, Strategic Environmental Research and Development Program, and Environmental Security Technology Certification Program by HydroGeoLogic, Inc., Reston, Virginia.

Huberty, C. J. 1994. Applied discriminant analysis. New York: Wiley.

Hutchinson, G. E. 1957. Concluding remarks. Cold Spring Harbor Symposia on Quantitative Biology 22:415–427.

Hylander, K. 2006. Riparian zones increase regional species richness by harboring different, not more, species: Comment. Ecology 87:2126-2128.

IUCN, Conservation International, and NatureServe. 2004. Global amphibian assessment. IUCN, Conservation International, and NatureServe. Washington, DC and Arlington, Virginia, USA.

Jakle, M.D. and T.A. Gatz. 1985. Herpetofaunal use of four habitats in the Middle Gila River drainage, Arizona. In: Riparian Ecosystems and Their Management: Reconciling Conflicting Uses. First North American Riparian Conference, April 16-18, 1985. U.S.D.A. Forest Service General Technical Report RM-120, p. 355-358.

Johnson, N. K. 1972. Breeding distribution and habitat preference of the Gray Vireo in Nevada. California Birds 3:73-78.

Johnson, R.R., S.W. Carothers, and J.M. Simpson. 1984. A riparian classification system. pp 375-382, In: R.E. Warner and K.M. Hendrix, eds., California Riparian Systems: Ecology, Conservation, and Productive Management. University of California Press, Berkeley.

Johnson, R.R. and L.T. Haight. 1985. Avian use of xeroriparian ecosystems in the North American warm deserts. In: Riparian Ecosystems and Their Management: Reconciling Conflicting Uses. First North American Riparian Conference, April 16-18, 1985. U.S.D.A. Forest Service General Technical Report RM-120, p. 156-160.

Jones, K.B. 1988. Distribution and habitat associations of herpetofauna in Arizona: comparisons by habitat type. In: Management of Amphibians, Reptiles, and Small Mammals in North America. Proceedings of the Symposium, July 19-21, 1988. U.S. Forest Service General Technical Report RM-166. p. 109-128.

Jorgensen, E.E., Demarais, S., Sell, S., and S.P. Lerich. 1998. Modeling habitat suitability for small mammals in Chihuahuan desert foothills of New Mexico. Journal of Wildlife Management 62(3):989-996.

Kassas, M. and M. Imam. 1954. Habitat and plant communities in the Egyptian Desert: III. The wadi bed ecosystem. Journal of Ecology 42:424–41.

Katz, G. L., Denslow, M. W., and J.C. Stromberg. 2012. The Goldilocks effect: intermittent streams sustain more plant species than those with perennial or ephemeral flow. Freshwater Biology 57:467–480.

Kellndorfer, J., Walker, W., LaPoint, E., Bishop, J., Cormier, T., Fiske, G., Hoppus, M., Kirsch, K., and J. Westfall. 2012. NACP Aboveground Biomass and Carbon Baseline Data (NBCD 2000), U.S.A., 2000. Data set. Available on-line at <http://daac.ornl.gov> from ORNL DAAC, Oak Ridge, Tennessee, U.S.A.

Kepner, W.G. 1978. Small mammals of the Black Canyon and Skull Valley planning units, Maricopa and Yavapai Counties, Arizona. U.S. Bureau of Land Management, Phoenix District Office. Technical Note 350.

Kirkpatrick, C., Conway, C.J., and D. LaRoche. 2007. Quantifying impacts of groundwater withdrawal on avian communities in desert riparian woodlands of the southwestern U.S. USGS Arizona Cooperative Fish and Wildlife Research Unit, Department of Defense, Legacy Resource Management Program, Project 06-290.

Kozma, J.M. and N.E. Mathews. 1995. Long-term monitoring of Neotropical migrants in Chihuahuan Desert arroyo-riparian habitat and adjacent upland.

Krausman, P.R., Rautenstrauch, K.R., and B.D. Leopold. 1985. xeroriparian systems used by desert mule deer in Texas and Arizona. In: Riparian Ecosystems and Their Management: Reconciling Conflicting Uses. First North American Riparian Conference, April 16-18, 1985. U.S.D.A. Forest Service General Technical Report RM-120, p. 144-149.

Krueper, D.J. 1993. Conservation priorities in naturally fragmented and human-altered riparian habitats of the arid West. USDA Forest Service. General Technical Report RM-43. <www.birds.cornell.edu/pifcapemay/krueper.htm>

Landis, J.R. and G.G. Koch. 1977. The measurement of observer agreement for categorical data. Biometrics 33(1):159–174.

Larned, S. T., T. Datry, D. B. Arscott, and K. Tockner. 2010. Emerging concepts in temporary-river ecology. Freshwater Biology 55:717-738.

Levick, L., Fonseca, J., Goodrich, D., Hernandez, M., Semmens, D., Stromberg, J., Leidy, R., Scianni, M., Guertin, D.P., Tluczek, M., and W. Kepner. 2008. The ecological and hydrological significance of ephemeral and intermittent streams in the arid and semi-arid American Southwest. U.S. Environmental Protection Agency and USDA/ARS Southwest Watershed Research Center. EPA/600/R-08/134, ARS/233046, 116 pp.

Levick, L., Hammer, S., Lyon, R., Murray, J., Birtwistle, A., Goodrich, D., Bledsoe, B., Guertin, P., and M. Laituri. *in progress*. An ecohydrological approach to managing intermittent and ephemeral streams on Department of Defense lands in the Southwestern United States. Strategic Environmental Research and Development Program. Project RC-1727.

Lynn, J. C., Chambers, C. L., and S.S. Rosenstock. 2006. Use of wildlife water developments by birds in southwest Arizona during migration. Wildlife Society Bulletin, 34:592–601.

Lyon, R. 2013. Using rainfall-runoff models to characterize the flow regime of desert streams in the U.S. southwest. M.S. Thesis, University of Arizona, Tucson.

MacArthur, R.H. and J.W. MacArthur. 1961. On bird species diversity. Ecology 42:594–598.

McArthur, E.D. and S.C. Sanderson. 1992. A comparison between xeroriparian and upland vegetation of Beaver Dam Slope, Utah, as desert tortoise habitat. In: Proceedings – Symposium on Ecology and Management of Riparian Shrub Communities. U.S. Dept. of Agriculture, General Technical Report INT-289, p. 25-31.

Magurran A.E. and B.J. McGill. 2011. Biological diversity: frontiers in measurement and assessment. Oxford University Press Inc., New York.

Mcfarland, T.M.,C. van Riper, III, and G.E. Johnson. 2012. Evaluation of NDVI to assess avian abundance and richness along the upper San Pedro River. Journal of Arid Environments 77:45-53.

Miller, S.N., Semmens, D.J., Goodrich, D.C., Hernandez, M., Miller, R.C., Kepner, W.G., and D.P. Guertin. 2007. The Automated Geospatial Watershed Assessment Tool. Journal of Environmental Modeling and Software 22:365.377

Mills, G.S., Dunning, J.B., and J.M. Bated. 1991. The relationship between breeding bird density and vegetation volume. Wilson Bulletin 103(3):468-479.

Morrison, M., Block, W.M., Hall, L.S., and H.S. Stone. 1995. Habitat characteristics and monitoring of amphibians and reptiles in the Huachuca Mountains, Arizona. The Southwestern Naturalist 40(2): 185-192.

Myers, L.M., Mathews, N.E., and J.M. Kozma. 1998. Final report: long term monitoring of Neotropical migrant and breeding bird populations in arroyos and uplands on Fort Bliss Military Reservation.

Naiman, R.J., Dé camps, H., and M. Pollock. 1993. The role of riparian corridors in maintaining regional biodiversity. Ecological Applications 3:209-212.

NatureServe. 2014. NatureServe Explorer: An online encyclopedia of life [web application]. Version 7.1. NatureServe, Arlington, Virginia. Available <http://explorer.natureserve.org>.

NOAA. 2012. National Oceanic and Atmospheric Administration's Precipitation Frequency Data Server. Precipitation dataset. Retrieved 04/25/2012, from <http://dipper.nws.noaa.gov/hdsc/pfds/>

National Research Council (NRC). 2002. Riparian areas: functions and strategies for management. National Academy of Science. Washington, DC.

Oberholser, H. C. 1974. The bird life of Texas. University of Texas Press, Austin.

Ohmart, R.D. and C.D. Zisner. 1993. Functions and values of riparian habitat to wildlife in Arizona, a literature review. Center for Environmental Studies, Arizona State University, Tempe, AZ. Submitted to Arizona Game and Fish Department, Contract Number G300-25B.

Pardieck, K.L., Ziolkowski, D.J. Jr., and M.-A.R. Hudson. 2014. North American Breeding Bird Survey Dataset 1966 - 2013, version 2013.0. U.S. Geological Survey, Patuxent Wildlife Research Center <www.pwrc.usgs.gov/BBS/RawData/>

Parker, K.C. 1986. Partitioning of foraging space and nest sites in a desert shrubland bird community. American Midland Naturalist, 115:255-267.

Patterson, B.D., Ceballos, G., Sechrest, W., Tognelli, M.F., Brooks, T., Luna,, L., Ortega, P., Salazar, I., and B.E. Young. 2003. Digital distribution maps of the mammals of the Western Hemisphere, version 1.0. NatureServe, Arlington, Virginia, USA.

Poole, A. (Editor). 2014. The birds of North America online: http://bna.birds.cornell.edu/BNA/. Cornell Laboratory of Ornithology, Ithaca, NY.

Powell, B.F. and R.J. Steidl. 2002. Habitat selection by riparian songbirds breeding in southern Arizona. Journal of Wildlife Management 66(4):1096-1102.

PRISM Climate Group. 2010. Oregon State University, <http://prism.oregonstate.edu>.

Qian, H., Kissling, W.D., Wang, X., and P. Andrews. 2009. Effects of woody plant species richness on mammal species richness in southern Africa. Journal of Biogeography 36:1685–1697

R Core Team. 2014. R: A language and environment for statistical computing. R Foundation for Statistical Computing, Vienna, Austria <http://www.R-project.org>

Radosavljevic, A. and R.P. Anderson. 2013. Making better MAXENT models of species distributions: complexity, overfitting and evaluation. Journal of Biogeography 41(4):629-643.

Ragotzkie, K.E. and J.A. Bailey. 1991. Desert mule deer use of grazed and ungrazed habitats. Journal of Range Management, 44(5):487-490.

RHJV (Riparian Habitat Joint Venture). 2004. The riparian bird conservation plan: a strategy for reversing the decline of riparian associated birds in California. California Partners in Flight. <http://www.prbo.org/calpif/pdfs/riparian_v-2.pdf>

Ridgely, R.S., Allnutt, T.F., Brooks, T., McNicol, D.K., Mehlman, D.W., Young, B.E., and J.R. Zook. 2003. Digital distribution maps of the birds of the Western Hemisphere, version 1.0. NatureServe, Arlington, Virginia, USA.

Rosen, P.C. and C.H. Lowe. 1996. Ecology of the amphibians and reptiles at Organ Pipe Cactus National Monument, Arizona. Tech. Report #53. Cooperative Park Studies Unit, The University of Arizona, Tucson.

Rosenberg, K.V., Ohmart, R.D., Hunter, W.C., and B.W. Anderson. 1991. Birds of the Lower Colorado River Valley. University of Arizona Press, Tucson.

Rosgen, D. 1994. A classification of natural rivers. Catena 22(3): 169-199.

Sabo, J. L. and C. U. Soykan. 2006. Riparian zones increase regional richness by supporting different, not more, species: Reply. Ecology 87:2128-2131.

Sabo, J. L., Sponseller, R., Dixon, M., Gade, K., Harms, T., Heffernan, J., Jani, A., Katz, G., Soykan, C., Watts, J., and A. Welter. 2005. Riparian zones increase regional species richness by harboring different, not more, species. Ecology 86:56-62.

Schlossberg, S. 2006. Abundance and habitat preferences of gray vireos (Vireo vicinior) on the Colorado Plateau. Auk 123:33-44.

Schwinning, S., Sandquist, D. R., Miller, D. M., Bedford, D. R., Phillips, S. L., and J. Belnap. 2011. The influence of stream channels on distributions of *Larrea tridentata* and *Ambrosia dumosa* in the Mojave Desert, CA, USA: patterns, mechanisms and effects of stream redistribution. Ecohydrology 4: 12–25.

Seavy, N.E., Viers, J.H., and J.K. Wood. 2009. Riparian bird response to vegetation structure: a multiscale analysis using LiDAR measurements of canopy height. Ecological Applications 19(7):1848-1857.

Sedgwick, J. A. 1987. Avian habitat relationships in pinyon-juniper woodland. Wilson Bulletin 99:413-431.

Shanahan, S.A., Nelson, S.M., Van Dooremolen, D.M., and J.R. Eckberg. 2011. Restoring habitat for riparian birds in the Lower Colorado River watershed: an example from the Las Vegas Wash, Nevada. 2011. Journal of Arid Environments 75(11):1182–1190.

Shannon, C.E. and W. Weaver. 1949. The mathematical theory of communication. The University of Illinois Press, Urbana, 117pp.

Shaw, J.R. and D.J. Cooper. 2008. Linkages among watersheds, stream reaches, and riparian vegetation in dryland ephemeral stream networks. Journal of Hydrology 350: 68-82.

Shcheglovitova, M. and R.P. Anderson. 2013. Estimating optimal complexity for ecological niche models: a jackknife approach for species with small sample sizes. Ecological Modelling 269:9-17.

Sing, T., Sander, O., Beerenwinkel, N., and T. Lengauer. 2005. ROCR: visualizing classifier performance in R. Bioinformatics, 21(20): 7881. <http://rocr.bioinf.mpi-sb.mpg.de>.

Skagen, S.K., Kelly, J.F., Van Riper, C., Hutto, R.L., Finch, D.M., Krueper, D.J., and C.P. Melcher. 2005. Geography of spring landbird migration through riparian habitats in southwestern North America. The Condor 107:212–227.

Steward, A. L., von Schiller, D., Tockner, K., Marshall, J.C., and S.E. Bunn. 2012. When the river runs dry: human and ecological values of dry riverbeds. Frontiers in Ecology and the Environment 10:202-209.

Stromberg J.C. 2007. Seasonal reversals of upland-riparian diversity gradients in the Sonoran Desert. Diversity and Distributions 13:70-83.

Stromberg, J.C., Hazelton, A.F., and M.S. White. 2009. Plant species richness in ephemeral and perennial reaches of a dryland river. Biodiversity Conservation 18:663-677.

Strong, T. R. and C. E. Bock. 1990. Bird species distribution patterns in riparian habitats in southeastern Arizona. Condor 92:866-885.

Sullivan, B.L., Wood, C.L., Iliff, M.J., Bonney, R.E., Fink, D., and S. Kelling. 2009. eBird: a citizen-based bird observation network in the biological sciences. Biological Conservation 142: 2282-2292.

Tews, J., Borse, U., Grimm, V., Tielborger, K., Wichmann, M.C., Schwager, M., and F. Jeltsch. 2004. Animal species diversity driven by habitat heterogeneity/diversity; the importance of keystone structures. Journal of Biogeography 31(1):79-92.

Thomas, J.W., Maser, C., and J.E. Rodiek. 1979. Edges. In: J.W. Thomas (Ed.), Wildlife Habitats in Managed Forest: the Blue Mountains of Oregon and Washington. USDA Forest Service Agricultural Handbook Number 553.

Tooth, S. 2000. Process, form and change in dryland rivers: a review of recent research. Earth-Science Reviews 51:67-107.

U.S. Army, Fort Bliss Integrated Natural Resources Management Plan, 2001. Prepared by Fort Bliss Directorate of Environment Conservation Division; Science Applications International Corp.; Center for Ecological Management of Military Lands; U.S. Army Corps of Engineers; and Geo-Marine, Inc.

U.S. Environmental Protection Agency (EPA). 2005. Letter from Benjamin H. Grumbles, Assistant Administrator, EPA, to Ms. Jeanne Christie, Executive Director, Association of State Wetland Managers, dated Jan. 9, 2005.

U.S. Geological Survey (USGS). 2006. National Hydrography Dataset (NHD) website, <http://nhd.usgs.gov/index.html>.

U.S. Geological Survey National Gap Analysis Program (USGS-GAP). 2007. Digital animal-habitat models for the Southwestern United States. Version 1.0. Center for Applied Spatial Ecology, New Mexico Cooperative Fish and Wildlife Research Unit, New Mexico State University

U.S. Geological Survey, Gap Analysis Program (GAP). May 2011. National land cover, version 2 <http://gapanalysis.usgs.gov/gaplandcover/>.

U.S. Geological Survey Gap Analysis Program (USGS-GAP). 2014. National species distribution models. Available: <http://gapanalysis.usgs.gov>. Accessed October 2014.

UNEP. 1992. World Atlas of Desertification. Edward Arnold, Sevenoaks, UK.

Vale, T. R., Parker, K.C., and A. J. Parker. 1989. Terrestrial vertebrates and vegetation structure in the western United States. The Professional Geographer 41(4):450-464.

Van Devender, T.R. 2002. The Sonoran desert tortoise: natural history, biology, and conservation. University of Arizona Press, Tucson.

Wagener, S. M., Oswood, M.W., and J. P. Schimel. 1998. Rivers and soils: parallels in carbon and nutrient processing. Bioscience 48:104-108.

Warren, P.L. and L.S. Anderson. 1985. Gradient analysis of a Sonoran Desert wash. In: Riparian Ecosystems and Their Management: Reconciling Conflicting Uses. First North American Riparian Conference, April 16-18, 1985. U.S.D.A. Forest Service General Technical Report RM-120, p. 150-155.

White Sands Technical Services. Britt, C., and C. Lundblad. 2007. Gray vireo status and distribution on Fort Bliss: 2007.

Whittaker, R.H. 1960. Vegetation of the Siskiyou mountains, Oregon and California. Ecological Monographs 30:279-338.

Wolff, J.O. 1995. On the limits of species-habitat association studies. Northwest Science 69:72-76.

Zia Engineering and Environmental Consultants. Hobert, J., Hartsough, M., and D. Burkett. 2010. Gray Vireo status and distribution on Sacramento Mountains portions of Fort Bliss – 2008.

Zia Engineering and Environmental Consultants. Griffin, D., Burkett, D., and R. Wu. 2012a. Surveys for avian species of concern in the Organ Mountains on Fort Bliss.

Zia Engineering and Environmental Consultants. Hanks, T., Schielke, B., and D. Burkett. 2012b.Gray Vireo surveys and nest monitoring on Ft. Bliss, Otero County, New Mexico.

Zia Engineering and Environmental Consultants. Griffin, D., and K. Stabinsky. 2013. 2012 Gray Vireo surveys and nest monitoring on Fort Bliss Military Reservation.

Zimmerman, J.A.C., DeWald, L.E., and P.G. Rowlands. 1999. Vegetation diversity in an interconnected ephemeral riparian system of north-central Arizona, USA. Biological Conservation. 90:217-228.

APPENDIX A – wildlife tables

Species Richness:
Table 1. Riparian-associated species occurring or possible at Fort Bliss, NM. Source of model or lack of availability indicated by USGS (National GAP), SW (Southwest Regional GAP), or None. Species with an asterisk in the model column were subspecies represented by the full species model or species represented by another GAP model because taxonomy changed. Inclusion in TERS group indicated with a Y (yes) or N (no). Season of use for birds indicated by S (summer), W (winter), YR (year-round), or M (passage migrant). Riparian-dependency indicated by N (No), F (Facultative), I (Important, but not obligate), O (Obligate), or "not RA" (not on the riparian-associated list).

Model Source	Scientific Name	Common Name	Taxon	TERS	Rip. Rank	Season
USGS	*Ambystoma tigrinum/mavortium*	Tiger salamander	A		I	
SW	*Anaxyrus/Bufo cognatus*	Great Plains toad	A		I	
SW	*Anaxyrus/Bufo debilis*	Green toad	A		I	
SW	*Anaxyrus/Bufo punctatus*	Red-spotted toad	A		O	
SW	*Anaxyrus/Bufo woodhousii*	Woodhouse's toad	A		I	
SW	*Hyla arenicolor*	Canyon tree frog	A		O	
SW	*Scaphiopus couchii*	Couch's spadefoot	A		N	
SW	*Spea bombifrons*	Plains spadefoot	A		N	
SW	*Spea multiplicata*	New Mexico/Mexican spadefoot	A		N	
USGS	*Accipiter cooperii*	Cooper's hawk	B		F or I	W,YR
USGS	*Accipiter striatus*	Sharp-shinned hawk	B		F or I	W,YR

Model Source	Scientific Name	Common Name	Taxon	TERS	Rip. Rank	Season
SW	*Agelaius phoeniceus*	Red-winged blackbird	B		O	YR
USGS	*Amphispiza belli/Artemisiospiza nevadensis*	Sage sparrow	B	N	F or I	W
USGS	*Amphispiza bilineata*	Black-throated sparrow	B		N	S
USGS	*Aphelocoma californica*	Western scrub-jay	B		F	YR
USGS	*Archilochus alexandrinus*	Black-chinned hummingbird	B		I or O	S
USGS	*Asio otus*	Long-eared owl	B		I	YR
USGS	*Asturina nitidus/Buteo plagiatus*	Gray hawk	B	Y	O	S
USGS	*Bubo virginianus*	Great horned owl	B		F	YR
USGS	*Buteo albonotatus*	Zone-tailed hawk	B	Y	I	S
USGS	*Buteo regalis*	Ferruginous hawk	B		N	W
USGS	*Buteo swainsoni*	Swainson's hawk	B		F	S
USGS	*Buteogallus anthracinus*	Common black-hawk	B	Y	O	S
USGS	*Callipepla gambelii*	Gambel's quail	B		I	YR
USGS	*Callipepla squamata*	Scaled quail	B	Y	F	YR
USGS	*Calypte costae*	Costa’s hummingbird	B	Y	F	S
USGS	*Cardinalis sinuatus*	Pyrrhuloxia	B		F or I	YR
USGS	*Carduelis lawrencei*	Lawrence’s goldfinch	B	Y	I	W
USGS	*Carduelis psaltria*	Lesser goldfinch	B		O	YR
USGS	*Carduelis tristis*	American goldfinch	B	N	F	W
USGS	*Cathartes aura*	Turkey vulture	B		F	S
None	*Catharus ustulatus*	Swainson’s thrush	B		NR	na
USGS	*Catherpes mexicanus*	Canyon wren	B		I	YR
USGS	*Ceryle alcyon*	Belted kingfisher	B		O	W

Model Source	Scientific Name	Common Name	Taxon	TERS	Rip. Rank	Season
USGS	*Chordeiles acutipennis*	Lesser nighthawk	B		F	S
USGS	*Cinclus mexicanus*	American dipper	B	Y	O	YR
USGS	*Cistothorus palustris*	Marsh wren	B	N	O	W
USGS	*Coccyzus americanus*	Yellow-billed cuckoo	B	Y	O	S
USGS	*Contopus sordidulus*	Western wood-pewee	B		F	S
USGS	*Corvus brachyrhynchos*	American crow	B		O	W
None	*Crotophaga sulcirostris*	Groove-billed ani	B		NR	na
None	*Dendroica fusca*	Blackburnian warbler	B		NR	na
None	*Dendroica occidentalis*	Hermit warbler	B		NR	na
None	*Dendroica palmarum*	Palm warbler	B		NR	na
None	*Dendroica pensylvanica*	Chestnut-sided warbler	B		NR	na
None	*Dendroica striata*	Blackpoll warbler	B		NR	na
None	*Dendroica virens*	Black-throated green warbler	B		NR	na
None	*Dolichonyx oryzivorus*	Bobolink	B		NR	na
USGS	*Elanus leucurus*	White-tailed kite	B	Y	F	YR
None	*Empidonax minimus*	Least flycatcher	B		NR	na
USGS	*Empidonax oberholseri*	Dusky flycatcher	B		F	M
USGS	*Empidonax occidentalis*	Cordilleran flycatcher	B		O	S
USGS	*Empidonax traillii extimus*	Southwestern Willow flycatcher	B	Y	O	S
USGS	*Empidonax wrightii*	Gray flycatcher	B	Y	I	S
None	*Euphagus carolinus*	Rusty blackbird	B		NR	na
USGS	*Euphagus cyanocephalus*	Brewer's blackbird	B		I	W,YR
USGS	*Falco femoralis*	Aplomado Falcon	B	Y	N	YR

Model Source	Scientific Name	Common Name	Taxon	TERS	Rip. Rank	Season
USGS	*Falco sparverius*	American kestrel	B		F	YR
USGS	*Geothlypis trichas*	Common yellowthroat	B		O	S
USGS	*Haliaeetus leucocephalus*	Bald eagle	B	Y	I	W
USGS	*Icteria virens*	Yellow-breasted chat	B	Y	I	S
USGS	*Icterus bullockii*	Bullock's oriole	B		F	S
USGS	*Icterus cucullatus*	Hooded oriole	B	Y	I	S
None	*Icterus galbula*	Baltimore oriole	B		NR	na
USGS	*Icterus parisorum*	Scott's oriole	B		N	S
USGS	*Ictinia mississippiensis*	Mississippi kite	B	Y	I	S
USGS	*Junco hyemalis*	Dark-eyed junco	B		N	W
USGS	*Lanius excubitor*	Northern shrike	B		N	W
USGS	*Melospiza georgiana*	Swamp sparrow	B		I	W
USGS	*Melospiza lincolnii*	Lincoln's sparrow	B	N	O	W
USGS	*Melospiza melodia*	Song sparrow	B		O	W
USGS	*Mimus polyglottos*	Northern mockingbird	B		N	YR
USGS	*Oporornis tolmei*	MacGillivray's warbler	B		I	S
USGS	*Oreoscoptes montanus*	Sage thrasher	B	N	N	W
USGS	*Otus/Megascops kennicotti*	Western screech-owl	B		I	YR
USGS	*Pandion haliaetus*	Osprey	B	Y	O	YR
USGS	*Parabuteo unicinctus*	Harris's hawk	B	Y	I	YR
None	*Parula americana*	Northern parula	B		NR	na
USGS	*Passerella iliaca*	Fox sparrow	B		I	W
USGS	*Passerina amoena*	Lazuli bunting	B		I	W

Model Source	Scientific Name	Common Name	Taxon	TERS	Rip. Rank	Season
USGS	*Passerina caerulea*	Blue grosbeak	B		F	S
USGS	*Passerina ciris*	Painted bunting	B		F	S
USGS	*Passerina cyanea*	Indigo bunting	B		I	S
USGS	*Passerina versicolor*	Varied bunting	B	Y	O	S
USGS	*Petrochelidon fulva*	Cave swallow	B	Y	I	S
USGS	*Petrochelidon pyrrhonota*	Cliff swallow	B		I	S
USGS	*Phainopepla nitens*	Phainopepla	B		I	S
None	*Pheucticus ludovicianus*	Rose-breasted grosbeak	B		NR	na
USGS	*Pheucticus melanocephalus*	Black-headed grosbeak	B		I	S
USGS	*Picoides pubescens*	Downy woodpecker	B		F	YR
USGS	*Picoides villosus*	Hairy woodpecker	B		F	YR
USGS	*Pipilo chlorurus*	Green-tailed towhee	B	N	F	W
None	*Pipilo erythrophthalmus*	Eastern towhee	B		NR	na
USGS	*Pipilo maculatus*	Spotted towhee	B		I	YR
USGS	*Pipilo/Melozone fuscus*	Canyon towhee	B		F or I	YR
USGS	*Piranga rubra*	Summer tanager	B		O	S
USGS	*Polioptila caerulea*	Blue-gray gnatcatcher	B		F	S
USGS	*Polioptila melanura*	Black-tailed gnatcatcher	B	Y	I	YR
None	*Protonotaria citrea*	Prothonotary warbler	B		NR	na
USGS	*Quiscalus mexicanus*	Great-tailed grackle	B		I	YR
USGS	*Riparia riparia*	Bank swallow	B		I	S
USGS	*Salpinctes obsoletus*	Rock wren	B		F	W
USGS	*Sayornis nigricans*	Black phoebe	B		O	YR

Model Source	Scientific Name	Common Name	Taxon	TERS	Rip. Rank	Season
USGS	*Sayornis phoebe*	Eastern phoebe	B		I	W
None	*Seiurus noveboracensis*	Northern waterthrush	B		NR	na
None	*Setophaga ruticilla*	American redstart	B		NR	na
USGS	*Sphyrapicus nuchalis*	Red-naped sapsucker	B	N	F	W
USGS	*Spizella atrogularis*	Black-chinned sparrow	B	Y	F	S,W
USGS	*Spizella pallida*	Clay-colored sparrow	B		N or F	W
USGS	*Stelgidopteryx serripennis*	Northern rough-winged swallow	B		I	S
USGS	*Strix occidentalis lucida*	Mexican spotted owl	B	Y	I	YR
USGS	*Tachycineta bicolor*	Tree swallow	B	N	O	W
USGS	*Thryomanes bewickii*	Bewick's wren	B		F	W
USGS	*Toxostoma dorsalis/crissale*	Crissal thrasher	B		O	YR
USGS	*Toxostoma rufum*	Brown thrasher	B		I	YR
USGS	*Troglodytes aedon*	House wren	B		F	W,YR
None	*Tyrannus tyrannus*	Eastern kingbird	B		NR	na
USGS	*Tyrannus vociferans*	Cassin's kingbird	B		I	S
None	*Vermivora chrysoptera*	Golden-winged warbler	B		NR	na
USGS	*Vermivora/Oreothlypis celata*	Orange-crowned warbler	B		F or I	S,W
USGS	*Vermivora/Oreothlypis luciae*	Lucy's warbler	B	Y	O	S
USGS	*Vermivora/Oreothlypis virginiae*	Virginia's warbler	B	Y	F	S
USGS	*Vireo bellii medius*	Bell's vireo	B	Y	I	S
USGS	*Vireo gilvus*	Warbling vireo	B		F or I	S
USGS	*Vireo huttoni*	Hutton's vireo	B		F	na
USGS	*Vireo plumbeus*	Plumbeous vireo	B		F or I	S

Model Source	Scientific Name	Common Name	Taxon	TERS	Rip. Rank	Season
USGS	*Vireo vicinior*	Gray vireo	B	Y	N	S
None	*Wilsonia citrina*	Hooded warbler	B		NR	na
USGS	*Xanthocephalus xanthocephalus*	Yellow-headed blackbird	B		F	W
USGS	*Zenaida asiatica*	White-winged dove	B		F	W
None	*Zonotrichia querula*	Harris's sparrow	B		NR	na
SW	*Ammospermophilus interpres*	Texas antelope squirrel	M	Y	N	
USGS	*Antrozous pallidus*	Pallid bat	M		I	
USGS	*Bassariscus astutus*	Ringtail	M		I	
None	*Chaetodipus eremicus*	Chihuahuan pocket mouse	M		NR	
SW	*Chaetodipus hispidus*	Hispid pocket mouse	M	Y	N	
USGS	*Chaetodipus intermedius*	Rock pocket mouse	M		F	
USGS	*Corynorhinus townsendii*	Townsend's big-eared bat	M	Y	F	
*	*Corynorhinus townsendii pallescens*	Pale lump-nosed bat	M	Y	F	
SW	*Dicotyles/Pecari tajacu*	Javelina / Collared peccary	M		I	
USGS	*Eptesicus fuscus*	Big brown bat	M		F	
SW	*Erethizon dorsatum*	Porcupine	M		F	
USGS	*Lasionycteris noctivagans*	Silver-haired bat	M		O	
USGS	*Lasiurus blossevillii*	Western red bat	M	Y	O	
USGS	*Lasiurus cinereus*	Hoary bat	M		F	
USGS	*Lynx rufus*	Bobcat	M		F	
SW	*Mephitis mephitis*	Striped skunk	M		F or I	
SW	*Microtus mogollonensis*	Mogollon vole	M		F	
USGS	*Mustela frenata*	Long-tailed weasel	M		I	

Model Source	Scientific Name	Common Name	Taxon	TERS	Rip. Rank	Season
USGS	*Myotis lucifugus*	Little brown myotis	M	Y	I	
USGS	*Myotis occultus*	Occult little brown bat / Arizona myotis	M		O	
USGS	*Myotis velifer*	Cave myotis	M	Y	O	
USGS	*Myotis volans*	Long-legged myotis	M		F	
USGS	*Myotis yumanensis*	Yuma myotis	M		O	
USGS	*Nyctinomops macrotis*	Big free-tailed bat	M	Y	F	
SW	*Odocoileus hemionus*	Mule deer	M		I	
USGS	*Peromyscus boylii*	Brush mouse	M		F	
SW	*Peromyscus leucopus*	White-footed mouse	M		F	
SW	*Pipi/parastrellus hesperus*	Western pipistrelle / Canyon bat	M		O	
SW	*Procyon lotor*	Raccoon	M		I	
USGS	*Puma concolor*	Mountain lion	M	Y	I	
SW	*Reithrodontomys megalotis*	Western harvest mouse	M		F	
SW	*Sigmodon hispidus*	Hispid cotton rat	M		F	
USGS	*Spilogale gracilis*	Western spotted skunk	M		I	
SW	*Sylvilagus audubonii*	Desert cottontail	M		F	
SW	*Sylvilagus floridanus*	Eastern cottontail	M		F	
USGS	*Tadarida brasiliensis*	Brazilian/Mexican free-tailed bat	M	Y	N	
SW	*Urocyon cinereoargenteus*	Gray fox	M		I	
USGS	*Ursus americanus*	Black bear	M		I	
USGS	*Arizona elegans*	Glossy snake	R		N	
USGS	*Aspidoscelis exsanguis*	Chihuahuan spotted whiptail	R		I	
USGS	*Aspidoscelis inornata*	Little striped whiptail	R		N	

Model Source	Scientific Name	Common Name	Taxon	TERS	Rip. Rank	Season
USGS	*Aspidoscelis neomexicana*	New Mexico whiptail	R		I	
USGS	*Aspidoscelis tesselata*	Checkered whiptail	R		F	
USGS	*Aspidoscelis tigris*	Western/Tiger whiptail	R	Y	F	
USGS	*Aspidoscelis uniparens*	Desert grassland whiptail	R		F	
None	*Chrysemys picta*	Painted turtle	R		O	
None	*Coluber constrictor*	Racer	R		F	
USGS	*Cophosaurus texanus*	Greater earless lizard	R		I	
SW	*Crotalus atrox*	Western diamondback rattlesnake	R		F	
SW	*Crotalus lepidus*	Rock rattlesnake	R		F	
*	*Crotalus lepidus klauberi*	Banded rock rattlesnake	R	Y	F	
*	*Crotalus lepidus lepidus*	Mottled rock rattlesnake	R	Y	F	
USGS	*Crotalus molossus*	Black-tailed rattlesnake	R		N	
USGS	*Crotaphytus collaris*	Eastern collared lizard	R		N or F	
SW	*Diadophis punctatus*	Ringneck snake	R		I	
SW	*Elaphe gutatta/Pantherophis guttatus*	Red cornsnake / Great Plains ratsnake	R		I	
USGS	*Holbrookia maculata*	Lesser earless lizard	R		F	
SW	*Hypsiglena chlorophaea*	Night snake	R		N	
SW	*Kinosternon flavescens*	Yellow mud turtle	R		O	
USGS	*Lampropeltis alterna*	Gray-banded kingsnake	R	Y	F	
USGS	*Lampropeltis getula*	Common kingsnake	R		N	
*	*Lampropeltis splendida*	Desert kingsnake	R	(Y)	N	
SW	*Leptotyphlops/Rena dulcis*	Texas blind/thread snake	R		F	
SW	*Leptotyphlops/Rena humilis*	Western blind/thread snake	R	Y	F	

Model Source	Scientific Name	Common Name	Taxon	TERS	Rip. Rank	Season
USGS	*Masticophis/Coluber flagellum*	Western coachwhip	R		F	
SW	*Masticophis/Coluber taeniatus*	Striped whipsnake	R		F	
USGS	*Phrynosoma modestum*	Roundtail horned lizard	R		F	
USGS	*Plestiodon obsoletus*	Great Plains skink	R		I	
USGS	*Rhinocheilus lecontei*	Longnose snake	R		F	
SW	*Salvadora grahamiae*	Mountain/Eastern patchnose snake	R		N	
SW	*Salvadora hexalepis*	Western patchnose snake	R		F	
*	*Salvadora hexalepis deserticola*	Big bend patchnose snake	R		F	
USGS	*Sceloporus magister*	Desert spiny lizard	R		F	
USGS	*Sceloporus poinsettii*	Crevice spiny lizard	R		F	
SW	*Sceloporus undulatus(?)*	Prairie lizard	R		F	
USGS	*Sistrurus catenatus*	Massasauga	R	Y	F	
SW	*Sonora semiannulata*	Western Ground snake	R		N	
SW	*Tantilla hobartsmithi*	Smith's/Southwestern black-headed snake	R		N	
SW	*Tantilla nigriceps*	Plains black-headed snake	R		F	
SW	*Thamnophis cyrtopsis*	Blackneck garter snake	R		I	
SW	*Thamnophis marcianus*	Checkered garter snake	R		O	
USGS	*Thamnophis sirtalis*	Common garter snake	R		O	
USGS	*Trimorphodon biscutatus*	Western/Texas lyresnake	R		F	
*	*Trimorphodon lambda*	Sonoran lyresnake	R	Y	F	
USGS	*Trimorphodon vilkinsonii*	Texas lyresnake	R	Y	F	
USGS	*Urosaurus ornatus*	Ornate tree lizard	R		I	
USGS	*Uta stansburiana*	Common side-blotched lizard	R		I	

Model Source	Scientific Name	Common Name	Taxon	TERS	Rip. Rank	Season
na	*Craugastor augusti*	Western barking frog	A		not RA	
na	*Accipiter gentilis*	Northern (Apache) goshawk	B		not RA	
na	*Aeronautes saxatilis*	White-throated swift	B		not RA	
na	*Aimophila cassinii*	Cassin's sparrow	B		not RA	
na	*Aimophila ruficeps*	Rufous-crowned sparrow	B		not RA	
na	*Ammodramus bairdii*	Baird's sparrow	B		not RA	
na	*Ammodramus leconteii*	Le Conte's sparrow	B		not RA	
na	*Ammodramus savannarum*	(Arizona) Grasshopper sparrow	B		not RA	
na	*Anthus rubescens*	American pipit	B		not RA	
na	*Anthus spraguei*	Sprague's pipit	B		not RA	
na	*Aquila chrysaetos*	Golden eagle	B		not RA	
na	*Asio flammeus*	Short-eared owl	B		not RA	
na	*Athene cunicularia*	Western burrowing owl	B		not RA	
na	*Auriparus flaviceps*	Verdin	B		not RA	
na	*Baeolophus ridgwayi*	Juniper titmouse	B		not RA	
na	*Bombycilla cedrorum*	Cedar waxwing	B		not RA	
na	*Buteo jamaicensis*	Red-tailed hawk	B		not RA	
na	*Buteo lagopus*	Rough-legged hawk	B		not RA	
na	*Calamospiza melanocorys*	Lark bunting	B		not RA	
na	*Calcarius lapponicus*	Lapland longspur	B		not RA	
na	*Calcarius mccownii*	McCown's longspur	B		not RA	
na	*Calcarius ornatus*	Chestnut-collared longspur	B		not RA	
na	*Campylorhynchus brunneicapillus*	Cactus wren	B		not RA	

Model Source	Scientific Name	Common Name	Taxon	TERS	Rip. Rank	Season
na	*Caprimulgus vociferus*	Whip-poor-will	B		not RA	
na	*Cardellina rubrifrons*	Red-faced warbler	B		not RA	
na	*Carduelis pinus*	Pine siskin	B		not RA	
na	*Carpodacus cassini*	Cassin's finch	B		not RA	
na	*Carpodacus mexicanus*	House finch	B		not RA	
na	*Carpodacus purpureus*	Purple finch	B		not RA	
na	*Catharus guttatus*	Hermit thrush	B		not RA	
na	*Certhia americana*	Brown creeper	B		not RA	
na	*Chondestes grammacus*	Lark sparrow	B		not RA	
na	*Chordeiles minor*	Common nighthawk	B		not RA	
na	*Circus cyaneus*	Northern harrier	B		not RA	
na	*Coccothraustes vespertinus*	Evening grosbeak	B		not RA	
na	*Colaptes auratus*	Northern flicker	B		not RA	
na	*Columba fasciata*	Band-tailed pigeon	B		not RA	
na	*Columbina inca*	Inca dove	B		not RA	
na	*Contopus cooperi*	Olive-sided flycatcher	B		not RA	
na	*Corvus corax*	Common raven	B		not RA	
na	*Corvus cryptoleucus*	Chihuahuan raven	B		not RA	
na	*Cyanocitta stelleri*	Steller's jay	B		not RA	
na	*Cypseloides niger*	Black swift	B		not RA	
na	*Cyrtonyx montezumae*	Montezuma quail	B		not RA	
na	*Dendroica coronata*	Yellow-rumped warbler	B		not RA	
na	*Dendroica graciae*	Grace's warbler	B		not RA	

Model Source	Scientific Name	Common Name	Taxon	TERS	Rip. Rank	Season
na	*Dendroica nigrescens*	Black-throated gray warbler	B		not RA	
na	*Dendroica petechia*	Yellow warbler	B		not RA	
na	*Dendroica townsendi*	Townsend's warbler	B		not RA	
na	*Empidonax hammondii*	Hammond's flycatcher	B		not RA	
na	*Eremophila alpestris*	Horned lark	B		not RA	
na	*Falco columbarius*	Merlin	B		not RA	
na	*Falco mexicanus*	Prairie falcon	B		not RA	
na	*Falco peregrinus*	Peregrine falcon	B		not RA	
na	*Geococcyx californicus*	Greater roadrunner	B		not RA	
na	*Glaucidium gnoma*	Northern pygmy-owl	B		not RA	
na	*Gymnorhinus cyanocephalus*	Pinyon jay	B		not RA	
na	*Hirundo rustica*	Barn swallow	B		not RA	
na	*Lanius ludovicianus*	Loggerhead shrike	B		not RA	
na	*Loxia curvirostra*	Red crossbill	B		not RA	
na	*Melanerpes formicivorus*	Acorn woodpecker	B		not RA	
na	*Melanerpes lewis*	Lewis woodpecker	B		not RA	
na	*Meleagris gallopavo*	Gould's wild turkey	B		not RA	
na	*Mniotilta varia*	Black-and-white warbler	B		not RA	
na	*Molothrus ater*	Brown-headed cowbird	B		not RA	
na	*Molothus aeneus*	Bronzed cowbird	B		not RA	
na	*Myadestes townsendi*	Townsend's solitaire	B		not RA	
na	*Myiarchus cinerascens*	Ash-throated flycatcher	B		not RA	
na	*Myioborus pictus*	Painted redstart	B		not RA	

Model Source	Scientific Name	Common Name	Taxon	TERS	Rip. Rank	Season
na	*Passerculus sandwichensis*	Savannah sparrow	B		not RA	
na	*Phalaenoptila nuttallii*	Common poorwill	B		not RA	
na	*Picoides scalaris*	Ladder-backed woodpecker	B		not RA	
na	*Piranga flava*	Hepatic tanager	B		not RA	
na	*Piranga ludoviciana*	Western tanager	B		not RA	
na	*Poecile gambeli*	Mountain chickadee	B		not RA	
na	*Pooecetes gramineus*	Vesper sparrow	B		not RA	
na	*Progne subis*	Purple martin	B		not RA	
na	*Psaltriparus minimus*	Bushtit	B		not RA	
na	*Regulus calendula*	Ruby-crowned kinglet	B		not RA	
na	*Regulus satrapa*	Golden-crowned kinglet	B		not RA	
na	*Sayornis saya*	Say's phoebe	B		not RA	
na	*Selasphorus platycercus*	Broad-tailed hummingbird	B		not RA	
na	*Selasphorus rufus*	Rufous hummingbird	B		not RA	
na	*Sialia currucoides*	Mountain bluebird	B		not RA	
na	*Sialia mexicana*	Western bluebird	B		not RA	
na	*Sialia sialis*	Eastern bluebird	B		not RA	
na	*Sitta canadensis*	Red-breasted nuthatch	B		not RA	
na	*Sitta carolinensis*	White-breasted nuthatch	B		not RA	
na	*Sitta pygmaea*	Pygmy nuthatch	B		not RA	
na	*Sphyrapicus thyroideus*	Williamson's sapsucker	B		not RA	
na	*Sphyrapicus varius*	Yellow-bellied sapsucker	B		not RA	
na	*Spiza americana*	Dickcissel	B		not RA	

Model Source	Scientific Name	Common Name	Taxon	TERS	Rip. Rank	Season
na	*Spizella breweri*	Brewer's sparrow	B		not RA	
na	*Spizella passerina*	Chipping sparrow	B		not RA	
na	*Sturnella magna*	Eastern meadowlark	B		not RA	
na	*Sturnella neglecta*	Western meadowlark	B		not RA	
na	*Tachycineta thalassina*	Violet-green swallow	B		not RA	
na	*Toxostoma curvirostre*	Curve-billed thrasher	B		not RA	
na	*Turdus migratorius*	American robin	B		not RA	
na	*Tyrannus verticalis*	Western kingbird	B		not RA	
na	*Tyto alba*	Barn owl	B		not RA	
na	*Vermivora peregrina*	Tennessee warbler	B		not RA	
na	*Vermivora ruficapilla*	Nashville warbler	B		not RA	
na	*Vireo cassinii*	Cassin's vireo	B		not RA	
na	*Vireo olivaceus*	Red-eyed vireo	B		not RA	
na	*Vireo philadelphicus*	Philadelphia vireo	B		not RA	
na	*Wilsonia pusilla*	Wilson's warbler	B		not RA	
na	*Zenaida macroura*	Mourning dove	B		not RA	
na	*Zonotrichia albicollis*	White-throated sparrow	B		not RA	
na	*Zonotrichia leucophrys*	White-crowned sparrow	B		not RA	
na	*(Neo)Tamias minimus*	Least chipmunk	M		not RA	
na	*Antilocapra americana*	Pronghorn	M		not RA	
na	*Canis latrans*	Coyote	M		not RA	
na	*Chaetodipus penicillatus*	Desert pocket mouse	M		not RA	
na	*Cratogeomys castanops*	Yellow-faced pocket gopher	M		not RA	

Model Source	Scientific Name	Common Name	Taxon	TERS	Rip. Rank	Season
na	*Cynomys ludovicianus*	Black-tailed prairie dog	M		not RA	
na	*Dipodomys merriami*	Merriam's kangaroo rat	M		not RA	
na	*Dipodomys ordii*	Ord's kangaroo rat	M		not RA	
na	*Dipodomys spectabilis*	Banner-tailed kangaroo rat	M		not RA	
na	*Geomys bursarius*	Plains pocket gopher	M		not RA	
na	*Lepus californicus*	Black-tailed jackrabbit	M		not RA	
na	*Myotis californicus*	California myotis	M		not RA	
na	*Myotis leibii/ciliolabrum*	(western) Small-footed myotis	M		not RA	
na	*Myotis thysanodes*	Fringed myotis	M		not RA	
na	*Neotoma albigula*	White-throated wood rat	M		not RA	
na	*Neotoma micropus*	Gray (southern plains) wood rat	M		not RA	
na	*Notiosorex crawfordi*	Desert/Crawford's Gray shrew	M		not RA	
na	*Onychomys arenicola*	Mearn's/Chihuahuan grasshopper mouse	M		not RA	
na	*Onychomys leucogaster*	Northern (short-tailed) grasshopper mouse	M		not RA	
na	*Ovis canadensis*	Desert bighorn sheep	M		not RA	
na	*Perognathus flavescens*	Plains/Apache pocket mouse	M		not RA	
na	*Perognathus flavus*	Silky pocket mouse	M		not RA	
na	*Peromyscus eremicus*	Cactus mouse	M		not RA	
na	*Peromyscus maniculatus*	Deer mouse	M		not RA	
na	*Peromyscus nasutus*	Northern rock mouse	M		not RA	
na	*Reithrodontomys montanus*	Plains harvest mouse	M		not RA	
na	*Spermophilus mexicanus/ Ictidomys parvidens*	Mexican ground squirrel	M		not RA	
na	*Spermophilus spilosoma*	Spotted ground squirrel	M		not RA	

Model Source	Scientific Name	Common Name	Taxon	TERS	Rip. Rank	Season
na	*Spermophilus variegatus*	Rock squirrel	M		not RA	
na	*Spermophilus/Ictidomys tridecimlineatus*	Thirteen-lined ground squirrel	M		not RA	
na	*Tadarida/Nyctinomops femorosacca/us*	Pocketed free-tailed bat	M		not RA	
na	*Tamias canipes*	Gray-footed chipmunk	M		not RA	
na	*Tamias cinereicollis*	Gray-collared chipmunk	M		not RA	
na	*Tamias quadrivittatusaustralis*	Organ Mountain Colorado chipmunk	M		not RA	
na	*Taxidea taxus*	Badger	M		not RA	
na	*Vulpes macrotis*	Kit fox	M		not RA	
na	*Vulpes vulpes*	Red fox	M		not RA	
na	*Bogertophis subocularis*	Trans-pecos (rat) snake	R		not RA	
na	*Coleonyx brevis(variegatus)*	western banded gecko	R		not RA	
na	*Crotalus scutulatus*	Mojave rattlesnake	R		not RA	
na	*Crotalus viridis viridis*	Prairie rattlesnake	R		not RA	
na	*Gambelia wislizenii*	leopard lizard	R		not RA	
na	*Gyalopion canum*	(Chihuahuan) western hooknose snake	R		not RA	
na	*Heterdon nasicus*	(Mexican) Western hognose snake	R		not RA	
na	*Lampropeltis triangulum*	(New Mexico) Milk snake	R		not RA	
na	*Phrynosoma cornutum*	Texas horned lizard	R		not RA	
na	*Phrynosoma douglasii(hernandesi)*	(Greater) short-horned lizard	R		not RA	
na	*Pituophis catenifer*	Bullsnake/Gophersnake	R		not RA	
na	*Terrapene ornata*	(Desert/)ornate box turtle	R		not RA	

Table 2. Conservation status of riparian-associated species occurring or possible at Fort Bliss, NM. NatureServe conservation ranks are G5, N5, and S5, unless otherwise noted. Details on meanings of ranking can be found at (http://explorer.natureserve.org/granks.htm); ranks are 5 (Secure), 4 (Apparently Secure), 3 (Vulnerable), 2 (Imperiled), 1 (Critically Imperiled), or H(Possibly Extinct or Presumed Eliminated), and are sometimes split by breeding (B) and non-breeding (N) range. Federal and State listing status is indicated by T (threatened), E (endangered), or P (proposed).

Scientific Name	Common Name	Tax.	Species of Concern Status			
			NatureServe		Listing	
			G/N	NM	Fed	NM
Asturina nitidus/Buteo plagiatus	Gray hawk	B	N1N, N3B			
Buteo albonotatus	Zone-tailed hawk	B	G4	S3		
Buteogallus anthracinus	Common black-hawk	B	G4G5/ N3B	S2B, S3N		T
Callipepla squamata	Scaled quail	B		S3B, S4N		
Calypte costae	Costa's hummingbird	B	N4N	S1		T
Carduelis lawrencei	Lawrence's goldfinch	B	G3G4			
Cinclus mexicanus	American dipper	B		S3B, S4N		
Coccyzus americanus	Yellow-billed cuckoo	B		S3	PT	
Elanus leucurus	White-tailed kite	B	N4	S2N		
Empidonax traillii extimus	Southwestern Willow flycatcher	B	G5T2	S1	E	E
Empidonax wrightii	Gray flycatcher	B		S3B, S5N		
Falco femoralis	Aplomado Falcon	B	G4T2/ N1	SHB, S1N	E	E
Haliaeetus leucocephalus	Bald eagle	B		S1B, S4N		T
Icteria virens	Yellow-breasted chat	B		S3B, S4N		
Icterus cucullatus	Hooded oriole	B		S3B, S4N		
Ictinia mississippiensis	Mississippi kite	B		S2B, S3N		

Scientific Name	Common Name	Tax.	Species of Concern Status			
			NatureServe		Listing	
			G/N	NM	Fed	NM
Pandion haliaetus	Osprey	B	N4N	S2B, S4N		
Parabuteo unicinctus	Harris's hawk	B		S2B, S3N		
Passerina versicolor	Varied bunting	B	N4B	S1		T
Petrochelidon fulva	Cave swallow	B	N4B	S3		
Polioptila melanura	Black-tailed gnatcatcher	B		S3		
Spizella atrogularis	Black-chinned sparrow	B		S3		
Strix occidentalis lucida	Mexican spotted owl	B	G3T3	S2	T	
Vermivora/Oreothlypis luciae	Lucy's warbler	B		S3B, S4N		
Vermivora/Oreothlypis virginiae	Virginia's warbler	B		S3B, S4N		
Vireo bellii medius	Bell's vireo	B	N4B	S2B, S3N	PS	T
Vireo vicinior	Gray vireo	B	G4/ N4B	S4B, S3N		T
Ammospermophilus interpres	Texas antelope squirrel	M	G4G5/ N4N5	S3		
Chaetodipus hispidus	Hispid pocket mouse	M		S3		
Corynorhinus townsendii	Townsend's big-eared bat	M	G3G4/ N3N4	S3		
Lasiurus blossevillii	Western red bat	M	N3	S3		
Myotis lucifugus	Little brown myotis	M	G3/N3			
Myotis velifer	Cave myotis	M	N4	S3S4		
Nyctinomops macrotis	Big free-tailed bat	M	N3N4	S3		
Puma concolor	Mountain lion	M		S3?		
Tadarida brasiliensis	Brazilian/Mexican free-tailed bat	M		S3S4		
Aspidoscelis tigris	Western/Tiger whiptail	R		S3		

Scientific Name	Common Name	Tax.	Species of Concern Status			
			NatureServe		Listing	
			G/N	NM	Fed	NM
Crotalus lepidus klauberi	Banded rock rattlesnake	R	N4	S2		
Lampropeltis alterna	Gray-banded kingsnake	R	N4	S1		E
Leptotyphlops/Rena humilis	Western blind/thread snake	R		S3?		
Sistrurus catenatus	Massasauga	R	G3G4	S3S4		
Trimorphodon vilkinsonii	Texas lyresnake	R	G4/N3			

Table 3. Riparian-associated breeding birds at Fort Bliss, NM. Nests were found for species highlighted in gray by Myers et al. (1998). Species marked with a * were added to the riparian associated list based on Myers' findings. Scores for use of each structure layer, season of presences, and occurrence in lowlands, foothills, or mountains are indicated. Season YR = year-round occurrence, S = summer occurrence.

		Vegetation Layer					Rip.				
Common Name	**Scientific Name**	**0.5-1m**	**1-4m**	**4-12m**	**>12m**	**Season**	**Rank**	**TERS**	**Lowlands**	**Foothills**	**Mountains**
Cooper's hawk	*Accipiter cooperii*			2	2	YR	F or I	N		●	●
Sharp-shinned hawk	*Accipiter striatus*		1	2	2	YR	F or I	N		●	●
Red-winged blackbird	*Agelaius phoeniceus*	2	2	1		YR	O	N	●	●	
*Rufous-crowned sparrow	*Aimophila ruficeps*	1				YR	KM RA	N	●	●	●
Black-throated sparrow	*Amphispiza bilineata*	2	1			YR	N	N	●	●	
Western scrub-jay	*Aphelocoma californica*		2	1		YR	F	N		●	●
Black-chinned hummingbird	*Archilochus alexandrinus*		2	2		S	I or O	N	●	●	●
Long-eared owl	*Asio otus*		2	1		YR	I	N	●	●	
Gray Hawk	*Asturina nitidus*			1	2	S	O	Y	●	●	
*Verdin	*Auriparus flaviceps*	1	2	1		YR	KM RA	N	●	●	
Great horned owl	*Bubo virginianus*	1	1	2	2	YR	F	N	●	●	●
Zone-tailed hawk	*Buteo albonotatus*			1	2	S	I	Y	●	●	●
Swainson's hawk	*Buteo swainsoni*		2	1		S	F	N	●	●	
Common black-hawk	*Buteogallus anthracinus*				2	S	O	Y	●	●	●
Gambel's quail	*Callipepla gambelii*	2	1			YR	I	N	●	●	
Scaled quail	*Callipepla squamata*	2	1			YR	F	Y	●	●	
Costa's Hummingbird	*Calypte costae*	2	2			S	F	Y	●	●	
Pyrrhuloxia	*Cardinalis sinuatus*		2			YR	F or I	N	●	●	
Lesser goldfinch	*Carduelis psaltria*		2	2	1	YR	O	N		●	●
*House finch	*Carpodacus mexicanus*		2	1		YR	KM RA	N	●	●	
Turkey vulture	*Cathartes aura*				1	S	F	N	●	●	●
Hermit thrush	*Catharus guttatus*	2	1			YR	KM RA	N		●	●
Canyon wren	*Catherpes mexicanus*					YR	I	Y			
Lesser nighthawk	*Chordeiles acutipennis*	1	1	1		S	F	N	●	●	
American dipper	*Cinclus mexicanus*					YR	O	Y			

Common Name	Scientific Name	Vegetation Layer				Season	Rip. Rank	TERS	Lowlands	Foothills	Mountains
		0.5-1m	1-4m	4-12m	>12m						
Western Yellow-billed cuckoo	*Coccyzus americanus*		2	1	1	S	O	Y	●	●	
Western wood-pewee	*Contopus sordidulus*	1	2	2	2	S	F	N		●	●
White-tailed kite	*Elanus leucurus*		1	2	2	YR	F	Y	●	●	
Cordilleran flycatcher	*Empidonax occidentalis*	1	2	1		S	O	N			●
Willow Flycatcher	*Empidonax traillii*	1	2	1		S	O	Y		●	●
Gray flycatcher	*Empidonax wrightii*	1	2	1		S	I	Y	●	●	●
Brewer's blackbird	*Euphagus cyanocephalus*	2	2	1		YR	I	N	●	●	●
Northern Aplomado Falcon	*Falco femoralis*			2		YR	N	Y	●	●	
American kestrel	*Falco sparverius*		1	2	1	YR	F	N	●	●	●
*Greater roadrunner	*Geococcyx californicus*		2			YR	KM RA	N	●	●	-
Common yellowthroat	*Geothlypis trichas*					S	O	N			
Blue grosbeak	*Guiraca/Passerina caerulea*	2	2	1		S	F	N	●	●	
Yellow-breasted chat	*Icteria virens*	2	1			S	I	Y	●	●	●
Bullock's oriole	*Icterus bullockii*		2	2	1	S	F	N	●	●	●
Hooded oriole	*Icterus cucullatus*		2	2		S	I	Y	●	●	●
Scott's oriole	*Icterus parisorum*		2	1		S	N	N	●	●	
Mississippi kite	*Ictinia mississippiensis*		1	2	2	S	I	Y	●	●	●
Northern mockingbird	*Mimus polyglottos*	1	2	1	1	YR	N	N	●	●	●
*Brown-headed cowbird	*Molothrus ater*					YR	KM RA	N	●	●	●
*Ash-throated flycatcher	*Myiarchus cinerascens*	1	2	1		S	KM RA	N	●	●	-
MacGillivray's warbler	*Oporornis tolmei*	2	1	1		S	I	N			●
Western screech-owl	*Otus kennicotti*		1	2		YR	I	N	●	●	●
Harris's hawk	*Parabuteo unicinctus*		2	2		YR	I	Y	●	●	
Painted bunting	*Passerina ciris*	2	2			S	F	N	●	●	●
Indigo bunting	*Passerina cyanea*	2				S	I	N	●	●	●
Varied bunting	*Passerina versicolor*	2	2			S	O	Y	●		
Cave swallow	*Petrochelidon fulva*					S	I	Y			
Cliff swallow	*Petrochelidon pyrrhonota*					S	I	N			
Phainopepla	*Phainopepla nitens*		2	1		S	I	N	●	●	●

Common Name	Scientific Name	Vegetation Layer				Season	Rip. Rank	TERS	Lowlands	Foothills	Mountains
		0.5-1m	1-4m	4-12m	>12m						
Black-headed grosbeak	*Pheucticus melanocephalus*		2	2		S	I	N	●	●	●
Downy woodpecker	*Picoides pubescens*		1	2	1	YR	F	N		●	●
Hairy woodpecker	*Picoides villosus*		2	2	2	YR	F	N		●	●
Canyon towhee	*Pipilo fuscus*	1	2			YR	I	N	●	●	●
Spotted towhee	*Pipilo maculatus*	2	2			YR	F or I	N	●	●	●
Summer tanager	*Piranga rubra*		2	2	1	S	O	N	●	●	●
Blue-gray gnatcatcher	*Polioptila caerulea*		1	2	1	S	F	N		●	●
Black-tailed gnatcatcher	*Polioptila melanura*	1	2	1		YR	I	Y	●	●	
Great-tailed grackle	*Quiscalus mexicanus*		1	2	2	YR	I	N	●	●	●
*Ruby-crowned kinglet	*Regulus calendula*	1	1	2	1	YR	KM RA	N			●
Bank Swallow	*Riparia riparia*					S	I	N	●		
Rock wren	*Salpinctes obsoletus*					YR	F	N			
Black phoebe	*Sayornis nigricans*		1			YR	O	N	●	●	●
Red-naped sapsucker	*Sphyrapicus nuchalis*		2	2	1	YR	F	N		●	●
Black-chinned sparrow	*Spizella atrogularis*	2				S	F	Y	●	●	●
Northern rough-winged swallow	*Stelgidopteryx serripennis*					S	I	N			
Mexican spotted owl	*Strix occidentalis*			1	1	YR	I	Y			●
Bewick's wren	*Thryomanes bewickii*	1	2	1		YR	F	N	●	●	●
Crissal thrasher	*Toxostoma dorsalis/crissale*	2	2			YR	O	N	●	●	
Brown thrasher	*Toxostoma rufum*	2	2			YR	I	N	●	●	●
House wren	*Troglodytes aedon*		2	2		YR	F	N	●	●	●
Cassin's kingbird	*Tyrannus vociferans*			2	2	S	I	N	●	●	●
Orange-crowned warbler	*Vermivora celata*	2	2			YR	F or I	N			●
Lucy's warbler	*Vermivora luciae*		2	2		S	O	Y	●	●	
Virginia's warbler	*Vermivora virginiae*	1	1			S	F	Y		●	●
Bell's vireo	*Vireo bellii*	2	2			S	I	Y	●		
Warbling vireo	*Vireo gilvus*		2	2	2	S	F or I	N	●	●	●
Plumbeous/Solitary vireo	*Vireo plumbeus*	1	2	1		S	F or I	N		●	●
Gray vireo	*Vireo vicinior*		2			S	N	Y		●	●
White-winged dove	*Zenaida asiatica*		2	2		YR	F	N	●	●	●

Table 4. Vegetative, hydrologic, and geomorphic variables used in analysis of stream reach species richness at Fort Bliss, NM.

Variable	Units	Description
Slope	%	Percent slope of the stream reach, from down- to upstream
Elevation	m	Elevation of the mid-point of the stream-line
FP	% year	Average annual flow permanence, from NEXRAD
Qp25	cub. m/sec	Peak flow of 25-year, 1-hour storm
Tsp25	kW/m	Total stream power of 25-year, 1-hour storm
W_area	sq. meters	Size of the contributing area for the stream reach
Percent Cover	%	Percent cover of all woody vegetation, from RE-NDVI
Veg_Ind Mean	n/a	Mean RE-NDVI value of woody vegetation in the stream reach
LiDAR 0.5-1	%	Percent of the reach with vegetation reaching 0.5-1 m
LiDAR 1-4	%	Percent of the reach with vegetation reaching 1-4 m
LiDAR 4-12	%	Percent of the reach with vegetation reaching 4-12 m
LiDAR >12Y-N	Y/N	Presence (Y) or absence (N) of vegetation >12 m
Shannon_LiDAR	n/a	Vegetation structural diversity, calculated from LiDAR
Landcover_var	cover types	Number of different ecological systems found within the stream reach
1m Width	m	Mean width of the 1m-flooded depth polygon for the reach
2m Width	m	Mean width of the 2m-flooded depth polygon for the reach
3m Width	m	Mean width of the 3m-flooded depth polygon for the reach
ER 2/3	unitless	Entrenchment ratio, 2m Width/3m Width
ER 1/3	unitless	Entrenchment ratio, 1m Width/3m Width
ER 0.5/3	unitless	Entrenchment ratio, 0.5m Width/3m Width
ER 1/2	unitless	Entrenchment ratio, 1m Width/2m Width
ER 0.5/2	unitless	Entrenchment ratio, 0.5m Width/2m Width
RSI	unitless	Rainfall Seasonality Index, precip of wettest month/annual precip

APPENDIX B – Distribution of potential Species Richness

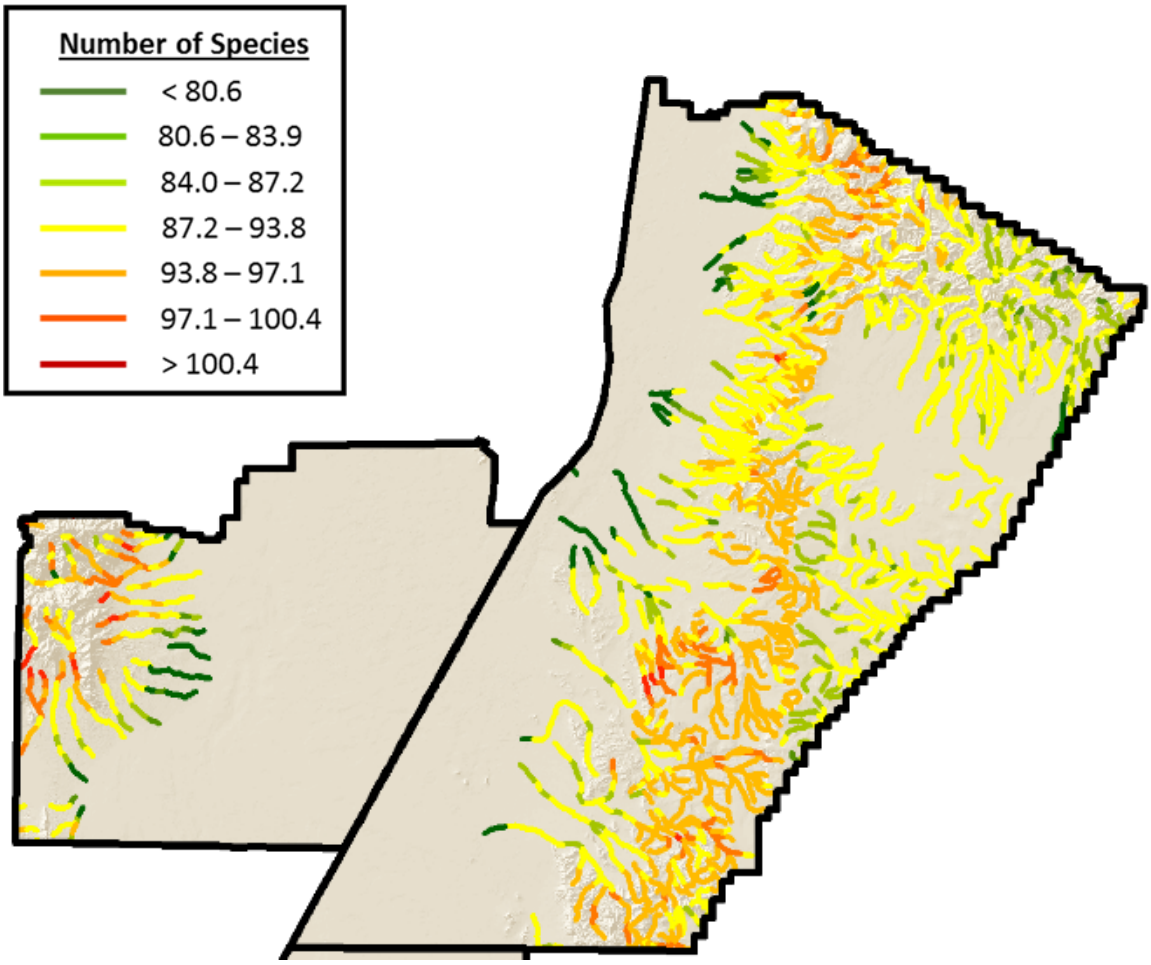


Figure 1. Distribution of all riparian-associated species in stream reaches at Ft. Bliss, NM. Potential species richness was derived by stacking GAP animal habitat distribution models downloaded on or before October 2014.

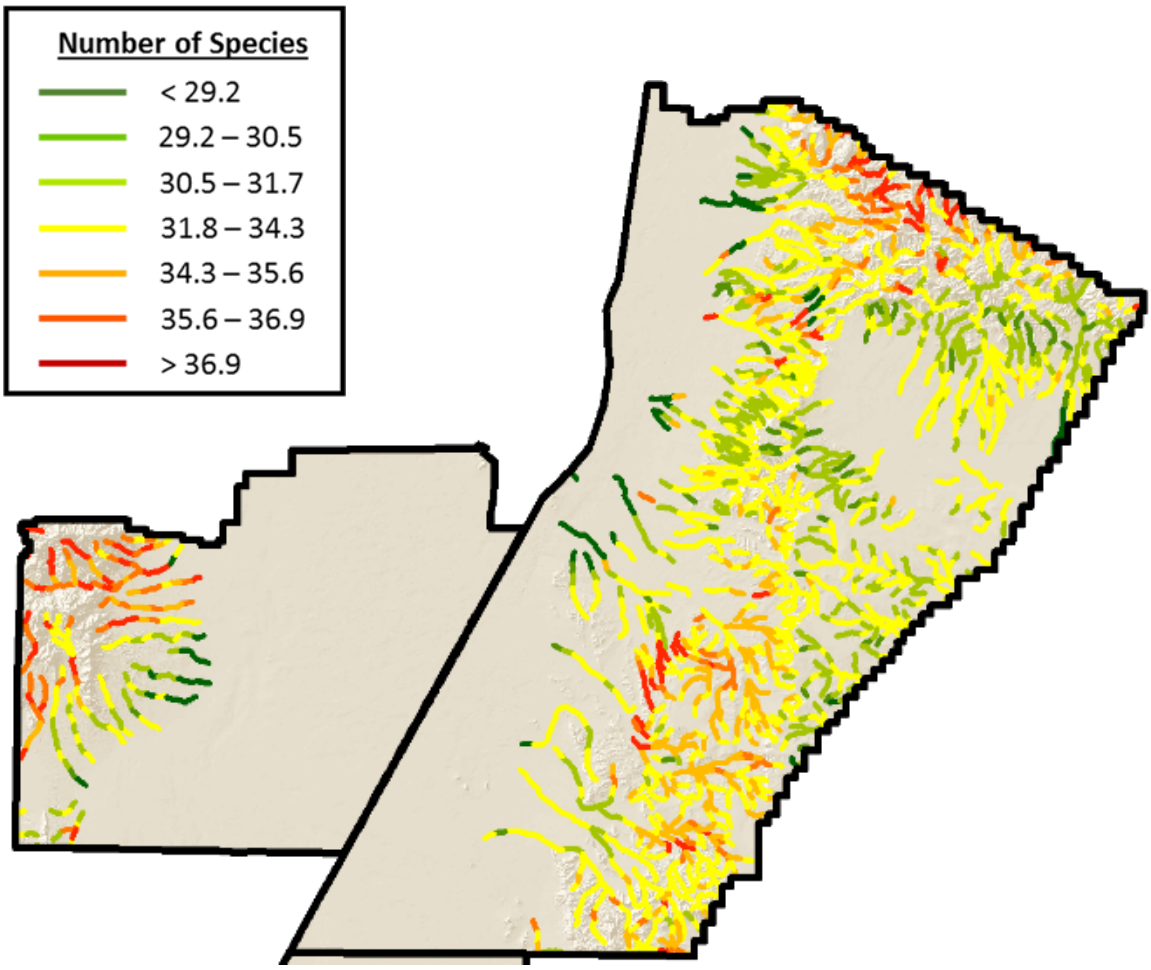


Figure 2. Distribution of all obligate riparian-associated species at Ft. Bliss, NM. Potential species richness was derived by stacking GAP animal habitat distribution models downloaded on or before October 2014.

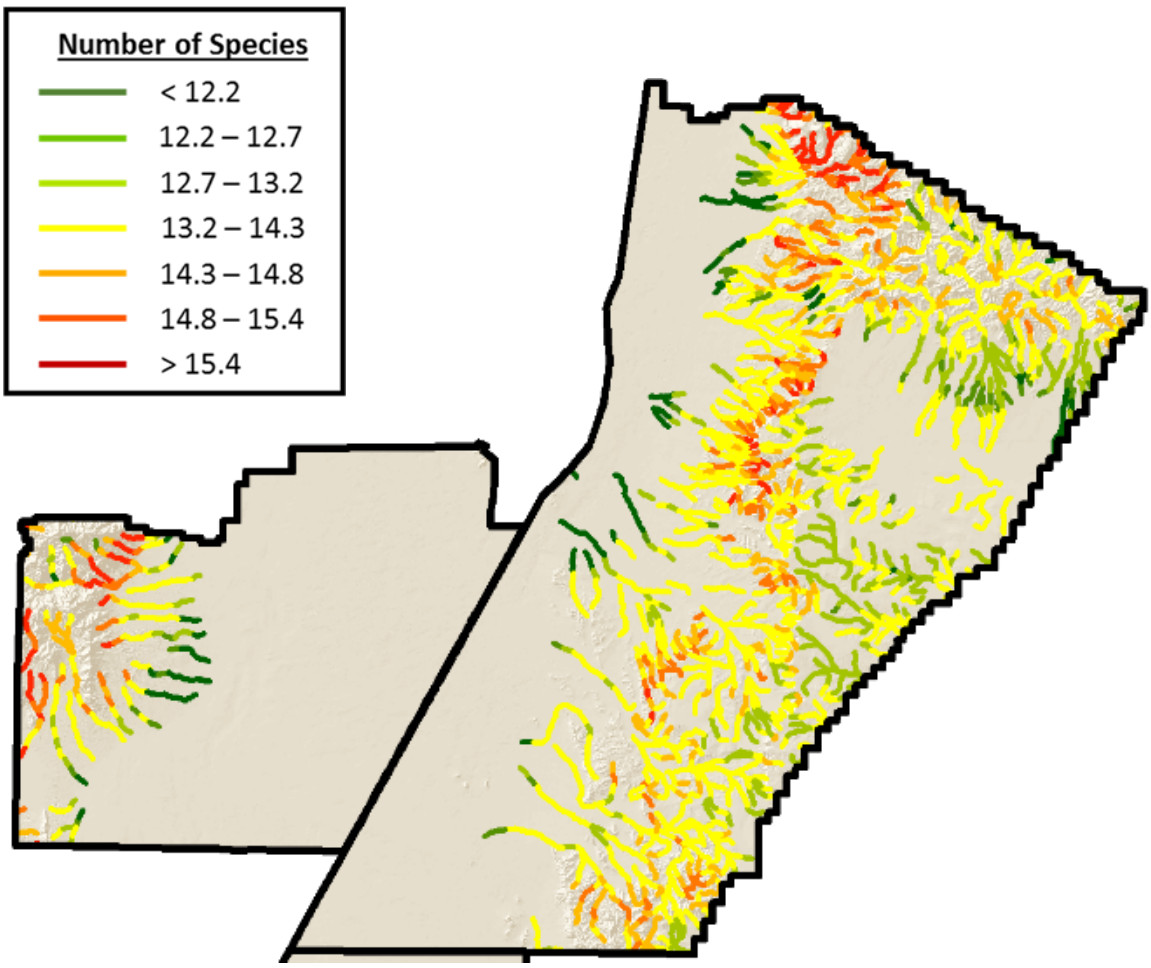


Figure 3. Distribution of all TER-S riparian associated species in stream reaches at Ft. Bliss, NM. Potential species richness was derived by stacking GAP animal habitat distribution models downloaded on or before October 2014.

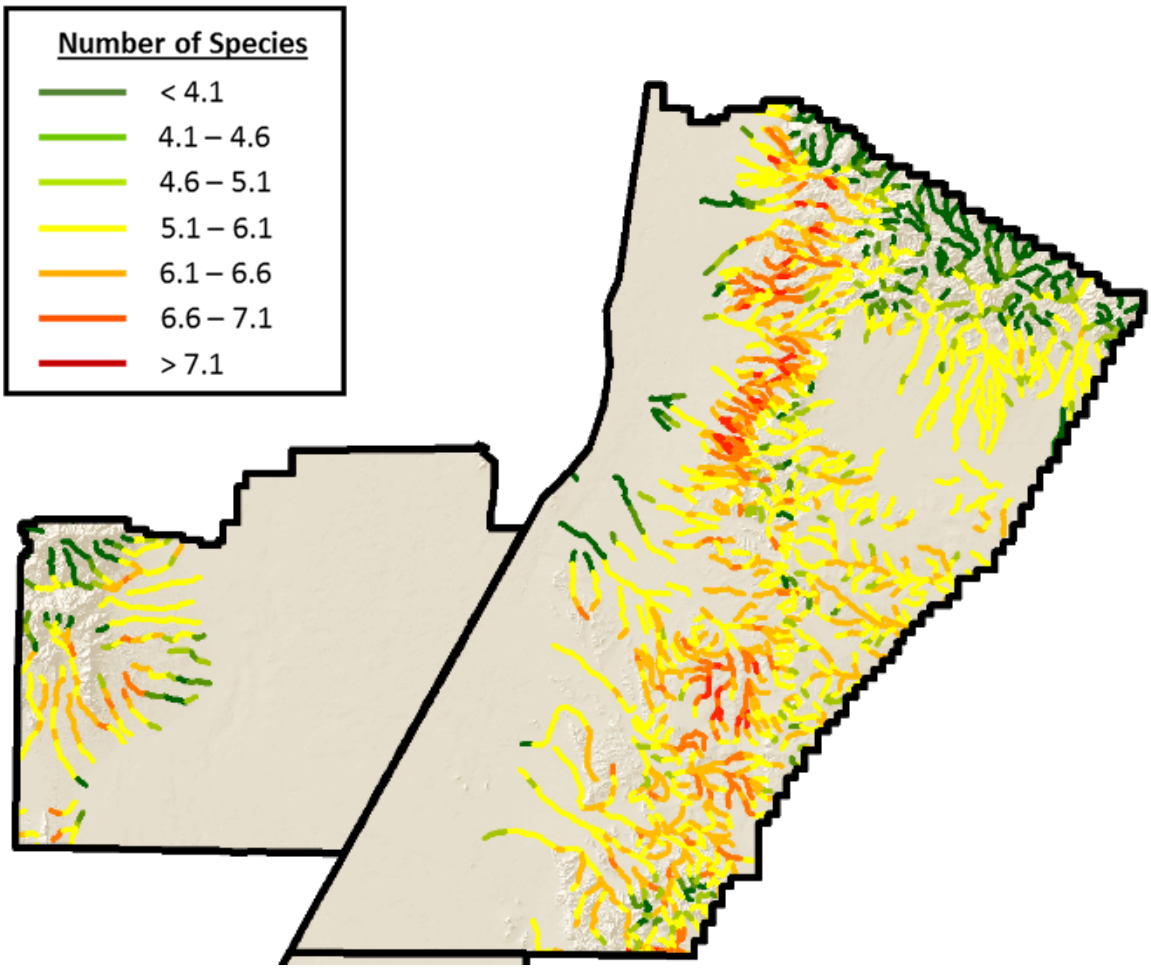


Figure 4. Distribution of riparian-associated amphibian species in stream reaches at Ft. Bliss, NM. Potential species richness was derived by stacking GAP animal habitat distribution models downloaded on or before October 2014.

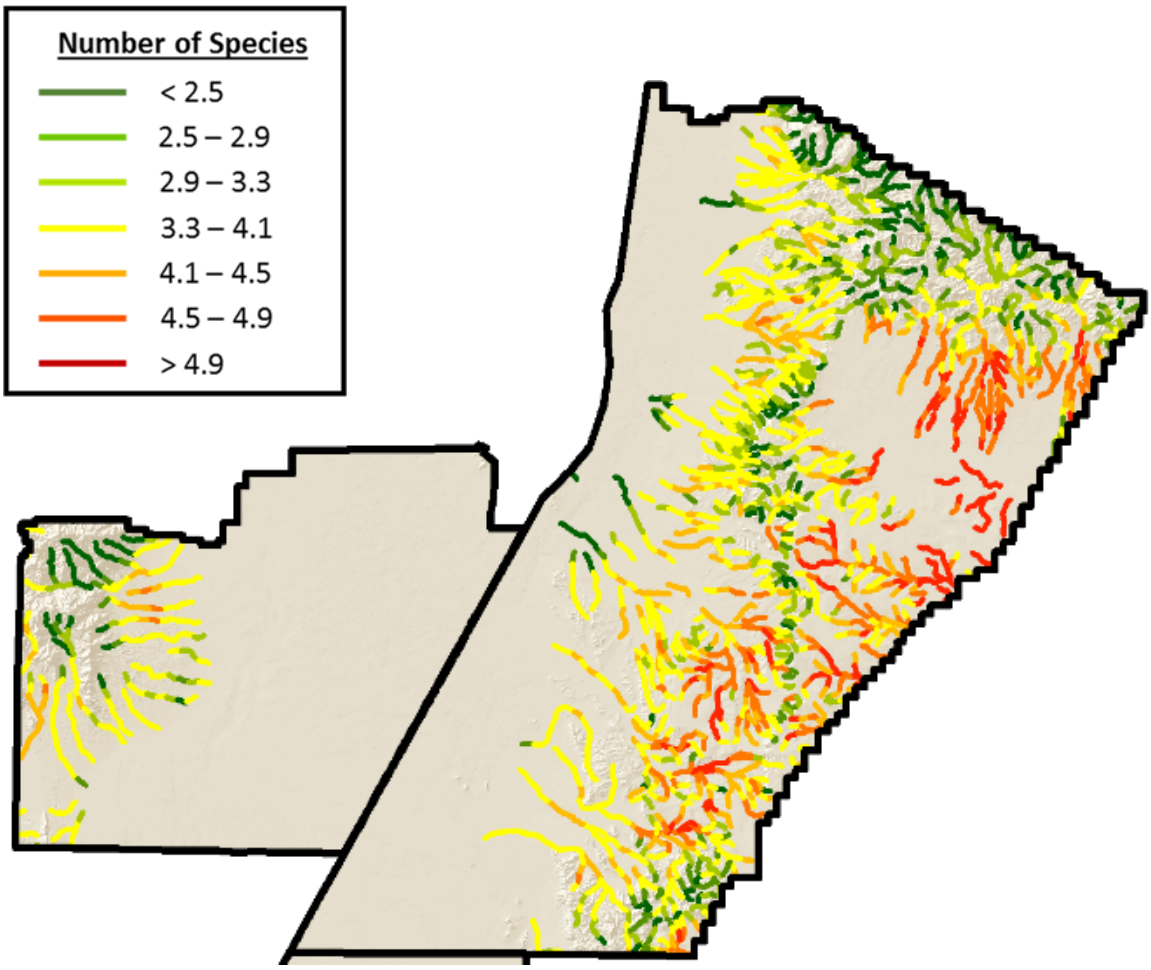


Figure 5. Distribution of obligate riparian-associated amphibian species in stream reaches at Ft. Bliss, NM. Potential species richness was derived by stacking GAP animal habitat distribution models downloaded on or before October 2014.

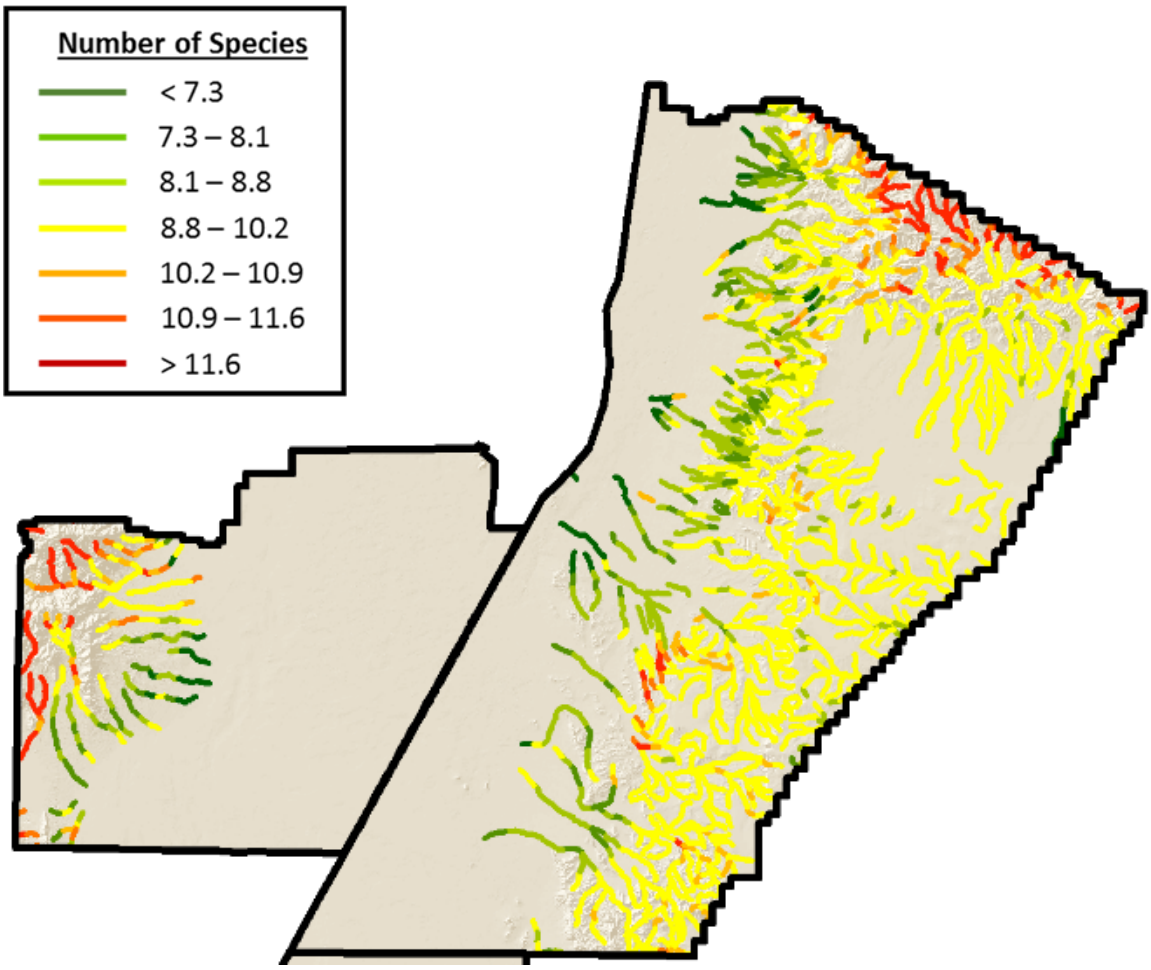


Figure 6. Distribution of riparian-associated summering bird species in stream reaches at Ft. Bliss, NM. Potential species richness was derived by stacking GAP animal habitat distribution models downloaded on or before October 2014.

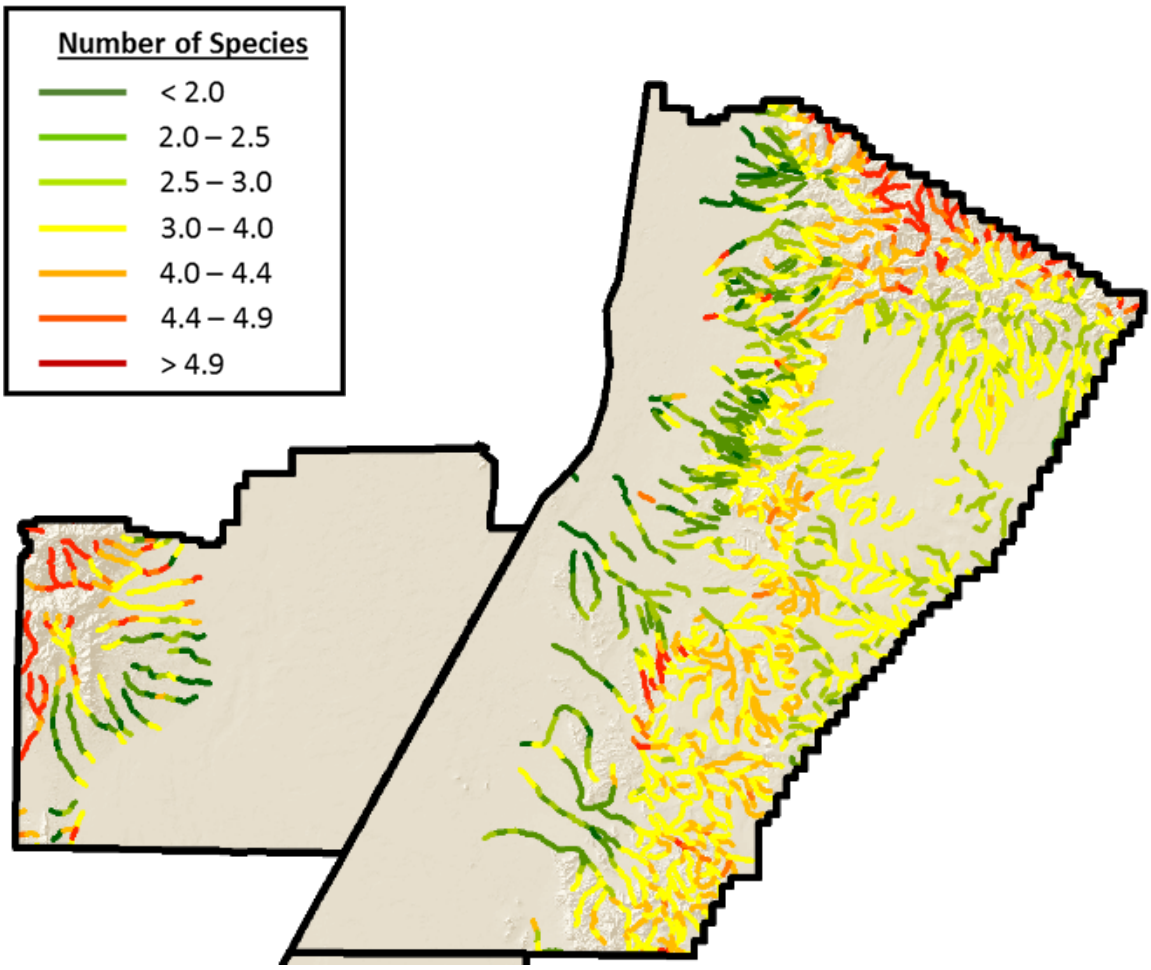


Figure 7. Distribution of obligate riparian-associated summering bird species in stream reaches at Ft. Bliss, NM. Potential species richness was derived by stacking GAP animal habitat distribution models downloaded on or before October 2014.

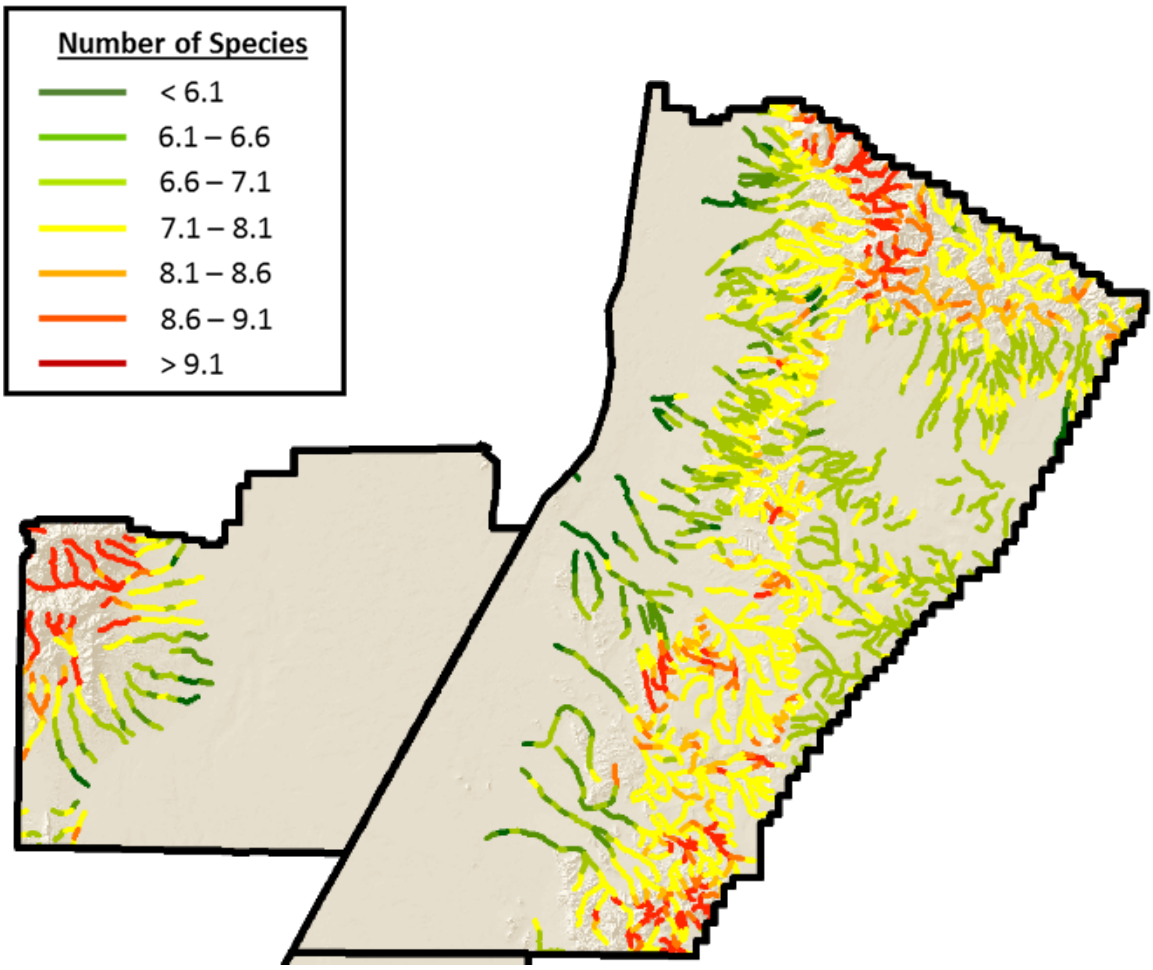


Figure 8. Distribution of riparian-associated wintering bird species in stream reaches at Ft. Bliss, NM. Potential species richness was derived by stacking GAP animal habitat distribution models downloaded on or before October 2014.

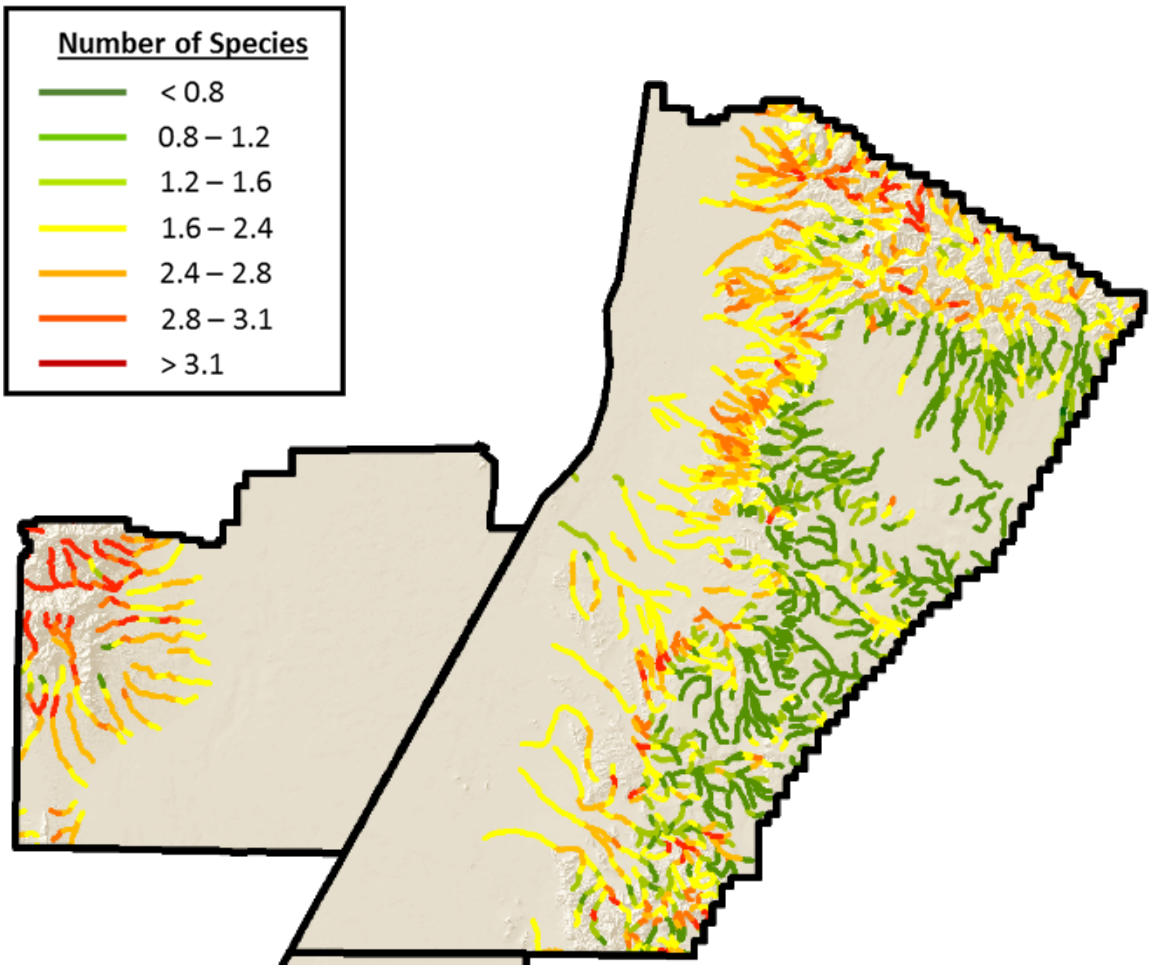


Figure 9. Distribution of obligate riparian-associated wintering bird species in stream reaches at Ft. Bliss, NM. Potential species richness was derived by stacking GAP animal habitat distribution models downloaded on or before October 2014.

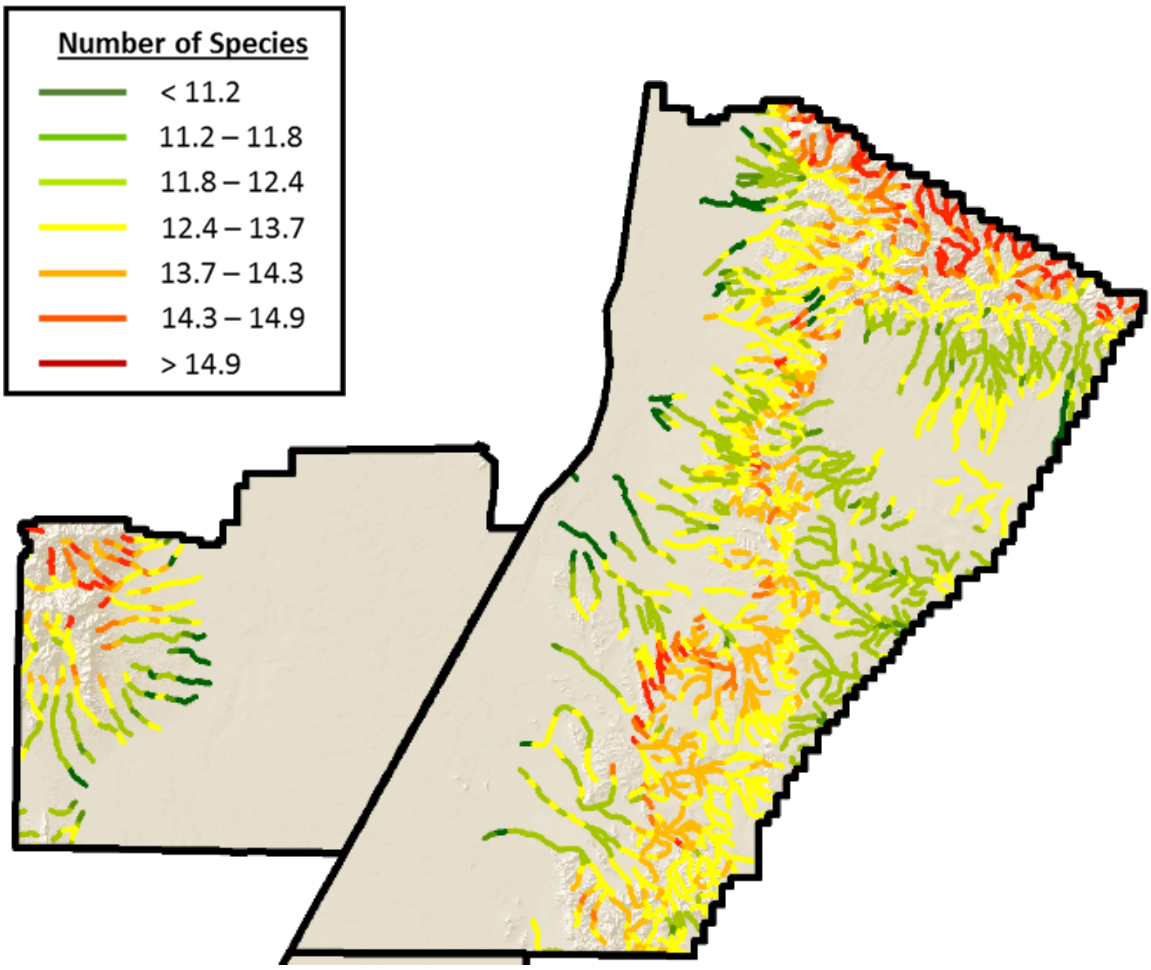


Figure 10. Distribution of riparian-associated year-round bird species in stream reaches at Ft. Bliss, NM. Potential species richness was derived by stacking GAP animal habitat distribution models downloaded on or before October 2014.

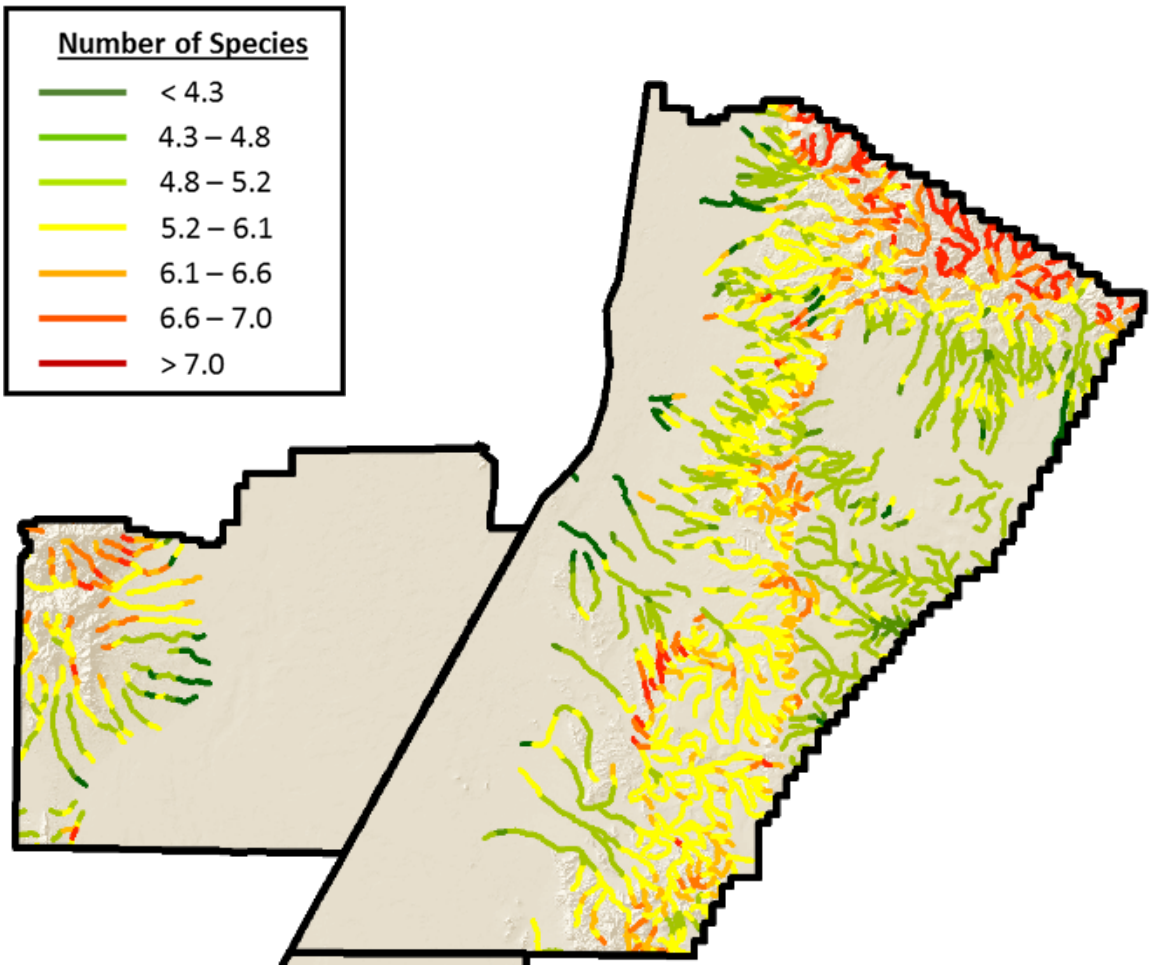


Figure 11. Distribution of obligate riparian-associated year-round bird species in stream reaches at Ft. Bliss, NM. Potential species richness was derived by stacking GAP animal habitat distribution models downloaded on or before October 2014.

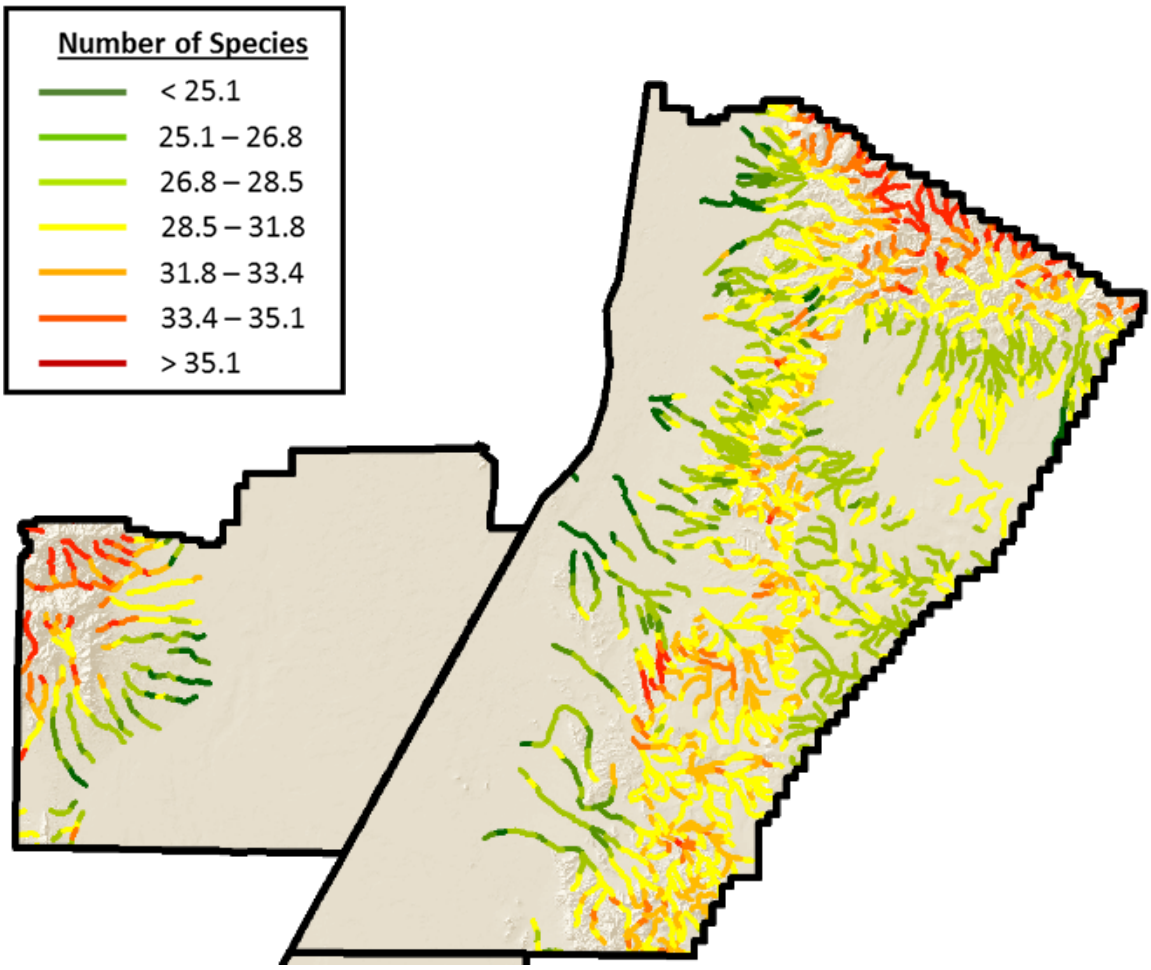


Figure 12. Distribution of all riparian-associated bird species in stream reaches at Ft. Bliss, NM. Potential species richness was derived by stacking GAP animal habitat distribution models downloaded on or before October 2014.

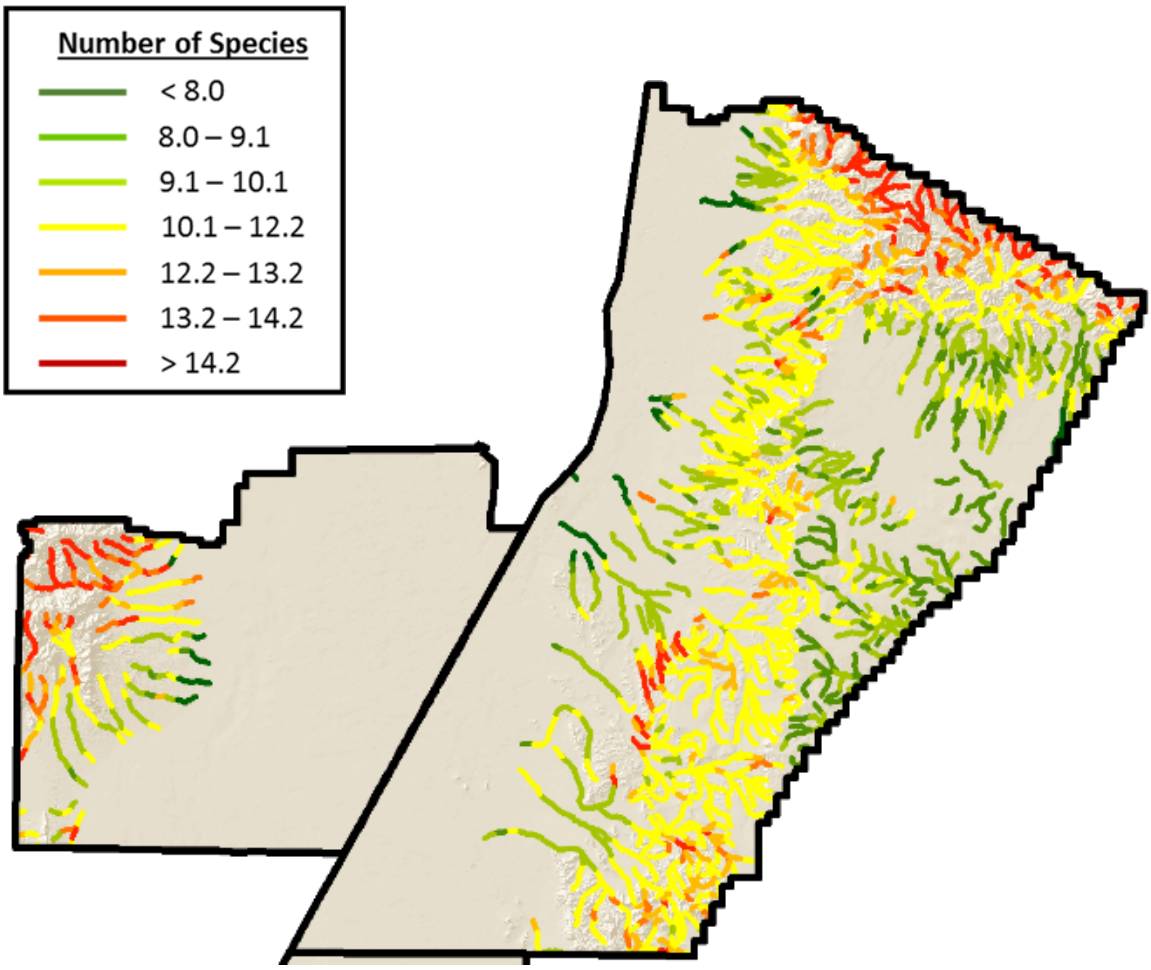


Figure 13. Distribution of all obligate riparian-associated bird species in stream reaches at Ft. Bliss, NM. Potential species richness was derived by stacking GAP animal habitat distribution models downloaded on or before October 2014.

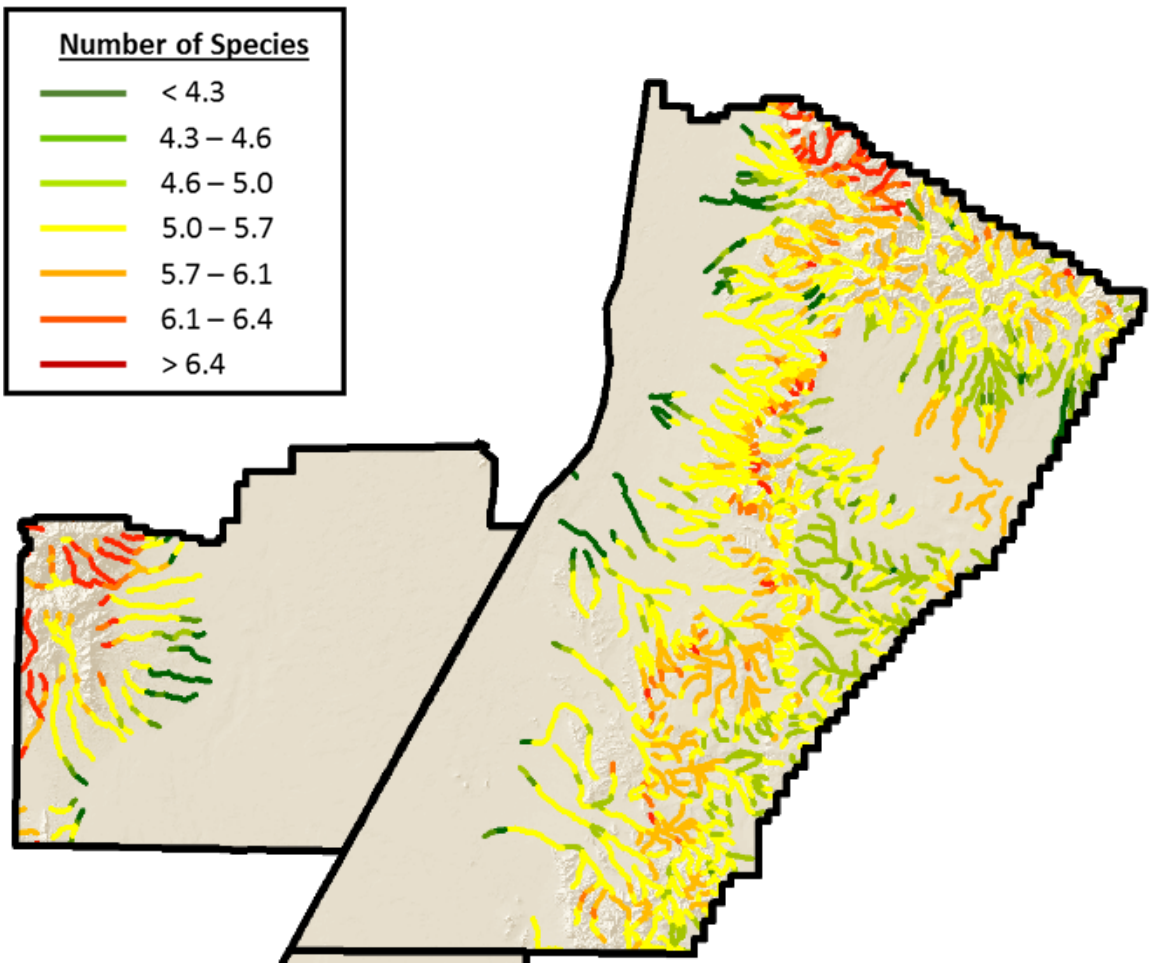


Figure 14. Distribution of all TER-S riparian associated bird species in stream reaches at Ft. Bliss, NM. Potential species richness was derived by stacking GAP animal habitat distribution models downloaded on or before October 2014.

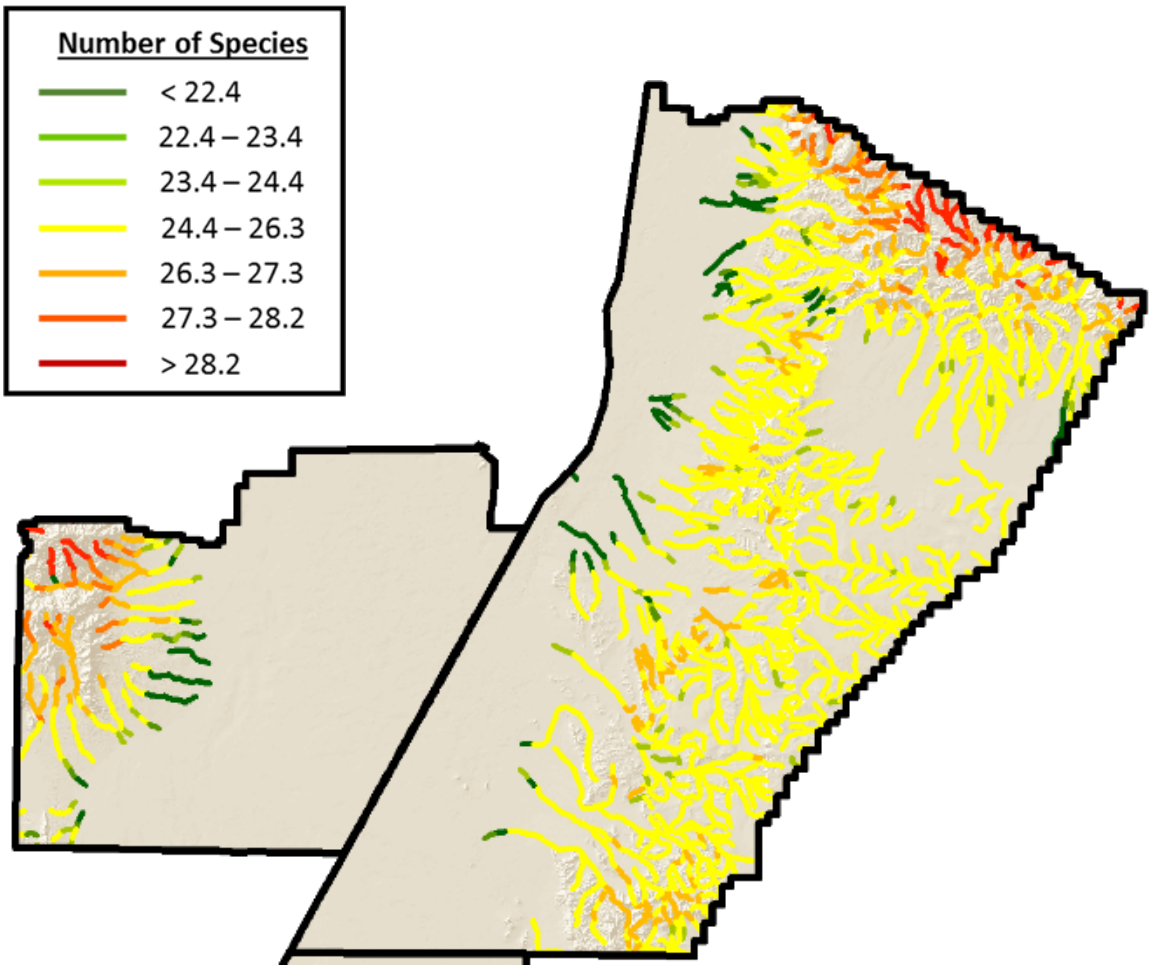


Figure 15. Distribution of riparian-associated mammal species in stream reaches at Ft. Bliss, NM. Potential species richness was derived by stacking GAP animal habitat distribution models downloaded on or before October 2014.

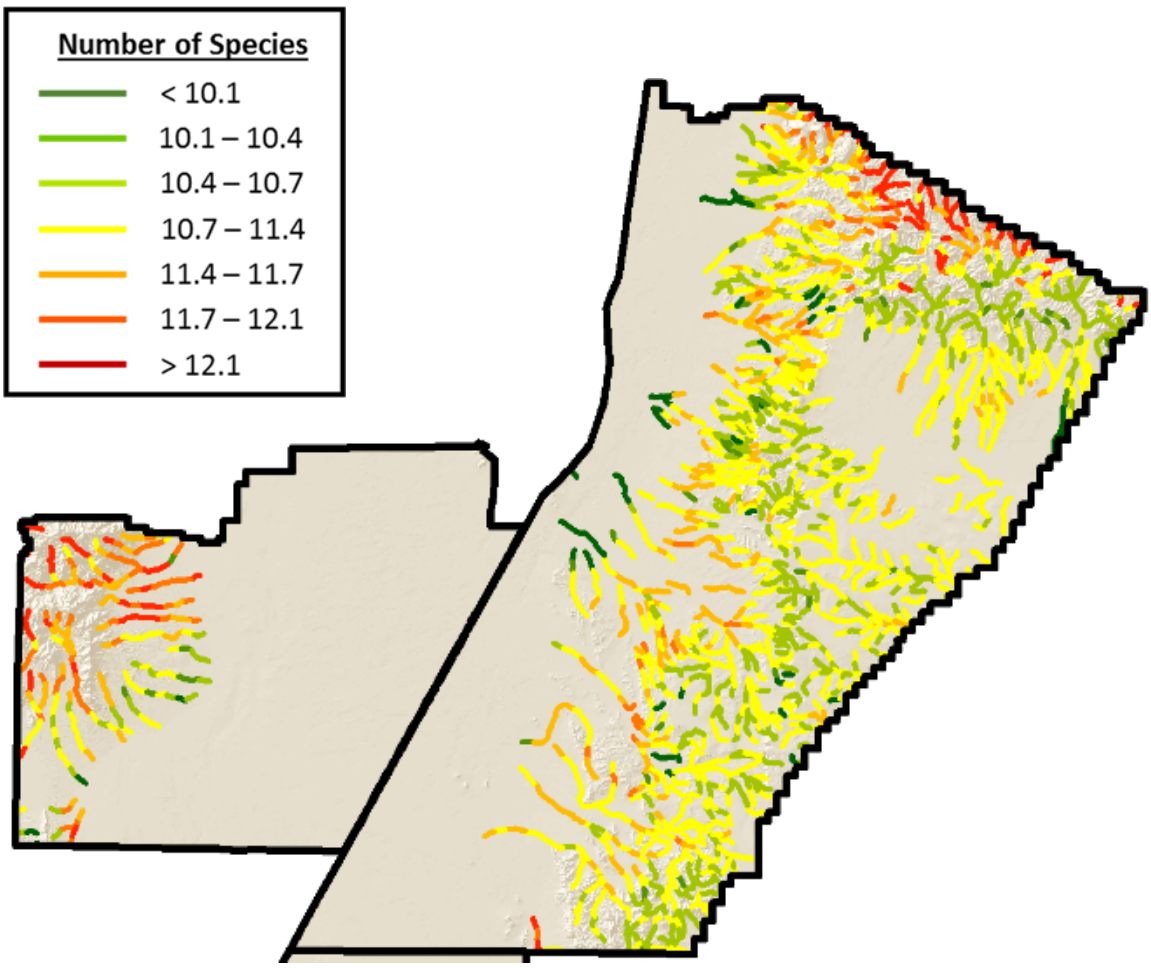


Figure 16. Distribution of obligate riparian-associated mammal species in stream reaches at Ft. Bliss, NM. Potential species richness was derived by stacking GAP animal habitat distribution models downloaded on or before October 2014.

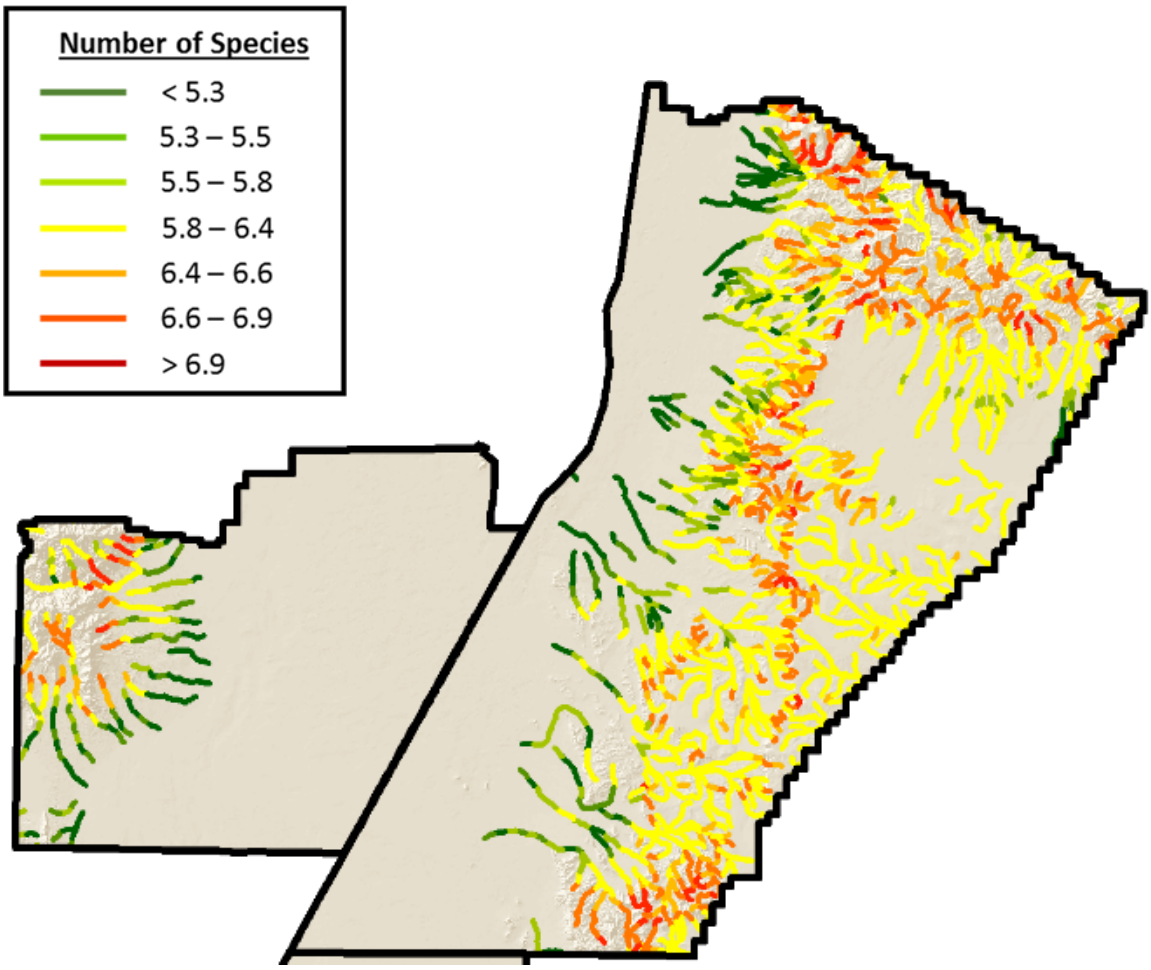


Figure 17. Distribution TER-S riparian associated mammal species in stream reaches at Ft. Bliss, NM. Potential species richness was derived by stacking GAP animal habitat distribution models downloaded on or before October 2014.

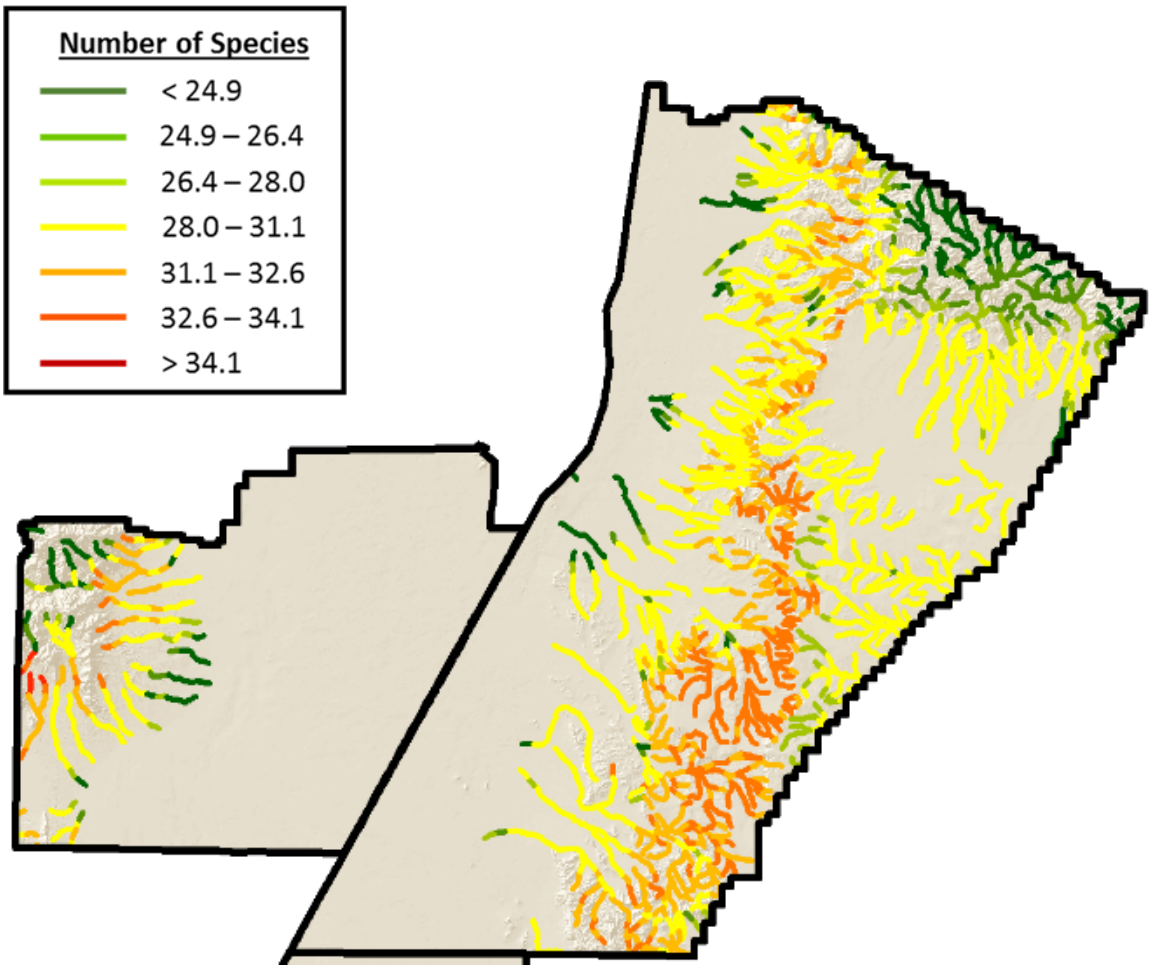


Figure 18. Distribution of riparian-associated reptile species in stream reaches at Ft. Bliss, NM. Potential species richness was derived by stacking GAP animal habitat distribution models downloaded on or before October 2014.

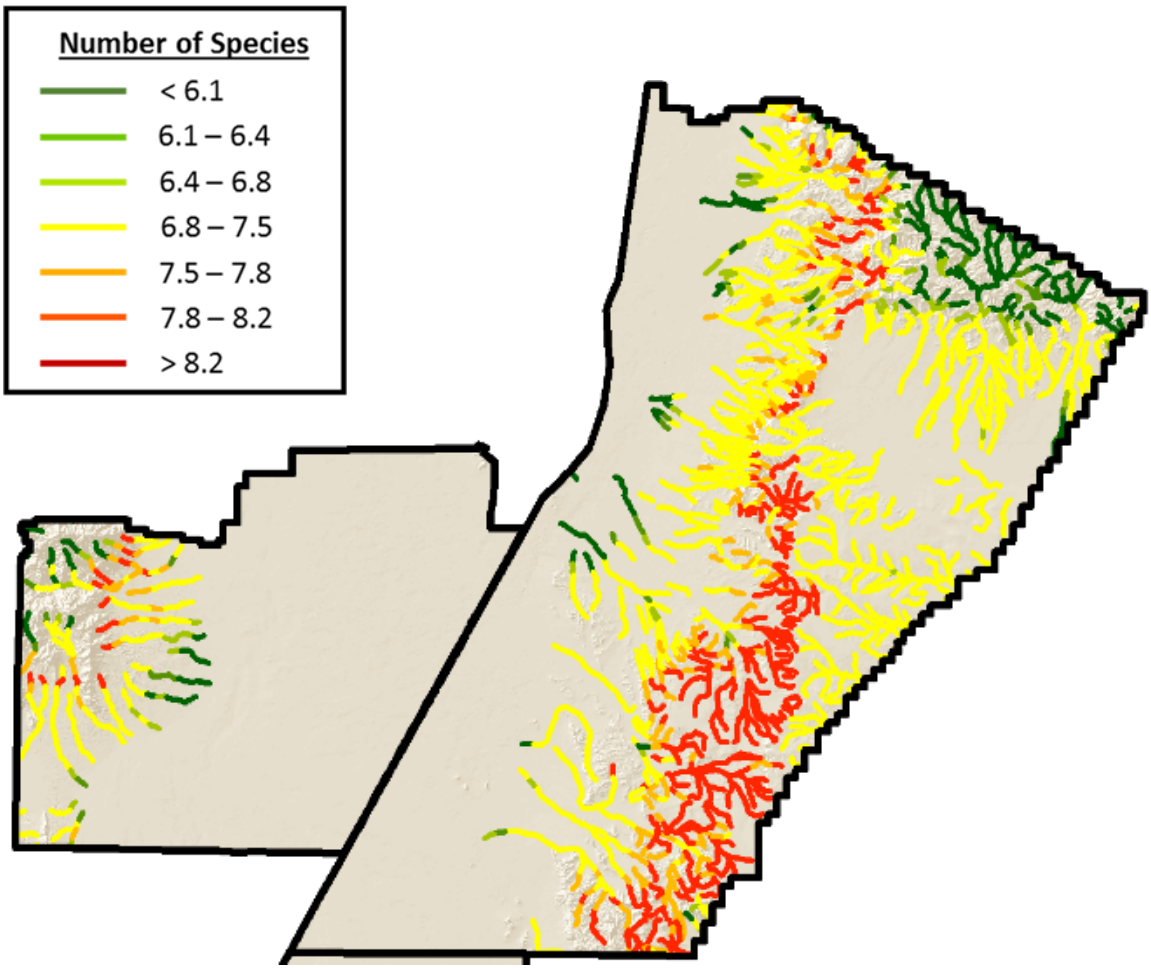


Figure 19. Distribution of obligate riparian-associated reptile species in stream reaches at Ft. Bliss, NM. Potential species richness was derived by stacking GAP animal habitat distribution models downloaded on or before October 2014.

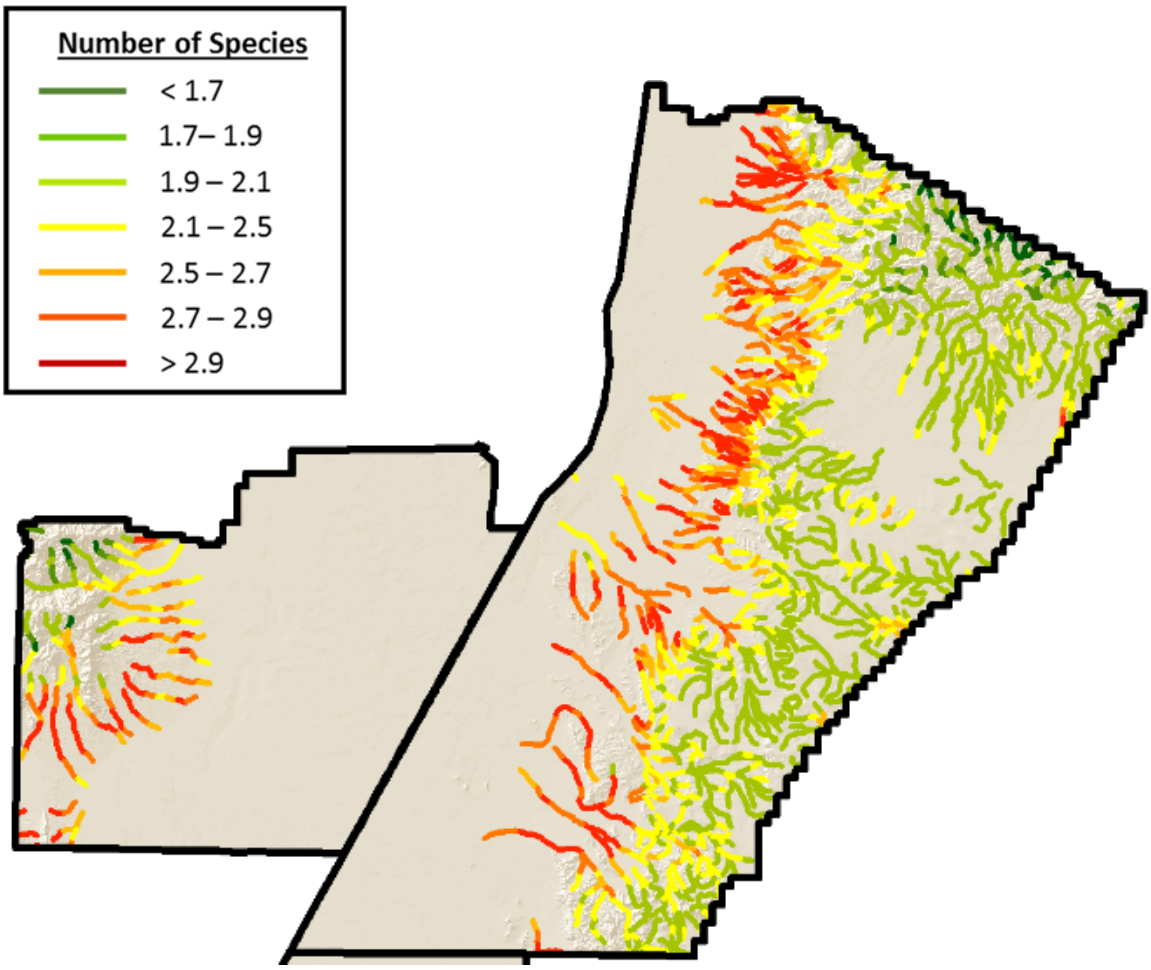


Figure 20. Distribution of TER-S riparian associated reptile species in stream reaches at Ft. Bliss, NM. Potential species richness was derived by stacking GAP animal habitat distribution models downloaded on or before October 2014.

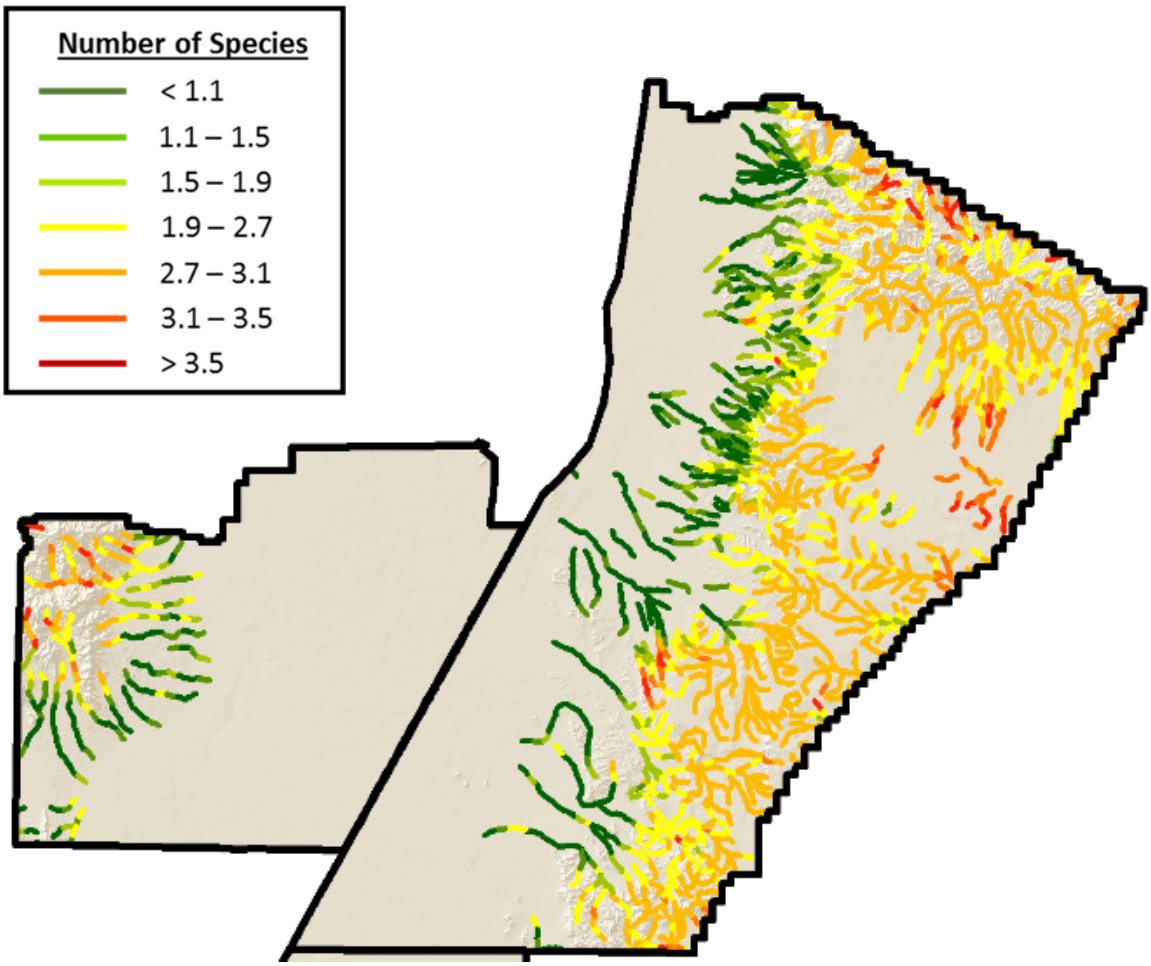


Figure 21. Distribution of riparian-associated passage migrant bird species in stream reaches at Ft. Bliss, NM. Potential species richness was derived by stacking GAP animal habitat distribution models downloaded on or before October 2014.

Appendix G. Russell Lyon Master's Thesis

USING RAINFALL-RUNOFF MODELS TO CHARACTERIZE THE FLOW REGIME OF DESERT STREAMS IN THE U.S. SOUTHWEST

By

Russell Lyon

A Thesis Submitted to the Faculty of the

SCHOOL OF NATURAL RESOURCES AND THE ENVIRONMENT

In Partial Fulfillment of the Requirements
For the Degree of

MASTER OF SCIENCE
WITH A MAJOR IN WATERSHED MANAGEMENT AND ECOHYDROLOGY
In the Graduate College
THE UNIVERSITY OF ARIZONA

2013

STATEMENT BY AUTHOR

This thesis has been submitted in partial fulfillment of requirements for an advanced degree at the University of Arizona and is deposited in the University Library to be made available to borrowers under rules of the Library.

Brief quotations from this thesis are allowable without special permission, provided that an accurate acknowledgement of the source is made. Requests for permission for extended quotation from or reproduction of this manuscript in whole or in part may be granted by the head of the major department or the Dean of the Graduate College when in his or her judgment the proposed use of the material is in the interests of scholarship. In all other instances, however, permission must be obtained from the author.

SIGNED: Russell Anthony Lyon

APPROVAL BY THESIS DIRECTOR

This thesis has been approved on the date shown below:

David P. Guertin
Professor of Watershed Hydrology
and Management

04/12/2013
Date

ACKNOWLEDGMENTS

I would like to thank the many people who have contributed to this work in one form or another. This research was made possible through funding provided by the Department of Defense's Strategic Environmental Research and Development Program (SERDP). I would like to express my gratitude to my committee members for their assistance and counseling throughout the completion of this project. Research Scientist and lead PI, Lainie Levick provided the knowledge and guidance to ensure that the work contained within was of the highest quality. Dr. Dave Goodrich offered an immense wealth of expertise and helped me to explore the various pathways to meet my objectives. My advisor, Dr. Phil Guertin, put forward the opportunity to work with the SERDP team while continuously trusting in my abilities. Dr. Shirley Papuga helped to advance my knowledge with her stimulating lectures while providing endless moral support.

I would also like to thank fellow SERDP team members Joel Murray and Samantha Hammer for making our countless expeditions into the desert both enjoyable and memorable, Kristin Jaeger for her expertise in helping to calibrate the models, and Hillary Nichols for sharing her Tidbit data results. Recognition is also due to both Shea Burns and Yoga Korgaonkar for providing enormous technical support in the setting up and execution of AGWA. Thank you to my family, friends, and professors who have stood by my side throughout my time at the University of Arizona. Such support has allowed me to continue the pursuit of my life-long goal of working to preserve and protect the natural environment from which we all depend.

TABLE OF CONTENTS

LIST OF FIGURES 6

LIST OF TABLES 7

ABSTRACT 8

1. INTRODUCTION 9

1.1 Purpose 9

1.2 Study objectives 10

2. LITERATURE REVIEW 11

2.1 Ecohydrology of semiarid riparian areas 11

2.2 Flow permanence 16

2.3 Peak flows 17

2.4 Rainfall-runoff models 18

2.5 NEXRAD data 19

2.6 Climate projections for the Southwest 20

3. METHODOLOGY 21

3.1 SERDP 21

3.2 Study sites 21

3.3 AGWA description 23

3.4 Watershed delineation and discretization 27

3.5 Soil and landcover parameterization 29

3.6 Precipitation input 31

3.7 Simulations and model execution 35

3.8 Calibration and validation of SWAT at Fort Huachuca....36
3.9 Calibration and validation of KINEROS2 at Fort Huachuca....38
3.10 Statistical analysis....38
3.11 Flow permanence....39
3.12 Flow permanence cutoffs....40
3.13 Peak flows....41
4. Results....42
4.1 Calibration and validation of SWAT at Garden and Huachuca Canyons....42
4.2 Calibration and validation of KINEROS2 at Ft Huachuca....49
4.3 Flow permanence....49
4.4 Peak flows....55
5. Discussion....58
5.1 Errors and assumptions....58
5.2 Flow permanence....60
5.3 Peak flows....60
5.4 Climate projection simulations....61
5.5 Suggestions for improvements....62
5.6 Future development and uses....63
6. Conclusion....64

APPENDICES....66
APPENDIX A: FLOW PERMANENCE MAPS....66
APPENDIX B: ABSOLUTE CHANGE FLOW PERMANENCE MAPS....69

REFERENCES 72

LIST OF FIGURES

Figure 1. Location of the four military installations. 22

Figure 2. National Climatic Data Center average monthly precipitation records from 1960-2012 at Fort Bliss, NM; Fort Huachuca, AZ; Yuma Proving Grounds, AZ; and Fort Irwin, CA.23

Figure 3. Diagram of AGWA workflow. 27

Figure 4. Graphical representation of thermal interpretation of streamflow from Gungle, 2005. 41

Figure 5. Depth-area ratios at Walnut Gulch for 2, 10, and 100-yr, 1-hour storms (Osborn *et al.,* 1980). 42

Figures 6 (a) and (b). Plot of simulated vs. observed average monthly volume totals at Upper Garden Canyon using NEXRAD-MPE precipitation input for (a) calibration and (b) validation time periods. 45

Figures 7 (a) and (b). Plot of simulated vs. observed average monthly volume totals at Upper Garden Canyon using rain gauge precipitation input for (a) calibration and (b) validation time period. 46

Figures 8 (a) and (b). Plot of simulated vs. observed average monthly volume totals at Upper Huachuca Canyon using NEXRAD-MPE precipitation input for (a) calibration and (b) validation time periods. 47

Figures 9 (a) and (b). Plot of simulated vs. observed average monthly volume totals at Upper Huachuca Canyon using rain gauge precipitation input for (a) calibration and (b) validation time periods. 48

Figure 10. Line plot of Tidbit sensor derived flow permanence compared to SWAT-NEXRAD derived flow permanence percentages for 2011. 57

Figure 11. Line plot of Tidbit sensor derived flow permanence compared to SWAT-rain gauge derived flow permanence percentages for the summer of 2011. 52

Figure 12. Flow permanence at Fort Huachuca using NEXRAD-MPE data and flow cutoffs. 53

Figure 13. Absolute change in flow permanence between 1981-2000 and 2081-2100 at Fort Bliss using GFDL CM2.1 climate projection data.....54

Figure 14. Photographs from Bug Scuffle watershed at Fort Bliss showing large channel and flood debris on tree 56

Figure 15. Photographs from Mojave Wash at Yuma Proving Grounds showing large channel and flood debris on tree.....57

Figure A1. Flow permanence at Fort Bliss using rain gauge precipitation data. 66

Figure A2. Flow permanence at Fort Irwin using rain gauge precipitation data 67

Figure A3. Flow permanence at Yuma Proving Grounds using rain gauge precipitation data 68

Figure B1. Absolute change in flow permanence between 1981-2000 and 2081-2100 at Fort Bliss using GFDL CM2.1 climate projection data 69

Figure B2. Absolute change in flow permanence between 1981-2000 and 2081-2100 at Fort Irwin using GFDL CM2.1 climate projection data 70

Figure B3. Absolute change in flow permanence between 1981-2000 and 2081-2100 at Yuma Proving Grounds using GFDL CM2.1 climate projection data.....71

LIST OF TABLES

Table 1. Paired T-test results from Upper Garden Canyon calibration and validation simulations. 44

Table 2. Statistical results for Upper Garden Canyon SWAT-NEXRAD and SWAT-rain gauge simulations with coefficient of determination (R^2) and Nash-Sutcliffe Efficiency (NSE) values for calibration and validation time periods. 44

Table 3. Paired T-test results from Upper Huachuca Canyon calibration and validation simulations. 44

Table 4. Statistical results for Upper Huachuca Canyon SWAT-NEXRAD and SWAT-rain gauge simulations with coefficient of determination (R^2) and Nash-Sutcliffe Efficiency (NSE) values for calibration and validation time periods. 44

Table 5. Stromberg research team's 2011 Tidbit Sensor flow permanence and SWAT derived flow permanence percentages at Fort Huachuca. 51

ABSTRACT

In the southwestern United States, the ephemeral nature of most streams often obscures the importance of the underlying ecohydrological processes that occur within them. The integrity of the riparian vegetation is primarily determined by the hydrologic regime of the adjacent stream channel. Determining the frequency and magnitude of streamflow events is an essential component of any assessment of riparian productivity. Flow permanence and peak flow are two key metrics that have been used to describe the flow regime in dryland environments; however, the lack of observational data collected from ephemeral or intermittent streams makes characterization difficult. The objectives of this study are to 1) develop a methodology for determining flow permanence values based on metrics derived from a continuous rainfall-runoff model, 2) determine peak flows from 2, 10, and 100-year, 1-hour design storms from an event orientated rainfall-runoff model, and 3) use climate projection data to explore flow regime changes in response to increasing temperatures to identify which areas would be most susceptible to climate change. Utilizing the Automated Geospatial Watershed Assessment (AGWA) toolkit to set up and run the Soil and Water Assessment Tool (SWAT) and the Kinematic Runoff and Erosion (KINEROS2) models, I was able to replicate hydrologic conditions and provide estimates for flow permanence and peak flow metrics. SWAT model calibration and validation were possible at two stream gauge locations where acceptable streamflow estimates were obtained at monthly intervals. A comparison between different SWAT precipitation inputs revealed that NEXRAD-MPE yielded as reasonable estimates as rain gauge data, justifying its use in areas where observational data are limited. Characterizing the hydrology of ephemeral and intermittent stream channels can allow land managers to better

assess riparian conditions and may be used to predict response to changes in the hydrologic regime associated with human disturbances. It can also be used to direct land use activities away from ecologically sensitive areas to help preserve ecosystem health and take into consideration some of the environmental concerns associated with future land use and climate change.

1. INTRODUCTION

1.1 Purpose

Conventional stream classifications based on flow attributes and/or channel morphology have primarily been focused on perennial stream networks common to mesic environments (Rosgen, 1994; Montgomery & Buffington, 1997; Puckridge *et al.,* 1998). In arid to semiarid systems, where ephemeral and intermittent streams are the dominant fluvial features, scarce observational data has hindered most attempts to perform similar stream classifications. While ephemeral and intermittent streams perform similar hydrologic and ecologic functions as their perennial counterparts (Levick *et al.,* 2008) they generally are not incorporated in most watershed-based assessments. This research aims to fill that void by developing a stream classification for ephemeral and intermittent streams based on hydrologic characteristics, mainly flow regime attributes, that can easily be related to vegetation attributes and can be used in defining ecohydrological relationships.

1.2 Study objectives

The work described in this paper is just one component of a larger research project working towards an ecohydrological classification of ephemeral and intermittent streams in the southwestern United States. This component of the project focuses primarily on the hydrologic component by characterizing the flow regime of streams based on the timing, duration, frequency, and volume of flows. The primary objectives are to: 1) develop a methodology for determining flow permanence values based on metrics derived from a continuous rainfall-runoff model, 2) determine peak flows from 2, 10, and 100-year, 1-hour design storms from an event orientated rainfall-runoff model, and 3) use climate projection data to explore flow regime changes in response to increasing temperatures to identify which areas would be most susceptible to climate change. The results from these characterizations will be used to create a classification of ephemeral and intermittent streams based on the timing and duration of flows and discharge patterns. Such a classification can be used to make correlations with vegetation characteristics such as canopy height and percent cover that can then be used to model riparian conditions and predict changes under different flow regimes associated with various land cover and climate change scenarios.

2. LITERATURE REVIEW

2.1 Ecohydrology of semiarid riparian areas

Scientists have recently begun to embrace a more interdisciplinary approach to improve our understanding of the links between hydrological, biogeochemical, and ecological processes (Rodriguez-Iturbe, 2000; Newman *et al.,* 2006). As a result, ecohydrology has emerged as a branch of science that explores the interactions between hydrological and ecological processes and their associated feedbacks across both spatial and temporal scales. The study of ecohydrology in arid and semiarid ecosystems is of particular importance due to the lack of water and the tight coupling of hydrological partitioning and ecological dynamics being more evident yet not as clearly understood (Jackson *et al.,* 2009). Ecohydrological research offers a holistic approach to ecosystem studies, but a solid understanding of underlying hydrologic processes must be in place prior to making any attempts to establish relationships.

Soil moisture has been identified as one of the key variables linking climate fluctuations and vegetation dynamics (Rodriguez-Iturbe, 2000). Distinct vegetation patterns have been observed along ephemeral and intermittent streams where greater soil moisture concentrations allow for increased plant biomass or the establishment of more mesic species. These riparian areas are a unique part of the landscape where hydrologic connectivity is maintained throughout the watershed to supply the water and nutrients needed to fuel downstream biogeochemical reactions. Riparian areas are especially important in desert landscapes because of their essential ecological role in providing nutrients, critical habitat, and migration routes for many species of wildlife.

Riparian ecology is controlled largely by local and regional flow patterns determined by the variability in the intensity, timing, and duration of precipitation interacting with terrain, soil texture, and evapotranspiration (Poff *et al.,* 1997). The interaction between a stream's flow regime and riparian communities are largely determined by how precipitation translates into moisture stored in the soil and other components of the water budget expressed in the equation:

$$P = R + ET + S + D$$

Where P = precipitation, R = runoff, ET = evapotranspiration, S = storage in soil, and D = deep aquifer recharge. Below I summarize how each component of the water budget is tied to a stream's flow regime and how they influence riparian vegetation communities.

Arid and semiarid systems are characterized by having a mean annual precipitation that is less than potential evapotranspiration rates (Allison & Hughes, 1983) creating conditions that limit surface water availability. For most streams, flow typically occurs in response to precipitation events resulting in ephemeral streams being the dominant fluvial features of the landscape. An ephemeral stream's flow regime is not influenced by groundwater inflow but is solely tied to the timing and magnitude of precipitation pulses that are in turn driven by seasonal to decadal climatic patterns (Loik *et al.,* 2004). In semiarid regions of the United States the majority of precipitation events are small (0 to <5mm) events with most of the rainfall returning to the atmosphere via evaporation resulting in less water available for plant uptake (Lauenroth & Bradford, 2009). More important are the less frequent, higher intensity summer convection storms that contribute to the local recharge and determine the amount of water available for desert riparian vegetation (Baillie *et al.,* 2007).

Riparian vegetation is influenced by flow regime characteristics such as presence of surface or groundwater flows and high and low flow conditions (Stromberg *et al.,* 2005). The

increased biodiversity and ecological function of riparian areas are attributed in part to the dynamic nature of the flow regime's regulation of soil moisture. The width of the riparian zones is largely determined by the size of the stream, the position of the stream within the watershed, the flow regime, and local geomorphology (Naiman *et al.,* 1993). Species richness in riparian zones varies greatly both spatially and temporally along the stream channel (Naiman *et al.,* 1993). The degree to which these vegetation changes occur is primarily regulated by the flow regime (Naiman *et al.,* 1993), which determines how much subsurface moisture travels from the hyporheic and parafluvial zones beneath the active channel to the riparian zone. It is within these areas where the majority of ecohydrological processes occur and where the other components of the water budget determine riparian characteristics (Naiman & Decamps, 1997).

Runoff is typically the smallest component of the water budget in arid and semiarid ecosystems, often accounting for less than 5% of the total annual budget (Wilcox, 2003). In regions of the southwestern United States subject to the North American monsoon, runoff is most often associated with high intensity, summer thunderstorms (Stone *et al.,* 2008). Runoff can also be generated from late summer and fall tropical depressions. In higher elevations where shallow soils and bedrock are common, runoff also occurs with rapid snowmelt and low intensity winter rainfall, enhanced by El Niño conditions (Woolhiser *et al.,* 1993). While topography and soil texture can influence runoff behavior, how it responds once it encounters vegetation is an important determinant of ecohydrological processes. Upland vegetation patches help obstruct runoff leading to sediment deposition and infiltration facilitating their own growth and promoting greater biological activity (Ludwig *et al.,* 2005). Riparian areas perform in a similar manner as upland vegetation patches, but are tied directly to the stream channel where the additional soil moisture supports more vegetation growth and/or can influence the flow regime.

Rates of evapotranspiration vary greatly depending on vegetation type, soil texture, and meteorological conditions. Plants are often organized into different functional groups (i.e. grasses, shrubs, trees) based on similar rooting densities and depths to better understand vegetation response to water fluxes (Jackson *et al.,* 1996). Semiarid riparian areas typically contain assemblages of these functional groups with a wide variety of canopy and rooting structures that can lead to complex interactions between evapotranspiration and soil moisture.

Evaporation in riparian areas occurs both at the vegetation canopy and at soil surfaces. Small precipitation events (<5mm) provide little moisture for vegetation uptake due to most of it being intercepted by the vegetation canopy and returning to the atmosphere via evaporation (Owens *et al.,* 2006). The amount that is lost from the canopy is controlled mainly by leaf area of the vegetation and referred to as interception loss. Evaporation from the soil surface is typically limited to the top 15cm (Wilcox, 2003). With larger intensity or longer duration storms, precipitation will exceed the storage potential of the canopy and reach the surface as throughfall or stemflow. Beneath the canopy of trees and large shrubs where shading from solar radiation regulates temperature and the accumulation of organic debris promotes infiltration, exists a microclimate that facilitates the establishment of understory shrubs and grasses. This is often reflected in riparian areas with a shrub or tree overstory contributing to the establishment of a grass understory (Scholes & Archer, 1997).

Water that is not lost to evaporation can infiltrate to deeper soil horizons where it becomes available for plant uptake and is used to cycle nutrients throughout the plant until it is eventually transpired through their stomata as water vapor. The amount of transpiration that takes place in riparian areas is related to the vegetation type and size with larger species having higher levels of transpiration compared to smaller sizes of the same species (Tong *et al.,* 2008).

The ratios of transpiration/evapotranspiration and evaporation/evapotranspiration have been shown to be highly regulated by precipitation seasonality with evaporation being the main component of evapotranspiration when small infrequent rain events occur, but later shifts to transpiration becoming the main component when precipitation events are more frequent and/or of greater intensity (Cavanaugh *et al.,* 2011).

When a tree is not transpiring it has the unique ability to transfer moisture from wet to dry areas of the soil via its root system. This important mechanism, known as hydraulic redistribution, influences both carbon and nutrient fluxes and can impact vegetation composition and structure. Sap flow measurements in *Prosopis velutina* Woot. (velvet mesquite) showed that significant amounts of soil water were redistributed both via hydraulic lift during the growing season and via hydraulic descent during winter dormancy (Hultine *et al.,* 2004; Scott *et al.,* 2008). Certain understory species (shrubs and grasses) may also benefit from overstory tree species delivering moisture from deep to shallow soil layers via hydraulic lift (Zou *et al.,* 2005). In riparian areas the results of such water movement can have considerable influence on the soil water budget through increases in transpiration or decreases in groundwater recharge and is an important consideration for any ecohydrological assessments.

The volume of flow in alluvium-dominant ephemeral channels tend to decrease as it travels downstream due to in channel infiltration of water, referred to as transmission loss, which can serve as the principal contribution to deep aquifer recharge (Lane, 1983; Goodrich *et al.,* 2004). Channel soil properties (e.g. soil texture, structure, antecedent soil moisture) determine infiltration rate and control if water will make it beyond the rooting depth of riparian vegetation to eventually recharge the deepwater aquifer. Recent hydrologic models suggest that for most arid to semiarid interdrainage areas, no deep drainage has occurred since the onset of the

Holocene some 10,000 - 15,000 years ago (Seyfried *et al.,* 2005). Therefore, it can be inferred that most deep drainage occurs at or near ephemeral channels, which would be partially regulated by transpiration of riparian vegetation (Goodrich *et al.,* 2004).

Some riparian species are able to facilitate their own establishment and growth by modifying the rate of hydrological processes through changes in roughness, albedo, and soil moisture beneath their canopy thereby promoting seedling establishment and plant growth (D'odorico *et al.,* 2010). These interactions between biotic and hydrologic processes result in a positive feedback that can influence riparian vegetation composition and structure. Biological feedbacks are complex processes that have tremendous impacts on hydrologic and vegetation interactions from individual stream reach to watershed scales and being able to explain how they relate to ecohydrological processes poses one of the greatest challenges to ecohydrologists today.

2.2 Flow permanence

Quantifying the relationship between flow regime and stream ecology in dryland ecosystems requires a measurement that captures the stochastic nature of flow pulses and accurately describes hydrologic connectivity throughout the stream. Flow permanence offers this by determining the degree of stream intermittency by quantifying the amount of time in a given period that flow is present in the channel (Leenhouts *et al.,* 2006). Aside from providing soil moisture for transpiration, flow pulses are responsible for initiating biogeochemical processes by stimulating microbial activity, cycling nutrients and organic matter, and transporting these resources to downstream areas where they are available to the adjacent riparian zone (Larned *et al.,* 2010). In effect, riparian areas exposed to longer periods of flow duration, or higher values of flow permanence, will be expected to have noticeable patterns, such

as greater vegetation biomass and height compared to interdrainage vegetation. A stream classification based on flow permanence can be used as a key indicator of the frequency in which soil moisture becomes available for riparian vegetation uptake and can be used to assign different levels of ecological importance among various stream reaches.

Several studies exist that have looked at the importance of the relationship between flow permanence and vegetation or aquatic species attributes. Hupp (2000) showed that for low-gradient coastal rivers a similar metric known as the hydroperiod, or the annual period of inundation, controls riparian vegetation distribution and is useful for assessing plant ecological patterns. Stromberg *et al.* (2005) showed that in a semiarid environment stream flow and soil moisture are positively associated with plant species richness suggesting that flow permanence could be used in ephemeral and intermittent streams as a possible indicator of riparian species composition. Arscott *et al.* (2010) analyzed benthic invertebrates species richness across a longitudinal intermittence gradient of an alluvium stream in New Zealand and found that 1.9 taxa/m^2 were added per 10% increase in flow permanence.

2.3 Peak flows

Large flood events that are common to ephemeral and intermittent streams are responsible for much of the changes in channel morphology and can have considerable influence on riparian plant species (Friedman & Lee, 2002). Peak flow represents the highest point of discharge on a hydrograph and is a useful metric for describing the magnitude of large flood events (Pitlick, 1994; Osterkamp & Friedman, 2000). It is also often used to assess the hydrologic response of a watershed to a particular storm event and can be used as a measurement of watershed condition (Hernandez *et al.,* 2000). Peak flow estimates are possible using a

rainfall-runoff model driven by design storms generated from precipitation frequency maps. These estimates can provide evidence of areas within a watershed that may experience large alterations in channel morphology and/or high loads of sediment transport (Friedman & Lee, 2002). These areas can then be considered in directing site or road development to more stable locations or used to justify culvert construction for existing roadways.

2.4 Rainfall-runoff models

Hydrologic models that measure rainfall-runoff relationships are often utilized to determine streamflow characteristics to address water resource problems in ungauged watersheds (Gassman *et al.,* 2007). Rainfall-runoff models calculate stream discharge by employing mathematical equations that partition rainfall into each of the hydrologic components based on the interactions with various watershed characteristics including topography, soil type, and vegetation cover (Arnold *et al.,* 1998). The output from these models can be used to assess the impact of management and climate on water supplies (Arnold & Fohrer, 2005). Rainfall-runoff models are useful for determining flow permanence because they operate at a daily time-step (Arnold *et al.,* 1998); the smallest practical unit of time used to determine the percent of time when flow is present in a stream reach.

One major challenge in determining flow permanence is the lack of observed data in ephemeral and intermittent channels; however, new methods that use hydrologic models to simulate flow regimes have begun to emerge. Kirkby *et al.* (2011) used a hydrological model to dynamically partition precipitation to estimate how much water was available for evapotranspiration and how much was left for runoff to determine when critical low-flow stages were present in semiarid rivers across Europe. Gallart *et al.* (2012) used rainfall-runoff

simulations to develop flow-permanence and seasonal predictability of zero flow period metrics that were used to classify ephemeral streams into distinct aquatic regimes.

Hydrologic models have also shown to be useful in determining additional streamflow metrics such as runoff depth and peak discharge. Hernandez *et al.* (2000) used two rainfall-runoff models to assess watershed condition by measuring runoff response to land cover change. Wollmuth & Eheart (2000) used a rainfall-runoff model to calculate discharge volumes so that they could distribute water allocations to meet both irrigation demand and environmental flows necessary to sustain riparian vegetation. Both of these studies indicate that with the absence of measured data, model simulated results can be used as a substitute, though some discretion must be used in the quantitative results of such efforts depending on whether model calibration and validation are possible.

2.5 NEXRAD data

The reliability of rainfall-runoff modeling results can vary depending on the level of detail of the precipitation data used as input into the model. The relatively few and remote location of rain gauges located in the southwestern United States and the highly variable nature of rainfall has led many modelers to look for alternative sources of precipitation data that better captures the spatial variability of non-uniform events. Consequently, Next Generation Weather Radar (NEXRAD) data has emerged as a viable option to improving modeled flow results. For instance, Moon *et al.* (2004) reported that NEXRAD was useful for capturing localized rainfall events in a large watershed in the Trinity River Basin in Texas and performed well in modeling streamflow. Wang *et al.* (2008) compared the performance of rain gage corrected NEXRAD Stage III dataset to the rain gage and satellite corrected NEXRAD Multisensor Precipitation

Estimation (NEXRAD-MPE) dataset using a high-density rain gauge network in the Upper Guadalupe River Basin of the Texas Hill Country and found that both datasets were better at detecting non-uniform precipitation events than rain gages alone, but that Stage III data tended to overestimate (20%) and MPE tended to underestimate (7%) precipitation values. Tobin and Bennett (2009) report that runoff model results using NEXRAD Stage III data outperformed rain gauge data (standard error +/- 13%) in two watersheds in the Middle Rio Grande at a monthly time scale.

2.6 Climate projections for the Southwest

The Intergovernmental Panel on Climate Change Working Group II's Contribution to the Fourth Assessment Report (Parry, 2007) describes how global climate change is influencing regional weather patterns that may be resulting in changes to local precipitation patterns. Such changes have the potential to negatively impact many terrestrial systems leading to declines in biodiversity and ecosystem goods and services (Parry, 2007). Understanding how climate change will affect the Southwest is key to any adaptation plans and is slowly becoming possible using spatially and temporally downscaled global climate data projections (Meehl *et al.,* 2007; Seager *et al.,* 2007). Meehl *et al.* (2007) used the combined results from 25 climate models that successfully explained past global climate changes to predict that a warming of 1.8-3.4°C is expected by the year 2100. Seager *et al.* (2007) reported that the multi-model mean from 19 climate models showed a transition to more arid conditions in the Southwest is expected in the late 21st century and should already be under way. A study by Cayan *et al.* (2010) used downscaled global climate data to predict a 2-4°C increase in temperature and a decrease in

precipitation by the end of the 21st century would lead to more extreme drought conditions in the Southwest.

3. **METHODOLOGY**

3.1 SERDP

The core of this research is funded by the Department of Defense's Strategic Environmental Research and Development Program (SERDP), which provided access to study areas at four military installations in the Southwest. These sites were chosen because they represent the main desert ecoregions (Chihuahuan, Sonoran and Mojave Deserts; Figure 1) and the natural variations in climatic conditions and precipitation (Figure 2) that naturally occur across the Southwest.

3.2 Study sites

Fort Irwin is a National Training Center located in the High Mojave Desert of Southern California. It covers approximately 1,180 mi^2 (3,056 km^2) and averages 4.33 inches (110 mm) of precipitation per year (NOAA's National Climatic Data Center [NCDC], http://www.ncdc.noaa.gov/). It is the only installation included in this study that is not influenced by the North America monsoon and receives most of its rainfall during the winter season (NOAA NCDC, http://www.ncdc.noaa.gov/). Yuma Proving Ground (YPG) is used mainly as a military equipment-testing center located in the Sonoran Desert of southwestern Arizona. It has an area of approximately 1,300 mi^2 (3,367 km^2) and is located in one of the driest parts of the United States receiving an average annual precipitation of only 3.65 inches

(92.7 mm; NOAA NCDC, http://www.ncdc.noaa.gov/). Fort Huachuca serves mainly as a communication center with minimal outdoor training activity and is located in the Sonoran-Chihuahuan transition zone in southeastern Arizona. Its eastern boundary runs adjacent to the town of Sierra Vista and includes parts of the Huachuca Mountains to its west, where the only perennial streams included in this study are found. It is the smallest of the four study areas covering approximately 127 mi^2 (329 km^2), but receives the most precipitation with an annual average of 15.6 inches (381 mm; NOAA NCDC, http://www.ncdc.noaa.gov/). Fort Bliss is an army post located in the Chihuahuan desert in southwestern New Mexico. It is the largest of the study areas at approximately 1,740 mi^2 (4,506 km^2) and receives an average of 8.66 inches (220 mm) of precipitation per year (NOAA NCDC, http://www.ncdc.noaa.gov/).

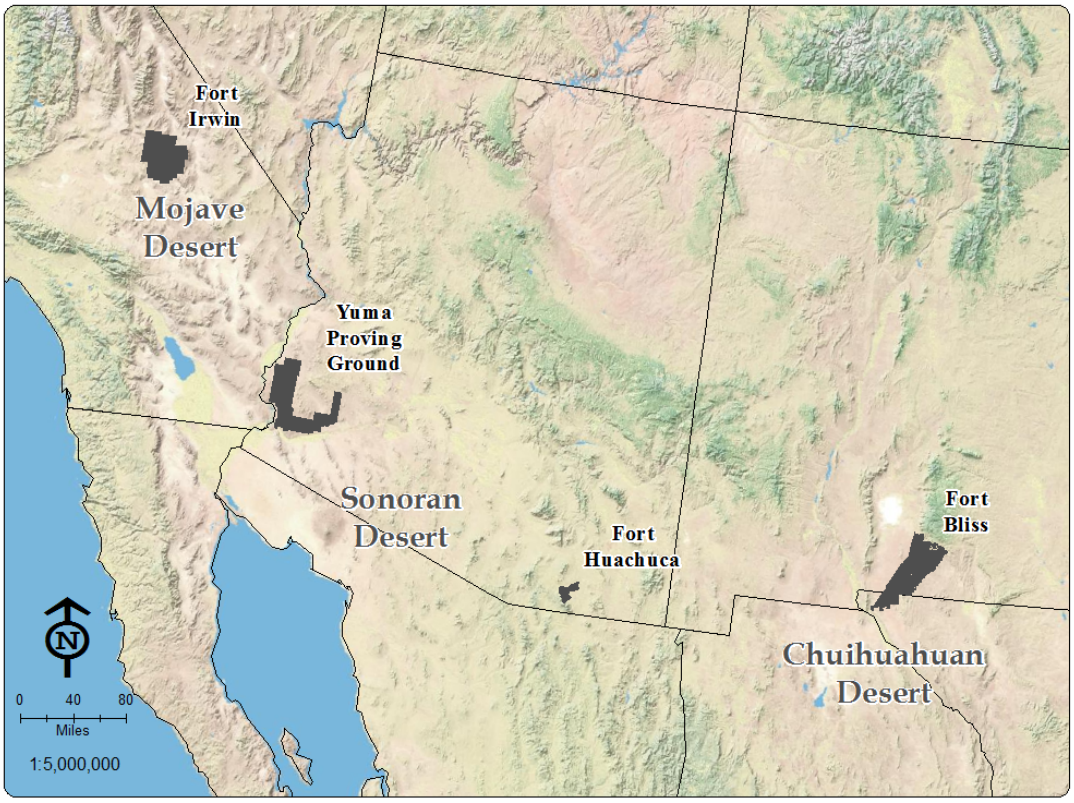


Figure 1. Location of the four military installations used as research sites for the SERDP project.

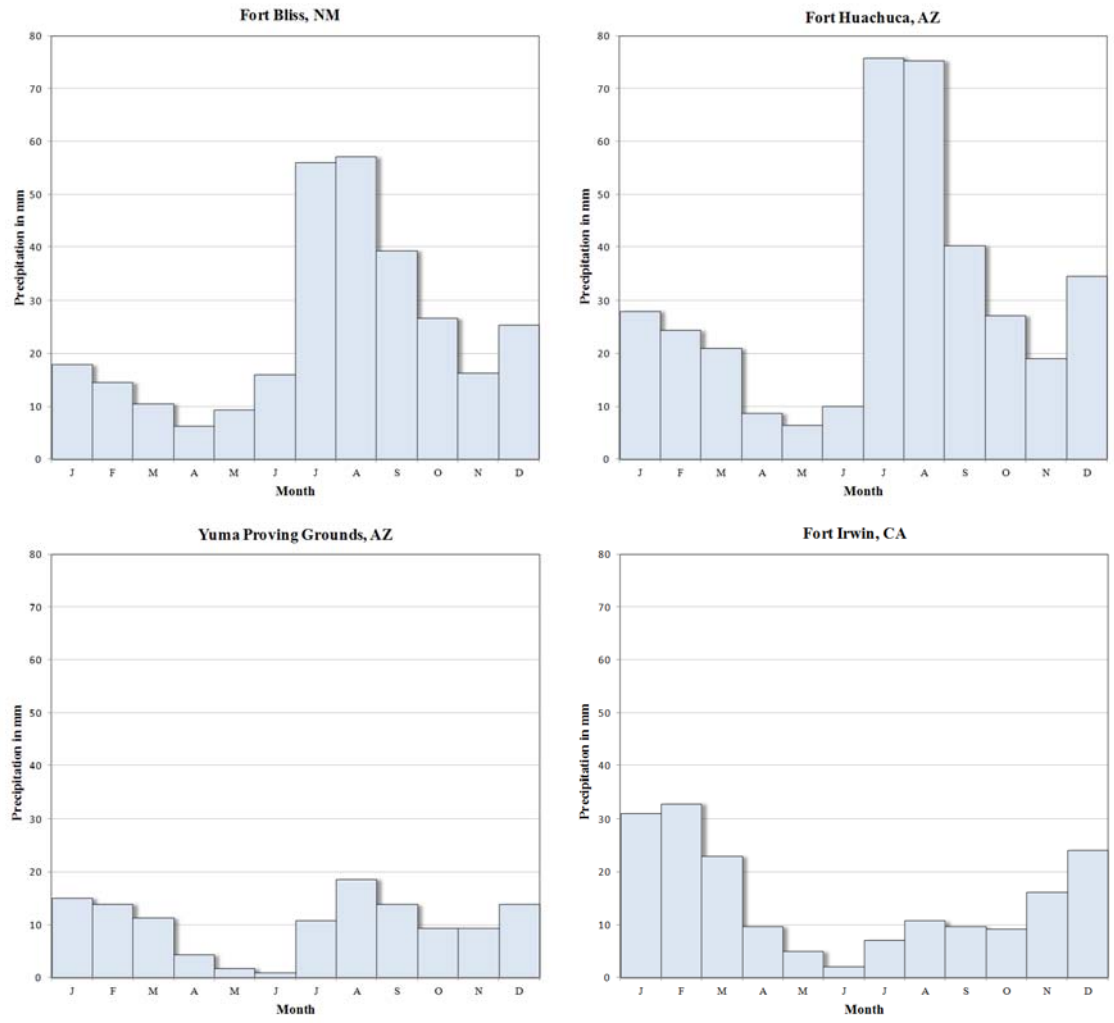


Figure 2. National Climatic Data Center (NOAA NCDC, www.ncdc.noaa.gov) average monthly precipitation records from 1960-2012 at Fort Bliss, NM; Fort Huachuca, AZ; Yuma Proving Grounds, AZ; and Fort Irwin, CA.

3.3 AGWA description

The Automated Geospatial Watershed Assessment (AGWA) toolkit was chosen for this study because of its consideration of each of the hydrologic components of the water budget within each of the two separate runoff models. An added benefit of using two separate models is that it allows the evaluation of the flow regime at different temporal scales permitting a wider analysis from varying perspectives. The first model uses long-term data to provide daily

measurements that are used to calculate flow permanence, or the average annual time period when flow is present in the channel, while the second model uses event-specific rainfall depth to determine peak discharge values. Combined these metrics can be used to develop different classes of stream types that can be used to establish relationships with different riparian attributes.

AGWA Version 2.0 is an open source toolkit that automates the tasks of assigning topographical, soil, and landcover parameters to watershed units in preparation for running a pair of hydrologic models (Miller *et al.,* 2007). AGWA is embedded in common geographic information system (ESRI ArcGIS) software where watershed boundaries are delineated and subdivided then overlain with spatial data to obtain the necessary information needed to run the models. At the core of AGWA are two distributed hydrologic models that allow for watershed assessment across spatial and temporal scales. The Soil and Water Assessment Tool (SWAT) is a continuous simulation model that was designed for predicting watershed response to land management practices for large basins over large periods of time (Arnold *et al.,* 1998). It uses a modified Curve Number methodology to partition rainfall into infiltration and overland flow and reports water and sediment yields on a daily time-step, monthly, or annual time-step (Miller *et al.,* 2007). The Kinematic Runoff and Erosion model (KINEROS2) is an event specific model that details the processes of interception, infiltration, surface runoff, and erosion from small watersheds (Woolhiser *et al.,* 1990; Goodrich *et al.,* 2012). AGWA is designed to lead the user through the process to parameterize and execute the chosen model and display the results for visual analysis and change detection in response to landscape alterations (Miller *et al.,* 2002a; Figure 3).

AGWA was developed jointly by the USDA Agricultural Research Service (ARS) Southwest Watershed Research Center branch, the United States EPA Office of Research and Development, and the University of Arizona (Miller *et al.,* 2007). The tool has been used to demonstrate hydrological impacts from decadal-scale landcover change, estimate post-fire impacts on runoff and sediment transport, and assess the potential impacts of rangeland management actions on soil erosion and sediment yields (Miller *et al.,* 2002b; Canfield *et al.,* 2005; Goodrich *et al.,* 2011). Recent improvements include a landcover modification tool that allows users to modify the landcover input layer to determine the hydrologic effects associated with changes from fire, urbanization, climate change or other natural or anthropogenic disturbances (Burns *et al.,* 2007). AGWA is under constant development to improve performance and incorporate additional features and planned additions include the representation and modeling of fire and drought; parameterization procedures based on Ecological Site Descriptions and State-and-Transition Models; tools to modify water locations, fences, and buffers; an economic analysis toolkit; and a web-based version of AGWA (Goodrich *et al.,* 2011).

AGWA is primarily designed to provide qualitative estimates of runoff and erosion useful for assessing relative change between simulation results or between the different subunits within the larger watershed; however with proper calibration, it can provide quantitative estimates as well (Miller *et al.,* 2002a). In this study, AGWA was used to characterize the flow regime of ephemeral, intermittent, and perennial stream channels in unmonitored basins within semiarid to arid parts of the southwestern United States. SWAT was used to determine historical and projected average annual flow permanence based on over a decade of observed rainfall data as well as downscaled climate projection data from a representative global circulation model.

KINEROS2 was used to estimate peak flows based on 2, 10, and 100-year, 1-hour design storms created from the National Oceanic and Atmospheric Administration's (NOAA) Atlas 14 point precipitation frequency estimates (NOAA Precipitation Frequency Data Server, 2012).

Prior to running the models several data layers and climate data were collected including, topography (http://viewer.nationalmap.gov), soil (http://soildatamart.nrcs.usda.gov), land cover (http://gapanalysis.usgs.gov/), and daily precipitation and temperature (http://www.ncdc.noaa.gov) values. Since the reliability of the modeling results will depend highly on the quality of the input data, a thorough examination of each data layer is included describing the potential benefits and limitations of each.

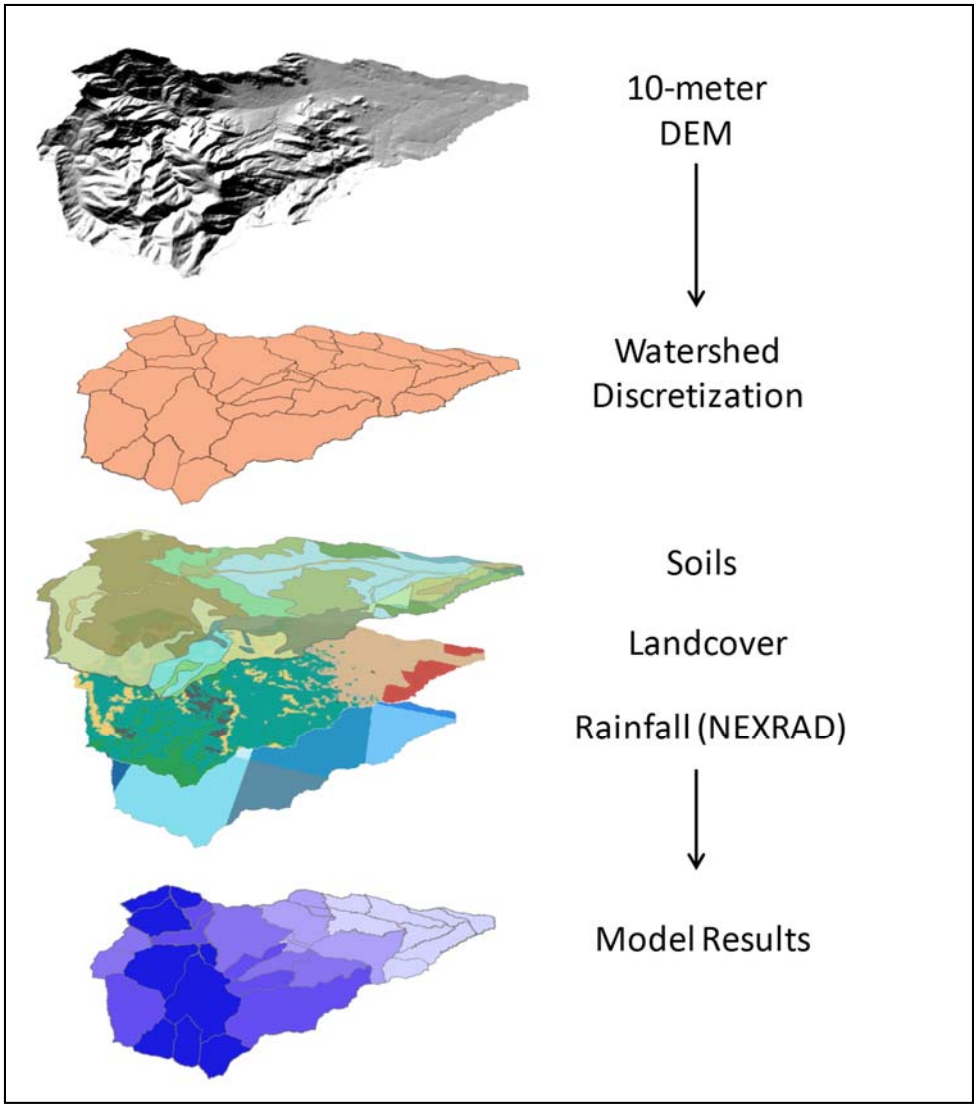


Figure 3. Diagram of AGWA workflow.

3.4 Watershed delineation and discretization

A tiled mosaic of Digital Elevation Model (DEM) raster data layers was necessary to delineate watershed boundaries and determine the flow routes needed to run the models. The United States Geological Survey (USGS) provides bare earth DEM data from the National Elevation Dataset (NED) of 1/3 arc-second (approximately 10-meter) resolution for the contiguous United States that has been corrected to remove artifacts, match edges, and account

for missing data (Gesch *et al.,* 2002). The 10-meter DEM data was deemed appropriate for use in this project as it captures the level of detail necessary to determine stream pathways, though some variance is expected, especially in areas of low relief. AGWA allows users to fill DEMs in order to remove any erroneous values (sinks). Then it is used to create a flow directional grid, a flow accumulation grid, and stream representation layer.

The size and shape of each watershed boundary was determined by the location of the watershed outlets that were chosen by overlaying the installation boundaries over the stream map. Some personal expertise was required in determining outlet locations due to the predominantly linear boundaries of the study areas not corresponding with the natural flow pathways and large parts of some watersheds being located outside the study areas. This resulted in two different classes of watershed sizes. The first class represents areas that are completely contained within the study area's borders and whose outlet location was based as close as possible on the USGS's Watershed Boundary Dataset for 12-Digit Hydrologic Units (HUC12). The second class is considerably smaller due to only a small portion of a watershed being located within the study area. The focus of the work is on the larger watersheds that predominantly lie within the study boundaries but may also incorporate some portions of the surrounding watersheds.

Upon delineation of the watershed boundary the user decides which model will be used before proceeding to discretize the watershed into the smaller subwatersheds, referred to as hydrologic response units (HRUs) within SWAT and planes within KINEROS2, due to each model having a different method for routing flow through the steam channels. SWAT uses a command structure to route runoff through the watershed by computing surface runoff and infiltration for each HRU before adding the runoff to each downstream stream segment (Arnold

& Fohrer, 2005). KINEROS2 conceptualize subwatersheds into rectangular overland planes and then routes flow to the channel from planes on either or both sides of the channel before routing it to the next downstream channel segment (Woolhiser *et al.,* 1990). It is during the discretization that the user decides on the size of the individual HRUs or planes and their associated stream segments by defining the contributing source area (CSA), which is adjusted to reflect the level of model complexity desired (Goodrich *et al.*, 2011). For this study the CSA was set to a flow accumulation area of 10,000 m^2, which was deemed an appropriate scale needed to meet the project's objectives.

3.5 Soil and land cover parameterization

The next step was to intersect soil and landcover data to each model element polygon and its associated stream segment. The soil databases used in this study include the Soil Survey Geographic (SSURGO) and the State Soil Geographic (STATSGO) databases, both created and maintained by the USDA's Natural Resource Conservation Service (Soil Survey Staff [SSS] Natural Resources Conservation Service [NRCS], 2011). The SSURGO dataset comes from digitized county-level maps that were created following standardized field methodologies and vary spatially from 1:12,000 to 1:63,360 (SSS NRCS, 2012). The STATSGO dataset is a coarser version of the soil survey maps, generalized to a scale of 1:250,000 to be more appropriate for state and regional uses (SSS NRCS, 2011). Comparing the differences between modeled runoff results in a more temperate area of the United States has shown that SSURGO-based results tend to be closer to observed values, whereas STATSGO-based results tend to underestimate runoff (Mednick, 2010). However, STATSGO has also been observed to be more accurate than SSURGO in some uncalibrated runs, although both were found to be within reasonable ranges

(Geza & McCray, 2008). Evaluating which soil database will prove to be the more accurate for areas covered in this study was not part of the original scope of this project and remains to be explored. Due to its availability at the time of the study, the finer resolution the SSURGO database was used at Fort Huachuca and most of Fort Bliss and Fort Irwin and the STATSGO was used at Yuma Proving Grounds and where SSURGO data was unavailable.

Land cover information on vegetation and land use patterns was acquired from the USGS's Gap Analysis Program (GAP) National Land Cover dataset (USGS National Gap Analysis Program, 2012). The GAP land cover data combines data generated by regional GAP projects with LANDFIRE data to provide information on the distribution of native vegetative types, modified and introduced vegetation, developed areas, and agricultural areas in a seamless coverage for the entire Unite States (USGS GAP, 2012). The southwest portion of the dataset was derived through the classification of 30-meter, multi-seasonal Landsat Enhanced Thematic Mapper Plus (ETM+) satellite images that were acquired between 1999-2001 (Lowry *et al.,* 2007). The imagery was classified into 590 land use classes following the NatureServe's Terrestrial Ecological Systems Classification framework for natural and semi-natural land cover (Comer *et al.,* 2003). Training data were used to validate the classification based on field work samples, aerial photography, digital orthophotoquads, or other remotely sensed imagery and agreement between the validation samples and map ranged in accuracy from 50-70% for the entire Southwest region (Lowry *et al.,* 2007). The GAP land cover data are available online and was downloaded for the 'Desert' Landscape Conservation Cooperative region from the GAP land cover data portal (USGS GAP, 2012).

In AGWA the vegetation type, interception, Manning's N, percent impervious, and curve number values based on the hydrologic soil group (A, B, C, and D) are all obtained from the land

cover layer using a land cover data look up table that is included within the AGWA2 data package (Burns *et al.,* 2007). These values were determined for each of the vegetation classes from expert opinion and previously published look-up tables (Miller *et al.,* 2002a). The original table included with AGWA, however, covers only parts of the Southwest and excluded some of the ecological classes in Southern California needed for this study. As a result, a new lookup table was created that incorporated these missing classes by assigning values from similar classes based on their physical description.

3.6 Precipitation input

Following the assignment of soil and landcover data to each HRU, the next step in running AGWA is to prepare the precipitation input data for the desired model. Accurate representation of precipitation events requires a high degree of spatial coverage and both rain gage and radar data were explored to assess which could most accurately simulate real world conditions. The representation of rainfall from rain gauge observations varied at each site depending on the number of gauges found in close proximity to the military installations. The finer resolution NEXRAD-MPE data were also used at all four installations to supplement for some of the areas with limited rain gage coverage.

SWAT precipitation input requires a table of daily precipitation (mm) values arranged chronologically by year and Julian calendar day that are associated with each rain gauge location. For multiple gauges, AGWA uses a built in tool that distributes the values using Thiessen polygons to compute the weighted rainfall depth falling on each subwatershed (Miller *et al.,* 2007). The daily climate data needed to run SWAT was obtained from the NOAA National Climatic Data Center's (NCDC) Global Historical Climatology Network (GHCN) Daily, Version 2 dataset accessed via the online interactive map application (NOAA GHCN,

2010). This dataset contains a composite of climate records from numerous sources that were merged and subjected to a suite of quality assurance reviews (NOAA GHCN, 2010). The dataset provides daily maximum and minimum temperatures, snowfall, and 24-hour precipitation totals that were obtained primarily from state universities or cooperatives and reported as part of the United States Cooperative Summary of the Day (NOAA GHCN, 2010).

Daily precipitation and temperature data were compiled for those rain gauges that were within a close proximity to the four study areas. Due to the relatively remote locations of the study sites only a limited number of rain gauges have been installed and maintained over the years. Some of the gauges have changed location or have been removed completely resulting in varied spatial coverage of the study areas. From the data available only the years with overlapping recorded observations will be used and any gaps or erroneous values will be replaced with averaged values from adjacent stations.

The following reports the number of the gauges with years available for each study site: eight gauges with 55 years of data (1956-2011) at Fort Huachuca, nine gauges with 51 years (1960-2011) at Fort Bliss, five gauges with 55 years (1956-2011) at YPG, and six gauges with 57 years (1954-2011) at Fort Irwin. Given that relatively few of the rain gauges recorded data continuously throughout these time periods, different subsets of years will be used at each installation, each with a varying number of rain gauges available.

Due to the limited spatial coverage of the GHCN rain gauge data additional precipitation estimates were obtained from next-generation radar (NEXRAD) data and from local meteorological stations at Fort Huachuca. NEXRAD data are collected through a network of 159 high-resolution Weather Surveillance Radar-1988 Doppler (WSR-88D) radars that constantly scan the near surface detecting precipitation and atmospheric movement using a

Precipitation Processing System (PPS) algorithm described in detail in Fulton *et al.* (1998). The data are organized to provide spatially continuous precipitation estimates over a 4x4 km^2 grid projected in the Hydrologic Rainfall Analysis Project (HRAP) coordinate system. The quality of NEXRAD data has evolved through various stages (I-IV), as new algorithms have been developed to remove bias and enhance accuracy (Young *et al.,* 2000). NEXRAD Stage IV observed precipitation data, also known as Multisensor Precipitation Estimation (NEXRAD-MPE) data, were downloaded from the NOAA Advanced Hydrologic Prediction Service as a series of daily shapefiles from 2005-2012 for the conterminous United States. An open source Python script designed by Mehmat Ercan at the University of South Carolina (http://grg.engr.sc.edu/mehmet/scripts.html) was used to create a table of daily precipitation values for the central point of each HRAP grid cell that intersected any part of the study area watersheds. These center points were then used as virtual rain gauge locations and used to drive SWAT. Fort Bliss NEXRAD-MPE data were obtained using HydroDesktop, a GIS program that allows a spatial query of hydrologic data sources and allows for the download and export of MPE data from the NWS regional River Forecasting Centers (Ames *et al.,* 2012).

In addition to the NEXRAD-MPE and rain gauge data sources, an array of six meteorological towers (met towers) located at Fort Huachuca within the installation boundaries provided precipitation and temperature data from 2000-2011 in 15-minute intervals. These data were evaluated as an input for SWAT and were used to create design storms needed for the KINEROS2 calibration efforts at Upper Garden and Huachuca Canyons.

To assess the impacts of climate change on the flow regime, climate projection data were obtained from the World Climate Research Programme's (WCRP's) third Coupled Model Intercomparison Project (CMIP3). These data have the advantage of previously being bias-

corrected and spatially and temporally downscaled (Maurer *et al.,* 2010). Created by the United States Department of the Interior's Bureau of Reclamation (Research and Development Office) and the Lawrence Livermore National Laboratory (LLNL) with the help from other federal agencies and the Santa Clara University Civil Engineering Department, these data are currently available for use in climate change studies including those that study changes in watershed hydrology. The Intergovernmental Panel on Climate Change's (IPCC) Fourth Assessment Report (AR4) incorporates the work of several climate modeling groups who have developed and produced hundreds of simulations of past and future climates (Parry *et al.,* 2007). Different scenarios have been developed based on various population and economic growth forecasts and technological advances that have been grouped into 4 different scenarios (A1, A2, B1 and B2) and subdivided into three groups (A1a, A1b, A1c etc.), each with a varying degree of CO_2 concentrations (Nakićenović *et al.,* 2000). For this study, climate projection data will be used based on the high forcing A2 scenario, where carbon emissions increase to 820ppm from 2000 to 2100 with an average global warming of 3.4°C (Meehl *et al.,* 2007). Of the various climate models included in the CMIP3 dataset, NOAA's Geophysical Fluid Dynamics Laboratory Climate Model version 2.1 (GFDL CM2.1) was shown to have a good representation of the multi-model ensemble mean for the Southwest and is one of the few models that provide continuous daily temperature and precipitation outputs (Seager *et al*., 2007; Cayan *et al.,* 2010). These data have a scale of 1.8° or approximately 12 km resolution and was accessed for free from the LLNL Green Data Oasis data storage website (http://gdo-dcp.ucllnl.org). The GFDL CM2.1 data were obtained for both historical (1981-2000) and future (2081-2100) time periods and were assigned to "virtual" rain gauge locations at grid centers before being used to create necessary SWAT precipitation input files.

Precipitation data required to run the KINEROS2 model were entered as depths (in) from a pre-defined table of precipitation frequency estimates based on a specific return interval and duration. NOAA's Precipitation Frequency Data Server (PFDS) allows for the input of geographical coordinates to determine precipitation depths based on a frequency analysis of partial duration series (NOAA PFDS, 2012). Design storms based on 2, 10, and 100-year, 1-hour storms were created from the PFDS data using the centroid coordinate for each watershed in the study areas. Applying a design storm created from a single point estimate across an entire watershed tends to result in an overestimation of runoff due to the failure to account for spatial heterogeneity of the input data (Miller *et al.,* 2002a). To account for discrepancies, an aerial reduction factor developed from paired rain gauge study in Southern Arizona (Osborn *et al.,* 1980) and expanded for other parts of the Southwest in NOAAs Technical Memorandum NWS HYDRO-40 (Zehr & Myers, 1984) was applied to the design storm depth estimates.

3.7 Simulations and model execution

Writing the SWAT simulation file involves selecting the appropriate precipitation and temperature files and the desired simulation start date and time period. Temperature data for the historical runs using rain gauge and NEXRAD-MPE were created from weather generator station data included within the program. Included with SWAT, the weather generator files contain statistical data for gauge locations that are used to estimate daily maximum and minimum temperature values by selecting the station closest to the watershed (Burns *et al.,* 2007). Temperature data included with GFDL CM2.1 projection data were formatted to match the temperature (.tmp) file structure used by SWAT at each virtual rain gauge location and were

selected based on proximity to watershed center. Lastly, a daily output frequency was selected to report streamflow data on a daily time-step, necessary for determining flow permanence.

KINEROS2 simulation files are written by selecting the discretized watershed and the desired design storm previously created. A saturation index slider allows the user to set the amount of soil moisture present prior to the model run and was adjusted based on the presence and duration of previous storms. A series of multipliers also make it possible to adjust hydraulic conductivity (Ks) and Manning's N in both the planes and channels and were determined from the calibration efforts. After creating the simulation files the desired model was chosen and executed and results were then imported back into the GIS viewer where AGWA allows for visual display of the modeling results using a graduated color ramp.

3.8 Calibration and validation of SWAT at Fort Huachuca

Calibration and validation were performed in order to improve model accuracy by adjusting several of the model input parameters until modeled and observed streamflow were in agreement. Calibration of SWAT was possible by comparing simulated and monitored streamflow values at the watershed outlet for yearly, monthly and daily time-steps. Streamflow observations are limited to two U.S. Geological Survey (USGS) stream gauges found on perennial streams in the higher elevations of Garden and Huachuca Canyons and are the only locations where calibration and validation of model output were possible. Daily discharge totals in cubic feet per second (cfs) were downloaded from the USGS Water Data website (http://waterdata.usgs.gov) for USGS 09470800 Garden Canyon and USGS 09471310 Huachuca Canyon stream gauges and average totals were calculated for a calibration and validation time period. The sums were then converted to depth by dividing by the watershed area (km^2) for

comparison to SWAT simulated results. Subsurface flows were determined using a Baseflow Filter Program based on methodology outlined in an Arnold and Allen (1999) study that reports a fraction used to separate surface and subsurface flow of the USGS data.

Compared to initial SWAT average annual basin outputs, it was determined that model parameter changes would be needed in order to better match actual streamflow conditions. Past studies in similar settings have indicated that the Curve Number (CN) parameter has the strongest influence on runoff values and can be adjusted to improve model efficiency (Hernandez *et al.,* 2000; Miller *et al.,* 2002a). CN is an empirical parameter that describes the amount of runoff or infiltration that occurs from rainfall excess and ranges from 30-100, with high numbers indicating greater runoff and low numbers indicating less runoff (United States Soil Conservation Service, 1983). Following the SWAT user guide instructions for calibration, surface flow estimates were adjusted by changing CN and soil available water content (SOL_AWC) values in the input model files until surface flow estimates and observations were similar. Baseflow contributions were then adjusted by changing the groundwater "revap" coefficient (GW_REVAP) until baseflow estimates and observations were similar. Adjustments were made incrementally and then assessed using common statistical tests at monthly and daily time-steps.

Calibration and validation was carried out at Upper Garden and Upper Huachuca Canyons for SWAT-rain gauge, SWAT-NEXRAD-MPE (from here on referred to as just NEXRAD), and SWAT-met tower simulations to compare and to assess the accuracy of each. Specifically, the SWAT-NEXRAD derived output was compared against the SWAT-rain gauge output to determine if it was a viable substitute for areas with a sparse rain gauge network. Calibration and validation of the climate projection simulations were not performed due to the

down-scaled data for the 1981-2000 time period showing little relation to actual observations and the goal of the study to look at the relative difference in flow permanence between different parts of a watershed under a climate change scenario.

3.9 Calibration and validation of KINEROS2 at Fort Huachuca

Calibration for the KINEROS2 model was attempted at Fort Huachuca at both Upper Garden and Huachuca Canyons based on USGS peak flow stream gauge reports and 15-minute met tower precipitation data. From 2000-2011 the Garden Canyon stream gauge reported twelve high-flow events from which seven had matching met tower data and were chosen for calibration. For the same time period, the Huachuca gauge reported eleven high-flow events from which three were used for calibration. Calibration was performed using AGWA multipliers to adjust several input parameters for KINEROS2 including saturated hydraulic conductivity (Ks) and Manning's N estimates for both planes and channels. Several model iterations using various multipliers were performed to calibrate the peak flows of one storm and were then applied to separate storms to determine if the changes were valid.

3.10 Statistical analysis

Agreement between observed and modeled streamflow values were assessed using a variety of statistical methods including a paired t-test, a linear regression, and the Nash-Sutcliffe model efficiency (NSE), with the latter two considered the most widely used statistics used for reporting hydrologic calibration and validation (Gassman *et al.,* 2007). The paired t-test was used to assess the null hypothesis of zero difference between the mean of the observed and simulated data sets at a 0.05 significance level ($\alpha = 0.05$). A standard linear regression statistic

was used to evaluate the strength of the linear relationship between the observed and simulated data using the coefficient of determination (R^2) to report the degree of correlation between simulated and observed regression lines. R^2 values can range from 0 to 1, with 0 indicating no correlation and 1 indicating the two lines are equal (Krause *et al.,* 2005). The NSE measures how well the simulated versus observed data match a regression line with a slope of 1 and ranges in values from -∞ to 1. Values less than 0 indicate that the mean of the observed data is a better predictor than the model output and a value of 1 indicate a perfect fit (Krause *et al.,* 2005). Accuracy assessment will follow the Moriasi *et al.* (2007) evaluation standard that model simulation results are satisfactory if R^2 and NSE values are > 0.5 at the monthly time-step. The increased sensitivity of R^2 and NSE values to outliers and insensitivity to a consistent over- or under-estimation can often limit the reliability of these statistical results despite meeting the acceptable limit (Legates and McCabe, 1999). To address this and further assess model accuracy line plots were created to compare simulated variation to observed variation.

3.11 Flow permanence

For this study, flow permanence refers to the percent of time of the year where surface flow is present for each stream reach. Presence was determined using the SWAT reach (.rch) output file, which reports daily runoff values for each modeled stream reach. Prior to formatting it was deemed necessary to add a 'YEAR' column to the reach output files and was accomplished running a C# script to append a year to each record. The tables were then imported into Excel and sorted by date and reach and then a series of Excel formulas were used to capture the number of days where flow was present in each reach. Threshold values reported in section 4.3 were assigned such that values that were greater were designated as having "flow present"

and those that were less as "flow absent" for each reach on each day. A simple ratio of the number of days with flow present to the total number days of the year resulted in annual percent time with flow that was calculated for each stream reach, both for the total year and wet season only. Average flow permanence was calculated for the entire period of record and the resulting table was joined to the stream feature class then exported and merged into a final spatial layer that covered each installation.

3.12 Flow permanence cutoffs

Due to SWAT's inability to simulate zero flow conditions (Kirkby *et al.,* 2011) it was necessary to establish cutoff values equivalent to zero to accurately describe flow permanence. Because of the large variation in stream channel sizes it was decided that the cutoff values would need to vary based on the contributing watershed area. In this study, a correlation between flow permanence and watershed area was performed at stream gauge and Tidbit sensor locations in Fort Huachuca. Tidbit data sensors log temperature data from within the channel at 15-minute intervals and have been shown useful in detecting the onset and cessation of streamflow using a thermograph interpretation technique (Gungle, 2006; Figure 4). Data from the Gungle (2006) study reported the timing and duration of flows over an 18-month time period in 2001-2002 from several locations in and around Fort Huachuca. Two locations in particular, one in Lower Garden and one in lower Huachuca Canyons, were especially important because they provided flow permanence observations for the low-lying alluvium dominated channels where more recent sensor data was unavailable. Additional Tidbit sensor data was also acquired from an active SERDP project being conducted by the Stromberg research group, which provided data from 2011 that was used to assign the flow cutoff-watershed area classes for higher elevation,

mountainous stream reaches. For each Tidbit sensor data location average annual flows were determined and compared to SWAT results. Flow presence cutoffs were increased in small increments until they were in close agreement with the observed and used to define the different classes based on contributing watershed area.

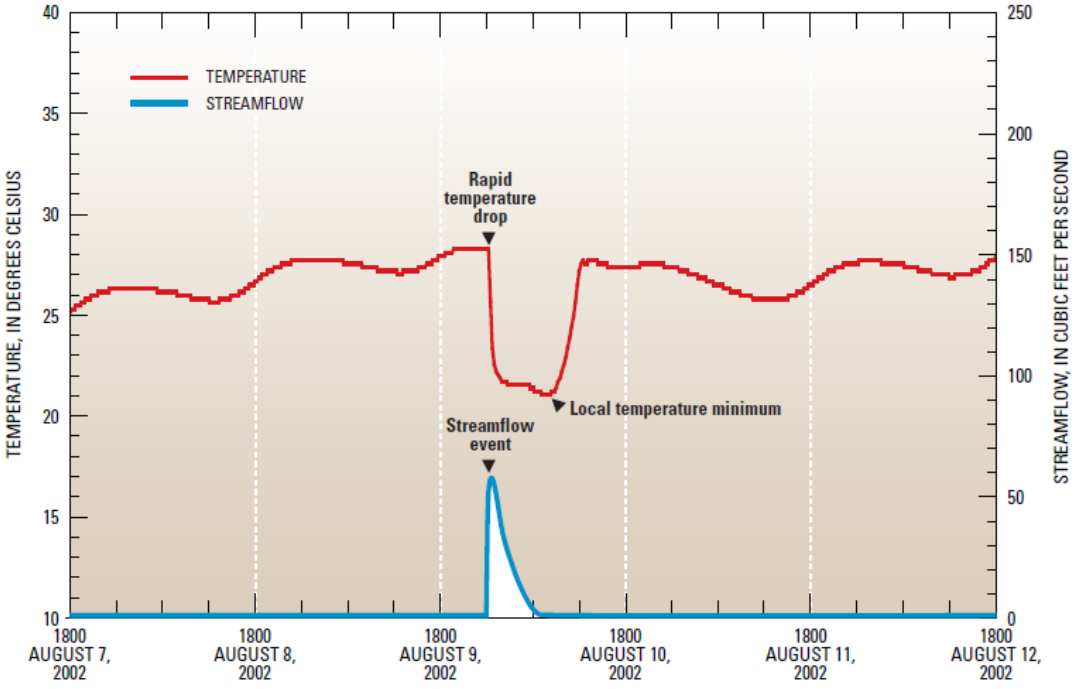


Figure 4. Graphical representation of thermal interpretation of streamflow from Gungle, 2006.

3.13 Peak flows

For each watershed center an aerial reduction factor was determined using area relationships developed from a paired rain gauge study at the Walnut Gulch Experimental Watershed by Osborn *et al.* (1980) for 2, 10, and 100-year, 1-hour storm events (Figure 5). These values were applied to each of the design storms created from NOAA's precipitation frequency maps prior to running KINEROS2. Following model execution peak flow (m^3/s) results were displayed in AGWA and individual spatial layers were then exported and merged to create a final coverage for each of the four study areas.

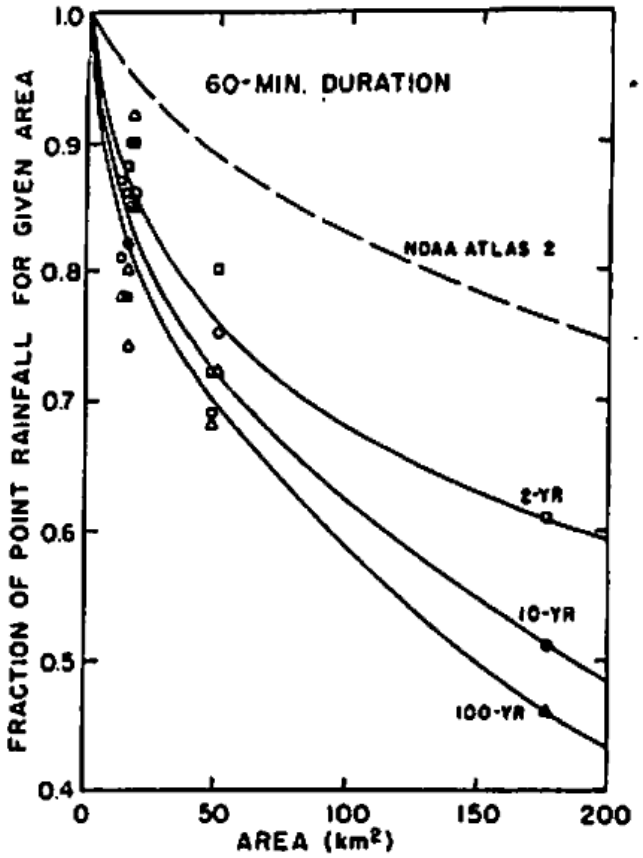


Figure 5. Depth-area ratios at Walnut Gulch for 2, 10, and 100-yr, 1-hour storms (Osborn *et al.,* 1980).

4. RESULTS

4.1 Calibration and validation of SWAT at Garden and Huachuca Canyons

Early SWAT-rain gauge, SWAT-NEXRAD, and SWAT-met tower simulations all displayed excessive surface runoff at Upper Garden Canyon. To correct for this a 20% decrease in CN values was applied to each subwatershed unit to increase infiltration within the subwatersheds. Further decreases to surface runoff were applied to the SWAT-NEXRAD runs by increasing the soil available water content (SOL_AWC) 0.08 at each soil horizon. Groundwater contributions were increased by adjusting the depth of groundwater evaporation

(GW_REVAP) values from the default value of 0.2 to 0.02 for SWAT-rain gauge and NEXRAD simulations and to 0.08 for SWAT-met tower simulations.

To assess the accuracy of the model simulations, statistical analyses were performed for average monthly totals and daily totals for both calibration and validation time periods. At Upper Garden Canyon, results from the paired T-test failed to reject the equal mean hypothesis for average monthly totals of all three precipitation inputs, but only SWAT-NEXRAD simulations failed to reject for daily totals (Table 1). Both SWAT-NEXRAD and SWAT-rain gauge simulations obtained acceptable levels of accuracy based on R^2 and NSE values for average monthly totals during both calibration and validation time periods (Table 2). However, upon plotting the data a trend of overprediction of large flow events and underprediction of small events was observed for both SWAT-NEXRAD simulations [Figures 6 (a) and (b)] and SWAT-rain gauge simulations [Figures 7 (a) and (b)]. The poor performance of the SWAT-met tower simulations at the monthly calibration time period (Table 2) may have been the result of data gaps in the met tower dataset considering that acceptable results were achieved during the validation period (Table 2).

At Upper Huachuca Canyon, results from the paired T-test also failed to reject the equal mean hypothesis for average monthly totals for each of the simulations minus the SWAT-NEXRAD validation time period; whereas all three simulations were rejected for the daily totals (Table 3). Acceptable R^2 values were obtained for both SWAT-NEXRAD and SWAT-rain gauge simulations at both time periods; however, NSE values were below the 0.5 limit (Table 4). Line plots revealed an over-prediction for small events and under-prediction for large events for the SWAT-NEXRAD simulations [Figures 8 (a) and (b)]; whereas SWAT-rain gauge simulations under-predicted small events and over-predicted large events [Figures 9 (a) and (b)].

The similarity between rain gauge and radar results observed at Upper Garden and Huachuca Canyons suggest that the NEXRAD-MPE data can serve as an accurate substitute for field observations where rain gauges are absent or possibly achieve better results where they are scarce.

Table 1. Paired T-test results from Upper Garden Canyon calibration and validation simulations.

Precipitation Data	Calibration					Validation				
	Years	Ave Monthly Total		Daily Total		Years	Ave Monthly Total		Daily Total	
		P-value	Reject H_Θ	P-value	Reject H_Θ		P-value	Reject H_Θ	P-value	Reject H_Θ
NEXRAD-MPE	2005-2008	0.81	No	0.17	No	2009-2012	0.17	No	0.17	No
Rain gauge	2000-2005	0.19	No	1.36E-15	Yes	2006-2011	0.97	No	0.27	No
Met tower	2000-2004	0.062	No	0.01	Yes	2005-2008	0.7	No	0.01	Yes

Table 2. Statistical results for Upper Garden Canyon SWAT-NEXRAD and SWAT-rain gauge simulations with coefficient of determination (R^2) and Nash-Sutcliffe Efficiency (NSE) values for calibration and validation time periods.

Precipitation Data	Calibration					Validation				
	Years	Daily		Monthly		Years	Daily		Monthly	
		R^2	NSE	R^2	NSE		R^2	NSE	R^2	NSE
Nexrad-MPE	2005-2008	0.50	-0.01	0.80	0.80	2009-2012	0.57	-0.38	0.90	0.86
Rain gage	2000-2005	0.46	0.44	0.95	0.92	2006-2011	0.34	-0.24	0.97	0.73
Met Tower	2000-2004	0.02	-6.9	0.06	-0.3	2005-2008	0.37	-0.21	0.99	0.78

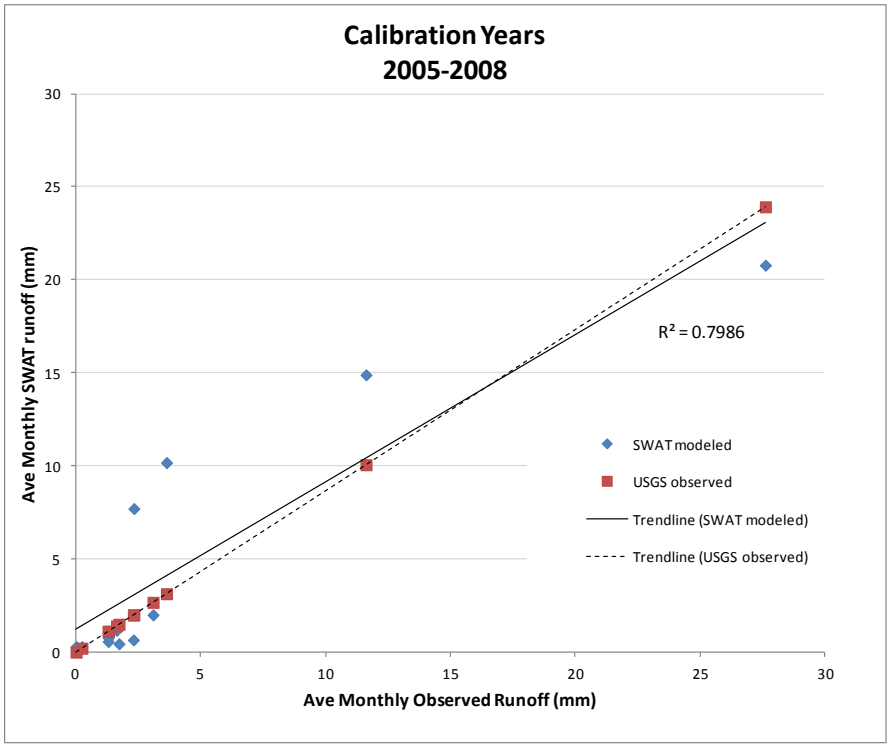
Table 3. Paired T-test results from Upper Huachuca Canyon calibration and validation simulations.

Precipitation Data	Calibration					Validation				
	Years	Ave Monthly Total		Daily Total		Years	Ave Monthly Total		Daily Total	
		P-value	Reject H_Θ	P-value	Reject H_Θ		P-value	Reject H_Θ	P-value	Reject H_Θ
NEXRAD-MPE	2005-2008	0.22	No	8.42E-07	Yes	2009-2012	0.02	Yes	3.79E-13	Yes
Rain gauge	2005-2007	0.18	No	2.24E-14	Yes	2008-2011	0.25	No	9.39E-07	Yes
Met tower	2005-2006	0.21	No	0.04	Yes	2007-2008	0.52	No	3.82E-09	Yes

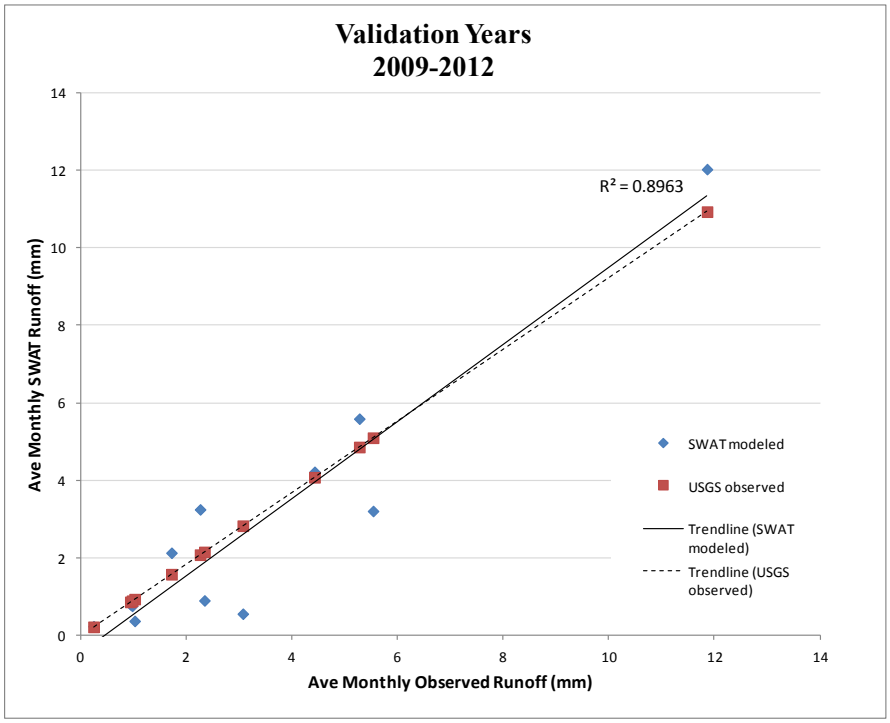
Table 4. Statistical results for Upper Huachuca Canyon SWAT-NEXRAD and SWAT-rain gauge simulations with coefficient of determination (R^2) and Nash-Sutcliffe Efficiency (NSE) values for calibration and validation time periods.

Precipitation Data	Calibration					Validation				
	Years	Daily (<1mm)		Monthly (<5mm)		Years	Daily (<1mm)		Monthly (<5mm)	
		R^2	NSE	R^2	NSE		R^2	NSE	R^2	NSE
Nexrad-MPE	2006-2008	0.12	0.02	0.53	0.14	2009-2012	0.05	-0.22	0.86	0.12
Rain gage	2005-2007	0.49	-1.05	0.97	-9.71	2008-2011	0.07	-7.08	0.83	-3.22
Met Tower	2005-2006	0.06	-2.56	0.66	-107	2007-2008	0.51	-20.4	0.16	-1.06

(a)

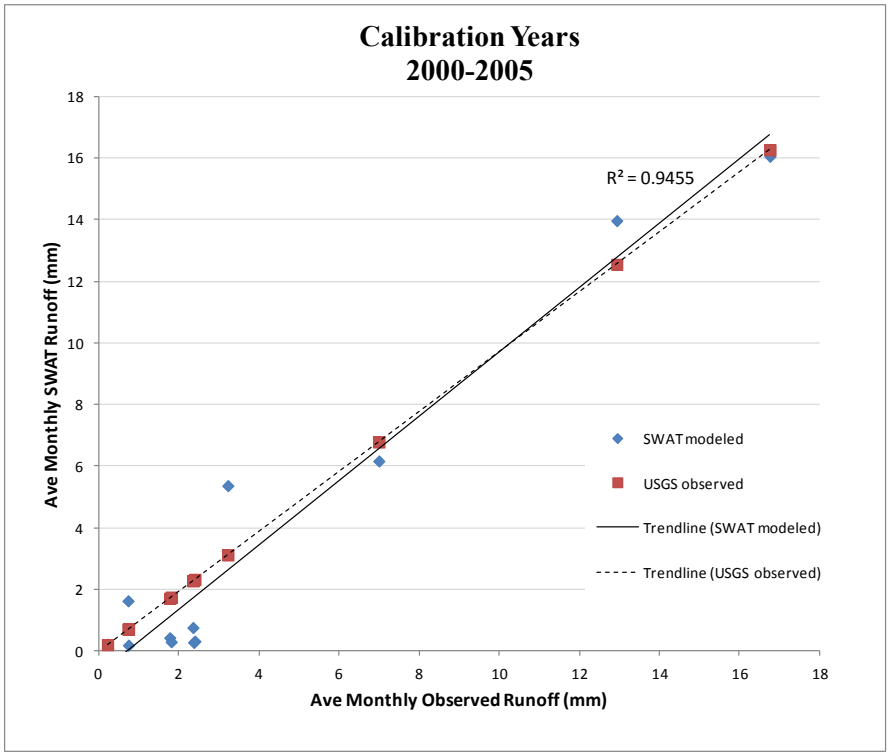


(b)

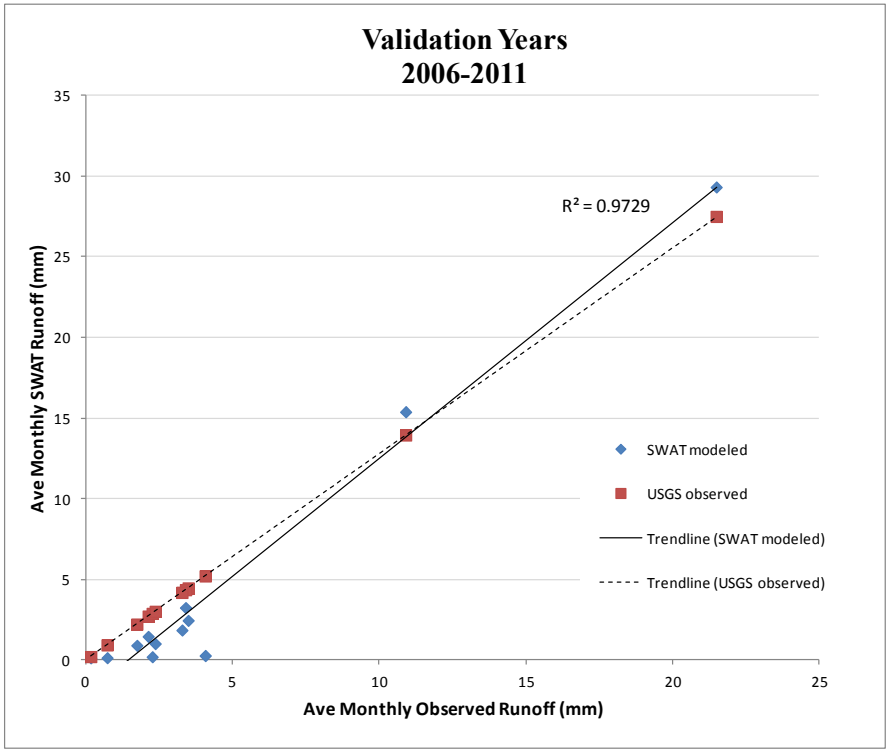


Figures 6 (a) and (b). Plot of simulated vs. observed average monthly volume totals at Upper Garden Canyon using NEXRAD-MPE precipitation input for (a) calibration and (b) validation time periods.

(a)

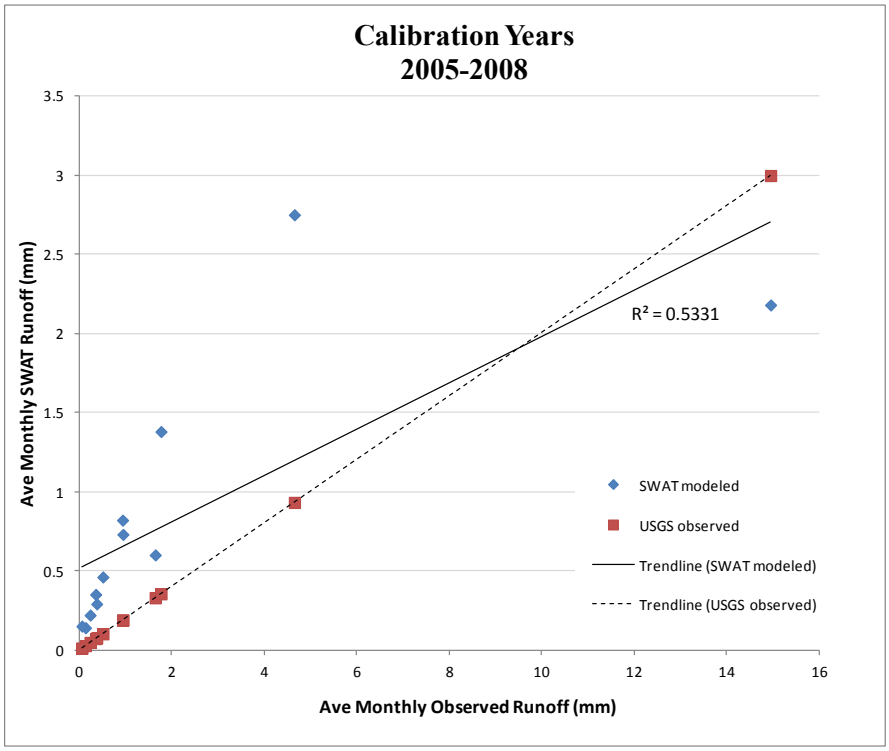


(b)

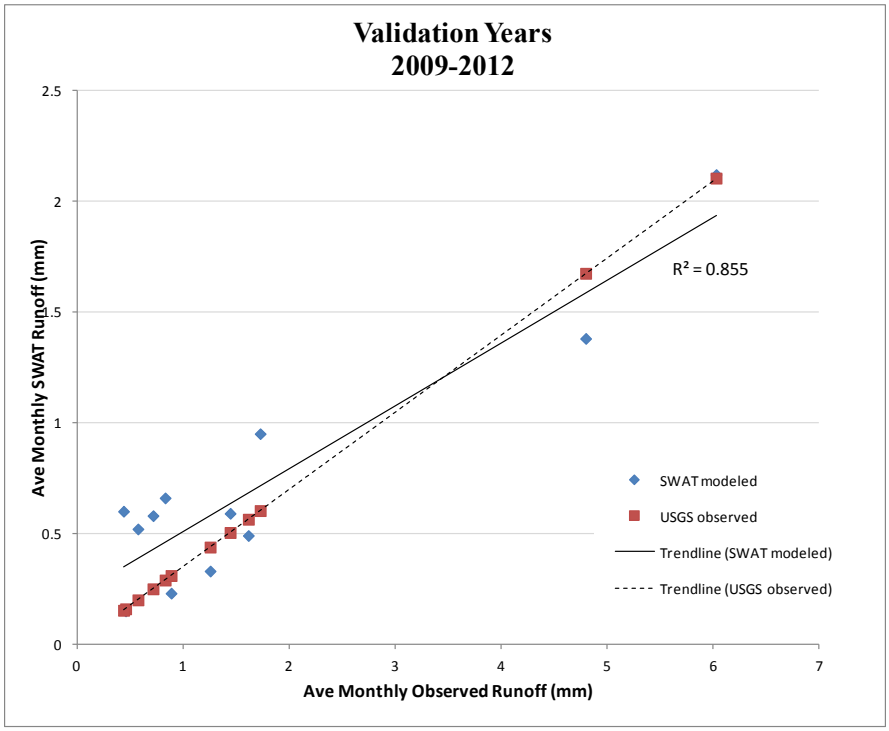


Figures 7 (a) and (b). Plot of simulated vs. observed average monthly volume totals at Upper Garden Canyon using rain gauge precipitation input for (a) calibration and (b) validation time period.

(a)

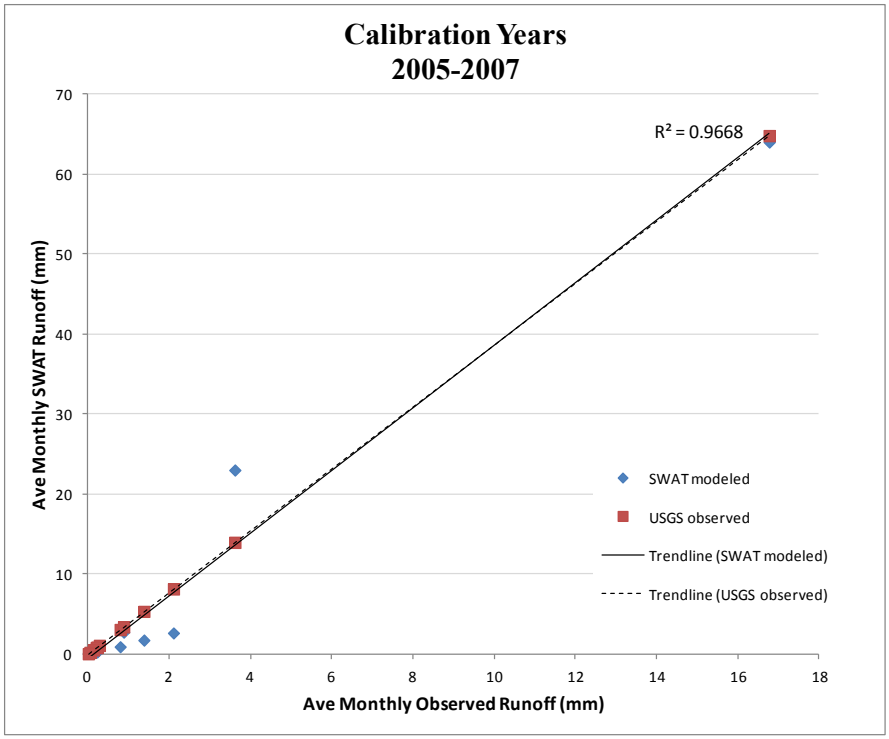


(b)

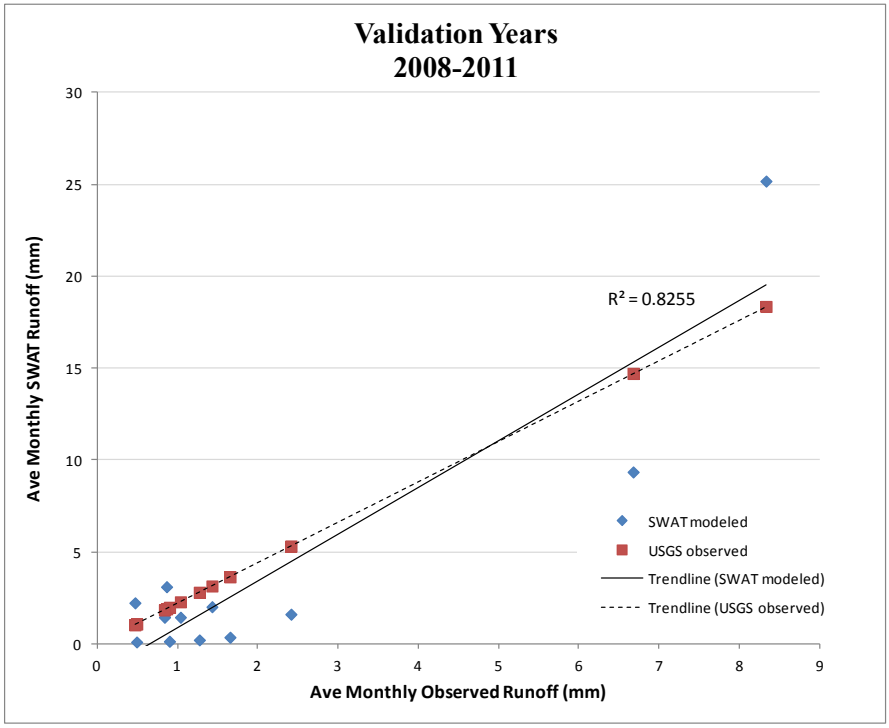


Figures 8 (a) and (b). Plot of simulated vs. observed average monthly volume totals at Upper Huachuca Canyon using NEXRAD-MPE precipitation input for (a) calibration and (b) validation time periods.

(a)



(b)



Figures 9 (a) and (b). Plot of simulated vs. observed average monthly volume totals at Upper Huachuca Canyon using rain gauge precipitation input for (a) calibration and (b) validation time periods.

4.2 *Calibration and validation of KINEROS2 at Fort Huachuca*

At Garden Canyon, non-calibrated simulations of KINEROS2 showed that of the nine high-flow events with met tower data, four showed under estimations of peak flows, two were marginally overestimated and two events (08/09/2007 and 08/05/2008) were largely overestimated. For Upper Huachuca Canyon met tower data for three high-flow events exist, however the closest met tower was found outside of the watershed and showed poor agreement between the timing of storm events and streamflow and were not considered practical for calibration. After considerable attempts of calibration it was determined that obtaining agreement between the observed and simulated peak flows was not possible given the wide range of estimated values. This was perhaps due to the high spatial variability of the summer thunderstorms with high rainfall intensities that often result in high-flow events. Another possibility is changing conditions in soil moisture within the watershed, though attempts were made to account for varying conditions by adjusting the saturation index in KINEROS2 based on whether any precipitation was recorded in the preceding days. Despite not being able to accurately calibrate KINEROS2 simulations, the relative difference of peak flows of each stream reach can still be useful in differentiating channels that see large magnitude flows from those that only experience low-flow events.

4.3 Flow permanence

Flow permanence values were successfully assigned to each stream reach within the four study areas using the SWAT-rain gauge and SWAT-NEXRAD results. Flow cutoffs, or the minimum streamflow values where flow was considered present in the channel, were established for the mountainous areas of Fort Huachuca based on the 2011 Stromberg Tidbit data sensors

(Table 5) located in the upper and middle parts of Garden Canyon, the middle tributary of the Buena School Area watershed, the southern tributary of Soldier Creek watershed, the upper part of Huachuca Canyon, and Upper Slaughterhouse Wash. Flow cutoffs were established for alluvium reaches of Garden Canyon, Woodcutters Wash, Graveyard Gulch, Soldier Creek, and Huachuca Canyons based on the Gungle 2001-2002 Tidbit sensor results. Three watershed size classes were assigned different flow cutoffs based on their contributing watershed area. Watersheds with an area <10 km^2 were assigned a cutoff of 0.0001 m^3/sec; between 10-34.9 km^2 a cutoff of 0.001 m^3/sec; and >35km^2 a cutoff of 0.35 m^3/sec. A statistical comparison between the Tidbit and SWAT flow permanence values revealed acceptable R^2 values for the SWAT-NEXRAD simulations for entire year 2011 (Figure 10) and SWAT-rain gauge simulations for the summer of 2011 (Figure 11). SWAT derived flow permanence values were assigned to stream reaches located within each of the four military installations based on these same cutoff values and divided into ten classes based on Jenks natural breaks (Figure 12, Appendix A).

Flow permanence values were also obtained using the 1981-2000 and 2081-2100 GFDL CM2.1 climate data at each of the four installations with absolute and percent differences calculated between the two time periods. Results varied among the different watersheds but overall indicated that higher elevation portions of watersheds would be most affected by decreased precipitation and increased temperatures predicted for the Southwest (Figure 13, Appendix B).

Table 5. Stromberg research team's 2011 Tidbit Sensor flow permanence and SWAT derived flow permanence percentages at Fort Huachuca (Monsoon time period includes Julian calendar days 166-258)

Watershed	TidBit Sensor			NEXRAD-MPE		Rain Gauge	
	Location ID	Annual %	Monsoon %	Annual %	Monsoon %	Annual %	Monsoon %
Buena School Area	GN	7.9	15.08	7.95	16.13	9.32	6.45
Soldier Creek	HN	7.47	12.12	1.37	4.3	0.27	1.08
Huachuca Canyon	HU	28.81	86.31	24.38	54.84	43.01	54.84
Garden Canyon	GU	88.74	84.95	69.59	74.19	56.71	60.22
Garden Canyon	GL	14.69	40.96	30.41	56.99	56.44	60.22
Ramsey Canyon	RU	82.33	53.76	90.14	82.8	71.78	65.59
Ramsey Canyon	RL	9.04	27.99	57.81	63.44	24.93	25.81

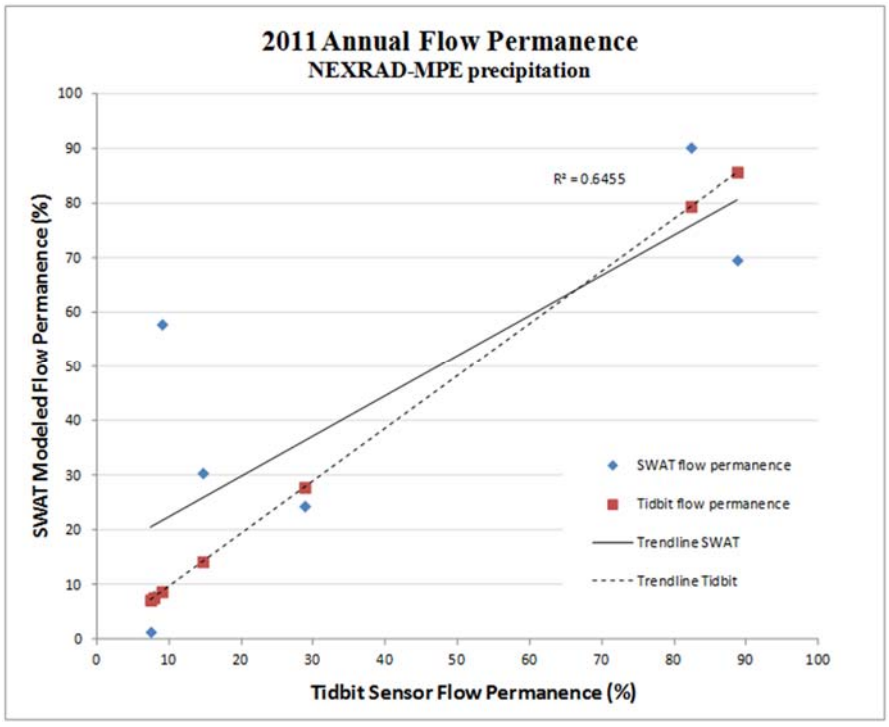


Figure 10. Line plot of Tidbit sensor derived flow permanence compared to SWAT-NEXRAD derived flow permanence percentages for 2011.

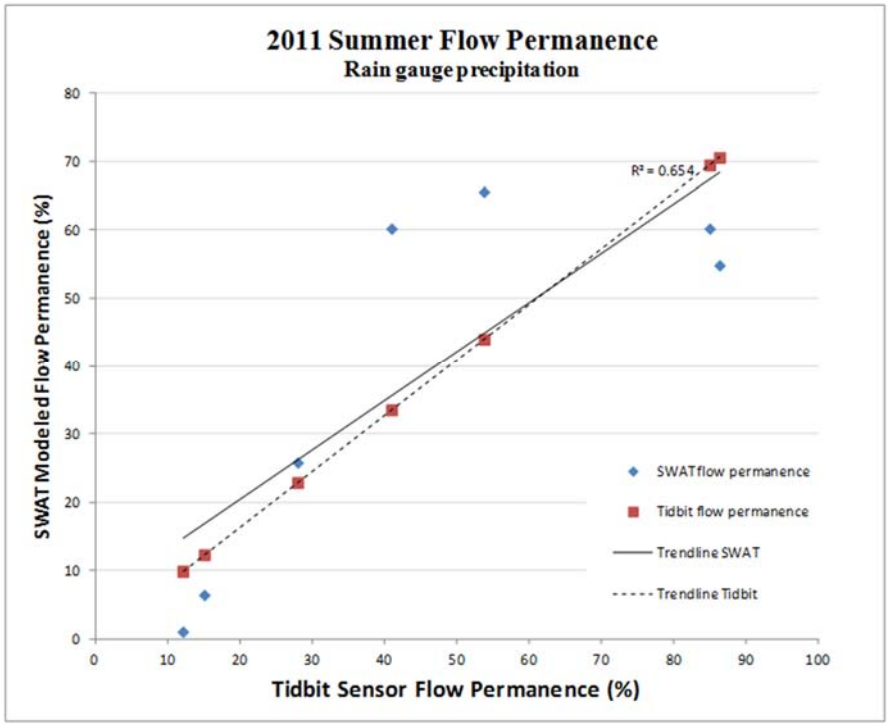


Figure 11. Line plot of Tidbit sensor derived flow permanence compared to SWAT-rain gauge derived flow permanence percentages for the summer of 2011.

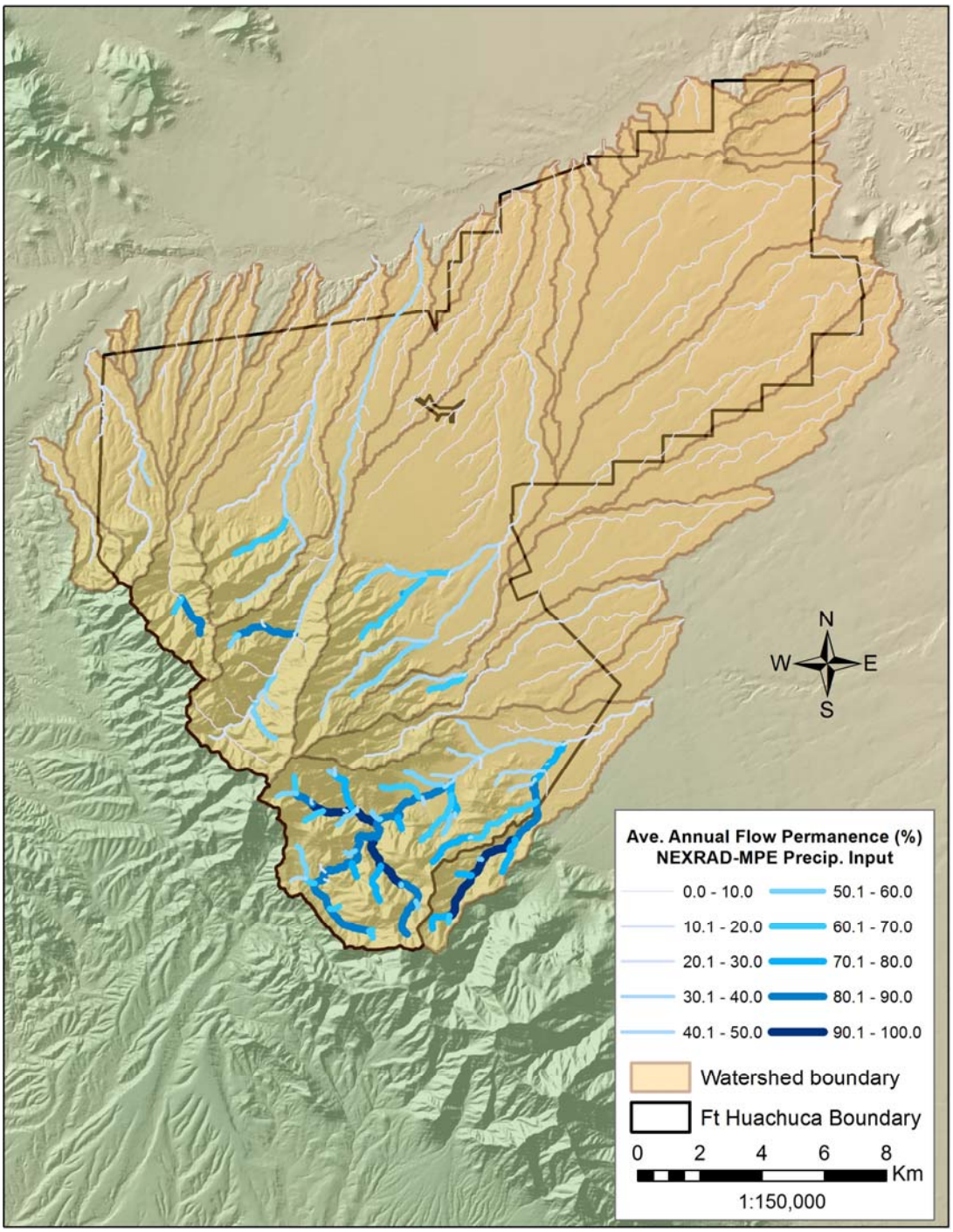


Figure 12. Flow permanence at Fort Huachuca using NEXRAD-MPE data and flow cutoffs.

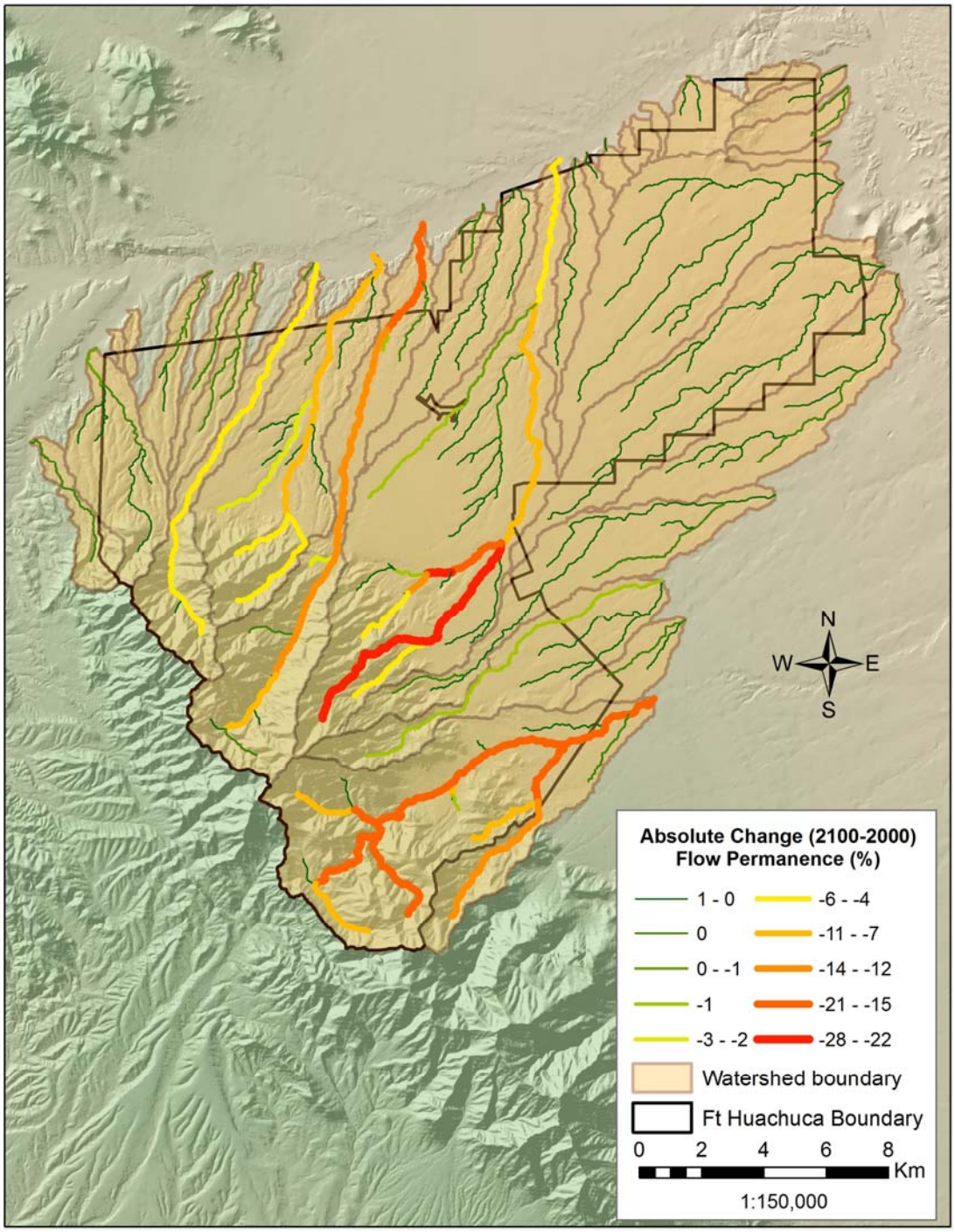


Figure 13. Absolute change in flow permanence between 1981-2000 and 2081-2100 at Fort Huachuca using GFDL CM2.1 climate projection data.

4.4 Peak flows

Due to the inability to calibrate KINEROS2, analysis of the peak flow model results were based on visual cues made during field operations. Indicators such as width of channel and height of flood debris on banks were examined for evidence of large flow events. At each of the installations the stream reaches with the highest simulated peak flows were often found to have wide braided channels indicating large magnitude flows. Figure 14 shows photographs from the Bug Scuffle watershed at Fort Bliss where channel width was approximately 15-meters and flood debris on a mid channel tree had a height over 1-meter. The modeled 100-year, 1-hour peak flow associated with this reach was 1,912 m^3/sec, which was the highest estimate for the entire watershed. Figure 15 shows evidence from Mojave Wash at Yuma Proving Grounds where channel width was approximately 50-meters with 1-meter high flood debris encountered on a mid-channel tree. The modeled 100-year, 1-hour peak flow associated with this stream reach was 2,094 m^3/sec, also the largest estimate for this watershed.



Figure 14. Photographs from Bug Scuffle watershed at Fort Bliss showing large channel and flood debris on tree.



Figure 15. Photographs from Mojave Wash at Yuma Proving Grounds showing large channel and flood debris on tree.

5. DISCUSSION

In the southwestern United States the ecological function of riparian areas is largely determined through the interaction between hydrological and ecological processes that take place within the hyporheic and parafluvial zones. Quantifying the flow regime of ephemeral and intermittent streams is a critical first step in establishing ecohydrological relationships within riparian environments. The methodology presented here attempts to advance the current knowledge of semiarid stream hydrology by examining how the timing, frequency, and magnitude of streamflow events vary throughout different parts of a watershed. By incorporating topographical relief, soil properties, and land cover patterns in rainfall-runoff model simulations, valuable insights were made on soil moisture distribution. This knowledge can be used to explore associations between hydrologic connectivity and sediment transport, seed dispersal, or aquatic species distribution. Furthermore, it can be used as a measure of how often flow pulses act as a catalyst for biogeochemical reactions that can influence the amount of nutrients available for plant uptake. This characterization of streams based on their flow regime can be used to gauge the ecological sensitivity of the adjacent riparian areas and be used to guide land use activities away from more vulnerable environments.

5.1 Errors and assumptions

The work described here is not without error and where observed data were available attempts were made to measure accuracy, but the inherent nature of certain types of error are largely unquantifiable. As with any modeling effort the level of accuracy is much dependent on the correctness of the input data. The high degree of spatial variability associated with summer

thunderstorms remains one of the key sources of error in rainfall measurements and biggest challenge to modeling efforts. Even fine resolution radar and local met tower data can fail to account for the variability of rainfall especially in areas with large elevation gradients related to orographic features. At the Walnut Gulch Experimental Watershed nearly 100 precipitation and runoff gages are required to accurately assess hydrologic conditions of a watershed that is approximately 150 km^2 (Garcia *et al.,* 2008).

Errors may also have been introduced as a result of equipment failure. Large gaps were often observed in some of the meteorological and rain gauge data and zero flow days reported by the stream gauges on days where rainfall was recorded. The various resolutions of the DEM, soil, and landcover data often result in an oversimplification of real-world conditions that can affect modeling results. A comparison of SWAT's performance in semiarid verses more mesic landscapes indicated that the model does not perform as well in dry conditions and that it had trouble reproducing short-term rainfall events (Van Liew *et al.,* 2007) This was due to a combination of factors including the need for a shorter computational time-step than one day and the inability of the model to accurately account for antecedent soil moisture conditions immediately prior to precipitation events, which affected the curve number method of partitioning rainfall into runoff (Van Liew *et al.,* 2007). Many of the parameters changed during model calibration and validation corrected most of the discrepancies within the different data layers; however, the accuracy of applying these same changes to different watersheds cannot be fully assessed due to the absence of observed data. The accuracy of using the Tidbit data to establish flow presence cutoff values may also have been affected by the placement of the sensor within the channel as high-flow events may alter channel morphology and resulted in a shift of the main channel away from the sensor's location. Also, the persistence of soil moisture long

after flow has ceased may result in an overestimation of time when flow was considered to be present.

5.2 Flow permanence

The results of this research indicate that determining flow permanence values using the SWAT model is a viable procedure that can quickly assess hydrologic conditions over large areas. The results at Fort Huachuca demonstrate that the accuracy of the simulated results can be established when field observations are available to allow calibration and validation of the model. However, in failing to establish acceptable statistical results below the monthly time-step indicates some uncertainty in the flow permanence values calculated on a daily time-step. Nevertheless these results, as well as those from the other installations, highlight the relative differences in flow permanence within a watershed that serve as a good measure of which areas are more sensitive to land-use change. For example, if a base manager was tasked with choosing a new site for ground training activities, they could choose areas that have streams with low flow permanence knowing that these areas would be associated with less riparian abundance and less potential wildlife habitat. Such information can be used to justify land management decisions that direct disturbance activities away from ecologically sensitive areas. It also allows land managers to evaluate hydrologic connectivity and assess how upstream activities could impair downstream ecohydrological processes.

5.3 Peak flows

KINEROS2 modeling efforts were able to determine peak flows using 2, 10, and 100-year, 1-hour storm events for all stream reaches within the four study sites. The relatively few

peak flow events reported for the time period prevented a successful calibration and determination of model accuracy at the stream gauge locations. However, field observations of channel morphology established that channel reaches with the highest modeled peak flows were typically the wider, more braided stream channels that form during large magnitude flow events. In addition, the reliability of results from the 100-year, 1-hour simulations can be assumed to be relatively accurate due to high volumes overwhelming any watershed or channel characteristics. These results provide a good indication of which parts of the watershed are most susceptible to high flow events and where channel geomorphology is most dynamic. This information can be used to assist base managers in road maintenance activities as well as in future site development assessments.

5.4 Climate projection simulations

Agreement among climate model projections indicates that a global rise in temperature will likely affect regional and local weather patterns. How these changes will be manifested in local precipitation patterns remains uncertain. Using spatially and temporally down-scaled climate data offers one look at how these changes will influence ephemeral and intermittent streamflow in the Southwest. The results of the comparison of the GFDL CM2.1 climate data for the historical and projected time periods show a wide variance in absolute and percent changes of flow permanence values. One pattern that emerged was a noticeable decrease in flow permanence in the higher elevation mountainous areas. These patterns indicate that these areas might be more sensitive to climate change and could be used to justify the directing of adaptation management strategies to focus on species located in these areas first.

5.5 Suggestions for improvements

The methodology described within this paper was designed using the appropriate rainfall-runoff models with best available geospatial data, but there exists areas where improvements can be made in both the modeling results and flow permanence determination. Model results are only as good as the input data used to run them and the scant amount of data in the Southwest limits calibration, validation, and assessment of the model output. A coarse representation of rainfall patterns is created from the scarce and infrequent scattering of rain gauges across the desert Southwest. Though improvements in radar and satellite detection of precipitation are being made, a local network of meteorological towers could deliver superior spatial and temporal scaled data that could be used to drive the models.

More streamflow measurements are needed to guide the calibration process and assess the accuracy of runoff models. With the exception of the two stream gauges in the upper watersheds of Ft Huachuca, no stream gauge data was available for model calibration forcing an analysis that looks at relative differences alone. Installing stream gauges at various points within some of the key tributaries would deliver data needed for accurate representation of streamflow volumes and make possible a measurement of sediment transport. Another less-costly option would be to expand this methodology to areas of similar terrain outside the study areas where streamflow data are available and then apply those results back to the study areas with the assumption that any differences between the areas would be minor.

Additional Tidbit sensor data are currently being collected in watersheds throughout Fort Huachuca and should soon become available. The addition of this data could lead to more accurate cutoffs for flow detection and determination of flow permanence. Additionally, creating smaller subwatersheds with shorter stream segments by setting smaller CSAs during the

discretization stage of modeling would create a more detailed stream representation for which flow permanence values could be assigned. The use of a CSA of 10,000 m^2 may have been appropriate for the larger study sites (Irwin, Bliss, and YPG); however a finer level of detail may be more appropriate for the smaller Fort Huachuca.

5.6 Future development and uses

The next phase of the SERDP study is to establish a relationship between the hydrologic characteristics collected in this study with both riparian vegetation and geomorphologic characteristics to develop an ecohydrologic classification of ephemeral and intermittent streams. Correlating channel geomorphology with the flow data can provide insight into how channel patterns influence the hydrologic budget. It can also highlight which parts of the landscape are more susceptible to change due to erosional and depositional processes. Hydrologic data can also be correlated to vegetation metrics derived from remotely sensed data. A combination of aerial imagery and LiDAR datasets can be used to measure the three-dimensional distribution of vegetation canopies and bare-ground topography allowing for accurate assessments of vegetation height, cover, and canopy structure. Correlating vegetation metrics from riparian areas to the flow regime could be used as an indicator of vegetation response to hydrologic change. A combination of these results could be used to create an ecohydrologic classification of ephemeral and intermittent streams that would provide a holistic understanding of some of the potential feedbacks that could occur from land use disturbances. Placing this knowledge in the hands of land managers would present them with a greater level of information that can be used to guide future base operations.

6. CONCLUSION

In semiarid to arid environments traditional stream measurements fail to fully describe the hydrology due to the ephemeral and intermittent nature of most flows. Despite the absence of continuous flow, an abundance of ecohydrological interactions are known to occur within these stream channels that require an improved method for characterizing the hydrologic flow regime. While frequency and magnitude of flows can determine hydrologic connectivity within the watershed and limit the amount of soil moisture and nutrients available for vegetation uptake, little observational data exists to accurately describe these parameters.

The results show that it is possible to use rainfall-runoff models to capture flow permanence and peak flow data that better characterizes the flow regime of ephemeral and intermittent streams. It demonstrates how the AGWA toolkit was used to setup and run the continuous simulation SWAT model, from which daily flow values were derived, and the event orientated KINEROS2 model, from which peak flows were estimated. Calibration and validation of both models were performed at two sites in Fort Huachuca that contained active stream gauges. Acceptable results were achieved for the SWAT simulations on a monthly time-step using NEXRAD-MPE precipitation data. The methodology developed herein illustrated using daily flow data it is possible to obtain average annual and wet season flow permanence using flow cutoff values based on Tidbit temperature sensor data from several stream channels at Fort Huachuca. These flow cutoff values can then be assigned to the unmonitored stream reaches based on the contributing watershed area. Additional model simulations using climate projection data were able to identify stream reaches that are most vulnerable under a hotter, drier scenario. While quantifiable results were achieved at the calibrated watersheds, an analysis of the

relative differences between different reaches within the watersheds provides enough information to guide decision-making.

This research demonstrates that it is possible to use free and easily obtainable datasets within AGWA to setup and simulate a rainfall-runoff time series to characterize stream hydrology in unmonitored watersheds. These results can be correlated to vegetation metrics to identify areas with increased ecological sensitivity. Such associations would make it possible to make vegetation change predictions that occur in response to hydrologic changes from future land-use development or climatic changes. Such knowledge would promote ecologically sensitive land management decisions that direct development away from critical habitat areas thereby preserving the integrity of the ecosystem.

APPENDICES

APPENDIX A: FLOW PERMANENCE MAPS

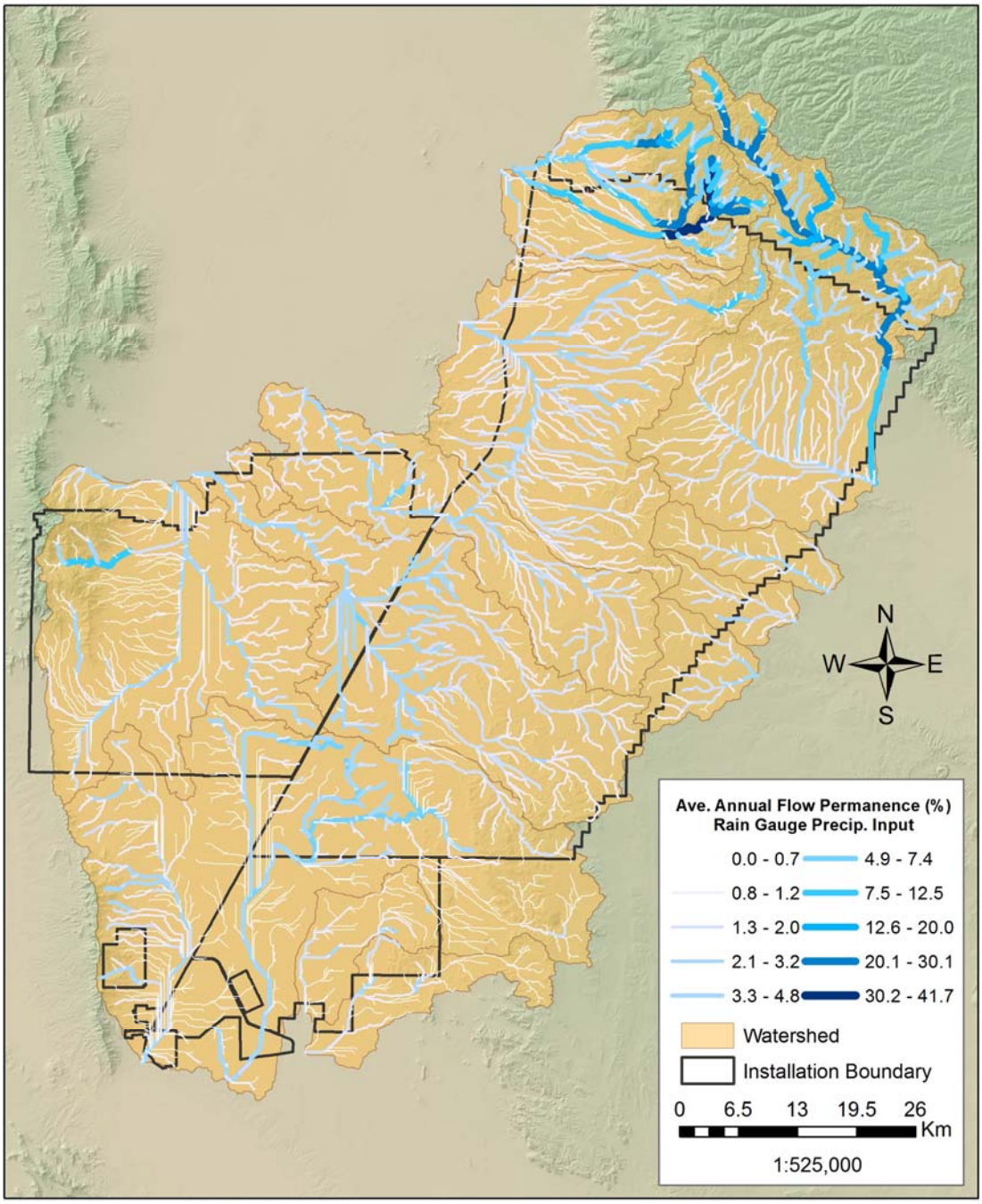


Figure A1. Flow permanence at Fort Bliss using rain gauge precipitation data.

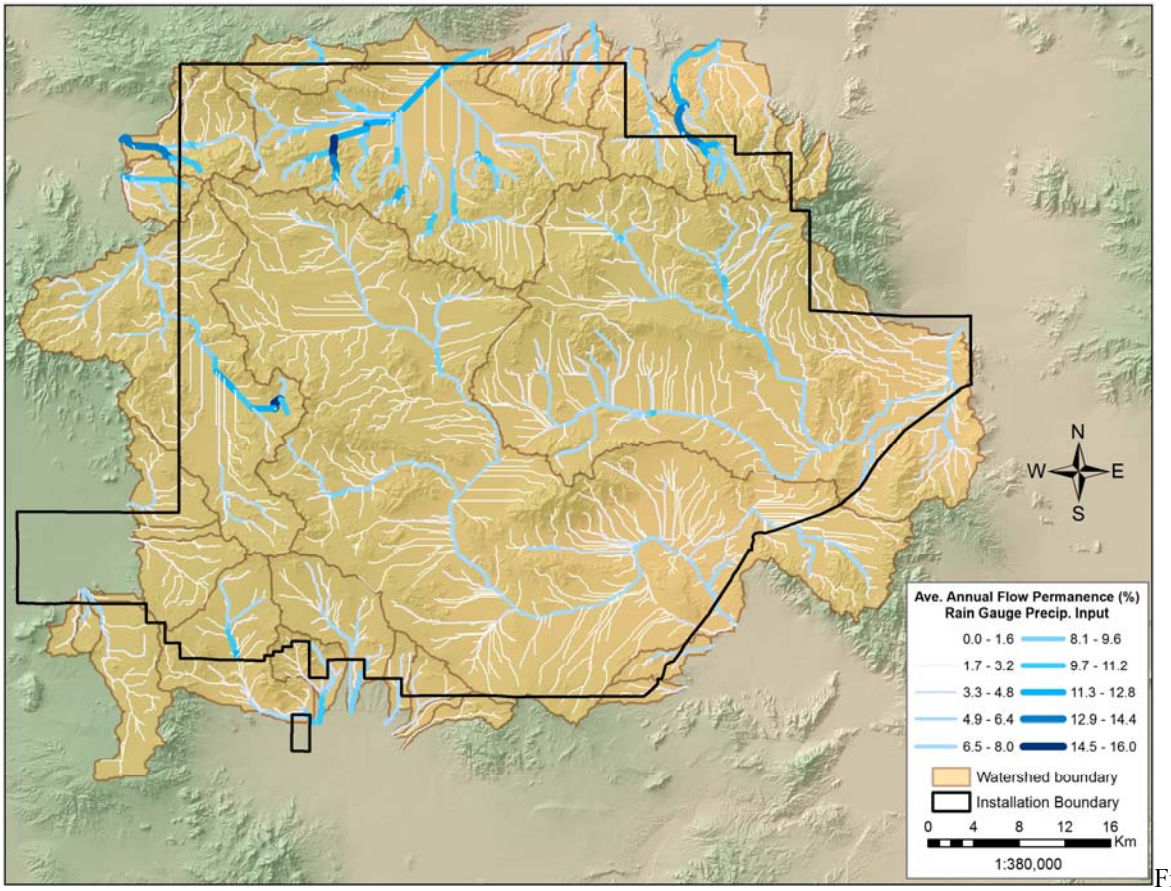


Figure A2. Flow permanence at Fort Irwin using rain gauge precipitation data.

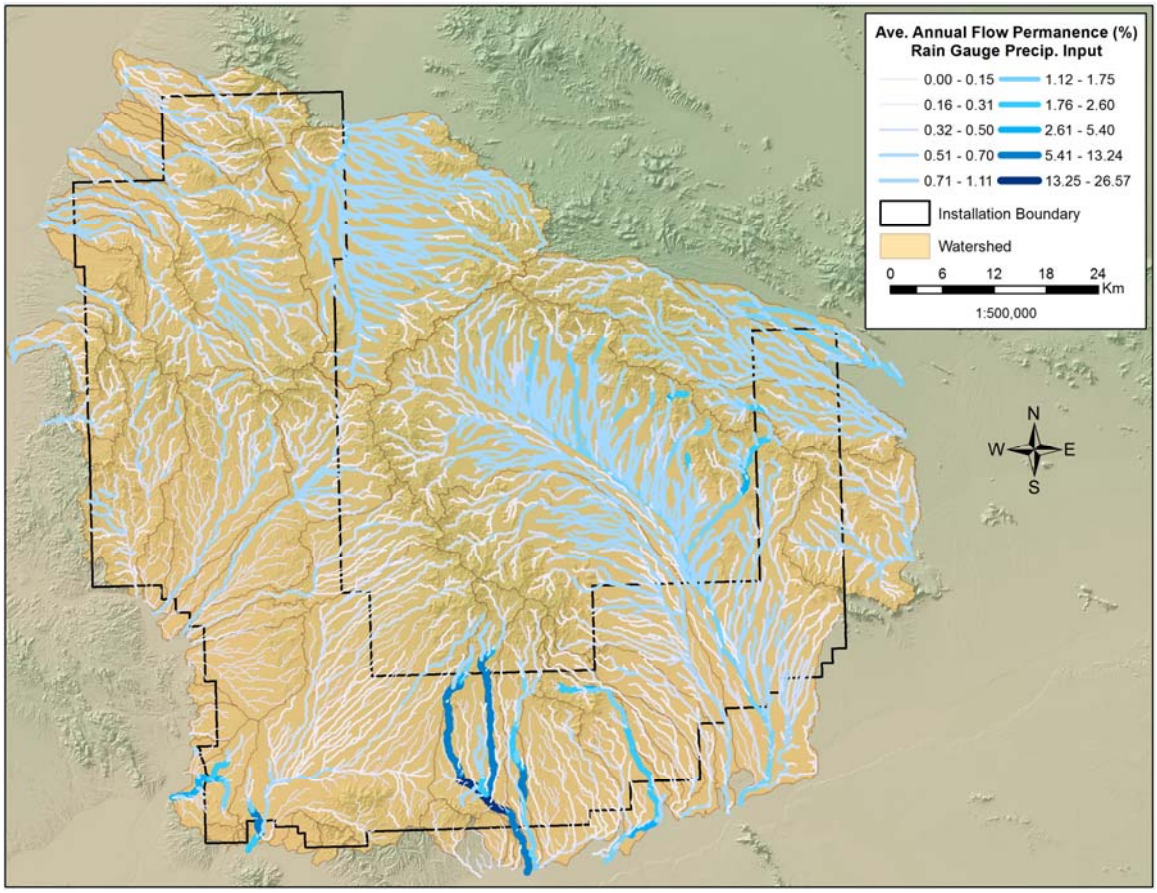


Figure A3. Flow permanence at Yuma Proving Grounds using rain gauge precipitation data.

APPENDIX B: ABSOLUTE CHANGE FLOW PERMANENCE MAPS

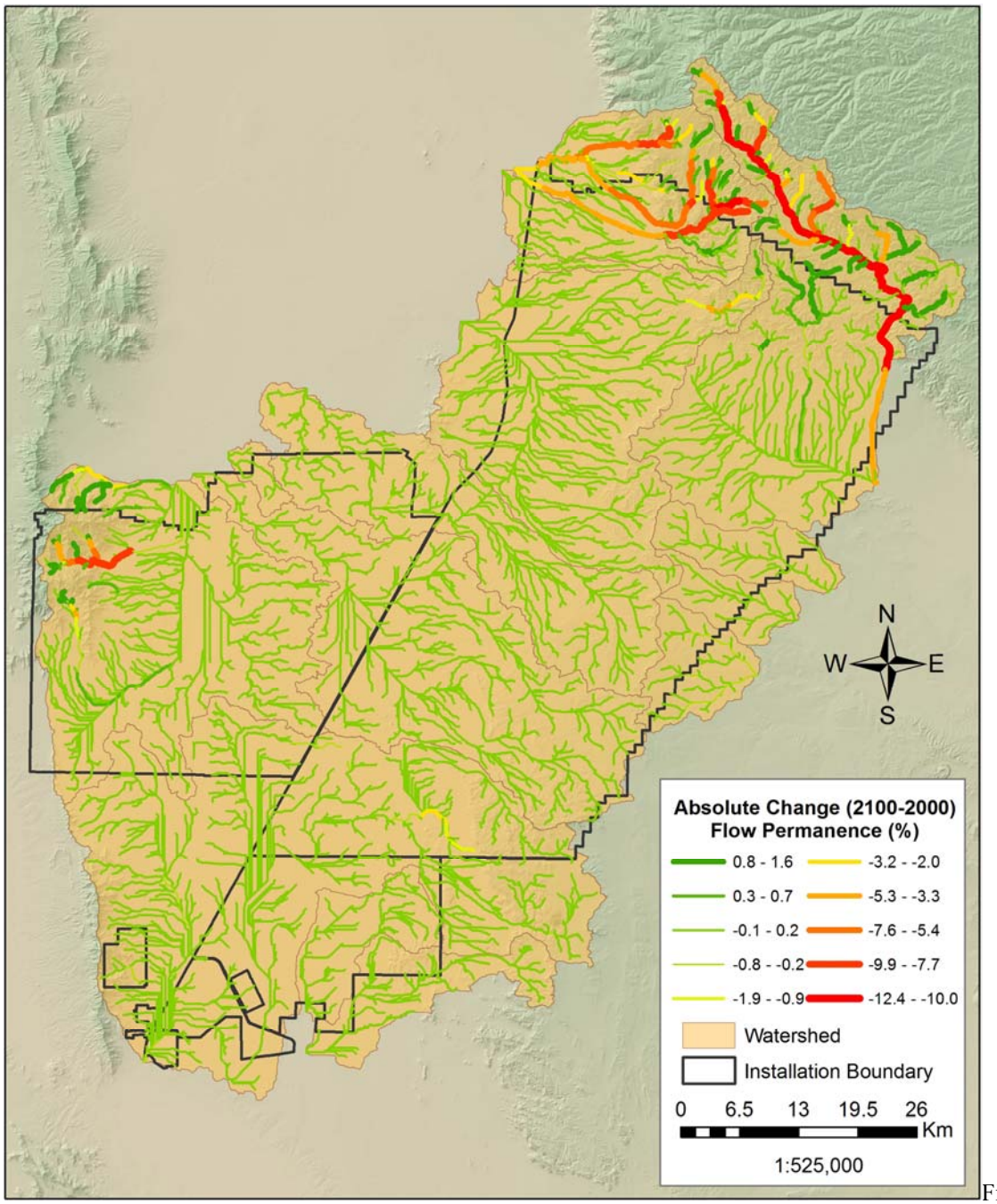


Figure B1. Absolute change in flow permanence between 1981-2000 and 2081-2100 at Fort Bliss using GFDL CM2.1 climate projection data.

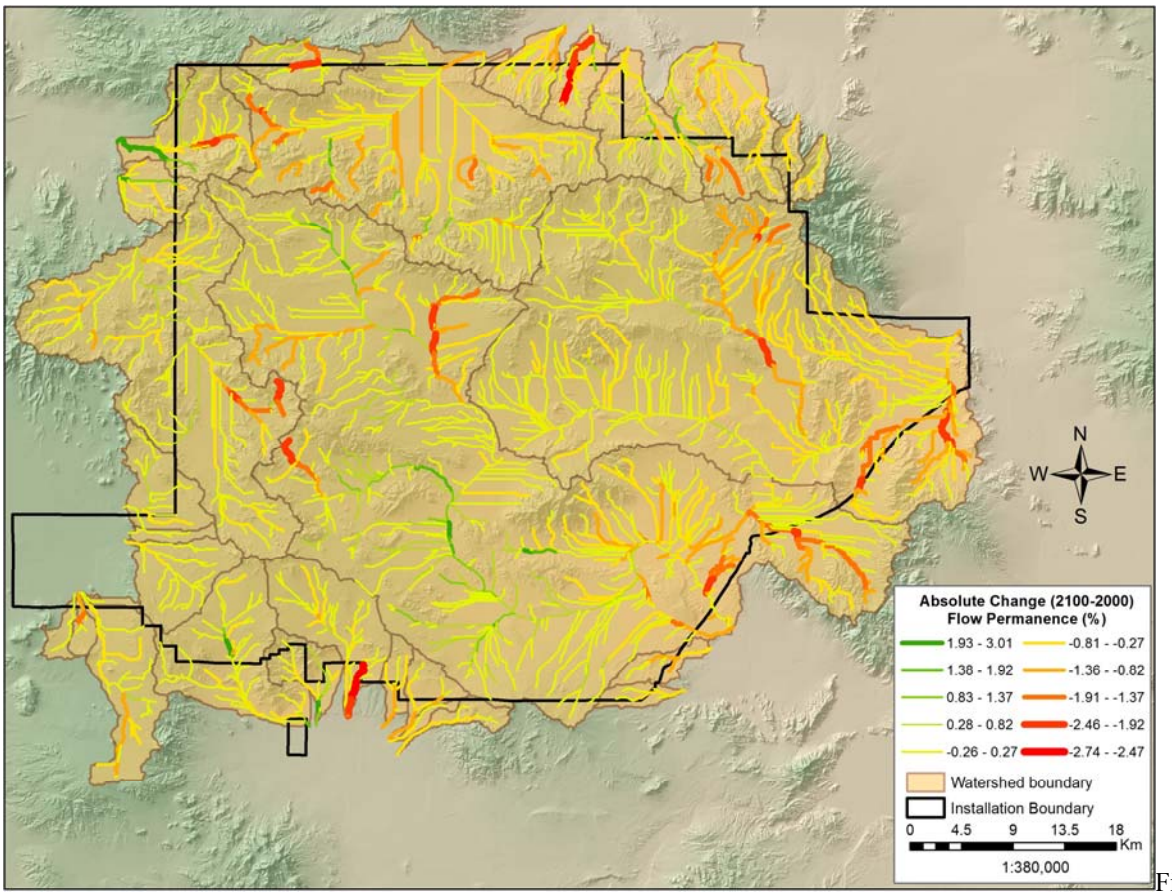


Figure B2. Absolute change in flow permanence between 1981-2000 and 2081-2100 at Fort Irwin using GFDL CM2.1 climate projection data.

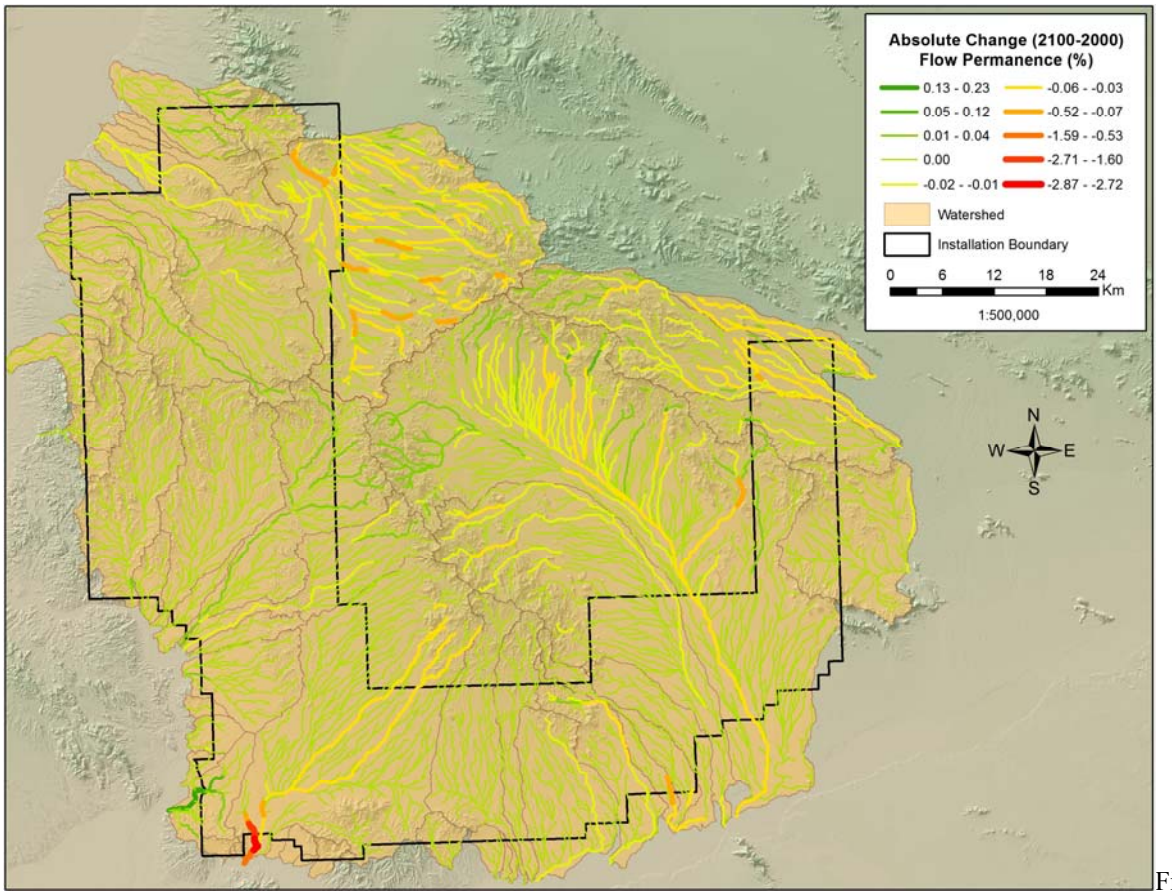


Figure B3. Absolute change in flow permanence between 1981-2000 and 2081-2100 at Yuma Proving Grounds using GFDL CM2.1 climate projection data.

REFERENCES

Allison, G., & Hughes, M. (1983). The use of Natural Tracers as Indicators of Soil-Water Movement in a Temperate Semi-Arid Region. *Journal of Hydrology, 60*(1-4), 157-173. doi:10.1016/0022-1694(83)90019-7

Ames, D. P., Horsburgh, J. S., Cao, Y., Kadlec, J., Whiteaker, T., & Valentine, D. (2012). HydroDesktop: Web services-based software for hydrologic data discovery, download, visualization, and analysis. *Environmental Modeling & Software, 37*, 146-156. doi:10.1016/j.envsoft.2012.03.013

Arnold, J. G., Srinivasan, R., Muttiah, R. S., & Williams, J. R. (1998). Large area hydrologic modeling and assessment - Part 1: Model development. *Journal of the American Water Resources Association, 34*(1), 73-89. doi:10.1111/j.1752-1688.1998.tb05961.x

Arnold, J., & Allen, P. (1999). Automated methods for estimating baseflow and ground water recharge from streamflow records. *Journal of the American Water Resources Association, 35*(2), 411-424. doi:10.1111/j.1752-1688.1999.tb03599.x

Arnold, J., & Fohrer, N. (2005). SWAT2000: current capabilities and research opportunities in applied watershed modelling. *Hydrological Processes, 19*(3), 563-572. doi:10.1002/hyp.5611

Arscott, D. B., Larned, S., Scarsbrook, M. R., & Lambert, P. (2010). Aquatic invertebrate community structure along an intermittence gradient: Selwyn River, New Zealand. *Journal of the North American Benthological Society, 29*(2), 530-545. doi:10.1899/08-124.1

Baillie, M. N., Hogan, J. F., Ekwurzel, B., Wahi, A. K., & Eastoe, C. J. (2007). Quantifying water sources to a semiarid riparian ecosystem, San Pedro River, Arizona. *Journal of Geophysical Research-Biogeosciences, 112*(G3), G03S02. doi:10.1029/2006JG000263

Burns, I.S., S.N. Scott, L.R. Levick, D.J. Semmens, S.N. Miller, M. Hernandez, D.C. Goodrich, & W.G. Kepner, 2007. Automated Geospatial Watershed Assessment 2.0 (AGWA 2.0) – A GIS-Based Hydrologic Modeling Tool: Documentation and User Manual; U.S. Department of Agriculture, Agricultural Research Service.

Canfield, H.E., D.C. Goodrich, and I.S. Burns, 2004. Selection of Parameters Values to Model Post-fire Runoff and Sediment Transport at the Watershed Scale in Southwestern Forests. ASCE Conference Proceedings 178 (48).

Cavanaugh, M. L., Kurc, S. A., & Scott, R. L. (2011). Evapotranspiration partitioning in semiarid shrubland ecosystems: a two-site evaluation of soil moisture control on transpiration. *Ecohydrology, 4*(5) doi:10.1002/eco.157

Cayan D.R., Das T., Pierce D.W., Barnett T.P., Tyree M., & Gershunova A. (2010). Future dryness in the Southwest US and the hydrology of the early 21st century drought. *Proc.Natl.Acad.Sci.U.S.A.Proceedings of the National Academy of Sciences of the United States of America, 107*(50), 21271-21276.

Comer, P. J., & NatureServe (Program). (2003). *Ecological systems of the United States: a working classification of U.S. terrestrial systems*. Arlington, Va.: NatureServe.

D'Odorico, P., Laio, F., Porporato, A., Ridolfi, L., Rinaldo, A., & Iturbe, I. R. (2010). Ecohydrology of Terrestrial Ecosystems. *Bioscience, 60*(11), 898-907. doi:10.1525/bio.2010.60.11.6

Friedman, J., & Lee, V. (2002). Extreme floods, channel change, and riparian forests along ephemeral streams. *Ecological Monographs, 72*(3), 409-425. doi:10.2307/3100097

Fulton, R. A., Breidenbach, J. P., Seo, D. J., Miller, D. A., & O'Bannon, T. (1998). The WSR-88D rainfall algorithm. *Weather and Forecasting, 13*(2), 377-395. doi:10.1175/1520-0434(1998)013<0377:TWRA>2.0.CO;2

Gallart, F., Prat, N., Garcia-Roger, E. M., Latron, J., Rieradevall, M., Llorens, P., . . . Froebrich, J. (2012). A novel approach to analyzing the regimes of temporary streams in relation to their controls on the composition and structure of aquatic biota. *Hydrology and Earth System Sciences, 16*(9), 3165-3182. doi:10.5194/hess-16-3165-2012

Garcia, M., Peters-Lidard, C. D., & Goodrich, D. C. (2008). Spatial interpolation of precipitation in a dense gauge network for monsoon storm events in the southwestern United States. *Water Resources Research, 44*(5), W05S13. doi:10.1029/2006WR005788

Gassman, P. W., Reyes, M. R., Green, C. H., & Arnold, J. G. (2007). The soil and water assessment tool: Historical development, applications, and future research directions. *Transactions of the ASABE, 50*(4), 1211-1250.

Gesch, D., Oimoen, M., Greenlee, S., Nelson, C., Steuck, M., & Tyler, D. (2002). Highlight Article - The National Elevation Dataset. *Photogrammetric Engineering and Remote Sensing., 68*(1), 5.

Geza, M., & McCray, J. E. (2008). Effects of soil data resolution on SWAT model stream flow and water quality predictions. *Journal of Environmental Management, 88*(3), 393-406. doi:10.1016/j.jenvman.2007.03.016

Goodrich, D. C., Williams, D.G., Unkrich, C.L., Hogan, J.F., Scott, R.L., Hultine, K.R., Pool, D., Coes, A.L., Miller, S. (2004). Comparison of methods to estimate ephemeral stream recharge, Walnut Gulch, San Pedro River Basin, Arizona. In: *Groundwater recharge in a desert environment: the southwestern United States*. Washington, DC: American Geophysical Union.

Goodrich, D. C., Guertin, D. P., Burns, I. S., Nearing, M. A., Stone, J. J., Wei, H., . . . Jolley, L. (2011). AGWA: The Automated Geospatial Watershed Assessment Tool to Inform Rangeland Management. *Society for Range Management Rangelands, 33*(4), 41-47.

Goodrich, D.C., Burns, I.S., Unkrich, C.L., Semmens, D.J., Guertin D.P., Hernandez, M., . . . Levick, L.R. (2012). KINEROS2 / AGWA: Model Use, Calibration, and Validation. *Transactions of the ASABE, 55*(4), 1561-1574.

Gungle, B., United States. Bureau of Land Management. & Geological Survey (U.S.). (2006). Timing and duration of flow in ephemeral streams of the Sierra Vista Subwatershed of the upper San Pedro basin, Cochise County, southeastern Arizona. Retrieved

Hernandez, M., Miller, S. N., Goodrich, D. C., Goff, B. F., Kepner, W. G., Edmonds, C. M., & Jones, K. B. (2000). Modeling runoff response to land cover and rainfall spatial variability in semi-arid watersheds. *Environmental Monitoring and Assessment, 64*(1), 285-298. doi:10.1023/A:1006445811859

Hultine, K., Scott, R., Cable, W., Goodrich, D., & Williams, D. (2004). Hydraulic redistribution by a dominant, warm-desert phreatophyte: seasonal patterns and response to precipitation pulses. *Functional Ecology, 18*(4), 530-538. doi:10.1111/j.0269-8463.2004.00867.x

Hupp, C. (2000). Hydrology, geomorphology and vegetation of Coastal Plain rivers in the south-eastern USA. *Hydrological Processes, 14*(16-17), 2991-3010. doi:10.1002/1099-1085(200011/12)14:16/17<2991::AID-HYP131>3.0.CO;2-H

Jackson, R. B., Canadell, J., Ehleringer, J. R., Mooney, H. A., Sala, O. E., & Schulze, E. D. (1996). A global analysis of root distributions for terrestrial biomes. *Oecologia, 108*(3) doi:10.1007/BF00333714

Jackson, R. B., Jobbagy, E. G., & Nosetto, M. D. (2009). Ecohydrology in a human-dominated landscape. *Ecohydrology, 2*(3), 383-389. doi:10.1002/eco.81

Kirkby, M. J., Gallart, F., Kjeldsen, T. R., Irvine, B. J., Froebrich, J., Lo Porto, A., . . . MIRAGE Team. (2011). Classifying low flow hydrological regimes at a regional scale. *Hydrology and Earth System Sciences, 15*(12), 3741-3750. doi:10.5194/hess-15-3741-2011

Krause, P., Boyle, D. P., & Bäse, F. (2005). Comparison of different efficiency criteria for hydrological model assessment. *Advances in Geosciences, 5*, 89-97.

Lane, L.J. (1983). Transmission losses. In: *National engineering handbook: IV: Hydrology.* Washington, D.C.: Soil Conservation Service, U.S. Dept. of Agriculture.

Larned, S. T., Datry, T., Arscott, D. B., & Tockner, K. (2010). Emerging concepts in temporary-river ecology. *Freshwater Biology, 55*(4) doi:10.1111/j.1365-2427.2009.02322.x

Lauenroth, W. K., & Bradford, J. B. (2009). Ecohydrology of dry regions of the United States: precipitation pulses and intraseasonal drought. *Ecohydrology, 2*(2) doi:10.1002/eco.53

Leenhouts, J. M., Stromberg, J. C., Scott, R. L., United States. Bureau of Land Management., & Geological Survey (U.S.). (2006). *Hydrologic requirements of and consumptive ground-water use by riparian vegetation along the San Pedro River, Arizona*. Reston, Va.: U.S. Geological Survey.

Legates, D., & McCabe, G. (1999). Evaluating the use of "goodness-of-fit" measures in hydrologic and hydroclimatic model validation. *Water Resources Research, 35*(1), 233-241. doi:10.1029/1998WR900018

Levick, L. R., Goodrich, D. C., Hernandez, M., Fonseca, J., Semmens, D. J., Stromberg, J. C., . . . United States. Environmental Protection Agency. Office of Research and Development. (2008). *The ecological and hydrological significance of ephemeral and intermittent streams in the arid and semi-arid American Southwest*. Washington, D.C.: U.S. Environmental Protection Agency, Office of Research and Development.

Loik, M. E., Breshears, D. D., Lauenroth, W. K., & Belnap, J. (2004). A multi-scale perspective of water pulses in dryland ecosystems: climatology and ecohydrology of the western USA. *Oecologia, 141*(2) doi:10.1007/s00442-004-1570-y

Lowry, J., Ramsey, R. D., Thomas, K., Schrupp, D., Sajwaj, T., Kirby, J., . . . Prior-Magee, J. (2007). Mapping moderate-scale land-cover over very large geographic areas within a collaborative framework: A case study of the Southwest Regional Gap Analysis Project (SWReGAP). *Remote Sensing of Environment, 108*(1), 59-73. doi:10.1016/j.rse.2006.11.008

Ludwig, J. A., Wilcox, B. P., Breshears, D. D., Tongway, D. J., & Imeson, A. C. (2005). Vegetation patches and runoff-erosion as interacting ecohydrological processes in semiarid landscapes. *Ecology, 86*(2) doi:10.1890/03-0569

Maurer, E. P., Hidalgo, H. G., Das, T., Dettinger, M. D., & Cayan, D. R. (2010). The utility of daily large-scale climate data in the assessment of climate change impacts on daily streamflow in California. *Hydrology and Earth System Sciences, 14*(6), 1125-1138. doi:10.5194/hess-14-1125-2010

Mednick, A. C. (2010). Does soil data resolution matter? State Soil Geographic database versus Soil Survey Geographic database in rainfall-runoff modeling across Wisconsin. *Journal of Soil and Water Conservation, 65*(3), 190-199. doi:10.2489/jswc.65.3.190

Meehl, G. A., Covey, C., Delworth, T., Latif, M., McAvaney, B., Mitchell, J. F. B., . . . Taylor, K. E. (2007). THE WCRP CMIP3 Multimodel Dataset: A New Era in Climate Change Research. *Bulletin of the American Meteorological Society, 88*(9), 1383-1394.

Miller, S.N., Semmens, D. J., Hernandez, M., Goodrich, D. C., Miller, W.P., Kepner, W.G., Ebert,D. (2002a) GIS-based hydrologic modeling: the Automated Geospatial Watershed

Assessment tool, in Proceeding of the Second Federal Interagency Hydrologic Modeling Conference, July 28 - August 1, 2002, Las Vegas NV, CD-ROM, 12 p.

Miller, S. N., Kepner, W. G., Mehaffey, M. H., Hernandez, M., Miller, R. C., Goodrich, D. C., . . . Miller, W. P. (2002b). Integrating landscape assessment and hydrologic modeling for land cover change analysis. *Journal of the American Water Resources Association, 38*(4), 915-929. doi:10.1111/j.1752-1688.2002.tb05534.x

Miller, S. N., Semmens, D. J., Goodrich, D. C., Hernandez, M., Miller, R. C., Kepner, W. G., . . . Special section: Advanced Technology for Environmental Modeling. (2007). The Automated Geospatial Watershed Assessment tool. *Environmental Modeling and Software, 22*(3), 365-377.

Montgomery, D., & Buffington, J. (1997). Channel-reach morphology in mountain drainage basins. *Geological Society of America Bulletin, 109*(5), 596-611. doi:10.1130/0016-7606(1997)109<0596:CRMIMD>2.3.CO;2

Moon, J., Srinivasan, R., & Jacobs, J. H. (2004). Stream flow estimation using spatially distributed rainfall in the Trinity River Basin, Texas. *Transactions of the ASAE, 47*(5), 1445-1451.

Moriasi, D. N., Arnold, J. G., Van Liew, M. W., Bingner, R. L., Harmel, R. D., & Veith, T. L. (2007). Model evaluation guidelines for systematic quantification of accuracy in watershed simulations. *Transactions of the ASABE, 50*(3), 885-900.

Naiman, R., & Decamps, H. (1997). The ecology of interfaces: Riparian zones. *Annual Review of Ecology and Systematics, 28*, 621-658. doi:10.1146/annurev.ecolsys.28.1.621

Naiman, R., DeCamps, H., & Pollock, M. (1993). The Role of Riparian Corridors in Maintaining Regional Biodiversity. *Ecological Applications, 3*(2), 209-212. doi:10.2307/1941822

Nakićenović, N., & Intergovernmental Panel on Climate Change. (2000). *Special report on emissions scenarios*. Cambridge: Cambridge University Press, published for the Intergovernmental Panel on Climate Change.

NOAA's Global Historical Climatology Network. Precipitation dataset. Retrieved 11/01/2010. From http://www.ncdc.noaa.gov/oa/climate/ghcn-daily/

NOAA's Precipitation Frequency Data Server. Precipitation dataset. Retrieved 04/25/2012. From http://dipper.nws.noaa.gov/hdsc/pfds/

Newman, B. D., Wilcox, B. P., Archer, S. R., Breshears, D. D., Dahm, C. N., Duffy, C. J., . . . Vivoni, E. R. (2006). Ecohydrology of water-limited environments: A scientific vision. *Water Resources Research, 42*(6), W06302. doi:10.1029/2005WR004141

Osborn, H. B., Lane, L. J., & Myers, V. A. (1980). Rainfall-Watershed Relationships for Southwestern Thunderstorms. *Transactions of the ASAE, 23*(1), 82-&.

Osterkamp, W., & Friedman, J. (2000). The disparity between extreme rainfall events and rare floods - with emphasis on the semi-arid American West. *Hydrological Processes, 14*(16-17), 2817-2829. doi:10.1002/1099-1085(200011/12)14:16/17<2817::AID-HYP121>3.0.CO;2-B

Owens, M. K., Lyons, R. K., & Alejandro, C. L. (2006). Rainfall partitioning within semiarid juniper communities: effects of event size and canopy cover. *Hydrological Processes, 20*(15) doi:10.1002/hyp.6326

Parry, M. L., & Intergovernmental Panel on Climate Change. Working Group II. (2007). *Climate change 2007: impacts, adaptation and vulnerability: contribution of Working Group II to the fourth assessment report of the Intergovernmental Panel on Climate Change*. Cambridge, U.K.; New York: Cambridge University Press.

Pitlick, J. (1994). Relation between Peak Flows, Precipitation, and Physiography for 5 Mountainous Regions in the Western Usa. *Journal of Hydrology, 158*(3-4), 219-240. doi:10.1016/0022-1694(94)90055-8

Poff, N. L., Allan, J. D., Bain, M. B., Karr, J. R., Prestegaard, K. L., Richter, B. D., . . . Stromberg, J. C. (1997). The natural flow regime. *Bioscience, 47*(11) doi:10.2307/1313099

Puckridge, J., Sheldon, F., Walker, K., & Boulton, A. (1998). Flow variability and the ecology of large rivers. *Marine and Freshwater Research, 49*(1), 55-72. doi:10.1071/MF94161

Rodriguez-Iturbe, I. (2000). Ecohydrology: A hydrologic perspective of climate-soil-vegetation dynamics. *Water Resources Research, 36*(1), 3-9. doi:10.1029/1999WR900210

Rosgen, D. (1994). A Classification of Natural Rivers. *Catena, 22*(3), 169-199. doi:10.1016/0341-8162(94)90001-9

Scholes, R., & Archer, S. (1997). Tree-grass interactions in savannas. *Annual Review of Ecology and Systematics, 28*, 517-544. doi:10.1146/annurev.ecolsys.28.1.517

Scott, R. L., Cable, W. L., & Hultine, K. R. (2008). The ecohydrologic significance of hydraulic redistribution in a semiarid savanna. *Water Resources Research, 44*(2), W02440. doi:10.1029/2007WR006149

Seager R, Ting M, Held I, Kushnir Y, Lu J, Vecchi G, . . . Naik N. (2007). Model projections of an imminent transition to a more arid climate in southwestern North America. *Science (New York, N.Y.), 316*(5828), 1181-4.

Seyfried, M. S., Schwinning, S., Walvoord, M. A., Pockman, W. T., Newman, B. D., Jackson, R. B., & Phillips, E. M. (2005). Ecohydrological control of deep drainage in arid and semiarid regions. *Ecology, 86*(2) doi:10.1890/03-0568

Soil Survey Staff, Natural Resources Conservation Service, United States Department of Agriculture. Soil Survey Geographic (SSURGO) Database for AZ, NM, TX, & CA. Retrieved 05/03/2012. From http://soildatamart.nrcs.usda.gov/

Soil Survey Staff, Natural Resources Conservation Service, United States Department of Agriculture. U.S. General Soil Map (STATSGO2) Database for AZ, NM, TX, & CA. Retrieved 06/28/2011. From http://soildatamart.nrcs.usda.gov/

Stone, J. J., Nichols, M. H., Goodrich, D. C., & Buono, J. (2008). Long-term runoff database, Walnut Gulch Experimental Watershed, Arizona, United States. *Water Resources Research, 44*(5), W05S05. doi:10.1029/2006WR005733

Stromberg, J. C., Bagstad, K. J., Leenhouts, J. M., Lite, S. J., & Makings, E. (2005). Effects of stream flow intermittency on riparian vegetation of a semiarid region river (San Pedro River, Arizona). *River Research and Applications, 21*(8) doi:10.1002/rra.858

Tobin, K. J., & Bennett, M. E. (2009). Using SWAT to Model Streamflow in Two River Basins with Ground and Satellite Precipitation Data. *Journal of the American Water Resources Association, 45*(1), 253-271. doi:10.1111/j.1752-1688.2008.00276.x

Tong, C., Gong, J., Marrs, R., Zhang, L., & Wang, W. (2008). Pattern of transpiration of four shrub species and water consumption from shrub stands in an eco-reclamation catchment in northwest China. *Arid Land Research and Management, 22*(3) doi:10.1080/15324980802183277

USGS, National Gap Analysis Program. Landcover dataset. Retrieved 07/10/2012. From http://gapanalysis.usgs.gov/

United States. Soil Conservation Service., & United States. Dept. of Agriculture. (1983). *National engineering handbook: Section 3: Sedimentation.* Washington, D.C.: Soil Conservation Service, U.S. Dept. of Agriculture.

Van Liew, M. W., Veith, T. L., Bosch, D. D., & Arnold, J. G. (2007). Suitability of SWAT for the conservation effects assessment project: Comparison on USDA Agricultural Research Service watersheds. *Journal of Hydrologic Engineering, 12*(2), 173-189. doi:10.1061/(ASCE)1084-0699(2007)12:2(173)

Wang, X., Xie, H., Sharif, H., & Zeitler, J. (2008). Validating NEXRAD MPE and Stage III precipitation products for uniform rainfall on the Upper Guadalupe River Basin of the Texas Hill Country. *Journal of Hydrology -Amsterdam-, 348*(1-2), 73-86.

Wilcox, B. P. (2003). Rangelands, water balance on. *Encyclopedia of Water Science,* DOI: 10.1081/E-EWS 120010097

Wollmuth, J., & Eheart, J. (2000). Surface water withdrawal allocation and trading systems for traditionally riparian areas. *Journal of the American Water Resources Association, 36*(2), 293-303. doi:10.1111/j.1752-1688.2000.tb04268.x

Woolhiser, D., Keefer, T., & Redmond, K. (1993). Southern Oscillation Effects on Daily Precipitation in the Southwestern United-States. *Water Resources Research, 29*(4), 1287-1295. doi:10.1029/92WR02536

Woolhiser, D. A., Smith, R. E., & Goodrich, D. C. (1990). *KINEROS: a kinematic runoff and erosion model: documentation and user manual.* [Washington, D.C.]: U.S. Dept. of Agriculture, Agricultural Research Service.

Young, C. B., Bradley, A. A., Krajewski, W. F., Kruger, A., & Morrissey, M. L. (2000). Evaluating NEXRAD Multisensor Precipitation Estimates for Operational Hydrologic Forecasting. *Journal of Hydrometeorology, 1*(3), 241.

Zehr, R. M., Myers, V. A., & United States. National Weather Service. (1984). *Depth-area ratios in the semi-arid southwest United States*. [Washington, D.C.?]: U.S. Dept. of Commerce, National Oceanic and Atmospheric Administration, National Weather Service.

Zou, C. B., Barnes, P. W., Archer, S., & McMurtry, C. R. (2005). Soil moisture redistribution as a mechanism of facilitation in Savanna tree-shrub clusters. *Oecologia, 145*(1) doi:10.1007/s00442-005-0110-8

Appendix H. AGWA Tool Guidance Document

Hydrologic Modeling Guidance Document: Using the Automated Geospatial Watershed Assessment Tool (AGWA) to Characterize the Flow Regime of Desert Streams in the North American Southwest

Table of Contents

Background 3

Purpose 3

AGWA Overview 3

AGWA Installation 4

Data Acquisition 5

Background: Study Area 6

Study Area Boundary 6

NHD Watershed Boundaries 6

Step 1: Download Data 6

Step 2: Unzip and Save 10

Part 1: Topography 10

Step 1: Download Data 10

Step 2: Unzip and Save 13

Part 2: Soil 14

Part 3: Land Cover 15

GAP Landcover 16

Part 4: Precipitation 17

SWAT Precipitation 17

KINEROS2 Precipitation 22

Data Management 38

Background: Extract Study Area Outline 38

Part 1: Projecting Data into a Common Coordinate System 39

Step 1: View the data in ArcMap 39

Step 2: Project the Data to a Common Coordinate System 41

Part 2: Clip the Data to a Suitable Project Area 43

Step 1: Create a Suitable Project Area Shapefile 43

Step 2: Clip the Input GIS Layers to the Project Area Shapefile 48

Part 3: Preparing the Precipitation Data 51

SWAT Precipitation 51

KINEROS2 NOAA Precipitation 57

Part 4: Preparing the Soils Database 59
Step 1: Import Tabular Data into SSURGO Database 59

AGWA Modeling 61

Study Area 61

Getting Started 62
GIS Data 62

SWAT 63
Part 1: Watershed Delineation and Discretization 63
Part 2: Soil and Landcover Parameterization 65
Part 3: Precipitation Input 67
Part 4: Simulations and Model Execution 69

KINEROS2 70
Part 1: Watershed Delineation and Discretization 71
Part 2: Soil and Landcover Parameterization 74
Part 3: Precipitation Input 75
Part 4: Simulations and Model Execution 76

Results 80
Part 1: Flow Permanence 80
Part 2: Peak Flow 85

References 87

Background

Conventional stream classifications based on flow attributes and/or channel morphology have primarily been focused on perennial stream networks common to mesic environments (Rosgen, 1994; Montgomery & Buffington, 1997; Puckridge et al., 1998). In arid to semiarid systems where ephemeral and intermittent streams are the dominant fluvial features, scarce observational data has hindered most attempts to perform similar stream classifications. While ephemeral and intermittent streams perform similar hydrologic and ecologic functions as their perennial counterparts (Levick et al., 2008) they generally are not incorporated in most watershed-based assessments. This guidance document addresses the hydrologic modeling portion of a larger research project that aims to fill that void by developing a stream type classification for ephemeral and intermittent streams based on a set of ecohydrologic characteristics, including flow regime attributes.

Purpose

This guidance document outlines the techniques used implement the Automated Geospatial Watershed Assessment tool (AGWA) that is used to characterize the flow regime of streams based on timing, duration, frequency, and volume of flow. Techniques presented include data acquisition, data management, model installation, implementation of AGWA, and interpretation of hydrologic model results. These techniques can be interpreted as a cohesive methodology or split as needed to fulfill other watershed based tasks. Fort Huachuca is used as the example study location, but the methods and data types can be applied to any location.

AGWA Overview

AGWA Version 3.0 is an open source toolkit that automates the tasks of assigning topographical, soil, and landcover parameters to watershed units in preparation for running a pair of hydrologic models (Miller et al., 2002). AGWA is embedded in common geographic information system (ESRI ArcGIS) software where watershed boundaries are delineated and subdivided then overlain with spatial data to obtain the necessary information needed to run the models. The tool leads the user through the process to characterize the watershed as well as to execute the chosen model and display the results for visual analysis and change detection in response to landscape alterations (Miller et al., 2002; Figure 3). AGWA contains the Soil and Water Assessment Tool (SWAT) and the Kinematic Runoff and Erosion model (KINEROS2). The two models operate at different spatial and temporal scales which allows for evaluation of the flow regime from two different perspectives.

SWAT is a continuous simulation model that was designed for predicting watershed response to land management practices for large basins over large periods of time (Arnold et al., 1998). It uses a modified Curve Number methodology to partition rainfall into infiltration and overland flow and reports water and sediment yields on a daily time-step, monthly, or annual time-step (Miller et al., 2007). It uses long-term data to provide daily measurements that are used to calculate flow permanence, or the average annual time period when flow is present in the channel. In contrast KINEROS2 is an event specific model that details the processes of interception, infiltration, surface runoff, and erosion from small watersheds (Woolhiser et al., 1990). KINEROS2 uses event-specific rainfall depth to determine peak discharge values. Combined, the outputs from SWAT and KINEROS2 can be used to develop different classes of stream types that can be used to establish relationships with different riparian attributes.

AGWA is primarily designed to provide qualitative estimates of runoff and erosion useful for assessing relative change between simulation results or between the different subunits within the larger watershed; however with proper calibration, it can provide quantitative estimates as well (Miller et al., 2002). For this study, AGWA will be used to characterize the flow regime of ephemeral, intermittent, and perennial stream channels in unmonitored basins within semiarid to arid parts of the southwestern United States. SWAT will be used to determine historical and projected average annual flow permanence based on over a decade of observed rainfall data as well as downscaled climate projection data from a representative global circulation model. KINEROS2 will be used to estimate peak flows based on 5, 10, 25, and 100-year, 1-hour design storms created from the National Oceanic and Atmospheric Administration's (NOAA) Atlas 14 point precipitation frequency estimates.

The results from these characterizations were used in a classification of ephemeral and intermittent streams for a larger project that includes four military installations in the southwestern U.S.: Fort Irwin (CA), Yuma Proving Ground (AZ), Fort Huachuca (AZ), and Fort Bliss (TX) (Figure 1). Such a classification can be used to make correlations with vegetation characteristics such as canopy height and total cover that can then be used to model riparian conditions and predict changes under different flow regimes associated with various land cover and climate change scenarios. The hydrologic modeling for Fort Huachuca will be used to illustrate these data acquisition and modeling techniques. This document is intended to complement the more detailed Tutorial and associated data supplied to each installation. Installation of the AGWA tool will be presented first, followed by steps for Data Acquisition, and Data Management. The final section will be a brief introduction to AGWA modeling; however, the Tutorial provided on this laptop is more comprehensive.

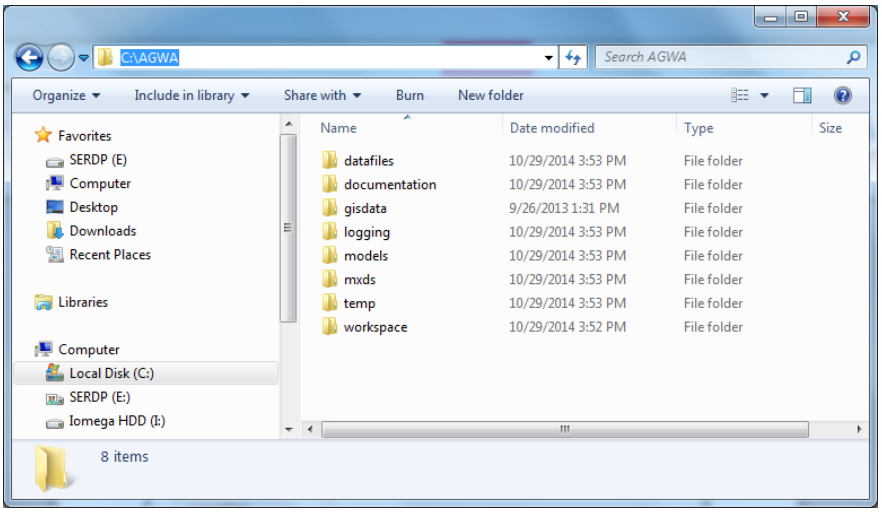
AGWA Installation

If AGWA is not already installed on your computer, all of the necessary data are provided on the AGWA website, http://www.tucson.ars.ag.gov/agwa/. AGWA has a Certificate of Networthiness (CON) for all of DoD. To install AGWA perform the following steps:

1. Download the AGWA add-in for ArcGIS and the supporting data:
    a. agwa_add-in_10.1-3.0.5.xxxx
    b. agwa_2.x_3.x_directory

2. Extract the contents of the agwa_add-in zip file to a permanent location of your choice on your hard drive.
    a. Double-click on the file "AGWA2 Desktop Add-In" file to install AGWA.
    b. Click the "Install Add-In" button when the ESRI ArcGIS Add-In Installation Utility form appears.
    c. Click "OK" when the "Installation Succeeded" form appears.

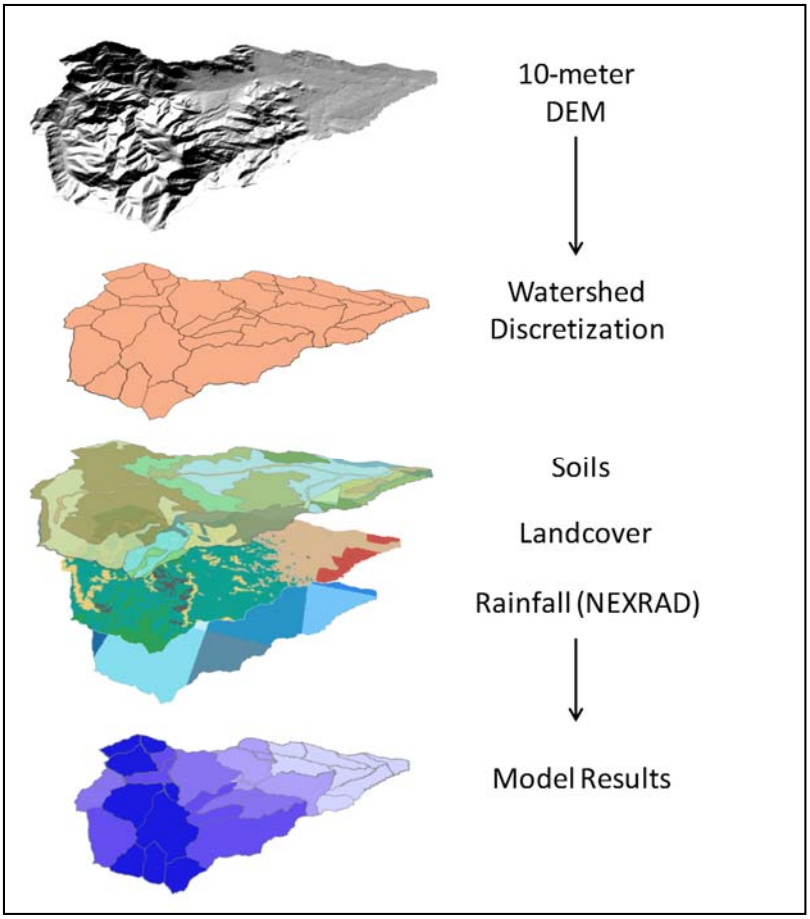
3. Extract the contents of the agwa directory zip file so the "AGWA" directory is located at the C:\ location. The directory structure should look like the illustration below. The *datafiles*, *documentation*, and *models* folders are the only critical folders that need to be in the *AGWA* directory, the other folders are shown as a suggested organizational aid.



Data Acquisition

The first step in any AGWA project is to obtain the necessary input data. Prior to running the models, several data layers and climate data need to be collected including topography, soil, land cover, and daily precipitation and temperature values (Figure 1). All of the data can be obtained for free from various federal and state websites. Since the accuracy of the modeling results will depend highly on the quality of the input data, a thorough examination of each data layer is included describing the potential benefits and limitations of each. These data will need to be stored in an easy to find location on your computer. We recommend creating a **GISdata** folder within the **C:\AGWA** directory with new folders for each study area. For example data relevant to Fort Huachuca data would be stored in the **C:\AGWA\GISdata\FortHuachuca** folder. A *downloads* folder should also be created because most downloaded data will need to be manipulated in order to utilize it within AGWA. All data acquired in this example will be saved to C:\AGWA\GISdata\FortHuachuca\downloads\.

This section outlines common data sources and methods to acquire datasets necessary to run the models within AGWA. However, the data mentioned in this section have already been compiled for you and are found in the Hydrologic Modeling folder on your laptop.



Background: Study Area

Study Area Boundary

The area you are interested in may be a wildfire boundary, an urban development, an incorporated city, or a Department of Defense Reserve or Installation Boundary. These boundaries can often be acquired online as shapefiles from the USGS National Map Viewer as well.

NHD Watershed Boundaries

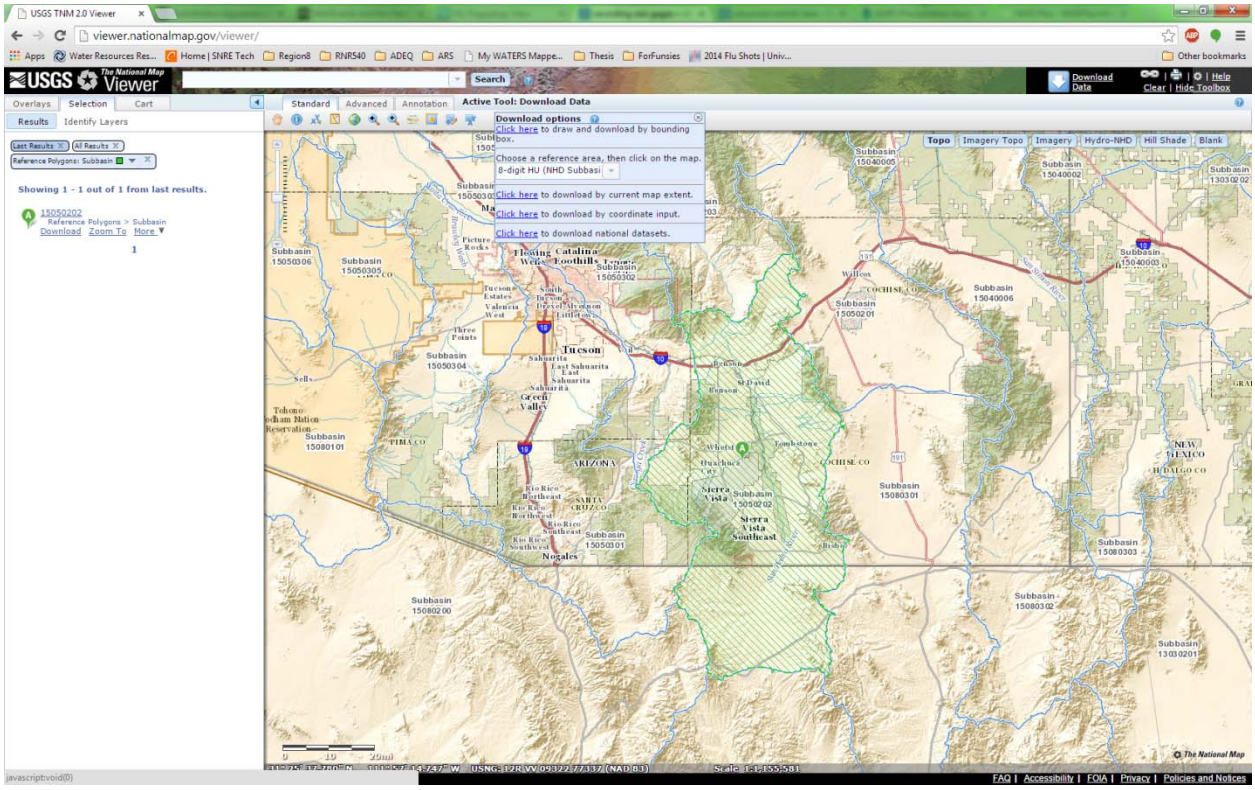
To get background information about the hydrography of your study area, we recommend the National Hydrography Dataset (NHD). NHD data can be found in many online locations; however, the easiest to navigate will be the USGS National Map Viewer. These areas of interest along with the NHD dataset will guide data download and influence which watersheds are modeled using AGWA.

Step 1: Download Data

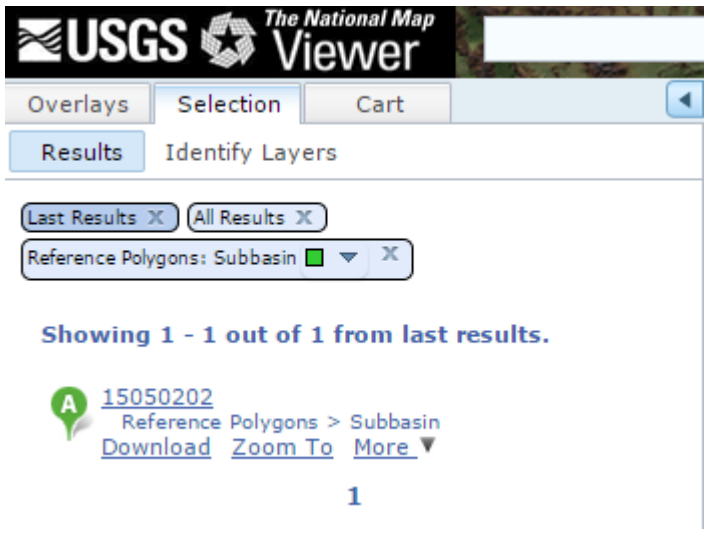
Start by visiting The National Map Viewer at viewer.nationalmap.gov/viewer/.

1. The Standard toolbar across the top of the map contains a download button which when selected gives the user multiple options to define an area from which to download data.
   1.1. For this application we will use the dropdown menu which allows the user to "Choose a reference area, then click on the map."
      1.1.1. Select 8-digit HU(NHD Subbasin) from the dropdown menu.

1.1.2. On the map, place the cursor on Subbasin 15050202 and click. This will highlight the Upper San Pedro Watershed.



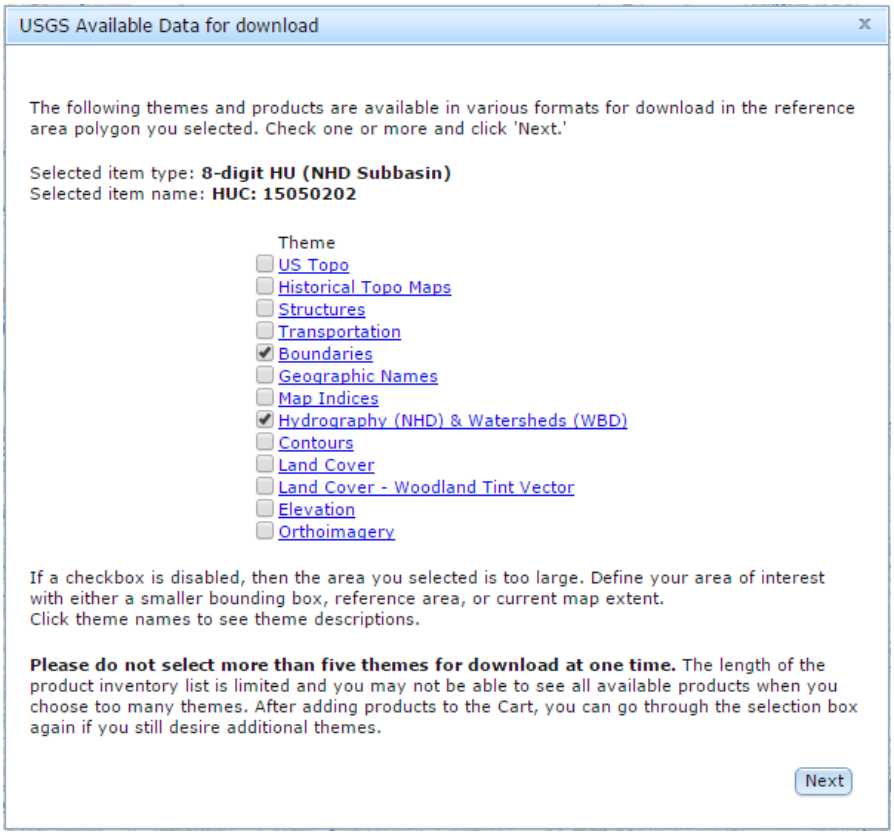
1.2. When this selection is made, the Selection tab will show the selected results.



1.3. Select Download.

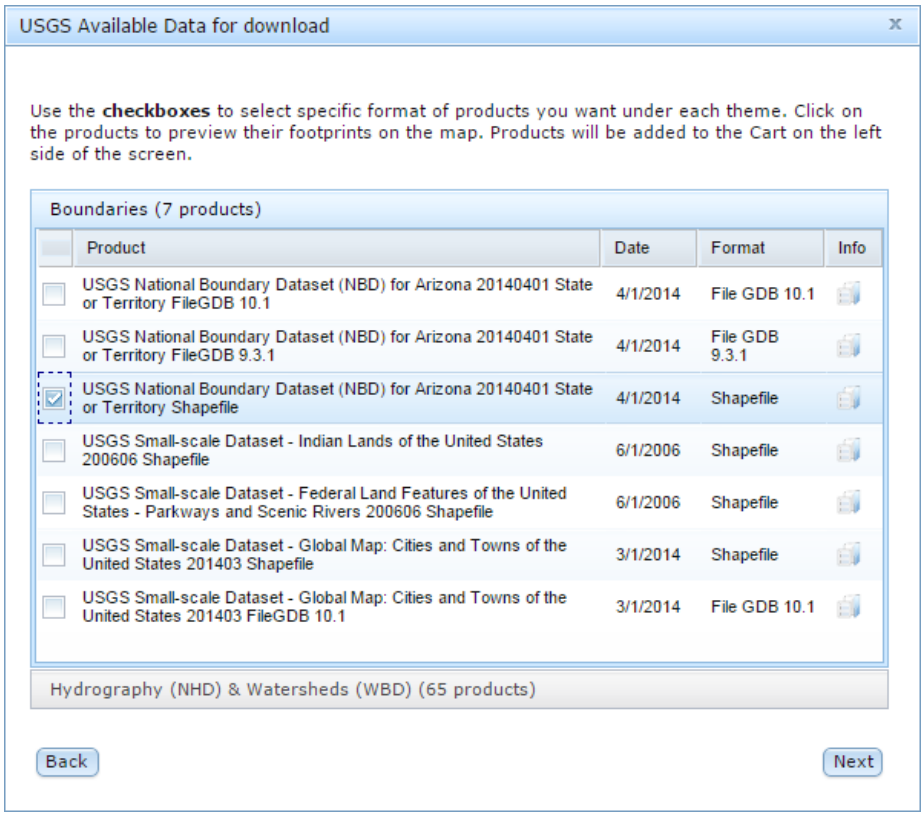
1.3.1. This brings up a new window *USGS Available Data for download*.

1.3.2. Check the boxes next to Boundaries and Hydrography (NHD) & Watersheds (WBD).

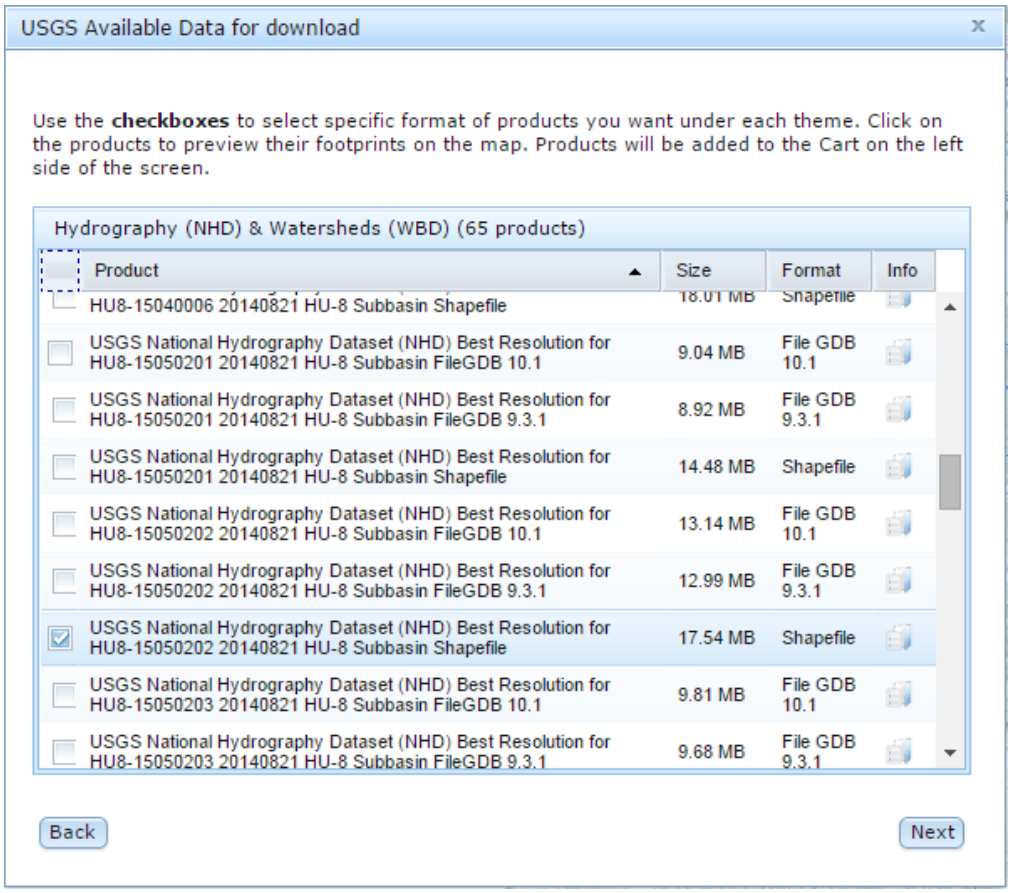


1.4. Click Next

2. The next window allows the user to select the specific boundary and hydrography datasets to order. There are many options available which may suit the needs of different watershed assessments and studies so explore these options as desired.
   2.1. For Boundaries, of the 7 products available select the USGS National Boundary Dataset (NBD) for Arizona 20140401 State or Territory Shapefile.



2.2. For Hydrography (NHD) & Watersheds (WBD), of the 65 products available, select USGS National Hydrography Dataset (NHD) Best Resolution for HU8-15050202 20140821 HU-8 Subbasin Shapefile.



2.3. Click Next.

3. Proceed to Checkout under the Cart Tab.
4. Enter the appropriate e-mail address from which you will download the data products you just ordered.

NOTE: The NBD dataset will arrive in your email inbox rather quickly; however the dynamic extract may take some time to process by the USGS and will arrive shortly after.

Step 2: Unzip and Save

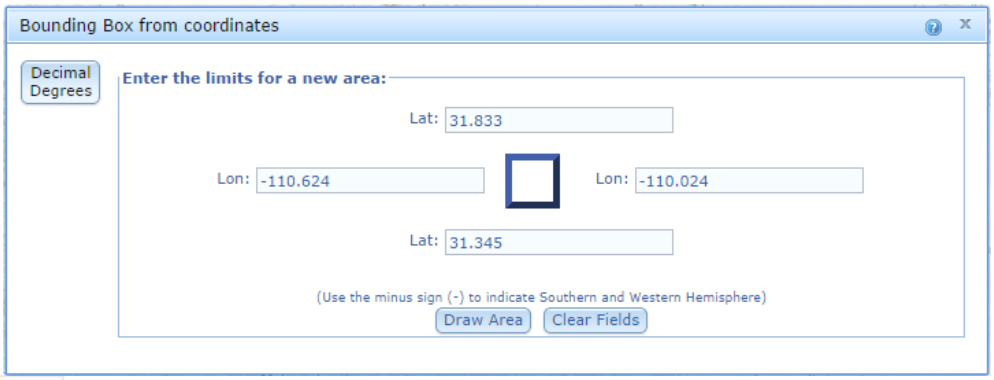
Part 1: Topography

A tiled mosaic of Digital Elevation Model (DEM) raster data layers is necessary to delineate watershed boundaries and determine the flow routes needed to run the models. The United States Geological Survey (USGS) provides bare earth DEM data from the National Elevation Dataset (NED) of 1/3 arc-second (approximately 10-meter) resolution for the contiguous United States that has been corrected to remove artifacts, match edges, and account for missing data (Gesch et al., 2002).

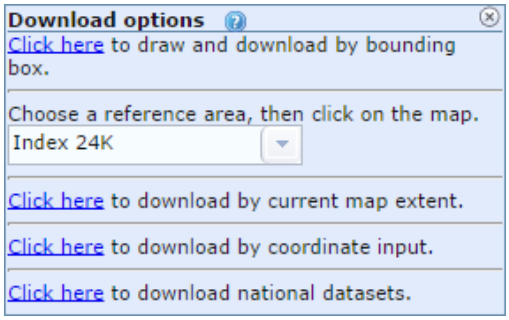
Step 1: Download Data

To download this DEM data visit the USGS National Map Viewer at viewer.nationalmap.gov/viewer/ and zoom into the area of interest, for this example Fort Huachuca in Southern Arizona.

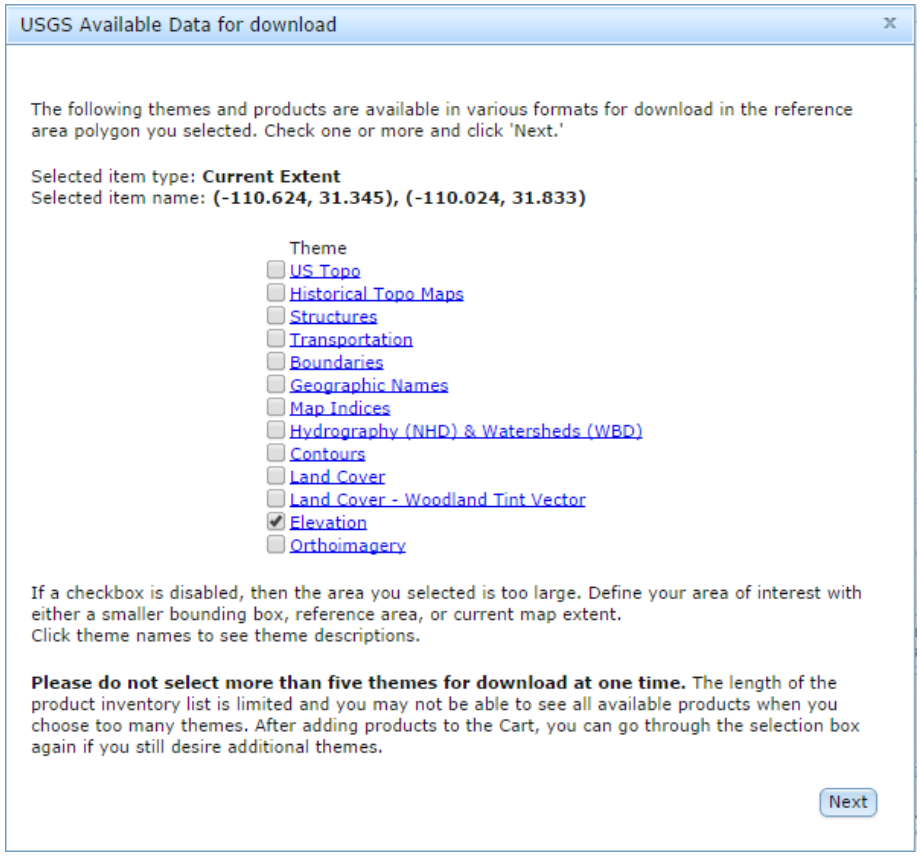
5. The Standard toolbar across the top of the map contains a download button which when selected gives the user multiple options to define an area from which to download data.
   5.1. While all options are easy to use, for this example we will download by coordinate input using the following coordinates.



NOTE: There are many options to download data in the National Map Viewer. Take a minute to explore those options as other methods may work better for different study areas or different scales.



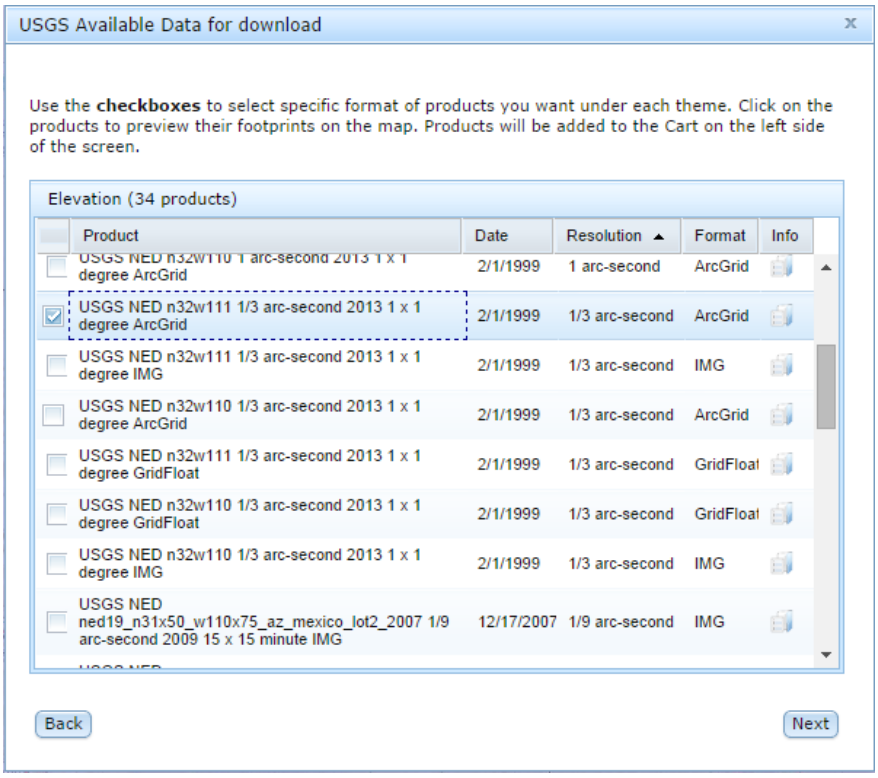
6. Click “Draw Area” which will bring up a new window displaying “USGS Available Data for download”.
   6.1. Check the box for Elevation.



NOTE: There are many spatial products available for download from the USGS National Map Viewer. Explore these products, some of which may be useful, especially the Land Cover products which contain National Land Cover Database from the years 1992 to 2011.

6.2. Click Next.

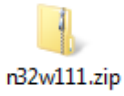
7. The next page will display all of the Elevation products available. For this study we will download the 10 meter DEM.
   7.1. Sort by Resolution so that you can view all data with 10 meter or 1/3 arc-second resolution.
   NOTE: The 10 meter (1/3 arc-second) DEM is sufficient for most watershed studies; however, consider using a 30 meter (1 arc-second) DEM for large watersheds and faster processing time (e.g. 4-Digit HUCs).
   7.2. Check the box as shown below; this is the only product to select for this example. Click Next.



8. This will bring you to the Cart menu which shows the user selected items and allows for checkout. If this does not automatically happen, select "Cart" in the upper left of the page.
9. Proceed to Checkout.
   9.1. Enter an e-mail that you have access to and select Place Order.

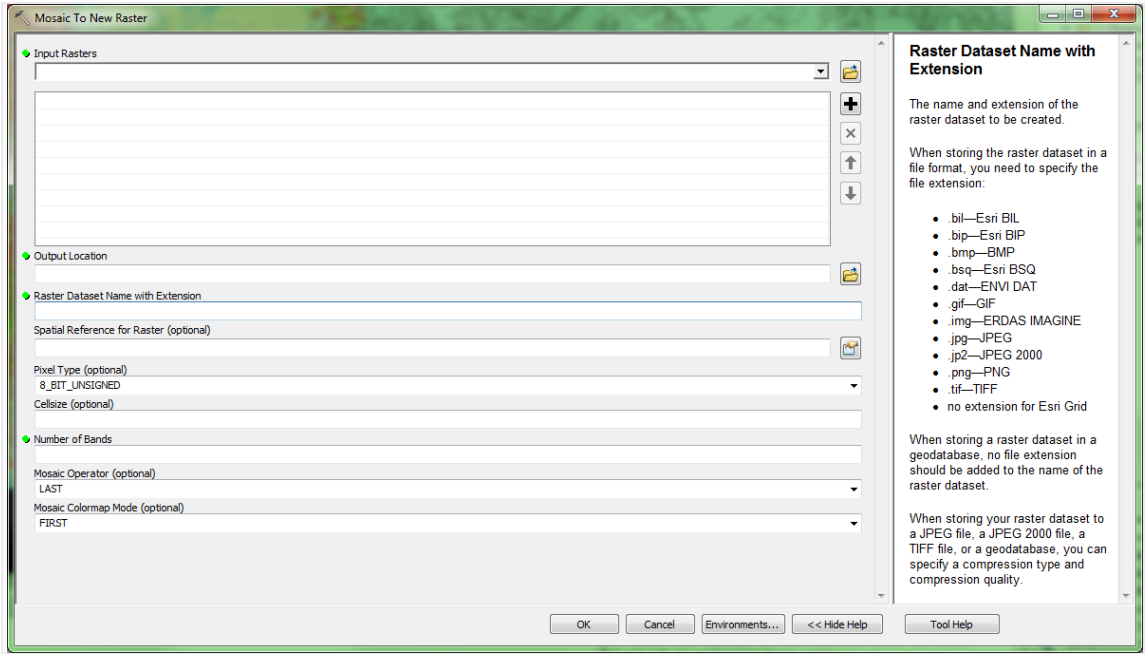
Step 2: Unzip and Save

10. The ordered file should arrive in your Inbox within a few minutes.
    10.1. Select the Download Link.
11. The file will download in a zip format which will need to be unzipped and saved in an accessible folder.
    11.1. To unzip the file, navigate to the zipped file, most likely in the computers Download folder.



    11.2. Right click on the folder with name n32w111.zip and select Extract All…
        11.2.1. Select the GISdata folder created (FortHuachuca) as the destination folder and click Extract.

NOTE: Fort Huachuca is small enough that one DEM tile covers the entire study area, however in larger areas more than one DEM tile may be needed and those tiles will need to be combined using the Mosaic tool in ArcCatalog or ArcMap. It is generally good practice to download data with coverage beyond your study area in case a watershed extends beyond the study area.

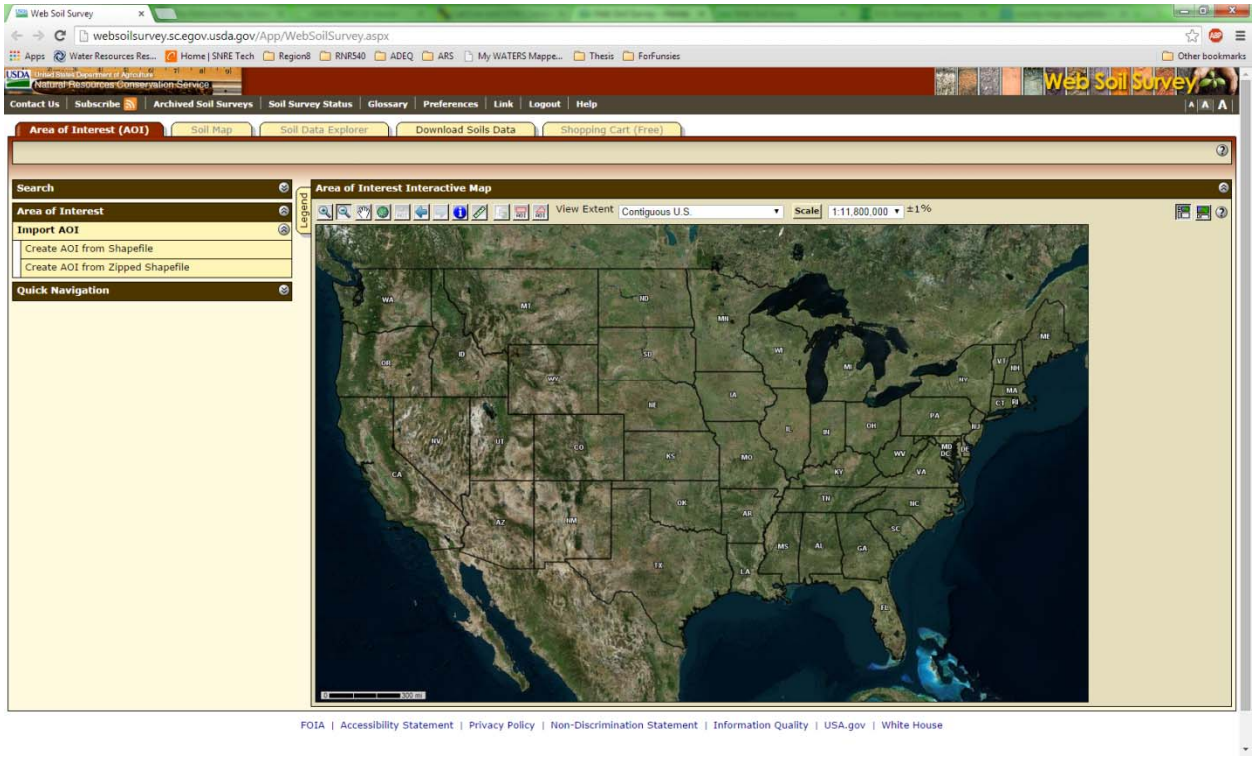


The downloaded DEM will be used to delineate watersheds using AGWA. Prior to delineation, AGWA allows users to fill DEMs to remove any erroneous values (sinks). The filled DEM is then used to create a flow directional grid, a flow accumulation grid, and a stream representation layer.

Part 2: Soil

The soil databases used in this study include the Soil Survey Geographic (SSURGO) and the State Soil Geographic (STATSGO) databases, both created and maintained by the USDA's Natural Resource Conservation Service (http://www.nrcs.usda.gov/wps/portal/nrcs/site/soils/home/). The SSURGO dataset was developed from digitized county-level maps that were created following standardized field methodologies and vary spatially from 1:12,000 to 1:63,360 (http://www.nrcs.usda.gov/wps/portal/nrcs/site/soils/home/). The finer resolution SSURGO database was used at Fort Huachuca.

12. Visit the Web Soil Survey maintained by the USDA NRCS at websoilsurvey.sc.egov.usda.gov/App/WebSoilSurvey.aspx.



13. Select the tab "Download Soils Data". You will use SSURGO data for this project.
    13.1. To download SSURGO data select the option Soil Survey Area (SSURGO).
        13.1.1. Under Options select the following:
            13.1.1.1. State: Arizona
            13.1.1.2. County: Cochise
            13.1.1.3. Sort by… Most recently updated
        13.1.2. Click the download link associated with Area Symbol AZ671.
        13.1.3. A zip folder under the name wss_SSA_AZ671_soildb_US_2003_[2013-12-15].zip will begin downloading.
14. Follow the steps outlined in Part 1-Step 2: Unzip and Save to handle this new download.

Part 3: Land Cover

AGWA has the capability to interpret different land cover datasets to characterize and parameterize watersheds. Gridded land cover datasets represent the distribution and variability of landscape classes across a study area. In general, it is recommended that users acquire land cover grids that extend beyond the boundaries of the study area and watershed for successful parameterization.

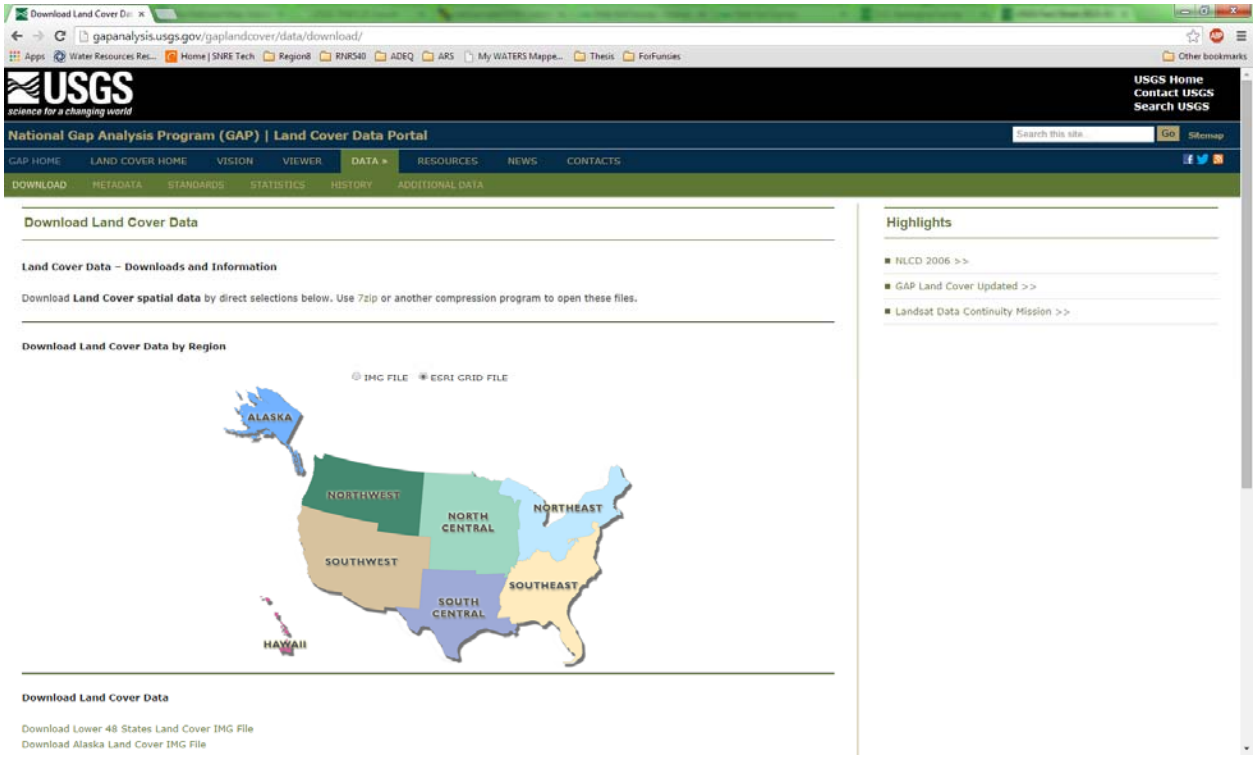
AGWA currently supports GAP, MLRC (NLCD), and NALC land cover grids. However, users may utilize other land cover datasets if an associated land cover look-up table exists or is created that matches the format of other look-up tables. In AGWA the cover type, interception, Manning's N, percent impervious, and curve number values (A, B, C, and D) are all obtained from the land cover layer using a land cover data look up table that is included within the AGWA data package (Burns et al., 2007). These values were determined for each of the

vegetation classes from expert opinion and previously published look-up tables (Miller et al. 2002).

GAP Landcover

Land cover information on vegetation and land use patterns was acquired from the USGS's Gap Analysis Program (GAP) National Land Cover dataset (USGS National Gap Analysis Program, 2012). The GAP land cover data combines data generated by regional GAP projects with LANDFIRE data to provide information on the distribution of native vegetative types, modified and introduced vegetation, developed areas, and agricultural areas in a seamless coverage for the entire United States (USGS National Gap Analysis Program, 2012). The southwest portion of the dataset was derived through the classification of 30-meter, multi-seasonal Landsat Enhanced Thematic Mapper Plus (ETM+) satellite images that were acquired between 1999-2001 (Lowry et al., 2007). The imagery was classified into 590 land use classes following the NatureServe's Terrestrial Ecological Systems Classification framework for natural and semi-natural land cover (Comer et al., 2003).

15. Visit the USGS GAP Analysis Downloads Webpage at gapanalysis.usgs.gov/gaplandcover/data/download/



16. Scroll down to the Download Data by Area section where a dropdown menu allows you to download by state.
    16.1. Download by State: Select Arizona
    16.2. Click Download ESRI GRID File
    16.3. The download will take less than five minutes depending on the internet connection.

NOTE: For some study sites downloading data by state will not be effective. Explore this page to get an idea of available coverage and data formats.

17. When the download is complete follow the steps outlined in Part 1- Step 2: Unzip and Save.
    17.1. Unzip the gaplndcov_az.zip folder into the **C:\AGWA\GISdata\FortHuachuca** folder.

Part 4: Precipitation

The next step in data preparation for running AGWA is to prepare the precipitation input data for the desired model. Accurate representation of precipitation events requires a high degree of spatial coverage. For this project a variety of climate data sources were explored to assess which could most accurately simulate real world conditions. The representation of rainfall from rain gage observations varied at each site depending on the number of gages found in close proximity to the bases. This section presents a variety of possible precipitation inputs to be used for SWAT or KINEROS2.

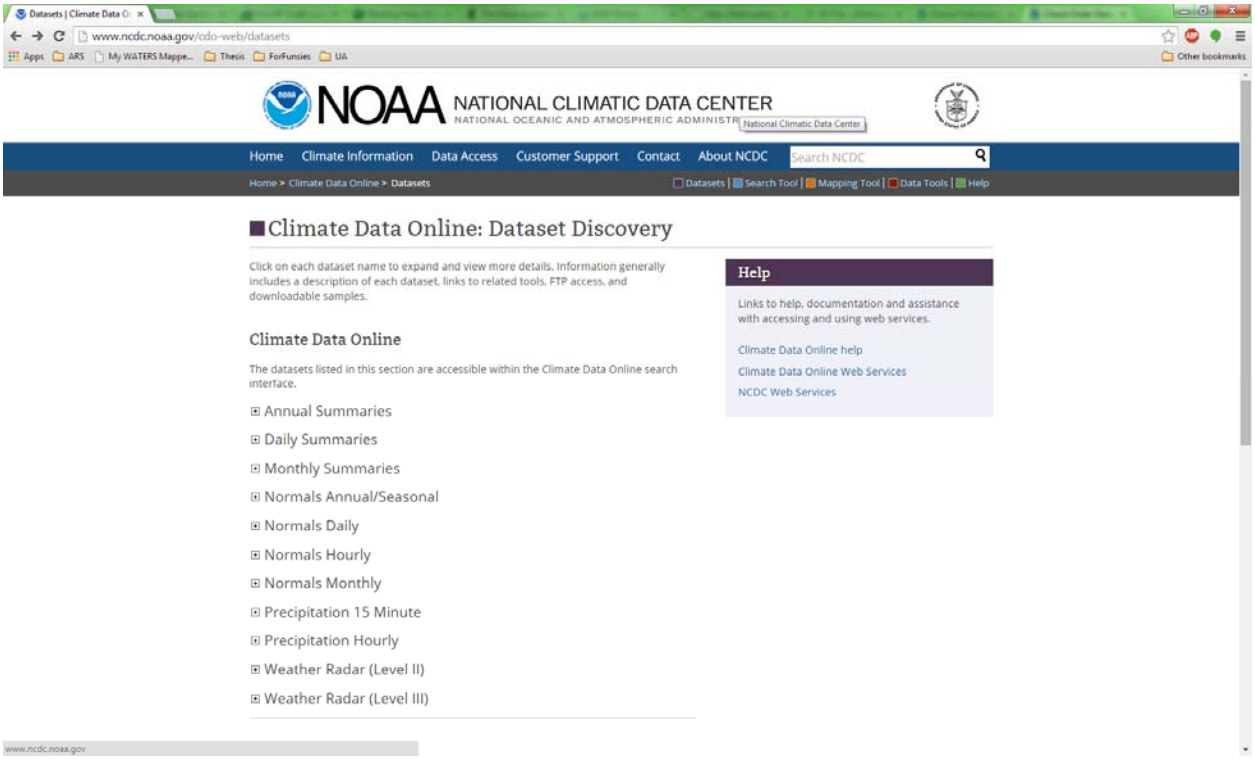
SWAT Precipitation

NOAA GHCN

SWAT precipitation input requires a table of daily precipitation (mm) values arranged chronologically by year and Julian calendar day that are associated with each rain gage location. For multiple gages, AGWA uses a built-in tool that distributes the values using Thiessen polygons to compute the weighted rainfall depth falling on each subwatershed (Miller et al., 2007). The daily climate data needed to run SWAT was obtained from the NOAA National Climatic Data Center's (NCDC) Global Historical Climatology Network (GHCN) Daily, Version 2 dataset accessed via the online interactive map application (NOAA GHCN, 2010). This dataset contains a composite of climate records from numerous sources that were merged and subjected to a suite of quality assurance reviews (NOAA GHCN, 2010). The dataset provides daily maximum and minimum temperatures, snowfall, and 24-hour precipitation totals that were obtained primarily from state universities or cooperatives and reported as part of the United States Cooperative Summary of the Day (NOAA GHCN, 2010). Currently, there are approximately 8,500 active stations across the United States that are recording precipitation and temperature maximum and minimum data and some have historical records that reach as far back as the late 1800's, though most begin around 1948 (NOAA GHCN, 2010).

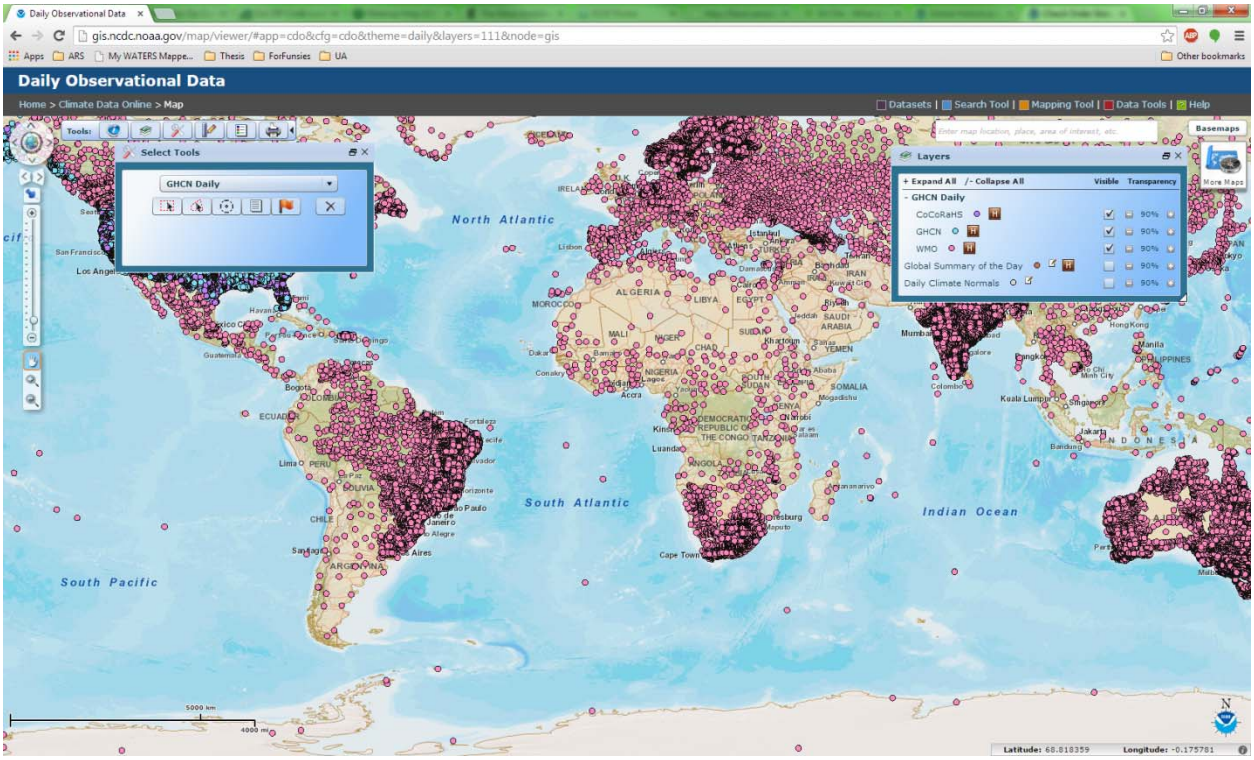
For this exercise we will look at one year of data from one station at Fort Huachuca. The data acquired here will be discussed in the Data Management section to demonstrate how this information will need to be adjusted for use as an input for SWAT.

18. Visit the NOAA NCDC Webpage for Climate Data Online at http://www.ncdc.noaa.gov/cdo-web/datasets



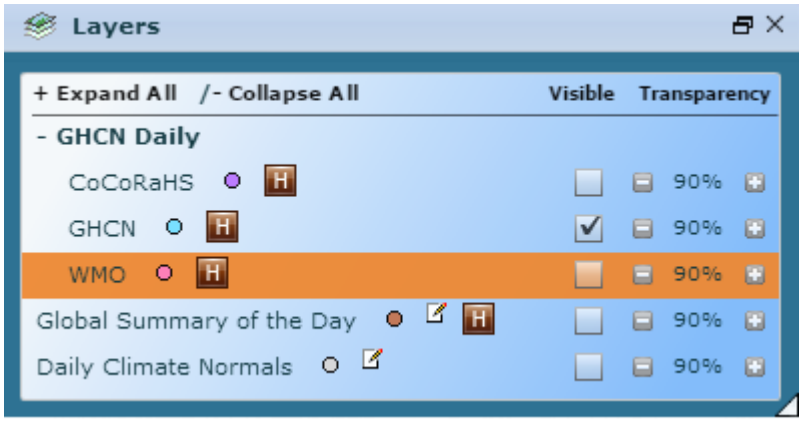
This website contains a lot of good information that may be used in other exercises. For example the Precipitation 15 Minute link may be utilized to find precipitation information to drive the KINEROS2 model in AGWA.

19. For this exercise, expand the section for Daily Summaries. At this point feel free to read more about these data.
20. Select the Mapping Tool 



20.1. Two windows appear on the map: the left window "Select Tools" contains five tools which allow the user to specify which gages they are interested in; the right window "Layers" is a legend for the map.

20.1.1. To start, there are three datasets that are visible; for this exercise we are only concerned with the GHCN dataset, so uncheck all other layers in the Layers window.



20.2. Use the Select By Attributes tool  in the Select Tools window.

20.2.1. Type Fort Huachuca

20.2.2. Click Search

20.3. A new window "Results" will appear.

20.3.1. Check the box in front of Fort Huachuca Sierra Vista Municipal Airport, AZ US.

20.3.2. Click Get Selected Data.

21. This brings you the Cart: Daily Summaries page where you further specify what kind of data to order.
    21.1. Select the output format: Custom GHCN-Daily CSV
    21.2. Select the Date and time range: 2012-01-01 to 2012-12-31. Click Apply.
    21.3. Review the items in your cart: Fort Huachuca Sierra Vista Municipal Airport, AZ US.
    21.4. Click Continue.
22. Select the data to order.
    22.1. Station Detail & Data Flag Options: Select Station Name and Geographic Location
    22.2. Select Data types for custom output:
        22.2.1. Expand Precipitation
            22.2.1.1. Select Precipitation (tenths of mm)
        22.2.2. Select Air Temperature
    22.3. Click Continue, and review the requested data. Enter your email address.
    22.4. Click Submit Order.
23. A notice will be emailed to you confirming the submittal of this data request.
24. Shortly after the actual data will be sent to your email for download.
25. Copy this csv file (the file name will be a 6-digit code with the csv file extension) into the GISdata/downloads folder.

NOTE: This short of a time period is not recommended for adequate watershed analysis; however, for the purpose of this demonstration a one year time period allows us to more easily walk through all necessary steps in formatting, model simulations, and interpretation.

NEXRAD

Due to the limited spatial coverage of the GHCN rain gage data additional precipitation estimates were obtained from Next-Generation Radar (NEXRAD) data and from local meteorological stations at Fort Huachuca. NEXRAD data is collected through a network of 159 high-resolution Weather Surveillance Radar-1988 Doppler (WSR-88D) radars that constantly scan the near surface, detecting precipitation and atmospheric movement using a Precipitation Processing System (PPS) algorithm described in detail in Fulton et al. (1998). The data are organized to provide spatially continuous precipitation estimates over a 4x4 km^2 grid projected in the Hydrologic Rainfall Analysis Project (HRAP) coordinate system. An open source Python script designed by Mehmat Ercan at the University of South Carolina was used to create a table of daily precipitation values for the central point of each HRAP grid cell that intersected any part of the study area watersheds. Center points were then used as virtual rain gage locations and used to drive SWAT. Fort Bliss NEXRAD Multisensor Precipitation Estimator (MPE) data were obtained using HydroDesktop, a GIS program that allows a spatial query of hydrologic data sources and allows for the download and export of NEXRAD-MPE data from the NWS's regional River Forecasting Centers (Ames et al., 2012). This tool can be found in the Hydrologic Modeling folder.

Meteorological Towers and Rain Gages

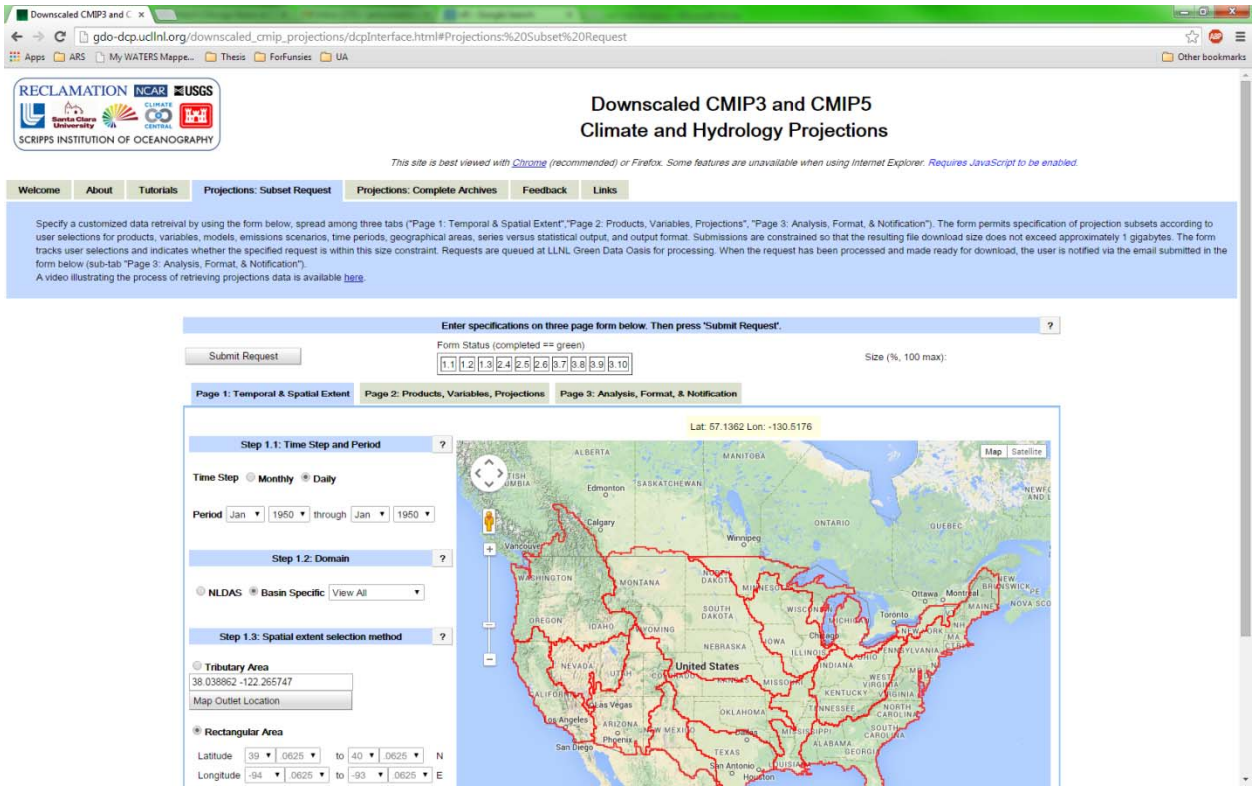
In addition to the NEXRAD and rain gage data sources, an array of six meteorological towers (met towers) located at Fort Huachuca within the installation boundaries provided precipitation

and temperature data from 2000-2011 in 15-minute intervals. These data were evaluated as an input for SWAT and used create design storms needed for the KINEROS2 calibration efforts at Upper Garden and Huachuca Canyons (for more detail see Lyon, 2013).

Climate Change

To assess the impacts of climate change on the flow regime, climate projection data were obtained from the World Climate Research Programme's (WCRP's) third Coupled Model Intercomparison Project (CMIP3). Of the various climate models included in the CMIP3 dataset, NOAA's Geophysical Fluid Dynamics Laboratory Climate Model version 2.1 (GFDL CM2.1) was shown to have a good representation of the multi-model ensemble mean for the Southwest and is one of the few models that provide continuous daily temperature and precipitation outputs (Seager et al. 2007; Cayan et al. 2010). The data have a scale of 1.8° or approximately 12 km resolution and were accessed for free from the LLNL Green Data Oasis data storage website. The GFDL CM2.1 data were obtained for both historical (1981-2000) and future (2081-2100) time periods and were assigned to "virtual" rain gage locations at grid centers before being used to create the SWAT precipitation input files.

An updated version of these data is available as a CMIP5 dataset with documentation and download options available here:
http://gdo-dcp.ucllnl.org/downscaled_cmip_projections/dcpInterface.html#Welcome
Use the Projections: Subset Request tab to download daily data for specific time periods by area.



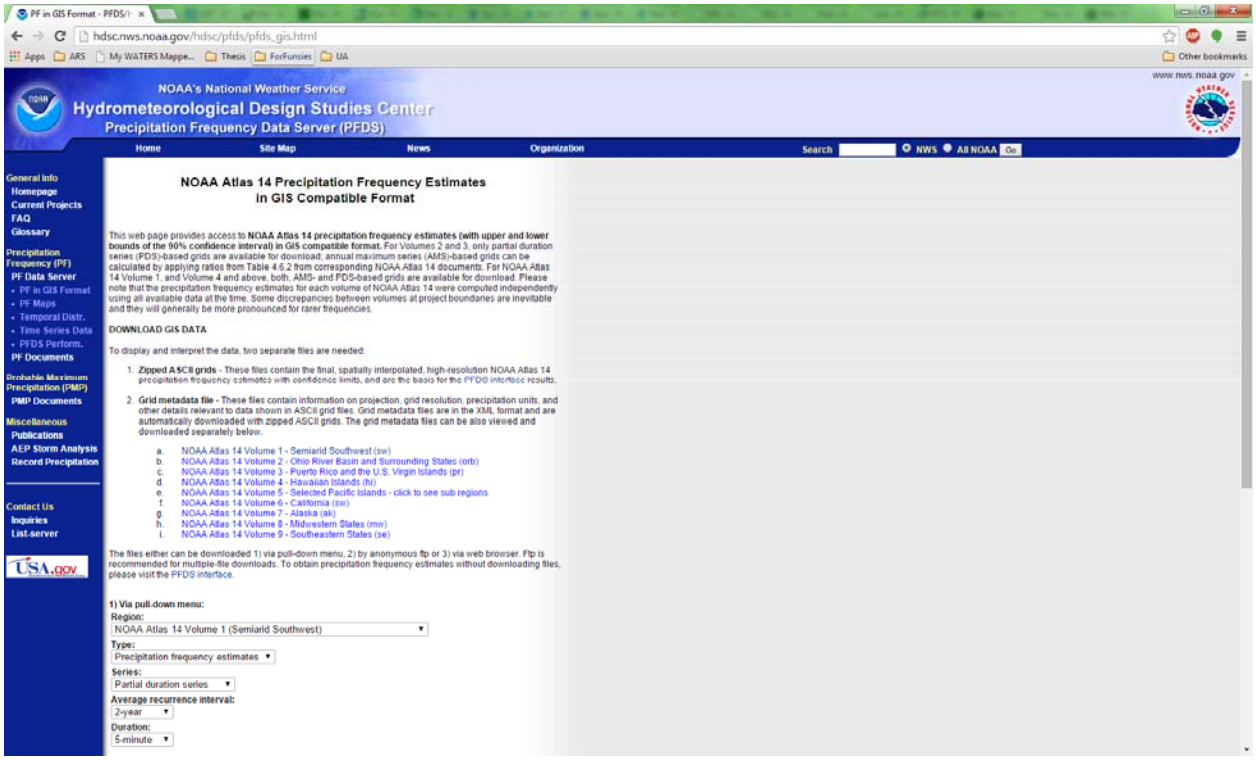
KINEROS2 Precipitation

Precipitation data required to run the KINEROS2 model were entered as depths (in) from a pre-defined table of precipitation frequency estimates based on a specific return interval and duration. NOAA's Precipitation Frequency Data Server (PFDS) allows for the input of geographical coordinates to determine precipitation depths based on a frequency analysis of partial duration series (NOAA PFDS, 2012). Design storms based on 5, 10, 25, and 100-year, 1-hour storms were created from the PFDS data using the centroid coordinate for each watershed in the study areas. Applying a design storm created from a single point estimate across an entire watershed tends to result in an overestimation of runoff due to the failure to account for spatial heterogeneity of the input data (Miller et al., 2002).

NOAA Precipitation Frequency

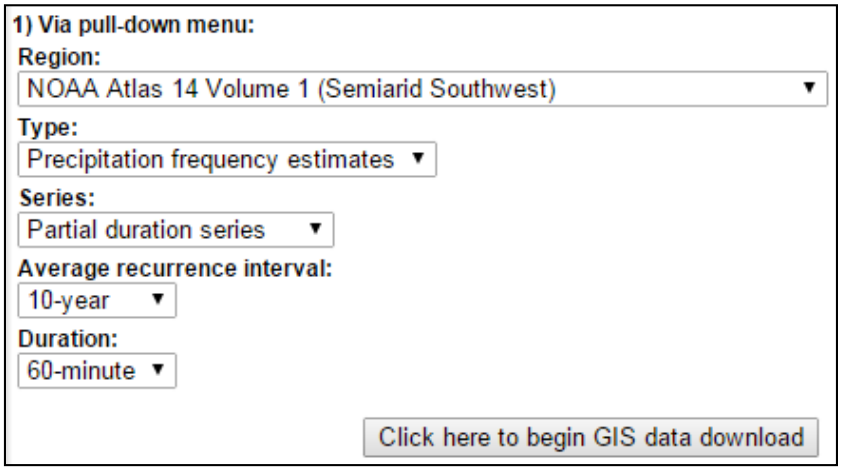
NOAA Atlas 14 Precipitation Frequency Estimates come in multiple formats; one of these is a GIS compatible format which is a gridded dataset that provides precipitation frequency estiamtes in partial duration series. The gridded dataset is available for most of the United States and is separated in Volumes 1-9 by region.

26. Visit NOAA Atlas 14 Precipitation Frequency Estimates in GIS Compatible Format at http://hdsc.nws.noaa.gov/hdsc/pfds/pfds_gis.html.



27. Scroll down to the series of dropdown menus and populate accordingly:
    27.1. Region: NOAA Atlas 14 Volume 1 (Semiarid Southwest)
    27.2. Type: Precipitation frequency estimates
    27.3. Series: Partial duration series

27.4. Average recurrence interval: 10-year
27.5. Duration: 60-minute



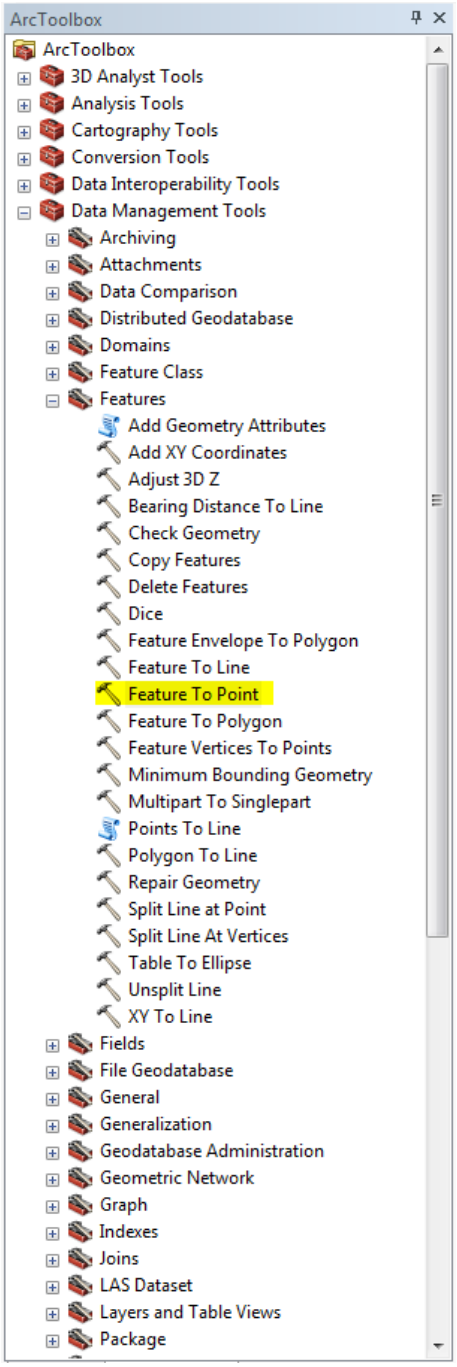
27.6. Click to begin download.
28. Unzip the file and save it to GISdata/precipitation

Database
AGWA has a built in design storm database which contains return period depths for specific locations. This table can be found in the AGWA/datafiles/precip folder with the file name dsgnstrm.dbf. Databases were also developed for each of the installations and can be found in the HydrologicModeling folder.

To use this precipitation input for KINEROS2, the dsgnstrm.dbf table must be added to the map document.

User-Defined Depth
This refers to a depth-duration measurement for which you will need the duration of the storm in hours along with the total depth of the storm over that time period in mm.

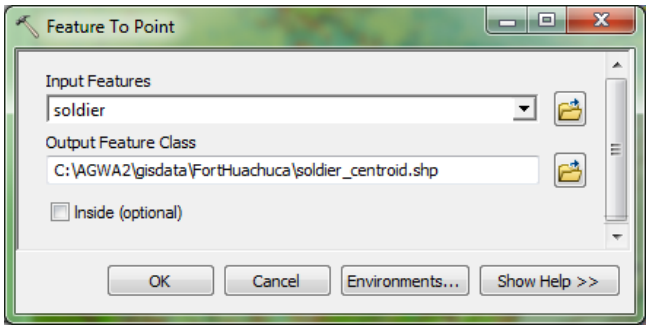
29. Watershed delineation is required to create the appropriate precipitation data.
    STOP: For this exercise, complete AGWA Modeling, SWAT, Part 1, Watershed Delineation, then return to Step 30 of Data Acquisition.
30. For the delineated Soldier Creek watershed, you will locate the watershed centroid using ArcToolbox.
    30.1. Locate and select the Feature to Point tool found under Data Management Tools and the subfolder Features.



30.2. Execute the tool.

30.2.1. Input Features will be the watershed in your study area.

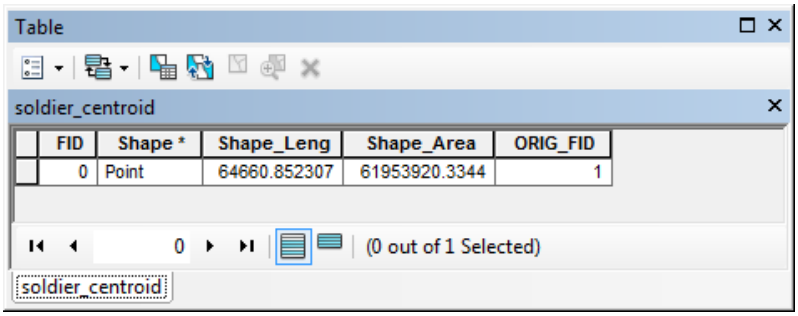
30.2.2. The Output Feature Class should be in a folder that is easily accessible. We recommend keeping all relevant data in the C:\AGWA\GISdata\FortHuachuca\ folder that was created earlier.



30.2.3. Click OK. This tool will find the centroid of the polygon and place that point in a shapefile titled "soldier_centroid.shp".

30.3. The point shapefile will be in a projected coordinate system (NAD 1983 UTM Zone 12N) which is converted to Decimal Degrees to find precipitation data using NOAA PFDS.

30.3.1. Open the soldier_centroid table by right clicking on the layer in ArcGIS table of contents and selecting Open Attribute Table.

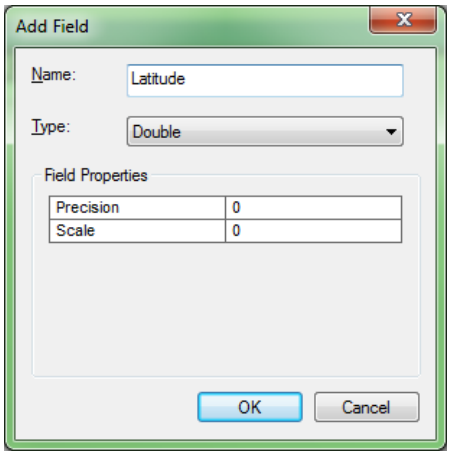


30.3.2. Add two fields to the table.

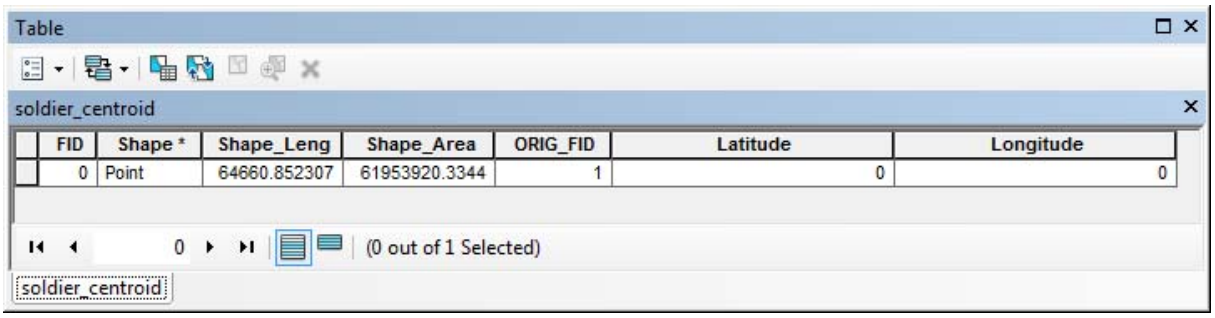
30.3.2.1. Open Table Options menu then select Add Field…

30.3.2.1.1. Name the first field Latitude.

30.3.2.1.2. Select Double as the field type.



30.3.2.1.3. Repeat and name the second field Longitude.

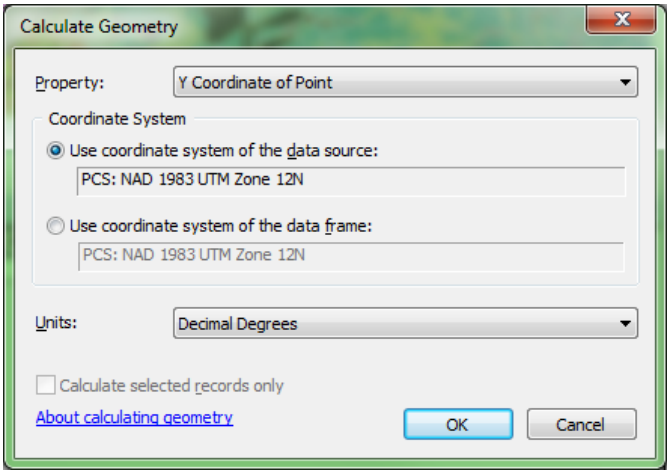


30.3.3. Populate these fields with X and Y Coordinate Locations.

30.3.3.1. Right click on Latitude and select Calculate Geometry. A warning message will appear asking if you would like to continue. Select Yes.

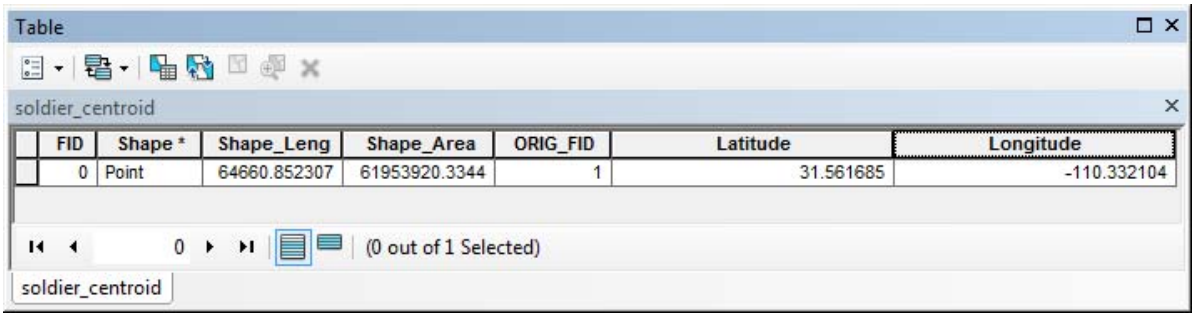
30.3.3.2. Select the Property: Y Coordinate of Point.

30.3.3.3. Select Units: Decimal Degrees



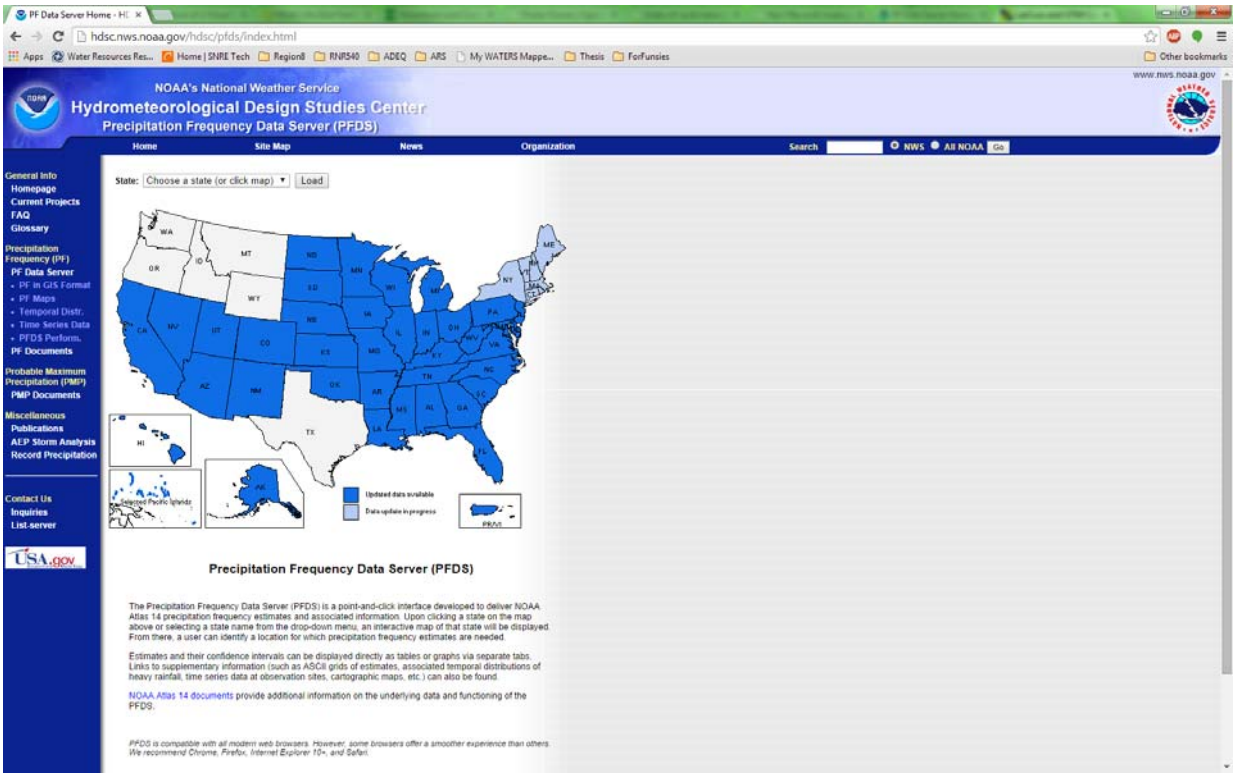
30.3.3.4. Click OK. Another warning may appear, select Yes.

30.3.3.5. Repeat for Longitude; selecting Property: X Coordinate of Point.

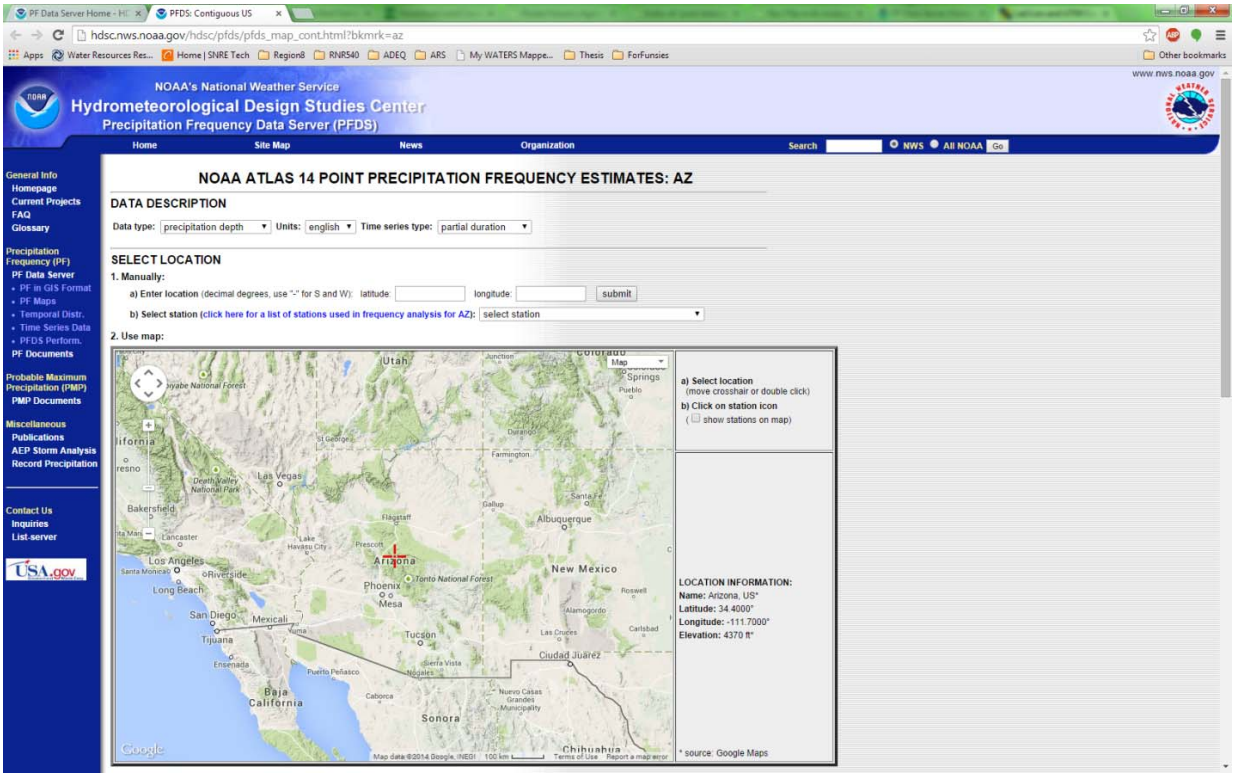


31. Use the coordinate location of this point for input in the NOAA PFDS.

31.1. Visit http://hdsc.nws.noaa.gov/hdsc/pfds/index.html



31.2. Select AZ using either the dropdown menu or interactive map.

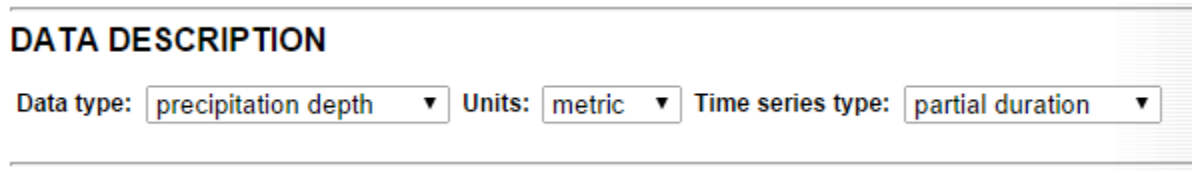


31.3. Select the Data Description options.

31.3.1. Data type: precipitation depth

31.3.2. Units: metric

31.3.3. Time series type: partial duration

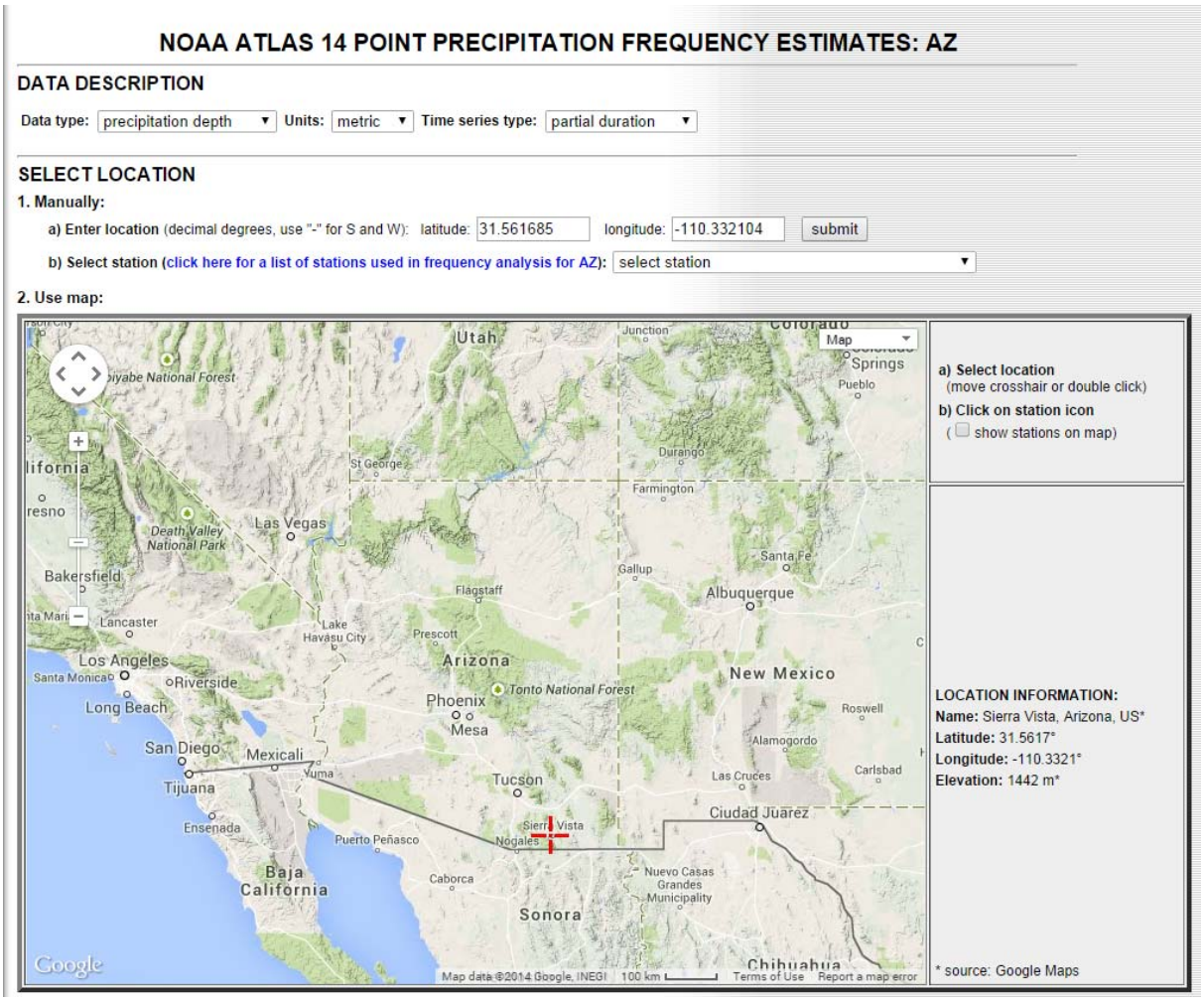


31.4. Select Location

NOTE: There are many options available to select locations using this interface. For this exercise we will use the latitude and longitude calculated in ArcMap; however, for other studies it may be more feasible to select stations from a list or simply navigate using the map. Explore these options for future use.

31.4.1. Manually enter the location using the latitude and longitude from the soldier_centroid table.

31.4.2. Click submit. The Map will update and move the crosshair to the input location.



32. Acquire precipitation data.
    32.1. Scroll down on the page until you see “Point Precipitation Frequency (PF) Estimates”.
    32.2. The PF tabular view shows Duration on the vertical axis and Average recurrence intervals (years) on the horizontal axis.

POINT PRECIPITATION FREQUENCY (PF) ESTIMATES

WITH 90% CONFIDENCE INTERVALS AND SUPPLEMENTARY INFORMATION
NOAA Atlas 14, Volume 1, Version 5

PF tabular | PF graphical | Supplementary information | Print Page

PDS-based precipitation frequency estimates with 90% confidence intervals (in millimeters)[1]

Duration	Average recurrence interval (years)									
	1	2	5	10	25	50	100	200	500	1000
5-min	7 (6-8)	9 (8-10)	12 (10-13)	14 (12-16)	17 (14-19)	19 (16-21)	21 (18-24)	23 (19-26)	26 (21-30)	28 (22-32)
10-min	11 (10-12)	14 (12-16)	18 (16-20)	21 (19-24)	25 (22-29)	29 (25-32)	32 (27-36)	35 (29-40)	39 (32-45)	42 (34-49)
15-min	13 (12-15)	17 (15-20)	22 (20-25)	26 (23-30)	31 (27-36)	35 (30-40)	39 (33-45)	43 (36-50)	48 (40-56)	52 (42-61)
30-min	18 (16-21)	23 (20-26)	30 (26-34)	35 (31-40)	42 (37-48)	48 (41-54)	53 (45-60)	58 (49-67)	65 (54-75)	71 (57-82)
60-min	22 (20-25)	29 (25-33)	37 (33-42)	44 (38-50)	52 (45-59)	59 (51-67)	65 (56-75)	72 (60-83)	81 (66-93)	87 (71-102)
2-hr	26 (23-29)	32 (29-37)	42 (37-47)	49 (43-55)	59 (52-67)	67 (58-76)	75 (64-86)	84 (70-96)	95 (79-110)	105 (85-122)
3-hr	27 (24-30)	34 (30-38)	43 (38-48)	51 (45-57)	61 (53-68)	69 (60-78)	78 (67-88)	87 (73-99)	100 (82-115)	110 (89-128)
6-hr	31 (27-35)	38 (34-43)	48 (43-55)	57 (50-64)	69 (60-77)	78 (67-88)	88 (75-100)	99 (83-113)	114 (93-132)	127 (101-148)
12-hr	34 (31-39)	43 (38-48)	54 (48-60)	63 (56-70)	75 (66-84)	85 (74-96)	96 (82-108)	107 (90-121)	122 (101-140)	134 (109-156)
24-hr	39 (37-43)	49 (46-53)	61 (57-66)	70 (65-76)	83 (76-90)	93 (85-101)	103 (94-112)	113 (102-123)	127 (114-142)	137 (122-158)
2-day	44 (41-48)	55 (51-59)	67 (62-73)	78 (72-84)	93 (85-100)	104 (95-113)	116 (105-126)	128 (116-140)	145 (129-159)	159 (140-175)
3-day	48 (45-52)	60 (56-65)	74 (69-80)	86 (80-93)	102 (94-111)	115 (105-125)	129 (117-140)	143 (129-156)	162 (144-178)	177 (156-195)
4-day	53 (49-57)	66 (61-71)	81 (75-88)	94 (87-102)	112 (103-121)	126 (116-137)	142 (129-154)	157 (141-171)	179 (159-196)	196 (172-216)
7-day	64 (59-69)	79 (73-86)	98 (91-106)	114 (105-123)	135 (124-146)	151 (138-163)	168 (153-182)	185 (167-202)	209 (186-228)	227 (201-250)
10-day	73 (68-79)	91 (85-98)	113 (105-121)	129 (120-139)	152 (140-163)	169 (155-182)	186 (170-201)	204 (185-221)	227 (204-247)	244 (218-267)
20-day	102 (94-109)	127 (118-137)	155 (144-167)	176 (163-190)	204 (188-219)	224 (206-241)	244 (223-263)	263 (240-284)	287 (260-312)	304 (274-332)
30-day	126 (117-136)	157 (146-169)	191 (177-206)	216 (200-232)	246 (228-265)	268 (248-289)	290 (267-312)	309 (284-334)	334 (305-363)	352 (320-383)
45-day	154 (144-166)	192 (179-206)	231 (215-248)	259 (240-277)	293 (272-314)	316 (293-340)	338 (313-364)	359 (331-387)	383 (352-415)	400 (367-435)
60-day	179 (167-191)	222 (207-238)	266 (248-285)	297 (277-318)	334 (311-358)	360 (334-386)	384 (356-413)	406 (376-438)	432 (398-467)	450 (413-488)

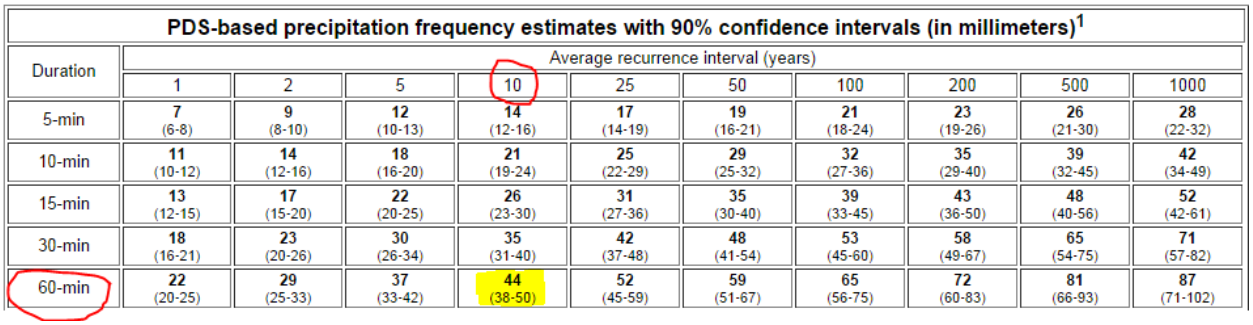
[1] Precipitation frequency (PF) estimates in this table are based on frequency analysis of partial duration series (PDS).

Numbers in parenthesis are PF estimates at lower and upper bounds of the 90% confidence interval. The probability that precipitation frequency estimates (for a given duration and average recurrence interval) will be greater than the upper bound (or less than the lower bound) is 5%. Estimates at upper bounds are not checked against probable maximum precipitation (PMP) estimates and may be higher than currently valid PMP values.

Please refer to NOAA Atlas 14 document for more information.

32.3. At this point, you can either download the csv format of this information or simply note the values of interest.

32.3.1. For this study we are going to use the 10-year 1-hour precipitation frequency estimate of 44mm.



PDS-based precipitation frequency estimates with 90% confidence intervals (in millimeters)[1]

Duration	Average recurrence interval (years)									
	1	2	5	10	25	50	100	200	500	1000
5-min	7 (6-8)	9 (8-10)	12 (10-13)	14 (12-16)	17 (14-19)	19 (16-21)	21 (18-24)	23 (19-26)	26 (21-30)	28 (22-32)
10-min	11 (10-12)	14 (12-16)	18 (16-20)	21 (19-24)	25 (22-29)	29 (25-32)	32 (27-36)	35 (29-40)	39 (32-45)	42 (34-49)
15-min	13 (12-15)	17 (15-20)	22 (20-25)	26 (23-30)	31 (27-36)	35 (30-40)	39 (33-45)	43 (36-50)	48 (40-56)	52 (42-61)
30-min	18 (16-21)	23 (20-26)	30 (26-34)	35 (31-40)	42 (37-48)	48 (41-54)	53 (45-60)	58 (49-67)	65 (54-75)	71 (57-82)
60-min	22 (20-25)	29 (25-33)	37 (33-42)	44 (38-50)	52 (45-59)	59 (51-67)	65 (56-75)	72 (60-83)	81 (66-93)	87 (71-102)

32.3.2. This information will be used to write the precipitation file for KINEROS2 in AGWA.

To account for discrepancies an aerial reduction factor, developed from paired rain gage study in Southern Arizona (Osborn et al., 1980) and expanded for other parts of the Southwest in NOAAs Technical Memorandum NWS HYDRO-40 (Zehr & Myers, 1984), can be applied to the design storm depth estimates. However, for this application we will not apply the reduction factor.

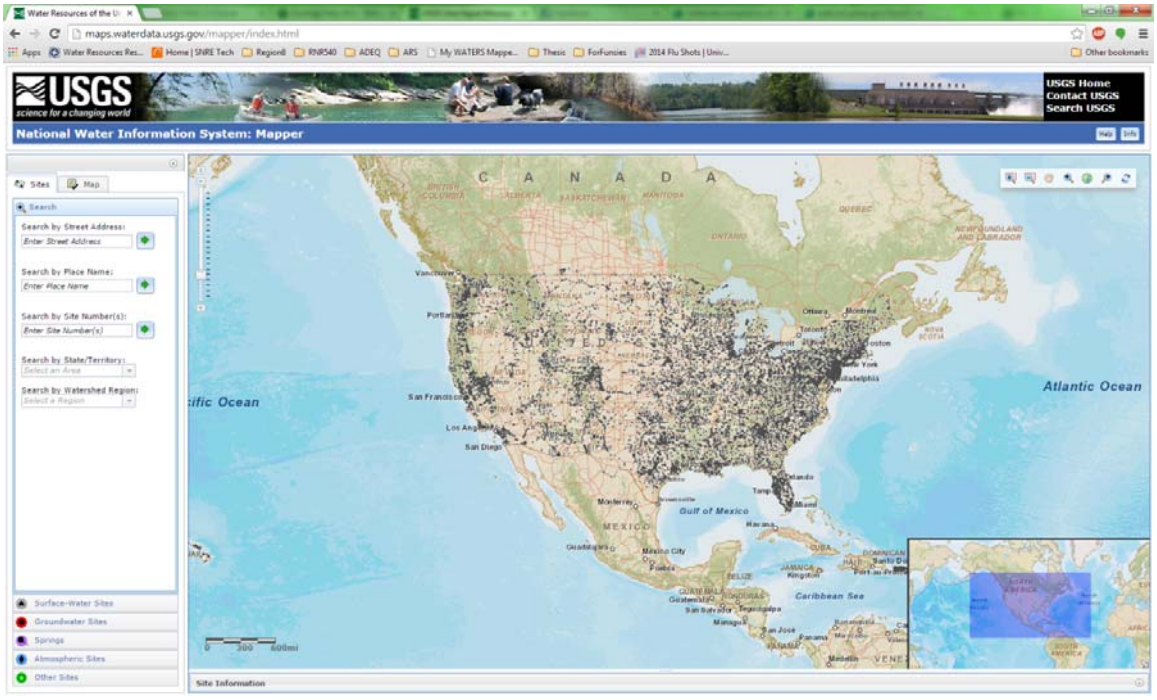
User-Defined Hyetograph

If users have their own event data, this information can be organized such that for each time step there is a corresponding depth in millimeters or intensity in mm per hour. This information can be used as a direct input for the KINEROS2 model.

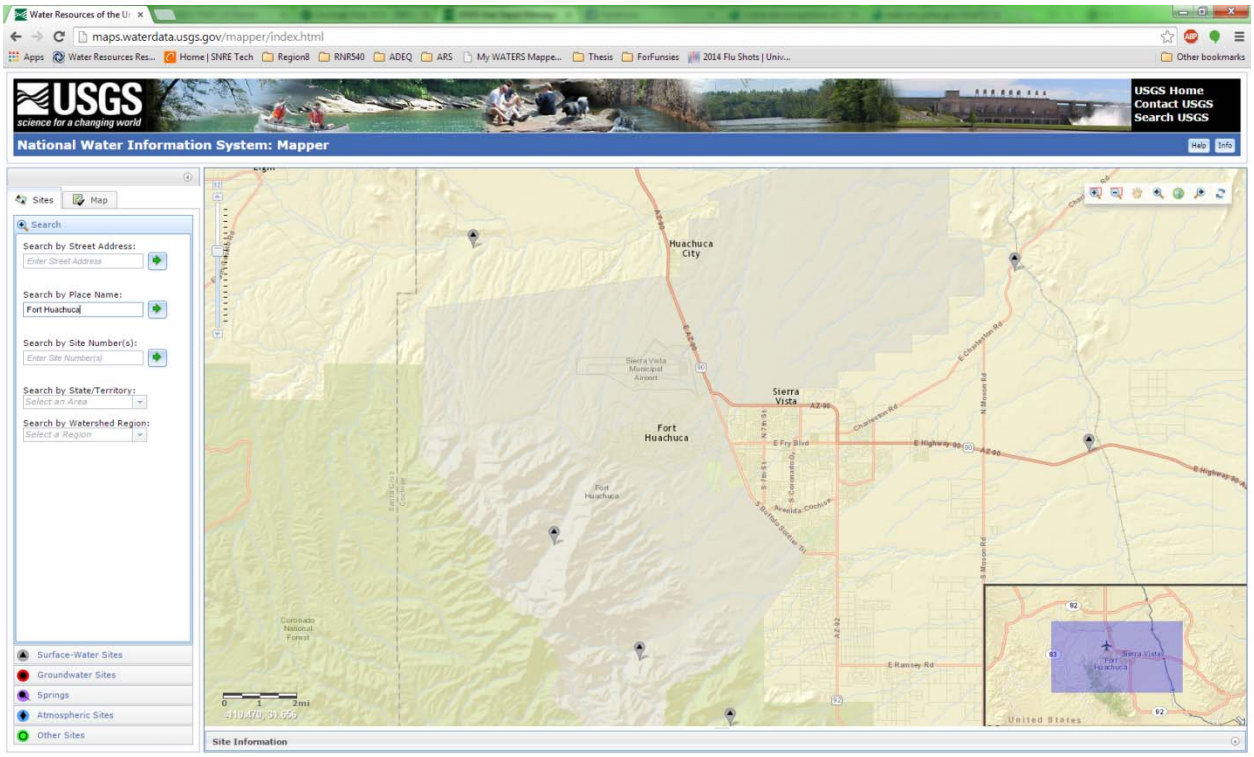
To acquire this information, various web based data repositories may be available, however the most detailed information will likely come from a local source familiar with the study area, the watershed, and any instrumentation on site. For the SERDP project, Lyon (2013) used local gage data obtained directly from Fort Huachuca personnel.

An online source that is used in this exercise is provided by the USGS: the National Water Information System: Mapper contains active and inactive sites that monitor surface water, groundwater, springs, atmospheric and more. Accessing these data requires a fair amount of user involvement to filter through precipitation information. This section will outline how to find the information and will use an event that has already been selected.

33. Navigate to the USGS National Water Information System: Mapper webpage at http://maps.waterdata.usgs.gov/mapper/index.html

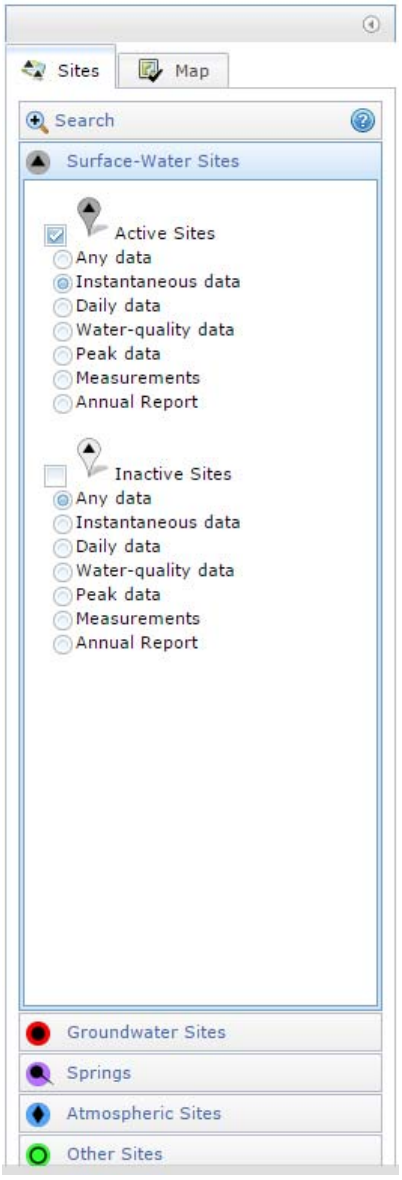


34. On the left panel under the tab Sites select Search by Place Name.
    34.1. Type: Fort Huachuca
    34.2. This will zoom to Fort Huachuca in Southeastern Arizona.

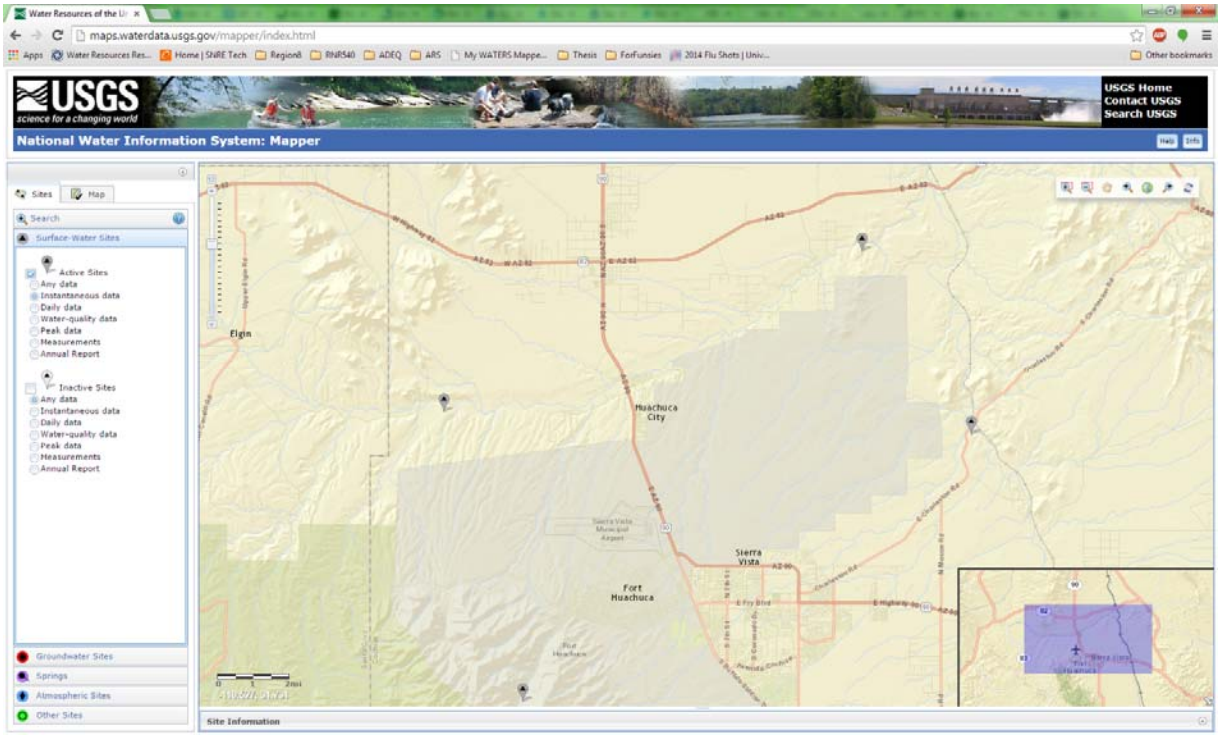


The default sites shown are Active Surface-Water Sites. These sites can record discharge, gage height, and precipitation; however, not all sites record all of this information. The sites also record at different temporal scales, which is important to recognize for this application.

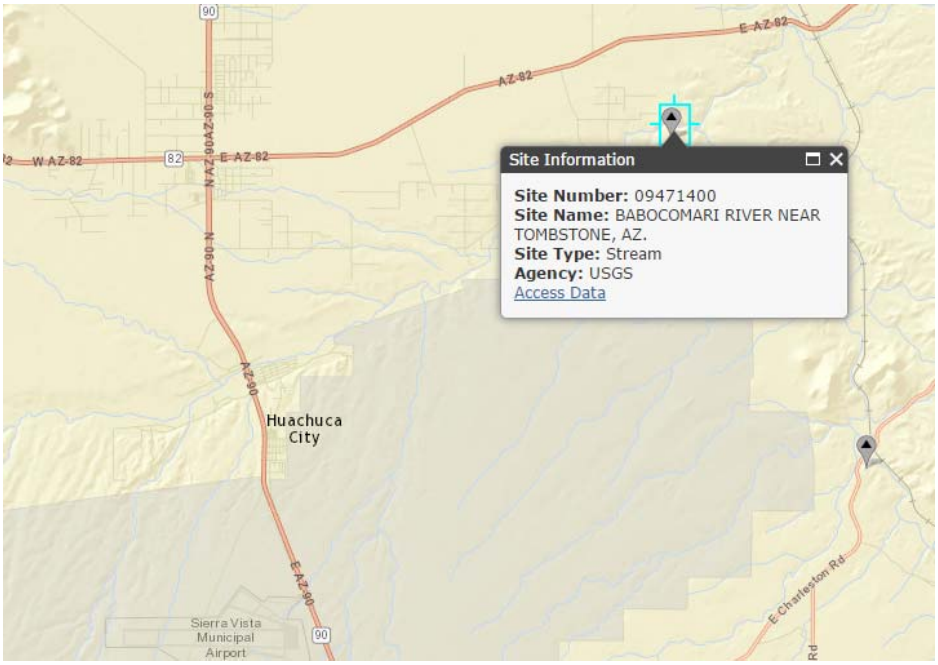
35. Below the Search window is the Surface-Water Sites window. Open this window.
    35.1. Select Active Sites.
        35.1.1. Select Instantaneous data



36. In the map viewer pan to the northeast of Fort Huachuca, bringing another gage into view.



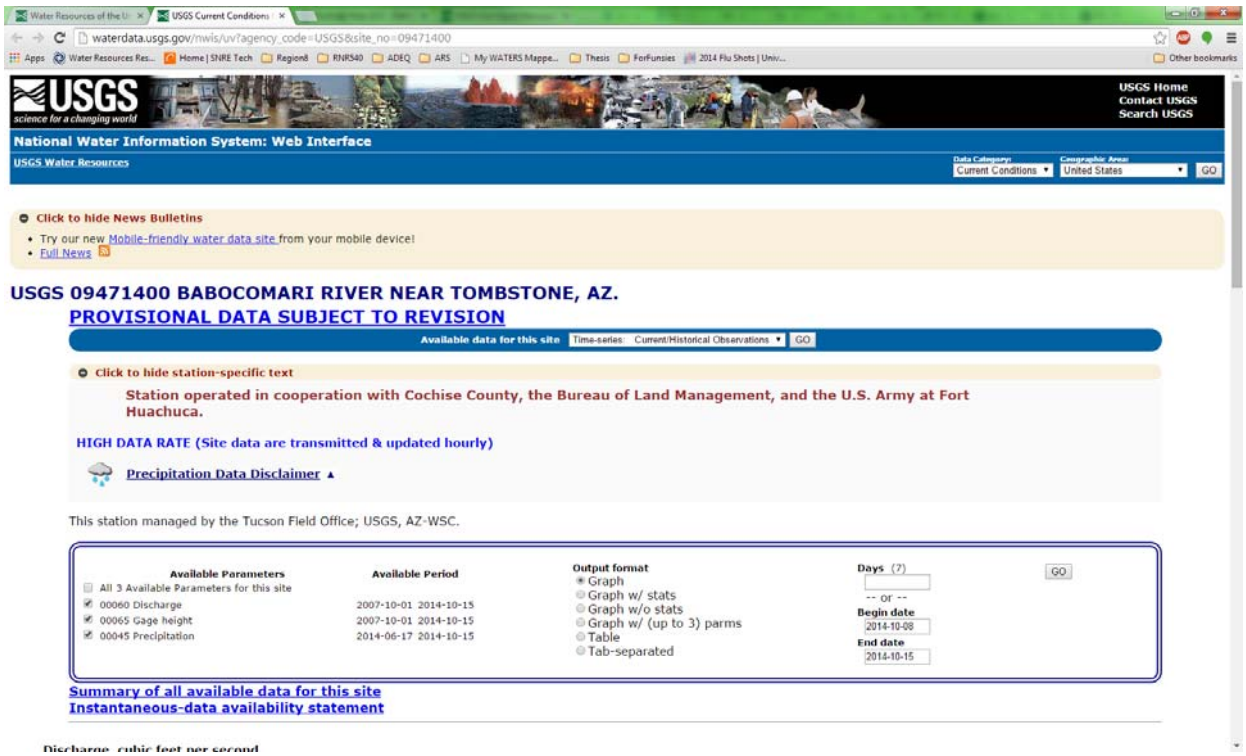
36.1. Click the northern-most site.



36.1.1. This will open a window as shown above.

36.1.2. Click Access Data.

37. A new page will open with Current Conditions for USGS 09471400 Babocomari River near Tombstone, AZ.



37.1. Make sure that the dropdown menu indicating Available data for this site is set to Time-series: Current/Historical Observations.



37.2. Below this menu is a list of user-driven properties that indicate the data to be downloaded

37.2.1. Available Parameters: Select only Precipitation

37.2.2. Output Format: Select Table.

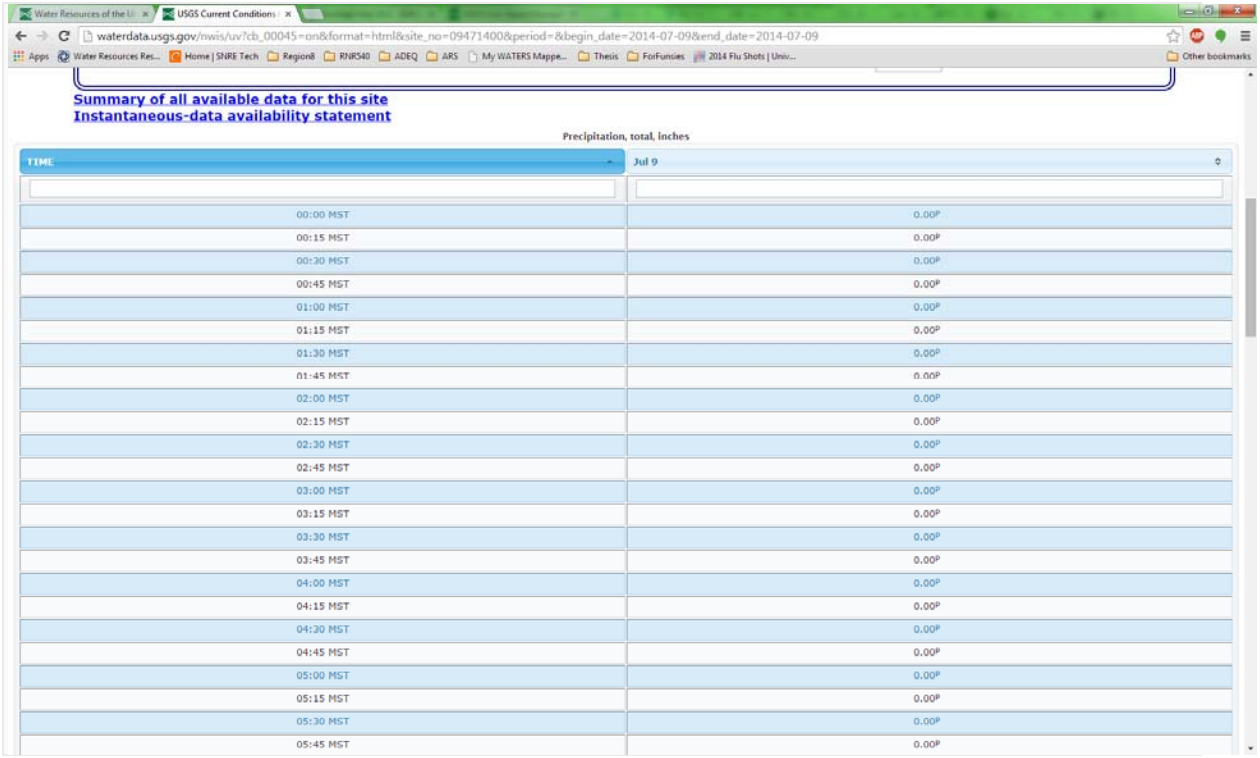
37.2.3. Begin Date: 2014-07-09

37.2.4. End Date: 2014-07-09

NOTE: The beginning and end date will need to cover a larger period of time if the user has not identified a storm to be modeled.

37.2.5. Click GO.

37.3. Scroll down until you see the table with time and precipitation in total inches.



37.4. The storm we are interested in starts at 16:00mst.

38. Open EXCEL

38.1. Populate the first four columns as follows:

Time (min)	Precip (in)	Cumulative Precip (in)	Cumulative Precip (mm)

This table will hold the hyetograph that will be used to drive KINEROS2 in AGWA.

38.2. We will copy the precipitation values in inches into the precip (in) column, starting at time 16:00mst and ending at time 17:30mst.

38.3. Time (min) will be populated from 0-90 in 15 minute increments.

Time (min)	Precip (in)
0	0
15	0.02
30	0.47
45	0.16
60	0.33
75	0.1
90	0.01

38.4. Cumulative precip (in) will be calculated in EXCEL by compounding the precipitation at each time step. For example, cumulative precip (in) at 30 minutes will be 0.47+0.02+0=0.49.

38.5. These values will then be converted to millimeters under the assumption that 25.4mm are in 1in. The results should look like this:

Time (min)	Precip (in)	Cumulative Precip (in)	Cumulative Precip (mm)
0	0	0	0
15	0.02	0.02	0.508
30	0.47	0.49	12.446
45	0.16	0.65	16.51
60	0.33	0.98	24.892
75	0.1	1.08	27.432
90	0.01	1.09	27.686

39. Save this EXCEL file in the gisdata/precipitation folder for Fort Huachuca to be used as an input for KINEROS2.

Data Management

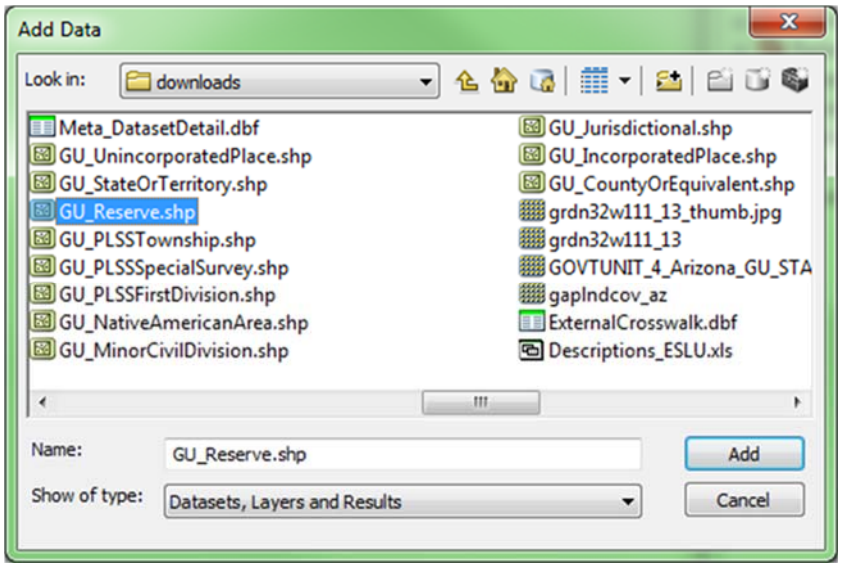
Acquiring data relevant to your project area is the first step: getting and data management is also important for proper implementation in AGWA. Some of the data acquired in the previous Data Acquisition section and saved to the **C:\AGWA\GISdata\FortHuachuca\downloads** folder will be used in this part of the guidance document. However, the data used to drive KINEROS2 and SWAT for the Tutorial have already been downloaded and organized; the steps in this section are only required when acquiring new data for new study areas. This section also focuses on a limited set of data sources; however, the same process can be used to organize and format different data.

Begin by opening ArcCatalog. Folder connections to drives and folders where your data are stored must be established if they are not already. To establish new folder connections, click the ***Connect To Folder*** button on the menu bar at the top of the screen. Select drive **(C:)**.

Background: Extract Study Area Outline

In this example, the study area boundary is a part of the larger NHD dataset that was downloaded in the Data Acquisition section that includes boundaries for the entire state of Arizona. If you already have a boundary layer of your study area, this part is not necessary.

1. Start ArcMap with a new empty map.
   1.1. Save the empty map document as **DataManagement** in the **C:\AGWA\GISdata\FortHuachuca** folder.
   1.2. Click on the ***Add Data*** button below the menu bar at the top of the screen, and navigate to **C:\AGWA\GISdata\FortHuachuca\downloads.** You may need to establish a folder connection as you did in ArcCatalog.
      1.2.1. Select the GU_Reserv.shp shapefile.



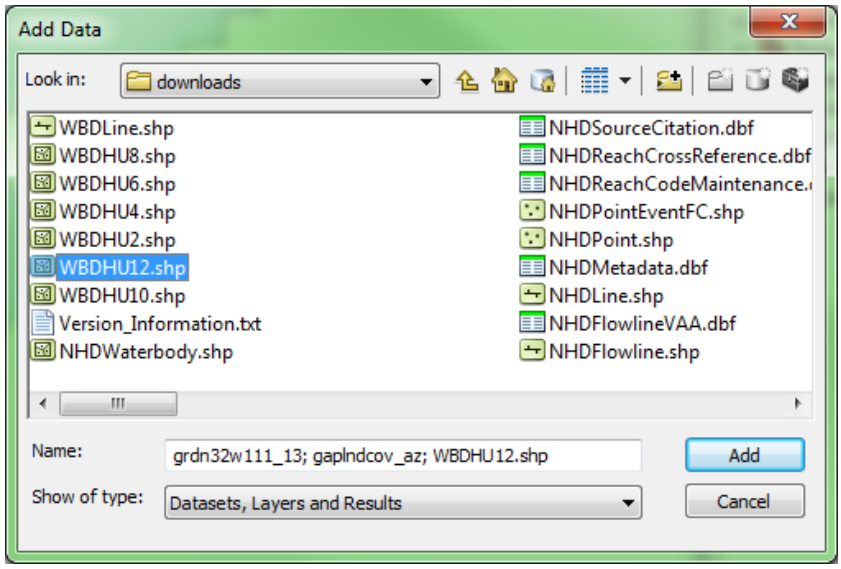
2. Click ***Add***.
3. Right click on the GU_Reserve layer to open the attribute table.

4. Sort the attribute table by name and scroll to Fort Huachuca.
5. Select this feature.
6. With this feature selected right click on GU_Reserve layer again; select Data, Export Data…
   6.1. Export: Selected features
   6.2. Navigate to GISdata/FortHuachuca and save the file as FtHua_Boundary.shp
   6.3. Click Save, then Click Okay.
   6.4. A dialogue will appear that asks if the exported data should be added to the map, click yes.
7. The GU_Reserve layer can then be removed from the map document.
8.

Part 1: Projecting Data into a Common Coordinate System

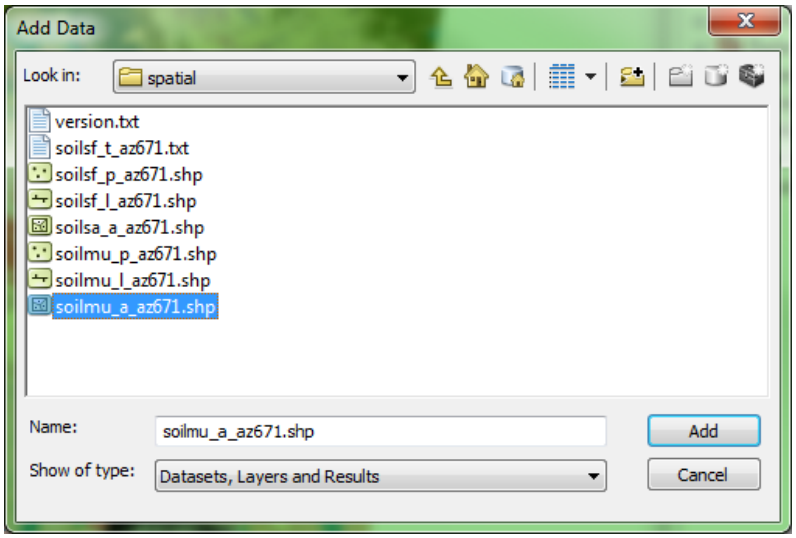
Step 1: View the data in ArcMap

9. Click on the ***Add Data*** button below the menu bar at the top of the screen, and navigate to **C:\AGWA\GISdata\FortHuachuca\downloads\.** You may need to establish a folder connection as you did previously in ArcCatalog.
   9.1. Select the DEM layer (grdn32111_13), the landcover layer (gaplndcov_az), and the NHD watershed boundary layer for HUC12 (WBDHU12.shp). In order select more than one layer click and hold the shift key or click and hold the control key.
   9.2. Click ***Add***.



NOTE: ARCMAP will ask if you would like to build pyramids for the raster datasets you are adding; click YES.

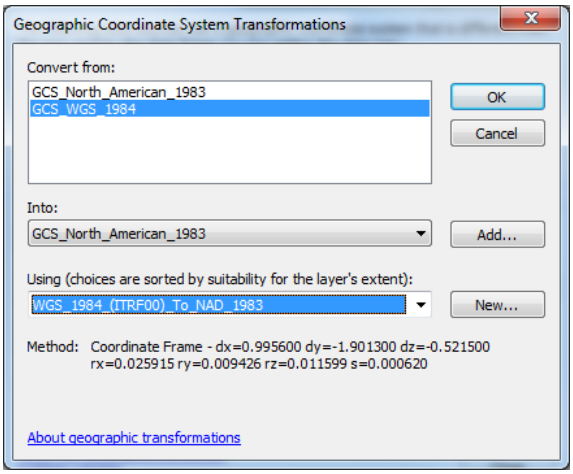
   9.3. Click the Add Data button again.
      9.3.1. This time, open the **AZ671** folder, and navigate to **C:\AGWA\GISdata\FortHuachuca\AZ671\spatial\soilmu_a_az671.shp**.



9.3.2. Click ***Add***.

9.3.3. A ***Geographic Coordinate Systems Warning*** window appears.

9.3.3.1. Click ***Transformations***. Make the following selections:



9.3.3.1.1. ***Convert from***: **GCS_WGS_1984**

9.3.3.1.2. ***Into***: **GCS_North_American_1983**

9.3.3.1.3. ***Using:*** **WGS_1984_(ITRF00)_To_NAD_1983**

9.3.3.2. Click ***OK*** to exit the ***Geographic Coordinate System Transformations*** window.

9.3.4. Click ***Close*** to exit the ***Geographic Coordinate Systems Warning*** window.

Look at the data you have available to you to familiarize yourself with the area. Layers can be reordered, turned on/off, and their legends collapsed to suit your preferences and clean up the display. If the layers cannot be reordered by clicking and dragging, the ***List By Drawing Order*** button  may need to be selected at the top of the ***Table Of Contents***. Place the ***gsmsoilmu_a_ca*** layer below the other layers, the ***FtHua_Boundary*** layer above all layers, and zoom to the ***HUC12*** layer.

Step 2: Project the Data to a Common Coordinate System

Projecting data into a common coordinate system is a necessary step to use the data in AGWA, and is a generally sound practice for any type of GIS analysis. This example explains how to project data to a common coordinate system for Fort Huachuca; you will need to determine the coordinate system for other locations.

10. View the current projection of the data frame.
    10.1. Right click on Layers in the Table of Contents and select Properties.
    10.2. In the Coordinate System tab
        10.2.1. Open the Projected Coordinate Systems
            10.2.1.1. Open UTM
                10.2.1.1.1. Open NAD 1983
                10.2.1.1.2. Select NAD 1983 UTM Zone 12.
11. A Warning will appear select Transformations…
    11.1. Convert From: GCS_WGS_1984
    11.2. Into: GCS_North_American_1983
    11.3. Using: WGS_1984_(ITRF00)_To_NAD_1983
    11.4. Click OK.
    11.5. Click Yes.
12. Click OK to leave the Data Frame Properties Window.
13. View the current projections of the layers.
    13.1. Coordinate systems for each of the layers can be found by double clicking on the layer then opening the Source tab.
    13.2. All of the data currently in this map document are unprojected. To correct this we will project rasters together and then project feature classes.
14. Reproject the raster layers to the ***NAD_1983_UTM_12N*** coordinate system.
    14.1. Open ArcToolbox using the ArcToolbox button in the Standard Toolbar in ArcMap.
        14.1.1. Navigate to ***Data Management Tools*** > ***Projections and Transformations***.
        14.1.2. Right-click on the ***Project*** tool, and select ***Batch***.
            14.1.2.1. ***Input Dataset or Feature Class***: double-click and select **FtHua_Boundary**.
            14.1.2.2. ***Output Dataset or Feature Class***: right-click, select ***Browse***.
                14.1.2.2.1. Navigate to the folder **C:\AGWA\GISdata\FortHuachuca**.
                14.1.2.2.2. Name the file **FH_Bound_utm12**.
            14.1.2.3. ***Output Coordinate System***: double-click and select the Spatial Reference Properties button .
                14.1.2.3.1. Expand the ***Projected Coordinate Systems*** folder, expand the ***UTM*** folder, expand the ***NAD 1983*** folder then select **NAD_1983_UTM_Zone_12N**.
            14.1.2.4. ***Geographic Transformation***: leave blank.
            14.1.2.5. ***Input Coordinate System***: do nothing.
        14.1.3. Click the Add Row button . Fill out the second row.
            14.1.3.1. ***Input Dataset or Feature Class***: double-click and select **WBDHU12**.
            14.1.3.2. ***Output Dataset or Feature Class***: right-click, select ***Browse***.
                14.1.3.2.1. Navigate to the folder **C:\AGWA\GISdata\FortHuachuca**.

14.1.3.2.2. Name the file **HUC12_utm12**.

14.1.3.3. ***Output Coordinate System***: double-click and select the Spatial Reference Properties button .

14.1.3.3.1. Select **NAD_1983_UTM_Zone_12N**.

14.1.3.3.2. ***Geographic Transformation*: leave at its pre-populated value-*WGS_1984_(ITRF00)_To_NAD_1983.**

14.1.3.3.3. ***Input Coordinate System*: do nothing.**

14.1.4. Click the Add Row button . Fill out the third row.

14.1.4.1. ***Input Dataset or Feature Class***: double-click and select **soilmu_a_az671**.

14.1.4.2. ***Output Dataset or Feature Class***: right-click, select ***Browse***.

14.1.4.2.1. Navigate to the folder **C:\AGWA\GISdata\FortHuachuca**.

14.1.4.2.2. Name the file **ssurgo_utm12**.

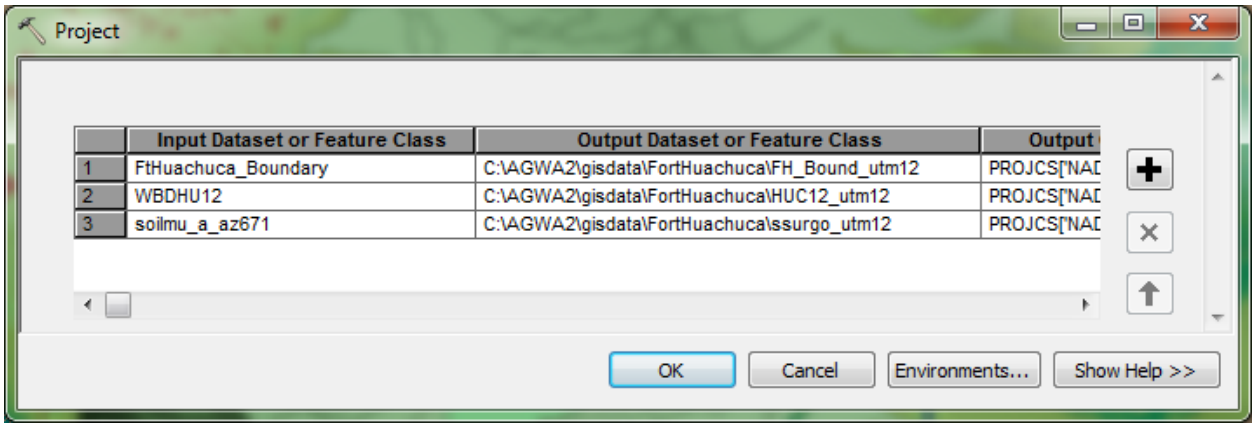
14.1.4.3. ***Output Coordinate System***: double-click and select the Spatial Reference Properties button .

14.1.4.3.1. Expand the ***Layers*** folder, and select **NAD_1983_UTM_Zone_12N**.

14.1.4.3.2. ***Geographic Transformation*: leave at its pre-populated value-*WGS_1984_(ITRF00)_To_NAD_1983.**

14.1.4.3.3. ***Input Coordinate System*: do nothing.**

14.1.5. **Click *OK*. Wait for the *Project* tool to run, which will create two new shapefiles.**



NOTE: Projected data will not automatically be added to the map; to add the data press the add data button and select these features, and remove the unprojected data.

14.2. **Return to ArcToolbox. Now reproject the raster layers.**

14.2.1. Navigate to ***Data Management Tools* > *Projections and Transformations* > *Raster***.

14.2.2. **Right-click on the *Project Raster* tool, and select *Batch*.**

14.2.2.1. ***Input Raster*: double-click and select grdn32w111_13.**

14.2.2.2. ***Output Raster Dataset*: right-click and select *Browse*.**

14.2.2.2.1. **Navigate to the folder C:\AGWA\GISdata\FortHuachuca**

14.2.2.2.2. Name the file **10mDEM_utm12**

14.2.2.3. ***Output Coordinate System*: double-click and select the** Spatial Reference Properties button .

14.2.2.3.1. **Expand the *Layers* folder, and select NAD_1983_UTM_Zone_12N**.

14.2.2.4. ***Resampling Technique*: click the drop-down arrow and select Bilinear.**

14.2.2.5. **Do not alter any of the other columns.**

14.2.3. Click the Add Row button . Fill out the second row.

14.2.3.1. ***Input Raster***: double-click and select **gaplndcov_az**

14.2.3.2. ***Output Raster Dataset***: right-click, select ***Browse***.

14.2.3.2.1. Navigate to the folder **C:\AGWA\GISdata\FortHuachuca**.

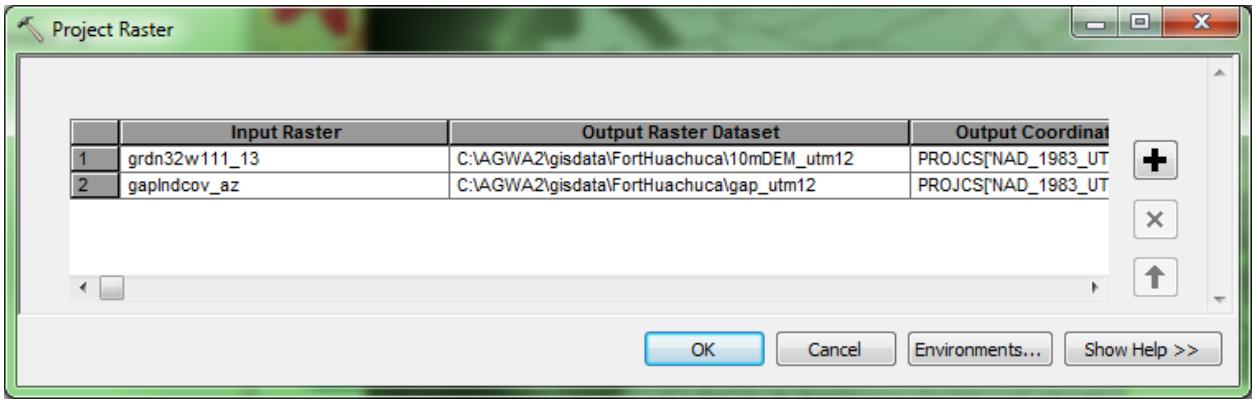
14.2.3.2.2. Name the file **gap_utm12**.

14.2.3.3. ***Output Coordinate System***: double-click and select the Spatial Reference Properties button .

14.2.3.3.1. Expand the ***Layers*** folder, and select **NAD_1983_UTM_Zone_12N**.

14.2.3.3.2. ***Resampling Technique*: leave at the default - Nearest.**

14.2.3.4. **Do not alter any of the other columns.**



14.2.4. **Click *OK*. Wait for the *Project Raster* tool to run, which will create two new rasters.**

NOTE: Remember reprojected data will not be added to the map automatically.

Part 2: Clip the Data to a Suitable Project Area

In Part 2, the reprojected data will be clipped to a project area. Depending on the original dataset sizes and the clipped areas of interest, this may significantly reduce processing time during AGWA steps involving raster data. In this exercise, the DEM, Land Cover layer, and soils layer are all regional in scale at this point, and should be clipped.

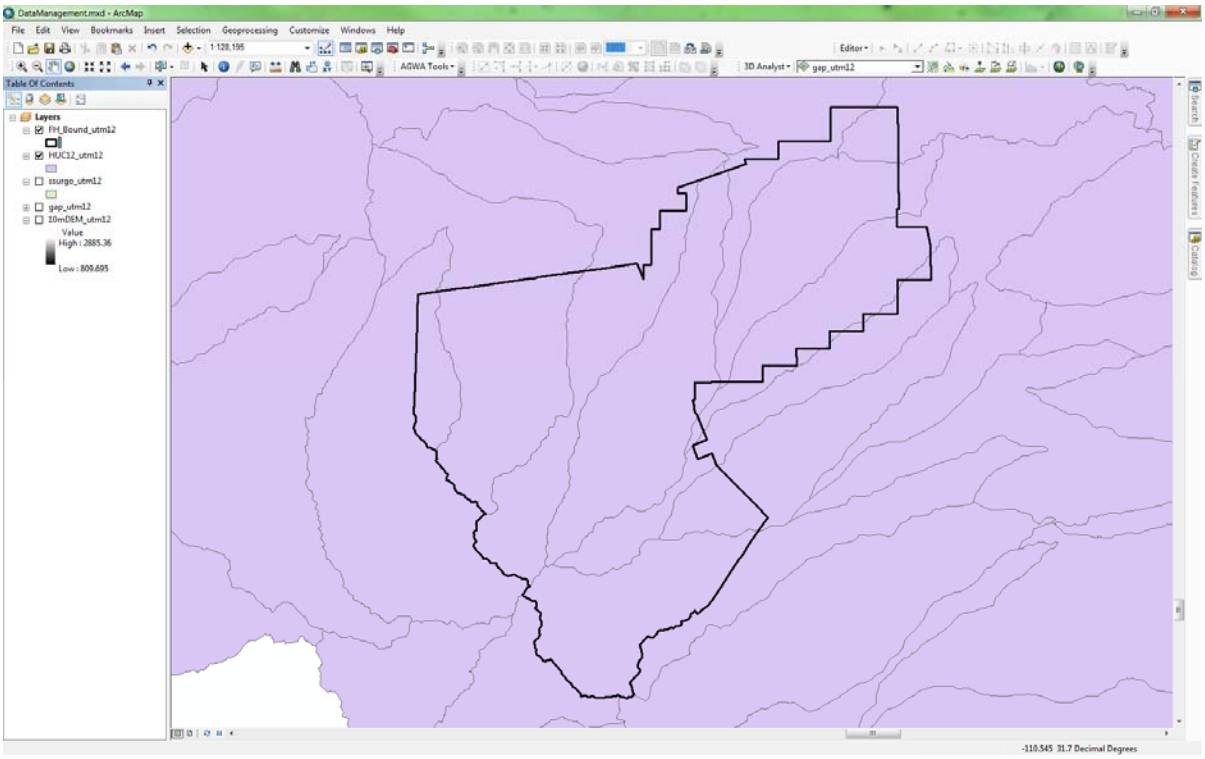
Step 1: Create a Suitable Project Area Shapefile

Deciding on a suitable clip size depends on your data and area of interest. For a burned area scenario, one might want to choose the fire perimeter as the project area. However, watersheds do not conform to the burn area, so a wider project area is needed. In this exercise, the intersection of the HUC12 and the Fort Huachuca boundary will be used.

15. View the scale of the project area.

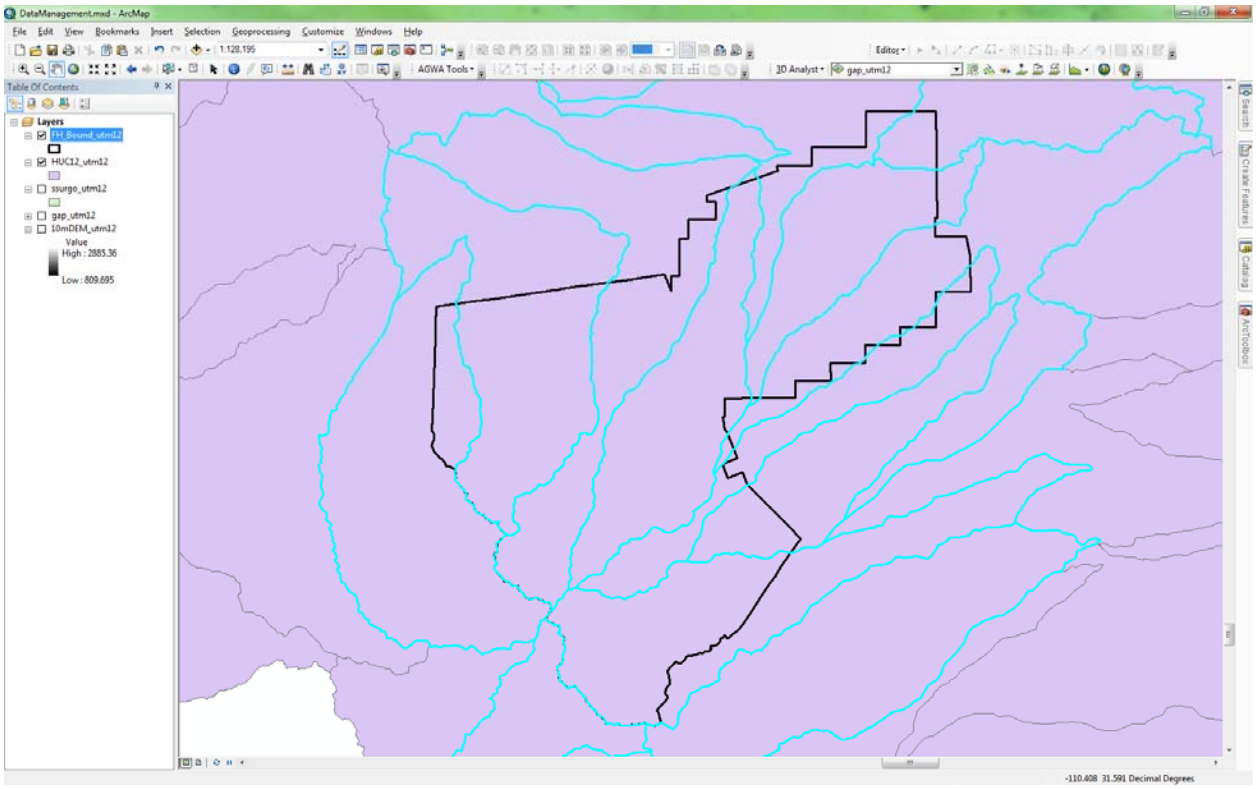
15.1. In the Table of Contents, turn on the ***HUC12_utm12*** and ***FH_Bound_utm12*** layers. Turn all other layers off. Drag the ***FH_Bound_utm12*** layer above the ***HUC12_utm12*** layer. Zoom to the ***FH_Bound_utm12*** layer.

15.2. Change the symbology of ***FH_Bound_utm12*** so it is hollow.



Notice that the boundary crosses various HUC12 watershed boundaries. To model all of the watersheds within Fort Huachuca, the clipped area should include all HUC12 watersheds that intersect Fort Huachuca.

16. Select all the HUC12s that intersect with the Fort Huachuca boundary.
    16.1. Under the ***Selection*** menu on the ArcMap menu bar, choose ***Select by Location …***
        16.1.1. ***Selection method***: select features from
        16.1.2. ***Target layer(s)***: check **HUC12_utm12**
        16.1.3. ***Source layer***: **FH_Bound_utm12**
        16.1.4. ***Spatial selection method for target layer feature(s)***: **intersect the source layer feature**
    16.2. Press ***OK***.



All the HUC12s that intersect with the Fort Huachuca boundary are now selected.

16.3. Open ArcToolbox again. Create a new shapefile of only the selected HUC12s.

16.3.1. Navigate to ***Analysis Tools > Extract***.

16.3.2. Double-click on the ***Select*** tool to open the tool.

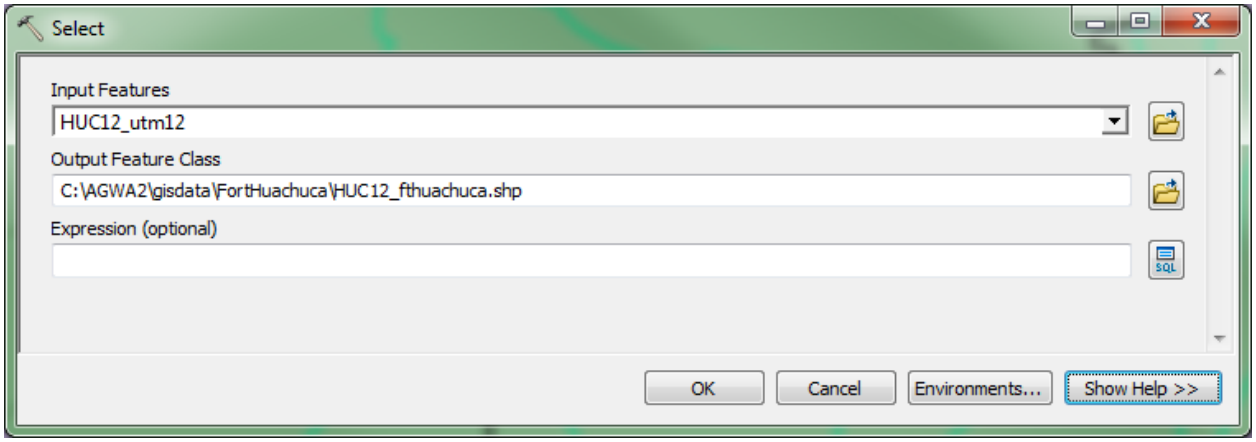
16.3.2.1. ***Input Features***: **HUC12_utm12**

16.3.2.2. ***Output Feature Class***: Click the ***Browse*** button.

16.3.2.2.1. Navigate to **C:\AGWA\GISdata\FortHuachuca\.**

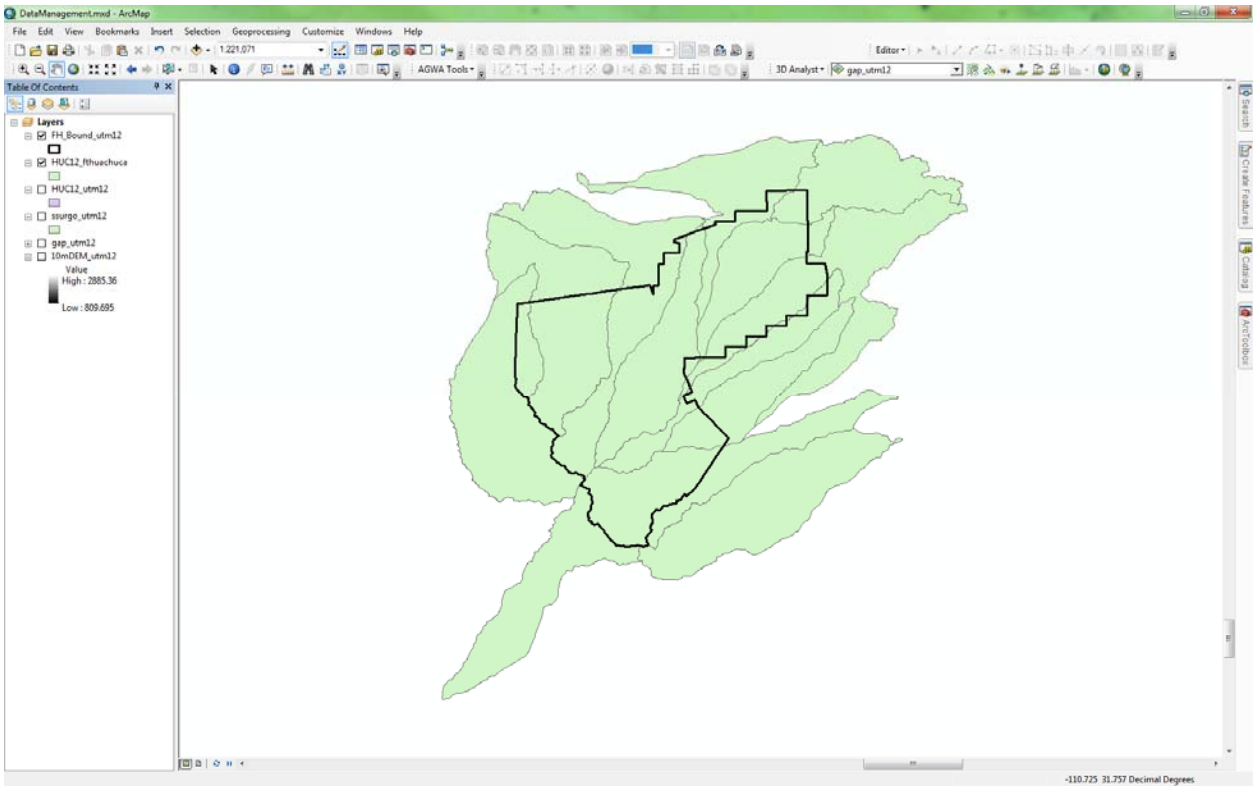
16.3.2.2.2. Name the file **HUC12_fthuachuca.shp**.

16.3.2.3. ***Expression (optional)***: leave blank.



16.4. Press ***OK***. **Wait for the *Select* tool to run, which will create a new shapefile of only the selected HUC12s.**

16.5. **Zoom to the new layer *HUC12_fthuachuca*, and place the boundary layer over it.**



17. Merge all the polygons within the project area, and buffer the polygon.

17.1. In the Table of Contents, turn off the ***FH_Bound_utm12*** layer.

17.2. In the ***Customize*** menu of the ArcMap menu bar, select ***Toolbars*** > ***Editor***. The Editor toolbar will appear.

17.2.1. In the ***Editor*** dropdown menu, select **Start Editing**.

17.2.2. In the ***Start Editing*** window, select **HUC12_fthuachuca**, and press ***OK***.

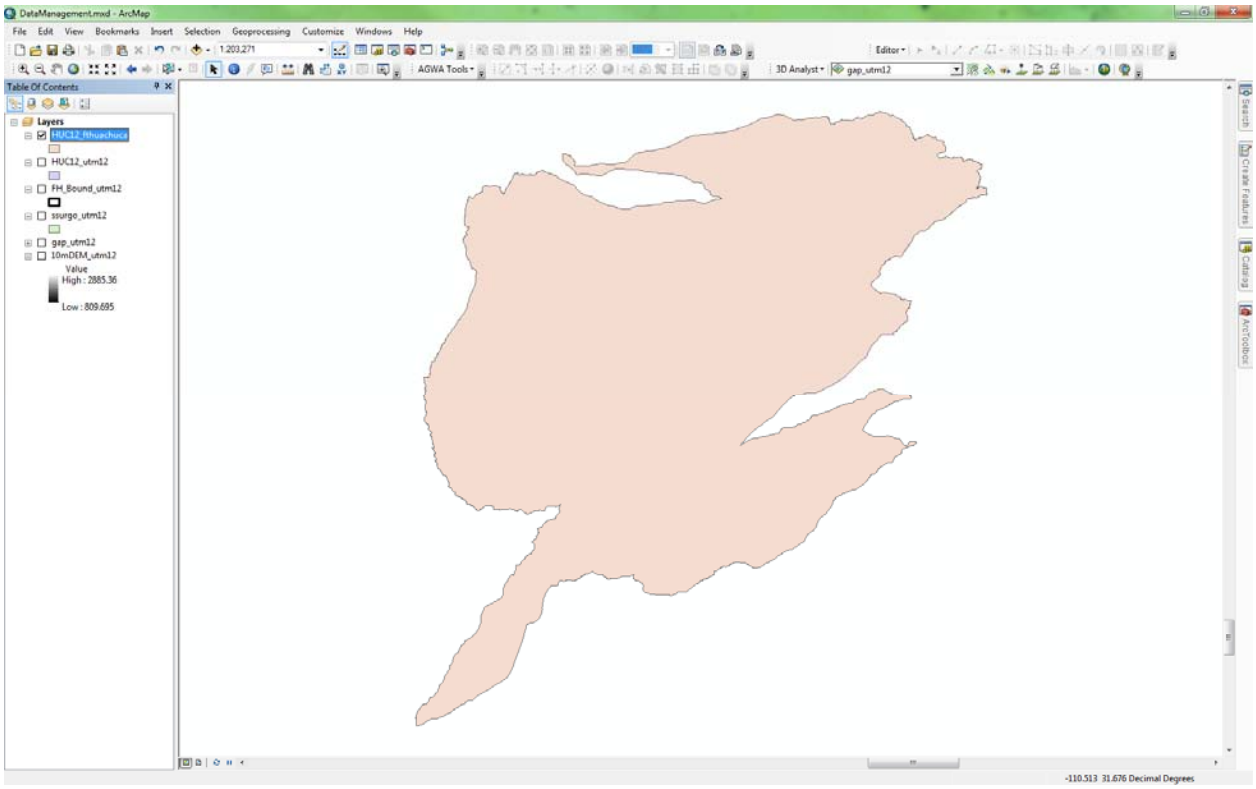
17.2.2.1. If the ***Start Editing*** window appears with warnings about Spatial references click ***Continue***.

17.2.3. In the Tools toolbar in ArcMap, click the Select Features button .

17.2.3.1. Click and drag a rectangle around the entire ***HUC12_fthuachuca*** layer, so all polygons are selected.

17.2.4. In the Editor dropdown menu, select **Merge…** and press ***OK***.

17.2.5. In the Editor dropdown menu, select **Save Edits** then **Stop Editing**.



Now that a suitable project area has been made, it is always good practice to buffer the area in case DEM drainages do not match the HUC maps exactly.

17.3. Open ArcToolbox again.

17.3.1. Navigate to ***Analysis Tools*** > ***Proximity***.

17.3.2. Double-click on the ***Buffer*** tool to open the tool.

17.3.2.1. ***Input Features***: **HUC_fthuachuca**

17.3.2.2. ***Output Feature Class***: press the ***Browse*** button.

17.3.2.2.1. Navigate to **C:\AGWA\GISdata\FortHuachuca**.

17.3.2.2.2. Name the file **HUC_buff1km.shp**.

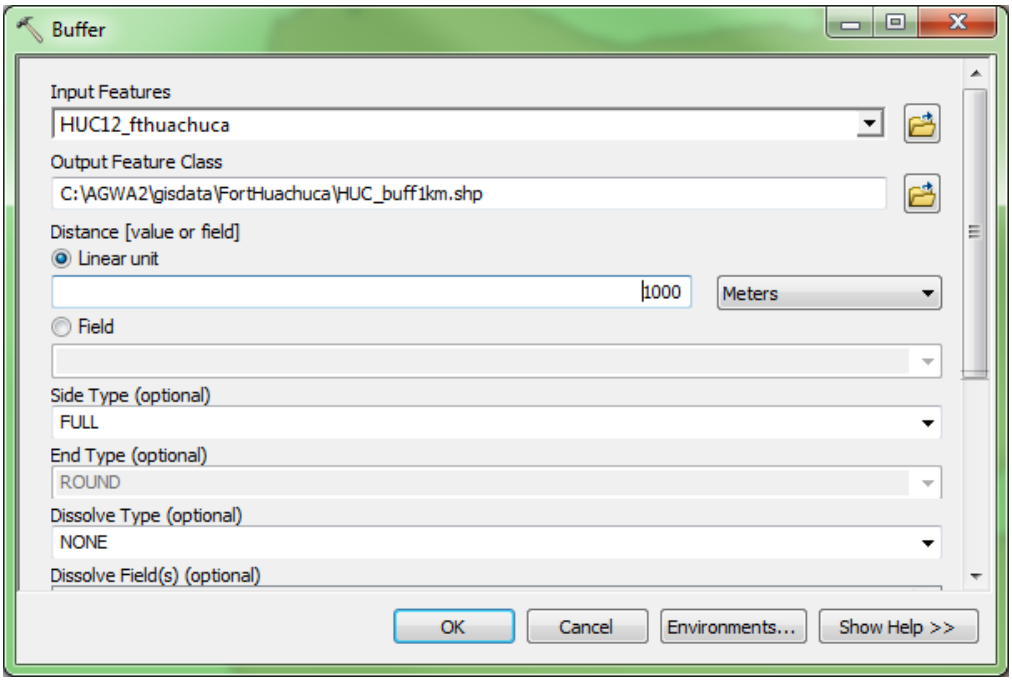
17.3.2.3. ***Distance [value or field]***:

17.3.2.3.1. Select the **Linear** unit radiobutton.

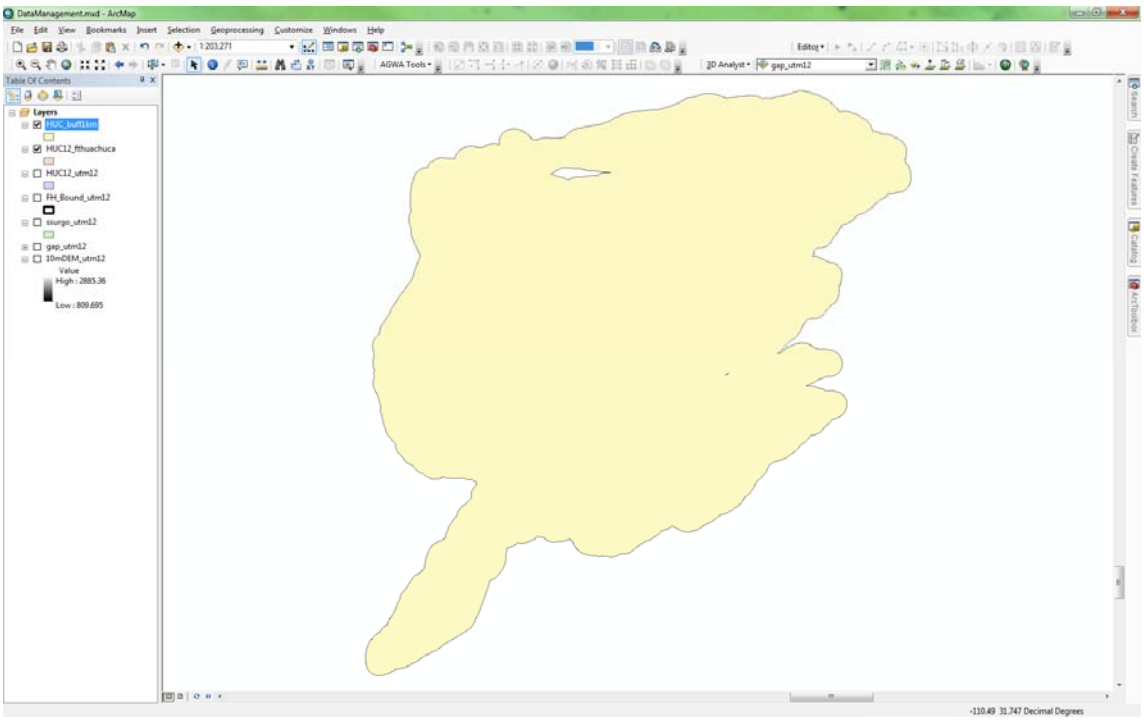
17.3.2.3.2. Type **1000**.

17.3.2.3.3. Keep the units as **Meters**.

17.3.2.4. Leave all other fields as the defaults.



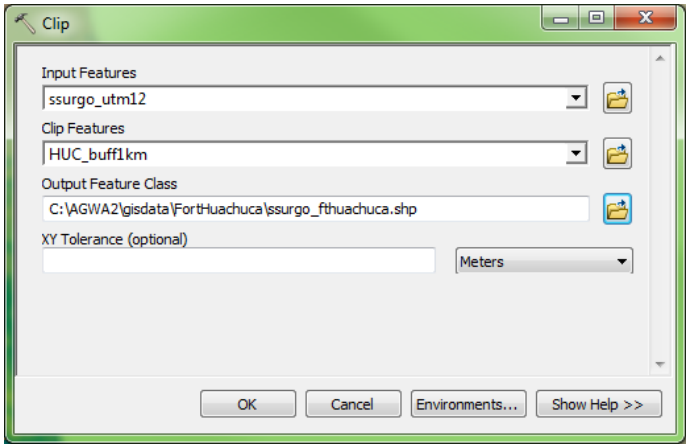
17.3.2.5. Press OK. **Wait for the *Buffer* tool to run, which will create a new shapefile.**



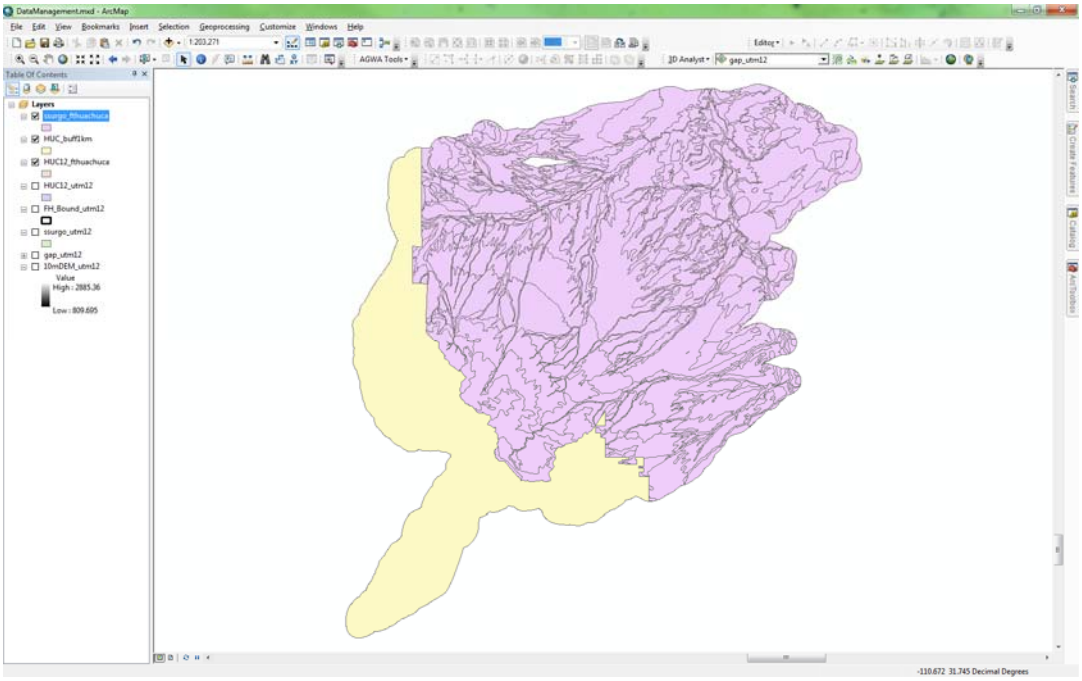
Step 2: Clip the Input GIS Layers to the Project Area Shapefile

Now that a suitable, buffered project area has been created, the large DEM, land cover, and soils layers can be clipped.

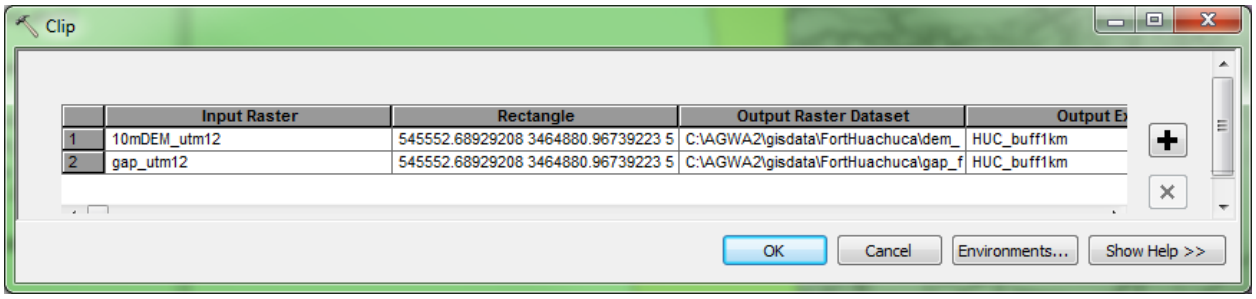
18. Use the Clip tool to clip the shapefile layers to the project area.
    18.1. Open ArcToolbox again.
        18.1.1. Navigate to ***Analysis Tools > Extract***.
        18.1.2. Double-click on the ***Clip*** tool to open the tool.
            18.1.2.1. ***Input Features***: **ssurgo_utm12**
            18.1.2.2. ***Clip Features***: **HUC_buff1km**
            18.1.2.3. ***Output Feature Class***: Press the ***Browse*** button.
                18.1.2.3.1. Navigate to **C:\AGWA\GISdata\FortHuachuca**.
                18.1.2.3.2. Name the layer **ssurgo_fthuachuca**.
            18.1.2.4. ***XY Tolerance (optional)***: do nothing.



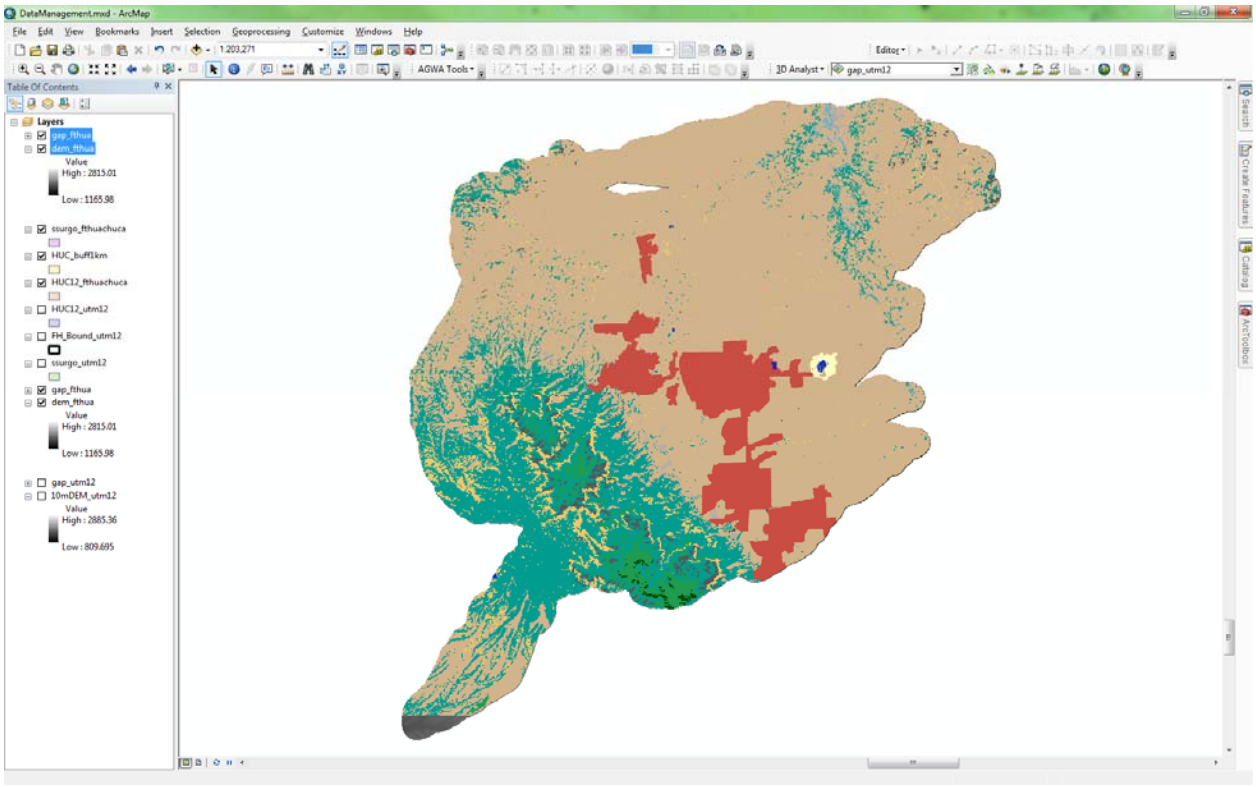
            18.1.2.5. Click ***OK***. **Wait for the *Clip* tool to run, which will create a new soils shapefile.**



19. Use the raster Clip tool to clip the rasters to the project area.
    19.1. Open ArcToolbox again.
        19.1.1. Navigate to ***Data Management Tools*** > ***Raster*** > ***Raster Processing***.
        19.1.2. Right-click on the ***Clip*** tool and select ***Batch***.
            19.1.2.1. ***Input Raster***: double-click and select **10mDEM_utm12**.
            19.1.2.2. ***Rectangle***: do nothing.
            19.1.2.3. ***Output Raster Dataset***: Right-click and select ***Browse***.
                19.1.2.3.1. Navigate to **C:\AGWA\GISdata\FortHuachuca**.
                19.1.2.3.2. Name the layer **dem_fthua**.
            19.1.2.4. ***Output Extent***: double-click and select **HUC_buff1km**.
            19.1.2.5. ***NoData Value***: do nothing
            19.1.2.6. ***Use Input Features for Clipping Geometry***: right-click and select Open
                19.1.2.6.1. Check the ***Use Input Features for Clipping Geometry*** box.
            19.1.2.7. ***Maintain Clipping Extent***: do nothing.
        19.1.3. Click the Add Row button ✚. Fill out the second row.
            19.1.3.1. ***Input Raster***: double-click and select **gap_utm12**.
            19.1.3.2. ***Rectangle***: do nothing.
            19.1.3.3. ***Output Feature Class***: Right-click and select ***Browse***.
                19.1.3.3.1. Navigate to **C:\AGWA\GISdata\FortHuachuca**.
                19.1.3.3.2. Name the layer **nlcd_mtnfire**.
            19.1.3.4. ***Output Extent***: double-click and select **HUC_buff1km**.
            19.1.3.5. ***NoData Value***: do nothing
            19.1.3.6. ***Use Input Features for Clipping Geometry***: right-click and select Open
                19.1.3.6.1. Check the ***Use Input Features for Clipping Geometry*** box.
            19.1.3.7. ***Maintain Clipping Extent***: do nothing.



        19.1.4. Click OK. **Wait for the *Clip* tool to run, which will create DEM and land cover rasters.**



20. Import renderers to enhance visualization of land cover.

Part 3: Preparing the Precipitation Data

SWAT Precipitation

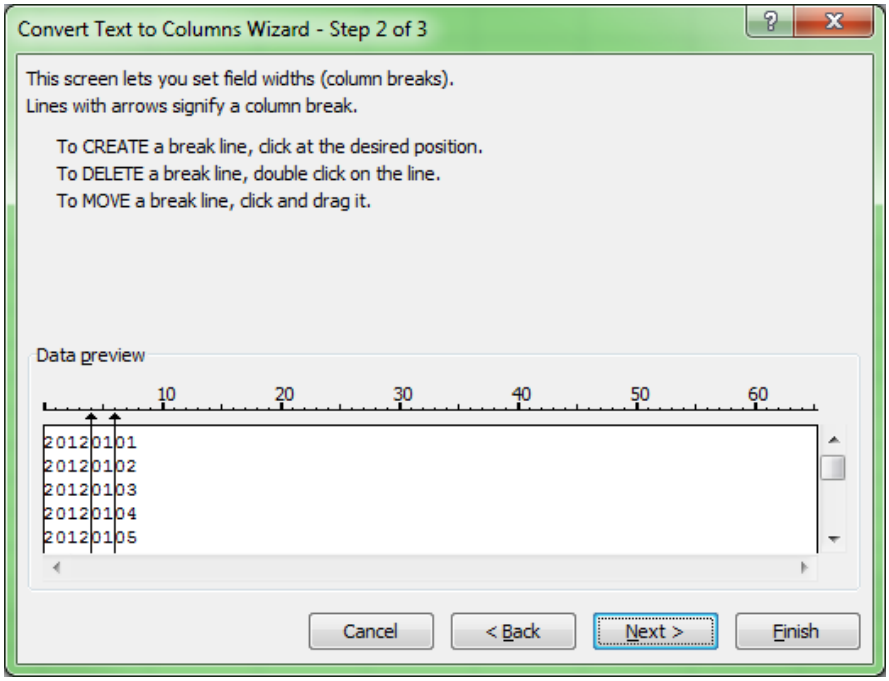
SWAT precipitation needs to be in a certain format for AGWA to read it as an input file. This is refered to as an unweighted precipitation file that contains a minimum of three fields: YEAR, DAY, and a gage field named G<gage id>. DAY is the Julian day of the year (1-366) with values repeating for each year in the record. It is recommended that to capture long term trends of a climatic region that at least 30 years of record are used in this step; however, due to data availability this may not always be possible. The gage id in the G<gage id> field must match the ids in the gage field of the rain gage point theme.

Weighted averages will be adjusted for missing or negative precipitation values. Missing data should be indicated with a -99.0. This section will guide you through creating a point file for rain gages and formatting the unweighted precipitation file for input. The example will be for only one rain gage acquired from GHCN; however, the same process can be repeated for multiple gages from any data source.

21. Open the GHCN csv file in Excel
    21.1. Save this file as 3124_pcp in the GISdata/FortHuachuca folder.
22. Format Precipitation Values
    22.1. Delete the first five columns of data (STATION, STATION_NAME, ELEVATION, LATITUDE, and LONGITUDE).
    22.2. Add two new columns: PRCP (mm) and G3124

22.3. Populate the PRCP (mm) column by dividing values in the PRCP column by 10
  22.3.1. C#=B#/10
22.4. Populate the G3124 by copying PRCP (mm) values into the new column
  22.4.1. Paste values only.
22.5. Clear contents in both the PRCP and PRCP (mm) columns, and leave these two blank columns there.

23. Format the Date
23.1. Select Column A
23.2. Use the Excel tool Text to Columns, usually found under the Data tab in Excel (depending on the version of Microsoft Office).
23.3. This opens a new window, Select Fixed Width.
23.4. Set spacers between the year, the month and the day.



23.5. Click Next
23.6. This creates a year, month and day column.

Year	Month	Day	G3124
2012	1	1	0
2012	1	2	0
2012	1	3	0
2012	1	4	0

23.7. Insert a new column titled Date between Day and G3124
23.8. Reformat date information into the format of MM/DD/YYYY
  23.8.1. Use the Excel formula = DATE(year,month,day)

23.9. Insert a new column titled Julian between Date and G3124.

23.9.1. Populate this column using the following formula:

=TEXT(D2,"yyyy")&TEXT((D2-DATEVALUE("1/1/"&TEXT(D2,"yy"))+1),"000")

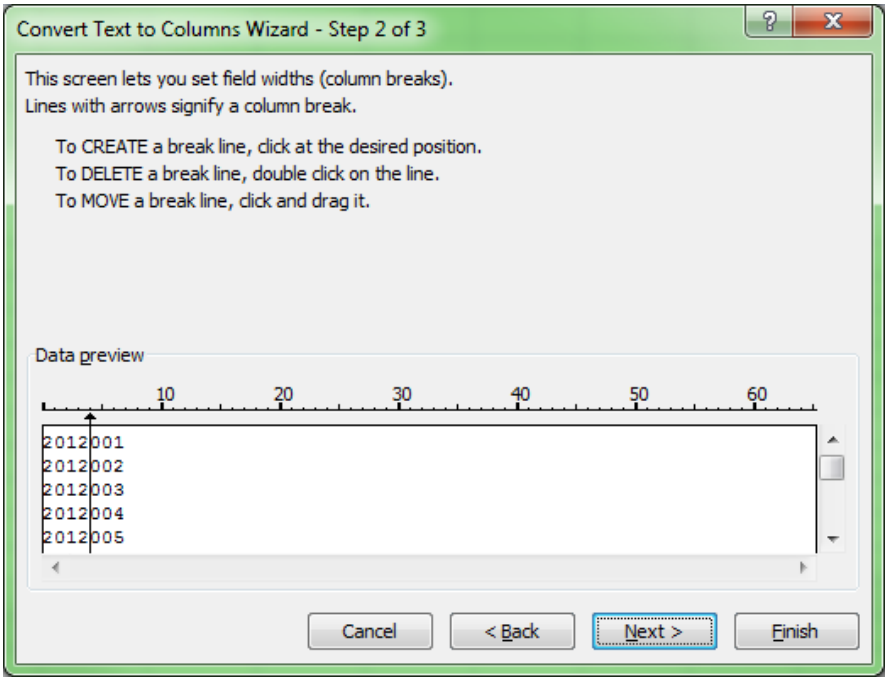
23.9.2. Copy this Column to the Year Column

23.9.3. Past values only.

23.10. Delete Columns C through E.

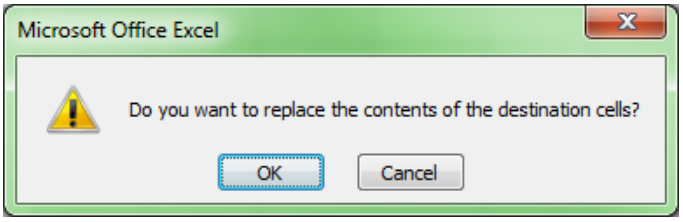
23.11. Use the Text to Columns tool again

23.11.1. Select Column A and used Fixed Width



23.11.2. Click Finish.

23.11.3. A Message will appear, click OK.



23.12. Rename Column A: YEAR

23.13. Rename Column B: DAY

23.14. Save this document and exit.

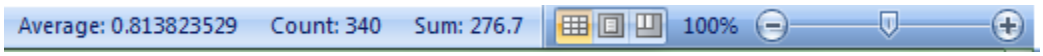
24. Populate Missing values with "-99"

24.1. Writing precipitation in AGWA will run smoothly if all of the input files are correctly configured. However, the configuration of these files can be very time consuming. This step will outline the process of adding missing dates and populating them.

24.2. First, start by looking through the data you downloaded. For this case we have data for 2012 which happens to be a leap year. So we expect to have 366 days of precipitation measurements (e.g. 366 cells below the heading G3124).

24.2.1. To check for missing data you can use any Excel counting tool.

24.2.1.1. For this example simply select all of the cells below G3124 to display a count in the lower right corner of Excel.



24.2.1.2. This indicates we are missing 26 days of data. With the date formatted in Julian day it should be easy to locate where these days are.

24.2.1.3. The first set of missing days is 12-16.

24.2.1.4. Starting at Julian day 17, drag down five rows of data, right click and select insert. This should result in 5 new rows to populate.

YEAR	DAY	G3124
2012	1	0
2012	2	0
2012	3	0
2012	4	0
2012	5	0
2012	6	0
2012	7	0
2012	8	0
2012	9	0
2012	10	0
2012	11	0
2012	17	0

24.2.1.5. Fill in the date accordingly then populate G3124 column with “-99”.

24.2.1.6. Continue this process identifying all gaps in data and populating them.

24.2.1.7. Save the file.

24.2.2. For larger datasets this may be automated using a variety of software products.

25. Create the rain gage point file.

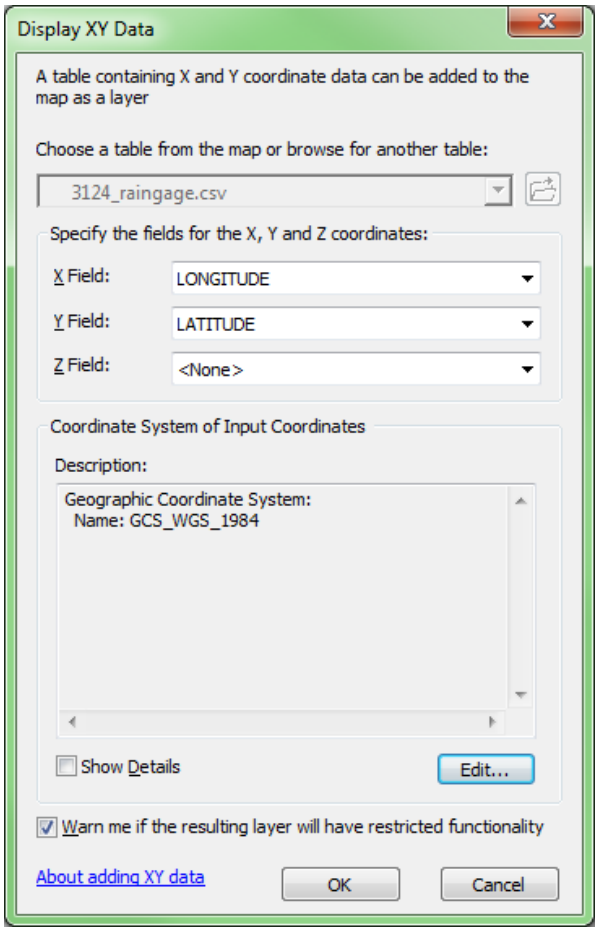
25.1. Open the raw GHCN csv file from the downloads folder.

25.2. Save it as 3124_raingage.csv in the GISdata folder

25.3. Delete everything except rows 1 and 2.

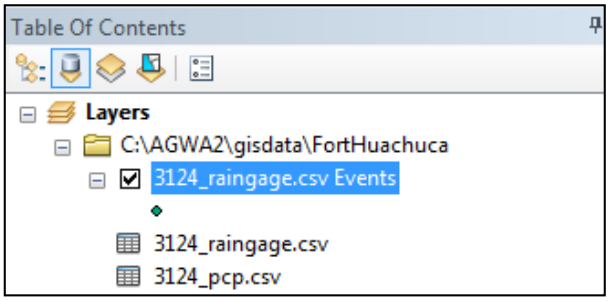
25.4. Add two new columns to the end: END_DATE and GAGE_ID
25.4.1. END_DATE will be populated with 20121231
25.4.2. GAGE_ID will be populated with 3124

26. Bring both of these files into ArcMap.
26.1. Use the Add Data button to add both the 3124_pcp.csv and the 3124_raingage.csv to the DataManagement map document.
26.2. In the table of contents, right click on the 3124_raingage.csv file
26.2.1. Select display XY Data.
26.2.1.1. X Field: Longitude
26.2.1.2. Y Field: Latitude
26.2.1.3. Z Field: None
26.2.1.4. Coordinate System of Input Coordinates: Select Edit
26.2.1.4.1. Search WGS 1984
26.2.1.4.2. Expand Geographic Coordinate Systems →World
26.2.1.4.3. Select WGS 1984
26.2.1.4.4. Click OK



26.2.1.5. Click OK
26.2.1.6. A dialogue will appear with “Table Does not Have Object-ID Field”. Click OK.

26.2.2. A new Event will appear in the table of contents. This will need to be exported to become a permanent shapefile.



26.3. Export the Event as a shapefile

26.3.1. Right click on the Event

26.3.2. Select data→Export Data…

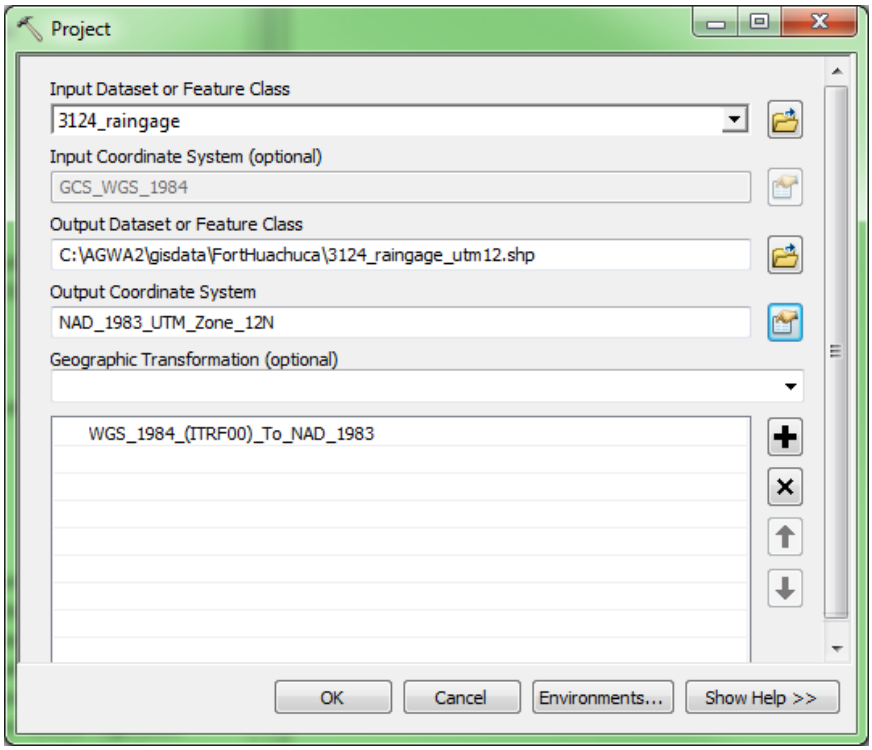
26.3.3. Browse to the GISdata/FortHuachuca folder and save the shapefile as 3124_raingage.shp

26.3.4. Click OK

26.3.5. When prompted to add the exported data to the map as a layer, Click Yes.

26.4. Project the new shapefile.

26.4.1. Open the Project Tool (See Part 1).



26.4.2. Click OK

27. Export the 3124_pcp.csv as a dBase Table.

27.1. Right click on the file in the ArcMap table of contents.

27.1.1. Select Data→Export Data…

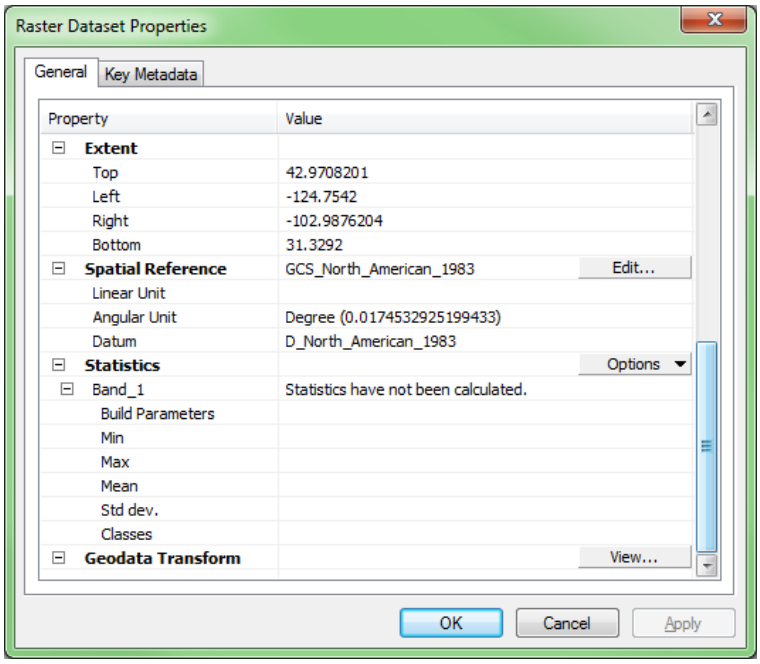
27.1.2. Browse to GISdata/FortHuachuca
27.1.3. Save this file
27.1.3.1. Name: 3124_pcp.dbf
27.1.3.2. Save as type: dBASE Table.
27.1.3.3. Click OK
27.1.3.4. Add the new table to the map document.

KINEROS2 NOAA Precipitation

KINEROS2 precipitation data needs to be in a certain format for AGWA to read it as an input file. This section will describe how to create a design storm input file using the NOAA Precipitation Frequency data.

28. Convert NOAA precipitation frequency grid to another format.

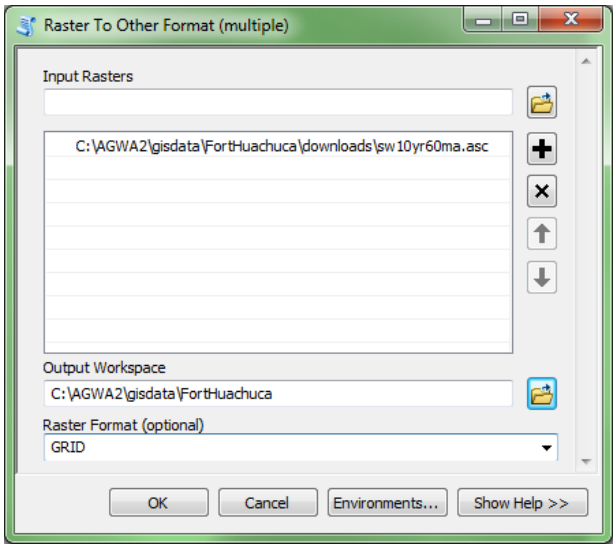
28.1. Open ArcCatalog in the DataManagement map document from the Standard toolbar.
28.1.1. Navigate to GISdata/FortHuachuca/downloads.
28.1.2. Right click on sw10yr60ma.asc in this folder.
28.1.3. Select Properties.
28.1.4. Scroll down to Spatial Reference which is undefined at this point.
28.1.5. Click Edit
28.1.5.1. Search NAD 1983
28.1.5.2. Expand Geographic Coordinate Systems→North America
28.1.5.3. Select NAD 1983
28.1.5.4. Click OK



28.1.6. Click Apply, then Click OK

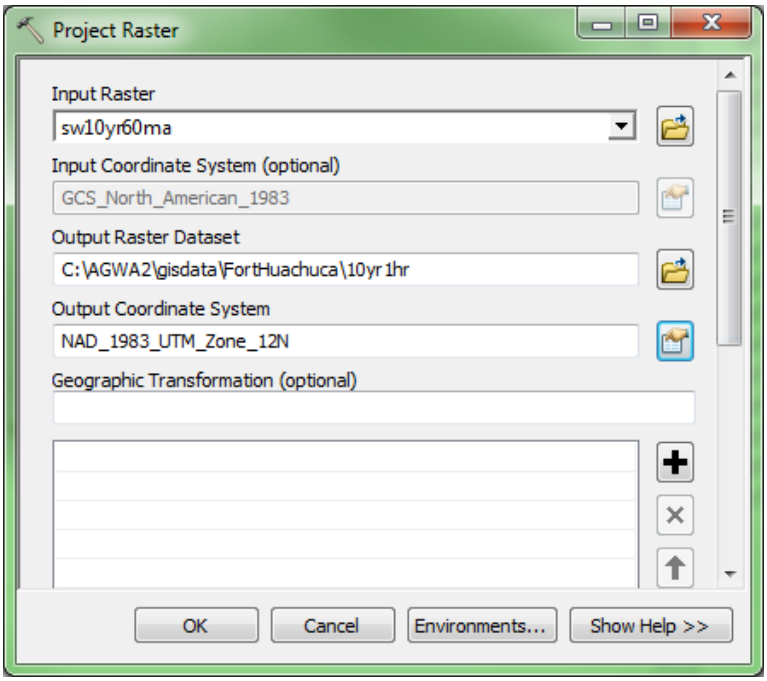
28.2. Add the sw10yr60ma.asc grid to the DataManagement map document. (Building Pyramids is optional)
28.3. An error message will appear with "Unknown Spatial Reference". We will address this issue shortly.
28.4. Add this grid to the Map Document by dragging it from the ArcCatalog window into the table of contents or viewer.

29. Convert the .asc grid to ESRI grid format.
29.1. Expand the Conversion Tools in ArcToolbox
29.2. Expand To Raster
29.3. Select Raster to Other Format (multiple)
29.3.1. Browse to the GISdata/downloads folder and select the sw10yr60ma.asc file as an input raster.
29.3.2. Designate the output workspace as GISdata/FortHuachuca
29.3.3. Select GRID as the Raster Format



29.3.4. Click OK.
29.3.5. The output Raster will need to be added to the map document.

30. Project the NOAA Grid
30.1. Go to Data Management → Projections and Transformations → Rasters
30.2. Open Project Raster.

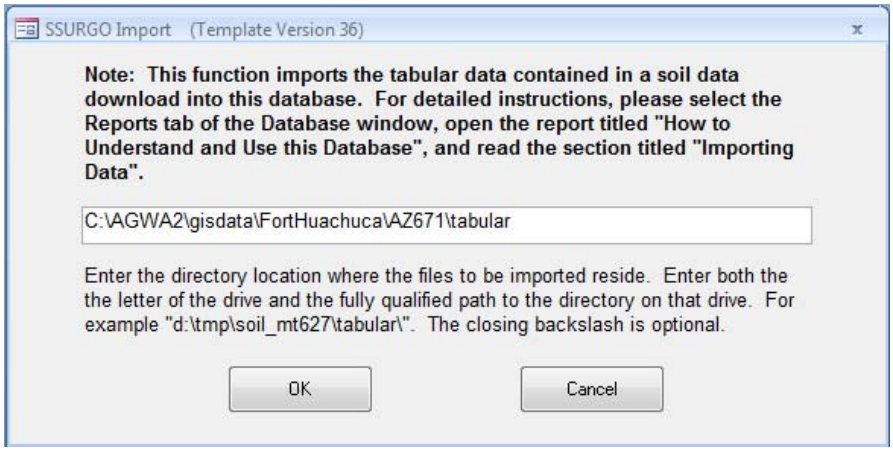


Part 4: Preparing the Soils Database

Although the GIS layers are ready for AGWA modeling, one final step is necessary. This involves importing the tabular soils data into to the SSURGO MS Access database. This is necessary for AGWA to access the correct soils information in the soils database.

Step 1: Import Tabular Data into SSURGO Database

31. Open the MS Access database and import tabular data.
    31.1. In Windows Explorer, navigate to **C:\AGWA\GISdata\FortHuachuca\AZ671\.**
        31.1.1. Open ***soildb_US_2003.mdb***.
            31.1.1.1. In the ***Action Failed*** window, select **Stop All Macros**.
            31.1.1.2. In the ***Security Warning*** banner at the top of the page, select Options...
                31.1.1.2.1. Select the ***Enable this content*** radiobutton, and click ***OK***.
            31.1.1.3. The SSURGO Import window will appear. In Windows Explorer, open the ***tabular*** folder.
                31.1.1.3.1. Select and copy the file path for this folder: ***C:\AGWA\GISdata\FortHuachuca\AZ671\tabular***.
            31.1.1.4. Paste the file path in the SSURGO Import window.



31.1.1.5. Press ***OK***. Wait for the database to import the data, then close the database. This dataset is now ready for use in AGWA

AGWA Modeling

Study Area

Fort Huachuca serves mainly as a communication center with minimal ground training activity and is located in the Sonoran-Chihuahuan transition zone in southeastern Arizona. Its eastern boundary runs adjacent to the town of Sierra Vista and includes parts of the Huachuca Mountains to its west, where the only perennial streams included in this study are found. It is the smallest of the four study areas in the SERDP project, covering approximately 127 mi^2 (329 km^2), but receives the most precipitation with an annual average of 15.6 inches (381 mm).

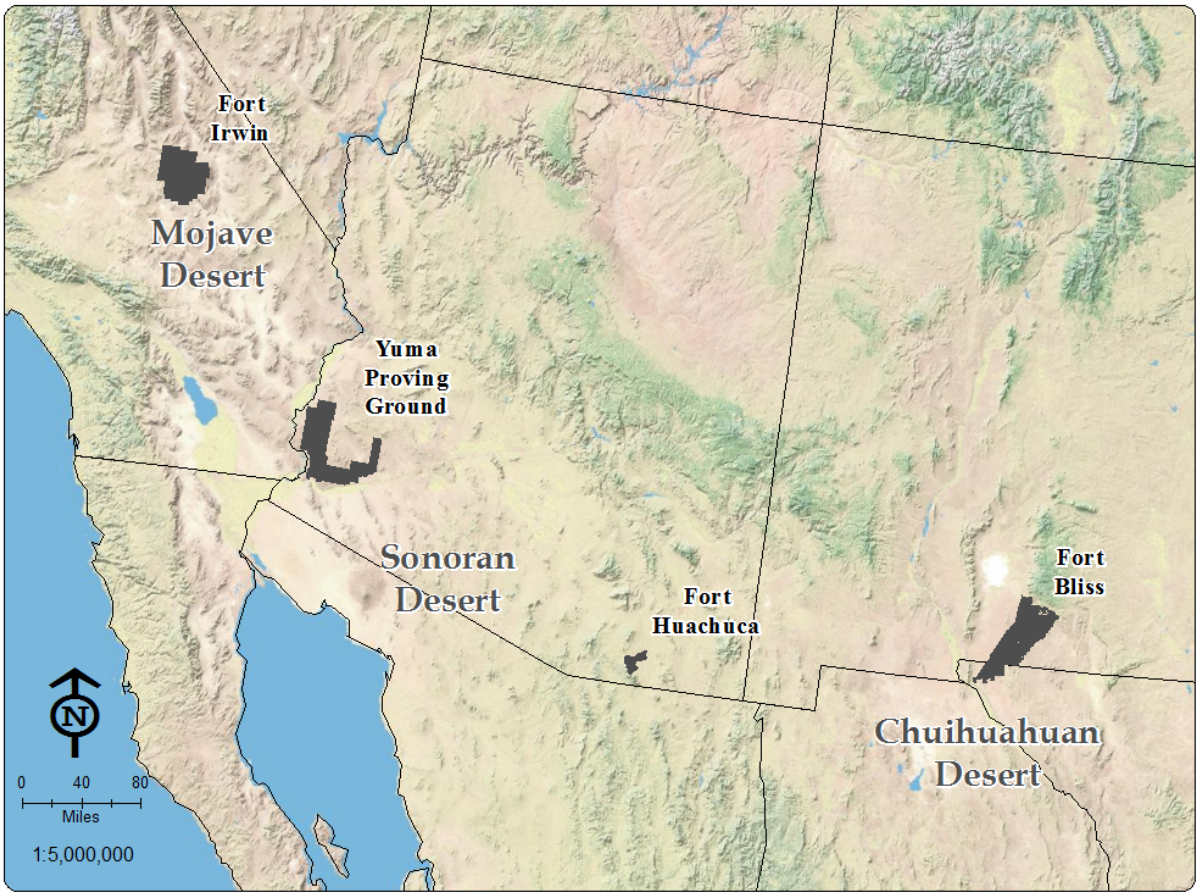


Figure 1. Location of the four military installations used as research sites for the SERDP project; Fort Huachuca is the focus of this guidance document.

Getting Started

Start ArcMap with a new empty map. Save the empty map document as **FortHuachuca** in the **C:\AGWA\mxds** directory. If the ***AGWA Toolbar*** is not visible, turn it on by selecting ***Customize → Toolbars → AGWA Toolbar*** on the ArcMap Main Menu bar. Once the map document is opened and saved, set the Home, Temp, and Default Workspace directories by selecting ***AGWA Tools → Other Options → AGWA Preferences*** on the ***AGWA Toolbar***.

- Home: **C:\AGWA**
- Temp: **C:\AGWA\temp**
- Default Workspace: **C:\AGWA\workspace\FortHuachuca**
  The default workspace location will need to be created by clicking on ***Make New Folder*** button in the window that opens.

The Home directory contains all of the look-up tables, datafiles, models, and documentation required for AGWA to run. If this is set improperly or you are missing any files, you will be presented with a warning that lists the missing directories or files that AGWA requires.

The Temp directory is where some temporary files created during various steps in AGWA will be placed. You may want to routinely delete files and directories in the Temp directory if you need to free up space or are interested in identifying the temporary files associated with your next AGWA use.

The Default Workspace directory is where delineation geodatabases will be stored by default. This can be a helpful timesaver during the navigation process if you have a deeply nested directory structure where you store AGWA outputs.

GIS Data

Add the GIS data to the map by clicking on the *Add Data* button  below the menu bar at the top of the screen. Navigate to the **C:\AGWA\GISdata\FortHuachuca** folder and add the following datasets and layers:

- **filldem_10m**
- **fdgfilldem_1**
- **facgfilldem_**
- **landcover**
- **SSURGO\soil_az671\spatial\soilmu_a_az671.shp**

Add the following files from C:\HydrologicModeling\FortHuachuca.mdb

- **Watersheds\WatershedOutlet**
- **Gauges\NEXRAD_Center**
- **NEXRAD_precip**
- **PrecipFreqInches**

You will also need to add the following files from the **C:\AGWA\datafiles** folder:

- **lc_luts\swgap_lut.dbf** –look-up table for Southwest GAP land cover
- **wgn\wgn_us83.shp** – weather generator stations for SWAT

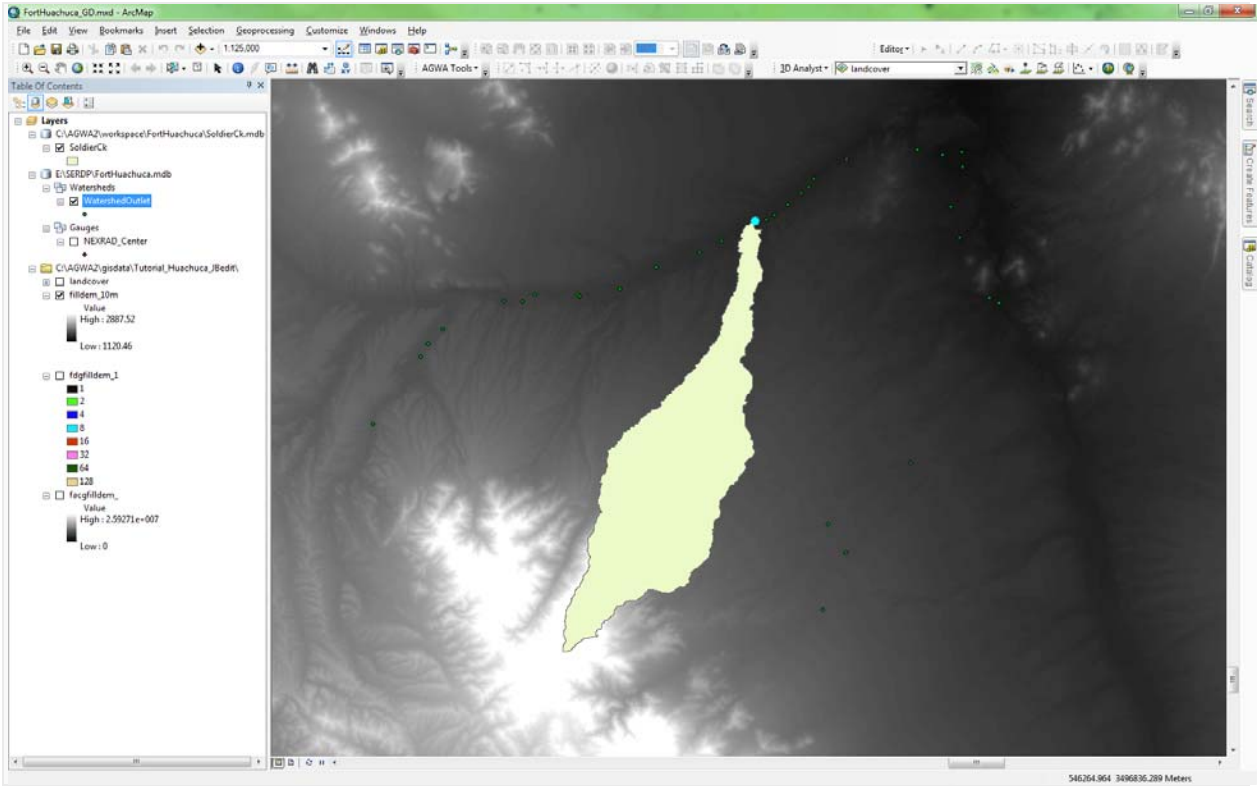
SWAT

The Soil and Water Assessment Tool was used to determine Flow Permanence for stream reaches at Fort Huachuca and the other three intallations for the SERDP project, using the water yield output. This section will outline the process for modeling watersheds using SWAT.

Part 1: Watershed Delineation and Discretization

Before beginning, turn off all layers except WatershedOutlet.shp and filldem_10m.

32. Perform the watershed delineation by selecting the ***Delineate Watershed*** menu item from the ***AGWA Tools → Delineation Options*** menu.
    32.1. ***Output Location*** box
        32.1.1. Workspace textbox: navigate to and select/create **C:\AGWA2\workspace\FortHuachuca**
        32.1.2. ***Geodatabase*** textbox: enter **SoldierCk**
    32.2. ***Input Grids*** box
        32.2.1. ***DEM*** tab: select **filldem_10m** (Do not click Fill)
        32.2.2. ***FDG*** tab: select **fdgfilldem_1** (Do not click Create
        32.2.3. FACG tab: select **facgfilldem_** (Do not click Create)
    32.3. ***Outlet Identification*** box
        32.3.1. ***Point Theme*** tab
            32.3.1.1. ***Outlets Theme***: Select **WatershedOutlet**
            32.3.1.2. Open the WatershedOutlet attribute table by right clicking on the shapefile in the table of contents.
            32.3.1.3. Select **ObjectID15**
            32.3.1.4. Close the attribute table
            32.3.1.5. Using the ***Select Feature*** button in the Delineator form, draw a rectangle around the selected point.
    32.4. CLICK ***Delineate***.



32.5. Save the map document and continue.

At this point, the Soldier Creek watershed is delineated. The workspace specified is the location on your hard drive where the delineated watershed is stored as a feature class in a geodatabase. The discretization created next will also be stored in the geodatabase.

33. Perform the watershed discretization by selecting the ***Discretize Watershed*** menu item from the ***AGWA →Discretization Options*** menu.

33.1. ***Input*** BOX

33.1.1. ***Delineation***: **SoldierCk**

33.2. ***Model Options*** BOX

33.2.1. ***Model***: **SWAT2000**

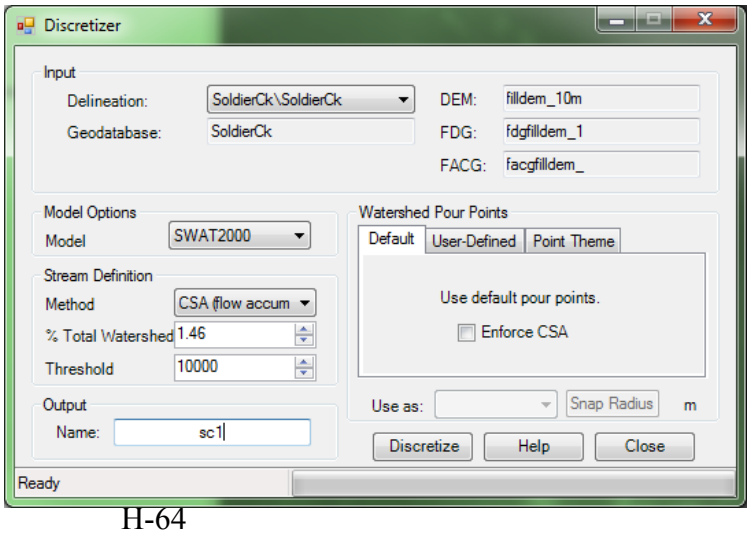
33.3. ***Stream Definition*** BOX

33.3.1. ***Method***: **CSA (flow accumulation)**

33.3.2. ***% Total Watershed***: DO NOTHING

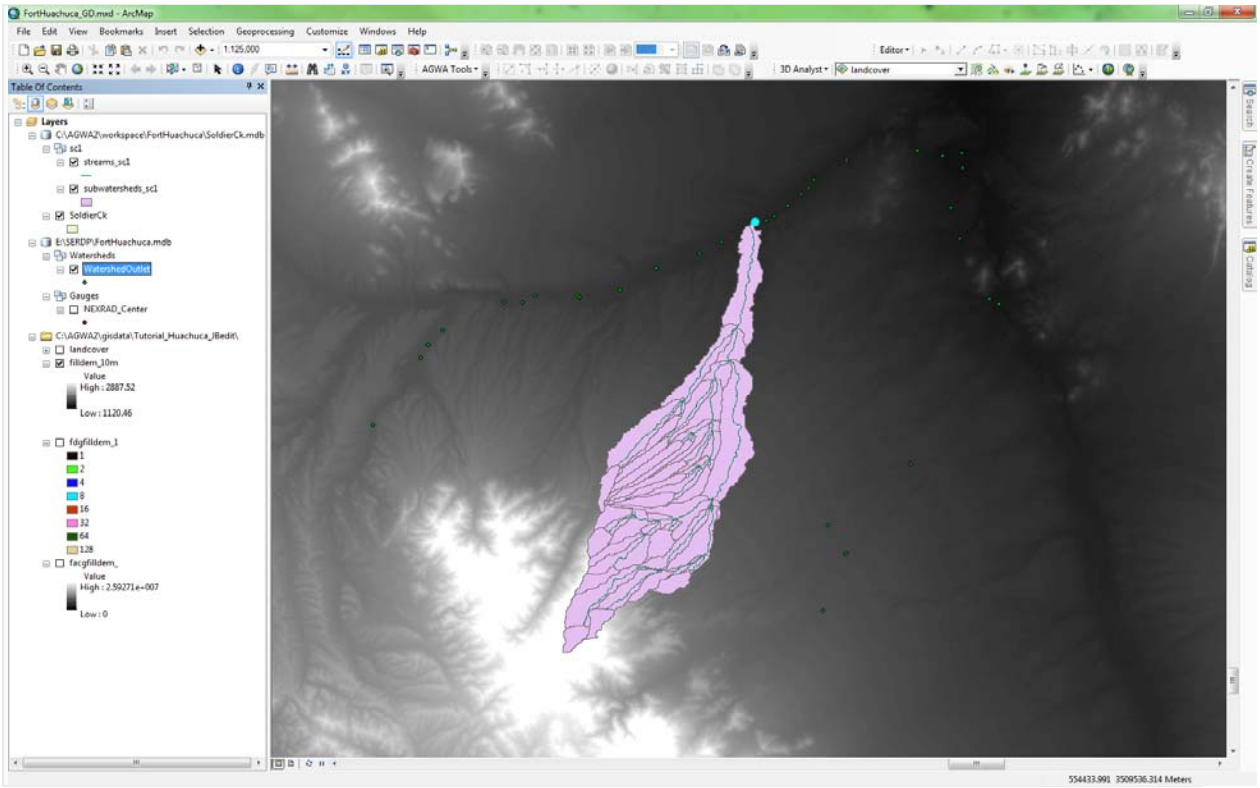
33.3.3. ***Threshold***: **10,000**

33.4. ***Output*** BOX



33.4.1. ***Name***: **sc1**

33.5. CLICK ***Discretize***



33.6. Save the map document and continue to the next step.

Discretizing breaks up the delineation/watershed into model specific elements and creates a stream feature class that drains the elements. The CSA, or Contributing/Channel Source Area, is a threshold value which defines first order channel initiation, or the upland area required for channelized flow to begin. Smaller CSA values result in a more complex watershed, and larger CSA values result in a less complex watershed. The default CSA in AGWA is set to 2.5% of the total watershed area. The discretization process created a subwatersheds layer with the name **subwatersheds_d1s1** and a streams map named **streams_d1s1**. In AGWA discretizations, are referred to with their geodatabase name as a prefix followed by the discretization name given in the *Discretizer* form, e.g. **d1\d1s1**.

Part 2: Soil and Landcover Parameterization

34. Perform the element, land cover, and soils parameterization of the watershed by selecting the ***Parameterize*** menu item from the ***AGWA Tools →Parameterize Options*** Menu

34.1. ***Input*** box

34.1.1. ***Discretization***: **SoldierCk\sc1**

34.1.2. ***Parameterization Name***: **gap**

34.2. ***Elements*** box

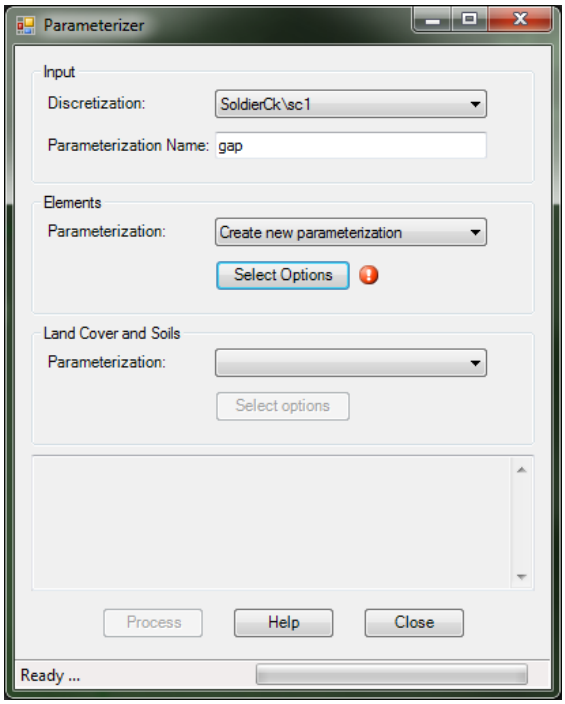
34.2.1. ***Parameterization***: **Create new parameterization**

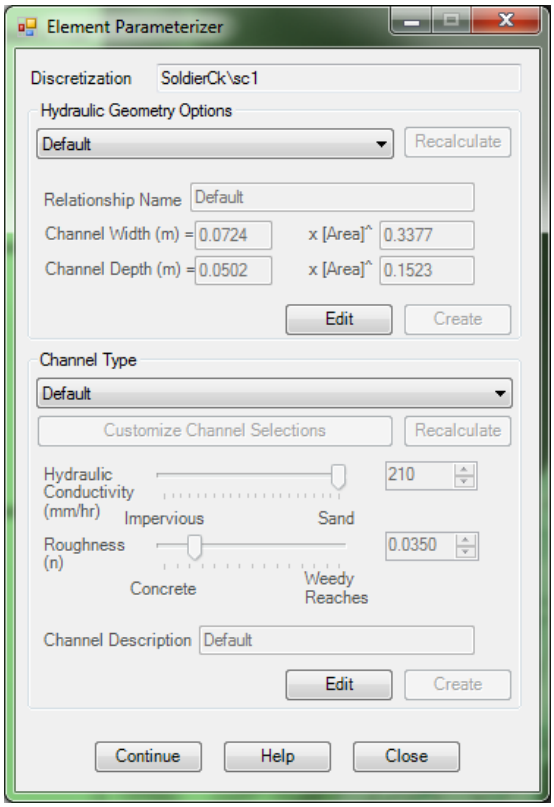
34.2.2. Click ***Select Options***

34.2.2.1. ***Hydraulic Geometry Options***: **Default**

34.2.2.2. ***Channel Type***: **Default**

34.2.2.3. Click ***Continue***





34.3. ***Land Cover and Soils***

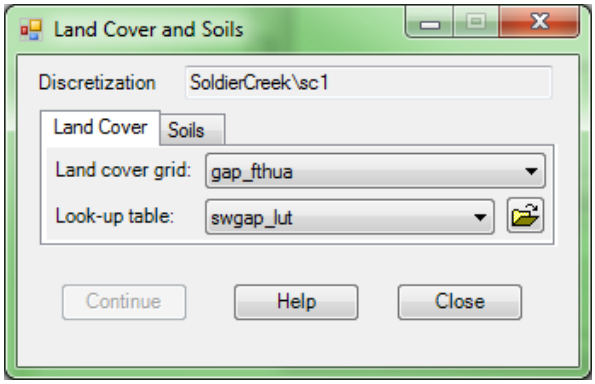
34.3.1. ***Parameterization***: **Create new parameterization**

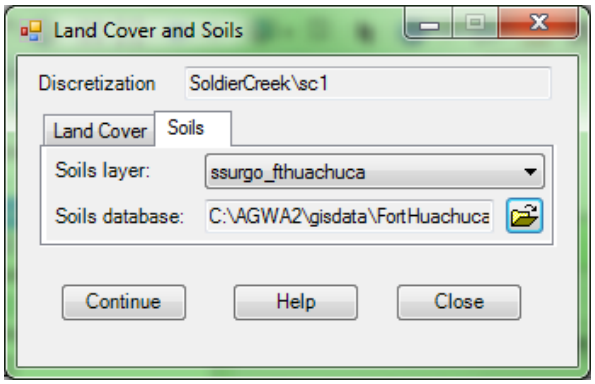
34.3.2. Click ***Select Options***

34.3.2.1. ***Land Cover*** tab

34.3.2.1.1. ***Land cover grid***: **landcover**

34.3.2.1.2. ***Look-up table***: **swgap_lut**





34.3.2.2. ***Soils*** tab

34.3.2.2.1. ***Soils layer***: **soilmu_a_az671**

34.3.2.2.2. ***Soils database***: navigate to and select **C:\AGWA\GISdata\FortHuachuca\AZ671and select soildb_US-2003.mdb**

34.3.2.3. Click ***Continue***

34.4. Click ***Process*** .

Part 3: Precipitation Input

AGWA provides a means for preparing rainfall files in SWAT- or KINEROS2-ready format. For SWAT, the user must have a *dbf* file containing the continuous, daily estimates of rainfall for the rain gages within the study area. Daily rainfall data for gages within and/or around the watershed are provided to you in multiple files in the Fort Huachuca personal geodatabase within the Hydrologic Modeling Folder shown in the following table. Points are found in the Gauges feature dataset. This example steps the user through modeling using the NEXRAD precipitation files.

Data Source	Point File Name	dBase File Name	Years of Record
Rain Gages	RainGauges	RG_precip2006	2006-2012
		RG_precip1982	1982-2005
		RG_precip1956	1956-1981
NEXRAD	NEXRAD_Center	NEXRAD_precip	2005-2012
Meterological Stations	MetTowers	MetPrecip2000	2000-2008
CMIP3	BCCA_CMIP3_VG	CMIP3_hist	1961-2000
		CMIP3_proj	2081-2100

When AGWA is used expressly as a hydrologic modeling tool it is critical that the rainfall data be spatially distributed across the watershed. A large body of literature exists regarding the crucial nature of spatially distributed rainfall data. In this exercise however, we will use a single rain gage to generate a uniform rainfall file across all the model elements. This is clearly a huge deviation from using distributed, observed data, but there is a sound reason for doing so in change detection work. We are interested in the impacts of land cover change on hydrologic response, but the spatial variability in rainfall can have confounding effects on the analysis, overwhelming the isolated changes within the subwatershed elements. Using uniform rainfall serves to isolate the effects of land cover change independent of the rainfall.

35. Write the SWAT precipitation file for the watershed by selecting ***AGWA →Precipitation Options →Write SWAT Precipitation.***

35.1. ***SWAT Precipitation Step 1*** form

35.1.1. ***Watershed Input*** box:

35.1.1.1. ***Discretization***: **SoldierCk\sc1**

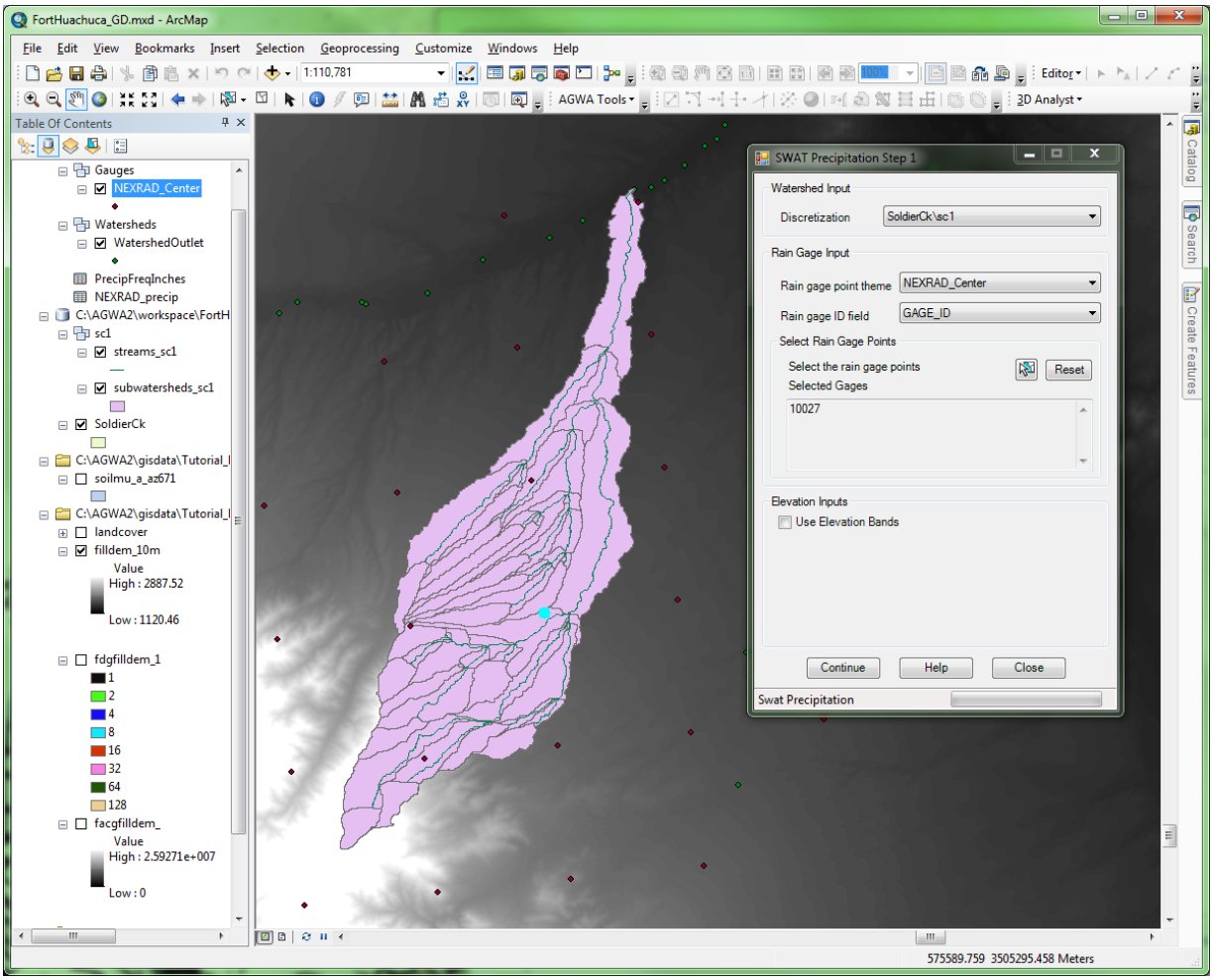
35.1.2. ***Rain Gage Input*** box:

35.1.2.1. ***Rain gage point theme***: **NEXRAD_Center**

35.1.2.2. ***Rain gage ID field***: **GAGE_ID**

35.1.3. ***Select Rain Gage Points*** box:

35.1.3.1. Click the ***Select Feature*** button to select ***Gage 10027***



35.1.4. ***Elevation Inputs*** box:

35.1.4.1. ***Use Elevation Bands*** checkbox: leave unchecked

35.1.5. Click ***Continue***

35.2. ***SWAT Uniform Precipitation*** Form

35.2.1. ***Write the *.pcp file*** box:

35.2.1.1. ***Selected discretization theme: SoldierCk\sc1***

35.2.1.2. ***Selected rain gage point theme: NEXRAD_Center***

35.2.1.3. ***Selected rain gage ID field: GAGE_ID***

35.2.1.4. ***Unweighted precipitation file:*** **NEXRAD_precip**

35.2.1.5. ***Enter a name for the precipitation file:*** **10027** (use the Gage ID as name)

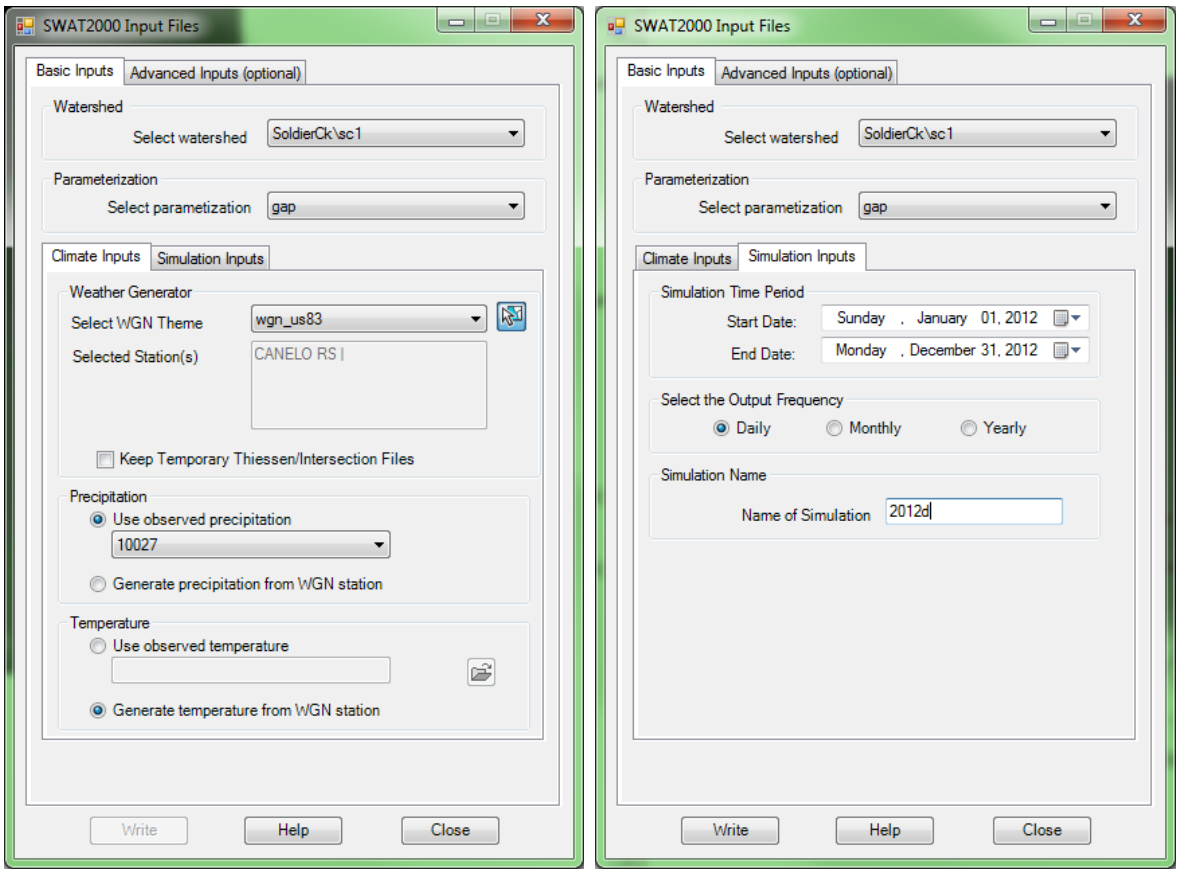
35.2.1.6. Click ***Write***

Part 4: Simulations and Model Execution

Writing the SWAT simulation file involves selecting the appropriate precipitation and temperature files and the desired simulation start date and time period. Temperature data for the historical runs using rain gage and NEXRAD-MPE was created from weather generator station data included within the program. Included with SWAT, the weather generator files contain statistical data for gage locations that are used to estimate daily maximum and minimum temperature values by selecting the station closest to the watershed (Burns et al., 2007). Temperature data included with GFDL CM2.1 projection data was formatted to match the temperature (.tmp) file structure used by SWAT at each virtual rain gage location and were selected based on proximity to watershed center. Lastly, a daily output frequency was selected to report streamflow data on a daily time-step, necessary for determining flow permanence.

Writing the model input files creates a simulation directory and writes all required input files for the model. When writing the input files, AGWA loops through features of the selected discretization and reads the model parameters from the parameterization look-up tables to write to the input files for the model.

36. Write the SWAT input files by selecting ***AGWA Tools → Simulation Options →SWAT 2000 Options →Write SWAT200 Input Files***
    36.1. ***Basic Inputs*** tab
        36.1.1. ***Watershed*** box: **SoldierCk\sc1**
        36.1.2. ***Parameterization*** box: **gap**
        36.1.3. ***Climate Inputs*** tab:
            36.1.3.1. ***Weather Generator*** box:
                36.1.3.1.1. ***Select WGN Theme***: **wgn_us83**
                36.1.3.1.2. ***Select Station***: **CANELO RS**
                36.1.3.1.3. ***Keep Temporary Thiessen/Intersection Files*** leave unchecked
            36.1.3.2. ***Precipitation*** box:
                36.1.3.2.1. ***Use observed precipitation***: **10027**
            36.1.3.3. ***Temperature*** box:
                36.1.3.3.1. ***Use observed temperature***: leave unchecked
                36.1.3.3.2. ***Generate temperature from WGN station***: **check the radio button**



36.2. ***Simulation Inputs*** tab

36.2.1. ***Simulation Time Period*** box: These dates depend on the precipitation data you are using so look at that data and determine the start and end dates you are interested in.

36.2.1.1. ***Start Data***: **Thursday, January 01, 2012**

36.2.1.2. ***End Date***: **Friday, December 31, 2012**

36.2.2. ***Select the Output Frequency***: **Daily**

36.2.3. ***Simulation Name***: **2012d**

36.3. Click ***Write***

37. Run the SWAT model for Soldier Creek watershed by selecting the ***Execute SWAT 2000 Model*** menu item from the ***AGWA Tools → Simulation Options → SWAT2000 Options*** menu.

37.1. ***Select the discretization***: **SoldierCk\sc1**

37.2. ***Select the simulation***: **2012d**

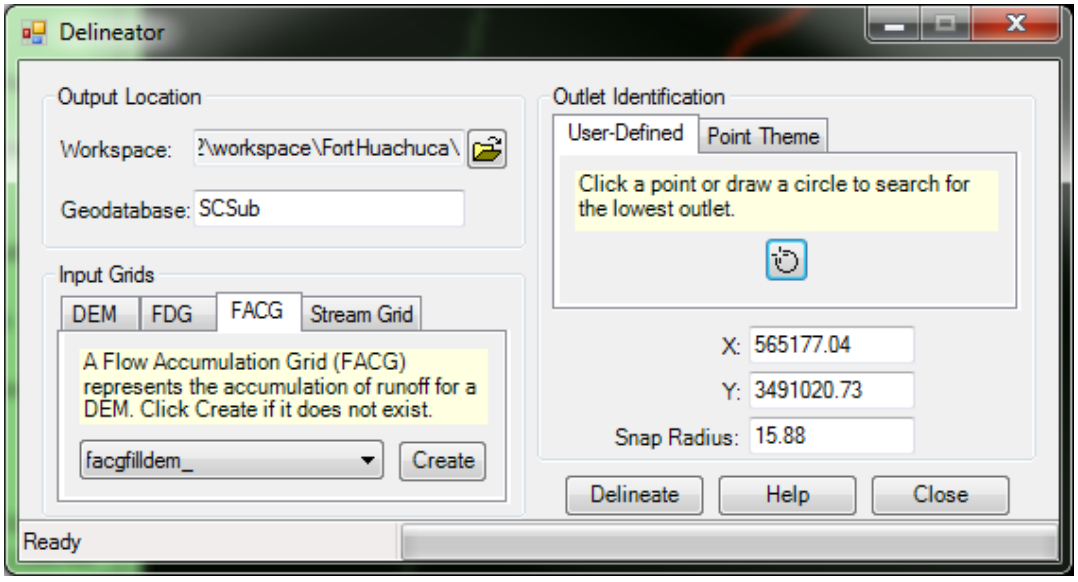
37.3. Click ***Run***

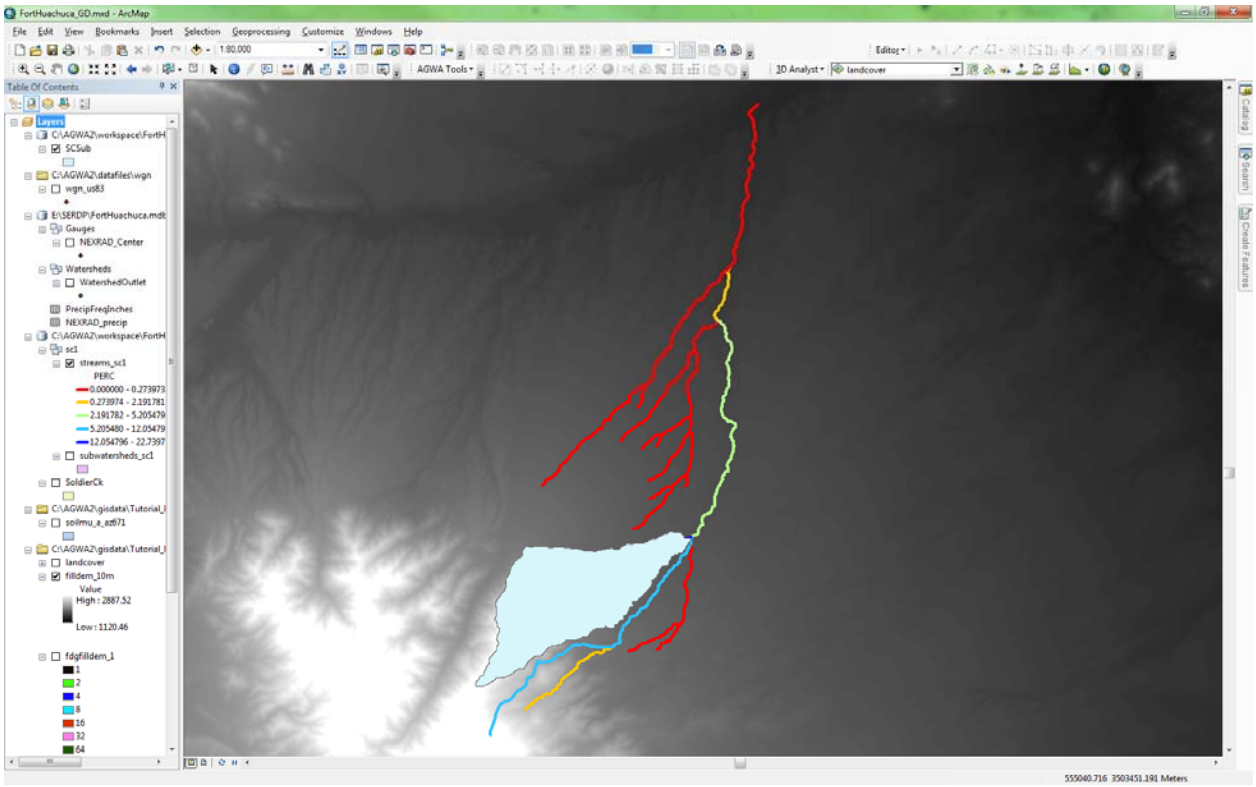
KINEROS2

Results from the Kinematic Runoff and Erosion Model (KINEROS2) were used to determine peak flow throughout Fort Huachuca and the other three installations.

Part 1: Watershed Delineation and Discretization

38. Perform the watershed delineation by selecting the ***Delineate Watershed*** menu item from the ***AGWA Tools → Delineation Options*** menu.
    38.1. ***Output Location*** box
        38.1.1. ***Workspace*** textbox: navigate to and select or create **C:\AGWA\workspace\FortHuachuca**
        38.1.2. ***Geodatabase*** textbox: enter **SCSub**
    38.2. ***Input Grids*** box
        38.2.1. ***DEM*** tab: select **filldem_fthua**
        38.2.2. ***FDG*** tab: select **fdgfilldem_f**
        38.2.3. ***FACG*** tab: select **facgfilldem_**
    38.3. ***Outlet Identification*** box
        38.3.1. ***User-Defined*** tab: Draw a circle around the outlet of any subwatershed in Soldier Creek. For this exercise we will select the watershed with the highest flow permanence. The following map depicts the subwatershed for analysis.





38.4. Click ***Delineate***

38.5. Save the map document and continue to the next step.

39. Perform the watershed discretization by selecting the ***Discretize Watershed*** menu item from the ***AGWA →Discretization Options*** menu.

39.1. ***Input*** BOX

39.1.1. ***Delineation***: **SCSub**

39.2. ***Model Options*** BOX

39.2.1. ***Model***: **KINEROS**

39.3. ***CSA*** BOX

39.3.1. ***Method***: **CSA (flow accumulation)**

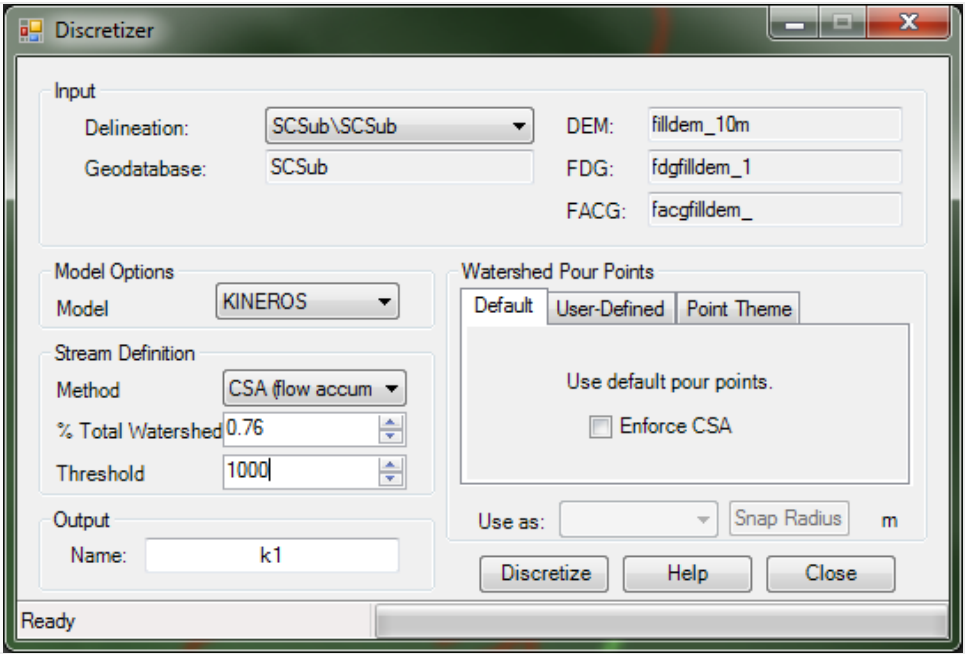
39.3.2. ***% Total Watershed***: DO NOTHING (this value will change when you set the threshold)

39.3.3. ***Threshold***: **1000**

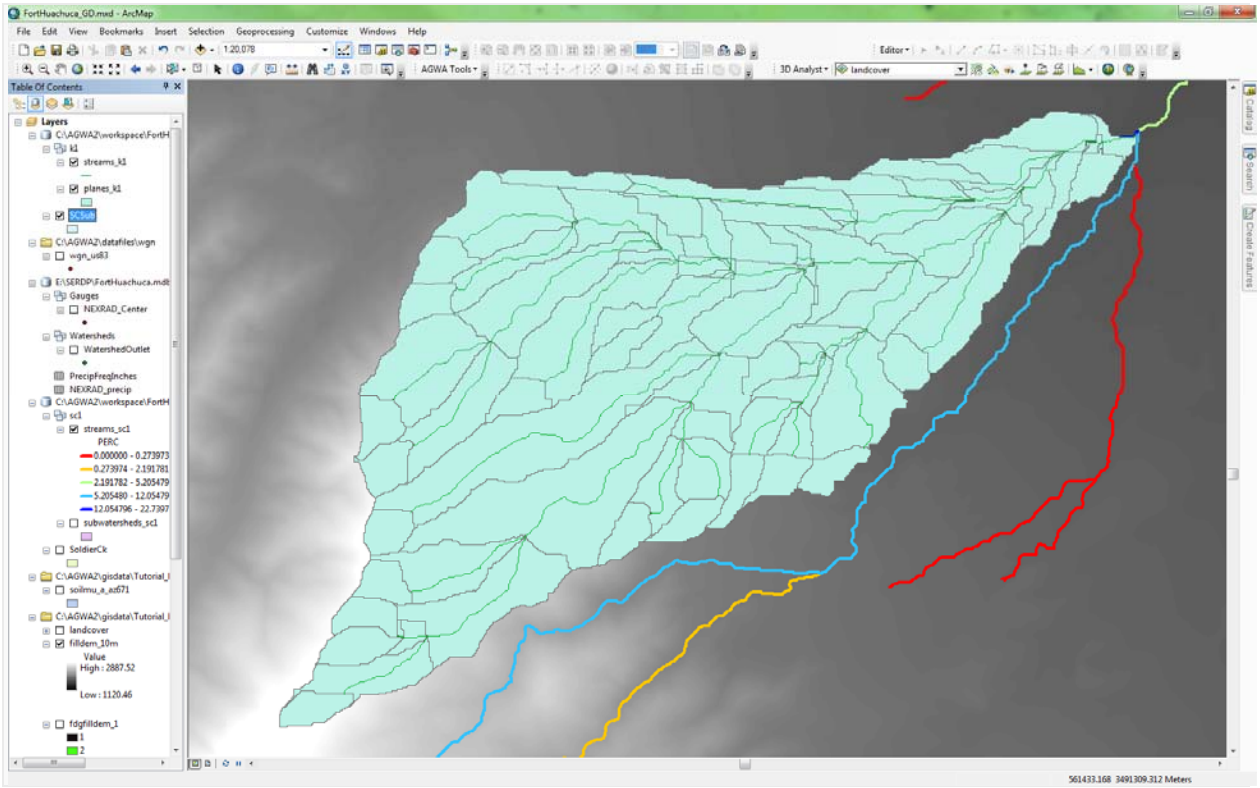
39.4. ***Output*** BOX

39.4.1. ***Name***: **k1**

39.5. CLICK ***Discretize***



39.6. Save the map document and continue to the next step.



Part 2: Soil and Landcover Parameterization

40. Perform the element, land cover, and soils parameterization of the watershed by selecting the ***Parameterize*** menu item from the ***AGWA Tools*** →***Parameterize Options*** Menu

40.1. ***Input*** box

40.1.1. ***Discretization***: **SCSub\k1**

40.1.2. ***Parameterization Name***: **gap**

40.2. ***Elements*** box

40.2.1. ***Parameterization***: **Create new parameterization**

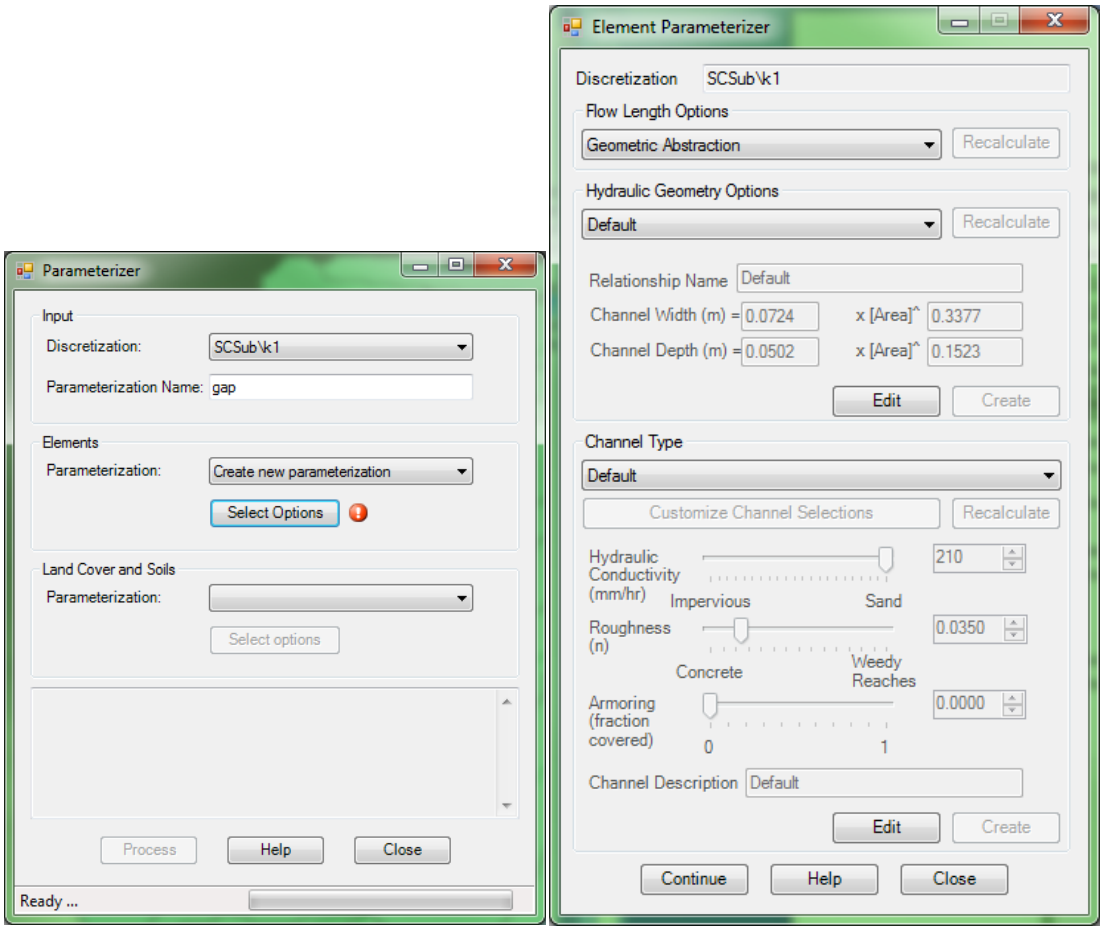
40.2.2. Click ***Select Options***

40.2.2.1. ***Flow Length Options***: **Geometric Abstraction**

40.2.2.2. ***Hydraulic Geometry Options***: **Default**

40.2.2.3. ***Channel Type***: **Default**

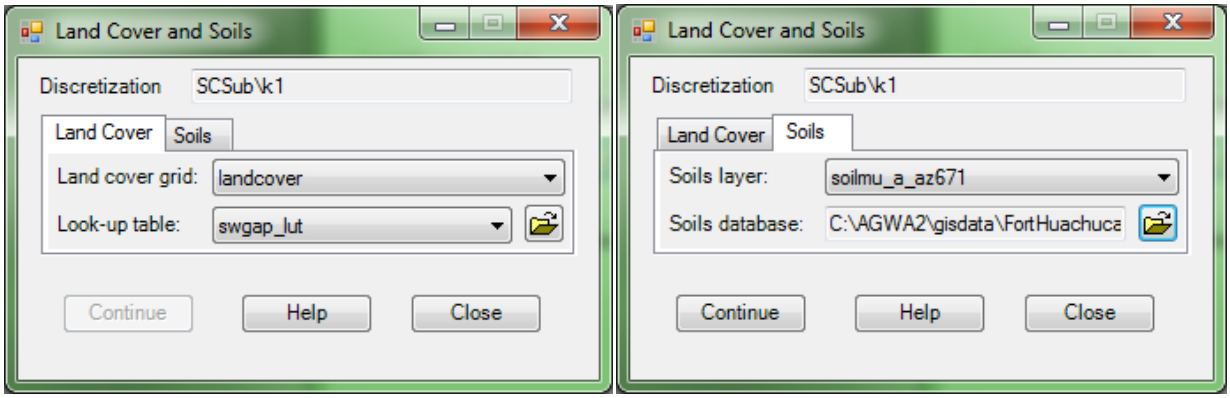
40.2.2.4. Click ***Continue***



40.3. ***Land Cover and Soils*** box

40.3.1. ***Parameterization***: **Create new parameterization**

40.3.2. Click ***Select Options***



40.3.2.1. ***Land Cover*** tab

40.3.2.1.1. ***Land cover grid***: **landcover**

40.3.2.1.2. ***Look-up table***: **swgap_lut**

40.3.2.2. ***Soils*** tab

40.3.2.2.1. ***Soils layer***: **soilmu_a_az671**

40.3.2.2.2. ***Soils database***: navigate to and select **C:\AGWA\GISdata\FortHuachuca\AZ671and select soildb_US-2003.mdb**

40.3.2.3. Click ***Continue***

40.4. Select ***Process***

Part 3: Precipitation Input

AGWA provides a means for preparing rainfall files in SWAT- or KINEROS2-ready format. For KINEROS2, users can define hyetographs, input a NOAA grid (See KINEROS2 Precipitation in the Data Acquisition and Management sections), define a depth and duration, or use a predefined database. For this example we will use a design storm database that was developed for this project. The database, PrecipFreqInches, should be added to the map document from Fort Huachuca Personal Geodatabase within the Hydrologic Modeling folder.

41. Write the KINEROS2 precipitation file for the watershed by selecting ***AGWA →Precipitation Options →Write KINEROS Precipitation***.

41.1. ***KINEROS Precipitation*** form

41.1.1. ***Select discretization***: **SCSub\k1**

41.1.2. ***Storm Depth*** box:

41.1.2.1. ***Database*** tab:

41.1.2.1.1. ***Database***: **PrecipFreqInches**

41.1.2.1.2. ***Location***: **SoldierCreek**

41.1.2.1.3. ***Storm frequency (yrs)***: **25**

41.1.2.1.4. ***Storm duration (hrs)***: **1**

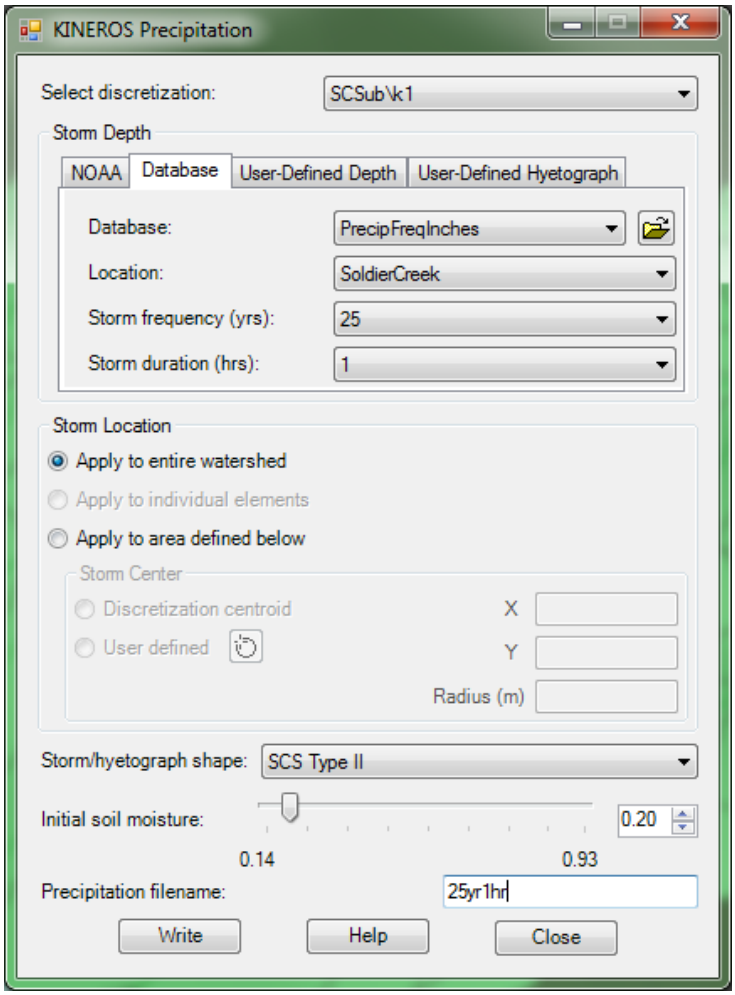
41.1.3. ***Storm Location*** box:

41.1.3.1. **Apply to entire watershed**

41.1.4. ***Storm/hyetograph shape***: **SCS Type II**

41.1.5. ***Initial soil moisture***: leave at 0.20

41.1.6. ***Precipitation filename***: **25yr1hr**



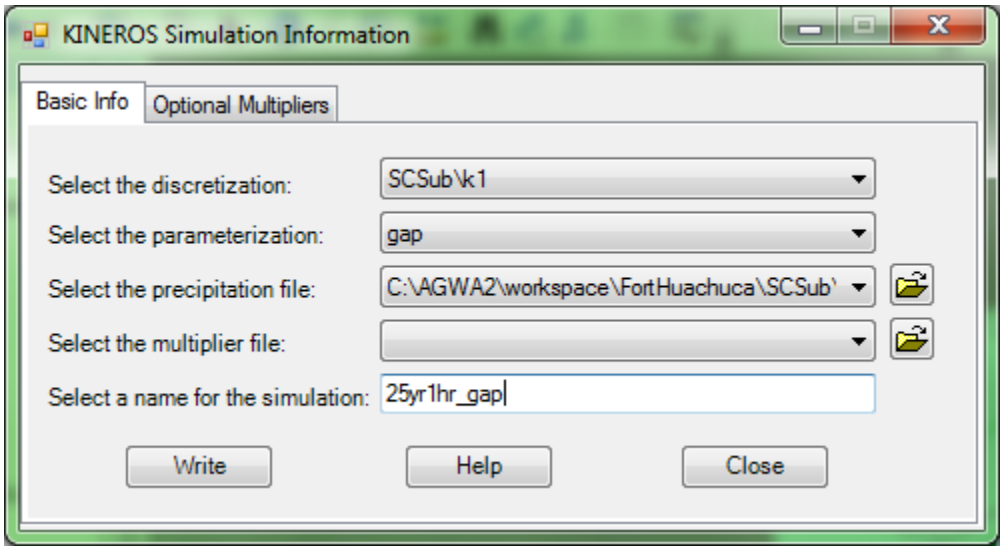
41.1.7. Click ***Write***

Part 4: Simulations and Model Execution

KINEROS2 simulation files are written by selecting the discretized watershed and the desired design storm previously created. An "Initial soil moisture" slider allows the user to set the amount of soil moisture present prior to the model run and was adjusted based on the presence and duration of previous storms. A series of multipliers also make it possible to adjust hydraulic conductivity (Ks), and Manning's N in both the planes and channels and were determined from the calibration efforts. After creating the simulation files the desired model was chosen and executed and results were then imported back into the GIS viewer where AGWA allows for visual display of the modeling results of Peak Flow using a graduated color ramp.

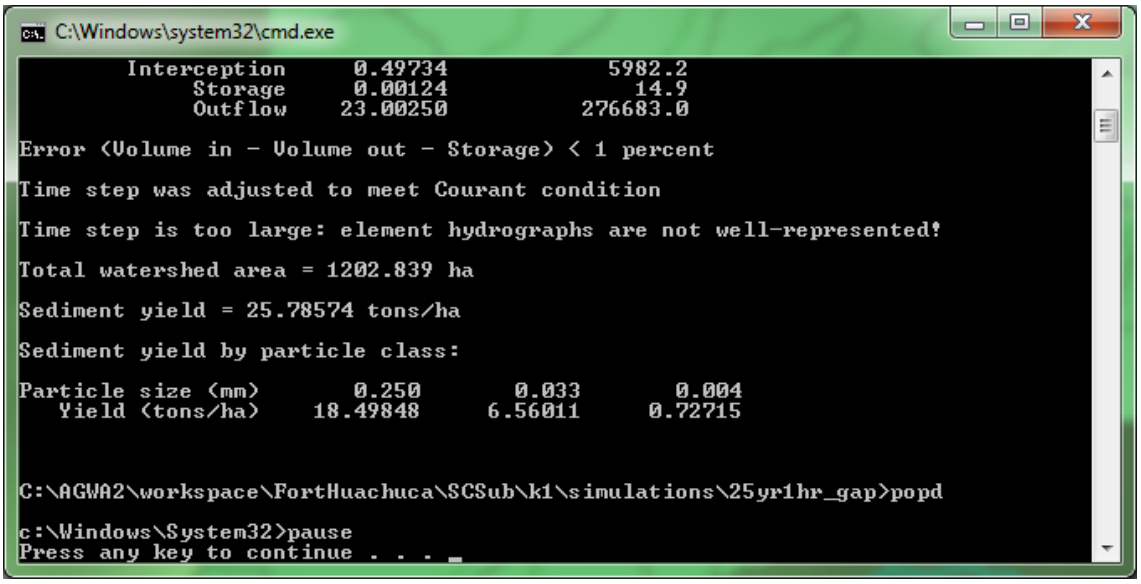
42. Write the KINEROS2 input files by selecting ***AGWA Tools → Simulation Options →KINEROS Options →Write KINEROS Input Files***
    42.1. ***Basic Info*** tab

42.1.1. ***Select the discretization***: **SCSub\k1**
42.1.2. ***Select the parameterization***: **gap**
42.1.3. ***Select the precipitation file***:
C:\AGWA\workspace\FortHuachuca\scsub1\precip\25yr1hr.pre
42.1.4. ***Select the multiplier file***: leave blank
42.1.5. ***Select a name for the simulation***: **25yr1hr_gap**

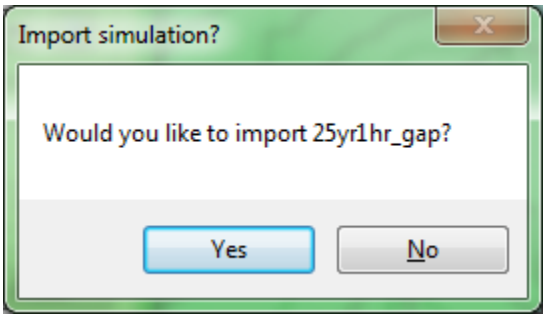


42.2. Click ***Write***

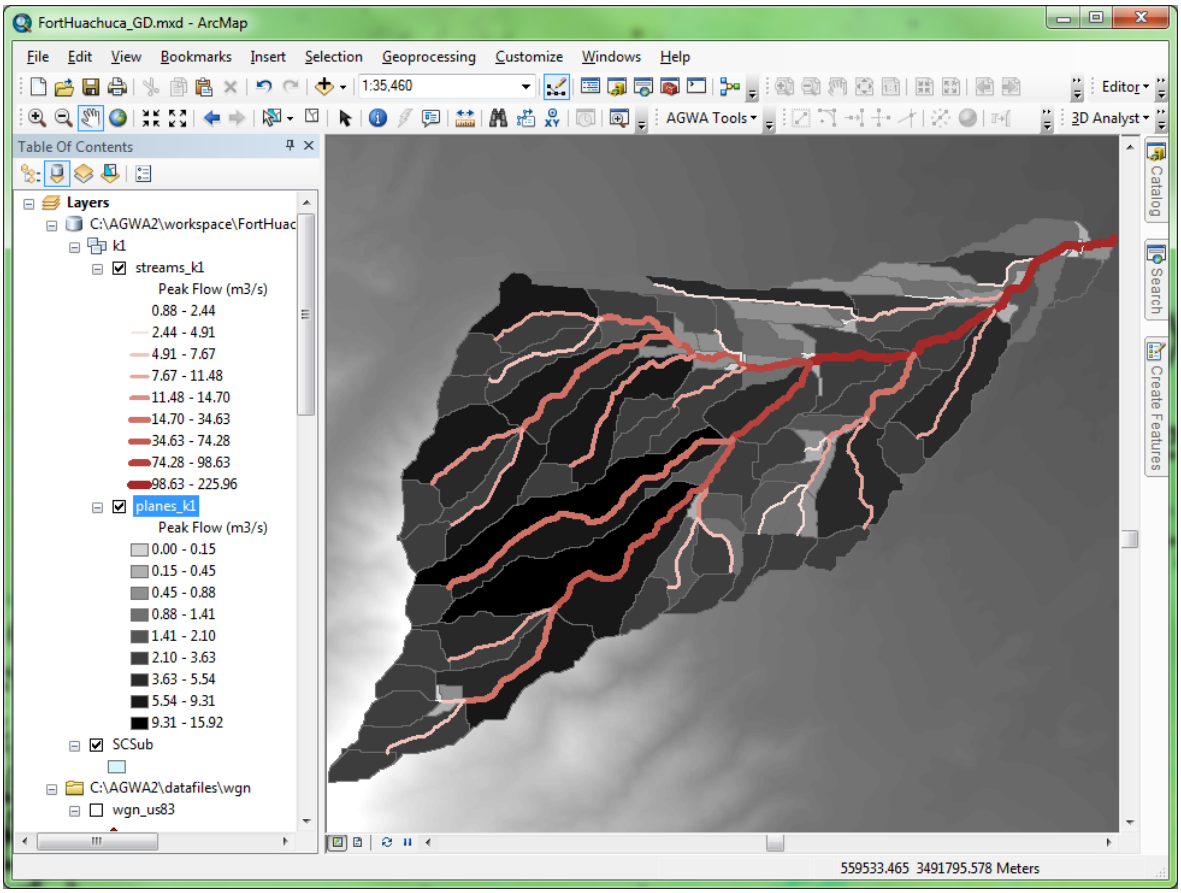
43. Run the KINEROS2 model for Soldier Creek subwatershed by selecting the ***Execute KINEROS Model*** menu item from the ***AGWA Tools → Simulation Options → KINEROS Options*** menu.
43.1. ***Select the discretization***: **scsub\k1**
43.2. ***Select the simulation***: **25yr1hr_gap**
43.3. Click ***Run***



44. Import and View KINEROS2 Results for Soldier Creek subwatershed by selecting ***View KINEROS Results*** menu item from the ***AGWA Tools → View Results →KINEROS Results***
    44.1. ***Results Selection*** box
        44.1.1. ***Watershed***: **SCSub\k1**
        44.1.2. ***Simulation***:
            44.1.2.1. Click ***Import***
                44.1.2.1.1. A window will pop up asking if you would like to import 25yr1hr_gap simulation, click ***Yes***.



            44.1.2.2. Select **25yr1hr_gap**.
        44.1.3. ***Output***: **Peakflow (m^3/s)**


FortHuachuca_GD.mxd - ArcMap
File Edit View Bookmarks Insert Selection Geoprocessing Customize Windows Help
1:35,460
Editor
AGWA Tools
3D Analyst
Table Of Contents
Layers
C:\AGWA2\workspace\FortHuac
k1
streams_k1
Peak Flow (m3/s)
0.88 - 2.44
2.44 - 4.91
4.91 - 7.67
7.67 - 11.48
11.48 - 14.70
14.70 - 34.63
34.63 - 74.28
74.28 - 98.63
98.63 - 225.96
planes_k1
Peak Flow (m3/s)
0.00 - 0.15
0.15 - 0.45
0.45 - 0.88
0.88 - 1.41
1.41 - 2.10
2.10 - 3.63
3.63 - 5.54
5.54 - 9.31
9.31 - 15.92
SCSub
C:\AGWA2\datafiles\wgn
wgn_us83
Catalog
Search
Create Features
559533.465 3491795.578 Meters

Results

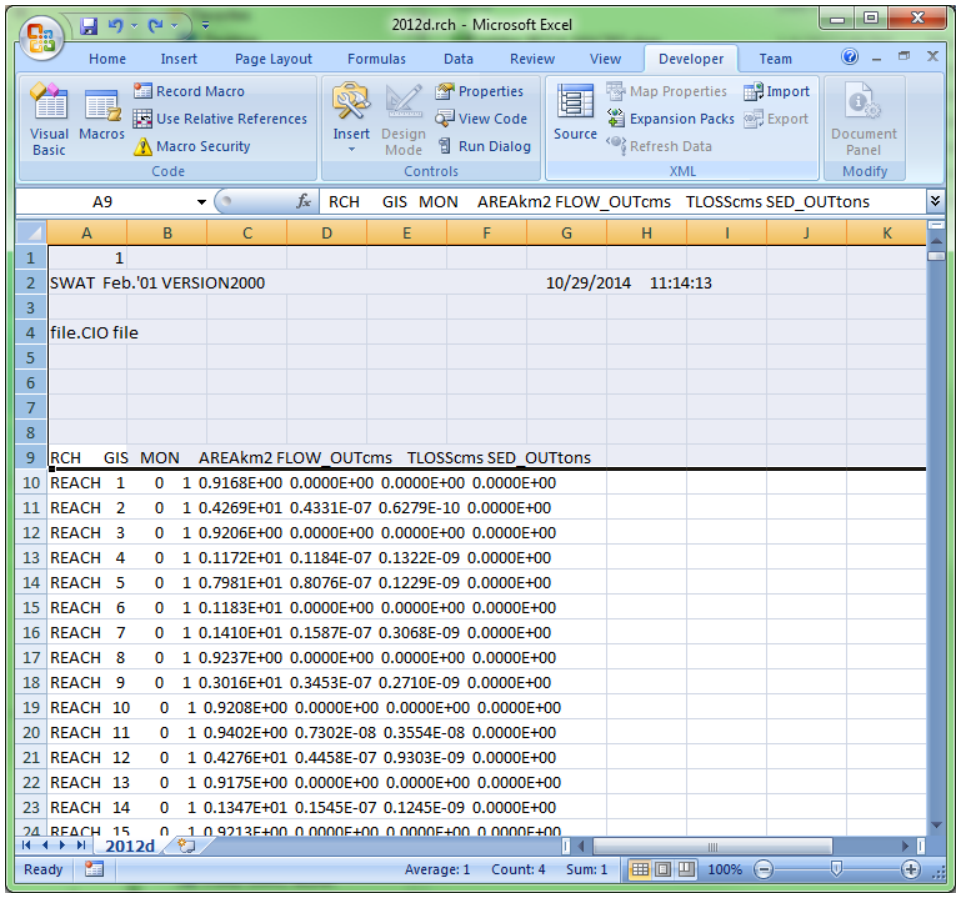
This section describes how the flow permanence and peak flow values were obtained for the SERDP project. Addional information is found in Lyon (2013).

Part 1: Flow Permanence

For this study, flow permanence refers to the percent of time of the year when surface flow is present for each stream reach. Presence was determined using the SWAT reach (.rch) output file, which reports daily runoff values for each modeled stream reach. Prior to formatting this file, a 'YEAR' column was added to the reach output files by running a C# script to append a year to each record. The tables were then imported into Excel and sorted by date and reach. Next, a series of Excel formulas were used to capture the number of days where flow was present in each reach. Threshold values, or cutoffs, were established and runoff values that were greater were designated as having "flow present" and those that were less as "flow absent" for each reach on each day. A simple ratio of the number of days with flow present to the total number days of the year resulted in annual percent time with flow that was calculated for each stream reach, both for the total year and wet season only. Average flow permanence was calculated for the entire period of record and the resulting table was joined to the stream feature class, exported and merged into a final spatial layer for each installation.

Flow permanence cutoffs were established for the mountainous areas of Fort Huachuca based on the 2011 Stromberg Tidbit data sensors located in the upper and middle parts of Garden Canyon, the middle tributary of the Buena School Area watershed, the southern tributary of Soldier Creek watershed, the upper part of Huachuca Canyon, and Upper Slaughterhouse Wash. Cutoffs were established for alluvial reaches of Garden Canyon, Woodcutters Wash, Graveyard Gulch, Soldier Creek, and Huachuca Canyons based on the Gungle 2001-2002 Tidbit sensor results. Three watershed size classes were assigned different cutoffs based on their contributing watershed area. Watersheds with an area <10 km^2 were assigned a cutoff of 0.0001 m^3/sec; between 10-34.9 km^2 a cutoff of 0.001 m^3/sec; and >35km^2 a cutoff of 0.35 m^3/sec.

45. Open the Excel document blank_MACRO.xlsm
46. Create a new worksheet.
47. Open the AGWA Reach output file
    C:\AGWA2\workspace\FortHuachuca\SoldierCk\sc1\simulations\2012d\2012d.rch
    47.1. Do not split this text, leave as is when opening in Excel.
    47.2. Delete the first 9 rows of text.



47.3. Copy the rest of the worksheet into the new worksheet created in blank_MACRO.xlsm

47.4. Close the 2012d.rch Excel file.

48. Run MACROS

48.1. Open the Developer tab.

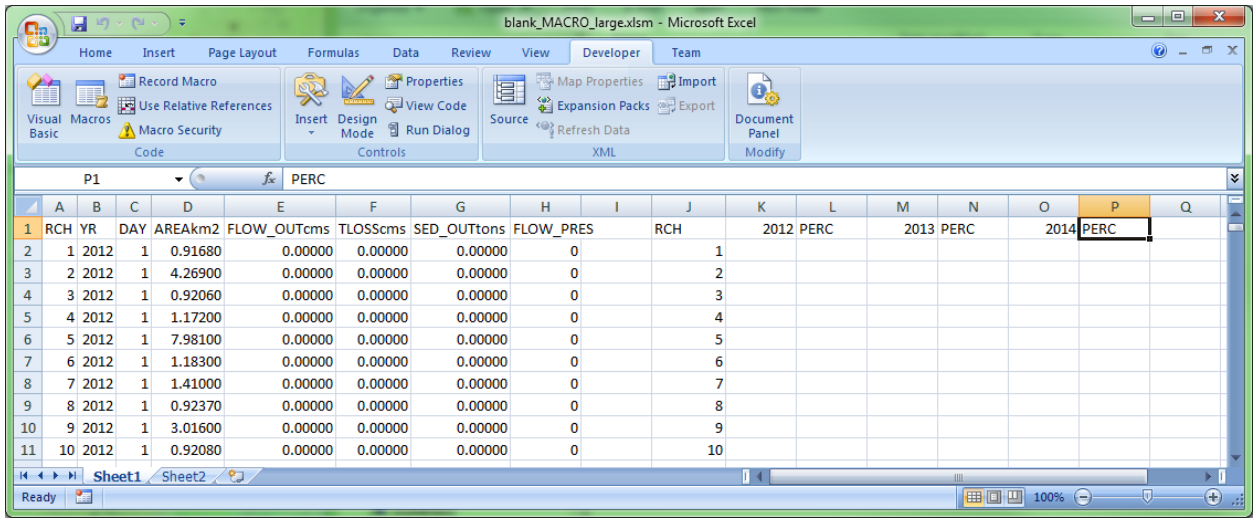
48.2. Select MACROS

48.3. Run A_FormatTable

48.4. Populate the YR column (Column B) with 2012

48.4.1. For this exercise there is only one year simulated so we can easily do this; for multiple years of simulations a program can be used to add this information to the table automatically.

48.5. Run B_FlowPresent



	A	B	C	D	E	F	G	H	I	J	K	L	M	N	O	P	Q
1	RCH	YR	DAY	AREAkm2	FLOW_OUTcms	TLOSScms	SED_OUTtons	FLOW_PRES		RCH	2012	PERC	2013	PERC	2014	PERC	
2	1	2012	1	0.91680	0.00000	0.00000	0.00000	0		1							
3	2	2012	1	4.26900	0.00000	0.00000	0.00000	0		2							
4	3	2012	1	0.92060	0.00000	0.00000	0.00000	0		3							
5	4	2012	1	1.17200	0.00000	0.00000	0.00000	0		4							
6	5	2012	1	7.98100	0.00000	0.00000	0.00000	0		5							
7	6	2012	1	1.18300	0.00000	0.00000	0.00000	0		6							
8	7	2012	1	1.41000	0.00000	0.00000	0.00000	0		7							
9	8	2012	1	0.92370	0.00000	0.00000	0.00000	0		8							
10	9	2012	1	3.01600	0.00000	0.00000	0.00000	0		9							
11	10	2012	1	0.92080	0.00000	0.00000	0.00000	0		10							

48.5.1. Edit the RCH Column and Column headers

48.5.1.1. RCH should contain only the number of reaches simulated in the watershed, delete all rows below RCH 53 in Column J

48.5.1.2. Delete Columns M-P as we only simulated one year in this exercise.

48.6. Run C_DaysPerYear

48.6.1. This will only run for RCH 1; drag the formula for Column 2012 (Column K) and Column PERC (Column L) through RCH 53.

48.7. Copy, Paste and Save Columns J-L in a new worksheet

48.7.1. Copy Columns J-L

48.7.2. Paste in Sheet2

48.7.3. Save document as C:\AGWA2\GISdata\FortHuachuca\2012d_flowperm.xlsx

NOTE: ARCMAP does not read .xlsm files so you will need to select a new format when you use the save as option.

49. Connect Flow Permanence Calculations to Stream Reaches in ArcMAP

49.1. Open FortHuachuca.mxd

49.2. Add Sheet2$ of 2012d_flowperm.xlsx

49.3. Join Sheet2$ with streams_sc1

49.3.1. Right click on streams_sc1

49.3.2. Select Joins and Relates →Join…

49.3.2.1. What do you want to join to this layer?: Join attributes from a table

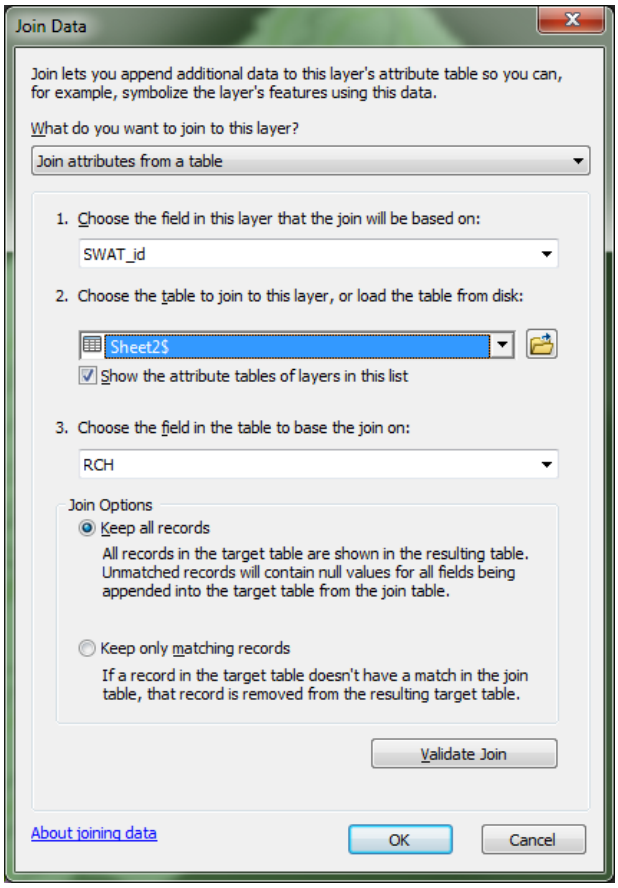
49.3.2.1.1. 1. Select SWAT_id

49.3.2.1.2. 2. Select Sheet2$

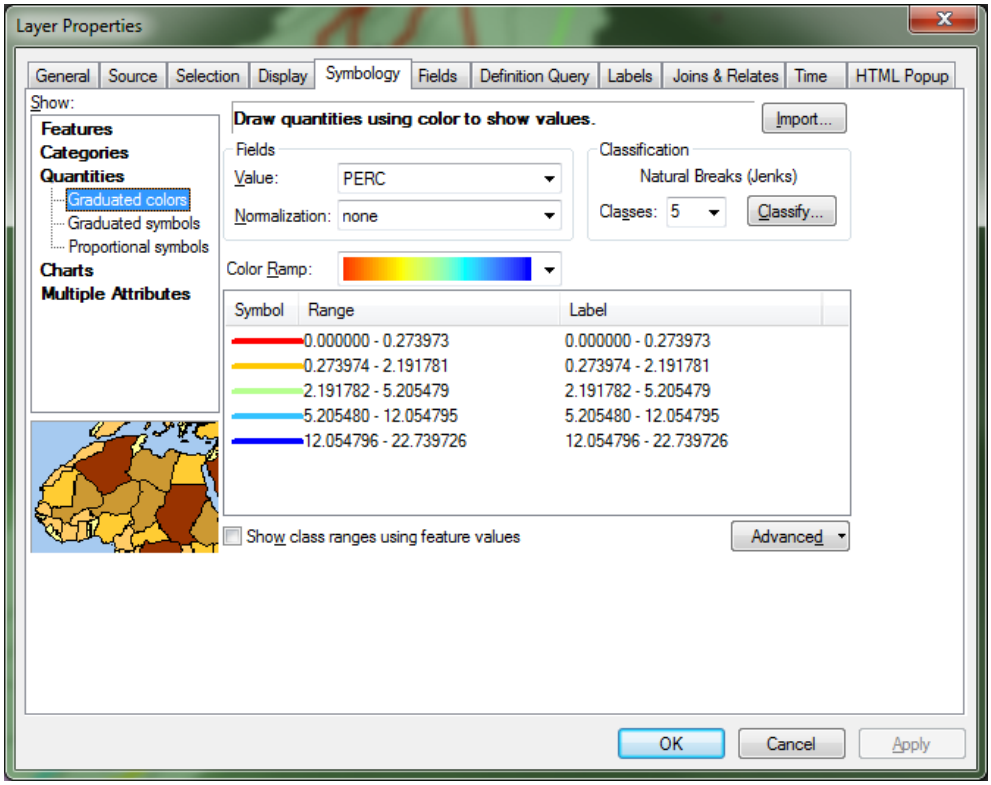
49.3.2.1.3. 3. Select RCH

49.3.2.1.4. Join Options: Select Keep All Records

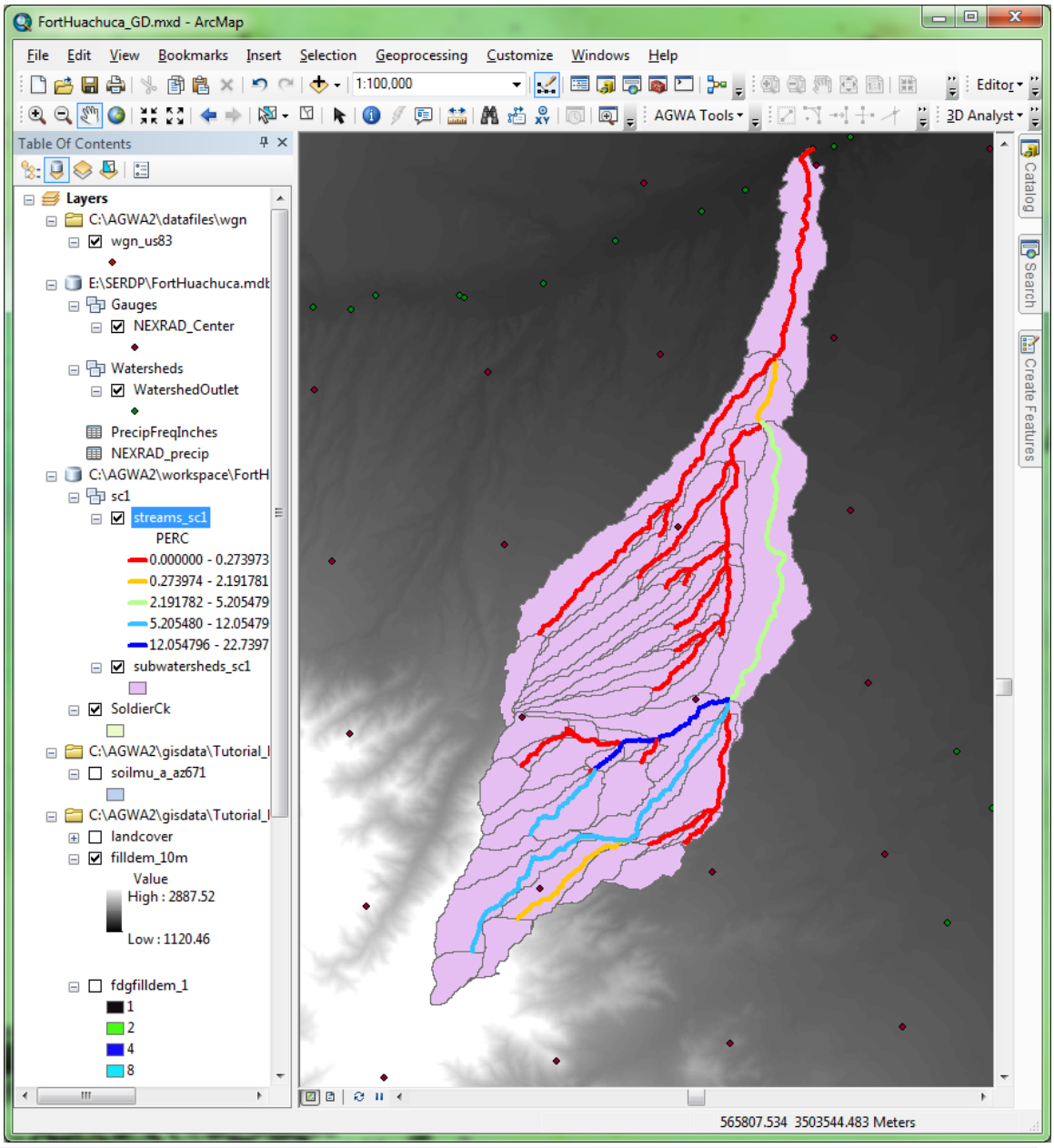
49.3.2.1.5. Click OK



50. Visualize Flow Permanence
    50.1. Open Properties of streams_sc1
    50.2. Open Symbology tab
    50.3. Show: select Quantities\Graduated Colors
        50.3.1. Fields box
            50.3.1.1. Values: PERC
            50.3.1.2. Normalization: none
        50.3.2. Color Ramp: Select whichever works best for your application
        50.3.3. Click Symbol to edit the weight of the line
            50.3.3.1. Select Properties for All Symbols
                50.3.3.1.1. Change Width to 3
                50.3.3.1.2. Click OK



50.4. Click Apply



NOTE: Adjust the classification break points by clicking CLASSIFY… in the classification box.

The output shown above can be interpreted as the percent of time during 2012 those stream reaches had flow present; flow presence is determined according to cutoffs largely based on watershed size.

Part 2: Peak Flow

For each watershed center an aerial reduction factor was determined using area relationships developed from a paired rain gage study at Walnut Gulch by Osborn et al. (1980) for the 5-, 10-, 25- and 100-year, 1-hour storm events. These values were applied to each of the design storms created from NOAA's precipitation frequency maps prior to running KINEROS2. Following

model execution peak flow (m^3/s) results were displayed in AGWA and individual spatial layers were then exported and merged to create a final coverage for the entire installation.

Part 4 of the KINEROS2 section demonstrates how these outputs are visualized; tables generated during the simulations were used as inputs for the classification of stream reaches.

References

Ames, D. P., Horsburgh, J. S., Cao, Y., Kadlec, J., Whiteaker, T., & Valentine, D. 2012. HydroDesktop: Web services-based software for hydrologic data discovery, download, visualization, and analysis. Environmental Modeling & Software, 37, 146-156.

Arnold, J. G., Srinivasan, R., Muttiah, R. S., & Williams, J. R. 1998. Large area hydrologic modeling and assessment - Part 1: Model development. Journal of the American Water Resources Association, 34(1), 73-89.

Burns, I.S., Scott, S.N., Levick, L.R., Semmens, D.J., Miller, S.N., Hernandez, M., Goodrich, D.C., & Kepner W.G. 2007. Automated Geospatial Watershed Assessment 2.0 (AGWA 2.0) – A GIS-Based Hydrologic Modeling Tool: Documentation and User Manual; U.S. Department of Agriculture, Agricultural Research Service.

Cayan D.R., Das T., Pierce D.W., Barnett T.P., Tyree M., and Gershunova A. 2010. Future dryness in the Southwest US and the hydrology of the early 21st century drought. Proc. Natl. Acad. Sci. U.S.A. Proceedings of the National Academy of Sciences of the United States of America, 107(50), 21271-21276.

Comer, P. J., & NatureServe (Program). 2003. Ecological systems of the United States: a working classification of U.S. terrestrial systems. Arlington, Va.: NatureServe.

Fulton, R. A., Breidenbach, J. P., Seo, D. J., Miller, D. A., & O'Bannon, T. 1998. The WSR-88D rainfall algorithm. Weather and Forecasting, 13(2), 377-395.

Gesch, D., Oimoen, M., Greenlee, S., Nelson, C., Steuck, M., & Tyler, D. 2002. Highlight Article - The National Elevation Dataset. Photogrammetric Engineering and Remote Sensing., 68(1), 5.

Levick, L., Fonseca, J., Goodrich, D., Hernandez, M., Semmens, D., Stromberg, J., Leidy, R., Scianni, M., Guertin, D.P., Tluczek, M., and Kepner, W. 2008. The Ecological and Hydrological Significance of Ephemeral and Intermittent Streams in the Arid and Semi-arid American Southwest. U.S. Environmental Protection Agency and USDA/ARS Southwest Watershed Research Center. EPA/600/R-08/134, ARS/233046, 116 pp.

Lowry, J., Ramsey, R. D., Thomas, K., Schrupp, D., Sajwaj, T., Kirby, J., . . . Prior-Magee, J. 2007. Mapping moderate-scale land-cover over very large geographic areas within a collaborative framework: A case study of the Southwest Regional Gap Analysis Project (SWReGAP). Remote Sensing of Environment, 108(1), 59-73.

Lyon, R. 2013. Using rainfall-runoff models to characterize the flow regime of desert streams in the U.S. southwest. M.S. Thesis, University of Arizona, Tucson.

Miller, S.N., Semmens, D. J., Hernandez, M., Goodrich, D. C., Miller, W.P., Kepner, W.G., Ebert,D. 2002. GIS-based hydrologic modeling: the Automated Geospatial Watershed Assessment tool, in Proceeding of the Second Federal Interagency Hydrologic Modeling Conference, July 28 - August 1, 2002, Las Vegas NV, CD-ROM, 12 p.

Miller, S.N., Semmens, D.J., Goodrich, D.C., Hernandez, M., Miller, R.C., Kepner, W.G. and Guertin, D.P. 2007. The Automated Geospatial Watershed Assessment Tool. J. Environmental Modeling and Software, 22:365.377

Montgomery, D., and Buffington, J. 1997. Channel-reach morphology in mountain drainage basins. Geological Society of America Bulletin, 109(5): 596-611.

National Oceanic and Atmospheric Administration's (NOAA) Global Historical Climatology Network (GHCN). Precipitation dataset. Retrieved 11/01/2010. From http://www.ncdc.noaa.gov/oa/climate/ghcn-daily/

National Oceanic and Atmospheric Administration's (NOAA) Precipitation Frequency Data Server. Precipitation dataset. Retrieved 04/25/2012. From http://dipper.nws.noaa.gov/hdsc/pfds/

Osborn, H. B., Lane, L. J., Myers, V. A. 1980. Rainfall-Watershed Relationships for Southwestern Thunderstorms. Transactions of the ASAE, 23(1):82.

Puckridge, J., Sheldon, F., Walker, K., Boulton, A. 1998. Flow variability and the ecology of large rivers. Marine and Freshwater Research, 49(1): 55-72.

Rosgen, D. 1994. A Classification of Natural Rivers. Catena, 22(3): 169-199.

Seager R, Ting M, Held I, Kushnir Y, Lu J, Vecchi G, . . . Naik N. 2007. Model projections of an imminent transition to a more arid climate in southwestern North America. Science (New York, N.Y.), 316(5828), 1181-4.

U. S. Geological Survey (USGS), National Gap Analysis Program. Landcover dataset. Retrieved 07/10/2012. From http://gapanalysis.usgs.gov/

Woolhiser, D. A., Smith, R. E., & Goodrich, D. C. 1990. KINEROS: a kinematic runoff and erosion model: documentation and user manual. U.S. Dept. of Agriculture, Agricultural Research Service, Washington, D.C.

Zehr, R. M., Myers, V. A., and United States National Weather Service. 1984. Depth-area ratios in the semi-arid southwest United States. Vol. 40 of NOAA technical memorandum NWS HYDRO. U.S. Dept. of Commerce, National Oceanic and Atmospheric Administration, National Weather Service.

Appendix I: Stream Type Classification Guidance Document

STREAM TYPE CLASSIFICATION GUIDANCE DOCUMENT

Table of Contents

Introduction **3**

Input Variables **3**

1. FORT IRWIN 4
   a) Elevation 4
   b) LiDAR Slope 4
   c) Flow Permanence 5
      Climate Change Analysis 6
   d) Peak Flow 6
   e) Total Stream Power 7
   f) LiDAR Vegetation Structure 7
   g) Percent Vegetation Cover 7
   h) Mean Vegetation Index 7
   i) Mean Riparian Widths 8
   j) Entrenchment Ratio 8
   k) Rainfall Seasonality Index (RSI) 8
   l) Cumulative Area 8
2. YPG 8
   a) Mean Elevation 9
   b) Slope 9
   c) Flow Permanence 9
      Climate Change Analysis 10
   d) Peak Flow 11
   e) Total Stream Power 12
   f) Percent Vegetation Cover 12
   g) Mean Vegetation Index 12
   h) Mean Riparian Widths 12
   i) Entrenchment Ratio 13
   j) Rainfall Seasonality Index (RSI) 13
   k) Cumulative Area 13
   l) LiDAR 13
3. FORT HUACHUCA 13
   a) Elevation 14
   b) LiDAR Slope 14
   c) Flow Permanence 14
      Climate change Analysis 15
   d) Peak Flow 16
   e) Total Stream Power 16
   f) LiDAR Vegetation structure 16
   g) Percent Vegetation Cover 16

h) Mean Vegetation Index 17
i) Mean Riparian Widths 17
j) Entrenchment Ratio 17
k) Rainfall Seasonality Index (RSI) 17
l) Cumulative Area 18

4. FORT BLISS 18
a) Elevation 18
b) LiDAR Slope 18
c) Flow Permanence 19
Climate Change Analysis 19
d) Peak Flow 20
e) Total Stream Power 21
f) LiDAR Vegetation Structure 21
g) Percent Vegetation Cover 21
h) Mean Vegetation Index 21
i) Mean Riparian Widths 21
j) Entrenchment Ratio 22
k) Rainfall Seasonality Index (RSI) 22
l) Cumulative Area 22

Literature Cited 22

Introduction

The purpose of the Stream Type Classification is to provide a means to evaluate stream reaches in terms of the hydrology, vegetation, and geomorphology, for analysis of wildlife habitat characteristics, and for other management requirements. This classification may be useful for management applications, such as identifying stream reaches that might have high peak flows or flashy runoff, or vegetation characteristics specific for wildlife use. This document describes the methods used to derive and prepare the variables for the stream type classification. Names of intermediate data layers are included for information only. Additional details used to derive the hydrologic, vegetation and geomorphic variables are found in those respective guidance documents, as noted in the text below. A complete description of the methods used for the classification is in the Final Report.

The Stream Type Classification was performed using an Agglomerative Hierarchical Clustering technique, in the R statistical analysis package (R Project, 2014; www.r-project.org) within the R-Studio interface (www.rstudio.com). This method is an unsupervised learning method that groups data into clusters based on their similarity. It was performed using the *hclust* technique with Euclidean distance and Ward's method, and uses a sub-set of variables to create the clusters. The resulting clusters are viewed in a dendrogram that illustrates the main stream type clusters, and that can be further subdivided to get additional stream types to provide more detailed information on the stream reach characteristics.

Input Variables

Several analyses were performed to determine the most informative variables for the classification. All variables were derived for the 1km stream reaches, with each reach having a unique identifier or a Unique_ID. A correlation matrix was analyzed in Excel to identify and remove highly correlated or redundant variables. A principal components analysis (PCA) was then performed in R to determine and confirm the most important variables. The final variables were selected and the cluster analyses were performed. Various Cluster Validity tests were performed to determine the optimal number of clusters. The results indicated that while there was usually one optimal cluster arrangement, there were several acceptable cluster configurations. Therefore, to select the final number of cluster, the dendrograms were analyzed, the different cluster arrangements were mapped, and site knowledge was used to select the arrangement that best captured the variability of stream characteristics across each installation. This method produced stream types based on the most informative vegetation, hydrologic and geomorphic variables, which are described in the next section. All analyses were performed in ArcGIS ArcMap (ESRI, http://www.esri.com/software/arcgis) unless otherwise noted.

The variables used for the stream type classification are:

1. Elevation (m)
2. Slope (%)
3. Flow Permanence (%)
4. Peak flow for the 25-year 1-hour storm (Qp, m^3/s)
5. Total stream power for the 25-year 1-hour storm (kW/m)

6. Vegetation structure/heights, from the LiDAR vegetation height layer, varies by installation (not available for YPG)
7. Vegetation cover (%), derived from the mean vegetation index
8. Vegetation density, derived from the mean vegetation index
9. Vegetation response to monsoonal precipitation, derived from Landsat 5TM data for pre- and post-monsoon dates, using the percent difference of the MSAVI2 vegetation index
10. Surface water width at inundation depth of 2m
11. Entrenchment Ratio, calculated from the 3m and 0.5m inundated depths
12. Rainfall seasonality index
13. Cumulative area above the reach (m^2)

1. FORT IRWIN

Data inputs used for each 1km stream reach are: Mean Elevation (from LiDAR), Reach slope (PercentSlope from LiDAR), Flow Permanence, Peak Flow (25 yr 1hr event), Total Stream Power (25 yr 1hr event), LiDAR Vegetation Structure (percent <0.25m, 0.25-1m, 1-4m, 4-12m), QuickBird Vegetation Cover from MSAVI2 classification, Mean Vegetation Index from QuickBird MSAVI2 values, Rainfall Seasonality Index, Cumulative Area above the reach (from AGWA results), Entrenchment Ratio (3m/0.5m water surface width), and 2m water surface width.

Note that the LiDAR does not extend all the way to the northern boundary of Fort Irwin, and does not include the Leach Lake Impact Area. Therefore, the final analyses are limited to the LiDAR extent. All data are based on the 1km stream reach – 3m flooded polygon layer IrwNHDPV2es_3mplyfld200mbuffinal.shp and irw3mplyfld200mbufClipLidar.shp (the area covering the LiDAR extent). All stream reaches are identified by a Unique ID.

a) Elevation

Use the LiDAR bareearth layer to get the elevation at the mid-point of each stream reach.

1. Use "Feature Vertices to Points" to get a point at the midpoint of each reach
    a. Input feature = IrwNHDPV2esLidarExtent.shp
    b. Point type = mid
    c. Output feature class = IrwNHDPV2esLidarExtent_MidPts.shp
2. Use "Extract Values to Points" (Spatial Analyst Tools/Extraction) to get the elevation at each point
    a. Input point feature class = IrwNHDPV2esLidarExtent_MidPts.shp
    b. Input raster = bareearth
    c. Output point features = Irw_LiDARExtent-lidelevmidpts.shp
        i. This layer has elevation "RasterValu", and Unique_IDs.

b) LiDAR Slope

Calculate Percent Slope from the LiDAR bare earth layer "barearth" and nhdplusIrwinEdit_Split.shp = PCTSlope.

1. Use 3D Analyst/Functional Surface/Add Surface Information, to add Z-max and Z-min (elevation max and min), and SLength (length of stream reach) to the table.
    a. Input feature class: nhdplusIrwinEdit_Split.shp
    b. Input surface: bareearth
    c. Output property: Select All
2. Export table and save as IrwLiDARSlope.xlsx. Calculate slope from outputs Z-max and Z-min, and SLength
    slope = (Z-max - Z-min)/SLength.
3. Multiply by 100 to get PCTSlope.

c) Flow Permanence

The AGWA results for flow permanence, peak flow, and cumulative area were developed from the AGWA hydrologic models. Detailed instructions for running AGWA to obtain these values are found in the AGWA Guidance Document, tutorial, and in the Master's thesis by Russell Lyon (Lyon, 2013), who conducted the modeling.

AGWA produces a stream network based on the DEM; however, this network does not align with the NHDPV2 streamline, so it was edited to relate the values to the NHDPV2 streamline and the Unique_IDs. The following steps were used to combine the AGWA data and relate it to the NHDPV2 streamline and Unique_IDs. Note that the original flow permanence values were derived from the AGWA results that used USGS Raingage data. Lyon determined that NEXRAD-MPE data produced better results for flow permanence, so additional steps added those results. Flow permanence values derived from the NEXRAD-MPE were used in the stream type classification.

1. Project RaingaugeFP.shp (in AGWA geodatabase FortIrwin.mdb) to WGS84, Irwin_ FP84.shp.
2. Edit so that each 1km polygon within IrwNHDPV2es_200mbuf.shp has one AGWA streamline with one value for flow permanence = Irwin_RG_FP84Edit.shp
3. Intersect to get UniqueIDs with IrwNHDPV2es_200mbuf.shp = IrwAGWAFlwPermEdit84Intersect.shp
4. This shapefile now has the average annual flow permanence results (field AVE_FL_PER) for each UniqueID but it is a line feature class.
5. Join IrwAGWAFlwPermEdit84Intersect.shp to IrwNHDPV2es_200mbuf.shp on UniqueID, then export to preserve join = IrwAGWAFlwPermUniqueID.shp
6. Export the table = IrwAGWAFlwPerm.dbf, save as IrwAGWAFlwPerm.xlsx
7. Get Flow Perm values from NEXRAD data = NEXRAD_FP.shp (in AGWA geodatabase FortIrwin.mdb). This layer has the same streamnum-contrib-seqnum as the rain gage file Irwin_RG_FP84Edit.shp, and has the code AGWA_Code.
8. Copy Irwin_RG_FP84Edit.shp to Irwin_RG_FP84EditCopy.shp, and delete extra fields (all the day & pct fields except the first and last).
9. Join IrwNEXRAD_FPcopy.shp on NexradCode to Irwin_RG_FP84EditCopy.shp on AGWA_Code. This joins the NEXRAD Flow Permanence values to the edited streamline.

10. Export to save join = IrwRG_FP84EditCopy_Nexrad.shp
11. Intersect IrwRG_FP84EditCopy_Nexrad.shp with IrwNHDPV2es_200mbuf.shp to get UniqueIDs and NEXRAD flow permanence values = IrwRG_FP84EditCopy_Nexrad_UniqueID.shp.
12. Clip to the LiDAR extent with IrwBoundaryLiDARExtent.shp = IrwRG_FP84EditCopy_Nexrad_UniqueIDclipLidar.shp

Climate Change Analysis

An analysis was conducted in AGWA/SWAT to estimate how projected climate change would impact flow permanence values. Downscaled climate projection data were obtained from the Coupled Model Intercomparison Project phase 3 (CMIP3) multi-model dataset. These data were created from global circulation model results included in the Intergovernmental Panel on Climate Change Fourth Assessment Report and were downscaled to a 12 km^2 spatial and daily temporal resolution using a BCCA technique (a description of the technique and CMIP3 data can be found at http://gdo-dcp.ucllnl.org). Included are projections of minimum temperature, maximum temperature, and precipitation from two time periods (1981-2000 and 2081-2100) generated by NOAA's Geophysical Fluid Dynamics Laboratory Climate Model 2.1 (http://www.gfdl.noaa.gov/) for the A2 emissions path that can be used to drive SWAT2000 and analyze for changes under a warming climate scenario.

BCCA_CMIP3_FP.shp has the projected and historic flow permanence values based on the BCCA CMIP3 data. These are downscaled at the same resolution, so are used together for the climate change scenario.

Add the BCCA Flow Permanence values for the Historic and Projected climate change data:

1. Edit to remove extra fields and add the code for StrmNum + Contrib + SeqNum = BCCA_CMIP3_FPCopyEdit.shp.
2. Join BCCA_CMIP3_FPCopyEdit.shp to IrwRG_FP84EditCopy_Nexrad_UniqueIDclipLidar.shp on the code

d) Peak Flow

All peak flow results were analyzed; however, only the 25-year 1-hour peak flow values were used in the stream type classification.

1. Use the AGWA shapefiles for peak flow All_5yr1h.shp, All_10yr1h.shp, All_25yr1hr.shp, and All_100yr1hr.shp
2. Project to WGS84: irw_5y1h_PF84.shp, irw_10y1h_PF84.shp, irw_25y1h_PF84.shp, and irw_100y1hrPF84.shp
3. Create AGWA codes to join these tables back to the Flow Permanence layer that has been edited and joined to have the Unique_IDs (IrwAGWAFlwPermUniqueID.shp). Repeat for all shapefiles: IrwAGWAFlwPermUniqueID.shp, irw_5y1h_PF84.shp, irw_25y1h_PF84.shp. QP_m3_s is the Peak flow value.
    a. Add field "strmnum_tx" as text type, calc = StreamNum
    b. Add field "contrib_tx" as text type, calc = CONTRIB

   c. Add field “seqnum_tx” as text type, calc = SeqNum
   d. Add field “AGWA_Code” as text type, calc = [strmnum_tx] + "_" + [contrib_tx] +"_" + [seqnum_tx]
4. Join irw_5y1h_PF84.shp, irw10y1h_PF84.shp, and irw_25y1h_PF84.shp to IrwAGWAFlwPermUniqueID.shp on AGWA_Code
5. Export the tables which have the Flow Permanence values, 5yr 1hr Peak Flow values, 10yr 1hr Peak Flow, and 25yr 1hr Peak Flow and Cumulative Area values for each Unique_ID, and save as excel files: IrwAGWA_FP_PF5y1h.xlsx, IrwAGWA_FP_PF10y1h.xlsx, and IrwAGWA_FP_PF25y1h.xlsx
6. To match the UniqueIDs for just the LiDAR extent, join these excel tables to Irw3mplyfld200mbufClipLidar.shp on UniqueID:
7. Add 100 year Peak Flow.
   a. Create the codes in irw_100y1h_PF84.shp = PF100Code
   b. Join to IrwRG_FP84EditCopy_NexradUniqueIDclipLidar.shp on NexradCode (make sure it has this code and the uniqueID)
   c. Export to preserve join = IrwRG_FPNexradclipLidar100ycodeTable.dbf/xlsx

e) Total Stream Power

Use LiDARSlope and AGWA Peak Flow for the 5, 10, 25 and 100 year events to calculate Total Stream Power. These calculations are in the “copy-edit” tab in the Irwin_reach.xlsx file. This file contains the final geomorphology data and calculations, but they were not used to calculate TSP. Only the 25 year TSP values were used in the stream type classification.

Q25TSP-AGWA = 9.81 * LiDARSlope * QP25yr = kW/m

f) LiDAR Vegetation Structure

Vegetation Structure represents the various zones or regions in vegetation that are typically used by wildlife, and the total amount of vegetation that is within that height layer.Vegetation structure is derived from the multi-return LiDAR vegetation height layer (calculated as canopy/first return minus ground/last return) and classified into vegetation height categories based on typical vegetation types: <0.25m, 0.25m-1m, 1-4m, 4-12m. Steps to derive the LiDAR Vegetation Structure layers are in the Riparian Vegetation Guidance Document.

g) Percent Vegetation Cover

Vegetation cover (%) is derived from the QuickBird satellite imagery, using a vegetation index (MSAVI2) to classify the 1km stream reaches into vegetation vs. bare ground or ground cover, with aerial photography and field photos as guides to verify vegetation pattern, abundance and cover. It is calculated as total area of vegetation pixels divided by total area of the 1km stream reach polygon. More details and steps to derive vegetation cover are in the Riparian Vegetation Guidance Document.

h) Mean Vegetation Index

The Mean Vegetation Index describes the relative vegetation density for each 1km stream reach, calculated using only the pixels classified as vegetation cover from the satellite imagery (i.e. the

pixels classified as bare ground or ground cover were not used to derive this variable). In areas of sparse vegetation, both vegetation and soil properties are represented by the vegetation index. Therefore, the Mean Vegetation Index can indicate the overall sparseness or density of vegetation.The Mean Vegetation Index is derived from the QuickBird satellite imagery, from the vegetation index (MSAVI2). Steps to derive mean vegetation index are in the Riparian Vegetation Guidance Document.

i) Mean Riparian Widths

The mean riparian width represents the mean value of the water surface extent at various inundation depths for each 1km stream reach polygon. Riparian width can be related to riparian vegetation extent, or channel bottom. It is derived using the Hydro-Geomorphic Valley Classification (HGVC) tool in ArcMap, to create a polygon delineating the water surface at the specified depth. The HGVC tool requires a filled DEM and a stream network (the edited NHD stream line). Riparian width is calculated as the area of each 1km stream reach polygon divided by the actual length of the 1km stream reach.

Steps to derive riparian widths are in the Geomorphic Data Guidance Document. The final values for widths 0.25m, 0.5m, 1m, 2m, and 3m are in IrwVariables.xlsx, rip-width tab. The 3m width polygon was used to calculate the riparian vegetation variables, the 2m width values were used in the stream type classification, and the 3m and 0.5m widths were used to calculate the entrenchment ratio.

j) Entrenchment Ratio

The entrenchment ratio indicates the degree of channel entrenchment or the vertical containment of the river. It is usually calculated as Flood Prone Width divided by Bankfull Width from field data. We did not collect those data in the field; therefore, it is calculated here using mean riparian widths: 3m / 0.5m. This assumes Water Surface Width at 3m inundation depth approximates Flood Prone Width, and Water Surface Width at 0.5m inundation depth approximates Bankfull Width. Lower values (closer to 1) for the entrenchment ratio indicate increased entrenchment.

k) Rainfall Seasonality Index (RSI)

The Rainfall Seasonality Index: describes precipitation characteristics and indicates the intensity of erosion potential due to precipitation characteristics, derived from PRISM 30 year normals (PRISM Climate Group, 2010), calculated as the mean precipitation of the wettest month divided by the mean annual precipitation, for the 30-year period 1980-2010. Steps to derive the rainfall seasonality index are in the Geomorphic Data Guidance Document.

l) Cumulative Area

Cumulative area above the reach (m2) represents the watershed area above the reach that contributes to stream flow at that reach, and is related to channel geometry and vegetation community differences. It is obtained from the AGWA model outputs. The AGWA results for cumulative area above each reach (cum_area) are from IrwAGWAFlwPermUniqueID.shp.

2. YPG

Data inputs used for each 1km stream reach are: Mean Elevation (from 10m DEM), Reach slope (PercentSlope from 10m DEM), Flow Permanence, Peak Flow (25 yr 1hr event), Total Stream

Power (25 yr 1hr event), RapidEye Vegetation Cover from Red Edge NDVI classification, Mean Vegetation Index from RapidEye Red Edge NDVI values, Rainfall Seasonality Index, Cumulative Area above the reach (from AGWA results), Entrenchment Ratio (3m/0.5m water surface width), and 2m water surface width. LiDAR exists for only small areas of YPG, therefore the vegetation height analysis cannot be performed.

All data are based on the 1km stream reach – 3m flooded polygon layer YPGNHDPV2es_3mplyfld200mbuffinal.shp. All stream reaches are identified by a Unique_ID.

a) Mean Elevation

Use the USGS 10m DEM, ypg10dem, to get the mean elevation for each 1km stream reach.

1. Use Zonal Statistics Tool "ZonesWOverlap"
    a. Zone layer: YPGNHDPV2es_3mplyfld200mbuffinal.shp
    b. Input Raster: ypg10dem
    c. Zone field: Unique_ID
    d. Output table: YPG_10mdemtable.dbf. Save as excel file .xlsx.

b) Slope

Calculate Percent Slope from the 10m DEM and YPG_NHDPlusV2_es.shp = PCTSlope.

1. Use 3D Analyst/Functional Surface/Add Surface Information to calculate slope from the 10m DEM ypg10dem_utm and YPG_NHDPlusV2_es.shp to add Z-max, Z-min, and SLength to the table.
2. Export the table as YPG10mSlope.dbf, save as xlsx.
3. Calc slope = (Zmax-Zmin)/SLength. These calcs are in YPG10mSlope.xlsx, copy-edit tab.
4. Calculate PCTSLOPE by multiplying by 100.

c) Flow Permanence

The AGWA results for flow permanence, peak flow, and cumulative area were developed from the AGWA hydrologic models. Detailed instructions for running AGWA to obtain these values are found in the AGWA Guidance Document, tutorial, and in the Master's thesis by Russell Lyon (Lyon, 2013), who conducted the modeling.

AGWA produces a stream network based on the DEM; however, this network does not align with the NHDPV2 streamline, so it was edited to relate the values to the NHDPV2 streamline and the Unique_IDs. The following steps were used to combine the AGWA data and relate it to the NHDPV2 streamline and Unique_IDs. Note that the original flow permanence values were derived from the AGWA results that used USGS Raingage data. Lyon determined that NEXRAD-MPE data produced better results for flow permanence, so additional steps added those results. Flow permanence values derived from the NEXRAD-MPE were used in the stream type classification.

1. Project YPG_RG_FP.shp, YPG_5yr1hr.shp, YPG_10yr1hr.shp and YPG_25yr1hr.shp to WGS84 = YPG_RGFP84.shp, YPG_5yr1hr84.shp, YPG_10yr1hr84.shp and YPG_25yr1hr84.shp
2. Edit to match the NHDPV2 flooded polygons. First combine the layers so all values are in one shapefile.
    a. Intersect YPG_5yr1hr84.shp, YPG_10yr1hr84 and YPG_25yr1hr84.shp = YPG_Qp5_10_25Intersect.shp
    b. Add YPG_RGFP84_edit.shp (this does not have the unneeded fields) = YPG_Qp5_10_25_FlPerm_Intersect.shp
    c. Copy to YPG_Qp5_10_25_FlPerm_Inters_edit.shp
3. Edit YPG_Qp5_10_25_FlPerm_Inters_edit.shp so that there is one AGWA line for each Unique_ID polygon.
4. Intersect to get UniqueIDs with YPGNHDPV2es_200mbuf.shp = YPG_AGWAStreamlines_UniqueID.shp
   This shapefile now has the average annual flow permanence results and all peak flow results for each UniqueID but it is a line feature class.
5. Join YPG_AGWAStreamlines_UniqueID.shp to YPGNHDPV2es_200mbuf.shp on UniqueID, then export to preserve join =YPG_AGWAResults_UniqueID.shp

Climate Change Analysis

An analysis was conducted in AGWA/SWAT to estimate how projected climate change would impact flow permanence values. Downscaled climate projection data were obtained from the Coupled Model Intercomparison Project phase 3 (CMIP3) multi-model dataset. These data were created from global circulation model results included in the Intergovernmental Panel on Climate Change Fourth Assessment Report and were downscaled to a 12 km^2 spatial and daily temporal resolution using a BCCA technique (a description of the technique and CMIP3 data can be found at http://gdo-dcp.ucllnl.org). Included are projections of minimum temperature, maximum temperature, and precipitation from two time periods (1981-2000 and 2081-2100) generated by NOAA's Geophysical Fluid Dynamics Laboratory Climate Model 2.1 (http://www.gfdl.noaa.gov/) for the A2 emissions path that can be used to drive SWAT2000 and analyze for changes under a warming climate scenario.

Get the NEXRAD and BCCA_CMIP3 climate change Flow Permanence values:
These data are in the YumaProvingGrounds.mdb AGWA geodatabase.
BCCA_CMIP3_FP.shp has the projected and historic flow permanence values based on the BCCA CMIP3 data. These are downscaled at the same resolution, so are used together for the climate change scenario.

1. Export all 3 Flow Permanence feature classes from the geodatabase YumaProvingGrounds.mdb to shapefiles. Delete extra fields from each of these shapefiles and save as BCCA_CMIP3_FPcopy.shp, NEXRAD_FPcopy.shp, RainGaugeFPcopy.shp
2. Spatial join BCCA_CMIP3_FPcopy.shp and NEXRAD_FPcopy.shp = YPG_BCCA_Nexrad_SplJn.shp

This now has the flow permanence values for all these two datasets, and the StrmNum, Contrib, and SeqNum that matches the code in YPG_AGWAStreamlines_UniqueID.shp which has been edited to match and has the Unique_IDs. Check to make sure this code matches.

3. Create this code in YPG_BCCA_Nexrad_ SplJn.shp = NewFPCode
4. Join to YPG_AGWAStreamlines_UniqueID.shp on the codes.

d) Peak Flow

All peak flow results were analyzed; however, only the 25-year 1-hour peak flow values were used in the stream type classification. The Peak Flow values were obtained at the same time as the Flow Permanence values, so the steps from that section are repeated here.

1. Project YPG_RG_FP.shp, YPG_5yr1hr.shp, YPG_10yr1hr.shp and YPG_25yr1hr.shp to WGS84 = YPG_RGFP84.shp, YPG_5yr1hr84.shp, YPG_10yr1hr84.shp and YPG_25yr1hr84.shp
2. Edit to match the NHDPV2 flooded polygons. First combine the layers so all values are in one shapefile.
    a. Intersect YPG_5yr1hr84.shp, YPG_10yr1hr84 and YPG_25yr1hr84.shp = YPG_Qp5_10_25Intersect.shp
    b. Add YPG_RGFP84_edit.shp (this does not have the unneeded fields) = YPG_Qp5_10_25_FlPerm_Intersect.shp
    c. Copy to YPG_Qp5_10_25_FlPerm_Inters_edit.shp
3. Edit YPG_Qp5_10_25_FlPerm_Inters_edit.shp so that there is one AGWA line for each Unique_ID polygon.
4. Intersect to get UniqueIDs with YPGNHDPV2es_200mbuf.shp = YPG_AGWAStreamlines_UniqueID.shp
   This shapefile now has the average annual flow permanence results and all peak flow results for each UniqueID but it is a line feature class.
5. Join YPG_AGWAStreamlines_UniqueID.shp to YPGNHDPV2es_200mbuf.shp on UniqueID, then export to preserve join =YPG_AGWAResults_UniqueID.shp
6. Add the 100 year event
    a. Project YPG_100yr1hr.shp to WGS84 = YPG_100yr1hr84.shp
    b. Intersect YPG_100yr1hr84.shp and YPG_25yr1hr84.shp = YPG_Qp25100Intersect.shp
    c. Create code in YPG_Qp25100Intersect.shp = Code25100 (use the second set of codes)
    d. Create code in YPG_Qp5_10_25_FlPerm_Inters_edit.shp = Code51025 (use the second set of codes)
    e. Join YPG_Qp25100Intersect.shp to YPG_Qp5_10_25_FlPerm_Inters_edit.shp
    f. Export to preserve join = YPG_Qp100IntersectEdit.shp

g. Join YPG_Qp100IntersectEdit.shp to YPG_AGWAStreamlines_UniqueID.shp on codes to get Unique_ID for the Qp100 values. Export to preserve join = YPG_Qp100UniqueID.shp

e) Total Stream Power

Use 10m DEM PCTSlope and AGWA Peak Flow for the 5, 10, 25 and 100 year events to calculate Total Stream Power. These calculations are in the GeomorphInputs tab. Only the 25 year TSP values were used in the stream type classification.

Q25TSP-AGWA = 9.81 * LiDARSlope * QP25yr = kW/m

f) Percent Vegetation Cover

Vegetation cover (%) is derived from the RapidEye satellite imagery, using a vegetation index (Red Edge NDVI) to classify the 1km stream reaches into vegetation vs. bare ground or ground cover, with aerial photography and field photos as guides to verify vegetation pattern, abundance and cover. It is calculated as total area of vegetation pixels divided by total area of the 1km stream reach polygon. More details and steps to derive vegetation cover are in the Riparian Vegetation Guidance Document.

g) Mean Vegetation Index

The Mean Vegetation Index describes the relative vegetation density for each 1km stream reach, calculated using only the pixels classified as vegetation cover from the satellite imagery (i.e. the pixels classified as bare ground or ground cover were not used to derive this variable). In areas of sparse vegetation, both vegetation and soil properties are represented by the vegetation index. Therefore, the Mean Vegetation Index can indicate the overall sparseness or density of vegetation.The Mean Vegetation Index is derived from the RapidEye satellite imagery, from the vegetation index (Red Edge NDVI). Steps to derive mean vegetation index are in the Riparian Vegetation Guidance Document.

h) Mean Riparian Widths

The mean riparian width represents the mean value of the water surface extent at various inundation depths for each 1km stream reach polygon. Riparian width can be related to riparian vegetation extent, or channel bottom. It is derived using the Hydro-Geomorphic Valley Classification (HGVC) tool in ArcMap, to create a polygon delineating the water surface at the specified depth. The HGVC tool requires a filled DEM and a stream network (the edited NHD stream line). Riparian width is calculated as the area of each 1km stream reach polygon divided by the actual length of the 1km stream reach.

Steps to derive riparian widths are in the Geomorphic Data Guidance Document. The final values for widths 0.25m, 0.5m, 1m, 2m, and 3m are in YPGVariables.xlsx, rip_width tab. The 3m width polygon was used to calculate the riparian vegetation variables, the 2m width values were used in the stream type classification, and the 3m and 0.5m widths were used to calculate the entrenchment ratio.

i) Entrenchment Ratio

The entrenchment ratio indicates the degree of channel entrenchment or the vertical containment of the river. It is usually calculated as Flood Prone Width divided by Bankfull Width from field data. We did not collect those data in the field; therefore, it is calculated here using mean riparian widths: 3m / 0.5m. This assumes Water Surface Width at 3m inundation depth approximates Flood Prone Width, and Water Surface Width at 0.5m inundation depth approximates Bankfull Width. Lower values (closer to 1) for the entrenchment ratio indicate increased entrenchment.

j) Rainfall Seasonality Index (RSI)

The Rainfall Seasonality Index: describes precipitation characteristics and indicates the intensity of erosion potential due to precipitation characteristics, derived from PRISM 30 year normals (PRISM Climate Group, 2010), calculated as the mean precipitation of the wettest month divided by the mean annual precipitation, for the 30-year period 1980-2010. Steps to derive the rainfall seasonality index are in the Geomorphic Data Guidance Document.

k) Cumulative Area

Cumulative area above the reach (m2) represents the watershed area above the reach that contributes to stream flow at that reach, and is related to channel geometry and vegetation community differences. It is obtained from the AGWA model outputs. The AGWA results for cumulative area above each reach (cum_area) are from YPG_AGWAResults_UniqueID.shp.

l) LiDAR

Minimal LiDAR exists for YPG; however, there are multi-return tiles for an area that includes the Mesquite Bosques, Game & Fish wildlife cameras, and streamlines in the northern Cibola region, near the headwaters of Mojave Wash. These tiles were processed for analysis of vegetation height and for analysis of the wildlife camera data.

Data: 2008

dem_60cm_a1_cibola_range_tile1.tif, dem_bare_60cm_cibola_range_tile1.tif
dem_60cm_a1_cibola_range_tile2.tif, dem_bare_60cm_cibola_range_tile2.tif
dem_60cm_a1_cibola_range_tile3.tif, dem_bare_60cm_cibola_range_tile3.tif
dem_60cm_a1_cibola_range_tile4.tif, dem_bare_60cm_cibola_range_tile4.tif
dem_60cm_a1_cibola_range_tile5.tif, dem_bare_60cm_cibola_range_tile5.tif
dem_60cm_a1_cibola_range_tile6.tif, dem_bare_60cm_cibola_range_tile6.tif
dem_60cm_a1_yuma_jerc2.tif, dem_bare_60cm_yuma_jerc2.tif

Data: 2010

dem_50cm_a1_yuma_jerc3.tif, dem_bare_60cm_yuma_jerc3.tif

3. FORT HUACHUCA

Data inputs used for each 1km stream reach are: Mean Elevation (from LiDAR), Reach slope (PercentSlope from LiDAR), Flow Permanence, Peak Flow (25 yr 1hr event), Total Stream Power (25 yr 1hr event), LiDAR Vegetation Structure (percent <1m, 1-4m, 4-12m >12m), MSAVI2 Vegetation Cover, MSAVI2 Mean, Rainfall Seasonality Index, Cumulative Area above the reach (from AGWA results), Entrenchment Ratio (3m/0.5m water surface width), and 2m water surface width.

All data are based on the 1km stream reach – 3m flooded polygon layer HuaNHDPV2es_3mplyfld200mbuffinal.shp. All stream reaches are identified by a Unique_ID.

a) Elevation

Use LiDAR bare earth layer, fth_be2013, to get the elevation at the mid-point of each stream reach.

1. Use "Feature Vertices to Points" to get a point at the midpoint of each reach.
   Input feature = Fth_hhdpv2splitedit.shp
   Point type = mid
   Output feature class = fth_nhdpv2splitedit_midpt.shp
   Use "Extract Values to Points" (Spatial Analyst Tools/Extraction) to get the elevation at each point =
   Input point feature class = fth_nhdpv2splitedit_midpt.shp
   Input raster = fth_be2013
   Output point features = fth_lidelevemidpts.shp
   This feature class has elevation "RasterValu", and Unique_IDs.
2. Join fth_lidelevmidpts.shp to fth_hhdpv2splitedit.shp on Unique_ID
3. Export to preserve join = hua_lidelevmidptsUniqueID.shp

b) LiDAR Slope

Calculate Percent Slope from the LiDAR bare earth layer fth_be2013 and fth_nhdpv2splitedit.shp = LiDARSlope.

1. Use 3D Analyst/Functional Surface/Add Surface Information, from NHDPV2 split streamline.
2. Calculate slope from outputs Z-max and Z-min, and SLength, slope = (Z-max - Z-min)/SLength.

c) Flow Permanence

The AGWA results for flow permanence, peak flow, and cumulative area were developed from the AGWA hydrologic models. Detailed instructions for running AGWA to obtain these values are found in the AGWA Guidance Document, tutorial, and in the Master's thesis by Russell Lyon (Lyon, 2013), who conducted the modeling.

AGWA produces a stream network based on the DEM; however, this network does not align with the NHDPV2 streamline, so it was edited to relate the values to the NHDPV2 streamline and the Unique_IDs. The following steps were used to combine the AGWA data and relate it to the NHDPV2 streamline and Unique_IDs. Note that the original flow permanence values were derived from the AGWA results that used USGS Raingage data. Lyon determined that NEXRAD-MPE data produced better results for flow permanence, so additional steps added those results. Flow permanence values derived from the NEXRAD-MPE were used in the stream type classification.

1. The AGWA flow permanence result using the rain gages, HuachucaAllRG_FP.shp, was edited to remove streamlines not within hua_nhdpv2se200mbuf.shp = HuaAGWAFlwPermEdit.shp, then projected to WGS84 = HuaAGWAFlwPermEdit84.shp
2. To get Unique_ID's: Intersect with fth_nhdpv2se200mbuf.shp = HuaAGWAFlwPermEdit84Intersect.shp
3. This shapefile now has the average annual flow permanence results (field AnnAve) for each Unique_ID, but there are multiple flow permanence values for each Unique_ID.
    a. Use the flow permanence value for the longest stream segment associated with each Unique_ID.
    b. Add field and calc "length". Export table and save in excel = hua_agwaflowpermtable.xlsx
4. New Flow Permanence values were generated using NEXRAD data (new data with superior results for flow permanence) = NEXRAD_FP.shp (in AGWA geodatabase FortHuachuca.mdb. This layer has the same streamnum-contrib-seqnum (AGWA-generated values) as the rain gage file used above. Create a code with these values in the NEXRAD_FP.shp file and in HuaAGWAFlwPermRG_NEXRAD.shp
    a. Add new field AGWA_code
    b. Calculate code in field calculator as: "streamnum" + "_" + "contrib" + "_" + "seqnum"
    c. Save shapefile as NEXRAD_FPCode.shp
    d. Join the two files on the codes, and export to preserve join = HuaAGWAFlwPermRG_NEXRAD.shp
    e. This shapefile now has both flow permanence values and the Unique_ID.

Climate change Analysis

An analysis was conducted in AGWA/SWAT to estimate how projected climate change would impact flow permanence values. Downscaled climate projection data were obtained from the Coupled Model Intercomparison Project phase 3 (CMIP3) multi-model dataset. These data were created from global circulation model results included in the Intergovernmental Panel on Climate Change Fourth Assessment Report and were downscaled to a 12 km^2 spatial and daily temporal resolution using a BCCA technique (a description of the technique and CMIP3 data can be found at http://gdo-dcp.ucllnl.org). Included are projections of minimum temperature, maximum temperature, and precipitation from two time periods (1981-2000 and 2081-2100) generated by NOAA's Geophysical Fluid Dynamics Laboratory Climate Model 2.1 (http://www.gfdl.noaa.gov/) for the A2 emissions path that can be used to drive SWAT2000 and analyze for changes under a warming climate scenario.

Two rainfall input files using both the historical and projected BCCA precipitation data were created from these data for use in the AGWA/SWAT model.
BCCA_hist.dbf (the historic rainfall data file, for 1981-2000)
BCCA_proj.dbf (the projected rainfall data file, for 2081-2100)
CMIP3_VG.shp (the shapefile with the location of the virtual gages)

BCCA_CMIP3_FP.shp has the projected and historic flow permanence values based on the BCCA CMIP3 data. These are downscaled at the same resolution, so are used together for the climate change scenario.

1. Spatial join BCCA_CMIP3_FPEdit.shp to HuaAGWAFlwPermEdit84Intersect.shp (has Unique_IDs), using a 10m distance for the intersection = HuaAGWAFlwPerm_BCCA.shp

d) Peak Flow

All peak flow results were analyzed; however, only the 25-year 1-hour peak flow was used in the stream type classification.

1. Use the AGWA shapefiles HuachucaStreams_5yr1hr.shp, HuachucaStreams_10yr1hr.shp, HuachucaStreams__25yr1hr.shp, and HuachucaStreams_100yr1h.shp
2. Project to WGS84: Hua_AGWAPkFlw5y1h84.shp, Hua_PkFlw10yr1hr84.shp, and Hua_PkFlw25yr1hr84.shp, Hua_PkFlw100yr1hr84.shp
3. Edit so that each 1km polygon within HuaNHDPV2es_200mbuffinal.shp has one AGWA streamline with one value for flow permanence = Hua_PkFlw10yr1hr84Edit.shp
4. Intersect to get UniqueIDs withHuaNHDPV2es_3mplyfld200mbuf.shp =HuaAGWAPkFlwEditIntersect.shp
5. This shapefile now has the 10 year 1 hour Peak Flow results (field Qp10m3s) for each UniqueID.
6. Export the table = HuaAGWAPkFlwEditIntersectTable.dbf
7. Add the 25year event. Add AGWA codes: StreamNum, Contrib, SeqNum to Hua_PkFlw25yr1hr84.shp and HuaAGWAPkFlwEditIntersect.shp
8. Join on the codes.

e) Total Stream Power

Use LiDARSlope and AGWA Peak Flow for the 10year and 25 year events to calculate Total Stream Power. These calculations are in the "copy-editCorrected" tab in the Huachuca_reach.xlsx file. This file contains the final geomorphology data and calculations, but they were not used to calculate TSP. Only the 25 year TSP values were used in the stream type classification.

Q25TSP-AGWA = 9.81 * LiDARSlope * QP25yr = kW/m

f) LiDAR Vegetation structure

Vegetation Structure represents the various zones or regions in vegetation that are typically used by wildlife, and the total amount of vegetation that is within that height layer.Vegetation structure is derived from the multi-return LiDAR vegetation height layer (calculated as canopy/first return minus ground/last return) and classified into vegetation height categories based on typical vegetation types: <1m, 1-4m, 4-12m, >12m. Steps to derive the LiDAR Vegetation Structure layers are in the Riparian Vegetation Guidance Document.

g) Percent Vegetation Cover

Vegetation cover (%) is derived from the QuickBird satellite imagery, using a vegetation index (MSAVI2) to classify the 1km stream reaches into vegetation vs. bare ground or ground cover,

with aerial photography and field photos as guides to verify vegetation pattern, abundance and cover. It is calculated as total area of vegetation pixels divided by total area of the 1km stream reach polygon. More details and steps to derive vegetation cover are in the Riparian Vegetation Guidance Document.

h) Mean Vegetation Index

The Mean Vegetation Index describes the relative vegetation density for each 1km stream reach, calculated using only the pixels classified as vegetation cover from the satellite imagery (i.e. the pixels classified as bare ground or ground cover were not used to derive this variable). In areas of sparse vegetation, both vegetation and soil properties are represented by the vegetation index. Therefore, the Mean Vegetation Index can indicate the overall sparseness or density of vegetation.The Mean Vegetation Index is derived from the QuickBird satellite imagery, from the vegetation index (MSAVI2). Steps to derive mean vegetation index are in the Riparian Vegetation Guidance Document.

i) Mean Riparian Widths

The mean riparian width represents the mean value of the water surface extent at various inundation depths for each 1km stream reach polygon. Riparian width can be related to riparian vegetation extent, or channel bottom. It is derived using the Hydro-Geomorphic Valley Classification (HGVC) tool in ArcMap, to create a polygon delineating the water surface at the specified depth. The HGVC tool requires a filled DEM and a stream network (the edited NHD stream line). Riparian width is calculated as the area of each 1km stream reach polygon divided by the actual length of the 1km stream reach.

Steps to derive riparian widths are in the Geomorphic Data Guidance Document. The final values for widths 0.25m, 0.5m, 1m, 2m, and 3m are in HuaVariables.xlsx, rip-width tab. The 3m width polygon was used to calculate the riparian vegetation variables, the 2m width values were used in the stream type classification, and the 3m and 0.5m widths were used to calculate the entrenchment ratio.

j) Entrenchment Ratio

The entrenchment ratio indicates the degree of channel entrenchment or the vertical containment of the river. It is usually calculated as Flood Prone Width divided by Bankfull Width from field data. We did not collect those data in the field; therefore, it is calculated here using mean riparian widths: 3m / 0.5m. This assumes Water Surface Width at 3m inundation depth approximates Flood Prone Width, and Water Surface Width at 0.5m inundation depth approximates Bankfull Width. Lower values (closer to 1) for the entrenchment ratio indicate increased entrenchment.

k) Rainfall Seasonality Index (RSI)

The Rainfall Seasonality Index: describes precipitation characteristics and indicates the intensity of erosion potential due to precipitation characteristics, derived from PRISM 30 year normals (PRISM Climate Group, 2010), calculated as the mean precipitation of the wettest month divided by the mean annual precipitation, for the 30-year period 1980-2010. Steps to derive the rainfall seasonality index are in the Geomorphic Data Guidance Document.

l) Cumulative Area

Cumulative area above the reach (m2) represents the watershed area above the reach that contributes to stream flow at that reach, and is related to channel geometry and vegetation community differences. It is obtained from the AGWA model outputs. The AGWA results for cumulative area above each reach (cum_area) are from Hua_AGWAFP_PkFl5JoinIntersecttable.dbf.

4. FORT BLISS

Data inputs used for each 1km stream reach are: Mean Elevation (from LiDAR), Reach slope (PercentSlope from LiDAR), Flow Permanence, Peak Flow (25 yr 1hr event), Total Stream Power (25 yr 1hr event), LiDAR Vegetation Structure (percent <0.5m, 0.5-1m, 1-4m, 4-12m, >12m), RapidEye Vegetation Cover from Red Edge NDVI classification, Mean Vegetation Index from RapidEye Red Edge NDVI values, Rainfall Seasonality Index, Cumulative Area above the reach (from AGWA results), Entrenchment Ratio (3m/0.5m water surface width), and 2m water surface width.

All data are based on the 1km stream reach – 3m flooded polygon layer BlsNHDPV2es_200mbufplyfldemfinal1.shp. All stream reaches are identified by a Unique_ID.

a) Elevation

Use LiDAR bare earth layer bareearth_original from geodatabase FtBliss_orig.gdb to get the elevation at the mid-point of each stream reach.

1. Use "Feature Vertices to Points" to get a point at the midpoint of each reach
    a. Input feature =nhdplusBlissEdit_Split.shp
    b. Point type = mid
    c. Output feature class = nhdplusBlissEditSplitmidpts.shp
2. Use "Extract Values to Points" (Spatial Analyst Tools/Extraction) to get the elevation at each point
    a. Input point feature class = nhdplusBlissEditSplitmidpts.shp
    b. Input raster = bareearth_original
    c. Output point features = Bls_lidelevemidpts.shp. This has elevation "RasterValu", and Unique_IDs.
3. Join to nhdplusBlissEditSplitmidpts.shp on Unique_ID
4. Export to preserve join = bls_lidelevmidptsUniqueID.shp

b) LiDAR Slope

Calculate Percent Slope from the LiDAR bare earth layer *bareearth_original* and BlsNHDPV2es_200mbufplyfld3mfinal2.shp = LiDARSlope.

1. Use 3D Analyst/Functional Surface/Add Surface Information, to add Z-max and Z-min (elevation max and min), and SLength (length of stream reach) to the table.
    a. Input feature class: BlsNHDPV2es_200mbufplyfld3mfinal2.shp
    b. Input surface: bareearth_original: Select All

2. Export table and save as BlsLiDARSlope.xlsx. Calculate slope from outputs Z-max and Z-min, and SLength
   slope = (Z-max - Z-min)/SLength

c) Flow Permanence

The AGWA results for flow permanence, peak flow, and cumulative area were developed from the AGWA hydrologic models. Detailed instructions for running AGWA to obtain these values are found in the AGWA Guidance Document, tutorial, and in the Master's thesis by Russell Lyon (Lyon, 2013), who conducted the modeling.

AGWA produces a stream network based on the DEM; however, this network does not align with the NHDPV2 streamline, so it was edited to relate the values to the NHDPV2 streamline and the Unique_IDs. The following steps were used to combine the AGWA data and relate it to the NHDPV2 streamline and Unique_IDs. Note that the original flow permanence values were derived from the AGWA results that used USGS Raingage data. Lyon determined that NEXRAD-MPE data produced better results for flow permanence, so additional steps added those results. Flow permanence values derived from the NEXRAD-MPE were used in the stream type classification.

1. Original shapefile Bliss_Flow_Perm_RG.shp, Project to WGS84 Bliss_Flow_Perm_RG84.shp
2. Edit to NHDPV2 streamlines: Copy Bliss_Flow_Perm_RG84.shp, rename to Bliss_Flow_Perm_RG84edit.shp
3. Clip to Bliss boundary with install_area_aggreg.shp (use Cartography Tools/Generalization/Aggregate Polygons to combine all polygons in Bliss boundary layer) = Bliss_FlowPermRG84_editclip.shp
4. Intersect with BlsNHDPV2EditSplit200mbuf.shp to get Unique_ID with Flow Permanence results = Bliss_FlowPermRG84edit_UniqID.shp. This is the final shapefile that has been edited to remove the duplicate unique_IDs.
5. Join to BlsNHDPV2es_200mbufplyfld3mfinal2.shp on Unique_ID to get a flow permanence value for each Unique_ID.

<u>Climate Change Analysis</u>

An analysis was conducted in AGWA/SWAT to estimate how projected climate change would impact flow permanence values. Downscaled climate projection data were obtained from the Coupled Model Intercomparison Project phase 3 (CMIP3) multi-model dataset. These data were created from global circulation model results included in the Intergovernmental Panel on Climate Change Fourth Assessment Report and were downscaled to a 12 km^2 spatial and daily temporal resolution using a BCCA technique (a description of the technique and CMIP3 data can be found at http://gdo-dcp.ucllnl.org). Included are projections of minimum temperature, maximum temperature, and precipitation from two time periods (1981-2000 and 2081-2100) generated by NOAA's Geophysical Fluid Dynamics Laboratory Climate Model 2.1 (http://www.gfdl.noaa.gov/) for the A2 emissions path that can be used to drive SWAT2000 and analyze for changes under a warming climate scenario.

The NEXRAD and BCCA_CMIP3 climate change Flow Permanence values are in the FortBliss.mdb AGWA geodatabase.
BCCA_CMIP3_FP.shp has the projected and historic flow permanence values based on the BCCA CMIP3 data. These are downscaled at the same resolution, so are used together for the climate change scenario.

1. Export all 3 Flow Permanence feature classes from the geodatabase FortBliss.mdb to shapefiles. Delete extra fields from each of these shapefiles and save them as BCCA_CMIP3_FPcopy.shp, NEXRAD_FPcopy.shp, RainGaugeFPcopy.shp
2. Spatial join BCCA_CMIP3_FPcopy.shp and NEXRAD_FPcopy.shp = BCCA_Nexrad_SplJn.shp
   This now has the flow permanence values for all these two datasets, and the StrmNum, Contrib, and SeqNum that matches the code in Bliss_FlowPermRG84edit_UniqID.shp which has been edited to match and has the Unique_IDs.
3. Create this code in BCCA_Nexrad_ SplJn.shp = NewFPCode
4. Join to Bliss_FlowPermRG84edit_UniqID.shp on the codes.

d) Peak Flow

All peak flow results were analyzed; however, only the 25-year 1-hour peak flow values were used in the stream type classification.

1. Use the AGWA shapefiles Bliss_Qp_5yr1hr.shp, Bliss_Qp_10yr1hr.shp, and Bliss_Qp_25yr1hr.shp
2. Project to WGS84: Bliss_Qp_5yr1hr84.shp, Bliss_Qp_10yr1hr84.shp, and Bliss_Qp_25yr1hr84.shp
3. Add AGWA codes to Bliss_Qp_10yr1hr84.shp and Bliss_Qp_25yr1hr84.shp (StreamNum, Contrib, SeqNum).
4. Spatial join Bliss_Qp_10yr1hr84.shp and Bliss_Qp_25yr1hr84.shp = BlsPkFlw10_25.shp
5. Delete extra fields, calc new field for Qp 10yr values.
6. Copy BlsPkFlw10_25.shp to BlsPkFlw10_25edit.shp
7. Edit BlsPkFlw10_25edit.shp to match Unique_ID polygons, using Bliss_FlowPermRG84edit_UniqID.shp as a guide, so there is one value for each polygon.
8. Join to Bliss_FlowPermRG84edit_UniqID.shp on Unique_ID, export table = BlsPkFlwPermCumAreaTable.dbf, sort on Unique_ID, save as .xlsx
9. Copy Peak Flow for 10 year and 25 year events to BlsVariables.xlsx, HydroInputs tab.
10. Add the 100 year 1 hour event = Bls_Qp_100yr1hr84.shp
11. Join BCCA_Nexrad_SplJn.shp to Bliss_FlowPermRG84edit_UniqID.shp = BCCA_Nexrad_SplJnUniqID.shp
12. Delete extra fields
13. Spatial join Bls_Qp10_25spjoin.shp to Bls_Qp_100yr1hr84.shp = BlsQp1025100.shp

14. Join BCCA_Nexrad_SplJnUniqID.shp (NewFPCode) to BlsQp1025100.shp (Qp10code) = BlsNexradQp1025100UniqIDAll.shp
15. Join on Unique_ID BlsPkFlw10_25UniqID.shp and BlsNexQp1025100UniqIDAll.shp. Export to preserve join = BlsNexQp1025100UniqIDAllcombined.shp

e) Total Stream Power

Use LiDARSlope and AGWA Peak Flow for the 10, 25 and 100 year events to calculate Total Stream Power. Only the 25 year TSP values were used in the stream type classification.

Q25TSP-AGWA = 9.81 * LiDARSlope * QP25yr = kW/m

f) LiDAR Vegetation Structure

Vegetation Structure represents the various zones or regions in vegetation that are typically used by wildlife, and the total amount of vegetation that is within that height layer.Vegetation structure is derived from the multi-return LiDAR vegetation height layer (calculated as canopy/first return minus ground/last return) and classified into vegetation height categories based on typical vegetation types: <0.5m, 0.5m-1m, 1-4m, 4-12m, >12m. Steps to derive the LiDAR Vegetation Structure layers are in the Riparian Vegetation Guidance Document.

g) Percent Vegetation Cover

Vegetation cover (%) is derived from the RapidEye satellite imagery, using a vegetation index (Red Edge NDVI) to classify the 1km stream reaches into vegetation vs. bare ground or ground cover, with aerial photography and field photos as guides to verify vegetation pattern, abundance and cover. It is calculated as total area of vegetation pixels divided by total area of the 1km stream reach polygon. More details and steps to derive vegetation cover are in the Riparian Vegetation Guidance Document.

h) Mean Vegetation Index

The Mean Vegetation Index describes the relative vegetation density for each 1km stream reach, calculated using only the pixels classified as vegetation cover from the satellite imagery (i.e. the pixels classified as bare ground or ground cover were not used to derive this variable). In areas of sparse vegetation, both vegetation and soil properties are represented by the vegetation index. Therefore, the Mean Vegetation Index can indicate the overall sparseness or density of vegetation. The Mean Vegetation Index is derived from the RapidEye satellite imagery, from the vegetation index (Red Edge NDVI). Steps to derive mean vegetation index are in the Riparian Vegetation Guidance Document.

i) Mean Riparian Widths

The mean riparian width represents the mean value of the water surface extent at various inundation depths for each 1km stream reach polygon. Riparian width can be related to riparian vegetation extent, or channel bottom. It is derived using the Hydro-Geomorphic Valley Classification (HGVC) tool in ArcMap, to create a polygon delineating the water surface at the specified depth. The HGVC tool requires a filled DEM and a stream network (the edited NHD stream line). Riparian width is calculated as the area of each 1km stream reach polygon divided by the actual length of the 1km stream reach.

Steps to derive riparian widths are in the Geomorphic Data Guidance Document. The final values for widths 0.25m, 0.5m, 1m, 2m, and 3m are in BlsVariables.xlsx, rip-width tab. The 3m width polygon was used to calculate the riparian vegetation variables, the 2m width values were used in the stream type classification, and the 3m and 0.5m widths were used to calculate the entrenchment ratio.

j) Entrenchment Ratio

The entrenchment ratio indicates the degree of channel entrenchment or the vertical containment of the river. It is usually calculated as Flood Prone Width divided by Bankfull Width from field data. We did not collect those data in the field; therefore, it is calculated here using mean riparian widths: 3m / 0.5m. This assumes Water Surface Width at 3m inundation depth approximates Flood Prone Width, and Water Surface Width at 0.5m inundation depth approximates Bankfull Width. Lower values (closer to 1) for the entrenchment ratio indicate increased entrenchment.

k) Rainfall Seasonality Index (RSI)

The Rainfall Seasonality Index: describes precipitation characteristics and indicates the intensity of erosion potential due to precipitation characteristics, derived from PRISM 30 year normals (PRISM Climate Group, 2010), calculated as the mean precipitation of the wettest month divided by the mean annual precipitation, for the 30-year period 1980-2010. Steps to derive the rainfall seasonality index are in the Geomorphic Data Guidance Document.

l) Cumulative Area

Cumulative area above the reach (m2) represents the watershed area above the reach that contributes to stream flow at that reach, and is related to channel geometry and vegetation community differences. It is obtained from the AGWA model outputs. The AGWA results for cumulative area above each reach (cum_area) are from BlsPkFlwFlwPermCumAreaTable. xlsx.

Literature Cited

Lyon, R. 2013. Using rainfall-runoff models to characterize the flow regime of desert streams in the U.S. southwest. M.S. Thesis, University of Arizona, Tucson.

Appendix J: Riparian Vegetation Analysis Guidance Document

RIPARIAN VEGETATION ANALYSIS GUIDANCE DOCUMENT

Table of Contents

Introduction **4**

Methods to obtain riparian vegetation variables **4**

1km Stream Reach layer 4

Riparian zone 5

Riparian vegetation Structure/height 5

Vegetation Cover and Density 6

Vegetation response to monsoonal precipitation (YPG only) 7

Methods to calculate Variables for each 1km stream reach polygon 8

Vegetation Variables for each installation **8**

Fort Irwin 8

Flooded polygon layer 8

QuickBird Data Processing 9

QuickBird Data Analysis 10

Vegetation Cover for each 1km stream reach polygon 12

MSAVI2 Mean values for each 1km stream reach polygon 13

Multi-Return LiDAR Data 13

LiDAR Processing: Terrain Dataset 13

LiDAR-Derived Vegetation Structure Groups 13

LiDAR analysis of extreme values 14

YPG 14

Flooded Polygon Layer 14

RapidEye Data Processing 15

RapidEye Data Analysis 15

Vegetation Cover for each 1km stream reach 17

Red Edge NDVI Mean values 18

Landsat Data Analysis 19

Fort Huachuca 20

Flooded Polygon Layer 20

QuickBird Data Processing 21

QuickBird Data Analysis 21

Vegetation cover for each 1km stream reach polygon 22

MSAVI2 Mean values for each 1km stream reach polygon 22

Multi-Return LiDAR Data 23

LiDAR Processing 23

LiDAR-Derived Vegetation Structure Groups 23
LiDAR Data analysis of extreme values 24
Fort Bliss 24
Flooded Polygon layer 25
RapidEye Data Processing 25
RapidEye Data Analysis 25
Vegetation Cover for each 1km stream reach 27
Red Edge NDVI Mean values 27
Multi-Return LiDAR Data 28
LiDAR Processing 28
LiDAR-Derived Vegetation Structure Groups 28
LiDAR analysis of extreme values 28

Vegetation Structure Classification 29

Literature Cited 32

Appendices 33

Appendix A: Vegetation Indices Background 33
Broadband Vegetation Indices 33
Narrowband Vegetation Indices converted to broadband values for the Red Edge band (RapidEye) 34

Introduction

The riparian vegetation analysis is part of the larger project goal to create an ecohydrologic stream type classification for DoD's southwest desert installations: Fort Irwin, YPG, Fort Huachuca, and Fort Bliss. The purpose of the vegetation analysis is to characterize the vegetation along the stream channels. These data were used for the stream type classification, for analysis of wildlife habitat use and value, and for the vegetation structure analysis. The criteria used to select the appropriate characteristics for analysis is based on features that wildlife requires for nesting, breeding, forage, and movement. Vegetation height/structure, cover, density, biomass, connectivity (patchiness) are some of the more important features for wildlife habitat. Riparian vegetation is important in determining the value of the stream reach to wildlife.

Methods to obtain riparian vegetation variables

The vegetation variables used in this project were vegetation structure or height (Fort Irwin, Fort Huachuca, and Fort Bliss only), vegetation cover, vegetation density and vegetation response to monsoonal precipitation (YPG only). These variables will be described briefly here and the methods used to derive those variables will be described in more detail in the next sections.

The riparian vegetation structure (height) groups were determined by analyzing multi-return LiDAR for all installations except YPG where no LiDAR was available at the start of the project. Structure groups are based on the general types of vegetation found in these deserts, and relate to the general region of plants used by wildlife: <1m, 1-4m, 4-12m, and >12m. Ground dwelling birds, small mammals and reptiles depend on ground cover, while some birds have preference for foraging or nesting in the middle or upper parts of the plant. Larger mammals (i.e. deer) depend on the taller vegetation to provide cover and protection from predators.

The vegetation cover and vegetation density variables were both derived from multi-spectral satellite imagery using a vegetation index. We obtained two types of imagery for this project: QuickBird (DigitalGlobe, Inc., http://www.digitalglobe.com/) and RapidEye (Spatial Energy, LLC., http://www.spatialenergy.com). We used the Red Edge Normalized Difference Vegetation Index (NDVI; Weichelt et al. 2012) with RapidEye and the Modified Soil Adjusted Vegetation Index (MSAVI2; Qi, 1994) from QuickBird imagery. Riparian vegetation cover is derived by classifying the vegetation index into vegetation vs. bare ground and ground cover. The mean vegetation index values are used to derive vegetation density.

We did not attempt to identify plant species since vegetation species cannot be determined using our methods or data, and this information can be obtained from existing vegetation mapping and reports at each military installation.

1km Stream Reach layer

The streamline from the USGS National Hydrography Dataset (NHD) Plus Version 2 dataset (USGS, 2006) was chosen for the stream network because it contained the most complete supporting data for use with the geomorphic analyses. Therefore the *flowlines* shapefile from this dataset was used for the vegetation analyses, and was also used for the stream type classification.

The unit of analysis was selected as the 1km stream reach, based on observations in the field regarding how frequently overall stream characteristics change. The NHDPlus V2 flowline was split into +/- 1km reaches using ET-GeoWizards (http://www.ian-ko.com/ET_GeoWizards/gw_main.htm). This tool splits each stream reach into equal segments as close to 1km as possible. The "length" of each split stream reach was calculated in the GIS. Each 1km stream reach was given a Unique_ID created by combining the NHDPlus V2 reach ID and the GIS FID (e.g. 30012345_200) for use in all the analyses.

Riparian zone

Because drylands don't always have a well-defined riparian vegetation zone that differs substantially from upland vegetated areas, we developed a method to delineate the riparian zone within which to perform our vegetation analyses. In many desert locations vegetation is sparse whether along the channels or in the uplands. Vegetation can be distributed fairly uniformly across the landscape, is not necessarily clustered along the channel edges, and can be green as a result of rainfall regardless of location (i.e. uplands vs. riparian zone) or season. Therefore, a surrogate "riparian zone" was defined by inundating a DEM to 3m using the Hydro-geomorphic valley classification Tool's Optional Inundation Feature (HGVC, E.A. Carlson, 2011). This depth of 3m was determined based on comparison with imagery and field photographs to best delineate the extent of vegetation that would be influenced by stream flow when it occurs. The result is a polygon map that is an acceptable delineation of the areas around the channels that might be flooded during stream flow and that would be influenced by that flow (i.e. indicating a riparian zone). When viewed using a base map or aerial photos, it generally includes the obvious denser shrub and tree vegetation associated with the channel. Seasonal forbs and grasses resulting from seasonal rainfall or episodic stream flow were not delineated since we are aiming to identify the more permanent vegetation structure and density for use in wildlife habitat analyses. This polygon layer was split into approximately 1km reach lengths, and the resulting polygons for each installation provided the area within which to calculate the vegetation metrics.

Create the "riparian zone" polygon layer using the HGVC Optional Inundation tool to flood the DEM to 3m. Use a filled 10m DEM or LiDAR bare earth DEM, and the NHDPlus V2 stream line. Aerial imagery and LiDAR or DEM hillshades were used to determine that 3m is the optimal depth to create the water surface width that captures the zone around the channel with the densest vegetation, indicating the area most influenced by streamflow. Create polygons at 0.25m, 0.5m, 1m, 2m, and 3m inundation depth, to be used for other analyses, including calculating an entrenchment ratio.

The HGVC Inundation tool creates a single polygon that must be split into the 1km stream reaches for use in the vegetation and other analyses. This was done by buffering the stream lines to 200m for each installation using "flat" ends. Intersecting this buffered stream line with the split NHDPlus V2 streamline produces a polygon layer that has been split into 1km reaches. The buffer of 200m was determined using imagery and aerial photographs to best capture the area around the NHDPlus V2 streamline that would be influenced by streamflow, but not extending too far beyond the stream. This buffer also reduces the width of stream reaches occurring in flat areas such as playas or sand dunes for use in the analyses.

Riparian Vegetation Structure/Height

Riparian vegetation structure (height) was obtained from the multi-return LiDAR data for Fort Huachuca, Fort Bliss and Fort Irwin. LiDAR was not available for YPG when this project began, so this analysis was not done for YPG. Vegetation structure represents the various vertical zones or regions in vegetation that are typically used by wildlife, and the total amount of vegetation that is within that height layer. Note that these values do not account for vegetation that is underneath that height category (i.e. the 1-4m high vegetation underneath the 4-12m high vegetation).

Vegetation height is derived from multi-return LiDAR by subtracting the bare earth layer from the canopy layer. The resulting vegetation height layer is then classified into height categories in the GIS. Determine percent of each height category in each 1km stream reach by intersecting the height layer with the riparian zone polygon layer and calculating the totals. Use the methods described in the previous section to calculate the percent of each structure category within each 1km stream reach polygon.

These are the vegetation height categories used:

% <0.25m (Fort Irwin), <0.5m (Fort Bliss), or <1m (Fort Huachuca)
% 0.25m - 1m (Fort Irwin), 0.5m – 1m (Fort Bliss)
% 1m – 4m
% 4m – 12m
% >12m

Vegetation Cover and Density

The Vegetation cover and density variables were derived from the satellite imagery for each 1km stream reach. QuickBird satellite imagery (2.4m resolution, B-G-R-NIR bands) was obtained from Fort Huachuca and purchased for Fort Irwin. RapidEye satellite imagery (5m resolution, B-G-R-RedEdge-NIR bands) was purchased for Fort Bliss and YPG. RapidEye imagery was purchased for these two installations because it is considerably less expensive than QuickBird imagery, and also included an additional band (the red edge band) that improves vegetation analysis. We were interested in determining if this type of data could also be used in our analysis. All imagery was atmospherically corrected. The QuickBird imagery was also georectified; the RapidEye imagery was purchased as Level 3A data, and was already orthorectified.

Vegetation indices were calculated from the imagery and used to manually classify the data into vegetation vs. bare ground or ground cover. Best results were achieved with MSAVI2 vegetation index with the QuickBird imagery for Fort Huachuca and Fort Irwin, and Red Edge NDVI with the RapidEye imagery at Fort Bliss and YPG. Percent vegetation cover and mean vegetation index (density) were calculated within each 1km reach of the riparian zone polygon layer.

Equation for MSAVI2: $$MSAVI2 = \frac{\left(2*NIR+1-\sqrt{(2*NIR+1)^2-8*(NIR-RED)}\right)}{2}$$

Equation for Red Edge NDVI: RENDVI = (NIR – RE) / (NIR + RE)

General Steps (described in more detail below for each installation):

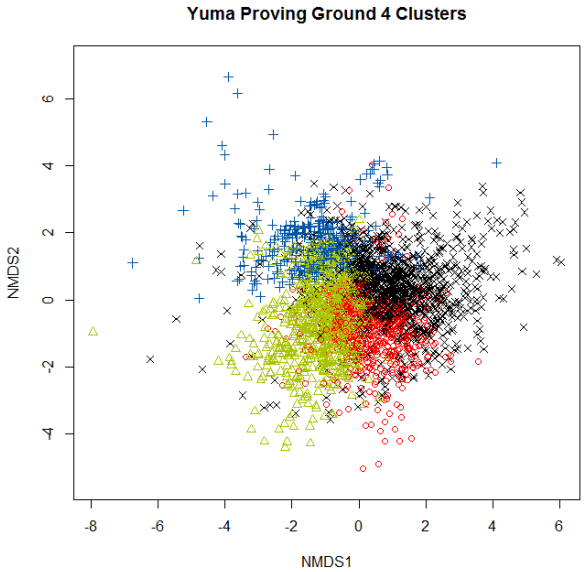
1. Calculate MSAVI2 or Red Edge NDVI for each tile in ArcMap.

2. Classify each tile into vegetation vs. bare ground or ground cover, making sure the classification is consistent across tiles (use aerial photographs and field photographs as guides). Actual values used to classify each tile are listed below in the sections for each installation.
3. Mosaic all resulting classified tiles in ERDAS Imagine (ERDAS, 2013) or any image processing software.
4. To get vegetation cover, tabulate total "vegetation" within each 1km polygon in ArcMap using the methods described previously.
5. To get Mean Vegetation Index (MSAVI2 and Red Edge NDVI) use the "mean" value obtained from the Zonal Stats W/Overlaps tool for each riparian zone polygon.

Vegetation response to monsoonal precipitation (YPG only)

Because we were unable to perform the LiDAR vegetation structure analysis at YPG for use in the stream type classification due to lack of LiDAR data, we investigated the use of Landsat 5 Thematic Mapper (TM) data to add to the vegetation characterization. Using the MSAVI2 vegetation index for a wet monsoon season, we calculated the percent difference for pre-monsoon (June 11, 2008) and post-monsoon (Oct. 1, 2008). The mean value for each 1km stream reach polygon was used as input to the classification.

Various statistical analyses were performed to evaluate whether this variable improved the classification results. Correlation analysis indicated that the Landsat variable was not correlated to any of the other variables. Principal components analysis (PCA) indicated that the variable was important in the second and third principal component. The cluster analysis in R was performed using both datasets, for 3 to 12 clusters. Nonmetric multidimensional scaling (NMDS) in R was used to view the structure of the datasets with and without the Landsat variable for each cluster result, and indicated that the addition of the Landsat variable resulted in more distinct clusters. The Landsat variable was used in the classification analysis for YPG.



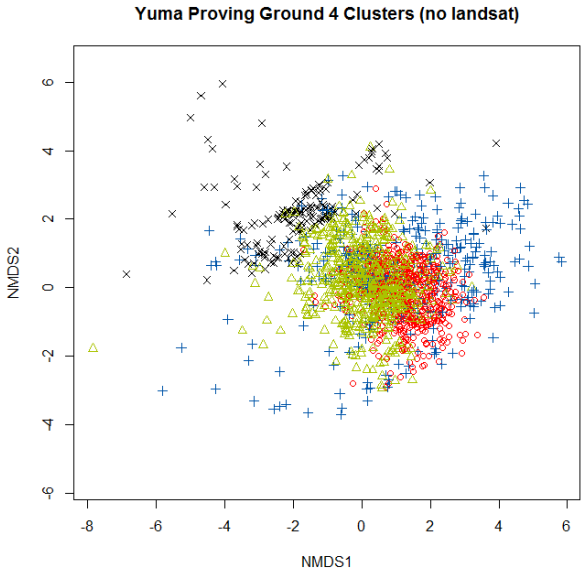


Figure 86. NMDS plots for 4 clusters at YPG, with (left) and without (right) the Landsat 5TM MSAVI2 variable for vegetation seasonal response to precipitation.

Methods to calculate Variables for each 1km stream reach polygon

The ArcGIS "Zonal Statistics as Table" tool does not work on overlapping polygons which occur when the buffered stream reach is intersected with the inundated polygon; it will only calculate the area of the first overlapped polygon, giving an incorrect total area for each Unique_ID, so alternative methods must be used.

1. Alternative method 1: ZONAL STATISTICS Tool "Zonal Stats w/ Overlaps" http://www.arcgis.com/home/item.html?id=b859b33c616a47d2b99b5e133942db02 (included as a zip file with the GIS data). Note: this may not be completely correct, so use the next method.
2. Alternative method 2: Multi-stepped analysis in the GIS
    a. "Intersect" the polygon layer with itself, to obtain only polygon portions that overlap.
    b. Use "Symmetrical Difference" to subtract the overlapped polygons from the original polygon layer to get the layer with only non-overlapping polygons, and the layer with overlapped polygons.
    c. Run "Tabulate Areas" on the non-overlapped polygon layer.
    d. For the Overlapped polygon layer "Dissolve" on Unique ID to remove multiple records for each Unique_ID
    e. Run "Tabulate Areas" on the dissolved overlapped polygon layer, to get the value for the first overlapped polygon.
    f. "Join" this layer back to the original overlapped polygon layer, delete all records that have values (these are the first overlapped polys).
    g. Run "Tabulate Areas" on the remaining overlapped polygons.
    h. "Join" the two overlapped results back to the non-overlapped result on the Unique_ID. This will combine all results into one table.
    i. Use "Summary Statistics" to combine the results for each Unique_ID (calculates the total for each Unique_ID). "Merge" for all three tables can also be used.

Vegetation Variables for each installation

Fort Irwin

Fort Irwin vegetation data were obtained from QuickBird satellite imagery and 1m Multi-Return LiDAR data. The general methods used to produce the vegetation structure, vegetation cover and mean vegetation index were described earlier in this document. Specific steps for Fort Irwin are described in this section.

Flooded polygon layer

The NHDPlus V2 streamline was used for the stream network. Steps to create the flooded polygon layer are:

1. Project the NHDPlus V2 flowline to WGS84 = NHDV2Flowline84Irwin.shp

2. Edit NHDV2Flowline84Irwin.shp to better match up with the LiDAR and QuickBird = NHDV2Flowline84IrwinEdit.shp
3. Split into 1km reaches or equal lengths using ET-GeoWizards = nhdplusIrwinEdit_Split.shp
4. Clip nhdplusIrwinEdit_Split.shp to Fort Irwin boundary = IrwNHDPV2es_bndry.shp
5. Add field and calculate "length".
6. Buffer nhdplusIrwinEdit_Split.shp to 200m = IrwNHDPV2es_200mbuf
7. Use HGVC Optional Inundation tool to flood 10m DEM to 3m using nhdplusIrwinEdit_Split.shp = IrwNHDPV2es_3mplyfld.shp
8. Clip IrwNHDPV2es_3mplyfld.shp with IrwNHDPV2es_200mbuf to eliminate playas = IrwNHDPV2es_3mplyfld200mbuf.shp (this step is actually not needed)
9. Intersect IrwNHDPV2es_3mplyfld.shp with IrwNHDPV2es_200mbuf to split it into 1km reaches and get the Unique_IDs back = IrwNHDPV2es_3mplyfld200mbufInt.shp
10. Dissolve IrwNHDPV2es_3mplyfld200mbufInt.shp on Unique_ID to combine polygons = IrwNHDPV2es_3mplyfld200mbufDis.shp
11. Join IrwNHDPV2es_3mplyfld200mbufDis.shp to IrwNHDPV2es_bndry.shp to get lengths back and export to save join = IrwNHDPV2es_3mplyfld200mbuffinal.shp

Calculate flooded polygon with LiDAR

1. Calculate Flooded Polygon and width with LiDAR
2. Use HGVC to create polygons at each depth using LiDAR bareearth layer
3. Irw2mPolyLidar.shp, Irw3mPolyLidar.shp, Irw1mPolyLidar.shp
4. Buffer the stream line IrwNHDPV2es.bndry.shp to 300m = IrwNHDPV3es_300mbuf.shp
5. Clip IrwNHDPV2es.bndry.shp to Irw3mPolyLidar.shp (some of these streamlines extend beyond the flooded polygon so the length will be incorrect) = IrwNHDPV2es_clipLidar.shp. Recalculate Length.
6. Clip Irw3mPolyLidar.shp with IrwNHDPV2es_300mbuf.shp = Irw3mPlyLidClip300mbuf.shp
7. Intersect IrwNHDPV2es_300mbuf.shp with Irw3mPlyLidclip300mbuf.shp to get the UniqueIDs = Irw3mPlyLid300mBufIntersect.shp
8. Dissolve to combine UniqueIDs: Irw3mPlyLid300mBufIntDislv.shp
9. Join back to IrwNHDPV2es_clipLidar.shp to get lengths back
10. Export to preserve join and calculate width = Irw3mPlyLid300mbufIntDislvWidth.shp
11. Recalculate area, add field Width, calculate width = area/length
12. Export table, use this Width in the classifications, and for the Entrenchment Ratio (use 3m/0.5m).

QuickBird Data Processing

QuickBird satellite imagery was purchased for Fort Irwin from DigitalGlobe (http://www.digitalglobe.com/). These are archived images with no cloud cover, for the entire installation. Five separate scenes were required to cover all of Fort Irwin; however we could not get all five with dates close together. Each scene was delivered as a set of tiff images (tiles)

which were mosaicked together based on date of acquisition, as follows, resulting in 6 tiles that were used for this analysis:

QuickBird Tile 1, ftirwinqb1.img, 052451131010_01_P001, Jan. 17, 2009, 12 tiles
QuickBird Tile 2, ftirwinqb2.img, 052548270020_01_P001, Jun. 2, 2008, 8 tiles
QuickBird Tile 3a, ftirwinqb3a.img, 052451131010_01_P004, Jan. 12, 2009, 12 tiles
QuickBird Tile 3b, ftirwinqb3b.img, 052451131010_01_P002, Jan. 04, 2009, 12 tiles
QuickBird Tile 4, ftirwinqb4.img, 052548270030_01_P001, Jul. 08, 2008, 7 tiles
QuickBird Tile 5, ftirwinqb5.img, 052548270050_01_P001, Aug. 28, 2004, 3 tiles

Steps used to process the imagery are as follows:

1. Atmospheric correction in ERDAS Imagine ATCOR2
    a. Compute statistics for each tiff image before performing the atmospheric correction.
    b. In ERDAS, Open the tiff image, right click on it to open the Layer Info, click on the "Σ" to compute statistics, make sure "Calculate on all Layers" is checked, change the Bin Function from *Default* to *Linear*, click OK.
    c. Get mean elevation of each tile in ArcMap. Use Zonal Statistics as Table with the "tile shape" shapefile to define the zone
    d. Get sensor and sun info from the metadata file for each tile.
    e. Run ATCOR2. Use scale factor = 4, and scene visibility = 100. Do not perform Haze Removal.
2. Review atmospherically corrected tiles with the LiDAR stream line to determine if Georectification is necessary. The stream locations in the QuickBird tiles were very close and acceptable in most places to the streamline layer, and it was determined that georectification would not improve the tiles. No georectification was done.
3. Use the atmospherically corrected QuickBird images. Mosaic in ERDAS Imagine to combine each date into one tile. Since the acquisition dates were so different, each tile was analyzed separately, and the final results combined after classification.
    ftirwinqb1.img
    ftirwinqb2.img
    ftirwinqb3a.img
    ftirwinqb3b.img
    ftirwinqb4.img
    ftirwinqb5.img

QuickBird Data Analysis

Fort Irwin vegetation is sparse, and is not significantly different along stream channels. Vegetation exists in any location that has a more favorable climate, including shaded, northern and eastern aspects, or low areas that collect water. Most washes that are wide enough to drive on are used as roads, and this further confounds classification attempts. The complex terrain at Fort Irwin results in various landforms being classified as vegetation (i.e. dark volcanic rock outcrops, limestone outcrops). The classification of denser or woody vegetation vs. ground cover or bare ground was checked with aerial imagery and field photographs. MSAVI2 was the

vegetation index used to classify vegetation across this varied terrain to distinguish vegetation from ground cover or bare ground.

Steps:

1. Calculate MSAVI2 for all 6 mosaicked tiles as described in Section II, Vegetation Cover and Density.
2. Classify each into 32 classes using Geometrical Interval
3. Determine the threshold for vegetation vs. ground cover or bare ground.
4. Check the MSAVI2 results for consistency across all tiles, adjust classifications as necessary
5. Reclassify each tile according to the final values listed below, into vegetation vs. ground cover or bare ground.
   irwqb1msv2cls, irwqb2msv2cls, irwqb4msv2cla, irwqb3ams2cls, irwqb3bms2cls, irwqb5msv2cls
6. Clip each reclassified tile (Extract by mask) to minimize overlap areas, SNAP to original QuickBird tiles depending on which has the longest common border (Environment settings, Processing Extent, Snap Raster). Use tile 1 as the first tile, and do NOT clip it.
   irwqb1msv2cls, irwqb2msv2clp, irwqb4msv2clp/irwqb4ms2clpa, irwqb3ams2clp, irwqb3bms2clp, irwqb5msv2clp
7. In ArcMap mosaic all to new raster = irwqbmsvi2mosa

The final values used to classify each tile are listed below. All 6 QuickBird MSAVI2 rasters are located in the geodatabase IrwQuickBirdMSAVI2.gdb

1. QuickBird Tile 1, ftirwinqb1.img (052451131010_01_P001), 09Jan17.
   This is the western part of Irwin, east of the Western Expansion Area. Dark rocks in some areas create classification errors. The Blue band of this tile (layer 1) is mostly dark, and possibly defective; however, it was not used in the MSAVI2 calculation.
   MSAVI2 = irw1msavi2, veg > 0.297916727

2. QuickBird Tile 2, ftirwinqb2.img, (052548270020_01_P001), 08Jun02
   This is the central area of Fort Irwin.
   MSAVI2 = irw2msavi2, veg > 0.248418109

3. QuickBird Tile 3, split into two tiles, see below, ftirwinqb3.img not used
   This was mosaicked from QB dataset 052451131010_01 P004 and P002. Because these two datasets have different dates, the final mosaic was not used and each dataset was mosaicked separately.
   09jan12_04corr_mos.img
   09jan04_02corr_mos.img

   QuickBird Tile 3a, ftirwinqb3a.img = 09jan12_04corr_mos.img, (052451131010_01_P004), 09jan12
   This tile includes the mountains at Panther Spring, south to the playas at Langford Lakes, making it difficult to classify all types of vegetation consistently.

MSAVI2 = irw3amsavi2, veg > 0.239740523, classified with natural breaks, 32 classes, excluding <0.

QuickBird Tile 3b, ftirwinqb3b.img = 09jan04_02corr_mos.img, (052451131010_01_P002), 09Jan04
This is the eastern portion, extending into the Eastern Expansion Area and including the Avawatz Mountains with dark rock outcrops and bright sand.
MSAVI2 = irw3bmsavi2, veg > 0.250370699 classified with natural breaks, 32 classes, excluding <0.

4. QuickBird Tile 4, ftirwinqb4.img, (052548270030_01_P001), 08Jul08
   This is the Western Expansion Area covered mainly with low shrubs < 1m, scattered Joshua Trees, and grasses.
   MSAVI2 = irw4msavi2, veg > 0.261085361; > 0.235063291 (revised March 27, 2014)

5. QuickBird Tile 5, ftirwinqb5.img, (052548270050_01_P001), 04Aug28
   This is the very eastern edge of the Eastern Expansion area.
   MSAVI2 = irw5msavi2, veg > 0.25470979

<u>Vegetation Cover for each 1km stream reach polygon</u>

1. Use mosaicked MSAVI2 data layer = irwqbmsv2mosa
2. Tabulate areas to get percent vegetation cover from msavi2 for overlapping polygons, using the intersect method described below
3. Intersect IrwNHDPV2es_3mplyfld200mbuffinal.shp with itself = irwnhdpv2es_intersect.shp, to create a layer with only the overlapping polygons.
4. Subtract the overlapped polygons from the original polygon layer to get a layer with only non-overlapping polygons. Use Symmetrical Difference: irwnhdpv2es_intersect.shp from IrwNHDPV2es_3mplyfld200mbuffinal.shp =irwnhdpv2es_symdif.shp
5. Run Tabulate Areas using the non-overlapped polygon layer irwnhdpv2es_symdif.shp on irwqbmsv2mosa to get table irwqbmsv2mosa_symdifTabAreas.dbf
6. For the Overlapped layer irwnhdpv2es_intersect.shp, dissolve on Unique ID to remove multiple records for each Unique_ID = irwnhdpv2es_intersect_dslv.shp
7. Run Tabulate Areas on the dissolved overlapped polygon layer irwnhdpv2es_intersect_dslv.shp with irwqbmsv2mosa, to get the value for the first overlapped polygon, to get table irwqbmsv2mosa_intersect1TabAreas.dbf
8. Join this table irwqbmsv2mosa_intersect1TabAreas.dbf back to the dissolved overlapped polygon layer irwnhdpv2es_intersect_dslv.shp
9. Export to new shapefile to preserve join = irwqbmsv2mosa_overlap1.shp, delete all records that have values (these are the first overlapped polys). This shapefile now has only overlapped polygons without msavi2 totals.
10. Run Tabulate Areas on the remaining overlapped polygons irwqbmsv2mosa_overlap1.shp to get table irwqbmsv2mosa_intersect2TabAreas.dbf

11. Join all three tabulate areas tables back to IrwNHDPV2es_3mplyfld200mbuffinal.shp shapefile on the Unique_ID. This will combine all results into one table.
12. Calculate the total vegetation cover in this table, or use "Summary Statistics" to combine the results for each Unique_ID (calculates the total for each Unique_ID).
13. Calculate msavi2 veg cover for each UniqueID as total vegetation/area of the polygon = msavi2_pct.
14. Clip to the LiDAR extent.

MSAVI2 Mean values for each 1km stream reach polygon

1. Mosaic all tiles with original MSAVI2 values: irw1msavi2, irw2msavi2, irw3amsavi2, irw3bmsavi2, irw4msavi2, irw5msavi2 = irw_qbmsv2all
2. Use Zonal Statistics Tool "ZonesWOverlaps" to get the mean value for each UniqueID.
   Zone layer: Irw3mplyfld200mbufClipLiDAR.shp
   Zone field: UniqueID
   Data layer: irw_qbmsv2all
   Output table: irw_qbmsv2all_zstats.dbf

Multi-Return LiDAR Data

Multi-return LiDAR data (1m resolution) were obtained from Fort Irwin as Terrain Datasets in October 2012. These are quick-viewing tools based on the raw LAS files, and were used to calculate the percent of each vegetation structure group.

LiDAR Processing: Terrain Dataset

Import the Terrain Datasets into ArcMap.
   NTC_LiDAR_2009.gdb (bare earth) Bare_Earth_Terrain
   FirstReturnLiDAR_09.gdb (first return) Terrain_Terrain

Convert to rasters in 3D Analyst Tools > Conversion > From Terrain > Terrain to Raster.
   Bare_Earth_Terrain converted to bareearth raster.
   First_Return_Terrain converted to firstreturn raster.

This raster had negative values to -100000 and was reclassified to convert all negative values to 0, to create new raster firstreturn1.
   Use "con" statement to convert all values less than 0 to 0.

LiDAR-Derived Vegetation Structure Groups

Create LiDAR vegetation height layer, classify into structure groups, and determine area of each structure group within each 1km reach polygon. Note that the LiDAR data does not extend to the northern part of Fort Irwin. This analysis was conducted on only those reaches within the LiDAR extent, using Irw3mplyfld200mbufClipLidar.shp.

1. Subtract bareearth from firstreturn1 = minus_fr_be, (FtIrwinVegHeight.gdb)
2. Reclassify minus_fr_be into 6 classes =IrwLidReclass
   1 = <0m, bare ground
   2 = <0.25m, bare ground
   3 = 0.25-1m, ground cover

4 = 1-4m
5 = 4-12m
6 = >12m

3. Use Model Builder Tabulate Areas of each structure group from IrwLidReclass within IrwNHDPV2es_3mplyfld200mbuffinal.shp to get table = IrwLidarAppend2.dbf
4. Save as excel file IrwLidarVegResults.xlsx and calculate percent of each structure group within each 1km stream reach.
5. Calculate percent of each structure layer within each UniqueID for the cluster analysis.

LiDAR analysis of extreme values

This analysis was performed to determine how many pixels were corrupt, and would therefore give an erroneous result for the bareearth – firstreturn differencing (i.e. the vegetation structure result). The goal was to determine where these bad pixels were and determine if they impact the final classification results for vegetation structure.
The firstreturn and bareearth layers were obtained from 2009 geodatabases, terrain dataset. The firstreturn layer has a large number of negative values all located in one area and not within any stream polygons.
Conclude that the corrupt pixels did not impact this analysis.

YPG

YPG vegetation data were obtained from RapidEye satellite imagery. Multi-return LiDAR data were not available in time for our use in this project. The general methods used to produce the vegetation structure, vegetation cover and mean vegetation index were described earlier in this document. Specific steps for YPG are described in this section.

Flooded Polygon Layer

The NHDPlus V2 streamline was used for the stream network. Steps to create the flooded polygon layer are:

1. Use NHD-Plus V2, split into 1km reaches using ET GeoWizards = YPG_NHDPlusV2_WGS84_Split.shp
2. Edit to match RapidEye imagery, World Imagery, orthophotos, and 10mDEM hillshade = YPG_NHDPV2_es.shp
    a. Note that this editing is especially important since we don't have LiDAR to use for the vegetation analysis, and the NHDPV2 lines don't follow the channels very well. Create a preliminary 3m inundation layer to help identify areas that don't follow the channels. Use the RapidEye and aerial imagery as much as possible to edit the lines, especially in the uplands where the 3m inundation is very narrow.
3. Buffer to 200m = YPGNHDPV2_es200mbuf.shp
4. Create 3m inundation depth polygon in HGVC using the 10m DEM = YPGNHDPV2es_3mplyfld.shp
5. Intersect YPGNHDPV2es_200mbuf.shp and YPGNHDPV2es_3mplyfld.shp to eliminate large flooded areas = YPGNHDPV2es_3mplyfld200mbuf.shp.

6. Dissolve YPGNHDPV2es_3mplyfld200mbuf.shp on FID_YPGNHD to combine polygons = YPGNHDPV2es_3mplyfld200mbufdis.shp
7. Join back to YPGNHDPV2es_3mplyfld200mbuf.shp and export to save the join = YPGNHDPV2es_3mplyfld200mbuffinal.shp
8. Additional modified versions to remove polys that extend up adjacent tributaries = ypg_inundatedpoly3m.shp (used to calculate widths)
    a. Created by intersecting YPGNHDPV2es_3mplyfld200mbuffinal.shp with itself and manually editing each polygon.

RapidEye Data Processing

RapidEye satellite imagery was purchased for YPG from Spatial Energy (http://www.spatialenergy.com/), with Level 3A correction, 13 tiles as tiff images. These images are radiometrically corrected, but need to be atmospherically corrected, and converted to reflectance values. Atmospherically correct each tile using the ATCOR2 module in ERDAS Imagine, to get percent reflectance. Use Layer Stack to rebuild the images. The tiles with different satellite azimuth angles cannot be analyzed together; therefore, each tile was analyzed separately.

1. Atmospheric Correction:
    a. Compute statistics for each tiff image before doing the atmospheric correction. In ERDAS Imagine, open the tiff image, right click on it to open the Layer Info, click on the "Σ" to compute statistics, check "Calculate on all Layers" , change the Bin Function from *Default* to *Linear*, click OK.
    b. Get mean elevation in ArcMap from the 10m DEM. Use Zonal Statistics with the udm.tif file to define the zone.
    c. Get sensor and sun info from the metadata file for each tile.
    d. Run ATCOR2. Use scale factor = 10, and scene visibility = 100. Do not perform Haze Removal.
2. Use Layer Stack in ERDAS to rebuild the images.
3. Calculate statistics for each tile.

RapidEye Data Analysis

YPG has many areas of dark desert pavement, interspersed with strips of vegetation within the rills and channels, and typical Sonoran Desert uplands consisting of scattered vegetation with little ground cover and bright soil. Various vegetation indices were analyzed to determine the best one for isolating vegetation from ground or ground cover, especially those using the Red Edge band. Red Edge NDVI produced the best results, and is best at picking up smaller vegetation clusters and producing the best overall representation of the vegetation patterns.

Red Edge NDVI = RENDVI = (NIR-RE) / (NIR+RE)

All RapidEye tiles were analyzed separately and were matched as closely as possible, based on the stream channels using the polyflood 3m polygon layer.

Steps for classification of vegetation vs. bare ground/ground cover:

1. Use the atmospherically corrected tiles to calculate the vegetation index Red Edge NDVI. First convert each band to "float", then calculate RENDVI using the YPG boundary as the analysis extent. Mosaic all RENDVI tiles to get raster ypg_rendviall that has the RENDVI values for all of YPG.
2. Classify each individual tile in ArcMap using Natural Breaks with 32 classes, excluding negative values.
3. Select the threshold value (listed below) that will classify each tile into vegetation vs. bare ground and ground cover, based on the most significant vegetation, noting that this is 5m resolution imagery, which will not pick up the smaller isolated vegetation such as individual cholla, or small creosote bushes.
4. Classify each tile in ArcMap using the values listed below into vegetation (1) vs. bare ground and ground cover (0).

The Red Edge NDVI (RENDVI) values used for each tile are:

1. Tile atm08t192702.img (ypg192702ndvi.gdb), 11/08/11
Red Edge NDVI = ypg702rendvi. Veg range > 0.129124392
Classify = ypg702rendvicl

2. Tile atm08t192703.img (ypg192703ndvi.gdb), 11/08/11
Red Edge NDVI = ypg703rendvi. Veg range > 0.093023255
Classify = ypg703rendvicl

3. Tile atm08t192706.img (ypg192706ndvi.gdb), 11/08/11
Red Edge NDVI = ypg706rendvi. Veg range 0.091089107
Classify = ypg706rendvicl

4. Tile atm08t191921.img (ypg191921ndvi.gdb), 12/08/11
Red Edge NDVI = ypg921rendvi. Veg range >0.100702576
Classify = ypg921rendvicl

5. Tile atm08t192710.img (ypg192710ndvi.gdb), 11/08/11
Red Edge NDVI = ypg710rendvi. Veg range >0.096989967
Classify = ypg710rendvicl

6. Tile atm08t192709.img (ypg192709ndvi.gdb), 11/08/11
Red Edge NDVI = ypg709rendvi. Veg range >0.090909094
Classify = ypg709rendvicl

7. Tile atm08t192010.img (ypg192010ndvi.gdb), 11/02/11
Note: This tile has been mosaicked with atm08t192713 to the west.
Red Edge NDVI = ypg010rendvi. Veg range > 0.090909094
Classify = ypg010rendvicl

8. Tile atm08t191953.img (ypg191953ndvi.gdb), 11/01/11
Red Edge NDVI = ypg953rendvi. Veg range > 0.10124334
Classify = ypg953rendvicl

9. Tile atm08t191037.img (ypg191037ndvi.gdb), 10/23/11
Red Edge NDVI = ypg037rendvi. Veg range > 0.096774191
Classify = ypg037rendvicl

10. Tile atm08t191041.img (ypg191041ndvi.gdb), 10/23/11
Red Edge NDVI = ypg041rendvi. Veg range > 0.097046413
Classify = ypg041rendvicl

11. Tile atm08t191738.img (ypg191738ndvi.gdb), 8/5/10
This tile was obtained at the end of the monsoon (8/5/10), so the vegetation density is higher than other tiles.
Red Edge NDVI = ypg738rendvi. Veg range > 0.120370373
Classify = ypg738rendvicl

12. Tile atm08t192026.img (ypg192026ndvi.gdb), 12/30/10
Red Edge NDVI = ypg026rendvi. Veg range > 0.106382981
Classify = ypg026rendvicl

13. Tile atm08t191535.img (ypg191535ndvi.gdb), 8/27/10
This tile was obtained at the end of the monsoon (8/27/10), and is upper Sonoran Desert, so the vegetation density is higher than other tiles.
Red Edge NDVI = ypg535rendvi. Veg range > 0.109090909
Classify = ypg535rendvicl

Vegetation Cover for each 1km stream reach

Use the RapidEye vegetation classifications from the Red Edge NDVI (RENDVI) analyses for each tile (previous step) to calculate the percent vegetation cover.

1. Use the tiles from the previous step that classified all tiles into vegetation vs. bare ground or ground cover (1, 0) based on the values listed above.
2. Mosaic to new raster in ArcMap = ypg_rendvi
3. Calculate percent vegetation cover for each 1km stream reach using the polygon intersection method. Intersect YPG_inudatedPoly3m_zone12.shp with itself to separate out areas that are overlapping from areas that are not overlapping = YPG_inudatedPoly3m_z12_intersect.shp. This shapefile has only areas that are overlapped.
4. Subtract the overlapped areas from the original layer to get only areas that are NOT overlapped. Use the ERASE tool:
   Input features: YPG_inudatedPoly3m_zone12.shp
   Erase features: YPG_inudatedPoly3m_z12_intersect.shp
   Output feature class = ypg_inundatedPoly3m_z12_int_dif.shp.

This shapefile has only the areas that are NOT overlapped.

5. Non-Overlapping polys: Run Tabulate Areas on the non-overlapped layer ypg_inundatedPoly3m_z12_int_dif.shp using the ypg_rendvi raster (classified into vegetation vs. bare ground or ground cover).
   Tabulate Area:
   Input raster or feature zone data = ypg_inundatedPoly3m_z12_int_dif.shp
   Zone field = Unique_ID
   Input raster = ypg_rendvi
   Output table = ypg_inundatedpoly3m_rendvi_table.dbf, save as excel file .xlsx
   This table has the vegetation vs. bare ground or ground cover totals for the non-overlapped areas.
6. Copy Unique_ID, VALUE_0 AND VALUE_1 to YPGVariables.xlsx, RapidEyPctCover tab, and calculate total non-overlapping area.
7. Overlapping polys: Use the Overlapped layer YPG_inudatedPoly3m_z12_intersect.shp Dissolve on Unique ID to remove multiple records for each Unique_ID = YPG_inunpoly3m_z12_int_dis.shp
8. Run Tabulate Areas on the overlapped poly layer YPG_inunpoly3m_z12_int_dis.shp to get tabulat_shp1. This has values for only the first overlapped poly, with no values for the underneath polys.
9. Join tabulat_shp1 to YPG_inunpoly3m_z12_int_dis.shp on Unique_ID. Export to save join = YPG_inunpoly3m_z12_intdis_tab1.shp
10. Make a copy of the shapefile = YPG_inunpoly3m_z12_intdis_tab1Copy.shp. In this copy, delete all records that contain values (the first overlapped polys). This layer now has only the underneath overlapped polys with Unique_IDs.
11. Run Tabulate Areas on YPG_inunpoly3m_z12_intdis_tab1Copy.shp = tabulat_shp2
12. Join this table to YPG_inunpoly3m_z12_int_dis.shp on Unique_ID. Export to save join = YPG_inunpoly3m_z12_intdis_tab2.shp
13. Join both tables to ypg_inundatedPoly3m_Zone12.shp. Export to save join = YPG_inundatedpoly3m_z12_overlappedpolys.shp.
14. Save table as YPG_inundatedpoly3m_z12_overlappedpolys.xlsx. This table now has the vegetation vs. bare ground or ground cover values for the two overlapped polygon tabulate area results.
15. The final values for each Unique_ID, area_sqm, VALUE_0, VALUE_1 (the first overlapped polys), VALUE_01, VALUE_12 (the second overlapped polys) are in YPGVariables.xlsx, RapidEyePctCover tab.
16. Add all overlapping and non-overlapping polygons values for vegetation vs. bare ground or ground cover, to get the total areas. Calculate percent vegetation cover.

<u>Red Edge NDVI Mean values</u>
Use projected polygon layer = ypg_inundatedPoly3m_Zone12.shp
Create RENDVI raster layer of just vegetation pixels within the 3m inundated polygon = ypg_rendviveg

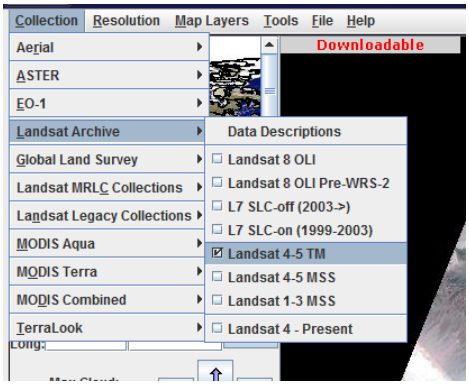
Calculate Mean values using ZonalStatsW/Overlap = ypg_rendviveg_table.xlsx

Landsat Data Analysis: Seasonal Vegetation Response Index (SVRI)
Landsat 5 TM archival data were used to analyze the seasonal response of riparian vegetation to monsoonal precipitation at YPG using a seasonal difference for the vegetation index, MSAVI2. This analysis was added to enhance the vegetation variables for the stream type classification in the absence of LiDAR data.

Percent difference was calculated directly from the MSAVI2 values in the Landsat grids for each grid cell, for June 11 and Oct. 1, 2008. These dates were selected because 2008 was a wet monsoon season with rainfall well distributed throughout July, August and September across Southern Arizona (Yuma, Phoenix, and Tucson; http://www.wrh.noaa.gov/twc/monsoon/monsoon.php). The percent difference between the vegetation indices from pre-monsoon to post-monsoon should show the vegetation response to rainfall. The mean value for each 1km stream reach polygon was used in this analysis. This value is called the Seasonal Vegetation Response Index, or SVRI, and was used in the stream type classification.

The steps to acquire and process the Landsat data and calculate the MSAVI2 vegetation index are listed below.

1. Landsat 5 TM was downloaded from http://glovis.usgs.gov/ using Bulk Application Downloader
    a. The scene that covers YPG is at Path: 38 and Row: 37
    b. To isolate the Landsat 5 TM scenes, go to the *Collection Tab → Landsat Archive → Landsat 4-5 TM* (Figure at Right)
    c. Level 1T Scenes with minimal cloud cover over the course of the monsoonal season were downloaded using the Add and Send to Cart buttons. LEVEL 1 Terrain Corrected or L1T are data products that provide "systematic radiometric accuracy, geometric accuracy by incorporating ground control points, while also employing a DEM for topographic accuracy." (http://landsat.usgs.gov/descriptions_for_the_levels_of_processing.php)



2. Each scene was processed using ENVI 5.0, and uploaded by the provided MTL text file which contains the metadata for the scene
3. Calibrating Reflectance
    a. Select Radiometric Correction in ENVI's Toolbox and change the Calibration Type to Reflectance, then save to an output file
4. Dark Object Subtraction (DOS)

   a. Use the Dark Object Subtraction tool on the output of the Radiometric Correction tool
   b. Performed to remove atmospheric scattering which can be best quantified in a dark object; the value generated in this process is subtracted throughout the image to remove the atmospheric scattering
5. Generate MSAVI2 values in ArcMap 10.2 using Band 4 (NIR) and Band 3 (Red) on the images resulting from the previous step, in Raster Calculator with the equation:
   (2* "%NIR Band%" + 1 - (SquareRoot (Square (2*"%NIR Band%"+1) - 8*("%NIR Band%" - "%Red Band%"))))/2
6. Mask the MSAVI2 image to isolate the study area and remove any cloud cover
7. Change the pixel resolution of the masked image from 30x30m to 5x5m for better results with the Zonal Statistics Tool
8. Change Float values to Byte Values
   a. Raster Calculator with the MSAVI2 scene and the equation:
   ("%FloatRaster%" + 1) * 127.5
9. Percent Difference Tool
   a. Raster Calculator with a Newer and Older raw Landsat MSAVI2 scene to calculate the Percent Difference between the two scenes with the equation:
   (("%Newer%" - "%Older%") / (("%Newer%" + "%Older%") / 2)) * 100
10. The 3m inundation layer was used to extract the Mean and Max values within each reach polygon from each MSAVI2 scene
   a. The 3m inundation layer was split into 4 groups to remove issues with overlapping polygons when running the *Zonal Statistics as Table* tool
   b. *Zonal Statistics as Table* tool was used with each of the four 3m feature classes and the selected MSAVI2 scene; the zonal stat tables from each feature class was then merged; this step was done on the raw scenes created in Step 8 and the Percent Difference values created in Step 9.
   c. Results are in Oct1_Jun11_08msavi2pd_3mWd.xlsx.
   d. The final MSAVI2 Mean values are in YPGVariables.xlsx, SVRI-LandsatMSAVI2 tab.

Fort Huachuca

Fort Huachuca vegetation data were obtained from QuickBird satellite imagery and 1m resolution Multi-Return LiDAR data. The general methods used to produce the vegetation structure, vegetation cover and mean vegetation index were described earlier in this document. Specific steps for Fort Huachuca are described in this section.

Flooded Polygon Layer

The NHDPlus V2 streamline was used for the stream network. Steps to create the flooded polygon layer are:

1. Split into 1km reaches or equal lengths using ET-GeoWizards
2. Project to WGS84 = fth_nhdpv2split84.shp

3. Edit to follow the LiDAR hillshade (fth_be2013hs1) to improve the result = fth_nhdpv2splitedit.shp
4. Flood the LiDAR bare earth layer to 3m using the HGVC Optional Inundation Depth function = HuaNHDPV2edit_3mplyfld.shp
5. Buffer fth_nhdpv2splitedit.shp to 200m = fth_nhdpv2se200mbuf.shp
6. Intersect fth_nhdpv2se200mbuf.shp with HuaNHDPV2edit_3mplyfld.shp to split the polygons into 1km reaches and reduce wide polygons in flat areas or playas = HuaNHDPV2edit_3mplyfld200mbuf.shp
7. Dissolve on FID_hua_nh to combine small polygons into adjacent larger ones, use "create multipart features", unsplit lines "no", = HuaNHDPV2es_3mplyfld200mbufdis.shp
8. Join back to HuaNHDPV2edit_3mplyfld200mbuf.shp on FID_hua_nh to get unique ID's back, and export to preserve join = HuaNHDPV2es_3mplyfld200mbuffinal.shp

QuickBird Data Processing

QuickBird satellite imagery was obtained from Fort Huachuca GIS personnel. The images were delivered as 6 tiles, 3 dated Nov. 20, 2009, and 3 dated Dec. 26, 2009.

All tiles were atmospherically corrected using the ATCOR2 module in ERDAS Imagine (http://www.erdas.com/products/ERDASIMAGINE/ERDASIMAGINE/Details.aspx), and georectified in ArcMap (ESRI, http://www.esri.com) using the LiDAR stream line generated in the Automated Geospatial Watershed Assessment Tool (AGWA; http://www.tucson.ars.ag.gov/AGWA; rastert_st350001.shp; CSA = 35,000). The LiDAR streamline was used because it was acquired at the same time as the imagery and produced a very accurate representation of the stream network.

QuickBird Data Analysis

Fort Huachuca has nearly total vegetation ground cover (grasses) in most areas, or total canopy cover in the mountains. Therefore, this classification was performed to isolate woody or permanent vegetation from grasses or bare ground by viewing the riparian areas within the 3m inundated polygon in areas with more open canopy. Aerial imagery and field photos were used to guide the classification. MSAVI2 was the vegetation index used to classify vegetation across this varied terrain.

Steps:

1. Calculate MSAVI2 for all six QuickBird tiles using the equation listed previously.
2. Classify into 32 classes, using Geometrical Interval and excluding negative values.
3. Check the MSAVI2 results for consistency across all tiles, adjust classifications as necessary, then reclassify each tile according to the final values (listed below), into vegetation vs. grasses or bare ground.
4. Clip each reclassified tile (02 – 06 only) to minimize overlap areas, SNAP to original QuickBird tiles depending on which has the longest common border (Environment settings, Processing Extent, Snap Raster).

5. Mosaic all clipped classified tiles in ERDAS Imagine (Edit > Set Overlap Function = Feather) = huamsvi2clmos.img
6. Convert to raster = huamsv2clmos

These tiles are in the order in which they were mosaicked, and are the final values used for classification. The final results are located in the geodatabases for each tile.

1. Tile 09nov20_01_corr10.img (fth01qb.gdb) East Range grasslands
   MSAVI2 = fth01msavi2. Vegetation range > 0.259949252 (geometrical interval, 32 classes); classified fth01msavi2cl; don't clip this tile

2. Tile 09dec26_05_corr11.img (fth05qb.gdb) Huachuca Mountains, forested, snow visible on the ground
   MSAVI2 = fth05msavi2. Vegetation range > 0.225240382 (geometrical interval, 32 classes); classified fth05msavi2cl; clipped with huaqb05clp = fth05ms2clclp

3. Tile 09dec26_04_corr1.img (fth04qb.gdb) Babocomari area
   MSAVI2 = fth04msavi2. Vegetation range > 0.239763164 (geometrical interval, 32 classes); classified fth04msavi2cl; clipped with fthqb04clp and snapped to QuickBird raster 09nov20_01_corr10.img to improve overlap = fth04ms2clclp

4. Tile 09nov20_02_corr1.img (fth02qb.gdb) Lower Garden & Coyote, this image is darker than the rest
   MSAVI2 = fth02msavi2. Vegetation range > 0.258331345 (geometrical interval, 32 classes); classified fth02msavi2cl; clipped with fthqb02clp and snapped to QuickBird raster 09dec26_05_corr11.img to improve overlap = fth02ms2clclp

5. Tile 09nov20_06_corr2.img (fth06qb.gdb) Upper Garden Canyon
   MSAVI2 = fth06msavi2. Vegetation range > 0.243871916 (geometrical interval, 32 classes); classified fth06msavi2cl; clipped with fthqb06clp and snapped to QuickBird raster 09dec26_05_corr11.img to improve overlap = fth06ms2clclp

<u>Vegetation cover for each 1km stream reach polygon</u>

1. Tabulate areas of huamsvi2clmos within HuaNHDPV2es_3mplyfld200mbuffinal.shp on Unique_ID (HuaMsavi2TabulateAreas.xlsx)
2. Calculate percent of total vegetation in this excel file using the total area from HuaNHDPV2es_3mplyfld200mbuffinal.shp, and VALUE_1. Name the field =msavi2_pct

<u>MSAVI2 Mean values for each 1km stream reach polygon</u>

Use the mean value for the MSAVI2 vegetation index.

1. Clip all tiles so the borders with "no data" are removed.
   Original tiles: fth01msavi2, fth02msavi2, fth03msavi2, fth04msavi2, fth05msavi2
   Clipped tiles: fth01msv2clp, fth02 msv2clp, fth03 msv2clp, fth04 msv2clp, fth05 msv2clp

2. Mosaic all tiles = hua_msavi2all
3. Use Zonal Statistics Tool "ZonesWOverlaps" to get the mean value for each UniqueID.
   Zone layer: HuaNHDPV2es_3mplyfld200mbuffinal.shp
   Zone field: Unique_ID
   Data layer: hua_msavi2all
   Output table: hua_msavi2all_zstats.dbf
4. Join this table to HuaNHDPV2es_3mplyfld200mbuffinal.shp on Unique_ID. Create raster layer using these values = hua_msv2mean

Multi-Return LiDAR Data

Multi-return LiDAR data were obtained from Fort Huachuca, and were used to calculate the percent of each vegetation structure group. The data were delivered as 21 tiles with 1m resolution.

LiDAR Processing

1. Bare Earth layer

In ERDAS Imagine, mosaic all 21 tiles from Army Geospatial Center (2009). These were cleaned up and mosaicked from the original 133 tiles. The bare earth layers are labeled as *dem_bare_1m_ft_huachuca_tilexx.tif.*
Final mosaicked bare earth layer is called fth_mos2012.img

Note: The area of the southernmost tiles (109, 110, 111, 112, 113, 119, 120) was corrupt, so the original LAS tiles were combined into an LAS Dataset in ArcMap 10.1 using the following steps:

a. Data Management Tools/LAS Dataset/Create LAS Dataset = las109110.lasd
b. In LAS Dataset Toolbar, add Filter for Ground, then Convert from LAS Dataset to Raster (value field = elevation, sampling value = 1) = las109230grnd
c. Mosaic with existing bare earth layer to new raster: fth_mos2012.img + las109120grnd = fth_be2013

Final new bare earth LiDAR layer is called fth_be2013

2. First Return layer

In ERDAS Imagine, mosaic all 21 tiles from Army Geospatial Center (2009). These were cleaned up and mosaicked from the original 133 tiles. They are labeled as *dem_1m_a1_ft_huachuca_tilexx.tif*
Final mosaicked first return layer is called fth_fr2012.img

LiDAR-Derived Vegetation Structure Groups

Create LiDAR vegetation height layer, classify into structure groups, and determine area of each structure group within each 1km reach polygon.

1. Subtract bare earth layer from first return to get vegetation structure/height: fth_fr2012.img – fth_be2013 = fth_veght2013
2. Classify in ArcMap to create fth_veght2013r using these classes:
   0 = <0m = bare ground

1 = 0-1m = ground cover or grasses
2 = 1-4m
3 = 4-12m
4 = >12m

3. Extract to just the Fort Huachuca boundary: fthvght2013rx
4. Export each class to a separate grid layer
5. Tabulate areas of each structure group from fthveght2013r within HuaNHDPV2es_3mplyfld200mbuffinal.shp to get table = HuaLidarTabArea.dbf
6. Save as excel file HuaLiDARTabAreaCalcs.xlsx
7. Calculate percent of each structure group for each Unique_ID for the Cluster analysis

LiDAR Data analysis of extreme values

In the *fth_fr2012.img* and *fth_be2013* data layers, there are many pixels where the bare earth layer values are larger than the first return values, resulting in large negative values for the vegetation structure layer. This analysis was performed to determine the location of these extreme pixels that would produce an erroneous result for the fth_be2013 – fth_fr2012.img differencing (i.e. the vegetation structure result). The goal is to determine the locations of these extreme pixels and determine if this impacts the final classification results for vegetation structure within the riparian zones.

Most of the larger negative values (>-2.0) are located on the uplands and do not affect the stream polygons. Most of the negative values within the stream polygons are between 0 to -0.5m.

1. Determine percentage of negative values within the 3m flooded polygon.
2. Classify fth_veght2013 into classes: -2.0, -1.0, -0.5, 0, >0 = fth_testclass
3. Tabulate areas = fth_testclasstabarea.dbf
4. Save as fth_testclasstabarea.xlsx and calculate the percentages.
5. Results show that while 18.41% of pixels are less than 0m, 18.28% are within 0 - -0.5m, and 0.13% are less than -0.5m. The pixels within 0 - -0.5m mostly occur in the channel bottoms and other open areas (based on visual analysis), and were grouped with the "ground" class of "less than 0".

Height	<-0.2	-0.2 - -0.1	-1.0 - -0.5	-0.5 - 0	0 - 89.950248	89.950248 - 161.960092
ID	VALUE_1	VALUE_2	VALUE_3	VALUE_4	VALUE_5	VALUE_6
total	223	3025	32064	4745063	21175918	2
percentage	0.00085914	0.01165421	0.12353073	18.28097192	81.58297631	0.00000771
total <0				18.4170		

6. Conclude that these data are adequate for this use, as classified.

Fort Bliss

Fort Bliss vegetation data were obtained from RapidEye satellite imagery purchased for this project, and 1.5m resolution Multi-Return LiDAR data obtained from DISDI. The general

methods used to produce the vegetation structure, vegetation cover and mean vegetation index were described earlier in this document. Specific steps for Fort Bliss are described in this section.

Flooded Polygon layer

The NHDPlus V2 streamline was used for the stream network. Steps to create the flooded polygon layer are:

1. Use NHDPlusV2, edited to follow the LiDAR Hillshade for improved vegetation analysis = nhdplusBlissEdit.shp
2. Split into +/-1km using ET GeoWizards = nhdplusBlissEdit_Split.shp.
3. Buffer to 200m to capture the entire 3m inundation zone = BlsNHDPV2EditSplit200mbuf.shp.
4. Create 3m inundation depth polygon in HGVC using the 10m DEM = bliss_polyflood3m.shp
5. Intersect BlsNHDPV2EditSplit200mbuf.shp with bliss_polyflood3m.shp to split into 1km reaches = BlsNHDPV2EditSplit_200mbufplyfld3m.shp.
6. Dissolve on "Unique_ID" = BlsNHDPV2EditSplit_200mbufplyfld3mdis.shp.
7. Join back to nhdplusblissEdit.shp to get stream lengths back and export to preserve join = BlsNHDPV2EditSplit_200mbufplyfld3mfinal.shp.

RapidEye Data Processing

RapidEye satellite imagery was purchased for Fort Bliss from Spatial Energy (http://www.spatialenergy.com/), with Level 3A correction. Nineteen (19) tiles were purchased; however, only 18 were required to cover the entire installation. Each tile was analyzed individually.

1. Perform Atmospheric correction in ERDAS Imagine ATCOR2 on all tiles. Use 10m DEM to get zonal statistics for atmospheric corrections (bliss10mdem1).

RapidEye Data Analysis

All RapidEye imagery is from September – October 2010 (following a wet summer), therefore it exhibits high vegetation greenness. This area gets approximately 9.43" annual rainfall, with more than half occurring during the summer monsoon (July – Sept). We conducted a field visit in Sept. 2010 and field photos show very green and lush conditions. In general, dense riparian vegetation exists within the larger channels, with minimal riparian zones extending beyond the channel banks, except for the very large braided channels like El Paso Draw where vegetation is in the channel bottom and a narrow band of riparian vegetation occurs along the channel edge where no downcutting exists. On Otero Mesa, the grasslands are pervasive across the terrain, and channels are mostly discontinuous with extensive sheetflood zones (wide swales of dense grasses and shrubs). Riparian vegetation zones are found along the smaller channels in the steeper sloped areas such as in the Sacramento Mountains, or piedmont headwaters, but are only 1-3m wide on average. There is a pronounced aspect effect with north & east facing slopes having significantly more and different vegetation than west and south facing slopes. The resolution of RapidEye imagery is 5m, making it difficult to distinguish small isolated shrubs and grasses.

All RapidEye tiles were analyzed separately and were matched as closely as possible, based on the stream channels in the 3m polyflood layer. The vegetation index Red Edge NDVI performed the best for picking up the smaller vegetation clumps and distinguishing vegetation across the various types of land cover and terrain.

Steps:
1. Convert the Red Edge and NIR bands (4 & 5) to FLOAT in ArcMap, then classify into 32 classes, using Jenks Natural Breaks, calculate unique values first, and set skip factor to 1.
2. Check for consistency across all tiles, adjust classifications as necessary, then reclassify each tile using the values below.

The Red Edge NDVI values used for each tile are:

1. Tile 6056 (bliss6056ndvi.gdb) Coppice sand dunes, straddling Hwy 54, TAs 5B, 5D, 32D, 32C
   Red Edge NDVI = re_ndvi6056. Veg range > 0.166666672

2. Tile 6062 (bliss6062ndvi.gdb) Western Dona Ana Range, Organ Mountains, Las Cruces
   Red Edge NDVI = re_ndvi6062. Veg range > 0.151419565

3. Tile 6160 (bliss6160ndvi.gdb) Cantonment and Castner Range
   Red Edge NDVI = re_ndvi6160. Veg range > 0.172932327

4. Tile 6163 (bliss6163ndvi.gdb) South Range
   Red Edge NDVI = re_ndvi6163. Veg range > 0.173202619

5. Tile 6219 (bliss6219ndvi.gdb) Western Dona Ana Range, Organ Mountains, Las Cruces
   Red Edge NDVI = re_ndvi6219. Veg range > 0.165938869

6. Tile 6220 (bliss6220ndvi.gdb) Western Dona Ana Range, Organ Mountains, Las Cruces
   Red Edge NDVI = re_ndvi6220. Veg range > 0.154205605

7. Tile 6221 (bliss6221ndvi.gdb) Northeast Dona Ana across Hwy 54 to McGregor Range
   Red Edge NDVI = re_ndvi6221. Veg range > 0.191275165

8. Tile 6224 (bliss6224ndvi.gdb) North Dona Ana Range, Organ Mountains
   Red Edge NDVI = re_ndvi6224. Veg range > 0.176803395

9. Tile 6229 (bliss6229ndvi.gdb) Cantonment and Castner Range
   Red Edge NDVI = re_ndvi6229. Veg range > 0.172131151

10. Tile 6231 (bliss6231ndvi.gdb) South Range, Southern McGregor Range
    Red Edge NDVI = re_ndvi6231. Veg range > 0.16883117

11. Tile 6232 (bliss6232ndvi.gdb) Dona Ana Range, Organ Mountains
    Red Edge NDVI = re_ndvi6232. Veg range >0.170731708

12. Tile 6240 (bliss6240ndvi.gdb) Southern portion of Otero Mesa
    Red Edge NDVI = re_ndvi6240. Veg range > 0.164772734 (Quantile, 32 classes)

13. Tile 6293 (bliss6293ndvi.gdb) – southeast corner, TAs 24, 25, 26
    Red Edge NDVI = re_ndvi6293. Veg range > 0.172000006

14. Tile 6294 (bliss6294ndvi.gdb) Central Otero Mesa, west to the sand dunes
    Red Edge NDVI = re_ndvi6294. Veg range > 0.164611416 (Geometric Interval, 32 classes)

15. Tile 6327 (bliss6327ndvi.gdb) – northwest corner, TAs 10-13, 33
    Red Edge NDVI = re_ndvi6327. Veg range > 0.181818187

16. Tile 6340 (bliss6340ndvi.gdb) – El Paso Draw, Otero Mesa
    Red Edge NDVI = re_ndvi6340. Veg range > 0.185185179

17. Tile 6341 (bliss6341ndvi.gdb) Otero Mesa
    Red Edge NDVI = re_ndvi6341. Veg range > 0.142284572

18. Tile 6342 (bliss6342ndvi.gdb) – Sacramento Mountains
    Red Edge NDVI = (NIR-RE)/(NIR+RE) =re_ndvi6342. Veg range > 0.14910537

Vegetation Cover for each 1km stream reach

1. Mosaic all classified Red Edge NDVI results in ArcMap, using FIRST for overlap = blsrendvimos
2. Use Model Builder to Tabulate Areas of total vegetation cover within each 1km polygon using BlsNHDPV2es_200mbufplyfld3mfinal.shp on Unique_ID = BlsRendviTable1a.dbf, export and save as BlsRendviTable1a.xlsx
3. Calculate percent total vegetation cover for each polygon using total area from BlsNHDPV2es_200mbufplyfld3mfinal.shp
4. Add field “veg_rendvi”
5. Calculate vegetation cover for each UniqueID as total vegetation/area of the polygon = rendvi_pct

Red Edge NDVI Mean values

Create layer of Red Edge NDVI values to use in the classification.

1. Mosaic all 18 re_ndvi tiles = bls_rendviall
2. Use Zonal Statistics Tool “ZonesWOverlaps” to get mean Red Edge NDVI values.
   a. Zone layer: BlsNHDPV2es_200mbufplyfld3mfinal1.shp
   b. Zone field: Unique_ID

c. Data layer: bls_rendviall
d. Output table: bls_rendviall_zstats.dbf, save as bls_rendviall_zstats.xlsx

Multi-Return LiDAR Data

Multi-return LiDAR data were obtained from the Defense Installations Spatial Data Infrastructure (DISDI) for 2006 = FtBliss_Orig.gdb, containing two rasters: bareearth_original and canopy_original.

LiDAR Processing

Create LiDAR vegetation height layer using the rasters from FtBliss_Orig.gdb

1. Subtract the bare earth layer (bareearth_original) from the first return layer (canopy_original) = minuscanbe

LiDAR-Derived Vegetation Structure Groups

Classify the vegetation height layer *minuscanbe* into structure groups. Determine area of each structure group within each 1km reach polygon.

1. Classify in ArcMap = blisslidveght
   1 = <0.5m
   2 = 0.5m - 1m
   3 = 1m – 4m
   4 = 4m – 12m
   5 = >12m

2. Use Model Builder to Tabulate areas of blisslidveght within the polyflood layer BlsNHDPV2EditSplit_200mbufplyfld3mfinal.shp, use zone field Unique_ID
3. Calculate percent of each structure group within each 1km stream reach. Final table = BlsNHDPV2es_200mbufplyfld3mfinal1Table.xlsx

LiDAR analysis of extreme values

This analysis is to determine how many pixels are corrupt, and would therefore give an erroneous result for the bareearth – canopy return differencing (i.e. the vegetation height result). The goal is to determine where these bad pixels are located and determine if they impact the final classification results for vegetation height.

Steps:

1. Reclassify minuscanbe (the vegetation height layer) into 32 classes so that values <0 are split into several classes to determine the range of negative values = bls_testcls2
   Remap table = bls_testclasstable2.dbf
2. Review this classification with aerial imagery for Unique_IDs and installation boundary extent.
3. Calculate statistics “Zonal Statistics as Table” for each of the 32 classes within each range at Fort Bliss = bls_testcls2_zstats.xlsx

4. Combine the remap table values and the statistics for each class in one file bls_testclasstable2.xlsx. Calculate the percentage of each class in each range. The results for the entire LiDAR height layer:

vegetation height	% of pixels
> 0m	93.45278
-0.5m to 0m	6.5455
<-0.5m	0.00223
-0.5m to 10m	99.94

4. For just the pixels within the 3m inundated polygons (bls_testcls3_zstatstable.xlsx):

vegetation height	% of pixels
< -10m	0
-10m to -0.5m	0.00074
-0.5m to 0m	3.39
0m to 12m (the vegetation structure range)	96.59
> 12m	0.028
12m to 20m	0.006
-0.5m to 12m	99.97

Visual analysis in ArcMap shows that nearly all pixels less than 0 are located along the very edge of the data, outside the boundary of Fort Bliss, and not within the stream polygons. There are several polygons with values between -0.5 – 0m but analysis of adjacent pixels in the first return and bareearth layers indicate that the actual vegetation height would still be close to 0m, and the final vegetation structure class would not change.
Conclude that these data layers are suitable for this analysis.

Vegetation Structure Classification

The vegetation structure data from the Multi-Return LiDAR were used to create an additional vegetation structure classification for all installations except YPG (no LiDAR data available). This classification provides additional information regarding riparian vegetation structure for use in management, but was not used in the stream type classification.

Steps to Classify into Vegetation Structure Classes using ERDAS Imagine

1. In ArcMap, create separate raster layers for each vegetation structure layer (polygon to raster)
2. In ERDAS Imagine, layer stack all separate vegetation structure layer rasters.
3. Perform Unsupervised Classification IsoData in ERDAS Imagine, using sample interval of 1, defaults for all other options. The number of classes is determined by trial and error using different number of classes, viewing the results in ArcMap, and analyzing the vegetation structure percentages to see what makes the most sense based on knowledge of the area and field work. Most results showed 7-9 classes as most explanatory.

a. From ERDAS Documentation, accessed online March 10, 2014 http://geomaticsjc.lboro.ac.uk/ven/software/Imagine2013/Foundation2013/Repository/ERDAS-Foundation/Doc/en/ERDAS%20Foundation%20Release%20Notes.pdf

b. The term "Iterative Self-Organizing Data Analysis Technique" (Isodata) describes a broad algorithmic approach to performing unsupervised classification on imagery. It is iterative in that it repeatedly performs an entire classification (outputting a thematic raster layer) and recalculates statistics. "Self-Organizing" refers to the way in which it locates the clusters that are inherent in the data. The Isodata method allows the user to set a range for the number of clusters to be produced. This is because the Isodata algorithm can perform cluster deletion, splitting, and merging between iterations, and provides for producing a greater number classes in the tails of the image histograms – the dark / shadowed areas and the bright areas.

4. Results for each installation.

a. Fort Irwin: 8 classes, irwlidvegstka.img is input image, irwlidvegstka_iso10.img is output image with 8 classes.

Veg Group	<0.25m	0.25-1m	1-4m	4-12m	>12m	Fort Irwin General vegetation structure description
1	99.75	0.24	0.01	0.00	0	mostly veg <0.25m, minor veg 0.25-4m
2	90.08	7.49	2.16	0.27	0	mostly veg <0.25m, some veg 0.25-1m, minor veg 1-12m
3	98.91	1.02	0.08	0.00	0	mostly veg <0.25m, minor veg 0.25-4m
4	96.84	2.90	0.26	0.00	0	mostly veg <0.25m, minor veg 0.25-1m, minor veg 1-4m
5	98.75	0.97	0.24	0.04	0	mostly veg <0.25m, minor veg 0.25-12m
6	99.65	0.33	0.02	0.00	0	mostly veg <0.25m, minor veg 0.25-4m
7	98.68	1.31	0.01	0.00	0	mostly veg <0.25m, minor veg 0.25-4m
8	99.27	0.72	0.01	0.00	0	mostly veg <0.25m, minor veg 0.25-4m

b. Yuma Proving Ground: No LiDAR available

c. Fort Huachuca: 7 classes, hualidvegstk.img is input image, hualidvegstkiso10.img is output image with 7 classes.

Veg Group	<1m	1-4m	4-12m	>12m	Fort Huachuca General vegetation structure description
1	39.9	23.4	31.7	4.9	diverse structure, mostly veg >1m, and veg >12m
2	85.2	12.3	2.5	0.0	mostly veg <1m, with some veg 1-12m
3	91.0	8.1	0.9	0.0	mostly veg <1m, with minor veg 1-12m
4	68.8	21.0	10.2	0.0	mostly veg <4m, with some veg 4-12m
5	67.8	15.3	14.9	2.0	diverse structure, mostly veg <1m, some veg 1-12m, minor veg >12m
6	93.0	6.3	0.7	0.0	mostly veg <1m, minor veg 1-12m
7	96.1	3.5	0.4	0.0	mostly veg <1m, minor veg 1-12m

d. Fort Bliss: 9 classes, blslidarvegstk.img is input image, blslidarvegstkiso10a.img is output image with 9 classes.

Veg Group	<1m	1-4m	4-12m	>12m	Fort Bliss General vegetation structure description
1	0.46	0.09	0.00	0.00	mostly veg <1m with minor veg 1-4m and minor veg >4m
2	1.05	0.49	0.15	0.01	mostly veg <1m with sparse veg 1-4m and minor veg >4m
3	1.64	0.39	0.00	0.00	mostly veg <1m with sparse veg 1-4m and minor veg 4-12m
4	3.10	0.82	0.00	0.00	mostly veg <1m with some veg 1-4m and minor veg 4-12m
5	2.52	1.68	0.04	0.00	mostly veg <1m with some veg 1-4m and sparse veg >4m
6	4.91	1.51	0.01	0.00	mostly veg <1m with moderate veg 1-4m and minor veg 4-12m
7	6.08	3.27	0.52	0.77	mostly veg 0.5-1m, sparse veg 1-4m with minor veg > 4m
8	9.33	3.09	0.02	0.00	mostly veg 0.5-4m with sparse veg 4-12m and minor veg >12m
9	16.57	17.63	4.89	0.17	mostly veg 1-12m with some veg >12m

Literature Cited

Carlson E.A. 2009. Fluvial Riparian Classifications for National Forests in the Western United States. Master's Thesis. Colorado State University: Fort Collins, CO; 194 pp.

Lyon, R. 2013. Using rainfall-runoff models to characterize the flow regime of desert streams in the U.S. southwest. M.S. Thesis, University of Arizona, Tucson.

Qi, J., Chehbouni, A., Huete, A.R., Kerr, Y.H., Sorooshian, S. 1994. A Modified Soil Adjusted Vegetation Index. Remote Sensing of Environment, 48:119-126

R Project. 2014. R version 3. www.r-project.org

U.S. Geological Survey (USGS). 2006. National Hydrography Dataset website, http://nhd.usgs.gov/index.html.

Weichelt, H., Rosso, P., Marx, A., Reigber, S., Douglass, K., Heynen, M. 2012. The RapidEye Red Edge Band White Paper. Accessed Nov. 26, 2012 http://blackbridge.com/rapideye/upload/Red_Edge_White_Paper.pdf

Appendices

Appendix A: Vegetation Indices Background

Vegetation indices and other analyses using reflectance properties in satellite imagery are typically employed to evaluate crop or plant health or stress related to water content, fertilization, biomass, carbon, or total leaf area. There are over 150 vegetation indices. The four main components of plant foliage involved in its spectral response are: pigments, water, carbon and nitrogen. Plant leaf pigment is the most relevant component for our analysis since we are not evaluating plant health (determined from carbon, nitrogen and water content), and we must assume that the vegetation at our desert locations are stressed. Therefore, all three categories of leaf pigment would be useful for analysis of desert vegetation: chlorophyll, carotenoids and anthocyanins.

Vegetation Indices include Broadband and Narrowband Indices, some of which were tested for this project and are described below (ENVI Online Help, 2005. ENVI User's Guide, Vegetation Indices, http://geol.hu/data/online_help/Vegetation_Indices.html). The narrowband indices require the red edge band so are only tested at Fort Bliss and YPG where we have RapidEye imagery. Broadband indices are tested at all locations.

Indices using the Red Edge Band (RapidEye) were tested to determine which provided the most information on arid lands vegetation. Most indices using the red edge band are narrowband indices, were developed for hyperspectral imagery, and specify bands with specific wavelengths. Although the RapidEye imagery bands have a broader range than the hyperspectral bands, several of these indices were calculated, using the RapidEye band with the closest narrowband value.

Broadband Vegetation Indices

1. Normalized Difference Vegetation Index (NDVI) is the normalized difference of green leaf scattering in NEAR-INFRARED, and chlorophyll absorption in RED. NDVI is most appropriate in highly vegetated areas with minimal soil cover.

    NDVI = NIR-RED / NIR + RED

    "The NDVI represents a measure of vegetation photosynthetic activity, and is sensitive to various biophysical vegetation characteristics, such as biomass and percentage cover (e.g. Huete and Jackson 1987)." From Wallace & Marsh 2005.

2. Simple Ratio Index (SRI) is the ratio of green leaf scattering in NEAR-INFRARED, and chlorophyll absorption in RED.

    SR = NIR / RED

3. Enhanced Vegetation Index (EVI) is an enhancement on the NDVI to better account for soil background and atmospheric aerosol effects.

    EVI = 2.5 (NIR – RED / NIR + 6RED – 7.5BLUE + 1)

4. Atmospherically Resistant Vegetation Index (ARVI) is an enhancement on the NDVI to better account for atmospheric scattering.

    ARVI = NIR – (2RED – BLUE) / NIR + (2RED – BLUE)

5. Greenness Index (GI) is the integral of scattered light in the GREEN spectral range that is sensitive to gaps in the vegetation canopy.

GI = GREEN/RED

6. Soil Adjusted Vegetation Index (SAVI) is related to NDVI but with a correction factor to adjust for soil brightness and low vegetation cover

SAVI = ((NIR – R) * (1 + L)) / (NIR +R+L)

Where L is from 0-1, with values near 1 for areas with low or no vegetation cover and bright soil, and 0 for total vegetation cover. For areas of unknown cover, use L = 0.5.

7. Modified Soil-adjusted vegetation index (MSAVI2, Qi et al, 1994)

The modified soil-adjusted vegetation index (MSAVI) and its later revision, MSAVI2, are soil adjusted vegetation indices that seek to address some of the limitation of NDVI when applied to areas with a high degree of exposed soil surface. The problem with the original soil-adjusted vegetation index (SAVI) is that it required specifying the soil-brightness correction factor (L) through trial-and-error based on the amount of vegetation in the study area. Not only did this lead to the majority of people just using the default L value of 0.5, but it also created a circular logic problem of needing to know what the vegetation amount/cover was before you could apply SAVI which was supposed to give you information on how much vegetation there was. Qi et al. (1994a) developed the MSAVI, and later the MSAVI2 (Qi et al. 1994) to more reliably and simply calculate a soil brightness correction factor.

The formula for calculating MSAVI itself is the same as the formula for calculating SAVI:

$$MSAVI = \frac{(NIR - RED)(1 + L)}{NIR + RED + L}$$

where RED is the red band reflectance from a sensor, NIR is the near infrared band reflectance, and L is the soil brightness correction factor. The difference between SAVI and MSAVI, however, comes in how L is calculated. In SAVI, L is estimated based on how much vegetation there is (but it's generally left alone at a compromise of 0.5). MSAVI uses the following formula to calculate L:

$$L = 1 - \frac{2 * s * (NIR - RED) * (NIR - s * RED)}{(NIR + RED)}$$

where S is the slope of the soil line from a plot of red versus near infrared brightness values. Qi et al. (1994b), starting with the MSAVI equation, substituted 1-MSAVI(n) for a range of N and then solved the equation recursively until MSAVI(n)=MSAVI(n-1). This yields the following formula, commonly called MSAVI2, which eliminates the need to find the soil line from a feature-space plot or even explicitly specify the soil brightness correction factor:

$$MSAVI2 = \frac{\left(2 * NIR + 1 - \sqrt{(2 * NIR + 1)^2 - 8 * (NIR - RED)}\right)}{2}$$

From: http://wiki.landscapetoolbox.org/doku.php/remote_sensing_methods:modified_soil-adjusted_vegetation_index

**For this project MSAVI2 was used in areas with bright soil backgrounds or highly contrasting vegetation communities like at Fort Huachuca with bright yellow/gold grasses and dark mesquite trees or shrubs, or Fort Irwin with bright sand/ground surface.

Narrowband Vegetation Indices converted to broadband values for the Red Edge band (RapidEye)

Rapid Eye multi-spectral satellite imagery includes the Red Edge band, which is not present in the QuickBird data, or in many other multi-spectral datasets. Several indices using this band were tested to determine which would most improve the vegetation analyses. These analyses

showed that many of the indices performed similarly, but the Red Edge NDVI gave the most consistent results across varied terrain and vegetation.

The Red Edge band (690-730 nm) covers the portion of the spectrum between the Red band (630-685 nm) and the NIR band (760-850 nm), and provides information on plant chlorophyll content, and leaf cell structure reflection. The Red Edge band includes the portion of the spectrum where reflectance increases rapidly, and therefore can add information regarding the variation in plant chlorophyll content and reflection, improving the ability to distinguish plant types, cover and density. (Dr. Horst Weichelt, Dr. Pablo Rosso, Alexander Marx, Sandra Reigber, Kim Douglass, Markus Heynen, The RapidEye Red Edge Band White Paper. http://blackbridge.com/rapideye/upload/Red_Edge_White_Paper.pdf)

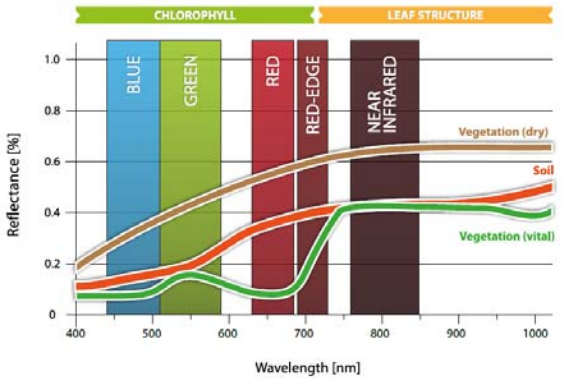


Figure 1: Typical spectral reflectance curves of selected surfaces in relation to the RapidEye spectral bands

Schuster et al. (2012) tested the use of the red edge band for land use classification and found that this band improved accuracy in areas of open landscapes such as bush vegetation.

The following indices (narrowband greenness) using the Red Edge band are from the website http://geol.hu/data/online_help/Vegetation_Indices.html, The ENVI User Guide, accessed November 27, 2012 which converted narrowband values to broadband values. The original equations use the wavelength values, where ρ_{750} indicates wavelength 750, and so on. These values were replaced in the revised equations with the closest broadband band, where ρ_{750} is replaced with the NIR band, ρ_{705} is replaced with the Red Edge band, and so on.

1. Red Edge Normalized Difference Index (RE_NDVI)
   Original equation $NDVI_{705} = \rho_{750} - \rho_{705} / \rho_{750} + \rho_{705}$
   Revised equation $NIR\text{-}RE/NIR + RE$

**This index was used at Fort Bliss and YPG where we have RapidEye imagery. It allowed for an improved and more consistent analysis of vegetation cover.

2. Modified Red Edge Simple Ratio Index (Re-Mod-SRI)
   Original equation $mSR_{705} = \rho_{750} - \rho_{445} / \rho_{705} - \rho_{445}$
   Revised equation Re-Mod-SRI = $NIR - B / RE - B$

3. Modified Red Edge Normalized Difference Vegetation Index
   Original equation = $NDVI_{705} = \rho_{750} - \rho_{705} / \rho_{750} + \rho_{705} - 2\rho_{445}$

Revised equation = Re-Mod-SRI = *NIR – RE / NIR + RE – 2B*

4. Modified Chlorophyll Absorption in Reflectance Index (MCARI; Daughtry et al. 2000) to minimize effects of soil reflectance and non-photosynthetic surfaces

MCARI = {((RedEdge – RED) – 0.2)(RedEdge-GREEN)](RedEdge/RED

5. Transformed Chlorophyll Absorption in Reflection Index (TCARI; Haboudane et al. 2002) to reduce background reflectance

TCARI = 3[(RedEdge – RED)-0.2(RedEdge-GREEN)(RedEdge/RED)]

Appendix K: Geomorphology Analysis Guidance Document

GEOMORPHOLOGY ANALYSIS GUIDANCE DOCUMENT

Table of Contents

Introduction 2

Data Acquisition 3

HUC 8, HUC 10, HUC 12, NHDPlus Flowline 3

Catchment Layer 5

Connecting Flowlines with each Watershed Boundary Polygon 6

Reach Layer 8

Derivation of the Attributes 9

HUC 8, HUC 10, HUC 12, and Catchment Metrics 10

Length, Width and Area 10
Elevation Max, Elevation Min, Relief Ratio and Slope 11
Drainage Density (HUC 10 and HUC 12 only) 13
GAP Majority and Variety (HUC 10, HUC 12 and CATCHMENT) 15
Rainfall Seasonality and Modified Fournier Index (HUC 12) 16
Weathered Products Texture (HUC 12) 18
NOAA Depth-Duration-Frequency (HUC 12) 21
Annual Flood Frequency, Drainage Condition Index, Hydrologic Group, K Factor (Catchment) 23

Reach Metrics 27

Rock Type and Lithology 27
Rainfall Seasonality and Modified Fournier Index 29
Reach Width at 0.25, 0.5, 1, 2 and 3 meters 30
National Flood Frequency: Linear Regression Equations 32
Contributing Area 32
Flood-Peak Discharge 35
Total Stream Power 35
Unit Stream Power 36

Literature Cited 37

Appendix A: Weathered Products Texture 39

Appendix B: Soil Properties aggregated from the National Soil Survey Handbook (NSSH): Part 618 (Subpart A) 40

Appendix C: Map Examples of Derived Data 41

Introduction

The geomorphic analysis is part of the larger project goal to create and ecohydrologic stream type classification. This document describes the geomorphologic, hydrologic, and vegetative data that were calculated at varying scales as parameters or variables for this analysis for the four DoD installations: Fort Bliss, Fort Huachuca, Yuma Proving Ground (YPG), and Fort Irwin. The Salford Predictive Modeler Software (http://www.salford-systems.com/ ;Salford Systems) was used to analyze these data within a Random Forest Statistical Model. The raw datasets utilized here are all freely available through various institutions and governmental organizations. These parameters and variables may be updated as improved datasets become available with the methodology as described here. Since these ecosystems are complex this dataset is by no means complete and there are likely to be additional parameters or variables that would be beneficial. The addition of other parameters or different scales may identify other important aspects in describing stream networks. This document describes the reasoning and methods behind the derivation and calculation of this suite of data.

Describing a system at multiple scales enhances the understanding of that system where multiple processes (biological, physical or chemical) simultaneously interact at varying spatial and temporal scales with each other. Reach scale channel characteristics are related to large scale features such as landcover type, soil characteristics, topography or disturbances within the uplands.

This methodology focuses on three hydrologic scales, but also takes into account larger spatial scales. The Water Boundary Dataset (WBD) within the NHDPlus Version 2 dataset maps the Hydrologic Unit Codes (HUCs) at several hierarchical scales across the conterminous US. The HUC 8 (Subbasin) scale was used to isolate the smaller scale hydrologic units (HUC 10, HUC 12 and Catchment) in the study areas. In these databases, the HUC 12 (Watershed Hydrologic Unit) and Catchment (Valley Hydrologic Unit) scales were of primary focus and many of the parameters/variables documented here were derived at these scales as well as the Reach scale. The USGS NHDPlus Version 2 Flowline layer, used as the reach layer, is a coarse resolution of the streams within these regions and many of the smaller channels are missed. In certain regions the Catchment dataset is not nested within the HUC 12 layer and therefore may skew data analyses in these areas. While this should not have an adverse effect on the outcomes of this research, it is important to take into consideration when analyzing results or in using these data.

Data Acquisition

The stream networks and data were obtained from the National Hydrography Dataset Plus[1] (High Resolution Dataset) and were downloaded by state (Table 1: *Flowline & HUC data*[2]). This includes the NHD Flowline network, and the hydrologic boundary feature classes: HUC 8, HUC 10 and HUC 12. The Catchment layer (*NHDPlusV21*_XX_XX_*NHDPlusCatchment_01.7z)* and Flow Accumulation Grid (*NHDPlusV21*_XX_XX_XX_*FdrFac_01.7z*) were downloaded by the HUC 2 Identifier (Table 1: *Drainage Area ID, VPU, and RPU*) through the Horizon Systems NHD Plus website[2].

Table 1: Downloading NHDPlus data from NHDftp[2] and Horizon Systems[3] website.

	Flowline & HUC data[2]	Catchment & Flow Accumulation Grid data[3]			
Base	**NHD Plus High Resolution Dataset**	**HUC 2 Name**	**Drainage Area ID**	**HUC 2 (VPU)**	**Raster Processing Unit (RPU)**
Fort Bliss	NHDH_NM_931v10.zip	Rio Grande	RG	13	13a, 13b, 13c
Fort Huachuca	NHDH_AZ_931v201.zip	Lower Colorado	CO	15	15a
YPG	NHDH_AZ_931v201.zip NHDH_CA_931v201.zip	Lower Colorado	CO	15	15b
Fort Irwin	NHDH_CA_931v201.zip	California	CA	18	18a

The NHDPlus (High Resolution Dataset) flowline network covers most streams in the US and identifies every stream as part of the network with a unique *ReachCode* identifier. When a stream intersects with another stream, the downstream section receives a new *ReachCode* identifier. In this analysis, the streams were split into smaller segments and an underscore and number were added to the end of the *ReachCode* ID. This became our unique identifier.

HUC 8, HUC 10, HUC 12, NHDPlus Flowline

1. Download and Unzip the NHDPlus (High Resolution Dataset), Catchment, and FAC grid data (the FAC grid data will be set aside for later use)

2. Open ArcMap 10.1 and locate the NHDH geodatabase (NHDH_*XX*.gdb)

3. Under the *WBD* subfolder in the geodatabase (Figure 1), import WBD_HU8, WBD_HU10 and WBD_HU12 into ArcMap 10.1 (the smaller the HUC number, the larger the spatial scale)

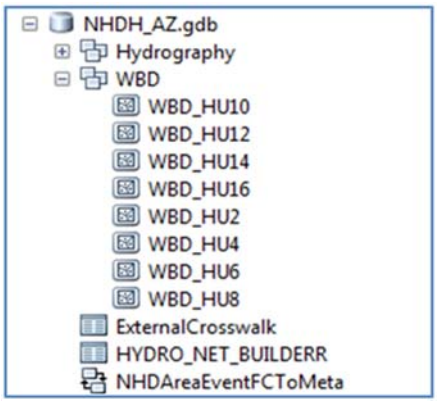


Figure 1: NHDPlus High Resolution geodatabase.

[1] ftp://nhdftp.usgs.gov/DataSets/Staged/States/FileGDB/HighResolution/ (US Geological Survey: National Hydrograph Dataset)

[2] http://www.horizon-systems.com/nhdplus/NHDPlusV2_home.php (Horizon Systems Corporation)

4. Upload the installation Boundary Layer
5. Overlay the Boundary Layer with the WBD_HU8 layer
6. Use the Select Tool  to select the intersecting WBD_HU8 polygons with the Boundary Layer (Figure 2, Table 2)
7. Use the **Select Tool** to extract the HUC 8 polygons that are identified in Table 2 under *Analysis -> Extract -> Select*
8. Use the **Clip Tool** to clip the HUC 10 and HUC 12 layers to the boundary of the HUC 8 layer that was just created, under *Analysis -> Extract -> Clip*
    a. *Input Features:* HUC 10, HUC 12
    b. *Clip Features:* HUC 8 output from the *Select Tool*
9. Import the NHDFlowline under the *Hydrography* subfolder (Figure 1) and follow **Step 8**, but with the Flowline layer as the input layer
10. Change Projection of the clipped HUC 8, HUC 10, HUC 12 and NHDFlowline layers to WGS 1984 UTM projection (refer to Table 2 for specific projection)
    a. To do this, use the **Project Tool** *(Data Management Tools -> Projections and Transformations -> Feature -> Project)*

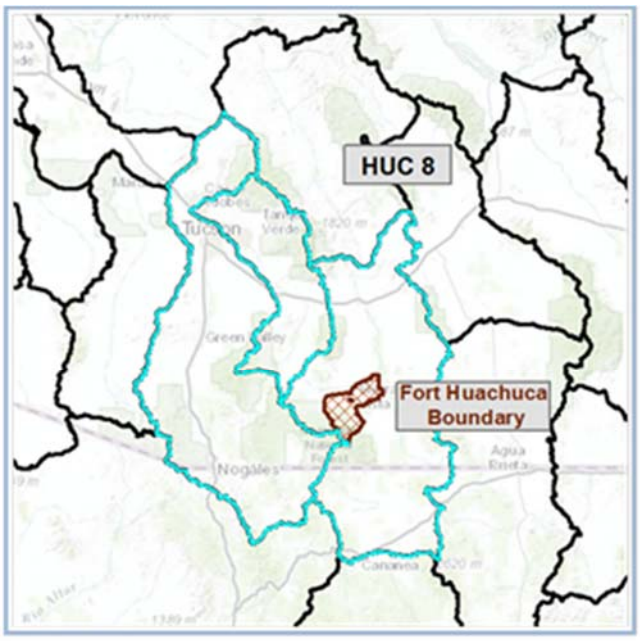


Figure 1: Selecting the HUC 8 layers that pertain to the study area.

Table 2: HUC 8 IDs that were selected in Step 6 and designated projection for each feature class in the end product.

Base	HUC 8 IDs Extracted in Step 6	Projected Coordinate System
Fort Bliss	13050003, 13030103, 13060010, 13050004,	WGS_1984_UTM_Zone_13N

	13040100, 13030102	
Fort Huachuca	15050302, 15050202, 15050301	WGS_1984_UTM_Zone_12N
YPG	15030106, 15030105, 15030104, 15070201, 15030107, 18100204, 15030108	WGS_1984_UTM_Zone_11N
Fort Irwin	18090204, 18090201, 18090207, 18090205, 18090206, 18090202, 18090208, 18090203	WGS_1984_UTM_Zone_11N

Catchment Layer

11. Upload the Catchment polygon layer in ArcMap 10.1 (Figure 3)
    a. The Catchment layer does not exactly match the HUC boundaries and therefore the Select Button was used to select the Catchment polygons that fall within the HUC 8 Boundary files (Figure 4)

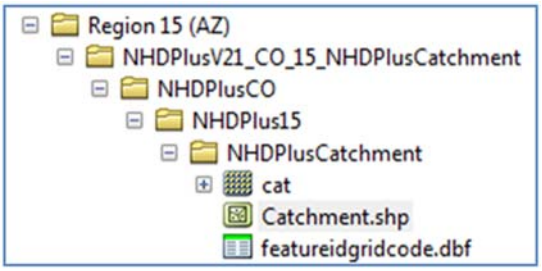


Figure 3: Location of Catchment Polygon after unzipped.

12. The **Select Tool** was used to extract the Catchment polygons *(Analysis -> Extract -> Select*)
13. The layer was re-projected as defined in Table 2 and Step 10

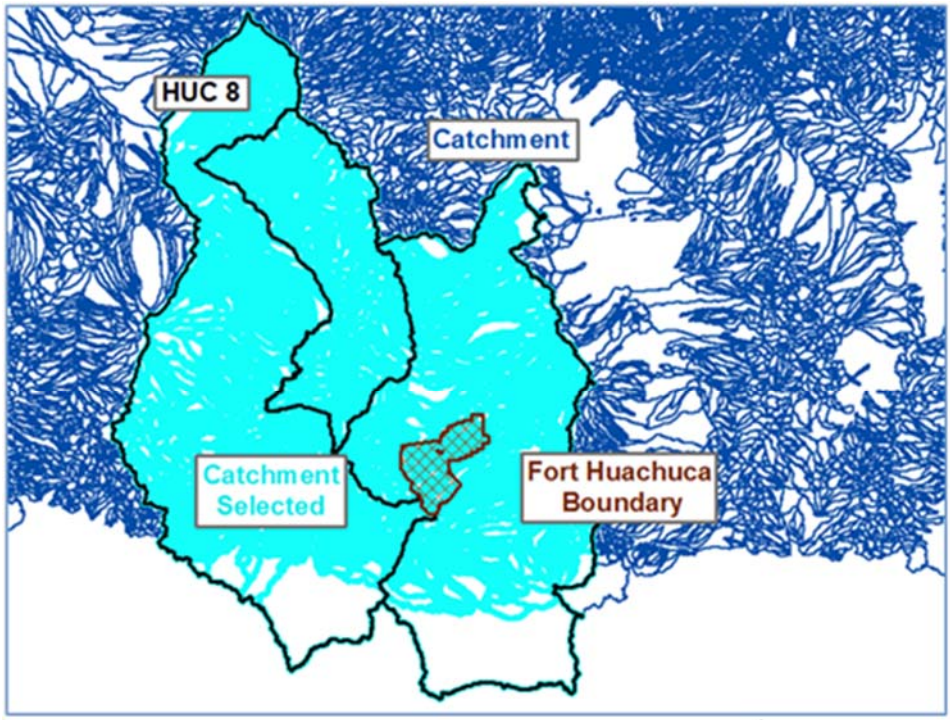


Figure 4: Selecting Catchment polygons.

Connect Flowlines with each Watershed Boundary Polygon
The NHDPlus Flowline layer was intersected with each NHDPlus Watershed Boundary layer so future joins between these layers could be easily executed. The unique common identifiers in Table 3 were transferred to the NHDPlus Flowline layer by the Intersecting Tool.

Table 3: The Fields in the Attribute Table that holds the Unique Identifier in each WBD Layer.

WBD Layer	Common Identifier	WBD Layer	Common Identifier
HUC 8	HUC_8	**HUC 12**	HUC_12
HUC 10	HUC_10	**Catchment**	GRIDCODE

14. **Spatial Join Tool** was used on each WBD Layer with the NHDPlus Flowline layer *(Analysis Tools -> Overlay -> Spatial Join)*

    a. *Target Features:* NHDPlus Flowline
    Join Features: HUC 8
    Join Operation (optional): JOIN_ONE_TO_ONE
    Match Option (optional): HAVE_THEIR_CENTER_IN

    b. Repeat for HUC 10, and HUC 12 and Catchment

15. In the original NHDPlus Flowline layer 4 new Fields were added by the ***Add Field*** button under the menu tab  (Figure 5)

    a. *Name:* HUC8ID
    Type: Text
    Length: 8

    b. *Name:* HUC10ID
    Type: Text
    Length: 10

    c. *Name:* HUC12ID
    Type: Text
    Length: 12

    d. *Name:* GRIDCODE
    Type: Long

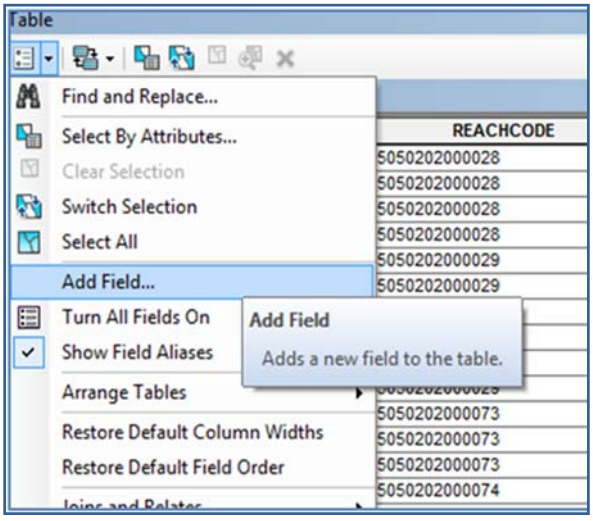


Figure 5: Adding Fields in the Attribute Table.

***The following Steps (16 to 18) were executed for each individual join before performing the next join; **Step 16** creates the join, **Step 17** transfers the data, then **Step 18** removes the join.

16. Each WBD layer was joined separately to the NHDPlus Flowline Layer by

    a. Right Clicking the NHDPlus Flowline layer in the *Table of Contents;* selecting ***Joins and Relates***, selecting ***Join…*** (Figure 6)

    b. In the *Join Data* GUI, join the Common ID of the associated field as seen in Table 3 to the same Common ID from the selected intersected layers created in **Step 14** (which is set in Item 2)

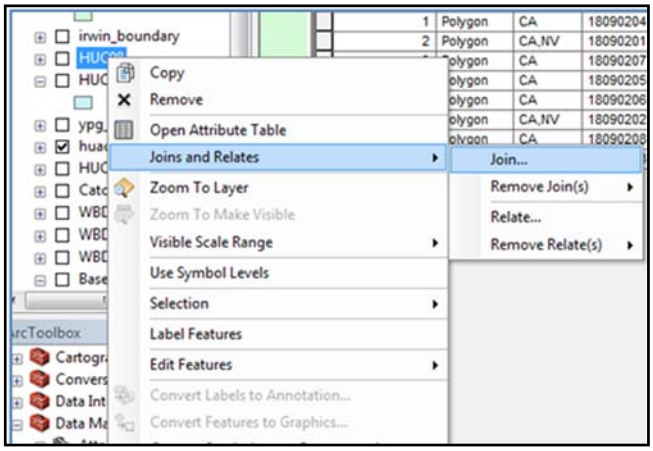


Figure 6: Joining two attribute tables in ArcGIS.

17. The **Field Calculator Tool** was used to transfer the Common ID from the intersected flowline layer to the main flowline layer by right clicking the column header and choosing ***Field Calculator…***; "*XXX*" represents the name given to the output layers from **Step 14**; the formulas that transferred the Common IDs per WBD Layer are as follows:

    a. *HUC8ID* = **[*XXX*:HUC_8]**

    b. *HUC10ID* = **[*XXX*:HUC_10]**

    c. *HUC12ID* = **[*XXX*:HUC_12]**

    d. *GRIDCODE* = **[*XXX*:GRIDCODE]**

18. Each Join was removed

    a. Right Click on Layer in Table of Contents; select ***Joins and Relates,*** then ***Remove Join(s),*** select Join to remove (Figure 7)

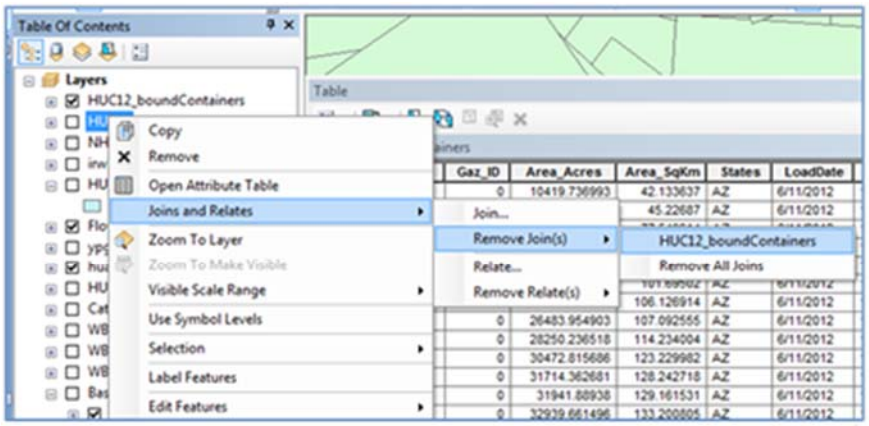


Figure 7: Removing Join by Right Clicking on Layer in the Table of Contents.

Reach Layer

19. The **Clip Tool** was used to create the Reach layer *(Analysis -> Extract -> Clip)*; (Figure 8)
    a. *Input Features:* The re-projected Flowline Layer created in **Steps 9 & 10**
    b. *Clip Features*: Boundary Layer (in the same Projection as the *Input Features*)
20. The ET Geo Wizards Tool was downloaded through ET Spatial Techniques[3] and uploaded into ArcMap 10.1 Toolbox. This tool was used to divide the reaches into equal lengths roughly around 1 km

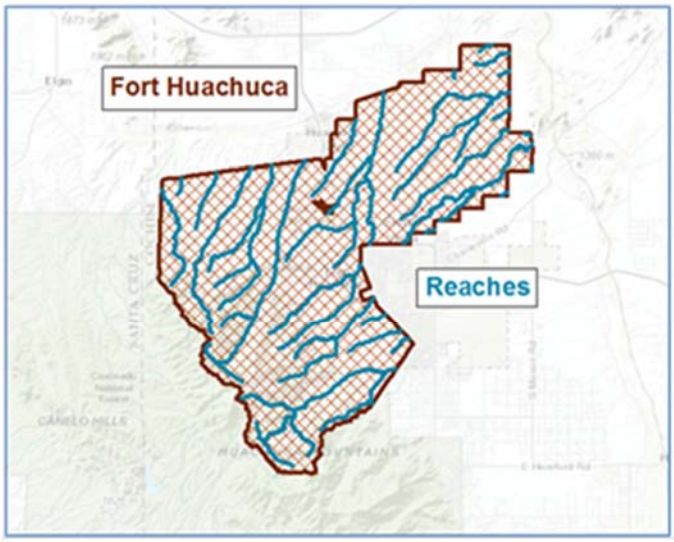


Figure 8: Clipping the NHDPlus Flowline to the base boundary.

21. The **Split Tolerance Tool** was used (Note: a License is required)
    a. *Input:* Base Boundary
    Flowline Layer
    Segment Length: 1 km
    Split Tolerance: Equal Length

22. In the Attribute Table, two new fields were created (**Step 15**, Figure 5)
    a. *Name:* ET_ID
    Type: Text
    Length: 5

[3] http://www.ian-ko.com (ET SpatialTechniques)

b. *Name:* UniqueID
Type: Text
Length: 25

23. The **Field Calculator Tool** was used to calculate the new columns (Right click on column header and choose *Field Calculator*….); the formulas are as follows:
    a. *ET_ID* = **[FID]**
    b. *UniqueID* = **[REACHCODE] & "_" & [ET_ID]**

**The *UniqueID* is the unique identifier that is used in the rest of this methodology to join and relate the Attribute Tables of the associated layers back to the reach scale and to link up the geodatabase tables of the end products to the spatial layers.

Derivation of the Attributes

After the HUCs, Catchment, NHDPlus Flowline, and Reach (at the Base scale) were all created, the next task was to derive the attributes using a variety of GIS functions and data sources, as identified in Figure 7. The HUC 8 and HUC 10 layers are at larger scales and therefore only a few parameters have been calculated for them. The HUC 12 or Watershed Scale and Catchment layers incorporate data that are generalized to the extents of each polygon. The Reach scale generalizes data along each 1 km reach that were created in **Steps 14 – 18**.

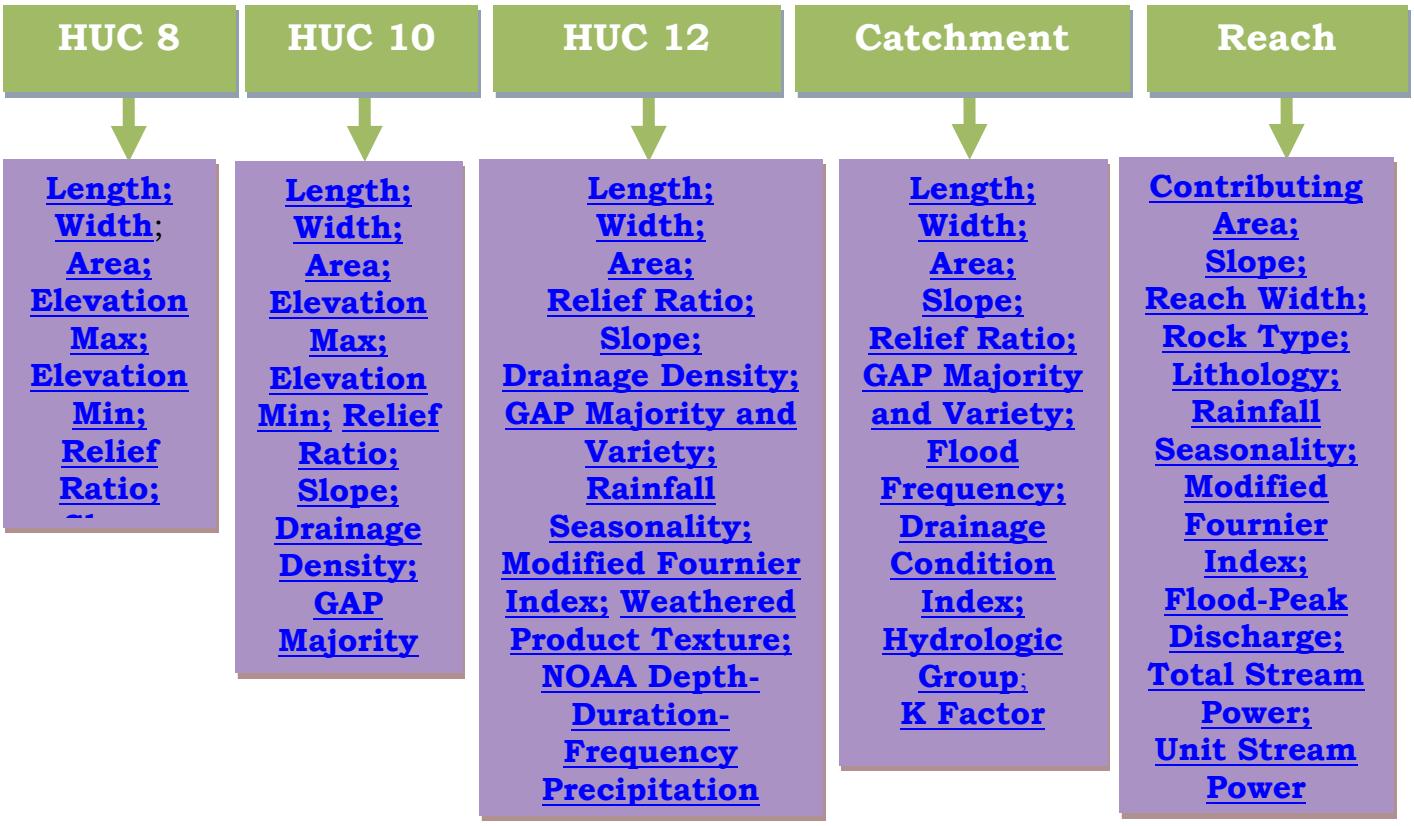


Figure 9: Spatial assignments of each parameter included within the geomorphic dataset. The items in this figure are linked to the area within this document that shows how the data were processed. To follow the link, use CTRL + Click.

Note that some parameters were calculated or derived from or include other variables, therefore the order in which the parameters are derived is important.

HUC 8, HUC 10, HUC 12, and Catchment Metrics

Length, Width and Area

The dimensions of the hydrologic units within the HUC 8, HUC 10, HUC 12 and Catchment layers were estimated. Length was used to calculate the average slope for each hydrologic unit within each spatial layer.

24. The **Minimum Bounding Geometry Tool** was used to calculate the Length and Width of each polygon within each feature class
    a. *Input:* HUC 8, HUC 10, HUC 12
       Geometry Type (optional): RECTANGLE_BY_AREA option
       Group Option (optional): None
       Check *Add geometry characteristics as attributes to output (optional)*
    b. The output feature class maintained each of the input attributes and added *MBG_Width, MBG_Length, MBG_Orient*
25. Two new fields were added in each NHDPlus Layer (**Step 15**, Figure 5)
    a. *Name:* Width_km
       Type: Float
    b. *Name:* Length_km
       Type: Float
26. The Main Layer was joined to the Minimum Bounding Geometry output shapefile using the Common Identifiers specified in Table 3 (**Step 16**, Figure 6)
27. The **Field Calculator** in the Attribute Table was used to transfer the data (refer to **Step 17**); note that the dimensions were in units of meters; dividing by 1000 in the **Field Calculator** puts the dimensions into km; "*XXX*" represents the name given to the output table from **Step 24**; the formulas used are as follows:
    a. *Width_km* = [*XXX*:**MBG_Width] / 1000**
    b. *Length_km* = [*XXX*:**MBG_Length] / 1000**
28. The Join was removed (**Step 18**, Figure 7)
29. Area was calculated for each Main Layer by adding another Field (**Step 15,** Figure 5)
    a. *Name:* Area_sqkm
       Type: Float

30. The area was calculated by right clicking on the field that was just created then selecting ***Calculate Geometry…*** (Figure 10)

    a. *Property:* Area
    Units: Square Kilometers [sq km]

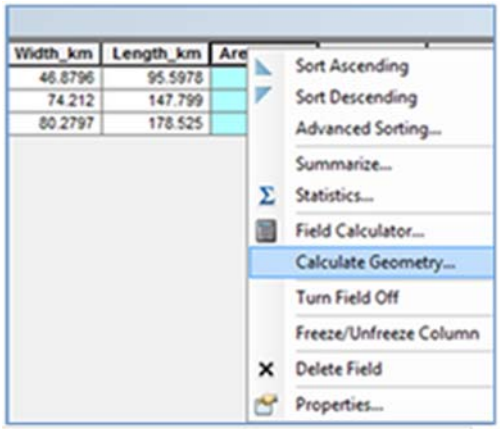


Figure 10: Calculate Geometry for a Field.

Elevation Max, Elevation Min, Relief Ratio and Slope

For these parameters, a Digital Elevation Model (DEM) was downloaded through the USGS National Map Viewer website[4] for each region for the extent of the NHDPlus layers. The specific DEMs used in this analysis were from the National Elevation Dataset (NED) 1/3 and have a spatial resolution of 10m or 1/3 arc-second and are delivered in an ArcGrid format with units in meters. The DEMs for each installation were mosaicked together to create a continuous data layer for each installation and surrounding area. Each DEM was used to acquire the Elevation Max and Min parameters. The Relief Ratio is calculated as the range between the highest and lowest elevation values within each NHDPlus unit. The slope (m/m) was calculated by dividing the Relief Ratio within the specific spatial unit by the length of that unit.

Table 4: Specific DEM Grid Code IDs (NED 1/3 arc-second) used in estimating Elevation and Slope parameters at the HUC extents. These grid layers were downloaded through the USGS: National Map Viewer[5].

Base	USGS NED 1/3 arc-second Grid ID				
Fort Bliss	n31 w105 n31 w106 n31 w107	n32 w105 n32 w106 n32 w107 n32 w108	n33 w105 n33 w106 n33 w107 n33 w108	n34 w106 n34 w107	n35 w106 n35 w107
Fort Huachuca	n32 w110 n32 w111 n32 w112	n33 w111 n33 w112			
YPG	n33 w114 n33 w115 n33 w116 n33 w117	n34 w113 n33 w114 n33 w115 n33 w116 n33 w117	n35 w114 n35 w115		
Fort Irwin	n35 w116	n36 w116	n37 w116	n38 w117	

[4] http://viewer.nationalmap.gov/viewer/ (US Geological Survey: The National Map Viewer)

	n35 w117 n35 w118 n35 w119	n36 w117 n36 w118 n36 w119	n37 w117 n37 w118 n37 w119	n38 w118 n38 w119	

31. The grids listed in Table 4 were downloaded through the USGS National Map Viewer website[5] and unzipped
32. All DEM grids per study area were uploaded into ArcMap 10.1
33. All DEM grids were projected into the WGS 1984 UTM projection as specified by Table 2 and **Step 10**
34. The **Mosaic Tool** was used to mosaic all the datasets into one target dataset *(Data Management Tools -> Raster -> Raster Datasest ->Mosaic)*
    a. *Input Rasters:* For each base, all but 1 of the Grids mentioned in Table 4
       Target Raster: The remaining Grids not used in *Input Rasters*, per base
35. To link up the Elevation Data to each of the NHDPlus Boundary layers, the **Zonal Statistics as Table Tool** was used *(Spatial Analyst Tools -> Zonal -> Zonal Statistics as Table)*
    a. *Input raster or feature zone data:* HUC 8, HUC 10, HUC 12 or Catchment
       Zone field: ***The Common Identifier shown in Table 3 was used***
       Input value raster: Mosaiced DEM created in **Step 34**
       Statistics type (optional): MIN_MAX
36. Four new fields were added to each NHDPlus layer (**Step 15**, Figure 5)
    a. *Name:* ElevMax_m
       Type: Float
    b. *Name:* ElevMin_m
       Type: Float
    c. *Name:* Relief Rat
       Type: Float
    d. *Name:* Slope
       Type: Float
37. A join (**Step 16**, Figure 6) was used to join the Zonal Statistics as Table output table **(Step 35)** to each NHDPlus layer with the Common Identifier shown in Table 3
38. After joined, the **Field Calculator** was used to transfer the Min and Max elevation data to the main NHDPlus layers. Note: the DEM input data is in meters and therefore the Min Max data is also in meters; "*XXX*" represents the name given to the output table; the formulas used are as follows:
    a. *ElevMax_m* = **[***XXX***:MAX]**

b. *ElevMin_m*= **[*XXX*:MIN]**

39. The Join was removed (See **Step 18**, Figure 7)
40. To calculate the Relief Ratio, the **Field Calculator Tool** was used (see **Step 17**); the formula used is
    a. *ReliefRat* = **[ElevMax_m] - [ElevMin_m]**
41. To calculate Slope, the **Field Calculator Tool** was used (see **Step 17**). Note: Relief Ratio was converted to km; the slope is unitless; the formula used is
    a. *Slope* = **([ReliefRat] / 1000) / [Length_km]**

Drainage Density (HUC 10 and HUC 12 only)

Drainage Density (km/km^2) estimates the ability of a watershed to drain, where larger drainage densities suggest higher peak floods, higher sediment yield, and steeper slopes (Dunne & Leopold, 1978; pg 500). Drainage Density is calculated by summing the length of all streams within a drainage area then dividing it by the area of the drainage area. While the NHDPlus Flowline layer is a coarse estimation of many of the streams in the southwest, this parameter is still useful as it identifies the larger streams. A finer Drainage Density would include the smaller streams and braided channels that are not located on the NHDPlus Flowline. It is important to note that the drainage densities derived from the NHDPlus dataset are likely to be under estimated (i.e. many values less than 1.0 km/km$^{2)}$. A Drainage Density of 0 indicates there are no stream channels present. In our dataset, this is most often seen at Fort Bliss in areas of little to no slope and high infiltration rates.

42. NHDPlus Flowline, HUC 10, and HUC 12 layers were opened in ArcMap 10.1
43. The **Intersect Tool** was used to join the Flowline layer with the HUC layers *(Analysis Tools -> Overlay -> Intersect)*
    a. *Input Features:* NHDPlus Flowline
    HUC 10
    Join Attributes (optional): ALL
    Output Type (optional): Input
44. **Step 43** was repeated for the HUC 12 layer
45. In the intersected Flowline layers, a new field was added (**Step 15,** Figure 5)
    a. *Name:* Length
    Type: Float
46. ***Calculate Geometry…*** was used on the field just created to calculate the length of all the reaches in km (**Step 30**, Figure 10)

a. *Property:* Length
Units: Kilometers [km]

47. All non-natural streams were removed, such as ditches, canals and pipelines

    a. In the Attribute Table **Select by Attributes…** was used; under the menu tab  (Figure 11)

    b. This equation was inserted:

    "FTYPE" = 'StreamRiver'

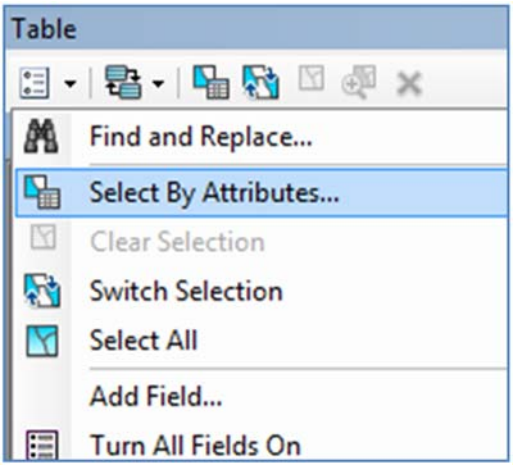


Figure 11: Select By Attributes…

48. Once all of the StreamRiver FTypes were selected the **Select Tool** was used, under *Analysis -> Extract -> Select*

49. The **Dissolve Tool** was used to dissolve the streams on the HUC 10 and HUC 12 Flowline; the unique Common Identifier was used to dissolve the flowlines (*Data Management Tools -> Generalization -> Dissolve*)

    a. *Input Features:* Output from **Step 48** (HUC10flowline or HUC12flowline layers)
    Dissolve: Check HUC_10 or HUC_12 depending upon input
    Statistics Field(s) (optional):
    Field: Length
    Statistics Type: SUM

50. The ***Sum_Length*** from the dissolved layer for the HUC 10 and HUC 12 layers were transferred to the main NHDPlus HUC 10 and HUC 12 layers by

    a. Adding a new Field (**Step 15**, Figure 5)

        i. *Name:* SumLen_km
        Type: Float

    b. Joining the tables (**Step 16**, Figure 6)

    c. Using Field Calculator (**Step 17**) with the formula:

        i. *SumLen_km* = **[*XXX*:Sum_Length]**

    d. Removing the Join (**Step 18**, Figure 7)

51. Drainage Density was now calculated

    a. A new field was added to the attribute table in the main NHDPlus HUC 10 and HUC 12 layers (**Step 15**, Figure 5)

i. *Name:* DrainDen
Type: Float

b. Field Calculator (**Step 17**) was used with the formula:

i. *DrainDen* = **[SumLen_km] / [Area_SqKm]**

GAP Majority and Variety (HUC 10, HUC 12 and CATCHMENT)

National Gap Analysis Program (GAP)[5] data were obtained for the Southwest and South Central Region. This raster dataset is delivered in the Albers Conical Equal Area Projection. The GAP dataare derived from the Landsat 7 ETM+ satellite imagery from 1999 through 2001 and digital elevation model (DEM) datasets. Each $30m^2$ cell within the dataset has been assigned an Ecological System or a land use value and description. This classification was created through a decision tree classifier (Gap Metadata[6]).

The GAP Majority variable estimates the majority of the landcover from the GAP model that occurs in each drainage unit within the HUC 10, HUC 12 and Catchment layers. The values created through this method should be considered categorical data and indicate a certain landcover type. The GAP Majority field of the NHDPlus layers can be joined to the GAP raster layer through the Value field to identify each landcover type. The GAP Variety estimates the diversity in landcover types within each drainage unit at each scale.

52. The Southwest and Southcentral GAP models were downloaded, unzipped, and uploaded to ArcMap 10.1
53. The Southwest and Southcentral GAP models were projected as defined by Table 2 using the **Project Raster Tool** *(Data Management Tools -> Projections and Transformations -> Project Raster)*
54. The Southwest GAP layers were then clipped to the NHDPlus extents by using **Extract by Mask Tool** *(Spatial Analyst Tools -> Extraction -> Extract by Mask)*
55. An extra step was required for Fort Bliss as a quarter of the study area falls into the Southcentral GAP region; **Step 54** was repeated for Fort Bliss using the Southcentral GAP raster layer
    a. After both GAP rasters were masked, they were merged together through the **Mosaic Tool** *(Data Management Tools -> Raster -> Raster Datasest ->Mosaic)*
        i. Input Rasters: Fort Bliss's re-projected and masked Southcentral GAP
        Target Raster: Fort Bliss's re-projected and masked Southwest GAP
56. To link the GAP Data to each of the NHDPlus layers, the **Zonal Statistics as Table Tool** was used *(Spatial Analyst Tools -> Zonal -> Zonal Statistics as Table)*

---

[5] http://gapanalysis.usgs.gov/gaplandcover/ (US Geological Survey, 2011)

[6] http://gapanalysis.usgs.gov/gaplandcover/files/2012/09/USGS_GAP_LandCover_Metadata.pdf (Gap Analysis Program, 2010)

a. *Input raster or feature zone data:* HUC 10, HUC 12 or Catchment
Zone field: ***Use Common Identifier shown in Table 3***
Input value raster: The associated GAP layer created in **Step 54**; Bliss: **Step 55**
Statistics type (optional): ALL

57. The *Majority* and *Variety* fields from the Tables created in **Step 56** for the HUC 10, HUC 12, and Catchment layers were transferred to the associated NHDPlus HUC 10, HUC 12, Catchment layers by

a. Add two new Fields (**Step 15**, Figure 5)

i. *Name:* GAPmaj
Type: Long

ii. *Name:* GAPvar
Type: Long

b. Join the NHDPlus layer to the appropriate Zonal Statistics Table (**Step 21**, Figure 8)

c. Using Field Calculator (**Step 17**)

i. *GAPmaj* = **[***XXX***:Majority]**

ii. *GAPvar* = **[***XXX***:Variety]**

d. Removing the join (**Step 18**, Figure 7)

Rainfall Seasonality and Modified Fournier Index (HUC 12)

Rainfall is an important driver in arid landscapes especially when rainfall events are temporally and spatially variable. Characterizing annual precipitation events can be an important indicator of channel form and degree of erodibility, and can impact vegetation. The Rainfall Seasonality Index (RSI) is calculated as the wettest month divided by the total annual precipitation to describe the seasonal differences in rainfall dynamics (Equation 1). By using the average of monthly rainfall over many years, the RSI can describe the regional rainfall seasonality.
The RSI is closely related to the Fournier Index which squares the precipitation of the wettest month. An extension of the Fournier Index, known as the Modified Fournier Index (MFI) measures the effects of rainwater on erosion where higher values equate to more erosibility potential (Elagib, 2011). The MFI is classified into five categories: very low (0 – 60), low (60-90), moderate (90-120), high (120-160) and very high (> 160) (Elagib, 2011). The Modified Fournier Index (MFI) takes the sum of the squares of the mean rainfall total per month for the annum then divides it by the mean annual precipitation amount (Equation 2). Several papers have described the MFI as a beneficial measure of rainfall erodibility potential using the above criteria (Elagib, 2011).

Equation 1: $$RS = \frac{Mean\ Monthly\ Precip\ of\ Wettest\ Month}{Mean\ Annual\ Precip}$$

Equation 2: $$MFI = \sum_{n=1}^{12} \left(\frac{(Month_n)^2}{Mean\ Annual\ Precip} \right)$$

The mean monthly and mean annual precipitation data used in the RSI and MFI equations were derived using the PRISM 30-Year Normals dataset[7]. The PRISM Data were downloaded through the Oregon State University as ascii layers (13 layers total) at an 800 meter resolution. These data were calculated using the HUC 12 and reach layer (**Steps 106-109**), calculating the RSI and MFI at the watershed and reach scale. Precipitation is downloaded in units of mm*100, so all precipitation values are divided by 100 to convert to mm.

58. After the Annual and Monthly 30-Year Normals[8] (.asc) data at the 800m resolution were download and unzipped, the 13 ascii layers were uploaded into ArcMap 10.1

59. The HUC 12 was projected to the same projection as the PRISM datasets (GCS North American 1983) by using the **Project Tool** *(Data Management -> Projections and Transformations -> Feature -> Project)*

    a. *Input:* HUC 12
    Output Coordinate System: GCS_North_American_1983
    Output Transformation (optional): WGS_1984_(ITRF00)_To_NAD_1983

60. To calculate the precipitation means within each HUC 12, the **Zonal Statistics as Table Tool** was used *(Spatial Analyst Tools ->Zonal -> Zonal Statistics as Table);* Batch tool expedited this step; these tables were saved as the first 3 letters: ann, jan, feb, mar, apr, may, jun, jul, aug, sep, oct, nov, dec

    a. *Input raster or feature zone data:* HUC 12
    Zone field: HUC_12
    Input value raster: ***1 of the 13 ascii files downloaded in Step 58***
    Statistics type (optional): MEAN

61. The MEAN precipitation values for each HUC 12 unit from the 13 tables created in **Step 60** were joined back to the HUC12 shapefile in the GCS coordinate system by

    a. Adding 13 new Fields (**Step 15**, Figure 5)

        i. *Name:* Ann; Jan; Feb; Mar; Apr; May; Jun; Jul; Aug; Sep; Oct; Nov; Dec
        Type: Float

    b. Joining each table separately (**Step 16**, Figure 6)

    c. Using Field Calculator (**Step 17**); (divide by 100 to convert the precipitation to mm)

        i. *Ann* = **[ann:MEAN]/100**

        ii. *Jan* = **[jan:MEAN]/100**

[7] http://www.prism.oregonstate.edu/normals/ (PRISM Climate Group, 2010)

iii. Et cetera…

d. Remove each join (**Step 18**, Figure 7)

62. The Attribute Table of the HUC 8 with each annual and monthly mean precipitation value was then extracted into a .dbf file (Select the menu button  in the attribute table, then ***Export…*** and save as a **dBASE Table**)

63. The .dbf file was uploaded into Excel

    a. In the adjacent cell to the **Dec** column, the ***=MAX()*** function was used to extract the Highest Precipitation Value for all months (the **Ann** column was not included in this formula)

    b. In the next column, the Rainfall Seasonality Index (RSI) was calculated by dividing the Highest Precipitation Value by the Annual Precipitation Value

    c. In the next column, the Modified Fournier Index (MFI) was calculated by following the MFI formula described in ***Equation 2***

64. The Excel document was saved, uploaded into ArcMap and the RSI and MFI data were transferred to the main HUC 12 layer by

    a. Adding 2 new Fields (**Step 15**, Figure 5)

        i. *Name:* RainfallSeas
        Type: Float

        ii. *Name:* ModFournier
        Type: Float

    b. Joining the HUC 12 to the excel (dbf) table (**Step 16**, Figure 6)

    c. Using Field Calculator (**Step 17**)

        i. *RainfallSeas*= **[***XXX***:RS]**

        ii. *ModFournier*= [*XXX*:**MFI**]

    d. Removing the join (**Step 18**, Figure 7)

Weathered Products Texture (HUC 12)

The Weathered Products Texture (WPT) parameter refers to the geologic parent material and is used to explain the availability of sediment potential within the watershed. This parameter is based on the USGS Mineral Resources Program: Geology Datasets, where the categories in the Rock Type 1 field were simplified into four categories: *Unconsolidated, Coarse, Fine* and *Unknown* (for rock type assignment refer to Appendix: A). These USGS GIS layers were compiled from State Geology maps and were downloaded per state[8]. The digital geology GIS

[8] For New Mexico and Texas: http://pubs.usgs.gov/of/2005/1351/ (Stoeser et al. 2007). For California and Arizona: http://pubs.usgs.gov/of/2005/1305/ (Lundington et al. 2007)

layers for California[9], Arizona[10], New Mexico[11] and Texas[12] were downloaded (ArcView shapefiles: *XX*geol_dd.zip). Background information about these layers and attributes tables can also be found at http://pubs.usgs.gov/of/2005/1351/documents/CONUSDocumentation.pdf.

65. The GIS versions of the State Geology layers were downloaded, unzipped and the *XX*geol_dd_polygon.shp layer was uploaded into ArcMap

66. An extra step was needed at Fort Bliss, where the Texas and New Mexico geology layers were merged together by using the **Merge Tool** *(Data Management -> General -> Merge)*

67. The **Project tool** was used to project the geology shapefile into the same projection as the HUC 12 layer as documented in Table 2 *(Data Management Tools -> Projections and Transformations -> Feature -> Project)*

68. The **Clip Tool** was used to clip the geology layer to the HUC extents *(Analysis Tool -> Extract -> Clip)*

69. The Geology polygons were then dissolved on the ROCKTYPE1 field using the **Dissolve Tool** *(Data Management ->Generalization -> Dissolve)*

    a. *Input Features:* Geology Layer
    Dissolve_Field(s) (optional): check ROCKTYPE1

70. A new field was added into the attribute table of the dissolved geology layer (**Step 15**, Figure 5)

    a. *Name:* WPT
    Type: Text
    Length: 50

    b. The four categories were added to the new field: *Unconsolidated, Coarse, Fine* and *Unknown* to reflect Appendix: A by using the **Editor Tool** *(Right click on layer in Table of Contents-> Edit Features -> Start Editing)*

71. The **Dissolve Tool** was used to aggregate the WPT classes *(Data Management -> Generalization -> Dissolve)*

    a. *Input Features:* Geology Layer
    Dissolve_Field(s) (optional): check WPT

---

[9] California Geology Layers (http://pubs.usgs.gov/of/2005/1305/#CA): *CAgeol_dd.zip*

[10] Arizona Geology Layers (http://pubs.usgs.gov/of/2005/1305/#AZ): *AZgeol_dd.zip*

[11] New Mexico Geology Layers (http://pubs.usgs.gov/of/2005/1351/#NM): *NMgeol_dd.zip*

[12] Texas Geology Layers http://pubs.usgs.gov/of/2005/1351/#TX): *TXgeol_dd.zip*

72. The geology polygon layer that includes the WPT field was then converted to a raster using **Polygon to Raster Tool** *(Conversion Tools -> To Raster -> Polygon to Raster)*

    a. *Input Features:* ***geology layer created in Step 71***
    Value field: WPT
    Cell assignment type (optional): Cell_Center
    Priority field (optional): NONE
    Cellsize (optional): 0.0001

73. **Zonal Statistics as Table Tool** was used to find the majority of the WPT index from the geology raster *(Spatial Analyst Tools -> Zonal -> Zonal Statistics as Table)*

    a. *Input raster or feature zone data:* HUC 12
    Zone field: WPT
    Input value raster: ***geology raster from Step 72***
    Statistics type (optional): MAJORITY

74. Since the Zonal Statistics calculated the Value field, the WPT was associated to the Value field by

    a. Adding a new Field in the Zonal Statistics Geology Table (**Step 15**, Figure 5)

        i. *Name:* WPT
        Type: Text
        Length: 50

    b. Joining the *Majority* field in the Zonal Statistics Geology Table to the *Value* field in the geology raster (**Step 16**, Figure 6)

    c. Using Field Calculator (**Step 17**)

        i. *WPT* = **[***XXX***:WPT]**

    d. Removing Join (**Step 18**, Figure 7)

75. The *WPT* field from the Zonal Statistics Geology Table was transferred to the main HUC 12 layer by

    a. Adding a new Field in the HUC 12 layer (**Step 15**, Figure 5)

        i. *Name:* WPT
        Type: Text
        Length: 50

    b. Joining the HUC 12 layer to the Zonal Statistics Table (**Step 16**, Figure 6)

    c. Using Field Calculator (**Step 17**)

        i. *WPT* = **[***XXX***:WPT]**

    d. Removing Join (**Step 18**, Figure 7)

NOAA Depth-Duration-Frequency (HUC 12)

The Depth-Duration-Frequency (DDF) estimates the depth of rainfall during extreme precipitation events as a function of duration for a specified return period. The frequency and magnitude of these events can be a major driver of fluvial geomorphological processes such as channel formation and sediment movement. The DDF estimates were calculated for rainfall depths at duration and frequency intervals of 10yr-30min, 10yr-60min, 10yr-2hr, 25yr-30min, 25yr-60min and 25yr-2hr; where the 10yr recurrence intervals have an annual exceedance[13] probability of 0.10 or a 10% chance of this type of event occurring each and every year, and the 25yr recurrence intervals have a probability of occurring of 0.04 or 4% chance each and every year (Dunne & Leopold, 1978, p 52-53).

The Precipitation Frequency raster data used in this research were developed through the Hydrometeorological Design Studies Center within the Office of Hydrologic Development of National Oceanic and Atmospheric Administration's (NOAA) National Weather Service (NWS) and are divided into volumes based on geographic location (Office of Hydrologic Development, 2014)[14]. At each DDF interval, the Semiarid Southwest (NOAA Atlas 14 Volume 1) were downloaded in ascii grid format and used on the associated installations. The resolution of this data is at 889 meters and is delivered in precipitation values of inches*1000 so that precipitation is in interval form. The precipitation was converted into millimeters with three significant figures.

Since Fort Bliss includes areas in Texas, DDF values for Texas were sourced separately through the *USGS: Atlas of Depth-Duration Frequency of Precipitation Annual Maxima for Texas*[15] contour maps (Asquith & Roussel, 2004). This document contains the DDF contour maps at varying duration and time scales. The precipitation depths were obtained for the same six Duration-Frequency scales as the NOAA DDF datasets and are documented in intervals at a tenth of an inch. This was approximated by georeferencing the contour maps and using the Editor Tool in ArcMap to add in the associated values. The DDF values were converted into millimeters and rounded to two significant figures.

76. The raster files from the ***NOAA Atlas 14 Volume 1 (Semiarid Southwest): Precipitation frequency estimates: Annual Maximum Series*** data were downloaded at each DDF interval and unzipped
    a. *Annual exceedance probability:* 1/10 (10 year)
        i. *Duration:* 30-minute, 60-minute and 2-hour
    b. *Annual exceedance probability:* 1/25 (25 year)

[13] *Annual exceedance* is a measure of a sample of all annual extreme rain events of a certain duration interval at a measuring station (Dunne & Leopold, 1978, p 52).

[14] NOAA Atlas 14 Precipitation Frequency Estimates in GIS Compatible Format: NOAA Atlas 14 Volume 1 – Semiarid Southwest (sw) (http://hdsc.nws.noaa.gov/hdsc/pfds/pfds_gis.html)

[15] USGS: Atlas of Depth-Duration Frequency of Precipitation Annual Maxima for Texas: http://pubs.usgs.gov/sir/2004/5041/ (Asquith & Roussel, 2004)

i. *Duration:* 30-minute, 60-minute and 2-hour

77. After layers were brought into ArcMap 10.1, the **Define Projection Tool** was used to project the DDF grids into the same projection (GCS North American 1983) as the HUC 12 layer created in **Step 59** *(Data Management -> Projections and Transformations -> Define Projection)*

78. To obtain the DDF means for each of the six intervals within each HUC 12 drainage area, the **Zonal Statistics as Table Tool** was used *(Spatial Analyst Tools ->Zonal -> Zonal Statistics as Table);* Batch tool expedited this step; these tables were saved as *sw10y30m, sw10y60m, sw10y2hr, sw25y30m, sw25y60m,* and *sw25y2hr*, respectively

    a. *Input raster or feature zone data:* HUC 12 (with GCS North American 1983 projection)
    Zone field: HUC_12
    Input value raster: ***1 of the 6 DDF grids***
    Statistics type (optional): MEAN

79. The MEAN precipitation values for each HUC 12 unit from the 6 tables created in **Step 78** were joined back to the *main* HUC12 shapefile

    a. Adding 6 new Fields (**Step 15**, Figure 5)

        1. *Name:* sw10y30m, sw10y60m, sw10y2hr, sw25y30m, sw25y60m, sw25y2hr
        Type: Float

    b. Join each table separately (**Step 16**, Figure 6)

    c. The following formulas were used in Field Calculator (**Step 17**) to convert the precipitation to mm and round it to the nearest tenth of a millimeter

        i. *sw10y30m* = **Round(([sw10y30m:MEAN]/1000*25.4), 1)**

        ii. *sw10y60m* = **Round(([sw10y60m:MEAN] /1000*25.4), 1)**

        iii. Et cetera…

    d. Each join was removed (**Step 18**, Figure 7)

80. Fort Bliss required an extra step where the *USGS: Atlas of Depth-Duration Frequency of Precipitation Annual Maxima for Texas* contour maps were used
    a. The DDF images were saved as a jpeg, then uploaded into ArcMap 10.1
    b. The images were georeferenced by adding at least 4 control points to each of the 6 DDF maps, (*Customize tab -> Toolbars -> Georeferencing)*
    c. **Editor Tool** was used on the HUC12 layer *(Right click on layer in Table of Contents-> Edit Features -> Start Editing)*
        i. The main HUC 12 layer was superimposed on each of the DDF contour map jpg's

ii. The average precipitation value from each DDF map was added to each HUC 12 polygon that intersected Texas; Used values between the contour lines, DDF values were averaged; all values were rounded to 2 significant figures

Annual Flood Frequency, Drainage Condition Index, Hydrologic Group, K Factor (Catchment)

The Annual Flood Frequency, Drainage Condition Index, Hydrologic Group and K Factor variables are products of the STATSGO and SSURGO datasets that were acquired for each region through the NRCS Geospatial Data Gateway Portal[16]. The STATSGO GIS data are provided at the state scale, while the SSURGO data are frequently mapped at the county level. When the SSURGO dataset was not available, the STATSGO dataset was used.

Annual Flood Frequency (see Appendix B) estimates the approximate number of times flooding occurs over a time period for a given area (USDA n.d., 618.30). There are a total of six Flood Frequency Classes, however the majority of the installations in this study have very little flooding possibilities and fall into the *None* (< 1% chance of occurring within 100 yrs, but >1% occurring in 500yrs) flood frequency class. Some areas have a slightly higher flood frequency potentials and are in the *Very Rare* (<1% chance of occurring within 100yrs) or *Rare* (1-5% chance of occurring within 100yrs) flood frequency classes. Fort Huachuca has a few areas that fall within the *Occasional* Flood Frequency Class where flooding has a 5-50% chance of occurring within 100 yrs (USDA n.d., 618.30). The flood frequency variable derived in this analysis is based on the dominant Annual Flood Frequency class within each SSURGO/STATSGO map unit.

The Drainage Condition Index consists of 7 classes that are based on landscape position and soil morphology and refers to the natural drainage condition of the soil. The classes range from Excessively Drained to Very Poorly Drained (See Appendix B) which provides information regarding the limitations and potentials of soil (USDA n.d., 618.18). The drainage variable used in this analysis was based on the dominant Drainage Condition within each SSURGO/STATSGO map unit.

The Hydrologic Groups are split into four distinct categories (A, B, C, or D) that display similar runoff patterns (See Appendix B). These classes refer to intake and transmission of water under the conditions of maximum yearly wetness, unfrozen soil, bare soil surface and maximum swelling of expansive clays; with the principle idea that soils found within a climatic region should be similar in the following factors: depth of a restrictive layer (includes water table), transmission rate of water, soil texture, structure and degree of swelling when saturated (USDA Natural Resources Conservation Services, 2007). Group A soils generally allow water to flow freely through the soil, have a low runoff potential even when soil is thoroughly wet and generally have less than 10% clay and more than 90% of sand or gravel. Group B soils generally

[16] http://datagateway.nrcs.usda.gov/ or

http://websoilsurvey.nrcs.usda.gov/app/WebSoilSurvey.aspx (Soil Survey Staff)

allow water to transmit through soil unimpeded, therefore have moderately low runoff potential even when thoroughly wet, and generally consist of 10-20% clay and 50-90% sand with some loamy sand or sandy loam textures. Group C soils have constrained water transmission rates causing a moderately high runoff potential when thoroughly wet, and are usually 20-40% clay and less than 50% sand with possibilities of loam, silt loam, sandy clay loam, clay loam, clay loam, and silty clay loam present. Group D soils have very poor water transmission rates through the soil causing high runoff potential when thoroughly wet, with greater than 40% clay, less than 50% sand and have clayey textures (USDA Natural Resources Conservation Services, 2007).

The KF factor is a soil erodibility factor that quantifies the ability of soil less than 2.0 mm (fine earth) to detach from the substrate via runoff and raindrop impact (USDA, n.d., 618.58). The KF factor is based on the interactions between five soil properties:

1) Percent of silt plus very fine sand
2) Percent of sand greater than 0.10mm
3) Organic matter content
4) Soil structure
5) Saturated Hydraulic Conductivity

The KF factor includes 14 classes: 0.02. 0.05, 0.10, 0.15, 0.17, 0.20, 0.24, 0.28, 0.32, 0.37, 0.43, 0.49, 0.55 and 0.64; where the spread of these classes represents the uncertainty associated with the K value, such that 0.10 has $\pm$ 0.025 units of uncertainty (USDA, n.d., 618.58).
Both the SSURGO and STATSGO spatial and tabulated data were downloaded. The tabulated data were opened in the Microsoft Access SSURGO template file supplied with each download through the NRCS Data Gateway website (http://datagateway.nrcs.usda.gov/). After the tabulated database was connected in Microsoft Access, it was then usable in ArcMap. The *muaggatt component* and *chorizon* files contain the relevant fields used here.

81. Download all relevant SSURGO and STATSGO data from the NRCS Data Gateway site
82. The soils data were unzipped as well as the soildb_US_2002 zip folder that is nested within
83. The Access database files were opened and the location of the tabulated folder was entered into the SSURGO Import GUI (this enabled the soils databases to be useable in ArcMap
84. The spatial data of the STATSGO/SSURGO dataset as well as the corresponding *muaggatt, component,* and *chorizon* tables from the soildb_US_2002 access database were brought into ArcMap 10.1
85. Five new fields were added to the soils shapefile (**Step 15**, Figure 5)
    a. *Name:* HydroGrp
       Type: Text
       Length: 5
    b. *Name:* Drainage

Type: Text
Length: 50

c. *Name:* FldFreq
Type: Text
Length: 25

d. *Name:* cokey
Type: Text
Length: 30

e. *Name:* KFfact
Type: Text
Length: 5

86. The *muaggatt* table was joined (**Step 16**, figure 6) through the mukey field to the soils shapefile; field calculator (**Step17**) was used to transfer the *hydgrpdcd* to the newly created HydrGrp field, *drclassdcd* to the newly created Drainage field, and *flodfreqdcd* to the new FldFreq field; then the join was removed (**Step 18**, Figure 7)

87. Similarly to **Step 86**, the *component* table was joined to the soils shapefile through the *mukey* so that the cokey could be transferred to the newly created cokey field; then the join was removed

88. Similarly to **Step 86**, the *chorizon* table was joined to the soils shapefile through the *cokey* from the previous step, which allowed the *kffact* field to be transferred to the KFfact field in the soil shapefile; then the join was removed

89. **Steps 81** to **88** were repeated for each soils layer in the study areas; a **Merge Tool** *(Data Management -> General -> Merge)* was used to merge all of the SSURGO shapefiles together and when the SSURGO dataset was not available, the STATSGO dataset was added (the **Erase** and **Merge Tool** was used to add in the non-overlapping dataset)

90. The final product of **Step 89** was projected to the relevant HUC projection (Table 2, **Step 10**) then clipped to the NHDPlus WBD extents (**Step 19**, Figure 8)

91. The merged soils shapefile was dissolved on each of the following fields: *HydroGrp, Drainage, FldFreq* and *KFfact fields* individually by using the **Dissolve Tool** *(Data Management Tools -> Generalization -> Dissolve)* to create four new shapefiles

    a. *Input Features:* Soils shapefile
    Dissolve Field: check one of the four fields mentioned above, individually

92. For each of the four dissolved layers created in **Step 91**, the **Select Tool** *(Analysis Tools -> Extract -> Select)* was used to remove the category with no data or in the case of the KF factor, the zeros; this was done by selecting all the non-empty categories (Figure 12)

93. Each of the four dissolved shapefiles were converted to a raster using the **Polygon to Raster Tool** (*Conversion -> To Raster -> Polygon to Raster)*

    a. *Input Features:* one of the four dissolved shapefile from **Step 92**
    Value field: the corresponding dissolved field (HydroGrp, Drainage, FldFreq or KFfact)
    Cell Size: 20

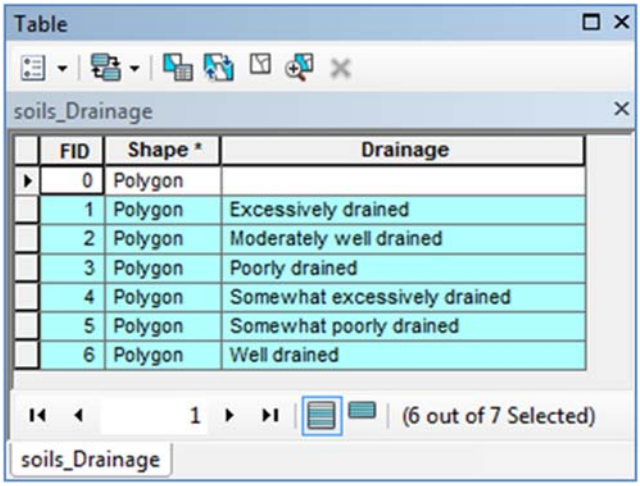


Figure 12: Using Select Tool to remove out the

94. To link each of the soils data to each of the Catchment layers, the **Zonal Statistics as Table Tool** was used *(Spatial Analyst Tools -> Zonal -> Zonal Statistics as Table)*

    a. *Input raster or feature zone data:* Catchment
    Zone field: GRIDCODE
    Input value raster: ***Each Raster layer created in Step 92, individually***
    Statistics type (optional): MAJORITY

95. The output tables from **Step 94** from the categorical data were transfer back into them

    a. Each table had a new field added (**Step 15**, Figure 5)
        i. *Name:* maj
        Type: Text
        Length: 50

    b. Each table was joined (**Step 16**, Figure 6) to the corresponding raster using the *MAJORITY* field from the Table and the *VALUE* field from the corresponding raster

    c. Field calculator was used to transfer the categories from the raster to the *maj* field for each table (**Step 17**)

    d. Each join was removed (**Step 18**, Figure 7)

96. The same fields in **Step 85** were added to the Catchment Layer

97. Each table was joined individually (**Step 16**, figure 6) to the Catchment layer through the GRIDCODE field; field calculator (**Step 17**) was used to transfer the *maj* to the corresponding newly created fields in the Catchment layer; then the joins were removed (**Step 18**, Figure 7)

Reach Metrics

Rock Type and Lithology

The Rock Type and Lithology can be important metrics in indentifying the type and character of the substrate and can also suggest distinctive weathering patterns. The USGS Mineral Resources Program: Geology Datasets include the dominant Rock or Lithology types and are displayed in a hierarchal order ranging from ROCKTYPE1 to ROCKTYPE2 and LITH 1 to LITH 5, where ROCKTYPE1 and LITH1 document the most dominant type. The USGS notes that the Geology Map Units are mapped on a relatively large scale (by state) and may force certain groupings to generalize the data at these scales and therefore may cause a generalization of the lithology categories; consequently, it is common that many of the Map Units contain more than one lithology (Lundington et al., 2007 & Stoeser, et al., 2007). Here LITH1 and LITH2 are assigned to each reach to help display the multiple lithologies.

Previously, ROCKTYPE1 was consolidated into the Weathered Texture Products in **Steps 65 - 75**. The same *XXgeol_dd_polygon* layers that were downloaded for the WPT metric from the USGS Mineral Resources Program: Geology Datasets were also used here. On the same website, the dbf file for each geology dataset was downloaded[17]. This dbf zipfile contains the lithology information that was linked to the geology shapefile through the UNIT_LINK field in both tables.

98. The same shapefile that was downloaded (for Fort Bliss, Texas and New Mexico were merged) and re-projected in **Steps 65 – 68** was uploaded into ArcMap 10.1
99. Three new fields were added to the geology shapefile for each installation (**Step 15**, Figure 5)
    a. *Name:* LITH1
       Type: Text
       Length: 50
    b. *Name:* LITH2
       Type: Text
       Length: 50
    c. *Name:* LITH_FORM
       Type: Text
       Length: 50

[17] California Geology Layers (http://pubs.usgs.gov/of/2005/1305/#CA): *California dbf files;*
Arizona Geology Layers (http://pubs.usgs.gov/of/2005/1305/#AZ): *Arizona dbf files;*
New Mexico Geology Layers (http://pubs.usgs.gov/of/2005/1351/#NM): *New Mexico dbf files;*
Texas Geology Layers http://pubs.usgs.gov/of/2005/1351/#TX): *Texas dbf files*

100. The [State] .dbf file that was downloaded from the same USGS website (see footnote 18) as the geology shapefile was unzipped and the *XX*LITH.dbf file was uploaded into ArcMap 10.1

101. A join was created between the shapefile and the *XX*LITH.dbf file through the UNIT_LINK field (**Step 16**, Figure 6)

102. The LITH1, LITH2 and LITH_FORM fields were transferred to the geology shapefile through Field Calculator (**Step 17**) and the join was removed (**Step 18**, Figure 7)

103. A point shapefile was created that contained the midpoints of each reach by

    a. Creating an x and y field (float) within the reach layer

    b. Using calculate geometry tool (**Step 30**, Figure 10) to acquire the x and y coordinates of the midpoints of each reach

    c. Exporting the attribute table as a dbf file (Select the menu button  in the attribute table, then ***Export…*** and save as a **dBASE Table**)

    d. In ArcCatalog, the exported file was selected and right clicked; then ***Create Feature Class*** **and** ***From XY Table…*** was selected (Figure 13); in the next GUI, the x and y fields were selected.

        i. The new point layer was projected to the same projection as the geology layer

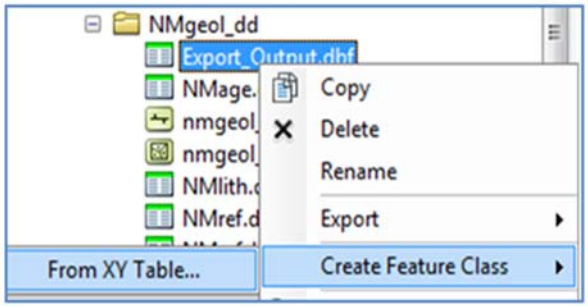


Figure 13: Creating a Feature Class from a dbf file.

104. The point layer was intersected with the geology layer *(Analysis Tools -> Overlay -> Intersect)*

105. The ROCKTYPE1, ROCKTYPE2, LITH1, LITH2 and LITHFORM of the intersected point layer was transferred back to the main reach Flowline layer by

    a. Adding the fields (**Step 15**, Figure 5) to the Reach Flowline layer

        i. *Name:* ROCKTYPE1
        Type: Text
        Length: 50

        ii. *Name:* ROCKTYPE2
        Type: Text
        Length: 50

        iii. *Name:* LITH1
        Type: Text
        Length: 50

iv. *Name:* LITH2
Type: Text
Length: 50

v. *Name:* LITH_FORM
Type: Text
Length: 50

b. Joining the tables through the *UniqueID* (**Step 16**, Figure 6)

c. Using Field Calculator to transfer each of the 5 geology metrics to the reach network (**Step 17**)

d. Removing the join (**Step 18**, Figure 7)

Rainfall Seasonality and Modified Fournier Index

The monthly PRISM grid layers were used to calculate the Rainfall Seasonality Index and the Modified Fournier Index of each reach. Calculating these metrics at the reach scale may show more subtle changes than as generalized at the Watershed (HUC 12) scale. Similar methods were utilized as described in the *Rainfall Seasonality and Modified Fournier Index* of the HUC 12 layer (**Steps 58 – 64)**; however, here the tool *Extract Multi Values to Points* was employed with the reach midpoint shapefile.

106. The Annual and Monthly 30-Year Normals[18] (.asc) data at the 800m resolution that were download in **Step 58**, were uploaded into ArcMap 10.1 (13 ascii layers)

107. The midpoint shapefile that was created in **Step 103** was projected to the same projection as the PRISM datasets (GCS North American 1983) by using the **Project Tool** *(Data Management -> Projections and Transformations -> Feature -> Project)*

    a. *Input:* Reach Midpoint Layer
    Output Coordinate System: GCS_North_American_1983
    Output Transformation (optional): WGS_1984_(ITRF00)_To_NAD_1983

108. **Extract Multi Values to Points Tool** was used to add the monthly and annual precipitation values as each point *(Spatial Analyst Tools -> Extraction -> Extract Multi Values to Points)*

    a. *Input point features:* Reach Midpoint Layer in GCS projection
    Input rasters: Annual and All months (together), named appropriately

109. The same methods were followed as described in **Steps 61 -64**; except the attribute table of the layer that was created in **Step 108** was used instead of the HUC 12 layer

[18] http://www.prism.oregonstate.edu/normals/ (PRISM Climate Group, 2010)

Reach Width at 0.25, 0.5, 1, 2 and 3 meters inundation depth

The water surface widths of streams at varying depths (Figure 14) can be an important indicator of channel hydro-geomorphology and may be used to identify bankfull width or channel incision. In this study, the mean widths at various inundation depths were calculated at each reach segment. The HGVC (Hydro-Geomorphic Valley Classification) extension tool (Carlson E.A., 2009) was used in ArcMap 10.1 to create the water surface extent polygons at different inundated depths. To create these layers, a DEM (LiDAR or 10m DEM) and flowline shapefile were used with the *Optional Inundation Depth Tool*. The polygons were created for 0.25, 0.5, 1.0, 2.0 and 3.0m depths.

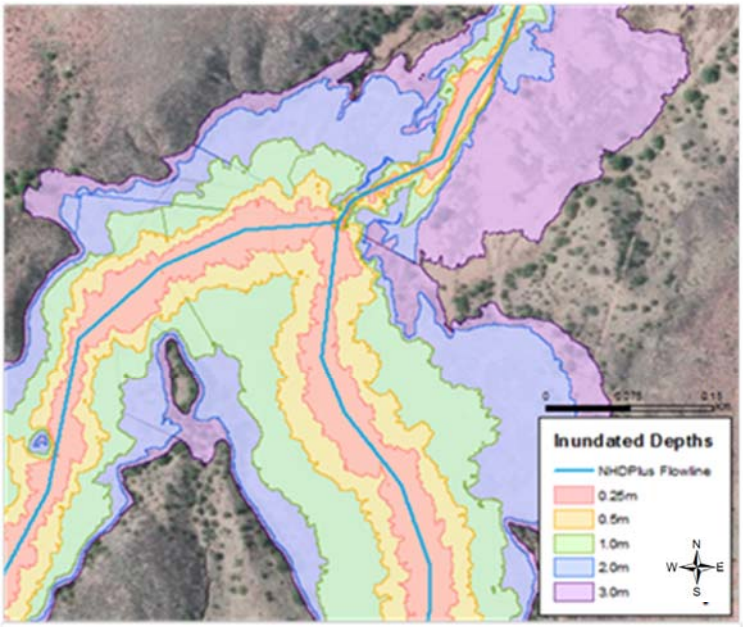


Figure 14: Inundated polygons at different depths at Fort Huachuca using the HGVC tool and LiDAR as the Digital Elevation Model.

110. The Reach Flowline Layer and DEM (LiDAR-Bare Earth or 10 DEM) were uploaded into ArcMap 10.1
111. The LiDAR or DEM were projected to the associated projection listed in Table 2
112. The HGVC 9.3 Toolset was added into ArcToolbox (by right clicking in ArcToolbox, selecting *Add Toolbox…* and navigating to location on computer), then the **Optional: Inundation Tool** was opened (*HGVC 9.3 Toolset -> Valley Segment Creation -> Optional: Inundation Depth)*
    a. *INPUT: Filled Surface Raster:* filled LiDAR or DEM
    INPUT: Stream Network Raster: Reach Flowline Layer
    INPUT: Unique Valley Analysis Area Shapefile: Base Boundary

Flood Depth (m) (optional): 3, 2, 1, 0.5, 0.25 (individually)

113. A 200 m buffer of the flowline was created to segment the inundated layers back into the reach segments *(Analysis Tools -> Proximity -> Buffer)*

    a. *Input Features:* Reach Flowline
    Distance [value or field]: 200 meters
    Side Type (optional): FULL
    End Type (optional): FLAT
    Dissolve Fields (optional): NONE

114. The Inundation Layer was clipped to the Reach Buffer Layer *(Analysis Tools -> Extract -> Clip)*

    a. *Input Features:* Buffered Reach Layer (**Step 113**)
    Clip Features: 3m Inundation Layer (**Step 112**)

115. The output layer from **Step 114** was manually edited to remove extraneous portions of the stream segments that were clipped near adjacent streams or confluences

    a. The Intersect tool was used to find areas of overlap within the inundated reach polygon layer *(Analysis Tools -> Overlay -> Intersect)*; Input Features: the inundation reach layer by itself

116. Once the 3m inundation layer was edited, the 2m Inundation Layer was clipped *(Analysis Tools -> Extract -> Clip)*

    a. *Input Features:* Edited 3m Inundation Layer (**Step 115**)
    Clip Features: 2m Inundation Layer (**Step 112**)

    b. **Step 115** was re-executed for the 2m Inundation Reach output

117. **Step 116** was repeated for the 1, 0.5, and 0.25m using the corresponding Input and Clip features for each inundation depth

118. Two new Fields were added into each of the finalized inundation layers (**Step 15**, Figure 5)

    a. *Name:* Area_sqm
    Type: Float
    b. *Name:* Width_m
    Type: Float

119. For the *Area_sqm* field, Calculate Geometry was used to determine the area of each reach polygon (**Step 30**, Figure 10)

    a. *Property:* Area
    Units: Square Meters [sqm]

120. For the *Width_m* field in each Inundated Reach Layer, Field Calculator (**Step 17**) was used

a. *Width_m*= **[Area_sqm] / [Length_m]**

121. In the main Reach Flowline Layer, five new fields were added (**Step 15**, Figure 5)

a. *Name:* Width3m, Width2m, Width1m, Width0_5m, and Width0_25m
Type: Float

122. The inundated widths were transferred to the main Reach Flowline Layer by

a. Joining each Inundated Table through the *UniqueID* (**Step 16**, Figure 6)

b. Using Field Calculator (**Step 17**) to transfer the *Width_m* field to the associated field created in **Step 121**

c. Each Join was removed (**Step 18**, Figure 7)

National Flood Frequency: Linear Regression Equations

The relevant documents that display the Linear Regression Equations were downloaded through the USGS Publications Warehouse. The documents used for Fort Bliss were *The Analysis of the Magnitude and Frequency of Peak Discharge and Maximum Observed Peak Discharge in New Mexico and Surrounding areas*[19] and *The National Flood-Frequency Program – Methods for Estimating Flood Magnitude and Frequency for Natural Basins in Texas, 2001*[20]. For Fort Irwin, the document used was *Methods for Determining Magnitude and Frequency of Floods in California, Based on Data through Water Year 2006*[21]. For YPG and Huachuca, the document *The National Flood-Frequency Program – Methods for Estimating Flood Magnitude and Frequency in Rural Areas in Arizona*[22] was used.

Contributing Area

The Contributing Area (CA) of a channel is defined as the area of the hillslopes above the channel that carry water during rain events into the channel. The CA used in this methodology was derived from the FAC grid layers included with the NHDPlus Version 2 Dataset which counts the number of cells within the HydroDEM that drains into each cell. Each cell in the FAC grid is 30 by 30 meters and therefore has an area of 900m^2 or 0.0009km^2. The CA values were used in the Flood Peak Discharge, Total Stream Power and Unit Stream Power Equations in the following sections.

123. The Flow Accumulation (FAC) Grid layers that were downloaded through the Horizon Systems NHD Plus website[23] in the Data Acquisition section were unzipped and uploaded into ArcMap 10.1 (Refer to Table 1: XXX*_FdrFac_01.7z.)*; at some bases, multiple grids were required.

---

[19] http://pubs.usgs.gov/sir/2008/5119/ (Waltemeyer, 2008)

[20] http://pubs.er.usgs.gov/publication/fs02201 (Sumioka, 2001)

[21] http://pubs.usgs.gov/sir/2012/5113/ (Gotvald, 2012)

[22] http://pubs.er.usgs.gov/publication/fs11198 (Mason, et al. 1999)

[23] http://www.horizon-systems.com/nhdplus/NHDPlusV2_home.php (Horizon Systems Corporation)

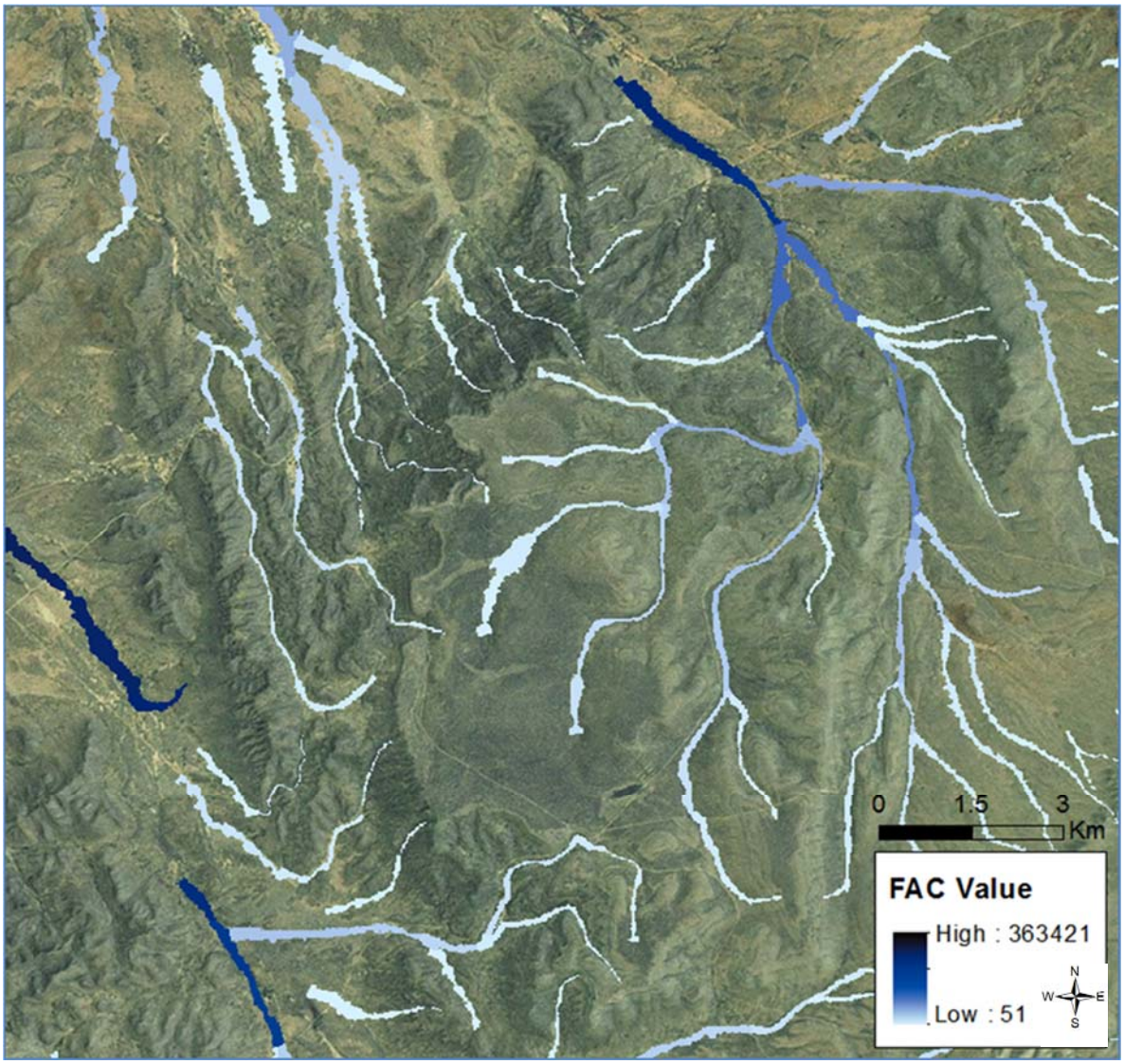


Figure 15: Flow Accumulation Values from the NHD Plus Version 2 dataset for each Reach at Fort Bliss. The FAC values were multiplied by 0.0009 to get the contributing area in square kilometers.

124. The 1m Inundation Layer created in **Steps 110 – 117** was used to find the maximum FAC value of each reach

    a. The confluences of the 1m reach polygons were removed to eliminate processing errors

        i. **Intersect** the 1m Inundation Layer with itself *(Analysis Tools ->Overlay -> Intersect)*

        ii. **Erase** the intersected area *(Analysis Tools ->Overlay -> Erase)*

            1. *Input Features:* 1m Inundation Layer
               Erase Features: Intersected layer from **Step 124.a.i**

2. This step erases some polygons resulting in incorrect FAC values, but this was mitigated in a later step

125. The newly created inundation layer was projected to the same projection as the FAC grid layer *(Data Management Tools -> Projections and Transformations -> Feature -> Project)*

    a. *Output Coordinate System:* NAD_1983_To_WGS_1984_1
    Geographic Transformation (optional): NAD_1983_To_WGS_1984_1

126. **Zonal Statistics as Table** was used to find the maximum FAC value within the reach polygons *(Spatial Analyst Tools -> Zonal -> Zonal Statistics as Table)*

    a. *Input raster or feature zone data:* 1m Inundated layer from **Step 125**
    Zone field: UniqueID
    Input value raster: FAC Grid
    Statistics type (optional): MAX
    b. This was completed for all overlapping grids in the study area

127. The values were transferred back to the original 1m Inundation Layer by

    a. Adding a new field to the Inundation Layer (**Step 15**, Figure 5)

        i. *Name:* fac
        Type: Long

    b. The tables were joined (**Step 16**, Figure 6) by the *UniqueID* field

    c. Field calculator was used to transfer the *max* field to the *fac* field (**Step 17**)

    d. The join was removed (**Step 18**, Figure 7)

128. Errors were corrected by using the *Symbology* Tab (Right click on the feature class, then select *Properties…*), selecting the *Graduated Colors* under the *Quantities* tab, then choosing the *fac* field as the Value class; this assisted the detection of incorrect or missing FAC values along the flowline network; any errors found were manually inserted into the *fac* field using the **Editor Tool**

129. After the FAC values were corrected, the attribute table was exported to a .dbf file and uploaded into excel

130. The fac values of each reach were converted into square miles to be used in the Discharge Linear Regression Equations by using the equation:

    Contributing Area (mi^2) = *fac value* * $0.009km^2$ * $0.386102mi^2/km^2$

Flood-Peak Discharge

The Linear Regression equations found in the corresponding state Magnitude and Frequency documents described in the National Flood Frequency Program introduction were applied to calculate the Flood-peak Discharge for the recurrence intervals 2, 5, 10, 25, 50, and 100 years and were displayed in cms. The equations are in US Customary units (cfs), and were converted to SI units (cms). The Contributing Area for each reach is in mi^2 and Q is calculated in cfs. For elevation, the elevation at the midpoint (feet) of the reach was used. After the magnitude of discharge was calculated, the volume was then converted back into cms by multiplying by 0.028316.

131. In Excel, the Contributing Area for each reach calculated in **Step 130** was inserted into the Regional Discharge Equations associated with each installation at the 2, 5, 10, 25, 50, and 100 year recurrence interval (**Table 5)**

Table 5: Regional Discharge Equations where A is the Contributing Area and Q_x is the Discharge at a specific recurrence interval.

Recurrence Interval	Fort Bliss	Fort Huachuca & YPG	Fort Irwin
Q_2	$= 146.5 \times A^{0.454}$	$= 10^{(6.38 - 4.29A^{-0.06})}$	$= 10.3 \times A^{0.506}$
Q_5	$= 277.7 \times A^{0.468}$	$= 10^{(5.78 - 3.31A^{-0.08})}$	$= 60.0 \times A^{0.506}$
Q_{10}	$= 387.8 \times A^{0.477}$	$= 10^{(5.68 - 3.02A^{-0.09})}$	$= 151 \times A^{0.506}$
Q_{25}	$= 553.7 \times A^{0.488}$	$= 10^{(5.64 - 2.78A^{-0.10})}$	$= 403 \times A^{0.506}$
Q_{50}	$= 695.5 \times A^{0.497}$	$= 10^{(5.57 - 2.59A^{-0.11})}$	$= 760 \times A^{0.506}$
Q_{100}	$= 851.8 \times A^{0.506}$	$= 10^{(5.52 - 2.42A^{-0.12})}$	$= 1{,}350 \times A^{0.506}$

132. The Discharge values were converted into cms by multiplying the results by $0.028316 m^3/ft^3$

Total Stream Power

The Total Stream Power (TSP) is an estimate of the ability of a stream to transport sediment and can be influential within fluvial systems. The equation for TSP in kW/m is

$$\Omega = \rho g Q S$$

Where ρ is the density of water at 1.0 kg/m^3, g (gravity) = $9.81 m/s^2$, Q = Flood-Peak Discharge for the given frequency event (m^3/s), S is slope (m/m). TSP was calculated for the same return intervals as the Flood-Peak Discharge by using the corresponding Q variable (2, 5, 10, 25, 50, and 100 years) calculated in the Flood-Peak Discharge section.

133. In Excel, the Discharge values (cms) for each recurrence interval were inserted into Equation 3, where Ω = kW/m

Equation 3:

$$\Omega = \mathbf{1.0}\,{}^{kg}/_{m^3} \times \mathbf{9.81}\,{}^{m}/_{s^2} \times \boldsymbol{Q}\,{}^{m^3}/_{s} \times \boldsymbol{Slope}\,{}^{m}/_{m}$$

Unit Stream Power

The Unit Stream Power (USP) is an estimate of the rate of energy expenditure per unit area of channel bed and has relevance in bed sediment entrainment, bedload transport rate and stream stability. The equation for USP in kW/m^2 is

$$\omega = \frac{\rho g S \sqrt{Q}}{a}$$

Where ρ, g, S and Q are the same variables in the Total Stream Power equation and *a* is a constant between 3.0 and 4.7 depending on the substrate. In this case, $a = 3.6\sqrt{s/m}$ was used. This equation was used to calculate USP for the corresponding Q variables in the Flood-Peak Discharge section.

134. In Excel, the Discharge values (cms) per each recurrence interval were inserted into Equation 4, where ω =kW/m^2:

Equation 4:

$$\boldsymbol{\omega} = \mathbf{1.0}\,{}^{kg}/_{m^3} \times \mathbf{9.81}\,{}^{m}/_{s^2} \times \boldsymbol{Slope}\,{}^{m}/_{m} \times \left. \sqrt{\boldsymbol{Q}\,{}^{m^3}/_{s}} \right/ \mathbf{3.6}\sqrt{{}^{s}/_{m}}$$

135. The Discharge, Total Stream Power and Unit Stream Power values were entered into a geodatabase table for each *UniqueID,* and can be joined to the reach Flowline layer to map these quantities across each base.

Literature Cited

Asquith W. H. and M. C. Roussel, 2004. Atlas of Depth-Duration Frequency of Precipitation Annual Maxima for Texas. U.S. Geological Survey Scientific Investigations Report 2004-5041. TxDOT Implementation Report 5-1301-01-1.

Bonnin, G. M., D Martin, B. Lin, T. Parzybok, M. Yekta, D. Riley. 2011. NOAA Atlas 14 Volume 1 Version 5.0, Precipitation-Frequency Atlas of the United States. Semiarid Southwest (Arizona, Southeast California, Nevada, New Mexico, Utah). NOAA, National Weather Service, Silver Spring, MD.

Dunne, T., and L.B, Leopold. 1978. Water in Environmental Planning, 2nd edn. W.H. Freeman, San Francisco.

Elagib, N. A. 2011. Changing Rainfall, Seasonality and Erosivity in the Hyper-Arid Zone of Sudan. *Land Degradation & Development* ***22*****(6)**:505-512.

ET SpatialTechniques: ET GeoWizards, Version 10.2. Faerie Glen, South Africa.

Gap Analysis Program: Metadata. 2010. National Land Cover Gap Analysis Project. Version 1.

Gotvald, A.J., Barth, N.A., Veilleux, A.G., and Parrett, Charles. 2012. Methods for determining magnitude and frequency of floods in California, based on data through water year 2006: U.S. Geological Survey Scientific Investigations Report 2012–5113, 38 p., 1 pl., available online only at http://pubs.usgs.gov/sir/2012/5113/.

Horizon Systems Corporation: National Hydrography Dataset Plus (NHDPlus Version 2). Herndon, Virgina.

Carlson, E.A. 2009. Fluvial riparian classification for national forests in the western United States. M.S. Thesis. Colorado State University.

Lundington, S., B. Moring, R. J. Miller, P. A. Stone, A. A. Bookstrom, D. R. Bedford, J. G. Evans, G. A. Haxel, C. J. Nutt, K. S. Flyn, M. J. Hopkins. 2007. Preliminary Integrated Geologic Map Databases for the United States, Western States: California, Nevada, Arizona, Washington, Oregon, Idaho and Utah. Version 1.3. U. S. Geological Survey: Open-File Report (2005-1305). (http://pubs.usgs.gov/of/2005/1305/).

Mason, R. R. Jr., J. N. King, O. Jr. Wilbert. 1999. The National Flood-Frequency Program—Methods for Estimating Flood Magnitude and Frequency in Rural Areas in Arizona. U.S. Geological Survey Fact Sheet 111-98.

National Hydrography Dataset Plus - NHDPlus Version 2. U.S. Environmental Protection Agency (USEPA) and the U.S. Geological Survey (USGS).

Office of Hydrologic Development, NWS, NOAA. April, 2014. Hydrometeorological Design Studies Center Quarterly Progress Report. Silver Spring, Maryland. (http://www.nws.noaa.gov/oh/hdsc/current-projects/progress/201404_HDSC_PR.pdf)

Perica S., S. Dietz, S. Heim, L. Hiner, K. Maitaria, D. Martin, S. Pavlovic, I. Roy, C. Trypaluk, D. Unruh, F. Yan, M. Yekta, T. Zhao, G. Bonnin, D. Brewer, L. Chen, T. Parzybok, and J. Yarchoan. 2011. NOAA Atlas 14 Volume 6 Version 2.0, Precipitation-Frequency Atlas of the United States, California. NOAA, National Weather Service, Silver Spring, MD.

PRISM Climate Group. 2010. Gridded climate data for the contiguous USA. http://prism.oregonstate.edu

Salford Systems: Salford Predictive Modeler (SPM). San Diego, California.

Soil Survey Staff, Natural Resources Conservation Service, United States Department of Agriculture. U.S. General Soil Map (STATSGO2).

Soil Survey Staff, Natural Resources Conservation Service, United States Department of Agriculture. Soil Survey Geographic (SSURGO).

Stoeser, D. B., G. N. Green, L. C. Morath, W. D. Heran, A. B. Wilson, D. W. Moore, and B. S. Van Gosen. 2007. Preliminary Integrated Geologic Map Databases for the United States, Central States: Montana, Wyoming, Colorado, New Mexico, North Dakota, South Dakota, Nebraska, Kansas, Oklahoma, Texas, Iowa, Missouri, Arkansas, and Louisiana. Version 1.2. U. S. Geological Survey: Open-File Report (2005-1351). (http://pubs.usgs.gov/of/2005/1351/).

Sumioka, S. S., K. G. Reis III. 2001. The National Flood-Frequency Program – Methods for Estimating Flood Magnitude and Frequency for Natural Basins in Texas, 2001. USGS Fact Sheet: 022-01.

USDA 2007. Natural Resources Conservation Services. Part 630 Hydrology National Engineering Handbook. Chapter 7: Hydrologic Soil Groups. Accessed: June 16, 2014. (http://directives.sc.egov.usda.gov/OpenNonWebContent.aspx?content=17757.wba)

USDA n.d. Natural Resources Conservation Services. National Soil Survey Handbook (NSSH): Part 618 (Subpart A). Accessed: June 16 2014. (http://www.nrcs.usda.gov/wps/portal/nrcs/detail/soils/survey/?cid=nrcs142p2_054223#39)

US Geological Survey. n.d. Gap Analysis Program (GAP). August 2011. National Land Cover, Version 2.

US Geological Survey. n.d. (b). National Hydrography Dataset: High Resolution.

US Geological Survey. n.d. (c). The National Map Viewer.

Waltemeyer, S.D. 2008. Analysis of the magnitude and frequency of peak discharge and maximum observed peak discharge in New Mexico and surrounding areas: U.S. Geological Survey Scientific Investigations Report 2008–5119, page 105.

Appendix A: Weathered Products Texture

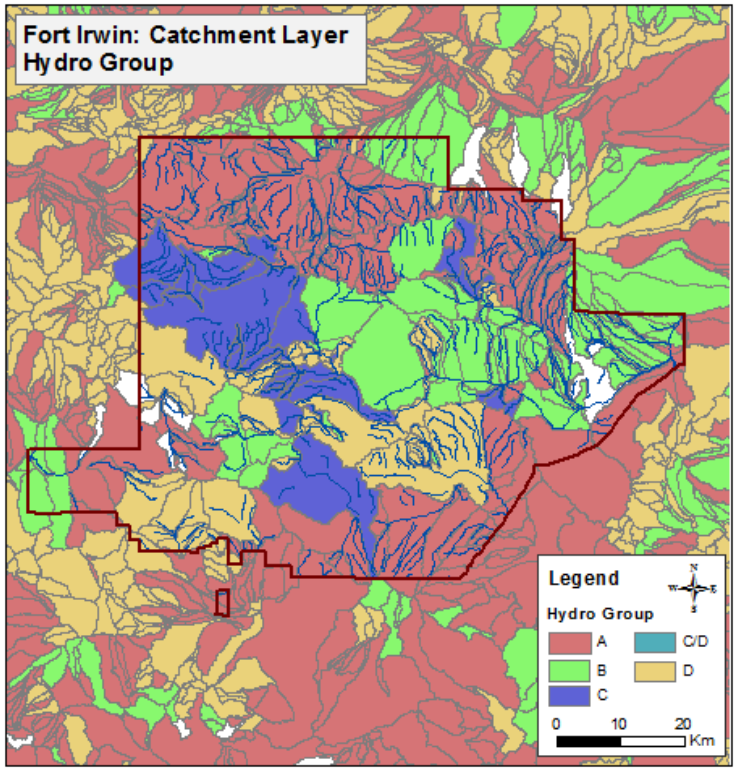
Rock Type reclassified into the Weathered Products Texture parameter. Rock Types not included in this table are classified as "Unknown".

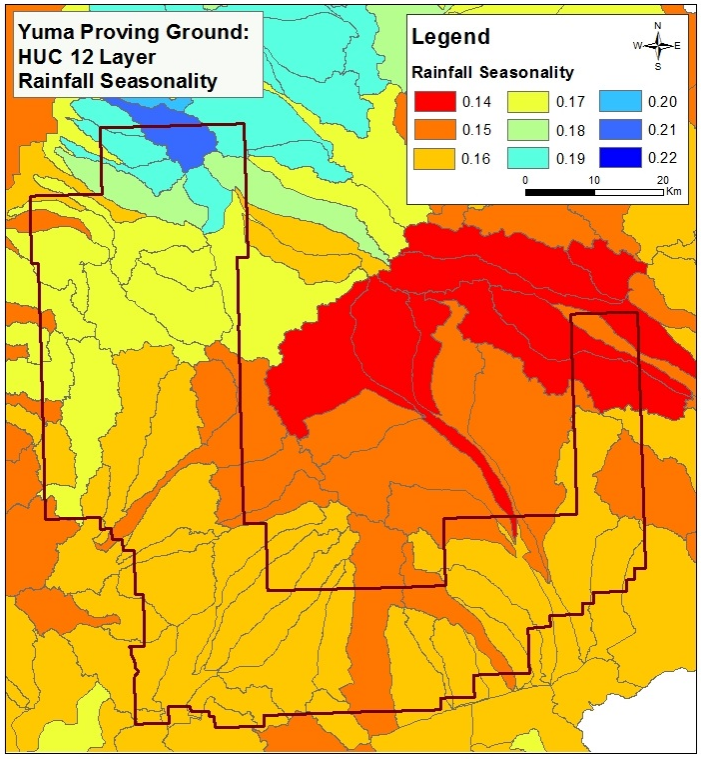
Rock Type	WPT	Rock Type	WPT
Alkaline Basalt	Fine	**Granite**	Coarse
Alluvial Fan	Unconsolidated	**Granodiorite**	Coarse
Alluvium	Unconsolidated	**Gravel**	Unconsolidated
Andesite	Fine	**Intermediate Volcanic Rock**	Fine
Argillite	Fine	**Lake or Marine Deposit (Non-Glacial)**	Unconsolidated
Basalt	Fine	**Lava Flow**	Fine
Carbonate	Fine	**Limestone**	Fine
Clastic	Coarse	**Metasedimentary Rock**	Fine
Clay or Mud	Unconsolidated	**Mica Schist**	Fine
Conglomerate	Coarse	**Mudstone**	Fine
Coarse Grained Mixed Clastic	Coarse	**Plutonic Rock (phaneritic)**	Coarse
Dacite	Fine	**Quartz Monzonite**	Coarse
Dolostone (dolomite)	Fine	**Quartz-Feldspar Schist**	Fine
Dune Sand	Unconsolidated	**Rhyolite**	Fine
Eolian	Unconsolidated	**Sand**	Unconsolidated
Felsic Volcanic Rock	Coarse	**Sandstone**	Coarse
Fine-Grained Mixed Clastic	Fine	**Schist**	Fine
Gabbro	Coarse	**Sedimentary Rock**	Fine
Gneiss	Coarse	**Shale**	Fine

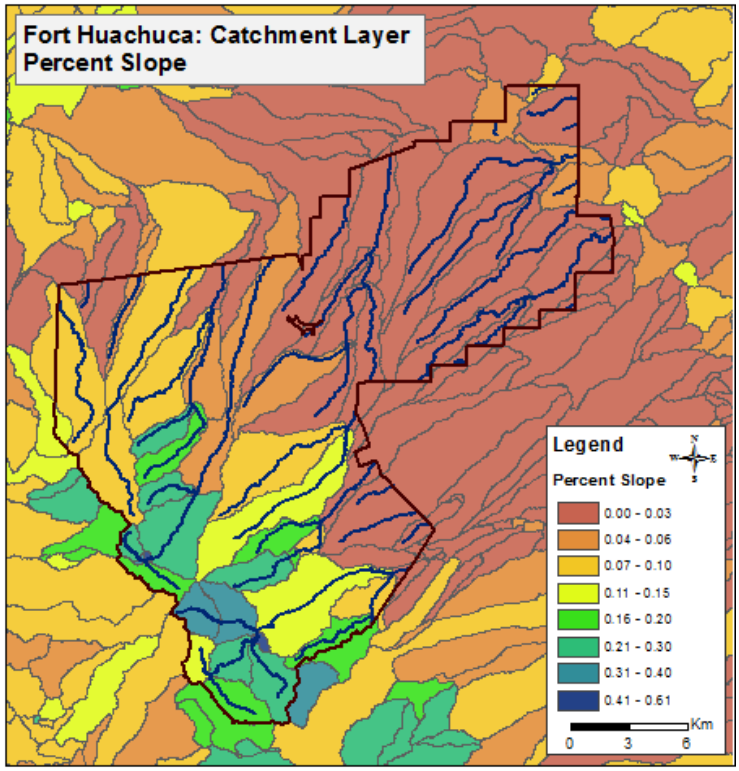
Appendix B: Soil Properties aggregated from the National Soil Survey Handbook (NSSH): Part 618 (Subpart A)

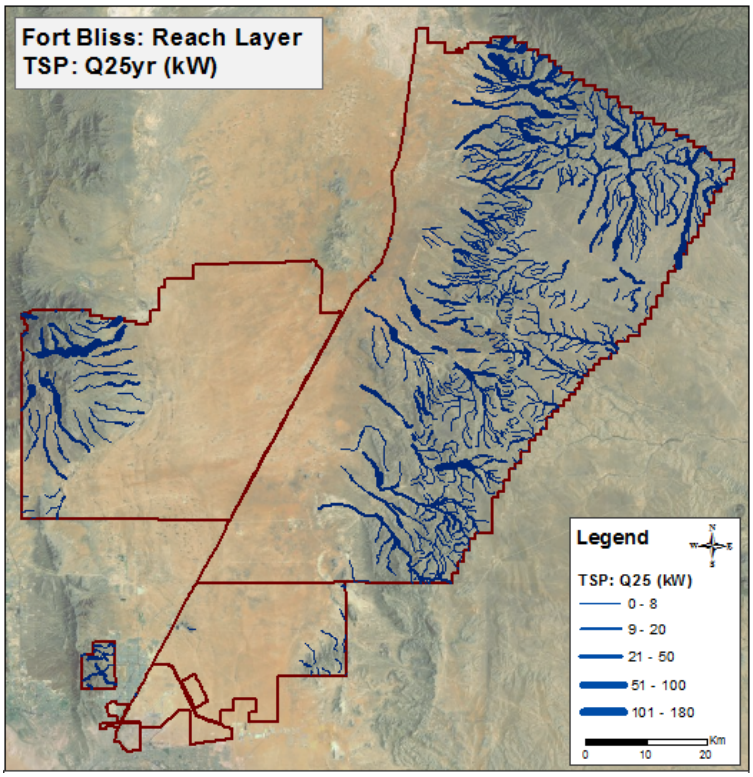
	Flood Frequency	Drainage Condition Index	Hydrologic Group	K Factor
Description	The annual probability of a flood event	The natural drainage condition of the soil refers to the degree, frequency and duration of wet periods.	A group of soils having similar runoff potential under similar storm and cover conditions.	Erodibility factor which quantifies the susceptibility of soil particles to detachment by runoff and raindrop impact.
Data Type	Categorical	Categorical	Categorical	Categorical
Classes	6	7	4	14
Variables	**1 = None** (possibility of flood occurring <1 time in 500 yrs) **2 = Very Rare** (possibility of flood occurring <1 time in 100yrs) **3 = Rare** (possibility of flood occurring 1-5 times in 100yrs) **4 = Occasional** (possibility of flood occurring 5-50 times in 100yrs) **5 = Frequent** (possibility of flood occurring is >50 times in 100yrs, but less than 50% chance of flood occurring in all mon/yr) **6 = Very Frequent** (possibility of flood occurring is >50 times in 100yrs, but more than 50% chance of flood occurring in all mon/yr)	1 = Excessive 2 = Somewhat Excessive 3 = Well Drained 4 = Moderately Drained 5 = Somewhat Poorly Drained 6 = Poorly Drained 7 = Very Poorly Drained	**A** = low runoff potential **B** = moderately low runoff potential **C** = moderate runoff potential **D, A/D, B/D, C/D** = high runoff potential	0.02 0.05 0.10 0.15 0.17 0.20 0.24 0.28 0.32 0.37 0.43 0.49 0.55 0.64
Table Name	muaggatt	muaggatt	muaggatt	chorizon
Field Name	flodfreqdcd	drclassdcd	hydgrpdcd	kffact
NHHS Source (USDA n.d.)	618.30 Flooding Frequency Class	618.18 Drainage Class	618.39 Hydrologic Group	618.58 Soil Erodibility Factors

Appendix C: Map Examples of Derived Data









Appendix K: Geomorphology Analysis Guidance Document